BIORHEOLOGY

THE OFFICIAL JOURNAL OF THE
INTERNATIONAL SOCIETY OF BIORHEOLOGY

An Affiliated Commission of the International Union for Pure and Applied Biophysics

Editors-in-Chief: Alfred L. Copley, New York, N.Y., U.S.A. *and* Alex Silberberg, Rehovot, Israel

Vol. 17
1980

LIST OF CONTENTS
AND
AUTHOR INDEX
VOLUMES 16 & 17, 1979 & 1980

PERGAMON PRESS

BIORHEOLOGY

Founded by A. L. Copley and G. W. Scott Blair

Editors-in-Chief

ALFRED L. COPLEY, Laboratory of Biorheology, Polytechnic Institute of New York, 333 Jay Street, Brooklyn, NY 11201, U.S.A. *OR*: 50 Central Park West, New York, NY 10023, U.S.A.
A. SILBERBERG, Polymer Department, The Weizmann Institute of Science, Rehovot, Israel

Board of Editors

E. FUKADA, Biopolymer Physics Laboratory, Rikagaku Kenkyusho (The Institute of Physical and Chemical Research), Wako-shi, Saitama 351, Japan (Haemorheology; Piezoelectricity of Biopolymers; Bone).
Y.C.B. FUNG, Department of Applied Mechanics and Engineering Sciences, M-005, University of California, San Diego, La Jolla, CA 92037, U.S.A. (Hemorheology; Lungs; Bolus).
H.L. GOLDSMITH, The Montreal General Hospital, 1650 Cedar Avenue, Montreal, Quebec, H3G 1A4, Canada (Hemorheology; Models).
R.D. HARKNESS, Department of Physiology, University College, London, Gower Street, London WC1E 6BT, England (Collagen).
J.C. HEALY, Laboratoire de Biophysique et d'Informatique Médicale, U.E.R. de Médecine, Université de Saint-Etienne, 30, rue Ferdinand Gambon, La Métare, 42023 Saint-Etienne Cédex, France (Hemorheology).
Y. HIRAMOTO, Biological Laboratory, Tokyo Kogyo Daigaku (Tokyo Institute of Technology) Ookayama, Meguro-Ku, Tokyo, Japan.
N. KAMIYA, Department of Cell Biology, National Institute for Basic Biology, Myodaiji, Okazaki 444, Japan (Protoplasm; Botanical Sciences).
M. LITT, Department of Bioengineering, University of Pennsylvania, College of Engineering and Applied Science, 289 Towne Building D3, Philadelphia PA 19104, U.S.A. (Mucus; Hemorheology).
A. MAROUDAS, Bone and Joint Research Unit, The London Hospital Medical College, University of London, Arthritis and Rheumatism Council Building, 25-29 Ashfield Street, London E1 2AD, United Kingdom.
S. OKA, National Cardiovascular Center Research Institute, 5-125 Fujishiro-dai, Suita, Osaka 565, Japan (Theory; Hemorheology; Hemodynamics).
E. PUCHELLE, Unité de Recherche de Physio-Pathologie Respiratoire, U 14 Inserm • Plateau de Brabois, 54500 Vandoeuvre Annexe 2, Nancy, France (Mucus).
D. QUEMADA, Laboratoire de Biorheologie et d'Hydrodynamique Physiologique, Université Paris VII, Tour 33/34, 2•etage, 2 Place Jussieu, 75221 Paris Cédex 05, France (Theory; Hemorheology).
R. SKALAK, Department of Civil Engineering, Columbia University, Seeley W. Mudd Building, New York, NY 10027, U.S.A. (Theory; Hemorheology).
V.I. VOROB'EV, Institute of Cytology, Academy of Sciences, Leningrad 190121, U.S.S.R. (Cell Biology).

Honorary Editorial Advisory Board

S.E. BERGENTZ, *Malmö, Sweden*
D.E. BROOKS, *Vancouver, Canada*
G. BUGLIARELLO, *New York, U.S.A.*
C.G. CARO, *London, England*
S.E. CHARM, *Boston, U.S.A.*
S. CHIEN, *New York, U.S.A.*
D. DANON, *Rehovot, Israel*
L. DINTENFASS, *Sydney, Australia*
F.R. EIRICH, *New York, U.S.A.*
L.E. GELIN, *Göteborg, Sweden*
J.F. GROSS, *Tucson, Arizona, U.S.A.*
H.H. HARTERT, *Kaiserslautern, F.R.G.*
A. LARCAN, *Nancy, France*
S.G. MASON, *Montreal, Canada*
Y. MASUDA, *Osaka, Japan*
G.E. PALADE, *New Haven, U.S.A.*
R.D. PRESTON, *Leeds, U.K.*
G. QUADBECK, *Heidelberg, F.R.G.*
R.S. RIVLIN, *Bethlehem, U.S.A.*
S. SENO, *Okayama, Japan*
B. TAMAMUSHI, *Tokyo, Japan*
R.L. WHITMORE, *Brisbane, Australia*
C.A. WIEDERHIELM, *Seattle, U.S.A.*

BIORHEOLOGY Executive Editorial Office: Polytechnic Institute of New York, 333 Jay Street, Brooklyn, NY 11201, U.S.A.

Publishing, Subscription and Advertising Offices: Pergamon Press Inc., Fairview Park, Elmsford, NY 10523, U.S.A.; or Pergamon Press Ltd., Headington Hill Hall, Oxford OX3 0BW, England.

PUBLISHED BIMONTHLY. *Annual Subscription Rates* including postage and insurance for libraries, university departments, government laboratories, industrial and other multiple-reader institutions: (1981) US $150.00. Two-year Rate (1981/82) US $285.00. *Specially Reduced Rates to Individuals:* In the interests of maximizing the dissemination of the research results published in this important international journal, we have established a two-tier price structure. Any individual whose institution takes out a library subscription, may purchase a second or additional subscription for personal use at a much reduced rate of US $45.00. Prices include surface postage and insurance; air mail subscriptions extra. Subscription inquiries should be sent to Pergamon Press Inc., Maxwell House, Fairview Park, Elmsford, NY 10523, USA.; or Pergamon Press Ltd., Headington Hill Hall, Oxford OX3 0BW, England.

Microform Subscriptions and Back Issues

Back issues of all previously published volumes are available in the regular editions and on microfilm and microfiche. Current subscriptions are available on microfiche simultaneously with the paper edition and on microfilm on completion of the annual index at the end of the subscription year.

Copyright © 1981 Pergamon Press Ltd. • Printed in the USA.

It is a condition of publication that manuscripts submitted to this journal have not been published and will not be simultaneously submitted or published elsewhere. By submitting a manuscript, the authors agree that the copyright for their article is transferred to the publisher if and when the article is accepted for publication. The copyright covers the exclusive rights to reproduce and distribute the article, including reprints, photographic reproductions, microform or any other reproductions of similar nature and translations. No part of this publication may be reproduced, stored in a retrieval system or transmitted in any form or by any means, electronic, electrostatic, magnetic tape, mechanical, photocopying, recording or otherwise, without permission in writing from the copyright holder.

U.S. Copyright Law Applicable to Users in the U.S.A.

The Article Fee Code on the first page of an article in this journal indicates the copyright owner's consent that, in the U.S.A., copies may be made for personal or internal use provided the stated fee for copying, beyond that permitted by Section 107 or 108 of the United States Copyright Law, is paid. The appropriate remittance should be forwarded with a copy of the first page of the article to the Copyright Clearance Center Inc., 21 Congress Street, Salem, MA 01970. If a code does not appear copies of the article may be made without charge, provided permission is obtained from the publisher. The copyright owner's consent does not extend to copying for general distribution, for promotion, for creating new works or for resale. Specific written permission must be obtained from the publisher for such copying. In case of doubt please contact your nearest Pergamon Office.

Cover by L. Alcopley

Contents of Volume 16, 1979

Number 1/2

Editorials

A. L. COPLEY — 1 Congress papers, Executive Editorial Office of Biorheology and other Editorial policy matters

E. FUKADA — 3 A message from the President of the International Society of Biorheology

5 The Council of the International Society of Biorheology 1978–1981

Symposium Papers

R. S. SNYDER and G. V. F. SEAMAN — 7 Experimentation in space and biorheology

S. L. KIMZEY — 13 A review of hematology studies associated with space flight

D. A. SAVILLE — 23 Flow processes in a micro-gravity environment

L. DINTENFASS — 29 Aggregation of red cells and blood viscosity under near-zero gravity

A. L. COPLEY — 37 Certain aspects of hemorheology in a near zero gravity environment

A. L. ADAMS and L. VROMAN — 51 Effects of gravity and the presence of erythrocytes on platelet and granulocyte adhesion in stagnant blood

Congress Papers

M. KING — 57 Interrelation between mechanical properties of mucus and mucociliary transport: effect of pharmacologic interventions

L. DINTENFASS — 69 Clinical applications of blood viscosity factors and functions: especially in the cardiovascular disorders

R. H. COX — 85 Regional, species, and age related variations in the mechanical properties of arteries

L. HOUBOUYAN, S. GAILLARD, A. GOGUEL and J. F. STOLTZ — 95 Influence of some antibiotics of the β-Lactam group upon rheological properties of blood and platelet aggregation

Non-Congress Papers

H. N. SABBAH and P. D. STEIN — 101 Contribution of semilunar leaflets to turbulent blood flow

P. CHATURANI and V. S. UPADHYA — 109 A two-fluid model for blood flow through small diameter tubes

Brief Communications

M. SINGH and N. A. COULTER, JR. — 119 Fahraeus–Lindqvist effect in oscillatory flow

P. CHATURANI and V. S. UPADHYA — 121 A note on Poiseuille flow of couple stress fluid

Abstracts — 123 Annual Meeting, German Society of Microcirculation

Announcement — 133 XII. International Conference on Medical and Biological Engineering and V. International Conference on Medical Physics

Number 3

Editorial

A. L. COPLEY — 135 Additional Instructions to Authors

Symposium Papers

K. JAN — 137 Red cell interactions in macromolecular suspension

G. B. THURSTON — 149 Rheological parameters for the viscosity, viscoelasticity and thixotropy of blood

Congress Papers

M. HORIMOTO, T. KOYAMA, H. MISHINA and T. ASAKURA — 163 Pulsatile blood flow in arteriole of frog web

I. ANADERE, H. CHMIEL, H. HESS and G. B. THURSTON — 171 Clinical blood rheology

Vol. 17
1980

I. Anadere, H. Chmiel and W. Laschner — 179 Viscoelasticity of "normal" and pathological synovial fluid

S. E. Charm, H. Paz and G. S. Kurland — 185 Reduced plasma viscosity among joggers compared with non-joggers

Y. Lanir — 191 The rheological behavior of the skin: experimental results and a structural model

S. Oka — 203 Physical theory of permeability of vascular walls in relation to atherogenesis

B. Obrecht, P. Rusch and J. C. Healy — 211 The mechanical transfer function of blood: modifications by some biological factors

H. Niimi — 223 Role of stress concentration in arterial walls in atherogenesis

Non-Congress Papers

T. Karino, H. H. M. Kwong and H. L. Goldsmith — 231 Particle flow behaviour in models of branching vessels—I. Vortices in 90° T-junctions

P. D. Stein, H. N. Sabbah, D. T. Anbe and F. J. Walburn — 249 Blood velocity in the abdominal aorta and common iliac artery of man

P. Péronneau and M. Nakache — 257 Relationship between hydrodynamic forces and vascular wall phenomena—I. Measurement of parietal friction by pulse type Doppler velocimeter

M. Nakache and P. Péronneau — 265 Relationship between hydrodynamic forces and vascular wall phenomena—II. Study of the influence of friction on the parietal microenvironment by the fixed enzyme method

Announcement — 277 An International Symposium on The Mechanical Properties of Biological Materials

Number 4/5

Symposium Papers

E. A. Evans — 279 Mechanical calorimetry of red cell membranes

R. F. Baker and L. J. Clark — 285 Structural and dynamic aspects of the red cell membrane. I. Phosphate–calcium induced fusion

V. A. Parsegian, R. P. Rand, N. Fuller, M. McAlister and L. J. Lis — 293 Molecular forces between and within lipid membranes

S. Weinbaum — 297 Theoretical models of vesicular transport and endothelial membrane interaction

M.-m. Poo — 309 Molecular movements of receptors on cell surface

Congress Papers

N. D. Panagiotacopulos, W. G. Knauss and R. Bloch — 317 On the mechanical properties of human intervertebral disc material

C. Marriott, C. K. Shih and M. Litt — 331 Changes in the gel properties of tracheal mucus induced by divalent cations

C. H. Tamblyn, F. J. Nordt, R. L. Swank, C. F. Zukoski, IV and G. V. F. Seaman — 339 Comparison of methods for the evaluation of microaggregate removal by blood transfusion filters

Non-Congress Papers

D. Hauger, D. M. Stasiw and L. C. Cerny — 347 Mixtures of artificial and whole blood

P. D. Stein, H. N. Sabbah and D. T. Anbe — 357 Comparison of disturbances of flow in the main pulmonary artery and ascending aorta of man

T. Shiga, N. Maeda, T. Suda, K. Kon, M. Sekiya and S. Oka — 363 Rheological and kinetic dysfunctions of the cholesterol-loaded, human erythrocytes

Program and Brief Report — 371 Réunion de Biorhéologie

Announcements — 373 The Fourth International Congress of Biorheology

375 Hemorheology and Diseases: European Symposium

Vol. 17
1980

Number 6

Congress Papers

P. CHATURANI — 377 Flow of couple stress fluid through narrow tubes by sigma phenomenon and marginal zone theory with applications to blood flow and cardiovascular diseases

Non-Congress Papers

S. FUJIHARA, R. YAMAMOTO and Y. MASUDA — 387 Viscoelastic properties of plant cell walls. IV. Physical meaning of parameter K in mathematical formulation for stress-relaxation and load-extension processes

A. GANSSEN, H. SCHMID-SCHÖNBEIN, H. MALOTTA and R. SCHNEIDER — 397 Fast determination of water mobility in blood plasma – investigation of clinical significance

M. S. KUNTAMUKKULA, L. V. MCINTIRE and E. A. NATELSON — 403 A rheological study of the kinetics of coagulation in normal and hemophilic blood plasma

F. J. WALBURN, E. F. BLICK and P. D. STEIN — 411 Effect of the branch-to-trunk area ratio on the transition to turbulent flow: implications in the cardiovascular system

P. CHATURANI and V. S. UPADHYA — 419 On micropolar fluid model for blood flow through narrow tubes

V. M. ZAIKO and A. N. SHARIKOV — 429 Mathematical model of substance diffusion in tissue with nonlinear consumption

F. AZELVANDRE, G. MANDRET and A. PETERS — 435 Rheological behaviour of stored blood cells

J. P. G. URBAN, A. MAROUDAS, M. T. BAYLISS and J. DILLON — 447 Swelling pressures of proteoglycans at the concentrations found in cartilaginous tissues

F. FALVO, C. RAMSEY, M. ZONGRONE, D. STASIW and L. C. CERNY — 465 The erythrocyte sedimentation rate in inclined tubes

V. SESHADRI, C. MCKAY and M. Y. JAFFRIN — 473 The effect of red blood cell flexibility on blood flow through tubes with diameters in the range 30 to 500 microns

Brief Communication

R. L. POWELL, W. H. SCHWARZ, J. A. HOUSE and J. B. EMERY — 485 Immunological and virological effects on the rheological properties of canine mucus

Abstracts

491 Second Annual Meeting of the Japanese Society of Biorheology

501 Fifth Annual Meeting of the International Society of Haematology, European and African Division

505 Hemorheology and Diseases: European Symposium

Report — 533 VIIth International Congress on Thrombosis and Hemostasis

Book Review

A. L. COPLEY — 535 Documentation Rheology

Errata — 537

Announcement — 539 7th Jean Julliard Prize

Author Index

Adams, A.L., 51
Anadere, I., 171, 179
Anbe, D.T., 249, 357
Asakura, T., 163
Azelvandre, F., 435

Baker, R.F., 285
Bayliss, M.T., 447
Blick, E.F., 411
Bloch, R., 317

Cerny, L.C., 347, 465
Charm, S.E., 185
Chaturani, P., 109, 121, 377, 419
Chmiel, H., 171, 179
Clark, L.J., 285
Copley, A.L., 1, 37, 135, 535
Coulter, N.A., 119
Cox, R.H., 85

Dillon, J., 447
Dintenfass, L., 29, 69

Emery, J.B., 485
Evans, E.A., 279

Falvo, F., 465
Fujihara, S., 387
Fukada, E., 3
Fuller, N., 293

Gaillard, S., 95
Ganssen, A., 397
Goguel, A., 95
Goldsmith, H.L., 231

Hauger, D., 347
Healy, J.C., 211
Hess, H., 171
Horimoto, M., 163
Houbouyan, L., 95
House, J.A., 485

Jaffrin, M.Y., 473
Jan, K., 137

Karino, T., 231
Kimzey, S.L., 13
King, M., 57
Knauss, W.G., 317
Kon, K., 363
Koyama, T., 163
Kuntamukkula, M.S., 403
Kurland, G.S., 185
Kwong, H.H.M. 231

Lanir, Y., 191
Laschner, W., 179
Lis, L.J., 293
Litt, M., 331

Maeda, N., 363
Malotta, H., 397
Mandret, G., 435
Maroudas, A., 447
Marriott, C., 331
Masuda, Y., 387
McAlister, M., 293
McIntire, L.V., 403
McKay, C., 473
Mishina, H., 163

Nakache, M., 257, 265
Natelson, E.A., 403
Niimi, H., 223
Nordt, F.J., 339

Obrecht, B., 211
Oka, S., 203, 363

Panagiotacopulos, N.D., 317
Parsegian, V.A., 293
Paz, H., 185
Peronneau, P., 257, 265
Peters, A., 435
Poo, M.-m., 309
Powell, R.L., 485

Ramsey, C., 465
Rand, R.P., 293
Rusch, P., 211

Sabbah, H.N., 101, 249, 357
Saville, D.A., 23
Schmid-Schoenbein, H., 397
Schneider, R., 397
Schwartz, W.H., 485
Seaman, G.V.F., 339
Sekiya, M., 363
Seshadri, V., 473
Sharikov, A.N., 429
Shiga, T., 363
Shih, C.K., 331
Singh, M., 119
Snyder, R.S., 7
Stasiw, D.M., 347, 465
Stein, P.D., 101, 357, 411
Stoltz, J.F., 95
Suda, T., 363
Swank, R.S., 339

Tamblyn, C.H., 339
Thurston, G.B., 149, 171

Upadhya, V.S., 109, 121, 419
Urban, J.P.G., 447

Vroman, L., 51

Walburn, F.J., 249, 411
Weinbaum, S., 297

Yamamoto, R., 387

Zaiko, V.M., 429
Zongrone, M., 465
Zukoski, IV, C.F., 339

Contents of Volume 17, 1979

Number 1/2

Editorials

A.L. Copley — 1 — Salutations to Maurice Joly, Harold Wayland and the new editors

A.L. Copley — 3 — On submission of communications for publication

A.L. Copley — 5 — On the practice of basic and clinical hemorheology at blood transfusion centers

Non-Congress Papers

I.J.A. Dawidson, L-E. Gelin and E. Haglind — 9 — Blood viscosity and red cell aggregation changes after hemodilution in vivo and in vitro: A comparison between different plasma substitutes

G. Heuser and R. Opitz — 17 — A Couette viscometer for short time shearing of blood

A. Downs, M. Litt and R.E. Kron — 25 — Low shear rate viscosity of fresh blood

Congress Symposium: Soft Tissues Around a Diarthrodial Joint

S.L-Y. Woo — 37 — Introduction

S.L-Y. Woo — 39 — Biorheology of soft tissues: The need for interdisciplinary studies

A.S. Hoffman — 45 — Comparison of enzyme probe techniques used to investigate tissue biomechanics in vitro

M.E. Nimni — 51 — The molecular organization of collagen and its role in determining the biophysical properties of the connective tissues

D.F. Betsch and E. Baer — 83 — Structure and mechanical properties of rat tail tendon

W.H. Akeson, D. Amiel and S.L-Y. Woo — 95 — Immobility effects on synovial joints: The pathomechanics of joint contracture

W.M. Lai and V.C. Mow — 111 — Drag-induced compression of articular cartilage during a permeation experiment

Congress Symposium: Muco-Ciliary Transport

J.R. Blake and H. Winet — 125 — On the mechanics of muco-ciliary transport

H. Winet and J.R. Blake — 135 — On the mechanics of muco-ciliary flows I. Observations of a channel model

G.T. Yates, T.Y. Wu, R.E. Johnson, A.T.W. Cheung and C.L. Frand — 151 — A theoretical and experimental study on tracheal muco-ciliary transport

F.A. Meyer and A. Silberberg — 163 — The rheology and molecular organization of epithelial mucus

D.F. Katz and S.A. Berger — 169 — Flagellar propulsion of human sperm in cervical mucus

Congress Symposium: Recent Advances in Hemorheology

E. Fukada and M. Kaibara — 177 — Viscoelastic study of aggregation of red blood cells

P. Gaehtgens — 183 — Flow of blood through narrow capillaries: Rheological mechanisms determining capillary hematocrit and apparent viscosity

Congress Paper

M. Bureau, J.C. Healy, D. Bourgoin and M. Joly — 191 — Rheological hysteresis of blood at low shear rate

Letter to the Editor-in-Chief

Y. Nubar — 205 — Comments on "A two-fluid model for blood flow through small diameter tubes"

Vol. 17
1980

Number 3

Editorial

A.L. Copley — 207 — Alex Silberberg, new Co-Editor-in-Chief and the revised editorial policy

Congress Symposium: Rheology of Blood Vessels

K. Hayashi, S. Nagasawa, Y. Naruo, A. Okumura, K. Moritake and H. Handa — 211 — Mechanical properties of human cerebral arteries

R.N. Vaishnav — 219 — Mathematical characterization of the nonlinear rheological behavior of the vascular tissue

K. Fronek and Y.C. Fung — 227 — Mechanical properties of arteries as a function of topography and age

Non-Congress Communications
Papers

P.L. Easthope and D.E. Brooks — 235 — A comparison of rheological constitutive functions for whole human blood

M. King — 249 — Relationship between mucus viscoelasticity and ciliary transport in guaran gel/frog palate model system

M. Kaibara and E. Fukada — 255 — An analysis of the clotting curves of complex dynamic rigidity for fibrinogen-thrombin solutions

T.M. Vatsala and M. Singh — 261 — Effects of hypercholesterolemia and onions on rheology of blood in rabbits

F.J. Walburn, E.F. Blick and P.D. Stein — 267 — Comparison of power density spectra of turbulent flow through tubes obtained with hot film and laser Doppler anemometers

P.D. Stein, F.J. Walburn and E.F. Blick — 275 — Damping effect of distensible tubes on turbulent flow: Implications in the cardiovascular system

Brief Communications

S.P. Sutera — 283 — A note on hemolysis during filtration through micropores

R. Glaser and A. Herrmann — 289 — The sedimentation velocity of individual human erythrocytes as a function of temperature

Report

J.F. Stoltz and P. Drouin — 293 — Symposium on "Hemorheology and Diseases"

Number 4

Obituary

297 — Alan Chadburn Burton (1904-1979)

Overview

P.D. Stein and H.N. Sabbah — 301 — Hemorheology of turbulence

Papers

D.P. Ly, D. Bellet, P. Boyer and C. Roques — 321 — Rheological behaviour of synovial fluids

T.-C. Hung, T.-K. Hung and G. Bugliarello — 331 — Blood flow in capillary tubes: Curvature and gravity effects

D.E. McMillan and N. Utterback — 343 — Maxwell fluid behavior of blood at low shear rate

D.E. McMillan, N.G. Utterback and J. Stocki — 355 — Low shear rate blood viscosity in diabetes

S. Shimura, S. Sato, T. Takishima, Y. Otsubo and K. Umeya — 363 — Relaxation behavior of sputum studied using the Raised Cosine Pulse method

N. Iida and T. Murata — 377 — Theoretical analysis of pulsatile blood flow in small vessels

S. Palosaari and K. Linko — 385 — Flow of blood in transfusion systems

W. Fabisiak and C.R. Huang — 391 — Mathematical analysis of the hysteresis rheogram of human blood

Vol. 17
1980

Number 5/6

Editorial

A.L. Copley and A. Silberberg — 397 Welcome to new Editors, the new format of BIORHEOLOGY and communications pertaining to clinical biorheology other than clinical hemorheology

Papers

P. Chaturani — 399 A note on plane Poiseuille flow of couple stress fluid

J.B. Shukla, S.P. Gupta and R.S. Parihar — 403 Biorheological aspects of blood flow through artery with mild stenosis: Effects of peripheral layer

J.P. Kirkpatrick, L.V. McIntire, J.L. Moake and D.M. Peterson — 411 Metabolic requirements of contractile force generation in platelet rich plasma. A rheological study.

P. Brunn — 419 On the rheology of viscous drops surrounded by an elastic shell

L. Arminski, S. Chien, R. Pfeffer and S. Weinbaum — 431 Steric hindrance effects on the time dependent diffusion of plasmalemma vesicles across vascular endothelium

D.E. McMillan, N.G. Utterback and J.B. Baldridge — 445 Thixotropy of blood and red blood cell suspensions

M.R. Beck, Jr. and E.C. Eckstein — 455 Preliminary report on platelet concentration in capillary tube flows of whole blood

P.Y. Tam, D.F. Katz and S.A. Berger — 465 Non-linear viscoelastic properties of cervical mucus

Brief Communication

G.B. Nash and S.J. Wyard — 479 Changes in surface area and volume measured by micropipette aspiration for erythrocytes ageing in vivo

Review Article

T. Shiga and N. Maeda — 485 Influence of membrane fluidity on erythrocyte functions

Abstracts

501 Abstracts of papers presented at the 1980 Annual Meeting of Japanese Society of Biorheology

511 *Announcements*

Author Index

Akeson, W.H., 95
Amiel, D., 95
Arminski, L., 431

Baer, E., 83
Baldridge, J.B., 445
Beck, Jr., M.R., 455
Bellet, D., 321
Berger, S.A., 169, 465
Betsch, D.F., 83
Blake, J.R., 125, 135
Blick, E.F., 267, 275
Bourgoin, D., 191
Boyer, P., 321
Brooks, D.E., 235
Brunn, P., 419
Bugliarello, G., 331
Bureau, M., 191

Chaturani, P., 399
Cheung, A.T.W., 151
Chien, S., 431
Copley, A.L., 1, 3, 5, 207, 397

Dawidson, I.J.A., 9
Downs, A., 25
Drouin, P., 293

Easthope, P.L., 235
Eckstein, E.C., 455

Fabisiak, W., 391
Frand, C.L., 151
Fronek, K., 227
Fukada, E., 177, 255
Fung, Y.C., 227

Gaehtgens, P., 183
Gelin, L-E., 9
Glaser, R., 289
Gupta, S.P., 403

Haglind, E., 9
Handa, H., 211
Hayashi, K., 211
Healy, J.C., 191
Herrmann, A., 289
Heuser, G., 17
Hoffman, A.S., 45
Huang, C.R., 391
Hung, T.-C., 331
Hung, T.-K., 331

Iida, N., 377

Johnson, R.E., 151
Joly, M., 191

Kaibara, M., 177, 255
Katz, D.F., 169, 465
King, M., 249
Kirkpatrick, J.P., 411
Kron, R.E., 25

Lai, W.M., 111
Linko, K., 385
Litt, M., 25
Ly, D.P., 321

Maeda, N., 485
McIntire, L.V., 411
McMillan, D.E., 343, 355 445
Meyer, F.A., 163
Moake, J.L., 411
Moritake, K., 211
Mow, V.C., 111
Murata, T., 377

Nagasawa, S., 211
Naruo, Y., 211
Nash, G.B., 479
Nimni, M.E., 51
Nubar, Y., 205

Okumura, A., 211
Opitz, R., 17
Otsubo, Y., 363

Palosaari, S., 385
Parihar, R.S., 403
Peterson, D.M., 411
Pfeffer, R., 431

Roques, C., 321

Sabbah, H.N., 301
Sato, S., 363
Shiga, T., 485
Shimura, S., 363
Shukla, J.B., 403
Silberberg, A., 163, 397
Singh, M., 261
Stein, P.D., 267, 275, 301
Stocki, J., 355
Stoltz, J.F., 293
Sutera, S.P., 283

Tam, P.Y., 465
Takishima, T., 363

Umeya, K., 363
Utterback, N., 343, 355, 445

Vaishnav, R.N., 219
Vatsala, T.M., 261

Walburn, F.J., 267
Weinbaum, S., 431
Winet, H., 125, 135
Woo, S.L-Y., 37, 39, 95
Wu, T.Y., 151
Wyard, S.J., 479

Yates, G.T., 151

BIORHEOLOGY Vol. 17 pp. 1-2 0006-355X/80/010001-02$02.00/0
Pergamon Press Ltd. 1980. Printed in the United States

Vol. 17
1980

EDITORIAL

SALUTATIONS TO MAURICE JOLY, HAROLD WAYLAND AND THE NEW EDITORS

It is with great regret that Maurice Joly and Harold Wayland, due to their retirement from the institutions they were associated with for many years, found it necessary to terminate their appointments as Editors of BIORHEOLOGY. The Publishers and I should like to express our gratitude to both of them for their many contributions to our Journal.

Maurice Joly has been an Editor of BIORHEOLOGY since the beginning of the journal in 1962. He also acted as Acting Co-Editor-in-Chief from June 1974 to September 1975 when he kindly took over the duties of George W. Scott Blair who was incapacitated due to an accident and eye operations. During this time he has been most helpful in making important editorial decisions and also in editing with me the Proceedings of the Second International Congress of Biorheology, held at the Weizmann Institute of Science in Rehovot, Israel. These congress contributions were published in several issues of our journal. As an Editor, he has been most helpful during the nineteen years of his association with our journal, including the past three years when BIORHEOLOGY became a journal for rapid publication, as well as since 1974, when BIORHEOLOGY became a bi-monthly publication.

The special issue for the Third International Congress of Biorheology Volume 15, Numbers 5/6, 1978 was dedicated to Maurice Joly. It contains a report I wrote on the Poiseuille Award dedicated to him by the International Society of Biorheology, Syoten Oka's presentation address at the Poiseuille Gold Medal Award Ceremony and Maurice Joly's Poiseuille Award Lecture. The double issue also listed nearly thirty main publications by Maurice Joly and associates. Maurice Joly's counsel in many editorial decisions, in particular during the past few years, has been most helpful to me and I should like to take this opportunity to thank him for all he did for our journal also in my capacity as member of the Council of our Society.

Harold Wayland served well as an Editor for the past three years and I regret that he could not complete his term of six years.

The Readers of BIORHEOLOGY will join me in our very best wishes to Maurice Joly and Harold Wayland for good health as well as for any scientific contributions they may make during their retirement. Our Readers will be interested to learn that both intend to continue, as much as possible, with their scientific research in biorheology and other areas of interest to them.

It is a tribute to Maurice Joly, Harold Wayland and our other Editors who have served or are serving that BIORHEOLOGY, the official journal of the International Society of Biorheology, is the leading journal in all fields of our growing science of biorheology and that our journal enjoys a high reputation in the scientific community.

It is with great pleasure that the Publishers and I welcome our new Edi-

tors, J.C. Healy of Saint-Etienne, France and Mitchell Litt of Philadelphia, Pennsylvania, U.S.A., who have taken on the duties of Maurice Joly and Harold Wayland.

I am confident that our Editors and Authors will continue to maintain the high standing of BIORHEOLOGY as a significant international scientific journal.

The Publishers and I extend our best wishes for 1980 to the Readers of BIORHEOLOGY.

Alfred L. Copley
Editor-in-Chief

Vol.
198

BIORHEOLOGY Vol.17, pp.3-4 0006-355X/80/010003-02$02.00/0
Pergamon Press Ltd. 1980. Printed in the United States

EDITORIAL

ON SUBMISSION OF COMMUNICATIONS FOR PUBLICATION

The Publishers and I must again ask the Authors to follow strictly the Instructions to Authors, printed on the inside back cover of each issue of BIORHEOLOGY. There have been delays of publication, because a communication accepted for publication on scientific merits had to be returned to the Authors for corrections and retyping, because of errors in presentation. Actually, such a technically faulty communication should never have been considered for review on scientific merits by the Editor, to whom it was submitted. Although we have cautioned our Editors, some of them or their secretarial assistants have overlooked the requirements, as given in the Instructions to Authors.

Some errors in a manuscript, submitted for camera-ready printing, occur frequently and, therefore, I should point out to them in order to facilitate publication as rapidly as possible, after a Paper or Brief Communication has been accepted by an Editor. They concern the following points:

1. Preparation or laysheets should be used as much as possible. In case these sheets cannot be quickly secured by Authors, eager to get their work published without delay, the limitation in size of the typing area should be followed as described in the Instructions to Authors. The typing area on each sheet should be utilized as fully as possible.

2. Key Words are always necessary and must be placed as a footnote after the wording "Key Words:" on the Title Page and not on a separate sheet.

3. Running Titles of not more than 45 typewriter spaces must be provided by the Author on a separate sheet or written in blue pencil on the top of the Title Page.

4. Figures

   a. Space of Figures on the preparation or laysheets must be provided, but not more than is necessary, and the legends will have to be placed next to or below the Figures.

   b. The Figures should be clear either on a glossy photograph or in the original. They can never be smaller than the required size, but can be larger.

   c. The lettering for each Figure has to be large enough to be easily readible after the 20% reduction which each manuscript sheet is subjected to.

   d. On the back of each Figure, the names of the Authors and the number of the Figure should be placed lightly in pencil.

   e. Figures cannot be placed in the text under Discussion.

5. The References must be followed in accordance to our Instructions to Authors. Surnames must be capitalized, the name of the journal and its volume must be underlined and in the case of a book, its title has to be underlined. If the book has particular Editors, their names must be provided in accordance with the Instructions. The last page number of a reference must be given together with the first.

Vol. 17
1980

6. Double spacing or $1\frac{1}{2}$ spacing is no longer permissible. Each text will need to be single-spaced. Each paragraph should begin with an indentation and should be separated from the following paragraph by double spacing. In this way a paragraph is clearly identified.

7. Regarding page charges, details are given in the Instructions to Authors. In case the communication exceeds the permissible number of pages, which are free of charge, the Authors are requested to submit a statement signed by them or their institution that the extra page charge of 50 U.S. dollars per every 2 pages will be paid to the Publishers.

8. Each Editor must send two forms to the Authors, when a communication is accepted for publication. One of these forms, which contains the Reprint Order Form, notifies the Author(s) that the communication has been accepted, while the other is the Copyright Form. An Author must complete both forms and send them without delay to the Executive Editorial Office (EEO) and not to the Publishers. The EEO is under my direction and is located at the Laboratory of Biorheology, Polytechnic Institute of New York, 333 Jay Street, Brooklyn, NY 11201, USA. The Reprint Order Form must also be completed, whether or not the purchase of reprints is requested.

We have only emphasized the need for corrections of errors which are usually made by the Authors. However, there are other points which are given under the Instructions to Authors which must also be strictly adhered to by the Authors. The Authors and their secretarial assistants must, therefore, acquaint themselves fully with the Instructions to Authors before the typing of a manuscript in camera-ready form. After the notification of acceptance of a communication by an Editor, the Authors must act also in accordance with the Instructions, some of which are reemphasized in the Editorial.

It should be pointed out that only the last revision of June 1979 of our Instructions to Authors contained in each issue beginning with Volume 16, Number 3 are valid.

Alfred L. Copley
Editor-in-Chief

Vol.
198

BIORHEOLOGY Vol.17, pp. 5-7 0006-355X/80/010005-03$02.00/0
© Pergamon Press Ltd. 1980. Printed in the United States

Vol. 17
1980

EDITORIAL

ON THE PRACTICE OF BASIC AND CLINICAL HEMORHEOLOGY AT BLOOD TRANSFUSION CENTERS

Basic and clinical hemorheology is more and more being practiced in hospitals and research institutions associated in particular with medical schools in many countries. Efforts are being made on a world-wide basis in establishing hemorheological investigations and testing procedures as an aid in the practice of medicine and surgery. However, the numerous blood transfusion centers and blood tranfusionists in different parts of the globe appear to be unaware of the existence of hemorheology and of its significance for the practice of the transfusion of blood and of its cellular and plasmatic components.

The Readers of BIORHEOLOGY, in particular those working in hemorheology, will be interested in my opening remarks which I gave as Président d'Honneur of the European Symposium Hemorheology and Diseases (Hémorhéologie et Pathologie) held 17.-19. October 1979 in Nancy, France. An excerpt of my address at the opening ceremony of this international conference follows:

"It is very gratifying to see the growing interest in hemorheology among researchers from different disciplines. This interest stems from many important studies during the past thirty years and, in particular, during the past decade. I believe, we are merely, so-to-speak, "at the tip of the iceberg" in exploring hemorheology. In likening hemorheology to inquiries about other natural phenomena, we could picture explorations of a jungle with its many plants, branches, twigs and leaves. Corrective examinations of such a tangled vegetation would make it more accessible to scientific exploration. In hemorheology we have passed such similar preliminary investigations. With the aid of tools, including those from other disciplines, and, what we need to be aware of, within the limitations of our insights, we can begin to do more than pruning the "jungle" of the flow of blood and its relations to vessel walls.

As you well know, hemorheology is a term for a science branch of biorheology which deals not merely with the rheology, that is, the flow properties and deformation of blood, but as well with the rheology of the vessel wall, viz., of all the structures with which the flowing blood and any of its components come into direct contact.

We all are well aware that hemorheology is not limited to the circulation of the blood in a mammalian organism, but concerns also any other classes of animals which are endowed with blood, contained and circulating within a cardio-vascular system. However, what this symposium will deal with is the mammalian organism, with special emphasis on the human species and its pathology.

It is particularly encouraging that quite a number of diseases and other pathological conditions benefit already from the advancement of knowledge in hemorheology. This is a development which is bound to affect human health and many pathological conditions in patients, in which the blood and the blood vessel wall are involved. There can hardly be any doubt that the new knowledge will be of direct aid to the diagnosis, therapy and prognosis of many diseases

and other pathological conditions. Hemorheology will also become increasingly important in the prevention of diseases and thus counter the threat to health and fight disease processes which may either cripple or lead to death.

Although many among us researchers here at this symposium are not involved in directly aiding or treating patients, it goes without saying that advancement of fundamental knowledge in hemorheology is most important for better understanding the physiology of the blood circulation towards more effective prevention and treatment of human disease. Advancement of knowledge of the flow properties of blood and many of its constituents is therefore essential. This is also true for the exchanges between the blood and the tissues, as well as with regard to the physical and chemical processes which are involved.

The organizers of this symposium have wisely chosen to invite contributions which will be presented in sessions dealing with theory, models, methodology, pathology, pharmacology and therapy.

You will probably be surprised in my referring to my previous journey in Europe, where six weeks ago I visited with my old friend Professor van Loghem in Amsterdam. He showed me the Central Laboratory of the Netherlands Red Cross Blood Transfusion Service which he directed until last year. I know Professor van Loghem since my first visit to Amsterdam in 1948, when we met in his small laboratory for blood group research, which he founded three years earlier. He expanded his laboratory of immuno-hematology over the years into a blood transfusion center, where now about 1,000 people work, including many who are engaged in scientific research in about fifteen departments.

I am mentioning this recent visit of mine for several reasons in association with the practice of hemorheology. As the flow of blood, so is the flow of a suspension of isolated platelets a rheological phenomenon. Following the transfusion of platelets, the hemorheological behavior of the circulating blood is altered. Platelet transfusions are increasingly being given therapeutically in a number of pathological conditions with often highly beneficial results to the patient. In this connection, I should like to acquaint you with the following story.

On my first post-war visit in Europe after participating in the First International Congress on Rheology at Scheveningen, Holland in 1948, I met also in Amsterdam the late Professor van Creveld, the pediatrician. He enthusiastically told me about the historical event of the first transfusion of platelets which was given to a patient of his who suffered of thrombocytopenic purpura. What pleased me was that a child benefited from this historical transfusion and that the method of the isolation of platelets, employed in Dr. van Loghem's laboratory, was developed by me together with my associate Dr. Houlihan in 1944 in my laboratory at the University of Virginia School of Medicine at Charlottesville. It was a cumbersome method which, I am glad, could be replaced by less laborious and even elegant ones.

When last month Professor van Loghem showed me the large blood transfusion center, I had to tell him that I am missing a very important activity, namely, a laboratory, if not a department, of hemorheology. In my appraisal,

a blood transfusion center anywhere must have a reasearch laboratory of hemorheology, as well as a hemorheology laboratory for routine testing of blood samples. In any hospital in the world, where blood transfusions are performed, the blood is tested for blood groups and other factors. It is very clear to everyone, including the lay public, that these are immunological tests for compatibility. However, it did not occur thus far to the medical profession in general and especially to many blood transfusionists that what they are dealing with are hemorheological phenomena on an immunological basis, namely, agglutination or the irreversible clumping of red blood cells, and hemolysis. It is not yet general knowledge, what we all here assembled take for granted, that there can be hemorheological phenomena on a non-immunological basis, which can lead following blood transfusion to disturbances in the circulation. As I pointed out to my friend van Loghem, there is a need for hemorheological studies and routine testing in a blood transfusion center, such as the one in Holland, and I reasserted my belief in such a necessity, when I was introduced to the new director of this large institution in Amsterdam.

I know that such hemorheology laboratories do not exist, for instance, as part of the New York Blood Center in the city, where I am residing, nor with the Blood Service of the American Red Cross in Washington, D.C. To my knowledge, the only blood transfusion center in the world, where hemorheological testing and research in hemorheology are being made, is here at the Centre Regional de Transfusion Sanguine et d'Hématologie. I am glad to say that both fundamental and clinical hemorheological research is being pursued here vigorously and with great enthusiasm. I, therefore, salute Professors Streiff, Larcan and Stoltz who had the foresight to include the practice of hemorheology as an integral activity of the transfusion center here at Nancy. The question may be asked, what kind of routine hemorheological testing can be done in a blood transfusion center? As I have been told yesterday by Dr. Stoltz, the following routine procedures are being employed here at the transfusion center: measurements of viscosity and viscoelasticity of blood and plasma, different filtration tests, and also electrophoresis tests of red blood cells and platelets. Since many hemorheological research studies are being made here, it can be expected that, as a result, several tests employed in these studies will then be applied as routine hemorheological tests for blood transfusion. It goes without saying that for routine hemorheological testing, measuring techniques and methods developed in other laboratories should be included as far as is feasible or practical, but deems necessary in preventive medicine and for clinical considerations.

I should like to emphasize that the practice of hemorheology is not merely imperative in any blood transfusion center, but also in any hospital and clinical laboratory, as part of the armamentarium in providing needed information to physicians and surgeons everywhere, for the betterment of medical care."

Alfred L. Copley

Laboratory of Biorheology
Polytechnic Institute of New York
Brooklyn, New York 11201, U.S.A.

Vol. 17
1980

BLANK
PAGE

Vol.
198

BIORHEOLOGY Vol.17, pp. 9-16 0006-355X/80/010009-08$02.00/0
© Pergamon Press Ltd. 1980. Printed in the United States

BLOOD VISCOSITY AND RED CELL AGGREGATION CHANGES AFTER HEMODILUTION IN VIVO AND IN VITRO. - A COMPARISON BETWEEN DIFFERENT PLASMA SUBSTITUTES

Ingemar J.A. Dawidson, Lars-Erik Gelin, and Eva Haglind
Department of Surgery I, University of Gothenburg, Sahlgren's Hospital, 413 45 Gothenburg, Sweden

(Received 26.7.1979; in revised form 31.10.1979.
Accepted by Editor Y.C. Fung)

ABSTRACT The viscosity of whole blood (WB), plasma (P), and packed cells (PC) was measured in a Wells-Brookfield cone plate viscometer on blood from dogs undergoing surgical shock and hemodilution with different plasma substitutes and on human ACD-blood diluted in vitro to comparable concentrations of colloids. Erythrocyte sedimentation rate (ESR) and microscopic red cell aggregate count were used as in vitro indices of red cell aggregation. During three hours of intestinal shock WB viscosity increased by 20 %, hematocrit increased from 50.9 to 59.1 %, P viscosity was unchanged and PC viscosity increased by 6 %. When compared at equal hematocrit drop, Ringer's acetate decreased WB viscosity more than albumin, ACD-plasma, dextran 70 and gelatin in this order both on blood diluted in vitro and in vivo. Since the duration of volume expansion in vivo after Ringer's solution was very transient the absolute decrease of viscosity was less than that observed after all other solutions except gelatin. P viscosity increased with dextran 70, was unchanged with ACD-plasma, dextran 40, and gelatin and decreased with albumin and Ringer's acetate dilution. A marked red cell aggregation occurred with dextran 70 and gelatin with increasing concentration. No aggregation of red cells was seen with dextran 40, albumin, or Ringer's acetate. It is concluded that lasting hemodilution in vivo is best achieved with albumin and dextran 40 based on their viscosity influences, volume expansion duration and their lack of red cell aggregation properties.

Vol. 17
1980

INTRODUCTION

Periferal vasoconstriction and cellular aggregation leading to venular stasis and microvessel obstruction are pathophysiological effects seen in various kinds of shock, resulting in reduced and uneven blood flow through the microcirculation (1-7). Surgical trauma and shock is associated with loss of proteins and water to the extravascular space, resulting in decreased circulating plasma volume and elevated hematocrit (8, 9). Hemoconcentration is a common cause of an increased viscosity of blood. Surgical trauma induces red cell aggregation by protein changes, mainly by increased fibrinogen concentration with increased blood viscosity especially at low shear rates (10, 11). These factors cause a decrease of venous return and cardiac output. An uneven blood flow distribution causes hypoxia and tissue acidosis (7, 12-14). Hemodilution is a therapeutic method in shock and other conditions associated with hemoconcentration. It will counteract the detrimental pathophysiologic defects in such conditions.

The purpose of these experiments was to compare the effects of different plasma substitutes on blood viscosity and red cell aggregation when used for hemodilution and when given in comparable volumes and doses.

MATERIAL AND METHODS

In vivo experiments

Sixty mongrel dogs of both sexes, weighing 20.0 $\pm$ 3.8 kg, were anesthetized with ketamine, initially 4 mg/kg, and continued with 1 mg/kg/hour. Pancuronum bromide was used as muscle relaxant at a dose of 1 mg/kg/hour. The animals were intubated and ventilated with room air. Catheters were inserted through the right carotid artery into the aorta for sampling and through the external jugular vein for injection of fluids and drugs. After control measurements shock was induced by laparotomy with splenectomy and exteriorization of the small intestine and placed in wet gauze for three hours. Then new measurements were made. The intestine was thereafter returned to the abdominal cavity and the abdomen closed. The dogs were randomized into eight groups. The test fluids were warmed to 37°C and given during a period of 20 minutes. The animals were followed for another four hour period.

In vitro experiments

Samples of human ACD-blood (hct = 43 %) were used for in vitro dilution experiments. Dilution to hct 30 was achieved by addition of 3 ml of plasma substitute to 7 ml of the ACD whole blood. Erythrocyte sedimentation rate (ESR) was examined for samples of whole blood (hct = 30) with increasing concentrations of colloid. The measurements were made in plastic tubes with a diameter of 3 mm and read after 60 minutes. Red blood cell aggregation was assessed in a hemocytometer chamber. Whole blood was diluted with serum (1:200) and the sample was added to the hemocytometer. Each monodispersed red cell or each red cell aggregate was counted after 10 minutes, at seven different concentrations of colloid from seven different blood donors.

Measurements

Whole blood (WB), plasma (P), and packed cell (PC) viscosities were estimated on 1 ml samples of heparinized blood diluted in vivo or on ACD-blood diluted in vitro at 37°C, using a Wells-Brookfield cone plate viscometer model LVT. After WB viscosity had been determined, plasma and red cells were separated by centrifugation at 2000 G for 15 minutes. Viscosities were then determined on plasma and on packed cell mass separately. WB viscosity was determined at shear rates 230, 115, 46, 23, and 11.5 sec^{-1}, P viscosity at 115 sec^{-1}, and PC viscosity at shear rate 11.5 sec^{-1}. Hematocrit was measured in duplicates in microhematocrit tubes after centrifugation at 12000 G for three minutes. No correction for trapped plasma was made.

Test solution and experimental groups

Group N: Eight animals were shocked, the intestine was returned to abdomen but no infusion was given. Group R: Eight animals were infused with Ringer's acetate. (Content: Na^+ 134 mEq/l, Ca^{2+} 1.8 mEq/l, Cl^- 111 mEq/l, acetate 31 mEq/l, osmolality 260 mOsm/l, pH 7.0). Group G: Eight animals were infused with gelatin (polypeptides) with an average weight molecular weight ($\bar{M}w$) = 35000 and an average number molecular weight ($\bar{M}n$) = 6000. Group D: Eight animals were infused with dextran 40 of $\bar{M}w$ = 40000 and $\bar{M}n$ = 26000. Group M: Eight animals were infused with dextran 70 of $\bar{M}w$ = 70000 and $\bar{M}n$ = 41000. Group P: Eight animals were infused with dog ACD-plasma. Group A: Five animals were infused with albumin Cohn, made from dog plasma according to the Cohn fractionation method, modified by Björling (15). (Content: Total protein 41 g/l, approximately 90 % of which was albumin (AB KABI, Stockholm, Sweden). Group E: Seven animals were infused with albumin PEG, made from dog plasma by fractionation with polyethylene glycol (PEG), according to the method of Björling (16). (Content: Total protein 41 g/l, approximately 80 % of which was albumin (AB KABI, Stockholm, Sweden).

All colloids were given as 3.5 % solutions in saline at a dose of 1.5 g/kg, corresponding to 43 ml/kg. Plasma was given in the same volume. Ringer's acetate was given in a volume three times larger, or 129 ml/kg.

Statistical methods

Standard statistical methods were used to compute mean values and standard deviations. The effect of infusion is defined as the mean difference between pairs of individual values at shock and values at different times after reposition of the intestine. The comparisons of different groups were carried out as univariate analysis of variance with the shock effect as a co-variate (17, 18).

RESULTS

The viscosity of different plasma substitutes dissolved in saline increased with increasing concentration (Fig. 1). Normal heparinized plasma had a viscosity of approximately 1.3 - 1.4 cp. ACD-plasma had about 15 % lower viscosity or 1.2 cp because of its dilution with the ACD-solution. At a colloid concentration of 3.5 %, albumin had a viscosity of 0.8 cp, dextran 40, and gelatin 1.3 cp, and dextran 70 1.6 cp. Gelatin in concentrations higher than 3.5 % was not available. In these experiments saline had a viscosity of 0.7 cp.

Plasma viscosity (P)

Total plasma protein concentration and albumin concentration decreased slightly to 96 % and 91 %, respectively, of the initial values (Table 1). Plasma protein and albumin concentrations changed after infusion in relation to the hemodilution effects of the various fluids.

P viscosity did not change during shock (Table 2). P viscosity increased after infusion of dextran 70 ($p < 0.001$). Ringer's acetate lowered P viscosity ($p < 0.001$). These influences were most pronounced one hour after infusion but were still effective at four hours after infusion ($p < 0.05$). Gelatin, dextran 40, and ACD-plasma did not change P viscosity significantly, while albumin Cohn caused a slight decrease. Similar relative changes were observed on samples diluted in vitro (Fig. 2).

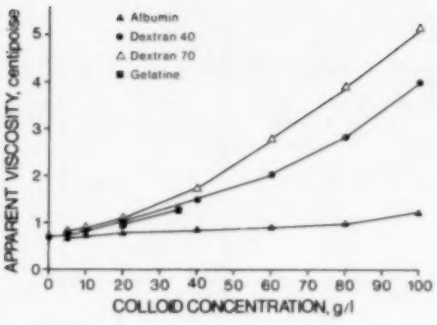

FIG. 1

Apparent viscosity versus concentration for different colloid solutions.

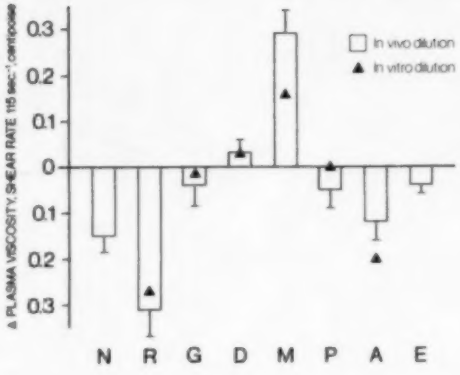

FIG. 2

Change in plasma viscosity after dilution in vitro and in vivo with 3.5 % colloid and Ringer's acetate solutions. Mean ± SEM. Legends as in Fig. 4.

Vol. 17
1980

TABLE 1

Total Plasma Protein, Albumin, and Hematocrit Changes during Shock

	Control	Shock	Effect of shock
Total protein g/l	62.6 ± 6.9 *	60.3 ± 6.6	-2.4 ± 5.6 **
Albumin (g/l)	25.3 ± 2.3	23.0 ± 2.5	-2.3 ± 2.1 **
Hematocrit (%)	50.9 ± 5.7	59.1 ± 5.9	+8.2 ± 4.2 **

* Mean ± SD. ** $p < 0.01$.

Whole blood viscosity (WB)

WB viscosity increased during shock at all shear rates, more so at lower shear rates (Fig. 3 and Table 2), concomitant with the increase of hematocrit from 50.9 to 59.1 %. All infusions decreased WB viscosity because of hemodilution. When comparing WB viscosity change at equal hematocrit decrements, Ringer's acetate lowered WB viscosity more than albumin Cohn, ACD-plasma, dextran 40, albumin PEG, dextran 70, and gelatin in this order. When blood was diluted in vitro with 3.5 % solutions the same relative influences were obtained with the different plasma substitutes (Fig. 4).

Packed cell viscosity (PC)

PC viscosity increased slightly during shock to 106 % of control values (Table 2), and was further elevated with dextran 70 and gelatin infusions in relation to all other groups

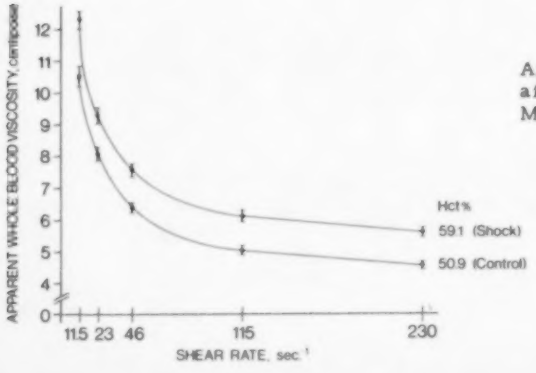

FIG. 3

Apparent whole blood viscosity before and after three hours of intestinal shock. Mean ± SEM.

($p < 0.001$). PC viscosity was unchanged after dextran 40 and ACD-plasma and decreased with albumin or Ringer's infusions. PC viscosity changes were similar in blood when diluted in vitro with colloids of 3.5 % concentrations (Fig. 5, Table 2).

TABLE 2

Viscosity Changes during three hours of Intestinal Shock

	Shear rate, sec^{-1}	Control	Shock	Effect of shock
WB Viscosity	230	4.55 ± 0.73*	5.60 ± 1.14	+ 1.05 ± 0.87 **
	115	5.07 ± 0.83	6.12 ± 1.24	+ 1.02 ± 0.93 **
	46	6.42 ± 1.09	7.55 ± 1.48	+ 1.12 ± 1.50 **
	23	8.08 ± 1.50	9.30 ± 1.84	+ 1.20 ± 1.46 **
	11.5	10.64 ± 2.26	12.34 ± 2.56	+ 1.67 ± 2.27 **
P Viscosity	115	1.32 ± 0.17	1.32 ± 0.19	0.00 ± 0.11
PC Viscosity	11.5	144 ± 20	153 ± 18	+ 10 ± 11 **

* Mean ± SD ** $p < 0.001$

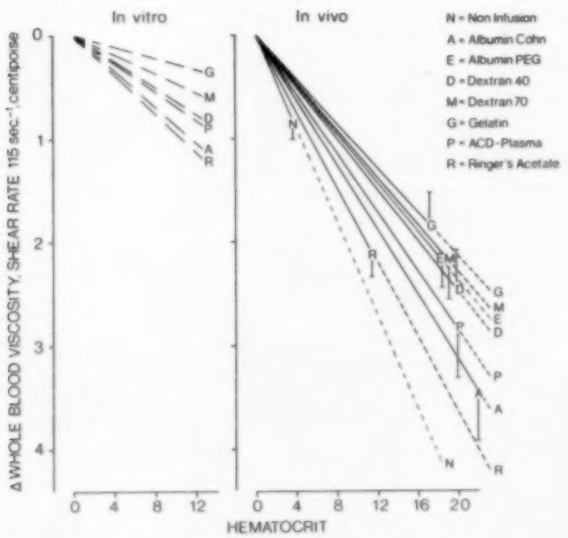

FIG. 4

Change in whole blood viscosity in relation to hematocrit change after dilution in vitro and in vivo with 3.5 % colloid and Ringer's acetate solutions. Mean ± SEM.

Erythrocyte sedimentation rate (ESR) in vitro

ESR increased with increasing concentrations of dextran 70 or gelatin, and was unchanged with increasing concentrations of dextran 40 or albumin (Fig. 6).

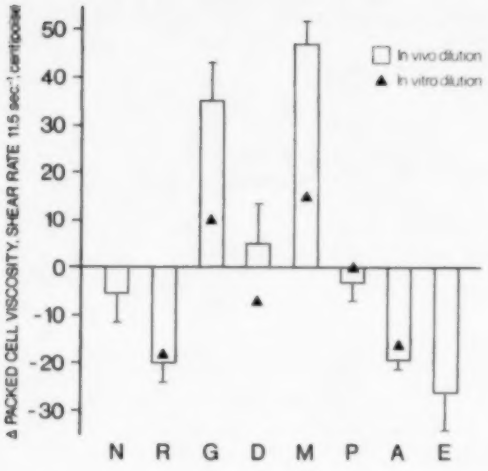

FIG. 5

Change in packed cell viscosity after dilution in vitro and in vivo with 3.5 % colloid and Ringer's acetate solutions. Mean ± SEM. Legends as in Fig. 4.

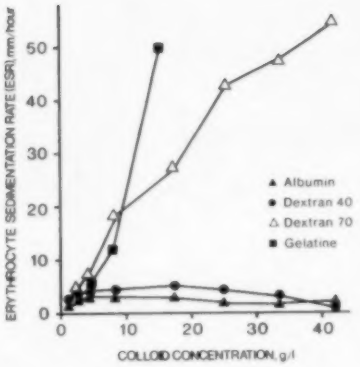

FIG. 6

Erythrocyte sedimentation rate versus concentration for different colloid solutions.

Vol. 17
1980

Microscopic red blood cell aggregation count in vitro

Approximately 50 % of red blood cells were aggregated in rouleaux formations in heparinized plasma and 20 % in serum. With increasing concentrations of dextran 70 or gelatin the number of free monodispersed cells decreased and the number of aggregates increased up to 12 g colloid substance per liter, above which concentration this system seemed to reach a saturation point, where no further cells were available for aggregation (Figs. 7 and 8).

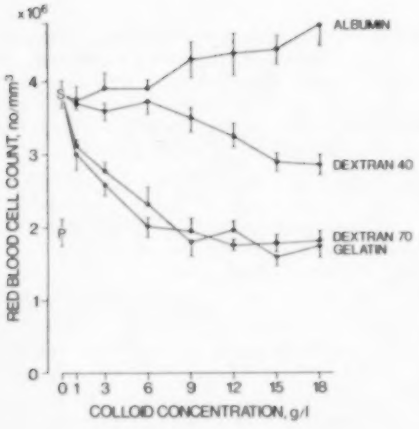

FIG. 7

Monodispersed red blood cell count versus increasing colloid concentration. Mean ± SEM. S = serum; P = plasma.

Albumin caused no aggregation. Dextran 40 did not aggregate at concentrations below 12 g/l. Exceeding this concentration a slight aggregation was seen but less than with normal plasma.

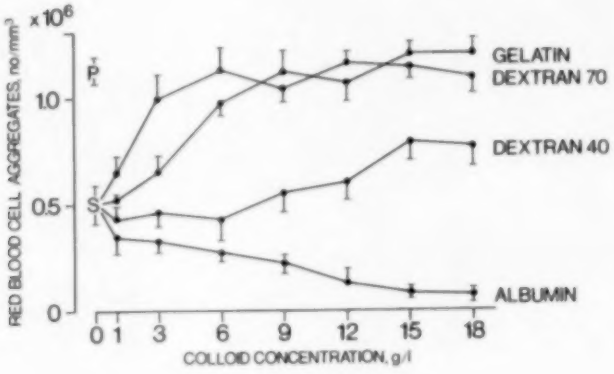

FIG. 8

Red blood cell aggregate count versus increasing colloid concentration. Mean ± SEM. S = serum; P = plasma.

DISCUSSION

The purpose of the present experiments was to study blood viscosity and red blood cell aggregation at comparable hemodilution and concentrations of colloids. Colloids have different inherent viscosity and aggregation effects depending upon their physicochemical properties (Figs. 1, 6-8). The in vitro viscosity of plasma and of whole blood after dilution will therefore be determined in a predicted way by the concentration and volume of a specific substitute used for dilution. Such in vitro experiments do not apply to the in vivo situation, where the hydration status further determines whether water will move in or out of vascular space, depending on the hydration of the recipient and the colloid osmotic activity or concentration of the fluid given (9, 13).

The different plasma substitutes had similar relative influences on blood viscosity both when diluted in vivo and in vitro, when compared at equal hematocrit change and concentration of colloids. The greater general decrease in whole blood viscosity in vivo per change of hematocrit was explained by a viscosity decrease even when no infusion was given (group N) (Fig. 4).

During shock total protein concentration did not change substantially which is consistent with unchanged plasma viscosity during shock.

Viscosity measurements in vitro reflect only a few flow determinants that are effective in vivo. Even if one accepts in vitro viscometry data as indicative of a trend, the pricise influence is difficult to analyse in quantitative terms. The peripheral vasoconstriction and cellular aggregation with blockage of small vessels resulting in uneven or maldistributed blood flow is probably of far greater importance and is only to a minor extent determined by in vitro viscosity measurements (1, 6, 7, 12).

Whole blood viscosity at higher shear rates (above 115 sec^{-1}) is mainly affected by hematocrit and the red cell deformability. At lower shear rates (almost zero) red blood cell aggregation plays an increasing role and causes blood viscosity to increase (19, 20). During shock, flow rates near or at zero exist, especially on the venous side of the capillary. This stasis causes increased viscosity and increased resistance to flow, resulting in elevated capillary pressure and efflux of fluid and proteins, with further loss of plasma volume (21). This effect is further potentiated by hemoconcentration seen in shock.

Packed cell viscosity is usually used in order to eliminate hematocrit variations and is believed to reflect direct cell to cell interactions and red cell deformability (20). The packed cell viscosity changes in the present study were similar when blood was diluted in vivo and in vitro. In addition, the changes in packed cell viscosity were consistent with those seen in erythrocyte sedimentation rate and in the microscopic aggregation test for the different plasma substitutes, suggesting that packed cell viscosity is influenced by changes in red cell aggregation.

Red blood cell aggregation occurs regularly after injury (4-6) and contributes to elevation of whole blood viscosity at low shear rates (19, 20). The degree of aggregation is directly

related to protein changes, mainly fibrinogen and globulins (22). Increased aggregation is reflected and measured by increased erythrocyte sedimentation rate (23). The in vivo consequence of cellular aggregation is capillary blockage, maldistribution of blood flow, tissue anoxia and tissue acidosis (1, 6, 12-14). Macromolecules, other than proteins, also cause red blood cells to aggregate. The difference between dextran 70 and dextran 40 is striking. The aggregating capacity depends on the concentration, the average molecular weight and the molecular weight distribution (23-26). The results in the present study regarding viscosity and red blood cell aggregation are consistent with those reported by Brooks, Jan, Chien, and Lim (24-27).

CONCLUSIONS

1. At dilution to equal hematocrit Ringer's acetate decreased whole blood viscosity more than albumin Cohn, ACD-plasma, dextran 40, albumin PEG, dextran 70, and gelatin, in this order.

2. Albumin Cohn and Ringer's acetate decreased plasma viscosity. ACD-plasma, dextran 40, and gelatin caused no change, and dextran 70 increased plasma viscosity.

3. These relative influences on blood viscosities from plasma substitutes were similar when blood was diluted in vitro and in vivo.

4. Albumin, dextran 40 and Ringer's acetate did not cause red cell aggregation in concentrations less than 12 g/l serum. Dextran 70 and gelatin caused marked red cell aggregation at corresponding concentrations.

5. It is concluded that lasting hemodilution in vivo is best achieved with albumin and dextran 40 based on their viscosity influences, volume expansion duration, and their lack of red cell aggregation properties.

Vol. 17
1980

ACKNOWLEDGEMENT

This investigation was supported by the Swedish Medical Research Council project No. B-79-17X-00660-13A, 14B, and 15C, and Göteborg Medical Society.

REFERENCES

1. BAECKSTRÖM, P., FOLKOW, B., KOVACH, A.G.B., LÖFVING, B., and ÖBERG, B.: Evidence of plugging of the microcirculation following acute haemorrhage. In 6th Europ. Conf. Microcirc., Aalborg (Karger, Basel), 1971, pp 16-22.

2. GELIN, L.-E., BERGENTZ, S.-E., HELANDER, C.-G., LINDER, E., NILSSON, N.J., and RUDENSTAM, C.-M.: Hemodynamic consequences from increased viscosity of blood. International Conference on Hemorheology (Reykjavik, 1966) Copley, 1968, pp 721-728.

3. GELIN, L.-E.: Studies in anemia of injury. Acta Chir. Scand. Suppl. 210, 1956, 132 pp.

4. GELIN, L.-E. and ZEDERFELDT, B.: Experimental evidence of the significance of disturbances in the flow properties of blood. Acta Chir. Scand. 122:336-342, 1961.

5. KNISELY, M.H., ELIOT, T.S., and BLOCH, E.H.: Sludged blood in traumatic shock. Arch. Surg. 51:220-236, 1945.

6. GELIN, L.-E.: A method for studying the aggregation of blood cells, erythrostasis, and plasma skimming in branching capillary tubes. Bibl. Anat. 4:362-375, 1964.

7. APPELGREN, L.: Perfusion and diffusion in shock. A study of disturbed tissue-blood exchange in low flow states in canine skeletalmuscle by a local clearance technique. Acta Phys. Scand. Suppl. 378, 1972.

8. ABEL, F.L. and MATTEW, B.W.: Increased capillary permeability to ^{125}I-labelled albumin during experimental hemorrhagic shock. Trans. NY. Acad. Sci. 35:243-252, 1973.

9. DAWIDSON, I., GELIN, L.-E., and HAGLIND, E.: Plasma volume, intravascular protein content, hemodynamic and oxygen transport changes during intestinal shock in dogs: comparison of relative effectiveness of various plasma expanders. Crit. Care Med., Febr., 1980 (In press).

10. CHIEN, S.: Blood rheology and its relation to flow resistance and transcapillary exchange with special reference to shock. Adv. Microcirc. 2:89-103, 1969.

11. BERGENTZ, S.-E., GELIN, L.-E., RUDENSTAM, C.-M., and ZEDERFELDT, B.: The viscosity of whole blood in trauma. Acta Chir. Scand. 126:289-293, 1963.

12. DAWIDSON, I., APPELGREN, L., GELIN, L.-E., and HAGLIND, E.: Skeletal muscle microcirculation in experimental intestinal shock. - A study on the efficiency of different plasma substitutes. (Submitted for publication)

13. DAWIDSON, I., ERIKSSON, B., GELIN, L.-E., and SÖDERBERG, R.: Oxygen consumption and recovery from surgical shock in rats: a study on the efficiency of different plasma substitutes. Crit. Care Med. 7 (10):460-465, 1979.

14. JENNISCHE, E., ENGER, E., MEDEGÅRD, A., APPELGREN, L., and HALJAMÄE, H.: Correlation between tissue pH, cellular transmembrane potentials, and cellular energy metabolism during shock and during ischemia. Circ. Shock 5:251-260, 1978.

15. BJÖRLING, H.: Plasma fractionation methods used in Sweden. Vox San. 23:18, 1972.

16. BJÖRLING, H.: A new plasma fractionation method based on polyethylene glycol (PEG) precipitation of albumin concentrate. (To be published).

17. ARMITTAGE, P.: Statistical methods in medical research. Blackwell, London, 1973.

18. MORRISON, D.F.: Multivariate statistical methods. McGrawhill, New York, 1967.

19. CHIEN, S., USAMI, S., DELLENBACK, R.J., and BRYANT, C.A.: Comparative hemorheology - hematological implications of species differences in blood viscosity. Biorheology 8:35-57, 1971.

20. CHIEN, S., USAMI, S., TAYLOR, H.M., LUNDBERG, J.L., and GREGERSEN, M.I.: Effects of hematocrit and plasma proteins on human blood rheology at low shear rates. J. Applied Physiol. 21:81-87, 1966.

21. CHIEN, S., DELLENBACK, R.J., USAMI, S., BURTON, D.A., GUSTAVSSON, P.E. and MAGAZINOVIC, V.: Blood volume, hemodynamic, and metabolic changes in hemorrhagic shock in normal and splenectomized dogs. Am. J. Physiol. 225:866-879, 1973.

22. DITZEL, J.: Relationship of blood protein composition to intravascular erythrocyte aggregation (sludge blood). Acta Med. Scand. Suppl., 343:10-63, 1959.

23. THORSEN, G. and HINT, H.: Aggregation, sedimentation, and intravascular sludging of erythrocytes. Acta Chir. Scand. Suppl. 154, 1950.

24. BROOKS, D.E. and SEAMAN, G.V.F.: Some effects of dextran on human erythrocyte interactions. Bibl. Anat. 11:272-280, 1973.

25. JAN, K.-M. and CHIEN, S.: Role of surface electric charge in red blood cell interactions. J. Gen. Physiol. 61:638-654, 1973.

26. CHIEN, S. and JAN, K.-M.: Red cell aggregation by macromolecules: roles of surface absorption and electrostatic repulsion. J. Supermolecular Structure 1:385-409, 1973.

27. LIM Jr., C., KOSTRZEWSKA, E., BERGENTZ, S.-E., and GELIN, L.-E.: Blood flow property changes following infusion with Dextran 40 and Dextran 70. Rev. Surg. 25:151, 1968.

BIORHEOLOGY Vol.17, pp. 17-24 0006-355X/80/010017-08$02.00/0
© Pergamon Press Ltd. 1980. Printed in the United States

A COUETTE VISCOMETER FOR SHORT TIME SHEARING OF BLOOD

G. Heuser and R. Opitz

Aerodynamisches Institut der RWTH Aachen, Germany

(Received 2.8.1979; in revised form 22.10.1979.
Accepted by Editor H. Schmid-Schönbein)

ABSTRACT

A Couette viscometer with axial flow is proposed which allows blood to be exposed to defined shear stresses of short duration. A prototype of this viscometer is tested. By measurements and simple calculations the range of application is established. Measurements with blood show the possibility to control the flow conditions which may lead to haemolysis.

Vol. 17
1980

INTRODUCTION

The damage of blood particles through shear stresses can be of essential importance for artificial organs. Not only the magnitude of the shearstresses but also the time they act on the particles is important. Various experimental set up were constructed through which both the influence of magnitude and time can be investigated. Figure 1 shows a summary of the ranges examined. Williams (1) and Champion et al. (2) use a cone and plate system. Leverett et al. (3), Nevaril et al. (4) and Whiffen et al. (5) carried out measurements in a combination of a cone-plate and a Couette system, Bacher et al. (6) and Keshavia et al. (7) in capillaries. Lambert (8) examined the deformation of erythrocytes in a narrow slit. Short loading times were reached by Rooney (9) with oscillating gas bubbles, by Williams et al. (10) with oscillating wires, by Bernstein et al. (11), Blackshear (12) and Forstrom et al. (13) with turbulent jets. Short shearing times are of particular interest, since in natural and artificial circulations hardly a constant shearstress will develop for minutes as in (1,2,3,4,5). Naumann (14) arrived at very short loading times of about 10^{-3} sec for the flow through an artificial heart valve or through a stenosis.

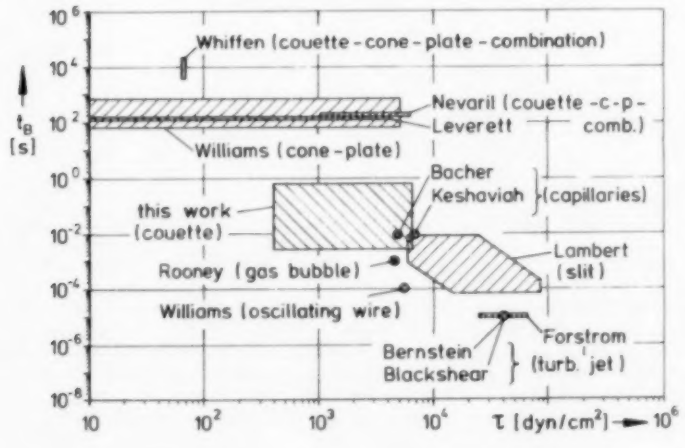

Fig. 1: Range of shear stresses and shearing times examined and test devices used by other authors

Well defined flow conditions are required for the investigation of shear induced haemolysis. The shear stress distribution as well as the duration of the load should be known. This is not the case in many experiments (9,10,11,12,13) either the estimate of the shear stress is not sufficiently accurate or the particles may be loaded repeatedly in the vortex motion of the flow. Clearly defined conditions are found in capillaries (6,7), but here the shear stress is not constant. In a slit (8) only one erythrocyte can be observed. The existing variation in its volume is taken as a measure of the amount of penetrated haemoglobin.

In this paper a Couette system is described, in which high shear stresses can be generated in short loading times. Both parameters can be varied independently. For this purpose the Couette system has an axial flow. The rotation of the inner cylinder controls the shear stress and the axial velocity regulates the loading time. This system is described and tested, and first measurements with blood will be presented in the following.

DEVELOPMENT OF A COUETTE SYSTEM WITH AXIAL FLOW

Reproducable shear stresses can be generated in the Couette system by the choice of the speed of rotation of the rotating inner cylinder, if the geometry and the viscosity of the medium are known. The diameter of the inner cylinder d_i = 58 mm and a gap width b = 0,115 mm produces a shear velocity of $\dot{\gamma} = 2.1 \cdot 10^3\ sec^{-1}$ for its maximum rotational speed n = 8000 R/min. The height of the cylinder is h = 5 mm. A proportioning pump produces a well known volume flow $\dot{V}$. Since the geometry is known, the shearing time t_B results to $t_B = h \cdot \pi \cdot d_i \cdot b/\dot{V}$. A sectional drawing of the system is shown in figure 2. Blood flows through the inlet A tangential into a toroidal channel with stationary walls, from here through the shearing region of the Couette system and from there into another toroidal channel with stationary walls and finally through the outlet B, where the probe is taken. The whole device is thermo-regulated at the outer cylinder and within the apparatus. The inner cylinder is fastened at the shaft which can be adjusted in axial and radial direction.

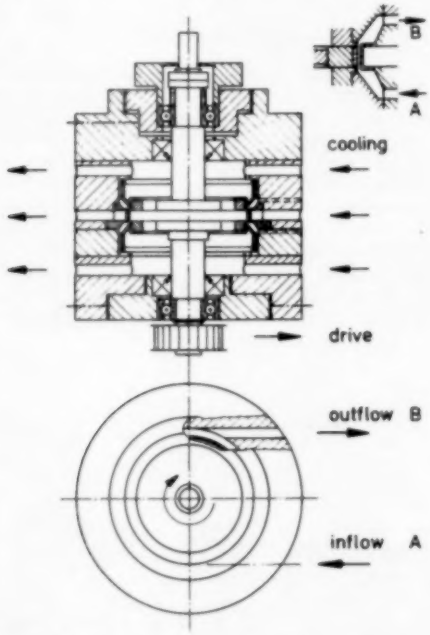

Fig. 2: Sectional drawing of the Couette viscometer

Since high shear stresses should be developed only within the Couette system by the rotating inner cylinder, this cylinder is stuffed against the stationary housing (sliding velocity $v_\Theta \leq 24$ m/sec). A suitable packing was found in an axial wheel shaft packing.*) The inner cylinder, consisting of backing coal, reinforced by an outside shrinked on stainless steel (V_2A) ring, moves on standing coale rings. The behaviour of the packing, the abrasion of which is indicated with 1 mm per 10^4 working hours will be described. The toroidal channels and the in- and outflow tubes were made out of titanium.

The flow in a Couette system with axial flow has been investigated by many authors. Chung and Astill (15) theoretically and Gravas and Martin (16) examined experimentally the onset of Taylor vortices depending on the mean axial velocity $\bar{v}$ and the rotations per unit time n of the inner cylinder. The flow

*) This packing was delivered by Fa. GOETZEWERKE, 567 Opladen

modes which developed are shown in figure 3.

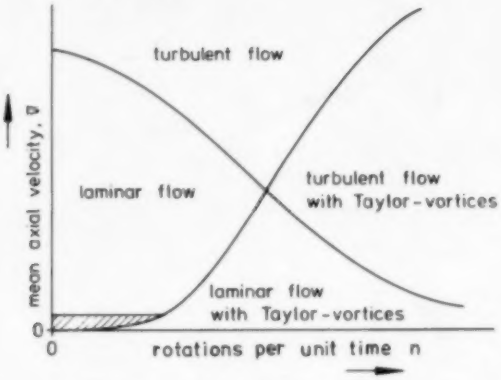

Fig. 3: Modes of flow which may develop in a Couette system with axial flow

In the system proposed here, neither the axial nor the tangential velocity profiles are fully developed. Astill et al. (17) investigated this flow experimentally and Coney and El-Shaarawi (18) theoretically. Velocity- and pressure distributions were obtained for the developing flow region, however not in a range of axial velocities and rotational speeds which are of interest here. Estimate of the two limiting cases, either rotating flow without axial flow or axial flow only show, that both profiles are developed at least after one tenth of the length which is given by the construction. Two requirements should be fulfilled: a) shear stresses caused by the rotation have to exceed those caused by the axial flow, b) haemolysis measurements should be done under laminar flow conditions only. These conditions establish the range, in which the system can work meaningful. This range is shaded in figure 3. The shear stresses given in some of the following figures are those caused by the rotation only and are thereby to be considered as the lower limiting case.

Since the axial flow causes a velocity profile, the residence time of blood particles in the gap will depend on their distance from the cylinder. An erythrocyte which is in a distance of 10μm from one cylinder will remain twice as long in the slit as one which is in the middle. The loading time t_B is the mean passage time through the gap.

First haemolysis measurements were done in the loading range which is shaded in figure 1. This range can be extended by changing the geometry of the gap by the interchangeable outer cylinder or by varying the viscosity of the test fluid.

TESTING THE SYSTEM

The Couette viscometer was tested repeatedly in order to ensure a reproducable and well defined flow field. The influence of possible error sources were estimated. For the operation of a Couette system it is essential that the cylinders are concentric. As was shown by Ullrich (19), the pressure loss caused by axial flow depends on the excentricity e of the cylinders (see figure 4). Measurements of the pressure loss show a good agreement between theory and experiment. This method allows only a rough checking as to whether or not the cylinders are concentric, since the differences in the measured pressure losses at e = 0 are small. A very sensitive method is to measure the static pressure at three locations uniformly distributed on the perimeter. Excentrically rotating cylinders will give an asymmetrical pressure distribution. Without axial flow the rotating inner cylinder is shifted relative to the outer cylinder and will provide a symmetric pressure distribution.

In- and outflow channels are symmetric to a plane normal to the axis of rotation. Different pressures in these channels at rotating inner cylinder without axial flow indicate an asymmetry to this plane. The inner cylinder is too high to too low with respect to the outer cylinder. The results of the measured pressure difference Δp between in- and outflow channel depending on the axial shifting distance s of the inner cylinder are shown in figure 5. The curves for the two directions of rotation are caused by the backlash of the bearing. After fixing the sense of rotation (inflow in direction of rotation) the pressure difference Δp is adjusted to zero.

Laminar flow should develop in the whole range of operation. In this case the axial pressure difference between in- and outflow channel depends linearly on the loading time t_B. As figure 6 shows, this is true for $\dot{\gamma} \leq 15.53 \cdot 10^4\ sec^{-1}$. It is concluded that for the pressure loss in the gap quadratic terms may be neglected. The deviation from this behaviour at higher shear velocities can be explained by a small remaining pressure difference even if the axial flow is zero (see figure 5). The straight lines are shifted

Vol. 17
1980

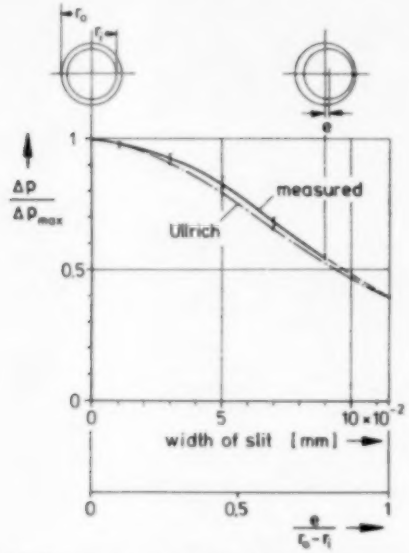

Fig. 4: Pressure loss of axial flow as a function of the excentricity e of the cylinders

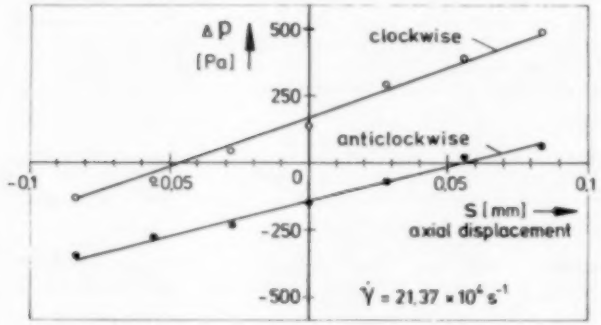

Fig. 5: Test of the axial symmetry. Clockwise or anticlockwise rotation when viewed from above

with increasing shear velocity at constant loading time to higher pressure differences.

As was shown by Karle (20), temperature influences the rate of haemolysis, too high temperatures damage the erythrocytes directly. Therefore the temperatures occuring in the Couette system should be known. The temperature is measured by means of a probe introduced through a pressure tap next to the fluid penetrating the gap. The rise in temperature is plotted against the time and the stationary end temperature is transferred into a $\dot{\gamma}$ - t_B -diagram. Points with constant temperature increase $\Delta\vartheta$ are connected and shown in figure 7. These curves are obtained without additional cooling in the thermostat reservoir. The whole system is heated up by the frictional heat produced by the axial wheel shaft packing. With additional cooling the temperature rise can be halfed. It was found to be independent of the viscosity η of the test fluids (1 cP $\leq \eta \leq$ 10 cP). The measurements with blood were carried out with a temperature of $\vartheta = 30^0$ C in the reservoir and additional cooling.

Because of the high shear velocities which are required, the angular velocity of the inner cylinder has to be increased to 800 sec^{-1}. In this case a pressure gradient within the cooling fluid inside the housing of the system is to be expected which may cause a leakage of cooling fluid through the axial wheel shaft packing into the blood. The leaking water volume was measured as a function of the shear velocity. Especially for measurements with blood not the absolute value of the leaking volume seems to be of interest but rather the percentage of volume leaving the outflow B coming from the cooling circuit. This is plotted in figure 8 as leakage in percent against the loading time. For $\dot{\gamma} < 4 \cdot 10^4$ sec^{-1} the packing in tight, for $\dot{\gamma} \geq 5 \cdot 10^4$ sec^{-1} the leakage volume is increased. The maximum loading time was 0.69 sec for experiments with blood which results in a leakage of 7 percent. To avoid osmotical haemolysis physiological solution of sodium chloride is used as cooling fluid in experiments with blood. Experiments with different coloured cooling water show the leakage to be apportioned half by half on each of the

sealing surfaces.

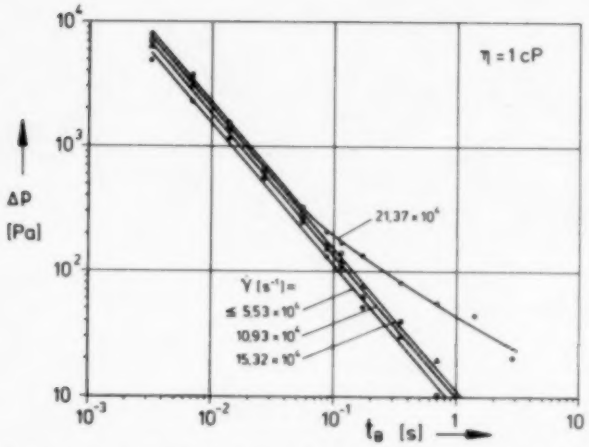

Fig. 6: Pressure loss in the gap by axial flow and rotating inner cylinder

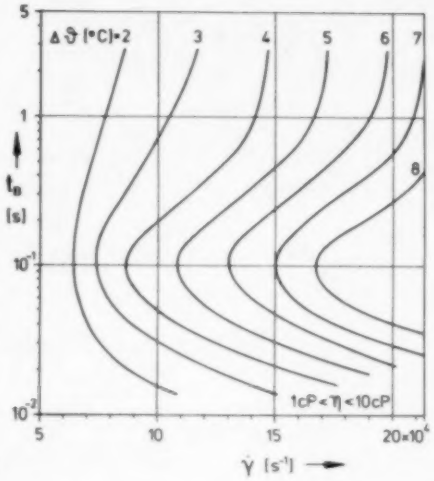

Fig. 7: Increase in temperature in the gap without additionalcooling

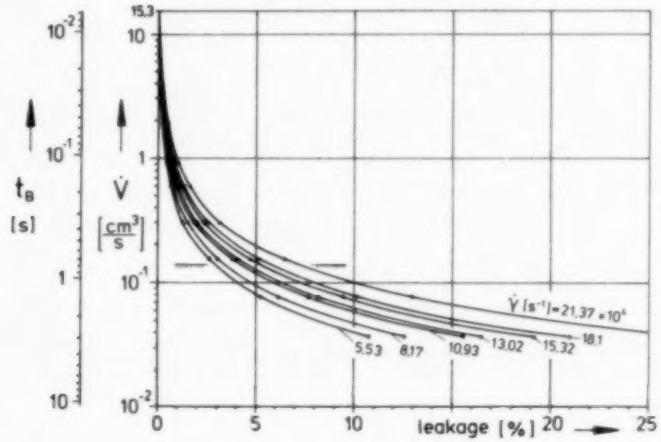

Fig. 8: Leakage through the axial wheel shaft packing

In experiments with blood it is necessary to rinse the blood leading system with physiological solution of sodium chloride and to keep the system filled with it to avoid blood air contact. The sodium chloride solution in the system is to be displaced by blood conveyed by the proportioning pump. The time required for this process is to be determined as a function of the operating conditions. Instead of the sodium chloride solution the system is filled with coloured water. The rinsing process is determined by measuring the colour concentration with a photometer. The process is completed if the concentration of the colour is below 1 % . The time which is known now allows one to calculate the volume to be displaced to get blood with known composition and load at the outflow. This volume V is plotted as a function of the loading time t_B in figure 9. Differences between axial flow with and without rotation exist only for $t_B > 0.1$ sec. The displaced volumes are independent from the shear velocity for axial flow with rotation. This displaced volumes cannot be used in experiments with blood.

The possible range of operation is demonstrated in figure 10. This range is limited by the maximum rotational speed which corresponds to a maximum shear velocity of $\dot{\gamma} = 21.37 \cdot 10^4$ sec^{-1}. Since the maximum wall shear stress τ_w should not increase above 10% of the shear stress caused by the rotation τ_{rot}, the possible loading time t_B is limited. Points of measurement on the left side of the curve $\tau_w = 1.1 \cdot \tau_{rot}$ are to be excluded. As an example a point $\dot{\gamma} = 15 \cdot 10^4$ sec^{-1} and $t_B = 0.1$ sec is considered. The diagram shows: a) the leakage of cooling water into the flowing blood is smaller than 1%, b) the temperature incrase $\Delta\vartheta$ will be 7°C without additional cooling, with cooling an increase of 3.5° C is to be expected, c) Taylor vortices will not develop in fluids which have a viscosity of $\eta > 2.3$ cP.

Vol. 17
1980

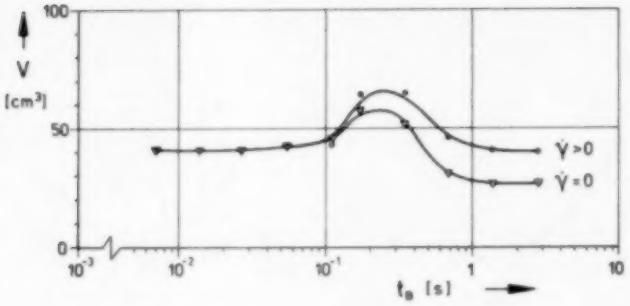

Fig. 9: Displaced volume to get blood with known composition and load

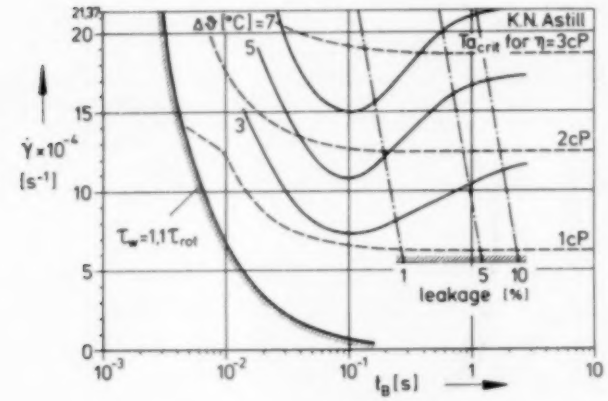

Fig. 10: Possible range of operation
——— constant increase in temperature (see Fig. 7)
—·—·— constant leakage (see Fig. 8)
– – – – onset of Taylor vortices depending on the viscosity η of the fluid (Astill (19))

HAEMOLYSIS MEASUREMENTS

The measurements of blood damage described below were done with fresh heparinised pig blood. The rate of haemolysis Hg is defined as the ratio of plasmahaemoglobin released during the load Δ Hb to the total amount of haemoglobin Hb in percent. The plasmahaemoglobin concentration at the beginning is PHb_o and at the end PHb of the experiment, the haematokrit Ht and the whole blood haemoglobin concentration VHb are to be measured at every sample. These values are evaluated with the formula

$$Hg = \frac{\Delta Hb}{Hb}[\%] = \frac{(1-Ht/100)(PHb - PHb_o)}{VHb} \cdot 100$$

The blood damage thus defined is plotted in figure 11 depending on shear velocity and loading time. In a pilot experiment could be shown that there was no blood damage detectable with axial flow alone. All curves show the same shape at constant loading time, although t_B is varied over more than two orders of magnitude. For $t_B < 3{,}4 \cdot 10^{-5}$ sec and $\dot{\gamma} < 3 \cdot 10^4$ sec^{-1} no haemolysis is detectable. The shape of the curves is similar to those obtained by Williams (1) who varied the shear stress at constant loading time of 5 minutes.

A diagram of haemolysis, in which the shear stress is plotted depending on the shearing time with the rate of haemolysis as parameter, can be obtained from figure 11. The viscosity of blood was chosen to be η = 3 cP. The diagram of haemolysis (figure 12) illustrates the influence of time on haemolysis. For

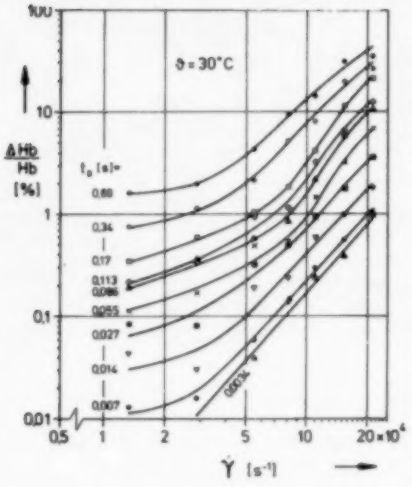

Fig. 11: Rate of haemolysis depending on shear velocity and loading time. Haemolysis for the operation of the loading pump alone is not detectable.

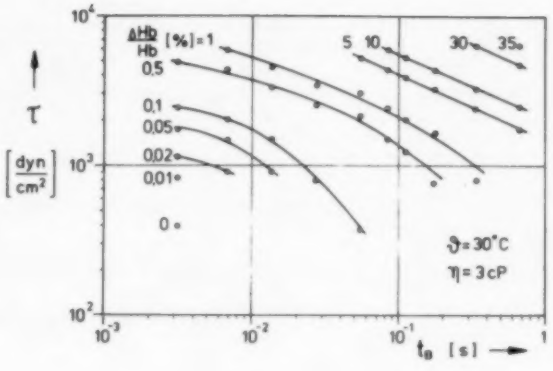

Fig. 12: Diagram of haemolysis

Vol. 17
1980

one shear stress a great intervall of time is needed to reach, beginning with Hg = 0, total haemolysis. Rates of haemolysis Hg > 5 % are represented by straight lines which are proportional to the loading quantity $\tau \cdot t_B^{1/2}$ as was already shown by Lambert (8). This dependence also results from a theoretical investigation by Richardson (21).

SUMMARY

A Couette viscometer with axial flow to generate high and clearly defined shear stresses and short shearing times is tested, for the projected range of operation. The concentricity of the cylinders is controlled by measuring the static pressure at three locations uniformly distributed on the perimeter. The symmetry to a plane normal to the axis of rotation is tested by the measurement of the static pressures in the toroidal channels with the inner cylinder rotating. With additional axial flow the results of the measurement of the pressure difference in these channels permit to neglect quadratic terms in the pressure loss in the gap. For the measurements with blood the increase in temperature, the leakage through the packing and the displaced volume which is required to get blood of known composition and load at the outflow are determined. The results of these measurements are summarized in the operating diagram. Experiments with pig blood show the applicability of the viscometer to measurements of blood damage by shear stresses. Shear stresses $\tau < 7 \cdot 10^3$ dyn/cm^2 and shearing times $t_B > 3 \cdot 10^{-3}$ sec can be obtained.

ACKNOWLEDGEMENTS

This study was sponsored by the Deutsche Forschungsgemeinschaft SFB 109.

REFERENCES

1. WILLIAMS, A.R. Shear induced fragmentation of the linear erythrocytes. Biorheology, 10, 303-311, 1973.

2. CHAMPION, J.V., NORTH, P.F., COAKLEY, W.T., WILLIAMS, A.R. Shear fragility of human erythrocytes. Biorheology, 8, 23-29, 1971.

3. LEVERETT, L.B., HELLUMS, J.D., ALFREY, C.P., LYNCH, E.C. Red blood cell damage by shear stress. Biophys.Journal, 12, 257-272, 1972.

4. NEVARIL, C.G., LYNCH, E.C., ALFREY, C.P., HELLUMS, J.D. Erythrocyte damage and destruction by shearing stress. J. Lab. and Clin. Med., 784790, 1973.

5. WHIFFEN, J.D., LIGHTFOOT, W.N., DENNIS, W.H., FORD, R.E., POWASER, M.M. SOLEN, K.A. A device to study the degradation of blood in a shear field with controlled wall effects. J. Biomed. Mater. Res. 5, 315-324, 1971.

6. BACHER, R.P., WILLIAMS, M.C. Hemolysis in capillary flow. J. Lab. and Clin. Med., 76, 485-495, 1970.

7. KESHAVIA, J., M.S. Thesis. University of Minnesota, Minneapolis, 1970.

8. LAMBERT, J. Die hämolysierende Wirkung hoher, kurzzeitiger, laminarer Schubspannungen. Diss. TH Aachen, 1976.

9. ROONEY, J.A. Hemolysis near an ultrasonic pulsating gas bubble. Science, 169, 869-871, 1970.

10. WILLIAMS, W.J. HUGHES, D.E., NYBORG, W.L. Hemolysis near a transversely oscillating wire. Science, 169, 871-873, 1970.

11. BERNSTEIN, E.F., BLACKSHEAR, P.L., KELLER, K.H. Factors influencing erythrocyte destruction in artificial organs. American J. Surg., 114, 126-138, 1967.

12. BLACKSHEAR, P.L. Mechanical hemolysis in flowing blood. In: Fung, Perrone, Anliker: Biomechanics, its Foundations and Objectives, Verlag Prentice Hall, Inc., Englewood Cliffs, N.J. 1972, p.501.

13. FORSTROM, R., BLACKSHEAR, P.L., KESHAVIA, P., DORMAN, F. Fluid dynamic lysis of red cells. Presented 3rd Joint Meeting AICHE, San Juan, Puerto Rico 1969.

14. NAUMANN, A. Strömung in natürlichen und künstlichen Organen und Gefäßen. Klin. Wschr., 53, 1007-1019, 1975.

15. CHUNG, K.C., ASTILL, K.N. Hydrodynamic instability of viscous flow between rotating coaxial cylinders with fully developed axial flow. J. Fluid Mech., 81, 641-655, 1977.

16. GRAVAS, N., MARTIN, B.W. Instability of viscous axial flow in annuli having a rotating inner cylinder. J. Fluid Mech., 86, 385-394, 1978.

17. ASTILL, K.N., GANLEY, J.T., MARTIN, B.W. The developing tangential velocity profile for axial flow in an annulus with a rotating inner cylinder. Proc. Roy. Soc., A.307, 55-69, 1968.

18. CONEY, J.E.R., EL-SHAARAWI, M.A.I. A contribution to the numerical solution of developing laminar flow in the entrance region of concentric annuli with rotating inner walls. Journal of Fluids Engineering, 333-340, 1974.

19. ULLRICH, H. Druckverlust und Wärmeübergang in laminar durchströmten Ringspalten mit beliebig geformtem Kern. Chem.Ing.Techn., 33, 606-608, 1961.

20. KARLE, H. Effect on red cells of a small rise in temperature: in vitro studies. Brit. J. Haemat., 16, 409-419, 1969.

21. RICHARDSON, E. Applications of a theoretical model for haemolysis in shear flow. Biorheology, 12, 27-37, 1975.

BIORHEOLOGY Vol 17, pp. 25-35 0006-355X/80/010025-11$02.00/0
© Pergamon Press Ltd. 1980. Printed in the United States

LOW SHEAR RATE VISCOSITY OF FRESH BLOOD

A. Downs, M. Litt and R. E. Kron
Department of Bioengineering, College of Engineering and Applied Science
and Department of Psychiatry, School of Medicine
University of Pennsylvania
Philadelphia, Pennsylvania 19104, U.S.A.

(Received 6.6.1979; in revised form 27.12.1979.
Accepted by Editor H.L. Goldsmith)

ABSTRACT A capillary viscosmeter is described which allows measurement of the shear rate dependency of fresh blood viscosity at low shear rates. The instrument has been used in a preliminary study to evaluate differences between fresh and EDTA anticoagulated blood. In a shear rate range of 0.5 to 1.3 sec^{-1} the viscosity of fresh blood is more strongly dependent on hematocrit than is the viscosity of EDTA anticoagulated blood. Also, the viscosity of anticoagulated blood is more sensitive to day-to-day variations than is that of fresh blood. For some subjects, such variations may amount to as much as 30%.

Vol. 17
1980

INTRODUCTION

There is a considerable body of literature on the rheological properties of blood, both normal and abnormal. At low shear rates whole blood is a pseudoplastic fluid. Furthermore, it has been well documented that both the absolute value and shear rate dependency of whole blood viscosity vary significantly in various abnormal or disease states (1).

Almost the entire literature dealing with whole blood rheology is based upon studies performed on anticoagulated samples. A number of investigations using fresh blood have given conflicting results: several conclude that there is no effect of anticoagulants on blood viscosity, while others suggest that there are differences in the viscosity of fresh vs. anticoagulated blood (2-5). Because most precise viscometric techniques require considerable set-up time, fresh blood viscosity measurements are usually limited to one shear rate value for each sample before significant clotting takes place. This paper describes a capillary ramp-response viscometer which can determine whole blood viscosity as a function of shear rate on a single sample of fresh blood. Measurements over a wide shear rate range can be completed in less than one minute after venipuncture. The method is capable of giving shear stress/shear rate data directly, giving true viscosity, as well as apparent viscosity, and is not dependent upon the a priori assumption of a specific rheological model.

DESCRIPTION OF THE INSTRUMENT

A block diagram of the instrument is given in Figure 1. The unusual feature of this capillary viscometer is that it is operated as a variable flow device, i.e., the flow rate is deliberately varied as a specific function of time. In the version described here the flow follows a linear ramp function and is in the pseudo-steady state regime; that is, the ramp time is large compared to the time constant of the system. The flow ramp is achieved by using a modified syringe pump (Harvard Model 990 Servo-Control Syringe Pump). A linear voltage ramp is generated by a suitable function generator. This signal drives the syringe pump controller, which then generates a flow output linearly varying with time. The ramp function generator output also drives the arm of an X-Y recorder, so that the X axis records a signal directly proportional to flow rate. The pressure drop across the capillary is measured by a differential transducer (Validyne Model GP-45 Transducer with Model CD-12 Transducer Indicator). The output of the transducer is recorded as the pen signal on the X-Y recorder. When a Newtonian fluid flows through the capillary, the result should be a linear plot whose slope is proportional to the viscosity of the fluid. When a non-Newtonian fluid flows through the

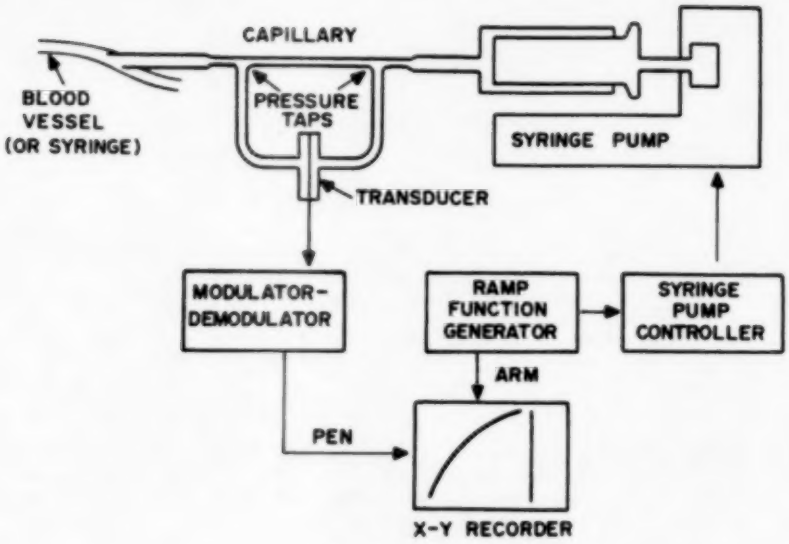

FIG. 1

Block Diagram of Capillary Ramp Function Viscometer

capillary, a nonlinear plot should be obtained whose slope at any point is proportional to the apparent viscosity at the average shear rate characterized by that particular flow. Using the Rabinowitch equation (6), the data at different flow rates can be transformed to give an absolute viscosity.

Characteristics of the instrument were studied and calibration was carried out using several sucrose solutions of varying viscosities (5 - 40 CP) as well as anticoagulated human blood. The pressure transducer was calibrated against a micromanometer. The viscosity determined from the ramp function response agreed well with values determined from steady state runs, indicating that the pseudo-steady state assumption was valid over the range of flows and viscosities used. Analysis of the transient characteristics of the system indicated that with the capillary and transducer used the time constant of the system was about 1 second for a viscosity of 24 CP. Experiments indicated that the optimum ramp times were on the order of 10 seconds; this gave a linear response over most of the output curve (for Newtonian samples) and failed to demonstrate any changes with anticoagulated blood that could be attributed to sedimentation or aggregation. Further details of the instrumentation and calibration can be found in Downs (7). This instrument is a modification for low shear rates of that developed by Kron (8).

To carry out a test, a constant initial flow was set and a decreasing ramp of flow vs. time was run. Data from a calibration run of this type are shown in Figure 2, for a sucrose solution. Overall time of the experiment is 10 seconds, starting from an initial shear rate of 5 sec^{-1}. There is an initial curvature of the plot due to the compliance of the pressure transducer. The curve then becomes linear, as expected of a Newtonian fluid. When the impressed flow falls to zero, however, the pressure is still above zero. This is due to the displacement of the transducer membrane; because of the high viscosity of the fluid in the capillary, it takes a finite time for the pressure to decay to zero. This behavior can be understood in terms of the following analysis. For a Newtonian fluid, assuming the Hagen-Poiseuille law for flow in a capillary obtains, we have

$$P = \frac{8\mu LQ}{\pi R^4} = k_2 \mu Q \qquad (1)$$

where P = pressure difference across the capillary of length L and radius R: and μ is the dynamic viscosity. The flow rate through the capillary Q has two components, as illustrated in Figure 3. Q_p is the induced flow due to the syringe pump; Q_t is the flow due to the displacement of the transducer diaphragm. The components are given by

$$Q_p = Q_{pi}\,(1 - t/t_e) \tag{2}$$

$$Q_t = \frac{-dV_t}{dt} \tag{3}$$

where V_t is the volume of the transducer. The total flow through the capillary is $Q = Q_p + Q_t$. It is assumed that the sidearms A and B are designed so that pressure drops in them are negligible. The flow due to the transducer is linearly dependent on the pressure measured by the transducer through the compliance k_1:

$$\frac{dV_t}{dt} = k_1 \frac{dP}{dt} \tag{4}$$

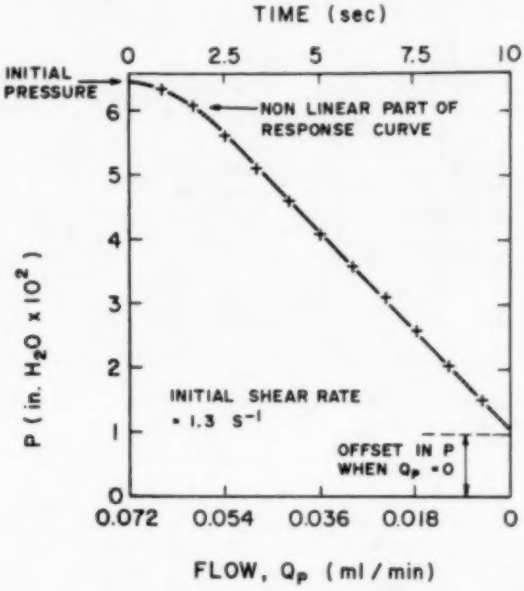

FIG. 2

Typical Pressure vs. Flow (or Time) Results from the Ramp Response of a Newtonian Fluid (24CP sucrose solution)

Combining these equations, we have

$$P = k_2\{Q_{pi}(1 - t/te) - k_1 \frac{dP}{dt}\} \tag{5}$$

$$0 \leq t \leq t_e$$

t_e being the time at which the pump is turned off. Solving this equation gives, for the pressure vs. time:

$$P = k_2\mu Q_{pi}\{(1 - t/t_e) + \frac{k_1 k_2 \mu}{t_e}\,(1 - e^{\frac{-t}{k_1 k_2 \mu}})\} \tag{6}$$

$$0 \leq t \leq t_e$$

From Equation (1), P_o, the initial pressure before starting the ramp, is given by $k_2\mu Q_{pi}$. Using this, we can solve Equation 6 explicitly for the viscosity, giving

$$\mu = \frac{t_e}{k_1 k_2}\,\{\frac{P/P_o + t/t_e - 1}{1 - \exp(-t/k_1 k_2 \mu)}\} \tag{7}$$

Vol. 17 1980

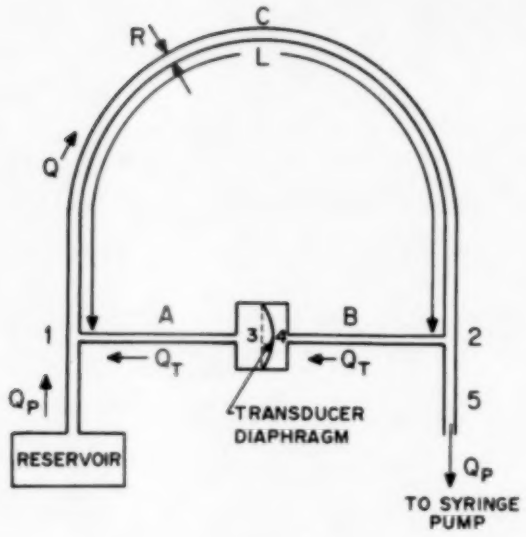

FIG. 3

Diagram of Capillary-Transducer Flow Circuit

For the parameters used in the present apparatus, after a few seconds the exponential term decays, giving

$$\mu = \frac{t_e}{k_1 k_2} \{P/P_o + t/t_e - 1\} \qquad (8)$$

where μ is the Newtonian viscosity (or apparent viscosity for non-Newtonian fluids). This explains the linear portion of the curve in Figure 2. Furthermore, it is apparent from Equation (8) that at $t = t_e$, i.e., at the end of the ramp, the pressure is not equal to zero, but is given by a finite value which is

$$\frac{P}{P_o} = \frac{k_1 k_2 \mu}{t_e} \qquad (9)$$

From Equations (7) and (9), it is seen that the term $k_1 k_2 \mu$ is the first order time constant of the system, and that the nonlinear effects can be minimized by making the time constant small compared to the ramp time. Within the constraints of maintaining transducer response and low shear rate, it was possible to obtain useful linear data over about 80% of the ramp. It should be noted that since k_1 is the only compliance term used, it effectively includes the entire system compliance.

For a non-Newtonian fluid, one can apply a similar analysis except that the middle portion of the plot will now also be curved because $\mu = f(Q)$. At each instant of time, an apparent Newtonian viscosity μ_{APP} can be calculated from Equation (8) which assumes the applicability of Poiseuille's law; the corresponding flow rate is obtained from Equation (2). From this and the pressure one can then calculate the Newtonian wall shear rate $\dot{\gamma}_{WN}$ and the wall shear stress τ_W:

$$\tau_W = \frac{R}{2}\left(\frac{\Delta P}{L}\right) \quad ; \quad \dot{\gamma}_{WN} = \frac{4Q}{\pi R^3} \qquad (10)$$

Using these data and the Rabinowitch equation, one can obtain the true non-Newtonian viscosity μ_{NN} at any shear rate via:

$$\frac{\mu_{NN}}{\mu_{APP}} = \frac{4}{3 + \frac{\log\dot{\gamma}_{WN}}{\log\tau_W}} \qquad (11)$$

Figure 4 shows a raw data plot for whole blood. The slight oscillations in the curves are due to residual noise from the syringe pump.

For the studies carried out here, a capillary of 2.108 mm diameter and 24.3 cm long was used. The usable shear rate range was from about 1.5 down to 0.1 sec^{-1}. The shear rate range can easily be extended by varying the gear setting of the pump and is ultimately limited by the sensitivity of the pressure transducer. The temperature was maintained at 37° by immersing the entire capillary-transducer assembly in a water bath.

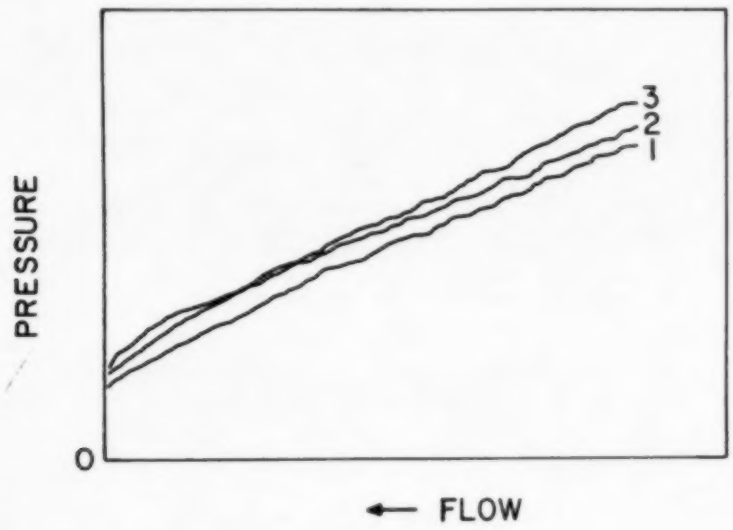

FIG. 4

Tracing of Actual Pressure-Flow Curves from X-Y Plotter. Fresh Blood Sample from Normal Subject. Curves 1-3 run on same sample approximately 20 seconds apart.

EXPERIMENTAL STUDY

1. Populations

An experiment to test the utility of the instrument was designed. The apparent viscosity of fresh vs. anticoagulated blood at low shear rates was determined. Subjects were students ranging in age from 18 to 23 years; there were 15 males and 4 females. Ramp tests were run with shear rates ranging from 1.5 down to 0.1 sec^{-1}. The data are reported at two shear rates, 1.3 and 0.5 sec^{-1}.

Because the results of previous work had indicated that significant viscosity variations could occur due to time of sampling and behavior of the subjects (time since last meal, stress from examinations, prior weekend partying, etc.), the study was carried out under as controlled conditions for the subjects as possible. Data from each subject were collected on each of the three successive days. These were Tuesday, Wednesday and Thursday mornings, which were selected as being the least stressful days of the students' week. A questionnaire was used to determine any relevant personal characteristics of the subject. Each subject was asked to come to the laboratory prior to breakfast and to refrain from eating or drinking anything after midnight of the night before.

Vol. 17
1980

2. Testing

As indicated in Fig. 1, samples can be introduced directly from the vein into the instrument, or from a syringe. In the present studies, all samples (10 ml) were drawn from the antecubital vein to a syringe and then loaded into the instrument, since repeated trials indicated that the instrument could be loaded just as rapidly in this fashion. Prior to use, the capillary was siliconized and the instrument flushed with blood to equilibrate all surfaces. It was then filled with saline. Experiments with anticoagulated blood demonstrated that about 4 ml of blood were needed to replace the saline in the capillary (volume 0.85 ml) to avoid dilution errors. Depending upon the skill of the operator, the instrument was ready for the initial run 20-30 seconds following withdrawal of the sample. Each run took 15 seconds, with 5 seconds between tests. Thus, in most cases, three or more complete replicate tests could be carried out on the same sample in a period of less than 2 minutes after venipuncture. After loading the machine with fresh blood, the remaining sample was introduced into a vacutainer (of appropriate size for the blood volume) which contained the proper amount of dry EDTA. The anticoagulated samples were run as soon as possible after the fresh ones, usually within one hour. Hematocrit was determined on the EDTA sample using the microhematocrit capillary tube method, on the same day. Between samples, the system was flushed with saline until clear. Also, the system was periodically cleaned more thoroughly by removing the capillary and reaming with a large pipe cleaner, followed by recoating. Recalibration after extended use indicated negligible changes.

In all, 57 blood samples drawn from 19 subjects were tested (one per day for each over 3 days). A limited number of tests were also carried out with samples from subjects showing various forms of vascular pathology, including stroke, TIA (transient ischemic attack), and sickle cell anemia. These tests were all made on EDTA anticoagulated blood, since it was not possible to transport the patients to the laboratory.

Vol. 198

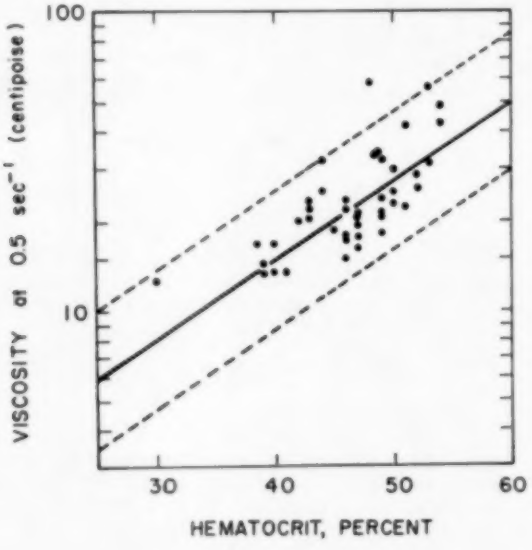

FIG. 5

Viscosity of Normal Fresh Blood as a Function of Hematocrit at 0.5 sec^{-1}. Solid Line: Least Squares Regression. Dashed Lines: 95% Confidence Interval.

RESULTS

A typical plot from a subject having a hematocrit of 50, in which three tests were carried out in succession, is shown in Figure 4. The tests are labelled 1-3 in the temporal order in which they were carried out. In this case the first test was completed in slightly under 1 minute. Each subsequent

test was completed 20 seconds later. There is a definite increase in the initial pressure P_0 for each repeat, which are all carried out at the same initial flow rate Q_{pi}. Therefore, there must be significant increase in viscosity over this time period, indicating that rheological changes associated with coagulation may be taking place from the moment of venipuncture. At 1 sec^{-1}, the results indicate an 8% increase in viscosity in 20 seconds. Over the same time period, similar repetitions using the EDTA anticoagulated blood were reproducible, indicating that sedimentation was not causing the variation seen in Figure 4. Allowing anticoagulation blood to remain undisturbed in the capillary for a long time (> 5 min) did produce changes that could be attributed to sedimentation.

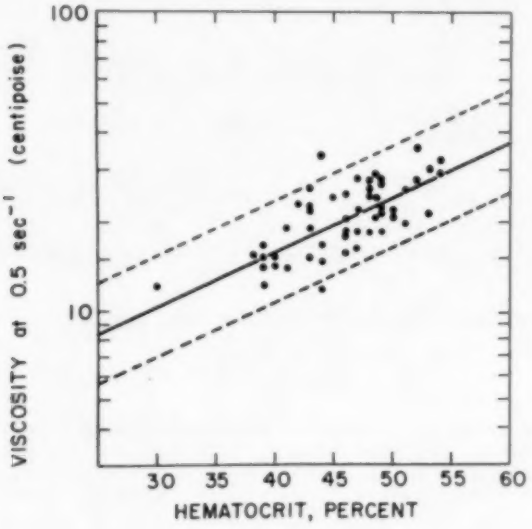

FIG. 6

Viscosity of Normal EDTA Anticoagulated Blood as a Function of Hemocrit at 0.5 sec^{-1}. Solid Line: Least Squares Regression. Dashed Lines: 95% Confidence Interval

Because of this, in the present study, the earliest results were used as representative of the "fresh" blood sample viscosity. Actually, a better method might have been to extrapolate viscosity values back to the moment of venipuncture, but this would have required much better control over and recording of samplestimes, with presumably individualized corrections for variations in coagulation rates between samples. Certainly further studies to quantitate this effect are in order.

A semi-logarithmic plot of fresh blood viscosity vs. hematocrit at a shear rate of 0.5 sec^{-1} is shown in Figure 5. A least squares regression line has been fit to the data. Also included are the 95% confidence limit bands for the individual measured values. A similar plot for the same samples after EDTA addition is given in Figure 6. The results of statistical analysis of these data and at a shear rate of 1.3 sec^{-1} are given in Table 1. The correlation coefficients for the regressions range from about 70 to 85%, indicating some scatter but highly significant correlations. These results indicate that the predicted slopes of the EDTA and fresh blood viscosity plots were significantly different at the 95% level at a shear rate of 1.3 sec^{-1}. At the lower shear rate, the difference in slopes was significant only at the 84% level. Interestingly enough, the two plots cross at hematocrit around 45, indicating that measurements on hematocrits in that range would tend to show no differences between fresh and anticoagulated blood. However, at conditions of extreme high and low hematocrit, which might be typical of abnormal states, there appears to be a significant difference in the viscosity/hematocrit behavior of fresh vs. anticoagulated blood.

A statistical analysis of the variation of the data, comparing fresh samples vs. EDTA anticoagulated samples, and for each type of sample the variation in viscosity vs. the days of collection, is summarized in Table 2.

Vol. 17
1980

TABLE 1

HEMATOCRIT DEPENDENCE OF FRESH AND EDTA ANTICOAGULATED BLOOD VISCOSITY

Data	N*	Slope	Intercept	Standard Error	95% Conf. Band	$r_{corr.}$
		A. Shear Rate = 1.3 sec^{-1}				
Fresh vs. HCT	53	0.058 (0.048 - 0.069)†	-0.163	0.160	±38%	0.840
EDTA vs. HCT	58	0.036 (0.027 - 0.045)	0.850	0.156	±37%	0.744
		B. Shear Rate = 0.5 sec^{-1}				
Fresh vs. HCT	57	0.060 (0.046 - 0.073)	0.302	0.243	±63%	0.764
EDTA vs. HCT	58	0.043 (0.033 - 0.053)	1.045	0.176	±42%	0.757

*Data from samples falling outside the 95% predicted range have been excluded from the analysis

†Figures in parentheses are minimum and maximum limits

Paired-t tests were carried out, and the significance levels for each of the comparisons are given. The analysis was carried out to examine the following hypotheses: that there were no differences between the viscosities of either fresh or EDTA blood with respect to test day, that there was no variation of

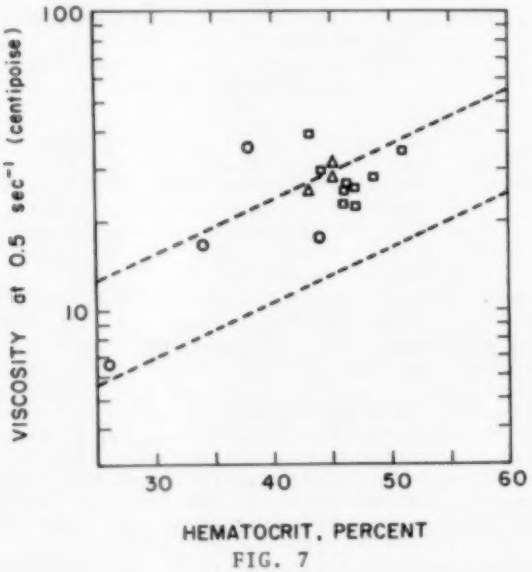

FIG. 7

Viscosity of EDTA Anticoagulated Blood from Patients with Disease at 0.5 sec^{-1} vs. Hematocrit. Dashed Lines are 95% Confidence Interval for Normal EDTA Blood.

□ stroke Δ TIA o sickle cell

the hematocrit from day to day, and that fresh blood did not significantly differ in its viscosity behavior day to day from EDTA blood. However, comparison of the fresh and EDTA blood viscosities of the same samples at a shear rate of 0.5 sec^{-1} shows a significant difference between the two, with fresh blood viscosity being, on the average, higher by 1.7 cp. At the higher shear rate of 1.3 sec^{-1}, there was still a difference, which was only significant at the 78% confidence level. The change in viscosity of EDTA blood from the second to third days of the test sequence was significant at the higher shear rate as well as at the lower.

Data on EDTA blood viscosity of abnormal patients are shown in Figure 7. The subjects include eight patients who had suffered recent acute cerebrovascular accidents (strokes), three subjects having recent transient ischemic attacks, and three subjects with sickle cell anemia. On this plot, the dotted lines represent the 95% confidence band for normal samples.

DISCUSSION

In the shear rate range used, the present instrument gives values of the viscosity with a reproducibility within 0.5 CP. The normal blood data showed a variation for individuals on a day-to-day basis that was in general significantly greater than this. The experiment had been designed in an attempt to minimize extraneous causes of variability, so as to determine the constancy of fresh blood viscosity as a possible clinical measure. To this end, the testing was carried out at midweek using a homogeneous population with respect to age, background and life style. The subjects were partially controlled as to diet in an attempt to reduce this factor. However, there were still some uncontrolled factors which have been shown to have an effect on blood viscosity (1). Of the 19 subjects, there were four females who were not controlled with regard to the menstrual cycle. There were two cigarette smokers of one pack per day, and one occasional smoker. One subject was slightly overweight, with moderately elevated blood pressure. A number of the subjects displayed stress reactions to the venipuncture and several had a family history of heart disease. These factors may have contributed to some of the variability noted. However, the day to day variability of most subjects was several times that of the minimum variability in the determination, with some individuals changing as much as 30% day to day. There was also some indication of hematocrit variation on a daily basis, which seemed to explain some but not all of the viscosity variation, particularly for the fresh blood. It would also appear that other factors are at work in determining daily variations in blood viscosity. These results indicate that one must be cautious in interpreting blood viscosity determinations on subjects who are thought to be representative of a particular environmental state or disease condition, since the individual fresh blood viscosity values of even healthy subjects may vary significantly over time, particularly if the tests are uncontrolled with regard to incidental level of stress and to diet.

The viscosity behavior as measured here is in line with that of previous investigators, although the absolute viscosity values appear to be significantly lower than those reported from some other studies. Dintenfass (1) reported the average viscosity at 1 sec^{-1} for normal males as ranging from 27 to 82 CP, with an average of 45. In the present study, EDTA blood at 1.3 sec^{-1} had an average viscosity of only 12.5 CP. In a more recent study of 100 healthy males ages 45-55, Dintenfass had an EDTA blood viscosity range of 21 to 37 CP for one standard deviation (9). Part of this difference may be due to age, but it is not likely to completely explain the result. Although previous studies on fresh blood using individual samples have been reported, no comparable studies of the type reported here have been made.

It is also apparent that significant changes in viscosity of fresh blood take place almost immediately after drawing of the sample. In most literature it is assumed that clotting is initiated after several minutes and that the viscosity, if measured within a time period of several minutes, would be indicative of fresh blood viscosity (2). Indeed, this is the basis of prior measurements of fresh blood viscosity. The present results show that significant changes in viscosity take place only one minute after venipuncture.

The difference in the viscosity-hematocrit behavior of fresh vs. anticoagulated blood shows that interactions between red cells and other factors determining fresh blood viscosity are significantly different in these two cases. The fresh blood appears to be significantly more sensitive to hematocrit variation, which may be related to differences in the chemistry of anticoagulated vs. fresh blood. In normal blood containing free calcium and other ions, the intercellular interactions are strongly influenced by the surface charge of the red cell due to the ionic double layer surrounding the cell. This surface charge behavior might be significantly changed due to

Vol. 17
1980

TABLE 2

TEMPORAL DEPENDENCE OF FRESH AND EDTA ANTICOAGULATED BLOOD VISCOSITY

Pairs		Paired t	D.F.	Normal t (95%)	Significance Level (%)
A. Shear rate = 1.3 sec^{-1}					
Fresh vs. EDTA, all samples		1.2192	53	2.007	78
Fresh:	First vs. Second days	0.2283	10	2.228	15
	Second vs. Third days	1.3266	17	2.110	79
	First vs. Third days	0.3801	14	2.145	25
EDTA:	First vs. Second days	0.9994	17	2.110	69
	Second vs. Third days	2.4012	20	2.086	97
	First vs. Third days	1.5602	17	2.110	84
HCT:	First vs. Second days	0.7154	16	2.120	51
	Second vs. Third days	1.6003	20	2.086	87
	First vs. Third days	0	18	2.101	0
Fresh vs. EDTA:	First days	0.9510	15	2.131	67
	Second days	0.6182	18	2.101	45
	Third days	0.4761	18	2.101	36
B. Shear rate = 0.5 sec^{-1}					
Fresh vs. EDTA, all samples		2.005	56	2.003	95
Fresh:	First vs. Second days	0.3133	17	2.110	16
	Second vs. Third days	0.4970	17	2.110	33
	First vs. Third days	0.5778	16	2.120	43
EDTA:	First vs. Second days	0.0560	17	2.110	10
	Second vs. Third days	1.9318	20	2.086	93
	First vs. Third days	2.4195	17	2.110	97
Fresh vs. EDTA:	First days	1.6376	17	2.110	87
	Second days	1.4372	19	2.093	82
	Third days	0.2563	18	2.101	20

chelation of the calcium ions by EDTA. There appears to be a fortuitous relationship in that at the average hematocrit of 45, the effect of EDTA appears to be minimal with much greater effect at lower and higher hematocrits. The importance of recognizing this factor when interpreting the viscosity behavior of abnormal blood samples is obvious. Also, the fresh blood viscosity shows less variation over time than the EDTA samples of the same blood, implying that EDTA may interfere with some mechanism tending to maintain constant viscosity.

Limited data on patients suffering from various cerebrovascular diseases indicate that the viscosity values are significantly elevated relative to what would be expected of the normal range at the given hematocrit. Of the 16 samples tested, 4 were outside the normal 95% confidence limits, whereas on statistical grounds only one would be expected to be. Furthermore, they were all elevated. Also, almost all the samples that were within the normal 95% band were above the best line, indicating that the results were skewed

towards higher values. Interestingly, three of the four sickle cell samples were within the normal band, although the samples had abnormally low hematocrits. These results would confirm data of previous investigators (10, 11) that there are significant viscosity changes in the case of vascular disease.

ACKNOWLEDGEMENTS

We thank Dr. A.L. Copley for his valuable advice during the course of this research. Supported by NIH Grant HL 17408.

Address correspondence and reprint requests to M. Litt.

REFERENCES

1. DINTENFASS, LEOPOLD. Blood Microrheology: Viscosity Factors in Blood Flow, Ischemia & Thrombosis. New York: Appleton Century-Crofts, 1971.

2. DINTENFASS, L. An application of a cone in cone viscometer to the study of viscosity, thixotropy and clotting of whole blood. Biorheology 1, 91, 1963.

3. MAYER, G. A. and KISS, O. Blood viscosity and in vitro anticoagulants. Am. J. Physiol. 208, 795, 1965.

4. MERRILL, E. W.; COKELET, G. R.; GILLILAND, E. R.; SHIN, H.; BRITTEN, A. and WELLS, R. E., JR. Rheology of human blood near and at zero flow. Biophys. J. 3, 199, 1963.

5. PIROFSKY, B. The determination of blood viscosity in man by a method based on Poiseuille's Law. J. Clin. Inv. 32, 292-298, 1953.

6. VAN WAZER, J. R.; LYONS, J. W.; KIM, K. Y. and COLWELL, R. E. Viscosity and Flow Measurement -- A Laboratory Handbook of Rheology. New York: Interscience 1963, p. 189.

7. DOWNS, A. The Day to Day Variation of Blood Viscosity in Healthy Human Subjects. M.S.E. thesis in Chemical Engineering, University of Pennsylvania, 1977.

8. KRON, R. E. 1974 U.S. Patent No. 3,720,097. A diagnostic apparatus and method to measure the viscosity of fresh mammalian blood.

9. DINTENFASS, L. Blood viscosity in healthy men, measured in rhombospheroid viscometer on EDTA blood: a comparison with the cone-in-cone viscometer data and those of Copley. Biorheology 11, 397, 1974.

10. SWANK, R. L. Blood viscosity in cerebrovascular disease. Neurol. 9, 553-560, 1959.

11. CHIEN, S.; USAMI, S.; JAN, K. M.; SMITH, J. A. and BERTES, John F., Blood rheology in sickle cell disease. Proceedings of the Symposium on Molecular and Cellular Aspects of Sickle Cell Disease, DHEW Publ. No. (NIH) 76-1007, 1976, p. 277.

Vol. 17
1980

BLANK
PAGE

Vol.
198

BIORHEOLOGY Vol.17, p.37 0006-355X/80/010037-01$02.00/0
© Pergamon Press Ltd. 1980. Printed in the United States

Vol. 17
1980

THIRD INTERNATIONAL CONGRESS OF BIORHEOLOGY

SYMPOSIUM ON SOFT TISSUES AROUND A DIARTHRODIAL JOINT

INTRODUCTION

This three hour symposium was presented during the 3rd International Congress of Biorheology in La Jolla, California U.S.A. on August 28, 1978. The purpose was to demonstrate the complexity of joint tissue structure and function, and to illustrate the need for a multidisciplinary approach in the study of joint rheology.

The invited lecturers included Dr. Eric Baer on "The Multicomposite Structure of Tendon Collagen - Relationship between Ultrastructure and Mechanical Properties", Dr. Paul D. Benya (on behalf of Dr. Marcel E. Nimni) on "Collagen: Its Structure and Function in Normal and Pathological Connective Tissues", Dr. Van C. Mow on "Biphasic Rheological Analyses of Cartilage Creep and Stress Relaxation", Dr. Allan S. Hoffman on "Application of Enzyme Probes in Connective Tissue Biomechanics", and Dr. Wayne H. Akeson on "Mechanical Imperatives for Synovial Joint Homeostasis: The Present Potential and Therapeutic Manipulation". I, as Chairman, also gave a short introduction on "Biorheology of Soft Tissues: The Need for Interdisciplinary Studies".

With Dr. A.L. Copley, the Editor-in-Chief's kind invitation, and with the urging of Professor Y.C. Fung, the Congress Chairman, I proceeded to solicit opinions from the lecturers about writing their lectures. All the invited lecturers graciously consented, and thus it became possible to present the aforementioned symposium in manuscript form. The minor changes in authorships and titles of present manuscripts as compared to those abstracts published in the Congress Proceedings are a reflection of more current contents which have been added since the Congress.

I am honored and privileged to organize this symposium and to serve as a guest editor for four of the articles. Special thanks are to be given to all the authors for their fine contributions and cooperation. I also wish to thank Dr. Copley for editing the remaining two articles.

Savio L-Y. Woo, Ph.D.
Guest Editor

BLANK
PAGE

Vol.
198

BIORHEOLOGY Vol.17, pp. 39-43 0006-355X/80/010039-05$02.00/0
© Pergamon Press Ltd. 1980. Printed in the United States

Vol. 17
1980

THIRD INTERNATIONAL CONGRESS OF BIORHEOLOGY

SYMPOSIUM ON SOFT TISSUES AROUND A DIARTHRODIAL JOINT

BIORHEOLOGY OF SOFT TISSUES: THE NEED FOR INTERDISCIPLINARY STUDIES

Savio L-Y. Woo

Division of Orthopedics and Rehabilitation
University of California, San Diego
La Jolla, California 92093 U.S.A.

(Received 1.11.1979. Guest Editor's Contribution Invited by Editor-in-Chief A.L. Copley)

The diarthrodial joints in the human body consist of bones and specialized soft connective tissues, each performing complex functions. For example, the articular cartilage in synovial joints must sustain high loads on the order of magnitude of several times body weight, and yet it must provide the very low coefficient of friction during joint motion. The ligaments and tendons around these joints must support the joint's stability and absorb rapid and high loads. Yet, these soft tissues must not limit joint mobility in functional axes. Naturally, the understanding of the mechanical function of these joint components, their homeostatic responses, their physiology, and ability to repair, are necessary prerequisites for the knowledge of joint function.

The purpose of this symposium is to demonstrate the importance and the need for multidisciplinary approach in the understanding of joint function. Fung (1,2) described the major features of the complex rheological behavior of soft tissues such as lung, heart, urethra, and blood vessels, etc. by showing all these living tissues are composite materials. Different components of the tissue will take up loads at different stress levels. The loading and unloading of soft tissues follow different and nonlinear paths. The tissues are anisotropic and possess time dependent viscoelastic properties. Furthermore, soft tissues have no natural state, i.e., the state a material remembers and always returns to when all external loads are removed, to serve as a unique reference for stress and strain measures. The soft tissues around the joints also possess these aforementioned special rheological features. In addition, effects of aging, physiological wear and tear, and the complex repair process of these biological materials are also of major concern to clinicians and surgeons. Articular cartilage, for example, is avascular and aneural and has little or no ability to repair itself, and yet it must survive for a life time. The healing of a lacerated digital flexor tendon not only involves the strength of repair, but also its gliding function with peritendinous sheath.

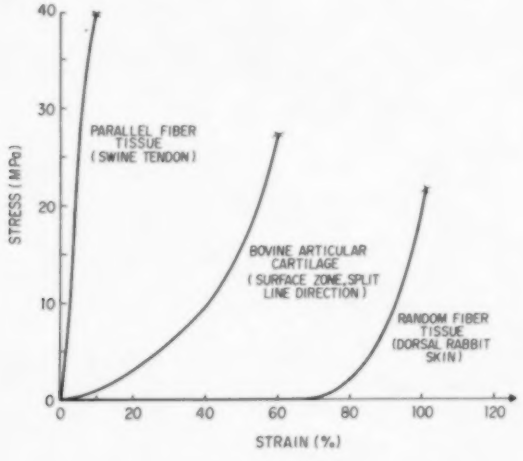

FIG. 1
Mechanical properties of various soft tissues. This diagram demonstrates the effects of fiber orientation on the tensile properties. Note that once the fibers are aligned, the slope of the stress-strain curves becomes similar for all tissues.

Current literature has documented general biomechanical behaviors of soft tissues under uniaxial tension. The stress-strain relationship is nonlinear with the slope increases with stress. Physical interpretation of this nonlinear behavior is that of recruitment of collagen fibers, followed by straightening and elongation of collagen fibers during tensile stretch (3). Thus, the organization of collagen fibers in the soft tissues will significantly alter the biomechanical response (3,4). Figure 1 shows data obtained in the author's laboratory where a wide range of tensile properties between tendon, articular cartilage, and skin was found. Tendon is a parallel-fibered tissue, and therefore, needs minimal recruitment before the fibers are elongated in tensile test as observed by Viidik and Ekholm (5) using polarized light. On the other hand, the skin consists of more randomly oriented fibers and a significant amount of recruitment and straightening of the wavy pattern is required before elongation of fibers. A simple model for such tissue was illustrated by Bull (6). When nylon threads are made into nylon fabric, the stress-strain behavior will have a much lower stiffness at low stress levels until the fibers are aligned into the loading direction.

It is clear that a close relationship exists between the mechanical properties and the structural organization of collagen fibers. Diamant, et al (7), using rat tail tendon as an experimental model, found that the collagen fibers in these tendons have a wavy appearance called "crimp" during the unstressed state. When a small stress is applied, the crimp gradually disappears. This portion of the stress-strain curve is characterized by a small change in the slope, called "toe region". Once the crimps disappeared, the slope of the stress-strain curve increased significantly. The crimping of fiber was modeled as a flexible hinge with interconnecting springs with the springs acting as the force to restore the crimp of fibers upon unloading.

Dr. Eric Baer, an invited lecturer of this symposium, presented a new morphological model for the previous crimp model (7). The first substructures of the mature rat tail tendon are 80 to 320 μm in diameter, and are called fascicles. Using a new methodology whereby the native water is replaced with liquids of refractive index near to that of collagen to eliminate light diffusion, Baer's group was able to observe the substructure of the fascicles. It was found that each fascicle consisted of a cylindrical array of plannar zig-zag crimped, 500 to 5,000 Å diameter collagen fibrils. The crimps of the collagen fibrils are predominantly sharp, rather than sinusoidal in appearance. With such clear understanding of the ultrastructural tendon hierarchy, Betsch and Baer (8) described the detailed tensile behavior of the rat tail tendon. Such correlative description between the ultrastructure and mechanical properties provided more valid and detailed information over previous models (3,7).

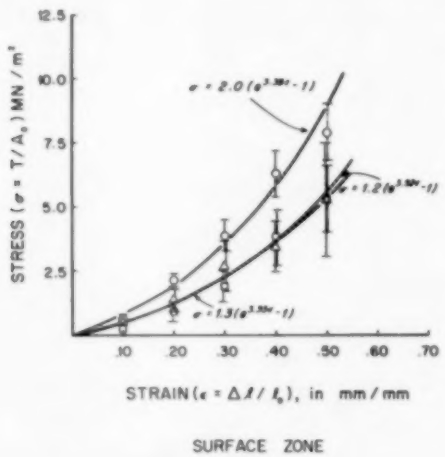

FIG. 2
Comparison of the directional properties of articular cartilage specimens taken from the surface zone. Note that circular, triangular and square symbols represent 0^{o} (split line direction), 45^{o} and 90^{o} specimens, respectively.

The tissues with more randomly oriented fibers have greater complexity with respect to morphological appearance and mechanical properties such as articular cartilage and skin. For example, using scanning electron microscopy, articular cartilage can be grossly divided into three zones, i.e., superficial, middle and deep zones. The superficial zone is composed of densely packed sheets or bundles of collagen fibers oriented predominantly in a

specific direction called "split line". In the middle zone the fibers are more randomly oriented, and in the deep zone the fibers are generally larger and are anchored radially into the subchondral bone (9,10). The tensile properties of articular cartilage have been studied following such morphological description (11,12,13). Figure 2 shows the distinct directional properties of articular cartilage taken from the surface zone. The specimen along the split line direction (0^{o}) is significantly stiffer than that taken 45^{o} and 90^{o} from the split line directions (12).

In addition to the ultrastructure, the biochemical composition of tissue also modifies its mechanical behavior. For example, the flexor tendons have significantly higher stiffness and strength than the extensor tendons from the same digits. (See Figure 3). Correspondingly, the biochemical composition also showed higher collagen concentration for the flexors (784 ± 4 mg/gm of fat free dry weight for flexor tendons as compared to 765 ± 6 mg/gm for the extensor tendons, $p<0.05$).

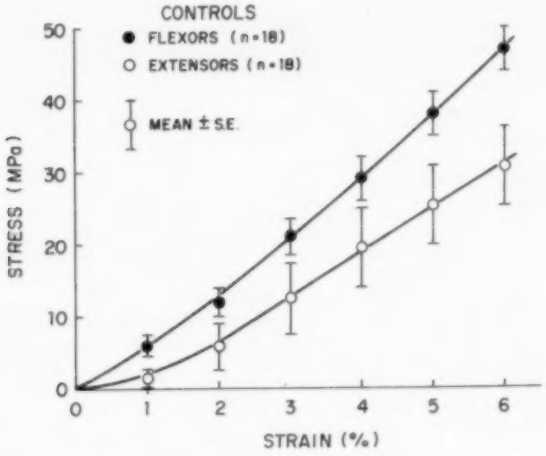

FIG. 3
Comparison of the tensile properties of the digital flexor and extensor tendons of the Yucatan swine*.

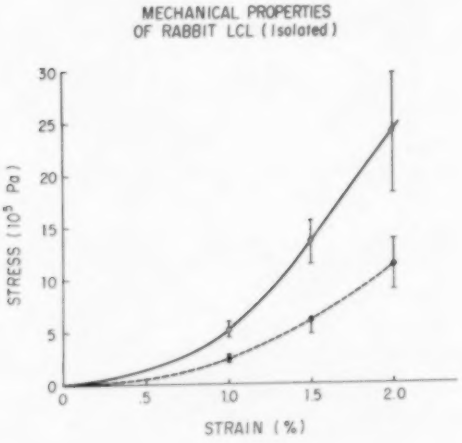

FIG. 4
Comparison of the tensile properties of the lateral-collateral ligaments obtained from control and 9-week immobilized rabbit knees. Open circles are from control specimens and closed circles are from experimental specimens (n=6).

*Obtained from the Kroc Foundation, Santa Ynez, California 93160.

Vol. 17
1980

The changes in tissue behavior secondary to immobilization and exercise can be best understood if biochemical constituent changes are known. Akeson, et al (14) demonstrated that immobilization of the knee joint of rabbits for a 9-week period resulted in an average of 30% decrease of glycosaminoglycans in the periarticular connective tissues. There was, however, no significant decrease in collagen concentration. The joint stiffness increased significantly, probably due to loss of tissue gliding function and increase in collagen cross-linking (15,16). The mechanical properties of individual tissue, such as the lateral-collateral ligament, appeared to be compromised following immobilization. (See Figure 4). On the other hand, exercise has positive effects on soft tissue homeostasis as reflected by strength characteristics. After 12 months of moderate exercise training, the digital extensor tendons of the swine showed a significant increase in size, as well as in mechanical properties (17). The biochemical analysis also shows the collagen concentration for these extensors was significantly increased (787 ± 4 mg/gm of fat free dry tissue for the exercised versus 765 ± 6 mg/gm of fat free dry tissue, $p<0.001$).

The preceding few examples are offered as a general overview for the purpose of illustrating the interrelationship of morphology, biochemistry and biorheology of soft tissues around diarthrodial joints. The following five symposium articles, which are the contribution of a group of distinguished investigators with widely different, but relevant backgrounds, will discuss this subject matter more thoroughly from the microscopic level to the entire joint composite. The relationship between morphological structure and mechanical properties will be described by macromolecular scientists using rat tail tendon as a model. The biomechanical and biochemical correlates of collagen at a molecular level will be discussed by a biochemist. The alteration of tissue biomechanical properties using enzyme to effect specific individual components of the soft tissues will be presented by a chemical engineer. The multiphasic behavior of articular cartilage and its relationship to joint function will be described by bioengineers using modern and advanced theories and confirmatory experiments. And finally, the biological and biomechanical changes of a synovial joint following prolonged immobilization will be discussed by a multidisciplinary group of inevestigators headed by a clinical scientist. It is hoped that as a result of this series of symposium articles, the need for multidisciplinary group approach to better understanding of the soft tissue behavior and its relationship to synovial joint function is reinforced and encouraged. It is only with rigorous collaborative efforts that mechanisms related to pathological joint diseases can be understood. Ultimately, the acquired knowledge and information can be given to clinical scientists and physicians for the prevention or therapeutic manipulation of diarthrodial joint diseases.

ACKNOWLEDGMENTS

Support from NIH Grants AM14918, GM24900 and AM00304 is gratefully acknowledged.

REFERENCES

1. FUNG, Y.C.B. Elasticity of soft tissues in simple elongation. Amer. J. of Physiology. Vol. 213, No. 6, 1532-1544, 1967.

2. FUNG, Y.C.B. Biorheology of soft tissues. Biorheology, Vol. 10, 139-155, 1973.

3. FRESEN, M., MAGI, M., SONNERUP, L., VIIDIK, A. Rheological analyses of soft collagenous tissue - I. Theoretical considerations. J. of Biomechanics, Vol. 2, 13-20, 1969.

4. VIIDIK, A. On the correlation between structure and mechanical function of soft connective tissues. Verh. Anat. Ges. 72.5. 75-89, 1978.

5. VIIDIK, A. EKHOLM, R. Light and electromicroscopic studies of collagen fibers under strain. Z A.anat.Entwickl.-Gesch., Vol. 127, 154-164, 1968.

6. BULL, H.B. Protein structure and elasticity. In: Tissue Elasticity. J.W. Remington (Ed.), Amer. Physiol. Society, Washington. 1957, pp. 32-42.

7. DIAMANT, J., KELLER, A., BAER, E., LITT, M. and ARRIDGE, R.G.C. Collagen: Ultrastructure and its relation to mechanical properties as a function of aging. Proc. Royal Society of London. B, Vol. 180, 293-315, 1972.

8. BETSCH, D.F. and BAER, E. Structure and mechanical properties of rat tail tendon. Biorheology, Vol. 17, 1980.

9. CLARKE, I.C. Articular cartilage: A review and scanning electron microscope study - I. The interterritorial fibular architecture. J. Bone and Joint Surg., Vol. 53B, 732-750, 1971.

10. MOW, V.C., LAI, M.W. and REDLER, I. Some surface characteristics of articular cartilage. I. Scanning electron microscopy studies of the theoretical model for the dynamic interaction of synovial fluid and articular cartilage. J. of Biomechanics, Vol. 7, 449-456, 1974.

11. KEMPSON, G.E. The mechanical properties of articular cartilage. In: Articular Cartilage. M.A.R. Freeman (Ed.) Grune and Stratton, New York, pp. 171-227, 1973.

12. WOO, S. L-Y., AKESON, W.H., JEMMOTT, G.F. Measurements of nonhomogeneous directional mechanical properties of articular cartilage in tension. J. of Biomechanics, Vol. 9, 785-791, 1976.

13. WOO, S. L-Y., LUBOCK, P., GOMEZ, M.A., JEMMOTT, G.F., KUEI, S.C. and AKESON, W.H.: Large deformation nonhomogeneous directional properties of articular cartilage in uniaxial tension. J. of Biomechanics, Vol. 12, 437-446, 1979.

14. AKESON, W.H., WOO, S. L-Y., AMIEL, D., COUTTS, R.D., DANIEL, D. The connective tissue response to immobility: Biochemical changes in periarticular connective tissues of the immobilized rabbit knee. Clin. Orthop. and Rel. Res., Vol. 93, 356, 1973.

15. WOO, S. L-Y., MATTHEWS, J.V., AKESON, W.H., AMIEL, D. and CONVERY, F.R. Connective tissue response to immobility: Correlative studies of biomechanical and biochemical measurements of normal and immobilized rabbit knee. Arthritis and Rheumatism, Vol. 18, No. 3, 257-264, 1975.

16. AKESON, W.H., AMIEL, D., MECHANIC, G.L., WOO, S. L-Y., HARWOOD, F.L. and HAMER, M.D. Collagen cross-linking alterations in joint contractures: Changes in the reducible cross-links in periarticular connective tissue collagen after nine weeks of immobilization. Conn. Tissue Res., Vol. 5, 15-19, 1977.

17. WOO, S. L-Y., RITTER, M.A., AMIEL, D., SANDERS, T.M., GOMEZ, M.A., KUEI, S.C., GARFIN, S.R. and AKESON, W.H. The biomechanical and biochemical properties of swine tendon - long term effects of exercise on the digital extensors. To appear in Connective Tissue Research, 1980.

Vol. 17
1980

BLANK
PAGE

Vol.
198

BIORHEOLOGY Vol 17, pp. 45-50 0006-355X/80/010045-06$02.00/0
© Pergamon Press Ltd. 1980. Printed in the United States

Vol. 17
1980

THIRD INTERNATIONAL CONGRESS OF BIORHEOLOGY

SYMPOSIUM ON SOFT TISSUES AROUND A DIARTHRODIAL JOINT

COMPARISON OF ENZYME PROBE TECHNIQUES USED TO INVESTIGATE TISSUE BIOMECHANICS IN VITRO

Allan S. Hoffman
Center for Bioengineering
University of Washington
Seattle, Washington 98195

(Received 1.11.1979. Accepted by Guest Editor S. Woo)

ABSTRACT

Enzymes are widely used to remove selectively various stress bearing components of connective tissues before, during or after application of stress. This paper surveys and critically reviews these techniques.

INTRODUCTION

Soft tissues, such as ligament, tendon, skin and blood vessels contain the three following major components which are pertinent to their mechanical behavior: (A) collagen, a stiff, fibrous protein, (B) elastin, a soft, rubber-like fibrous protein, (C) glycosaminoglycans (GAG) which form, along with relatively large amounts of water, the soft, hydrogel material called "ground substance" which fills in the matrix between the fibers and cells. Some GAG molecules probably associate with the collagen and elastic fibers at the interface of these fibers with the matrix (1).

Other minor components of soft tissues may include: (D) microfibrillar protein, MFP (e.g., the sheath material at the interface between elastin and the GAG matrix (2)), (E) muscle cells (present in significant amounts in muscular artery only), (F) lipids and lipoproteins (e.g., as lipid deposits in the arterial wall), (G) mineral deposits (e.g., in the arterial wall) and (H) fibroblasts.

If soft tissues are viewed in this way as composite materials, then one must recognize that their mechanical behavior is optimized in nature by an effective sharing of stress between the different phases. Several excellent reviews of the mechanics of soft tissues have been published (3,4,5).

A number of techniques have been developed to remove various components of tissues, such that the biomechanical properties may be measured before and after treatment, with any changes being ascribed to the missing component(s). These methods include, for example, the use of warm formic acid (6), warm 0.1N NaOH (7) or autoclaving (8) to remove collagen and GAG and thus to isolate elastin. Guanadine hydrochloride has been used to remove the microfibrillar protein of the elastic fiber (9). Acetone has been used to de-fat the whole tissue (10,11).

Most of these techniques are crude, relatively non-selective and can be potentially "damaging" to the structure and composition of the remaining tissue, especially if biomechanical measurements are to be made. The use of enzymes, as proteases or polysaccharidases, both selective and general, is a much more satisfactory technique for removing individual components or classes of components in tissues (e.g., 10, 12-32). This article gives a summary of the general methodologies which utilize enzyme probes in soft tissue biomechanics.

BIOMECHANICAL TESTING AND THE USE OF ENZYME PROBES

There are a number of important experimental considerations involved in biomechanical testing in general and in particular with the use of enzyme probes. Many of these are listed in Table 1.

The animal source and its history of diet, drugs, etc. plus its general state of health and the method of sacrifice may all be important factors. Washing, storage and cutting of the specimen may contribute in different ways to the subsequent biomechanical behavior. For example, the question of specimen orientation is quite critical, and it is well known that the arrangement of the collagen and elastic fiber networks differ from one tissue to another or within one tissue from point to point, as the biomechanical

enviroments and requirements differ. Ligament and tendon are mainly stressed longitudinally and their axial fibrous orientations reflect this. Specimens should be cut along and across this fiber axis for testing. Aorta is mainly stressed circumferentially, although in vivo longitudinal forces should not be overlooked (33-35). Arteries and skin are subject to biaxial stress in vivo. Biaxial tests may show effects which are not revealed by the simple uniaxial tests (36).

TABLE I

Biomechanical Testing and the Use of Enzyme Probes: Some Important Experimental Considerations

1) History of tissue source
2) Sample preparation and characterization
3) Sample storage conditions
4) Randomization of samples and test procedures
5) Biomechanical preconditioning
6) Calculation and homogeneity of sample "stress" or "strain"
7) Effects of stress or strain levels on biomechanics
8) Test rates and dynamic, static, or failure testing
9) Enzyme source and protocols
10) Statistical significance of data

Specimens should be carefully measured and representative sections removed at various points for assaying the composition and water contents; both dimensions and composition can vary significantly in any one tissue.

Test specimens may be stored in buffered saline plus a bacteriostat (e.g., NaN_3) in the refrigerator, but they will still "age" under those conditions. Such aging can cause an initial stiffening of the specimen. Different components may age at different rates, and, as noted above, it is well known that the collagen and elastin contents in the aorta change distally along this artery (12).

In addition, connective tissues do not often display linear viscoelasticity and their responses may be stress (or strain) as well as time dependent. Thus, one must take care to randomize not only the selection of test specimens from storage but also the order of test conditions.

There are two basic types of static mechanical testing: stress-strain, where a specimen is strained at a constant rate, and stress relaxation (or creep), where the specimen is fixed at a constant strain (or load) level and the time course of load relaxation (or length extension) is measured. Both of these techniques have been applied to biological tissues, from several types of animals as well as humans. The stress relaxation technique is preferred, since it may permit a more fundamental analysis of the mechanism of viscoelasticity in the relaxing specimen (37). Irreversible testing (i.e., to rupture) seldom yields reproducible, comparative biomechanical data, and despite the relative ease of this test technique, it is not generally recommended.

It is important to try to define clearly the in vitro strain level, in hopes of relating in vitro data to the in vivo condition. This question has rarely even been mentioned in the literature; we have recently considered it in detail for canine artery(38). Since enzymolysis or autoclaving may change the specimen length (e.g., elongate or shrink the specimen) it is important to compare specimens at equivalent "states of strain" based on the length of the untreated, unstressed specimen (38, 39). It is also difficult to define the true stress on a specimen due to the lack of knowledge of the actual cross-section of the components being stressed.

There are three possible regions of strain which may be observed in testing biological tissues: 1) an initial region during which any "slack" in the specimen is taken up, including both gross slack due to the specimen being held loosely in the grips and slack due to loose fibers not yet participating in stress bearing; 2)an intermediate region which may be most representative of the reversible biomechanical functioning of the tissue in vivo; and 3) a final region in which there can be irreversible damage done to the tissue as it approaches rupture.

Fung (40-42) has also emphasized the need to "pre-condition" specimens by straining them one or more times into region II before testing them. It has been noted by Daly et al (43), however, that this pre-conditioning effect can be demonstrated in vivo (in the periodontal ligament in this case) followed by a rapid recovery from the effects of several loading cycles,again in vivo. These results imply that connective tissue which

is subject to random loads can exhibit properties which vary as a function of this loading history. This effect is additional to the normal, expected viscoelastic responses of the specimen. Furthermore, it must be acknowledged that the total time sequence between excision, storage, pre-conditioning and testing will have a complex influence on the test results. When the pre-conditioning step is restricted in the region of strains where total reversibility is retained (region II above), then it may also be used to "pre-characterize" the specimens before enzymolysis for comparison with the same specimens after enzymolysis (21, 22).

When enzyme probes are used, the source, purity (specificity) and specific activity of each particular enzyme can all critically influence the validity of comparisons between results with different specimens. A particular enzyme to substrate ratio should be selected, and for this, one must assay the enzyme activity as well as estimate the concentration of the specific tissue component in each test specimen. A low enzyme to substrate ratio (e.g., 0.05 to 0.1) is recommended in order to minimize the effects of non-specific, enzymatic impurities. Inhibitors (e.g., soybean trypsin inhibitor and and N-ethyl maleimide) may also be added to the enzyme preparation. Table II summarizes some of the enzyme protocols which we have used.

It may be concluded that it is a significant experimental challenge to obtain comparable and meaningful biomechanical test data on soft connective tissues, especially when using enzyme probes.

GENERAL TECHNIQUES FOR USE OF ENZYME PROBES (TABLE III)

There are three general protocols for using enzyme probes in biomechanics studies:

1) Enzymolysis is accomplished before mechanical testing. This has been the most commonly used technique.

2) Enzymolysis occurs during mechanical testing, with the specimen immersed in the enzyme bath at the start of testing. The simultaneous processes of diffusion of the enzyme into the specimen and the viscoelastic response of the specimen, complicate interpretation of data from this technique.

3) Enzymolysis occurs during mechanical testing of specimens which have been pre-saturated with enzyme before the start of testing. Conditions of pH and/or temperature may be adjusted so that minimal enzymolysis occurs during the pre-saturation step. Then the enzyme is activated by bringing the Ph to the optimum level (for the particular enzyme concerned) and raising the temperature to 37°C. This newer technique permits analysis of viscoelastic processes due to removal of specific components (24, 25).

Variations within such protocols include mechanical testing after different times of enzymolysis or using different enzymes on the same specimen, either together or in a sequence of tests. The progress of enzymolysis may be followed by (1) assaying the supernatant for enzymolysed fragments (e.g., for hydroxyproline with collagenase or for amino acids with elastase); (2) assaying the remaining tissue for the component being removed, using either biochemical or gravimetric techniques; (3) observing the specimen at various depths using histological slides, or scanning or transmission electron miscroscopy. These visual observations may also help one to formulate a physical model of the tissue and its biomechanical response.

CONCLUSIONS

The use of enzymes to probe the contributions of individual components to the biomechanics of soft connective tissues is increasing along with the increasing availability of more and purer enzymes. A number of factors important to this experimental approach have been discussed in this article.

Vol. 17
1980

TABLE II

Examples of Enzyme Protocols

Enzyme (Source)	Type	Substrate Site	Optimum pH and Buffer Used*	Specific Enzyme Inhibitors	Use Inhibitor With:
Elastase Swine Pancreas (Worthington)	Endopeptidase	O ‖ -C-CH- | R (R-Aliphatic Hydrocarbon)	pH=8.8 0.01% NaN_3	D.F.P. (Diisopropyl fluoro phosphate)	Collagenase Solutions
Collagenase Clostridia Histolyticum (Worthington)	Endopeptidase	-P-X-Gly-P-Y (P-Pro or Hypro)	pH=7.4 0.001M $CaCl_2$ 0.01% NaN_3	EDTA N-Ethyl Maleimide**	Elastase Solutions
Trypsin Bovine Pancreas (Worthington)	Endopeptidase	Lys, Arg	pH=7.8 0.01M $CaCl_2$ 0.01% NaN_3	Soybean Trypsin Inhibitor -- D.F.P.	Elastase or Collagenase Solutions -- Collagenase Solutions
Hyaluronidase Bovine Testes (Worthington)	Endomucopoly-saccharidase		0.75M NaCl pH=4.8 0.01% NaN_3		
β-Glucuronidase Beef Liver (Worthington)	Exomucopoly-saccharidase		0.75M NaCl pH-4.8 0.01% NaN_3		

* NaN_3 is a bacteriostat
** Inhibits sulfhydryl protease impurities

TABLE III

Enzyme Probes in Biomechanics: General Protocols

1. Wash, cut, store specimens
2. Characterize each sample (e.g., dimensions; water, collagen, elastin contents)
3. Precondition samples biomechanically
4. Assay enzyme-solvent system
5. Treat parallel samples in solvent or enzyme-solvent solutions:

   A. Before biomechanical testing; test after different times of enzymolysis

   B. During biomechanical testing, but before specimen is saturated with enzyme

   C. During biomechanical testing, but only after specimen is saturated with enzyme

6. Assay supernatant solutions and/or samples for extent of enzymolysis
7. Repeat 5 and 6 on any one specimen, using a sequence of different enzymes
8. Observe samples (e.g., histology; SEM, TEM)
9. Analyse data; model the biomechanical behavior

REFERENCES

1. WIGHT, T.N. and ROSS, R. Proteoglycans in Primate Arteries - I. Ultrastructure Localization and Distribution in the Intima. J. Cell Biology 67:660, 1975).

2. ROSS, R. and BORNSTEIN, P. Elastic Fibers in the Body. Sci. Amer. 224(6):43, 1971.

3. MILLINGTON, P. F., GIBSON, T., EVANS, J. H. and BARBENEL, J. C. Structural and Mechanical aspects of Connective Tissue. In: Adv. in Biomed. Eng. I. R. M. Kenedi (Ed). London: Academic Press, 1971, p. 189.

4. VIIDIK, A. Functional Properties of Collagenous Tissues. Intern'l Rev. Conn. Tissue Res. 6:127, 1973.

5. DOBRIN, P. B. Mechanical Properties of Arteries. Physiol. Revs. 58:397, 1978.

6. HASS, G. M. Elastic Tissue. Arch. Path. (Chicago) 35:29, 1943.

7. LANSING, A.I. ROSENTHAL, T. B., ALEX, M. and DEMPSEY, E. W. Structure and Chemical Characterization of Elastic Fibers as Revealed by Elastase and Electron Microscopy. Anat. Rec. 114:555, 1952.

8. PARTRIDGE, S. M. Isolation and Characterization of Elastin. In: Chemistry and Molecular Biology of the Intercellular Matrix. E. A. Balasz (Ed). Academic Press 1970, p. 593.

9. ROSS, R. and BORNSTEIN, P. The Elastic Fiber - I. The Separation and Partial Characterization of Its Macromolecular Components. J. Cell. Biol. 40:366, 1969.

10. WOOD, G. C. Some Tensile Properties of Elastic Tissue. Biochim. Biophys. Acta 15:311, 1954.

11. LAKE, L. W. and ARMENIADES, C. D. Structure-Property Relations of Aortic Tissue. Trans. Amer. Soc. Artif. Intern. Organs 18:202, 1972.

12. HARKNESS, M. L. and HARKNESS, R. D. Effect of Enzymes on Mechanical Properties of Tissues. Nature 183:1821, 1959.

13. ROBERT, B. and ROBERT, L. Studies on the Structure of Elastin and the Mechanism of Action of Elastolytic Enzymes. In: Chemistry and Molecular Biology of the Intercellular Matrix. E. A. Balasz (Ed). Academic Press, 1970.

14. HALL, D. A. and CZERKAWSKI, J.W. The Reaction between Elastase and Elastic Tissue. Biochem. J. 80:134, 1961.

15. COULSON, W. F. and LINKER, A. Cardiovascular Studies of the Copper-Deficient Swine, XI Mucopolysaccharides and the Mechanical Properties of the Aorta. Biochem. Biophys. Acta 158:117, 1968.

16. TURINO, G. M., LOURENCO, R. V. and MC CRACKEN, G. H. Role of Connective Tissues in Large Pulmonary Airways. J. Appl. Physiol. 25:645, 1968.

17. DALY, C. H. The Biomechanical Characteristics of Human Skin. Ph.D. Thesis, University of Strathclyde, Glasgow, Scotland, 1966.

18. DALY, C. H. The Role of Elastin in the Mechanical Behavior of Human Skin. Paper #18-7 Proc. of 8th ICEMB, Chicago, p. 18, 1969.

19. COULSON, W. F. The Effect of Proteolytic Enzymes on the Tensile Strength of Whole Aorta and Isolated Aortic Elastin. Biochim, Biopys. Acta 237:378, 1971.

20. HOFFMAN, A. S., PARK, J. B. and ABRAHAMSON, J. Sequential Enzymolysis of Ligament and Resultant Stress-Strain Behavior. Biomat., Med. Dev., Art. Org. 1:453, 1973.

21. HOFFMAN, A. S., GRANDE, L. A., GIBSON, P., PARK, J. B., DALY, C. H., BORNSTEIN, P. and ROSS, R. Contributions of Collagen, Elastin and GAG's to the Low Strain Behavior of Arterial Tissue. In: Perspectives in Biomedical Engineering. R. M. Kenedi (Ed) London: University Park Press, 1973, p. 173.

22. HOFFMAN, A. S. GRANDE, L. A. and PARK, J. B. Sequential Enzymolysis of Human Aorta and Resultant Stress-Strain Behavior. Biomat., Med. Dev., Art. Org. 5:121, 1977.

23. GIBSON, P. H. Mechanical Behavior of Bovine Ligamentum Nuchae Before, During and After Enzymolysis. M.S.E. Thesis, University of Washington, Seattle, Washington, 1973.

24. KOLP, J. J. A Study of the Stress Relaxation of Canine Aorta Using Enzymolysis Techniques. M.S.Ch.E. Thesis, University of Washington, Seattle, Washington, 1974.

25. PENROSE, R. T. An In Vivo-In Vitro Study of the Contribution of Elastin to the Biomechanics of the Aorta. M.S. Metall. Eng. Thesis, University of Washington, Seattle, Washington, 1974.

Vol. 17 1980

26. MINNS, R. J. and STEVEN, F. S. Scanning Electron Microscopy of Stretch Elastin Fibres. Micron 5:127, 1974.

27. MINNS, R. J., SODEN, P. D. and JACKSON, D. S. The Role of the Fibrous Components and Ground Substance in the Mechanical Properties of Biological Tissues. J. Biomech. 6:153, 1973.

28. MUKHERJEE, D. P., HOFFMAN, A. S. and FRANZBLAU, C. The Physical Properties and Molecular Structure of Ligamentum Nuchae Elastin. Biopolymers 13:2447, 1974.

29. YANNAS, I. V., BURKE, J. F., HUANG, C. and GORDON, P. L. Correlation of In Vivo Collagen Degradation Rate with In Vitro Measurements. J. Biomed. Mater. Res. 9:623, 1975.

30. HUANG, C. and YANNAS, I. V. Mechanochemical Studies of Enzymatic Degradation of Insoluble Collagen Fibers. J. Biomed. Mater. Res. Sympos. No. 8, p. 137, 1977.

31. DAMUDE, L. C., COPE, D. A. and ROACH, M. R. The Effects of Enzymatic Digestion on the Elastic Properties of Isolated Human Cerebral Arteries. Can. J. Physiol. Pharmacol. 55:161, 1977.

32. OAKES, B. W. and BIALKOWER, B. Biomechanical and Ultrastructural Studies on the Elastic Wing Tendon from the Domestic Fowl. J. Anat. 123:369, 1977.

33. BERGEL, D. H. The Static Elastic Properties of the Arterial Wall. J. Physiol. 156:445, 1961.

34. PATEL, D. J. and FRY, D. L. In Situ Pressure-Radius-Length Measurements in Ascending Aorta of Anesthetized Dogs. J. Appl. Physiol. 19:413, 1964.

35. PATEL, D. J. and FRY, D. L. Longitudinal Tethering of Arteries in Dogs. Circ. Res. 24:1, 1969.

36. LANIR, Y. and FUNG, Y. C. Two-dimensional Mechanical Properties of Rabbit Skin - II. Experimental Results. J. Biomechanics 7:171, 1974.

37. TOBOLSKY, A. V. Properties and Structure of Polymers. J. Wiley and Sons, N.Y. Chapters IV and V, 1962.

38. PARK, J. B., DALY, C. H. and HOFFMAN, A. S. Contribution of Collagen to the Mechanical Response of Canine Artery at Low Strains. Frontiers Matrix Biol. 3:318, 1976.

39. SODEN, P. D. and KERSHAW, I. Tensile Testing of Connective Tissues. Med. and Biol. Eng. 12:510, 1974.

40. FUNG, Y. C. Elasticity of Soft Tissue in Simple Elongation. Amer. J. Physiol. 213:1532, 1967.

41. FUNG, Y. C. Stress-Strain History Relations of Soft Tissues in Simple Elongation. In: Biomechanics: Its Foundations and Objectives. Fung, Y.C., D. Perone and M. Anlinker (Eds), New Jersey: Prentice-Hall, 1972, p. 181.

42. FUNG, Y. C. Biorheology of Soft Tissues. Biorheol. 10:138, 1973.

43. DALY, C. H., NICHOLLS, J. I., KYDD, W. L. AND NANSEN, P. D. The Response of the Human Periodontal Ligament to Torsional Loading - I. Experimental Methods. J. Biomechanics 7:517, 1974.

BIORHEOLOGY Vol.17, pp. 51-82 0006-355X/80/010051-32$02.00/0
© Pergamon Press Ltd. 1980. Printed in the United States

THIRD INTERNATIONAL CONGRESS OF BIORHEOLOGY

SYMPOSIUM ON SOFT TISSUES AROUND A DIARTHRODIAL JOINT

THE MOLECULAR ORGANIZATION OF COLLAGEN AND ITS ROLE IN DETERMINING THE BIOPHYSICAL PROPERTIES OF THE CONNECTIVE TISSUES

Marcel E. Nimni

Department of Orthopaedics, Medicine, and Biochemistry
University of Southern California and Orthopaedic Hospital
of Los Angeles, California 90007

(Received 9.11.1979. Accepted by Guest Editor S. Woo)

ABSTRACT

Crosslinking of collagen is a prerequisite for the collagen fibers to withstand the physical stresses to which they are exposed. Significant progress has been made in understanding the functional groups on the molecule which are involved in the formation of crosslinks. Chemical agents, in particular bifunctional aldehydes such as glutaraldehyde, have found applications in the area of bioprostheses. They increase the resistance of collagen to biological degradation while increasing its mechanical resistance and decreasing its immunogenicity. It is to be expected that our increasing understanding of the molecular structure of collagen will allow us to further modulate its process of biosynthesis and turnover as well as to benefit from the use of chemically modified collagen fibers in the development of novel bioprostheses.

Vol. 17
1980

INTRODUCTION

Collagen is the single most abundant animal protein. In mammals it accounts for about 30% of all proteins. The collagen molecules, after being secreted by the cells which synthesize it, assemble into a characteristic fiber organization and as such are responsible for the functional integrity of tissues such as bone, cartilage, skin and tendon, where they account for the overwhelming majority of the proteins present, and for the structural integrity of many other structures such as blood vessels and most organs, to which they contribute a framework within which the tissue functions. A variety of human conditions, normal and pathological, involve the ability of tissues to repair and regenerate this collagenous framework. Some are characterized by excessive deposition of collagen (liver cirrhosis, scleroderma, keloid, glomerular nephritis). Following trauma or surgery, abnormal deposition of collagen may impair function (adhesions following repair of long tendons, scar formation during healing, etc.). In addition, many disabling conditions result from changes in the nature and organization of collagen (heart-valve lesions, osteoarthritis, rheumatoid arthritis, and congenital collagen diseases such as Marfan's syndrome and Ehlers-Danlos syndrome, osteogenesis imperfecta, etc.).

How do the collagen molecules in cartilage differ from those in cornea, tendon, bone matrix, dermis, the parenchyma of organs, periodontal ligaments, and so many other locations within the organism? Why is cornea transparent, tendon tough and inelastic and able to sustain significant stresses, and cartilage so resilient and viscoelastic? What kind of uniqueness is there in their chemical structures to enable these tissues to perform such specific biological functions? What regulates fiber diameter, orientation, concentration of fibers in a particular volume of tissue, and packing of the fibers into larger bundles? How can we approach the problem of aging of connective tissues and changes related to pathology? Is it possible that mesenchymal cells that have acquired the ability to make a particular type of collagen can be influenced by environmental factors, and in so doing change the rate and nature of the particular collagen molecules that they are able to synthesize.

This paper will focus on various fundamental steps associated with the anabolism and catabolism of collagen. The functional aspects of tissues, especially as they relate to the structure of collagen and to the functional groups responsible for specific molecular interactions, as well as the unique types of collagen present in cartilage and basement membranes and some disease-associated changes will be discussed. The crosslinking of collagen plays a major role in the ability of the collagen fibers to withstand stress. Therefore the normal mechanism by which crosslinks are formed will be compared with the crosslinks that can be introduced by chemical agents such as glutaraldehyde, and which provide a useful means of stabilizing collagen fibers against biological degradation and immunological rejection.

THE COLLAGEN MOLECULE

The coil arrangement of the amino acids, which make up the collagen molecule, is shown schematically in Fig. 1. Every third residue is glycine. Proline and OH-proline follow each other relatively frequently, and the (gly, pro, hyp) sequence makes up about 10% of the molecule. The triple helical structure generates a symmetrical pattern of three left-handed helical chains, which are in turn slightly displaced to the right, superimposing an additional "supercoil" with a pitch of approximately 86 Å. The amino acids within each chain are displaced by a distance h = 2.91 Å, with a relative twist of -110°, making the number of residues per turn 3.27 and the distance between each third glycine 8.7 Å. The individual residues are nearly fully extended in the collagen structure, since the maximum value within the fully stretched chain would be approximately 3.6 Å. This separation is nevertheless such that it will not allow intrachain bonds to form (as does occur in the α helix), and only interchain hydrogen bonds are possible(1). The exact number of H bonds that stabilize the triple helical structure is not certain. The model that Ramachandran and Kartha described has two hydrogen bonds for every three amino acids, whereas the Rich and Crick versions assume one H bond for every three residues(2). More recent studies using synthetic polypeptides of the type (gly, pro, pro) and others have shed further light on the molecular structure of collagen (3-7).

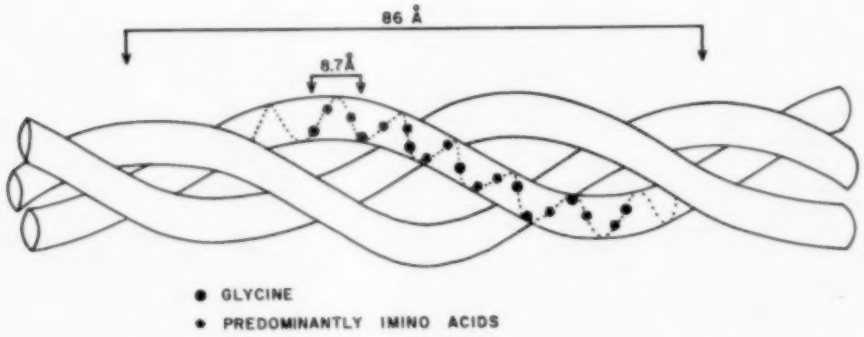

FIG. 1

Schematic drawing showing the collagen triple helix. The individual α chains are left-handed helices with approximately three residues per turn. The α chains are in turn coiled around each other following a right-handed twist. The hydrogen bonds (which are not shown) form between residues of the different chains (interpeptide hydrogen bonding).

In addition to these intramolecular conformational patterns there seems to exist a supermolecular coiling. Microfibrils, which could represent intermediate stages of packing, can be formed, and various models have been postulated (8-12). Recent interpretations of x-ray diffraction patterns suggest that a microfibril is formed when five collagen molecules aggregate with 670-Å axial stagger with an azimuthal displacement of 108° between nearest neighbors. This arrangement would repeat after five 670 Å periods and have a fivefold screw axis. The collagen molecules thus follow a superhelical path of pitch of 600 to 1000 Å around the microfibril.

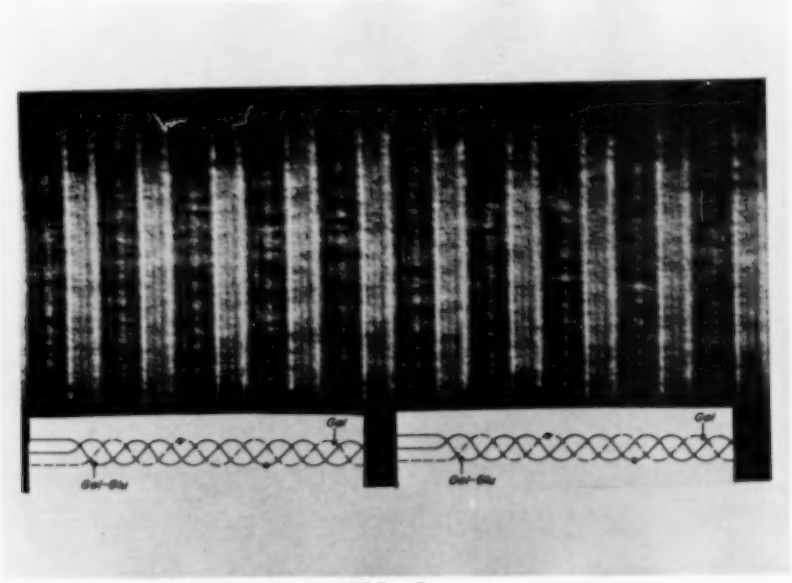

FIG. 2

Native collagen fiber stained with phosphotungstic acid showing the 680-Å periodicity and a schematic representation of a collagen molecule measuring 2800-Å, located in such a position as to generate the banding pattern. (Electron micrograph courtesy of Dr. John Petruska.)

Fig. 2 shows a native collagen fiber with its repeating 640-A periodicity alongside a schematic drawing of a collagen molecule (3000 A length). The relationship between the length of the molecule and the periodicity can be clearly seen, a fact that prompted the quarter-staggered theory of packing (13). Further details of this arrangement can be seen in the lower part of the figure. Stacking of collagen molecules to give rise to SLS crystallites (Fig. 3) has provided a very useful tool for understanding the dimensions of the molecule, and more recently to order the peptides originating after CNBr cleavage of the molecule.

The process of self-assembly that causes the collagen molecules to organize into fibers is illustrated schematically in Fig. 4. The thermodynamics of such a system involve changes in the state of the water molecules associated with the nonpolar regions of the collagen molecule. Also illustrated is the role of the polar groups on the surface of collagen, which we now know are distributed in such a way as to aid in the quarter-staggered packing arrangement (14, 15).

Intracellular Events

1. Synthesis of messenger-RNA specific for collagen.

2. Polyribosome clusters are formed, most noticeably in very active fibroblasts, and probably result from interactions with nascent collagen chains still attached to the ribosomes.

Vol. 17
1980

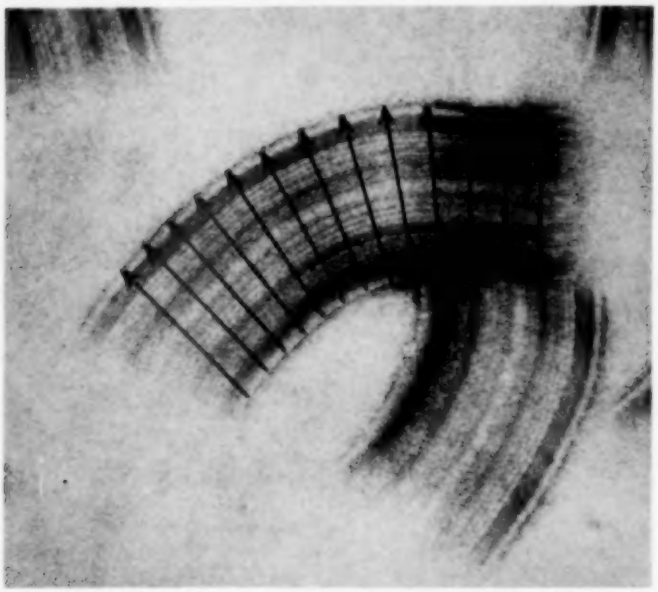

FIG. 3

Segment-long-spacing crystallites (SLS) formed when ATP (adenosine tryphosphate) is added to a solution of collagen. The negatively charged ATP will cause the molecules to aggregate side by side in register in such a way that the molecules can now be visualized. The arrows indicate the positions of the molecules in the crystallite and are meant to represent the orientation of the individual molecules present in the aggregate. (Electron micrograph courtesy of Dr. John Petruska.)

3. Association of the polyribosomes and the endoplasmic reticulum seems to be necessary for collagen secretion to occur.

4. Polypeptides which are not in a helical conformation occur at both the N and C terminal ends of the collagen molecule. The complete molecule with non-helical extensions at both ends is known as procollagen. The N terminal extensions of the three alpha chains may be the first parts of the nascent collagen polypeptide to recognize each other and facilitate the subsequent alignment and coiling of the molecule to give rise to the helix.

5. Certain peptide-bound proline and lysine residues are hydroxylated by specific enzymes. This seems to occur as nascent polypeptide chains are being synthesized, since proline hydroxylase has been shown not to be able to hydroxylate proline residues after the collagen molecule has acquired the triple helical configuration. This reaction requires vitamin C and is inhibited by a series of ion chelators.

6. Once the procollagen molecule is complete, and the central part of the molecule has acquired the triple helical configuration and the specific proline and lysine residues are hydroxylated, the molecule seems to be transported to the Golgi apparatus where it is glycosylated. In the first step, galactose is linked to hydroxylysine and in some instances this is followed by glucose, which when added gives rise to glucosyl-galactosyl-hydroxylysine. This reaction requires a UDP galactose and UDP glucose transferase which is known to be present in connective tissues.

7. The completed procollagen molecules are now packaged into vesicles and translocated to the surface of the cell where, by a process of exocytosis, they are expelled into the extracellular environment. This process requires the activity of microfilaments and microtubules, and agents which interfere with their motility are able to block the secretion of collagen; in particular the mitotic inhibitor colchicine has been found effective in preventing collagen secretion. Somewhere close to cell's surface, specific proteases are involved in the removal of the N and C terminal non-helical polypeptides. The sequence of removal has not been completely

Vol. 198

elucidated but it seems to occur in steps. Pulse-chase experiments coupled with autoradiographs show that in chick embryo calvaria, the amino propeptides are removed about the time that the procollagen molecule leaves the cell. The carboxypropeptides are cut off later on, probably extracellularly (16).

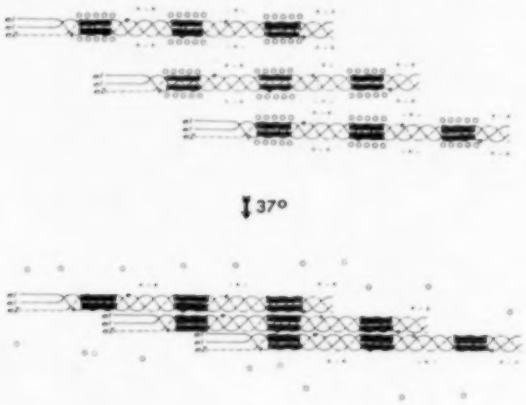

FIG. 4

Soluble collagen can be extracted from most tissues by cold neutral salt solutions. If these solutions are warmed to 37°C the collagen molecules assemble into native fibers. The upper part of the drawing represents molecules that have begun to align in a quarter-staggered overlap. The alignment is primarily due to interaction of opposing electrostatic changes as depicted by the + and - signs. As the temperature approaches 37°C the hydrogen-bonded water molecules (open circles), which are clustered around the hydrophobic regions of collagen, "melt" and expose these nonpolar surfaces. Exclusion of water allows these surfaces to interact with each other, giving rise to hydrophobic bonds that greatly enhance the stability of the fiber. The driving force results from an increase of entropy of the system. The release of "organized" water from initial sites and its transformation into "random" water increases the state of disorder or entropy of the system.

PROCOLLAGEN MOLECULE

This is a precursor to the collagen molecule. The diagrammatic representation of procollagen Type I is shown in Figure 6. The major segment of the molecule is arranged in a triple-stranded conformation involving the three alpha chains characteristic of collagen.

At both ends of this triple helical segment one can find globular extensions--each one of these extensions (there are six of them) is comprised of approximately one hundred amino acids.

Vol. 17
1980

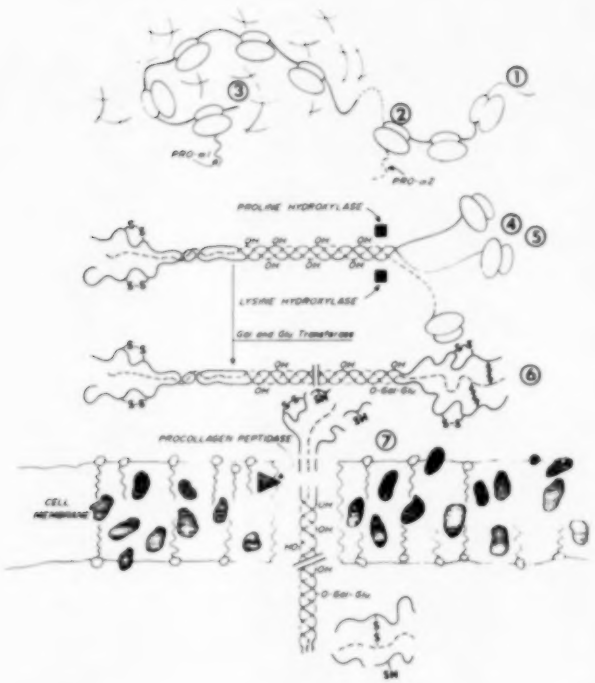

FIG. 5

Intracellular events leading to the completion of a collagen molecule. 1. Synthesis of specific m-RNA for collagen. 2. Translation of message by ribosomes. 3. Clustering of polysomes and association with endoplasmic reticulum. 4. Recognition and alignment of α chains aided by registration peptides. 5. Coiling of chains and hydroxylation of specific proline and lysine residues. 6. Glycosylation of specific hydroxylysine residues. 7. Extrusion of the completed molecule.

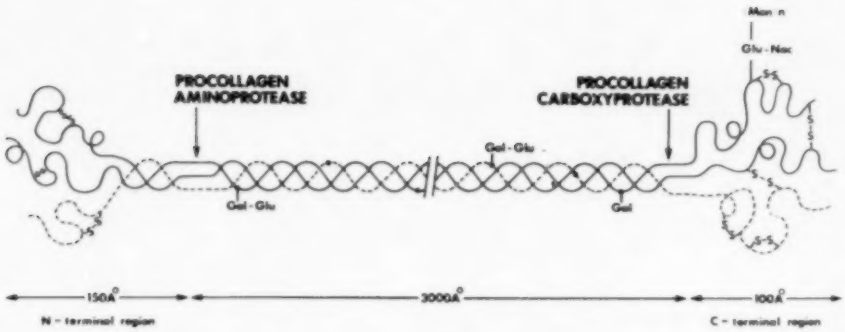

FIG. 6

Diagrammatic representation of a procollagen molecule depicting the 2 non-helical extensions at either end cleared by specific proteases prior to conversion to collagen.

The polypeptides from the C-terminal extension are linked to each other by disulfide bridges whereas the polypeptides in the N-terminal region have disulfide bridges which are intrapeptide in nature. In addition, the N-terminal region contains a small segment of collagen helix interspersed within the non-helical configuration. The dimensions occupied by the different regions of the molecule are shown schematically in the diagram. The C-terminal region contains N-acetyl-glucosamine and mannose covalently linked to the polypeptide backbone. The function of these extensions and the sequence of removal is not clear. It has been postulated that they play a role in preventing intracellular fiber formation and may provide aid in aligning the three collagen polypeptides for the purpose of folding. In particular, the C-terminus may play some function in determining the extracellular organization of the collagen fibers.

Peptidases that cleave the non-helical extensions of procollagen are found in bone, tendons, skin, and fibroblasts cell culture media in connective tissues. There are two enzymes, one which cleaves the amino extension and another one that cleaves the carboxyl extension (17). The physiological sequence of events seems to suggest that the first endopeptidase to act is the amino-procollagen-peptidase which removes the amino propeptides and subsequently the carboxyl procollagen peptidase which cleaves the carboxyl propeptide yielding α-chains (18).

Extracellular Events

8. Specific lysine and hydroxylysine residues in collagen are oxidatively deaminated to give rise to the corresponding peptide-bound aldehydes. This modification is mediated by an enzyme, lysyl oxidase, which requires Cu^{++}. Even though the location of this enzyme is not clear, its mode of action would suggest that it could be associated with the cell surface. Nevertheless, because this enzyme continues to act after the collagen molecules have been extruded, we tend to place it extracellularly.

9. Formation of intramolecular cross-links occur soon after the lysines located near the N-terminal region have been converted to aldehydes. This

Vol. 17 1980

cross-link involves an aldol condensation product that gives rise to an α-β-unsaturated aldehyde. This is a spontaneous, nonenzymatic reaction that seems to occur more readily when the collagen molecules are packed into fibers.

10. New aldehydes appear on the helical region of some collagens, particularly those that are involved in extensive cross-linking, such as in skin and bone.

11. Intermolecular cross-links form between peptide-bound aldehydes and unmodified-NH_2 groups of other lysine and OH-lysine residues. This reaction is of the Schiff base type. Further stabilization involving reduction or addition to the double bond seems to be necessary to render these cross-links heat- and acid-stable. These intermolecular cross-links are physiologically the most important ones.

FIG. 7

Extracellular events leading to fiber formation. 8. Biosynthesis of aldehydes near the N-terminal region. 9. Aldol condensation leading to formation of intramolecular cross-links. 10. Appearance of aldehydes in the helical region of collagen. 11. Formation of intermolecular cross-links (Schiff bases). 12. Staggering of collagen molecules within a fiber to generate the 680-Å periodicity (640-Å in the dry state). Arrows indicate the potential sites for intermolecules cross-linking (for rat skin collagen).

12. The collagen fibers found in the extracellular matrix of connective tissue vary in diameter and distribution. These differences in appearance

seem to reflect some intrinsic structural characteristics, as well as the composition of the extrafibrillar matrix (proteoglycans, glycoproteins, etc.)

TISSUE-SPECIFIC COLLAGENS

Approximately ten years ago it became apparent that not all the collagen molecules in a single species were identical. Heterogeneity in chain composition and amino acid sequence were shown to exist in spite of the fact that under the electron microscope the characteristic banding of collagen did not reflect such differences. Chick sternal cartilage and bovine articular cartilage collagen were shown to contain three identical alpha chains, in contrast to the more ubiquitous collagen previously isolated from bone, skin, and most other connective tissues which contained two identical α1 chains and one distinct alpha chain known as α2. (19 - 21). Because skin collagen was the first molecular species to be characterized, it was identified as Type I collagen. The newly discovered cartilage collagen was labeled Type II collagen. Subsequently another kind of collagen was found to be present in significant amounts in blood vessels and to a lesser extent in skin (22). This collagen, which was labeled Type III, also contains three identical chains and is unique in the sense that it contains interchain disulfide crosslinks in the helical region of the molecule. Type III collagen is found always in association with Type I collagen and the relative proportions of Type I and Type III collagens seem to vary with age and in a variety of pathological conditions. The insoluble forms of Type I and III collagens can be extracted from skin and other tissues after limited proteolysis with pepsin. These collagen species can be separated by differential salt precipitation or by differential denaturation and renaturation(23). The latter procedure takes advantage of the presence of the intrahelical disulfide crosslink, since the denatured alpha chains of Type III collagen tend to renature more readily, and can be selectively precipitated into native collagen fibers.

Vol. 17
1980

In addition, several other collagens have been partially characterized: Type IV from basement membrane (24), $\alpha A[\alpha B]_2$ from placental membranes (25), A and B chains from a variety of basement membrane-containing tissues (26), TSD4 collagen from a teratocarcinoma cell line (27), and X_2Y collagen from chondrocytes and their progeny (28). The use of type-specific, anti-collagen fluorescent antibodies has allowed (29) to demonstrate the simultaneous synthesis of Tupe I and III collagens by fibroblasts. Thus the collagen phenotype of a single cell may consist of more than one collagen type and necessitate the selective expression of the complex family of collagen genes. Regulation of this process, both quantitatively and qualitatively, is important for the maintenance of specific, functional extracellular matrices.

Figure 8 shows, in a schematic fashion, the major differences between collagen Types I, II, and III. Type I collagen is relatively poor in hydroxylysine and associated carbohydrates. Type II collagen, which is the sole component of hyaline articular cartilage, is found mixed with Type I collagen in fibro-cartilage and related structures. In addition to the three identical chains, the other major difference which is illustrated in the diagram is the increased content of hydroxylysine (represented by the dots), and the increased content of glucose and galactose bound to hydroxylysine. Type III collagen, as mentioned earlier, is always associated with Type I collagen. It is present in large amounts in blood vessels (up to 50%) and may account for 10-20% of the skin collagen, depending on the age of the animal. Like Type II collagen, it contains three identical chains different from those present in Types I and II, but exhibiting the unique characteristic of possessing intrachain disulfide crosslinks located in the helical region of the molecule close to the C terminal end.

Type IV collagen is a basement membrane collagen (Figure 9). It has unusual features such as a high proportion of 3-hydroxyproline (in contrast to interstitial collagens which contain almost exclusively 4-hydroxyproline). Since basement membrane collagen requires a combination of various procedures such as reduction and alkylation and enzyme digestion for its solubilization, characterization of its non-helical ends has proven more difficult. Some similarity seems to exist therefore between basement membrane collagen and the intact procollagen molecules isolated from

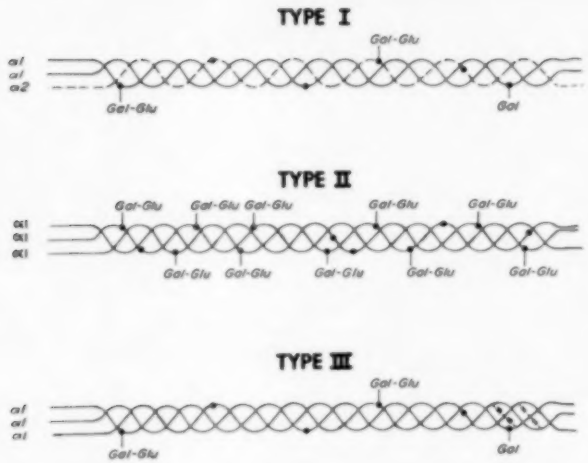

FIG. 8

Skin and bone collagen (Type I), Cartilage collagen (Type II) and Vascular or Embryonic collagen (Type III). These collagens exist usually as mixtures in various connective tissues, and only seldomly as single entities. The dots represent hydroxylysine residues. Type III has intramolecular disulfide bridges.

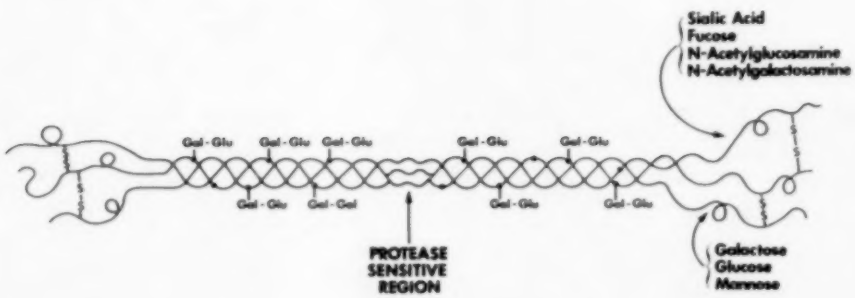

FIG. 9

Simplified diagram of a basement membrane collagen molecule (Type IV). Indicates disulfide bridged non-helical regions at both ends and approximate areas to which carbohydrate residues are attached. Also there seems to exist a somewhat enzyme sensitive region that may be responsible for cleavage of the molecule during purification, although this still remains a subject of great controversy.

Vol. 198

interstitial tissues. Also, smaller molecular weight collagen-like products which appear in the digest cannot be clearly identified as to their origin. Therefore in an attempt to summarize its structure one has to indulge in a significant degree of speculation. In addition to glucose and galactose, hexoses normally found to be associated with interstitial collagens, fucose, mannose, hexosamine and sialic acid have also been identified in Type IV collagen. A protease-sensitive region (probably resistant to pepsin and trypsin) may occur in the midst of the helical region, which may allow cleavage of the molecule into smaller helical fragments during extraction from tissues and purification. These observations are schematically summarized in Figure 9.

Table I lists a variety of tissues from several mammalian species (man, bovine and rat) which have been analyzed for their collagen types. Whenever possible, the type listed first constitutes the most abundant collagen species present (30-38)

TABLE I

Distribution of Collagen Types in Various Connective Tissues

Tissue	Collagen Types Present
Skin	I, III, A, B
Bone	I
Hyaline Cartilage	II
Perichondrium	I, II
Uterus	I, III
Basement Membrane	IV, A, B
Blood Vessels	I, III
Granulation Tissue	I, III
Annulus Fibrosus	I, II
Nucleus Pulposus	II, I
Muscle:	
Epimysium	I, III, IV
Perimysium	III
Endomysium	III, IV
Tendon:	
Bundles	I
Endotendinium	III, IV
Kidney Stroma	I, II
Gingiva	I, III
Cementum	I
Dentine	I
Periodontal Ligament	I, III

Vol. 17
1980

WOUND HEALING

There is inherent tendency of tissues to repair after they have been damaged. The nature of the repair process varies with the site and mode of injury. Connective tissues repair by regenerating their extracellular matrices. Therefore, a major part of the process involves the deposition of newly-synthesized collagen and proteoglycans. Healing of artificially-induced skin lesions has been studied extensively as an experimental model. In general, the cellular population of healing wounds changes from one associated with the initial inflammatory response, that is granulocytes and macrophages, to that associated with a proliferative and anabolic response involving fibroblasts. During the earliest phase of wounding, no obvious fibroblasts are present. Before recognizable fibroblasts enter the wound, cells that appear like immature fibroblasts are seen in the perivascular connective tissue. The development of these cells into mature fibroblasts has been followed during the different stages of wound repair by Ross and his associates. Collagen synthesis has been reported to increase significantly by 24 hours in open rat skin wounds (39). Bailey et al (40) reported that a high proportion of Type III collagen was produced in response to turpentine injection or to sponge implantation. Gay et al (41), using indirect immunofluorescent techniques, also observed an increase in Type III collagen synthesis associated with the initial phase of wound repair in humans. More recent and more quantitative studies on the nature of collagen synthesized during the early phase of wound healing (42) show an increase

in synthesis of Type III collagen 10 hours after inflicting the wound. By 24 hours, the percentage of Type III collagen synthesized returned to a normal skin value of 20%. The early increase in Type III collagen observed by these investigators is probably derived from local fibroblasts which are activated by the wounding process. The early Type III collagen deposited may be important in establishing the initial wound structure and provide a basic lattice for subsequent healing events. However, it is unlikely that Type III collagen contributes significantly to wound tensile strength because the greatest increase in tensile strength is not observed until later phases of wound repair (43). This change in collagen pattern associated with injury is of interest due to the fact that alteration in the normal distribution of the various collagen types is seen with increasing frequency in a variety of pathological states (44-46). Further studies on the quantitative and qualitative distribution of collagen types in a variety of normal and injured tissues might provide us with further insight into the specific role that the different collagen types possess in relationship to the normal structure and function of the connective tissues.

COLLAGEN CROSSLINKING

After the collagen molecules have self-assembled to form a collagen fiber, it is essential for the stability of such a fiber that crosslinks be generated between the individual molecules (47). absence of such crosslinks, such as is seen in certain experimental and human diseases, causes the collagen fibers to be extremely weak and friable. These are therefore not able to perform the mechanical functions associated with normal body functions. Chemical studies of commercial gelatins and subsequent analyses of purified collagens showed the presence of aldehyde groups in these polypeptides. These aldehydes are derived from an enzymatic modification of the amino acids lysine and hydroxylysine. An enzyme, lysyl-oxidase, has been isolated from connective tissues, which is known to convert specific lysine and hydroxylysine residues in collagen and elastin into peptide bound aldehydes. The reaction involves an oxidative deamination of the ε-amino-carbon yielding the corresponding delta-semialdehyde (Fig. 10).

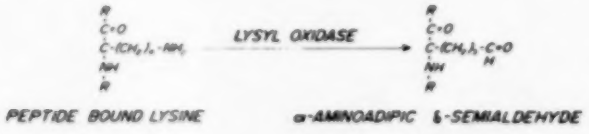

FIG. 10

Oxidative deamination of peptide-bound lysine by the enzyme lysyl oxidase generates the aldehydes associated with the collagen molecule.

Lysyl-oxidase from embryonic chick cartilage has been purified to constant specific activity and a single protein band on sodium dodecyl sulfate acrylamide gel electrophoresis. This band has an apparent molecular weight of 62,000. The purified enzyme is active with both insoluble elastin and embryonic chick skin or bone collagen which has been precipitated as reconstituted native collagen fibers. It exhibits very low activity towards collagen molecules in solution, indicating that this enzyme has a specificity for ordered aggregates. The lathyrogens such as β-aminopropionitrile (BAPN) will irreversibly inhibit lysyl-oxidase in vitro and in vivo. All collagen fractions so far tested show some lysyl-oxidase activity, which suggests a tight association between collagen and this enzyme. It is not clear at what time or place this enzyme acts upon the recently secreted collagen molecules, nor if this is a time dependant modification. Evidence exists that the more insoluble collagen fractions seem to accumulate larger numbers of aldehyde residues. Lysyl-oxidase seems to have a particular affinity for the lysine residue located near the N-terminal region of the molecule. Oxidative deamination of this particular lysine

is very rapid and may occur before the collagen molecule assembles into its final position in the fiber. On the other hand, additional aldehydes form in the helical portion of the molecule during maturation and the average number and approximate location of such aldehydes in rat skin collagen has been reported (48). The more insoluble, yet extractable, fractions of bone collagen also contain a significantly large amount of aldehydic residues (49). The co-factors required for the oxidative deamination of lysine have not been completely elucidated. Chelating agents abolish this activity which can be restored by cupric ions. Activity is absent from copper deficient chicks which induces a state similar to that seen in osteolathyrism. Requirement for pyridoxal or other such cofactors frequently associated with other amine-oxidases has not been established. The inhibition of lysyl-oxidase by BAPN has proven to be of major value in attempting to elucidate the mechanism of the crosslinking of collagen.

BIOSYNTHESIS OF INTRAMOLECULAR AND INTERMOLECULAR CROSSLINKS

It should be quite clear that the aldehydes found on collagen are the precursors of both the intramolecular and intermolecular crosslinks in collagen. To obtain an insight into the overall process of aldehyde formation of intramolecular and intermolecular crosslinks, neutral salt-soluble collagen was aged in vitro. The collagen fibers became increasingly insoluble as a function of time. Within the first 2 weeks some of the collagen could be redissolved by simply cooling the preparation to 4°C, but later the fibers became completely insoluble. Following this period and for another 2 weeks some of the collagen could be solubilized by 0.5-M acetic acid or 0.2-M cysteamine, pH 7.0 . But later on even these agents were unable to solubilize collagen. In order to interpret these findings, the various collagen fractions were reduced with NaB^3H_4 and analyzed on an amino acid analyzer for tritium incorporation . After removal of the uncrosslinked collagen by cooling to 4°C, the residue, which remained insoluble, was treated with NaB^3H_4. It showed the presence of various amounts of Schiff bases in addition to reduced aldehyde and aldol condensation products. The Schiff bases identified earlier as lysinonorleucine and hydroxylysinonorleucine increase rapidly during the first 2 weeks of incubation. Intramolecular crosslinks of the aldol type seem to be restricted to the N-terminal region of the molecule, and it is not clear whether all collagens have such crosslinks. In collagens from soft tissues there is a good correlation between the amount of β components seen after denaturation and the concentration of α-β-unsaturated aldol. In bone this point is less clear, and it is possible that β components arise from intermolecular cross-links of the Schiff base type. Removal of the N-terminal nonhelical peptides by limited cleavage with CNBr or by enzymes depletes soluble collagen of the aldol crosslinks and generates slightly shortened α chains, which migrate like the corresponding α_1 and α_2 chains in the parent molecule. The exact significance of intramolecular crosslinking is not known.

The reactions leading to the formation of the intramolecular (aldol) and intermolecular crosslinks (Schiff base) are shown in Figs. 11 and 12. In addition to the compound shown in Fig. 12, which illustrates lysinonorleucine, a compound first identified in elastin, other Schiff bases have been identified. These are hydroxylysinonorleucine , which results from the association of a lysine-derived aldehyde with a hydroxylysine residue, and dihydroxylysinonorleucine , which originates from a hydroxylysine-derived aldehyde and an unmodified hydroxylysine residue. These hydroxylysine-containing crosslinks seem to be the most prevalent intermolecular crosslinks in native insoluble collagen. The chemical structures of the principal crosslinks identified in collagens are shown in Figure 13.

In addition, the contributions by lysine, hydroxylysine and histidines to the formation of the structures are illustrated by enclosing in dotted lines the basic skeleton of these amino-acids. These structures represent the compounds which originate after the crosslinks have been reduced with sodium borohydride which makes them stable to acid hydrolysis. The sites of reduction are indicated by the asterisk and generate useful markers particularly if tritiated sodium borohydride is used as a reducing agent; then the tritium incorporated at these locations serves as a tag to identify and quantitate these crosslinks. Of significance in this connection is the greater chemical stability of the crosslinks which involve hydroxy-

Vol. 17
1980

lysine residues.

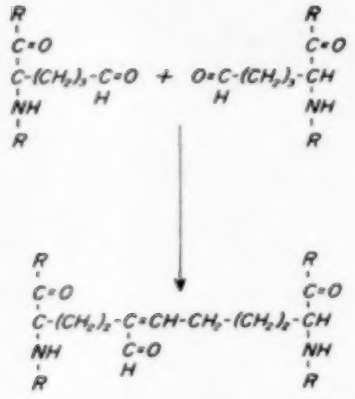

FIG. 11

Aldol condensation reaction involving lysine-derived aldehydes located near the N-terminus of the molecule. This aldol condensation is responsible for the formation of the intramolecular crosslink.

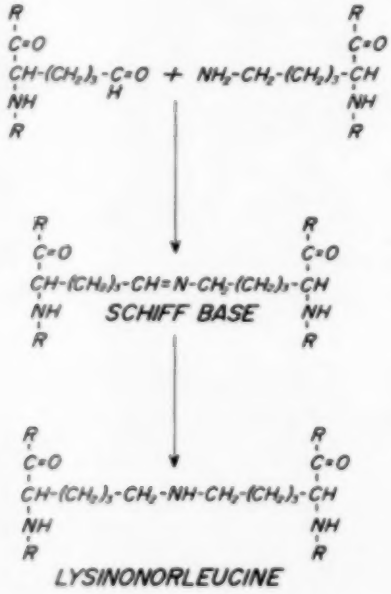

FIG. 12

Schiff base reaction occurring between a lysine-derived aldehyde and an unmodified ε-amino group. This interaction is primarily responsible for the formation of intermolecular crosslinks and can involve either lysine or hydroxylysine. It is acid-labile and seems to require further stabilization to render the collagen fiber heat- and acid-stable. The reduced form (lysinonorleucine or its hydroxylated derivatives) can be isolated after reduction or after in vitro aging collagen. It is not yet clear to what extent the reduced compound is a physiological stabilizer of the collagen assembly, nor which is the major stable crosslink in collagen.

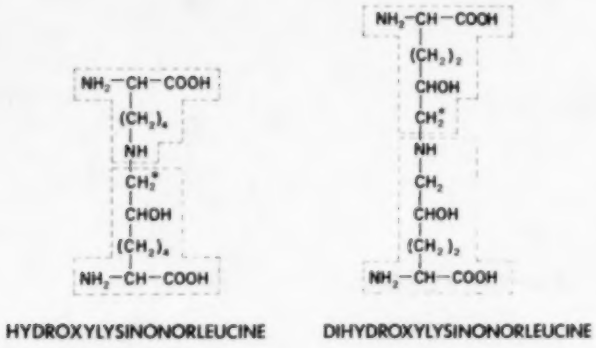

FIG. 13

Structures of the most abundant crosslinks isolated from collagens after reduction with $NaBH_4$. The asterisk indicates the site of insertion of tritium when radioactive isotope is used for reduction.

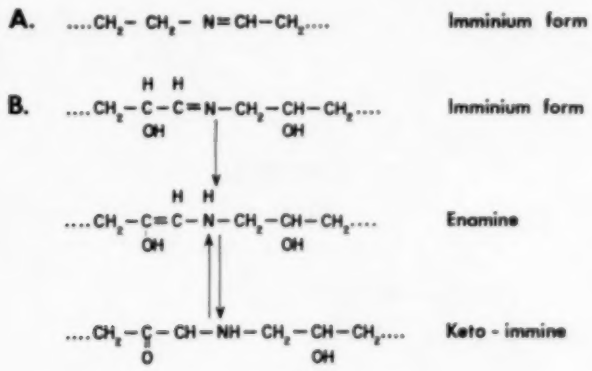

FIG. 14

Two types of crosslinks are illustrated. (A) A crosslink between a lysine from one collagen polypeptide and a lysine derived aldehyde from another. The Schiff base formed is in the imminium configuration and the double bond is susceptible to cleavage by acetic acid and certainly 6 N HC2 under conditions used for acid hydrolysis. (B) A crosslink formed between a hydroxylysine derived from one molecule and a hydroxylysine derived aldehyde from another molecule. This crosslink is prevalent in bone and in collagens rich in hydroxylysine. The initial imminium form contains a hydroxyl group conjugated with the N=C bond. This can form the enamine which readily tautomerizes to the ketoimine. The tautomeric form is stable to acid hydrolysis and explains the insolubility of bone collagen (50).

Figure 14 illustrates the resonating forms of the hydroxylysine derived crosslinks. The initial imminium form contains a hydroxyl group conjugated with the N=C. This can form the enamine which rarely tautomerizes to the ketoimine.

Vol. 17
1980

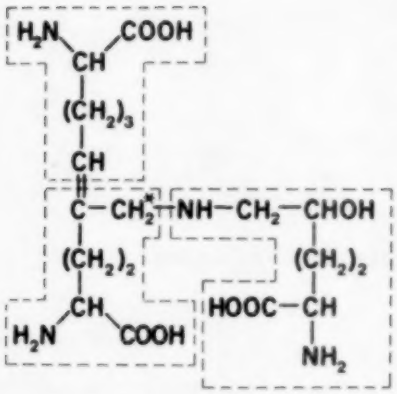

HYDROXYMERODESMOSINE

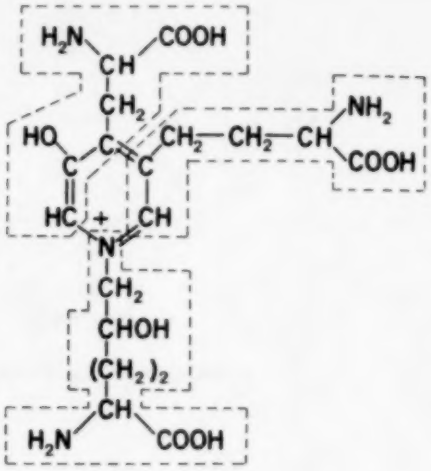

PYRIDINOLINE

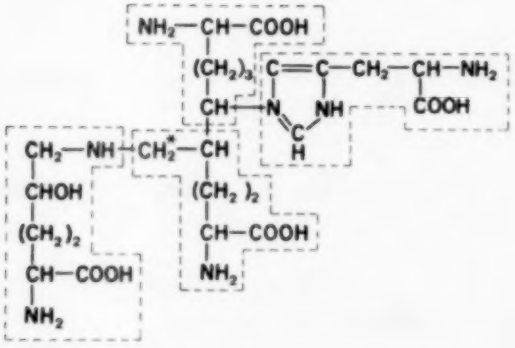

HISTIDINO-HYDROXYMERODESMOSINE

FIG. 15

Crosslinks found in various proportions in collagens from different tissues. The individual amino acids which give rise to these crosslinks, mostly lysine and lysine derived aldehydes and histidine, are identified enclosed within dotted areas.

THIOLISM: A DEFECT INDUCED BY PENICILLAMINE

Administration of penicillamine to animals and humans causes an accumulation of neutral salt-soluble collagen in various tissues (51-54).

The unusual features of penicillamine posed an interesting question as to how crosslinking of collagen could be impaired. As will become apparent later, two of the more characteristic properties of penicillamine, namely the ability to trap carbonyl compounds and to chelate heavy metals, are of primary significance in this connection. The former property manifests itself over all the effective dose ranges studied, whereas the latter seems to occur only at high dosages, far beyond that administered to humans. The mechanisms by which penicillamine inhibits crosslinking of newly formed collagen and by which it depolymerizes incompletely crosslinked insoluble collagen will be briefly discussed.

The collagen extracted from tissues of animals treated with D-penicillamine is able to form stable fibers *in vitro* and is not deficient in aldehydes like that from βAP-treated animals. As a matter of fact, its aldehyde content is even higher than normal. This suggested that the mechanism of action of βAPN and penicillamine had to be different.

Using the method of equilibrium dialysis, it was observed that cysteine, penicillamine and other analogues bind specifically to free aldehydes on collagen. Both the free amino and sulphydryl groups are necessary for binding to occur. The collagen-mercapto-ethylamine product is in equilibrium with its constituents and can be completely dissociated by exhaustive dialysis.

Although all collagen preparations are able to form native collagen fibers with native 640Å periodicity, only those containing significant amounts of aldehydes form stable crosslinks. The collagen from the animals treated with high levels of penicillamine is incapable of forming stable crosslinks when reconstituted *in vitro*, and in this connection behaves like lathyritic collagen.

One can conclude from these experiments that penicillamine has the ability both to block aldehydes and to inhibit lysyl oxidase activity. At lower dosage, it acts primarily by blocking the aldehyde residues present on the collagen molecule, whereas at the higher dose it also affects the activity of lysyl oxidase (55). This latter observation agrees with the fact that 10^{-4} M penicillamine partially blocked lysyl oxidase activity *in vitro* while 10^{-2} M inhibited it completely . Although the mechanism operating under these circumstances has not been defined, it may be related to the ability of penicillamine to chelate divalent cations or to interact with other cofactors (Fig. 16).

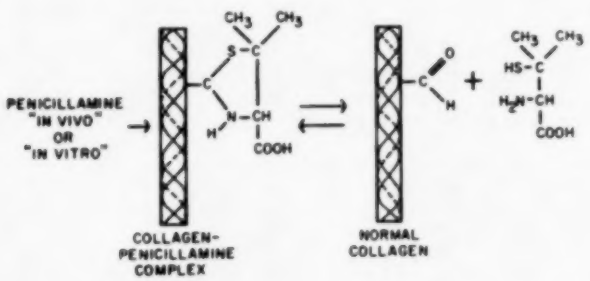

FIG. 16

Schematic drawing summarizing the mode of action of penicillamine. This compound *in vivo* as well as *in vitro* will interact with aldehydes on collagen, preventing their subsequent participation in the formation of intramolecular and intermolecular crosslinks. The reversibility of the collagen defect seen when penicillamine therapy is discontinued can be explained by the instability of the thiazolidine complex formed between penicillamine and the peptide-bound aldehydes.

Vol. 17
1980

DEPOLYMERIZATION OF INCOMPLETELY CROSSLINKED INSOLUBLE COLLAGEN

Fractionation of collagen according to its solubility has proven to be of value in revealing the process of collagen maturation and crosslinking. After rat skin has been extracted exhaustively with 0.45 M NaCl, an additional amount of collagen can be dispersed either by dilute organic acids (citric, acetic) or by compounds such as cysteamine or penicillamine (56).

In rats less than 60 days old, practically all the skin collagen can be dispersed by amino-thiols to yield a collagen soluble in neutral salt. The intrinsic viscosity of this material, 20-25 dl/g (tropocollagen 13 dl/g) reflects a mixture of tropocollagen with polymeric aggregates. This collagen will withstand centrifugation at forces greater than 100,000 g for several hours without appreciable precipitation. In older animals the amount of collagen soluble in dilute organic acids and amino-thiols becomes progressively less.

In addition to preventing the crosslinking of newly synthesized collagen fraction which otherwise would remain insoluble, this particular collagen fraction rendered soluble by administration of penicillamine seems to be equivalent to that able to be dissolved in vitro by amino-thiols and by 0.5N acetic acid. The fact that both in vivo and in vitro one is able to generate a collagen enriched in aldehydes suggests that penicillamine enhances the solubility of collagen by labilizing Schiff base type crosslinks (57, 58).

The size of this degradable pool is inversely proportional to the age of the animal. Penicillamine given to young animals exhibits maximum effect. Because of the rapid rate of collagen synthesis and turnover, the pool of thiol-degradable material is extremely large at this time. By using total skin mass as an index of absolute changes caused by penicillamine, a decline in the amount of total insoluble collagen during the first two weeks of treatment was observed. Continued administration of D-penicillamine failed to affect the remaining insoluble collagen. The soluble collagen that continues to accumulate during treatment may be a part of a rapidly-turning-over pool or may correspond to the more recently synthesized material which has not been allowed to mature. Taking into account the variability in rates of collagen synthesis with age, it is possible to estimate that the half-life of this form of collagen containing labile Schiff bases is around ten days in two-month-old rats. This period reflects the rate at which the Schiff base from the crosslink is transformed into a more stable form of a covalent crosslink by reduction, addition to double bond or other means.

The ability of various agents to affect the stability of Schiff bases using the model compounds has been investigated in the attempt to correlate this property with the in vivo depolymerizing activity (47).

Schiff bases formed between pyridoxal phosphate and γ-amino butyric acid (GABA) are quite unstable at acid pH. This instability of Schiff bases at acid pH can explain the solubilizing effects of dilute organic acids on certain forms of polymeric collagen.

On the other hand, base catalyzes the reaction of aminothiols with a Schiff base made from pyridoxal phosphate and GABA D-penicillamine showed a slight increase in reactivity as the pH was raised from pH 7 to 9, while reactions of L-cysteine and cysteamine were markedly accelerated by a rise in the pH of the media. This can explain our earlier observation that the effectiveness of cysteamine to solubilize insoluble skin collagen markedly increased over the pH range 6.0 to 9.0.

Recent studies by Siegel (59) have shed additional light on the mechanism of action of penicillamine on the inhibition of collagen crosslinking. One of the puzzling observations associated with the mode of action of penicillamine related to the fact that this compound seemed selectively to inhibit the crosslinking of soft-tissue collagen and was much less effective than the β-aminopropionitrile lathyrogens in affecting bone collagen. This collagen, with a high hydroxylysine content, is relatively unaffected in experimental animals fed penicillamine, although increased N^6:6'-dehydro-

5.5'-dihydroxylysinonorleucine is found. Actually it was observed, contrary to expectations, that the synthesis of bifunctional crosslinks involving hydroxylysine increased in those animals treated with penicillamine. In the case of hydroxylysine derived crosslinks, the thiazolidine ring interactions may not be sufficiently strong to block the synthesis of the bifunctional crosslinks involving these intermediates or those favored by the geometry of the fibril. These findings would therefore explain why the effects of penicillamine are significantly greater on soft tissues than on bone, since the former involve lysine-derived aldehyde intermediates, which will more readily form thiazolidine structures.

The stability of the ketoimine form was demonstrated by Mechanic and co-workers by determination of their reduced precursors in bone and dentin collagen . The stability of such a crosslink, derived from two hydroxylysine residues, may explain how such a crosslink can occur in the presence of physiological levels of penicillamine in the tissues. Such a crosslink may be favored over the thiazolidine structure which forms when lysine derived aldehydes are involved. Figure 14 illustrates the chemical composition of these crosslinks, involving lysine or hydroxylysine derived residues.

More recently, Amiel et al (60) looking at the periarticular collagen from immobilized rabbits treated with penicillamine to decrease contractures observed an almost complete inhibition of crosslinks formation. On the other hand, the untreated animals synthesized normal crosslinks (hydroxylysinonorleucine, dihydroxylysinonorleucine and histidinomerodesmosine) in their soft periarticular capsule. It is therefore now apparent why the action of penicillamine varies from tissue to tissue. Its ability to block crosslinking depends on the types of crosslinks that stabilize that particular collagen fiber.

Vol. 17
1980

INTRODUCTION OF ARTIFICIAL CROSSLINKS INTO COLLAGEN

Unless the molecules of collagen which are present within a collagen fiber are adequately crosslinked, either by native biosynthesized crosslinks or by artificially introduced chemical crosslinks, they will not be able to withstand any significant mechanical stresses. Tensile stress would cause the molecules to slip side by side along each other causing the fiber to easily rupture. The relatively weak ionic bonds and hydrophobic interactions which caused the random molecules to associate into fibers are not enough to resist such stresses, therefore the need for intermolecular crosslinks. Too many crosslinks, on the other hand, will cause a fiber to become brittle and inelastic and to easily fracture under mechanical stress. It is obvious therefore that an optimum amount of crosslinking is essential for a collagen framework to adequately perform its supportive function. The effects of the lack of crosslinks on dermal collagen is clearly illustrated in table 2.

TABLE II

Actual tensile strength (W) of dorsal skin from control and treated rats, values calculated on collagen cross-sectional basis (S_x) and after cross-linking with glutaraldehyde (53)

Group	W	Tensile strength per collagen cross-section, S_x		After cross-linking with 10^{-1} M glutaraldehyde
		Per total collagen cross-section	Per insoluble collagen cross-section	
	g	g/mm^2	g/mm^2	g
Control	2505	2980	3550	5214
β-Aminopropionitrile.	1270	1780	4275	3540
Penicillamine.....	275	315	1560	4510

Young growing rats which were treated with either β-amino-propionitrile or penicillamine, agents which are known inhibitors of collagen crosslinking, exhibit a marked decline in the physical strength of their collagen. In particular, penicillamine which we have shown to very specifically inhibit crosslinking in soft tissue collagen, was particularly effective; we have therefore labeled it a dermal lathyrogen. Correlating with these changes in mechanical resistance are marked changes in the response of crosslinked and uncrosslinked collagen to heat denaturation. Native collagen fibers are known to exhibit a shrinkage phenomena in the vicinity of 62-64° C, depending on the conditions under which this test is performed (rate of heating, ionic strength, pH, dielectric constant of the solvent, etc.). The mechanism by which the various lathyrogenic agents inhibit collagen crosslinking is summarized in the following diagram (Fig. 17).

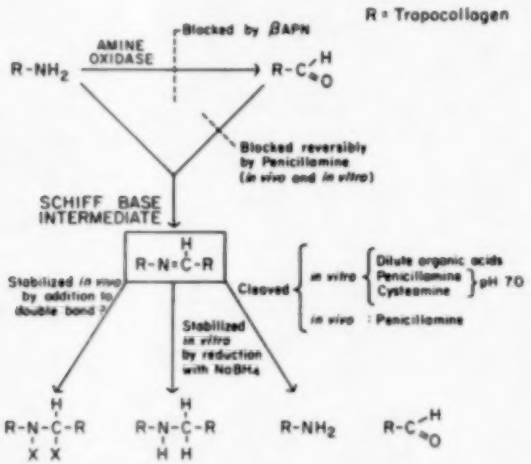

FIG. 17

Site of action of various agents which inhibit formation of crosslinks or cleave them after they are formed.

Because of the conditions of the experiment, the BAPN was not able to completely inhibit crosslinking and enough crosslinks existed within the collagen fibers to cause shrinkage at the time of denaturation of the individual collagen molecule. On the other hand, the collagen fibers from animals treated with D-penicillamine, which almost completely inhibited the formation of new intra-molecular crosslinks, and disrupted most of the pre-existing crosslinks, did not show any shrinkage response. Therefore, in this latter case, denaturation of the collagen molecules was followed by slippage of the denatured alpha-chains since not enough force was developed to counteract the resistance offered by the device used to measure shrinkage. Therefore this collagen devoid of intermolecular crosslinks became a suitable model for evaluating the capacity of various chemical agents to restore native characteristics to the collagen fiber. Figure 19 shows the shrinkage response exhibited by these dermal collagen fibers from D-penicillamine treated animals which were now exposed to various concentrations of glutaraldehyde (10^{-5} to 10^{-1} Molar) prior to being assayed for shrinkage. Fig. 19 shows how introducing crosslinks by means of a bifunctional aldehyde such as glutaraldehyde can restore the shrinkage response in the normal temperature range. The amount of contraction increased and the temperature range required for total contraction to occur was extended. At higher concentrations of glutaraldehyde (1 molar) and with the use of other aldehydes such as formaldehyde (2 molar) and glyoxal (1.5 molar) the temperature

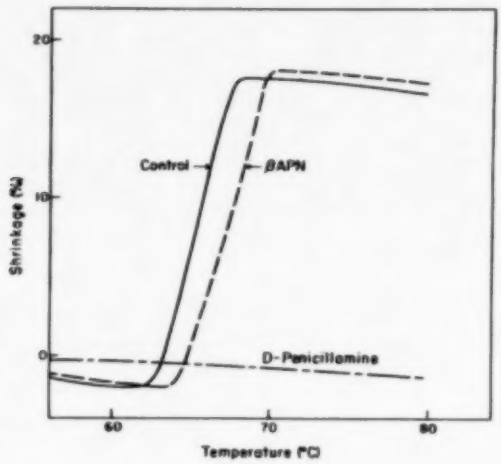

FIG. 18

Thermal shrinkage pattern of strips of dorsal skin (5x50 mm) of normal animals and animals treated for 45 days with either β-aminopropionitrile (BAPN) or D-penicillamine (0.58 mmole per day) (62).

Vol. 17
1980

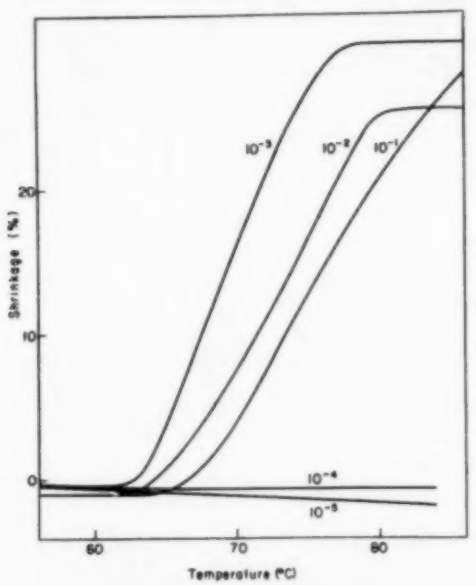

FIG. 19

Strips of dorsal skin obtained from D-penicillamine-treated rats were incubated for 45 min in the cold in the presence of different concentrations of glutaraldehyde (10^{-1} to 10^{-5} M). The basic medium consisted of 0.15 M NaCl buffered with 0.02 M sodium phosphate to pH 7.0 (53).

required to elicit shrinkage increased significantly due to the higher density of crosslinks. The role of the intermolecular covalent bonds, both the naturally biosynthesized ones and those introduced with glutaraldehyde to the non-crosslinked penicillamine collagen is illustrated schematically in Figure 20. The unfolding of the helix which occurs during heat denaturation is reflected by a collapse of the structural framework. Shrinkage parallel to longitudinal axis of the fibers results from the covalent bonds which remain bridging the unfolding protein strands. In the absence of such heat stable crosslinks, the randomly coiling chains slip alongside each other without a significant change in the shape of the amorphous extracellular matrix. Although glyoxial, formaldehyde, and other aldehydes tested were able to restore the shrinkage capability to uncrosslinked dermal collagen, except for the situation with glutaraldehyde, the effect was transient. That is, the changes could be reversed by prolonged washing of the crosslinked fibers with buffered saline solutions, indicating that the crosslinks introduced were unstable. The use of glutaraldehyde as a crosslinking reagent has increased significantly in the last few years. Although it is one of the most extensively used reagents, its chemistry and mechanism of reaction has remained elusive. An excellent review on chemical crosslinking reagents by Peters and Richards addresses itself to this question (61).

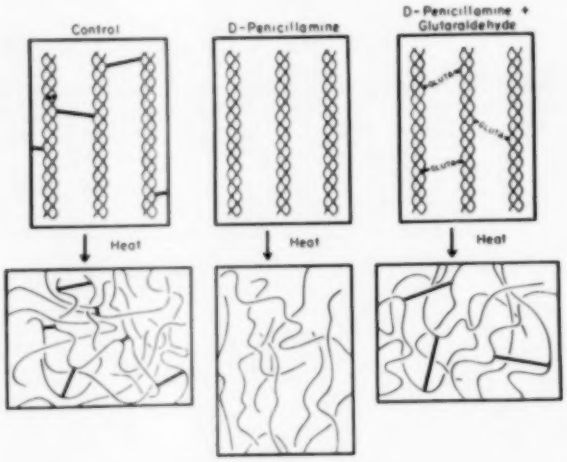

FIG. 20

Schematic representation of the changes occurring during thermal shrinkage of normally cross-linked collagen fibers, of fibers in which the tropocollagen subunits are not intermolecularly crosslinked (penicillamine-treated rats), and of non-crosslinked collagen treated with glutaraldehyde (53).

Some of the known facts which may allow us to understand the mechanism of glutaraldehyde crosslinking and the nature of the bonds formed can be summarized by the following observations. (A) Addition of glutaraldehyde to a protein or simple amine solution produces a yellow color that disappears on reduction with borohydride. (B) Amino acid analysis of a crosslinked protein shows a marked loss of lysine (lysine is not regenerated during 24 hr at 110° in 6 N HCl). No other amino acids are affected. (C) At neutral or acid pH the positive charge of the original ε-amino group is retained, but the pK_a of the new function is about 1 pH unit more acidic than the original primary amine.

Commercial solutions labeled 25%-glutaraldehyde were found by gas chromatography and NMR to contain 79% H_2O, 3% monomeric glutaraldehyde, and 18% derivatives of higher molecular weight that could be broken down to glutaraldehyde. At acidic pH glutaraldehyde is in equilibrium with

its cyclic hemiacetal and polymers of the cyclic hemiacetal (Figure 21A) as proposed by Hardy et al (62). The commercial solutions of glutaraldehyde have a pH of 3.1. However, when the pH is raised to the neutral or slightly basic range at which crosslinking is carried out, the dialdehyde undergoes an aldol condensation with itself, followed by dehydration, to generate α, β unsaturated aldehyde polymers (Figure 21B). As the pH is raised, n increases until the polymer precipitates from solution.

A

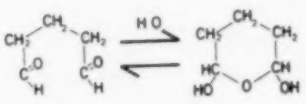

pH = 3.0

B

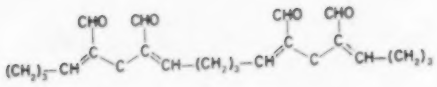

pH = 7.0

FIG. 21A, 21B

Solutions of glutaraldehyde can give rise to a hemiacetal structure at pH=3.0 and to aldol-condensed polymers at pH near neutrality and above

When crosslinking is carried out at pH 3, Schiff base linkages of glutaraldehyde with two lysine residues are formed. These products are unstable toward acid hydrolysis, which is contrary to the observation that the glutaraldehyde crosslinked complexes usually obtained do not regenerate lysine on acid hydrolysis. Therefore the acid-stable products cannot be a result of Schiff base formation with glutaraldehyde itself. Since crosslinking is normally carried out at higher pH the predominant reactive species is the α,β unsaturated aldehyde. The Schiff base that forms with the aldehyde is in conjugation with a double bond. It is therefore the resonance interaction of the Schiff base with the ethylenic double bond which probably leads to the stability of the crosslinked product to acid hydrolysis. The terminal aldehyde groups (few in number) will not be involved in acid-stable crosslinks, as they are not in conjugation with a double bond.

Another mechanism to explain the mode of crosslinking of proteins by glutaraldehyde was proposed by Hardy, Nicholls and Rydon as a result of their study of the interaction of glutaraldehyde with 6-aminohexenoic acid and with α-N acetyl lysine. They were able to isolate and characterize a 1,3,4,5, tetra-substituted pyridinium compound very similar to the amino acids desmosine and isodesmosine present in elastin. The structure of such a compound involving the 6-amino group of lysine with glutaraldehyde condensates is shown in Figure 20. Also shown in this figure are ways in which the glutaraldehyde molecule can condense in order to generate this cyclic pyridinium structure. The presence of some sort of aromatic system is strongly supported by the UV and NMR spectra, electrometric titration and amino acid analysis. The later data showed that the amino group

Vol. 17
1980

disappeared at the same time that it was being replaced by a very strong basic group which could very well be a quaternary pyridinium structure. This was supported by the sensitivity of the chromophore to the nucleophiles hydroxide and hydride (or borohydride) ions, in agreement with the known properties of pyridinium salts. There are also indications in the literature that although the reactions of straight chain aliphatic aldehydes with amines are seldom simple ones, there is in general a tendency to generate ultimately dihydro-pyridines. N-butyraldehyde for example initially forms a Schiff's base with butylamine which undergoes further condensation with the aldehyde to give 1-n-Butyl-3,5-diethyl-2-m-propyl dihydropyridine.

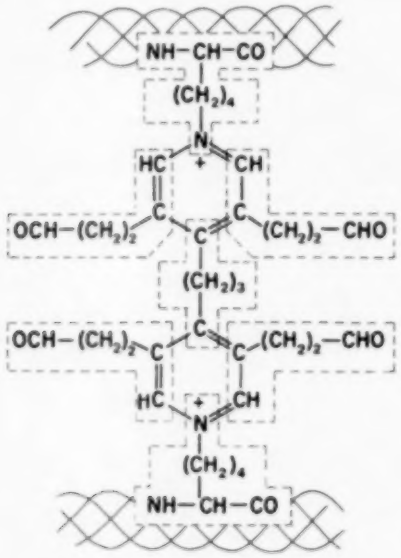

TETRASUBSTITUTED PYRIDINIUM

FIG. 22

Di-pyridinium structure postulated to occur when solutions of glutaraldehyde react with the ε-NH_2 groups of lysines present in adjacent collagen molecules.

Although none of the experiments so far completed in this area of glutaraldehyde chemistry is conclusive, the validity of these assumptions are significantly substantiated by comparing the models proposed with those known to originate from the native patterns of crosslinking of collagen and elastin. If we look back at the pyridinolin structure recently proposed by Fujimoto and his associates (63) as one of the native crosslinks present in collagen, and particularly if one reviews the structures of desmosine and isodesmosine isolated earlier in elastin, the likelihood that glutaraldehyde is generating structures of similar configuration looks quite substantial. Therefore, either the pyridinium ring as proposed by Hardy and his coworkers, or the Schiff's base that forms with the aldehyde in conjugation with a double bond are to be considered likely possibilities.

BIO PROSTHESES UTILIZING ARTIFICIALLY CROSSLINKED COLLAGEN FIBERS

As an example of how technology of the crosslinking of collagen can be of practical significance, in the area of tissue implants, we now see how animal heart valves which have been treated with glutaraldehyde have been stabilized physically, chemically and biologically, in such a way

that they can be implanted in another species, in this case man. Figure 23 shows a series of oriented collagen fibers as they are present in the cusp of the aortic valve of a pig. Figure 24 shows similar fibers at higher magnification (270,000 X). In both instances, the classical collagen pattern with its 760 A repeating period can be seen. The Hancock valve is an aortic pig valve which has been crosslinked with glutaraldehyde, and mounted on a dacron covered plastic ring to facilitate the implantation by the surgeon (Figure 25). Figure No. 26 shows the collagen fibers present in a cusp of a Hancock porcine heart valve which was implanted for eight years and 4 months in a patient. A specimen from the same explant is seen in Figure 27, this time in cross-section. In both these specimens, a fuzy material can be seen surrounding the collagen fiber, similar to that described by Dr. Ferrams and his coworkers (64) . If the explanted valves are placed in a trypsin solution (0.5 mg of trypsin per ml, 0.5 M tris , pH 7.5) the fuzy material which surrounds the collagen fibers disappears and leaves behind collagen fibers which are now undistinguishable from those seen in the fresh porcine tissue prior to implantation (Figure 28, 29). It is therefore clear that morphologically the collagen fibers, after such a long implantation period, in this case 8 years, have still retained their ultrastructure intact. The fuzziness which obscured the banding pattern does not therefore reflect the deterioration of the collagen fibers but seems rather to be an indication of deposition of host material in the peri-fibrillar spaces. To ascertain if these collagen fibers have retained their physical-chemical properties, it was decided to look at their resistance to denaturation. We know that native collagen fibers exposed to guanidine hydrochloride denature and that the rate of denaturation is inversely proportional to the degree of crosslinking. That is, recently synthesized collagen fibers such as those found in the skin of infants, is much more easily denatured than the mature collagen fibers found in the skin of adult individuals.

Vol. 17
1980

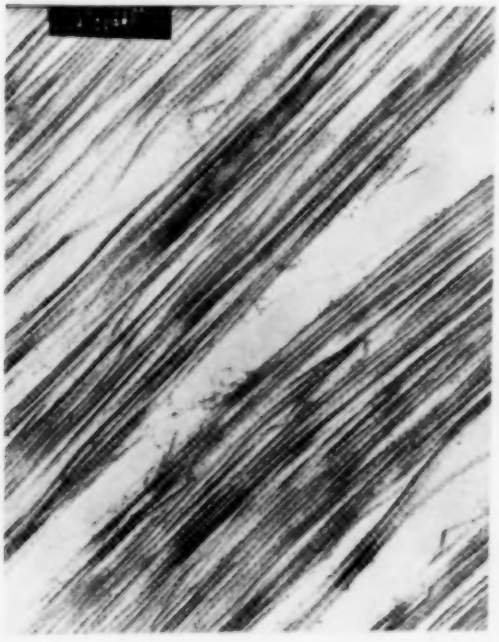

FIG. 23

Collagen fibers present in the cusp of a pig heart valve.

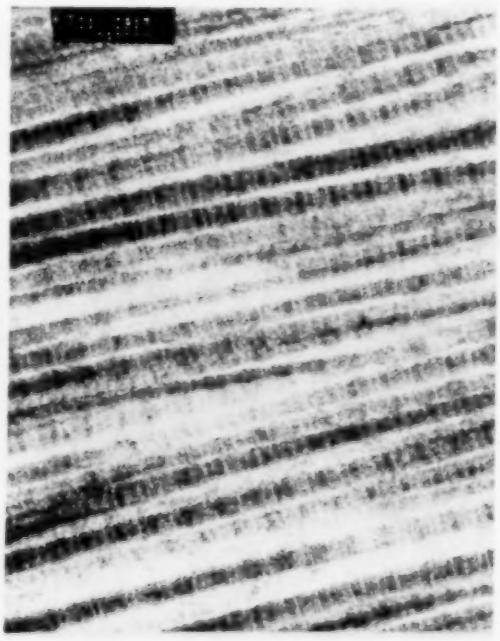

FIG. 24

Same tissue at higher magnification (270,000 X).

Denaturation under electron microscope shows up as an unfolding of the fiber as seen in Figure 30. This figure shows how guanidine hydrochloride disrupts the fibrillar structure of collagen fibers present in the cusp of an aortic valve, which has been placed for one hour in a solution of guanidine hydrochloride at room temperature.

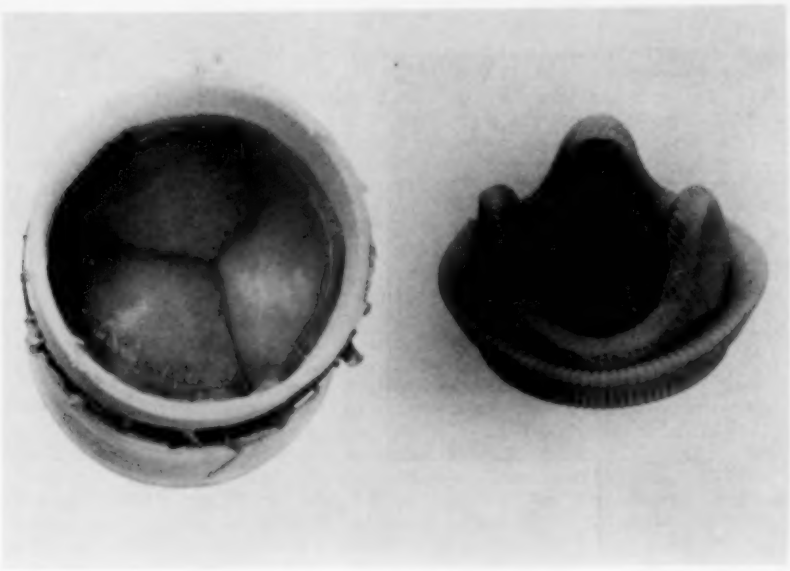

FIG. 25

Hancock glutaraldehyde treated porcine valve ready to be implanted.

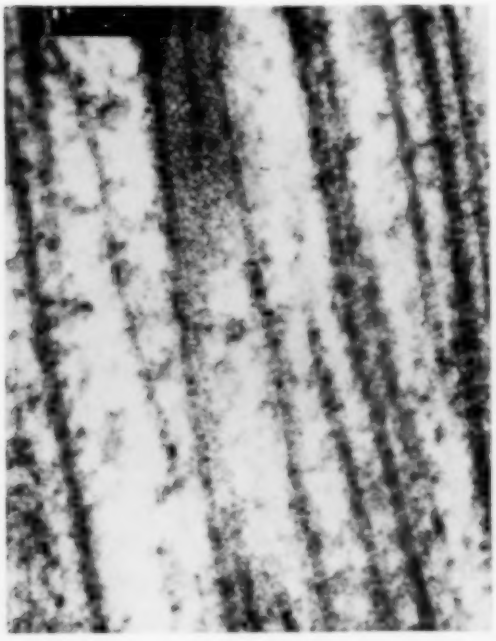

FIG. 26

Collagen and extra fibrillar deposits as they appear in a Hancock valve implanted for over 8 years.

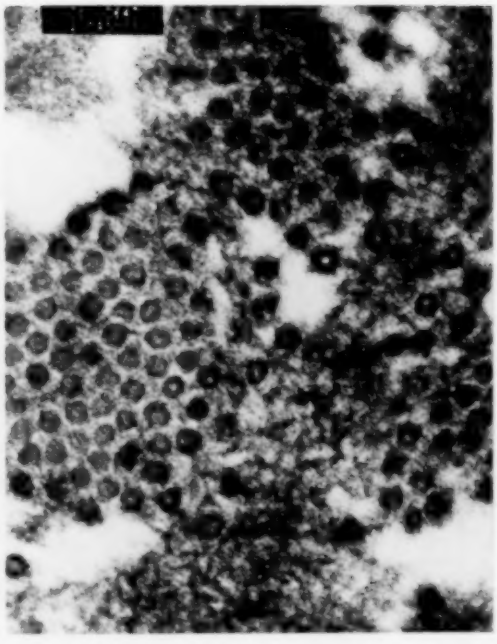

FIG. 27

Cross-section of specimen seen in Figure 21.

Figure 31 shows the behavior of a specimen obtained from the eight year implanted heart valve treated in a fashion similar to that of the fresh valve seen in Figure 7. No significant differences can be seen

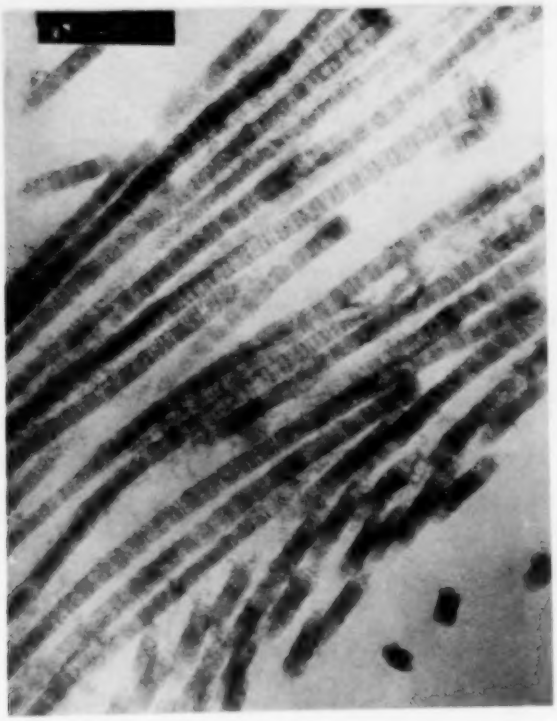

FIG. 28

Recovered Hancock valve treated with trypsin to expose the collagen fibers. Native periodicity becomes clear, as well as the integrity of the fibers. The fuzziness has disappeared.

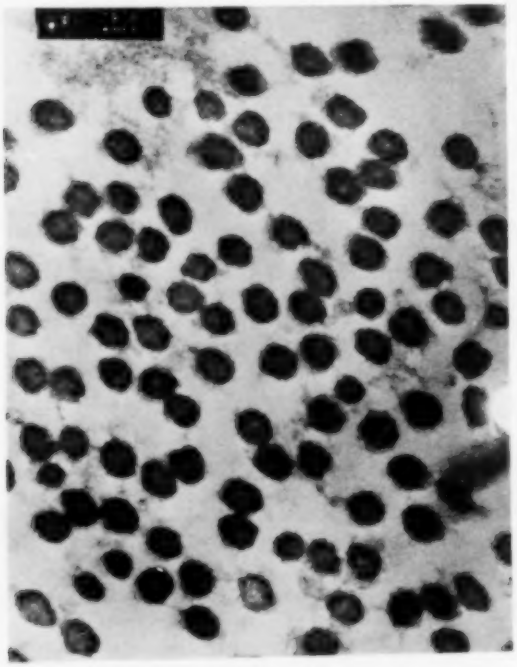

FIG. 29

Same as 25 but showing a cross-sectional view of the fiber bundles after exposure to trypsin.

Vol. 17
1980

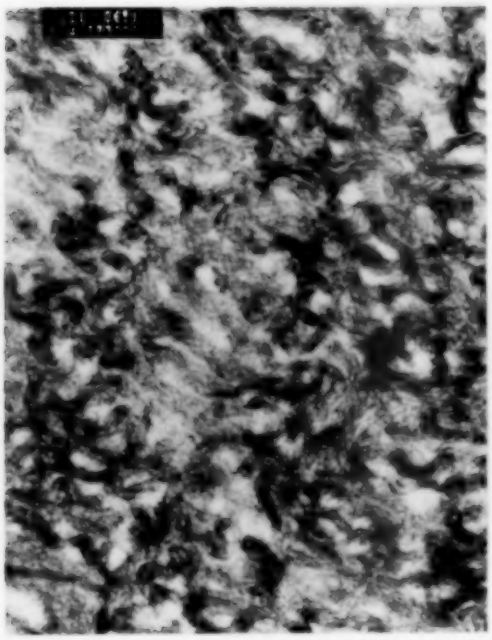

FIG. 30

Unfolding of collagen fibers caused by guanidine HCl. This reflects the absence of added crosslinks, such as those that can be introduced by glutaraldehyde.

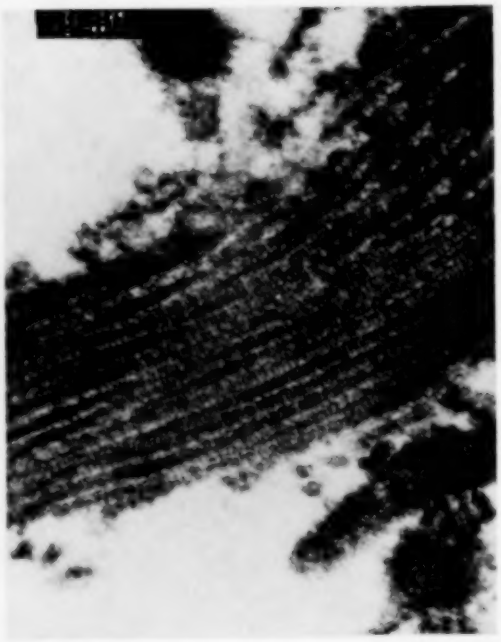

FIG. 31

Hancock valve recovered after 8 years of implantation and exposed to guanidine HCl. It behaves in a way similar to non-implanted glutaraldehyde fixed tissue.

between such an explanted valve and one recently processed by the glutaraldehyde treatment. It can be noted that the ultrastructure of collagen was preserved intact. In this particular case, because the specimen was not priorly treated with trypsin, the fuzy material which surrounds the fibers is present and represents the inter-fibrillar material which accumulated over the years, but which, as shown previously, does not seem to alter the ultrastructural morphology of collagen. It is therefore clear that the crosslinks introduced by glutaraldehyde into collagen fibers render it stable enzymatically and chemically. This example is a good indication of how the technology of crosslinking can be applied to the stabilization of collagen fibers prior to the use as bioprosthetic devices.

ACKNOWLEDGMENTS

I would like to express my appreciation to Drs. T. Quijano and N. Jaffe for allowing me to reproduce unpublished material in this manuscript. Also, to Ms. Arsha Apardian and Mary Duda for typing and editing the manuscript. This work was partially supported by NIH Grants AM-10358 and AM-16404.

REFERENCES

1. RAMACHANDRAN, G.N. Treatise on Collagen. *New York, Academic*, p 103, 1967.

2. RICH, A. and CRICK, F.H.C. The molecular structure of collagen. *J Mol Biol* 3:483, 1961.

3. ENGEL J., KURTZ, J., TRAUB, W., BERGER, A. and KATCHALSKI, E. in FITTON

JACKSON,S. et al (eds). Structure and Function of Connective and Skeletal Tissue. *London, Butterworths*, p. 241, 1965.

4. BROWN, F.R. III, di CORATO, A., LORENZI, G.P. and BLOUT, E.R. Synthesis and structural studies of two collagen analogues: Poly(L-prolyl-L-seryl-glycyl) and poly(L-prolyl-L-alanyl-glycyl). *J Mol Biol* 63:85, 1972.

5. TRAUB, W. and PIEZ, K.A. in ANFINSEN,C.B. Jr., EDSALL, J.T. and RICHARDS, F.M. (eds). Advances in Protein Chemistry. *New York, Academic*, p 243, 1971.

6. TRAUB, W., YONATH, A. and SEGAL, D.M. On the molecular structure of collagen. *Nature* 221:914, 1969.

7. SEGREST, J.P. and CUNNINGHAM, L.W. Unit fibril models derived from the molecular topography of collagen. *Biopolymers* 12:825, 1973.

8. VEIS, A., ANESEY, J.R. and MUSSELL, S. A limiting microfibril model for the three-dimensional arrangement within collagen fibers. *Nature* 215:931, 1967.

9. GRANT, R.A., HORNE, R.W. and COX, R.W. New model for the tropocollagen macromolecule and its mode of aggregation. *Nature* 207:824, 1965.

10. COX, R.W., GRANT, R.A. and HORNE, R.W. The structure and assembly of collagen fibrils. *J Royal Microscop Soc* 87:123, 1967.

11. MILLER, A. and PARRY, D.A.D. Structure and packing of microfibrils in collagen. *J Mol Biol* 75:441, 1973.

12. PETRUSKA, J.A. In SLAVKIN,H.C. (ed). The comparative molecular biology of extracellular matrices. *New York, Academic* p.387, 1973.

13. PETRUSKA, J.A. and HODGE, A.J. A subunit model for the tropocollagen macromolecule. *Proc Natl Acad Sci USA* 51:871, 1964.

14. BAIRATI, A., PETRUCCIOLI, M.G., TORRI TARELLI, L. Studies on the ultrastructure of collagen fibrils. I. Morphological evaluation of the periodic structure. *J Submicr Cytol* 1:113, 1969.

15. HULMES, D.J.S., MILLER, A., PARRY,D.A.D., et al. Analysis of the primary structure of collagen for the origins of molecular packing. *J Mol Biol* 79:137, 1973.

16. MORRIS, N.P., FESSLER, L.I., WEINSTOCK, A. and FESSLER, J.H. *J Biol Chem* 250:5719, 1975.

17. BORNSTEIN, P. *Ann Rev Biochem* 43:567, 1974.

18. DAVIDSON, J.M., McENEANY, L.S.G. and BORNSTEIN, P. *Biochemistry* 14:5188, 1975.

19. MILLER, E.J. and MATUKAS, V.J. Chick cartilage collagen: A new type of α1 chain not present in bone or skin of the species. *Proc Natl Acad Sci USA* 64:1264, 1969.

20. MILLER, E.J. Isolation and characterization of a collagen from chick cartilage containing three identical α-chains. *Biochemistry* 10:1652, 1971.

21. STRAWICH, E. and NIMNI,M.E. Properties of a collagen molecule containing three identical components extracted from bovine articular cartilage. *Biochemistry* 10:3905, 1971.

22. MILLER, E.J., EPSTEIN, E.H. and PIEZ, K.A. Identification of three genetically distinct collagens by cyanogen bromide cleavage of insoluble human skin and cartilage collagen. *Biochem Biophys Res Commun* 42:1024, 1971.

23. CHANDRARAJAN, J. Separation of type III collagen from type I collagen and pepsin by differential denaturation and renaturation. *Biochem Biophys Res Commun* 83:180, 1978.

Vol. 17
1980

24. KEFALIDES, N.A. Basement membranes: structural and biosynthetic considerations. *J Invest Dermatol* 65:85, 1975.

25. BURGESON, R.E., EL ADLI, F.A., KAITILA, I.I. and HOLLISTER, D.W. Fetal membrane collagens: identification of two new collagen alpha chains. *Proc Nat Acad Sci USA* 73:2579, 1976.

26. CHUNG, E., RHODES, R.K. and MILLER, E.J. Isolation of three collagenous components of probable basement membrane origin from several tissues. *Biochem Biophys Res Commun* 71:1167, 1976.

27. LITTLE, C.D., CHURCH, R., MILLER, R.A. and RUDDLE, F.H. Procollagen and collagen produced by a teratocarcinoma-derived cell line, TSD4: evidence for a new molecular form of collagen. *Cell* 10:287, 1977.

28. BENYA, P.D., PADILLA, S.R. and NIMNI, M.E. The progeny of rabbit articular chondrocytes synthesize collagen types I and II and type I trimer, but not type II. Verification by cyanogen bromide peptide analysis. *Biochemistry* 16:865, 1977.

29. GAY, S., MARTIN, G.R., MULLER, P.K., TIMPL, R. and KUHN, K. Simultaneous synthesis of types I and III collagen by fibroblasts in culture. *Proc Natl Acad Sci, USA* 73:4037, 1976.

30. DUANCE, V.C., RESTALL, D.J., BEARD, H., BOURNE, F.J. and BAILEY, A.J. The location of three collagen types in skeletal muscle. *FEBS Letters* 79:248, 1977.

31. TRELSTAD, R.L. Human aorta collagens: evidence for three distinct species. *Biochem Biophys Res Comm* 57:717, 1974.

32. BUTLER, W.T., BIRKEDAL-HANSEN, H., BEEGLE, W.F., TAYLOR, R.E. and CHUNG, E. Proteins of the Periodontium: Identification of collagens with the $[\alpha 1(I)]_2\alpha 2$ and $[\alpha 1(III)]_3$ structures in bovine periodontal ligament. *J Biol Chem* 250:8907, 1975.

33. CHRISTNER, P., ROBINSON, P. and CLARK, C.C. A preliminary characterization of human cementum collagen. *Calcif Tiss Res* 23:147, 1977.

34. WICK, G., NOWACK, H., HAHN, E., TIMPL, R. and MILLER, E.J. Visualization of type I and II collagens in tissue sections by immunohistologic techniques. *J Immunol* 117:298, 1976.

35. WOHLLEBE, M. and CARMICHAEL, D.J. Type-I Trimer and type-I collagen in neutral-salt-soluble lathyritic-rat dentine. *Eur J Biochem* 92: 183, 1978.

36. EYRE, D. and MUIR, H. Collagen polymorphism: two molecular species in pig intervertebral disc. *FEBS Letters* 42:192, 1974.

37. LENAERS, A. and LAPIERE, Ch.M. Type III procollagen and collagen in skin. *Biochim Biophys Acta* 400:121, 1975.

38. WU, C.H., ROJKIND, M., RIFAS, L. and SEIFTER, S. Biosynthesis of type I and type III collagens by cultured uterine smooth muscle cells. *Arch Biochem Biophys* 188:294, 1978.

39. COHEN, I.K., MOORE, C.D. and DIEGELMANN, R.F. *Proc Soc Exp Biol Med* 160:458, 1979.

40. BAILEY, A.J., SIMS, T.J., LELOUS, M. and BAZIN, S. *Biochem Biophys Res Commun* 66:1160, 1975.

41. GAY, S., VILJANTO, J., RAEKALLIO, J. and PENTTINEN, R. *Acta Chir Scand* 144:205, 1978.

42. CLORE, J.N., COHEN, I.K. and DIEGELMANN, R.F. Quantitation of collagen types I and III during wound healing in rat skin. *Proc Soc Exp Biol Med* 161:337, 1979.

43. KLUGER, J., REIDENBERG, M., TYBERG, T., LLOYD, V., ELLIS, G., HAYES, J. and DRAYER, D. *Clin Res* 26:244A, 1978.

44. POPE, F.M., MARTIN, G.R., LICHTENSTEIN, J.R., PENTTINEN, R., GERSON, B., ROWE, D.W. and MCKUSICK, V.A. *Proc Natl Acad Sci, USA* 72:1314, 1975.

45. MCCULLAGH, K.A. and BALIAN, G. *Nature, London* 258:73, 1975.

46. NIMNI, M.E. and DESHMUKH, K. Differences in collagen metabolism between normal and osteoarthritic human articular cartilage. *Science* 181:751, 1973.

47. NIMNI, M.E. Collagen: Its structure and function in normal and pathological connective tissues. *Semin Arthritis Rheum* 4:95, 1974.

48. DESHMUKH, K. and NIMNI, M.E. Characterization of the aldehydes present on the cyanogen bromide peptides from mature rat skin collagen. *Biochemistry* 10:1640, 1971.

49. DESHMUKH, K. and NIMNI, M.E. Soluble collagen with high aldehyde content extracted from insoluble collagen with mercaptoethylamine. *Biochim Biophys Acta* 154:258, 1968.

50. MECHANIC, G.and TANZER, M.L. Biochemistry of collagen crosslinking isolation of a new crosslink, hydroxylysinohydroxynorleucine, and its reduced precursor, dihydroxynorleucine, from bovine tendon. *Biochem Biophys Res Commun* 41:1597, 1970.

51. NIMNI, M.E. Accumulation of a collagen precursor in the skin of penicillamine-treated rats. *Biochim Biophys Acta* 111:576, 1965.

52. NIMNI, M.E. and BAVETTA, L.A. Collagen defect induced by penicillamine. *Science* 150:905, 1965.

53. NIMNI, M.E. A defect in the intramolecular and intermolecular crosslinks of collagen caused by penicillamine. I. Metabolic and functional abnormalities in soft tissues. *J Biol Chem* 243:1457, 1968.

54. HARRIS, E.D. Jr. and SJOERDSMAN, A. Effect of penicillamine on human collagen and its possible application to treatment of scleroderma. *Lancet* 2:996, 1966.

55. NIMNI, M.E., DESHMUKH, K. and GERTH, N. Tissue lysyl oxidase activity and the nature of the collagen defect induced by penicillamine. *Nature* 240:220, 1972.

56. NIMNI, M.E. Extraction of α and β components from insoluble collagen by thiol compounds. *Biochem Biophys Res Commun* 25:434, 1966.

57. NIMNI, M.E., DESHMUKH, K and BAVETTA, L. Turnover and age distribution of a collagen fraction extractable from rat skin by mercaptoethylamine. *Arch Biochem Biophys* 122:292, 1967.

58. ROJIKIND, M. and JAUREZ, H. The nature of the collagen defect in lathyrism. *Biochem Biophys Res Commun* 25:481, 1966.

59. SIEGEL, R.C. Collagen cross-linking. Effect of D-penicillamine on cross-linking in vitro. *J Biol Chem* 252:254, 1977.

60. AMIEL, D., AKESON, W.H., HARWOOD, F.L., SCHMIDT, D.A. and MECHANIC, G.L. Effect of low dosage schedule of D-penicillamine on collagen cross-linking in a nine-week immobilized rabbit knee. *Connect Tiss Res* 5:179, 1977.

61. PETERS, K. and RICHARDS, F.M. Chemical cross-linking: reagents and problems in studies of membrane structure. *Ann Rev Biochem* 46:523, 1977.

62. HARDY, P.M., NICHOLLS, A.C. and RYDON, H.N. *J Chem Soc Perkin Trans* 1:958, 1976.

63. FUJIMOTO, D., TAKAHIKO, M., ISHIDA, T. and HAYASHI, H. The structure of pyridinoline, a collagen crosslink. *Biochem Biophys Res Commun* 84:52, 1978.

Vol. 17
1980

65. QUIJANO, R.C., JAFFE, N.R., OTT, D. and NIMNI, M.E. Durability of the Hancock Bioprosthesis. In press, 1980.

64. FERRANS, V.J., SPRAY, T.L., BILLINGHAM, M.E. and ROBERTS, W.C. Structural changes in glutaraldehyde-treated porcine heterografts used as substitute cardiac valves. *Am J Cardiol* 41:1159, 1978.

Vol.
198

BIORHEOLOGY Vol.17, pp. 83-94 0006-355X/80/010083-12$02.00/0
© Pergamon Press Ltd. 1980. Printed in the United States

THIRD INTERNATIONAL CONGRESS OF BIORHEOLOGY

SYMPOSIUM ON SOFT TISSUES AROUND A DIARTHRODIAL JOINT

STRUCTURE AND MECHANICAL PROPERTIES OF RAT TAIL TENDON

D. F. Betsch and E. Baer

Department of Macromolecular Science
Case Institute of Technology
Case Western Reserve University
Cleveland, Ohio 44106

(Received 7.12.1979. Accepted by Guest Editor S. Woo)

Vol. 17
1980

INTRODUCTION

Connective tissue takes part in the structure of most organs, and the main protein component of such tissue is collagen. Collagen is produced extracellularly by fibrocytes which extrude amino acids into a mucopolysaccharide matrix. The basic unit formed in this way is the three-stranded tropocollagen molecule.

After the formation of tropocollagen, this protein takes no part in metabolism; it is inert. The amino acids do not exchange and the macromolecules are not broken down and renewed. Consequently, collagen has a property unique among proteins - it ages. Aging of collagen has been an active area of research for many years.

This work will deal with only rat tail tendon (hereafter RTT). RTT is a very convenient connective tissue specimen from the standpoint of availability and ease of sample collection. Experiments with RTT were done to characterize its structure and properties as early as 1954; it has been used in surgery and medicine since before 1900.

The object of this paper is to describe the currently accepted hierarchical structure of RTT and relate this structure to various mechanical properties.

STRUCTURE

Several chemical substances comprise tendon; among these are the protein collagen, the polysaccharides chondroitin sulfates B and C, hyaluronic acid, various proteoglycans, cellular materials, and water. The complexity of the tissue is further increased by a hierarchical organization of structures. This section describes the structural aspects of RTT as they are presently understood.

Water comprises about 65% of the native wet weight of RTT (1,2) depending on the age of the specimen and method of determination. Water associates with the collagen helix, polar side chains, and the matrix material and is described respectively as structural, bound, or free (3). Four states of water identifiable by calorimetry are non-freezeable water, freezeable water with heat and temperature of fusion different from those of bulk water, freezeable water with only the temperature of fusion different from that of bulk water, and freezeable water which is indistinguishable from bulk water (4). Much work has been done to understand the role of water in connective tissues (5,6).

The most important structural component of RTT is the protein collagen, which represents nearly 99% of the tendon dry weight (7). Three 10_3 left-handed helical collagen chains, two $\alpha 1$ type and one $\alpha 2$ type, combine to form a right-handed triple-helical tropocollagen molecule. Tropocollagen has a molecular weight about 300,000, length about 280 nm, and diameter about 1.5 nm (8).

The primary structure of the 1,052 residues in the $\alpha 1$ chain and about half of the residues in the $\alpha 2$ chain has been solved (9). Little variation in the sequence occurs among tendons from different species, and the salient features are as follows. The helical region of the chains contains 1011 residues, and 9-25 residues at each terminus are in non-helical regions. Every third residue, without exception, is glycine. If the sequence were represented as Gly-X-Y, then proline or hydroxyproline fills position X perferentially. The complete residue composition approximates 33% glycine, 22% proline or hydroxyproline, 11% alanine, 22% polar residues, and 12% miscellaneous (6). Various hydrophopic, hydrophilic, and covalent interactions are possible with such a primary structure, and these interactions are partly responsible for the hierarchical aggregation of tropollagen molecules.

The matrix, or ground substance, of RTT is responsible for less than 1% of the dry weight (10). Consequently, characterization of the ground substance lags behind that of the collagen. It is known that chondroitin sulfates B and C, hyaluronic acid, and proteoglycans are present in the matrix (17). Achilles tendon contains albumin, transferrin, haptoglobin, hemopexin, γ-globulin, and a glycoprotein called mucoid 2 (11). Such an elaborate analysis of the ground substance of RTT is not available, but is expected to be similar.

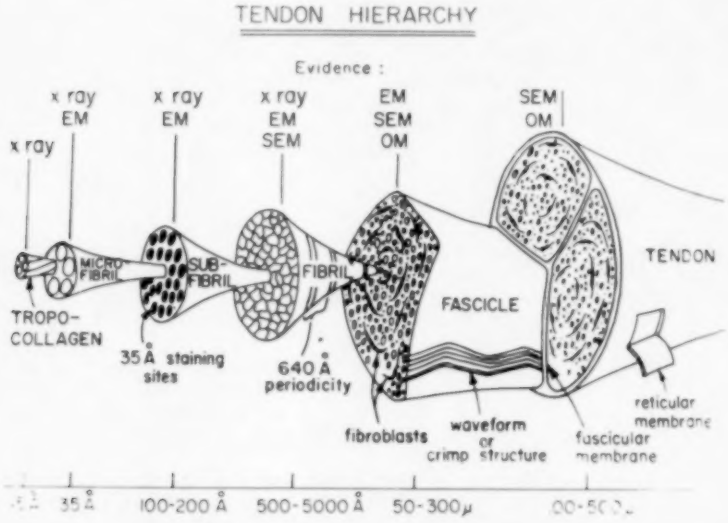

FIG. 1

Hierarchical Organization of Tendon (30)

These tendon components assemble in a multi-level structural hierarchy (12) (fig.1). The study of structure-property relationships is consequently more difficult and interesting. Although the term "collagen" has been applied to each level of organization, there are structure and proeprty variations from one level to the next.

Structure on the molecular level has already been discussed. Essential features at this lowest level of organization are the single collagen chain with sequence $(Gly\text{-}X\text{-}Y\text{-})_n$ and the tropocollagen triple helix with length 280 nm and diameter 1.5 nm. To form the next higher level of organization, five tropocollagen molecules are intertwined in a slow helical twist and are staggered by roughly one fourth their length along the fiber axis (13). This so-called "microfibril" has a diameter of 35Å and has been reported in longitudinal sections, stained cross-sections, and freeze-fractured specimens of RTT (14).

A level only recently included in this scheme is the "subfibril" of 10 to 20 nm diameter. Eveidence for this classification has come from chemically or mechanically disrupted material and from embryonic tissue (14). X-ray diffraction evidence of a subfibrillar level has been reported in the case of native RTT (12).

The next higher entity, the "fibril", encompasses a range of diameters from 50-500 nm and is the level of the familiar 65 nm (67 nm wet) periodicity in EM or X-ray (14). This banding pattern is thought to be caused by the quarter stagger arrangement of tropocollagen molecules within the microfibril and be preserved by appropriate packing at the higher structural levels. Fibrils also show crimped waveform. The crimped fibrils, together with the ground substance, form the next larger assembly, the "fascicle". Fascicle diameters between 80 and 320 μm are common with a distribution maximum for mature RTT at 200 to 240 μ (14). There is approximate cylindrical symmetry in the packing of cirmped fibrils into fascicles. Occasional evidence for a reticular membrane around fascicles has been found.

The tendon itself is comprised of one to ten fascicles, though it is uncommon for this number to exceed four. Tendon diameters are between 200 and 600 μm with a distribution maximum about 350 nm for mature RTT (14). Tendon samples are easily removed from the rat tail and sometimes are surrounded by a reticular membrane (14,1).

Crimping

Much of the recent work in our laboratory on RTT has involved the study of the fibrillar crimped waveform. A survey of collagen from a wide variety of sources has shown that the waveform is present in many tissues, but only in tissues which are subjected to tensile stress (15). Furthermore, data from muscle contraction studies suggest that only the strain levels corresponding to crimped fibril straightening are biologically relevant in vivo.

Despite the ubiquity of crimping in collagenous tissue, the causes thereof are unknown. An early explanation relied on the contraction of elastin fibers within the collagen structure to generate the crimps (14). However, it is accepted that RTT is without elastin. Dale et. al. (7) have proposed that contraction of the mucopolysaccharide matrix, in which the fibrils are embedded, buckles the fibrils. Their model system, high-modulus fibers in a soft-elastic matrix, closely paralleled tendon morphology and properties. The major drawback of their model is that it incorporated a much larger fraction of matrix than is present in tendon. A "wedge dislocation" mechanism has been recently proposed, but lack of hard evidence relegates this proposal to only speculation (14).

From Gathercole and Keller (15) we have several features of crimping in biological tissues. Crimping occurs only in collagenous tissues which undergo biological strain, and seems to be a common phenomenon in biological fibrillar aggregates which include only a small fraction of matrix. Crimping is independent of collagen chain type, as the $(\alpha I)_2(\alpha II)_1$ type tropocollagen is found both in bone, which has no waveform morphology, and RTT and skin, which show crimping. In addition, fibril crimping has been observed in newborn RTT, so the origins of crimping are somewhere within the foetal development (16).

Vol. 17
1980

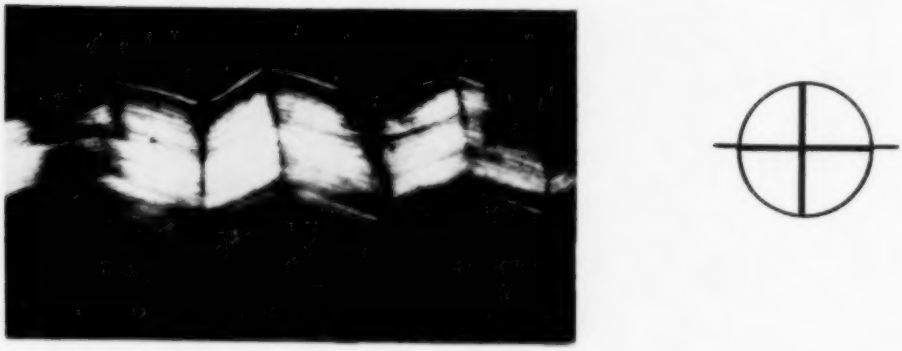

FIG. 2

Optical Micrograph of a Fascicle (120x) with Crossed Polarizers as Shown (17)

Polarizing optical microscopy has been the most important technique for studying the crimped morphology of intact, mature, wet RTT specimens (17) (Fig. 2). Diamant and coworkers deduced, from the behavior of the banding patterns with rotations about the microscope axis and tendon axis, that the arrangement of crimps is planar rather than helical, and that the crimp shape approximates a zig-zag rather than a sine curve. For specimens from mature rats, the wavelength of crimping is between 20 and 100 μm and the angle between the fibril and the tendon axis is between 15° and 20°. Straining the tendon decreases the crimp angle until, at some critical strain, the banding pattern disappears (Fig. 3). Teased and thereby disrupted tendons reveal fibrils with a wavy structure corresponding to the banding periodicity in the intact sample (Fig. 4).

Transmission electron microscopy has been used to verify the conslusions listed above (18). By sectioning samples at various angles, the planarity of crimping was confirmed. Additionally, the existence of sharp crimp apices was directly observed. Scanning electron microscopy of intact, freeze-dried tendons showed little information; however, teased specimens were seen as collections of flattened ribbons of parallel arrays of fibrils which had a waveform of the requisite dimensions (19).

A specially designed experiment allowed additional verification of these ideas by x-ray diffraction (20). Splitting of the reflections provided a "micro x-ray topography"

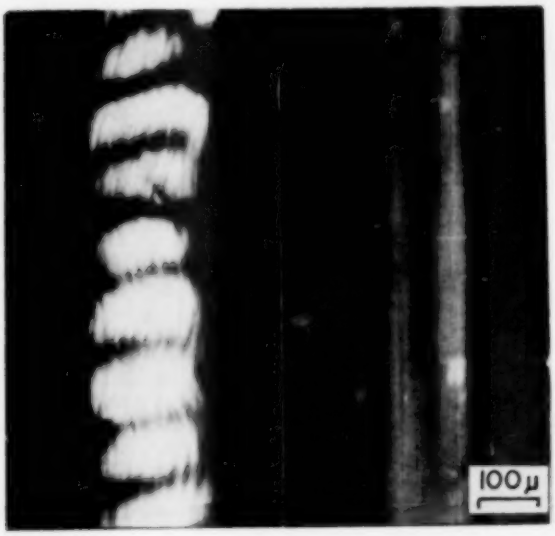

FIG. 3

Optical Micrographs of Tendon Fixed without Applied Tension (left) and with 1% Extension to Straighten Fibrils (right) (30)

FIG. 4

Fibril Bunch Separated from Fascicle Shows Planar Zig-zag Crimping (14)

technique for the 100 μm range. Crimp angles can be determined from the angle of the azimuthal split for the situation in which the beam is perpendicular to the crimping plane (Fig. 5). Previous workers in this area had chosen to avoid this splitting, which they considered problematic, by recording diffraction from stretched fibers (21).

Age Effects

An understanding of the aging process is an important motivation for much of the connective tissue research. A problem inherent in such research is to define a biological age of a specimen. Biological age has been assigned on the basis of tendon swelling (22), fatigue (23), solubility (22), chemical contraction (22), and thermal denaturation (24,25,26) experiments. Studies of aging have unfortunately clarified only the effects of aging rather than the causes, and without direct application of the results to living systems.

The difference betweeen aging and maturation ought to be clarified. Maturation refers to development from birth to sexual maturity, which occurs at 3-4 months in rats.

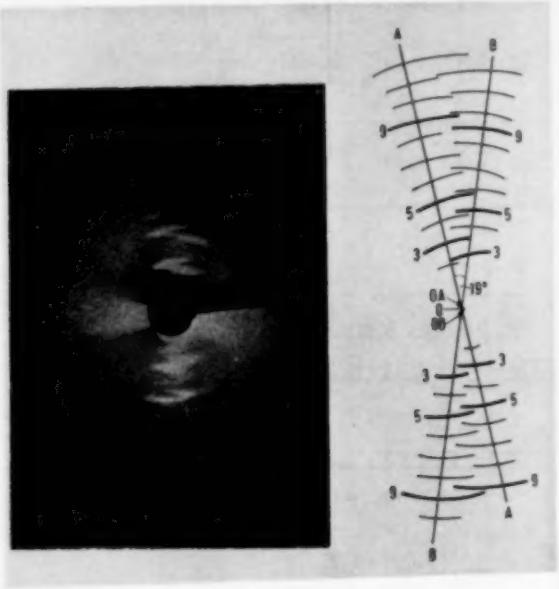

FIG. 5

Low Angle X-ray Diffraction of Rat Tail Tendon Unit
Photographed with X-ray Beam Perpendicular to the Crimp
Plane (left) and an Enlarged Tracing Thereof (right) (20)

Vol. 17
1980

Aging refers to changes in the animal after maturity has been reached. Age-growth related data will be discussed with this distinction in mind.

Cross-linking of the collagen chains, both intra- and intermolecular, is a well accepted effect of aging of RTT (22,26,27). The nature of these cross-links is not completely understood. From isometric melting experiments, evidence for aldimine cross-links between lysine ahd hydroxylysine residues that become more thermally stable with age has been proposed. Chemical reduction reactions have pointed to N-terminal aldehydes as cross-link percursors (28). In both of these series of experiments, the cross-link density was constant with age but the stability of cross-links increased.

Much is known about the changes in the hierarchical structure with aging. The cellular content of tendon is about 45% at birth, declines to 30% by 0.5 months, 10% by 1.5 months, and stabilizes about 3% at maturity (2). The 35 nm microfibrils have been described as loosely packed in new-born tendon and tightly packed in tendons older than 0.5 months. Several descriptions of the changes in the fibril diameter distribution with aging are available (2,29), one of which is presented in figure 6. After maturity, the fibril diameter does not change significantly; however, fusion of two fibrils into one irregularly shaped structure has been observed (2).

The crimp parameters, wavelength and angle, change with maturation and aging. Foetal RTT fibrils have crimp angles of 35 to 45° and wavelengths of 12 μm (16). Progressively smaller angles and longer wavelengths with maturation and aging are summarized in table 1. The increase in wavelength corresponds to the increase in tail length so that the number of crimps is constant (2000 ± 300) throughout the lifetime of the animal (17).

TABLE I

Values of Crimp Parameters, Length and Angle, for Tendons of Various Age (17)
Age of Animal Number of Samples

Age of Animal	Number of Samples	Wavelength (μm)	Crimp Angle (deg.)
2 wks.	9	21 ± 1	20.0 ± 0.5
3 wks.	7	46 ± 2	19.4 ± 1.4
2 mo.	5	64 ± 5	18.6 ± 0.5
5 mo.	6	86 ± 5	17.5 ± 0.7
13 mo.	5	92 ± 2	15.4 ± 0.5
29 mo.	4	110 ± 5	12.5 ± 1.5

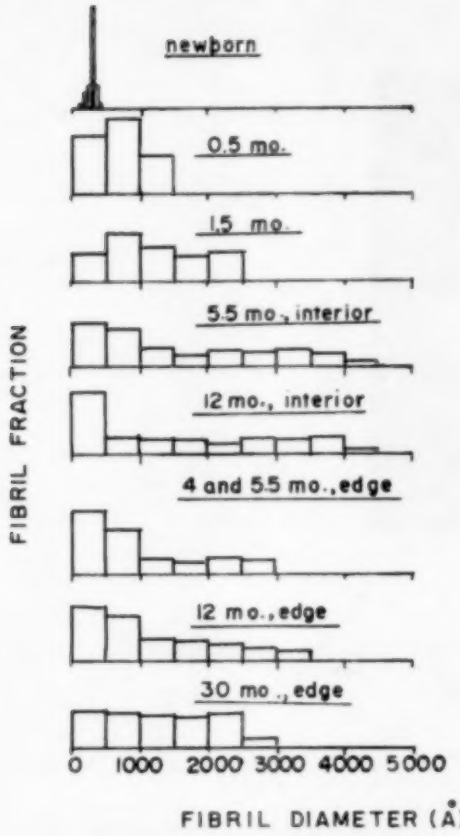

FIG. 6

Histograms of Fibril Diameter for Ages from Newborn to 30 Months. Total of 3,000 fibrils from RTT was Used (2)

STRUCTURE-PROPERTY RELATIONSHIPS

Because tendon serves as the link between muscle and skeleton, it must have a reasonably high modulus and toughness while simultaneously being able to flex at joints, absorb shock, and retract when muscles are relaxed. The multicomposite structure of tendon suits well these requirements. The mechanical and physical properties of RTT are important to the study of implant devices, theories of aging, and understanding of connective tissue generally.

The most frequently reported mechanical test has been tensile fracture, from which a stress vs. strain curve is constructed. A comparison of the work of various contributors is difficult, because of differences in age, strain rate, the definition of zero strain, and the equipment used. Results of tensile fracture experiments from Kastelic et. al. (30) are shown in Figure 7. Four regions are obvious on the curves for mature RTT; a "toe" region, linear region, and two yield regions. The strain rate was 8%/minute and zero strain was defined as the point at which the specimen was first pulled taut. Diamant (17) has published similar results for which the strain rate was 8%/minute and zero strain was defined as the tightest sample position that maintains the native banding structure under crossed polaroids. Again four regions can be identified for mature rats. The results of Nathan (31) and Morein et. al. (32) are from experiments at 160%/minute strain rate with zero strain being the point of the first needle deflection on the force recorder. Despite the huge difference in strain rate, the values for stress and strain at fracture fall within the same range (4.0 to 6.3 kg/mm^2 at 12 to 14% strain). These latter two curves display only one yield region however. Van Brocklin and Ellis (33) have reported increases in the linear modulus with increased strain rate.

Chvapil and Hruga (34) reported the fracture stress and strain of RTT at different loading rates. They found that the maximum fracture stress occurred over the loading range 600-1200 g/min and the maximum elongation occurred over the loading range 180-600 g/min. These values of load are not directly comparable to strain rate data, but a consideration of the average diameter of RTT and shape of the stress-strain curve shows that maximum strength of the tendon occurred between 8 and 16% per minute strain rate

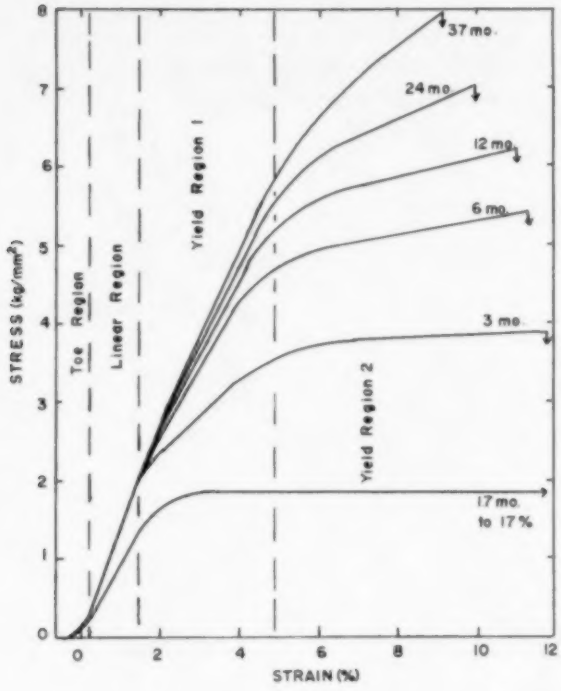

FIG. 7

Stress-strain Behavior as a Function of Age (30)

and maximum elongation was achieved with a 2 to 8% per minute strain rate. According to their data, a strain rate of 160%/minute would produce values of fracture stress and strain for lower than one half these maximum values, which is in conflict with the results from Kastelic, Diamant, Nature, and Morein listed above.

The significance of the "toe" region in the deformation experiment is recognized. Up to some critical strain, at which all fibrils are straight, there is a gradual decrease in the crimp angle. The linear region of the curves is thought to correspond to the elastic deformation of the fibrils. Within both yield regions the deformation is irreversible, which suggests that structural damage occurs at these strains. Mechanisms involving slippage of microfibrils and loss of cohesion between microfibrils are implicated to explain behavior in both yield regions (30).

Attempts have been made to describe the particular contributions of each structural component to the mechanical behavior. Dale (7) treated RTT with hyaluronidase and with trypsin; hyaluronidase-digestible material included hyaluronic acid and chondroitin sulfates C and possibly B; trypsin digestible material was non-collagen protein. He concluded that hyaluronidase-digestable material maintains cohesion within the 200 nm fibril and is critical for tendon strength and elasticity, and that trypsin-digestible material maintains lateral cohesion between fibrils and is not crucial to the strength or elasticity. Earlier work with the same enzymes was not conclusive because of difficulties with the precision of stress-strain data(10).

Water is very important to the mechanical properties of RTT. Recent experiments in our laboratory have shown that tendons, when dehydrated to 15% water, can reach fracture stress and strain values of over 40 kg/mm^2 and 20% respectively. The values exceed the maximum estimate for individual collagen fibrils of 15-30 kg/mm^2 (35). Interesting curve shapes and the disappearance of the "toe" region are other features of the work with dehydrated and only partially dehydrated RTT (fig. 8).

The linear modulus increases, the area of the hysteresis loop decreases, and the maximum stress in each cycle decreases for cyclic loading into the "toe" regions (2% strain) of RTT (Fig. 9). After ten cycles, for example, the modulus has increased by 20 to 40% (2). Rigby (36) has reported similar results together with additional evidence

Vol. 17
1980

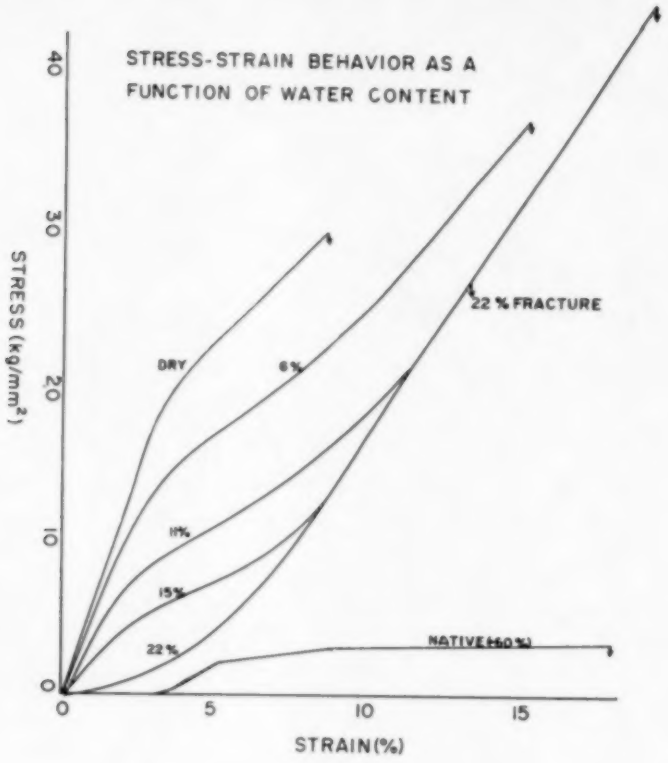

FIG. 8

Stress-strain Behavior of RTT as a Function of Water Content of the Tissue, from 3 Month Old Rats (unpublished results)

of sharpening of the x-ray diffraction pattern, and explained these results in terms of improved orientation. Periods of rest after cycling, for as long as fourteen hours, showed that the values of maximum stress and the hysteresis-loop area returned to their initial values (2).

When tendon is deformed into the linear regions, cyclic measurements indicate some changes in mechanical properties, but these are reversible after periods of rest. Crimp parameters do not change with cycling. Significant changes resulting from damage to the tendon structure do result from cycling into the first yield region, the most important of which is the decrease in linear modulus. Cyclic deformation into the first yield region also causes re-crimping, which is the appearance of smaller crimped waveforms superimposed on the initial waveform.

Rigby et.al. (37) conducted stress-relaxation measurements with RTT from 4-5 month old rats and plotted the data in terms of percentage change of stress as a function of log time. For RTT deformed and held at 3.5% strain, the stress leveled at 15% of the original value after 24 hours, with a linear region between 0 and 60 minutes and a second linear region after 60 minutes. RTT deformed and held at 7.5% relaxed to zero stress after 24 hours and the curve shape was different. Temperature changes affected the 3.5% samples in a reversible manner, but any change in stress level with changing temperature was permanent for the 7.5% samples. This relaxation behavior was not variable in the temperature range 0 to 37°C.

Hooley and Cohen (38) have modelled creep deformation for human digital flexor tendon with the assumption that the low-strain viscoelastic behavior of tendon results first from shearing of the matrix and then stretching of the straightened fibrils. By invoking a crimp angle distribution, they were able to model their experimental data. The general features of their results are that plots of isochronal creep strain and creep rate against stress bend downwards as stress increases. They observed that the non-linear viscoelastic behavior of tendon is opposite in several ways to that found for conventional polymers. We know of no such study for RTT, but would anticipate very similar results.

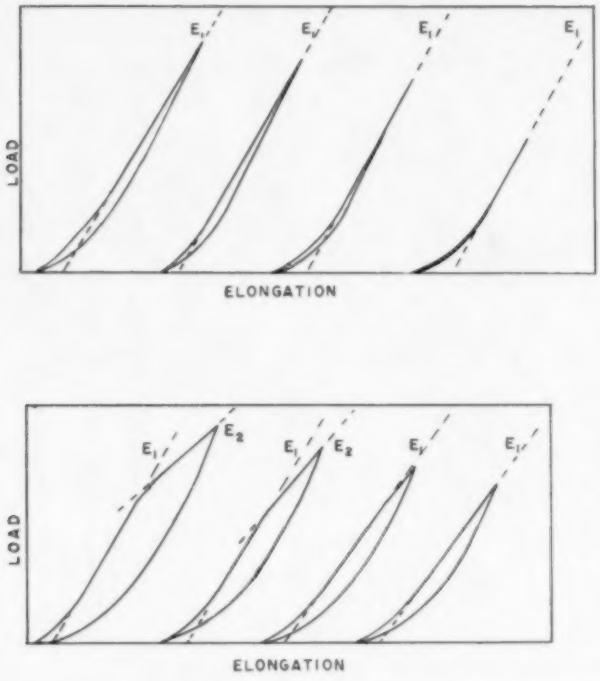

FIG. 9

Typical Cyclic Stress-strain Hysteresis Loops at Constant Maximum Strain for Deformation into the Linear Regions (above) and Yield Region (below) (2)

Age Effects

Some change in the mechanical properties is the result of the aging of tendon in vivo. The previously mentioned structural changes with age cause mechanical property changes, some of which we describe here. In figure 7 the increase of apparent modulus in both yield regions with age is depicted. These changes are due to increased inter-fibrillar interactions via-cross-linking, which hinder the principal damage mechanism, fibril dissociation. Additionally, it is important to notice that immature RTT shows only one yield region, and that the modulus of the linear region remains constant with age (30). These data are in accord with previous work (17). The effect of aging on the modulus is reasonable since deformation in the linear region is dominated by the collagen fibrils. Changes in fibril diameter which occur during maturation are responsible for the increase in modulus; after maturity, no fibril diameter increase occurs and consequently the modulus does not change.

Aged tendon responds to enzyme treatment in the same way as 3 month old RTT, but to a lesser degree (7). There is a loss of polysaccharides, especially hyaluronic acid, with aging and the remaining non-collagen components become more resistant to extraction.

Modelling the Stress-Strain Nonlinearity

Modelling of the stress-strain behavior has been almost entirely concerned with the "toe" region and crimped waveform. Early attempts have come from workers in the textile industry who concentrated on the behavior of single crimped fibers. Other models have made use of various non-morphological structural assemblies. Viidik (39) modelled tendon behavior with springs, dashpots, and slack elements. Lovin (40) reasoned that the waveform is induced by contraction of elastin fibers within the tendon; RTT is devoid of elastin fibers.

Diamant et. al. (8) defined a planar zig-zag with infinitely rigid apices so that the concepts of contilever bending could apply. Their results were quite good except in the case of high loads or young animals. Cominou and Yannas (41) considered both single isolated sinusoidal fibers and a composite of these. The fit was fair for isolated fibers but worsened when the composite was considered.

Vol. 17
1980

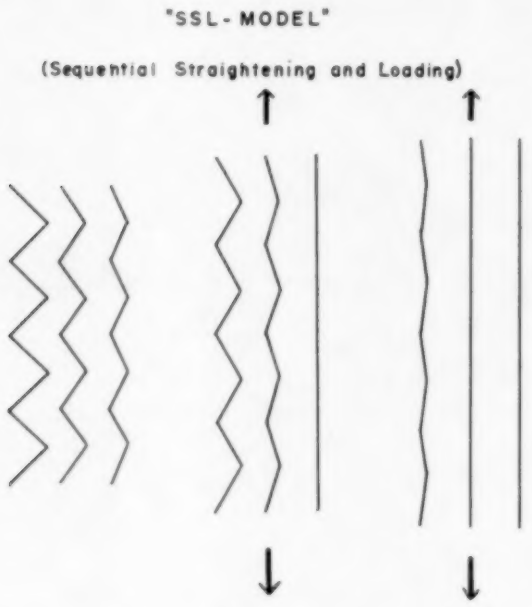

FIG. 10

The Mechanism of Resistance to Extension in the Sequential Straightening and Loading Model (14)

Kastelic (14) has proposed two models which assume a blunted zig-zag waveform. The first attributes the stress-strain non-linearity to elastic shear in the matrix. The second and more attractive proposal is that a range of crimp angles is present in tendon, and therefore, greater numbers of fibrils become straightened and bear load as the experiment progresses (figure 10). Crimped fibrils are assumed to have no resistance to strain. There is some evidence for a crimp angle distribution, and the closeness of the model fit makes this a reasonable proposal.

In the interest of the concise presentation, many details about RTT have been omitted. Crimping has been treated preferentially herein, as it has in recent literature, because of its significance to the mechanics of the living systems. The thrust of current research in this area is in applying in vitro data to the living system. One key to this comparison is the influence of water as a transport agent and property modifier. Another key is to further characterize the non-collagen components of tendon for a better understanding of the enzymatic processes which occur. Finally, emphasis is shifting to the causes of aging rather than the effects.

ACKNOWLEDGMENTS

This work is generously supported by NIH grant #00361-20.

REFERENCES

1. Yannas, I.V., and Huang, C., Fracture of Tendon Collagen, J. Polymer Sci., A-2 10, 577-584 (1972).

2. Torp, S., Ph.D. Thesis, Structure-Property Relationships in Tendon, Case Western Reserve University (1974).

3. Nomura, S., Hiltner, A., Lando, J.B., Baer, E., Interaction of Water with Native Collagen, Biopolymers 16, 231-246 (1977).

4. Haly, A.R. and Snaith, J.W., Calorimetry of Rat Tail Tendon Collagen before and after Denaturation: The Heat of Fusion of its Absorbed Water, Biopolymers 10, 1681-1699 (1971).

5. Elden, H., Physical Properties of Collagen Fibers, Int. Rev. Conn. Tiss. Res. 4, 238-348, (1968).

6. Ramachandran, G.N., Molecular Structure of Collagen, Int. Rev. Conn. Tiss. Res., 1, 127-182, (1963).

7. Dale, W.C., Ph.D. Thesis, A Composite Materials Analysis of the Structure, Mechanical Properties, and Aging of Collagenous Tissues. Case Western Reserve University (1974)

8. Diamant, J., Keller, A., Baer, E., Litt, M., and Arridge, R.G.C., Collagen; Ultrastructure and its Relation to Mechanical Properties as a Function of Aging, Proc. R. Soc. Lond. B180, 293-315 (1972).

9. Fietzek, P., and Kuhn, K., The Primary Structure of Collagen, Int. Rev. Conn. Tiss. Res. 7, 1-60, (1976).

10. Partington, F.R., and Wood, G.C., The Role of Non-collagen Components in the Mechanical Behavior of Tendon Fibers, Biochim.et Biophys. Acta 69, 485-495 (1963).

11. Anderson, J.C., Glycoproteins of the Connective Tissue Matrix, Int. Rev. Conn. Tiss. Res., 7, 251-322 (1976).

12. Baer, E.,Gathercole, L.J., and Keller, A., Structure Hierarchies in Tendon Collagen; an Interim Summary,J.Colston Papers 26, 189-195 (1975).

13. Miller, A., and Wray, J.S., Molecular Packing in Collagen, Nature, 238, 437 (1971).

14. Kastelic, J., Ph.D. Thesis, Structure and Mechanical Deformation of Tendon Collagen, Case Western Reserve University (1979).

15. Gathercole, L.J., and Keller, A., Light Microscopic Waveforms in Collagenous Tissues and the Structural Implications, Colston Papers, 26, 153-187, (1975).

16. Gathercole, L.J., and Keller, A., Early Development of Crimping in Rat Tail Tendon; A Polarizing Optical and SEM Study, Micron 9, 83-89, (1978).

17. Diamant, J., Master's Thesis, Ultrastructural-Mechanical Property Relationships in Collagen, Case Western Reserve University (1970).

18. Dlugosz, J., Gathercole, L.J., and Keller, A., Transmission Electron Microscope Studies and Their Relation to Polarizing Opitcal Microscopy in Rat Tail Tendon, Micron, 9, 71-82 (1978)

19. Gathercole, L.J., Keller, A., and Shah, J.S., The Periodic Wave Pattern in Native Tendon Collagen; Correlation of Polarizing with Scanning Electron Microscopy, J. Micro., 102, 95-106, (1974).

20. Gathercole, L.J., and Keller, A., X-ray Diffraction Effects Related to Superstructure in Rat Tail Tendon Collagen, Biochim. et. Biophys. Acta 535, 253-271 (1978).

21. Cowan, P.N., North, A.C.T., and Rondall, J.T., X-ray Diffraction Studies of Collagen Fibers, Symposia of the Society for Experimental Biology, 9, 115-126 (1955).

22. Bartos, Fr., Aging of Collagen in Vitro, Gerontologia 13, 81-85, (1967)

23. Everitt, A.V., Olsen, G.G., Burrows, G.R., The Effect of Hypophysectomy on the Aging of Collagen Fibers in the Tail Tendon of the Rat, J. Geront, 23, 333-336, (1968).

24. Zs-Nagy, I., N-Toth, V., and Vezar, F., High Resolution Electron Microscopy of Thermal Collagen Denaturation in Tail Tendons of Young, Adult, and Old Rats, Conn. Tiss., 2, 265-272 (1974).

25. Rigby, B.J., and Mitchell, T.W., Effect of Some Alcohols on in Vivo and in Vitro Aged Collagen, Biochim et. Biophys. Acta 532, 65-70 (1978).

26. Mitchell, T.W., and Rigby, B.J., In Vivo and in Vitro Aging of Collagen Examined Using an Isometric Melting Technique, Biochim et. Biophys. Acta 393, 531-541, (1975).

27. Elden, H.R., Effect of Cross-linking by Formaldehyde on the Contraction-Relaxation of Rat Tail Tendon, Nature, 183-332, (1959).

28. Deshmukh, K., A Comparative Study of the Cross-linking Precursors Present in Rat Skin and Tail Tendon Collagen, Conn. Tiss. Res., 2, 95-100 (1974).

29. Parry, D.A.D., Barnes, G.R.G., and Craig, A.S., A Comparison of the Size Distribution of Collagen Fibrils in Connective Tissues as a Function of Age and a Possible

Vol. 17
1980

Relation between Fibril Size Distribution and Mechanical Properties, Proc. R. Soc. Lond. B203, 305-321, (1978).

30. Kastelic, J., and Baer, E., Deformation in Tendon Collagen, Society for Experimental Biology, 34th Symposium on the Mechanical Properties of Biological Materials.

31. Nathan, H., Goldgefter, L., Kobyliansky, E., Goldschmidt-Nathan, M., and Morein, G., Energy Absorbing Capacity of Rat Tail Tendon of Various Ages, J. Anat. 127, 589-593 (1978).

32. Morein, G. Goldgefter, L., Kobyliansky, E., Goldschmidt-Nathan, M., and Nathan, H., Changes in the Mechanical Properties of Rat Tail Tendon During Postnatal Ontogenesis, Anat. Embroyoe., 154, 121-124, (1978).

33. Van Brocklin, J.D., and Ellis, D.G., A Study of the Mechanical Behavior of Toe Extensor Tendons under Applied Stress, Arch. Phys. Med. and Rehab 46, 369 (1965).

34. Chvapil, M., and Hruga, Z., Physical and Physical-chemical Heterogeneity of Collagen Fibers from Rat Tail Tendon, Gerontologia, 6, 102 (1962).

35. Elliott, D.H., Structure and Function of Mammalian Tendon, Biol. Rev., 40, 392, (1965)

36. Ribgy, B.J., Effect of Cyclic Extension on the Physical Properties of Tendon Collagen and its Possible Relation to Biological Aging of Collagen, Nature, 202, 1073, (1964).

37. Rigby, B.J., Hirai, N., Spikes, J., Eyring, H., The Mechanical Properties of Rat Tail Tendon, J. Gen. Physio. 43, 265-283, (1959).

38. Hooley, C.J., and Cohen, R.E., A Model for Creep Behavior of Tendon, Int. J. Biol. Macro. in press.

39. Viidik, A., Functional Properties of Collagenous Tissues, Int. Rev. Conn. Tiss. Res. 6, 127, (1973).

40. Lanir, Y., Structure-Function Relations in Mammalian Tendon: The Effect of Geometrical Nonuniformity, J. Bioeng. 2, 119-128, (1978).

41. Cominou, M., and Yannas, I.V., Dependence of Stress-Strain Nonlinearity of Connective Tissues on the Geometry of Collagen Fibers, J. Biomechanics 9, 427-433, (1976).

Vol. 198

BIORHEOLOGY Vol.17, pp. 95-110 0006-355X/80/010095-16$02.00/0
© Pergamon Press Ltd. 1980. Printed in the United States

THIRD INTERNATIONAL CONGRESS OF BIORHEOLOGY

SYMPOSIUM ON SOFT TISSUES AROUND A DIARTHRODIAL JOINT

IMMOBILITY EFFECTS ON SYNOVIAL JOINTS THE PATHOMECHANICS OF JOINT CONTRACTURE

Wayne H. Akeson, David Amiel and Savio L-Y. Woo

Division of Orthopedics and Rehabilitation
University of California, San Diego
La Jolla, California 92093 U.S.A.

(Received 21.12.1979. Guest Editor's Contribution Invited by Editor-in-Chief A.L. Copley)

ABSTRACT The purpose of this paper is to review the present knowledge of the effects of immobility on fibrous connective tissue and to outline present theories about the pathogenesis of joint contracture. A severe disordering of connective tissue homeostasis appears when the diarthrodial joints are subjected to prolonged immobilization. Not only are bone, muscle and cartilage affected by disuse, but the fibrous connective tissue structures are functionally disturbed. We found that the tissues lose significant lubricating and buffering volume of water and glycosaminoglycan in concert with increased inter- and intra-molecular cross-links of collagen which resulted in joint stiffness. The potential application of D-penicillamine and 17β-estradiol in pharmacological doses are being investigated for the therapeutic manipulation of reduction of strength of contracture.

Vol. 17
1980

INTRODUCTION

The effects of reduced stress and motion on the homeostasis of bone and muscle are well known. The loss of muscle mass, termed atrophy of disuse, is obvious. The atrophy of bone secondary to disuse is observed by Orthopedic surgeons routinely on x-rays of limbs treated with casts for the management of fractures or major ligament injuries. The effects of immobility on soft tissues are less obvious, even though the process is intuitively recognized. Prolonged restriction of joint motion results in contracture, and the widespread recognition of contracture as the principal complication of fracture treatment using cast immobilization emphasizes the importance of the process and the need for its detailed understanding. The purpose of this paper is to review the present knowledge of the effects of immobility on fibrous connective tissue and to outline present theories about the pathogenesis of joint contracture.

PERIARTICULAR CONNECTIVE TISSUE COMPOSITION AND ORGANIZATION

Periarticular connective tissue consists mostly of the organic molecule collagen on a dry weight basis. Collagen represents approximately 80 percent of the total dry weight of tissues in tendon, ligament, and capsule, as well as fascia. Collagen is also the only tensile resistant protein in these tissues, with the exception of the presence of small amounts of elastin in some connective tissues. The other major constituents present in these connective tissues are water and proteoglycan. Together the water and proteoglycan create a gel-like material which acts as a lubricant and spacing buffer system between the collagen fibers. The water and proteoglycan impart very important viscoelastic properties to the composite. The cells involved in the fibrous connective tissue are almost entirely fibroblasts and fibrocytes, and in addition, there exists a network of small vessels with associated mesenchymal cells. However, the blood flow in most of these structures is not great. The structure of these fibrous connective tissues is highly specific and the variations in the structural details result in marked differences in the mechanical properties of each system. In this regard, the simplest structure to consider is the relatively linear pattern of aggregation seen in most tendons and collateral ligaments of the knee. Here the origin and insertion of the principal fibers conform to a relatively straight line. When any of the fibers are placed under tension, most of the rest of the fibers are also under tension. Under low magnification microscopy, the tendon and ligament structure is crimped (1). The effect of the crimp is to impart quasi-elasticity to the system. The crimp permits extension of several percent before the fiber is fully extended. This fact explains the difference in the stress-strain diagram between tendon and a single collagen fiber (2).

Other structures which conform to a spiral pattern are the cruciate ligaments. The effect of this type of arrangement is such that not all of the fibers are under tension at any one time. Therefore, under conditions of early failure, the fibers under maximum tension fail, while those under less tension do not, and incomplete failure is possible, as commonly seen in human cruciate ligament injuries. Even more complicated fiber arrangements which influence the physical properties are seen in structures such as the capsule of joints, where an analogy between the fiber orientation to fabric mesh has been suggested (3). The effect of this fiber pattern is to permit a relatively long "toe region" on the stress-strain diagram. An example of the effect of fiber weave is seen in the Chinese finger trap which is commonly used for upper extremity fracture treatment in the emergency ward. The finger trap device is made of small cables in a mesh-like configuration which, when placed under tension, causes the diameter of the trap to be reduced as the system lengthens.

In summary, while a single material, collagen is the major structural constituent of all connective tissues, the physical properties of these tissues may vary widely according to the configuration of the fibers. However, without independent fiber mobility, functional properties of structural aggregates are compromised. This point emphasizes an important principle of connective tissue rheology, i.e. the imperative of gliding freedom of individual fibers in order to maintain normal connective tissue mobility. The importance of the principle will be illustrated in the study of the contracture process.

PATHOLOGY OF JOINTS SECONDARY TO IMMOBILIZATION

The gross and microscopic changes in joint contracture described in experimental animal models are similar to those observed in human pathologic materials in most respects. These changes can be conveniently divided into 1) periarticular and synovial tissue changes, and 2) articular cartilage and subchondral bone changes.

1. Periarticular and synovial tissue changes

The consistent feature of the gross appearance of the periarticular and synovial tissues of immobilized joints is a fibro-fatty connective tissue proliferation within the joint space. In knee immobilization models, this phenomenon is seen prominently in the intercondylar notch, but is also observed in other joint recesses (4,5,6). The proliferative fibro-fatty connective tissue covers exposed intra articular soft tissue structures such as the cruciate ligaments and the under-surface of the quadriceps tendon. It also blankets the non-articulating cartilage surfaces. With the passage of time, adhesions develop between the exposed tissue surfaces as the fibro-fatty connective tissue is transformed into more mature scar. The proliferation of this type of tissue is relatively the same in such diverse species as the rabbit (5), rat (7), dog (8) and primate (5). Similar changes are also prominent in human posterior intervertebral joints (9) and in human knee joints (10).

2. Articular cartilage and subchondral bone

The changes which occur secondary to immobility affecting articular cartilage can be separated into those in non-contact areas, and those in contact areas. The changes in the non-contact areas are thought to be in part secondary to the fibro-fatty connective tissue proliferation described above. The ingrowth of connective tissue which fills the joint space soon covers the joint surfaces. In the rat model studied by Evans, et al (4) in which the process was evaluated on a progressive time base, there was coverage of the articular surfaces by thirty days. The connective tissue became more dense and adherent during the subsequent month and remained relatively constant thereafter. The surface cartilage cells gradually became confluent with the overlying connective tissue. By sixty days the tangential layer of cartilage cells was lost in many of the animals. There was consistent evidence of thinning of the cartilage grossly beginning peripherally where the adhesions first occurred. Fibrillation of the cartilage was also seen and variable loss of staining of matrix was observed. Staining changes were also described by Baker, et al (9) in human spinal facet joints after anterior spine fusion. These changes included first a zone of loss of staining around the cells peripheral to the cellular lacunae. Ultimately, loss of definition of lacunae occurred, and the cartilage cells became stellate with poorly defined margin. Such change in staining characteristics of cartilage matrix had been described much earlier by Reyher in 1874 (8). Baker, et al (9) described similar changes and termed them "Weichselbaum's space" (11). Parker and Keefer (12) observed this process in cartilage beneath rheumatoid pannus and proposed that it represented a metaplastic process of cartilage cells transformed into fibroblasts, a view which Baker, et al (9) endorsed.

In the contact areas, mild to severe changes of articular cartilage are observed depending on the rigidity of immobilization, the position of immobilization, and most important, the degree of compression (5,13,14). Typically, the mild changes consist of loss of intensity of staining of the matrix. In areas of greater compressive forces there

are varying degrees of destruction up to and including full thickness ulceration of cartilage with cellular distortion and necrosis, fibrillation of matrix, and erosion of matrix down to subchondral bone.

The major areas of alteration in the subchondral bone occur beneath cartilage lesions in joints immobilized sixty days or longer (4). Hyperemia in the subadjacent marrow spaces is noted with proliferation of fascular connective tissue. In some areas this tissue penetrated the subchondral plate and hindered the calcified layer of articular cartilage. Trabecular atrophy and resorption in the areas subadjacent to cartilage lesions are also seen. Subchondral cysts sometimes develop in this location in animals followed for longer periods.

OUR EXPERIMENTAL STUDIES OF SOFT TISSUE RESPONSE TO IMMOBILITY

The changes in joint structure and function in immobilized limbs have been the subject of considerable interest with respect to the underlying processes involved, and with respect to the possibility of modifying the responses through the use of drugs or hormones. In an experimental model designed to evaluate the soft tissues response to immobility in our laboratory, the hind limbs of dogs and rabbits were immobilized using internal fixation procedures for up to nine weeks, and the periarticular connective tissues were examined (15,16).

Description of the Rabbit Experimental Animal Model

The left knee of the rabbit was fixed in acute flexion by means of a 2.4 mm diameter, threaded stainless steel pin inserted through the mid-diaphysis of the tibia, passed posterior to the popliteal fossa, while remaining within the skin-fold of the leg. The pin was then bent and hooked over the proximal femur through a short lateral incision. A nut was then tightened against the tibia to force the knee into full flexion. (See Figure 1).

Vol. 17
1980

FIG. 1
A roentgenogram demonstrating the internal fixation used for immobilizing the knee of the experimental animal.

The right knee remained free to serve as the control. After nine weeks of fixation the animals were sacrificed. The joint was dissected and all muscle attachments to the knee were divided circumferentially 4 cm above and 3 cm below the joint line. (See Figure 2).

Biomechanical Changes in the Immobilized Knees

The knee contracture was assessed immediately after sacrifice utilizing an apparatus called "arthrograph" (see Figures 3a and 3b). The arthrograph is designed to measure the joint stiffness in knees in terms of a torque-angular deformation (T-θ) diagram (17). The knees of the experimental and control from each animan were mounted on the arthrograph and cycled at a frequency of 0.2 Hz. Two ranges of motion, five cycles each, were used in sequence: the first was 50° to 80°, and the second 45° to 95° of knee angles. Each cycle of flexion and extension was recorded on the X-Y recorder (Figure 4). Recording of the first cycle

of the contracture knee was particularly important because subsequent cycles required substantially less energy. In addition, the amount of torque required to extend the knee from 50° to 65° from acute flexion during the first cycle was also significantly higher than that of subsequent cycles (Figure 5 at $\theta = 65^{\circ}$). The significant increases in torque and area of hysteresis were used as measures of increase in joint stiffness or severity of joint contracture.

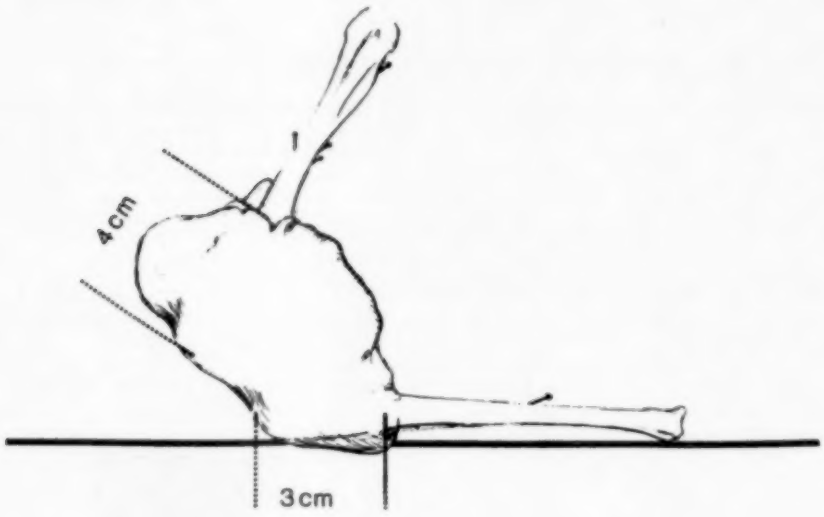

FIG. 2
An artist's view of the dissected rabbit knee specimen from the experimental animals.

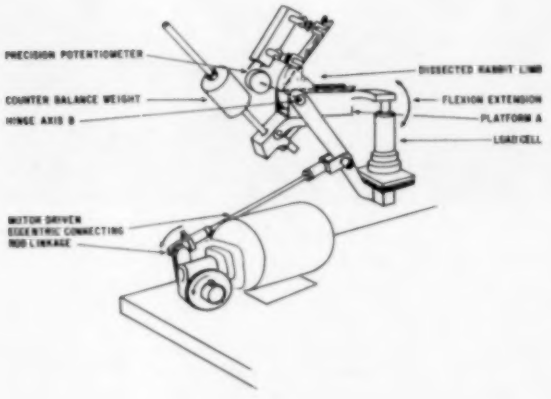

FIG. 3
A schematic diagram of the arthrograph system.

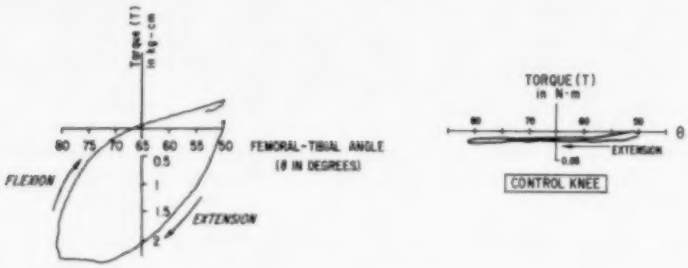

FIG. 4
X-Y recording of the typical torque-angular deformation (T-θ) diagram during the first cycle of extension-flexion of the rabbit knee. Note that the left diagram represents the 9-week immobilized knee and the right diagram represents the contralateral control, non-immobilized knee.

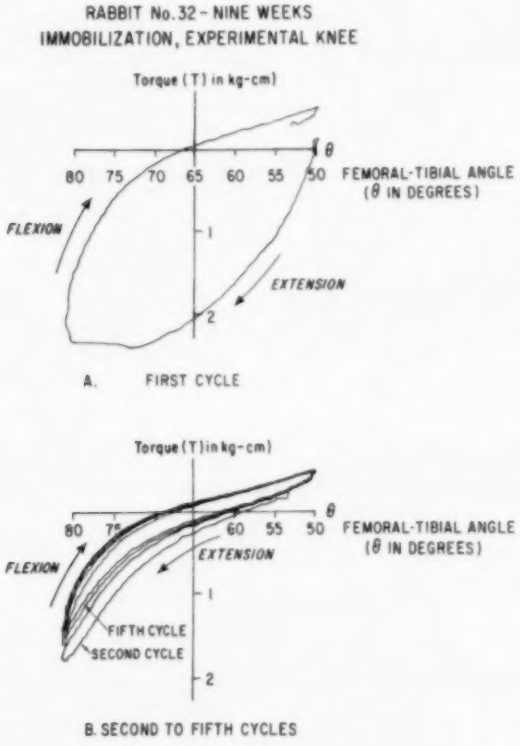

FIG. 5
X-Y recording of T-θ diagram of an experimental contracture rabbit knee showing the differences between the first and successive cycles.

PERIARTICULAR CONNECTIVE TISSUE COMPOSITION CHANGES

Periarticular connective tissues exist as discrete tendinous, ligamentous, fascial, capsular and synovial structures. As described earlier, these tissues share a composite nature consisting of collagen fibers plus an interstitial matrix of proteoglycan and water. Both elements of the structure are affected by stress deprivation. The matrix changes in the periarticular connective tissue from experimental limbs will be detailed, including alterations in the extracellular fluid volume, glycosaminoglycan content and collagen chemistry.

1. Extracellular fluid volume changes

The water content of fibrous connective tissues is in the range of 65 to 70 percent. As

Vol. 17
1980

the population of cells is relatively sparce in this tissue, the majority of this water is perforce in the extracellular space. On gross inspection, the dissected tissues from the immobilized limb appear less glistening and more "woody" in texture. Chemical analysis shows a statistically significant decrease in water content of 4 to 6 percent as compared to the control side (15,16). It seems likely that this amount of water loss is functionally significant. Fluid movement, which plays such an important role in articular cartilage load bearing and lubrication, is probably equally important in performing the same role in fibrous connective tissue. It has recently been established that hyaluronic acid and its attached or entrapped water is the principal fibrous connective tissue lubricant (18).

It is presumed that the interstitial fluid in a densely fibrous "connecting" anatomical structure serves as a spacer between individual collagen fibers or fibrils, permitting discrete movement of one fiber or fibril past the adjacent fibers. The importance of interstitial fluid to tissue rheology is obvious as the concept of viscoelasticity of connective tissue rests upon the dual fluid and solid nature of these systems.

2. Glycosaminoglycan changes

The largest change found in the composition of the stress deprived periarticular connective tissue is reduction in the concentration of glycosaminoglycans (GAG) (16,19). The decreases in chondroitin-4 and 6 sulfate (30%) and hyaluronic acid (40%) are statistically significant, while the percent change of dermatan sulfate thought to be associated with fibers is smaller. Decreased concentration of GAG and water would be expected to alter the plasticity and pliability of connective tissue matrices, and to reduce lubrication efficiency. Biochemical analyses of articular cartilage and meniscus from the experimental knees also show a reduction of 24 percent and 31 percent, respectively, of glycosaminoglycan content in these tissues (16). The total collagen remained unchanged.

Water content appeared to parallel the GAG ranges in concert with the known facts concerning the high water binding capacity of GAG. The preferential loss of GAG is also consistent with known facts about their rapid turnover half-life (1.7 to 7 days) (20, 21) as compared with collagen (half-life of 300 to 500 days) (22). Turnover studies utilizing tritium labeled acetate show that the decrement in specific activity of hyaluronic acid with time after preliminary labeling is the same for control and immobilized limbs. The conclusion is therefore that there is no acceleration of degradation, but rather, a reduction in the synthesis of hyaluronic acid in the immobilized extremities (23). The fibroblasts of the fibrous connective tissue matrix apparently respond to physical forces by a homeostatic feedback loop to maintain the proper balance of connective tissue constituents.

A gel-like structure created by the interaction between water and glycosaminoglycans is currently well accepted by physiologists working with interstitial fluid flow questions (24). Clearly, the gel structure is severely compromised in the connective tissue deprived of mechanical stimulation. It is postulated that the GAG and water changes are permissive in so far as qualitative changes in collagen are concerned, as fiber-fiber distances must be reduced when water and GAG volumes are reduced.

It is presumed that the lubricating and volume separating effects provided by hyaluronic acid and water permit the independent gliding of microfibrils past one another, facilitating the tissue adaptation to motion permitted by the particular connective tissue weave pattern. Loss of this volume separating and lubricating property provides for fibril-fibril friction as well as the potential for adhesions or cross-linking between adjacent collagen fibrils. Any newly synthesized collagen is apt to be randomly dispersed and to create interference with the functional gliding between fibers necessary for normal mobility. This is particularly so, since in the stationary attitude maturation processes may encourage fibril growth in diameter by including these newly synthesized random fibrils within the fiber structure of units. Such mismatch with respect to functional elongation needs and weave without regard to the usual physical force and motion may contribute to joint stiffness.

3. Collagen changes in joint contracture

The processes seen in the studies described above which rely on the techniques of anatomic pathology, suggest that connective tissue proliferation or simple granulation tissue production is the basis of joint contractures. However, collagen turnover studies are difficult to reconcile with this concept at first examination. For example, the studies by Brooke and Slack (25) showed that collagen precursor uptake was actually reduced in denervated rat limbs compared to controls. However, the collagen synthesis did proceed, but at a reduced level. Peacock (26) used saline solubility of collagen to estimate the amount of new collagen synthesized and found no differences in immobilized and control joints except for the posterior capsular area where there was increased collagen solubility. However, as he used pin fixation with a placement proximate to the posterior cap-

sule, the significance of finding total collagen mass changes became uncertain. Our laboratory was unable to demonstrate changes in total collagen by percentage or by total joint mass evaluation using the whole periarticular connective tissue unit (16). Recent studies of Klein (27) using long term labeling techniques which are more sensitive for this purpose, found small increases in collagen mass in the denervated limbs.

We feel, however, strategic placement of anomalous cross-links of newly synthesized collagen fibrils in the contracture process is of importance. These cross-links can act as bridges between existing functionally independent fibers with divergent tracking patterns. Using a simplified model, i.e., the Chinese finger trap mechanism, it can be seen that fixed contact at just a few nodal points defeats the functional gliding of the whole apparatus (Figure 6). Demonstration of such changes within the weave of the joint capsule is quite difficult because of right to left variability in micro-architecture and the small degree of change necessary to effect a mechanical impediment. However, it is easy to be convinced that such a process must play a role in the synovial joint contracture process. The disorganization which occurs in the cruciate ligament of a rabbit after nine weeks of immobilization is seen in Figure 7. The pattern of cellular alignment is obviously distorted, almost certainly reflecting a more random matrix organization.

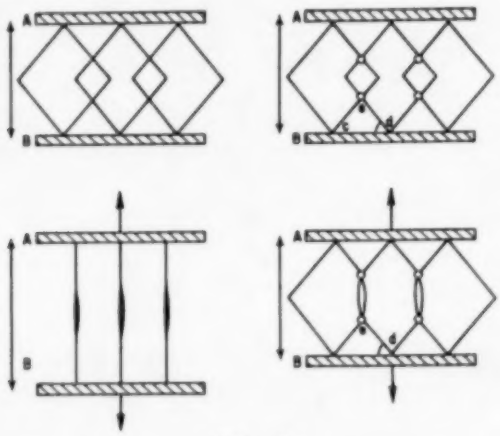

FIG. 6
A diagram showing the idealized weave pattern of collagen fibers. It can be demonstrated that fixed contact at strategic sites (e.g. points d and e) can severely restrict the extension of this collagen weave.

a. Collagen cross-link alterations

The studies of quantitative changes in the cross-linking of collagen from the immobilized rabbit knee periarticular connective tissue show significant increases in the sodium borohydride reducible intermolecular cross-links (28). A typical radioactive eltuion profile from column 1 of a 3N p-toluene sulfonic acid hydrolysate of $[^3H]NaBH_4$ reduced periarticular connective tissue from control and immobilized joints is shown in Figure 8, and the rechromatography on an extended basic column (column 2) of the aldolhistidine-dihydroxylysinonorleucine peaks show a two-fold increase in DHLNL on the immobilized side (Figure 9). It can be seen that dihydroxylysinonorleucine (DHLNL), hydroxylysinonorleucine (HLNL) and histidinohydroxymerodesmosine (HHMD) are the major cross-links which increase following immobilization (Table I). No change in hydroxylysine/lysine ratio between the immobilized and control periarticular connective tissue collagen is detected.

It can be speculated that the increased intra and intermolecular collagen cross-links are important in the contracture process. How do such cross-links interact at a molecular level? To begin with, it is unlikely that a fiber to fiber distance is bridged by a lysine-lysine or lysine-hydroxylysine reaction. The distances are much too great and the forces too small to create the nodal fiber to fiber cross-link which is proposed to hamper joint motion. Rather, it is presumed that the nodeal fiber to fiber cross-links are brought about by aggregation of new fibrils with preexisting fibers of the matrix. The process may proceed in the usual manner of aggregation of fibrils into fibers, then incorporating bridges of newly synthesized collagen fibril elements into pairs of existing fibers as illustrated in Figure 10. Such structures become mechanically constraining at the time when the joint is mobilized.

Vol. 17
1980

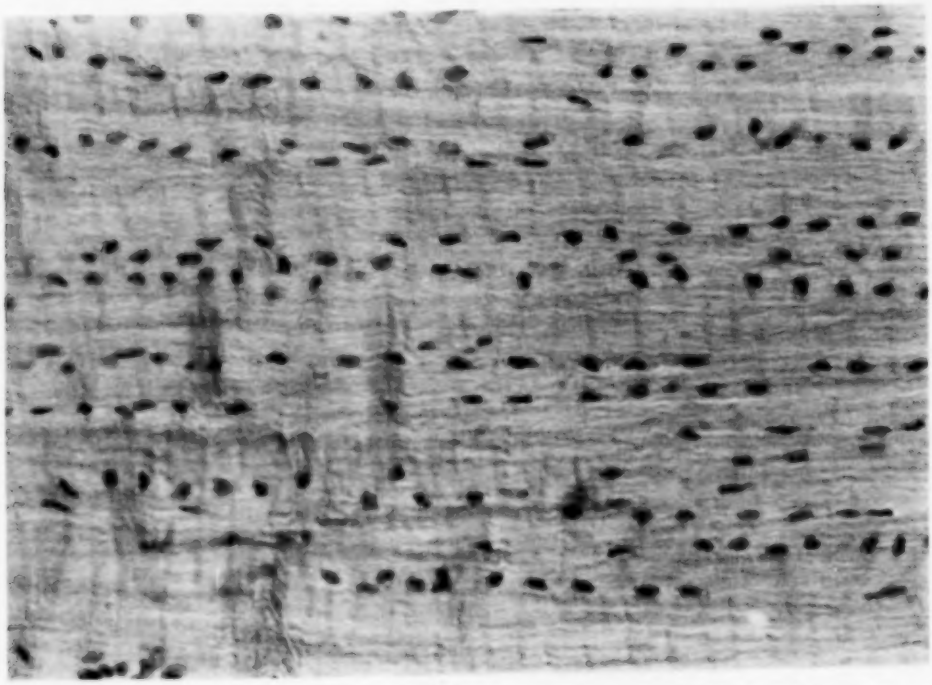

Anterior cruciate ligaments from contralateral control, non immobilized rabbit knee
(final magnification X 1,000)

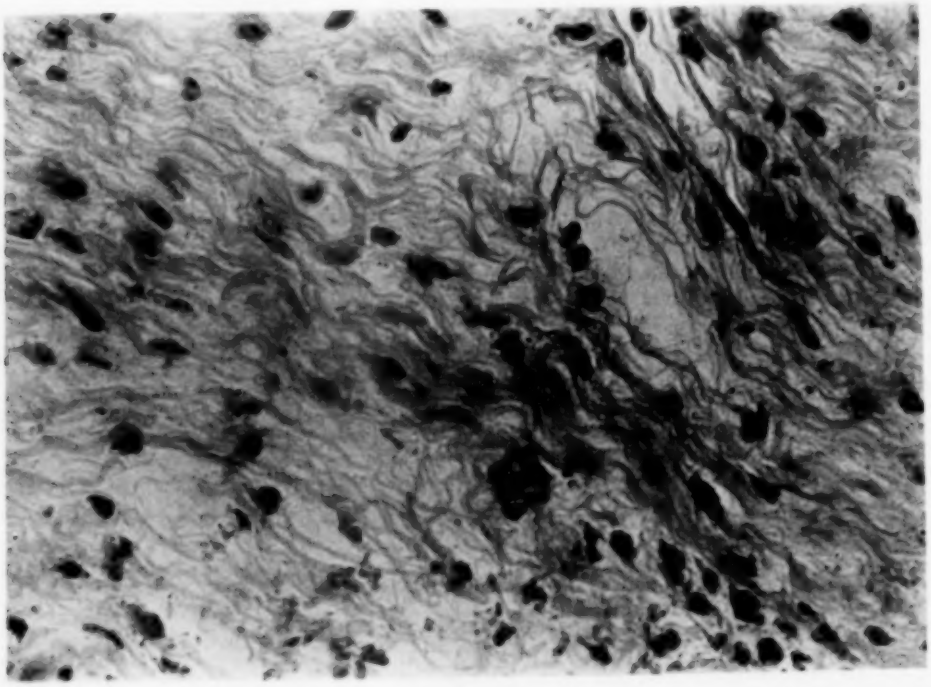

Anterior cruciate ligaments from 9-week immobilized rabbit knee
(final magnification X 1,000)

FIG. 7

Vol.
198

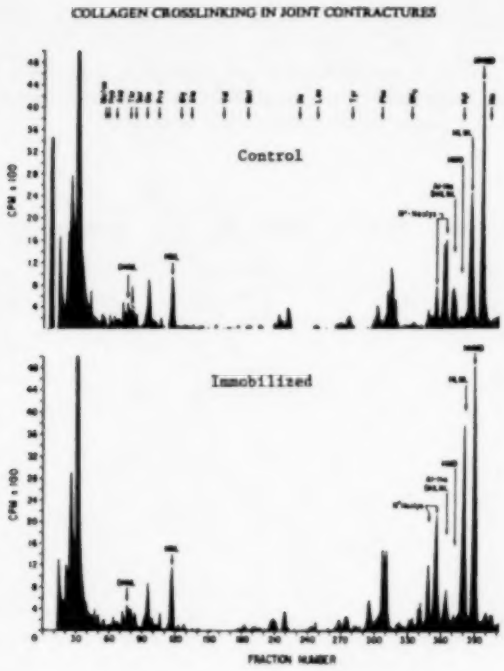

FIG. 8
Radioactive elution profile of a 3N p-toluene sulfonic acid hydrolysate of [^{3}H] $NaBH_4$ reduced collagen from control and immobilized periarticular connective tissue from rabbit knee. The abbreviatiations for the radioactive compounds are DHNL, dihydroxynorleucine; HNL, hydroxynorleucine; N^{ε}-hexlys, N^{ε}-hexosyllysine; Al-His, Aldol-histidine; DHLNL, dihydroxylysinonorleucine; HMD, Hydroxymerodesmosine; HLNL, hydroxylysinonorleucine; HHMD, histidinohydroxymerodesmosine.

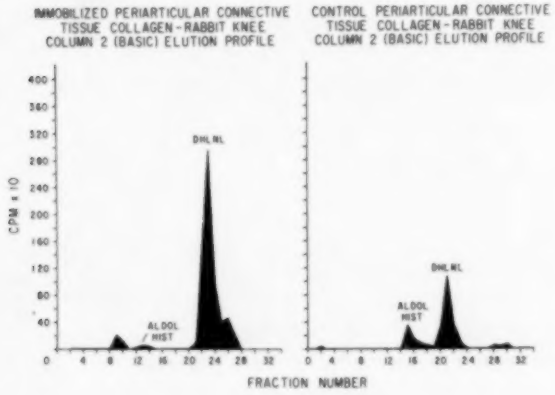
IMMOBILIZED PERIARTICULAR CONNECTIVE TISSUE COLLAGEN-RABBIT KNEE COLUMN 2 (BASIC) ELUTION PROFILE
CONTROL PERIARTICULAR CONNECTIVE TISSUE COLLAGEN-RABBIT KNEE COLUMN 2 (BASIC) ELUTION PROFILE
CPM x 10
DHLNL
ALDOL / HIST
FRACTION NUMBER

FIG. 9
Elution profiles of the aldol-histidine - dihydroxylysinonorleucine peak from the control and experimental periarticular connective tissue collagen rechromatographed on an extended basic column.

Vol. 17
1980

TABLE I

MEAN VALUES IN THE CHANGES IN THE REDUCIBLE CROSS-LINKS IN NORMAL AND IMMOBILIZED PERIARTICULAR CONNECTIVE TISSUE FROM RABBIT KNEES FROM 8 ANIMALS.

REDUCED CROSS-LINKS	E-C/C x 100	PAIRED T-TEST
HLNL	+ 49%	$p<.005$
DHLNL	+ 116%	$p<.005$
HHMD	+ 29%	$p<0.05$

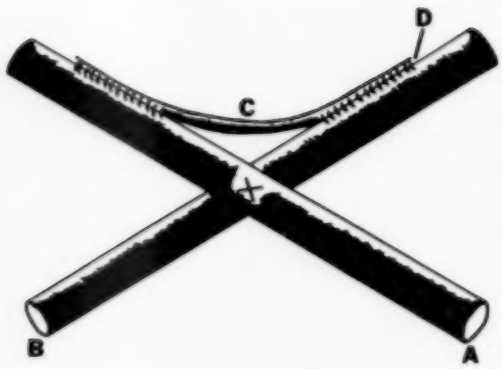

FIG. 10

An idealized model demonstrating the collagen cross-links interaction at the molecular level. Note that -

A and B - represent the preexisting fibers,

C - represents the newly synthesized fibril,

D - represents the cross-links created as the fibril becomes incorporated into the fiber, and

X - represents the nodal point at which adjacent fibers are normally freely moveable past one another.

b. Collagen typing changes

Since the formation of reducible cross-links follows collagen synthesis (29), and since the presence and relative amounts of these cross-links may in part depend on the type of collagen being synthesized (30), it is important to examine the type or types of periarticular connective tissue collagen synthesized during the period of immobilization. Examination of the densitometric scan of the SDS gel of the CNBr cleaved peptides from control and immobilized tissue reveals no alteration in the type of collagen being synthesized during the period of immobilization (31). One can see in Figure 11 that the peptides α_1 [III] CB(8&3) characteristic of type III collagen are absent in the CNBr digest of the control and immobilized periarticular connective tissue collagen. Furthermore, these results are confirmed by amino acid analysis and SDS gel electrophoresis performed on intact α components separated by CM cellulose chromatography. These results provide additional supportive evidence that only type I collagen is found in the dense fibrous structures of normal and contracture knees.

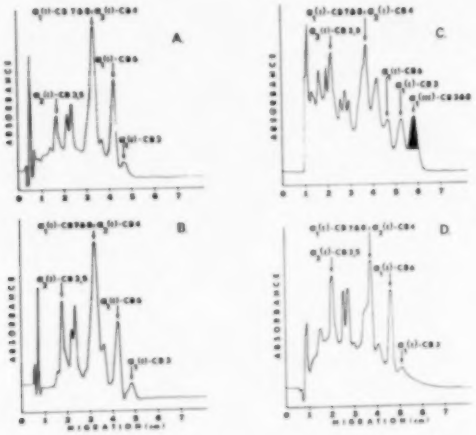

FIG 11
SDS gel electrophoresis of the CNBr peptide cleaved from -

A. PCT collagen from control knees.
B. PCT collagen from immobilized knees.
C. Types I & III (50% mixture) standard collagen.
D. Type I standard collagen.

Note that no type III collagen was present in the immobilized and control periarticular connective tissue collagen.

POTENTIAL THERAPEUTIC MANIPULATION OF CONTRACTURE DEVELOPMENT

Effects of 17β-estradiol on joint contracture

It has been postulated that the levels of water and GAG (hyaluronic acid, in particular) have a role in maintaining pliability, interfibrillar distance and lubrication in the periarticular connective tissue (17,18,32). In the study of the effect of 17β-estradiol on connective tissue from immobilized joints, our laboratory has shown that administration of 17β-estradiol is beneficial in the reduction of biomechanical measurements of joint stiffness (32). (See Figure 12). The 17β-estradiol appears to exert a protective effect against contracture on immobilized tissue by minimizing the loss of water and glycosaminoglycan. These results are consistent with studies on skin reported by other investigators (34-38).

It is thought that the lessening of joint stiffness observed in the 17β-estradiol treated animals may in part be due to maintenance of critical interfibrillar distance within the matrix by protection against loss of water and glycosaminoglycan. 17β-estradiol deserves further consideration as a therapeutic agent for short-term treatment of the female population in which injuries or diseases result in enforced immobilization and places them at risk for contracture.

Vol. 17
1980

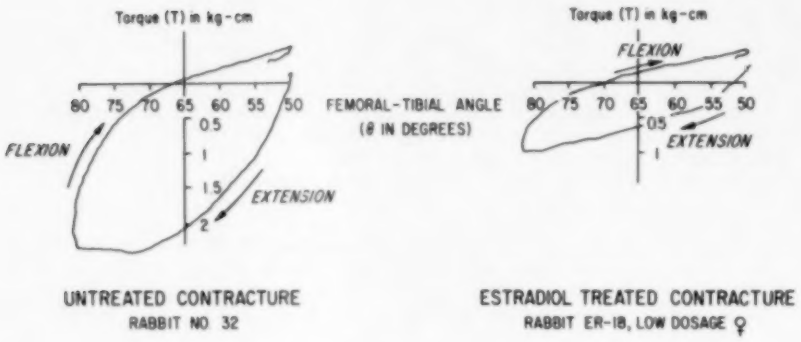

FIG. 12
The T-θ diagram during first cycle of extension-flexion of untreated and 17β-estradiol-treated rabbit knees after 9 weeks of immobilization.

Effects of D-penicillamine on joint contracture

Indirect evidence that D-penicillamine may interfere with the process of intermolecular cross-links has been demonstrated (39). It has been suggested that cysteamine and penicillamine form thiozolidine complexes with the lysine derived aldehydes, thereby preventing schiff base formation. Nimni (40) further suggests that D-penicillamine at low dosage acts primarily as a blocking agent of the aldehyde residues; whereas, at high doses it

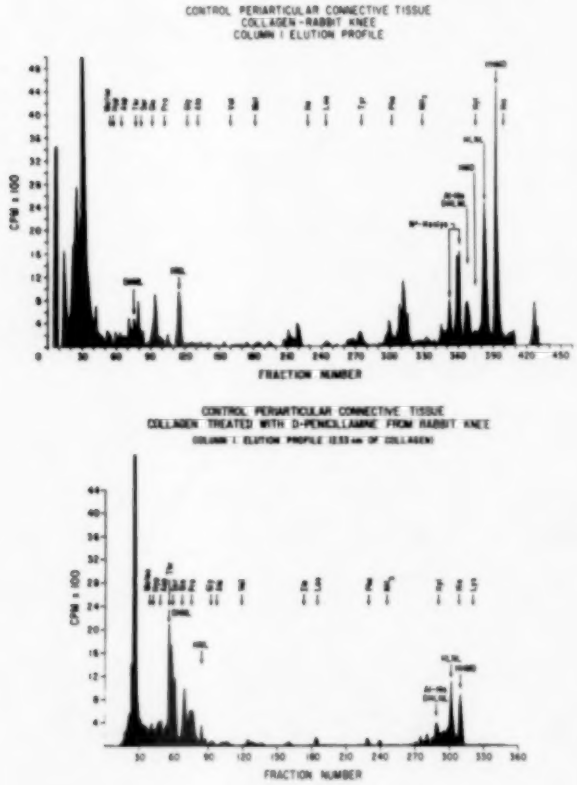

FIG. 13
Radioactive elution profile of a 3N p-toluene sulfonic acid hydrolysate of a $[^3H]$ $NaBH_4$ reduced control periarticular connective tissue collagen from rabbit knees. Note the significant reduction in the reducible cross-links as a result of D-penicillamine treatment.

also reduces the activity of lysyl oxidase which is involved in aldehyde formation. The potential of D-penicillamine as a therapeutic agent to inhibit the joint contracture process has been examined (41). Significant decreases in the formation of cross-links in the control and immobilized rabbit knees in the treated animals as compared to the untreated animals are found (Figures 13 and 14) when a dosage schedule of 60 mg/kg body weight three times weekly is used. D-penicillamine blocked the increase in DHLNL, HLNL and HHMD as previously demonstrated in immobilized rabbit knees. (See Table II). These data report evidence that penicillamine does inhibit schiff base formation and simultaneously promotes an increase in peptidyl aldehyde in rabbit connective tissue (41). Our work represents the first demonstration that in vivo administration of D-penicillamine directly inhibits the cross-linking reaction in collagen.

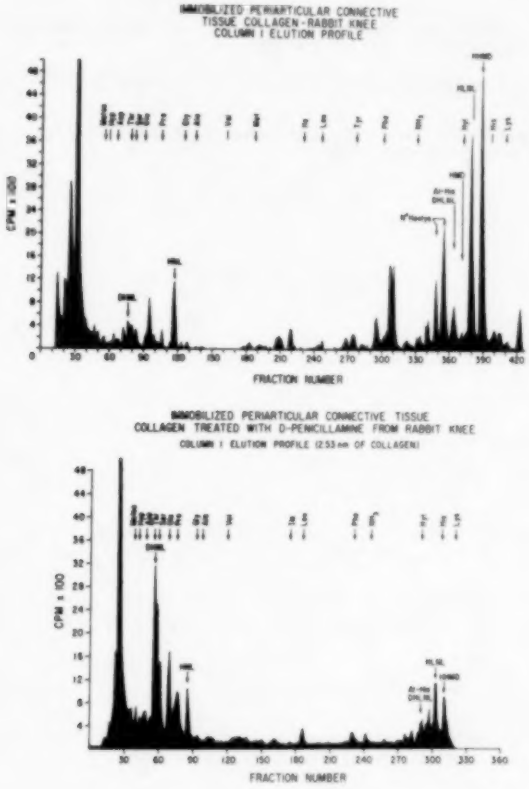
IMMOBILIZED PERIARTICULAR CONNECTIVE TISSUE COLLAGEN-RABBIT KNEE COLUMN I ELUTION PROFILE
CPM x 100
FRACTION NUMBER
IMMOBILIZED PERIARTICULAR CONNECTIVE TISSUE COLLAGEN TREATED WITH D-PENICILLAMINE FROM RABBIT KNEE
COLUMN I ELUTION PROFILE (2.53 mM OF COLLAGEN)
CPM x 100
FRACTION NUMBER

FIG. 14
Radioactive elution profile of a 3N p-toluene sulfonic acid hydrolysate of a $[^3H]$ $NaBH_4$ reduced immobilized periarticular connective tissue collagen from rabbit knees. Note the significant reduction in the reducible cross-links as a result of D-penicillamine treatment.

SUMMARY

We have reviewed the present status of understanding of the effects of stress and motion deprivation on diarthrodial joints. The biochemical, pathological and biorheological observations described indicate a severe disordering of connective tissue homeostasis when immobilization is enforced. Not only are bone, muscle and cartilage affected by disuse, but the fibrous periarticular connective tissue structures are functionally disturbed. Losses of significant lubricating and buffering volume of water and glycosaminoglycan in concert with increased collagen cross-links of DHLNL, HLNL and HHMD resulted in the increase of joint stiffness. New therapeutic modalities are on the horizon as a result of improved basic understanding of the contracture process. The application of drugs and hormones may offer hope in the modification of treatment for patients with high risk of joint contracture.

Vol. 17
1980

TABLE II

	E/C* PRECURSOR CROSS-LINKS+	E/C* CROSS-LINKS++
IMMOBILIZED 9 WEEKS (6 ANIMALS)	1.4 ± 0.4	1.5 ± 0.2
IMMOBILIZED 9 WEEKS PLUS D-PENICILLAMINE ADMINISTRATION (7 ANIMALS)	2.1 ± 0.5	1.0 ± 0.0

+ PRECURSORS PER NM OF COLLAGEN: DHNL, HNL
++ CROSS-LINKS PER NM OF COLLAGEN: DHLNL, HLNL, HHMD
* E=EXPERIMENTAL KNEE (IMMOBILIZED)
C=CONTROL KNEE((OPPOSITE LIMB)

RATIO OF MEAN VALUES IN THE CHANGES IN THE REDUCIBLE CROSS-LINKS AND PRECURSORS PER NANOMOLES OF COLLAGEN FROM-

a. CONTROL AND IMMOBILIZED PERIARTICULAR CONNECTIVE TISSUE IN RABBIT KNEE

b. CONTROL AND IMMOBILIZED PERIARTICULAR CONNECTIVE TISSUE IN RABBIT KNEE TREATED WITH D-PENICILLAMINE.

Ratio of mean values of the reducible cross-links and cross-link precursors per nanomoles of collagen from D-penicillamine treated and untreated rabbits.

ACKNOWLEDGMENTS

The authors gratefully acknowledge the sponsorship of NIH grants AM14918, AM00304 and GM24900 for this work.

REFERENCES

1. DIAMANT, J., KELLER, A., BAER, E., LITT, M. and ARRIDGE, R.G.C. Collagen: Ultrastructure and its relation to mechanical properties as a function of aging. Proc. Royal Society of London. B, Vol. 180, 293, 1972.

2. VIIDIK, A. and EKHOLM, R. Light and electromicroscopic studies of collagen fibers under strain. Z.A. anat. Entwickl. Gesch., Vol. 127, 154, 1968.

3. BULL, H.B. Protein structure and elasticity. In: Tissue Elasticity. J.W. Remington (Ed.) American Physiol. Society, Washington, 1957, pp. 32-42.

4. CLARK, D.D. and WECKNESSER, E. The influence of triamcinolone acetonide on joint stiffness in the rat. J. Bone and Joint Surg., 53A, 1390, 1971.

5. SALTER, R.B. and FIEL, P. The effects of continuous compression on living articular cartilage. J. Bone and Joint Surg., 42A, 31, 1960.

6. THAXTER, T.H., MANN, R.A. and ANDERSON, C.E. Degeneration of immobilized knee joints in rats. J. Bone and Joint Surg., 47A, 567, 1965.

7. EVANS, E.B., EGGERS, G.W.N., BUTLER, J.K. and BLUMEL, J. Experimental immobilization and remobilization of rat knee joints. J. Bone and Joint Surg., 42A, 737, 1960.

8. VON REYHER, C. On the cartilage and synovial membranes of the joints. J. Anat. Physiol. 8, 261, 1874.

9. BAKER, W.C., THOMAS, T.G. and KIRKALDY-WILLIS, W.H. Changes in the cartilage of the posterior intervertebral joints after anterior fusion. J. Bone and Joint Surg., 51B, No. 4, 737, 1969.

10. ENNEKING, W.F. and HOROWITZ, M. The intra articular effects of immobilization on the human knee. J. Bone and Joint Surg., 54A, 973, 1972.

11. WEICHSELBAUM, A. Die Feineren Veranderungen des Gelenk knorpels bei fungoser Synovitis und Caries der Gelenkenden. Virchows Archiv., 73, 461, 1878.

12. PARKER, F. and KEEFER, C.S. Gross and histologic changes in the knee joint in rheumatoid arthritis. Arch. of Path., Vol. 20, No. 4, 507, 1935.

13. GINSBERG, J.M. EYRING, E.J. and CURTISS, P.H. Continuous compression of rabbit articular cartilage producing loss of hydroxyproline before loss of hexosamine. J.

Bone and Joint Surg., 51A, 467, 1969.

14. TRIAS, A. Effect of persistent pressure on the articular cartilage. J. Bone and Joint Surg., 43B, 376, 1961.

15. AKESON, W.H. An experimental study of joint stiffness. J. Bone and Joint Surg., 43A, 1022, 1961.

16. AKESON, W.H., WOO, S. L-Y., AMIEL, D., COUTTS, R.D. and DANIEL, D. The connective tissue response to immobility: Biochemical changes in periarticular connective tissue of the immobilized rabbit knee. Clin Orthop. and Rel. Res., No. 93, 356, 1973.

17. WOO, S. L-Y., MATTHEWS, J.V., AKESON, W.H., AMIEL, D. and CONVERY, R. Connective tissue response to immobility. Correlative study of biomechanical and biochemical measurements of normal and immobilized rabbit knees. Arthritis and Rheumatism, Vol. 18, No. 3, 257, 1975.

18. SWANN, D.A., RADIN, E.L. and NAZIMIEC, M. Role of hyaluronic acid in joint lubrication. Ann. Rheum. Dis., 33, 318, 1974.

19. AKESON, W.H., AMIEL, D. and LA VIOLETTE, D. The connective tissue response to immobility. A study of chondroitin 4 and 6 sulfate and dermatan sulfate changes in periarticular connective tissue of control and immobilized knees of dogs. Clin. Orthop. and Rel. Res., 51, 183, 1967.

20. SCHILLER, S., MATTHEWS, M.D., CIFONELLI, J. and DORFMAN, A. The metabolism of mucopolysaccharides in animals. Further studies on skin utilizing C^{14} glucose, C^{14} acetate, and S^{35} sodium sulfate. J. of Biol. Chem., 218, 139, 1956.

21. SCHILLER, S., MATTHEWS, M.B., GOLFABER, L., LUDOWIEG, J. and DORFMAN, A. The metabolism of mucopolysaccharides in animal studies in skin utilizing labeled acetate. J. Biol. Chem., 212, 531, 1955.

22. NEUBERGER, A. and SLACK, H.G.B. The metabolism of collagen from liver, bones, skin and tendon in the normal rat. Biochem. J., 53, 47, 1953.

23. AKESON, W.H., AMIEL, D. and LA VIOLETTE, D. The connective tissue response to immobility; A study of hyaluronic acid turnover in periarticular connective tissue of control and immobilized knees of dogs. Biochemie et Physiologie du Tissue Confonctif. 1966, pp. 679-689.

24. GUYTON, A.C., BARBER, B.J. and MOFFATT, D.S. Theory of interstitial pressures. In: Tissue Fluid Pressure and Composition, Chapter 2. A. Hargens (Ed.), W.S. Wilkins, Co., Baltimore, Maryland. 1980 In Press.

25. BROOKE, J.S. and SLACK, H.G.B. Metabolism of connective tissue in limb atrophy in the rabbit. Ann. Rheum. Dis., 18, 129, 1959.

26. PEACOCK, E.E. Comparison of collagenous tissue surrounding normal and immobilized joints. Surg. Forum, 14, 440, 1963.

27. KLEIN, L., DAWSON, M.H. and HEIPLE, K.G. Turnover of collagen in the adult rat after denervation. J. Bone and Joint Surg., Vol. 59A, No. 8, 1065, 1977.

28. AKESON, W.H., AMIEL, D., MECHANIC, G.L., WOO, S. L-Y. and HARWOOD, F.L. Collagen cross-linking alterations in joint contractures: Changes in the reducible cross-links in periarticular connective tissue collagen after nine weeks of immobilization. Conn. Tissue Res., 5, 15, 1977.

29. BAILEY, A.J. and ROBINS, S.P. Development and matruation of the cross-links in the collagen fibers of skin. Frontiers of Matrix Biology, Vol. 1, 130, 1973.

30. JACKSON, D.S. and MECHANIC, G. Cross-link patterns of collagens synthesized by cultures of 3T6 and 3T3 fibroblasts and by fibroblasts of various granulation tissues. Biochemica and Biophysica Acta, 336, 1974.

31. AMIEL, D., AKESON, W.H., HARWOOD, F.L. and MECHANIC, G.L. Effect of nine week immobilization of the types of collagen synthesized in periarticular connective tissue from rabbit knees. Trans. of Orth. Res. Society, Vol. 5, 1980.

32. AKESON, W.H., WOO, S. L-Y., AMIEL, D. and MATTHEWS, J.V. Biochemical and biomechanical changes in the periarticular connective tissues of the immobilized rabbit knee. Conn. Tissue Res., Vol. 2, 315, 1974.

Vol. 17
1980

33. AKESON, W.H., WOO, S. L-Y., AMIEL, D., DOTY, D. and RUTHERFORD, L. Value of 17β-oestradiol in prevention of contracture formation. Ann. Rheum. Dis., 35, 429, 1976.

34. GROSMAN, N.E. Age dependence of the effect of oestrogenic treatment on the acid mucopolysaccharide pattern in the skin of mice. Acta Pharmacol. 31, 550, 1972.

35. SMITH, Q.T. and ALLISON, D.J. Study of the uterus, skin and femur of rats treated with 17β-oestradiol benzoate from one to twenty-one days. Acta Endocr. 53, 598, 1966b.

36. YANG, S.L., OKAMURA, H. and BEER, A.E. The effect of estrogen on collagen synthesis at the site of a skin autograft. Amer. J. of Obstet. and Gynec. 116, 694, 1973.

37. HENNEMAN, D.H. Effect of estrogen on in vivo and in vitro collagen biosynthesis and maturation in old and young female guinea pigs. Endocrinology, 83, 678, 1968.

38. SMITH, Q.T. and ALLISON, D.J. Changes of collagen content in skin, femur, and uterus of 17β-oestradiol benzoate treated rats. Endocrinology, 69, 486, 1966a.

39. NIMNI, M.E. A defect in the intramolecular and intermolecular cross-linking of collagen caused by penicillamine. J. Biol. Chem., 243, 1457, 1968.

40. NIMNI, M.E., DESHMUKH, K. and GERTH, N. Collagen defect induced by penicillamine. Nature, 240, 220, 1972.

41. AMIEL,D., AKESON, W.H., HARWOOD, F.L. and SCHMIDT. Effect of low dosage schedule of D-penicillamine on collagen cross-linking in a nine week immobilized rabbit knee. Conn. Tissue Res., 5, 179, 1977.

BIORHEOLOGY Vol. 17, pp. 111-123 0006-355X/80/010111-13$02.00/0
© Pergamon Press Ltd. 1980. Printed in the United States

THIRD INTERNATIONAL CONGRESS OF BIORHEOLOGY

SYMPOSIUM ON SOFT TISSUES AROUND A DIARTHRODIAL JOINT

DRAG-INDUCED COMPRESSION OF ARTICULAR CARTILAGE DURING A PERMEATION EXPERIMENT

W. Michael Lai and Van C. Mow
Department of Mechanical Engineering, Aeronautical Engineering & Mechanics
Rensselaer Polytechnic Institute
Troy, New York 12181

(Received 28.12.1979. Accepted by Guest Editor S. Woo)

ABSTRACT Linear and nonlinear theories are used to study the one-dimensional permeation problem of liquids flowing through soft tissues under applied pressure gradients. It is found that the strain field induced by the drag of permeation is nonuniform with respect to depth, causing nonuniform permeability in the tissue sample for which the permeability is to be measured. As a consequence, permeability experiments on soft, porous and permeable tissues can only measure their apparent permeabilities. The concept of "intrinsic" permeability is introduced to define the permeability of the tissue under an imposed, uniform clamping strain and a vanishly small imposed pressure gradient during a flow permeation experiment. Extrapolating from our experimental results for decreasing pressure gradients, we obtained the following intrinsic permeability function:

$$k_{intrinsic} = k_o \exp(M_o e)$$

where k_o and M_o are constants and e is the true strain. By using a nonlinear theory which incorporates the above intrinsic permeability function to describe the permeation experiment, we found that the dependence of apparent permeability on pressure gradient observed in our experiments can be predicted reasonably well by the theory. The results thus show that the intrinsic permeability function could be used to provide a better biphasic model whenever fluid flow becomes an important factor during the deformation of a soft, porous, permeable medium such as articular cartilage.

Vol. 17
1980

INTRODUCTION

Articular cartilage, a soft biomaterial, can be described as a composite organic solid matrix that is swollen by water. In normal, fully hydrated tissues, the fluid is fairly constant, ~ 85% by weight, for the upper 25% of the cartilage. With increasing depth, the degree of hydration decreases in a linear manner to ~ 70% [1]. However, these percentages may differ with the age, site in the joint and pathology of the specimen [2-6]. For example, it has been shown that cartilage, excised from the knee joints of dogs in which osteoarthritis (OA) has been experimentally induced, has a higher than average water content early in the development of OA lesions [4]. Such changes in volumetric porosity may have profound biomechanical implications in terms of tissue permeability [7] and joint lubrication and wear [8-13].

In this connective tissue, about 90% of the organic solid matrix is extracellular material, ~ 65% of which is collagen. In 1969, Miller and Matukas discovered that cartilage collagen is unusual in that it is composed of three α_1 chains [14,15], designated as type II, and that these fibrils are unable to form large fiber bundles. It is believed that this latter characteristic permits a maximum dispersion of the fibrils through the other major organic component, i.e., proteoglycans [2-6,16,17,18]. Cartilage collagen is also stronger than type I (bones, teeth and arterial walls), type III (embryonic tissues and scars), or type IV (synovium and basement membranes) collagen. Presumably, this is to enable the cartilage to sustain the large tensile stresses created within the tissue during joint articulation [19,20].

Cartilage collagen has a highly specific ultrastructural arrangement [18,20-25]. Most investigators regard the tissue as a layered medium composed of four separate histological and ultrastructural zones. The most superficial zone, the superficial tangential zone, is composed of sheets of tightly woven collagen fibers randomly oriented in the plane of the surface [18,21-25]. This zone has been determined biochemically to be more enriched in collagen than the remaining layers of the tissue [8]. The fibers of the middle zone are

Key Words: Theory, experiment, drag induced, compression, cartilage.

randomly oriented and homogeneously dispersed. The percentage of collagen by weight remains constant throughout the middle and deep zones of the tissue [8]. In the deep zone, the random fibers from the middle zone are partially anastomosed to form larger, radially oriented bundles. These bundles of fibrils cross the deep zone and insert into the calcified zone across the tidemark - the regular but wavy demarcation between the noncalcified zone and the calcified zone of cartilage [26]. In the calcified zone, the bundles of fibrils branch repeatedly to form an interlocking network of fibrils that serve to anchor the tissue to its bony substrate. A schematic representation of this ultrastructural arrangement is shown in Fig.1.

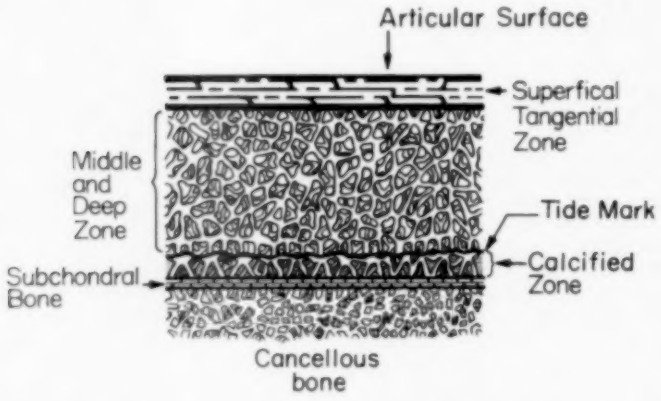

FIG.1

A Schematic Representation of Articular Cartilage's Collagen Ultrastructure as a Function of Depth (Mow, Lai and Redler [24].)

Proteoglycans constitute the other major organic component of the solid matrix. The conformation and physical properties of these polydispersed macromolecules, consisting of 50 to 100 glycosaminoglycan chains covalently bonded at the serine residues to a protein core, are of paramount importance to the biomechanical function of the tissue. The glycosaminoglycans making up the proteoglycan subunits (PGS) are chondroitin 4-sulfate (N-acetyl-galactosamine with an SO_4^{--} on the 4-carbon position and glucuronic acid), chondroitin 6-sulfate (N-acetyl-galactosamine with an SO_4^{--} on the 6-carbon position and glucuronic acid) and to a lesser degree - ~ 10% of the total polysaccharide content - keratan sulfate (N-acetyl-glucosamine with an SO_4^{--} on the 6-carbon position and galactose) [5,27,28]. In cartilage, many proteoglycan subunits are bound to a linear chain of hyaluronic acid (which comprises < 1% of the dry weight of the tissue) to form an enormous proteoglycan aggregate (PGA) with a molecular weight ranging up to 200 million. Two protein link components are also bound to the aggregate and appear to increase its conformational stability. The binding of the proteoglycan subunits to hyaluronic acid involves a specific site on the polypeptide backbone, the globular end, which has a high affinity for certain specific sites on the hyaluronate [29].

In the tissue, the carboxyl and sulfate groups of the proteoglycan aggregate endow it with a polyanionic characteristic. Maroudas, Muir and Wingham [30] determined the correlation of the negative fixed charged density in articular cartilage with its glycosaminoglycan content and found that it generally increases with depth from the articular surface. Because of these negatively charged groups on the glycosaminoglycan chains, the proteoglycan aggregates always seek their maximum solvent domain. In cartilage this is mediated by the large volume of interstitial water. Being hydrophilic, highly charged and immobilized in the fine collagen network, the proteoglycans impede fluid flow and resist the compressive loads of joint articulation. Presumably, the biomechanical function of the hyaluronate is to aggregate the proteoglycans and immobilize them in the extracellular material [5]. The exact nature of these interactions, i.e., collagen-proteoglycan aggregate interactions, proteoglycan-proteoglycan interactions, etc., is not known. It is known, however, that the proteoglycan aggregate-collagen matrix behaves, in a mechanical sense, like a soft, porous and permeable solid material. A schematic representation of this molecular model of articular cartilage is shown in Fig.2a.

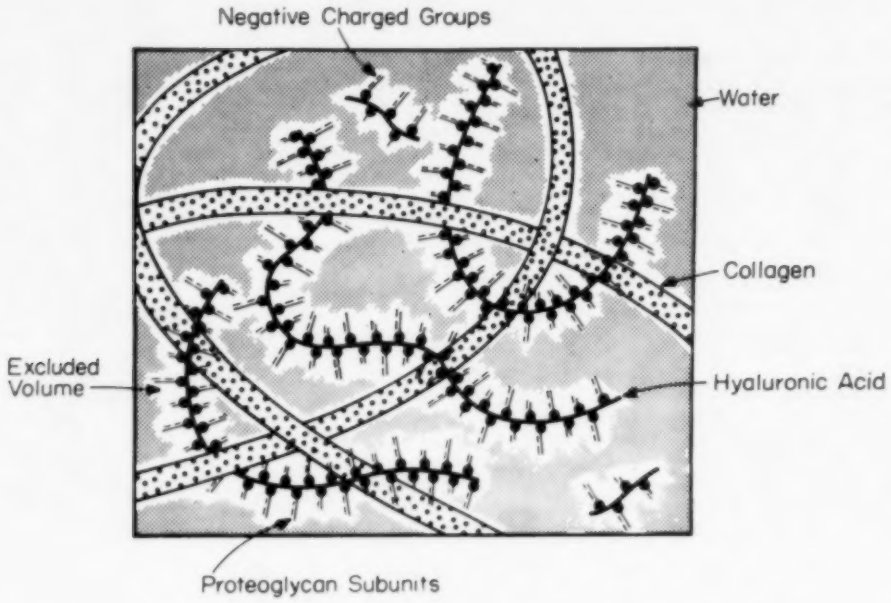

FIG. 2a

A Model Depicting the Dispersion of Collagen/Proteoglycan Organic Matrix Throughout Water (Mow and Lai [13].)

Vol. 17
1980

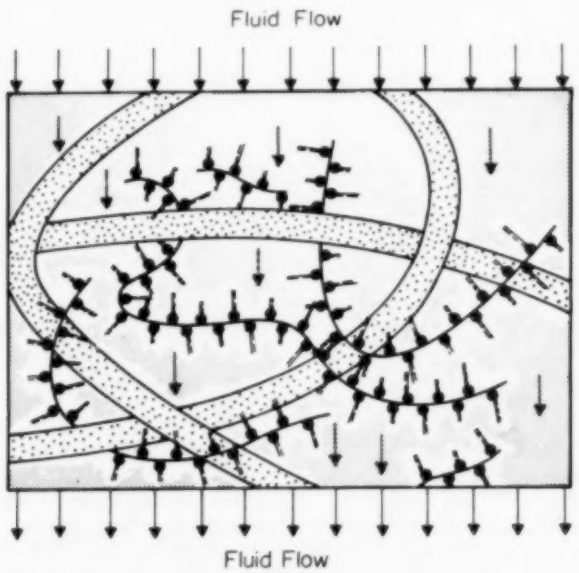

FIG. 2b

Schematic Illustration of the Compaction of the Solid Organic Matrix Due to the Diffusive Drag of Permeation.

PERMEABILITY

The movement of the interstitial fluid within the cartilage and across the articular surface are two fundamental phenomena that govern the tissue's mechanical response, its biomechanical function (e.g., the lubrication of synovial joints), and its biological integrity (e.g., the nutrition required by the chondrocytes of the adult tissue) [8-13,31-37]. There are two primary fluid transport mechanisms through the cartilage matrix: 1) The interstitial fluid may be transported through the porous permeable matrix via the application of a direct fluid pressure gradient across the tissue. The transport of the fluid increases with increasing pressure. For one-dimensional permeation flows through a finite thickness h of the tissue, an apparent permeability k_{app} is often defined by Darcy's law in the form of $Q = Ak_{app}P_A/h$ where Q is the volume flow rate across an area A of the cartilage, and P_A is the pressure drop across the thickness h of the specimen. Average values of this apparent permeability coefficient were first determined by McCutchen [11] to be 0.58×10^{-15} $m^4/N \cdot s$. Such a small value of permeability indicates a very high frictional resistance to fluid flow. It was also observed that permeability decreases with depth, with a value of 0.76×10^{-15} $m^4/N \cdot s$ near the middle region and a value of 0.43×10^{-15} $m^4/N \cdot s$ for the underlying cartilage. 2) Fluid transport can be achieved by deformation of the cartilage matrix. Exudation can be accomplished by squeezing the tissue between two rigid, porous platens with the fluid in the pores of the platen at ambient pressure. When this is done, the compressed solid matrix causes a rise of the internal pressure acting on the fluid within the tissue. This creates a pressure gradient across the surface of the specimen favoring the exudation of the interstitial fluid. This mechanism is known as flow due to consolidation.

In 1976, Mansour and Mow [7] measured the nonlinear interaction between the tissue's deformation and its resistance to permeation. More recently, using the same apparatus, one designed to clamp the tissue with precise amounts of applied compression before permeation, we empirically demonstrated an exponential decrease of tissue permeability with the clamping strain ϵ_{cla} [13,38]. Figure 3 shows a one-parameter (P_A) family of permeability curves as a function of applied clamping strain ϵ_{cla}. The pressure drop P_A for maintaining steady permeation was taken to be the parameter of the experiment. An empirical exponential law

$$k_{app} = A(p_A)\exp[\alpha(p_A)\epsilon_{cla}] \tag{1}$$

was used to curve-fit this set of data. Here $A(p_A)$ and $\alpha(p_A)$ depend on the applied pressure P_A and are determined experimentally by a curve-fitting procedure [39]. The solid lines of Fig.3 are plots of this exponential law and the points are from one experimental set of data. We have obtained ten such sets of data, all of which can be empirically described in the same manner.

The decrease of permeability with increasing compressive strain can be explained on the basis that compaction of the tissue decreases the average pore size of the tissue thereby making it more difficult for the permeating liquid to flow through it. However, there are two sources of such compaction in our permeation experimental set-up. One is the compaction due to the clamping strain ϵ_{cla} imposed on the tissue before the permeation; the other is the additional compaction due to the action of the diffusive drag during the permeation, see Fig.2b. The latter source originates from the applied pressure drop required for the maintenance of the steady permeation. This could be the mechanism that caused the decrease of permeability with pressure as originally observed by Mansour and Mow [7]. The applied clamping strain ϵ_{cla} is uniform whereas the drag-induced strain is nonuniform. The nonuniform strain in the tissue results in a nonuniform permeability so that such permeation experiments can only measure the "apparent" permeability. It seems logical then to introduce the concept of "intrinsic" permeability, which we define as the permeability function that depends only on the uniform strain. This condition could be achieved under the limiting condition of $P_A \to 0$, i.e., when the nonuniform strain field becomes vanishingly small. Even though such an experimental condition is impossible to achieve in reality, the intrinsic permeability function can be obtained by extrapolating results such as those shown in Fig.3 to the limit of $P_A \to 0$. In other words, the intrinsic permeability function is the permeability function that corresponds to a vanishingly small pressure gradient during a flow permeation experiment where the tissue is subjected to a uniform clamping strain ϵ_{cla}. The intrinsic permeability curve of Fig.3 was obtained by such an extrapolation procedure. This intrinsic permeability curve can be described by the expression [40]:

$$k_{intrinsic} = k_o \exp(M_o\epsilon) \tag{2}$$

where k_o and M_o are constants and ϵ is the true strain. Values of these constants for one set of data obtained from normal bovine tissues will be given later (see also [40]). However,

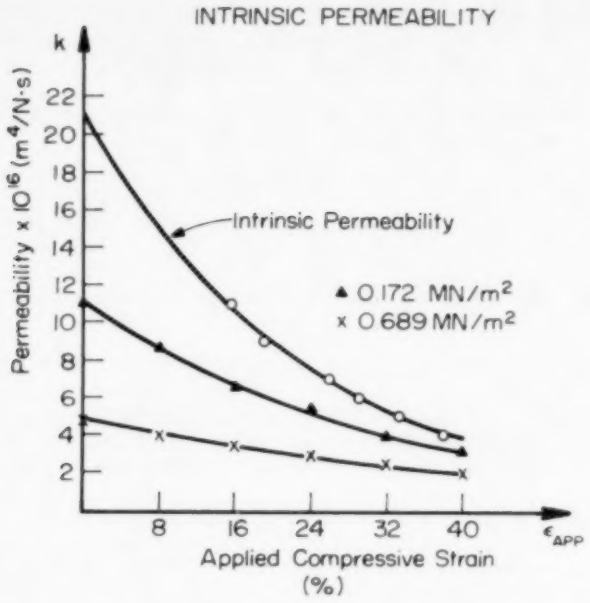

FIG.3

Permeability of Articular Cartilage, at Two Levels of Pressure P_A, as a Function of the Applied Clamping Strain. The intrinsic permeability is obtained from the limiting case of $P_A \to 0$ from six levels of P_A [42].

Vol. 17
1980

once this concept has been established, we propose that Eq.(2) may be used in the field to describe the pointwise variation of the permeability throughout the tissue.

The two objectives of this investigation are: (1) to obtain analytically the solutions for the drag-induced nonuniform compaction of a soft, porous, permeable matrix during a permeation experiment and (2) to demonstrate that the intrinsic permeability function as given by Eq.(2) can be used as a field variable to predict the pressure dependence of the apparent permeability function, Eq.(1).

BIPHASIC CONSTITUTIVE EQUATIONS

The general linear constitutive equations for a nonreacting biphasic mixture of an intrinsically incompressible solid and intrinsically incompressible liquid are as follows [13]:

(i) The solid apparent stress tensor:

$$\underset{\sim}{T}^s = -\alpha p \underset{\sim}{I} + \hat{A} e \underset{\sim}{I} + 2N \underset{\sim}{e} + \lambda_s (\text{div } \underset{\sim}{v}^s) \underset{\sim}{I} + 2\mu_s \underset{\sim}{D}^s - 2K_c \underset{\sim}{\Gamma} \tag{3}$$

where $\underset{\sim}{v}^s$ is the solid phase velocity field, $\underset{\sim}{e}$ and $\underset{\sim}{D}^s$ are the infinitesimal strain tensor and the rate of deformation tensor, respectively, $e = \text{tr } \underset{\sim}{e}$, $\underset{\sim}{\Gamma}$ is the spin tensor of the solid phase relative to the fluid phase, p is the pressure, α is the solid content ratio given by the initial volumes (V_s/V_f); and $\hat{A}$, N, λ_s, μ_s, and K_c are intrinsic material constants of the solid phase.

(ii) The fluid apparent stress tensor:

$$\underset{\sim}{T}^f = -p \underset{\sim}{I} + \lambda (\text{div } \underset{\sim}{v}^f) \underset{\sim}{I} + 2\mu \underset{\sim}{D}^f + 2K_c \underset{\sim}{\Gamma} \tag{4}$$

where $\underset{\sim}{v}^f$ is the fluid phase velocity field, $\underset{\sim}{D}^f$ is the rate of deformation tensor and λ and μ are intrinsic material constants of the fluid phase.

(iii) The continuity equation for this biphasic mixture:

$$\text{tr } \underset{\sim}{D}^f = -\alpha \, \partial e/\partial t , \tag{5}$$

(iv) The diffusive resistance on each of the phases of the mixture during relative motion:

$$-\underset{\sim}{\pi}^{f} = \underset{\sim}{\pi}^{s} = b(\text{grad } e) - K(\underset{\sim}{v}^{s} - \underset{\sim}{v}^{f}) \tag{6}$$

where b is an additional material constant and K is the diffusive coefficient. Equations (6) are to be used as body forces in the equation of motion, i.e.,

$$\text{div } \underset{\sim}{T}^{s} + \underset{\sim}{\pi}^{s} = \rho^{s} \underset{\sim}{a}^{s} \tag{7}$$

and

$$\text{div } \underset{\sim}{T}^{f} + \underset{\sim}{\pi}^{f} = \rho^{f} \underset{\sim}{a}^{f} \tag{8}$$

where $\underset{\sim}{a}^{s,f}$ are the acceleration vectors of the solid and the fluid phases, respectively.

LINEAR THEORY OF PERMEATION

In the following, we shall formulate a linear theory and a nonlinear theory of permeation, both for infinitesimal strain theory, using a simplified model of the biphasic medium where λ_s, μ_s, λ, μ, K_c, and b are taken to be zero. The linear theory of permeation assumes the diffusive resistance coefficient K to be a constant. For articular cartilage, we refer to such a biphasic medium as the linear KLM model for articular cartilage [42]. This linear model was used to describe the creep and stress relaxation behaviors of articular cartilage measured from confined compression experiments. The nonlinear KLM theory for articular cartilage [42] assumes the diffusive resistance coefficient to be strain dependent given by some form such as $K = K_o \exp(-M_o e)$ [13,41,42]. The results of the linear theory will show that the compaction of the tissue during permeation is nonuniform and thereby will demonstrate the need of a nonlinear theory. Furthermore, the relationship between permeability and diffusive resistance coefficient derived from the linear theory together with Eq.(2) motivates the use of the functional form of K to be used in the nonlinear theory.

Let us now consider a typical one-dimensional filtration experiment, in the z-direction, where a precisely prepared specimen of tissue ~ 200 μm in thickness and 31.8 mm in diameter is used as the filter. When subject to a steady-state condition where a constant pressure drop P_A is applied across the specimen, fluid flow velocity will also be a constant, designated by V. The constitutive equations for the simplified biphasic theory for articular cartilage ($\lambda_s = \mu_s = \lambda = \mu = 0$) reduce to

$$T^{s}_{zz} = -\alpha p + H_A \, du/dz \tag{9}$$

and

$$T^{f}_{zz} = -p \tag{10}$$

where u denotes the z-component of the displacement of the solid matrix and $e \equiv du/dz$. The equations of motion for the biphasic mixture ($b = 0$) reduce to

$$-\alpha \, dp/dz + H_A d^2u/dz^2 - K(-V) = 0 \tag{11}$$

and

$$-dp/dz - KV = 0 \tag{12}$$

where $H_A = \hat{A} + 2N$. From Eqs.(11) and (12) one can easily solve for u:

$$d^2u/dz^2 = -(1+\alpha)KV/H_A . \tag{13}$$

The solution of Eq.(13) is:

$$u(z) = -(1+\alpha)(KV/H_A)(z^2/2) + C_1 z + C_2 \tag{14}$$

where K = constant and C_1 and C_2 are constants of integration. Let us assume that the following conditions prevail at the downstream surface of the tissue at z = h:

(i) The supporting porous and permeable substrate is rigid,

$$u(h) = 0 .$$

(ii) The ambient pressure of the filtrate, e.g., water, is zero,

$$T^f_{zz}(h) = -p(h) = 0 .$$

Alternatively, condition (ii) expresses the fact that the supporting load is borne completely by the solid matrix. Applying boundary condition (i), we obtain

$$u(z) = \frac{(1+\alpha)KV}{2H_A}(h^2 - z^2) + C_1(z-h) . \tag{15}$$

To assess the constant C_1, we make use of the equation of equilibrium for the mixture as a whole. In this one-dimensional permeation case, we have

$$d(T^s_{zz} + T^f_{zz})/dz = 0 . \tag{16}$$

Therefore, the total stress must be a constant across the complete specimen. In particular, this condition yields

$$T^s_{zz}(0) + T^f_{zz}(0) = -P_A = T^s_{zz}(h) + T^f_{zz}(h) . \tag{17}$$

Here, $z = 0$ is taken as the upstream surface of the specimen and P_A is the applied pressure at this surface.

Applying boundary condition (ii), we obtain

$$T^s_{zz}(h) = -P_A \tag{18a}$$

or

$$H_A du/dz = -P_A \text{ at } z = h . \tag{18b}$$

Combining Eqs.(15) and (18b), we find that the constant C_1 is given by

$$C_1 = (1+\alpha)(KVh/H_A) - (P_A/H_A) . \tag{19}$$

Therefore, the complete linear theory solution for the steady state, drag-induced compaction of a soft, porous and permeable matrix during a permeation experiment is given by

$$u(z) = \frac{(1+\alpha)KV}{2H_A}(h^2 - z^2) + \left[\frac{(1+\alpha)KVh}{H_A} - \frac{P_A}{H_A}\right](z-h) \tag{20}$$

and the change of volume per unit initial volume is given by

$$e = du/dz = \frac{-(1+\alpha)KVz}{H_A} + \left[\frac{(1+\alpha)KVh}{H_A} - \frac{P_A}{H_A}\right] . \tag{21}$$

THE RELATION BETWEEN K AND k

The diffusive resistance K provides a measure of drag whenever there is relative motion between the two phases of the biphasic mixture. The apparent permeability constant k_{app} is defined by

$$k_{app} = \frac{(Q/A)}{(P_A/h)} \tag{22}$$

where Q is the volume discharge per unit time and A is the area used for permeation. Because the permeation speed V is related to Q by the expression $V = Q(1+\alpha)/A$, we have

$$k_{app} = \frac{Vh}{(1+\alpha)P_A} . \tag{23}$$

On the other hand, Eq.(12) and boundary condition (ii) give us

$$p(z) = KV(h - z) . \tag{24}$$

Vol. 17
1980

Let us now assume that the following boundary conditions prevail at the upstream surface of the specimen:

$$T^{s}_{zz}(0) = -(1-\beta)P_A \tag{25}$$

$$T^{f}_{zz}(0) = -\beta P_A . \tag{26}$$

The coefficient β is a parameter used to partition the applied stress at the surface of a porous medium [42]. On the upstream side, Eqs. (10) and (24) may be combined to yield

$$\beta P_A = KVh . \tag{27}$$

Therefore, Eqs. (23) and (27) may be used to determine k_{app} as a function of K:

$$k_{app} = \frac{\beta}{1+\alpha}\,(1/K) . \tag{28}$$

For the case where V is extremely small, such as those measured for articular cartilage during the permeation experiments, we assume that the partition coefficient β may be set equal to the surface porosity:

$$\beta = \frac{1}{1+\alpha} . \tag{29}$$

Hence, the apparent permeability k_{app} is related to the diffusive resistance K by

$$k_{app} = \frac{1}{K(1+\alpha)^2} . \tag{30}$$

Equation (27) may be used to simplify the drag-induced compaction expression, Eq. (20):

$$u(z) = \frac{KV}{H_A}\left\{\frac{(1+\alpha)}{2}\,(h^2 - z^2) + h\left[(1+\alpha) - \frac{1}{\beta}\right](z-h)\right\} \tag{31}$$

and

$$e = \frac{du}{dz} = \frac{KV}{H_A}\left\{-(1+\alpha)z + h\left[(1+\alpha) - \frac{1}{\beta}\right]\right\} . \tag{32}$$

For the slow permeation experiment, we have, by virtue of Eq. (29)

$$u(z) = \frac{KV}{H_A}\,\frac{(1+\alpha)}{2}\,(h^2 - z^2) \tag{33}$$

$$e = \frac{du}{dz} = \frac{-KV(1+\alpha)}{H_A}\,z = \frac{P_A}{H_A}\left(\frac{z}{h}\right) . \tag{34}$$

Figure 4 depicts the normalized displacement provided by Eq. (33) for the case where the parameter $KV(1+\alpha)/2H_A = 0.25$.

First, we note from Eq. (30) that the apparent permeability for a tissue of finite thickness h is inversely proportional to the diffusive resistance coefficient. We used this inverse proportionality to estimate the average apparent permeability for bovine patellar-femoral tissues in the confined compression creep experiment [13]. Taken over the entire creep deformational range of approximately 25% apparent compressive strain, the estimated value of $k_{app} = 1.09 \pm 0.43 \times 10^{-14}$ $m^4/N \cdot s$ was obtained*. This value of apparent permeability is an order of magnitude larger than those obtained from our direct permeability experiment over the entire range of applied compressive strain, Fig. 3. From the predictions of linear theory on fluid exudation occurring during the creep process, we can conclude that our curve-fitting procedure used to obtain these values of k_{app} favors the early periods of the creep data when copious exudation is occurring at the higher values of permeability [13].

For completeness, we also mention here that in the confined compression experiment, the aggregate elastic modulus $H_A (= 2N + \hat{A})$ of the solid matrix is obtainable at equilibrium, ~ 10,000 seconds. This modulus is independent of the fluid flow occurring during the creep

---

* These values are corrected from those computed in [13] where we assume the proportionality factor to be unity. The correct value is $1/(1+\alpha)^2 = 0.7$.

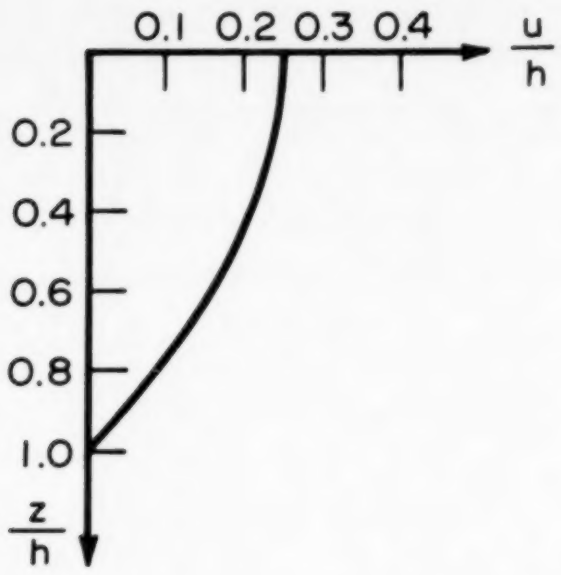

FIG.4

Displacement of the Solid Matrix as Predicted by Eq.(34) due to the Diffusion Drag of Permeation for the Case $KV(1+\alpha)/H_A = 0.50$. A nonhomogeneous linearly varying strain field is predicted; K = constant.

Vol. 17
1980

process. The equilibrium strain versus the equilibrium stress shows a remarkable linear relationship for strain up to ~ 25% [13]. For normal bovine patella-femoral tissues, the aggregate modulus is 0.70 ± 0.06 MPa at a 95% confidence level of the data population.

Second, we see from Eqs.(33) and (34) that, with K (and therefore k) assumed to be strain independent, a nonuniform compaction of the matrix occurs. These results, even though very simple, are very important because they point to the difficulty of measuring permeability by the direct permeation method. For permeation to take place, a pressure gradient must be applied. This causes the permeability to vary with the depth and thereby making the measurement not what it appears to be at first glance. However, if we extrapolate the results of the experimental curves, Fig.3, to the limit of $P_A \to 0$, at which the strain field in the tissue becomes uniform (e.g., via clamping), we obtain the "intrinsic" permeability function described by Eq.(2). In the following, we will use this relationship in the field to formulate a nonlinear permeation theory to describe the variation of the apparent permeability with applied pressure P_A.

NONLINEAR THEORY OF PERMEATION

In this theory, we assume that the apparent stress tensors T^s_{zz} and T^f_{zz} are still given by Eqs.(9) and (10), and the equations of motion are given by Eqs.(11) and (12) except that the diffusive resistance coefficient is now assumed to be a function of strain e instead of a constant. Guided by our linear analysis of the permeation experiment and our concept of the intrinsic permeability, we now assume that the diffusive drag is given by

$$K = K_o \exp(-M_o e) \tag{35}$$

where $e = du/dz$ and K_o is inversely proportional to the k_o of Eq.(2). With K given by Eq.(35), Eq.(13) becomes

$$d^2u/dz^2 = [-K_o V(1+\alpha)/H_A]\exp(-M_o\, du/dz)\,. \tag{36}$$

Integrating Eq.(36) once, we obtain

$$M_o(du/dz) = \ell n[-K_o V M_o(1+\alpha)z/H_A + c_1]\,. \tag{37}$$

The constant c_1 can be obtained from the boundary condition Eq.(18) so that

$$M_o du/dz = \ell n \left\{\exp(-M_o P_A/H_A) - K_o V M_o (1+\alpha)(z-h)/H_A\right\}. \tag{38}$$

Equation (38) expresses the nonuniform strain distribution with the depth according to this nonlinear theory of permeation.

Equation (12) for the fluid pressure p(z) is now given by

$$dp/dz = -K_o V \exp(-M_o du/dz). \tag{39}$$

By making use of Eq.(38), Eq.(39) can be integrated to give the fluid pressure p:

$$p(z) = \frac{H_A}{M_o(1+\alpha)} \ell n \left[1 - \frac{K_o V M_o (1+\alpha)}{H_A}(z-h)\exp(M_o P_A/H_A)\right] \tag{40}$$

where the condition $p(h) = 0$ has been used.

Applying the slow flow condition (29), $p(0) = \beta P_A = \frac{1}{1+\alpha} P_A$, we obtain

$$V = \frac{H_A}{K_o M_o (1+\alpha) h}\left[1 - \exp(-M_o P_A/H_A)\right]. \tag{41}$$

Now by substituting Eq.(41) into Eq.(23), we find the relationship for the apparent permeability to be:

$$k_{app} = \frac{k_o}{(M_o P_A/H_A)}\left[1 - \exp(-M_o P_A/H_A)\right] \tag{42}$$

where $k_o = \frac{1}{K_o(1+\alpha)^2}$. We note that as $M_o P_A \to 0$, $k_{app} \to k_o$; consistent with the linear theory. We see, therefore, that this nonlinear theory predicts that the apparent permeability depends exponentially on the applied permeation pressure P_A, which is the cause for the nonuniform strain in the tissue. Equation (42) can be used to curve-fit our experimental results of Fig.3 for $\epsilon_{cla} = 0$ by choosing $k_o = 17.1 \times 10^{-16}$ $m^4/N \cdot s$ and $M_o = 4.3$. A comparison of this predicted result and the experimental data is shown in Table 1.

TABLE 1

A Comparison of Experimentally Obtained Apparent Permeability and the Predicted Apparent Permeability from our Nonlinear Permeation Theory with $k_o = 17.1 \times 10^{-16}$ $m^4/N \cdot s$ and $M_o = 4.3$.

P_A	0.072	0.345	0.670	1.033	MPa
k_{app} [Eq.(42)]*	11.0	7.63	4.50	2.98	$\times 10^{-16}$ $m^4/N \cdot s$
k_{app} (experimental)**	11.0	7.20	4.70	3.60	$\times 10^{-16}$ $m^4/N \cdot s$

* One-dimensional analysis; ** axisymmetric experiment.

Substituting Eq.(41) into Eq.(38) we obtain

$$M_o(du/dz) = \ell n\left[1 - [1 - \exp(-M_o P_A/H_A)](z/h)\right]. \tag{43}$$

We see that if either $P_A \to 0$ or $M_o \to 0$, this relationship reduced to

$$M_o(du/dz) = \ell n\left\{1 - \frac{M_o P_A}{H_A}\left(\frac{z}{h}\right)\right\} \to -\frac{M_o P_A}{H_A}\left(\frac{z}{h}\right). \tag{44}$$

This result is identical with that obtained from our linear theory, see Eq.(34). For completeness, we integrate Eq.(43) to obtain u(z):

$$M_o u(z) = (\gamma z + 1)[\ln(\gamma z + 1) - 1]/\gamma + c_2 \tag{45}$$

where $\gamma = -[1 - \exp(-M_o P_A/H_A)]/h$ and $c_2 = -[h(1 + M_o P_A/H_A)\exp(-M_o P_A/H_A)/[1 - \exp(-M_o P_A/H_A)]$. Here $u(h) = 0$ has been used to obtain the constant of integration c_2.

More generally, if we subject the tissue to both a clamping strain ε_{cla}, before the permeation, and a pressure P_A and if we assume that the permeated tissue surfaces remain in contact with the rigid porous platens, then by using our nonlinear permeation theory we can, in a similar manner, calculate k_{app}:

$$k_{app}(\varepsilon_{cla}, P_A) = k_o \exp[-M_o(P_T - P_A)/H_A][1 - \exp(-M_o P_A/H_A)]/(M_o P_A/H_A)\,. \tag{46}$$

Here, P_T denotes the total pressure borne by the solid matrix at $z = h$ and is given by:

$$P_T = H_A\{\varepsilon_{cla} + (P_A/H_A)/[1 - \exp(-M_o P_A/H_A)] - 1/M_o\}\,. \tag{47}$$

The first term of Eq.(47) is the pressure that results from the clamping strain ε_{cla} whereas the second and third terms together give that which results from the nonlinear diffusive drag law, Eq.(35). Under the conditions stated, Eqs.(46) and (47) yield the relationship between the apparent permeability k_{app} and the clamping strain ε_{cla} and the applied pressure P_A. These two equations taken together are in the same form as our empirically obtained law of Eq.(1).

Vol. 17
1980

CONCLUSION

For soft, porous, permeable biphasic materials, the diffusive drag of permeation is sufficient to cause a substantial compaction of the matrix, Fig.4. This compaction, for very slow permeation experiments, is described by a parabolic displacement field, Eq.(33), and a nonhomogeneous strain field, Eq.(34), if P_A is small. Otherwise, Eq.(45) and Eq.(44) must be used to describe these quantities. It is this drag-induced compaction mechanism that is responsible for the experimentally observed pressure dependence of permeability. The limiting case of $P_A \to 0$ eliminates this nonhomogeneous strain field and yields the intrinsic permeability relationship described by Eq.(2) [40]. For soft, porous, permeable materials such as articular cartilage, a nonlinear biphasic theory, one in which Eq.(2) is used to describe the permeability function, can provide a better model for problems when fluid flow is an important factor.

These concepts of intrinsic matrix properties of biphasic materials such as articular cartilage provide a clear idea of what needs to be measured. Future studies on the correlations between biochemical alterations of proteoglycan conformations and composition and collagen structure and composition, and biomechanical properties such as the intrinsic elastic and viscoelastic moduli of the matrix and intrinsic permeability functions of the matrix must be pursued.

ACKNOWLEDGEMENT

This work was sponsored by the National Science Foundation Grant Number ENG 77-21247 and the National Institutes of Health Grant Number AM 19094. We thank Ms. Joan J. Sevon for her astute editing of this manuscript.

REFERENCES

1. LIPSHITZ, H., ETHERIDGE, R. and GLIMCHER, M.J. Changes in the hexosamine content and swelling ratio of articular cartilage as a function of depth from the surface. J. Bone & Jt. Surg., Vol.58A, 1976, pp.1149-1153.

2. BRANDT, K.D., PALMOSKI, M.J. and PERRICONE, E. Aggregation of cartilage proteoglycans. Arth. and Rheum., Vol.6, 1976, pp.1308-1314.

3. INEROT, S., HEINEGÅRD, D., AUDELL, L. and OLSSON, S.E. Articular cartilage proteoglycans in aging and osteoarthritis. Biochem. J., Vol.169, 1978, pp.143-156.

4. McDEVITT, C.A. and MUIR, H. Biochemical changes in the cartilage of the knee in experimental and natural osteoarthritis in the dog. J. Bone & Jt. Surg., Vol.58B, 1976, pp.94-101.

5. MUIR, H. Molecular approach to understanding of osteoarthrosis. Annals of the Rheumatic Diseases, Vol.36, 1977, pp.199-208.

6. ROSENBERG, L.C. Structure of cartilage proteoglycans. In: Dynamics of Connective Tissue Macromolecules. P.M.C. Burleigh and A.R. Poole (Eds.) Amsterdam: North Holland Pub. Co., 1975, pp.105-128.

7. MANSOUR, J.M. and MOW, V.C. The permeability of articular cartilage under compressive strain and at high pressures. J. Bone & Jt. Surg., Vol.58A, 1976, pp.509-516.

8. LIPSHITZ, H., ETHERIDGE, R. and GLIMCHER, M.J. In vitro wear of articular cartilage. J. Bone & Jt. Surg., Vol.57A, 1975, pp.527-534.

9. MALCOM, L.L. An Experimental Investigation of the Friction and Deformation Responses of Articular Cartilage Interfaces to Static and Dynamic Loading. Ph.D. Dissertation, The University of California, San Diego, 1976, pp.1-272..

10. MANSOUR, J.M. and MOW, V.C. On the natural lubrication of synovial joints: Normal and degenerate. J. Lub. Tech., Vol.99, 1977, pp.163-173.

11. McCUTCHEN, C.W. The frictional properties of animal joints. Wear, Vol.5, 1962, pp.1-17.

12. TORZILLI, P.A. and MOW, V.C. On the fundamental fluid transport mechanisms through normal and pathological articular cartilage during function. II. The analysis, solution and conclusions. J. Biomech., Vol.9, 1976, pp.587-606.

13. MOW, V.C. and LAI, W.M. Mechanics of animal joints. Ann. Rev. Fluid Mech., Vol.11, 1979, pp.247-288.

14. MILLER, E.J. and MATUKAS, V.J. Chick cartilage collagen: A new type of α_1 chain not present in bone or skin of the species. Proc. Nat. Acad. Sci (USA), Vol.64, 1969, pp.1264-1268.

15. EYRE, D.R. and MUIR, H. Distribution of different molecular species of collagen in fibrous, elastic and hyaline cartilages of pig. Biochem. J., Vol.151, 1975, pp.595-602.

16. SHEPARD, N. and MITCHELL, N. The localization of articular cartilage proteoglycans by electron microscopy. Anatomical Record, Vol.187, 1977, pp.463-476.

17. THYBERG, J., LOHMANDER, S. and FRIBERG, V. Electron microscopic demonstration of proteoglycans in guinea pig epiphyseal cartilage. J. Ultrastructure, Vol.45, 1973, pp.407-427.

18. LANE, J.M. and WEISS, C. Review of articular cartilage collagen research. Arth. and Rheum., Vol.18, 1975, pp.553-563.

19. KEMPSON, G.E., MUIR, H., POLLARD, C. and TUKE, M. The tensile properties of the cartilage of human femoral condyles related to the content of collagen and glycosaminoglycans. Biochimica et Biophysica Acta, Vol.297, 1973, pp.456-472.

20. ASKEW, M.J. and MOW, V.C. The biomechanical function of the collagen ultrastructure of articular cartilage. J. Biomech. Eng., Vol.100K, 1978, pp.105-115.

21. CLARKE, I.C. Surface characteristics of human articular cartilage: A scanning electron microscope study. J. Anat., Vol.108, 1971, pp.23-59.

22. REDLER, I. and MOW, V.C. Biomechanical Theories of Ultrastructural Alterations of Articular Surfaces of the Femoral Head. In: Proc. Symp. on Bioengineering and Arthritis of the Hip, W. Harris (Ed.) St. Louis: C.V. Mosby Co., Vol.23, 1974, pp.23-59.

23. WOO, S.L-Y, AKESON, W.H. and JEMMOTT, C.P. Measurement of nonhomogeneous, directional mechanical properties of articular cartilage in tension. J. Biomech., Vol.9, 1976, pp.785-791.

24. MOW, V.C., LAI, W.M. and REDLER, I. Some surface characteristics of articular cartilage. Part I: A scanning electron microscopy study and a theoretical model for the dynamic interaction of synovial fluid and articular cartilage. J. Biomech., Vol.7, 1974, pp.449-456.

Vol. 198

25. MUIR, H., BULLOUGH, P. and MAROUDAS, A. The distribution of collagen in human articular cartilage with some of its physiological implications. J. Bone & Jt. Surg., Vol.52B, 1970, pp.554-563.

26. REDLER, I., MOW, V.C., ZIMNY, M. and MANSELL, J. The ultrastructure and biomechanical significance of the tidemark of articular cartilage. Clinical Orthopaedics and Related Topics, Vol.112, 1975, pp.357-362.

27. ROSENBERG, L.C., HELLMANN, W. and KLEINSCHMIDT, A.K. Electron microscopic studies of proteoglycan aggregates from bovine articular cartilage. J. Biol. Chem., Vol.250, 1975, pp.1877-1883.

28. SCHUBERT, M. and HAMERMAN, D. The chemistry of the fibers of connective tissues. A Primer on Connective Tissues Biochemistry. Philadelphia: Lea & Febiger, 1968, pp.5-52.

29. HARDINGHAM, T.E. and MUIR, H. Binding of oliogosaccharides of hyaluronic acid to proteoglycans. Biochem. J., Vol.135, 1973, pp.905-908.

30. MAROUDAS, A., MUIR, H. and WINGHAM, J. The correlation of fixed negative charge with glycosaminoglycan content of human articular cartilage. Biochim. Biophys. Acta, Vol.177, 1969, pp.492-500.

31. COLETTI, J.M., AKESON, W.H. and WOO, S.L-Y. A comparison of the physical behavior of normal articular cartilage and the arthroplasty surface. J. Bone & Jt. Surg., Vol.54A, 1972, pp.147-160.

32. HIGGINSON, G.R. Squeeze films between compliant solids. Wear, Vol.46, 1978, pp.387-395.

33. LAI, W.M. and MOW, V.C. Flow fields in a single layer model of articular cartilage created by a sliding load. Advances in Bioengineering, Trans. ASME, M.K. Wells (Ed.), 1979, pp.101-104.

34. MANKIN, H. and THRASHER, A.Z. Water content and binding in normal and osteoarthritic human cartilage. J. Bone & Jt. Surg., Vol.57A, 1975, pp.76-80.

35. MAROUDAS, A. Physicochemical properties of cartilage in the light of ion exchange theory. Biophys. J., Vol.8, 1968, pp.575-595.

36. MAROUDAS, A. Biophysical chemistry of cartilaginous tissues with special reference to solute and fluid transport. Biorheology, Vol.12, 1975, pp.233-248.

37. SALTER, R.B. and FIELD, P. The effects of continuous compression on living articular cartilage. J. Bone & Jt. Surg., Vol.42A, 1960, pp.31-49.

38. GORDON, S.S., MOW, V.C., LEE, R. and GRODZINSKY, A.J. Permeability and Transport Properties of Articular Cartilage. Proc. 3rd Int. Cong. of Biorheology, La Jolla, CA, 1978, p.175.

39. GORDON, S.S. Permeability and streaming potential of normal and trypsin treated articular cartilage. M.S. Thesis, Rensselaer Polytechnic Institute, Troy, NY, 1978, pp.1-79.

40. LAI, W.M. and MOW, V.C. Intrinsic strain dependent permeability of a soft porous biomaterial. Submitted for publication. First World Biomaterials Congress, Vienna, Austria, April 8-12, 1980.

41. EISENFELD, J., MOW, V.C. and LIPSHITZ, H. The mathematical analysis of stress relaxation in articular cartilage during compression. Math. Biosci., Vol.39, 1978, pp.97-111.

42. MOW, V.C. and LAI, W.M. Selected unresolved problems in synovial joint biomechanics. Biomechanics Symposium, Trans. ASME. W. Van Buskirk (Ed.), 1979, pp.19-52.

Vol. 17
1980

BLANK
PAGE

Vol.
198

BIORHEOLOGY Vol.17, pp. 125-134 0006-355X/80/010125-10$02.00/0
© Pergamon Press Ltd. 1980. Printed in the United States

THIRD INTERNATIONAL CONGRESS OF BIORHEOLOGY

SYMPOSIUM ON MUCO-CILIARY TRANSPORT

ON THE MECHANICS OF MUCO-CILIARY TRANSPORT

J.R. Blake and H. Winet
CSIRO Division of Mathematics and Statistics,
P.O. Box 1965, Canberra City, ACT 2601, Australia,
and Department of Physiology, Southern Illinois
University at Carbondale, Carbondale, Illinois 62901
U.S.A.

(Received 1.7.1979. Accepted by Guest Editors T.Y. Wu and S. Berger)

ABSTRACT Although the internal structure of cilia on micro-organisms and in the lung is identical the mechanical principles of fluid (mucous) transport may be vastly different. Cilia on micro-organisms are generally quite long, less densely packed on the epithelium, have a pronounced aperiodic beating pattern and a highly coordinated metachronal wave compared to the short densely packed, multicellular coordination of cilia found in the lung. A simple hydrodynamic theory using two layers of Newtonian fluid of differing viscosity is developed to model muco-ciliary transport. Features include estimates for the mean force distribution, the likelihood that a cilium is located at a given height above the epithelium for an idealised beat pattern, and allowance for the retardation of the serous layer by the cilia. Initial calculations suggest that if the cilia just penetrate the upper, much more viscous, layer that mucous transport rates are substantially enhanced. Other features of the results are the significant retardation of flow in the serous layer and the 'plug' flow in the mucous layer.

Vol. 17
1980

INTRODUCTION

The internal structure of cilia on micro-organisms and in the lung are identical (Sleigh (18)) showing the well-known 9+2 fibril complex associated with cilia and flagella. The cilia bend due to the relative motion of the fibrils (Satir (17)). Although the structural and functional (the movement of the micro-organism or fluid) aspects of cilia on micro-organisms and in the lung are the same, the actual mechanisms of transport may be vastly different. In this paper we present several theoretical concepts which support this view.

Morphologically the cilia lining the airways of the lung are different from those on micro-organisms. The cilia in the lung are short, often around 5μm. in length, while those on fast swimming micro-organisms are 7-15μm. long. The frequency of beat appears to be similar in both circumstances, 10-30Hz, although it has been observed by Iravani (9) that the cilia beat frequency in the lung increases in the cranial direction.

On internal mechanical grounds Sleigh (18) suggests that cilia have a minimum radius of curvature around 2μm. Thus, the longer cilia on micro-organisms can develop a very asymmetric beat pattern characterised by the familiar pendular effective stroke and the "limp" recovery stroke near the epithelium surface. There are excellent hydro-dynamic grounds why this

asymmetric beat is desirable and these have been outlined previously by Blake (1), Blake et al. (4,5) and Sleigh (18). On the other hand the shortness of lung cilia probably limits the beat pattern to sharp pendular motions in both the effective and recovery strokes, something similar to that depicted by Cheung et al. (6). In the lung, cilia are densely packed on the epithelia with only a few diameters separating adjacent cilia (6-10 cilia/$(\mu m)^2$) compared to the relatively spacious arrangement on the fast swimming Paramecium (0.1-0.25 cilia/$(\mu m)^2$) Machemer (14), Blake et al. (5).

Coordination of the cilia on micro-organisms is well developed into metachronal waves whereas in the lung the coordination is more on a multi-cellular level. That is, the phase change may be from cell to cell rather than from row of cilia to row of cilia found in micro-organisms. Iravani et al. (10) observed patches of metachronal fields in rats although they were very irregular in size and shape varying from a few cells to hundreds.

Mucus is secreted by mucous cells. They are abundant on the epithelia of the trachea and larger bronchial airways, but are much less frequent in the smaller bronchioles, disappearing altogether in the terminal bronchioles (Sleigh (18)). At the terminal bronchioles level other secretory cells exist producing a watery liquid similar to that in the serous fluid and in the osmiophilic liquid lining the alveoli.

Iravani et al. (10) have reported that mucous transport initiates in the form of small flakes, 4-70μm. in diameter. These small flakes then aggregate to form plaques and then streams of mucus. These streams possibly coalesce further up the lung to form the mucous blanket so often reported in the literature (Lucas et al. (13); Sade, et al. (16)). Muco-ciliary clearance rates vary widely depending on location and circumstances.

Recent studies of muco-ciliary transport systems (Winet (19) and Gilboa et al. (7)) suggests that mucus increases transport rates and in the case of the frog palate is essential for transport. When the mucous supply is depleted transport is minimal and can only be regenerated by the addition of more mucus or a substance with polymer-like properties. Studies of the ultra-structure of the mucous blanket by Reissig et al. (15) support the view that cilia penetrate the blanket.

In this paper we use a simple theoretical hydrodynamic model using two layers of differing viscosity. If the cilia just penetrate the upper much more viscous layer it will be seen that flow rates can be substantially increased. We would suggest that one explanation why the cilia in the lung are so short is so they can sustain these heavily increased loads that are required in the transport of mucus. In normal, unloaded circumstances the cilia are probably acting sub-optimally, and essentially just "wafting" around in the serous fluid.

Most theoretical models of ciliary transport have restricted their attention to micro-organism locomotion in Newtonian fluids. A review of the various models can be found in Blake et al. (4,5). Suffice to say that two models have been developed to represent ciliary action; in one, the envelope model replaces the cilia by an "enveloping" surface over the tips of the cilia, the other attempts to incorporate the whole length of cilia within the sublayer and hence is called the cilia sublayer model. The theory for the cilia sublayer model has been further developed by Keller et al. (11) and by Liron et al. (12). In their models the action of the cilia has been replaced by either a volume or a line distribution of force. The replacement of the ciliary beat by a line distribution of force is more physically and geometrically reasonable than the volume force representation but this gain has to be balanced against the (mathematical) analytical simplicity of the volume force representation. An extension of the Keller et al. (11) model to an 'active porous medium' approach was suggested by Blake (3). This is perhaps more appropriate for the case when cilia are densely packed on the epithelium as occurs for example in Opalina and in the lung. We will develop a hybrid model in this paper.

FLUID-MECHANICAL MODEL

In the mathematical model, we restrict the geometry to two dimensions (x,y). We will suppose we have two Newtonian fluids; a serous layer of viscosity μ_1 and depth h, and on top of this a mucous layer of viscosity μ_2 and depth (H-h) (see Fig. 1.). Thus, the depth of the combined mucous and serous layer will be H. The depth of the cilia sublayer (the layer in which the cilia operate) will be taken equal to ℓ. In the analysis, we will consider two cases (i) $\ell < h$, when the cilia do not penetrate the mucous layer and (ii) $h < \ell < H$ when the cilia do penetrate into the layer. Actually from the mathematical viewpoint, we may ignore the region $\ell \leq y \leq H$ as this moves in a 'plug' flow with velocity $U(\ell)$.

Reducing the mathematical analysis to the simplest level we use only the mean-field equation with a mean volume force f dependent only on the height y (see Keller et al. (11)). Thus, the relevant equation in the serous layer ($0 \leq y \leq h$) is

$$\mu_1 \frac{d^2U}{dy^2} + f_1 = 0 \qquad (1a)$$

and in the mucous layer ($h \leq y \leq H$),

$$\mu_2 \frac{d^2U}{dy^2} + f_2 = 0 \qquad (1b)$$

where μ_1 and μ_2 are the viscosities in the serous and mucous layer respectively. The boundary conditions and matching conditions at the interface between the two Newtonian fluids are,

$$U(0) = 0 \qquad (2a)$$
$$U'(H) = 0 \qquad (2b)$$
$$U(h^-) = U(h^+) \qquad (2c)$$
$$\mu_1 U'(h^-) = \mu_2 U'(h^+) \qquad (2d)$$

where the dash implies differentiation with respect to y.
Equations (2c) and (2d) imply continuity of velocity and stress across the interface respectively.

In presenting the solution to these sets of equations it is much clearer if we separate the cases where the cilia do and do not penetrate the mucous layer. The solutions are formally presented in terms of integrals. For the case when the cilia do not penetrate the mucous layer ($\ell < h$),

$$U(y) = \frac{1}{\mu_1} \int_0^{\ell} K(y,\xi)\, f(\xi)\, d\xi \qquad (3a)$$

where

$$K(y,\xi) = \begin{cases} y, & 0 \leq y < \xi \\ \xi, & \xi < y \leq \ell \,. \end{cases} \qquad (3b)$$

In this case the mucous layer moves with the same velocity as the top of the serous layer in a plug flow.

For the case when the cilia do penetrate the mucous layer we have,

Vol. 17
1980

$$U(y) = \begin{cases} \frac{1}{\mu_1}\int_0^h f(\xi)K(y,\xi)d\xi + \frac{y}{\mu_1}\int_h^\ell f(\xi)d\xi; & 0 \leq y \leq h \\ \frac{1}{\mu_1}\int_0^h \xi f(\xi)d\xi + \frac{1}{\mu_2}\int_h^\ell f(\xi)K(y,\xi)d\xi & \\ + \frac{1}{\mu_2}(\theta-1)h\int_h^\ell f(\xi)d\xi; & h \leq y \leq \ell \\ \frac{1}{\mu_1}\int_0^h \xi f(\xi)d\xi + \frac{1}{\mu_2}\int_h^\ell \xi f(\xi)d\xi & \\ + \frac{1}{\mu_2}(\theta-1)h\int_h^\ell f(\xi)d\xi; & \ell \leq y \leq H \end{cases} \quad (4)$$

where $\theta = \mu_2/\mu_1$.

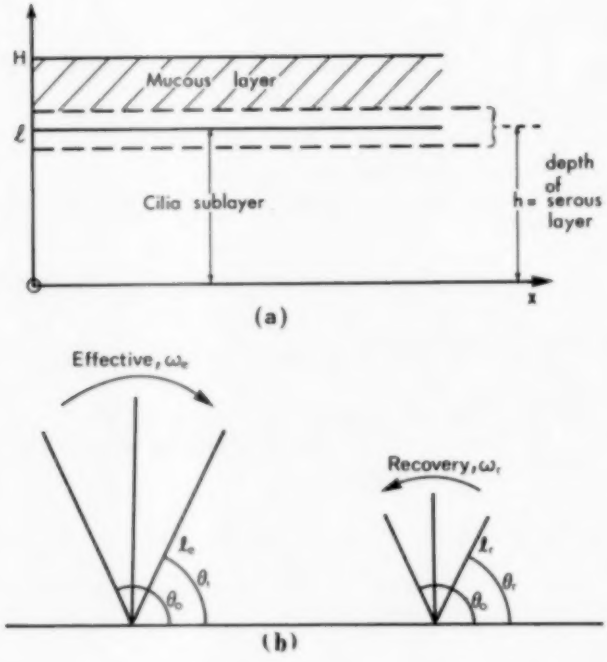

FIG. 1

(a) Illustrates geometry and arrangement of layers used in the mathematical model. (b) Idealised ciliary beat pattern used in analysis.

In a single Newtonian fluid Wu (20) has suggested that one optimal solution for a given rate of working allows for the force f to vary as $\sin \frac{\pi y}{\ell}$. We can do likewise in this double fluid model with the additional condition that the force distribution is also linearly proportional to the viscosity. This implies there will be a discontinuity in the force distribution at the interface. If we substitute this sinusoidal force dependence into both equations (3) and (4) we find for the case when θ=1000 and the penetration

depth into the mucous of 0.1ℓ that the flow rates are increased by a factor of 50 for the case when the cilia penetrate the mucus. This suggests that the penetration of the cilia into the mucus in this model is the predominant mechanism for transport. This contrasts with the action of cilia in propelling micro-organisms where the pronounced aperiodicity and asymmetry of the ciliary beat between effective and recovery stress is the prime mechanism for transport. This model also suggests a massive increase in the rate of working of the cilia when they penetrate the mucous layer. Presumably the cilia are capable of coping with this increased work load.

However there is a major inconsistency with this model. For high mucous flow rates we calculate an almost constant shear zone (Couette flow) in the serous layer. This is the main weaknesses of this model as it does not account for the additional resistance of the cilia due to the higher flow rates.

SUBLAYER RESISTANCE MODEL

For any realistic model we need to account for the additional resistance of the cilia due to increased flow rates attributed to the much more viscous upper layer. The force distribution acting on a cilium is directly proportional to the difference between the cilium's velocity and the local fluid velocity. To obtain an average volume force distribution we need to average over both space and time for a given ciliary beat cycle (see e.g. Keller et al. (11)). The aim of this paper is to illustrate, in a qualitative manner, the important physical processes involved with muco-ciliary transport. To do this we will make certain assumptions about the volume force distribution and ciliary beat cycle. We will suppose that

$$f_i(y) = \mu_i \, \Omega^2 \, (U_c(y) - \in(y)U(y)), \qquad i = 1,2 \tag{5}$$

where $U_c(y)$ is an averaged cilium velocity, $\in(y)$ is the average over a cycle of the cosine of the angle between the normal to the cilium and the x-axis as a function of height y and Ω is a cilia density parameter with dimensions of inverse length. In the next section a method of deriving both $U_c(y)$ and $\in(y)$ for an idealised ciliary will be presented.

IDEALISED CILIARY BEAT PATTERN

We will suppose that the effective stroke of the ciliary beat cycle consists of a pendular clockwise rotation from θ_o to θ_1 (see Fig. 1(b)). The cilium length will be taken as equal to ℓ_e with radian frequency ω_e. Likewise in the recovery stroke, we will suppose that we have an anti-clockwise rotation from θ_1 to θ_o: the effective cilium length now being ℓ_r and with radian frequency ω_r. The cartesian coordinate expressions for the beat pattern are then,

Effective stroke

$$\left.\begin{aligned} x &= s\cos(\theta_o - \omega_e t) \\ y &= s\sin(\theta_o - \omega_e t) \end{aligned}\right\} \qquad 0 \leq t \leq \frac{\theta_o - \theta_1}{\omega_e}, \; 0 \leq s \leq \ell_e \tag{6a}$$

Recovery stroke

$$\left.\begin{aligned} x &= s\cos(\theta_1 + \omega_r t) \\ y &= s\sin(\theta_1 + \omega_r t) \end{aligned}\right\} \qquad \frac{\theta_o - \theta_1}{\omega_e} \leq t \leq (\theta_o - \theta_1)\left(\frac{1}{\omega_e} + \frac{1}{\omega_r}\right), \; 0 \leq s \leq \ell_r \tag{6b}$$

Vol. 17
1980

Here s is the length along the cilium. It is convenient if we non-dimensionalize the linear dimensions with respect to ℓ, and velocities with respect to $f\ell$ (where f is the frequency of the ciliary beat). This non-dimensionalization produces

$$Y = y/\ell \qquad U^* = U/f\ell, \qquad U^*_c = U_c/f\ell$$

and $T = \Omega t$. The force distribution on the model cilium is obtained by using the formula from the appendix of Blake (2) and by averaging over time we obtain the following expression.

$$U_c^*(Y) = \begin{cases} 0; & 0 \leq Y \leq L_r \sin\theta, \\ Y[\theta_o - \theta_1 - 2\cos^{-1}(\frac{Y}{L_r})]; & L_r \sin\theta_1 \leq Y \leq L_r \\ 2Y\cos^{-1}(Y/L_e); & L_r \leq Y \leq L_e \end{cases} \tag{7}$$

To obtain this expression we have set $L_r = L_e \sin\theta_1$ where $L_r = \ell_r/\ell$ and $L_e = \ell_e/\ell$. We would obtain slightly different profiles if we used either inequality, but the profile is simplified by assuming equality.

The three layers of the profile correspond to (i) the region in which the cilia rotates in both effective and recovery stroke. To derive this expression we are considering the time integral of the force and hence the velocity because of the linear dependence between the two. However, since we return to the same location, this integral must be identically equal to zero. (ii) In this region the cilium is always present in the effective stroke, but only for part of the recovery stroke. (iii) Only the effective stroke operates in this region.

We can also obtain $\in(Y)$ for this special beat pattern.

$$\in(Y) = \begin{cases} \in_o = [\frac{1+1/\gamma}{2} + \frac{(1-1/\gamma)\sin 2\theta_1}{2(\theta_o-\theta_1)}]; & 0 \leq Y \leq L_r\sin\theta_1 \\ \quad [\frac{1+1/\gamma}{2(1+\omega_e/\omega_r)} + \frac{(1-1/\gamma)\sin 2\theta_1}{2(\theta_o-\theta_1)(1+\omega_e/\omega_r)} \\ \quad + \frac{(1+1/\gamma)}{(1+\omega_r/\omega_e)(\theta_o-\theta_1)}\cos^{-1}(Y/L_r) \\ \quad + \frac{(1-1/\gamma)}{(\theta_o-\theta_1)(1+\omega_r/\omega_e)}\frac{Y}{L_r}(1-\frac{Y^2}{L_r^2})^{\frac{1}{2}}]; & L_r\sin\theta_1 \leq Y \leq L_r \\ \quad [\frac{(1+1/\gamma)\cos^{-1}(Y/L_e)}{(\theta_o-\theta_1)(1+\omega_e/\omega_r)} + \frac{(1-1/\gamma)}{(\theta_o-\theta_1)(1+\omega_e/\omega_r)} \\ \quad \frac{Y}{L_r}(1-\frac{Y^2}{L_e^2})^{\frac{1}{2}}]; & L_r \leq Y \leq L_e \end{cases} \tag{8}$$

To calculate $\in$ we have neglected the mean of the time dependent components of the velocity and the orientation tensor. However $\in(Y)$ recognises the fact that the cilium is only located at a given height for only part of its effective and

recovery strokes and hence is very important in determining the resulting velocity profile. In Figure 2(a) graphs of $U_c^*(Y)$ and $\in(Y)$ are shown for the above idealised beat pattern.

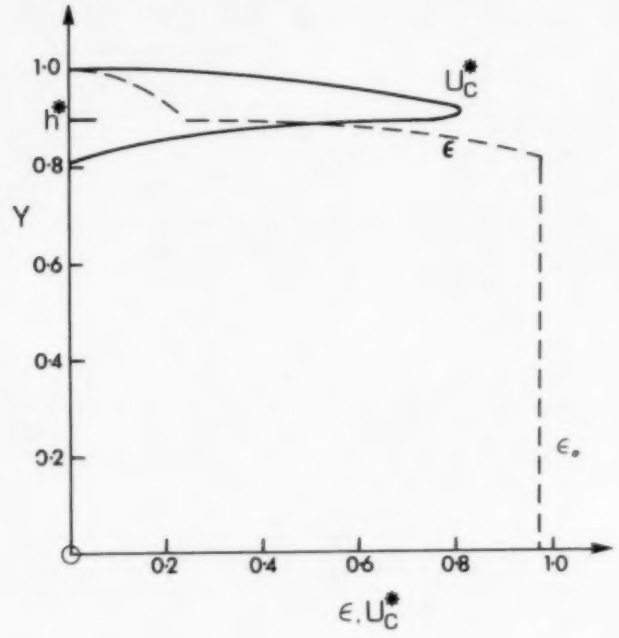

FIG. 2

The functions U_c^* and $\in$ as defined by (7) and (8) respectively. To obtain this plot we have taken $\omega_e/\omega_r = 3.0$.

NUMERICAL SOLUTION

To develop a better model we solve,

$$\frac{d^2U}{dY^2} + T^2(U_c^*(Y) - \in(Y)U(Y)) = 0 \qquad (9)$$

numerically for the values of U_c^* and $\in$ given in (21) and (22).

Actually in the region $0 \leq Y \leq L_r \sin\theta$ with $U_c^* = 0$ and $\in = \in_o$ we can obtain an analytic expression for the velocity

$$U = U_o \sinh T \in_o^{\frac{1}{2}} Y \qquad (10)$$

with U_o an unknown being determined from the numerical solution at $Y = L_r \sin\theta$.

If $T \gg 1$ we might expect that the 'active porous medium' result of Blake (3)

$$U(Y) \sim U_c^*(Y)/\in(Y) \qquad (11)$$

will be a good approximation.

Vol. 17
1980

This, however, neglects the possible importance of thin 'boundary layers' near the serous/mucous layer interface.

Before discussing the result, we need to estimate the numerical range of T. In the calculations we have assumed that γ, the ratio of normal to tangential resistance coefficients is two (in reality it will be somewhat less than 2). Likewise we can obtain an estimate for T from the normal resistance coefficients of a regular array of cylinders (see Happel et al. (8)) as follows,

$$T = \left(\frac{4\pi}{\log\left(\frac{d}{r_o}\right) - \frac{1}{2}} \right)^{\frac{1}{2}} \frac{\ell}{d} \qquad (12)$$

where ℓ, d and r_o are the length, spacing and radius of the cilium respectively. It seems that T_o lies in the range 5 - 25. We consider examples at both extremes of this range in Figure 3.

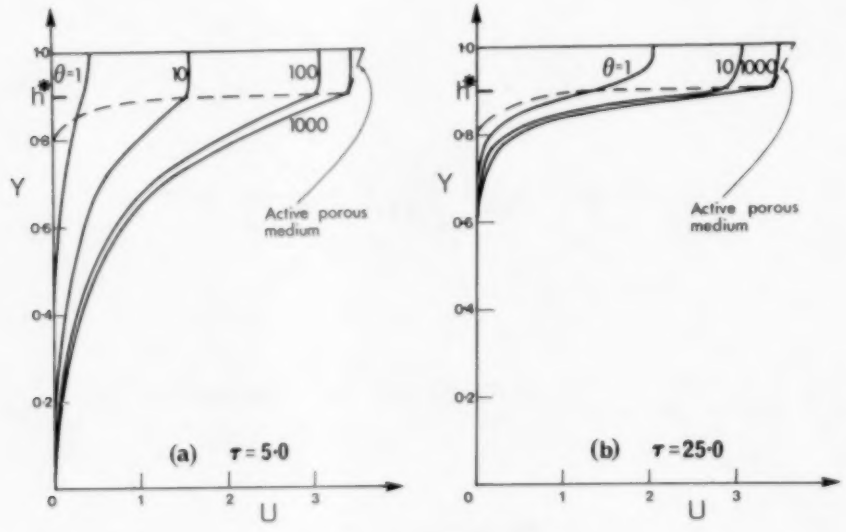

FIG. 3

Velocity profiles obtained by solving (23) numerically for (a) T = 5 and (b) T = 25. Values of θ (=1,10,100 and 1000) are indicated on the diagrams ($h^* = 0.9 = \sin^{-1}\theta_1$). The 'active porous medium' velocity profile given by (11) is also sketched on the diagrams.

In Fig. 3(a) we have taken T = 5 and plotted the velocity profile for increasing θ. The θ = 1 example corresponds to the case when the lower and upper fluid have the same viscosity or when the cilia lie entirely within the serous layer. For increasing θ the velocity of the fluid increases until it approaches close to the maximum velocity for θ = 1000. In this example the flow rate of the mucous has increased by an order of magnitude for θ = 1000 over θ = 1. Thus penetration of the cilia into the mucous layer substantially increases the flow rate in this example. Other important features to notice are the retardation of the velocity in the serous layer by the cilia and the almost constant 'plug' flow of the mucous layer. Also in Fig. 3(a) we have included the profile corresponding to (11). Fig. 3(b) is similar to Fig. 3(a), but with two enhanced features of the velocity profile. The first concerns the much larger velocity of the mucous layer in the case of θ = 1, such that increasing the viscosity of the upper layer a thousand fold only doubles the velocity. The second feature is the almost total retardation of

flow in the serous layer, in fact it closely approaches the 'active porous medium' profile which is also included in this figure.

This example suggests that the penetration of cilia, although still important for enhanced flow rates, does not produce the profound increase in flow rate. It seems that cilia density on the epithelial surface may play an important role in the efficiency of mucous transport.

CONCLUSIONS

The theoretical models suggest that the penetration of cilia into the mucous layer enhances transport, but the extent of the enhancement is still the subject of debate. Two other features that are important are the 'plug' flow in the mucous layer and the retardation of mean flow in the serous layer. To develop such a simple model many assumptions were used in the analysis, although all the essential physical features of muco-ciliary transport were included except for the very important aspect that the fluid in the mucous layer is non-Newtonian. The memory effects of the mucus may well provide another important mechanism for transport because of the aperiodicity of the ciliary beat. To study this analytically, even for linear models, would involve a much more detailed analysis of the full unsteady equations of motion.

REFERENCES

1. BLAKE, J.R. A model for the microstructure in ciliated micro-organisms. J. Fluid Mech. 55, 1-23, 1972.

2. BLAKE, J.R. Hydrodynamic calculations on the movement of cilia and flagella. Part 1. Paramecium. J. Theor. Biol. 45, 183-203, 1974.

3. BLAKE, J.R. A porous medium model for ciliary propulsion. J. Theor. Biol. 64, 697-701, 1977.

4. BLAKE, J.R. and SLEIGH, M.A. Mechanics of ciliary locomotion. Biol. Rev. 49, 85-125, 1974.

5. BLAKE, J.R. and SLEIGH, M.A. Hydromechanics of ciliary propulsion. In: Swimming and Flying in Nature. T.Y. Wu, C.J. Brokaw and C. Brennen (Eds.). N.Y.: Plenum, 1975, pp. 185-209.

6. CHEUNG, A.T.W. and JAHN, T.L. Determination of the movement pattern of the epithelial cilia of rabbit trachea and the clearance mechanism of the tracheal muco-ciliary clearance system. In: Swimming and Flying in Nature. T.Y. Wu, C.J. Brokaw and C. Brennen (Eds.). N.Y.: Plenum, 1975, pp.289-299.

7. GILBOA, A. and SILBERBERG, A. In situ Rheological characterization of epithelial mucus. Biorheology 13, 59-65, 1976.

8. HAPPEL, J. and BRENNER, S. Low Reynolds Number Hydrodynamics. Englewood Cliffs, N.J.: Prentice Hall, 1965, 553pp.

9. IRAVANI, J. Flimmerbewegung in den intrapulmonalen luftwegene der Ratte. Pflügers Arch. Ges Physiol. 297. 221-237, 1967.

10. IRAVANI, J. and VAN AS. Mucus transport in the tracheo-bronchial tree of normal and bronchitic rats. J. Path. 106, 81-93, 1972.

11. KELLER, S.R., WU, T.Y. and BRENNEN, C. A traction layer model for

Vol. 17
1980

ciliary propulsion. In: Swimming and Flying in Nature. T.Y. Wu, C.J. Brokaw and C. Brennen (Eds.) N.Y.: Plenum, 1975, pp.253-271.

12. LIRON, N. and MOCHON, S. The discrete cilia approach to propulsion of ciliated micro-organisms. J. Fluid Mech. 75, 593-607, 1976.

13. LUCAS, A.M. and DOUGLAS, L.C. Principles underlying ciliary activity in the respiratory tract. II. A comparison of nasal clearance in man, monkey and other mammals. Archs Otolaryngol. 20, 518-541, 1934.

14. MACHEMER, H. Ciliary activity and metachronism in protozoa. In: Cilia and Flagella. M.A. Sleigh (Ed.) London and New York: Academic Press, 1974, pp.199-286.

15. REISSIG, M., BANG, B.G. and BANG, F.B. Ultrastructure of the muco-ciliary interface in the nasal mucosa of the chicken. Am. Rev. of Resp. Dis. 117, 327-341, 1978.

16. SADE, J., ELIEZER, N., SILBERBERG, A. and NERO, A.C. The role of mucus in transport by cilia. Am. Rev. Resp. Dis. 102, 48-52, 1970.

17. SATIR, P. The present status of the sliding microtubule model of ciliary motion. In: Cilia and Flagella. M.A. Sleigh (Ed.), London: Academic Press, 1974, pp.131-142.

18. SLEIGH, M.A. The nature and action of respiratory tract cilia. In: Respiratory Defense Mechanisms, J.D. Brain, D.F. Proctor and L.M. Reid (Eds.), New York: Marcel Dekker, 1977, Pt. 1 pp.247-

19. WINET, H. Ciliary propulsion of objects in tubes: wall drag on swimming tetrahymena (Ciliata) in the presence of mucin and other long chain polymers. J. Exp. Biol. 64, 283-302, 1976.

20. WU, T.Y. Introduction to the scaling of aquatic animal locomotion. In: Scale Effects in Animal Locomotion. T.J. Pedley (Ed.), London: Academic Press, 1977, pp.203-232.

Vol. 198

BIORHEOLOGY Vol.17, pp. 135-150 0006-355X/80/010135-16$02.00/0
© Pergamon Press Ltd. 1980. Printed in the United States

THIRD INTERNATIONAL CONGRESS OF BIORHEOLOGY

SYMPOSIUM ON MUCO-CILIARY TRANSPORT

ON THE MECHANICS OF MUCOCILIARY FLOWS I. OBSERVATIONS OF A CHANNEL MODEL

H. Winet and J.R. Blake

Department of Physiology and School of Medicine,
Southern Illinois University, Carbondale, IL 62901 &
California Institute of Technology; and
CSIRO Division of Mathematics and Statistics,
P.O. Box 1965, Canberra City A.C.T., Australia, 2601

(Received 1.7.1979. Accepted by Guest Editors T.Y. Wu and S. Berger)

ABSTRACT Cilia-generated fluid flow between two strips of frog palate epithelium has been measured and flow velocity profiles have been obtained from the data. The strips are mounted in a covered chamber so as to form a ciliated channel and fluid motion is marked by suspended 1.0 μm polystyrene latex spheres which act as tracers. Results from a control non-mucus system and a 40% - 50% v/v mucus system are compared with predictions of a theoretical model. This theory for flow in mucociliated channels incorporates flow due to a static pressure drop between the channel ends and a difference in the cilia tip speeds between the two strips.

Vol. 17
1980

INTRODUCTION

Cilia which propel liquids in tubes of mammals are found in the otolaryngeal (e.g. Eustachian tube), respiratory (e.g. tracheal tube), nervous (e.g. brain ependyma) and reproductive (e.g. oviduct and ductuli efferentes) systems. In the Eustachian tube cilia help prevent large changes of pressure in the middle ear by clearing out liquid plugs, (1). In the trachea cilia remove mucus and particulate matter. In the ductuli efferentes cilia may keep spermatozoon suspensions moving toward the epididymis and in the ampulla of the oviduct they are the main source of propulsion for the ovum (2). In the brain ependyma cilia enhance transmural transport (3) by reducing the unstirred layer.

Morphologically the cilia lining biological tubes such as the trachea, cervix and oviduct are different from those of protozoa. Typically the tubal cilia are short, usually around 5 μm in length while those of fast swimming protozoa are 7 - 15 μm long. The beat frequency appears to be similar in both circumstances, 10 - 30 Hz, although it may change with time, as a function of estrus cycle phase, (4) (however, see also (5)) and location (as a function of distance from the cranial end of the lungs (6)) in tubal epithelium.

Cilia of ciliated epithelium are usually crowded into tufts on cells which may be separated from other ciliated cells. In the lung where ciliated cells form continuous layers only a few diameters separate adjacent cilia (6 - 10 cilia/μm^2). In the oviduct where ciliated cells comprise 40 - 80% of surface cells, and carry 200 - 300 cilia each (7) the spacing is of the order of 0.05 to 0.15μm or 8 cilia/μm^2 (measured from (7)). In contrast the spacing of cilia over the surface of the fast swimming Paramecium is 0.1 - 0.25 cilia/μm^2 (8, 9).

The fluid propulsion generated in tubes is termed "internal flow" because the liquid is bounded on at least two opposing sides. There are well established fluid mechanical grounds for expecting that cilia-generated internal flows are different from "external flows" (flow in fluids bounded on one side only) particularly with respect to the existence of a pressure gradient along the internal system. Accordingly, we cannot normally use external flow systems as experimental models for internal flow models.

In mucociliated epithelium of both the respiratory and reproductive tracts "secretory cells" which contain glycoprotein granules and Clara cells are interspersed with ciliated cells (10) in varying degrees. The concentration not the oligosacharide ratio of glycoprotein suspensions secreted from secretory cells appears to be the main determinant of its rheology. Thus low concentration (< 0.5% w/v) suspensions with Newtonian rheology are secreted from serous secretory cells and high concentration (> 0.5% w/v) glycoprotein suspensions with non-Newtonian rheology (at lower shear rates) from mucous cells. The glycoprotein secretions from mucous cells of the cervix will reach concentrations as high as 7.5% (w/v) (11), and during ovulation low enough such that the fluid can be considered Newtonian. In the lung and oviduct the secreted glycoprotein concentrations cover a wide range simultaneously. At one extreme they are great enough to form a blanket layer (12, 13, 14) over the cilia and at the other extreme they form a watery serous layer amongst the cilia. The transition to the mucus blanket state apparently begins, in the lungs at least, when small aggregates or flakes of mucus gel, 4 - 70 μm in diameter are transfered from their secretion sites to points of aggregation where they form larger plaques and then streams of mucus (15). These streams possibly coalesce downstream into blankets.

The ultimate internal flow experimental model would be the mucociliated tube. But development of merely ciliated tube biological models has been hampered by an inability to resolve the flow paths of tracer particles in the lumen. So-called transparent tube walls are simply not transparent enough to allow the special illumination optics (e.g. darkfield, Nomarski interference and Hoffman modulation contrast) which are needed to resolve small tracer particles. Fiber optics in conjunction with "windows" in the tube wall have improved resolution considerably; but the fiber interferes with flow.

In contrast, flow in ciliated channels places no optical obstruction other than the cilia (or "mucocilia") between the observer and the light source so fluid tracer particles are easily illuminated. Moreover, it has been shown by Liron (16) that ciliated channel flow velocity profiles are qualitatively similar to those of ciliated

tubes. Accordingly, the ciliated channel is a reasonable qualitative approximation for ciliated tube flow and a significantly more correct experimental model than the external flow system.

We report here observations of cilia-generated flow in both ciliated and mucociliated channels. Both sets of observations are compared with predictions of flow velocity profiles from fluid mechanical theory described below. The experimental models are constructed with frog palate epithelium.

METHODS

The Experimental Setup

Large ($\geq$ 7 cm body length) *Rana pipiens* and *R. catesbiana* are maintained in plastic containers with ca. 1 cm deep distilled H_2O at 16 - 17 °C in an incubator. Frogs are removed as needed and immediately processed on a cervical dislocator (Cervical Dislocators, Inc.). The dorsal part of the head is then excised and immersed in c. 20 ml amphibian phosphate buffer solution APBS (17) until needed. The mucus is collected by mounting the severed end of the excised head on the open end of a graduated centrifuge tube and allowing it to drain for about 10 minutes.

Vol. 17
1980

The epithelium is then prepared by carefully excising it from the palate with microsurgical scissors in one or two (first cut along the midline) pieces. The pieces are then placed cilia-down on APBS-moistened filter paper and allowed to 'walk off' excess mucus. This walk-off also serves as a check for cilia motility. Ciliated strips are obtained by gently teasing the epithelium into a flattened position and cutting longitudinally through both the epithelium and filter paper. Both length and width of strips vary but a minimum for each of 5 mm is maintained. Maximum length does not exceed 15 mm. During and after cutting the epithelium is kept moist with APBS. The freshly-cut strips are then gently drawn onto a coverglass panel to which they are tied with nylon (#50) thread.

Two ciliated panels are then placed in the observation chamber as shown in Figure 1. The chamber contains either a control solution APBS+, which is APBS with less than one drop/20 cc of 1 μm polystyrene latex spheres added, or APBSm which is APBS+ mixed with the drained-off mucus collected earlier. The various dilutions of APBSm are obtained by adding APBS+ and mixing vigorously with a wooden rod.

As indicated in Figure 1 the observation chamber fluid is continuous with a fluid reservoir and completely surrounds the ciliated panels such that the midpoint of the chamber between the two ciliated panels is at least 1mm from a rigid wall. The ciliated channel width which is the distance between the parallel ciliated panels is adjusted by simply sliding the panels. The chamber construction also allows the alignment of the panels so that their cilia may beat in opposite directions.

Flow of the polystyrene fluid tracers and the various ciliary beat parameters are recorded on motion picture film through a Nikon microscope (LKe) utilizing Hoffman Modulation Contrast optics and

strobed—by camera—xenon arc illumination. Focus during filming is maintained in the vertical midplane. Where channel width exceeds the microscope field, overlapping field sequences are filmed at each ciliated panel and the channel width is measured at a lower magnification with a calibrated Whipple disc.

Each series of observations consists of filming at various channel widths with the widths being varied in a random fashion. Random channel width variation is necessitated by a possible relationship between time following excisement and ciliary activity as indicated by the generally short duration of ciliary activity in our chamber as compared with the ciliary activity of an uncovered epithelium still attached to the excised dorsal head (cf 18).

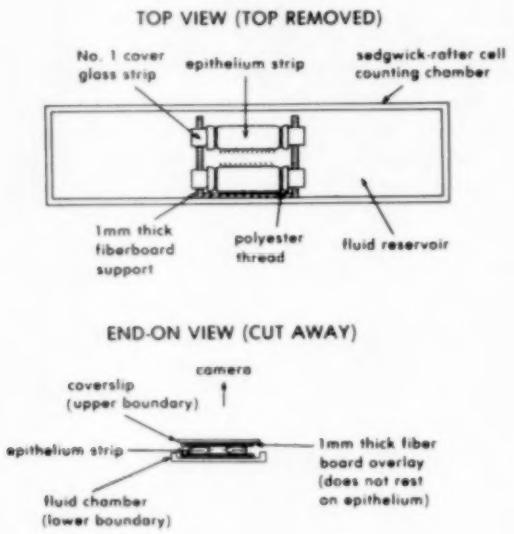

FIG. 1

Frog ciliated epithelium biological model.

The films resulting from the above observations are analyzed with the aid of a NAC film reader. The fluid tracer motion of the polystyrene spheres is plotted frame-by-frame and the average velocity of a particle or group of particles at a given distance from the epithelium determines each point of a flow velocity profile plot. Where ciliary beat frequency f cannot be resolved directly, and wave velocity c and wave length λ can, f is calculated from

$$c = f\lambda$$

The Fluid Mechanical Theory

We suppose the cross-section of the ciliated channel is as illustrated in Figure 2. The distance between the tips of the cilia sublayer (the extra-ciliary width) is $D'=2b$ $(=D - 2\ell)$. The depth of the chamber is much greater than D' so we can neglect the variation in the x direction. The velocities generated by the cilia at the top of the

sublayers are U_1 and U_2 in a direction out of the page (i.e. in the z direction). When mucus is present it is assumed to be completely penetrated by the cilia and so is taken to have a layer depth of $\ell-\delta$ where δ is the thickness of the serous fluid.

In the following analysis all fluids are taken to be Newtonian with a known density and viscosity μ although we can consider the fluid in the layer closest to the epithelium (the serous layer) to have a lower viscosity as previously discussed by Blake & Winet (20). Because of the low flow rates and small dimensions the Reynolds numbers are very small, allowing us to apply the Stokes flow equations in one dimension

$$\frac{dp}{dz} = \mu \frac{\partial^2 U}{\partial y^2}$$

where p is the pressure, and U the fluid velocity in the z direction.

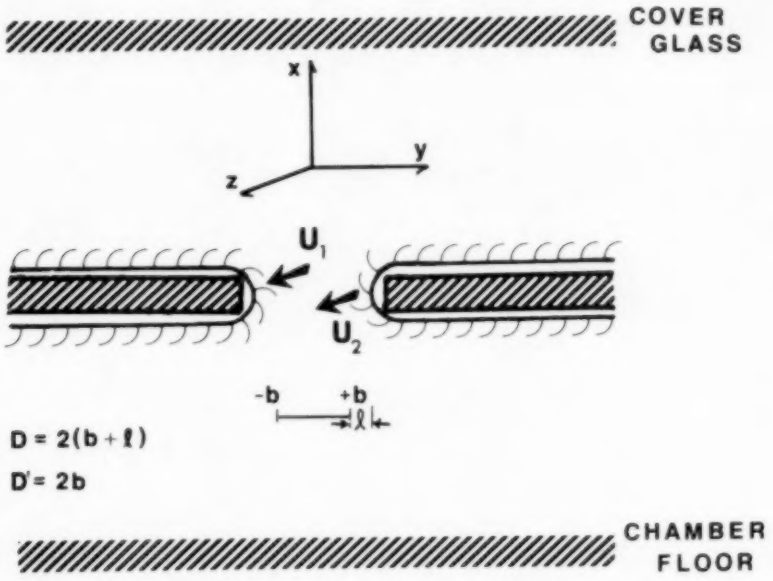

FIG. 2

The theoretical fluid mechanical model

The flow-field can be divided into two parts; (i) the two cilia sublayers and (ii) the central lumen region. Any pressure gradient will have an extremely limited effect on the fluid velocities in the cilia sublayer because of the increased resistance due to the surface area presented by the cilia. Accordingly, we will suppose that in the cilia sublayer the flow is due entirely to the beating of the cilia. In a previous paper (20) we described a simple theoretical model using serous and mucus layers of vastly differing viscosities to model aspects of mucociliary transport. In this report it is sufficient to approximate the flow field in the cilia sublayer as follows,

Vol. 17
1980

$$U_c(y) = \begin{cases} 0; & -(b+\ell) \le y \le -(b+\ell-\delta) \\ & b+\ell-\delta \le y \le b+\ell \\ U_1; & b \le y \le b+\ell-\delta \\ U_2; & -(b+\ell-\delta) \le y \le -(b+\ell). \end{cases}$$

That is, the mucus section (of depth $\ell-\delta$) of the ciliary layer moves along as a blanket with a constant velocity U_m (U_1 or U_2), while the serous layer is presumed totally retarded by the dense mat of cilia. This is probably a reasonable approximation for channels in chambers where chamber depth >>D as is the case with the present model. Such a conclusion is suggested by our previous theory (20). (There is evidence ——— a damping of fluid flow by the glass walls ——— that the approximation is not valid for chambers with thicknesses of the order $2(b+\ell)$ or less (19).)

For the non-mucus control we have to match the sublayer flow with the external flow in one continuous profile but since our experimental model shows only the extra sublayer flow, we shall present only this part of the flow equation which is the same in both the control and mucus models.

In modelling flow in the central lumen we divide the velocity field into two components induced by (i) the pressure drop along the apparatus and (ii) the cilia

$$U(y) = U_p(y) + U_c(y) \qquad (4)$$

where

$$U_c(y) = \frac{U_1 + U_2}{2} + \frac{y}{D'}(U_1 - U_2) \qquad (4a)$$

and

$$U_p(y) = \frac{1}{2\mu}\frac{dp}{dz}\left(y^2 - \frac{D'^2}{4}\right) = \frac{1}{2\mu}\frac{dp}{dz}(y^2 - b^2) \qquad (4b)$$

The volumetric flow rate per unit length in this system is

$$Q(D') = 2(\ell-\delta)(U_1+U_2) + \int_{-b}^{b} U(y)dy = 2(\ell-\delta)(U_1+U_2)b - \frac{2}{3\mu}\frac{dp}{dz}b^3 \qquad (5)$$

We can usually neglect the first term on the right hand side of (5) as it is small in comparison to the other terms; and in the following analysis it will be dropped. To uniquely determine the flow velocity profile either Q or the total pressure drop per unit length $\Delta P/L = \nabla P$ (where L is the length of the sealed chamber) must be prescribed. Once one is known the other can be obtained from (5) by using the substitution $dp/dz = \nabla P$. Unfortunately, neither Q nor ∇P was obtained in this experiment but we can use the observed flow velocity profile to obtain a measure of ∇P and at the same time check to see if the present level of approximation in the theory is acceptable for predicting profiles with a reasonable fit to the data. The evaluation of the theory, accordingly, will consist of plotting the

observed profiles and then using measured U_m values to calculate and plot U(y) for different values of ∇P using (4). The ∇P giving the best fit will then be considered the best estimate of the experimental model ∇P. The remaining parameter μ will be kept constant at that of water although it will be considered as a parameter for the mucociliary systems where mucus may invade the lumen of the channel.

EXPERIMENTAL RESULTS

Control-APBS+

Flow velocity profiles for APBS+ in three ciliated channel widths D are shown in Figure 3. All values are non-dimensionalized by their reference. Here ℓ is the thickness of the cilia sublayer and r is the extended length of a single cilium. We take $\ell = r = 5$ μm for this report. Also U_m is the maximum particle velocity. The measured U_m is assumed to be the true U_m even though the magnifications utilized do

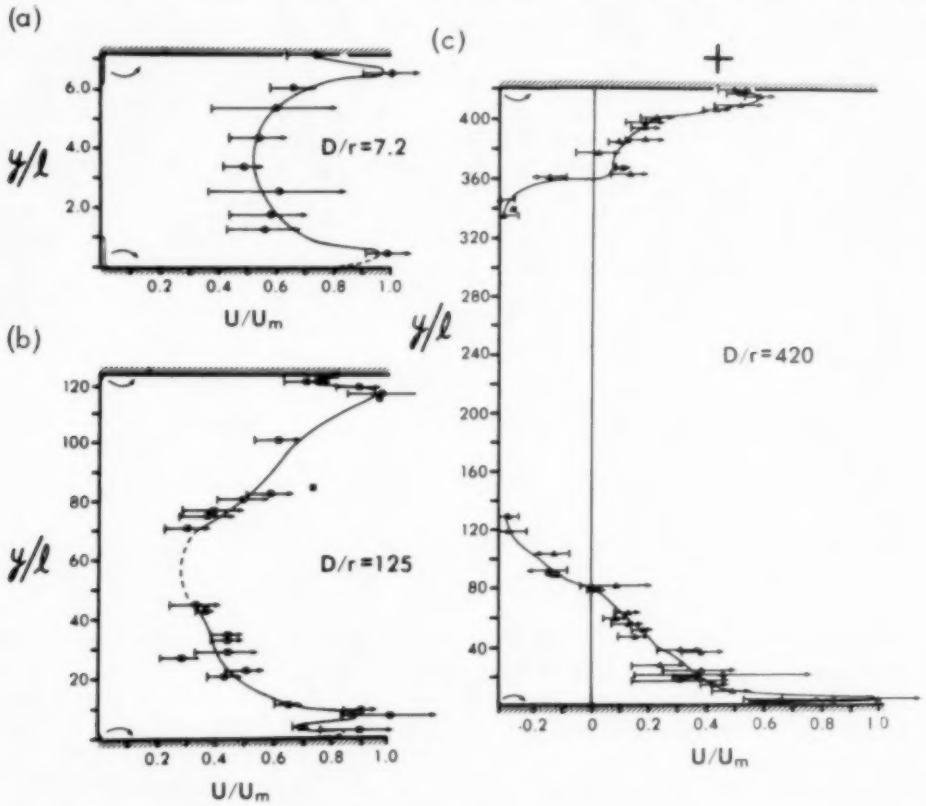

FIG. 3

Control flow velocity profiles for ciliated channels of three widths. Ordinate is reduced distance from lower epithelium surface. Abscissa is reduced velocity. Curved arrows indicate direction of cilium effective stroke. Arrows at data points indicate flow sense and length of arrows indicate standard deviation of the sample. Only the largest U_m is used to non-dimensionalize in each case. Symbols defined in text.

Vol. 17
1980

not allow measurement of U within the sublayer. This assumption is based upon earlier observations in which Cheung & Winet (19) indicated that the true U_m lies outside the sublayer.

In most preparations the ciliary activity on both ciliated panels do not match. Moreover, when D exceeds the microscope field and two overlapping film sequences are required, it is possible that there is a change in ciliary activity during the scene shift. Accordingly, even though the profiles illustrated represent the best panel matches, one can detect in 3b & c that U_m is achieved at one panel only.

Table 1 presents the various U_m's as well as the variations in the distance from the panel surface at which particle velocities drop to 50% of U_m.

As one follows the curves toward the channel center from the U_m position a rather rapid decrease in U occurs. The rate of this decrease is greatest in the narrowest channel but not smallest in the widest channel as indicated in the last column of Table 1.

Backflow is present in channels as wide as $D/\ell = 420$ but is absent in those as narrow as $D/\ell = 125$. The dashed part of the Figure 3b curve is an acknowledgement of the lack of tracers at the very center of the channel which would have provided more direct evidence of the lack of backflow.

TABLE 1.

$\frac{D}{r} = \frac{D}{\ell}$	U_m in $\mu m\ sec^{-1}$		$\frac{y}{\ell}$ at 50% U_m
	U_1	U_2	
7.2	373	378	absent
125	236	230	18 - 47
420	97	168	9 - 18

The point at which flow changes direction (U = 0) is not the same on both sides of the $D/\ell = 420$ channel (Fig. 3c). On the side with the larger U_m, the transition point is $y/\ell = 80$ but on the other side (upper part of the figure) U = 0 at $y/\ell = 60$ (420 - 360).

Some measurements of U_m as a function of f have been obtained and are presented along with the assumed point $U_m = 0$ at f = 0 in figure 4. In all cases f is calculated from measured c and λ values. U_m used in each case is the average velocity of the fastest particle observed (i.e. not the average for all particles at that distance from the ciliated surface; it is felt that the fastest particle is the most 'unencumbered' tracer, other particles may have small strands of mucin attached which may be stuck to slower-moving surfaces).

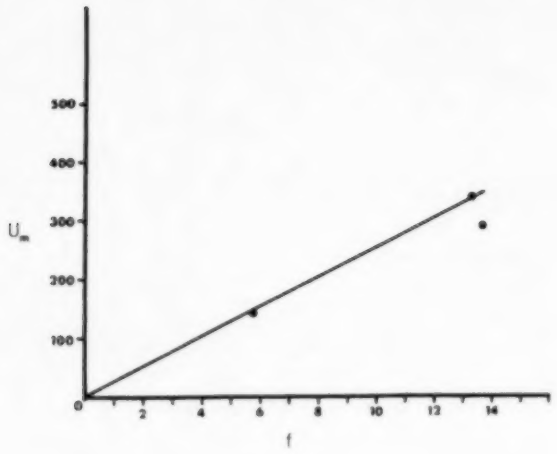

FIG. 4

Flow velocity of fastest measured tracer particles as a function of beat frequency f. Plot is extrapolated back to the point (0, 0). U_m is in 10^{-6} ms^{-1} and f is in Hz.

Vol. 17
1980

Mucociliary Channel-APBSm

"Vigorous mixing" of APBS+ with drained palate mucus suspension does not result in a homogeneous suspension. Strands of mucus are still evident in the mucociliated channels particularly when the two epithelia are allowed to touch and then separated. Even without the aid of Hoffman Modulation Contrast illumination one can see an intermittent series of mucus strands and patches wafting over the cilia. We record no data when the thickness of this mucus 'layer' appears to be greater than ℓ. The vigorous mixing does allow a somewhat random distribution of mucus patches in the reservoir fluid so that the channel has a constant supply.

Flow velocity profiles for APBSm in three ciliated channel widths are shown in Figure 5. The percentage values are in volume of drained mucus divided by the total suspension volume. The graph variables are the same as in Figure 3 and so are the apparent sources of U_m variation. In the narrowest mucociliary channel, however, the difference in motility between the two ciliated surfaces is so great than an adjusted curve is added to Figure 5a. Of the two curves the solid line is based upon the absolute U_m (which is U_2) and the dashed line is a split of the plot with the upper part based on U_1 and the lower part based on U_2. The resulting curve which is formed by matching U_1 and U_2 -based curves is more symmetrical than the plot based on one U_m.

The U_1 and U_2 values in figures 5b & c match fairly well so a splitting of U_m is not warranted.

The various U_m's and 50% U-drop distances for the mucociliated channel are presented in Table 2 as a parallel to Table 1.

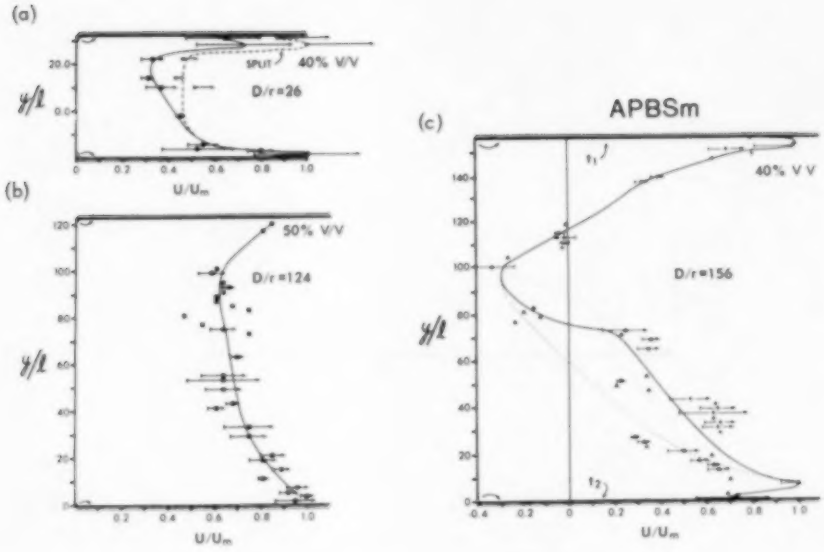

FIG. 5

Flow velocity profiles for mucociliated channels of three widths. Upper part of 5a is drawn for two values of U_1 the solid line is referenced to U_2 near the 'lower' epithelium and the broken line to U_m near the 'upper' epithelium (the true U_1). The symbols t_1 and t_2 in 5c indicate that the two epithelia were not photographed simultaneously. Other quantities and symbols are defined in the text or legend to Figure 3.

2.

TABLE

$\frac{D}{r} = \frac{D}{\ell}$	U_m in $\mu m\ sec^{-1}$		$\frac{y}{\ell}$ at 50% U_m
	U_1	U_2	
26	148	203	5
124	90	106	>62
156	212	200	14 - 36

In general the values of U_m are smaller for 'mucocilia' than they are for the control.

The decrease in U following the profile from U_m toward the chamber center follows the same general pattern as the control; i.e. the narrowest channel exhibits the greatest slope and the mid-width channel the smallest slope.

One notable difference between the control and mucociliary flow profiles is the latter's apparent non-uniform approach to backflow with increase in channel width. In the control the minimum particle velocity U_o decreases with increase in channel width in both its dimensional form (U_o) and its non-dimensional form U_o/U_m. In the mucociliary channel the non-dimensional values (see Figure 5) increase before they decrease, but the dimensional values decrease uniformly with increase in channel width as shown in Table 3 which compares the two systems.

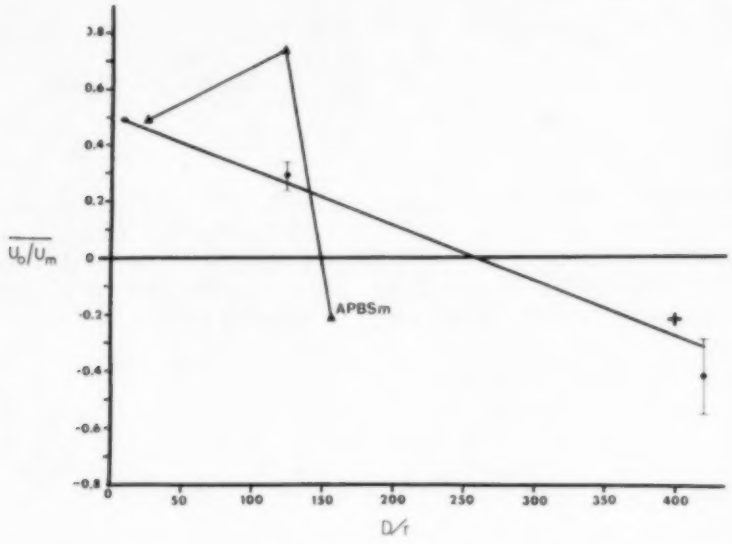

FIG. 6

Reduced flow velocity of the slowest or most negative measured tracer particles as a function of channel width. In each case U_o/U_m was calculated for each epithelium of a channel and the two resulting values averaged. Error bars are standard error of the sample. Other symbols are defined in text.

CONCLUSIONS FOR EXPERIMENTAL RESULTS

The differences between ciliary and mucociliary flows in these experiments are major only in the values of U_m attained in comparable channel widths and the drop in particle flow velocity from U_m to U_o. Since no measurements of f were obtained from the mucociliary systems, we cannot be sure that these differences were simply rheological effects of the mucus. Moreover, no bulk viscosity measurements were obtained so the difference in mechanical load upon the cilia of the two systems cannot be assessed. We can, however, be reasonably sure from the observations of Machemer (8) that the change in load from 40% to 50% suspensions is not sufficient to cause a significant change in f. Accordingly, the APBSm results may be lumped together as a representative unit.

Vol. 17
1980

3.

TABLE

$\frac{D}{r}$	System	U_o/U_m	U_o in $\mu m\ sec^{-1}$	$U_m - U_o$
7.2	+	0.54	203	173
26	m	0.46	81	95
124	m	0.62	61	37
125	+	0.275	64	169
156	m	-0.30	-29	126
420	+	-0.30	-72	312

The generally lower U_m values for mucociliary flow are probably not the result of a reduction in f because these are the velocities at which the mucus layer moves and with the exception of the med-width channel compare well (see Table 2) with the 167 $\mu m\ s^{-1}$ mucus layer velocity measured by Gilboa and Silberberg (18).

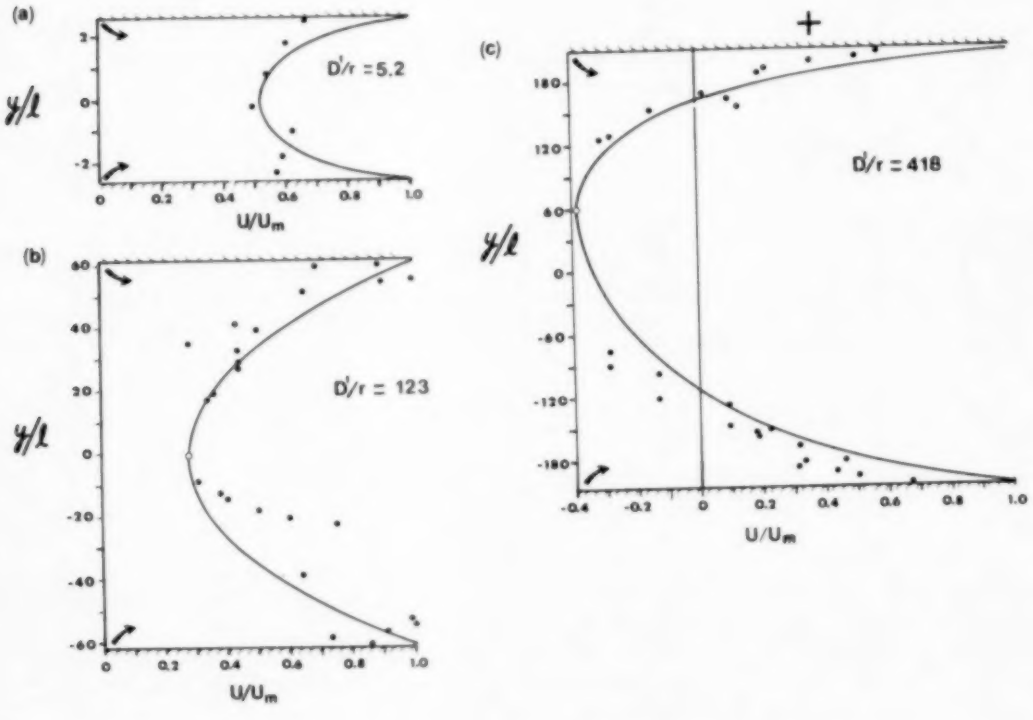

FIG. 7

Comparison of theoretical with experimental control models via predicted vs. measured flow velocity profiles in ciliated channels. Heavy line plots are theoretical. Solid circles are data points from Figure 3. Open circles are extrapolated data points. All symbols are defined in the legend of Figure 3 or the text.

It is evident that at some channel width in the range $124<D/\ell<420$, $U_o = 0$ (the transition point). Beyond this point $U_o<0$. If U_o/U_m is a linear function of D/ℓ then the control plot drawn in Figure 6 is valid and the transition point is around $D/\ell = 270$. If U_o/U_m is a nonlinear function of D/ℓ as suggested by the APBSm plot of the figure, then more observations will be necessary before the form of the relationship is clear. The data summarized in Figure 6 suggest that mucus allows backflow to appear in narrower channels than the control does. In the present cases the control channel has to be almost twice as wide as the mucociliary channel before backflow appears. More data for both regimes will be necessary, however, before any conclusion is possible.

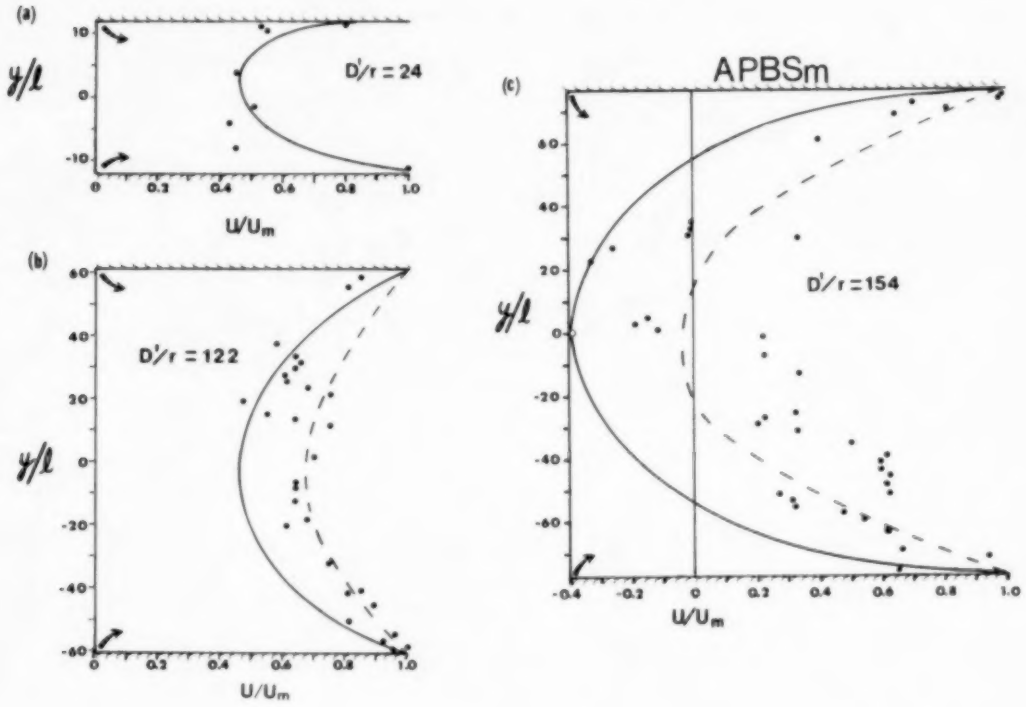

FIG. 8

Comparison of theoretical with experimental models via predicted vs measured flow velocity profiles in mucociliated channels. Format for plots is described in the legend for Figure 7. All symbols are defined in the legend for Figure 5 or the text.

DISCUSSION

The Agreement Between Theory and Experiment

The critical test of a theoretical model is the degree to which it conforms to the experimental model. Theoretical and experimental results are compared in Figures 7 and 8. Here the plots from Figures 3 and 5 are reproduced with data points and the theoretical results

Vol. 17
1980

from equations (4) are added as solid lines. In some cases dashed lines representing better "by-eye" fits are added for comparison.

In all cases the theoretical curves were generated by requiring that they run through three points, U_1, U_2 and the minimum value of U, U_0. In cases where data was lacking for U_0 the extrapolated values from figures 3 and 5 were used. Figure 7 represents a ciliated channel propelling a single Newtonian fluid (the control). We might expect these profiles to compare best with the data because of minimized error due to the absence of mucus. (Slow-moving strands of mucus can pull attached tracers back and/or fast-moving mucus strands which have just broken can pull attached tracers forward during their rapid recoil.) There is indeed better agreement between the Newtonian fluid data and theory than between non-Newtonian fluid data and theory which is plotted in Figure 8. The ∇P's and values of U_0 are compared in Table 4.

4

TABLE

$\frac{D'}{\ell}$	Conditions	U_{min}/U_m	∇P dynes-cm^{-2}
5.2	+	0.515	2.17×10^{2}
123	+	0.281	3.56×10^{-1}
418	+	-0.398	4.2×10^{-2}
24	m	0.478	5.47×10^{0}
122	m	0.688	1.06×10^{-1}
154	m	-0.403	3.87×10^{-1}

The variation in data from the mucociliary channel is not limited to fluctuations about a smooth theoretical curve as shown in Figure 8. Indeed an auxiliary curve had to be drawn (dashed line) for the D'/ℓ = 124 & 156 cases; the latter to allow for the probability that U_1 & U_2 changed between t_1 and t_2. Also, if the point-to-point variation in the data characteristic of the mucus channel plots may be attributed to mucus strands pulling tracers, the relative flatness of the D'/ℓ = 124 channel profiles cannot. This result has to be due to the smaller U_m values (see Table 2) which is probably due in turn to reduced ciliary activity.

One important feature to note in both the theory and experiments is the importance of the width of the channel D or D', the viscosity of the fluid in the central lumen and the presence of no-slip side boundaries on fluid flow. For a given positive pressure gradient ($dp/dz > 0$), *the wider the channel the weaker the flow in the central section* and in the widest channels of those included in our observations the flow actually reverses (see Figures 3c, 5c, 7c, 8c).

Similarly, the wider the channel the more important the retardation effect of the no-slip (slide and cover-glass of chamber) walls will be; although in the present model the spaces between the epithelium and the chamber walls reduces this factor considerably. However, increasing the fluid viscosity has an opposite effect, although it may well reduce the fluid velocities near the cilia tips and overall in the channel as indicated in the comparative values of Tables 1 and 2. An increase in viscosity will reduce the influence of the pressure gradient which must now balance the increased viscous stresses. One consequence of this prediction is less parabolic central flow velocity profiles which is indeed observed as indicated by a comparison of Figures 3ab with 5a (split) and b.

REFERENCES

1. Sade, J., *Ann. Otol. Rhinol. Laryngol.*, 80, 336-341. 1971.
2. Halbert, S. A., P. Y. Tam and R. J. Blandau. *Science*. 191, 1052-1053. 1976.
3. Nelson, D. J. and E. M. Wright, *J. Physiol.*, 243, 63-78. 1974.
4. Critoph, F. N. and K. J. Dennis, *Brit. J. Obst. Gynec.*, 84, 216-218. 1977.
5. Westrom, L.,P. A. Mardh, C. von Mecklenbrug and C. H. Hakansson, *Fert. Steril.* 28, 955-961. 1977.
6. Iravani, J., *Pflugers Arch. Ges. Physiol.* 297, 221, 1967.
7. Anderson, R. G. W., *J. Cell Biol.* 60, 393-404. 1974.
8. Machemer, H., *J. exp. Biol.* 57, 239-260. 1972.
9. Blake, J. R. and M. A. Sleigh, *Biol. Rev.* 49, 85-125. 1974.
10. Jones, R. and L. Reid, *Brit. Med. Bull.* 34, 9-16. 1978.
11. Davajan, V. and R. M. Nakamura in S. J. Behrman and R. W. Kistner (eds.) *Progress in Infertility*, Little: Boston, 1975.
12. Lucas, A. M. and L. C. Douglas, *Arch. Otolaryng*, 20, 518. 1934.
13. Sade, J., N. Eliezer, A. Silberberg and A. C. Nevo, *Am. Rev. Resp. Dis.* 102, 48. 1970.
14. Jansen, R. P. S., *Science* 201, 349-351. 1978.
15. Iravani, J. and A. Van As, *J. Path.* 106, 81. 1972.
16. Liron, N., *J. Fluid Mech.* 86, 705-726. 1978.
17. Nevo, A. C., Z. Weismann and J. Sade, *Different*, 3, 79-90. 1975.
18. Gilboa, A. and A. Silberberg in E. F. Aharonson, A. Ben-David and

Vol. 17
1980

M. A. Klingber (eds.) *Air Pollution and the Lung* NY: Halstead 49-63. 1975.

19. Cheung, A. T. W. and H.Winet in T. Y. Wu, C. J. Brokaw and C. Brennen (eds.) *Swimming and Flying in Nature Vol. I.* Plenum: NY 223-234. 1975.

20. Blake, J. R. and H.Winet, *Biorheology*, 1980.

BIORHEOLOGY Vol.17, pp. 151-162 0006-355X/80/010151-12$02.00/0
© Pergamon Press Ltd. 1980. Printed in the United States

THIRD INTERNATIONAL CONGRESS OF BIORHEOLOGY

SYMPOSIUM ON MUCO-CILIARY TRANSPORT

A THEORETICAL AND EXPERIMENTAL STUDY ON TRACHEAL MUCO-CILIARY TRANSPORT

George T. Yates*, Theodore Y. Wu*, Robert E. Johnson**, Anthony T. W. Cheung*** and Carol L. Frand*

* California Institute of Technology, Pasadena, California 91125
** University of Illinois at Urbana, Urbana, Illinois 61801
*** Loyola Marymount University, Los Angeles, California 90045

(Received 1.11.1979. Guest Editor's Contribution Invited by Editor-in-Chief A.L. Copley)

ABSTRACT A series of experiments have been carried out to investigate the muco-ciliary transport in the trachea of rat, rabbit and chicken with cinemicrographic analyses of the movement, beat pattern and metachrony of the tracheal cilia. As a principal test case of the cilia-tip-penetration-into-mucus hypothesis, detailed studies have been made on the transport of a biochemically viable mucous plug artificially introduced into the chicken trachea both with and without a pressure differential across the mucous plug. Guided by the result of these pilot experiments, a theoretical two-layer model of the muco-ciliary transport is introduced, in which the cilia are assumed to penetrate shallowly into the overlaying mucous layer during the effective stroke and to withdraw from the mucous layer during the recovery stroke. Both the mucus and the serous fluid are assumed to be Newtonian and with widely differing viscosities. Based on this model the mucus transport rate is found to depend linearly on the ciliary beat frequency and also on the time of ciliary tip penetration in the mucus. Results are also given on the propulsive force contributed by each individual cilium and an estimate of shear and shear rates within the mucous layer.

Vol. 17
1980

INTRODUCTION

Muco-ciliary systems occur in various organs in mammals (and most vertebrates), such as in the respiratory and reproductive tracts and in olfactory, auditory and other sense organs. Although they differ in physiological functions and there is considerable morphological variation in different organs, the muco-ciliary systems in the respiratory and reproductive tracts are essentially for the purpose of transporting biological and extraneous matter. The present study is devoted to an interdisciplinary investigation, both in theory and experiment, of the hydromechanical, biophysical and some physiological aspects of muco-ciliary transport in the mammalian trachea. The tracheal muco-ciliary system is selected for its relative simplicity and its lack of other perplexing factors such as the muscular contractile movement in oviduct. The biomedical significance of this research is relevant to certain diseases of and hazard to the respiratory tract that either are caused by or can result in abnormal muco-ciliary function including cystic fibrosis, chronic bronchitis, and adsorption of radioactive or biochemically-active pollutants.

The tracheal muco-ciliary system essentially consists of a mucous layer, a serous layer and epithelial cells. The epithelium is comprised of three main types of cells: cilia attached ciliated cells, mucus secreting goblet cells, and the underlining basal cells, through a more refined classification further includes brush cells, serous cells and migratory cells (for a review see Jaffery and Reid [1]). Mucus, an aqueous suspension of the glycoproteins (2-4%) and salts (1-2%) in water (95-97%) [2], is thought to have a transition from a gel upper layer (5-10 μm) to a sol lower layer ($\sim$6 μm) as the effects of ciliary activities increase toward the ciliated region [3-6]. The mucus has been observed to behave like a visco-elastic, shear-thinning medium under laboratory controlled conditions [7-9]. While a great deal of such experimental studies have been made, it may be stressed that adequate rheological properties of the mucus are generally not known for the *in vivo* conditions with the strain and strain rate approaching the level in typical operating states. On the other hand, the serous fluid is generally accepted to be an aqueous fluid [8, 10] though its density and viscosity have not been well quantified. Ross and Corrsin

[11] estimate it to be a Newtonian fluid with viscosity of 0.1 poise, which is 10 times that of water, this being due to the presence of many protein molecules. In comparison, the viscosity coefficient of the mucus, which is a sensitive function of the mucin concentration, is known to be three orders of magnitude or greater than that of the serous fluid.

Although the tracheal cilia and the cilia in micro-organisms have the same microstructure, they differ considerably in the mechanical principles of fluid transport and in various other aspects that characterize their movement. Relatively speaking, the tracheal cilia are short (generally 6-7 μm in length), densely distributed (3-11/μm^2), with a tip-to-tip spacing of 0.3 - 0.6 μm which is about twice the cilia diameter at the base, 0.2 - 0.25 μm [12]. It should be pointed out that this figure for the cilia concentration is for the densely ciliated patches and the overall average density, including non-ciliated areas, will be somewhat less. It has been observed in the rabbit trachea [13], the frog pharynx [6] and in other cases [14, 15] that tracheal cilia beat in a planar fashion, with little shape deviation during both effective and recovery strokes except near the basal end, where most of the active bending takes place, and near the tip which has been observed (by tracing and analysis of high-speed cinemicrographic data carried out in the present study) to bend more during the recovery stroke. Typically the effective stroke occupies about 1/4 to 1/3 of the cycle and the slower recovery stroke lasts the remainder at frequencies ranging over 12-25 Hz. The form of ciliary beat and angle of sweep, however, seem to be more species dependent; the form generally appear to be considerably less flexible and less varied than that in most ciliates, and the angular amplitude ranges over 35^0 - 60^0. (For further observations on these aspects see Cheung [16]; Cheung and Jahn [13, 17].) Regular metchronal waves of ciliary motion as found in micro-organisms are less conspicuous in the tracheal ciliary system; the tracheal cilia seem to beat in patches, with phase changes raised from the cilium level to the cell level. Nevertheless, the metachrony in most tracheal systems can still be discerned as antiplectic, with a metachronal wavelength ranging from 10-12 μm [6] to about 40 μm [18].

The interaction between cilia and muco-serous fluid has been extensively studied. Lucas and Douglas [10] reported qualitatively on the behavior of the two-layer system and on their finding that only the tips of the cilia appear to pentrate into the mucus. There are further recent evidences supporting the tip penetration hypothesis that this mechanism is believed to be essential in achieving an effective mucus transport [13, 17, 19, 20]. However, it is still not clear as to what extent the mucus transport is due to the ciliary tip penetration into the mucus on the one hand and the metachronal wave of the ciliary-tip envelope on the other. Previous biomechanical studies have used a variety of models, including the envelope model [11, 21, 22], the sublayer model [23, 24] and the traction-layer model [24]. It may be remarked that as all these models were first introduced to study the locomotion of ciliates, most applications of these models to muco-ciliary transport problems seem to have inherited much of the original concept without a firm grasp of the major differences between the two cases.

In this paper a theoretical model is introduced in which the cilia are assumed to have periodic penetration into the bottom of the overlaying mucous layer during the main stage of the effective stroke. Disengagement of the cilia from the mucous layer during the recover stroke by means of an increased bending near the cilia tip is believed essential to result in an efficient mucus transport. The effects of ciliary movement with symmetric strokes on the cyclic component of the serous flow may be neglected in the calculation of the mean transport because of the large difference between the viscosity coefficients of the mucus and the serous fluid. Based on this model the mucus transport rate is found to depend linearly on the beat frequency of the tracheal cilia and also on the time of contact between the cilia tip and the mucous layer.

Interrelated experimental investigations have been carried out to measure the important parameters characterizing the beat pattern of the tracheal cilia of various small animals and the mucus transport rate under different physiological conditions. Data have been obtained on the transport of a biochemically viable mucous plug artificially introduced into the chicken trachea with and without a pressure differential across the mucous plug. These results have been used in this work to determine the power expenditure, the mean propulsive force contributed by each individual cilium and to estimate the shear and rate-of-shear distributions within the mucous layer under different operating conditions.

EXPERIMENTAL METHODS

Experiments were carried out using three different kinds of tracheal muco-ciliary systems: (i) the trachea of rats (provided by Caltech Beckman Laboratory), the trachea of chickens (from live specimens commercially supplied), and the palate of large Southern grass frogs (Carolina Biological Supply House). In all tests the animals used were normal healthy individuals. The ciliated tissue or organ was excised from the

animal immediately after either cervical dislocation in the case of the frog, exsanguination by jugular severance in the case of the chicken, or ether anesthesia in the case of the rat, and was placed in a bath of culture medium (Medium 199 with 25 mM Hepes buffer and Hank's salt, Grand Island Biological Company) and allowed to equilibrate to room temperature (20^{b} - 24^{o}C). No unusual care outside of keeping the tissue moist with culture medium was required for the chicken trachea and the frog palate, and both remained functioning for up to four hours, and cilia motion was often observed even after 48 hours. The rat trachea was less durable with several specimens being rejected for very poor or no ciliary activity. This may have been due to the use of ether as well as to difficulties in handling such a small trachea (10 mm long with a diameter of 2 mm compared to the chicken trachea which was 100 mm long with a diameter of 6 mm). The durability of the chicken and frog cilia allowed repetition of experiments on the same tissue, thus giving more confidence in their results.

The tracheae were removed intact and, after removal of connective and fatty tissue, were sufficiently transparent under strong back lighting to permit visual observation of the artificially introduced mucus, which was dyed with blue food coloring (Schilling). The mucus motion was recorded on video tape for later analysis of the transport rates. For the frog palate and the rat trachea a low power dissection microscope (Bausch and Lomb) was used.

RESULTS AND OBSERVATIONS

Series of tests were conducted to compare the transport of various fluids and particles on ciliated epithelia. These included, india ink, food dye, Dow Corning 200 fluid (a silicone fluid) of viscosity 100 and 100,000 centistokes, glass beads, and human mucus collected from the sputum of healthy subjects. Similar transport rates were measured for all these materials introduced on the ciliated palate of frogs. Dow Corning's 100,000 centistokes fluid and human mucus showed similar transport rates on chicken trachea. In order to avoid any (unknown) physiological incompatability of the Dow Corning fluid and since sufficient quantities of chicken or rat mucus were difficult to obtain, human mucus was used in all the experiments described below. All further references to mucus will denote human mucus unless specifically stated otherwise.

Vol. 17
1980

With the trachea oriented horizontally and with both ends open to the atmosphere a mucous plug which completely occluded the trachea was introduced into the distal end of the trachea. The mucus plug was transported over the entire length of the trachea with no visible deformation and only trace amounts of blue dye remaining behind on the epithelium. When the mucous plug reached the proximal end of the trachea it could be removed and reintroduced at the distal end, and the same motion observed.

To measure the ciliary force a mucous plug was introduced in the same manner as before. After clear motion of the plug was observed both ends of the trachea were sealed from the atmosphere and the differential pressure caused by the compression of the air on the proximal side and the expansion of the volume on the distal side of the plug was monitored using a high sensitivity pressure transducer (Validyne, MP-45). For the chicken trachea typical pressures were 15 mm of water, depending on the size of the mucus plug. These values are in agreement with the measurements of Hilding [25]. When the ends were sealed the plug gradually came to a halt, then began to deform and flow along the trachea wall due to shear forces delivered by the beating cilia (Fig. 1).

Typical results for the rat trachea are shown in Fig. 2 (a) and (b). When both distal and proximal ends of the trachea are left open to atmospheric pressure ($\Delta P = 0$) the mucous plug travels along the trachea at the rates indicated by the slope of the lines given in Fig. 2(a). For the plug with both ends sealed from the atmosphere the pressure difference across the plug gradually increases and the plug slowly stops and moves only very slightly in comparison to the case when $\Delta P = 0$. This pressure difference must be balanced by the cilia which produce a shear stress τ acting along the cilia-mucus contact area. The mean ciliary shear stress is independent of the mucus viscosity and can be calculated from

$$\tau = \frac{\pi R^2}{2\pi RL} \Delta P = \frac{R}{2L} \Delta P \quad , \qquad (A)$$

where R is the inside radius of the trachea, and L is the axial length of the plug. The result is shown in Fig. 2(b).

The same experiment was performed using the chicken trachea and typical results are presented in Fig. 3(a) and (b). Here the transport rates are substantially above those measured in the rat, however, the ciliary shear stresses are in good agreement.

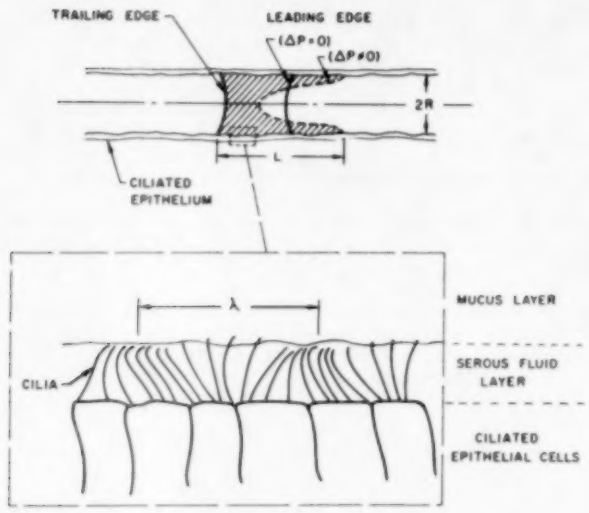

FIG. 1 The mucous plug is shown inside the trachea with and without a pressure gradient. In the insert the cilia density has been expanded to help illustrate the mucus, serous fluid, and cilia interaction.

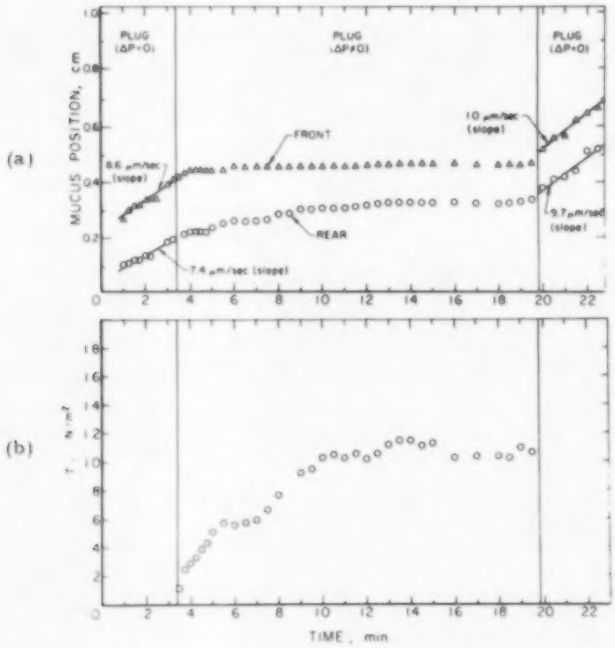

FIG. 2 Mucus transport rate (a) and shear stress (b) for the rat trachea as a function of time.

In a final experiment the plug was subjected to a pressure difference until the cilia action along the walls deformed the mucous plug sufficiently to cause the breaking of the plug and the formation of an annular coating on the inner walls of the trachea. When this occurred ΔP immediately dropped to zero and the annular mucous blanket, which now more closely approximates the natural state of operation in the respiratory tract, moved at a velocity similar to the plug with $\Delta P = 0$ as seen in Fig. 4(a) and (b).

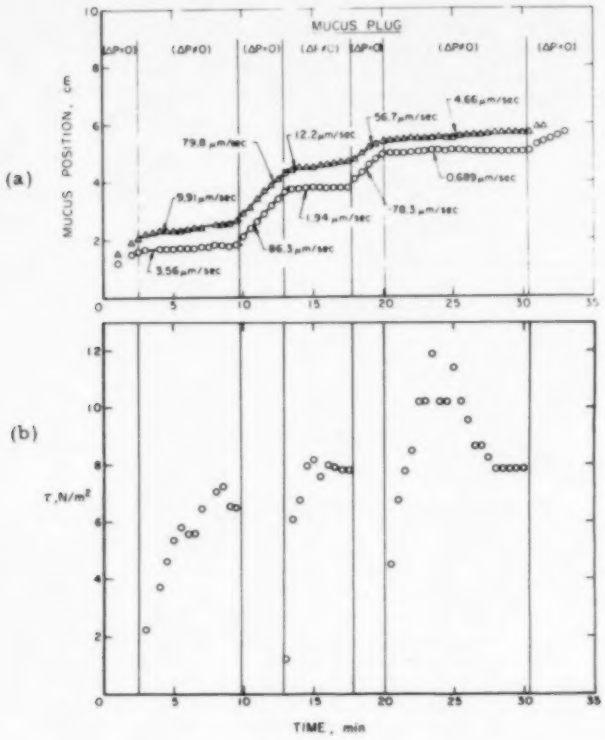

FIG. 3 Mucus transport rate (a) and shear stress (b) for the chicken trachea as a function of time.

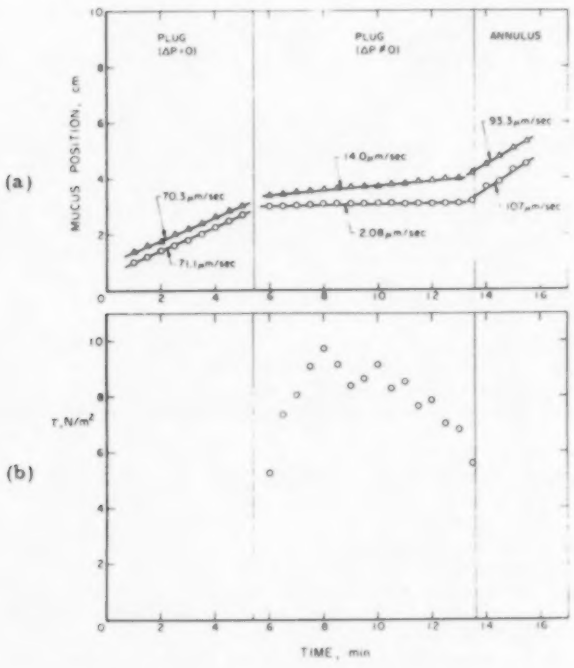

FIG. 4 Mucus (plug and annulus) transport rate (a) and shear stress (b) for the chicken trachea as a function of time.

Vol. 17
1980

A total of 8 experiments performed on four rats and 20 experiments on five chickens gave the mucus transport rates and shear stresses listed in Table 1. The results were more consistent for a given animal with larger variations between individual animals. More confidence is placed in the chicken data since the rat data might be subject to the effects of ether anesthesia and various handling difficulties as discussed earlier.

TABLE 1

Summary of Experimental Results

	Mucus Plug velocity ($\Delta P=0$) ($\mu m/sec$)	Mucus Plug velocity ($\Delta P \neq 0$) ($\mu m/sec$)	Mucus Annulus velocity ($\mu m/sec$)	Maximum τ (N/m^2)
Rat	0.66 - 15.9	0 - 5.9	————	1.3 - 11.5
Chicken	57 - 183	0 - 10	93 - 262	5.2 - 21.4

DISCUSSION OF EXPERIMENTAL RESULTS

Table 1 shows that the maximum shear stress for the rat and the chicken tracheae are of the same order in magnitude. Thus, both of these ciliated epithelia have similar working capabilities per unit area of ciliated epithelium. Knowing the mucus transport rates, it is possible to estimate the rate at which work is done (the power expenditure), and on this basis a maximum value of 5.6×10^{-3} W/m^2 is obtained. Maxwell [26] and Bowditch [27] obtained the value of 2×10^{-2} and 1.1×10^{-2} W/m^2, respectively, for the frog palate. Both these and our power measurements signify the rate at which useful mechanical work is being performed by the cilia. The total energy requirements of the tissue will be in excess of this due to energy wastes in the movement of serous fluid and in executing the return stroke of the cilia, and further due to the efficiency of the biochemical energy conversion. Our experiment as well as those of Maxwell and Bowditch seem to subject the cilia to abnormally strenuous conditions and thus are expected to yield higher work rates than that experienced during normal operation. Our somewhat lower value of the power expenditure may in part be due to the use of a different epithelium. The present experiment is believed to approximate more closely the natural functioning of the muco-ciliary system and, although it is still believed to give inflated results, it should give a more realistic estimate of the in vivo rate of working by the tracheal cilia.

Taking a cilia density of 5 cilia per square μm [28] the force exerted by an individual cilia can be calculated. We get a maximum of 4×10^{-12} N/cilia with values ranging to one quarter of this. This is believed to be the first estimate of the force producing capabilities of an individual respiratory cilia. Yoneda [29] obtains $0.5 - 3.0 \times 10^{-9}$ N for the large abfrontal gill cirrus of the marine bivalve Mytilus edulis. Although Yoneda does not specify the number of cilia participating in his force measurement, Baba [30] found such cirrus to contain upwards of 100 cilia, which would bring our results into his range. Yoneda subjected his cilia to unnatural and perhaps more demanding conditions which should result in a larger value of the cilia force than in the normal functioning.

An estimate of the cilia tip velocity of 313 $\mu m/sec$ is obtained when we take the beat frequency to be 19 Hz, the power stroke to endure 1/3 of the total beat period, the cilia to be 7 μm long, and the power stroke to subtend an angle of 45 degrees. Thus the ratio of the mucus transport velocity to the cilia tip velocity for chicken trachea with $\Delta P = 0$ is,

$$\frac{U_m}{U_c} = 0.18 - 0.84 \qquad (B)$$

The wide variation may be explained in two ways. First, the estimate of U_c may be in error since it was assumed to depend linearly on frequency, and the frequency was measured separately but was not monitored during the mucous transport tests. We used U_c for active healthy epithelium and if the tissue should have suffered damage the actual U_c would be reduced and the ratio U_m/U_c increased. Second, the variation in cilia beat pattern, and cilia tip penetration and duration of cilia-mucus contact might vary among individual specimens and thus causing some spread in U_m/U_c. The role of these parameters will be discussed in the next section. To fully explain the muco-ciliary transport mechanism, more detailed data on the mucus-cilia-serous fluid interaction and the concurrent beat frequency will be needed.

A THEORETICAL TWO-FLUID-LAYER MODEL

We now propose a theoretical model for the tracheal muco-ciliary system with the following assumptions. (i) The cilia beat mostly immersed in the serous layer; only during the effective stroke do they penetrate through the serous-mucus interface into the mucous layer. During the recovery stroke the ciliary tip bends somewhat more to avoid contact with the mucous layer. (ii) The cilia otherwise maintain the same slender shape throughout the beating cycle. (iii) The depth of penetration into the mucous layer by the ciliary tip is assumed small compared to ciliary length. (iv) The serous fluid is assumed to be Newtonian, as generally accepted. In addition, the mucus is also assumed to behave like a Newtonian fluid within the operating range of shear rate, with a viscosity much greater than that of the serous fluid.

Some of these assumptions are based on high-speed cinemicrographic observations made in the present study and elsewhere. Assumption (i) may be called the tip-penetration hypothesis, which is made almost by necessity under the circumstance of observation (ii) as described earlier. According to the basic principle for viscosity-dominant flows, assumption (ii) alone should imply that transport of serous fluid would be very inefficient if the cilia remained wholly immersed in the serous layer (without ever penetrating into the overlaying mucous layer) since the fluid particles should then have to almost recover all their initial positions at completion of each beating cycle. Based on this reasoning, the periodic component of the serous flow which is generated by nearly symmetric effective and recovery strokes of force-exerting cilia can be ignored in calculating the mean motion of the serous fluid because first of all, this component has little effect on the motion of a much more viscous mucus. Further, this unsteady component, being of zero mean, is of no direct interest. We shall therefore make this assumption for the benefit of simplifying the analysis with practically no loss of accuracy in the final result of the mucus transport rate.

Vol. 17
1980

Finally, we note that the assumption of mucus being a Newtonian fluid is made partly to render the problem tractable, and partly to regard the solution as a reference state for estimating the shear rates at the operating condition rather than those artificially established. It seems that the mucous plug flow, for which experimental results have been obtained, is a simple test case for evaluating the validity of the present model.

For the muco-ciliary plug flow in a mammalian trachea, we consider the axisymmetric two-layer flow within a circular cylinder of radius $r = R_o \equiv R + \ell$, its inner surface being lined with a layer of epithelial cilia of depth ℓ embedded in the serous fluid ($R < r < R_o$), and its core filled with a mucous plug ($0 < r < R$). As the basic flow we take a longitudinal segment which is of length equal to the metachronal wavelength and situated far from the two end surfaces of the plug so that the end effects can be neglected (see figure 2). For simplicity we further neglect the effect of cilia gaps in both longitudinal and asimuthal directions since flow variations of the scale of ciliary gaps are of no importance. With this simplification the flow becomes axisymmetric. Further, the inertial effects are negligible since the characteristic Reynolds number (based on the maximum cilia tip speed and ciliary length) is generally very small, being of order 10^{-3}.

In terms of the cylindrical coordinates (x, r, θ), the velocity $\underline{u}(x, r) = (u, v, w = 0)$ and the pressure $p(x, r)$ within the mucous layer satisfy the Stokes equations

$$\frac{\partial u}{\partial x} + \frac{1}{r}\frac{\partial}{\partial r}(rv) = 0 , \tag{1}$$

$$\frac{\partial p}{\partial x} = \mu \nabla^2 u , \tag{2}$$

$$\frac{\partial p}{\partial r} = \mu\left(\nabla^2 v - \frac{v}{r^2}\right) , \tag{3}$$

where μ is the viscosity coefficient of the mucus. The velocity $\underline{u}' = (u', v', w' = 0)$ and the pressure p' of the serous fluid $(R < r < R + \ell)$ also satisfy (1) - (3) with μ replaced by μ', the viscosity coefficient of the serous fluid. As already explained, we assume that

$$\mu/\mu' \gg 1 . \tag{4}$$

Now let the basic flow lie in the range $-\lambda/2 < x < \lambda/2$, $\lambda = 2\pi/k$ being the metachronal wavelength, k its wave number. Suppose over a central stretch $(-c < x < c)$ a patch of cilia have penetrated into the mucous layer and have their tips moving with a velocity distribution

$$u_c = U_c \cos Kx \qquad (-c < x < c, \quad c < \lambda/2) , \tag{5}$$

where U_c is the maximum cilia tip velocity and K is a constant. Physically this signifies that the x-component of tip velocity of the cilia away from the central station (x = 0) falls off according to this cosine distribution with 'wavelength' $\Lambda = 2\pi/K$. We further denote

$$\nu \equiv \lambda/\Lambda = K/k \ , \qquad x_o \equiv \pi/2K = \Lambda/4 \ . \tag{6}$$

These quantities can be expressed in terms of the phase angle θ as

$$\theta = kx, \quad kx_o = \frac{1}{2}\pi(k/K) = \pi/2\nu \equiv \alpha_o, \quad kc = \alpha, \quad Kx = \nu\theta \ . \tag{7}$$

The boundary conditions of the basic flow can now be prescribed as

$$u = u' = u_c = U_c \cos \nu\theta \qquad (r = R, \ |\theta| < \alpha) \ , \tag{8}$$

$$v = v' = 0 \qquad (r = R, \ |\theta| < \alpha) \ , \tag{9}$$

$$u = u', \ v = v' \qquad (r = R, \ \alpha < |\theta| < \pi) \ , \tag{10}$$

$$\sigma_{rr} - p = \sigma'_{rr} - p' \qquad (r = R, \ \alpha < |\theta| < \pi) \ , \tag{11}$$

$$\sigma_{xr} = \sigma'_{xr} \qquad (r = R, \ \alpha < |\theta| < \pi) \ , \tag{12}$$

where

$$\sigma_{rr} = 2\mu \frac{\partial v}{\partial r} \ , \qquad \sigma_{xr} = \mu \left(\frac{\partial u}{\partial r} + \frac{\partial v}{\partial x}\right) \ . \tag{13}$$

In addition, we have the no-slip condition at the epithelial surface

$$u' = v' = 0 \qquad (r = R + \ell \ , \quad |\theta| < \pi) \ , \tag{14}$$

and

$$u^2 + v^2 < \infty \qquad (r = 0 \ , \quad |\theta| < \pi) \ , \tag{15}$$

the last being the boundedness condition at the central axis. Here, conditions (8), (9) are in fact an approximation to the no-slip condition on the interfacial fluids in contact with the tips of the cilia patch for shallow depth of penetration. Condition (10) gives requirement on the continuity of velocity while conditions (11), (12) on the continuity of both normal and shear stresses across the part of interface which is free. These three conditions are the first approximation for small displacement of the free interface.

In seeking the solution, it is convenient to adopt the Oberbeck potential representation, by which u, v, and p can be written for the flow in the mucous plug $(0 < r < R, \ -\pi < \theta < \pi)$ as

$$u = P_o r^2 + U + \sum_1^\infty [A_n r_n I_1(r_n) + B_n R_n I_o(r_n)] \cos n\theta \ , \tag{16}$$

$$v = \sum_1^\infty [A_n r_n I_2(r_n) + B_n R_n I_1(r_n)] \sin n\theta \ , \tag{17}$$

$$p/2\mu = 2P_o x + \sum_1^\infty nk \, A_n I_o(r_n) \sin n\theta \ , \tag{18}$$

where $I_m(r_n)$ is the modified Bessel function of the first kind, and

$$P_o = \frac{1}{4\mu} \overline{\frac{\partial p}{\partial x}} \ , \quad U = \overline{u(0, x)}, \quad r_n = nkr \ , \quad R_n = nkR \ . \tag{19}$$

We see that P_o is proportional to the mean pressure gradient imposed on the plug, which can be arbitrary, and U is equal to the mean velocity of the mucous plug at the central axis.

For the flow in the serous layer, we have argued that the periodic component of zero mean can be neglected. Consequently we have for $R < r < R_o = R + \ell$, $-\pi < \theta < \pi$,

$$u' = P'_o(r^2 - R_o^2) + A' \log (r/R_o) \ , \qquad v' = 0 \ , \tag{20}$$

Vol. 198

$$p' = 4\mu' P'_o x \tag{21}$$

where $$P'_o = (\mu/\mu')P_o = \frac{1}{4\mu'}\overline{\frac{\partial p}{\partial x}} = \frac{1}{4\mu'}\overline{\frac{\partial p'}{\partial x}} \ . \tag{22}$$

Substituting the expressions (16) - (22) in the boundary conditions (8) - (14), and subsequently using the approximation $\ell/R \ll 1$ and the asymptotic expansion of $I_m(R_n)$ for large $R_n = nkR = 2\pi nR/\lambda$, we obtain the following dual Fourier series equations

$$\frac{1}{2}a_o + \sum_1^\infty a_n \cos n\theta = \cos \nu\theta - \phi \qquad (0 < \theta < \alpha) \tag{23}$$

$$\sum_1^\infty n a_n \cos \theta = 0 \qquad (\alpha < \theta < \pi) \tag{24}$$

where

$$\frac{1}{2}a_o = \frac{U}{U_c} = \Gamma \ , \qquad a_n = \frac{A_n}{U_c}(2\pi R_n)^{-1/2} e^{R_n} \qquad (n = 1, 2, \ldots) \tag{25}$$

$$\phi = P_o R^2/U_c = \frac{1}{4\mu}\overline{\frac{\partial p}{\partial x}}\frac{R^2}{U_c} \ . \tag{26}$$

Thus, U and A_n can be determined from the dual equation (23), (24) and the solution to the mucus flow is completed by the relations

$$B_n = -A_n(4R_n - 3)/(4R_n + 3) \qquad (n = 1, 2, \ldots) \ . \tag{27}$$

The above dual Fourier-series equations can be immediately inverted in closed form by Tranter's formula (Sneddon [31], p. 163). In particular, the constant coefficient a_o is found to be

$$\Gamma = \frac{U}{U_c} = \frac{1}{2}a_o = \Gamma_o - \phi \ , \tag{28}$$

$$\Gamma_o = \frac{1}{2}[P_{\nu-1}(\cos\alpha) + P_\nu(\cos\alpha)] \ , \tag{29}$$

where $P_\nu(\cos\alpha)$ denotes the Legendre function of order ν, ν being given by (6). This result provides the ratio of the mean velocity U of the plug at the central axis to the maximum cilia tip speed U_c. The pressure gradient is seen to affect the velocity ratio Γ through an additive term ϕ, as should be expected from the fact that this problem is linear. It therefore suffices only to discuss Γ_o, which is the velocity ratio at zero pressure gradient.

As shown in Fig. 5, Γ_o depends on two parameters, α and ν. The parameter α is a measure of the size of the cilia patch in contact with the mucous layer, while ν indicates the rate of decrease in longitudinal tip velocity of the off-center cilia from the maximum tip speed. If the patch size is small compared with the metachronal wavelength, α is small and Γ_o is not far less than 1 over a range of moderate values of ν. From our experimental measurement of the mean transport rate of an unobstructed mucus plug, we have estimated (see Eq. B) that

$$U/U_c = 0.18 - 0.84 \ . \tag{30}$$

This suggests that if $\alpha = \pi/3$, which corresponds to the duration of effective stroke equal to 1/3 of the metachronal period, then ν would lie in the range $1 < \nu < 2$. While this estimate seems to be quite reasonable, critical comparison between theory and experiment will require some sophisticated optical systems to locate and track the muco-serous interface, which has already proven to be a challenging feat.

From (13), (16) - (19) we obtain the first term in the axial shear stress evaluated at $r = R$ as

$$\sigma_{xr} = \frac{1}{2}\overline{\frac{\partial P}{\partial x}}R \ , \tag{31}$$

which of course agrees with (A). This same expression when used in evaluating the mean cilia shear stress yields the estimate of 5 - 21 N/m^2 for the chicken tracheal cilia. Under physiologically normal operation (i. e. when $\partial P/\partial x = 0$) we would anticipate the actual shear stress to be somewhat less.

Vol. 17
1980

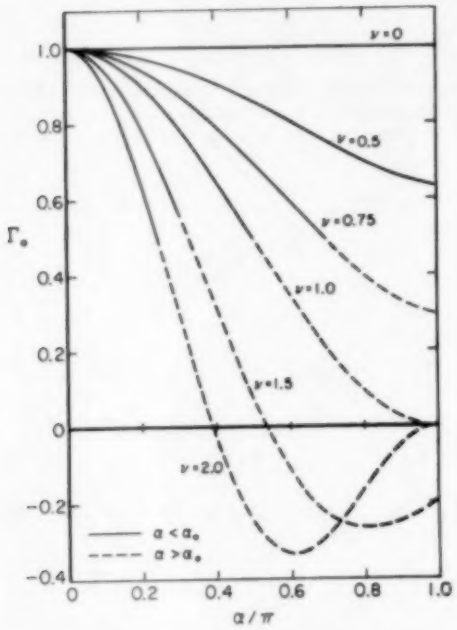

FIG. 5 Γ_o plotted as a function of the two parameters α and ν.

CONCLUSION

The present theoretical model of the tracheal muco-ciliary transport process based on two-layer Newtonian fluids hypothesis seems to provide reasonable results in comparison with experiments. A definitive assessment of the model, however, cannot be accomplished without acquiring further experimental data on several important parameters including the depth and duration of penetration by cilia tip into the mucus layer, the metachronal wavelength and phase velocity, as well as the velocity distribution of the cilia tips during the penetration period. Prior to such a critical examination, the present Newtonian fluid model should not be implied to indicate that any of the non-Newtonian fluid behavior of the mucus does not play an appreciable role in muco-ciliary transport. It is quite feasible that the elastic and shear-thinning properties of the mucus may prove important in evaluating local flow quantities, in the physiological functioning, and in enhancing the optimal operation of the muco-ciliary system. These problems appear as primary areas for further research. Along this direction it is hoped that the present study has helped in isolating the parameters of importance for future investigations.

ACKNOWLEDGMENT

This work was jointly sponsored by the National Science Foundation Grant ENG 77-21236-A01, the Office of Naval Research Contract N00014-76-C-0157-NR 062-230 and the National Institute of Health BRSP Grant RR07003.

REFERENCES

1. JAFFERY, P. K. and REID, L. M. The respiratory mucous membrane. Resp. Def. Mech. 5, 1977, pp. 193-254.

2. SCHLESINGER, R. B. Mucociliary interaction in the tracheo-branchial tree and environmental pollution. Bioscience 23, 1973, pp. 567-573.

3. KEISER-NIELSEN, H. Mucin. Dansk Videnskabs Forlag, 1953.

4. SADE, J. and ELIEZER, N. Secretory ottis media and the nature of the muco-ciliary system. Acta Otolargyngol. 70, 1970, pp. 351-357.

5. SADE, J., ELIEZER, N., SILBERBERG, A. and NEVO, A. C. The role of mucus in transport by cilia. Amer. Rev. Res. Dis. 102, 1970, pp. 48-52.

6. WILSON, G. B., JAHN, T., QUINTON, P. M., and FONSECA, J. R. Studies on ciliary beating of frog pharyngeal epithelium in vitro II. Relationship between beat form, metachronal coordination, fluid flow and particle transport. Swimming and Flying in Nature, T. Y. Wu, C. J. Brokaw and C. Brennen (eds.), Plenum Press: New York, Vol. 1, 1975, pp. 301-316.

7. HWANG, S., LITT, M. and FORSMAN, W. Rheological properties of mucus. Rheo. Acta, 8, Heft 4, 1969, pp. 438-448.

8. LITT, M. Mucus rheology. Arch. Intern. Med. 126, 1970, pp. 417-423.

9. WINET, H. Ciliary propulsion of objects in tubes: wall drag on swimming tetrahymena in the presence of mucin and other long chain polymers. J. Exp. Biol. 64, 1975, pp. 283-302.

10. LUCUS, A. M. and DOUGLAS, L. C. Principles underlying ciliary activity in the respiratory tract II. A comparison of nasal clearance in man, monkey and other mammals. Arch. Otolaryng. 20, 1934, pp. 518-541.

11. ROSS, S. M. and CORRSIN, S. Results of an analytical model of mucociliary pumping. J. Appl. Physiol. 37, 1974, pp. 333-340.

12. FAWCETT, D. W. and PORTER, K. R. A study of the fine structure of ciliated epithelia. J. Morphol. 94, 1954, pp. 221-281.

13. CHEUNG, A. T. W. and JAHN, T. L. Determination of the movement pattern of the epithelial cilia of rabbit trachea and the clearance mechanism of the tracheal muco-ciliary clearance system. Swimming and Flying in Nature, T. Y. Wu, C. J. Brokaw and C. Brenned (eds.), Plenum Press:New York, Vol. 1, 1975, pp. 289-299.

14. PROETZ, A. W. Applied Physiology of the Nose. Annals:St. Louis, 1941.

15. SLEIGH, M. A. The nature and action of respiratory tract cilia. Resp. Def. Mech. 5, 1977, pp. 247-288.

16. CHEUNG, A. T. W. Determination of ciliary beat of Opalina obtrigonoidea and in rabbit tracheal explants. Doctoral Thesis, University of California at Los Angeles, 1973.

17. CHEUNG, A. T. W. and JAHN, T. L. High speed cinemicrographic studies on rabbit tracheal (ciliated) epithelia: Determination of the beat pattern of tracheal cilia. Pediatr. Res. 10, 1976, pp. 140-144.

18. MILLER, C. E. The kinematics and dynamics of ciliary fluid systems. J. Exp. Biol. 49, 1968, pp. 617-629.

19. LITT, M. Flow behavior of mucus. Ann. Otolaryngol. 80, 1971, pp. 330-335.

20. REISSIG, M., BANG, B. G. and BANG, F. B. Ultrastructure of the mucociliary interface in the nasal of mucosa of the chicken. Am. Rev. Resp. Dis. 117, No. 2, 1978, pp. 327-341.

21. ROSS, S. M. A wavy wall analytical model of mucociliary pumping. Ph. D Thesis, The Johns Hopkins University, Baltimore, Md., 1971.

22. LARDNER, T. J. and SHACK, W. J. Cilia transport. Bull. Math. Biophys. 34, 1972, pp. 325-335.

23. BLAKE, J. R. Mucus flows. Math. Biophys. 17, 1973, pp. 301-313.

24. BLAKE, J. R. and WINET, H. On the mechanics of muco-ciliary transport. The 3rd Intern. Conf. Biorheology, La Jolla, Ca., 1978.

25. HILDING, A. C. Role of ciliary action in production of pulmonary atelectasis. Vacuum in paranasal sinuses and in otitis media. Trans. Amer. Acad. Ophthalmology and Otolaryngology, July-August, 1944.

Vol. 17
1980

26. MAXWELL, S.S. The effect of salt-solution on ciliary activity. Amer. J. Physiol. 13, 1905, pp. 154-170.

27. BOWDITCH, H.P. Force of ciliary motion. Boston Medical and Surgical J., 1876, pp. 159-164.

28. BRENNEN, C. and WINET, H. Fluid mechanics of propulsion by cilia and flagella. Ann. Rev. Fluid Mech. 9, 1977, pp. 339-398.

29. YONEDA, M. Force exerted by a single cilium of Mytilus edulis I. J. exp. Biol. 37, 1960, pp. 461-468.

30. BABA, S.A. Flexural rigidity and elastic component of cilia. J. exp Biol. 56, 1972, pp. 459-467.

31. SNEDDON, I.N. Mixed Boundary Value Problems in Potential Theory. North-Holland Publ. - Amsterdam, 1966.

Vol.
198

BIORHEOLOGY Vol.17, pp. 163-168 0006-355X/80/010163-06$02.00/0
© Pergamon Press Ltd. 1980. Printed in the United States

THIRD INTERNATIONAL CONGRESS OF BIORHEOLOGY

SYMPOSIUM ON MUCO-CILIARY TRANSPORT

THE RHEOLOGY AND MOLECULAR ORGANIZATION OF EPITHELIAL MUCUS

F.A. Meyer and A. Silberberg

Polymer Department, Weizmann Institute of Science, Rehovot, Israel

(Received 1.11.1979. Accepted by Guest Editors T.Y. Wu and S. Berger)

ABSTRACT In most instances where sliding transport has to occur over an epithelial tissue surface, the surface is covered by a system of cells capable of secreting a thick flowing fluid, mucus. The sliding motion can involve the transport of the whole organism, the transfer of food, the facilitation of sperm or ovum movement, the clearance of respiratory air ways, etc. There is considerable evidence that the major biopolymeric component involved is a glycoprotein, 80% of whose weight is carbohydrate and 20% is protein. The carbohydrate is attached in the form of short oligomeric side chains to about 4/5 of the protein backbone leaving 1/5 of its length bare. The bare part of the protein involves disulphide bridges which may or may not be intramolecular. These glycoproteins are crosslinked into a weak gel i.e. a system which is viscoelastic and is endowed with long, if not infinite, mechanical relaxation times.

Where, as is often the case, mucus is in mechanical contact with an array of metachronously beating cilia it acts as coupler in facilitating transport by ciliary propulsion. In relation to the period of the ciliary beat its characteristic relaxation time is sufficiently long so that the response of the mucus layer lying on top of the bed of beating cilia is that of a semi-solid sheet having an essentially rigid interaction with the moving wave. The requirements are strongly linked to ciliary beat characteristics. While solid-like properties are essential they must fall into a certain class. The characteristics of an incipient gel are most favourable in establishing transport.

Mucus also possesses properties whose effects and purposes are not yet understood. Mucus, for example is unstable and its gel-like structure declines with time. This occurs rather slowly at body, but more rapidly at higher temperature. Hence the crosslinks of mucus are labile and of a character not yet established. The glycoprotein molecules building the networks are but for the crosslinks molecularly disperse. This is indicated by measurements of the hydraulic permeability of mucus which is far too low for any other arrangement of the glycoprotein strands to be considered.

INTRODUCTION

In many instances when materials have to be moved over the surface of an interior passage in a living system, an epithelium is used where some cells carry a large number of metachronously beating cilia and where others secrete a thickly flowing glycoprotein based fluid designated as mucus (1). For transport both types of cells are important. There is obviously no motion without the mechanical propulsion of the cilia, but, as we have shown, the ciliary beat is ineffective unless the presence of mucus couples it to the load (2). We want to discuss what makes this system function, and renders mucus in particular so special that in its absence there is no transport and no epithelial clearance.

KEY WORDS Mucus, Mucus glycoprotein, Transport, Ciliary beat, Muco-ciliary clearance, Muco-ciliary epithelium.

Vol. 17
1980

DESCRIPTION OF THE SYSTEM

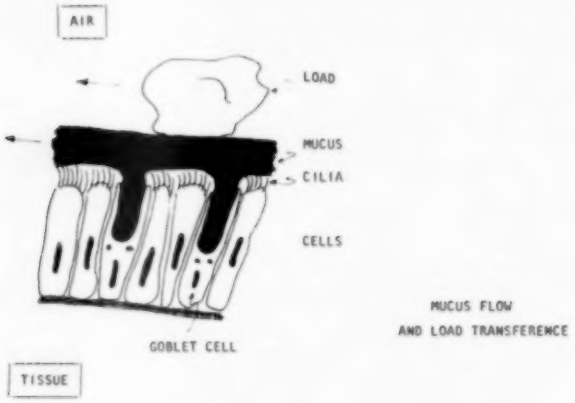

FIG. 1

Schematic Representation of a Muco-ciliary Epithelium

Fig. 1 outlines the essential features of a mucociliary epithelium of the kind under discussion. The epithelium as indicated is composed mainly of two types of cells. There are some 200 to 300 cilia very close to each other per ciliated cell. So close are cilia to each other, wall to wall, that there would be both difficulty for them to move out of unison and for very large macromolecules, particularly a system of crosslinked macromolecules, such as mucus, to penetrate between them. When therefore mucus is secreted from its source in the goblet cells, it distributes above and not between cilia. Moreover, in the absence of a mucus cover, capillary action alone would cause interstitial fluid, whether from the tissue or from cells, to rise between the cilia and to cover them up to their tips. Hence, the fluid in which the cilia actually move, the perciliary fluid does not contain the glycoprotein molecules typical of mucus (2). Its composition, probably, is reminiscent of interstitial fluid since it is in some kind of steady state balance with the epithelial cells.

It should be pointed out that mucus is stored in the goblet cell in the form of submicron sized lipid membrane covered granules. Only during the act of secretion are these granules made to open, probably by combining their membrane with the plasma membrane of the goblet cell, and their contents allowed to mix. If mucus, as subsequently collected, were, therefore, a permanent gel, whose macromolecules constituted a macroscopic covalently linked network, crosslinking could not have occurred throughout the system prior to secretion but only subsequent to it. On the other hand, there is no objection on these grounds for the contents of the granules to have been pre-crosslinked. The "seals" entered into, however, between the contents, subsequent to secretion, would probably be of a much weaker and more temporary kind.

The purpose of the system as a whole is to provide a means of transference of both cellular debris and airborne pollutants. We have shown that when the local supply of mucus is exhausted (by repeatedly loading a piece of excised muco-ciliary tissue) transference will stop, but can be restored by re-applying mucus from the outside (2). Hence mucus, or as it turns out a suitable substitute, is essential for this function (3). Ciliary beat continues both in the normal and the depleted conditions unless the tissue is allowed to lose water. Working in a totally humidified atmosphere, however, as is probably the case in the air passages of the nose, lungs and ears, the ciliary activity of excised tissue will maintain itself for days on the basis of the cells' stored metabolic fuel.

It is believed, therefore, that, in order to conserve mucus it will be secreted only when and where it is needed and that normally the mucus cover will either be entirely absent or extremely thin. Such an assumption is almost necessary in the lungs since an impossible "traffic" problem would arise in the trachea if all the minor airways were to discharge a continuous stream of mucus, even if in only a micron thick layer as probably is the case. The extra mucus load passing through trachea in disease is probably due to what happens when a discharge of mucus is actually being forced to occur over a major portion of the air/tissue interface of the lung.

Rheological Characteristics of Normal Mucus

A depleted excised piece of muco-ciliary tissue is a convenient system on which to test which properties of mucus are required in order to restore transport rate in full. For this purpose, we have used the excised palate of the frog as an easily accessible and conveniently sized source of tissue (2).

One performs two experiments simultaneously. One measures the rheological properties of the mucus (or mucus substitute) and one measures the velocity with which it permits arrested loads to be transferred. The rheological property tested is the viscoelasticity of the sample as characterized by its dynamic response over the frequency range of interest (4).

The samples tested are then varied in their properties by changing the number of cross-links and a curve of restored transport rate against viscoelastic character can be plotted. It could be shown that of the two frequency dependent functions which characterize the mucus, the frequency dependent dynamic viscosity and the frequency dependent dynamic elasticity, i.e. the loss and storage modulus respectively, only the latter is determining for transference. If one varies viscosity considerably without changing elasticity the extent of transference restored is unaffected. If the storage modulus is changed on the other hand, an optimum value can be shown to exist. Measured at a radial frequency of about 3-4 rad/sec the value of this optimum lies around 1.6 dynes/cm^2.

This optimum is characteristic of a loosely crosslinked system having a good number of relaxation mechanisms appreciably longer than the period of the ciliary beat. This gives a sizable elastic response in the frequency range of the ciliary beat.

Significance of the Rheological Characteristics of Normal Mucus

In order to appreciate the fine tuning of the system, some thought must be given to the likely mode of interaction between mucus and the underlying wave of synchronized ciliary motion. The thickness of the periciliary fluid layer within which the cilia move, is, in the absence of mucus adjusted, perhaps by capillarity, to match the mean height of the ciliary tips in their beat. The cilia are thus bathed mainly by periciliary fluid, but the forces which can be transmitted by ciliary movement through a fluid of this kind of viscosity would not be high enough to achieve the transference of power per cilium at the rate required for mucus movement. Only if cilium and mucus layer interact in a direct, solid-like fashion, i.e. essentially without slip, will energetic coupling be efficient enough. Such an interaction requires the penetration of each cilium at least partially, into the mucus and a movement of the tip of the cilium so fast, during the power stroke of the ciliary beat cycle, that no slip occurs. On the other hand, during parts of the remainder of the cycle the cilium must have adequate time first to engage and then to disengage from the mucus, "duck" under the level of the periciliary fluid/mucus interface by foreshortening, and to complete the cycle out of direct contact with mucus.

The following features have thus to characterize mucus, rheologically: The time over which a cilium straightens up, contacts the mucus layer and enters it from below and the time over which the structure of the mucus relaxes sufficiently, so as to permit penetration, must be matched. During the very brief period of the power stroke, on the other hand, during which the cilium moves between its two extreme positions, the mucus layer must react elastically, i.e. with minimum relative slip. Then, over the beginning of the recovery stroke, a period of sufficient length must again be granted for the cilium to release itself from the contact with the mucus. If either of these opposing tendencies is not fulfilled, we will have a failure of transport. If the storage modulus of mucus is too low, at the frequency of the power stroke, no coupling will take place. If storage modulus of the mucus is too high, at the frequency of ciliary penetration or release, no penetration will take place. Again no coupling and no clearance will occur. We can see, therefore, why an optimum arises and why it should be linked to the value of the frequency dependent dynamic storage modulus (4).

THE MACROMOLECULAR ORGANIZATION OF MUCUS

We have seen that for the transference function considered a purely rheological requirement can be put up and it is not surprising, therefore, that substitute systems of requisite characteristics can function as well (3). From the point of view of mucus molecular pathology, however, and from the point of view of properties needed for other functions of mucus not yet considered, and perhaps not yet understood, the macromolecular build-up of the glycoprotein strands which provide the network responsible for mucus elasticity is most important. It is, moreover, a very interesting system.

It turns out at first sight to be most difficult to dilute mucus, i.e. to breakup the network structure and disperse the glycoprotein component. Mucus seems to have all the appearance of being permanently crosslinked. Thus, dissolution is most easily effected by breaking covalent bonds. For example, reagents which disrupt disulphide bonds and

reagents, enzymes, which digest peptide chains bring about rapid dissolution. A glycoprotein macromolecular unit of about 500,000 Dalton eventually results. It almost looks as though a covalently linked network is at the basis of mucus structure and as though specific points of crosslinkage are involved. Nevertheless this is highly unlikely.

Some of the crosslinks would have to be closed only upon secretion, for the reasons already discussed. Such a reaction would have to arise moreover any time when two mucus blobs unite upon contact.

Most convincingly, however, mucus quite spontaneously goes into solution when left standing (5,6). The speed of this process of dissolution depends only upon the temperature. At low temperatures, mucus samples will maintain themselves for months, (and thus seem to be stable) but at higher temperatures, particularly at close to 100°C, the breakup occurs in minutes. When the process is further monitored by measuring the changes in the viscosity of the solution as a function of temperature, it turns out that the same activation energy and, therefore, the same mechanism characterizes the entire accessible temperature range. Moreover, the final breakdown product could very reasonably be the same 500,000 Dalton unit which results from the chemical attack. What also turns out is that the rate of breakdown is essentially independent of the chemical characteristics of the environment, as determined by the presence of various additives known to affect drastically the kind of secondary bonds usually entered into by proteins and glycoproteins (6). The breakdown of the network does not, therefore, require a direct attack on the primary bond system nor is the secondary bond structure involved in any of the usual ways.

It is known, moreover, that mucus glycoproteins from a variety of animal species and a variety of organs possess strong compositional and organizational similarity (7-10). Both the amino acid and the sugar compositions are rather similar and of late it has become increasingly evident that also the same 500,000 Dalton unit is involved. Where more detailed investigations have been performed, the structural principle illustrated by Fig. 2 was found to apply (10). Of particular interest from the point of view of crosslinking is the naked peptide region which, as indicated, contains a large number of half cystine moieties, all that the mucus glycoprotein seems to contain. The naked peptide is also the site of attack by trypsin. The resulting product is thus of almost unaltered molecular weight since the small peptide tail constitutes a contribution of only some 20,000 Dalton to the overall molecular weight.

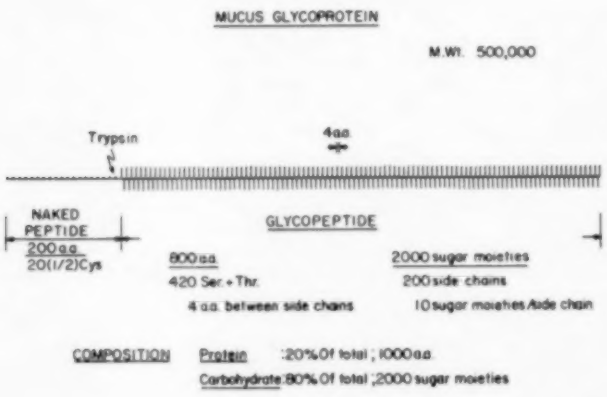

FIG. 2

Schematic Structure of the Mucus Glycoprotein Macromolecular Unit

The nature of the crosslink, how it is formed and broken, is thus unknown and unusual. Some entirely new principle of interaction may be involved based, perhaps, upon purely mechanical linkages. A possible model along these lines is illustrated in Fig. 3. This is not meant as a definite proposal but only as a means to fix ideas. The naked peptide is assumed to be rolled up into a ring held together by disulphide bonds. This ring is assumed threaded over the bottle brush-like glycoprotein region of the chains. It can slide along it by Brownian motion, due to local conformational adjustments, and thus break links. The process, however, would be very slow, as slow in fact as required by the observations. Either breaking disulphide bonds or tryptic digestion opens or dissolves the rings and frees the basic structural unit. Such a model could, therefore, account for mucus dissolution under all the circumstances so far known. It is unclear, however, how the crosslinks would form in the first instance. How much crosslinking occurs in the granule. How do mucus blobs "seal" to each other so rapidly during secretion.

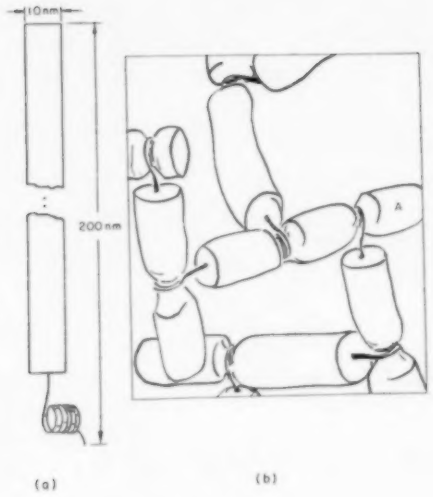

FIG. 3

Possible Mechanically Linked Network of Mucus Glycoprotein Molecules

(a) Structural Unit; (b) Network Assembly
Molecule A which has two rings slipped over the sugar coated region acts as a crosslink.

Vol. 17
1980

Much has been argued, particularly in the case of cervical mucus, that the network is composed of strands of rather substantial thickness. The gaps between these strands are believed to be big enough to permit sperm to pass between and to guide them towards the uterus (11). This structure is not very consistent with the chemical evidence so far discussed. Moreover, most mucus is not usually two phase (turbid) as a thick fiber system would tend to make it.

We have, however, even more conclusive evidence. Hydraulic permeability of a gel is a very sensitive test of the relative arrangement and degree of dispersion of the immobile phase. This, in the case of mucus, is the mucus glycoprotein. It is easily seen that the lowest permeability, the highest resistance to flow, corresponds to a molecularly disperse uniform arrangement where each part of the network phase is as thin as possible and as molecularly disperse as possible. Expressing flux J_v in terms of the Darcy constant K we have

$$J_v = (K/\eta)(-\nabla p)$$

when η is the solvent viscosity and $(-\nabla p)$ the applied pressure gradient. K can be expressed as (12)

$$K = \eta(1-\phi)/\phi\hat{f}_g$$
$$= (1-\phi)(2/3\pi)(1/L)$$

where ϕ is the volume fraction of the mucus glycoprotein, $\phi\hat{f}_g = 6\pi\eta a(L/4a)$ is the force on the gel substance in unit volume of mucus at unit relative velocity, a is the radius of the spherical beads, spaced a distance 4a apart, which hydrodynamically can replace the network strand, and L is the length of glycoprotein network strands per unit volume of mucus. Experimentally it is found that $K = 845\ nm^2$ when the mucus glycoprotein concentration is 1.75×10^{-3} gm/ml (13). One finds, therefore, that

$$L = 2.4 \times 10^{-4}\ nm^{-2}$$

and that a section of strand corresponding to the 500,000 Dalton mucus glycoprotein should be about 114 nm long. We have independently estimated this length to be 200 nm based on the dilute solution behavior of the breakdown products (14) (see Fig.3). This corresponds to a fairly extended peptide backbone. There may thus be some pairing of strands in the network but the lower effective length is more likely due to some hydrodynamic shielding between chains in the region of the crosslinks. It is quite out of

question that a drastic reduction in the value of L, such as would be required to build up the kind of fibers or "micelles" seen in a dried mucus sample (11), can be consistent with the permeability data. These fibers are thus a drying artefact.

CONCLUSIONS

We can summarize the above analysis of epithelial mucus as follows:

1. Mucus is a network of strands of single mucus glycoprotein molecules.
2. The network is thermally unstable and involves what is perhaps a rather unique crosslink.
3. Mucus must be a weak gel for muco-ciliary clearance. For effective coupling to the ciliary beat, there exists an optimum for the dynamic storage modulus of mucus over the frequency range of the beat. This requirement can be linked to a model for the cilium/mucus interaction.

ACKNOWLEDGMENTS

The work quoted was supported in part by a grant No. RO1 NS 10048 from the National Institutes of Health, U.S.A.

REFERENCES

1. See for example "Secretory Otitis Media and Its Sequelae"., J. Sadé (Ed.) Churchill Livingston, New York, 1979.

2. SADÉ, J., ELIEZER, N., SILBERBERG, A. and NEVO, A.C. The role of mucus transport by cilia. *Am.Rev.Resp.Dis.* 102, 48-52, 1970.

3. KING, M., GILBOA, A., MEYER, F.A. and SILBERBERG, A. On the transport of mucus and its rheological simulants in ciliated systems. *Am.Rev.Resp.Dis.* 110, 740-745, 1974.

4. GELMAN, R.A. and MEYER, F.A. Mucociliary transference rate and mucus viscoelasticity. Dependence on dynamic storage and loss modulus. *Am.Rev.Resp.Dis.* (in press).

5. MEYER, F.A. Mucus structure: relation to biological transport function. *Biorheology* 13, 49-58, 1976.

6. MEYER, F.A., to be published.

7. MEYER, F.A., ELIEZER, N., SILBERBERG, A., VERED, J., SHARON, N. and SADÉ, J. An approach to the biochemical basis for the transport function of epithelial mucus. *Bull-Physio-path.resp.* 9, 259-274, 1973.

8. MEYER, F.A. Comparison of structural glycoproteins from mucus of different sources. *Biochim.Biophys.Acta* 493, 272-282, 1977.

9. MEYER, F.A., VERED, J. and SHARON, N. Studies of glycoproteins from mucociliary secretions, In: *Mucus in Health and Disease*, M. Elstein and D.V. Parke (Eds.), Plenum Press, New York, 1977, 239-249.

10. SILBERBERG, A. Physico-chemical characteristics of epithelial mucus and mucus glycoprotein, In: *Secretory Otitis Media and Its Sequelae*, J. Sadé (Ed.). Churchill Livingston, New York, 1979; Chapter 16.

11. ODEBLAD, E. Physical properties of cervical mucus. In: *Mucus in Health and Disease*, M. Elstein and D.V. Parke (Eds.), Plenum Press, New York, 1977, pp. 217-226.

12. WEISS, N. and SILBERBERG, A. Permeability of gels, *Polymer Preprints* 16(2), 289-292, 1975

13. VAN VLIET, T., WEISS, N. and SILBERBERG, A. (to be published).

14. MEYER, F.A. and SILBERBERG, A. Structure and function of mucus. In: *Respiratory Tract Mucus*. Ciba Foundation Symposium No. 54 (New Series); Elsevier, Excerpta Medica, North-Holland; Amsterdam, 1978, pp. 203-218.

BIORHEOLOGY Vol.17, pp. 169-175 0006-355X/80/010169-07$02.00/0
© Pergamon Press Ltd. 1980. Printed in the United States

THIRD INTERNATIONAL CONGRESS OF BIORHEOLOGY

SYMPOSIUM ON MUCO-CILIARY TRANSPORT

FLAGELLAR PROPULSION OF HUMAN SPERM IN CERVICAL MUCUS

D.F. Katz[1] and S.A. Berger[2]

[1]Department of Obstetrics and Gynecology, School of Medicine, University of California, Davis, California 95616, and [2]Department of Mechanical Engineering, University of California, Berkeley, California 94720

(Received 3.12.1979. Guest Editor's Contribution Invited by Editor-in-Chief A.L. Copley)

ABSTRACT

A new model was developed to characterize the hydrodynamics of the interaction between spermatoza and cervical mucus. In this model the local environment about a length element of a spermatozoon in the mucus is represented as a *cell* consisting of a Newtonian fluid within a rigid, cylindrical no-slip boundary. Such a *cell* models the mucous microstructure in the sense of "hydrodynamically equivalent" properties. A simple resistive force theory for sperm hydrodynamics was developed and applied to a human spermatozoon swimming within a mucous *cell*. The results included the prediction that the drag on the sperm head has a substantial effect on swimming speed. This prediction was tested experimentally, by analyzing high-speed cine films of normal and headless human spermatozoa swimming in mucus. The theoretical result was confirmed, and a *cell* size of the order of 2 μm was suggested.

Vol. 17
1980

INTRODUCTION

Immediately following insemination, the spermatozoa of many mammals must negotiate a mucus-filled cervical canal as they begin their migration toward the egg (1,2). The cervix thus performs a crucial role in mammalian sperm transport, acting during the periovulatory period to admit and possibly to store normal viable spermatozoa, while simultaneously blocking the entrance of morphologically abnormal spermatozoa and pathogenic material. During non-ovulatory phases of the female reproductive cycle, and during pregnancy, no spermatozoa or other material are admitted. Much of this regulatory capacity of the cervix can be attributed to its mucous secretion. The cervical mucus, like the secretions of other epithelial tissues, is a hydrogel. Ninety to 99.5% of the mucus consists of the aqueous phase, which is similar in composition to blood serum and contains soluble proteins and inorganic salts. The solid phase is comprised of a carbohydrate-rich glycoprotein (the mucin) of high molecular weight. The three dimensional organization and integrity of the mucous microstructure depend upon interacting electro-chemico-physical properties of the mucin and mucous plasma (3).

The migration *in vivo* of spermatozoa into and through cervical mucus is a transport process whose mechanics depend upon: the active undulations of the sperm flagellum; the morphological and possibly electrical properties of the sperm body; the micro and macro-physical characteristics of the cervical mucus as time and space-dependent entities; the geometry of the cervical canal, the pattern of mucosal folding and distribution of cilia; and the activity of the female reproductive tract, including the ciliary beat (where present) and muscular contractions of the viscera. Hydrodynamic interactions among these factors, with physical and chemical modulation at the molecular level, determine the swimming trajectories of spermatozoa during passage through the cervix. It is presently believed that active swimming by spermatozoa is a necessary if not sufficient component of the mechanics of sperm transport through the cervix (2). Attempts at describing this element of the sperm-mucus interaction should characterize both the sperm and the mucus in terms of parameters that relate to first principles of biomechanics and that are amenable to experimental measurement.

There exist a small number of theoretical studies directly addressed to the fundamental hydrodynamics of the sperm-mucus interaction (4,5,6). These preliminary treatments modeled the sperm body as a two-dimensional, small amplitude wavy sheet of infinite length. The representation of mucous properties included the presence of adjacent undulating sheets as a model of the mucin macromolecules. Not surprisingly, these studies indicated that the nearby presence of the mucous microstructure could significantly influence the flagellar

hydrodynamics. As compared with swimming in an infinite fluid, higher propulsive velocities and rates of hydrodynamic working were predicted. However, interpretation and experimental verification of these predictions have been limited, due to the inherent geometrical restrictions of the wavy sheet model. These include the absence of a sperm head, the infinite length of the body, and the constraint of small amplitude flagellar waveforms. Moreover, the two-dimensionality of the model overestimates the hydrodynamic effects of the adjacent boundaries; i.e. the spacial decay of fluid disturbances created by the movements of three-dimensional organisms of finite length is more pronounced (7). Thus, as is the case for swimming in an infinite fluid, the value of the wavy sheet model in the study of the sperm-mucus interaction is primarily as an initial qualitative approach.

Considerably more attention has been devoted experimentally than theoretically to the properties of mucus and the sperm-mucus interaction (1,8). Much of this attention has been clinical, involving the diagnosis and treatment of human infertility and the design of new contraceptives. Consequently, the existence of a relationship between the properties of cervical mucus and the movements of spermatozoa therein has been appreciated empirically for many years. Objective, quantitative investigations of this relationship are, however, relatively scarce (9). For the most part, the rheological and other biophysical properties of cervical mucus have been assessed on a scale that encompasses aggregations of the mucin macromolecules. This scale is large compared to that of the movements and fluid disturbances created by individual motile spermatozoa, which is of the order of a sperm body length or less (10). Consequently, relatively little is appreciated about the properties of mucus as experienced by spermatozoa. Recent work in our laboratory has begun to investigate further the properties of cervical mucus *vis a vis* the sperm-mucus interaction. A number of observations have provided the motivation for the present study. Quantitative high-speed cinemicrographic studies of the movements of human spermatozoa in fresh, ovulatory cervical mucus have indicated alterations in the flagellar beat kinematics as compared with those in structure-less, Newtonian fluids of low viscosity (11). These alterations can be mimicked by increasing the viscosity of the simple media via addition of Ficol or methylcellulose, cf. Figure 1. Thus, there appears to be a significant amplification in the local forces and bending moments acting along a sperm body while swimming in the mucus, i.e. a strong, local "wall effect". Our qualitative visual observations have suggested that morphologically abnormal but actively motile headless or "pinhead" spermatozoa tend to swim faster in cervical mucus than do their normal counterparts with heads. These results imply that the entire sperm body, i.e. flagellum plus head, must be in close proximity to numbers of the mucin macromolecules.

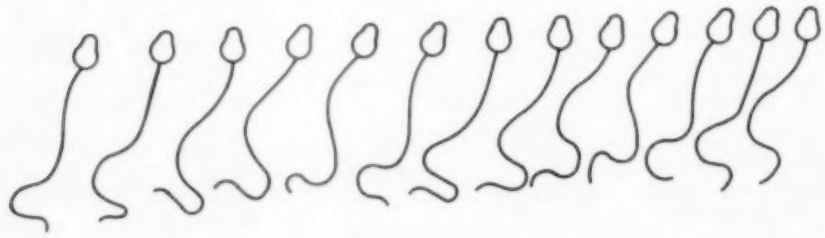

FIG. 1
Typical "figure-of-eight" beat shape of a spermatozoon in cervical mucus. These drawings are tracings from a high-speed cine film, 0.05 sec apart.

The present study was designed to take advantage of our recent experimental observations, and to begin the development of a new, more incisive biomechanical theory of the sperm-mucus interaction. Our approach was to characterize the local environment in the mucus about a spermatozoon as a *cell* comprised of a Newtonian fluid surrounded by a rigid cylindrical no-slip boundary. This boundary acted, thus, as the *hydrodynamic equivalent* of the many mucin macromolecules with which the sperm interacted. Our characterization of the mucous microstructure in terms of a hydrodynamically equivalent interstitial dimension is in the same spirit as the use of a hydraulic radius for flow in pipes (12), or the concept of a radius of gyration to describe macromolecules (13). We have developed a simple resistive force theory, which relates parameters of sperm swimming to the dimensions of the mucous *cell*. Preliminary experimental data for human sperm movement in ovulatory human cervical mucus have been obtained, and have been applied to the new theory. Estimates of the size of the mucous *cell* have consequently

been obtained.

EXPERIMENTAL METHODS AND RESULTS

Samples of cervical mucus were obtained at midcycle from two ovulating women with normal reproductive function. The specimens were collected via gentle suction into a polyethylene catheter (I.D. 1.40 mm, O.D. 1.90 mm) after the catheter had been advanced through the external os 1-2 cm into the cervical canal. The mucus in the proximal end of the catheters thus had its origin in the superior portion of the canal, i.e. the endocervix. Approximately 50 µl of this mucus was expressed onto a microscope slide, and immediately covered by a #1 1/2 coverglass, 22 mm X 22 mm, that had thin ridges of vaseline on three sides. The depth of the resulting preparation was approximately 200 µm. Fresh human semen was then injected via a Pasteur pipette under the open side of the coverglass, such that it contacted the mucus and filled the open space. A different semen specimen was applied to each mucous sample. The specimens were obtained by masturbation from normal healthy young men of proven fertility, and were utilized immediately after liquification. The open side of the coverglass was then sealed, and the completed slide preparation was placed on the stage of a microscope maintained at 37°C by an air curtain incubator.

Ten minutes after initial semen-mucus contact, high speed cinemicrography was used to assess the movement characteristics of the forwardmost, vanguard spermatozoa migrating into the mucus. A number of fields were chosen at random on each preparation. Cine films were taken at 100 frames/sec using a Locam high-speed camera. A timing light generator provided a precise measure of framing rate. Dry phase contrast optics were employed, using a 20X planachromatic objective and a 3.3X ocular. Processed cine films were analyzed frame-by-frame. Spermatozoa with normal head morphology, and also headless sperm were chosen randomly and assessed over two seconds of elapsed real time. All such sperm exhibited the "figure-of-8" beat shape common in normal, ovulatory mucus (11), cf. Figure 1. The time-average propulsive swimming speed V_p (µm/sec), flagellar beat frequency f (beats/sec), and beat amplitude b(µm) were obtained for each spermatozoon.

Vol. 17
1980

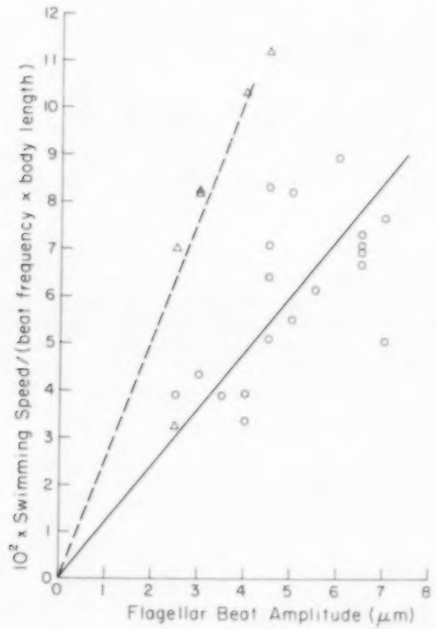

FIG. 2
Experimental data, obtained from high-speed cinemicrography, on the movement characteristics of human spermatozoa in ovulatory human cervical mucus. The triangles and circles are for headless and normal sperm, respectively. The broken and solid lines are the respective regression lines, fitted through the origin.

The pooled data are illustrated in Figure 2, in which the dimensionless swimming speed or "kinetic efficiency" V_p/fL has been plotted vs. beat amplitude. Here L is the length of the sperm body, which is 50 μm for a human spermatozoon. The straight lines in Figure 2 are linear regression lines fitted through the origin. The slopes of these lines are 1.17 for the normal sperm, and 2.49 for the headless sperm, and they differ significantly ($P < 0.01$). The legitimacy of this comparison procedure was established by determining that at a 5% significance level the unconstrained regression lines were linear and had intercepts not significantly different from zero. These data indicate that a headless spermatozoon tends to swim approximately twice as fast in the mucus as a normal sperm exhibiting identical beat frequency and amplitude (viz. beat shape).

THEORETICAL DEVELOPMENTS

As an initial new approach for describing the hydrodynamics of the sperm-mucus interaction, a simple *resistive force theory* was developed (14). The mucous microstructure experienced locally by length elements among a sperm body was represented by a rigid cylindrical no-slip boundary. This model of the hydrodynamic influence of the microstructure was motivated by our contemporary, qualitative understanding of its geometrical properties. The mucin network in the mucous native gel state is comprised of filamentous macromolecules whose length and diameter are small compared to a sperm flagellum. These macromolecules are organized such that the interstices among them vary in shape and orientation. A typical interstitial size is also small compared to the length of a sperm body. Thus, a spermatozoon swims in very close proximity and interacts hydrodynamically with numbers of the mucin macromolecules. The local force on each length element of the sperm body is assumed to depend upon the velocity of that element only. Such an approximation is relatively accurate for a structureless Newtonian fluid of infinite extent (15,16,17). The mucin macromolecules may, in fact, shield local elements of the sperm body from direct hydrodynamic interaction, therefore increasing the rationale for the resistive force approach.

The following resistive force coefficients were employed, cf. (18):

$$C_L = \frac{2\pi\eta}{\ell n(h/r_o) + 1} \tag{1}$$

$$C_N = \frac{4\pi\eta}{\ell n(h/r_o) - 1} \tag{2}$$

$$C_H = \frac{6\pi a_H \eta \left[1 - 0.7586\left(\frac{a_H}{h}\right)^5\right]}{1 - 2.1050\left(\frac{a_H}{h}\right) + 2.0865\left(\frac{a_H}{h}\right)^3 + 0.7260\left(\frac{a_H}{h}\right)^6} \tag{3}$$

Here C_L and C_N are respectively the longitudinal and normal force coefficients for the flagellum, and C_H is the force coefficient for the sperm head, assumed spherical; η is the viscosity of the surrounding fluid, assumed Newtonian; r_o and a_H are respectively the radii of the flagellum and head; and h is the separation distance between the centerline of the sperm body and the outer boundary. Use of these expressions is predicated on the assumption that the sperm swims undirectionally along the centerline of the cylindrical cavity. It follows that a simple analytic expression can be derived for the propulsive velocity or kinetic efficiency, (14), viz.

$$\frac{V_p}{f_L} = \left(\frac{\Lambda}{L}\right)\frac{(1-\beta)\left[1 - (C_L/C_N)\right]}{1 - \beta + (C_L/C_N)\beta + C_H/LC_N} \tag{4}$$

Here Λ is an effective wavelength as measured along the flagellum; and β is the mean-square value of the cosine of the local slope angle of the flagellum with respect to the axis of propulsion.

In order to model the figure-of-8 beat of human speramtozoa in cervical mucus, the waveform depicted in Figure 3 was used. The sperm head, if present, was represented by a sphere of radius 1.25 μm. The flagellum was taken as a circular cylinder of length 45 μm and radius 0.25 μm. The proximal 10 μm segment of the flagellum, which undergoes little bending, was modeled as a rigid circular cylinder. The distal 35 μm of the flagellum was then taken to propagate traveling sine waves. Three combinations of amplitude (b) and

wavelength (λ) were applied for these waves: b = 2 μm, λ = 25 μm; b = 4 μm, λ = 25 μm; and b = 5 μm, λ = 25 μm. Here λ is the wavelength as measured along the axis of propagation.

Figure 4 displays the results of the application of these waveforms to Eq. 4 for spermatozoa with or without heads. The theoretical model predicts that for cell sizes of the order of 2 μm, headless spermatozoa would swim approximately twice as fast as normal spermatozoa with heads and exhibiting the same beat.

FIG. 3
The model beat shape used in the theoretical calculations of a human sperm swimming in cervical mucus.

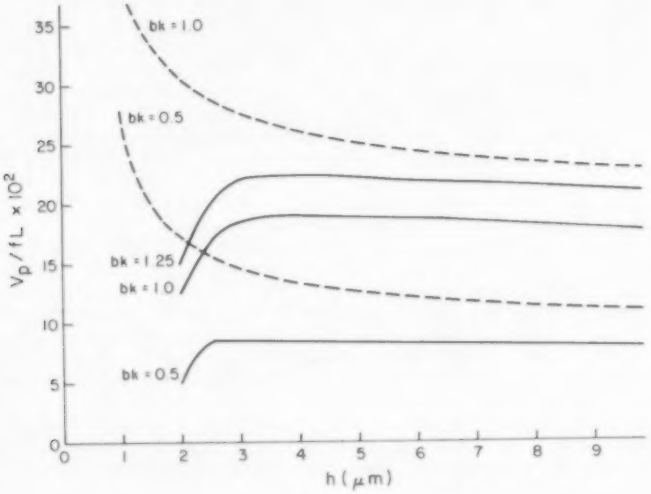

FIG. 4
Results of the theoretical model of a human spermatozoon swimming in cervical mucus. The symbols are: V_p = propulsive swimming speed; f = flagellar beat frequency; b = beat amplitude; k = 2π/(beat wavelength); L = length of sperm body (50 μm); and h = *cell* size. The broken lines are for headless spermatozoa. The solid lines are for normal sperm with heads.

DISCUSSION

The swimming of a spermatozoon within cervical mucus is a phenomenon in which hydrodynamic interactions between the sperm and the mucous microstructure are strong. This can be appreciated by reference to the theoretical model developed here with, for example, a *cell* size h = 2 μm, a beat amplitude b = 4 μm, and a wavelength λ = 25 μm. In such a case, the model predicts that a normal sperm (with a head) would have a kinetic efficiency (dimensionless swimming speed) approximately 50% higher in the mucus than while swimming with the same beat in a simple Newtonian fluid of infinite extent. This distinction arises from the amplification within the mucus of the local forces acting on the sperm body. For example, the normal resistive force coefficient C_N increases threefold in the mucous *cell* as compared with unbounded Newtonian fluid of the same local viscosity. The consequent increase in local bending moments acting along the flagellum undoubtedly contributes to the altered beat shape of mammalian sperm in the mucus as compared to simple Newtonian media of low viscosity, see e.g. (19,20,21). The increased drag on the sperm head, resulting in an altered "boundary condition" for the flagellar contraction mechanism is also likely to be a contributing factor (22). For example, the drag coefficient on the sperm head increases fourfold in the mucous *cell* as compared to an unbounded Newtonian fluid of the same local viscosity. Thus, the tradeoff between the increased drag on the sperm head and the increased forces acting upon and generated by the flagellum may be directly involved in modulating both the beat shapes and swimming speeds of spermatozoa in cervical mucus.

Vol. 17
1980

In this regard, it is interesting to note that the theoretical plots of kinetic efficiency vs. *cell* size, cf. Figure 4, contain maxima.

It should be appreciated that the values of mucous *cell* size h inherent to our theorectical model do not necessarily typify the geometrical distance between adjacent filaments of the mucous microstructure. That distance appears to be small compared to length of the flagellum (23,24) and a motile spermatozoon interacts hydrodynamically with numbers of the mucin filaments at different distances from it. Therefore, a typical *interstitial* size within the mucus would be smaller than the *cell* size depicted here.

If the experimentally determined 2:1 correspondence between the kinetic efficiencies of headless and normal sperm is used as the basis for predicting cell size, then the value $h \approx 2$ μm is suggested by the data of our study. Notably, both the cell size and related interstitial size suggested here are smaller than the diameter of what were formerly regarded as large, liquid-filled channels within the mucus, (cf. the chapters in ref. 8). Our related studies of micro-hydrodynamic phenomena in sperm-free cervical mucus provide confirmation of this distinction (24). Indeed, a spermatozoon swimming within the mucus may be in very close proximity to numbers of the microfilaments. To that extent, the rigid body drag inherent to the present model would underestimate that experienced by real spermatozoa. This could account at least in part for our lower theoretical than experimental values of kinetic efficiency. Stress-relaxation within the mucus might also contribute, since cervical mucus does exhibit viscoelastic behavior (3,25,26). These preceding studies indicate stress-relaxation times of the order of one second or more, which are large compared to the flagellar beat period of a typical human spermatozoon, beating at 15-25 Hz in the mucus (11). Delayed stress-relaxation in the local mucus adjacent to a motile sperm flagellum might reduce the ratio of thrust to drag on the sperm body, thereby slowing the sperm. That is, relaxation in the local mucus strained by the undulating sperm body might not be completed until the sperm had swum some distance away. To this extent, the sperm would not regain the elastic energy initially expended, and its rate of working would contain an elastic component in addition to the viscous one.

Physiologically speaking, flagellar propulsion does appear to play a role in sperm transport through the mucus within the mammalian cervix (2). It seems unlikely, however, that sperm motility is responsible for the very rapid transit of a few spermatozoa into and through the mucus *in vivo* immediately after insemination. This is probably due to the pumping action of the female reproductive tract. Rather, sperm motility may be responsible for the distribution of spermatozoa during the colonization of the cervix that follows insemination (27). Since the colonizing sperm population is likely to contain the fertilizing spermatozoa, it can be inferred that such cells do necessarily swim through the mucus (2). The kinetics of this passage appear to be very subtle, and may well be modulated by hydrodynamical interactions between spermatozoa and mucus of different properties in different regions of the cervical canal (28). The present study provides an initial description of the biomechanics of these interactions, describing them in terms of parameters amenable to experimental measurement and suggesting a basis for further experimental and theoretical study.

ACKNOWLEDGEMENT

This work was supported by NIH grant 1-RO1-HD12971.

REFERENCES

1. DAVAJAN, V., NAKAMURA, R. M. and KHARMA, K. Spermatozoan transport in cervical mucus. Obstet. Gynec. Surv. 25,1-43, 1970.

2. OVERSTREET, J.W. and KATZ, D. F. Sperm transport and selection in the female genital tract. In: Mammalian Development. M. H. Johnson (Ed.). Amsterdam, Elsevier/North Holland. 1977, pp. 31-65.

3. WOLF, D. P., BLASCO, L., KHAN, M. and LITT, M. Human cervical mucus. I. Rheological characteristics. Fertil. & Steril. 28, 41-46, 1977.

4. KATZ, D. F. On the biophysics of in vivo sperm transport. Ph.D. Dissertation, University of California, Berkeley, 1972.

5. SMELZER, R. E., SHACK, W. J. and LARDNER, T. L. The swimming of spermatozoa in an active channel. J. Biomech. 7, 349-355, 1974.

6. SHUKLA, J. B., RAO, B. R. P. and PARIHAR, R. S. Swimming of spermatozoa in cervix.

Effects of dynamical interaction and peripheral layer viscosity. J. Biomech. 11, 15-19, 1978.

7. KATZ, D. F. On the propulsion of microorganisms near solid boundaries. J. Fluid Mech. 64, 33-49, 1974.

8. ELSTEIN, M., MOGHISSI, K. and BERTH, R. Cervical Mucus in Human Reproduction. Copenhagen: Scriptor. 1973, pp. 1-163.

9. BLASCO, L., SOKOLOSKI, J. and WOLF, D. P. A practical, objective approach to evaluation of sperm and cervical mucus in humans. Fertil. Steril. 32, 55-60, 1979.

10. KATZ, D. F. and SINGER, J. R. Water mobility in bovine cervical mucus. Biol. Reprod. 17, 843-849, 1978.

11. KATZ, D. F., MILLS, R. N. and PRITCHETT, T. R. The movement of human spermatozoa in cervical mucus. J. Reprod. Fertil. 53, 259-265, 1978.

12. SCHLICHTING, H. Boundary Layer Theory. 6th ed. New York: McGraw-Hill, 1968, 747 pp.

13. TANFORD, C. Physical Chemistry of Macromolecules. New York: John Wiley and Sons, 1961, 710 pp.

14. GRAY, J. and HANCOCK, G. J. The propulsion of sea urchin spermatozoa. J. Exp. Biol. 32, 802-814, 1955.

15. JOHNSON, R. E. and BROKAW, C. J. Flagellar hydrohynamics: A comparison between resistive-force theory and slender-body theory. Biophys. J. 25, 113-127, 1979.

16. HIGDON, J. J. L. A hydrodynamic analysis of flagellar propulsion. J. Fluid Mech. 90, 685-711, 1979.

17. DRESDNER, R. D., KATZ, D. R., and BERGER, S. A. The propulsion by large amplitude waves of uniflagellar microorganisms of finite length. J. Fluid Mech. 1980 (in press).

18. HAPPEL, J. and BRENNER, H. Low Reynolds Number Hydrodynamics. Englewood Cliffs, NJ: Prentice Hall, 1965, 553 pp.

19. BROKAW, C. B. Computer simulation of flagellar movement. II. Influence of external viscosity on movement of the sliding filament model. M. Mechanochem. Cell Motility 1, 203-212, 1972.

20. BROKAW, C. J. Effects of viscosity and ATP concentration on the movement of reactivated sea-urchin sperm flagella. J. Exp. Biol. 62, 701-719, 1975.

21. RIKMENSPOEL, R., JACKLETT, A. C., ORRIS, S. E., and LINDEMANN, C. B. Control of bull sperm motility. Effects of viscosity, KCN and thiourea. J. Mechanochem. Cell Motility 2, 7-24, 1973.

22. RIKMENSPOEL, R. The equation of motion for sperm flagella. Biophys. J. 23, 177-206, 1978.

23. CHRETIEN, F. C., CERNIGON, C., DAVID, G., and PSYCHOYOS, A. The ultrastructure of human cervical mucus under scanning electron microscopy. Fertil. Steril. 24, 746-751, 1973.

24. TAM, P. Y., KATZ, D. F. and BERGER, S. A. Flow permeation studies of cervical mucus. Presented at the Third International Congress of Biorheology, La Jolla, August 28-September 1, 1978 (Abstract: Biorheology 15, 459, 1978).

25. HWANG, S. W., LITT, M. and FORSMAN, W. C. Rheological properties of mucus. Rheolog. Acta 8, 438-448, 1969.

26. ELIEZER, N. Viscoelastic properties of mucus. Biorheology 11, 61-68, 1974.

27. FORDNEY SETTLAGE, D. S., MOTOSHIMA, M. and TREDWAY, D. R. Sperm transport from the external cervical os to the fallopian tubes in women: A time and quantitation study. Fertil. Steril. 24, 655-661, 1973.

28. KATZ, D. F. and OVERSTREET, J. W. Mammalian sperm movement in the secretions of the male and female genital tracts. In: Testicular Development, Structure and Function. E. Steinberger and A. Steinberger (Eds.). New York, Raven Press. 1980, pp. 481-489.

BLANK
PAGE

Vol.
198

BIORHEOLOGY Vol.17, pp. 177-182 0006-355X/80/010177-06$02.00/0
© Pergamon Press Ltd. 1980. Printed in the United States

THIRD INTERNATIONAL CONGRESS OF BIORHEOLOGY

SYMPOSIUM ON RECENT ADVANCES IN HEMORHEOLOGY

VISCOELASTIC STUDY OF AGGREGATION OF RED BLOOD CELLS

Eiichi Fukada and Makoto Kaibara

The Institute of Physical and Chemical Research, Saitama, Japan

(Received 10.10.1979. Accepted by Guest Editor S. Chien)

ABSTRACT

The flow curves of rabbit blood, human fetal blood, and human adult blood show no hysteresis, a little hysteresis and considerable hysteresis, corresponding to their capacity of forming rouleaux. After the cessation of the steady flow, which was used to remove the original aggregation of cells, the time variations of the rigidity modulus G' and the loss modulus G" were determined at 1 Hz. For rabbit blood, almost no time change for G' and G" and no erythrocyte sedimentation was observed. For human adult blood, G' and G" first increased to a miximum value and then decreased. The rate of erythrocyte sedimentation was correlated to the rates of increase and decrease of G' and G". These observations were accounted for by considering the change of structure of blood: i.e. the formation of rouleux, the association of rouleux, and the formation of nonhomogeneous structure.

Vol. 17
1980

INTRODUCTION

The viscoelasticity of blood and red cell suppension has been investigated by many authors[1-3]. The blood shows small elasticity because of the interactions between red blood cells as well as the rigidity of cell walls. The rigidity modulus of blood has been found to be in the order of 1 dyne/cm^2. In this paper the viscoelastic properties of blood have been examined in relation to the aggregation of red blood cells. The bloods of rabbit, horse and man were investigated. The blood collected from human umbilical cord was also investigated. As an anticoagulant, 3.8 % sodium citrate solution was added in a volume ratio of 1 to 9. The steady flow viscosity and the dynamic modulus of blood were determined by means of a coaxial cylinder viscoelastometer.

METHODS

The flow curve of blood was measured by a rotating viscometer with concentric double cylinders[4]. The dynamic rigidity modulus $G = G' + iG"$ of blood was also determined by this apparatus. The outer cylinder was sinusoidally oscillated at 1 Hz. The torque in the inner cylinder transmitted from the blood sample was electrically detected. The outputs indicating the shear stress and the shear strain of sample were led to the two axes of an XY recorder and plotted a lissajous' figure as shown in Fig. 1. From the analysis of this figure, the real part of dynamic modulus or the storage modulus G' and the imaginary part of dynamic modulus or the loss modulus G" were determined. The amount of the sample was about 5 ml, the maximum shear strain in the sample was 0.06, and the detectable torque was about 0.01 dyne-cm.

RESULTS

Figure 2 shows examples of flow curves for rabbit blood, human fetal blood, and human adult blood. The shear stress in samples is plotted against the cyclic change of shear rate from zero to 3 or 4 sec^{-1} in a few minutes.

For rabbit blood, the relation between shear stress and shear strain is a little non-linear but no hysteresis is observed. For human fetal blood, a slight hysteresis is observed in the flow curve and for human adult blood a large hysteresis was observed as well as non linear relationship between shear stress and shear rate.

The difference in the steady flow viscosity for these samples should reflect the difference in the interaction between red blood cells or the degree of aggregation of red blood cells.

Figure 3 shows the microscopic observation of rabbit, human fetal and adult bloods. A small drop of blood was dropped on a slide glass and a cover glass was placed over it. Then photographs were taken under a microscope.

Red blood cells of rabbit are dispersed independently and do not form any aggregate. Red blood cells of man form rod like aggregates called rouleau. The rouleaux make lateral association and form a network structure as shown in the figure. Red blood cells of human fetal blood also form rouleaux. But the length of rouleaux is much shorter than those for adult blood. The lateral association between rouleaux is also weak. The tendency of aggregation of red blood

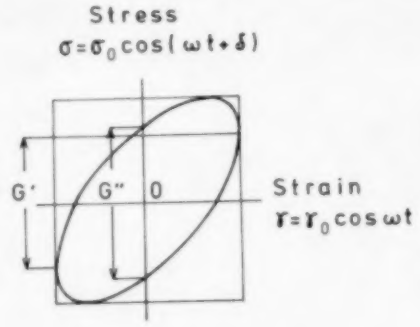

FIG.1
Lissajous' figure of dynamic shear stress σ and dynamic shear strain γ.

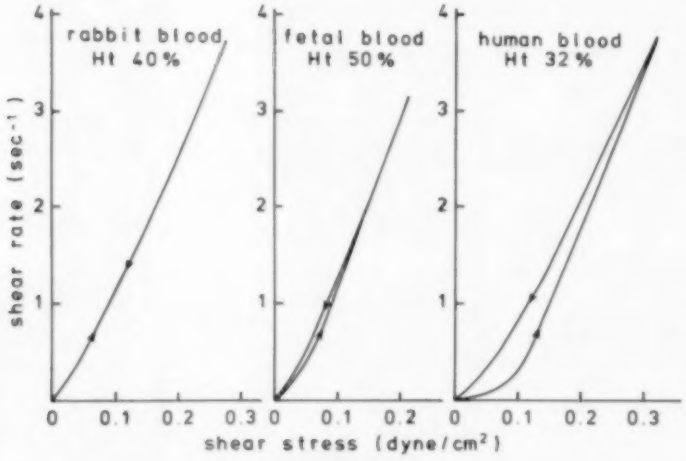

FIG.2
Flow curves for rabbit blood, human fetal blood, and human adult blood, 3.8 % sodium citrate solution was added in a volume ratio of 1 to 9.

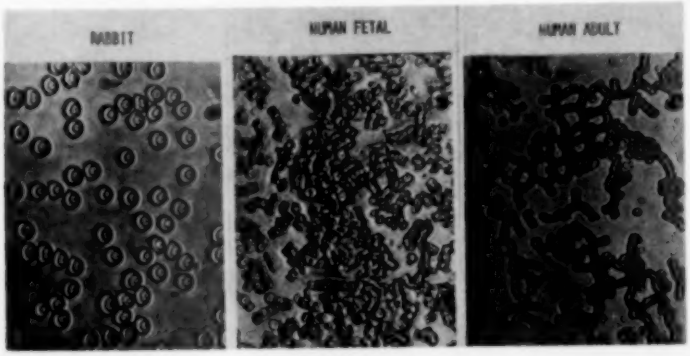

FIG.3
Microscopic observation of rouleaux formation in rabbit, human fetal and adult bloods.

cells in fetal blood is in between rabbit and human adult bloods.

The hysteresis in flow curves shown in Fig. 2 can be understood from these observations. For rabbit blood, the cells are dispersed separately and no hysteresis is observed. For human blood, the network structure connecting red blood cells is deformed and destructed by the applied shear stress. Consequently the large hysteresis is produced. Human blood shows a kind of thixotropy. Since fetal blood possesses a weak structure, a slight hysteresis is observed in its flow curve.

Since blood is thixotropic, the rigidity modulus depends on the structure formed by red blood cells, which easily changes by external disturbances. In order to set a standard condition, we applied to the blood sample a steady flow with a mean shear rate $\dot{\gamma} = 66\ sec^{-1}$ for 1 minute before starting the measurement of the dynamic modulus G' and G". It is known that rouleaux are broken in the steady flow with a shear rate of about $10\ sec^{-1}$. Therefore, the shear rate $66\ sec^{-1}$ employed in this study should break all rouleaux.

The origin of time was set when this steady flow was stopped. At this stage no aggregation was present between red blood cells and G' was nearly zero. Then oscillatory flow was applied to the sample and the recording of Lissajous' figure was started.

The aggregation of red blood cells gradually takes place after the cessation of the steady flow. Since the amplitude of oscillation is very small, the oscillatory flow would not give disturbance to the aggregation of cells. Nevertheless, the values of dynamic rigidity G' and G" gradually change during a period of measurement for 10 - 15 minutes after the cessation of the steady flow.

Figure 4(a) shows the time variation of storage modulus G' and loss modulus G" for rabbit blood with 40 % hematocrit. The value of G' is as small as 0.2 dyne/cm^2. It only slightly increases with time. The upper part of the figure shows the erythrocyte sedimentation, ES. No sedimentation was observed for rabbit blood.

Figure 4(b) shows the time change of G' and G" as well as ES for fetal blood with 53 % hematocrit. The value of G' increases slightly for 2 - 3 minutes after the cessation of the steady flow and levels off at about 0.8 dyne/cm^2. Owing to the large hematocrit, the values of G' and G" are greater than those for adult bloods. Almost no sedimentation was observed for fetal blood.

Figure 4(c) shows the time variation of G' and G" for human adult blood with 40 % hematocrit. G' increases for about 3 minutes to the value of about 0.5 dyne/cm^2 and then gradually decreases with time. For human adult blood erythrocyte sedimentation was obviously observed as shown in the upper part of the figure.

Since the elasticity of blood should originate from the interactions between red blood cells, the time variation of G' seems to reflect the

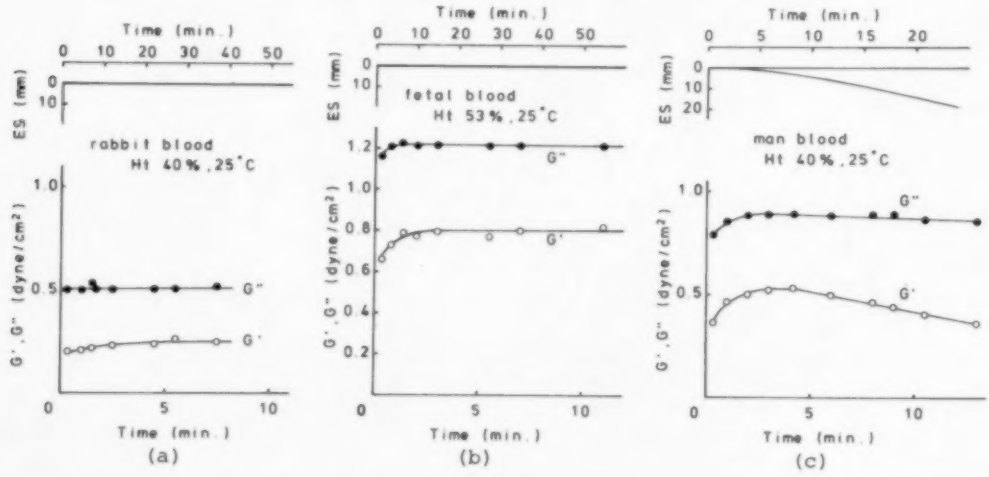

FIG.4
The rate of erythrocyte sedimentation(ES), the rigidity modulus(G') and the loss modulus(G") for rabbit blood(a), human fetal blood(b), and human adult blood(c).

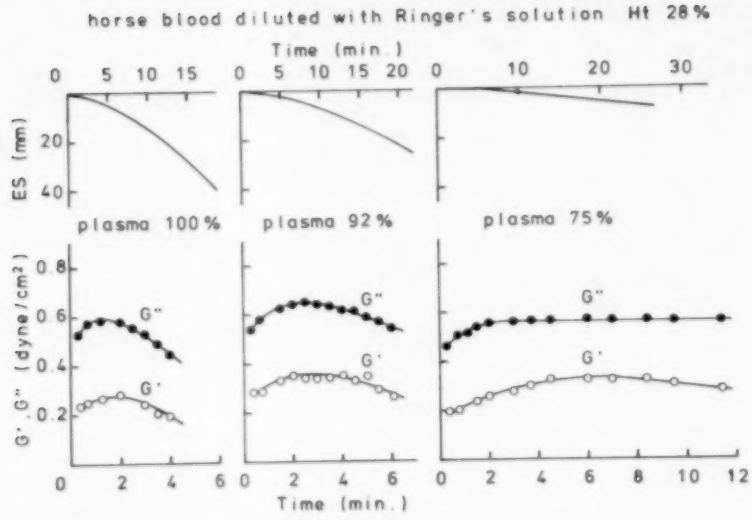

FIG.5
The effect of plasma dilution on the rate of erythrocyte sedimentation ES and the time variation of rigidity G' and loss G" for horse blood.

variation of the structure of blood which is formed by the aggregation of red blood cells. The rate of sedimentation of erythrocyte should be also related to the structural change of blood.

Since the interaction between erythrocytes is infuenced by the plasma proteins, we have undertaken experiments to investigate the effect of dilution of plasma.

Figure 5 shows the result for horse blood, which has properties similar to human blood. The blood of horse was diluted by Ringer's solution keeping its hematocrit at 28 %.

The left figure shows the erythrocyte sedimentation and the time variation of G' and G" for non-diluted horse blood denoted as plasma 100 %. G' and G" show an increase followed by a decrease with time similar to the human blood.

The data when the plasma is diluted by Ringer's solution are shown in the middle and right of the figure. The time required for G' to reach the maximum becomes longer and the rate of decrease of G' becomes smaller. It is also noticed that the rate of sedimentation of erythrocytes decreases with the dilution of plasma. When the plasma was completely substituted by Ringer's solution no time variation of G' and no sedimentation of cells were observed, similar to the rabbit blood. These observations suggest a correlation between the rate of erythrocyte sedimentation and the time variation of G' and G".

In Fig 6, the time required for G' to reach the maximum and the rate of decrease of G' after having passed through the maximum are plotted against the rate of erythrocyte sedimentation, ESR. Good correlations are present between them. If the sedimentation rate ESR is smaller, G' takes the longer time to reach the maximum and at the same time the rate of decrease of G' becomes smaller.

It is obvious that the increase and decrease of G' is influenced by the amount of plasma proteins and that the aggregation of red blood cells is governed by the presence of the plasma proteins.

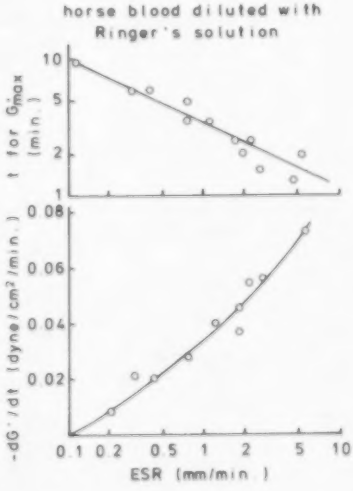

FIG.6
The time required for G' to reach a maximum and the rate of decrease of G' plotted against the erythrocyte sedimentation rate for horse blood.

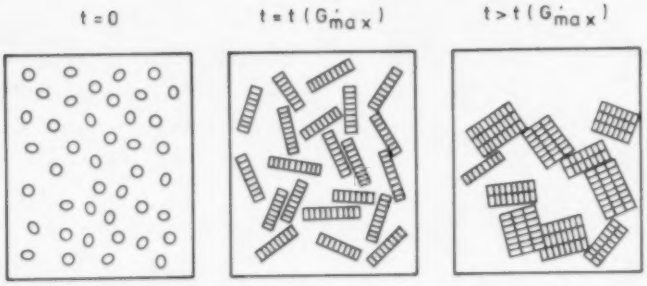

FIG.7
Schematic diagram of the structure of blood which is produced by the aggregation of red blood cells.

DISCUSSION

Figure 7 visualizes schematically the structure of blood of human or horse caused by the aggregation of red blood cells. At time zero when the steady flow is stopped, all cells are disintegrated and there is no aggregation between red cells. In 2 or 3 minutes, red cells aggregate to form reuleaux with the shape of long rod. These rouleaux associate laterally and form a three dimensional network, causing the increase of G'. Meanwhile the lateral association of rouleaux gradually developes the local assemblies of rouleaux and lead to a nonhomogeneous structure resembling to a pattern of islands in sea, in which G' is smaller compared to the homogeneous network structure.

Similar change of structure in blood should take place during the measurement of sedimentation rate. If the aggregation tendency of cells is greater, the rate of sedimentation is also greater.

As shown in Fig. 5, if the content of plasma proteins is normal, then the time variation of G' and sedimentation rate are large. However, if the content of plasma is reduced by dilution, both the time variation of G' and sedimentation become smaller. The aggregation of red blood cells must be governed by the plasma proteins, which interconnect red blood cells to each other.

The experimental results for human adult, human fetal and rabbit bloods are summarized in Table 1. For human and horse blood, the red blood cells form rouleaux with a long length. These rouleaux form assemblies. The sedimentation rate is therefore large. Because applied shear stress disturbs the aggregation of cells, large hysteresis is observed in the flow curve. Because the assemblies of rouleaux are formed, G' decreases with time.

On the other hand, for the rabbit blood, there is no aggregation of red blood cells. Therefore no sedimentation of cells, no hysteresis in flow curve, and no decrease of G' take place.

The fetal blood is in between them. The red blood cells form only short rouleau and the lateral association between rouleaux is weak. Therefore almost no sedimentation, only slight hysteresis in flow curve and no decrease of G' are observed. It is known that hematocrit in normal fetal blood is higher than 50 % and higher than that for normal adult blood, and that the amount of plasma proteins in fetal blood, particularly fibrinogen is lower than that for adult blood. The higher value of hematocrit could be understood by the necessity of oxygen supply to placenta. The high hematocrit should result in the high viscosity of blood. However, the low content of fibrinogen in fetal blood may serve to prevent the aggregation of red cells and to reduce the viscosity of blood in spite of high hematocrit.

The data of protein analysis for human fetal bloods are shown in Table 2. The content of total protein for fetal blood is 0.8 compared to adult blood. The ratio for albumin contents of fetus and adult is about 0.93. However, the ratio for globulin is 0.69 and the ratio for fibrinogen is only 0.48. these small contents of globulin and fibrinogen should be the origin for weak interactions between red blood cells in fetal blood.

Vol. 17
1980

TABLE 1 Comparison of results for different bloods

	rabbit (cow)	human fetal	human adult (horse)
aggregation of RBC	no	short rouleaux	long rouleaux
erythrocyte sedimentation rate	no	very small	large
hysteresis in flow curve	no	slight	large
decrease of G'	no	no	large

TABLE 2 The data of protein analysis of human fetal bloods by Dr. Manabu Kaibara, Tokyo University Branch Hospital

	total protein (g/dl)	albumin (g/dl)	globulin (g/dl)	fibrinogen (mg/dl)
adult	7.23	3.84	3.75	246
fetus	5.82	3.23	2.58	119
ratio	0.80	0.93	0.69	0.48

ACKNOWLEDGEMENT

The authors wish to express their gratitude to Dr. Manabu Kaibara of Tokyo University Branch Hospital for supplying us the samples of fetal blood and the results of protein analysis.

REFERENCES

1. THURSTON, G. B. Viscoelasticity of human blood. *Biophys. J.* 12, 1205 - 1217, 1972.

2. USAMI, S., KING, R. G., CHIEN, S., SKALAK, S., HUANG, C. R. and COPLEY, A. L. Microcinephotographic studies on red cell aggregation in steady and oscillatory shear - a note. *Biorheology* 12, 323 - 325, 1975.

3. CHIEN, S., KING, R. G., SKALAK, R., USAMI, S. and COPLEY, A. L. Viscoelastic properties of human blood and red cell suspensions. *Biorheology* 12, 341 - 346, 1975.

4. FUKADA, E. and KAIBARA, M. *Thrombosis Research* Suppl II 8, 49 - 58, 1976.

BIORHEOLOGY Vol.17, pp. 183-189 0006-355X/80/010183-07$02.00/0
© Pergamon Press Ltd. 1980. Printed in the United States

THIRD INTERNATIONAL CONGRESS OF BIORHEOLOGY

SYMPOSIUM ON RECENT ADVANCES IN HEMORHEOLOGY

FLOW OF BLOOD THROUGH NARROW CAPILLARIES: RHEOLOGICAL MECHANISMS DETERMINING CAPILLARY HEMATOCRIT AND APPARENT VISCOSITY.

Peter Gaehtgens
Institute for Normal and Pathological Physiology, University of Köln, Germany

(Received 15.7.1979; in revised form 5.11.1979.
Accepted by Guest Editor S. Chien)

ABSTRACT The dynamic volume concentration of red cells in a narrow capillary tube is a resultant of several mechanisms which take place either at the capillary orifice or within the tube. Both types of mechanisms have been studied in experiments in vitro. Human red cell suspensions were perfused through glass capillaries (I.D. 3.3 - 12µm) branching from a larger feed channel. In addition, relative apparent viscosity was measured as a function of tube hematocrit. The results indicate that the red cell flow fraction is determined by the flow rate distribution at the branching point, and may even be reduced to zero if the fraction of flow diverted into the capillary orifice is decreased. At any discharge hematocrit the hematocrit within the tube is further reduced due to the velocity difference between cells and plasma. At equal tube hematocrit, the relative apparent viscosity showed a minimum at a tube diameter of approx. 5µm, whereas the dynamic hematocrit reduction was maximal at approx. 15µm. These results were correlated with observations of the dynamic flow behaviour of the red cells in a "travelling capillary" which indicate that red cells tend to travel in groups rather than equally spaced, show a hematocrit dependent transition from single-file to multi-file arrangement in tubes larger than 6µm, and, even in the smallest capillaries, exhibit a distinctly non-symmetric shape, regardless of flow rate and hematocrit.

Vol. 17
1980

The presence of a particle in the flow of a continuous medium through a cylindrical tube causes a disturbance of the flow field which leads to an alteration of the viscous pressure dissipation associated with flow. The magnitude of this effect depends not only on the dimensions of the particle relative to that of the tube, but also on its dynamic behaviour during flow which determines its "effective volume" (1). This can be reduced for instance by shear-induced deformation or membrane rotation. For any given particle with defined microrheological properties the disturbance effect may increase with increasing particle volume concentration since additional sources of pressure dissipation (interactions between particles or between particles and the tube wall) come into the play. Thus, the phenomena determining the level of particle volume concentration in the flowing suspension represent a significant mechanism determining the increase of pressure necessary to maintain flow.

Ever since the classical work of FAHRAEUS and LINDQVIST (2) in tubes between approximately 300 and 30µm in diameter it is known that the relative viscosity of human blood decreases as the diameter of the tube is reduced, and this observation has been attributed to the changes of hydrodynamically effective ("dynamic") volume concentration of the red blood cells (3,4).+

+Historical footnote: Although the discovery of this phenomenon is commonly attributed to FAHRAEUS and LINDQVIST (1931), it might be noted that one year earlier P.MARTINI, A.PIERACH, and E.SCHREYER described very careful experiments in which the same results were obtained (5). Thus the decrease of apparent viscosity with tube radius might correctly be called the MARTINI-PIERACH-SCHREYER-FAHRAEUS-LINDQVIST-effect or, more simple, the MPSFL-effect.

In describing the results of our recent studies of blood flow into and through very narrow capillary tubes whose diameter is equal to or even smaller than that of the resting red cells, it is useful to differentiate two types of mechanisms by which cellular volume concentration can be affected (Fig. 1):

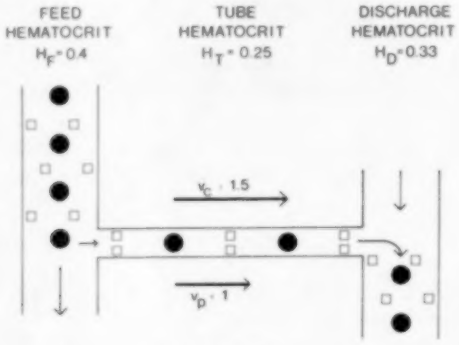

FIG.1
Schematic illustration of phenomena determining intracapillary (tube) hematocrit. Exclusion effects are described by the ratio H_D/H_F, whereas the FAHRAEUS effect is quantified by the ratio H_T/H_D. Velocity of cells (v_c, black dots) is arbitrarily assumed to exceed that of plasma (v_p, open squares) by 50%.

A. An exclusion of the cells from the entrance into the capillary may occur as a result of
   a. size limitation (tube diameter close to the so-called "critical capillary diameter, 2.7µm)
   b. radial inhomogeneity of cell distribution in the feeding tube or vessel ("plasma skimming")
   c. flow phenomena at the bifurcation which due to displacement of streamlines cause the cells to escape from the flow regions feeding the capillary orifice ("screening effect, 6).

B. The volume concentration of the cells within the capillary will decrease relative to that in the blood entering the capillary, if the average travelling speed of the cells exceeds that of the continuous medium. This effect has first been described by FAHRAEUS (7) and has therefore been called the FAHRAEUS-effect.+

The in vitro system used in the present studies was designed in an attempt to simulate a capillary vessel branching from a larger feeding arteriole. To this end glass capillaries (I.D. 3.3 - 12µm) were mounted at right angles to a cylindrical flow channel (I.D. 1.5mm) drilled through a lucite block. The feed channel was perfused at constant but variable flow rates with human red cell suspensions from a reservoir, and capillary flow was initiated by applying negative hydrostatic pressure at the downstream and of the capillaries.

The results obtained in this system showed that red cell exclusion from the capillary orifice is extremely sensitive to the flow rate distribution between feeding channel and the capillary. The ratio H_D/H_F, by which this phenomenon can be quantified, increases with increasing capillary flow rate and with decreasing flow rate in the feeding vessel. Fig. 2 gives some results obtained

+Historical footnote: It should be stressed that in the literature the definitions of this effect are variable. In his original publication (7) FAHRAEUS clearly excluded any "filter effect" from his considerations: "Consider a suspension flowing from a reservoir A through a capillary to another reservoir B. If the particles are small relative to the inner diameter of the capillary, such that a filter effect does not occur, the volume concentration in B will be the same as in A. As soon as steady-state flow has been established (....) particles and suspending fluid must enter or leave the A- or B-end of the capillary at the same volume concentration present in the original suspension. If we further assume that particles and suspending fluid exhibit different speed while flowing through the capillary, such that - as is really the case - the particles are faster (due to axial accumulation), then it follows that the residence time of the particles in the tube will be shorter that that of the fluid. Thus the particles must occupy a smaller volume fraction in the part of the suspension flowing through the tube compared to the original suspension." (Translated from the German text).

in a 6.3µm capillary the orifice of which was positioned either flush with the wall or in the centerline of the feeding channel. It is obvious that in both cases the ratio H_D/H_F varies between zero and a maximum value which is significantly less than unity if the capillary is fed from the marginal regions of the feed channel, but approaches unity in the absence of plasma skimming.

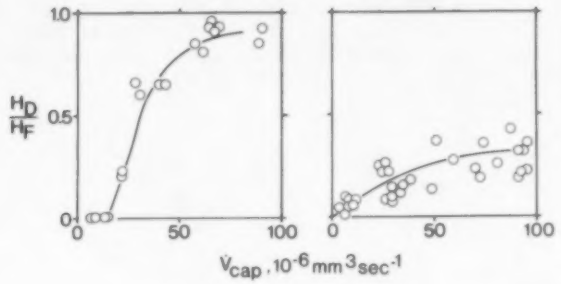

FIG. 2
Effect of variation of capillary flow rate ($\dot{V}_{cap}$) on the magnitude of cell exclusion at constant flow rate in the feeding channel (1.8ml/min). Left: capillary orifice in the center-stream, right: capillary orifice at the wall of the feeding channel.

This exclusion effect is clearly dependent on the diameter of the capillary. The experiments showed that the magnitude of this effect is negligibly small at tube diameters exceeding approximately 11µm, but increases with reduction of diameter, until, at the "critical" diameter of 2.7µm infinite flow forces are needed to force the cells into the branching capillary orifice (Fig.3).

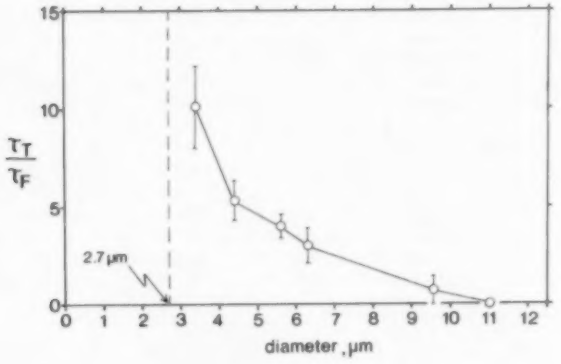

FIG. 3
The variation of cell exclusion effects with capillary diameter. The parameter on the ordinate is the ratio of average shear stresses in the capillary (τ_T) and in the feeding channel (τ_F), at which the ratio H_D/H_F equals 0.5.

Further experimental data which have been (8) or will be reported elsewhere in more detail have shown that modification of the flow properties of the cell suspensions greatly alters the magnitude of the exclusion effect: changes in continuous phase osmolarity in either direction, as well as increased aggregation tendency of the cells result in increased cell exclusion from the orifice. These observations indicate that the entrance of red cells into a narrow capillary orifice from a larger feeding vessel is a funtion of the equilibrium of forces exerted on the individual cells, but is, in addition, influenced by the microrheological properties of the cells. It is of physiological interest to stress that the entrance exclusion effects lead to a flow-dependent variation of the red cell flow fraction through the capillary: this observation suggests that the relationship between the transport capacity for oxygen in capillary flow and the capillary flow rate is distinctly non-linear (9).

Under any given flow conditions at the capillary entrance the red cell volume concentration of the blood entering the capillary tube is further reduced

Vol. 17
1980

within the capillary owing to the FAHRAEUS-effect. The present measurements made in very narrow capillary tubes indicate that this dynamic hematocrit reduction decreases with decreasing capillary diameter. Fig. 4 shows a summary of the present results and data obtained by several previous investigators. These data demonstrate that the FAHRAEUS-effect reaches a maximum in tubes or vessels of approximately 15µm and disappears as the tube diameter approaches the "critical" diameter of 2.7µm. The observed alteration of the magnitude of the FAHRAEUS-effect is clearly the result of the varying fraction of the tube cross-section which is occupied by the red blood cells. The surprizing magnitude of the dynamic hematocrit reduction in tubes smaller than the resting cell diameter is thus a consequence of the capacity of the cells to adapt to local flow conditions by deformation.

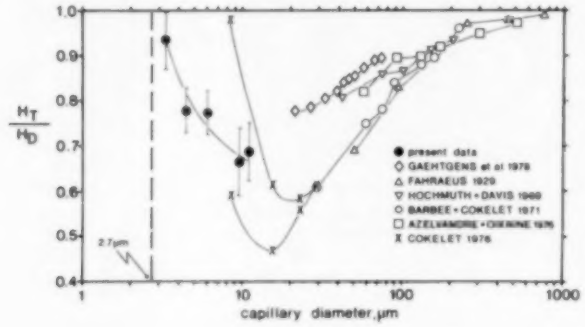

FIG. 4
Magnitude of the FAHRAEUS-effect in capillary tubes of various diameters. The maximum of the effect is expected at approximately 15 - 20µm.

By virtue of this dynamic reduction of volume concentration the disturbance effect caused by the red cells in the flow of plasma is relatively small. This conclusion is based on the determinations of the relative apparent viscosity in these capillaries which are given in Fig. 5 along with data obtained by previous investigators. However, the reduction of hydrodynamic flow resistance reaches a maximum at tube diameters considerably lower (4 - 6µm) than the reduction of dynamic volume concentration. The reason for this discrepancy is not entirely clear but it indicates that the total amount of pressure dissipation in these small tubes is not simply equal to the sum of the disturbance effects of each individual particle present, but is also affected by additional phenomena. This conclusion is substantiated by the observation in our experiments that at any capillary diameter the apparent relative viscosity was found to increase in a curvilinear fashion with increasing dynamic hematocrit.

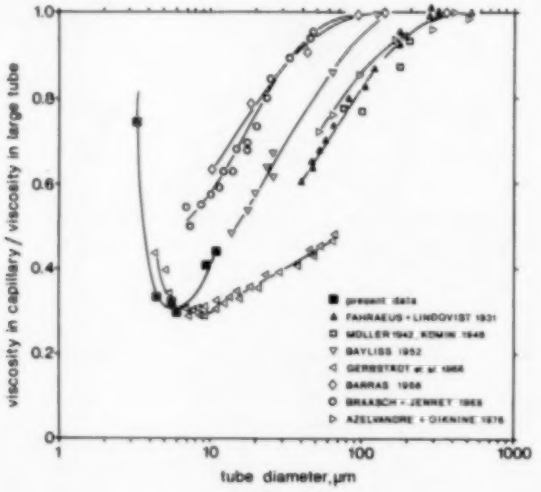

FIG. 5
The relative apparent viscosity of blood decreases with tube diameter to a minimum at approx. 4-6µm, and increases again at even smaller tube diameters.

This finding is in agreement with observations made in nuclepore filter systems and in glass capillary arrays (11,12). According to theory (10) one would rather expect an approximately linear increase at lower volume concentrations which might level-off somewhat in the higher concentration range.

In an attempt to elucidate the possible causes of these findings we have used the "travelling capillary" method (13) in order to study the dynamic flow behaviour of the red cells within the capillaries. The results of these studies provide several relevant observations:

1. Longitudinal grouping: In contrast to the assumptions underlying most theoretical analyses the longitudinal cell distribution was found quite inhomogeneous (14), regardless of capillary diameter or flow velocity. This may be the result of seizing-up behind single red cells exhibiting slower than average travelling speed due to differences in size and/or deformability. Theoretically, the formation of cell groups leads to a reduction of total pressure drop across the capillary length (10). Thus, it may be possible that the effect of cell grouping becomes less significant with increasing volume concentration, thus giving rise to a higher increase of apparent resistance than expected on the basis of equal spacing at all cell concentrations. Furthermore, the observations made in the larger capillaries (7-12µm) showed that cell-to-cell interactions occur frequently as a result of continuous rearrangement of both radial and longitudinal cell distribution (Fig. 6).

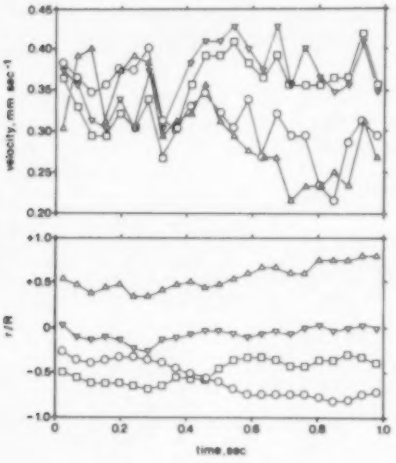

FIG. 6: Variation of axial velocity (top) and radial position (below) of four individual red cells during flow through a 12µm glass capillary at a tube hematocrit of 0.30.

2. Single-file to multi-file transition: The additional pressure drop caused by a particle in capillary flow is most importantly dependent on the effective cell to tube diameter ratio. Obviously, the radial cell distribution is constant in the very small diameter range (less than 6µm) where single-file flow was observed regardless of the volume concentration of the cells. However, in tubes of 7µm (and even more so in the larger capillaries) single-file to multi-file transition can occur if the tube hematocrit is increased. Typically, this results in the formation of "zipper"-flow (Fig. 7) at increased volume concentrations, which leads to a significant reduction of the marginal plasmatic sheath. As was shown earlier (14), this transition is also associated with a reduction of the FAHRAEUS-effect. It is conceivable that under these conditions the total pressure drop is increased beyond the value expected on the basis of the volume concentration alone. This is even more so, if the transition from single-file to zipper-flow occurs concomitantly with cell grouping, as was rather often observed. Under these conditions the occurrence of cell-to-cell and possibly even cell-to-wall interactions in groups of cells in a "zipper" arrangement cannot be excluded and thus additional sources of pressure dissipation may appear possible.

3. Finally, the analysis of red cell shape in the narrow capillaries both by cinephotography and by electron microscopy after fixation (15) clearly revealed a distinctly non-symmetric cell configuration. This is the result of the displacement of the intracellular hemoglobin solution within the folded-over biconcave red cells. It is, however, not clear whether the non-symmetrical shape of the human red cells during passage through very narrow capillaries would significantly modify the pressure drop calculated for an axially symmetrical particle.

Vol. 17
1980

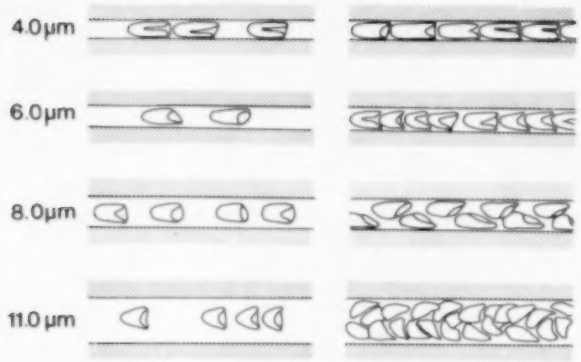

FIG. 7
Schematic drawings made from cinefilm taken of a "travelling capillary". Single-file flow is always present in the smaller capillaries whereas transition to "zipper" or multi-file flow may occur at increased volume concentrations in tubes larger than approximately 7µm.

In summary, the present study of blood flow in very narrow capillaries suggests that the mechanisms of hematocrit reduction discussed represent an important, but possibly not the only phenomenon determining viscous pressure dissipation during steady-state flow of blood. Nevertheless, the results demonstrate that by virtue of these phenomena the hydrodynamic disturbance effect resulting from the presence of red cells in the flowing plasma may be rather small in the appropriate diameter range, yielding only an increase of the hydrodynamic resistance by approximately 10% in capillaries of 4 - 6µm, which may be regarded as appropriate models for most of the nutritive capillary vessels in the microcirculation.

Vol.
198

REFERENCES

1. CHIEN, S.: Present state of blood rheology. In: Hemodilution (Eds. K.Messmer and H.Schmid-Schönbein), Basel: Karger, 1-40, 1972

2. FAHRAEUS.R., LINDQVIST,T.: The viscosity of blood in narrow capillary tubes Amer.J.Physiol. 96, 562-568, 1931

3. FAHRAEUS.R.: The suspension stability of the blood. Physiol. Rev. 9, 241-274, 1929

4. COKELET,G.R.: Comments on the Fahraeus-Lindqvist effect. Biorheology 4,123-126, 1967

5. MARTINI,P., PIERACH,A., SCHREYER,E.: Die Strömung des Blutes in engen Gefäßen. Dtsch. Arch. Klin. Med. 169, 212-222, 1930

6. COKELET,G.R.: Macroscopic rheology and tube flow of human blood. In: Microcirculation (Eds. J.Grayson and W.Zingg), New York: Plenum Publ. Corp., Vol.1, 9-31, 1976

7. FAHRAEUS,R.: Die Strömungsverhältnisse und die Verteilung der Blutzellen im Gefäßsystem. Klin. Wschr. 7, 100-106, 1928

8. GAEHTGENS,P., ALBRECHT,K.H., KREUTZ,F.: Capillary hematocrit as a function of screening and Fahraeus effect. AIChE Symposium Series 182, Vol.74, 61-64 1978

9. GAEHTGENS,P., PRIES,A., ALBRECHT,K.H.: Model experiments on the effect of bifurcations on capillary blood flow and oxygen transport. Pflügers Arch. ges. Physiol. 380, 115-120, 1979

10. SKALAK,R., CHEN,P.H., CHIEN,S.: Effect of hematocrit and rouleaux on apparent viscosity in capillaries. Biorheology 9, 67-82, 1972

11. LINGARD,P.: Capillary pore rheology of erythrocytes.IV: Effect of pore diameter and hematocrit. Microvasc. Res. 13, 59-78, 1977

12. LINGARD,P.: Capillary pore rheology of erythrocytes. V: The glass capillary array - effect of velocity and haematocrit in long bore tubes. Microvasc.Res., in press

13. GOLDSMITH,H.L.: Some flow properties of erythrocytes and rouleaux. Bibl. anat. (Karger/Basel) 9, 259-265, 1967

14. ALBRECHT,K.H., GAEHTGENS,P., PRIES,A., HEUSER,M.: The Fahraeus effect in narrow capillaries (I.D. 3.3 to 11.Oμm). Microvasc.Res. 18, 33-47, 1979

15. DÜHRSSEN,C., GAEHTGENS,P., KREUTZ,F., ZIEROLDT,K.: Deformation of human red blood cells during capillary flow. Pflügers Arch. ges. Physiol. 377 (Suppl.), R11, 1978

ACKNOWLEDGEMENTS: This work was supported by the Deutsche Forschungsgemeinschaft. The experimental results were obtained in cooperation with K.H.Albrecht, C.Dührssen, L.Glahé, M.Heuser, F.Kreutz, A.Pries.

Vol. 17
1980

BLANK
PAGE

Vol.
198

BIORHEOLOGY Vol.17, pp. 191-203 0006-355X/80/010191-13$02.00/0
© Pergamon Press Ltd. 1980. Printed in the United States

Vol. 17
1980

THIRD INTERNATIONAL CONGRESS OF BIORHEOLOGY

RHEOLOGICAL HYSTERESIS OF BLOOD AT LOW SHEAR RATE

M. Bureau*, J.C. Healy**, D. Bourgoin and M. Joly
Laboratoire de Biophysique, Faculté de Médecine Pitié Salpêtrière
91 boulevard de l'Hôpital, 75013 Paris, France

(Received 16.2.1979; in revised form 30.4.1979.
Accepted by Editor G.V.F. Seaman.
Received by Executive Editorial Office 4.12.1979)

ABSTRACT A Couette type servo-controlled microviscometer associated with a low frequency generator modulating the rotational speed of the viscometer outer cylinder has been used to plot the rheological hysteresis curves of blood. It has been shown that the shape of these curves largely depends on the values of the parameters α and t_m characterizing the linear variation of the rate of shear with time : $\dot{\gamma} = \alpha t$ for $0 < t < t_m$ and $\dot{\gamma} = \alpha(2t_m - t)$ for $t_m < t < 2t_m$. Two sets of α and t_m have been selected in order to obtain rheograms showing preferentially the viscoelastic or the thixotropic behaviour of blood. This technic is used to compare normal human bloods with bloods submitted to various physical or chemical treatments, or with different pathological bloods. Some interpretations are proposed from considerations on changes in the deformability or aggregability of blood cells.

INTRODUCTION

It is well known that the properties of viscoelasticity, shear thinning and thixotropy of a flowing liquid are easily revealed only if variations of the shear rate, with time or position, exist in the corresponding flow. That is the reason why these behaviours are generally detected and studied accurately by experiments in vitro when the rheological determinations are performed under periodic or transient flow conditions, for instance by measuring the dynamic response of the fluid to a sinusoidal test or to rectangular or triangular steps of rate of shear. These methods are perfectly suitable for the rheological study of blood (1-8) which at low shear rates (less than few reciprocal seconds) behaves typically as a shear thinning non Newtonian liquid exhibiting viscoelasticity and thixotropy. These properties are all the more important to know for blood as the shear rate in the circulating blood mass, owing to the geometrical complexity of the blood vessel system and the pulsatory character of the blood flow, shows great differences in its values according to the considered points and moments. This entails large variations in the apparent viscosity of blood and consequently in the resistance to blood circulation.

The method of rectangular or triangular steps of shear rate, in a Couette flow between coaxial cylinders or in a laminar flow in a cone-plate viscometer, appears to be the most sensitive one proposed to date for showing the peculiarities of the mechanical behaviour of rheologically complex liquids (9). We have developed it in our laboratory during the last years for a precise study of the rheological properties of blood (10-14).

In the present paper, we shall give the results obtained by the technique of the hysteresis loops (triangular steps of shear rate). Our purpose is to compare the behaviour of normal human blood with that of pathological and modified bloods, i.e. physically, chemically or enzymatically treated bloods. The hysteresis curve method had been used before in blood study by Huang and others (7), but in a different range of rates and amplitude of variation of the shear rate, which did not lead to a sensitivity as high as that we have obtained with our technique.

APPARATUS AND METHOD

We have employed a semi-automatic coaxial cylinder microviscometer constructed by Chaix-Meca (Anvar contract n° 6912800 LE) from a laboratory made prototype designed by D. Bourgoin and M. Joly.

* Present address : Unité INSERM n° 13, Hôpital Claude Bernard, 10 avenue de la Porte d'Aubervilliers. 75019 Paris. France.
** Present address : Service de Biophysique, UER Médicale, 30 rue Ferdinand Gambon, 42000 St Etienne. France.

TABLE I

Empirical Parameters of the Type A Rheograms.

$\dot{\gamma} = 0.0085\ t$ for $0 \leqslant t \leqslant 6.5$ s and $\dot{\gamma} = 0.0185\ (13 - t)$ for $6.5\ s \leqslant t \leqslant 13$ s

($t_m = 6.5$ s ; $\dot{\gamma}_m = 0.12\ s^{-1}$)

Parameters	Definitions	Errors (±)
σ_m	Value of the stress σ at the maximum value $\dot{\gamma}_m$ of $\dot{\gamma}$	6%
σ_1	Stress along the forward branch of the hysteresis curve	
σ_2	Stress along the backward branch of the hysteresis curve	
$\sigma_{2,0}$	Value of σ_2 at $\dot{\gamma} = 0$	6%
$\sigma_{2,M}$	Maximum of σ_2	6%
$\dot{\gamma}_M$	Value of $\dot{\gamma}$ for which $\sigma_2 = \sigma_{2,M}$	3%
$\sigma_{1,M}$	Value of σ_1 at $\dot{\gamma} = \dot{\gamma}_M$	6%
ξ	$\xi = \sigma_2 - \sigma_1$ at a given value of $\dot{\gamma}$	10%
ξ_M	Value of ξ at $\dot{\gamma} = \dot{\gamma}_M$	3.5%
Δ	Maximum of ξ	13.5%
$\dot{\gamma}_\Delta$	Value of $\dot{\gamma}$ for which $\xi = \Delta$	6.5%
$\sigma_{2,\Delta}$	Value of σ_2 at $\dot{\gamma} = \dot{\gamma}_\Delta$	

TABLE II

Empirical Parameters of the Type B Rheograms.

$\dot{\gamma} = 0.043\ t$ for $0 \leqslant t \leqslant 23.8$ s and $\dot{\gamma} = 0.043\ (47.6 - t)$ for $23.8\ s \leqslant t \leqslant 47.6$ s

($t_m = 23.8$ s ; $\dot{\gamma}_m = 1.02\ s^{-1}$)

Parameters	Definitions	Errors (±)
σ_m	Value of the stress σ at the maximum value $\dot{\gamma}_m$ of $\dot{\gamma}$	5%
σ_1	Stress along the forward branch of the hysteresis curve	
σ_2	Stress along the backward branch of the hysteresis curve	
$\dot{\gamma}_X$	Value of $\dot{\gamma}$ at the crossing point of the forward and backward branches of the hysteresis loop	3%
σ_X	Value of σ at $\dot{\gamma} = \dot{\gamma}_X$	8.5%
$\sigma_{2,0}$	Value of σ_2 at $\dot{\gamma} = 0$	8%
ξ	$\xi = \sigma_1 - \sigma_2$ at a given value of $\dot{\gamma}$	8.5%
Δ	Maximum of $-\xi$ for $\dot{\gamma} < \dot{\gamma}_X$	10%
$\dot{\gamma}_\Delta$	Value of $\dot{\gamma}$ for which $-\xi = \Delta$	12%
$\sigma_{2,\Delta}$	Value of σ_2 at $\dot{\gamma} = \dot{\gamma}_\Delta$	5.5%
Δ'	Maximum of ξ' for $\dot{\gamma} > \dot{\gamma}_X$	2%
$\dot{\gamma}_{\Delta'}$	Value of $\dot{\gamma}$ for which $\xi = \Delta'$	6%
$\sigma_{1,\Delta'}$	Value of σ_1 at $\dot{\gamma} = \dot{\gamma}_{\Delta'}$	

The outer cylinder is driven by a motor coupled to a tachometer dynamo and equipped with a servo-controlled device regulating the speed of rotation according to a tension programmed by a low frequency function generator. The inner cylinder is rigidly bound to a galvanometer frame located in a magnetic circuit. A generator supplies the galvanometer circuit with a current the intensity of which is modulated by a photoelectric device coupled with this generator so that the deviation of the inner cylinder should be constantly zero during the rotation of the outer cylinder. This intensity is proportional to the stress transmitted by the liquid at the wall of the inner cylinder. An XY recorder associated with the microviscometer makes it possible to plot the curves of the variations of the stress σ as a function of time t or shear rate $\dot{\gamma}$ (10-14).

In the present case of a non Newtonian fluid flowing in a Couette type viscometer the significance of the shear rate must be emphasized, taking into account the difficulty of knowing the exact distribution of shear rates in the gap of the apparatus. Since the calculation of the shear rate at the wall of the inner cylinder is complicated even when using approximate formula (15) we have chosen as $\dot{\gamma}$ an apparent mean shear rate which is the mean value of the shear rate in a Newtonian fluid for the same rotation speed of the outer cylinder and the same width of the gap between the cylinders. The corresponding apparent viscosity η of a non Newtonian liquid at this value of $\dot{\gamma}$ is defined as the value of the viscosity of a Newtonian liquid giving rise to the same shear stress at the inner cylinder wall for the same values of gap and rotation speed respectively.

In a previous paper (12) we have defined, by comparison with the behaviour of purely viscoelastic and purely thixotropic liquids (9), the optimal conditions of rate and amplitude of the linear shear rate variation, for which the observed rheological behaviour of blood is predominantly viscoelastic or thixotropic.

Indeed, for the triangular steps of shear rate, the shape of the hysteresis loops

of normal human blood $\sigma(\dot{\gamma})$, with $\dot{\gamma} = \alpha t$ for $0 \leq t \leq t_m$ and $\dot{\gamma} = \alpha(2t_m - t)$ for $t_m \leq t \leq 2t_m$, α and t_m being constant parameters, depends on α and t_m. With $t_m < 30$ s the viscoelastic character prevails at low values of α (5×10^{-3} $s^{-2} < \alpha < 5\times10^{-2}$ s^{-2}) and the superposed thixotropic character is all the more pronounced as the values of α are greater. On the other hand, for rather low values of $\dot{\gamma}_m = \alpha t_m$ (0.1 or 0.3 s^{-1} for instance) the viscoelastic character decreases and the thixotropic one increases with decreasing α, that is to say with increasing t_m. For very low values of α ($\alpha < 10^{-3}$ s^{-2} for instance) a quasi stationary flow would be practically reached at every point of the rheogram : there would no longer be a hysteresis loop but only a curve of shear softening the interpretation of which would be rendered difficult by a time dependent drift of the stationary stress at low shear rate due to the sedimentation of the red blood cells. Likewise, when t_m is long enough to allow the rate of shear to exceed, after a time $t_n < t_m$, the value $\dot{\gamma}_n = \alpha t_n$ above which blood behaves as a Newtonian fluid, the hysteresis curve is reduced to a straight line in the shear range $\dot{\gamma}_n$ — $\dot{\gamma}_m$ (14).

As a consequence of this great diversity of behaviour, it is necessary to define very accurately the experimental conditions, and to keep them rigorously constant for the comparison between the rheograms of different blood samples to be significant. Based on these considerations, and according to the geometrical and mechanical characteristics of the employed microviscometer, we have chosen two laws of linear variation of $\dot{\gamma}$ as a function of time leading to two types of rheogram :

Rheogram A - $\dot{\gamma} = 0.0185\ t$ for $0 \leq t \leq 6.5$ s and $\dot{\gamma} = 0.0185(13 - t)$ for $6.5\ s \leq t \leq 13s$.

Rheogram B - $\dot{\gamma} = 0.043\ t$ for $0 \leq t \leq 23.8$ s and $\dot{\gamma} = 0.043(47.6 - t)$ for $23.8\ s \leq t \leq 47.6s$.

The corresponding values of $\dot{\gamma}_m$ and t_m are 0.12 s^{-1}, 6.5 s and 1.03 s^{-1}, 23.8 s respectively. Tables I and II show the definitions of the empirical rheological parameters measured on these rheograms and the accuracy of their determination.

Each blood sample was measured at 25 ± 0.5°C the same day it had been taken in EDTA anticoagulating agent. The haematocrit has always been adjusted to the value H = 0.45. In order to obtain reproducible and significant rheograms it is necessary to respect very strict experimental procedure. Thus, every measurement must be performed 5 minutes after mixing by agitation ; the duration of any rheogram recording must be shorter than 1 minute. The justification of this procedure has been developed elsewhere (13,14). Moreover verifications have been made with Newtonian liquids in the same ranges of viscosity and shear rate to show that the shapes of the hemorheograms obtained are not artefacts ; they characterize the true rheological behaviour of the studied bloods.

Vol. 17
1980

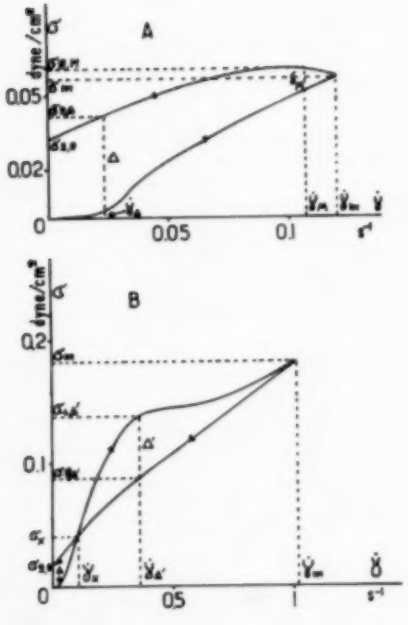

FIG. 1
Rheograms A and B of a sample of normal human blood.

EXPERIMENTAL RESULTS

We shall describe now, as a reference, the rheograms of a sample of a given human blood considered as normal with respect to the hematological criterion, and then we shall give the mean values and the scattering of the empirical rheological parameters of a set of hematologically normal human bloods. Afterwards, examples of abnormal or pathological bloods will be shown. Lastly we shall examine the rheological properties of bloods submitted to various physical, chemical or enzymatic treatments, and compare them with those of the corresponding non treated samples.

Normal human blood

The recorded rheograms A and B of a normal human blood are given in Fig. 1.

Rheogram A (t_m = 6.5 s, $\dot{\gamma}_m$ = 0.12 s^{-1}) shows the superposition of a marked viscoelasticity and a slight thixotropy. For $\dot{\gamma} = \dot{\gamma}_m$ the stress σ_m is equal to 5.7×10^{-2} dyne/cm² corresponding to an apparent viscosity of 47.5 centipoises. One observes that at a given $\dot{\gamma} < \dot{\gamma}_m$ the stress σ_1 on the forward curve is always smaller than the stress σ_2 on the backward curve, which is typical of the viscoelastic liquids. Besides, whereas the stationary stress at $\dot{\gamma} = 0.05$ s^{-1} for the same blood sample is $\sigma_s = 4.3\times10^{-2}$ dyne/cm², the stresses in transitory flow at the same value

TABLE III
Mean Values and Dispersion of the Empirical Rheological Parameters of the Normal Human Blood

Rheograms A				Rheograms B			
Parameters	Units	Mean values	Dispersion	Parameters	Units	Mean values	Dispersion
σ_m	10^{-2}dyne/cm^2	7.2	5.5 - 8.5	σ_m	10^{-1}dyne/cm^2	2.26	1.9 - 2.5
$\sigma_{2,M}$	-	7.6	6 - 8.65	$\sigma_{1,\Delta'}$	-	1.8	1.35 - 2
$\sigma_{1,M}$	-	6.15	5 - 6.70	σ_X	10^{-2}dyne/cm^2	7.1	4 - 8.3
$\sigma_{2,\Delta}$	-	5.2	4.15 - 6.75	$\sigma_{2,\Delta}$	-	4	2.3 - 4.8
$\sigma_{2,0}$	-	3.8	3.2 - 4.5	$\sigma_{2,0}$	-	3.1	1.7 - 4.1
$\dot\gamma_M$	10^{-2} s^{-1}	10.2	9.1 - 11.6	$\dot\gamma_X$	10^{-1} s^{-1}	1.3	1 - 1.55
$\dot\gamma_\Delta$	-	2.6	2.05 - 3.25	$\dot\gamma_{\Delta'}$	-	3.8	3.35 - 4
δ_M	10^{-2}dyne/cm^2	1.45	0.95 - 1.95	Δ	10^{-2}dyne/cm^2	3.55	2 - 4.9
	-	4.6	3.8 - 5.15	Δ'	-	5.65	5 - 6.7
σ_s at $\dot\gamma$=0.05 s^{-1}	10^{-2}dyne/cm^2	4.75	3.7 - 6.4	σ_s at $\dot\gamma$= 1 s^{-1}	10^{-1}dyne/cm^2	2.2	1.8 - 2.5

of $\dot\gamma$, 0.05 s^{-1}, are $\sigma_1 = 2.3\times10^{-2}$ dyne/cm^2 and $\sigma_2 = 5.15\times10^{-2}$ dyne/cm^2, which shows the amplitude of the retardation effect due to the elasticity. The maximum of the difference $\sigma_2 - \sigma_1$ occurs at $\dot\gamma = \dot\gamma_\Delta = 2.3\times10^{-2}$ s^{-1} and is equal to $\Delta = 3.85$ dyne/cm^2. The residual stress at zero shear rate on the backward curve is $\sigma_{2,0} = 3.2\times10^{-2}$ dyne/cm^2. The maximal stress on this backward branch of the hysteresis loop, $\sigma_{2,M} = 6.1\times10^{-2}$ dyne/cm^2, occurs at $\dot\gamma = \dot\gamma_M = 1.07\times10^{-1}$ s^{-1} for which the difference $\delta_M = \sigma_{2,M} - \sigma_{1,M} = 10^{-2}$ dyne/cm^2.

The shape of the rheogram A looks very roughly like that exhibited by the simplest viscoelastic liquid, the Maxwell's liquid. For such a liquid the curve $\sigma_1(\dot\gamma)$ is concave towards the increasing values of σ at any value of $\dot\gamma$. However, in the case of blood, as shown on figure 1, the curves $\sigma_1(\dot\gamma)$ bend in the opposite direction from a certain value of $\dot\gamma$ and become practically linear, and even in some cases slightly concave towards the higher values of $\dot\gamma$. This is probably the result of the superposition of a shear thinning to the viscoelasticity ; this shear softening most likely corresponds to the progressive disorganization of the network of the red cell rouleaux followed, close to $\dot\gamma_m$, by the beginning of the dissociation of the rouleaux themselves.

Rheogram B (t_m = 23.8 s, $\dot\gamma_m$ = 1.02 s^{-1}) shows an important thixotropic effect upon which a viscoelastic effect is superposed at low value of $\dot\gamma$. Indeed, forward and backward curves cross at $\dot\gamma = \dot\gamma_X$(nearly 0.1 s^{-1}). For $\dot\gamma_X < \dot\gamma < \dot\gamma_m$, at every value of $\dot\gamma$, the forward curve is always above the backward curve ($\sigma_2 < \sigma_1$), which is characteristic of thixotropic systems. For $0 \leq \dot\gamma < \dot\gamma_X$ on the contrary $\sigma_2 > \sigma_1$, and at $\dot\gamma = 0$ there is a residual stress $\sigma_{2,0}$ slowly relaxing that characterizes a viscoelastic behaviour. At $\dot\gamma = \dot\gamma_m$ the stress $\sigma_m = 1.9\times10^{-1}$ dyne/cm^2 corresponding to an apparent viscosity of 18.7 centipoises. The slope of the forward branch of the hysteresis loop, successively concave, convex, and again concave towards the increasing stresses, is also characteristic of the superposition, from $\dot\gamma = \dot\gamma_X$, of an important shear thinning to the viscoelasticity which on the contrary is prevailing at $\dot\gamma < \dot\gamma_X$. The extent of the shear thinning on this forward branch at $\dot\gamma > \dot\gamma_X$ can be easily characterized by evaluating the ratio R of the values of σ_1 at $\dot\gamma$ = 0.2 and 1 s^{-1}. This ratio $\sigma_1(0.2)/\sigma_1(1)$ would be equal to 0.2 for a Newtonian liquid, and greater than 0.2 for a shear softening liquid. Therefore the number $\rho = R - 0.2$ can be used as an empirical shear thinning index. In the present case $\rho = 0.33$.

At $\dot\gamma$ = 1 s^{-1} on the forward curve $\sigma_1 = 1.89\times10^{-1}$ dyne/cm^2 whereas the stress σ_s in stationary flow conditions at the same shear rate is equal to 2.15×10^{-1} dyne/cm^2, which shows that a slight effect of retardation due to the viscoelasticity remains. In order to give an idea of the relative importance of the viscoelastic behaviour on rheograms A and B one can compare, for instance, the ratio $\varepsilon = (\sigma_s - \sigma_1)/\sigma_s$ at $\dot\gamma$ = 1 s^{-1} for rheogram B and at $\dot\gamma$ = 0.05 s^{-1} for rheogram A where the viscoelastic effect prevails ; the corresponding value is only 0.12 in case B while it reaches 0.465 in case A. In the range $0 < \dot\gamma < \dot\gamma_X$ on rheogram B the maximum of $\delta = \sigma_2 - \sigma_1$ is $\Delta = 2.2\times10^{-2}$ dyne/cm^2 at $\dot\gamma_\Delta = 3.4\times10^{-2}$ s^{-1} ; in the range $\dot\gamma_X < \dot\gamma < \dot\gamma_m$ the maximum of $\delta' = \sigma_1 - \sigma_2$ is $\Delta' = 5\times10^{-2}$ dyne/cm^2 at $\dot\gamma_{\Delta'} = 3.6\times10^{-1}$ s^{-1}.

It has been shown (13) that different human bloods, though considered as hematologically normal, may have different values of some of their rheological parameters, which would indicate that rheological measurements provide a very sensitive tool of investigation and discrimination for blood studies. Table III gives the mean values and the dispersion of the empirical rheological parameters of a set of about 20 normal human bloods for rheograms A and B, and those of the stresses in stationary conditions at $\dot\gamma$ = 0.05 and 1 s^{-1}.

The viscoelasticity character is all the more marked as the ratios $\sigma_{2,M}/\sigma_m$, δ_M/σ_m, Δ/σ_m, $\sigma_{2,0}/\sigma_m$ and $\sigma_{2,0}/\sigma_X$ are greater. The thixotropic character increases when the ratios

Δ'/σ_m, $\sigma_{1,\Delta'}/\sigma_m$ increase and the ratio σ_X/σ_m decreases. As it has been shown elsewhere (14) the error on these ratios is rather small because each of the concern data are measured on the same recorded curve. Thus, the relative error on $\sigma_{2,M}/\sigma_m$, δ_M/σ_m, Δ/σ_m, $\sigma_{2,0}/\sigma_m$, Δ'/σ_m, $\sigma_{1,\Delta'}/\sigma_m$ and $\sigma_{2,0}/\sigma_m$ are $\pm$ 1.5%, $\pm$ 10.5%, $\pm$ 4%, $\pm$ 2,5%, $\pm$ 6%, $\pm$ 2%, $\pm$ 4.5% and $\pm$ 7.5% respectively.

Blood from umbilical cord

As a first example of abnormal blood we have studied one sample of a blood from umbilical cord.

The salient feature of this blood compared to normal blood for the same value of the haematocrit is a large decrease of the apparent viscosity in stationary flow : about 31.5% at $\dot{\gamma} = 0.05\ s^{-1}$ and 34% at $\dot{\gamma} = 1\ s^{-1}$. Figure 2 shows rheograms A and B of a sample of blood from umbilical cord and those averaging a set of normal human bloods (see table III). As in stationary flow the apparent viscosity in transient flow, at any value of $\dot{\gamma}$, is smaller for cord blood than for normal blood. Moreover one observes a slight increase of the viscoelastic character of the rheogram A, but on the contrary a decrease of the residual viscoelastic character at low shear rate is shown on rheogram B. Likewise, a very large decrease of the shear thinning and thixotropy appears on this latter rheogram, as shown on table IV. As a conclusion, the blood from umbilical cord, though slightly more viscoelastic, is considerably less viscous, shear softening and thixotropic than normal blood. One can roughly say that in the range of shear rate 0.2 - 1 s^{-1} the cord blood behaves a little more like a Newtonian liquid than a normal blood does.

The rheological behaviour of blood from umbilical cord can be interpreted by assuming, as a first approximation, that the size of the rouleaux in such a blood is smaller than in normal blood. The diminution of the length of the rouleaux explains not only the decrease of the viscosity at low shear rate but also the decrease of the shear thinning and thixotropy as a consequence of a less complete orientation of the rouleaux in the flow, and of smaller traction forces on them at the same shear rate, which reduces their mechanical dissociation.

Vol. 17
1980

Blood of a patient suffering from diabetes

The blood of a diabetic patient has been compared with the same "average normal blood" we have used in the study of a blood from umbilical cord.

In stationary flow, and at the same haematocrit value, the blood of this diabetic patient is less viscous than the normal blood at very low shear rate (at $\dot{\gamma} = 0.05\ s^{-1}$ the viscosity is equal to 60 cP instead of 95 cP) but more viscous at higher shear rate (at $\dot{\gamma} = 1\ s^{-1}$, η_s = 32 cP instead of 22 cP) which is in agreement with the results obtained by other authors (16,17). Figure 3 shows rheograms A and B for diabetic and normal blood. One remarks that the viscoelastic character on rheogram A and the residual viscoelasticity at low shear rate on rheogram B are largely diminished in the case of the abnormal blood. There is also a decrease of the shear thinning and of the thixotropy as shown on table V. This decrease of the shear softening explains the change of sign of the difference between the stationary viscosities at $\dot{\gamma} = 0.05\ s^{-1}$ and $\dot{\gamma} = 1\ s^{-1}$, and can be related to the fact that rouleaux are present in the arterioles of diabetic patients (18).

Taking into account the fact that the viscosities of the plasma are of the same order of magnitude in diabetic and normal bloods, the rheological properties of the diabetic blood can be tentatively interpreted by assuming the length of the rouleaux to be shorter and their mechanical stability greater than in normal blood. The shortening of the rouleaux explains the lower viscosity at low shear rate, and the strengthening of the resistance to mechanical dissociation gives the reason of the less extent of shear thinning and thixotropy accompanied by an important relative increase of the viscosity with increasing shear rate. On the other hand the decrease of the viscoelastic character at low shear rate might be due to a weaker cohesion and greater deformability of the rouleau network compared to those of normal blood. In addition to this one must not forget, in the case of diabetic patients, the effects of the possible modifications of the erythrocytes themselves on the blood rheological behaviour.

Blood of a patient suffering from anaemia of medular origin

The rheological behaviour of this blood sample, after the haematocrit has been readjusted to 0.45, is very similar to that of the above-mentioned blood of a diabetic patient, as shown on figure 4 and table IV.

Effect of hypotonicity. Dilution of plasma with 10% distilled water

In order to see the effect of small variations of the plasma tonicity, a sample of normal human blood the haematocrit of which was adjusted at H = 0.45 was divided into two parts. One of these has been studied directly as above and used as a reference sample. In the other one, red cells and plasma were separated by centrifugation, and 10% of the plasma has been substituted by an equal volume of distilled water before the red cells were redispersed in it. Under these conditions, the osmotic pressure of the plasma has varied from 0.32 to 0.29 moles.

Despite the slight diminution of the plasma viscosity one observes an increase of

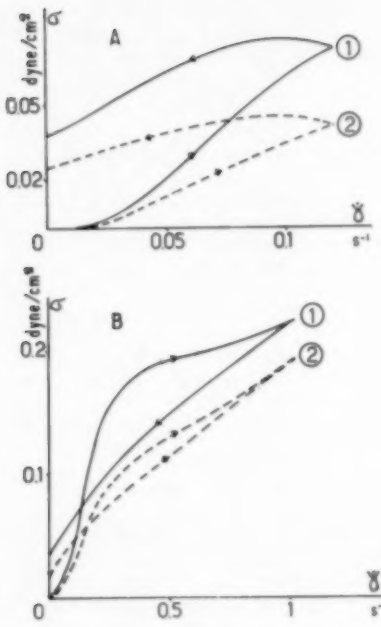

FIG. 2
Rheograms from umbilical cord blood
1 : normal blood ; 2 : umbilical cord blood

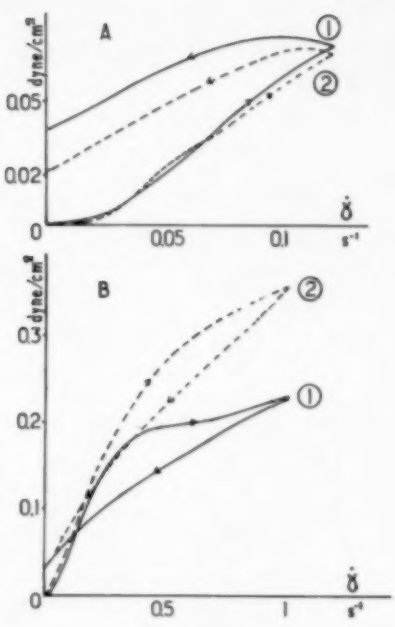

FIG. 3
Blood from a diabetic patient
1 : normal blood ; 2 :pathological blood

TABLE IV
Blood from Umbilical Cord

Blood	$\dot{\gamma} = 0.05$ s^{-1}	RHEOGRAM A							
	$10^2\sigma_s$ dyne/cm²	$10^2\sigma_m$ dyne/cm²	$10^2\sigma_{2,0}$ dyne/cm²	$10^2\Delta$ dyne/cm²	$10^2\delta_{M_2}$ dyne/cm²	ε	$\frac{\sigma_{2,0}}{\sigma_m}$	$\frac{\Delta}{\sigma_m}$	$\frac{\delta_M}{\sigma_m}$
Normal	4.75	7.2	3.8	4.6	1.45	0.58	0.53	0.63	0.20
Cord	3.75	4.1	2.5	2.8	0.8	0.615	0.61	0.685	0.195
	RHEOGRAM B								
	$10\sigma_m$ dyne/cm²	$10^2\sigma_{2,0}$ dyne/cm²	$10^2\sigma_X$ dyne/cm²	$10^2\Delta'$ dyne/cm²	$\frac{\sigma_{2,0}}{\sigma_X}$	$\frac{\sigma_{2,0}}{\sigma_m}$	$\frac{\Delta}{\sigma_m}$	ρ	$\frac{\Delta'}{\sigma_m}$
Normal	2.25	3.1	7.1	5.65	0.435	0.135	0.155	0.36	0.25
Cord	1.95	1.7	5.4	2.0	0.315	0.09	0.13	0.20	0.105

the blood viscosity in stationary flow of about 20% with respect to the viscosity of the reference sample. Other authors have obtained similar results for the effect of hypotonicity (19). One finds also an increase of the viscosity on rheograms A and B (see fig.5). Furthermore, still compared to the reference samples, the relative importance of viscoelasticity on rheogram A and of residual viscoelasticity on rheogram B slightly increases, whereas there is a decrease in the importance of the shear thinning and thixotropy, as shown on table VI.

The results are difficult to interpret without ambiguity. Indeed the increase in viscosity might suggest an increase of aggregation of the red cells. But, due to the hypotonicity, water has penetrated the blood cells and consequently their dimensions and shape have been modified. Such changes may have induced a decrease of the cell deformability leading to an augmentation of the blood viscosity.

Vol. 17
1980

Action of heat on red cells

The blood viscosity is increased by heating at a temperature higher than 45°C. This allows us to explain the blocking of the microcirculation observed in dogs the blood of which has been heated for about 30 s at 55°C (20). But, as heating leads to a beginning of plasma protein denaturation and floculation, it was interesting to study the action of heat on the red cells themselves. The method used was as follows :

A sample of normal human blood (haematocrit = 0.45) was divided into two parts. The first one was kept as a reference sample and studied directly. In the second one, red cells were separated from plasma by centrifugation and washed three times in a phosphate buffer, pH 7, the composition of which was : 0.20 g KH_2PO_4, 1.44 g Na_2HPO_4, 0.20 g KCl and 8 g NaCl in 1 liter of distilled water (π = 300 milliosmoles). The red cells, dispersed in this solution, were heated for 15 min. at 49°C for experiment I or 45 s at 55°C for experiment II. After these treatments the buffer was eliminated and replaced by plasma, and the haematocrit readjusted at 0.45. This second sample was then studied in the usual manner.

In these two experiments the viscosity in stationary flow of the treated samples is smaller than that of the reference blood sample. The decrease at $\dot{\gamma}$ = 0.05 s^{-1} and $\dot{\gamma}$ = 1 s^{-1} is 11% and 6% respectively with red cells heated for 15 min. at 49°C, and 49.5% and 38.5% respectively with blood cells heated for 45 s at 55°C.

Figures 6 and 7 give the rheograms A and B for the experiments I and II, and table VII shows the corresponding values of the main parameters. In addition to the decrease of the apparent viscosity one observes an important decrease of the viscoelasticity and thixotropy. There is also a marked diminution of the shear softening on rheograms B. Furthermore, on the forward curves of rheograms A, a rather large shear thinning appears, which modifies the retardation effect of the viscoelasticity. Thus, the ratio $\sigma_1(0.4)/\sigma_1(0.12)$, which is respectively equal to 0.225 and 0.2 for the reference samples I and II, reaches the values 0.33 in experiment I and 0.41 in experiment II. One can also remark that the variation of $\sigma_2(\dot{\gamma})$ on rheogram B in the range of $\dot{\gamma}$ between 0.2 and 1 s^{-1} is similar to that provided by a Bingham liquid (linear relationship between σ and $\dot{\gamma}$). It is to be observed that for a sample of blood heated in the presence of its plasma for 45 s at 55°C, though the stationary viscosity compared with that of non heated blood increases from 1.03 to 1.18 P at $\dot{\gamma}$ = 0.05 s^{-1} and from 23 to 33 cP at $\dot{\gamma}$ = 1 s^{-1} and σ_m on rheogram A increases from 7.3×10^{-2} to 9.45×10^{-2} dyne/cm^2, the concavity of the curve $\sigma_1(\dot{\gamma})$ on this rheogram is directed, from $\dot{\gamma}$ = 0.3 s^{-1}, towards the increasing $\dot{\gamma}$, which indicates also an important contribution of the shear thinning to the rheological behaviour in this case.

The decrease of the viscosity can be partly attributed to the fact that for the same haematocrit value the volume of plasma trapped between the red cells is increased by the heating of the blood cells. Indeed, if a blood sample initially at H = 0.45 is heated for 45 s at 55°C, and if the haematocrit is measured again after heating, one finds H = 0.49. Therefore, in experiments I and II, though the haematocrit has the same value for the reference sample and the treated sample, the number of red cells per volume unit is smaller in the treated sample than in the reference one. Moreover it has been shown that heating entails an irreversible rigidification of the red cells (21), which has been verified by the technique of Bessis and Mohandas (22). The decrease in viscoelasticity and thixotropy, the appearance of shear thinning from the very low values of $\dot{\gamma}$ and its diminution at higher values of $\dot{\gamma}$ can probably be explainded as a consequence of a large decrease of the interactions between the blood cells involving an easier deformation and dissociation of the rouleaux. This, leading to a diminution of the average equilibrium size of the rouleaux at a given shear rate, contributes also to the decrease in viscosity. Likewise, it is known that there is a complete dissociation of the rouleaux when the red cells are rigidified by glutaraldehyde.

Action of neuraminidase

Neuraminidase is an enzyme which modifies the membrane of the red cells by releasing sialic acid. Consequently the number of negative surface charges diminishes, leading to a decrease of the electrostatic repulsive forces between the red cells ; therefore the aggregation of blood cells increases (23). The experimental procedure was as follows.

The red cells were separated from plasma by centrifugation and then washed three times with an isotonic pH 7 buffer the composition of which was 0.20 g KH_2PO_4, 1.44 g Na_2HPO_4, 0.20 g KCl and 8 g NaCl per liter of distilled water. A solution of neuraminidase containing 100 units per ml was prepared from a commercial 5000 units solution in pH 5.5 acetate buffer by diluting it with the preceding phosphate buffer. A volume of this solution was added to a volume of washed red cells, the final pH being 6.5. This suspension of red cells was incubated for 1 hour at 37°C in a water-bath, after which the blood cells were washed again three times in the phosphate buffer, and the haematocrit readjusted at 0.45.

Independently of the action of neuraminidase, washing and incubation might have modified the mechanical properties of blood. For this reason two reference samples were compared with the neuraminidase treated blood : a sample of the initial blood and a sample of the same blood after the red cells have been washed and incubated in the absence of neuraminidase but before reintroduction of the plasma.

It was found that washing and incubation induce a decrease of the viscosity in

TABLE V
Bloods from Diabetic and Anaemic Patients

Blood	$\dot{\gamma} = 0.05$ s^{-1}	RHEOGRAM A							
	$10^2\sigma_s$ dyne/cm^2	$10^2\sigma_m$ dyne/cm^2	$10^2\sigma_{2,0}$ dyne/cm^2	$10^2\Delta$ dyne/cm^2	$10^2\delta_M$ dyne/cm^2	ξ	$\frac{\sigma_{2,0}}{\sigma_m}$	$\frac{\Delta}{\sigma_m}$	$\frac{\delta_M}{\sigma_m}$
Normal	4.75	7.2	3.8	4.6	1.45	0.58	0.53	0.63	0.20
Diabetic	3	6.9	2.2	3.1	0.90	0.20	0.32	0.45	0.135
Anaemic	4.05	6.75	2.15	3.1	0.62	0.46	0.32	0.46	0.09
	RHEOGRAM B								
	$10\sigma_m$ dyne/cm^2	$10^2\sigma_{2,0}$ dyne/cm^2	$10^2\sigma_X$ dyne/cm^2	$10^2\Delta'$ dyne/cm^2	$\frac{\sigma_{2,0}}{\sigma_X}$	$\frac{\sigma_{2,0}}{\sigma_m}$	$\frac{\Delta}{\sigma_m}$	ρ	$\frac{\Delta'}{\sigma_m}$
Normal	2.25	3.1	7.1	5.65	0.435	0.135	0.155	0.36	0.25
Diabetic	3.55	3.1	11.0	5.05	0.28	0.085	0.115	0.17	0.14
Anaemic	3.15	3.7	11.0	5.0	0.33	0.115	0.135	0.175	0.16

TABLE VI
Effect of Hypotonicity

Blood	$\dot{\gamma} = 0.05$ s^{-1}	RHEOGRAM A							
	$10^2\sigma_s$ dyne/cm^2	$10^2\sigma_m$ dyne/cm^2	$10^2\sigma_{2,0}$ dyne/cm^2	$10^2\Delta$ dyne/cm^2	$10^2\delta_M$ dyne/cm^2	ξ	$\frac{\sigma_{2,0}}{\sigma_m}$	$\frac{\Delta}{\sigma_m}$	$\frac{\delta_M}{\sigma_m}$
Normal	5.15	7.25	3.55	4.4	1.3	0.6	0.49	0.61	0.18
Treated	6.2	8.7	4.55	5.7	2.2	0.6	0.525	0.655	0.25
	RHEOGRAM B								
	$10\sigma_m$ dyne/cm^2	$10^2\sigma_{2,0}$ dyne/cm^2	$10^2\sigma_X$ dyne/cm^2	$10^2\Delta'$ dyne/cm^2	$\frac{\sigma_{2,0}}{\sigma_X}$	$\frac{\sigma_{2,0}}{\sigma_m}$	$\frac{\Delta}{\sigma_m}$	ρ	$\frac{\Delta'}{\sigma_m}$
Normal	2.45	3.4	8.3	5.55	0.41	0.14	0.15	0.265	0.225
Treated	2.9	4.45	10.5	6.15	0.425	0.155	0.19	0.245	0.21

stationary flow whereas neuraminidase treatment leads to an increase of the blood viscosity. The diminution is about 25% at $\dot{\gamma} = 0.05$ s^{-1} and 28% at $\dot{\gamma} = 1$ s^{-1}. The increases due to neuraminidase action at the same shear rates are 33% and 37%.

The rheograms A and B are shown on fig. 8, and their main parameters on table VIII. One observes in rheograms A that the viscoelastic effect is reduced by washing and incubation of red cells whereas it is increased by the neuraminidase action. Similar variations occur for the residual viscoelastic effect in rheograms B. On the contrary, both treatments induce a diminution of the shear thinning and thixotropy. One can remark that the variation of σ_2 as a function of $\dot{\gamma}$ in the range 0.2 - 1 s^{-1} is practically the same as that shown by a Bingham liquid (σ linear function of $\dot{\gamma}$).

The modification of the rheological behaviour in the presence of neuraminidase can be explained by an increase of the interactions between red cells, which enhances the mechanical stability of the rouleaux, increases their average equilibrium size for all values of $\dot{\gamma}$ and their rate of reaggregation after dissociation, and improves the cohesion of the rouleau network at rest and at very low shear rate.

Action of polyvinylpyrolidone

The polyvinylpyrolidone (PVP) we have used is a polymer of mean molecular weight

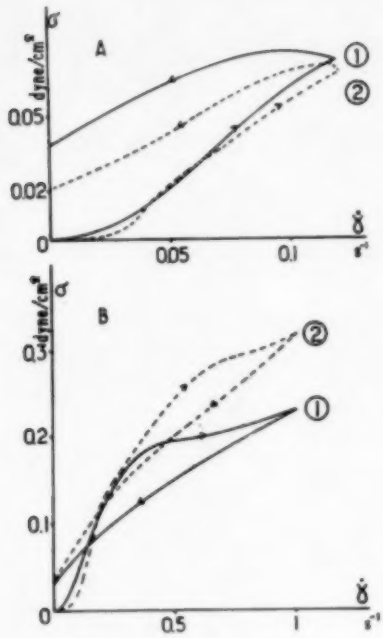

FIG. 4
Blood from a patient suffering from anaemia
(Same notation as for fig. 3)

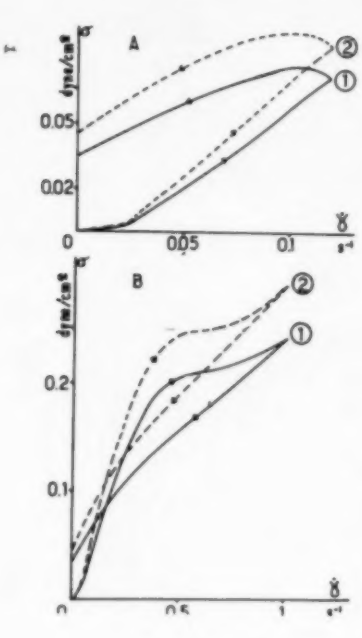

FIG. 5
Effect of plasma dilution
1 : normal blood ; 2 : treated blood

Vol. 17
1980

TABLE VII
Action of Heat and Red Cells

Blood	$\dot{\gamma}$ = 0.05 s^{-1}	RHEOGRAM A							
	$10^2\sigma_s$ dyne/cm^2	$10^2\sigma_m$ dyne/cm^2	$10^2\sigma_{2,0}$ dyne/cm^2	$10^2\Delta$ dyne/cm^2	$10^2\delta_M$ dyne/cm^2	ξ	$\frac{\sigma_{2,0}}{\sigma_m}$	$\frac{\Delta}{\sigma_m}$	$\frac{\delta_M}{\sigma_m}$
Normal I	6.4	8.45	4.85	5.55	1.6	0.57	0.575	0.87	0.19
Treated I	5.7	8.55	3.45	3.9	0.2	0.37	0.405	0.455	0.025
Normal II	4.85	7.1	3.8	4.4	1.05	0.59	0.535	0.62	0.15
Treated II	2.45	4.45	1.4	1.6	0	0.02	0.315	0.36	0
	RHEOGRAM B								
	$10\sigma_m$ dyne/cm^2	$10^2\sigma_{2,0}$ dyne/cm^2	$10^2\sigma_X$ dyne/cm^2	$10^2\Delta'$ dyne/cm^2	$\frac{\sigma_{2,0}}{\sigma_X}$	$\frac{\sigma_{2,0}}{\sigma_m}$	$\frac{\Delta}{\sigma_m}$	ρ	$\frac{\Delta'}{\sigma_m}$
Normal I	2.5	4.1	7.7	6.7	0.535	0.165	0.22	0.345	0.27
Treated I	2.35	2.9	5.6	3.55	0.52	0.125	0.165	0.285	0.15
Normal II	2.0	2.8	6.0	5.4	0.47	0.135	0.155	0.315	0.27
Treated II	1.25	1.0	2.15	1.85	0.465	0.08	0.105	0.28	0.15

about 25,000. The treatment of blood by PVP has consisted in replacing a maximum volume of plasma by an equal volume of a solution containing 3.5 g PVP, 0.8 g NaCl, 0.042 g $CaCl_2$ and 0.0005 g $MgCl_2$ per 100 ml distilled water. The viscosity of this solution is equal to 4 cP, much greater than that of plasma ; this should be taken into account for comparing and interpreting the behaviours of normal and PVP treated blood.

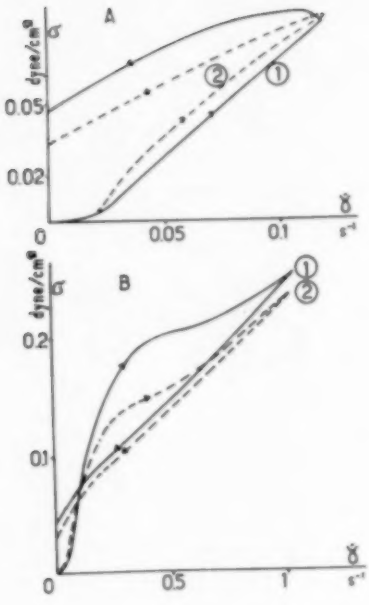

FIG. 6
Action of heat on red cells
(15 min. at 49°C)
(Same notations as for fig. 5)

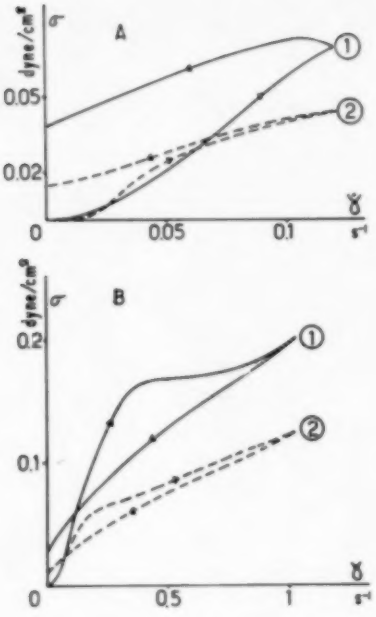

FIG. 7
Action of heat on red cells
(45 s. at 55°C)
(Same notations as for fig. 5)

TABLE VIII
Action of Neuraminidase

Blood	$\dot{\gamma}$=0.05 s^{-1}	RHEOGRAM A							
	$10^2\sigma_s$ dyne/cm^2	$10^2\sigma_m$ dyne/cm^2	$10^2\sigma_{2,0}$ dyne/cm^2	$10^2\Delta$ dyne/cm^2	$10^2\delta_M$ dyne/cm^2	ξ	$\frac{\sigma_{2,0}}{\sigma_m}$	$\frac{\Delta}{\sigma_m}$	$\frac{\delta_M}{\sigma_m}$
Normal	4.4	5.8	3.15	3.75	1.05	0.525	0.545	0.65	0.18
Incubated	3.3	4.95	2.4	2.55	0.88	0.455	0.485	0.575	0.18
Treated	5.85	8.15	4.55	5.55	2.1	0.59	0.78	0.68	0.26
	RHEOGRAM B								
	$10\sigma_m$ dyne/cm^2	$10^2\sigma_{2,0}$ dyne/cm^2	$10^2\sigma_X$ dyne/cm^2	$10^2\Delta'$ dyne/cm^2	$\frac{\sigma_{2,0}}{\sigma_X}$	$\frac{\sigma_{2,0}}{\sigma_m}$	$\frac{\Delta}{\sigma_m}$	ρ	$\frac{\Delta'}{\sigma_m}$
Normal	1.9	1.6	4.1	4.7	0.39	0.084	0.089	0.28	0.245
Incubated	1.6	1.25	2.75	3.6	0.455	0.078	0.078	0.255	0.225
Treated	3.0	3.7	9.25	5.8	0.4	0.185	0.155	0.24	0.195

It can be remarked that in stationary flow the viscosity of the tretaed blood increases by only 2.5% at $\dot{\gamma}$ = 0.05 s^{-1} while at $\dot{\gamma}$ = 1 s^{-1} the increase is 57%. Figure 9 shows rheograms A and B ; the characteristic parameters are given on table IX.

One sees on these rheograms that the action of the polymer is indicated by a slight increase of σ_1 at low values of $\dot{\gamma}$ (< 0.15 s^{-1}). At higher values of $\dot{\gamma}$, the increase becomes progressively more important. For instance, at $\dot{\gamma}$ = 1 s^{-1}, the stress σ_1 in the treated blood is about twice as large as in the normal blood. On the contrary, one observes a marked diminution of the viscoelasticity and a very large decrease of the thixotropy and shear thinning. In the range 0.2 - 1 s^{-1} of $\dot{\gamma}$ on rheogram B the behaviour of σ_2 on the

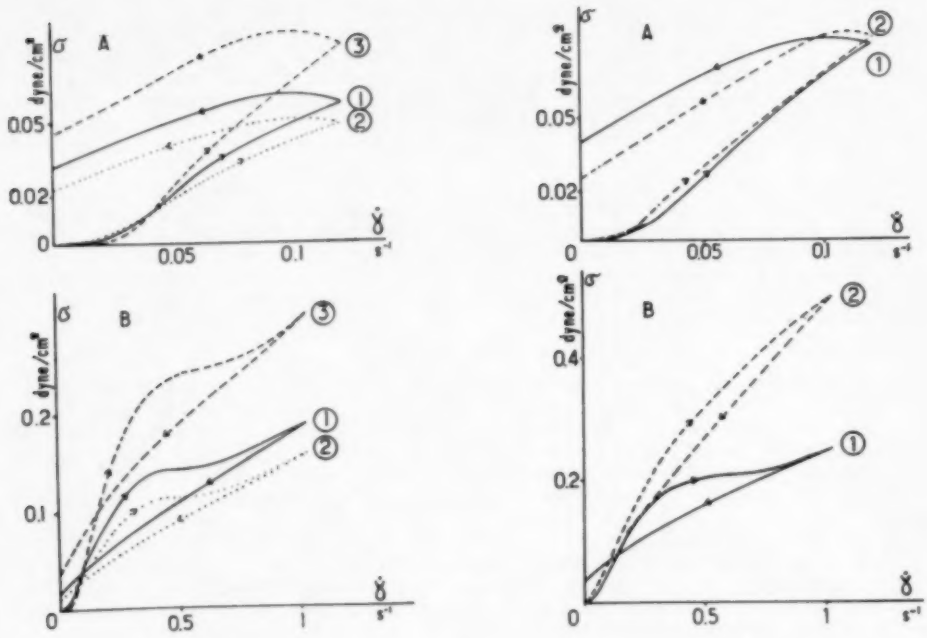

FIG. 8
Action of Neuraminidase
1:normal blood ; 2:blood with washed and incubated cells ; 3:neuraminidase treated blood

FIG. 9
Action of Polyvinylpyrolidone
(Same notations as for fig. 5)

TABLE IX
Action of Polyvinylpyrolidone

Blood	$\dot{\gamma}$ = 0.05 s^{-1}	RHEOGRAM A							
	$10^2\sigma_s$ dyne/cm²	$10^2\sigma_m$ dyne/cm²	$10^2\sigma_{2,0}$ dyne/cm²	$10^2\Delta$ dyne/cm²	$10^2\delta_M$ dyne/cm²	ξ	$\frac{\sigma_{2,0}}{\sigma_m}$	$\frac{\Delta}{\sigma_m}$	$\frac{\delta_M}{\sigma_m}$
Normal	6.0	8.0	4.1	4.9	1.35	0.58	0.515	0.615	0.17
Treated	6.15	8.3	2.6	3.4	0.85	0.505	0.315	0.41	0.10
	RHEOGRAM B								
	$10\sigma_m$ dyne/cm²	$10^2\sigma_{2,0}$ dyne/cm²	$10^2\sigma_X$ dyne/cm²	$10^2\Delta'$ dyne/cm²	$\frac{\sigma_{2,0}}{\sigma_X}$	$\frac{\sigma_{2,0}}{\sigma_m}$	$\frac{\Delta}{\sigma_m}$	ρ	$\frac{\Delta'}{\sigma_m}$
Normal	2.5	3.35	7.85	5.65	0.43	0.135	0.14	0.185	0.225
Treated	5.0	2.65	9.3	5.4	0.285	0.06	0.06	0.105	0.105

backward branch of the hysteresis curve is practically similar to that observed with a Bingham liquid (linear relationship between σ_2 and $\dot{\gamma}$).

It seems that it is possible to account for these results by assuming that the size of the rouleaux is not appreciably modified, even slightly reduced. This explains the difference between the viscosities of treated and normal blood in stationary flow at $\dot{\gamma}$ = 1 s^{-1}, taking into account the difference of the viscosity of PVP solution and plasma. Moreover the cohesion of the rouleau network is probably diminished, which may justify the small difference in the apparent viscosities at $\dot{\gamma}$ = 0.05 s^{-1}, and chiefly the large decrease of the viscoelasticity on rheogram A and of the residual viscoelasticity on rheogram B. On

Vol. 17
1980

the other hand the rouleaux must have a much greater mechanical stability than in normal blood, which could explain the large reduction of the shear softening and thixotropy. So the observed behaviour is very different from that of blood treated by low molecular weight dextran (MW = 40,000). In this case the substitution of a 10% dextran solution for the plasma entails a complete dissociation of the rouleaux involving a considerable drop in viscosity. For instance, at $\dot{\gamma} = 0.05\ s^{-1}$ in stationary flow the blood viscosity is divided by a factor 2.75 though the viscosity of a 10% dextran solution is much higher than that of plasma (10 - 13).

It is to be noted that these results on the PVP action are rather different from those obtained by J.C. Healy (10) who has found an aggregation effect, but using a PVP of molecular weight 70,000, and replacing only a part of the plasma by the PVP solution. This confirms the importance of the molecular weight in the action of polymers on red cell aggregation. Moreover it is known that low molecular weight PVP (MW 30,000) does not notably modify the sedimentation rate of blood cells whereas high molecular weight PVP (MW 70,000) increases it markedly (24,25).

Action of dextran

The dextran we have used is a polyglucoside of mean molecular weight 40,000. As in the case of polyvinylpyrolidone the treatment of blood by dextran consisted in replacing a maximum volume of plasma by an equal volume of a solution containing 100 g dextran and 9 g NaCl per liter distilled water. The viscosity of this solution is equal to 5 cP at 25°C. The mean feature in the action of dextran is a large decrease of the blood viscosity in stationary flow though the viscosity of the dextran solution is much greater than that of plasma. At $\dot{\gamma} = 0.05\ s^{-1}$ σ_s is equal to 1.45×10^{2} dyne/cm^2 for the treated blood while $\sigma_s = 3.7 \times 10^{2}$ dyne/cm^2 for the untreated sample. At $\dot{\gamma} = 1\ s^{-1}$ the corresponding values of σ_s are 2.4×10^{-1} and 2.2×10^{-1} dyne/cm^2 respectively. In the absence of dextran the ratio $\sigma_s(1)/\sigma_s(0.05) = 6.7$, which means a considerable shear thinning, whereas for the treated blood $\sigma_s(1)/\sigma_s(0.05) = 16.5$, which corresponds to a rather low shear softening since the ratio of the shear rates is 20. In rheogram A the stress $\sigma_{2,0}$ vanishes and Δ is very small, about 5×10^{-3} dyne/cm^2, therefore the viscoelasticity is very reduced by dextran. In rheogram B the thixotropic effect disappears completely : curves $\sigma_1(\dot{\gamma})$ and $\sigma_2(\dot{\gamma})$ coincide. The maximum stress $\sigma_m = 2.65 \times 10^{-1}$ dyne/cm^2 while for untreated blood $\sigma_m = 2.15 \times 10^{-1}$ dyne/cm^2. One sees a slight shear thinning, the index ρ being equal to 0.04 whereas $\rho = 0.38$ for the untreated sample. The ratio $\sigma_1(1)/\sigma_1(0.2)$, which is equal to 5 for Newtonian liquids, is equal to 4.2 for the dextran treated blood, and to 1.7 for the normal sample, which shows the great shear thinning of the reference blood.

All these results confirm that the dextran entails an almost complete rouleau dissociation, as shown before by optical and rheological techniques (10 - 13).

CONCLUSION

All the preceding results confirm the sensitivity of the hysteresis loop method for the detection and study of the changes in the rheological properties of normal, artificially modified and pathological bloods. Further studies by this method, if possible associated with optical techniques (26) and with determinations of the mechanical transfer function of blood (27), will be necessary to improve the interpretation of the observed behaviours.

ACKNOWLEDGEMENT

The authors acknowledge partial support received from the D.G.R.S.T. for this work (contract n° 74-7-0953).

REFERENCES

1. KUNZ, A.L. and COULTER, N.A. Non Newtonian behavior of blood in oscillatory flow. Biophys. J. 7, 25-36, 1967.

2. COULTER, N.A. and SIGH, M. Frequency dependence of blood viscosity in oscillatory flow. Biorheology 8, 115-124, 1971.

3. EVANS, R.L., KIRKWOOD, R.B. and OPSAHL, D.G. The dynamic viscosity of some human blood. Biorheology 8, 125-128, 1971.

4. EVANS, A. and WALDER, D.N. Starting transients in haemoviscosimetry. Biorheology 10, 77, 1973.

5. COKELET, G.R. and SMITH, J.H. The effect of concentric-cylinder viscometer gap size on the experimental rheological properties of human blood. Biorheology 10, 51-56, 1973.

6. THURSTON, G.B. Frequency and shear rate dependence of viscoelasticity of human blood. Biorheology 10, 375-381, 1973.

7. HUANG, C.R., SISKOVIC, N., ROBERTSON, R.W.J., FABISIAK, W., SMITHERBERG, E.H. and COPLEY, A.L. Quantitative characterization of thixotropy of whole human blood. Biorheology 12, 279-282, 1975.

8. CHIEN, S., KING, R.G., SKALAK, R., USAMI, S. and COPLEY, A.L. Viscoelastic properties of human blood and red cell suspensions. Biorheology 12, 341-346, 1975.

9. JOLY, M. Remarques sur le comportement rhéologique en cisaillement de certaines classes de systèmes condensés et sur ses méthodes d'étude. Cahiers Groupe Français Rhéologie 4, 176-182, 1977.

10. HEALY, J.C. Etude expérimentale des associations réversibles entre les globules rouges. Thèse Doctorat d'Etat ès Sciences Physiques. Univ. Paris 6, 1973, 70 pp.

11. HEALY, J.C. and JOLY, M. Rheological behaviour of blood in transient flow. Biorheology 12, 335-340, 1975.

12. APELBLAT, A., BOURGOIN, D., BUREAU, M., HEALY, J.C. and JOLY, M. Transient behaviour and hysteresis of human whole blood in Couette flow. In : Proc. 7th Intern. Congress on Rheology. C. Klason and J. Kubat (Ed.) Göteborg : Chalmers Univ. Technology 1976, pp. 570-571.

13. BUREAU, M. Propriétés rhéologiques du sang in vitro en écoulement de Couette en régime transitoire. Thèse Doctorat 3ème cycle Biophysique. Univ. Paris 6, 1977, 95 pp.

14. BUREAU, M., HEALY, J.C., BOURGOIN, D. and JOLY, M. Etude expériemntale in vitro du comportement rhéologique du sang en régime transitoire à faible vitesse de cisaillement. Rheol. Acta, 17, 612-625, 1978.

15. APELBLAT, A. HEALY, J.C. and JOLY, M. Shear rate in the Couette viscometer with a narrow annular gap between cylinders. A new approximate formula. Rheol. Acta 14, 976-978, 1975.

16. SKOVBORG, F., NIELSEN, A.V., SEHLICHTKRULL, J. and DITZEL, J. Blood viscosity in diabetic patients. Lancet 1, 129-131, 1966.

17. DITZEL, J. and MOINAT, P. Changes in serum proteins, lipoproteins and protein bound carbohydrates in relation to pathologic alterations in the microcirculation of diabetic subjects. J. Lab. clin. Med. 54, 843-859, 1959.

18. DITZEL, J. The nature of the intravascular erythrocyte aggregation in disease with particular reference to diabetes mellitus. Acta med. scand. 152, 372-384, 1955.

19. RAND, P.W., AUSTIN, W.H., LACOMBE, E. and BURKER, N. pH and Blood Viscosity. J. Appl. Physiol. 25, 550-559, 1968.

20. MASON GUEST, M. and BOND, T.P. Effect of heat-traumatized blood on microcirculatory dynamics. Int. World Congress for Microcirculation Toronto 1975. Communication no. 173.

21. RAKOW, A.L. and HOCHMUTH, R.M. Thermal transition in the human erythrocyte membrane : effect on elasticity. Biorheology 12, 1-3, 1975.

22. BESSIS, M. and MOHANDAS, N. A diffractometric method for the measurement of cellular deformability. Blood Cells 1, 307-313, 1975.

23. TENFORDE, T. Microelectrophoretic studies on the surface chemistry of erythrocytes. Adv. in Biol. Med. Physics 13, 43-105, 1970.

24. HINT, H. Relationships between the chemical and physico-chemical properties of dextran and its pharmacological effects. In : Dextrans, Current Concepts of Basic Action and Clinical Applications. J.R. Derrick and M. Mason Guest (Ed.) Springfield : C.C. Thomas Publ. 1971, pp. 3-26.

25. GREGERSON, M.I. Effect of artificial expander agents on blood viscosity. Comparison with human albumin and T.A.M.E.S. (synthetic polypeptide of glutamic acid). In : Dextrans, Current Concepts of Basic Action and Clinical Applications. J.R. Derrick and M. Mason Guest (Ed.) Springfield : C.C. Thomas Publ. 1971, pp. 27-38.

26. KING, R.G. and COPLEY, A.L. Some new accessories to the Weissenberg rheogoniometer. Biorheology 12, 355-360, 1975.

27. OBRECHT, B., RUSCH, P. and HEALY, J.C. The mechanical transfer function of blood : modifications by some biological factors. Biorheology 15, 468, 1978.

Vol. 17
1980

BLANK
PAGE

Vol.
198

BIORHEOLOGY Vol.17, pp. 205-206 0006-355X/80/010205-02$02.00/0
© Pergamon Press Ltd. 1980. Printed in the United States

Vol. 17
1980

LETTER TO THE EDITOR-IN-CHIEF

COMMENTS ON "A TWO-FLUID MODEL FOR BLOOD FLOW THROUGH SMALL DIAMETER TUBES"

YVES NUBAR
14 Horatio Street, New York, N.Y. 10014

(Received 30.10.1979; in revised form 5.11.1979.
Accepted by A.L. Copley)

May I refer to a recent paper by Chaturani and Upadhya (1), a theoretical study of the flow of blood viewed as a composite fluid with a couple stress fluid core and a peripheral shell of plasma. This is a valuable work, well organized and discussed with care. One is however somewhat jarred by the unconcern and casualness with which the authors set the flow velocity at the boundaries equal to zero. This unquestioning espousal and use of the handy "no-slip" hypothesis, the simplest possible of all boundary conditions, is not uncommon among students of fluid flow, due perhaps to ingrained habit, prevailing attitudes, or the path of least resistance. The fact is, however, that a number of studies of blood flow, both theoretical and experimental, have suggested, some by implication, others outright, the likely presence of slip (or a velocity discontinuity) at the flow boundaries (or in their immediate vicinity) - thus making the "no-slip" hypothesis one of uncertain validity.

Among these studies - some of them discussing slip in some detail and at some length - may be cited those by L.E. Bayliss (2,3), L. Bennett (4), E.H. Bloch (5), G. Bugliarello and J.W. Hayden (6), A.L. Copley (7), I. Isenberg (8), A.L. Jones (9), A.B. Metzner (10), Y. Nubar (11,12), G.W. Scott Blair (13), V. Vand (14). H. Bateman (15) and S. Goldstein (16) give summaries of the history of slip in addition to discussing boundary conditions in general.

If slip at the wall is indeed present in the flow of blood, as appears probable, ignoring it as a boundary condition in theoretical flow studies would be inaccurate. This applies equally in the case of experimental, viscometric studies of blood flow in which slip in the viscometers would affect the readings materially, unless it is detected and corrected for - something rarely, if ever, attempted. This is doubly inopportune, since these readings are normally used as criteria in testing and evaluating theoretical studies of blood flow.

REFERENCES

1. CHATURANI, P. and UPADHYA, V.S. A two-fluid model for blood flow through small diameter tubes. Biorheology 16, 109-118, 1979.

2. BAYLISS, L.E. Rheology of blood and lymph. In: Deformation and Flow in Biological Systems. A. Frey-Wyssling (Ed.) New York: Interscience Publ. 1952, pp. 355-418.

3. BAYLISS, L.E. The anomalous viscosity of blood. In: Flow Properties of Blood and Other Biological Systems. A.L. Copley and G. Stainsby (Eds.) New York: Pergamon Press, 1960, pp. 29-62.

4. BENNETT, L. Red cell slip at wall in vitro. Science 155, 1554-1556, 1967.

5. BLOCH, E.H. A quantitative study of hemodynamics in the living macrovascular system. Amer. J. Anat. 110, 125-153, 1962.

6. BUGLIARELLO, G. and HAYDEN, J.W. High-speed microcinematographic studies of blood flow in vitro. Science 138, 981-983, 1962.

7. COPLEY, A.L. Apparent viscosity and wall adherence of blood systems. In: Flow Properties of Blood and Other Biological Systems. A.L. Copley and G. Stainsby (Eds.) New York: Pergamon Press, 1960, pp. 97-121.

8. ISENBERG, I. A note on the flow of blood in capillary tubes. Bull. Math. Biophys. 15, 148-152, 1952.

9. JONES, A.L. On the flow of blood in a tube. Biorheology 3, 183-188, 1966.

10. METZNER, A.B. Flow of non-Newtonian fluids. In: Handbook of Fluid Dynamics. V.L. Streeter (Ed.) New York: McGraw Hill Book Co. 1961, pp. 7-2 -- 7-30.

11. NUBAR, Y. Effect of slip on the rheology of a composite fluid: application to blood. Biorheology 4, 133-150, 1967.

12. NUBAR, Y. Blood flow, slip and viscometry. Biophys. J. 11, 252-264,1971.

13. SCOTT BLAIR, G.W. Discussion of "Apparent viscosity and wall adherence of blood systems". In: Flow Properties of Blood and Other Biological Systems. A.L. Copley and G. Stainsby (Eds.) New York: Pergamon Press, 1960, p. 118.

14. VAND, V. Viscosity of solutions and suspensions. J. Phys. Colloid Chem. 52, 277-321, 1948.

15. BATEMAN, H. General physical properties of a viscous fluid. In: Hydrodynamics. H.L. Dryden, F.P. Murnaghan and H. Bateman. New York: Dover Publ. 1956, pp. 89-332.

16. GOLDSTEIN, S. Modern Developments in Fluid Dynamics. New York: Dover Publ. 1965, Vol.2, 680 pp.

Vol. 198

BIORHEOLOGY, Vol. 17, pp. 207-209, 1980
Printed in the USA. All rights reserved.

0006-355X/80/030207-02$02.00/0
Copyright (c) 1980 Pergamon Press Ltd

Vol. 17
1980

EDITORIAL

This Editorial deals with different matters which, for the convenience of our Readers, are given under several headings.

I. Alex Silberberg, Co-Editor-in-Chief

For the past two years, since the retirement of Dr. George W. Scott Blair, the position of Co-Editor-in-Chief of BIORHEOLOGY has not been filled. In my judgment, I thought it important to have the responsibility for editorial policy shared by a colleague. Upon my recommendation, the Publishers invited Professor Silberberg to act as Co-Editor-in-Chief and we are very glad that he accepted to be active in this capacity. It is with great pleasure that the Publishers and I welcome Professor Silberberg as Co-Editor-in-Chief. Beginning with the next issue, Alex Silberberg and I shall decide editorial policy or/and any revision deemed necessary. As an Editor-in-Chief, Alex Silberberg will no longer edit communications submitted to him in his former position of Editor. The Publishers and I should like to thank him for the fine work he did as an Editor for many years. Any Letters to the Editors-in-Chief can be either submitted to him or to me. As before, the Executive Editorial Office (EEO) of BIORHEOLOGY will be under my direction and communications concerning the technical presentation of communications should be directed to the EEO.

II. Revised Editorial Policy Concerning Additional Editors

It became necessary to increase our Editorial Board to a total of twenty-four Editors. However, not all new positions will be filled this year. This policy was initiated to decrease the burden on each Editor and also insure more rapid publication. As is mentioned in the first paragraph under Instructions to Authors, each Author may submit a communication to an Editor of his/her choice.

The following colleagues accepted the invitation to serve as Editors: E. Puchelle (France), D. Quemada (France) and R. Skalak (USA). The Publishers and I are pleased to welcome them as Editors of BIORHEOLOGY.

III. Communications Concerning Clinical Hemorheology and the new journal entitled "CLINICAL HEMORHEOLOGY. A Companion Journal of BIORHEOLOGY".

A new biorheological journal will begin publication this year by Pergamon Press. Its name is CLINICAL HEMORHEOLOGY with the subtitle "A Companion Journal of BIORHEOLOGY". During the past few years there has been a marked increase in the number of original contributions in the fields of clinical hemorheology, and communications in this field have been published in BIORHEOLOGY, as well as in other journals.

The founding of CLINICAL HEMORHEOLOGY as a separate journal became necessary, because otherwise BIORHEOLOGY would have become mainly a medical journal. As there is a growing need for an international journal on clinical hemorheology to serve as an aid to the practice of medicine in all its fields, whenever applicable, I have founded the new journal with the cooperation of the Publishers of BIORHEOLOGY.

The aims of CLINICAL HEMORHEOLOGY are to be of service to clinical investigations and to hemorheological testing in the clinical laboratory or in blood transfusion centers towards better medical care. Professor Siegfried Witte, F.R. Germany is Co-Editor-in-Chief of CLINICAL HEMORHEOLOGY. Papers and Brief Communications on clinical hemorheology will no longer be accepted for publication in BIORHEOLOGY, but, when submitted to any of our Editors of BIORHEOLOGY, they have been advised to send the manuscript to an Editor of CLINICAL HEMORHEOLOGY.

As is the case with BIORHEOLOGY, the new journal will be for rapid publication and a total of twenty-four Editors will be appointed although not all twenty-four positions will be filled this year.

Readers of BIORHEOLOGY who wish to have their communications published in CLINICAL HEMORHEOLOGY are asked to submit them to any of the following Editors of their choice: Ben Aronson (Israel), Takehiko Azuma (Japan), P.I. Brånemark (Sweden), Shu Chien (USA), L. Dintenfass (Australia), J. Ditzel (Denmark), John A. Dormandy (UK), Albrecht M. Ehrly (F.R. Germany), Alan C. Groom (Canada), H. Hartert (F.R. Germany), Yukihide Isogai (Japan), Donald E. McMillan (USA), Holger Schmid-Schönbein (F.R. Germany), Geoffrey V.F. Seaman (USA), and J.F. Stoltz (France). The exact addresses of any of the above mentioned Editors of CLINICAL HEMORHEOLOGY will be sent by the EEO upon request. It should be noted that the selection of the Board of Editors has not yet been completed.

It should be noted that since Professor H. Schmid-Schönbein and Professor G.V.F. Seaman switched their editorial activities from BIORHEOLOGY to CLINICAL HEMORHEOLOGY, they will no longer accept communications for BIORHEOLOGY. However, they will attend to the editing of communications, which were already submitted to them as Editors of BIORHEOLOGY, for the remaining three issues of volume 17, 1980. The Publishers and I thank them for their activities as Editors.

CLINICAL HEMORHEOLOGY is, as implied in the subtitle, a companion journal of BIORHEOLOGY. The new journal will, however, publish review articles in all fields of hemorheology upon the invitation of the Editors-in-Chief.

The address of the EEO of CLINICAL HEMORHEOLOGY will be the same as that of BIORHEOLOGY, viz., at Polytechnic Institute of New York and under my direction.

It should be noted that BIORHEOLOGY will, of course, continue to publish communications on non-clinical hemorheology, as well as of clinical biorheology other than clinical hemorheology.

Laysheets of manuscripts for CLINICAL HEMORHEOLOGY differ from those which were employed for the past few years for BIORHEOLOGY. They are 24 cm ($9\frac{1}{2}$ inches) high and 16 cm ($6\frac{1}{2}$ inches) wide. Laysheets for CLINICAL HEMORHEOLOGY as well as Instructions to Authors can be secured from the EEO or from any of the Editors of CLINICAL HEMORHEOLOGY mentioned above.

CLINICAL HEMORHEOLOGY will be published in six issues per volume. The first two issues of volume 1 will appear this year and the first issue is scheduled for August. The remaining four issues (3-6) of volume 1 will be published in 1981. With volume 2, published in 1982, CLINICAL HEMORHEOLOGY will become a bi-monthly journal as is BIORHEOLOGY.

IV. New Journal Size of BIORHEOLOGY and Revised Instructions to Authors

It was found desirable to change the format and size of BIORHEOLOGY to that of a smaller size. These changes were made because the smaller size ensures better readibility of texts on each page. The remaining issues of BIORHEOLOGY, viz., numbers 4, 5 and 6 of volume 17, 1980 will be the last issues, published in the present format and size. However, beginning in 1981 with issue number 1 of volume 18, BIORHEOLOGY will be published in the new format and the smaller size, which will be the same as CLINICAL HEMORHEOLOGY.

Readers, who wish to submit their communications for publication in volume 18 of BIORHEOLOGY, will need to use the new laysheets. The EEO as well as each Editor of BIORHEOLOGY will supply the new laysheets upon request.

Both our Editors and Authors, whose communications are being considered for publication, are advised to attend without delay to the editing and any possible revision of a submitted manuscript, respectively. The editorial review and any requested revision of manuscripts will have to be handled most rapidly so that for the remaining issues of volume 17 communications can be received at the EEO not later than November 14, 1980.

The Instructions to Authors had to be revised as of June 1980 for some of the reasons mentioned above, as well as for the completion of copyright and reprint order forms. These forms will be sent to Authors by Editors when a manuscript is accepted for publication. The Author must then forward without delay the completed forms to Pergamon Press, Inc., Maxwell House, Fairview Park, Elmsford, NY 10523 in order to ensure most rapid publication of the accepted communication. Authors must submit reprint order forms immediately after their manuscripts are accepted for publication, as otherwise they cannot expect the reprint orders to be filled by the Publisher for the same prices as given on the form. The reprint order form always has to be submitted, even if no reprints are ordered. If copyright forms are not completed, an Author's communication cannot be published.

V. The Fourth International Congress of Biorheology

Since BIORHEOLOGY is the official journal of the International Society of Biorheology, it will publish announcements by the President of our Society and Conference Chairman Professor E. Fukada, as well as announcements by any of its committees, in subsequent issues. As has been the case in the past, the abstracts and congress material will be published in BIORHEOLOGY as well.

As the Fourth International Congress of Biorheology will be held July 27 to August 1, 1981 at Tokyo, Japan, our Readers are advised to secure information about the Congress including travel and submission of abstracts by writing to Professor Yaso'o Matunobu, Secretary General, The Fourth International Congress of Biorheology, Department of Physics, Keio University, Hiyoshi, Kohoku-ku, Yokohama 223, Japan. News items about the Congress will be published in forthcoming issues as quickly as possible.

All abstracts accepted by the scientific committee of the Congress will be published in BIORHEOLOGY rapidly. The journal will also publish all invited lectures and other congress material, as well as all communications which have been accepted for publication by our Editors soon after the Congress.

Scientific Papers, the abstracts of which have been submitted to the Congress and accepted for presentation by its scientific committee, will be published in BIORHEOLOGY when accepted by one of its Editors, with the exception of Papers on clinical hemorheology. The latter will need to be submitted to Editors of CLINICAL HEMORHEOLOGY. However, all abstracts pertaining to all fields of hemorheology will be published in both journals. CLINICAL HEMORHEOLOGY will also publish all invited lectures pertaining to all fields of hemorheology.

VI. Review Articles and Other Texts in Future Issues of BIORHEOLOGY

Recently, several Review Articles in the various fields of biorheology have been invited by me. However, in the future, Review Articles and other texts will be invited both by Alex Silberberg and me as Editors-in-Chief. These contributions are not merely meant to inform our Readers, but to stimulate them for new research in the many fields of biorheology.

Alfred L. Copley
Editor-in-Chief

Vol. 17
1980

BLANK
PAGE

Vol.
198

BIORHEOLOGY, Vol. 17, pp. 211-218, 1980
Printed in the USA. All rights reserved.

0006-355X/80/030211-08$02.00/0
Copyright (c) 1980 Pergamon Press Ltd

Vol. 17
1980

THIRD INTERNATIONAL CONGRESS OF BIORHEOLOGY

SYMPOSIUM ON RHEOLOGY OF BLOOD VESSELS

MECHANICAL PROPERTIES OF HUMAN CEREBRAL ARTERIES

Kozaburo Hayashi, Shiro Nagasawa*, Yoshito Naruo*,
Atsushi Okumura*, Kouzo Moritake* and Hajime Handa*

National Cardiovascular Center Research Institute
Fujishirodai 5, Suita, Osaka 565, Japan
*Kyoto University Medical School, Department of Neurosurgery
Sakyo-ku, Kyoto 606, Japan

(Received 1.9.1979. Accepted by Guest Editor K. Fronek.
Received by Executive Editorial Office 16.5.1980)

ABSTRACT

Mechanical properties of human intracranial arteries and their age-related variations are quantitatively compared with those of extracranial arteries, using the stiffness parameter proposed by the authors and the incremental elastic modulus proposed by Bergel both of which are calculated from the pressure-diameter data. The intracranial arteries are much stiffer than the extracranial arteries throughout all ages. The high wall stiffness of the intracranial arteries under the forties is attributable to the high elastic modulus of wall material, while the wall thickening is a reason for the low distensibility observed in the older intracranial arteries. The extremely thin walls of the intracranial arteries under the forties develop very high stresses, which are more than twice as much as those in the extracranial arteries and the older intracranial arteries. Relative contents of collagen to elastin are much higher in the intracranial arteries than in the extracranial arteries. The activation of smooth muscle by vaso-constricting agents reduces the wall stiffness and increases the maximum diameter response of the intracranial arteries more effectively than of the extracranial arteries. These mechanical and morphological features of the intracranial arteries might be related to the pathogenesis of the cerebrovascular lesions.

INTRODUCTION

Morphological features peculiar to the cerebral arteries have been given a considerable amount of attention (1). However, there have been very few studies on their mechanical properties (2-7) which are very important not only to understand the physiology of the blood circulation in the brain but also to investigate the pathogenesis of cerebrovascular lesions like aneurysms, arteriosclerosis and vasospasm. For example, saccular aneurysms, which are one of the most troublesome cerebrovascular diseases, are common in the cerebral arteries and rather rare elsewhere in the body. There are many theories on the etiology of cerebral saccular aneurysms: congenital hypotheses, acquired hypotheses, or a combination of both. From the standpoint of biomechanics, the formation and rupture of aneurysms are considered to be a breakdown of the arterial wall caused by some force induced by blood pressure and blood flow (5, 7, 8). We cannot elucidate the mechanisms of these vascular lesions without a full understanding of the mechanical properties of blood vessel walls.

In this paper, the mechanical properties of human cerebral arteries and their age-related change are quantitatively compared with those of extracranial arteries, using a few parameters calculated from their pressure-diameter data. The effects of smooth muscle activation on the mechanical relations are also discussed together with the regional variations of histology and wall dimensions.

EXPERIMENTAL PROCEDURE

From 18 autopsy subjects who had neither systemic nor cerebral vascular lesions, we obtained tubular segments of basilar and vertebral arteries from the intracranial sites. For comparison, common carotid, internal carotid and vertebral arteries were taken from the extracranial sites. These arterial segments were resected within 10 hours post mortem after they were carefully dissected free from the surrounding connective tissues, and immediately stored in a Krebs-Ringer solution at 4°C.

In all mechanical tests, which were carried out within 15 hours post mortem, each

cylindrical segment was placed in a bath which contains the Krebs-Ringer solution kept at 37°C and continuously oxygenated with a 95% oxygen and 5% carbon dioxide gas mixture as depicted in Fig. 1. The segment was mounted horizontally to two short stainless steel tubes at its both ends, and inflated with the Krebs-Ringer solution from a reservoir through one of these tubes. The intraluminal pressure was measured by a strain gage manometer which was connected to the vessel segment via the other stainless steel tube and a short catheter. The external diameter of the specimen was measured by means of a specially designed displacement transducers (9), by putting the tubular specimen between the end parts of L-shaped stainless steel arms stemmed from two mutual inductance transformers of rotating type.

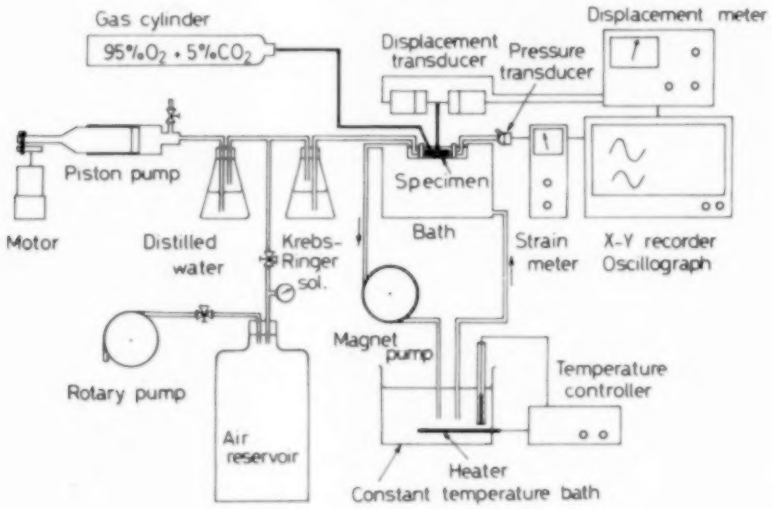

FIG. 1

Schematic representation of the testing apparatus used in the in vitro experiments.

After being kept at 100 mmHg for 30 minutes, the intraluminal pressure of a specimen was elevated up to 200 mmHg and then lowered to 0 mmHg at the rate of 3 mmHg/sec. After this specific preconditioning by the repetition of inflation and deflation, a stable pressure-diameter relation was finally obtained, and recorded for the elasticity analysis while the pressure was elevated from 0 to about 200 mmHg. After measuring the control pressure-diameter data on a specimen immersed in the Krebs-Ringer solution, the intraluminal pressure was again raised to 100 mmHg. Potassium or norepinephrine was then added to the Krebs-Ringer solution to the concentration of 50 mM or 10^{-5} M, respectively. After the peak contraction was reached, the pressure was lowered to 0 mmHg and then again elevated up to 200 mmHg at the rate of 1 mmHg/sec. The pressure-diameter relation of the activated blood vessel was recorded in this pressure elevation process. After these mechanical tests, a thin slice of about 1 mm in thickness was cut out from the middle portion of the segment which was again rinsed in the Krebs-Ringer solution, and was used to measure its unstressed internal and external diameter by a tool micrometer.

The compositions of connective tissues in each arterial wall were determined chemically by a modified method of the procedure employed by Neuman and Logan (10, 11). The collagen and elastin contents were measured by a colorimetric assay of hydroxyproline, and expressed by percentages of the dry defatted weight.

EXPERIMENTAL RESULTS AND DISCUSSION

Pressure-Diameter Relation

Figure 2 (a) illustrates the relations between the intraluminal pressure and the external diameter of an intracranial vertebral artery obtained from a 50 years old man. The solid curve was measured under the control condition in the Krebs-Ringer solution, while under the activated condition in the Krebs-Ringer solution mixed with potassium the relation expressed by the broken line was obtained. As widely known (13-16), the arterial wall under the physiological state yields nonlinear pressure-diameter relation as shown by the control curve in this figure, having higher distensibility in the lower pressure range and

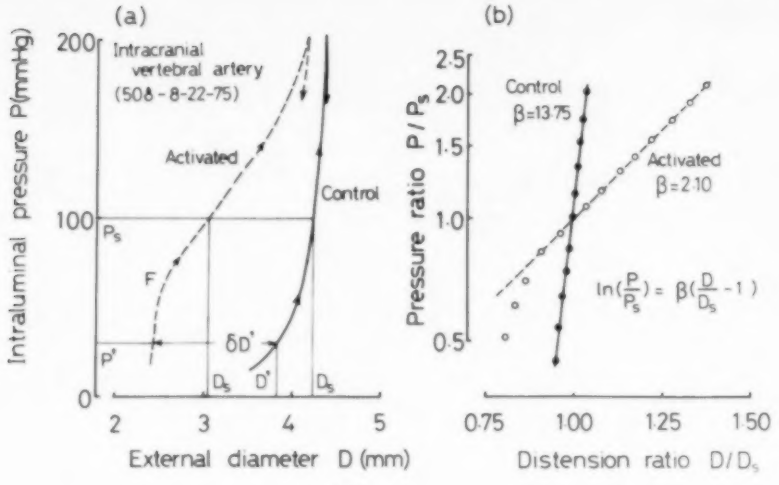

FIG. 2

Pressure-diameter relations (a) and their replotting as the logarithm of pressure ratio versus the distension ratio (b) of a control (solid line) and activated (broken line) intracranial vertebral artery.

losing it at progressively higher pressures. If we plot this curve as the logarithm of pressure ratio versus the distension ratio, a linear relation is obtained in the physiological pressure range with extremely high correlation coefficient as shown in Fig. 2 (b), which is described by:

$$ln\ (P/P_s) = \beta\ (D/D_s - 1), \qquad (1)$$

where P_s is the standard pressure and D_s is the wall diameter at the standard pressure. In this study, 100 mmHg was taken for P_s, relevant for the normal arterial blood pressure. To express the stiffness of nonlinear vascular wall quantitatively, we proposed the stiffness parameter, β, which is the slope of the line (4, 5, 17, 18).

The activation of vascular smooth muscle, on the other hand, yields a two-phasic pressure-diameter curve which is characterized by a flection point, F, as shown in Fig. 2 (a). Only a very slight change in wall diameter was detected below the intraluminal pressure at F-point. Above this pressure, however, the diameter increases rather rapidly with the pressure elevation, at a significantly higher rate than that of the control artery. The appearance of F-point in the pressure-diameter curve in the activated artery might be attributable to the release of the compressive stress which is developed in the connective tissues by the contracted smooth muscle below the pressure at F-point (12). Again in the case of the activated vascular wall, the pressure-diameter relation is described by Eq. (1) as shown in Fig. 2 (b) if we limit the pressure level to the normal blood pressure range above F-point. The pressure-diameter data in this case deviate from Eq. (1) below F-point.

Stiffness and Elastic Modulus

Figure 3 (a) summarizes β-values of 5 kinds of non-activated arterial segments, two of which were obtained from intracranial sites. Subjects were divided into two age groups: 'Young' for less than 45 years of age and 'Old' for over 45 years. This age grouping was established considering that the wall dimensions of intracranial arteries change remarkably in the forties and also that the atherosclerosis in the systemic arteries starts from around 45 years of age (12, 18). As a whole, the intracranial arteries have higher β-values in both age groups than the extracranial arteries. As reported elsewhere, the intracranial arteries, which have high β-values already at birth, start to increase in their stiffness soon after birth, and have significantly higher β-values at the age of around 20 years compared with the extracranial arteries (12, 18). Such a high stiffness as in the intracranial arteries of 'Young' group corresponds to the common occurrence of saccular aneurysms not only in the elderly but also in the middle aged persons (4, 7, 19). In contrast to the intracranial arteries, the low wall stiffness of the common carotid artery in childhood is retained until 40 years of age (12, 17), which gives fairly low β-value in the 'Young' common carotid artery as shown in Fig. 3 (a). The extracranial vertebral artery and internal carotid artery, which locate just outside the brain, yield very slight change of

Vol. 17 1980

wall stiffness with aging.

As understood from Eq. (1), the stiffness parameter, β, defines the slope of pressure-diameter relation, and express the indistensibility of a tubular wall. However, it does not necessarily represent the inherent elastic properties of wall material since the stiffness parameter involves not only the elastic modulus of the material but also the wall dimensions such as wall diameter and thickness. The parameter, β, is thought of as representing the apparent wall stiffness which includes these two factors comprehensively. To express the elastic modulus of the nonlinear material like a vascular wall, Bergel proposed the "Incremental elastic modulus" (20) which is described by:

$$E_{inc} = \frac{\Delta P}{\Delta R_o} \frac{2(1-\nu^2)R_i^2 R_o}{(R_o^2 - R_i^2)}, \qquad (2)$$

where R_o, R_i and ν are the external radius, internal radius and Poisson's ratio, respectively. While the stiffness parameter, β, is used to represent the apparent stiffness of a tubular wall, the incremental elastic modulus, E_{inc}, can be applied to study the inherent elastic properties of wall material.

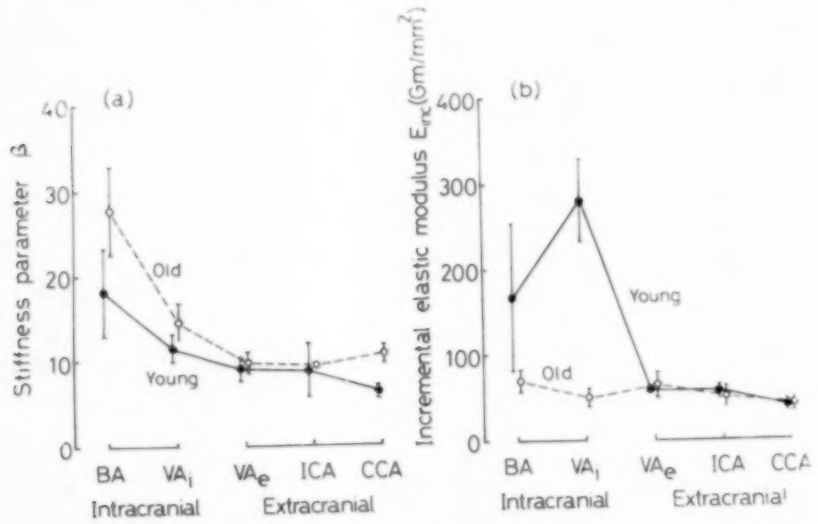

FIG. 3

Averaged values of stiffness parameter and incremental elastic modulus of 'Young' (younger than 45 years old) and 'Old' (older than 45 years) groups of intracranial and extracranial arteries. Vertical lines mean ± SE.

Regional and aging dependence of the incremental elastic modulus of arterial wall, which was calculated at the transmural pressure of 100 mmHg, is shown in Fig. 3 (b). Two intracranial arteries of 'Young' group have remarkably higher elastic moduli than the extracranial arteries. The incremental elastic moduli of the intracranial arteries are very high already at birth and remain almost unchanged with age until early in the forties (18). Contrary to the significant increase in β-values of intracranial arteries from the 'Young' to 'Old' ages, their incremental elastic moduli decrease tremendously with aging. These contrastive change of β-value and E_{inc}-value of the intracranial artery with age is attributable to its ramarkable change of wall thickness as shown later. The high wall stiffness of the intracranial artery under the forties is due to the high elastic modulus of its wall material, while the wall thickening is a major reason for the low distensibility in the 'Old' intracranial artery. The incremental elastic moduli of 'Old' intracranial arteries are almost similar to or somewhat higher than those of the extracranial arteries which exhibit almost no difference of their elastic moduli between these two age groups. Learoyd and Taylor also reported that the E_{inc}-values at 100 mmHg of the peripherally located arteries like the iliac and femoral arteries showed a tendency to decrease with age, while the elastic modulus of the thoracic aorta increases with age (21). There might be some change in the quality of wall components as well as their infrastructures during aging.

Stress and Wall Dimension

Stresses developed in the arterial walls by the transmural pressure of 100 mmHg are shown in Fig. 4, where the stress is the circumferential stress averaged through the wall thickness, calculated according to the membrane shell theory (22). While the stresses in the walls of extracranial arteries are all within a range between 5 to 12 Gm/mm^2 regardless of their age, the 'Young' intracranial arteries have tremendously high stresses above 20 Gm/mm^2. These high wall stresses in the 'Young' intracranial arteries, which are ascribed

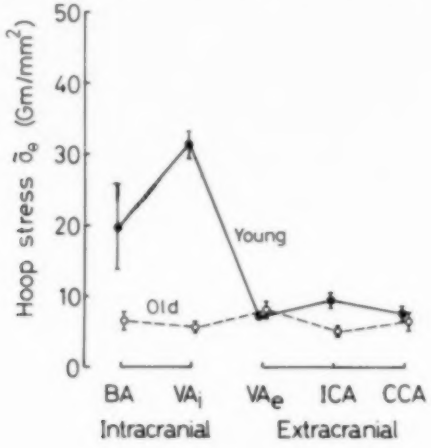

FIG. 4

Regional and age-related variations of circumferential wall stress expressed as mean ± SE.

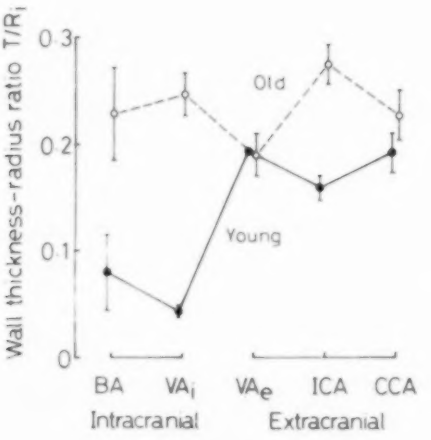

FIG. 5

Regional and age-related variations of the ratio of wall thickness to internal radius, expressed as mean ± SE.

to their extremely thin walls as understood from Fig. 5, are also considered to be one of the major contributors to the initiation and development of cerebrovascular lesions. After 40 years old, the wall thickness as well as the wall thickness-radius ratio of the intracranial arteries increase rather rapidly with age, which brings about the reduction of their wall stresses to almost the same level as those observed in the extracranial arteries. The decrease in wall stress with age was reported by Bader (23) on the human thoracic aorta and also suggested by Busby and Burton (2) on the human vertebral artery. There might be some force-sensible mechanism in arterial walls which change their wall dimensions so as to have a low wall stress during aging.

Vol. 17
1980

Connective Tissue Content

It has been believed that the passive elastic properties of blood vessels are roughly determined by the relative amounts of easily stretchable elastin fiber and inextensible collagen fiber (15, 16, 24-26). There is comparatively less elastin in the 'Young' intracranial arteries than in the extracranial arteries as shown in Fig. 6 (a) and (b), which might be a reason for their high elastic moduli. However, the relative contents of the connective tissues, which are represented by the weight ratios of collagen to elastin, are still significantly higher in the 'Old' intracranial arteries than in the extracranial ones in spite of the fact that the incremental elastic moduli of the 'Old' intracranial arteries converge to the same levels as in the extracranial arteries as shown in Fig. 3 (b). The reason for the discrepancy between the aging changes of wall elasticity and connective tissue contents observed in the intracranial arteries is not clarified yet at this stage. The change in compactness and quality of connective tissues with age should be studied further in detail. As for the major extracranial arteries, we obtained fairly good correlations between the E_{inc}-value at 20 mmHg and the elastin content and also between the E_{inc}-value at 180 mmHg and the collagen content (28),which are the similar results to those obtained by Cox (16).

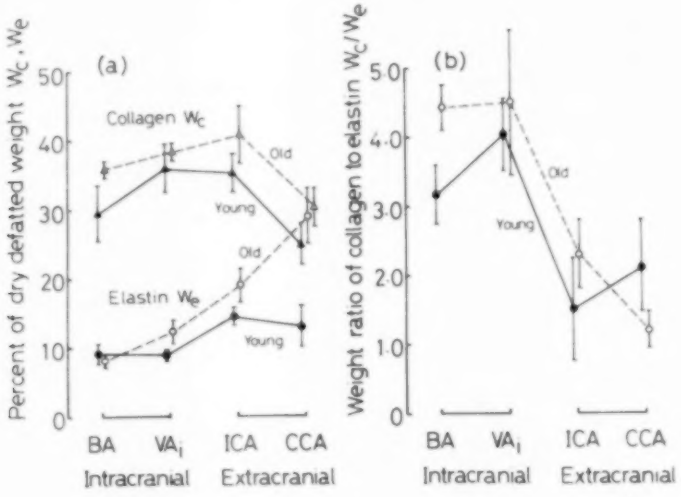

FIG. 6

Comparison of connective tissue contents and relative amount of collagen to elastin between intracranial and extracranial arteries. Each value is expressed as mean ± SE.

Effect of Activation of Smooth Muscle

Since the smooth muscle in the basilar artery was activated very poorly possibly due to the ligation of its small branches for the prevention of leakage, several intracranial and extracranial vertebral arteries, internal and common carotid arteries of 40 to 55 years old subjects were used to study the mechanical response to vaso-constricting substances. As shown in Fig. 2 (a), the activation of vascular smooth muscle makes the pressure-diameter curve shift to the left and changes the shape of the curve, accompanying with the appearance of F-point. The slope of the pressure-diameter curve above F-point is fairly lower than that of the control, non-activated artery, which is clearly demonstrated in Fig. 2 (b). The decrease of β-value caused by the activation of vascular smooth muscle is shown in Fig. 7 (a). Such a decrease in β-value or an increase in the distensibility of arterial wall by the activation of vascular smooth muscle was observed not only in these human arteries but also in experimental animals (29). It is very interesting to note in this figure that the vaso-constricting agent reduces the wall stiffness of intracranial vertebral artery much more effectively than that of the extracranial arteries.

Effect of the activation of vascular smooth muscle on the pressure-diameter relation is also expressed by the diameter response utilized by Cox (30) which is expressed by $\delta D'/D'$, where $\delta D'$ is the diameter change between the control and activated condition at each pressure level and D' is the diameter under the control, passive condition as shown in Fig. 2 (a). As understood in Fig. 2 (a), the diameter response depends upon the intraluminal

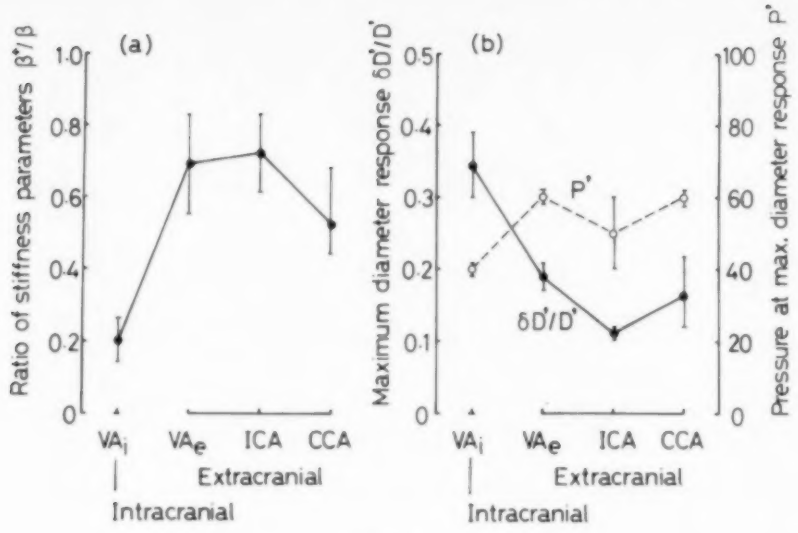

FIG. 7

Effects of the activation of vascular smooth muscle on the wall stiffness and dimension. Each vertical line indicates error range.

Vol. 17
1980

pressure, and becomes maximum at a certain pressure level. The diameter response is generally highest at a lower pressure level of around 50 mmHg as seen in Fig. 7 (b) and decreaes progressively at higher pressures (12). Fig. 7 (b) shows the maximum diametr response of each artery and the pressure value at which the maximum diameter response occurs. The intracranial vertebral artery manifests significantly larger maximum diameter response at somewhat lower pressure level than the extracranial arteries, although with the increase in pressure the diameter response of this particular artery decreases more rapidly than the others, which results in the lower β-values of the intracranial arteries than of the extracranial arteries. These mechanical and morphological effects of the activation of vascular smooth muscle in the case of intracranial artery might be related to the preferential occurrence of vasospasm in the cerebral artery.

REFERENCES

1. STEHBENS, W. E. *Pathology of Cerebral Blood Vessels*. St. Louis: Mosby, 1972, 661 pp.

2. BUSBY, D. E. and BURTON, A. C. The effect of age on the elasticity of the major brain arteries. *Can. J. Physiol. and Pharmacol.* 43, 185-202, 1965.

3. CHALUPNIK, J. D., DALY, C. H. and MERCHANT, H. C. *Material Properties of Cerebral Blood Vessels*. Final Report on Contract No. NIH-69-2232, 1971, 50 pp.

4. MORITAKE, K. Biomechanical studies on the pathogenesis of cerebral aneurysms and the mechanism of their growth and rupture, Part I Structures and mechanical behavior of cerebral arteries. *Arch. Jap. Chir.* 44, 87-107, 1975.

5. MORITAKE, K., HANDA, H., OKUMURA, A., HAYASHI, K. and NIIMI, H. Stiffness of cerebral arteries - Its role in the pathogenesis of cerebral aneurysms. *Neurologia medico-chir.* 14, 47-53, 1974.

6. SCOTT, S., FERGUSON, G. G., and ROACH, M. R. Comparison of the elastic properties of human intracranial artery and aneurysms. *Can. J. Physiol. and Pharmacol.* 50, 328-332, 1972.

7. MORITAKE, K. Biomechanical studies on the pathogenesis of cerebral aneurysms and the mechanism of their growth and rupture, Part II Hemodynamics at cerebral arterial bifurcations and in cerebral aneurysms. *Arch. Jap. Chir.* 44, 108-123, 1975.

8. FERGUSON, G. G. Physical factors in the initiation, growth and rupture of human intracranial saccular aneurysms. *J. Neurosurg.* 37, 616-677, 1972.

9. HAYASHI, K., OKUMURA, A., MORITAKE, K., NIIMI, H. and HANDA, H. A newly designed displacement transducer for the measurement of blood vessel diameter. *Jap. J. Medical Instrumentation* 48, 567-571, 1978.

10. NEUMAN, R. E. and LOGAN, M. A. Determination of hydroxyproline. *J. Biol. Chem.* 184, 299-305, 1950.

11. LANSING, A. I., ROSENTHAL, T. B., ALEX, M. and DEPSEY, E. W. The structure and chemical characterization of elastic fibers as revealed by elastase and by electron microscopy. *Anat. Rec.* 114, 555-575, 1952.

12. NAGASAWA, S., NARUO, Y., OKUMURA, A., HANDA, H. and HAYASHI, K. Mechanical properties of canine femoral artery smooth muscle, to be published.

13. BERGEL, D. H. The properties of blood vessels. In: *Biomechanics - Its Foundations and Objectives*. Y. C. Fung, N. Perrone and M. Anliker (Eds.) New Jersey: Prentice-Hall, 1972, pp. 105-139.

14. PATEL, D. J. and VAISHNAV, R. N. The rheology of large blood vessels. In: *Cardiovascular Fluid Dynamics, Vol. 2*. D. H. Bergel (Ed.) London: Acedemic Press, 1972, pp. 1-64.

15. DOBRIN, P. B. Mechanical properties of arteries. *Physiol. Rev.* 58, 397-460, 1978.

16. COX, R. H. Regional, species, and age related variations in the mechanical properties of arteries. *Biorheology* 16, 85-94, 1979.

17. HAYASHI, K. Present status of biomechanics (1) Application of solid mechanics to cardiovascular system. *Science of Machine* 27, 855-859, 1975.

18. HAYASHI, K., HANDA, H. NAGASAWA, S., OKUMURA, A. and MORITAKE, K. Stiffness and elastic behavior of human intracranial and extracranial arteries. to be published.

19. LOCKSLEY, H. B. Report on the cooperative study of intracranial aneurysms ans subarachnoid hemorrhage, Section 5, Part I. *J. Neurosurg.* 25, 219-239, 1966.

20. BERGEL, D. H. The static elastic properties of the arterial wall. *J. Physiol.* 156, 445-457, 1961.

21. LEAROYD, B. M. and TAYLOR, M. G. Alterations with age in the viscoelastic properties of human arterial walls. *Circ. Res.* 18, 278-292, 1966.

22. TIMOSHENKO, S. and YOUNG, D. H. *Elements of Strength of Materials (5th Edition)*. Princeton: D. Van Nostrand, 1968, 377 pp.

23. BADER, H. Dependence of wall stress in the human thoracic aorta on age and pressure. *Circ. Res.* 20, 354-361, 1967.

24. ROACH, M. R. and BURTON, A. C. The reason for the shape of the distensibility curves of arteries. *Can. J. Biochem. and Physiol.* 35, 681-690, 1957.

25. HOFFMAN, A. S. and GRANDE, L. A. Sequential enzymolysis of human aorta and resultant stress-strain behavior. *Biomat. Med. Dev. Art. Org.* 5, 121-145, 1977.

26. TAIRA, S., HAYASHI, K., SATO, M., HANDA, H., and MORITAKE, K. Biomechanical studies of vascular walls (Stress analysis of vascular walls by finite element method). *J. Soc. Materials Sci., Japan* 23, 437-443, 1974.

27. HAYASHI, K., SATO, M., HANDA, H. and MORITAKE, K. Biomechanical study of the constitutive laws of vascular walls. *Exp. Mech.* 14, 440-444, 1974.

28. NARUO, Y., NAGASAWA, S., OKUMURA, A., HANDA, H. and TAKEDA, T. Regional and aging change of collagen and elastin contents of human intracranial arteries. *Proc. 2nd Annual Meeting of Jap. Soc. of Biorheology* 141-143, 1979.

29. OKUMURA, A. Experimental studies of the role of vascular smooth muscle in mechanical properties of canine arterial walls. *Arch. Jap. Chir.* 46, 244-257, 1977.

30. COX, R. H. Mechanics of canine iliac artery smooth muscle in vitro. *Am. J. Physiol.* 230, 462-470, 1976.

Vol. 1980

BIORHEOLOGY, Vol. 17, pp. 219-226, 1980
Printed in the USA. All rights reserved.

0006-355X/80/030219-08$02.00/0
Copyright (c) 1980 Pergamon Press Ltd

THIRD INTERNATIONAL CONGRESS OF BIORHEOLOGY

SYMPOSIUM ON RHEOLOGY OF BLOOD VESSELS

MATHEMATICAL CHARACTERIZATION OF THE NONLINEAR RHEOLOGICAL BEHAVIOR OF THE VASCULAR TISSUE

Ramesh N. Vaishnav

Professor of Engineering
The Catholic University of America
Washington, D. C. 20064

(Received 1.11.1979. Accepted by Guest Editor K. Fronek.
Received by Executive Editorial Office 16.5.1980)

ABSTRACT

Elastic and viscoelastic characterizations of the nonlinear rheological behavior of incompressible, curvilinearly orthotropic aortic tissue are presented. For the elastic characterization, it is assumed that there exists for the tissue a strain energy density function which, for the usual physiological loading consisting of an intravascular pressure and a longitudinal force, can be represented as a polynomial of the second or third degree in the Green-St. Venant strains in the circumferential and longitudinal directions, involving three or seven constitutive constants, respectively. In vitro experiments on segments of the canine middle descending thoracic aorta indicate that these formulations (particularly the latter) characterize satisfactorily the large elastic deformations of this tissue. For characterizing the nonlinear viscoelastic behavior, it is assumed that the circumferential and longitudinal stresses are functionals of the histories of the two Green-St. Venant strains. Expressing these functionals in terms of series of multiple integrals and truncating these series at the first two levels yields nonlinear viscoelastic characterizations involving four and ten constitutive functions which are determined from experiments on canine aortic segments.

Vol. 17
1980

INTRODUCTION

To understand the mechanics of the circulatory system in health and disease, it is necessary to characterize the rheology of the vascular tissue realistically and in as much detail as possible. While earlier attempts at characterization of vascular rheology were based on elementary application of the classical theory of isotropic materials, considerable progress has been made by various investigators toward characterizing the vascular tissue more fundamentally, taking into consideration its capability of undergoing rather large deformations.

Several works (1-7) have adequately reviewed the recent, as well as the early, work in the field of vascular rheology. In this communication we outline our own attempts of the past several years toward mathematical characterization of the nonlinear rheological properties of the tissue of the large arteries. Specifically, we present formulations to describe the hyperelastic, elastic, and viscoelastic characterizations of the tissue and indicate an approach to its thermoviscoelastic characterization. We sketch here only an outline of these formulations, referring the reader to our original publications (8-11) for further details. Of these (8) and (11) treat the subject formally in contrast with the simplified heuristic approach used here.

For convenience, we restrict our discussion to the rheological behavior of the tissue from a straight, uniform segment of a canine middle descending aorta. It is well-known that the arterial tissue is capable of undergoing large deformations, and its stress-strain behavior in terms of the usual definitions of stress and strain is nonlinear. It is also known that the tissue is viscoelastic in nature. However, for many purposes (such as in determining the speed of pulse propagation in an artery) only the elastic characteristics of the tissue response are important. It is reasonable to assume that the arterial tissue is incompressible (12) and that no higher degree of anisotropy than orthotropy need be attributed to the tissue (13). Many other interesting aspects of vascular rheology have been documented (14,15). On the basis of these and other such findings, it appears reasonable to develop a theory for characterization of the tissue response on the basis of the following assumptions: (a) The tissue is a one-phase homogeneous continuum; (b) The tissue is incompressible; (c) The tissue is curvilinearly orthotropic; (d) The tissue can be treated as hyperelastic, elastic, viscoelastic, or thermoviscoelastic, depending upon the degree of

detail required in characterization. These assumptions concern the basic tissue characteristics. We shall make additional assumptions as and when necessary. For a detailed discussion of these assumptions, see (16).

ELASTIC RESPONSE OF THE TISSUE

Consider a thin-walled cylindrical arterial segment whose length, midwall radius, and the thickness are L, R, and h, respectively, when it is in a deformed state under the simultaneous action of a steady intravascular pressure P and a longitudinal force F. For convenience, we will refer to such loading of the tissue segment as "physiological loading". Let L_o, R_o, and h_o be the corresponding dimensions of the tissue segment in the undeformed or "natural" configuration that it would assume if the intravascular pressure and force were gradually removed. Although, in a strict sense, such a natural state does not exist for the tissue, a close approximation to it can indeed be made. We refer the deformed and the undeformed configuration of the tissue to a polar cylindrical coordinate system, r, θ, z oriented along the geometric axes of the cylindrical segment. Since the tissue is curvilinearly orthotropic, the deformed state of the segment can be characterized solely in terms of the three extension ratios or stretches λ_θ, λ_z, and λ_r, in the circumferential, longitudinal, and the radial directions, respectively. They define the lengths, in the deformed configuration, of infinitesimal line or arc elements in the θ, z, and r directions, respectively, as multiples of the corresponding dimensions in the undeformed configuration. In terms of the vessel dimensions, the stretches λ_θ, λ_z, and λ_r are given by

$$\lambda_\theta = R/R_o \qquad [1]$$

$$\lambda_z = L/L_o \qquad [2]$$

$$\lambda_r = h/h_o \qquad [3]$$

For an incompressible, orthotropic tissue under physiological loading, these stretches are interrelated through the incompressibility condition

$$\lambda_\theta \lambda_z \lambda_r = 1 \qquad [4]$$

which shows that only two of the three stretches can be independently prescribed. We also introduce the Green-St. Venant strains

$$a = \tfrac{1}{2}(\lambda_\theta^2 - 1) \qquad [5]$$

$$b = \tfrac{1}{2}(\lambda_z^2 - 1) \qquad [6]$$

$$c = \tfrac{1}{2}(\lambda_r^2 - 1) \qquad [7]$$

which also describe the deformation of the segment. These are often more convenient to use in mathematical characterizations of nonlinear defomrations than the conventional strains $\lambda_\theta - 1$, $\lambda_z - 1$, and $\lambda_r - 1$, since a squared length appears more naturally in the mathematical analysis of the geometry of deformation. In terms of a, b, and c, the incompressibility condition, Eq. [4], becomes

$$(1 + 2a)(1 + 2b)(1 + 2c) = 1 \qquad [8]$$

since, according to Eqs. [5] - [7],

$$\lambda_\theta^2 = 1 + 2a \qquad [9]$$

$$\lambda_z^2 = 1 + 2b \qquad [10]$$

$$\lambda_r^2 = 1 + 2c \qquad [11]$$

From Eq. [8] we see that only two of the three Green-St. Venant strains a, b, and c can be independently prescribed. Note that in the undeformed configuration $\lambda_\theta = \lambda_z = \lambda_r = 1$ and $a = b = c = 0$. The state of stress in a thin-walled segment can be described in terms of the three normal stresses S_θ, S_z, and S_r, in the θ, z, and r directions, respectively. In terms of the intravascular pressure and the longitudinal force, the stresses are given by

$$S_\theta = P\left(\frac{R}{h} - \frac{1}{2}\right) \qquad [12]$$

$$S_z = P\left(\frac{R}{2h} - \frac{1}{2}\right) + \frac{F}{2\pi Rh} \quad [13]$$

$$S_r = -P/2 \quad [14]$$

Equations [12] and [13] are obtained from simple equilibrium considerations (4,16). Equation [14] arbitrarily assigns a value to S_r equal to the mean of the values at the intimal and the adventitial surfaces. We note that the stresses given by Eqs. [12] - [14] are the "true" or Cauchy stresses and represent the forces on unit area elements perpendicular to the θ, z, and r axes in the deformed configuration.

The elastic response of the tissue, under physiological deformation, can be characterized by determining the relation between the state of stress given by S_θ, S_z, and S_r and the state of deformation given by λ_θ, λ_z, and λ_r or a, b, and c. For an incompressible material the state of strain is described by only two quantities, for example, λ_θ and λ_z or a and b. However, these quantities determine the stresses to only within a hydrostatic pressure since addition of an arbitrary amount of hydrostatic pressure to a deformed incompressible tissue cannot change its deformation and therefore cannot be determined from the deformation. Therefore, for an incompressible material only the non-hydrostatic or the deviatoric part of the stress can be determined from the knowledge of the deformation. However, the components of the deviatoric part, namely, $S_\theta - S_h$, $S_z - S_h$, and $S_r - S_h$, where $S_h = 1/3(S_\theta + S_z + S_r)$ is the hydrostatic stress, can all be determined from the knowledge of a pair of stress differences such as $S_\theta - S_r$ and $S_z - S_r$. The constitutive relation for the tissue can therefore be written as

$$S_\theta - S_r = (1 + 2a)f(a,b) \quad [15]$$

$$S_z - S_r = (1 + 2b)g(a,b) \quad [16]$$

where f and g are arbitrary functions of a and b. The factors $(1 + 2a) = \lambda_\theta^2$ and $(1 + 2b) = \lambda_z^2$ are introduced in Eqs. [15] and [16] for later convenience.

For practical application, the forms of the functions f and g must be determined. To this end one must postulate the functional forms on the basis of preliminary analyses or observations, and then carry out proper experiments to determine if these forms consistently describe the tissue behavior reasonably well over the range of variables studied. If functional forms are validated by means of experiments covering a physiologically significant domain of independent variables, these forms can be used as phenomenological descriptors of the tissue response. For example, we may assume that the functions f and g are polynomials in a and b. Then Eqs. 15 and 16 become

$$S_\theta - S_r = (1 + 2a)(A_0 + A_1a + A_2b + A_3a^2 + A_4ab + A_5b^2) \quad [17]$$

$$S_z - S_r = (1 + 2b)(B_0 + B_1a + B_2b + B_3a^2 + B_4ab + B_5b^2) \quad [18]$$

if we restrict the polynomials to contain terms in a and b of degree two. If we require that the undeformed configuration is stress-free, the constitutive parameters A_0 and B_0 can be set to zero. If we restrict the polynomials to contain only the first order terms in a and b, we get the first-order formulation given by

$$S_\theta - S_r = (1 + 2a)(A_0 + A_1a + A_2b) \quad [19]$$

$$S_z - S_r = (1 + 2b)(B_0 + B_1a + B_xb) \quad [20]$$

We may write various higher-order representations by including terms containing higher powers of a and b. We may of course postulate representations containing selected terms of various orders if a priori observations support it. If the constitutive constants in Eqs. [17] and [18] or in [19] and [20] were known, these equations could be used to evaluate $S_\theta - S_r$ and $S_z - S_r$ for any given state of deformation within the domain of applicability.

If we set $A_0 = B_0 = 0$, then Eqs. [17] and [18] contain ten unknown constitutive parameters, and Eqs. [19] and [20] contain four. Experimentally, by determining $S_\theta - S_r$ and $S_z - S_r$ corresponding to a pair of values of a and b, we obtain two equations corresponding to each state of deformation. Thus a minimum of five and two states of deformations, respectively, are required to determine the constitutive constants in Eqs. [17] and [18] or in [19] and [20]. More states of deformations provide additional equations which would permit a least-squares solution for the constitutive constants.

Equations [17] and [18] and [19] and [20] simplify somewhat if we assume that the tissue is hyperelastic, that is, there exists for the tissue a stored-energy or strain-energy

Vol. 17
1980

function W(a,b) which is a unique function of a and b. If W represents the energy stored by a unit volume of the undeformed configuration (which for an incompressible material is the same as the volume in the deformed configuration) the stress differences $S_\theta - S_r$ and $S_z - S_r$ are given by the expressions (4,16,17)

$$S_\theta - S_r = \lambda_\theta \frac{\partial W}{\partial \lambda_\theta} = \lambda_\theta^2 \frac{\partial W}{\partial a} = (1 + 2a)\frac{\partial W}{\partial a} \qquad [21]$$

$$S_z - S_r = \lambda_z \frac{\partial W}{\partial \lambda_z} = \lambda_z^2 \frac{\partial W}{\partial b} = (1 + 2b)\frac{\partial W}{\partial b} \qquad [22]$$

If W(a,b) is assumed to be of a polynomial form, for example, as

$$W(a,b) = Aa^2 + Bab + Cb^2 + Da^3 + Ea^2b + Fab^2 + Gb^3 \qquad [23]$$

or as

$$W(a,b) = Aa^2 + Bab + Cb^2 \qquad [24]$$

we get from Eqs. [21] and [22],

$$S_\theta - S_r = (1 + 2a)(2Aa + Bb + 2Da^2 + 2Eab + Fb^2) \qquad [25]$$

$$S_z - S_r = (1 + 2b)(Ba + 2Cb + Ea^2 + 2Fab + 3Gb^2) \qquad [26]$$

or

$$S_\theta - S_r = (1 + 2a)(2Aa + Bb) \qquad [27]$$

$$S_z - S_r = (1 + 2b)(Ba + 2Cb) \qquad [28]$$

for the formulations of W given by Eqs. [23] and [24], respectively. We note that Eqs. [17] and [18] reduce to Eqs. [25] and [26] and Eqs. [19] and [20] to Eqs. [27] and [28] if

$$A_2 = B_1 = B; \quad A_4 = 2B_3 = 2E; \quad 2A_5 = B_4 = 2F \qquad [29]$$

Vaishnav et al (8) carried out experiments on segments from middle descending thoracic aortas of dogs for experimental determination of the elastic constitutive constants. Typically, an 8-cm long segment was preconditioned by subjecting it to two cycles of inflation and deflation over a range of 25-200 cm H_2O pressure. The vessel was connected to a reservoir filled with oxygenated blood at room temperature (26-28°C) and the intraluminal pressure was varied from 20 to 200 cm H_2O in steps of 25 cm H_2O. At each step of pressure, five levels of extra longitudinal force (0, 25, 50, 75, 100 g) were applied in addition to the longitudinal force due to the intravascular pressure. Throughout the experiment the vessel segment was kept moist using saline at room temperature. The length of the segment and the external diameter of the segment were recorded at each level of pressure and longitudinal force. Subsequent to the experiment the segment was slit open longitudinally and its volume and undeformed configuration dimensions were determined. The Green-St. Venant strains a and b and the stresses at each data point were determined using Eqs. [1] - [7] and Eqs. [12] - [14]. A λ_θ range of 1.12 to 1.82 and a λ_z range of 1.17 to 1.60 were covered by these experiments. Eight equations from 40 data points were solved simultaneously for the seven and three constitutive constants using the method of least squares. Average values of these constants are given in Table 1. An analysis of goodness-of-fit of the two models showed that the seven-constant constitutive model fit the experimental data very well. The fit of the three-constant model was considered fair, but adequate for qualitative considerations. For further details, see Vaishnav et al (8).

1

TABLE

Average Values (± SEM) of Nonlinear Elastic Constitutive Constants From In Vitro Experiments on Segments of the Middle Descending Thoracic Aortas From 13 Dogs Based on Assuming Uniform Wall Stress Distribution

Constant	3-Constant Formulation	7-Constant Formulation
	$dyn/cm^2 \times 10^3$	$dyn/cm^2 \times 10^3$
A	332 ± 11	323 ± 19
B	315 ± 18	34 ± 54
C	252 ± 14	247 ± 20
D		25 ± 12
E		68 ± 28
F		862 ± 411
G		-41 ± 32

Adapted from (8) ; reproduced by permission of The Rockefeller University Press.

In a subsequent paper, Vaishnav et al (9) outlined a procedure for determination of the constitutive constants without invoking the assumption that the circumferential stresses are uniformly distributed through the thickness of the arterial wall, and computed the distribution of the circumferential and the longitudinal stresses in the arterial wall. Table 2 gives the constitutive constants based on the thick-wall theory. A comparison of Table 3 with Table 2 shows that properly accounting for the distribution of stresses through the

2

TABLE

Average Values (± SEM) of Nonlinear Elastic Constitutive Constants From In Vitro Experiments on Segments of the Middle Descending Thoracic Aortas From 13 Dogs Based on Assuming Nonuniform Distribution of Circumferential Stress Through the Wall Thickness

Constant	3-Constant Formulation	7-Constant Formulation
	$dyn/cm^2 \times 10^3$	$dyn/cm^2 \times 10^3$
A	266 ± 13	342 ± 24
B	386 ± 30	-35 ± 59
C	185 ± 18	302 ± 32
D		-58 ± 9
E		220 ± 31
F		111 ± 75
G		-57 ± 40

Adapted from (9); reproduced by permission of American Heart Association, Inc.

vessel wall has a significant effect on the constitutive constants. Therefore, in critical work the coefficients should be calculated on the basis of the thick-wall theory. It is these corrected constants that would correspond to those one would obtain using a two-dimensional test on a rectangular specimen of an arterial segment. Table 3 shows the effect of intravascular pressure on the peak values of stresses and strain energy density at the

Vol. 17
1980

intimal surface. Note that increasing the intravascular pressure from 100 to 150 cm H_2O causes a more than two-fold increase in the values of peak circumferential stress and the strain energy density.

3

TABLE

Effect of Intravascular Pressure on Stresses and Strain Energy Density at the Endothelial Surface

				Normalized Values at the Endothelial Surface			
($cm^P H_2O$)	λ_θ	λ_z	R/h	S_θ	S_z	S_r	W
100	1.39	1.48	10.5	1	1	1	1
125	1.52	1.48	12.3	1.48	1.18	1.26	1.49
150	1.66	1.48	14.6	2.10	1.51	1.52	2.22

P = intraluminal pressure, λ_θ = circumferential stretch, λ_z = longitudinal stretch, R/h = ratio of midwall radius to thickness, S_θ = circumferential stress, S_z = longitudinal stress, S_r = radial stress, and W = strain energy density. Reproduced from (9) by permission of American Heart Association, Inc.

VISCOELASTIC RESPONSE OF THE TISSUE

Although in the preceding development we treated the arterial tissue as elastic (or hyperelastic), it is in fact viscoelastic. When an arterial strip is subjected to a sinusoidal stress of small amplitude, the resulting sinusoidal strain lags the stress by a small amount. Under a constant stress, the tissue deformation gradually increases. When held at a constant deformation, the stress in the tissue relaxes. To account for this viscoelastic behavior we need a nonlinear viscoelastic formulation for the arterial tissue. We therefore outline briefly our own work in this area. For details see (10 and (11).

We use as our starting point the constitutive relations

$$S_\theta(t) - S_r(t) = [1 + 2a(t)]\,\mathcal{F}_{\tau=-\infty}^{t}[a(\tau), b(\tau)] \qquad [30]$$

$$S_z(t) - S_r(t) = [1 + 2b(t)]\,\mathcal{G}_{\tau=-\infty}^{t}[a(\tau), b(\tau)] \qquad [31]$$

where $\mathcal{F}$ and $\mathcal{G}$ are functionals of the arguments $a(\tau)$ and $b(\tau)$, which, in turn, are the histories of the Green-St. Venant strains undergone by the tissue from the distant past ($\tau = -\infty$) to the present time ($\tau = t$). Equations [31] and [32] are generalizations of Eqs. [15] and [16]. They are based on assuming that the tissue is incompressible and curvilinarly orthotropic and that we are interested in considering only physiological loading of the tissue. To develop a practically tractable formulation, we expand the functions $\mathcal{F}$ and $\mathcal{G}$ in Eqs. [30] and [31] into a series of multiple integrals and arbitrarily restrict the expansion to terms involving the first and second order integrals only. Accordingly we have

$$\begin{aligned} S_\theta(t) - S_r(t) = [1 + 2a(t)][&\int_{-\infty}^{t} A_1(t-\tau)\dot{a}(\tau)d\tau + \int_{-\infty}^{t} A_2(t-\tau)\dot{b}(\tau)d \\ &+ \int_{-\infty}^{t}\int_{-\infty}^{t} A_3(t-\tau_1, t-\tau_2)\dot{a}(\tau_1)\dot{a}(\tau_2)d\tau_1 d\tau_2 \\ &+ \int_{-\infty}^{t}\int_{-\infty}^{t} A_4(t-\tau_1, t-\tau_2)\dot{a}(\tau_1)\dot{b}(\tau_2)d\tau_1 d\tau_2 \\ &+ \int_{-\infty}^{t}\int_{-\infty}^{t} A_5(t-\tau_1, t-\tau_2)\dot{b}(\tau_1)\dot{b}(\tau_2)d\tau_1 d\tau_2] \end{aligned} \qquad [32]$$

$$S_z(t) - S_r(t) = [1 + 2b(t)][\int_{-\infty}^{t} B_1(t-\tau)\dot{a}(\tau)d\tau + \int_{-\infty}^{t} B_2(t-\tau)\dot{b}(\tau)d\tau + \int_{-\infty}^{t}\int_{-\infty}^{t} B_3(t-\tau_1, t-\tau_2)\dot{a}(\tau_1)\dot{a}(\tau_2)d\tau_1 d\tau_2 + \int_{-\infty}^{t}\int_{-\infty}^{t} B_4(t-\tau_1, t-\tau_2)\dot{a}(\tau_1)\dot{b}(\tau_2)d\tau_1 d\tau_2 + \int_{-\infty}^{t}\int_{-\infty}^{t} B_5(t-\tau_1, t-\tau_2)\dot{b}(\tau_1)\dot{b}(\tau_2)d\tau_1 d\tau_2] \quad [33]$$

where a dot denotes differentiation with respect to τ.

Equations [32] and [33] are the viscoelastic counterparts of Eqs. [17] and [18] and contain 10 constitutive kernel functions, $A_1, \ldots, A_5$, $B_1, \ldots, B_5$ which must be determined experimentally. Once these are determined, and the formulation judged to be satisfactory, Eqs. [32] and [33] can be used to compute stress differences at any time corresponding to prescribed histories of the strains a and b.

By dropping the second-order kernel functions A_3, A_4, A_5, B_3, B_4, and B_5, we get a simpler four-function formulation which can be used in a similar manner. This formulation would be the viscoelastic counterpart of Eqs. [19] and [20].

Young et al (10) experimentally determined the constitutive functions for the viscoelastic formulation by performing experiments on canine aortic segments. Thirty-eight steps in radial and longitudinal strains were simultaneously applied and the relaxation of the intravascular pressure and the longitudinal force continuously recorded. Each state of strain was maintained for 100 sec. At the end of the experiment the dimensions of the segment in the undeformed state were measured. In these experiments the step in λ_θ ranged in value from 1.17 to 1.82 and that in λ_z ranged in value from 1.28 to 1.61. Using this experimental data, values of relaxation functions for the 10- and 4-function formulations were computed for 20 different instants of time. Table 4 presents the average relaxation functions in the form $K(t) = K_f + (K_i - K_f)\exp(-\alpha t^{-\beta})$ which was found to describe all functions well. In this form K_f denotes the final value of K(t), K_i the initial value and α and β are empirical parameters. Because of the difficulties associated with the determination of the values of P and F at low values of t, the fitted values of K_i may not be quite accurate.

Vol. 17
1980

4

TABLE

The Average Relaxation Functions ($dyn/cm^2 \times 10^3$) for the Middle Descending Thoracic Aortas From 7 Dogs Expressed in the form $K(t) = K_f + (K_i - K_f)\exp(\alpha t^{-\beta})$

	4-Function	10-Function
$A_1(t)$	$564 + 44\exp(-0.47t^{0.47})$	$494 + 46\exp(-0.23t^{0.57})$
$A_2(t)$	179	$189 - 19\exp(-0.06t^{0.82})$
$A_3(t,t)$		51
$A_4(t,t)$		$-8 - 14\exp(-0.16t^{0.50})$
$A_5(t,t)$		$29 + 28\exp(-0.25t^{0.50})$
$B_1(t)$	$270 + 16\exp(-1.67t^{0.22})$	32
$B_2(t)$	$534 + 56\exp(-0.51t^{0.44})$	640
$B_3(t,t)$		$200 + 22\exp(-0.66t^{0.61})$
$B_4(t,t)$		$-26 - 34\exp(-0.34t^{0.53})$
$B_5(t,t)$		$30 + 75\exp(-0.22t^{0.61})$

Adapted from (10); reproduced by permission of Pergamon Press, Inc.

A NOTE ON THE THERMOVISCOELASTIC RESPONSE OF THE TISSUE

We have recently developed a formulation for describing the thermoviscoelastic response of an incompressible, curvilinearly orthotropic viscoelastic tissue under physiological loading. To develop this formulation we express the stress tensor, heat flux vector, specific internal energy and the specific entropy as functionals of the histories of deformation

and temperature. By applying various general restrictions and restrictions arising from the nature of the tissue, we arrive at a thermoviscoelastic formulation for the arterial tissue. We are in the process of developing an experimental approach to arrive at the appropriate constitutive functions.

ACKNOWLEDGMENTS

I acknowledge with thanks the contribution of my former student Dr. J. T. Young who collaborated with me in the elastic and viscoelastic characterizations. I am particularly grateful to Dr. D. L. Fry in whose laboratory at The National Institutes of Health the experimental work was carried out, and Dr. D. J. Patel, who has been my collaborator in most of my work in vascular rheology. Support of NSF Grant ENG76-02911 is gratefully acknowledged.

REFERENCES

1. BERGEL, D. H. The visco-elastic properties of the arterial wall. Ph.D. Thesis, University of London, 1960.

2. McDONALD, D. Blood Flow in Arteries. Baltimore: Williams and Wilkins, 1974, 396 p.

3. PATEL, D. J. and VAISHNAV, R. N. The rheology of large blood vessels. In: Cardiovascular Fluid Dynamics. Academic Press, 1972, Vol. 2, pp. 1-64.

4. PATEL, D. J., VAISHNAV, R. N., GOW, B. S., and KOT, P. A. Hemodynamics. Annual Reviews of Physiology, Annuals Reviews, Inc., Palo Alto, Calif., 36, 125-154, 1974.

5. ROACH, M. R. Biophysical analyses of blood vessel walls and blood flow. Annual Reviews of Physiology, Annual Reviews, Inc., Palo Alto, Calif., 39, 51-71, 1977.

6. FUNG, Y. C. B. Biomechanics, its scope, history, and some problems of continuum mechanics in physiology. Applied Mechanics Reviews 21, 1-20, 1968.

7. DOBRIN, P. B. Mechanical properties of arteries. Physiological Reviews 58, 397-460, 1978.

8. VAISHNAV, R. N., YOUNG, J. T., JANICKI, J., and PATEL, D. J. Nonlinear anisotropic elastic properties of the canine aorta. Biophysical Journal 12, 1008-1027, 1972.

9. VAISHNAV, R. N., YOUNG, J. T., and PATEL, D. J. Distribution of stresses and of strain energy density through wall thickness in a canine aortic segment. Circulation Research 32, 577-583, 1973.

10. YOUNG, J. T., VAISHNAV, R. N. and PATEL, D. J. Nonlinear anisotropic viscoelastic properties of canine arterial segments. Journal of Biomechanics 10, 549-559, 1977.

11. VAISHNAV, R. N., YOUNG, J. T., and PATEL, D. J. Nonlinear viscoelasticity of large blood vessels. Chapter 16 in: Cardiovascular System Dynamics. J. Baan, A. Noordergraaf, and J. Raines (Eds.). The M.I.T. Press, 1978, pp. 140-153.

12. CAREW, T. E., VAISHNAV, R. N., and PATEL, D. J. Compressibility of the arterial wall. Circulation Research 23, 61-68, 1968.

13. PATEL, D. J. and FRY, D. L. The elastic symmetry of arterial segments in dogs. Circulation Research 24, 1-8, 1969.

14. FUNG, Y. C. B. Rheology of blood vessels. In: Microcirculation. G. Kaley and B. M. Altura (Eds.), Baltimore, Md.: University Park Press, Vol. 1, pp. 299-327.

15. FUNG, Y. C. B. Mechanical properties of blood vessels. In: Peripheral Circulation. P. C. Johnson (Ed), New York: John Wiley and Sons, 1978, pp. 45-79.

16. PATEL, D. J. and VAISHNAV, R. N. Basic Hemodynamics. Baltimore, Md.: University Park Press, 1980. (In Press).

17. BIOT, M. Mechanics of Incremental Deformations. New York: John Wiley and Sons, 1965, 504 p.

BIORHEOLOGY, Vol. 17, pp. 227-234, 1980
Printed in the USA. All rights reserved.

0006-355X/80/030227-08$02.00/0
Copyright (c) 1980 Pergamon Press Ltd

THIRD INTERNATIONAL CONGRESS OF BIORHEOLOGY

SYMPOSIUM ON RHEOLOGY OF BLOOD VESSELS

MECHANICAL PROPERTIES OF ARTERIES AS A FUNCTION OF TOPOGRAPHY AND AGE

K. Fronek and Y. C. Fung

Department of AMES-Bioengineering,
University of California, San Diego

(Received 30.5.1980. Guest Editor's Contribution Invited by Editor-in-Chief A.L. Copley)

ABSTRACT

Mechanical properties of the arteries have been analyzed from mathematical and physiological viewpoints. 1)A mathematical expression of stress-strain relationship should fit experimental data over the full range and the parameters should correlate experimental variables systematically. For this purpose two forms of strain energy function were compared: polynomial and exponential. The efficacy of the mathematical presentation was tested in terms of the ability to fit the experimental data over full range of strains of interest and in terms of the usefulness of the parameters in distinguishing the members of a family of stress-strain curves. In both cases, the exponential strain energy function exhibits less variations of the constants, the fit with experimental data is better and it is easier to ascribe physical meaning to the constants. 2)The stress-strain relationship was analyzed in relation to the topography and age with the special reference to the physiological pressure range. The compliance decreases from the carotid artery caudad to the iliac arteries. It is assumed, that the change in compliance is determined by the structural configuration of the connective tissue fibers since no correlation of mechanical properties was found neither with collagen nor with elastin content or with their relative ratio. With age, the compliance of rabbit arteries further increases. All arteries, regardless of topography or age, had no significant differences in the circumferential stresses over the physiological pressure range. On the other hand, circumferential strain seems to be a good index of the mechanical properties in various arteries.

Vol. 17
1980

INTRODUCTION

Mechanical properties of the arterial wall are not only important as factors influencing circulatory hemodynamics, but may serve also as indices of various physiological and pathophysiological conditions. Our main area of interest are changes in the arterial wall due to a variety of endogeneous and exogeneous influences covering different physiologic and pathophysiologic conditions (e.g. aging, atherosclerosis). Obviously, the mechanical properties of the arterial wall could serve as one of the clinically investigated functions.

In view of the complexity of the topic, from the methodological as well as analytical point of view, we investigated the experimental and analytical approaches which would yield the most sensitive and specific differentiation and at the same time simple enough to permit the evaluation of large experimental series.

The first part of this presentation is devoted to methodology - experimental and analytical. The second part includes examples from several experimental series in which the influence of topography and age is examined.

METHODOLOGY

On perusing the literature and summarizing our initial experience, it seems necessary to identify all the factors that may influence the experimental results on the mechanical properties of the arteries, and try to develop a protocol that will reduce variation of experimental data caused by experimental procedure. Then an analytical approach should be developed which is simple enough to be used routinely and at the same time sufficiently reliable. In the following, we shall first describe our experimental procedure and equipment, then discuss the experimental parameters and sources of variation of experimental data. An analytical investigation then follows.

Selected rabbit arteries were cannulated from both ends and quickly removed from anesthetized animals. One end of the artery was connected to a fixed support with a T junction, where a pressure transducer (Micron Instr. M-15) and a pressure bottle were connected. The other end of the artery was connected to the arm of a balance via a force transducer (Statham green cell) which recorded the force necessary to maintain the vessel at its in vivo length. Axial stress changes were introduced by a slide mechanism on which the balance arms were fixed.

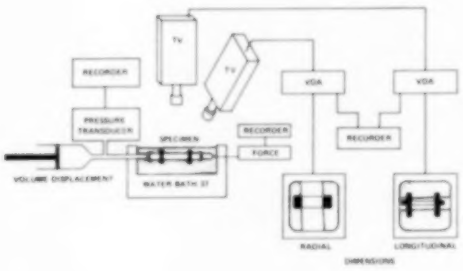

FIG. 1

Dimensional changes in the blood vessels are sensed optically be means of a closed-circuit television system and a video-dimensional analyzer (VDA). We used two VDA's connected to two television cameras which were positioned perpendicular to each other in order to monitor changes in longitudinal and transverse dimensions. The silk tags provided the needed optical contrast in the longitudinal direction. Suitable darkening of the background of the saline bath was necessary to display the vessel in a spotlight in order to obtain the necessary optical density contrast in measuring the vessel diameter. Following the acquisition of a good image, the dimensional changes were tracked automatically (1).

The vessel was preconditioned. During the experimental run, the vessel was pressurized via a pressure bottle from 0 to 180 mmHg. Three runs were recorded for each vessel, which was maintained at its in vivo length. The diameter changes were continuously monitored while the pressure was varied.

The unstretched vessel wall thickness (h_o) was determined microscopically. From the initial length (L_o), the outer diameter (D_o) and the wall thickness (h_o) the blood vessel volume was calculated. Under the assumption that the arterial wall is incompressible, the thickness (h) was calculated for each pressure level.

The following methodologic questions were analyzed:

1. The effect of the initial length.

During all experiments the in vivo length was reproduced in vitro. Because some arteries are dissected from the animal in an unphysiological position - as for instance the carotid artery, the accuracy of measurement of the in vivo length can be questioned.

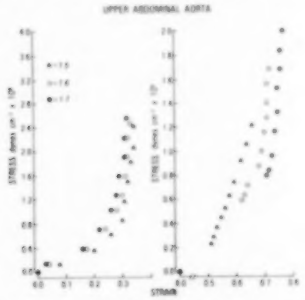

FIG. 2

The figure illustrates the influence of the three different longitudinal extension ratios on the circumferential stress as given by the left hand panel. The right hand panel illustrates the variation in stress in longitudinal direction during a pressure cycle, even when the longitudinal extension ratio is "maintained". Some changes in longitudinal direction could always be detected.

2. The effect of different stress loading.

In a series of experiments two different types of stress loading were analyzed: a, continuous pressurization at 2 cycles per minute and b, stepwise pressurization, each step lasting for 20 seconds. These two different techniques yielded the same stress-strain relationship. No significant difference was found in the final results.

3. The effect of smooth muscle.

In order to eliminate possible sources of variability which may be contributed by smooth muscle reactivity, the stress and strain relationship of the carotid artery was determined first in a bath using a standard oxygenated Krebs solution and then in a bath containing calcium free Krebs solution with EGTA to eliminate completely the effect of smooth muscle tone. Comparison of these two sets of data showed that there was no significant difference in the stress-strain relationship, indicating that vascular smooth muscle in non-activated state does not affect the overall mechanical properties of the arteries.

4. Forms of mathematical expression.

It is well known that the arteries are inelastic, anistropic and their stress-strain relationship is not linear. Since these properties are interrelated, it is quite difficult to describe the mechanical properties of arteries in a simple but accurate form. A practical solution of this problem is needed when one wishes to express the variations observed due to topography, aging, or experimental interventions. A more comprehensive treatment of this topic was recently described (2) and in the following only a brief outline is given so far as it pertains to the present discussion.

In spite of the fact that there is a large variety of mathematical expressions to describe the stress-strain relationship in uniaxial tests, in the case of biaxial or triaxial tests the selection can be reduced to the application of polynomials (3-6) or exponential functions (7-19).

The problem is reduced to the experimental measurement of strain energy function $\rho_o W^{(2)}$ as a function of strain in the circumferential and axial directions, $E_{\theta\theta}$ and E_{zz} respectively. Capital letter E is used here for the finite strain defined in the sense of Green's strain. A form of strain energy function used by Patel and Vaishnav (5) is

$$\rho_o W^{(2)} = Aa^2 + Bab + Cb^2 + Da^3 + Ea^2b + Fab^2 + Gb^3 \qquad (1)$$

where $a = E_{\theta\theta}$, $b = E_{zz}$, and A, B, ...G are material constants. As it can be seen, there are seven constants in this polynomial.

As an alternative, we proposed the following exponential strain energy function:

$$\rho_o W^{(2)} = \frac{C}{2} \exp \left[a_1 E_{\theta\theta}^2 + a_2 E_{zz}^2 + 2a_4 E_{\theta\theta} E_{zz} \right] \qquad (2)$$

where C, a_1, a_2 and a_4 are four material constants. We applied these two approaches to our experimental results obtained from the carotid artery, upper and lower abdominal aorta and iliac artery.

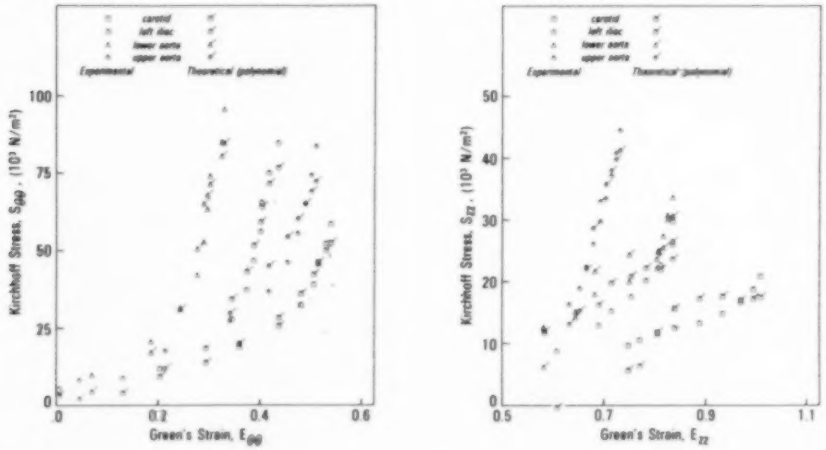

FIG. 3

Comparison of the stress-strain relationships obtained from polynomial strain energy function given by Eq. 1 with experimental data on four normal rabbit arteries. The symbols are defined in the upper left corner. Left side shows $S_{\theta\theta}$ vs $E_{\theta\theta}$. The right side shows S_{zz} vs

E_{zz}. The curves joining experimental data points (read from digital voltmeter) are not always smooth because stresses and strains in the two dimensions are coupled and any disturbances in E_{zz} results in a kink in the $S_{\theta\theta}$ vs $E_{\theta\theta}$ curve, and vice versa. Figure 4 shows a similar comparison of experimental results with the exponential strain energy function given in Eq. 2.

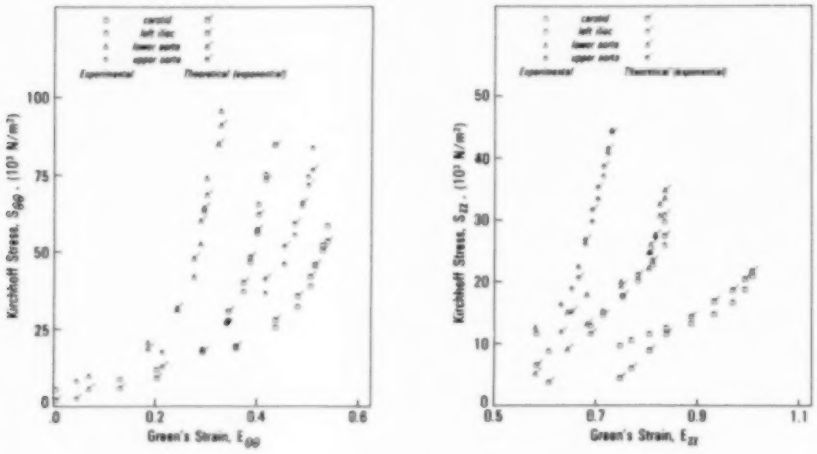

FIG. 4

Comparison of the stress-strain relationships obtained from the exponential strain energy function given by Eq. 2 with experimental data on four normal rabbit arteries. The symbols are defined in the upper left corner. Left side shows $S_{\theta\theta}$ vs $E_{\theta\theta}$. Right side shows S_{zz} vs E_{zz}. The curves joining experimental data points (read from digital voltmeter) are not always smooth because stresses and strains in the two dimensions are coupled and any disturbance in E_{zz} results in a kink in the $S_{\theta\theta}$ vs $E_{\theta\theta}$ curve, and vice versa. It can be seen that the correlation is better and it is also easier to ascribe physical meaning to a smaller number of constants.

TOPOGRAPHICAL AND MECHANICAL PROPERTIES

The examination of stress and strain in different arteries is important for the following reasons: a. It represents a frame of reference for future studies. b. Difference in stress-strain relationship may offer some clues to the intriguing yet unanswered question of varying incidence of atherosclerosis in different arteries.

Topographical differences of stress-strain relationship.

In an analysis of the stress-strain relationships of the carotid artery, upper and lower abdominal aorta and iliac artery obtained in earlier stages of our investigation, it was found that the carotid artery is more compliant and that the compliance decreases towards the iliac artery. (See Fig. 5)

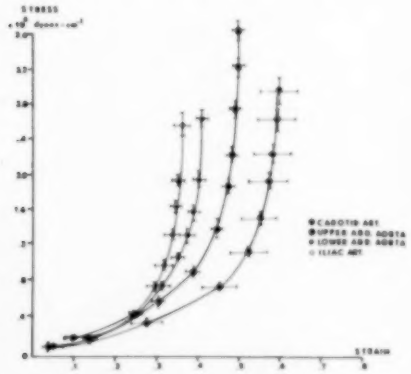

FIG. 5

The decrease in compliance of the arteries in the direction from carotid to the lower body seems to represent a uniform pattern regardless of age. One can speculate that the high compliance of the carotid artery may be related to the high mobility requirements related to the anatomical location. The decreased compliance of the abdominal aorta and iliac arteries may reflect in turn, limited mobility requirements.

The application of the tangential incremental modulus (20) as function of pressure yields similar results. See Fig. 6.

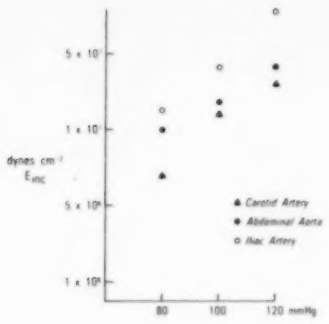

FIG. 6

The figure illustrates the incremental (tangential) modulus (E_{inc}) for the three arteries over a physiological pressure range. E_{inc} in rabbit arteries is higher than in those from dog or man. The carotid artery exhibits the lowest incremental modulus while the iliac artery has the highest incremental modulus of elasticity.

Topographic differences of circumferential stress and strain in the physiological pressure range.

In view of the topographical differences of the stress-strain relationship described above, the question arises whether it is the stress or the strain that contributes more to these differences.

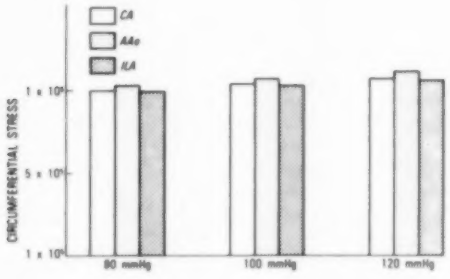

FIG. 7

The figure illustrates changes in circumferential stress (y axis) over the physiological pressure range (x axis) for three arteries studied. CA = carotid artery, AAO = abdominal aorta, ILA = common iliac artery. It shows that there are no significant differences in the stress in the three investigated samples over the range of physiological pressure.

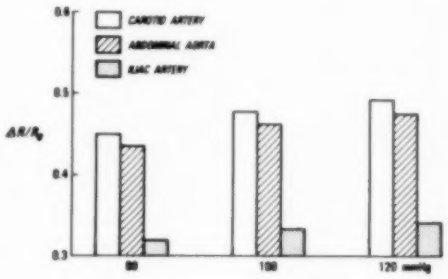

FIG. 8

Figure 8 illustrates changes in circumferential strain for the same blood vessel in the same experiment. Strain expressed as ΔR/Ro on y axis is compared over the physiological pressure range. Figure 8 documents a progressive decrease in circumferential strain along the arterial tree, the strain (for a given stress) being smallest in the iliac artery.

Correlation of chemical composition and mechanical properties.

In view of the topographic differences in mechanical properties and chemical composition of the arteries, the correlation between mechanical properties on one side and elastin and collagen on the other was investigated.

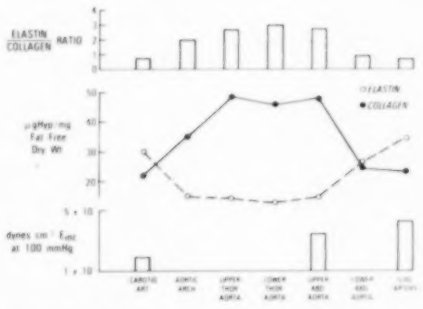

FIG. 9

Elastin and collagen content were biochemically determined in selected sections from the whole aorta taken from six rabbits. The results are normalized by the dry weight of defatted vascular tissue. These data are illustrated in the middle part of the graph. The upper part expresses the elastin collagen ratio and the bottom part gives E_{inc} at 100 mmHg for blood vessels which have been studied. As depicted, there is no relationship with mechanical properties which could be established whether relating them with content of elastin, of collagen or their ratios.

Vol. 17
1980

On the basis of this seris of experiments, we have to conclude that differences in structural configuration of these long-chain protein molecules may have a pronounced effect on the resulting mechanical properties.

The effect of age.

In order to simplify the comparison, the circumferential incremental moduli at 80, 100, and 120 mmHg for three different arteries (carotid artery, abdominal aorta and iliac artery) were compared in samples from young and old animals.

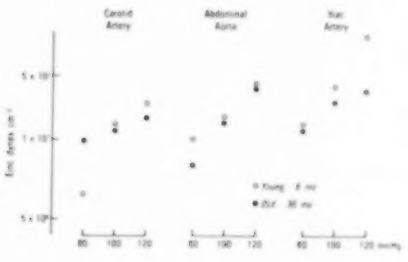

FIG. 10

The description of the figure is the same as that in Figure 6. In addition the study includes the comparison between arteries from 6 month and 36 month old rabbits. The incremental moduli were reduced in the arteries from old animals except in the carotid artery at 80 mmHg.

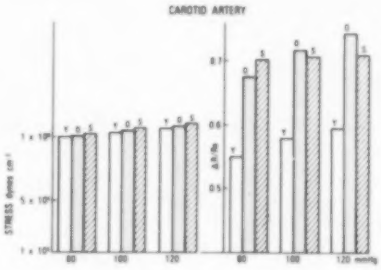

FIG. 11

Description of this graph is the same as in Figure 7 and 8. Column labelled "Y" illustrates the results from 6 month old animals. "O" column are for the blood vessels from old animals. "S" stands for blood vessels from chemically sympathectomized rabbits.

Finally, changes in stress and strain were examined as to their participation in the age induced differences.

As depicted in Figure 11 in the carotid artery there was no significant change in stress, while the circumferential strain in arterial samples from older animals was significantly higher (in the physiological pressure range). Similar results were obtained from the abdominal aorta and from the iliac artery as well.

Although it is generally accepted that human arteries become stiffer with increasing age, there is an uncertainty whether the same sequence of events applies to arteries of experimental animals, e.g. rats and rabbits. Hume (21) and Berry, et al (22) were able to show that adult rat aortas up to 600 days old do not exhibit any changes in elasticity Saxton (23) has demonstrated a decrease in the modulus of elasticity with age in the thoracic aorta segment of rabbits.

In humans, for instance, Leoroyd and Taylor (24) using human autopsy samples, observed that in the case of the thoracic aorta, the values of the incremental modulus were increased in older (older than 35 years) individuals compared to young individuals (younger than 35 years). For the peripheral arteries, e.g. the femoral and common iliac artery, however, this relationship was reversed with the younger having a higher elastic modulus as illustrated in Figure 12 which is based on data from Learoyd and Taylor's paper (24).

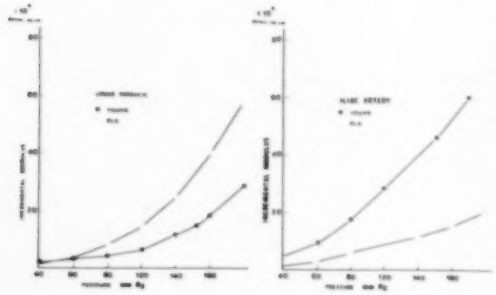

FIG. 12

The incremental modulus is expressed as function of pressure. Human arteries from young subjects and older subjects are compared. The left side illustrates this relationship for the thoracic aorta, the right side is for the femoral arteries.

Leoroyd and Taylor see the reason for this behavior of mechanical properties in the change of the relationship of the wall thickness and inner radius with age. The wall thickness increases with age, but the radius increases proportionally less. In addition this change is coupled with increased circumferential strain of the vessel at the given pressure. The calculated incremental modulus is influenced by combination of both factors. It is conceivable that arteries become, with age, more distensible in the circumferential direction and only when coupled with decreased ratio of wall thickness and radius, the incremental modulus may increase.

The circumstance that the age-related changes can be detected in changes of circumferential strain rather than stress, may turn out to be rather helpful from a clinical diagnostic point. It is well known that currently there are no reliable techniques available which would permit to identify non-invasively, the mechanical properties in man as a function of age or atherosclerosis. In view of the described results and with the advent of ultrasonic dynamic imaging, this question can be now focused, mainly because the circumferential strain changes can be monitored.

SUMMARY AND CONCLUSIONS

1. Experimental methodology used may influence the resulting characteristics of mechanical properties and therefore must be carefully defined.

2. The four-constant exponential expression represents very well the actual stress-strain relationship. The smaller number of constants makes this approach more practical and physiologically more meaningful.

3. Collagen, elastin or their ratios has no direct relationship with observed mechanical properties. It seems that the structural configuration has a more pronounced effect.

4. Changes in circumferential strain are good indices of changes in mechanical properties of different arteries in the rabbit. In contrast, circumferential stress at 100 mmHg pressure seems to be the same in all investigated arteries irrespective of the sites.

5. Similarly, circumferential stress at 100 mmHg intramural pressure seems to be the same in all arteries from young and old rabbits, while the circumferential strain is increased in old animals.

REFERENCES

1. FRONEK, K., SCHMID SCHOENBEIN, G. and FUNG, Y. C. A non-contact method for three-dimensional analysis of vascular elasticity in vivo and in vitro. J. Appl. Physiol. 40, 634-637, 1976.

2. FUNG, Y. C., FRONEK, K. and PATITUCCI, P. Pseudoelasticity of arteries and the choice of its mathematical expression. Am. J. Physiol. 237(5), H620-H631, 1979.

3. GREENFIELD, J. C. and PATEL, D. J. Relation between pressure and diameter in the ascending aorta of man. Circ. Res. 10, 778-781, 1962.

4. PATEL, D. J. and VAISHNAV, R. N. The rheology of large blood vessels. In: Cardiovascular Fluid Dynamics, D. H. Bergel (Ed). Academic, New York, Vol. 2, Chapter 11, p. 2-65, 1972.

5. VAISHNAV, R. N., YOUNG, J. T., JANICKI, J. S. and PATEL, D. J. Nonlinear anisotropic elastic properties of the canine aorta. Biophys. J. 12, 1008-1027, 1972.

6. WESLEY, R. L. R., VAISHNAV, R. N., FUCHS, J. C. A., PATEL, D. J. and GREENFIELD, J. C. Static linear and nonlinear elastic properties of normal and arterialized venous tissue in dog and man. Circ. Res. 37, 509-520, 1975.

7. AYORINDE, O. A., KOBAYASHI, A. S. and MERATI, J. K. Finite elasticity analysis of unanesthetized and anesthetized aorta. In: Proceedings of the Biomechanics Symposium, ASME, 1975, p. 79.

8. BRANKOV, G., RACHEV, A. and STOYCHEVE, S. On the mechanical behavior of blood vessels. Biomechanica, Bulgarian Acad. Sci. Sofia 1, 27-37, 1974.

9. DEMIRAY, H. J. A note on the elasticity of soft biological tissue. J. Biomech. 5, 309-311, 1972.

Vol. 17
1980

10. FUNG, Y. C. Stress-strain history relations of soft tissues in simple elongation. In: Biomechanics: Its Foundations and Objectives, Y. C. Fung, N. Perrone and M. Anliker (Eds.) Englewood Cliffs, New Jersy, Prentice-Hall, 1972, p. 181-208.

11. FUNG, Y. C. Biorheology of soft tissues. Biorheology 10, 139-155, 1973.

12. FUNG, Y. C. On mathematical models of stress-strain relationship for living soft tissues. Mech. Polymerov USSR 10, 850-867, 1975.

13. GOU, P. E. Strain energy function for biological tissues. J. Biomech. 3, 547-550, 1970.

14. HAYASHI, K. SATO, M., HANDA, H. and MORITAKE, K. Biomechanical study of the constitutive laws of vascular walls. Exp. Mech. 14, 440-444, 1974.

15. KASYANOV, V. The anisotropic nonlinear model of human large blood vessels. Mech. Polymerov USSR 874-884, 1974.

16. KASYANOV, V. and KNETS, I. Strain energy function for large human blood vessels. Mech. Polymerov USSR 122-128, 1974.

17. PURINA, B. G., VILKA, Y., KASYANOV, V. and CEDERS, E. Change of some mechanical properties of human large blood vessels with age. Mech. Polymerov USSR 129-138, 1974.

18. SNYDER R. W. Large deformation of isotropic biological tissue. J. Biomech. 5, 601-606, 1972.

19. TANAKA, T. T. and FUNG, Y. C. Elastic and inelastic properties of the canine aorta and their variation along the aortic tree. J. Biomech. 7, 357-370, 1974.

20. BERGEL, D. H. The static elastic properties of the arterial wall. J. Physiol. 156: 445-457, 1961.

21. HUME, J. F. The sensitivity of the rat's aorta as influenced by age, environmental temperature and certain toxic substances. Am. J. Hyg. Sect. A. 29, 11, 1939.

22. BERRY, C. L., GREENWALD, S. E. and RIVETT, J. F. Static mechanical properties of the developing and mature rat aorta. Cardiovasc. Res. 9, 669-678, 1975.

23. SAXTON, J.A. Jr. Elastic properties of the rabbit aorta in relation to age. Arch. Pathol. 34, 262, 274, 1942.

24. LEOROYD, B.M. and TAYLOR M. G. Alteration with age in the viscoelastic properties of human arterial walls. Circ. Res. 18, 278-292, 1966.

Vol. 198

BIORHEOLOGY, Vol. 17, pp. 235-247, 1980
Printed in the USA. All rights reserved.

0006-355X/80/030235-13$02.00/0
Copyright (c) 1980 Pergamon Press Ltd

A COMPARISON OF RHEOLOGICAL CONSTITUTIVE FUNCTIONS FOR WHOLE HUMAN BLOOD

Peter L. Easthope* and Donald E. Brooks+[1]
Departments of Pathology*+ and Chemistry+,
University of British Columbia,
Vancouver, British Columbia, Canada, V6T 1W5

(Received 22.11.1979; in revised form 29.1.1980.
Accepted by Editor G.V.F. Seaman)

ABSTRACT A constitutive function describing the flow properties of whole blood relates the shear stress measured in a viscometer to the shear rate and hematocrit of the sample. Eleven functions derived from various sources were examined for their ability to fit Couette flow data from blood from thirty-one healthy individuals, eleven of whom were using oral contraceptives. A nominal shear rate range of 0.031 to 120 s^{-1} was used at hematocrits from 0.29 to 0.55 . A non-linear curve fitting procedure allowed an ordering of the functions to be established with respect to their goodness of fit. The function first employed by Walburn and Schneck

$$T = X1 \exp(X2\ H + \frac{X4}{H^2})\ D^{1-X3\ H}$$

where T = shear stress, D = shear rate, H = hematocrit and X1 to X4 are adjustable parameters, was found to be the most successful. Population averages for the parameter values of best fit are given for the two most successful functions. There were no significant differences between the groups using and not using oral contraceptives.

Vol. 17
1980

INTRODUCTION

When a certain stress is applied to a material an associated deformation takes place. The rate at which this deformation occurs is known as the shear rate[2]. The function specifying the relationship between shear rate and stress is called the constitutive function (CF) of the material and is a characterization of its flow properties. Whereas the CF of a Newtonian fluid such as plasma is completely determined by one number, its dynamic viscosity, the CF of a non-Newtonian fluid can be considerably more complicated. The CF of blood is physically determined principally by the plasma viscosity, the flexibility of red cells and the degree of cell-cell interaction. Due to the complexity of the cellular flow process no fundamental theoretical model relating the plasma and cellular properties to the macroscopic CF has been presented. The practical value of such a function seems clear. One application, for instance, would be in the treatment of blood flow problems encountered in physiology and in the design of prosthetic devices where an analytical expression describing the flow properties of blood would be useful. A further application would be in interpretation of clinical hemorheological data. Since the cellular parameters on which the CF of blood depend vary significantly in many disease states (2) full exploitation of clinical hemorheological data might well provide hitherto unavailable diagnostic and prognostic information.

At present, major problems arise in the interpretation and comparison of clinical hemorheological data primarily because blood is a non-Newtonian fluid whose properties depend strongly upon the hematocrit, a parameter which differs between people and can change in an individual by significant amounts. To compare data from different individuals it is necessary either to prepare blood samples at a consistent hematocrit when making viscosity

Keywords: blood rheology, blood flow velocity, constitutive function, oral contraceptives.
[1] To whom correspondence should be directed.
[2] We choose shear rate = r(dw/dr) rather than (r/2)(dw/dr) (w=angular speed, r=radius); transformation of strain into cylindrical polar coordinates is explained in (1).

measurements, a procedure which is difficult experimentally, or to use some established mathematical expression to 'correct' viscosity values determined at the actual hematocrit to a standard one. To compare individuals, viscosity values must also be referred to a consistent shear rate. In a rheological examination of a blood sample, the shear rates are not accurately predetermined, particularly in the low shear rate range ($D<10s^{-1}$), since they depend upon the constitutive character of the individual sample as well as on the boundary conditions of the experimental flow field. Therefore there is difficulty in obtaining data referred to consistent conditions of hematocrit and shear rate. Yet, if actual data points are to be utilized, comparison of hemorheological information in any other way is not valid.

These problems may be overcome by fitting a function (the CF) to shear stress data derived over a range of shear rates and hematocrits and using the parameters of the function as the basis for comparison among individuals. This procedure has the additional advantage that fitting of the curve provides a statistical averaging of the data which reduces random experimental error. Use of the CF approach should facilitate comparisons of clinical hemorheological data as advocated by Huang and Fabisiak (3).

In recent years there have been several CFs presented with the intention of either achieving greater accuracy in representing experimental data or developing a stronger theoretical basis for the explanation of blood flow. The CF which has gained greatest prominence in the past is that of Casson (4). It may be written

$$T = [\, k_0^{1/2} + (k_1 D)^{1/2} \,]^2 \qquad [1]$$

where k_0 = yield stress

k_1 = viscosity parameter

Quemada (5) developed a function having zero yield stress which he showed to be an improvement over Casson's function. Phillips and Deutsch (6) hypothesized a general CF in tensor form, linear in stress, strain and their first derivatives with respect to time, thereby implying viscoelastic properties. Walburn and Schneck (7) used a computer routine which began with one independent variable and progressively added more variables until a function depending upon hematocrit, concentration of total protein less albumin and shear rate was constructed. Huang (8) has presented several expressions based upon the theory of non-equilibrium thermodynamics.

The CF which is chosen to represent clinical data should be that which, averaged over the population, conforms most closely to observations. The theoretical foundation of the function is of secondary concern, although it would be fortunate if the best fitting function had a sound theoretical basis. In the present work, CFs selected from the literature and constructed by ourselves were fit to data from a population of normal individuals and the values of the relevant parameters for each function obtained. The function of best fit was selected using a standard deviation estimator.

THEORETICAL

Our method is to consider a function $T(D,e,H,\{Xi\})$ where

- T = shear stress
- D = shear rate
- e = plasma viscosity
- H = hematocrit expressed as volume fraction
- {Xi}= set of parameters which determine the specific form and allow adjustment of the function in question; i = 1,...p

This function will be called the CF although we have tested it only in Couette flows. Moreover, the stress and shear rate referred to throughout are the values deduced from the instantaneous output signal of the rheometer in either steady state or transient flow conditions. Time dependent features do not appear in the CFs considered. The set of parameters, {Xi}, takes on specific values to characterize a particular sample of blood. Beginning with an initial estimate, the {Xi} are adjusted until the fit of the equation to the data is optimized. The concepts and techniques of nonlinear curve fitting and parameter estimation have been fully explained by Bard (9). Theoretically, an abnormal condition such as strong aggregation should be associated with abnormal values of one or more of the parameters found.

Goodness of fit

Each function was fit to the data by finding the {Xi} which minimizes

$$g = \sum_j (T_j - B_j)^2 = \sum [T(D_j, e, H_j, \{Xi\}) - B_j]^2 \qquad [2]$$

j = index denoting observations

T_j = shear stress predicted from function being fit

B_j = observed shear stress

The sum is taken over the observations on one individual at a series of hematocrits. The non-linear minimization problem and its solution are discussed in the appendix.

The standard deviation of fit, s, which measures goodness of fit, is given by:

$$s = \left(\frac{1}{n} g \right)^{1/2} \qquad [3]$$

where n = number of data points for each blood sample

Equation [3] implies that minimization of g results in the same parameter values as would minimization of s. As indicated schematically in Figure 1 the magnitude of s values displayed a population distribution. The mean of the distribution was denoted sm and its standard deviation was denoted sd.

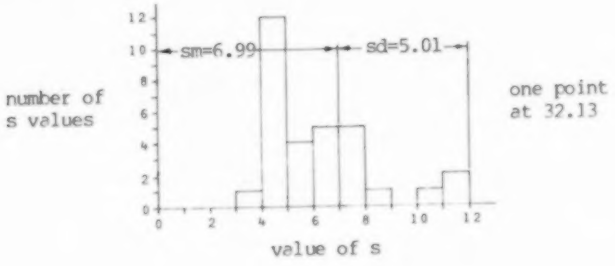

FIG. 1
The distribution of s values for function 7, Table 2A, steady state, S1 shear rate range with mean and standard deviation indicated.

The ordering of sm values - smallest to largest - was recorded for both sub-populations examined (taking or not taking oral contraception). For each function the difference in sm between the two subpopulations was tested for statistical significance via the t test and for the function of best fit differences in the {Xi} were likewise tested for significance. The population averages for the {Xi} and their standard deviations were calculated for the two most successful functions.

History of functions

The functions compared, listed in Table 1, were obtained from a variety of sources. In a number of cases the hematocrit dependence is given by a factor of exp(parameter H) since approximately this dependence has been observed experimentally for whole blood by a number of authors (10,11). In none of the equations is a specific parameter associated with erythrocyte aggregation included. Function 1 is a simplified form of the Walburn-Schneck function (see below) having only 2 parameters. Functions 2 through 6 were formed by combining a linear shear rate dependence with one which goes exponentially to zero at small D and adding a hematocrit dependence. When H --> 0 they reduce to the Newtonian representation of plasma; otherwise they have no theoretical background. Function 7 was first presented by Walburn and Schneck (7) who used a computer routine which determined the function of best fit in the shear rate range of 24 s^{-1} to 230 s^{-1}. As originally presented the parameter X4 was multiplied by the concentration of total protein less albumin in an attempt to remove individual variability from the value of X4. We have eliminated this factor albeit with some loss of consistency amongst samples from different people. Quemada (5) derived function 8 and showed that it fit data better than Casson's function. Functions 9 and 10 are based on the equation of Phillips and Deutsch (6). These authors did not include an H dependence so this variable was introduced in two ways as shown in Table 1. It is experimentally observed for some samples that when ln(T) is plotted versus ln(D) two quasi-linear regions appear. Function 11 represents this behaviour with X4 being a measure of the shear rate at which the slope changes. No function used successfully had more than

Vol. 17
1980

TABLE 1
Features of the functions considered

Function \ Attribute	$T(D,e,H,\{Xi\})$	$\lim_{D\to 0} \frac{T}{D}$	$\lim_{D\to\infty} \frac{T}{D}$	$\lim_{H\to 0} \frac{T}{D}$
blood	empirically determined	uncertain	$e<(\ )<\infty$	e
1	$e\exp(X1\ H)D^{1-X2\ H}$		0	e
2	$X4\ (\exp(X1\ H)D+X2\ H(1-\exp(-X3\ D)))$	$X4\ (\exp(X1\ H)+X2\ X3\ H)$	$X4\ \exp(X1\ H)$	X4
3	$X4\ (\exp(X1\ H)D+X2\ (1-\exp(-X3\ HD)))$	$X4\ (\exp(X1\ H)+X2\ X3\ H)$	$X4\ \exp(X1\ H)$	X4
4	$X4\ (D+X1\ H(1-\exp(-X2\ D)))\exp(X3\ H)$	$X4\ (1+X1\ X2\ H)\exp(X3\ H)$	$X4\ \exp(X3\ H)$	X4
5	$X4\ (D+X1\ (1-\exp(-X2\ HD)))\exp(X3\ H)$	$X4\ (1+X1\ X2\ H)\exp(X3\ H)$	$X4\ \exp(X3\ H)$	X4
6	$X4\ D(1+X1\ (1-\exp(-X2\ HD)))\exp(X3\ H)$	$X4\ (1+X1\ X2\ H)\exp(X3\ H)$	$X4\ (1+X1\ )\exp(X3\ H)$	X4
7	$X1\ \exp(X2\ H+X4\ /H^{2})D^{(1-X3\ H)}$	∞	0	$\infty(X4<0)$
8	$X4\ D\left\{\frac{1+X1\ D^{-1\ -1/2}}{1-X2\ H+(1-X2\ X3\ H)X1\ D^{-1\ -1/2}}\right\}^2$	$\left\{\frac{X4}{1-X2\ X3\ H}\right\}^2$	$\frac{X4}{1-X2\ H}$	X4
9	$X1\ \exp(X4\ H)\left\{\frac{1+X2\ D^{2}}{1+X3\ D^{2}}\right\}D$	$X1\ \exp(X4\ H)$	$\frac{X1\ X2}{X3}\exp(X4\ H)$	$X1\left\{\frac{1+X2\ D^{2}}{1+X3\ D^{2}}\right\}$
10	$X1\ \exp(X4\ H)\left\{\frac{1+X2\ HD^{2}}{1+X3\ HD^{2}}\right\}D$	$X1\ \exp(X4\ H)$	$\frac{X1\ X2}{X3}\exp(X4\ H)$	X1
11	$e\ D\exp\left\{A\left\{X1\ -X2\ V-\frac{X3\ (V-X4\ )}{1-\left[\frac{V}{X4}\right]^{3D}}\right\}\right\}$ $V=\ln(D)+5$	∞	0	e

four Xi parameters.

Convergence of the optimization routine was never obtained with any of the four forms of the function presented by Huang and Fabisiak (3). Consequently it is not included in Table 1. These authors presented their function in the following form and specified numerical values for c, A, n and t_o.

$$T = eD \pm cAD^{n} \exp(-cD^{n} t_o) \qquad [4]$$

The + sign is taken for a dilatant fluid and the - sign for a pseudoplastic or shear-thinning fluid. With the hematocrit introduced the function was examined in the following forms:

$$T = eD \pm X1\ D^{X2}\ \exp(X4\ H - X3\ D^{X2}) \qquad [5]$$

$$T = e^{X4\ H}\ (eD \pm X1\ D^{X2}\ \exp(-X3\ D^{X2})) \qquad [6]$$

The choice of + or - sign and two forms of hematocrit dependence gave four different forms, all of which were tested.

METHODS

1. Acquisition of blood samples

One sample was obtained from each of 30 women ranging in age from 19 to 44 years and three samples were obtained from one male aged 23 years. All donors were healthy and not taking any medication with the exception of oral contraception used by 11 of the women. With the donor in a seated position and a cuff applied to the upper arm, blood was drawn from an antecubital vein into a plastic syringe using a 21-gauge needle and discharged into a commercial EDTA tube (Sherwood Medical Industries). Results from samples taken without the cuff were not significantly different from those taken with it. Blood was routinely withdrawn between 0730 and 1000 h. Less than 10% of the samples appeared lipemic, i.e. had visibly cloudy plasma. Cloudy plasma was treated as outlined below.

2. Rheometry

The rheometer used was a Contraves LS-2 with a concentric cylinder measuring system; inner cylinder stationary, outer cylinder rotating. The dimensions of the annular sample space were: 11 mm inside diameter, 12 mm outside diameter and 8 mm height. A guard ring, which prevents transmission of stress near the liquid surface was made from poly(methylmethacrylate). This device provided no measurable effect when standardizing oil was tested but was found to be necessary to obtain Newtonian behaviour for plasma. A water circulator maintained the sample temperature at 25.0±0.1 C. The signal, proportional to shear stress, was recorded continuously on a chart recorder. The proportionality constant was determined with oils of known viscosity.

3. Manipulations

Measurements were made at 10 shear rates ranging in geometric progression from approximately 0.031 s^{-1} to 120 s^{-1} at various hematocrits. In some cases calculations were done with a subset of only six shear rates. These two ranges of shear rates will be denoted by:

$$S1 = \{ \text{shear rates} \mid .031\ s^{-1} \leq \text{shear rate} \leq 3.1\ s^{-1} \}$$
$$S2 = \{ \text{shear rates} \mid .031\ s^{-1} \leq \text{shear rate} \leq 120\ s^{-1} \} \qquad [7]$$

The volume fraction of erythrocytes, H, was determined with an IEC microhematocrit centrifuge. The correction for intercellular space (≈1%) was insignificant compared to other errors and was neglected. The values of H ranged from 0.29 to 0.55. The measurements at physiological hematocrits were run with the blood taken directly from the sampling tube. The plasma and erythrocytes were then separated by centrifugation at 1000 g for 180 to 300 s so that the majority of platelets remained in the plasma. Platelets were removed from the plasma by centrifugation at 24,000 g for 120 to 180 s and the chosen artificial hematocrits were obtained by remixing plasma and cells. The occasional cloudy plasma was filtered through a 0.45 μm cellulose acetate filter (Millipore Corporation). The sample volume used in the viscometer was 0.7 mL. Prior to measurement at each shear rate the sample was mixed by raising and lowering the inner cylinder six times through a displacement of about 5 mm. No more than 35 s elapsed between completion of mixing and initiation of shearing. The adequacy of the mixing between each shear rate was tested by completing measurements at the ten shear rates and then repeating this series. Duplication of the results proved that the first sequence of measurements did not influence the second. Measurements on any sample over the range of shear rates were completed within 30 minutes of sample preparation. The data so obtained agreed well with other published values taken over the appropriate range of shear rate (12). The plasma viscosity was determined at 25.0±0.1 C using a capillary tube viscometer with a flow time for water of 72 s.

4. Interpretation of observations

Either one or two pieces of data were taken from a viscometer chart record. The steady state value taken when the shear stress became constant provided one datum. When a peak value occurred it was always within the first 30 s of the record and was taken as the second datum; both were obtained from most records. The shear stress at the surface of the inner cylinder of the viscometer was deduced directly from the chart recordings. Evaluation of the corresponding shear rate utilized equation [7] taken from Krieger and Elrod's paper (13).

$$D(B) = \frac{w}{\ln(s)}[1+\ln(s)Z\ln(w)+\frac{1}{3}[\ln(s)Z\ln(w)]^2+\frac{1}{3}[\ln(s)Z]^2\ln(w)] \quad [8]$$

w = angular speed of cup relative to fixed bob

$$s = \frac{\text{radius of cup}}{\text{radius of bob}}$$

$$Z = \frac{d}{d(\ln(B))}$$

B = observed stress

Evaluation of the right hand side of this equation requires a representation of ln(rotational speed of viscometer) versus ln(observed stress) which was achieved numerically by fitting a cubic spline to each set of data points (14).

RESULTS AND DISCUSSION

Table 1 lists the functions tested and some of their limiting characteristics which are of interest for theoretical interpretation. All functions have zero yield stress. All functions have positive viscosity at zero shear rate although in some cases this viscosity is infinite. The CFs tested are not considered to apply at zero shear rate although it is of interest that good fits were obtained at low shear rates without including yield stresses in the functions. When D becomes large the viscosity should remain larger than the continuous phase viscosity but finite. Unfortunately, with the Walburn-Schneck function this limit is zero. For blood T(D,e,H,{Xi}) is an odd function of D; i.e.

$$T(-D,e,H,\{Xi\}) = -T(D,e,H,\{Xi\}) \quad [9]$$

Of all functions considered only those of Phillips and Deutsch (functions 9 and 10) have this symmetry.

TABLE 2A
Population averages and standard deviations of standard deviations of best fits

Steady state; S1 shear rate range; units: mPa

	No oral contraceptives			Using oral contraceptives			
function	sm	sd	order	sm	sd	order	p
1	1.71	0.79	3	1.28	0.32	4	0.05
2	3.76	1.47	9	2.54	1.20	8	0.03
3	2.82	1.61	8	2.05	0.83	7	0.07
4	1.59	1.07	2	1.14	0.25	2	0.10
5	1.93	0.86	6	1.26	0.37	3	0.01
6	2.46	0.58	7	1.99	0.56	6	0.05
7	1.44	0.68	1	1.00	0.23	1	0.03
8	13.35	9.39	10	12.79	8.49	9	0.44
9	1.74	0.67	4	1.28	0.21	4	0.02
10	1.79	0.75	5	1.48	0.24	5	0.11

Steady state; S2 shear rate range; units: mPa

	No oral contraceptives			Using oral contraceptives			
function	sm	sd	order	sm	sd	order	p
1	18.77	6.81	8	20.72	5.67	9	0.22
2	9.52	5.83	3	7.70	1.52	3	0.16
3	10.84	5.74	5	8.44	2.00	4	0.12
4	8.96	5.87	2	6.66	1.59	2	0.13
5	9.72	5.92	4	8.55	2.43	5	0.28
6	16.11	6.02	6	12.86	2.39	6	0.05
7	7.67	5.96	1	5.71	2.03	1	0.15
8	61.97	42.81	11	72.51	47.76	11	0.26
9	19.08	7.04	10	17.06	6.02	8	0.21
10	16.58	5.73	7	13.79	4.41	7	0.09
11	18.91	9.19	9	21.22	5.81	10	0.23

The standard deviation values for each function applied to samples of various hematocrits for each individual have been averaged over the two subpopulations of individuals taking and not taking oral contraception to obtain sm characterizing each function and the standard deviation about this mean has been denoted as sd. These two parameters are given in Tables 2A and 2B and are the results on which the goodness of fit

TABLE 2B
Population averages and standard deviations of standard deviations of best fits

Peak data; S1 shear rate range; units: mPa

	No oral contraceptives			Using oral contraceptives			
function	sm	sd	order	sm	sd	order	p
1	2.16	0.59	5	1.97	0.69	3	0.22
2	2.72	1.16	9	2.60	0.65	7	0.38
3	2.51	1.21	8	2.33	0.86	6	0.35
4	1.70	0.64	2	1.88	0.54	2	0.27
5	2.21	0.88	7	2.31	0.70	5	0.39
6	2.18	0.75	6	3.24	1.59	8	0.06
7	1.44	0.59	1	1.38	0.43	1	0.40
8	19.55	10.53	10	20.07	8.14	9	0.45
9	1.93	0.48	3	1.97	0.56	3	0.41
10	2.12	0.62	4	2.11	0.55	4	0.48

Peak data; S2 shear rate range; units: mPa

	No oral contraceptives			Using oral contraceptives			
function	sm	sd	order	sm	sd	order	p
1	21.02	4.91	8	22.10	5.05	9	0.28
2	9.92	5.70	2	9.16	1.41	3	0.34
3	11.73	5.40	5	11.12	2.18	5	0.36
4	8.51	5.80	1	7.77	1.16	1	0.34
5	10.22	6.07	3	8.78	1.23	2	0.23
6	21.27	4.93	10	18.24	3.12	8	0.04
7	10.98	3.23	4	9.63	1.53	4	0.10
8	47.60	39.81	11	60.76	41.58	11	0.21
9	17.81	7.12	7	18.02	5.45	7	0.47
10	17.29	6.35	6	16.04	3.33	6	0.28
11	20.08	7.17	9	26.27	11.84	10	0.04

Vol. 17
1980

estimation was based for the various functions in each subpopulation. The results for different shear rate ranges and steady state and peak value data are specified in these tables.

The most notable feature of Tables 2A and 2B is that the Walburn-Schneck function yields the smallest value of sm in six of the eight cases. Equation 4 fits best in the remaining two cases and has the second lowest sm value for all other sets of conditions. It can be seen from the p values given (p = probability that two subpopulations have same sm; derived from the t test) that in only 4/42 of the comparisons was $p<0.05$. The two subpopulations did not differ significantly, therefore, with regard to the ability of the functions tested to represent the shear stress. The ordering of the fidelity of the functions in fitting the data was in every case identical between the subpopulations for the two of best fit, functions 7 and 4.

The function of Quemada was found to have some s values comparable to those for the Walburn-Schneck function while others were larger than 100 mPa. Small values of s indicate curves fitting well while large values of s may be associated with a singularity occurring when the denominator of function 8 goes to 0; i.e.

$$1 - X2\ H + \frac{1-X2\ X3\ H}{X1\ D^{1/2}} = 0 \qquad [10]$$

Conditions leading to the singularity might have been avoided by constraining the parameters but this was not attempted. Another possible cause of bad fit (i.e. local minima) is discussed in the appendix.

Table 3 gives average and standard deviation values of the parameters for each type of data (steady state, peak) over the two ranges of shear rates for functions 7 and 4. The averages are taken over the entire sample population since no significant differences were found between the two subpopulations when the {Xi} were examined via the t test. 'Average' CFs for the population result if the parameter averages from Table 3 are substituted into their respective functions. The standard deviations quoted demonstrate how widely the parameters vary within the population studied.

Figures 2 to 8 show various samples of data with fit curves for the Walburn-Schneck function. Figures 2 to 7 are for data from sample 29. This case was chosen because it gave the best fit amongst all steady state data fit over the S2 shear rate range. Figures 2 and 3 show the results of fitting over S2 and S1 shear rate ranges respectively for the steady state data. Figures 4 and 5 give analogous information for the peak data. Figure 6 refers

TABLE 3
Population averages and standard deviations of parameters of best fit
These numerical values apply when shear rate is expressed in s^{-1}
and stress is expressed in mPa.

function	X1	sd(X1)	X2	sd(X2)	X3	sd(X3)	X4	sd(X4)
				Steady state; S2 shear rate range				
7	1.38	1.29	5.53	1.35	0.433	0.030	0.0633	0.0572
4	31.6	5.9	0.138	0.075	1.73	0.57	2.71	0.73
				Steady state; S2 shear rate range				
7	1.34	0.84	6.13	1.20	0.71	0.13	0.034	0.044
4	8.52	13.25	4.36	3.29	3.70	0.71	1.91	0.91
				Steady state; S2 shear rate range				
7	1.53	0.98	5.51	1.19	0.509	0.045	0.0479	0.0413
4	36.5	35.0	0.232	0.046	1.69	0.51	2.7	0.67
				Steady state; S2 shear rate range				
7	2.40	3.14	6.03	1.44	0.768	0.0722	0.0315	0.0549
4	9.41	12.6	3.19	2.41	3.55	0.80	2.41	1.32

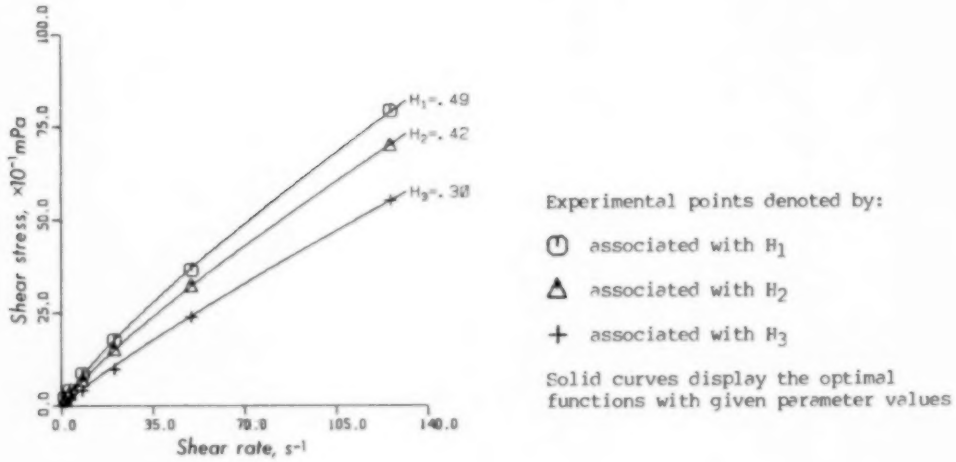

FIG. 2
Sample 29, function 7,
steady state data fit over S2,
see text for explanation
X1 = 2.70
X2 = 3.66
X3 = 0.389
X4 =-0.00495

to the same data and range of shear rates of fit as figure 4, but only the S1 range is plotted. This magnifies the region of figure 4 near the origin so that the discrepancies of fit at low shear rates are visible. Figure 7 refers to the same data as Figure 5. Here parameters derived by fitting over S1 are used to plot function 7 over the S2 shear rate range so that the effect of extrapolation is displayed. Figure 8 shows the results for sample 18 in the steady state data fit over S2 where it is the second from worst fit for this function. Even in this case the curves are seen to represent the data reasonably well.

In almost all cases the s values for the steady state data are smaller than the corresponding values derived from peaks of the shear stress - time output. This probably reflects the greater variability in the peak values rather than the inability of the functions used to follow the shear rate dependence. The reason for the appearance of peaks in the torque - time records is not completely clear. It has been suggested that it is due to a wall effect in the rheometer, representing a migration of cells away from the flow boundaries (15). Alternatively, since it is only present in aggregated suspensions it seems possible that it could represent a shear-dependent build up of aggregation. Phillips and Deutsch have shown that a simple viscoelastic fluid could also exhibit such behaviour (6). In any event, since the peak stresses are often used as an indication of the degree of aggregation present in a sample (16) their values were included in the analysis.

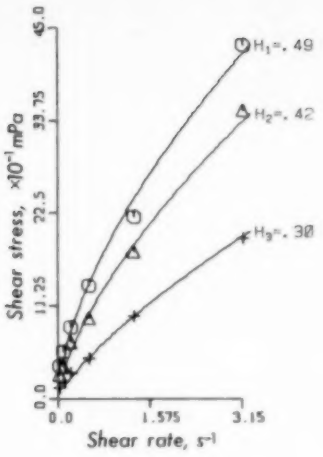

FIG. 3
Sample 29, function 7,
steady state data fit over S1
X1 = 4.32
X2 = 3.58
X3 = 0.798
X4 =-0.0407

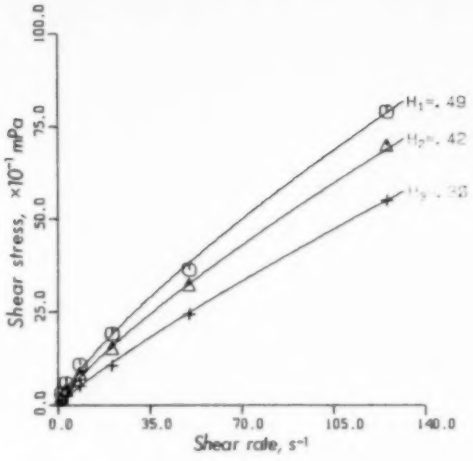

FIG. 4
Sample 29, function 7,
peak data fit over S2
X1 = 1.772
X2 = 4.67
X3 = 0.451
X4 = 0.0145

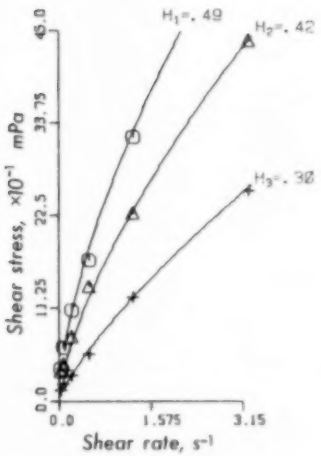

FIG. 5
Sample 29, function 7,
peak data fit over S1
X1 = 1.22
X2 = 6.27
X3 = 0.761
X4 = 0.0227

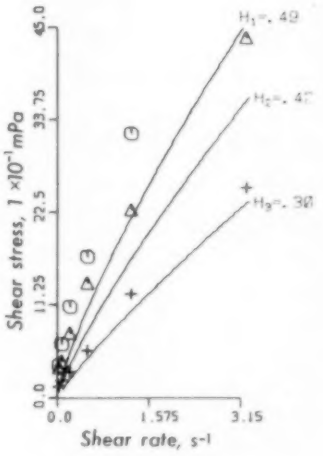

FIG. 6
Sample 29, function 7,
peak data fit over S2
X1 = 1.772
X2 = 4.67
X3 = 0.451
X4 = 0.0145

It is noteworthy, and somewhat disheartening, that no single set of parameters seems to adequately represent the shear rate dependence of shear stress over the whole range of D examined. It is apparent from Figures 6 and 7 that stresses at high shear rates cannot be accurately predicted from low shear rate values, nor can the low shear behaviour be derived safely from curves fit to data taken over the full range accessible (where the high shear values dominate the fitting procedure). This would suggest that none of the equations examined have much fundamental significance with respect to the basic fluid mechanics of these systems. On the other hand, function 7 is the best form in this regard among those tested. It is clear from the results presented in Table 3 that the parameters of best fit for the S1 and S2 shear rate ranges are very similar for this equation, in contrast to the other functions tested, typical of which in this regard is the behaviour of equation 4.

Vol. 17
1980

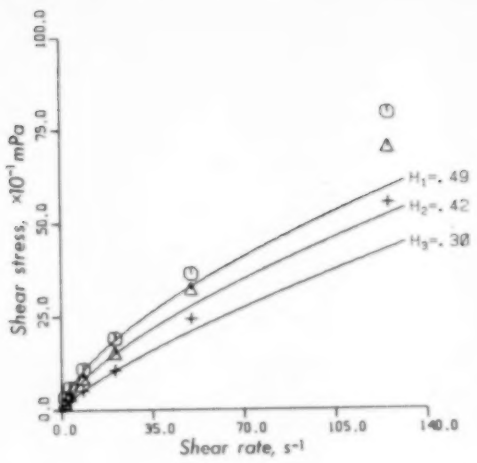

FIG. 7
Sample 29, function 7,
peak data fit over S1
X1 = 1.22
X2 = 6.27
X3 = 0.761
X4 = 0.0227

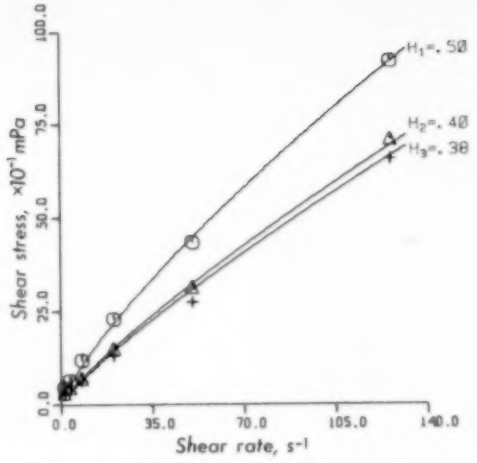

FIG. 8
Sample 18, function 7,
steady state data fit over S2
X1 = 0.845
X2 = 6.08
X3 = 0.441
X4 = 0.0487

Apparently the power law dependence of shear stress on shear rate most accurately represents the behaviour of anticoagulated whole blood in Couette flow. Our results also show that the hematocrit dependence of T is more complex than can be represented by an exponential whose exponent is linear in H. It remains to be seen whether or not there is any underlying physical reason for these observations.

Our results indicate that in the population studied, there are no significant differences between blood from women taking oral contraception and those not on such medication. Functions 7 and 4 were both able to fit the data from the two subpopulations with little difference, although in one case for equation 7 sm was significantly lower ($p=.03$) in the oral contraceptive subpopulation. If anything, the oral contraceptive data showed less variability than that from the remainder of the population. Likewise, the parameters characterizing the optimum fit of function 7 did not vary significantly in the t test ($p>.05$; data breakdown not shown). The constitutive functions for oral contraceptive and non-medicated blood are therefore indistinguishable in the populations examined.

Among the functions considered, then, that of Walburn and Schneck, function 7, would appear to be the most satisfactory. The four parameters characterizing this function can therefore be used to compare the flow behaviour of blood obtained from various sources. The unsatisfactory limit of viscosity when $D \rightarrow 0$ is one limitation on the applicability of this function, however. Future work might be directed towards combining the Walburn-Schneck hematocrit dependence with other shear rate dependencies that eliminate the above objection and allow more rapid changes in slope at low shear rates. Such a function might well provide a consistent fit over all accessible rates of shear.

ACKNOWLEDGEMENTS

This work was supported by grants from the Vancouver Foundation, the British Columbia Heart Foundation and the Medical Research Council of Canada. Portions of this work were carried out by P. E. in partial fulfilment of the requirements for the M. Sc. degree in Experimental Pathology. The authors thank Dr. Russell Greig and members of the UBC Computing Center for helpful discussion and Mandy Hoskins for meticulous technical assistance.

APPENDIX

Optimization

Suppose that a function, g, is to be minimized with respect to {Xi}. One might begin by forming the p algebraic equations:

$$\frac{\partial g}{\partial Xi} = 0 \qquad i = 1,\ldots p \qquad [11]$$

The problem is now identified as being in one of two categories. It is 'algebraically solvable' if the system of equations can be solved to provide explicit functions mapping the data into {Xi}. Otherwise it is not algebraically solvable. Unfortunately the problem at hand falls into the latter category. Thus it may be dealt with in one of two ways:

1. A transformation may be introduced which distorts the problem so that the new algebraic system is solvable. For example consider the problem of fitting T(D,k,m) to observations, where

$$T = kD^m \qquad (X1=k, X2=m) \qquad [12]$$

Statistical analysis of the errors using the theory of maximum likelihood (Bard (9) pp. 61-64) leads to the criterion of fit commonly called the least squares criterion. In this case it requires minimization of g with respect to k,m where

$$g = \sum_j^m (kD_j - B_j)^2 \qquad [13]$$

$$\frac{\partial g}{\partial k} = \sum_j^m 2(kD_j - B_j)D_j^m = 0 \quad \Longrightarrow \quad \sum_j^{2m} kD_j = \sum_j^m B_jD_j$$

$$\Longrightarrow \qquad k = \frac{\sum_j^m B_jD_j}{\sum_j^{2m} D_j} \qquad [14]$$

$$\frac{\partial g}{\partial m} = \sum_j^m 2(kD_j - B_j)kD_j^m \ln(D_j) = 0 \quad \Longrightarrow \quad \sum_j^m (kD_j - B_j)D_j^m \ln(D_j) = 0 \qquad [15]$$

Equation [15] is not algebraically solvable for m.

To transform the problem the natural logarithm is applied to equation [12] above giving

$$\ln(T) = \ln(k) + m\ln(D) \qquad [16]$$

Minimization of g with respect to k,m is replaced without justification by minimization of g' with respect to k,m where

$$g' = \sum_j [\ln(T_j) - \ln(B_j)]^2 = \sum_j [\ln(k) + m\ln(D_j) - \ln(B_j)]^2 \qquad [17]$$

$$\frac{\partial g'}{\partial \ln(k)} = \sum_j 2[\ln(k) + m\ln(D_j) - \ln(B_j)] = 0$$

$$\Longrightarrow \quad n\ln(k) + \left(\sum_j \ln(D_j)\right)m = \sum \ln(B_j) \qquad [18]$$

$$\frac{\partial g'}{\partial m} = \sum_j 2[\ln(k) + m\ln(D_j) - \ln(B_j)]\ln(D_j) = 0$$

$$\Longrightarrow \quad \left[\sum_j \ln(D_j)\right]\ln(k) + \left[\sum_j (\ln(D_j))^2\right]m = \sum_j \ln(B_j)\ln(D_j) \qquad [19]$$

Explicit formulas for k,m are obtainable from equations [18] and [19]. This transformation of the problem is referred to as linearization when the algebraic equations of the transformed problem are linear although in general any set of solvable equations is sufficient. The routine employed by Walburn and Schneck (7) utilized linearization.

The difficulty with linearization is that since it is not just a scaling it changes the relative size of different terms in the sum of squares and thus results in a different solution {Xi} than that which minimizes g. The errors occurring when the problem is

Vol. 17
1980

linearized may be appreciable. Colquhoun ((17) pp. 257-272) gives an example of a two parameter function fit by both methods and has found the errors of the parameters to be 4.8% and 5.9% when the problem is solved numerically versus 24.7% and 45.6% when linearization is used.

When the problem is reduced to a system of linear algebraic equations the question of uniqueness of the solution can be answered completely. Any linear algebraic system has either 0, 1 or ∞ solutions. Zero solutions would correspond to absence of a minimum and an infinite set of solutions would result from minimization of a function which is just a constant value; neither of these cases are of physical importance. The solution of the linearized problem will therefore be unique. However, the situation is not this definite in the more general case.

2. The second way of handling minimization problems which are not algebraically solvable is to solve the original problem by numerical methods. This is more accurate than linearization since no arbitrary distortion is involved. This approach was followed using an algorithm based on the method of conjugate directions devised by Powel (18). Other algorithms were tried but of those available at the UBC Computing Center (Bird and Moore Lee, (19)) that of Powel was found to be most robust. A FORTRAN program with single precision variables was used. Unfortunately the theory of nonlinear optimization and estimation is not well developed so it was necessary to use the minimum value of

$$s = \left[\frac{1}{n} \sum_j (T_j - B_j)^2 \right]^{1/2} \qquad [20]$$

as an estimate of the standard deviation of the observations from the predictions. The error introduced by this approximation in the linear case can be evaluated as follows. For a linear function $T(D,e,H,\{Xi\})$, $1 \le i \le p$, the unbiased estimator of standard deviation is

$$s = \left[\frac{1}{n-p} \sum_j (T_j - B_j)^2 \right]^{1/2} \qquad [21]$$

For n=28, p=4 the fractional error in our estimator versus the correct estimator, for the linear case would be

$$\frac{\left[\frac{1}{n} \sum\right]^{1/2} - \left[\frac{1}{n-p} \sum\right]^{1/2}}{\left[\frac{1}{n-p} \sum\right]^{1/2}} = \left[\frac{n-p}{n}\right]^{1/2} - 1 = 0.07 \qquad [22]$$

It therefore seems likely that the error in the nonlinear case would also be small. In any event the parameter, s, used is a measure of goodness of fit.

The possibility of a nonlinear problem having several solutions certainly exists. No general theorem specifying the criteria for existence or non-existence of a unique solution or determining the number of solutions of a non-linear optimization problem is known. Therefore, if one minimum is found in a particular problem it may be a local minimum, while the global minimum remains to be found. Which minimum is found when an optimization routine is applied depends on the location of the initial point used. Roughly speaking, a minimum close to the initial point will be found. Thus it is possible that some large values of s are associated with local minima whereas in only some cases the global minimum was obtained. We did not attempt to pursue this problem but present the data with the intention of displaying the general utility of the functions examined.

REFERENCES

1. FUNG, Y. C. Foundations of Solid Mechanics. New York, London, Sydney, Toronto, New Delhi and Tokyo: Prentice-Hall Inc., 1965, p. 114.

2. DINTENFASS, L. Rheology of Blood in Diagnostic and Preventative Medicine. London and Boston: Butterworth and Co. Ltd., 1976.

3. HUANG, C. R. and FABISIAK, W. A rheological equation characterizing both the time-dependent and the steady state viscosity of whole human blood. American Institute of Chemical Engineers 70th Annual Meeting, fiche #49. New York: American Institute of Chemical Engineers, 1977.

4. CASSON, N. A flow equation for pigment-oil suspensions of the printing ink type. In: Rheology of Disperse Systems. C. C. Mill [Ed]. New York, London, Paris and Los Angeles: Pergamon Press, 1959, p. 84.

5. QUEMADA, D. Hemorheologie. Aggregation des hematies et proprietes non-Newtonian du sang: nouvelle loi rheologie et validite de la loi de Casson pour le sang. C. R. Hebd. Seances Acad. Sci., Serie D Sci. Nat. 281,747-750,1975.

6. PHILLIPS, W. M. and DEUTSCH, S. Toward a constitutive equation for blood. Biorheology 12,383-389,1975.

7. WALBURN, F. J. and SCHNECK, D. J. A constitutive equation for whole human blood. Biorheology 13,201-210,1976.

8. HUANG, C. R. A thermodynamic approach to generalized rheological equations of state for time-dependent and time-independent non-Newtonian fluids. Chem. Eng. J. 3,100-104,1972.

9. BARD, Y. Nonlinear Parameter Estimation. New York and London: Academic Press, 1974.

10. WEAVER, J. P. A., EVANS, A. and WALDER, D. N. The effect of increased fibrinogen content on the viscosity of blood. Clin. Sci. 36,1-10,1969.

11. DORMANDY, J. A. Medical and engineering problems in blood viscosity. Biomed. Eng. 9,284-303,1974.

12. COPLEY, A. L., HUANG, C. R. and KING, R. G. Rheogoniometric studies of whole human blood at shear rates from 1000 to 0.0009 sec^{-1} Part I - experimental findings. Biorheology 10,17-22,1973.

13. KRIEGER, I. M. and ELROD, H. Direct determination of the flow curves of a non-Newtonian fluid. II Shearing rate in the concentric cylinder viscometer. J. Appl. Phys. 24,134-136,1953.

14. MOORE LEE, C. UBC CURVE. Vancouver: University of British Columbia Computing Center, 1978, pp. 61-66.

15. COKELET, G. R., MERRILL, E. W., GILLILAND, E. R., SHIN, H., BRITTEN, A. and WELLS, R. E. The rheology of human blood - measurement near and at zero shear rate. Trans. Soc. Rheol. 7,303-317,1963.

16. BROOKS, D. E., GOODWIN, J. W. and SEAMAN, G. V. F. Rheology of erythrocyte suspensions: Electrostatic factors in the dextran-mediated aggregation of erythrocytes. Biorheology 11,69-77,1974.

17. COLQUHOUN, D. Lectures on Biostatistics. Oxford, London and Toronto: Oxford University Press, 1971, pp. 257-272.

18. POWEL, M. J. D. An efficient method for finding the minimum of a function of several variables without calculating derivatives. Comput. J. 7,155-162,1965.

19. BIRD, C. and MOORE LEE, C. UBC NLP. Vancouver: University of British Columbia Computing Center, 1975.

Vol. 17
1980

BLANK
PAGE

BIORHEOLOGY, Vol. 17, pp. 249-254, 1980
Printed in the USA. All rights reserved.

0006-355X/80/030249-06$02.00/0
Copyright (c) 1980 Pergamon Press Ltd

RELATIONSHIP BETWEEN MUCUS VISCOELASTICITY AND CILIARY TRANSPORT IN GUARAN GEL/FROG PALATE MODEL SYSTEM.[1]

Malcolm King

Meakins Christie Laboratories,
McGill University Clinic,
Royal Victoria Hospital,
Montreal, Canada

(Received 21.9.1979; in revised form 25.1.1980.
Accepted by Editor H.L. Goldsmith.
Received in final form by Executive Editorial Office 24.3.1980)

Vol. 17
1980

ABSTRACT

Guaran gels, when placed on cilio-active but mucus-depleted frog palate, are transported by ciliary action. The relationship between the rate of ciliary transport of these gels and their viscoelastic properties was investigated. The mechanical properties were determined by the magnetic rheometer technique; this gave elasticity G' and tan δ (ratio of energy loss to storage) at various frequencies. Transportability was determined by comparing the linear velocity of the gel with that of endogenous palatal mucus. Because of aging effects, both G',and tan δ for a single gel change considerably over the course of several days. It was thus possible to obtain gels where tan δ at constant G' varied by a factor of 8 and G' at constant tan δ by more than an order of magnitude. Transport was found to decrease significantly as both G' and tan δ increased. However, the importance of tan δ on transport was much greater; the rate of decrease of transport with increasing tan δ being approximately 4 x that with increasing G'. The findings confirm those found previously for the transport of whole canine tracheal mucus.

INTRODUCTION

In a recent study (1),relationships between the dynamic mechanical properties of canine tracheal mucus and its velocity of ciliary transport on the mucus-depleted frog palate were reported. For fresh mucus samples from healthy tracheostomized dogs, linear correlations of negative slope were found relating ciliary transport velocity (V_{rel}) with the logarithm of mucus elasticity (G') at constant loss tangent (tan δ) and with tan δ at constant G' where G' and tan δ were determined at 1 radian /sec. The correlations obtained can be expressed as the following single equation:

$$V_{rel} = 1.61 - 0.221 \log G'(1) - 0.768 \tan \delta(1) \qquad (1)$$

The predictive values of this relationship (90% confidence) for individual mucus samples is about 0.16 (i.e., ± 16%) for 20 dyn/cm^2 < G'(1) < 600 dyn/cm^2 and 0.2 < tan δ(1) < 0.5.

---

[1]Presented at 1979 FASEB Meeting. Dallas, Texas. Supported by the Medical Research Council of Canada.

[2]Keywords: Mucociliary transport, mucus rheology, frog palate.

Negative relationships between ciliary transport and mucus elasticity had been reported by others authors (2,3) but the above mentioned study was the first to report a negative correlation between V_{rel} and tan δ. Because of the scatter in the data and the rather small range of variation in tan δ vis-à-vis G', the correlation between V_{rel} and tan δ was weak (r= -0.45). It was thus desired to confirm its existence in a system where tan δ could vary over a broader range. To this end, the present study was undertaken, using guaran gels as rheological simulants of mucus since they transport well on the frog palate (4) and since their mechanical properties can be manipulated more readily than those of whole mucus.

EXPERIMENTAL METHODS

Gels of guaran, a vegetable polysaccharide, containing from 1 to 2% solids were prepared in amphibian Ringer's solution. A self-gelling guar gum (Jaquar 315-FC2 from Stein Hall) was used for this purpose. The viscoelastic properties of each gel were determined with an oscillating ball magnetic rheometer (5), the same instrument that had been used to analyze the tracheal mucus. G' and G", the storage and loss modulus respectively, were determined at 23°C and at three frequencies — 1, 10, and 80 rad/s. G' is commonly termed elasticity and will be referred to as such in the presentation that follows. The mechanical loss tangent, tan δ, is the ratio G"/G' at any given frequency.

For the rheological measurements, the samples were placed in open-topped containers and layered with light paraffin oil to prevent evaporation. For the ciliary transportability assays, each sample was washed free of paraffin with petroleum ether and transferred to a 30°C 100% RH chamber where it was placed on the mucus-depleted excised palate of a frog. The leading edge velocity of the guaran sample was computed from the transit time over a 5 mm path along the midline of the palate. A mean of 4 to 6 readings were taken to compute a mean velocity. This was then expressed as a ratio of the mean velocity, before and after guaran, of frog palate mucus over the same path. The resulting ratio is known as V_{rel}, the relative ciliary transport velocity. In general, efforts were made to keep experimental conditions the same as those used in the tracheal mucus study, including the use of comparably sized samples, i.e., 5-10 µl.

After the frog palate assay, the guaran sample was transferred back to a sample container, re-layered with paraffin, and its viscoelastic properties re-determined. With freshly prepared gels the viscoelastic properties can change rapidly. When this happened, the mean values of G' and tan δ before and after the transport measurements were used in the subsequent analysis.

ANALYSIS OF RESULTS

Because of the kinetics of gel formation, the gels took several days to age, during which time G' increased considerably with only a modest increase in G". As a result, it was possible to choose pairs of guaran gels of different ages and concentrations in which only one viscoelastic parameter (G' or tan δ) was different, and test them on the same frog palate. The effect that changing a single viscoelastic variable had on transport is illustrated in Table I, in which are shown G'(1), tan δ(1), and V_{rel} four guaran gels. The first pair of gels illustrate the change in V_{rel} that occurs when G' and G" increase by the same ratio. For an 8-fold increase in G' at constant tan δ, ciliary transportability decreased by 30%. The second pair show the change in V_{rel} when two gels of the same storage modulus but grossly different loss modulus are compared on the same frog palate. In this case, an approximately 3-fold increase in tan δ at constant G' resulted in a more than 3-fold decrease in V_{rel}. The dependence of ciliary transport velocity on mucus viscoelasticity illustrated in this table was representative of the behaviour of all of the gels examined in this study; that is, the changes in loss tangent had a much more important effect on mucociliary transport than changes in elasticity.

TABLE I

Sample	G' (1 rad/s) (dyn/cm^2)	tan δ (1 rad/s)	V_{rel}
1	76	0.18	0.90
2	590	0.18	0.63
3	98	0.26	0.64
4	95	0.83	0.20

Figure 1 shows the plot of ciliary transport velocity against tan δ at 1 rad/s for all the guaran gels studied. In this case, the primary correlation was highly significant without having to adjust the data for any regression due to elasticity, as had been required in the tracheal mucus study (1). The slope and maximum range of the canine tracheal mucus data are shown here for comparison. The guaran slope is comparable to the one found previously, although the whole curve is shifted downward. This downward shift would suggest that there is some specific difference between the two gel systems; this will be dealt with below. The important point, though, is the way in which V_{rel} changes with the loss tangent and this is a common feature to both. The V_{rel} tan δ correlation shows up more strongly here simply because tan δ was allowed to vary over twice the range that it varied over for the whole mucus samples.

When the ciliary transport velocity is plotted against the elasticity of the guaran gels, as shown in Figure 2, there is no significant correlation, whereas there was one for the tracheal mucus samples (1). The reason for this lack of correlation is the dominating influence of the viscosity/elasticity ratio in V_{rel} in the guaran system. The V_{rel} data can be normalized for this effect, however, by applying the regression line from the previous figure. The result of this statistical procedure is shown in Figure 3, which gives the relationship between ciliary transport velocity and guaran elasticity at constant loss tangent. The correlation is now significant. The relationship is qualitatively similar to the one found for tracheal mucus, although the slope is somewhat less negative, and again the whole curve is shifted downward. Because the primary correlation coefficient between V_{rel} and G' is so close to zero, the relationship between adjusted V_{rel} and tan δ at constant G' is virtually indistinguishable from that shown in Figure 1, and is therefore not shown here. As in the tracheal mucus system, the relationship between V_{rel} and viscoelasticity for guaran gels can be expressed as a single equation, viz.

$$V_{rel,guaran} = 1.13 - 0.123 \log G'(1) - 0.697 \tan \delta(1) \qquad (2)$$

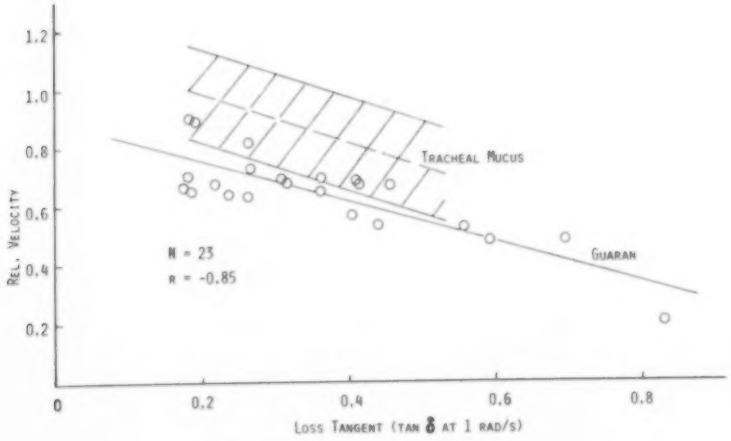

FIG.1

Ciliary transport velocity of guaran gels on frog palate (relative to frog palate mucus) vs. tan δ(1). Correlation for canine tracheal mucus (best fit line ± 1 SD) taken from Fig. 9 of Ref. 1.

Vol. 17
1980

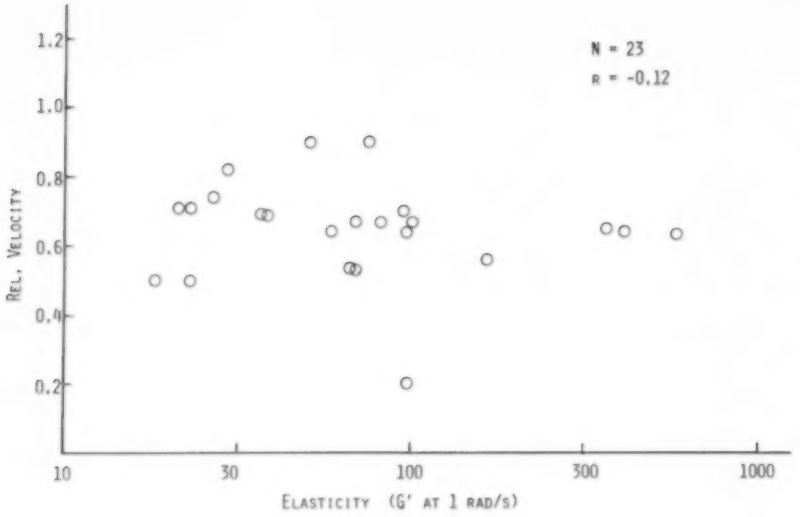

FIG. 2

Relative ciliary transport velocity of guaran vs. G' (1), plotted logarithmically.

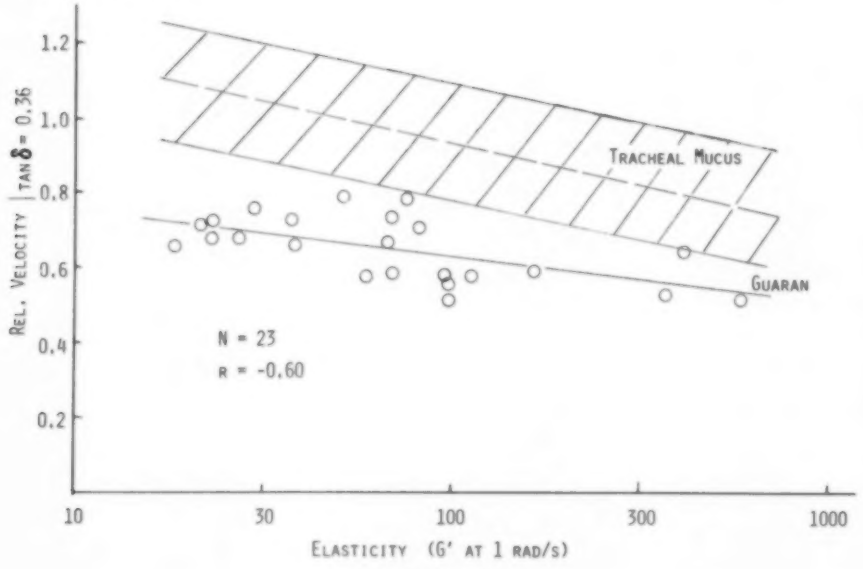

FIG. 3

Relative ciliary transport velocity of guaran adjusted for variation due to tan δ vs. G'(1). Corresponding correlation for canine tracheal mucus (best fit line ± 1 SD) taken from Fig. 8 of Ref. 1.

In Figure 4, unadjusted V_{rel} is plotted against guaran loss modulus. It is interesting to note that there is a mild negative correlation here where there was none for G' (Figure 2). The reason for this is the fact that G" is, of course, the product of G' and tan δ, one of which showed a strong negative correlation with transport, while the other showed no correlation at all. Thus, the product shows the intermediate relationship seen.

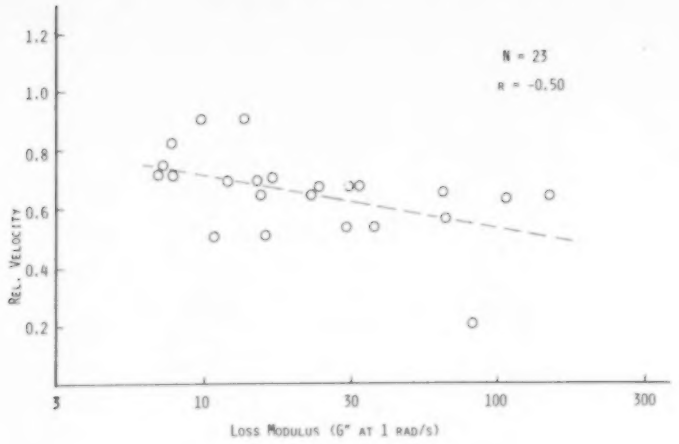

FIG.4

Relative ciliary transport velocity of guaran vs. G", plotted logarithmically.

At least part of the reason for the downward shift in ciliary transport velocity versus loss tangent for guaran is explainable by examining the way in which the correlations change when the viscoelastic properties are determined at frequencies other than 1 radian per second. This is illustrated in Figure 5, which shows ciliary transport velocity at constant mucus elasticity versus tan δ measured at three different frequencies. 80 rad/s (12.7 Hz) was chosen as representative of the frog palate ciliary beat frequency at 30°C. (Gilboa and Silberberg (6) reported frequencies of 8-20 Hz).

Vol. 17
1980

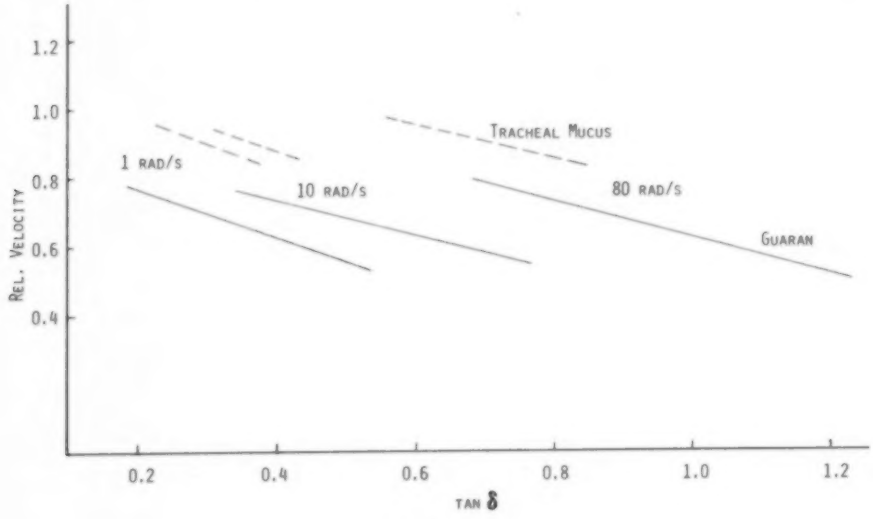

FIG.5

Relative ciliary transport velocity vs. tan δ at 1, 10 and 80 rad/s. Correlation lines for guaran (solid) and canine tracheal mucus (dashed) are shown for each frequency.

At a given V_{rel}, tan δ increased more rapidly with increasing frequency in the guaran than in the tracheal mucus system. In both systems the range of tan δ values also increased with frequency, while the accuracy of the rheological method decreased. As a result, for tracheal mucus, it was found that the correlation between V_{rel} and tan δ was stronger at 1 rad/s than at 80 rad/s. The same observation was made for guaran by itself; i.e., the

correlation coefficient was greater at 1 rad/s than at 80 rad/s. However, when the correlations for the two gel systems are compared, it is apparent that the vertical gap between them is reduced at the higher frequency. This suggests that the dynamic mechanical properties at 80 rad/s are a more appropriate determinant of frog palate ciliary transport than those at 1 rad/s. Nevertheless, for canine tracheal mucus by itself, a better predictive relationship between ciliary transportability and mucus viscoelasticity was obtained by determining viscoelasticity at 1 rad/s.

CONCLUSION

These results confirm the findings of the previous study, namely, that mucociliary transport velocity decreases with increasing mucus elasticity when storage and loss modulus increase in parallel, i.e., when mechanical loss tangent does not change. With elasticity held constant, mucociliary transport velocity also decreases with increasing mechanical loss. The latter relationship is interpreted as indicating that dissipation of ciliary energy by the mucus is important. In fact a given change in tan δ has a much greater effect on ciliary transportability than the same fractional change in G'.

REFERENCES

1. KING, M. Interrelation between mechanical properties of mucus and mucociliary transport: Effect of pharmacologic interventions. Biorheol. 16: 57-68, 1979.

2. DULFANO, M.J., and ADLER, K.B. Physical properties of sputum VII. Rheologic properties and mucociliary transport. Amer. Rev. Respir. Dis. 112:341-347, 1975.

3. GIORDANO, A.M., HOLSCLAW, D., and LITT, M. Mucus rheology and mucociliary clearance: Normal physiologic state. Amer. Rev. Respir. Dis. 118:245-250, 1978.

4. KING, M., GILBOA, A., MEYER, F.A., and SILBERBERG, A. On the transport of mucus and its rheologic simulants in ciliated systems. Amer. Rev. Respir. Dis. 110:740-745, 1974.

5. KING, M., and MACKLEM, P.T. Rheological properties of microliter quantities of normal mucus. J. Appl. Physiol. 42:797-802, 1977

6. GILBOA, A., and SILBERBERG, A. Characterization of epithelial mucus and its function in clearance by ciliary propulsion. IN: Air Pollution and the Lung. E.F. Aharonson, A. Ben-David, and M.A. Klingberg (Eds). New York, Wiley, 1976, pp. 49-63.

BIORHEOLOGY, Vol. 17, pp. 255-259, 1980
Printed in the USA. All rights reserved.

0006-355X/80/030255-05$02.00/0
Copyright (c) 1980 Pergamon Press Ltd

AN ANALYSIS OF THE CLOTTING CURVES OF COMPLEX DYNAMIC RIGIDITY FOR FIBRINOGEN-THROMBIN SOLUTIONS

Makoto Kaibara and Eiichi Fukada
The Institute of Physical and Chemical Research
Wako, Saitama 351, Japan

(Received 14.1.1980. Accepted by Editor S. Oka.
Received in final form by Executive Editorial Office 26.3.1980)

ABSTRACT

The clotting of fibrinogen solution is divided into three steps: (1) the transformation of fibrinogen to fibrin monomer by the action of thrombin, (2) the polymerization of fibrin monomer to fibrin polymer, and (3) the crosslinking of fibrin polymers to form network. Each process is assumed to be the first order reaction. Assuming appropriate values for the rate constants for three steps, the sigmoidal clotting curves of the dynamic rigidity and viscosity are calculated in good agreement with the observed data.

Vol. 17
1980

INTRODUCTION

During the clotting of fibrinogen-thrombin solution, the dynamic rigidity and the dynamic viscosity vary with time in many orders of magnitude. The analysis of the clotting curves of rigidity and viscosity is useful to understand the molecular mechanism in the gelation process of fibrinogen. Several equations have been already proposed to describe the rigidity-time relation for clotting blood and fibrinogen-thrombin system(1-2). The authors have also proposed an equation and examined its applicability under various experimental conditions(3-5). The equation reproduced fairly well the observed results but failed to show the sigmoidal shape of clotting curves at the initial period. In this paper we shall propose an improved equation which represents the sigmoidal nature of the clotting curves.

EXPERIMENTAL

Sample:

Bovine fibrinogen(90 percent clottable) obtained from Miles was dissolved into phosphate buffer solution with pH 7.5, consisting of NaH_2PO_4, Na_2HPO_4 and NaCl, at the concentration of 1.0g/100ml. Bovine thrombin with an activity of 26.8 unit/mg was also dissolved in the buffer solution at the concentration of 10mg/100ml. At the start of measurement, the thrombin solution and fibrinogen solution were mixed at the volume ratio of 1 to 3.

Experiment:

The dynamic rigidity G' and the loss modulus G" were measured by a parallel plate type viscoelastorecorder, which was reported previously(6). The imposed shear strain was 0.1 and the frequency was 1 Hz. It is known that fibrin gels show nonlinear viscoelasticity at the shear strain higher than 0.01(6,7). In our apparatus only linear response was detected by the use of phase sensitive detector circuits, which eliminated the higher harmonic components.

RESULTS AND DISCUSSIONS

The complex dynamic modulus G is expressed by $G = G' + iG"$, where G' is the dynamic rigidity and G" is the loss modulus, which is the product of the dynamic viscosity and the angular frequency. In order to describe the time variation of G' and G" for fibrinogen-thrombin solutions during clotting, we

KEY WORDS: Fibrinogen, Viscoelasticity, Clotting curve, Crosslink.

have previously proposed the following equations(3).

$$G' = G'_{1s}[1-C'e^{-k'_1(t-t'_1)}] + G'_{2s}[1-e^{-k'_2(t-t'_2)}] \quad (1a)$$

$$G'' = G''_{1s}[1-C''e^{-k''_1(t-t''_1)}] + G''_{2s}[1-e^{-k''_2(t-t''_2)}] \quad (1b)$$

where G'_{1s}, G'_{2s}, G''_{1s} and G''_{2s} are the saturated values of G'_1, G'_2, G''_1 and G''_2, k'_1 k'_2, k''_1 and k''_2 ($k'_1 > k'_2$, $k''_1 > k''_2$) are the rate constants, t the time elapsed from the moment when thrombin was added to the sample, t'_1, t'_2, t''_1 and t''_2 ($t'_1 \simeq t'_2$, $t''_1 \simeq t''_2$) the time when G'_1, G'_2, G''_1 and G''_2 begin to increase and C' and C" the coefficients which were put unity in the previous report.

It was assumed in eq.(1) that both G' and G" consist of two processes of the first order reaction. The increase of G' is caused firstly by the crosslinking reaction between fibrin polymers and secondly by the association of fibrin fibers around crosslinked regions. The increase of G" is caused firstly by the polymerization of fibrin monomers and secondly by the interaction between crosslinked fibrin fibers.

Figure 1 shows an example of the application of eq.(1) to the experimental data for a fibrinogen solution with ionic strength 0.5. The observed curves with open circles were divided into two curves with suffixes 1 and 2, which were derived according to eq.(1). It is seen that eq.(1) represents the experimental data fairly well except the initial rise of curves(3). Eq.(1) shows that both G' and G" should increase abruptly at the time t'_1 or t''_2 and can not represent the sigmoidal variation of the clotting curves.

In Fig. 1, G'_1 indicates the rigidity caused by crosslinking between fibrin polymers and G''_1 the dynamic viscosity caused by polymerization of fibrin monomers. These reactions are represented by a single first order reaction scheme. It has been observed that the second terms in eq.(1), G'_2 and G''_2 disappears when the ionic strength of the fibrinogen solution is lowered below 0.2. With low ionic strength, the fibrin fibers become thick and rigid and lateral association and interaction between fibrin fibers are much reduced. However, the sigmoidal nature of the clotting curves of G' and G" is still present. An example of the clotting curves G' and G" for a fibrinogen solution with ionic strength of 0.15 is shown in Fig. 2.

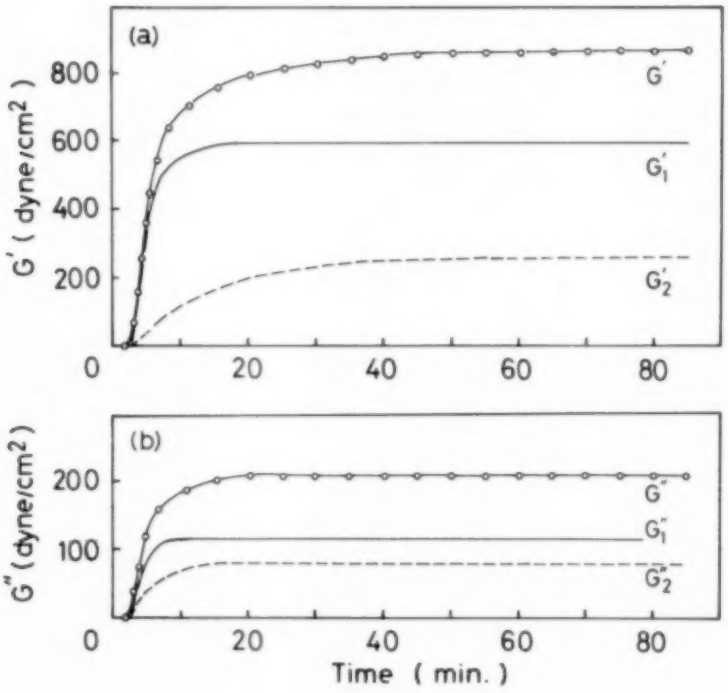

FIG.1

The clotting curves of the dynamic rigidity G' and loss modulus G" for the fibrinogen solution with ionic strength 0.5. The experimental curves with open circles are represented by the sum of solid and dashed curves calculated by eq.(1). $G' = G'_1 + G'_2$ and $G'' = G''_1 + G''_2$.

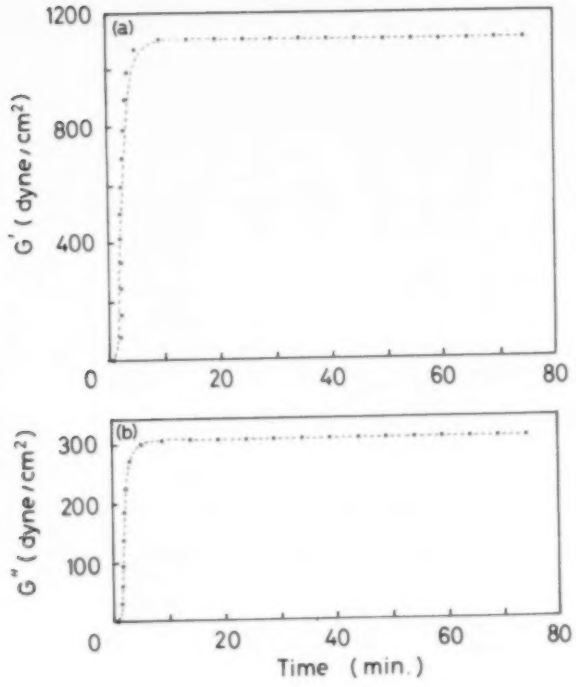

FIG.2

The clotting curves of G' and G" for the fibrinogen solution with ionic strength 0.15. The open circles are the experimental data. The dotted curves were calculated by eqs.(7) and (9) assuming $\alpha_1 = 2.4\ min^{-1}$, $\alpha_2 = 1.2\ min^{-1}$, $\alpha_3 = 0.94\ min^{-1}$, $G'_s = 1110\ dyn/cm^2$, and $G''_s = 310\ dyn/cm^2$.

In this paper, we wish to propose a simple theory which explain the sigmoidal curves of G' and G", and which takes into account only the polymerization reaction of fibrin monomers and the crosslinking reaction of fibrin polymers. In other words, we shall deal with the clotting curves of G' and G" which can be expressed only by the first terms in eq.(1).

Now we consider the gelation of fibrin gel proceeds in three steps:

Step 1 Fibrinogen(F) $\xrightarrow{\alpha_1}$ Fibrin Monomer(F_m),

Step 2 Fibrin Monomer(F_m) $\xrightarrow{\alpha_2}$ Fibrin Polymer(F_p),

Step 3 Fibrin Polymer(F_p) $\xrightarrow{\alpha_3}$ Fibrin Network(F_n),

where (F) is the number of fibrinogen, (F_m) the number of fibrin monomer activated by the enzymatic reaction of thrombin, (F_p) the number of fibrin monomer unit composing fibrin polymers, (F_n) the number of fibrin monomer unit in fibrin polymers which were crosslinked and thus incorporated into the network of the gel, and α_1, α_2, α_3 are rate constants for each step. We assume that(F_p) is proportional to the dynamic viscosity G''_1 and that(F_n) is proportional to the rigidity G'_1. We also assume that each step can be represented by the first order reaction(8-9), neglecting the reaction in backward direction. Then we have the following equations.

$$\frac{d(F)}{dt} = -\alpha_1(F) \tag{2}$$

$$\frac{d(F_m)}{dt} = \alpha_1(F) - \alpha_2(F_m) \tag{3}$$

$$\frac{d(F_p)}{dt} = \alpha_2(F_m) - \alpha_3(F_p) \tag{4}$$

Vol. 17
1980

$$\frac{d(F_n)}{dt} = \alpha_3(F_p) \tag{5}$$

Integration of eqs. (2), (3), (4) and (5) may give the time variation of (F), (F_m), (F_p), and (F_n), if the values of α_1, α_2 and α_3 are assumed. The rate constant α_1 for enzymatic reaction of thrombin on fibrinogen should be very large. The rate constant for polymerization process, α_2, is the same as k_1'' in eq. (1). The rate constant for crosslinking process, α_3, is the same as k_1' in eq. (1). There is the relation $\alpha_1 > \alpha_2 > \alpha_3$.

If the reaction rate with α_1 is rapid, we may assume the initial condition that the number of fibrinogen is equal to the number of fibrin monomer and neglect eq. (2). Then integrating (3), (4), and (5), we have

$$(F_n) = (F_o)\left(1 - \frac{\alpha_3}{\alpha_3-\alpha_2} e^{-\alpha_2 t} + \frac{\alpha_2}{\alpha_3-\alpha_2} e^{-\alpha_3 t}\right) \tag{6}$$

where (F_o) is the initial number of fibrin monomer. If the number of fibrin monomer in the network (F_n) is proportional to the rigidity G_1', eq. (6) is rewritten as

$$G_1' = G_{1s}'\left(1 - \frac{\alpha_3}{\alpha_3-\alpha_2} e^{-\alpha_2 t} + \frac{\alpha_2}{\alpha_3-\alpha_2} e^{-\alpha_3 t}\right) \tag{7}$$

For the time longer than several minutes, eq. (7) can be approximated to

$$G_1' = G_{1s}'\left(1 + \frac{\alpha_2}{\alpha_3-\alpha_2} e^{-\alpha_3 t}\right) \tag{8}$$

Compared to the first term of eq. (1a), $C'=\alpha_2/(\alpha_2-\alpha_3)$ is obtained.

If the second term in eq. (1b), i.e., the increase of G" due to the interaction between fibrin fibers in gel structure is ignored, the loss modulus G_1'' can be assumed to be proportional to the number of fibrin monomer in fibrin polymers(F_p). Then ignoring eq. (5), from eqs. (2), (3) and (4), we derive

$$G_1'' = G_{1s}''\left(1 - \frac{\alpha_2}{\alpha_2-\alpha_1} e^{-\alpha_1 t} + \frac{\alpha_1}{\alpha_2-\alpha_1} e^{-\alpha_2 t}\right) \tag{9}$$

For the time longer than several minutes, eq. (9) can be approximated to

$$G_1'' = G_{1s}''\left(1 + \frac{\alpha_1}{\alpha_2-\alpha_1} e^{-\alpha_2 t}\right) \tag{10}$$

Compared to the first term in eq. (1b), $C''=\alpha_1/(\alpha_1-\alpha_2)$ is obtained.

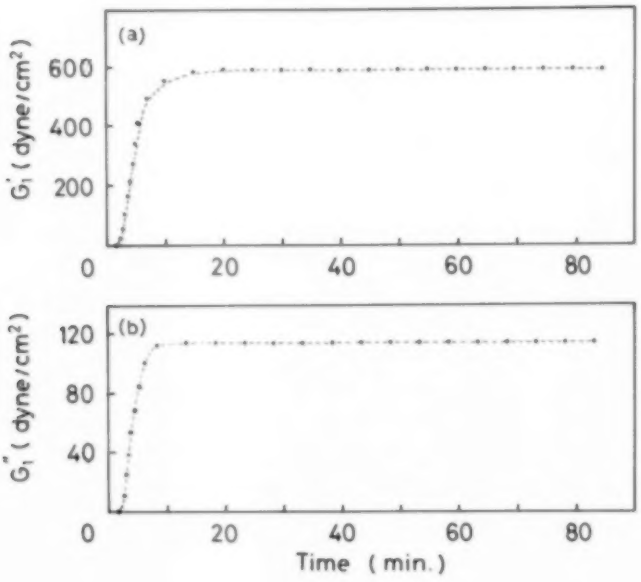

FIG. 3

The clotting curves of G_1' and G_1'' shown by open circles were derived from FIG.1. The dotted curves were calculated by eqs. (7) and (9) assuming $\alpha_1 = 1.5\ min^{-1}$, $\alpha_2 = 0.51\ min^{-1}$, $\alpha_3 = 0.40\ min^{-1}$ $G_{1s}' = 600\ dyn/cm^2$, $G_{1s}'' = 115\ dyn/cm^2$.

Eqs. (7) and (9) represent the sigmoidal curves for G_1' and G_2'', when the reactions corresponding to the second terms in eq. (1) are absent. Figure 2 shows the comparison of experimental and theoretical results of G' and G" for a fibrinogen solution with ionic strength 0.15. The open circles are the measured points and the dotted line has been calculated assuming $\alpha_1 = 2.4\ min^{-1}$, $\alpha_2 = 1.2\ min^{-1}$, and $\alpha_3 = 0.94\ min^{-1}$. The whole clotting curves of G' and G" including the initial sigmoidal parts are well represented by eqs. (7) and (9).

Figure 3 shows the similar application of eqs. (7) and (9) to calculate the time variation of G_1' and G_1'' for the fibrinogen solution with ionic strength 0.5, which were separated from the whole clotting curves of G' and G" shown in Fig. 1 by means of eq. (1). By assuming $\alpha_1 = 1.5\ min^{-1}$, $\alpha_2 = 0.51\ min^{-1}$, and $\alpha_3 = 0.40\ min^{-1}$, the dotted curves calculated by eqs. (7) and (9) represent well the observed data shown by circles.

CONCLUSION

We have assumed the simple kinetic equations of the first order for transformation of fibrinogen to fibrin monomer, the polymerization of fibrin monomers, and the crosslinking of fibrin polymers. The derived equations (7) and (9) with appropriate rate constants can represent satisfactorily the time variation of the rigidity modulus and loss modulus observed for the fibrinogen-thrombin solutions at low ionic strength. When the ionic strength of the fibrinogen solution is high, the second terms in the previously proposed equations (1) must be considered, which represent the association and interaction between fibrin fibers in the network.

The authors wish to thank Prof. M. Hori of the Tokyo Institute of Technology for inspiring this work.

Vol. 17
1980

REFERENCES

1. SCOTT BLAIR, G.W. and BURNETT, J. An equation to describe the rate of setting of blood and milk. Biorheology 1, 183-191, 1963.

2. GLOVER, C.J., McINTIRE, L.V., BROWN III, C.H. and NATELSON, E.A. Mechanical trauma effect on clot structure formation. Thrombosis Res. 10, 11-25, 1977.

3. KAIBARA, M. Dynamic viscoelastic study of the formation of fibrin networks in fibrinogen-thrombin systems and plasma. Biorheology 10, 61-73, 1973.

4. FUKADA, E. and KAIBARA, M. The dynamic rigidity of fibrin gels. Biorheology 10, 129-138, 1973.

5. KAIBARA, M. and FUKADA, E. Effect of temperature on the dynamic viscoelasticity during the clotting reaction of fibrin. Biochim. Biophys. Acta 499, 352-361, 1977.

6. FUKADA, E. and KAIBARA, M. Rheological measurement of fibrin gels during clotting. Thrombosis Res. 8, Suppl. II, 49-58, 1976.

7. ROBERTS, W.W., LORAND, L. and MOCKROS, L.F. Viscoelastic properties of fibrin clots. Biorheology 10, 29-42, 1973.

8. STURTEVANT, J.M., LASKOWSKI, M. Jr., DONNELLY, T.H. and SCHERAGA, H.A. Equilibria in the fibrinogen-fibrin conversion. III. Heats of polymerization and clotting of fibrin monomer. J. Am. Chem. Soc. 77, 6168-6172, 1955.

9. MIHALYI, E. and BILLICK, I.H. Transformation of fibrinogen into fibrin III. Kinetics of the pH change associated with the clotting of fibrinogen. Biochim. Biophys. Acta 71, 97-108, 1963.

BLANK
PAGE

Vol.
198

BIORHEOLOGY, Vol. 17, pp. 261-266, 1980
Printed in the USA. All rights reserved.

0006-355X/80/030261-06$02.00/0
Copyright (c) 1980 Pergamon Press Ltd

EFFECTS OF HYPERCHOLESTEROLEMIA AND ONIONS ON RHEOLOGY OF BLOOD IN RABBITS

T.M. Vatsala and Megha Singh
Biomedical Engineering Division
Indian Institute of Technology
Madra - 600 036, India

ABSTRACT An investigation has been made on the variation of the rheological parameters during induced hypercholesterolemia in rabbits. The animals were divided into three groups and were fed with control (Group I), Cholesterol (0.5 %) (Group II) and Cholesterol (0.5 %) plus extract of 20g fresh onions (Group III) diets. The samples of blood were collected up to six months. Blood viscosity, plasma viscosity, and ESR are higher in Group II than in Group I, whereas, for Group III blood viscosity, PCV, and plasma viscosity are higher than that of Group II. The erythrocytes shape in Group II shows crenation of its membrane, whereas, for Group III the shape is comparable with the normal shape of Group I, even though the cholesterol levels are comparable. Various factors which may be contributing towards the variation in blood rheology of these groups are discussed.

(Received 15.6.1979; in revised form 5.11.1979.
Accepted by Editor H. Schmid-Schönbein.
Received by Executive Editorial Office 2.4.1980)

Vol. 17
1980

INTRODUCTION

In atherosclerosis the pathological, histopathological and biochemical changes are well established (1-2). But little has been mentioned about the rheological changes during induced atherosclerosis. Excellent reviews have been written on blood rheology (3-5). These articles mentioned briefly the effect of hypercholesterolemia on blood viscosity. The detailed analysis of various rheological parameters during induced atheroclerosis has not been reported.Therefore, we aim to study the variation of these parameters in induced atherosclerosis in rabbits. To produce these changes in cardiovascular system, the animals are fed with hypercholesterolemic diet. This diet has further been supplemented for another group of animals with the extract of fresh onions to observe the rheological changes. Our work on onion extract has been motivated by the research carried out by several authors who pointed out that lipid levels in blood tend to decrease with the intake of onions (6-9).

METHODS

White albino rabbits of same age (2-3 months) and sex were maintained on normal laboratory diet (Rabbit feed, Hind lever Ltd.) and divided into three groups with ten animals in each group. Group I served as normal controls. Group II animals were fed with atherogenic diet (normal diet + 0.5 % cholesterol). Group III animals were fed with atherogenic diet plus extract of 20g fresh onions (10).

Blood was drawn by ear vein puncture and was collected with and without ammonium oxalate, as an anticoagulant, upto six month. The blood sample without anticoagulant was used for the determination of serum cholesterol levels (11). Using anticoagulated blood the erythrocyte sedimentation rate (ESR) and packed cell volume (PCV) were determined by Wintrobe method. Blood and plasma viscosities were determined (12) using cappilary viscometer (13). The hemoglobin level was determined by Drabkin's method (14) and plasma fibrinogen by the method of Goodwin (15). For microscopic observations of erythrocytes shape after six months the slides were prepared fresh ear vein blood.and were observed under Leitz microscope at a magnification of 1000.

Key words: Hypercholesterolemia, onion, blood rheology

RESULTS

Fig. 1 (a-c) shows the erythrocytes shape of various groups after six months (a) shows the erythrocytes shape for Group I (normal), (b) for Group II (crenated) and (c) for Group III (normal). Although the cholesterol content of the Groups II and III are comparable, the erythrocytes shape differs significantly.

Fig. 2 (a,b) defines the relationship between the blood viscosity and plasma viscosity with respect to the duration of observation for the above mentioned groups. The blood viscosity for Group I tends to remain constant, whereas, for Group II it decreases initially and for Group III it does not show any significant variation, but it is still higher than control group and Group II. The plasma viscosity tends to increase in Group II and Group III, and is more for Group III, whereas, for Group I, this does not show much variation.

The levels of various constituents which may influence the plasma viscosity, which in turn influences blood viscosity, are given in Table I. The increase in fibrinogen level in Group I is less (75 %) compared to Groups II and III (about 275 %), whereas, the cholesterol levels increase significantly for Groups II and III and not for Group I. Hemoglobin level does not show any significant variation.

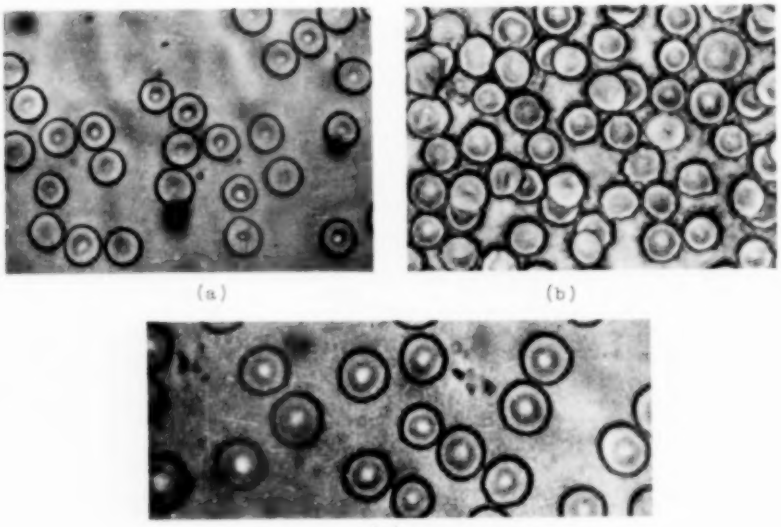

Fig. 1: Erythrocytes of (a) control group, (b) animals fed atherogenic diet and (c) animals fed with atherogenic diet plus onion extract.

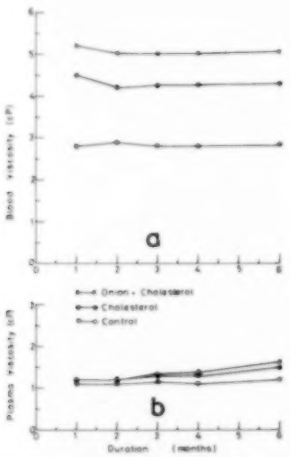

Fig. 2: The variation of blood viscosity and plasma viscosity with respect to the duration of observation at 50 sec^{-1}.

TABLE I

COMPARISON OF THE VARIOUS CONSTITUENTS OF BLOOD IN THREE GROUPS WITH RESPECT TO TIME DURATION

Duration (months)	Fibrinogen (mg %)		
	Group I	Group II	Group III
0	160 ± 10.5	158 ± 9.8	160 ± 8.5
1	170 ± 8.2	270 ± 8.2	265.5 ± 10.3
2	185 ± 8.1	356 ± 7.97	313.7 ± 6.17
3	200 ± 10.1	402.8 ± 13.0	391 ± 4.85
4	260 ± 12.3	604.7 ± 8.6	548.26 ± 21.8
6	280 ± 10.2	620 ± 5.78	600 ± 10.17

	Cholesterol (mg %)		
0	85 ± 5.4	87 ± 10.8	87 ± 9.5
1	93 ± 5.7	450 ± 39.3	427 ± 31.5
2	97 ± 6.5	544 ± 15.7	457 ± 11.1
3	98 ± 7.2	825 ± 10.2	800 ± 8.8
4	99 ± 7.5	1050 ± 12.5	1000 ± 12.9
6	105 ± 8.5	1200 ± 28.5	1178 ± 32.0

	Hemoglobin (mg %)		
0	14.5 ± 0.95	14.2 ± 1.2	14.5 ± 1.5
1	14.8 ± 1.2	14.64 ± 1.5	14.94 ± 1.66
2	16.4 ± 1.8	14.60 ± 1.3	12.67 ± 2.36
3	16.4 ± 1.3	16.38 ± 2.7	16.15 ± 2.36
4	16.0 ± 1.4	15.2 ± 1.9	15.1 ± 1.4
6	16.3 ± 1.3	15.4 ± 1.6	15.3 ± 1.5

Vol. 17
1980

Table II shows the variation of PCV and ESR. The PCV values for Group I show less variation compared to Groups II and III. This decrease is more for Group II compared to Group III. Similarly, ESR for Groups II and III shows an increase during the period of observation. This increase is more for Group II compared to Group III.

TABLE II

Duration (months)	ESR (mm/hour)			PCV (%)		
	Group I	Group II	Group III	Group I	Group II	Group III
0	2.8 ± 0.35	3.0 ± 0.50	2.8 ± 0.57	41.0 ± 1.5	40.0 ± 1.2	40.1 ± 1.5
1	3.0 ± 0.73	3.1 ± 0.87	3.0 ± 0.77	43.2 ± 1.7	36.9 ± 1.22	36.7 ± 1.4
2	2.1 ± 0.45	7.3 ± 1.18	5.1 ± 0.79	42.0 ± 1.4	35.1 ± 1.37	37.0 ± 1.4
3	2.0 ± 0.66	6.6 ± 0.77	5.4 ± 0.53	45.3 ± 2.1	32.0 ± 1.9	34.5 ± 1.5
4	2.1 ± 0.63	7.1 ± 0.52	5.4 ± 0.48	38.8 ± 1.1	31.6 ± 1.71	34.8 ± 1.2
6	2.1 ± 0.45	8.1 ± 0.78	6.1 ± 0.47	39.2 ± 1.3	32.1 ± 1.8	34.9 ± 1.1

DISCUSSION

Our results indicate that the blood rheology during induced hypercholesterolemia is different than that under normal conditions. Various parameters which influence the blood rheology under normal conditions, tend to vary during hypercholesterolemia.

It has been pointed out that the erythrocytes while subjected to a medium with altered plasma composition attain an altered membrane structure (15). Our present observations show that in Group II the erythrocytes have an altered membrane shape i.e., crenation of membrane. This effect may be due to the higher levels of cholesterol or fibrinogen or both. Recently Rogausch has also reported similar findings in guinea pigs (17). The normal shape of the erythrocytes in the presence of onion extract is an interesting finding.

The factors responsible for the variation of blood viscosity are either the varied levels of plasma constituents or erythrocytes shape or both. Similar observations are also made by others (3-5, 17-20). In the present studies, the levels of fibrinogen and cholesterol are significantly higher than that of the control group and these factors could be responsible for the increase in blood viscosity. With the increase of time duration, the change in PCV is more for Group II compared to Group III. The ESR for one hour, for Group II is higher than Group III to wards the end of six months. This may be due to a decrease in hematocrit compared to other groups.

Thus, it is observed that the rheology of blood during atherosclerosis is different that under normal flow conditions. The plasma constituents show an increasing pattern, which in turn may influence the erythrocytes and finally the blood viscosity. As it has been observed that the hemolytic tendency of crenated cells, under identical conditions, is more than in the normal cells (Vatsala and Singh, unpublished results), the decrease in PCV may be explained by this mechanism or it may be due to the impairment of the production of red cells in bone marrow due to higher plasma constituents. The absence of such crenation of Group III erythrocytes at comparable levels of cholesterol indirectly points out that the presence of the whole onion extract or any constituent of the onion extract counterbalances the deleterious effect of cholesterol and helps to retain the normal shape of erythrocytes and thus maintains the constant blood viscosity which is higher than for other Groups.

Recently we have reported that the erythrocytes of Group II regained their normal shape by incubation in the plasma of Group I or Group III, whereas, the normal cells of Group I or Group III get crenated after incubation in the plasma of Group II (21). This further supports the preventive action of onion extract on erythrocytes.

Thus, there may be a possible link between the blood rheology and the levels of various constituents of the suspending medium in induced hypercholesterolemia. Further studies in this direction concerning the viscoelastic behaviour of erythrocytes with the variation of plasma constituents are in progress.

REFERENCES

1. PAOLETTI, R. and GOTTO, A.M. Atherosclerosis Reviews, Vol. 1, New York: Raven Press,1976

2. PAOLETTI, R. and GOTTO,A.M. Atherosclerosis Reviews, Vol. 2, New York: Raven Press,1977

3. MERRILL, E.W. Rheology of blood, Physiol. Rev. 49, 863-888, 1969.

4. SCHMID-SCHÖNBEIN, H. and WELLS, R.E., Jr. Rheological properties of human erythrocytes and their influence upon the anomalous viscosity of blood. Ergeb. Physiol. Biol. Chem. Exp. Pharmakol. 63, 146-219, 1971.

5. CHIEN, S. Biophysical behaviour of red cell in suspension. In: The Red Blood Cell. D. MacN. Surgenor (ed.) New York, San Francisco, London: Acad. Press, Vol. 2, 1975, pp. 1032-1121.

6. MENON, I.S., KENDAL, R.Y., DEWAR, H.A. and NEWELL, D.J. Effects of onions on blood fibrinolytic activity. Brit. Med. J. 3, 351-355, 1968.

7. BORDIA, A., BANSAL,H.C. ARORA, S.K. and SINGH,S.V. Effects of essential oils of garlic and onions on hyperlipemia. Atherosclerosis. 21, 15-19, 1975.

8. SHARMA, K.K., CHOUDHARY, N.K. and SHARMA, A. L. Studies on hypocholesterolemic activity of onion: Effects on serum cholesterol diet. Ind. J. Nutr. Diet. 12, 388-391, 1975.

9. SHARMA,K.K. CHOUDHARY, N.K. and SHARMA, A.L. Long term effects of onion on experimentally induced hypercholesterolemia and consequently decrease fibrinolytic activity in rabbits. Ind. J. Med. Res. 63, 1629-1634, 1975.

10. STOLL, A. and SEEBECK, E. Chemical investigations on allin, the specific principle of garlic, In: Adv. Enzymol. F.F. Nord (ed.) New York: Interscience 11, 377-399, 1951.

11. ABELL, L.L. LEVY, B.B., BRODIE, B.B. and KENDALL, F.E. A simplified method for estimation of total cholesterol in serum and demonstration of its specificity. J. Biol. Chem. 195, 357, 1952.

12. SINGH, M. and COULTER, N.A., Jr. Influence of dextrans on rheological properties of blood. Biorheology. 11, 217-225, 1974.

13. VATSALA, T.M. and SINGH, M.A. new capillary viscometer for viscosity measurement of biological fluids. In: Proc. VII All India Biomed. Engn. Symp. Osmania Univ. Hyderabad, 17-18, 1978.

14. DRABKIN, D.L. Metabolism of hemin chromoproteins. Physiol. Rev. 31, 374-376, 1951.

15. GOODWIN, J.F. Determination of plasma fibrinogen: salting out procedure. Am. J. Clin. Pathological 35, 227-229. 1961.

16. BESSIS, M., WEED, RI. and LEBLOND, P.F. Red cell shape. New York, Heidelberg and Berlin: Springer -Verlag, 1973, P.180.

17. BOGAUSCH, H. Red cell deformability and adaptation in cholesterol-fed guinea pigs. Pflugers Archiv. 373, 39-42, 1978.

18. DINTENFASS, L. and KAMMER, S. Plasma viscosity in 615 subjects. Effects of fibrinogen globulin and cholesterol in normals, periferal vascular disease, retinopathy and melanoma. Biorheology. 14, 247-251, 1977.

19. SINGH, M. and COULTER, N.A. Jr. Rheology of blood: Effect of dilution with various dextrans. Microvas. Res. 5, 123-130, 1973.

Vol. 17
1980

20. SINGH, M. and COULTER, N.A., Jr. Dextrans and the rheology of blood. Ind. J. Med. Res. 62, 630-639, 1974.

21. VATSALA. T.M. and SINGH, M. In vitro changes and recovery of erythrocytes shape in induced atherosclerosis. Current Science, 48, 797-799, 1979.

BIORHEOLOGY, Vol. 17, pp. 267-273, 1980
Printed in the USA. All rights reserved.

0006-355X/80/030267-07$02.00/0
Copyright (c) 1980 Pergamon Press Ltd

COMPARISON OF POWER DENSITY SPECTRA OF TURBULENT FLOW THROUGH TUBES OBTAINED WITH HOT FILM AND LASER DOPPLER ANEMOMETERS

Frederick J. Walburn, Edward F. Blick*, and Paul D. Stein

Departments of Medicine and Surgery, Henry Ford Hospital, Detroit, MI 48202, USA, and
*School of Medicine, Nuclear and Mechanical Engineering, University of Oklahoma
College of Engineering, Norman, Oklahoma 73019, USA

(Received 20.6.1979; in revised form 27.9.1979.
Accepted by Editor H.L. Goldsmith.
(Received by Executive Editorial Office 30.4.1980)

ABSTRACT In order to assess the capability of a hot film anemometer to measure high frequency velocity fluctuations, the power spectra of turbulence obtained with a hot film anemometer were compared to the power spectra obtained with a laser Doppler anemometer. The spectra obtained with a hot film anemometer and the laser Doppler anemometer were within 6 dB of each other throughout approximately 12% of the frequencies calculated to be present in turbulence in this system. This included measurements well into the Kolmogorov region. The hot film anemometer measured frequencies to approximately 35% of the frequencies calculated to be present; whereas the laser Doppler anemometer measured frequencies to approximately 20% of the frequencies thought to be present. Consequently, higher frequencies were measured with the hot film anemometer. The amount of power measured with either the hot film anemometer or the laser Doppler anemometer was over 99% of the power contained in the turbulence. The hot film anemometer showed frequencies to 900 Hz at a Reynolds number of 11,000 using an overheat ratio of 1.02, and somewhat higher frequencies were measured at an overheat ratio of 1.14. These observations showed that the measured frequencies of fluctuating velocities depended upon the energy of fluctuations. Both the hot film anemometer and the laser Doppler anemometer were capable of measuring frequencies within the portion of the power spectral density curve that contained the great majority of power.

Vol. 17
1980

INTRODUCTION

Important investigative tools for the measurement of turbulent flow are the hot film and hot wire anemometers (1) and more recently,the laser Doppler anemometer (2). In spite of wide use of these instruments, there have been few attempts to determine the actual frequency response to flow fluctuations, in contradistinction to the electrical frequency response. The frequency response of hot film anemometers has been stated to be 10 kHz, although supporting data was not given (3). Actual investigations of the ability of hot film probes to measure velocities in water have been reported at frequencies as high as 1000 Hz only in one study (4). Others investigated oscillating velocities only at relatively low frequencies, 12 Hz (5) and 20 Hz (6). An attenuation of amplitude with increasing frequencies was reported by some (4); whereas an amplification of amplitude (5) or no change (6) at lower frequencies was also reported. Under optimal conditions, a time resolution of 100 sec, equivalent to a frequency response of 10 kHz, has been reported with a laser Doppler anemometer (7). The electrical frequency response of a hot film anemometer has been reported to be 18.6 kHz (8) and for the laser Doppler anemometer it is on the order of 100 kHz (9). In view of the sparse and varying information about these instruments this investigation was undertaken to compare the power spectra of turbulence obtained with hot film and laser Doppler anemometers.

METHODS

Turbulence was measured during the steady flow of saline through a rigid polyvinyl-chloride tube with an internal diameter of 19.1 mm. The flow system is shown schematically in Figure 1. Saline, .9 gm/100 ml (viscosity .0102 poise, density 1.006 gm/ml) was pumped from a collection tank into a reservoir in order to dissipate any large scale fluctuations. A 12.7 mm diameter cannulating electromagnetic flow transducer (Biotronex Laboratories, Inc., Kensington, Md.) was attached to the orifice of the test section. After passing through the test section, the saline flowed into a collection tank from which it was recirculated by a centrifugal pump. Steady flow from 0 to 10,800 ml/min could be produced, which permitted us to attain Reynolds numbers of 11,000.

Key Words: Hemodynamics, blood flow velocity, flowmeters, rheology, turbulence

The cannulating electromagnetic flow transducer at the orifice of the test section acted as a turbulence generator. The purpose of the turbulence generator was to cause the transition to turbulent flow to occur near the orifice. Therefore, fully developed flow was likely to be present at the site of measurement, 110 cm downstream from the orifice.

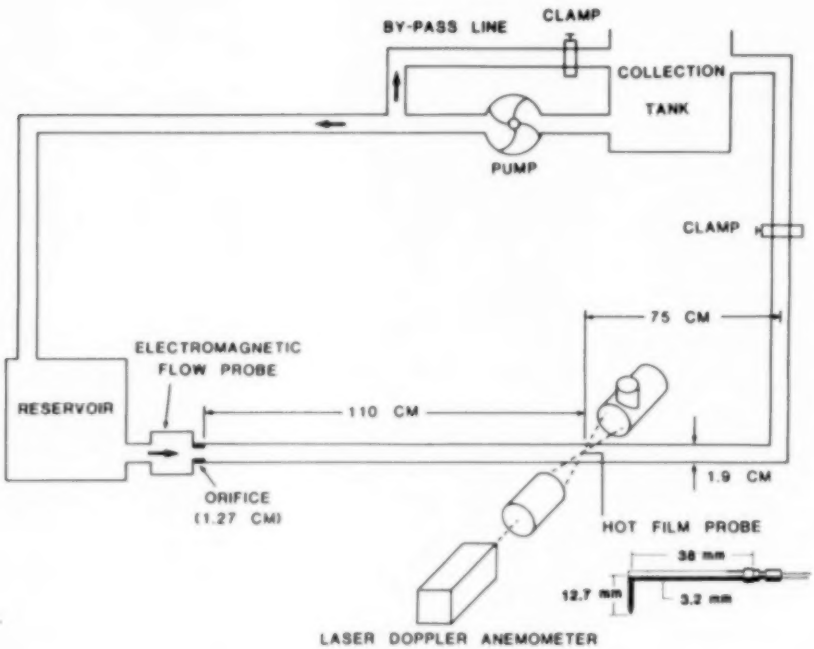

FIG. 1

Diagram of the flow system, not to scale, showing the location of the hot film probe and laser Doppler anemometer. The dimensions of the hot film probe are also shown.

The laser Doppler anemometer (Thermo-Systems, Inc., St. Paul, Minn.) was operated in the differential Doppler mode with forward scattering (10). In this mode a collimated, coherent, monochromatic, plane-polarized Gaussian laser beam is passed through a beam splitter and focused to a common point in the flow. The resulting destructive and constructive interference produces intimately spaced planar interference fringes in the beam intersection region. A particle moving through the beam intersection region will intercept the interference fringes. The light scattered by the particle will alternate between a maximum (particle crossing a fringe) and zero (particle between fringes). The receiving optics (consisting of a lens and a photodiode) collects the scattered light and generates an electrical current which has an amplitude proportional to the amount of scattered light collected. The frequency of this current is proportional to the rate at which the particle intercepts the fringes. The photodiode signal is processed by a velocity tracker--which is essentially a tracker filter. The incoming signal is passed through a narrow band voltage tuned filter and into a frequency discriminator whose output is proportional to the input frequency. The output of the frequency discriminator is then fed back through a filter to the voltage tuned filter. This enables the filter to "track" the frequency of the incoming signal. The components were mounted on an optical bench which, in turn, was fastened to the carriage of a lathe. The lathe carriage was attached to a drill press platform. Thus, the measuring volume could be moved incrementally in all directions. The longitudinal tube axis was perpendicular to the plane of the laser beams in order to measure the axial velocity component. Scattering particles consisting of 1.5 micron diameter silicon carbine particles (specific gravity = 3.2) were added to the flow system when the laser Doppler anemometer was used.

Instantaneous local velocity was also measured with an L-shaped conical tip hot film probe (TSI-1231) in combination with a TSI-1050 constant temperature anemometer and linearizing system (Thermo-Systems, Inc., St. Paul, Minn.). Based upon the probe diameter of 1.5 mm, the percentage of the total cross-sectional area of the tube occupied by the probe was less than one percent. Hence, blockage of the flow by the probe was minimal. The constant temperature anemometer was operated at overheat ratios of 1.02 and 1.14, which limited the temperature of the heated film to 2.7°C and 18.5°C respectively, above the

ambient temperature. The probe was calibrated at both overheats in a rotating reservoir and used at room temperature (23.6°C). Thus, the highest temperature of the probe was 42.1°C, well below the range where bubble formation would be expected to occur. The temperature of the saline was adjusted at frequent intervals to maintain it at 23.6°C.

The tip of the hot film probe and the measuring volume of the laser Doppler anemometer were positioned 110 cm downstream from the inlet at the center of the tube along the axis of flow. Voltage spectra were measured sequentially with a Model SD360 Spectrum Analyzer (Spectral Dynamics Corporations, San Diego, California) and displayed on a Model 135A-02-X-Y plotter (Hewlett Packard, Palo Alto, California). The hot film probe was left in place during the laser Doppler measurements. The length of the sampling time for each spectrum was approximately four minutes. Prior to measurements with the hot film system, the fluid was filtered to reduce the effect of changing heat transfer characteristics on the signal measured. Six spectra were obtained at each flow rate for both anemometers, and the reported results represented the average. The one dimensional energy density spectrum was calculated as $(\text{velocity})^2/\text{frequency}$ and plotted as a function of frequency, f, and wave number, $k = 2\pi f/\bar{U}$ where $\bar{U}$ is mean axial velocity.

The viscosity of the saline was measured at room temperature with a cone-in-plate viscometer (Brookfield Engineering Laboratories, Inc., Stoughton, Mass.) at shear rates of 450 sec^{-1} and 900 sec^{-1}. Density was measured with a hydrometer.

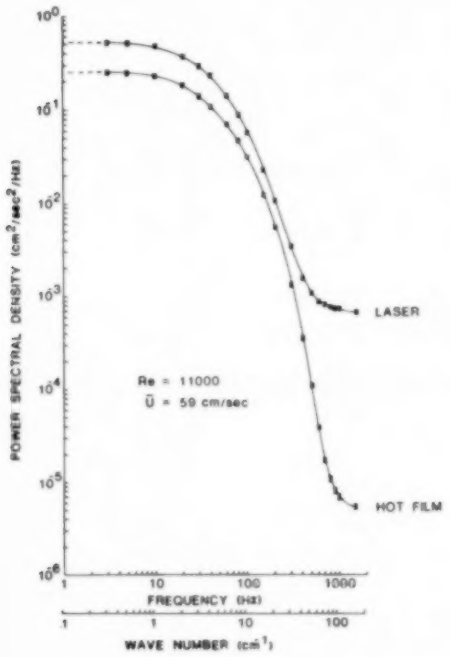

FIG. 2

Power spectral density shown as a function of both the frequency and wave number at a Reynolds number (Re) of 11,000. Mean axial velocity, U, was 59 cm/sec. The hot film probe was used at an overheat ratio of 1.14. Measured data are shown as the mean ± SEM.

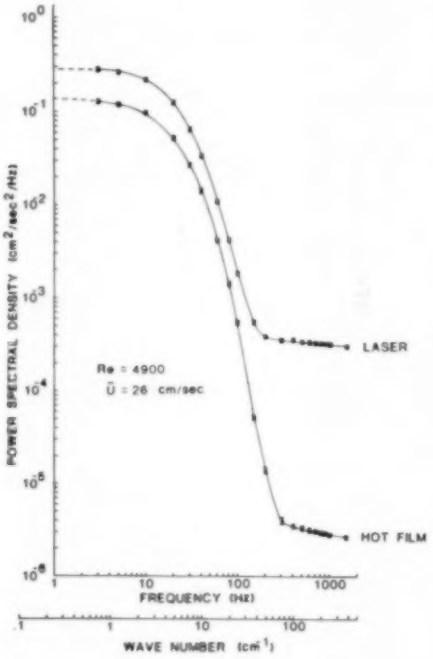

FIG. 3

Power spectral density shown as a function of the frequency and wave number at a Reynolds number of 4,900. The hot film probe was used at an overheat ratio of 1.14. Abbreviations are as in Fig. 2.

RESULTS

At wave numbers below approximately 6 cm^{-1}, which correspond to the region of energy containing eddies, the spectrum of frequencies obtained with the hot film anemometer used at an overheat ratio of 1.14 paralleled the spectrum obtained with the laser Doppler anemometer, but velocities were somewhat lower in the former (Figs. 2, 3). The region at which the power spectral density shows a slope of approximately -5/3 is defined as the inertial subrange. In our system, at the Reynolds numbers we studied, the inertial subrange was from wave numbers of approximately 6 cm^{-1} to 11 cm^{-1} in spectra obtained both with the hot film anemometer and the laser Doppler anemometer. At higher wave numbers, the beginning of Kolmogorov microscale region, the negative slope of the power spectral density increased. The spectrum obtained with the laser Doppler anemometer failed to

Vol. 17
1980

diminish above a wave number of 30 cm^{-1}; whereas the spectra obtained with the hot film probe showed a continuing sharp slope until 70 cm^{-1} to 100 cm^{-1}. Lower magnitudes of spectral density could be obtained with the hot film anemometer than the laser Doppler anemometer. The spectra obtained with the hot film anemometer and the laser Doppler anemometer were within 6 dB of each other throughout approximately 12% of the frequencies calculated to be present in turbulence in this system. (11). This included measurements well into the Kolmogorov region.

The frequencies that correspond to the inertial subrange and Kolmogorov region depend upon the Reynolds number. In our system, at a Reynolds number of 11000, the beginning of the inertial subrange was at 56 Hz, while the Kolmogorov region began at 103 Hz. The frequencies that correspond to the inertial subrange and the Kolmogorov range decreased as the Reynolds number decreased. At a Reynolds number of 4900, the inertial subrange began at about 25 Hz, and the Kolmogorov range began at about 45 Hz.

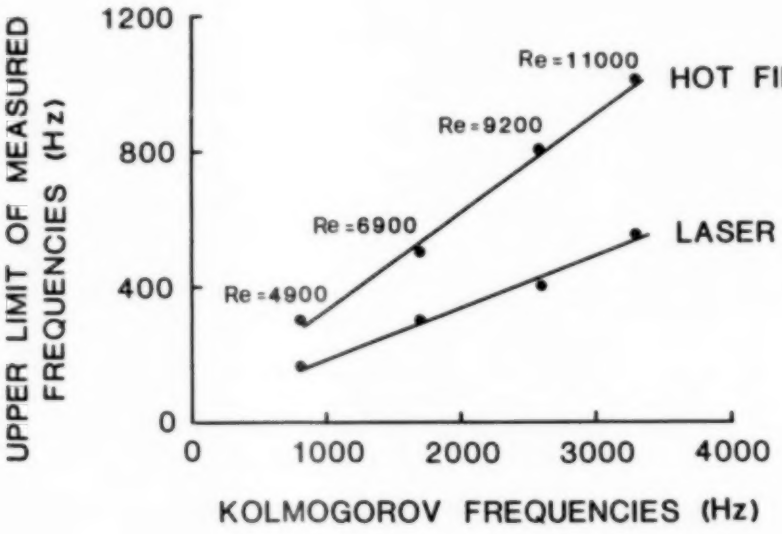

Approximate upper limit of frequencies measured with the hot film and laser Doppler anemometers shown relative to the highest frequencies calculated to be present (the Kolmogorov frequencies) at various Reynolds numbers (Re).

The energy density spectrum obtained with the laser Doppler anemometer at a Reynolds number of 11,000 showed a diminished negative slope at about 400 Hz and it was essentially flat about 1000 Hz indicating that valid measurements were not obtained in that region. The spectra obtained with the hot film anemometer began to show a reduced negative slope at about 1000 Hz, beyond which measurements did not appear to be valid. At a lower Reynolds number, 4900, the spectrum obtained with the laser Doppler aneomometer showed a diminished negative slope around 150 Hz and by 250 Hz it was flat indicating that the measurements were not valid at those frequencies. The spectra obtained with the hot film anemometer showed a constant slope until about 300 Hz beyond which valid measurements ceased to be obtained.

The approximate upper limit of frequencies that were measured with the hot film anemometer and laser Doppler anemometer at various Reynolds numbers are shown relative to the upper limit of frequencies calculated to be present in turbulent flow in this system (the Kolmogorov frequency) (Fig. 4). The Kolmogorov frequency was calculated as $\sqrt{\rho \bar{U}^3 / D\mu}$, where $\bar{U}$ is mean axial velocity, D is the tube diameter, ρ is density and μ is viscosity. The hot film anemometer measured frequencies to approximately 35% of those calculated to be present. The laser Doppler anemometer measured frequencies to about 20% of frequencies thought to be present. However, the amount of power measured with either the laser Doppler anemometer or the hot film anemometer (Fig. 5) constituted over 99% of the power contained within the turbulence. This is readily apparent from Figure 5, which shows that the area under the power spectral density curve of the laser Doppler aneomometer at frequencies above 550 Hz was small.

The spectrum obtained with the hot film anemometer at an overheat ratio of 1.14 was comparable to the spectrum obtained at an overheat ratio of 1.02 until a frequency of

900 Hz was reached (Fig. 6). Higher frequencies appeared to be measured when a higher overheat was used.

DISCUSSION

The frequency spectra for isotropic turbulence has been described in terms of regions (11). In order of increasing frequency and wave number, they are 1) the region of largest permanent eddies; 2) the region of energy containing eddies; 3) the inertial subrange; and 4) the region of the Kolmogorov microscales (11). The more permanent eddies contain less energy than the energy containing eddies, although it may amount to as much as 20% of the total kinetic energy (11). As the wavenumber (and frequency) increase, inertial interactions produce smaller eddies and transfer energy from the larger eddies to the smaller ones (11). The energy in the smallest eddies is then dissipated into heat due to viscosity. In the inertial subrange, inertial transfer of energy is the dominating factor (11) and the spectra are proportional to $k^{-5/3}$ (11). At higher frequencies, where the energy spectrum no longer diminishes at a slope of -5/3, is the region of eddies whose size and velocities are described as the Kolmogorov microscales. These eddies are the smallest that occur in a turbulent flow. This is the range at which viscous dissipation of turbulent kinetic energy dominates. The highest frequencies that exist in the Kolmogorov region can be calculated (11). In our system, at a Reynolds number of 11000, we estimated by these calculations that turbulent velocity fluctuations would reach approximately 350 Hz and at a Reynolds number of 4800 the frequency would reach approximately 950 Hz.

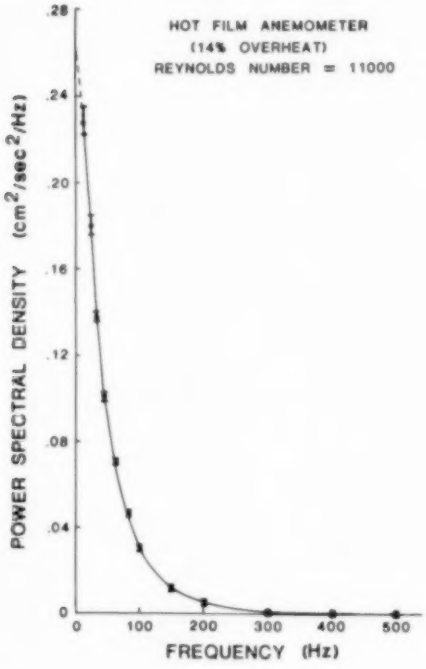

FIG. 5

Power spectral density shown as a function of frequency on rectilinear coordinates. Little power was present at frequencies above 300 Hz, as shown by the area under the curve at higher frequencies.

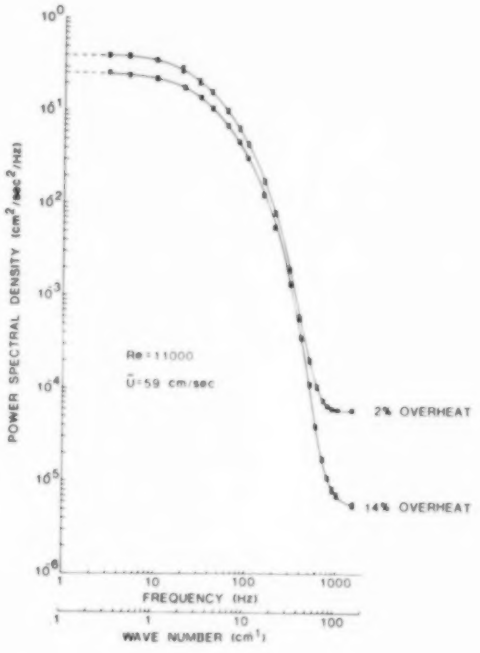

FIG. 6

Power spectral density curves obtained with a hot film anemometer using overheat ratios of 1.02 and 1.14 at a Reynolds number (Re) of 11,000 and a mean axial velocity (U) of 59 cm/sec.

Both the hot film and laser Doppler anemometers showed energy spectra which compare favorably to spectra predicted by theory through the first 20% to 35% of frequencies contained in turbulence in our system. The hot film anemometer appeared to measure somewhat higher frequencies than did the laser Doppler anemometer.

The leveling out of the curve representative of the power spectral density at higher frequencies (wave numbers greater than 11) for the laser Doppler anemometer is thought to be due to a limitation of the size of the sampling volume through which the beam passes (12). This is sometimes referred to as Doppler ambiguity, and is produced by the finite

Vol. 17
1980

transit time of particles through the scattering volume (12). It is possible that a somewhat higher frequency could be attained before ambiguity occurs by use of a digital counter. Another method for the reduction of ambiguity noise is by use of a cross correlation technique (13). When the characteristic wavelength of the turbulent fluctuations approximates the dimensions of the sampling volume, the laser Doppler anemometer would reach the limits of its sensitivity. For the laser Doppler anemometer used in our study, the sampling dimension was approximately 1 mm. It can be shown that the Kolmogorov eddy sizes for these tests were of an order of magnitude of .01 mm (11). In our system, at a Reynolds number of 11,000, a frequency of 100 Hz corresponded to a wave length of approximately 1 mm. As expected, therefore, at a frequency of around 400 Hz (which is the same order of magnitude as 100 Hz) the power spectral curve obtained with the laser Doppler anemometer at a Reynolds number of 11,000 began to flatten out. The power spectral density curve obtained with the hot film anemometer did not flatten out until higher frequencies. The recorded power spectrum of the flattened curve probably represented electronic noise in the circuits.

When discussing the frequency response and range of hot film and laser Doppler anemometers, it is important to recognize that there is a marked difference between the frequency response of the electronics itself and the response to a change in actual fluid velocity. Regarding the electrical response of hot film anemometers, one investigator used a shock tube to impose a step rise in the surface heat transfer on a hot wire and hot film probe and found a frequency limit of 200 kHz for his equipment (14). Another investigator used the thoery of a constant temperature anemometer to calculate a theoretical fluctuation response of 31 kHz which was comparable to 23 kHz obtained from applying a square wave test signal across an arm of a Wheatstone bridge (15). Experimenters have considered the energy balance for a cylindrical hot film probe as one arm of a Wheatstone bridge (8). It was reported that the cutoff frequency of the hot film anemometer can be estimated by means of a sine wave test. A cutoff frequency of 18.6 kHz was found for a typical anemometer system, but it was suggested that, in practice, boundary layer effects may be the limiting factor prior to the electronic limit (8).

In only a few cases have investigators measured the actual frequency response of a hot wire or hot film anemometer in liquids. Oscillating a probe in still water at a frequency of 12 Hz showed 20% amplification of the velocity (5). Others, however, found a flat amplitude response with oscillation of a probe in water to frequencies of 20 Hz (6). Clark (4) examined the frequency response of a conical tip and cylindrical tip hot film probes in water. The probes were held stationary in a pulsating flow for frequencies of 1 to 15 Hz. At higher frequencies, which reached 100 Hz, the probes were oscillated with a mechanical oscillator in a steady stream. The ratio of the measured amplitude of velocity to actual amplitude of velocity was examined as a function of the Strouhal number. (Strouhal number = $2\pi fl/U$, where f is the frequency, l is the distance from the leading edge of the probe to the thin film gauge, and U is mean axial velocity). For the conical tip probe, the measured amplitude of the fluctuating velocity did not differ from the actual amplitude at Strouhal numbers $\leq$ .15. Therefore, for example, there would be no attenuation of velocity to 29 Hz with their probe at a mean velocity of 60 cm/sec. For Strouhal numbers between .15 and .30, the amplitude ratio decreased 2.4 dB/decade. Therefore, at 57 Hz, there would be a 15% attenuation in the amplitude of velocity if the mean velocity were 60 cm/sec. For Strouhal numbers greater than .30, the amplitude ratio decreased at .92 dB/decade. Therefore, at a frequency of 1000 Hz, the velocity amplitude ratio would be attenuated 22% at a mean velocity of 60 cm/sec. The Strouhal number was reported to be the appropriate parameter since the amplitude diminished with variation of the frequency and the axial velocity.

The frequency response of hot film probes has been measured in air (16). The amplitude of velocity was found to be 35% to 58% less than the actual velocity of the moving hot film probe in air. It was stated that this effect was due to thermal feedback from the substrate of the thin film. It was predicted that there would be little attention of the amplitude of velocity due to thermal feed back from the substrate when hot film probes were used in water (16). However, no actual tests were made.

Few studies have been performed to determine the actual frequency response of a laser Doppler anemometer. The primary problem is to determine if the fluctuations of the scattering particles are the same as the fluctuations of the fluid itself. Theoretical considerations are far from complete (17). However, it has been reported that an actual frequency response of up to 10 kHz is possible under optimal conditions (7). An electrical frequency response of 10 kHz has been reported (7, 18).

Relatively low overheat ratios have been used for hot film anemometer measurements of velocity in patients (19) in order to prevent the deposition of fibrin upon the film (4). It is pertinent, therefore, that power spectral densities showed comparable values at overheat ratios of 1.02 and 1.14 to frequencies of 900 Hz. Beyond that frequency, signals of lower energy were recorded at a higher overheat ratio.

In conclusion, observations of the spectra obtained with a hot film anemometer and a laser Doppler anemometer showed that the measured frequencies of fluctuating velocities depended upon the energy of the fluctuations. Higher frequencies were measured with the hot film anemometer. Both the hot film anemometer and the laser Doppler anemometer were capable of measuring frequencies contained within the portion of the power spectral density curve that contained the great majority of power.

Supported under project R38820 from funds supplied by Henry Ford Hospital
via a Ford Foundation grant
and by U.S. PUblic Health Service -
National Heart, Lung and Blood Institute grant HL 23669-01

REFERENCES

1. SANDBORN, V.A. Laboratory instrumentation in turbulence measurements. In: Handbook of Turbulence - Volume 1: Fundamentals and Applications. W. Frost and T.H. Moulden (Eds). New York, Plenum Press. 1977, pp. 315-368.

2. CLIFF, W.C. Optical and acoustical measuring techniquess. In: Handbook of Turbulence - Volume 1: Fundamentals and Applications. W. Frost and T.H. Moulden (Eds). New York, Plenum Press. 1977, pp. 403-432.

3. LING, S.C., ATABEK, H.B., FRY, D.L., PATEL, D.J., JANICKI, J.S. Application of heated-film velocity and shear probes to hemodynamic studies. Circ. Res. 23, 789-801, 1968.

4. CLARK, C. Thin film gauges for fluctuating velocity measurements in blood. J. Sci. Instruments 7, 548-556, 1974.

5. SEED, W.A. and WOOD, N.B. Development and evaluation of a hot-film probe for cardiovascular studies. Cardiovasc. Res. 4, 253-263, 1970.

6. CLARK, C. and SCHULTZ, D.L. Velocity distribution in aortic flow. Cardiovasc. Res. 7, 601-613, 1973.

7. ITEN, P.D. and MASTNER, J. A laser Doppler velocimeter offering high spatial and temporal resolution. In: Flow - Its Measurement and Control in Science and Industry. R.B. Dowdell (Ed). Instrument Society of America, 1971, Vol. 1, pp. 1007-1013.

8. FREYMUTH, P. Theory of frequency optimisation for hot-film anemometers. J. Phys. E.: Sci. Instrum. 11, 177-179, 1978.

9. JONES, W.B. Laser fluid velocity sensor. In: Flow - Its Measurement and Control in Science and Industry. R.B. Dowdell (Ed). Instrument Society of America, 1974, Vol. 1, pp. 1015-1024.

10. RUDD, M.J. The laser anemometer - a review. Optics and Laser Technology 3, 200-207, 1971.

11. HINZE, J.O. Turbulence. New York, N.Y.: McGraw-Hill Book Co., 1975, pp. 221-231.

12. GEORGE, W.K., LUMLEY, J.L. The laser-Doppler velocimeter and its application to the measurement of turbulence. J. Fluid Mech. 60, 321-362, 1973.

13. VAN MAANEN, H.R.E., VAN DER MOLEN K., BLOM, J. Reduction of ambiguity in laser-Doppler velocimetry by a crosscorrelation technique. Proc. LDA-Symposium Copenhagen 81-88 , 1975.

14. DAVIS, M.R. The dynamic response of constant resistance anemometers. J. Phys. E.: Sci. Instrum. 3, 15-20, 1970.

15. WOOD, N.B. A method for determination and control of the frequency response of the constant-temperature hot-wire anemometer. J. Fluid Mech. 67, 769-786, 1975.

16. BELLHOUSE, B.J., SCHULTZ, D.L. The determination of fluctuating velocity in air with heated thin film gauges. Fluid Mech. 29, 19-25, 1966.

17. SOMERSCALES, E.F.C. Fluid velocity mesurement by particle tracking. In: Flow: Its Measurement and Control in Science and Industry. R.B. Dowdell (Ed). Instrument Society of America, 1974, Vol. 1, pp. 795-808.

18. CHUNG, J.S., GRAEBEL, W.P. Laser anemometer measurements of turbulence in non-Newtonian pipe flows. Phys. Fluids, 15, 546-554, 1972.

19. STEIN, P.D., SABBAH, H.N. Turbulent blood flow in the ascending aorta of humans with normal and diseased aortic valves. Circ. Res. 39, 58-65, 1976.

Vol. 17
1980

BLANK
PAGE

Vol.
198

BIORHEOLOGY, Vol. 17, pp. 275-281, 1980
Printed in the USA. All rights reserved.

0006-355X/80/030275-07$02.00/0
Copyright (c) 1980 Pergamon Press Ltd

DAMPING EFFECT OF DISTENSIBLE TUBES ON TURBULENT FLOW: IMPLICATIONS IN THE CARDIOVASCULAR SYSTEM

Paul D. Stein, Frederick J. Walburn, and Edward F. Blick*

Departments of Medicine and Surgery
Henry Ford Hospital, Detroit, Michigan 48202, U.S.A. and
*School of Aerospace, Nuclear and Mechanical Engineering, University of Oklahoma
College of Engineering, Norman, Oklahoma 73019, U.S.A.

(Received 5.31.1980; in revised form 7.5.1980.
Accepted by Editor H.L. Goldsmith)

ABSTRACT The effects of compliant tubes upon turbulent flow were measured because of the possibility that the compliance of arteries may affect the magnitude of disturbances of flow in the cardiovascular system. Turbulence was measured with a hot film anemometer during the steady flow of saline in a rigid tube, a latex rubber tube with a wall thickness of .16 cm and a latex rubber tube with a wall thickness of .08 cm. The latter had distensibility characteristics comparable to the human aorta. Throughout the range of Reynolds numbers tested (3,000 to 11,000) the relative intensity of turbulence (ratio of root-mean-square value of the fluctuating velocities to mean centerline velocity) was lower in the distensible tubes. The more compliant tube (.08 cm wall) showed a relative turbulence intensity 14% lower than in the rigid tube at a Reynolds number of 5,500 ($P < .001$) and a reduction of 10% at a Reynolds number of 10,500 ($P < .001$). The absolute intensity of turbulence was also lower in the compliant tubes. These observations indicate that the compliance of arteries may be a physiological factor that contributes to the reduction of turbulence in the cardiovascular system.

Vol. 17
1980

INTRODUCTION

Studies of the characteristics of blood flow in the human body have shown that flow is undisturbed in the descending aorta (1). Even in the region of the bifurcation of the aorta and the common iliac arteries, turbulence was not observed (1). These observations are contrary to predictions made on the basis of flow in rigid tubes at bifurcations (2). Moreover, we have shown prominent differences of the magnitude of turbulence in the aorta and the pulmonary artery which do not appear to be explained entirely on the basis of differences of blood velocity in these two vessels (3). Several physiological mechanisms may participate in determining the amplitude of disturbances at various sites in the human body. Among these are the pulsatile nature of flow (4), the number of erythrocytes (5), the deformability of erythrocytes (6), tapering of the vessels (7), and the branch-to-trunk area ratio (8). An additional physiological factor, that we speculate may tend to damp disturbances, is the compliance of the arteries. The possibility that the compliance of the blood vessels may attenuate turbulence is suggested by observations of damping of turbulence by compliant coatings over flat plates (9). However, there is a paucity of information related to the effects of compliant tubing upon the characteristics of flow. Therefore, this investigation was undertaken to determine if compliant tubes may attenuate turbulence.

METHODS

Turbulence was measured sequentially during the steady flow of saline through a rigid tube, and through latex rubber tubes of two different distensibilities. The flow system is shown schematically in Figure 1. Saline, .9 gm/100 ml (viscosity .0102 poise, density 1.006 gm/cm^3) was pumped from a collection tank into a reservoir in order to dissipate any large scale fluctuations. A 1.27 cm diameter cannulating electromagnetic flow transducer (Biotronex Laboratories, Inc., Silver Springs, Maryland) was attached to the orifice of the test section. After passing through the test section, the saline flowed into a collection tank from which it was recirculated by a centrifugal pump. Steady flow from 0 to 10,800 ml/min could be produced which permitted us to attain Reynolds numbers of 11,000.

The internal diameter of the rigid tubing was 1.91 cm and it was fabricated from polyvinyl chloride. The distensible tubes were natural latex rubber (Reichhold Chemicals, Inc., Cuyahoga Falls, Ohio) with a wall thickness of .08 cm and .16 cm. The unstretched internal diameter of the rubber tubing was also 1.9 cm. Care was taken to attach the

Key Words: Turbulence, distensibility, damping effect, hot film anemometer, turbulence intensity, cardiovascular system

distensible tubing with no tension in the walls. Each test section was 185 cm in length. The cannulating electromagnetic flow transducer at the orifice of the test section acted as a turbulence generator. The purpose of the turbulence generator was to cause the transition to turbulent flow to occur near the orifice. Therefore, fully developed flow was present at the site of measurement, 110 cm downstream from the orifice. The additional 75 cm length of tubing downstream from the probe reduced the chance of downstream effects from geometric discontinuities and wave reflections.

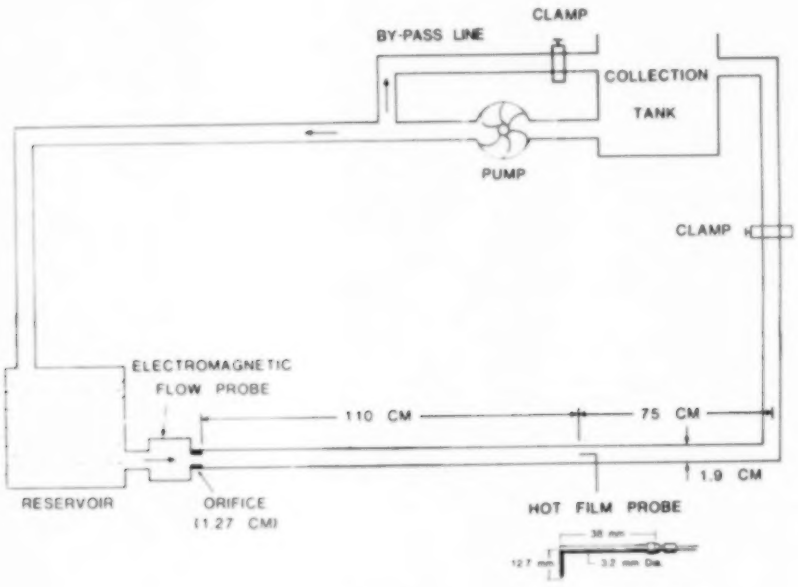

FIG. 1

Diagram (not to scale) of the flow system and hot film probe.

Instantaneous local velocity was measured with an L-shaped conical tip hot film probe (TSI-1231) in combination with a TSI-1050 constant temperature anemometer and linearizing system (Thermo-Systems, Inc., St. Paul, Minn.). The constant temperature anemometer was operated at an overheat of 1.14 which limited the temperature of the heated film to 18.5°C above the ambient temperature. Probes were calibrated and used at room temperature (23.6°C). In our laboratory we showed that the spectral density of turbulence measured with the hot film anemometer was comparable to that measured with a laser Doppler anemometer (Thermo-Systems, Inc.) to 400 Hz.

The tip of the hot film probe was positioned 110 cm downstream from the inlet at the center of the tube along the axis of flow. The absolute intensity of turbulence was measured as the root-mean-square value of the fluctuating velocities (10) using a true RMS voltmeter (Thermo-Systems, Inc., Model 1076). The root-mean-square value of the fluctuations of velocity were averaged over 100 sec after steady flow was established for a period of three minutes.

The relative intensity of turbulence was calculated as the ratio of the root-mean-square value of the fluctuating velocities to mean centerline axial velocity (10). The latter was determined from the mean electrical output of the hot film probe. Mean velocity was obtained with the hot film probe. This value was compared with velocity calculated from electromagnetically measured flow. The electromagnetic flowmeter was calibrated with a stopwatch and graduated cylinder. Mean velocity measured with the hot film probe differed an average of 8% from velocity measured with the electromagnetic flowmeter. The Reynolds number was based upon the tube diameter and mean centerline velocity at the site of measurement. The internal diameter of the .16 cm wall thickness tube at a Reynolds number of 3,000 was 1.91 cm and it increased to 1.94 cm at a Reynolds number of 11,000, which caused the cross-sectional area to increase 3%. The internal diameter of the .08 cm wall thickness tube was 1.92 at a Reynolds number of 3,000 and it increased to 2.06 cm at a Reynolds number of 11,000, which caused the cross-sectional area to increase 15%. At a Reynolds number of 3,000 the difference of diameter between the rigid and most compliant tube was 0.5% (cross-sectional area difference 1%) and at a Reynolds number of 6,000, the difference of diameter was 2% causing a 4% cross-sectional area difference.

The viscosity of the saline was measured at room temperature with a cone-in-plate viscometer (Brookfield Engineering Laboratories, Inc., Stoughton, Mass.) at shear rates

of 450 sec^{-1} and 900 sec^{-1}. The density was measured with a hydrometer. Flow and velocity were recorded on an Electronics for Medicine (White Plains, N.Y.) VR-12 recorder at paper speeds that ranged from 10 to 500 mm/sec. The frequency response of this instrument was flat from 0 to 2500 Hz. Tests were performed at least six times in each tube over a period of several days. The temperature of the saline was adjusted at frequent intervals to maintain it at 23.6°C. The tubing was occluded to establish a zero baseline after each measurement.

The distensibility of the rubber tubing was measured as the ratio of the change of internal radius that occurred with a change of pressure (11). A segment of tubing was occluded and incremental volumes of water were added through a stopcock. Pressure within the tube was measured with a catheter-tip micromanometer (Millar, Houston, Texas). Following each volumetric increment, the external diameter of the tube was measured with a micrometer, and the internal radius was calculated assuming that the volume of the tube wall material remained constant. The distensibility of the .16 cm wall thickness tubing was .67 $\times 10^{-3}$ cm/mm Hg; and the distensibility of the .08 cm thickness tubing was 2.2 $\times 10^{-3}$ cm/mm Hg.

RESULTS

Throughout the range of Reynolds numbers studied, the absolute intensity of turbulence in the compliant tubes was lower than in the rigid tube (Fig. 2). The absolute intensity of turbulence in the more distensible tube (.08 cm wall thickness) was 10% to 14% lower than in the rigid tube ($P < .001$), depending upon the Reynolds number.

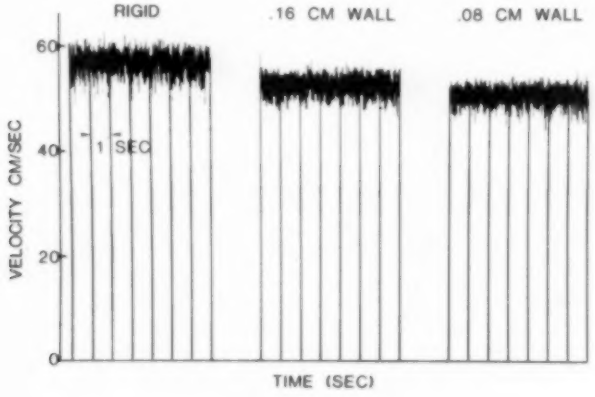

Re = 10800	Re = 10200	Re = 10500
$\bar{U}$ = 57 CM/SEC	$\bar{U}$ = 52 CM/SEC	$\bar{U}$ = 51 CM/SEC
D = 1.91 CM	D = 1.94 CM	D = 2.06 CM
u' = 2.8 CM/SEC	u' = 2.5 CM/SEC	u' = 2.3 CM/SEC
u'/$\bar{U}$ = .049	u'/$\bar{U}$ = .048	u'/$\bar{U}$ = .045

FIG. 2

Instantaneous velocity in the rigid tube and 1.6 mm and .8 mm wall thickness rubber tubes. The Reynolds number (Re), mean axial velocity ($\bar{U}$), internal diameter (D), absolute turbulence intensity (u') and relative turbulence intensity (u'/$\bar{U}$) are shown.

The relative intensity of turbulence in the compliant tubes was lower than in the rigid tube at each of the observed Reynolds numbers (Fig. 3). In the more compliant tube (.08 cm wall thickness), it was 14% lower than in the rigid tube at a Reynolds number of 5500 ($P < .001$) (unpaired t-test), and it was 10% lower at a Reynolds number of 10,500 ($P < .001$). The thinner wall (.08 cm) rubber tube showed a lower relative intensity of turbulence than the .16 cm wall tube ($P < .001$), and the latter showed less turbulence than the rigid tube ($P < .05$ to $P < .01$ depending upon the Reynolds number) (Fig. 3). The relative turbulence intensity, as it relates to distensibility is shown in Fig. 4.

Vol. 17
1980

DISCUSSION

This study showed that turbulence was less intense in compliant tubes than in rigid tube. The possibility that compliant surfaces may reduce turbulence, or turbulence induced skin friction drag, has been explored by aerodynamicists and naval engineers (9). It was suggested that the dolphin's compliant skin was responsible for its ability to swim at high speeds (12). Kramer believed that the dolphin's skin absorbed and dissipated the oscillatory energy from the boundary layer, and this retarded transition to turbulent flow and extended the area of laminar flow over the dolphin's body (12).

Theoretical analyses have suggested that the stability of laminar boundary layers can be altered by compliant boundaries. These analyses have been summarized in a review of skin friction drag reduction by compliant surfaces (13). Turbulence over compliant plates was found to be less than turbulence over a hard surface plate (9). On the other hand, some investigators have failed to find a reduction of drag induced by compliant surfaces (13). Blick, in his review of drag reduction by compliant coatings, concluded that the percentage of successful drag reduction experiments was "not too high" and little theory was available to guide experimenters (13).

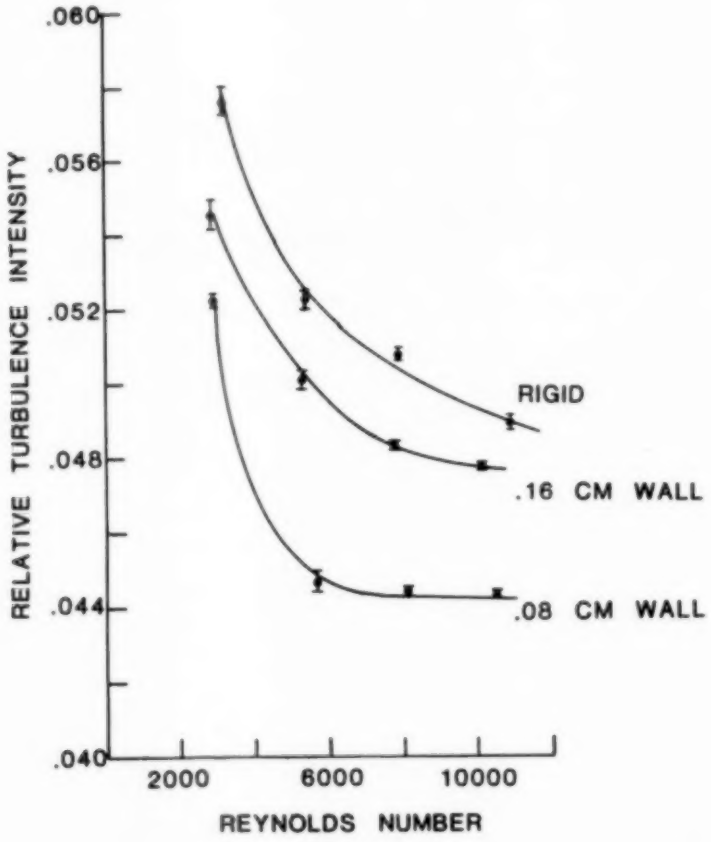

FIG. 3

Relative turbulence intensity in the various tubes shown as a function of the Reynolds number.

Regarding studies of flow in pipes, we are aware of only two investigations, and these were studies of drag reduction by flexible tubes. It was found that the skin friction in pipes could be reduced by as much as 35 percent by lining the pipe with a flexible tube (14). The annular space between the flexible tube and the pipe was filled with damping fluids. Others investigated the flow of water through damped flexible tubes and found a friction reduction in excess of 20 percent (15).

The reduced relative intensity of turbulence in the distensible tubes does not seem to be a reflection of the increased diameter of the distensible tubes that occurred at higher Reynolds numbers. The internal diameter of the more distensible tube (.08 cm wall thickness) increased from an unstretched diameter of 1.9 cm to 2.06 cm at a Reynolds number of 10,000.

In order to determine if this increased diameter may have caused the reduction of the relative intensity of turbulence, we repeated our measurements in a rigid tube with an internal diameter of 2.06 cm. Repeated measurements at a Reynolds number of 10,000 showed that flow in the larger diameter tube was even more turbulent. The relative turbulence intensity in the compliant tube was .044, in the 1.91 cm diameter rigid tube it was .049, and in the 2.06 cm diameter rigid tube it was .054 (Table I). Therefore, our observations do not appear to reflect minor variations of diameter that resulted from high flow through a distensible tube.

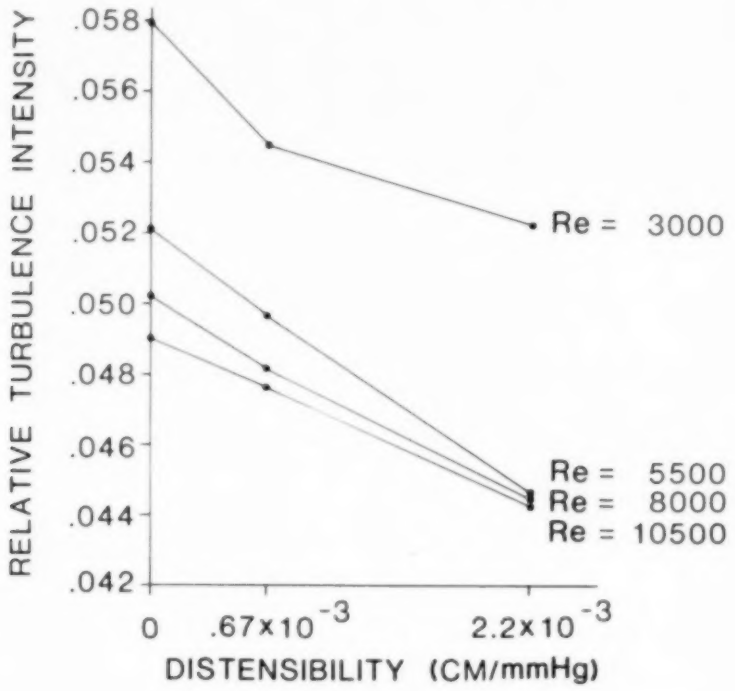

FIG. 4

Relative turbulence intensity at various Reynolds numbers (Re) shown as a function of the distensibility of the tubes.

The observations in this study are applicable to understanding the process involved in modifying disturbances of flow in the cardiovascular system. We found that disturbed or turbulent flow is present in the ascending aorta of patients with normal aortic valves, particularly when the cardiac output is elevated (16). The normal semilunar valves project into the stream of flow during ejection, and turbulence is initiated at the free margin of the cusps (17). Presumably the pulmonary valve acts similarly in initiating disturbances. However, we observed less turbulence (both absolute and relative) in the pulmonary artery than in the aorta (3). A lower blood velocity in the pulmonary artery may contribute to the lower amplitude of disturbances. Based upon this study of flow in flexible tubes, perhaps the compliance of the pulmonary artery also contributes to the reduction of turbulence in that vessel.

TABLE I

RELATIVE TURBULENCE INTENSITY AT A REYNOLD$ NUMBER OF 10,000 IN THE DISTENSIBLE TUBE AND RIGID TUBES OF 1.91 AND 2.06 CM DIAMETER

Type of Tube	Diameter (cm)	Relative Turbulence Intensity
Rigid	2.06	.054
Rigid	1.91	.049
Distensible (.08 cm wall)	2.06*	.044

*Internal diameter during flow

Vol. 17
1980

The distensibility of the ascending aorta and pulmonary artery of patients has been measured (11, 18). The .08 cm wall thickness latex rubber tubing used in this study had pressure-diameter characteristics comparable to the human aorta (2.2×10^{-3} cm/mm Hg in the rubber tube and 2.5×10^{-3} cm/mm Hg in the aorta) (11). The compliance of the pulmonary artery was greater (11.9×10^{-3} cm/mm Hg) (18). Therefore, based upon the observations in this study of less turbulence with more compliant tubing, disturbances in the pulmonary artery would tend to be lower than in the aorta.

Studies of disturbances of flow in branches of rigid tubes suggested that turbulence would occur in the common iliac artery (19, 20); although we did not observe disturbed flow (1). The compliance of these vessels may have contributed to the reduction of turbulence, although other factors such as a favorable branch-to-trunk area ratio of the vessels (8) and tapering (7) also may have contributed. In addition, in the cardiovascular system the number of red cells and their deformability relate to the magnitude of disturbances; and these effects are independent of viscosity (5, 6). Turbulence intensity was shown to be highest at hematocrits of 20 and 30 ml/100 ml (5). Nondeformable erythrocytes caused more disturbances than normal red cells (6).

In conclusion, at all Reynolds numbers tested, turbulence in compliant tubing was attenuated. This suggests that the compliance of arteries may be a physiological factor that participates in reducing turbulence in the cardiovascular system.

Supported in part by U.S. Public Health Service -
National Heart, Lung and Blood Institute grant HL23669-01

REFERENCES

1. STEIN, P.D., SABBAH, H.N., ANBE, D.T., WALBURN, F.J. Blood velocity in the abdominal aorta and common iliac artery of man. Biorheology 16: 249-255, 1979.

2. WESLOWSKI, S.A., FRIES, C.C., SABINI, A.M., and SAWYER, P.N. Turbulence, intimal injury, and atherosclerosis. In: Biophysical Mechanisms in Vascular Homeostasis and Intravascular Thrombosis. P.N. Sawyer (Ed). New York: Appleton-Century-Crofts. 1965, pp. 147-157.

3. Stein, P.D., SABBAH, H.N., and ANBE, D.T. Comparison of disturbances of flow in the main pulmonary artery and ascending aorta of man. Biorheology 16: 357-362, 1979..

4. PARKER, K.H. Instability in arterial blood flow. In: Cardiovascular Flow Dynamics and Measurements. Hwang, N.H.C., and Normann, N.A. University Park Press, Baltimore 1977, pp. 633-663.

5. STEIN, P.D., SABBAH, H.N., BLICK, E.F. Contribution of erythrocytes to turbulent blood flow. Biorheology 12: 293-299, 1975.

6. SABBAH, H.N., STEIN, P.D. Effect of erythrocytic deformability upon turbulent blood flow. Biorheology 13: 309-314, 1976.

7. WALBURN, F.J., STEIN, P.D. Effect of vessel tapering on the transition to turbulent flow: Implications in the cardiovascular system. (Abstract) Fed. Proc. 39: 1068, 1980.

8. WALBURN, F.J., BLICK, E.F., and STEIN, P.D.: Effect of the branch-to-trunk area ratio on the transition to turbulent flow: Implications in the cardiovascular system. Biorheology 16: 411-417, 1979.

9. FISHER, D.H. and BLICK, E.F. Turbulent damping by flabby skins. J. Aircraft 3: 163-164, 1966.

10. HINZE, J.O. Turbulence. New York: McGraw-Hill, 1959, p. 1-4.

11. GREENFIELD, J.C., Jr., and PATEL, D.J. Relation between pressures and diameter in the ascending aorta of man. Circ. Res. 10: 778-781, 1962.

12. KRAMER, M.O. The dolphins' secret. J. Am. Soc. Naval Engrs. 73: 103-107, 1961.

13. BLICK, E.F. Skin friction drag reduction by compliant coatings. International Conf. Drag Reduction. Sponsored by BHRA Fluid Engineering. Cranfield, Bedford, England, Sept. 1974, pp. F2-23 - F2-36.

14. PELT, R. A preliminary investigation of surface damping effects on fluid flow through flexible tubes. Ph.D. Dissertation, Dept. of Chem. Eng., University of Pittsburgh, 1964. Quoted by Blick, E.F. (Reference 12).

15. KLINZING, G.E., KUBOVCIK, R.J. and MARMO, J.F. Frictional losses in foam-damped flexible tubes. Ind. Eng. Chem. Process Design Develop. 8: 112-114, 1969.

16. STEIN, P.D. and SABBAH, H.N. Turbulent blood flow in the ascending aorta of humans with normal and diseased aortic valves. Circ. Res. 39: 58-65, 1976.

17. SABBAH, H.N. and STEIN, P.D. Contribution of semilunar leaflets to turbulent blood flow. Biorheology 16: 101-108, 1979.

18. GREENFIELD, J.C., Jr. and GRIGGS, D.M., Jr. Relation between pressure and diameter in main pulmonary artery of man. J. Appl. Physiol. 18: 557-559, 1963.

19. STEHBENS, W.E. Turbulence of blood flow. Quart. J. Exptl. Physiol. 44: 110-117, 1959.

20. KROVETZ, L.J. The effect of vessel branching on haemodynamic stability. Phys. Med. Biol. 10: 417-427, 1965.

Vol. 17
1980

BLANK
PAGE

Vol.
198

BIORHEOLOGY, Vol. 17, pp. 283-287, 1980
Printed in the USA. All rights reserved.

0006-355X/80/030283-05$02.00/0
Copyright (c) 1980 Pergamon Press Ltd

Vol. 17
1980

B R I E F C O M M U N I C A T I O N

A NOTE ON HEMOLYSIS DURING FILTRATION THROUGH MICROPORES

S. P. Sutera

Mechanical Engineering Department
Washington University, St. Louis

(Received 1.10.1979; in revised form 7.1.1980.
Accepted by Editor H.L. Goldsmith.
Received in final form by Executive Editorial Office 14.2.1980)

INTRODUCTION

One experimental technique which has been employed for the assessment of relative erythrocyte deformability involves the passage of cells through filters with pores in the 2 to 4 μm range (1,2). Typically, Nuclepore filters, which have cylindrical pores of highly uniform diameter, are used. Erythrocyte suspensions are driven at a controlled rate through the filter and the pressure drop across the filter is continuously recorded. Relative deformability is taken to be indicated by the time course of the pressure drop. The less deformable the cells, the higher the initial pressure drop across the filter and the more rapidly the pressure drop rises with time.

At sufficiently high flow rates (and pressure drops) hemolysis occurs. Experience has shown that significant hemolysis of normal erythrocytes flowing through 3 μm pores begins to occur when the pressure drop approaches 100 mm Hg. The flow conditions necessary to hemolyze a cell depend, of course, on the pore diameter, the overall deformability of the cell, i.e., its ability to fold and conform to the narrow cylindrical passage, and the ultimate strength of the cell membrane. It is the primary purpose of this note to analyze the forces which act on an individual cell as it moves through a typical micropore and the tension induced in the cell membrane by those forces. With this information and a knowledge of the mechanical properties and limitations of the erythrocyte membrane it should be possible to predict the hemolytic limit in filtration.

GEOMETRY OF DEFORMED CELL

The form taken by an erythrocyte passing through a capillary 4 μm or less in diameter is quite familiar from both microscopic observations (3) and model studies (4). In such small capillaries a human erythrocyte folds about a diametral line and fills the capillary lumen like a nearly cylindrical capsule, as shown in Fig. 1. Under the action of the driving pressure gradient the leading end inflates to a convex, quasi-spherical cap, while the trailing end collapses inward to an irregular, concave cup. The average thickness of the lubricating plasma layer, denoted by δ in Fig. 1, is extremely small and a function of cell speed, increasing to an asymptotic value with speed. The observations of Hochmuth et al. (3) indicated an asymptotic plasma-layer thickness of about 0.6 μm in a 4.5 μm capillary. Overall cell length, ℓ_c, tends to be very close to the normal disc diameter of the relaxed cell (3), say 8 to 9 μm, and a reasonable estimate for the length of the lubricating plasma layer, ℓ', would be one capillary radius less than ℓ_c.

FORCES ACTING ON CELL

Let the pressures existing instantaneously in the neighborhood of the upstream (trailing) and downstream (leading) ends of the cell be P_u and P_d, respectively. Then, if the cell cross-section be taken as approximately circular, the net pressure force driving the cell through the capillary is

$$F_p = \frac{\pi}{4}(D-2\delta)^2 \cdot (P_u - P_d). \qquad (1)$$

Opposing the cell's motion is the shear stress acting over the cell membrane. The axial resultant of the shear force is due primarily to the stress acting over that portion of the membrane which is adjacent to the lubricating plasma layer. That stress is nearly uniform

This work was sponsored by the National Heart, Lung and Blood Institute, U.S. Public Health Service, through Grant HL 12839.

Key words: hemolysis, filtration, Nuclepore filters.

and given by

$$\tau = \mu_p U/\delta \ , \tag{2}$$

where μ_p is the plasma viscosity and U the cell velocity. It follows, then, that the axial shear resultant would be approximately

$$\begin{aligned} F_s &= \tau \cdot \pi(D-2\delta)\ell' \\ &\equiv \pi\mu_p U(D-2\delta)\ell'/\delta \end{aligned} \tag{3}$$

This force acts in the upstream direction, i.e., in opposition to the driving pressure force, F_p.

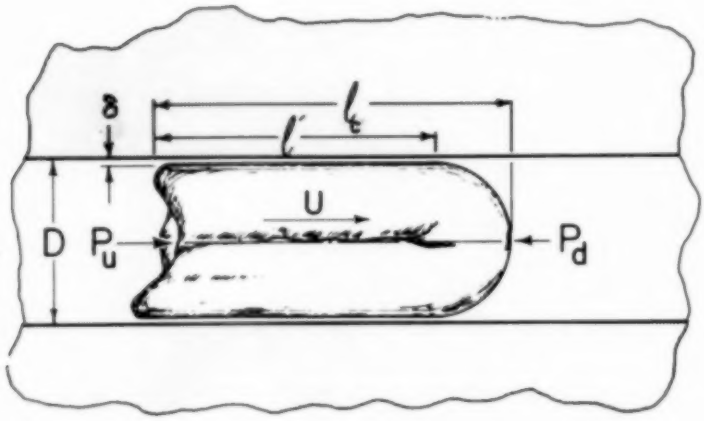

FIG. 1

Sketch of erythrocyte passing through 4.5 μm capillary (based on Ref. 4).

In the filtration experiments of interest here, overall pressure drops (across the filter) as high as 100 mm Hg have been imposed. Simple estimates based on Poiseuille flow through a 3 μm pore indicate that the corresponding average velocity through the pore would be nearly 30 cm/s. However, even at this relatively high velocity (about two orders of magnitude greater than the maximum capillary velocities observed in vivo) the Reynolds number of the cell motion will be less than unity, which means that inertial or acceleration effects can be neglected. Therefore, an instantaneous balance of the opposing forces F_p and F_s can be assumed; whereupon setting Eqs. (1) and (3) equal leads to

$$\Delta P_c = P_u - P_d = \frac{4\mu_p \ell' U}{\delta(D-2\delta)} \ . \tag{4}$$

This gives the pressure drop ΔP_c directly across a cell moving at velocity U which, it should be emphasized, very nearly equals the volumetric average velocity through the pore.

Now, consider the total pore length to be L and suppose a single cell is passing through it. Suppose further that along the unobstructed sections of the pore upstream and downstream of the cell, of net length $L-\ell_c$, the plasma flow can be described as simple Poiseuille flow. The total pressure drop along these pure plasma zones would be

$$\Delta P_p = \frac{32\mu_p (L-\ell_c)U}{D^2} \ . \tag{5}$$

This, of course, is an approximation which neglects flow-development lengths at the entrance and exit of the pore as well as in the immediate vicinity of the cell. From Eqs. (4) and (5) the ratio of the two pressure drops ΔP_p and ΔP_c, which together add up to the total drop across the filter, can be calculated.

$$\frac{\Delta P_p}{\Delta P_c} = 8\left(\frac{\delta}{D}\right)\left(1-2\frac{\delta}{D}\right)\left(\frac{L}{\ell_c} - 1\right) . \qquad (6)$$

While this ratio appears to be a function of geometry only, it must be remembered that the thickness δ is really dependent on cell speed (3).

Typically the thickness of Nuclepore filters is quite small, ranging from 10 to 20 μm. Thus, if $\ell_c \approx 8$ μm, the factor $(L/\ell_c - 1)$ would be less than 1.5. The thickness δ is estimated to be less than 0.5 μm, so that δ/D for a 3 μm diameter pore would be on the order of 0.1. It follows that $\Delta P_p/\Delta P_c$ would be about unity, which means that the total pressure drop along the pore would be divided roughly evenly between the cell and the rest of the pore. Of course, if δ were in fact much less than 0.5 μm, the pressure-drop contribution of the moving cell could become dominant.

MEMBRANE TENSION

The forces acting on the moving cell result in a state of tensile stress in those portions of the cell membrane which comprise the convex "cap" and the quasi-cylindrical surface of the "capsule". It is assumed that the membrane comprising the interior folds and the relatively limp concave trailing "cup" remains relaxed and nearly stress free. Thus, the pressure in the static liquid interior of the cell is essentially in equilibrium with P_u so that the full pressure difference $\Delta P_c = P_u - P_d$ must act across the convex membrane cap. Because of the longitudinal fold that runs along the cylindrical portion of the cell, one can argue that the circumferential component of membrane stress must be very small there. Thus, the state of membrane stress in this region is primarily one of axial tension, with magnitude decreasing approximately linearly from a maximum at the cap end to zero at the trailing end.

It follows from this simplified model of the stressed, capsule-like cell that the pressure within the thin lubricating layer of plasma is constant and approximately equal to P_u. The drop in the plasma pressure from P_u to P_d occurs rather abruptly at the forward end of the layer where the flow relative to the cell is being dragged into a rapidly converging channel by the pore wall.

If one now makes the approximation that the cell is an axisymmetric capsule with a spherical cap, it becomes possible to make a simple calculation of the maximum tensile stress in the membrane. According to this model the membrane loading and the resulting stress distribution would be axisymmetric as well. Figure 2 is a simplified diagram showing the pressure and shear forces acting on the stressed portions of the cell membrane. The

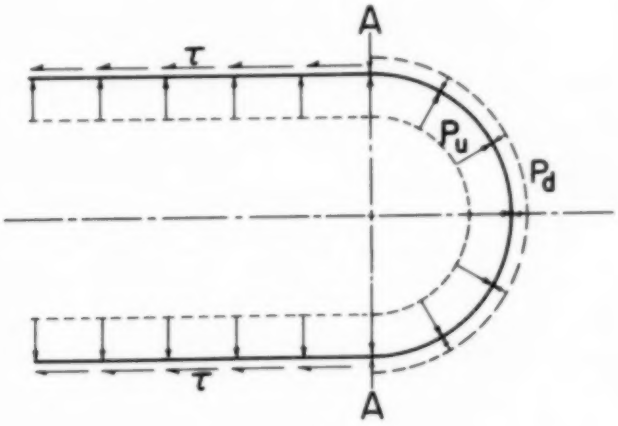

FIG. 2

Simplified diagram of pressure and shear stress distributions on meridian section of cell membrane.

membrane comprising the spherical cap, loaded by a uniform pressure differential, is in a state of uniform isotropic tension. The corresponding lineal tension σ (force per unit of membrane length) is first exposed by cutting the membrane at the transverse section A-A (Fig. 2). The two resulting free body diagrams are shown in Fig. 3. Equilibrium of axial forces on each of these free bodies requires that

Vol. 17
1980

$$\sigma = \Delta P_c \left(\frac{D-2\delta}{4}\right) = \frac{\mu_p U \ell'}{\delta} \quad . \tag{7}$$

This is the membrane tension which would exist instantaneously presuming a quasi-static balance of internal and external forces.

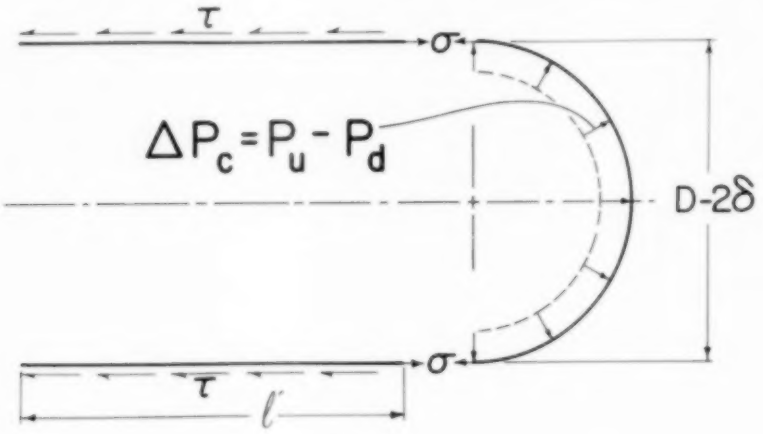

FIG. 3

Free body diagrams of cylindrical and spherical segments of axisymmetric capsule membrane.

The preceding equality relating σ to ΔP_c shows that the influence of cell motion on σ is solely through the parameter δ. Now the ratio δ/D is always very small, varying from 0 to perhaps 0.1 as cell speed increases. Thus, the influence of cell motion is very weak and σ is determined essentially by the static pressure load across the spherical cap. Consider, for example, a case in which 100 mm Hg is imposed across a Nuclepore filter with pores 3 μm in diameter by 10 μm long. In this case the deformed cell would very nearly fill the entire pore length, so it can be assumed that the entire pressure drop (100 mm Hg = 1.33×10^5 dyn/cm^2) acts across the cell. The upper bound on σ becomes

$$\sigma_{max} = \Delta P_c \cdot D/4 = 10 \text{ dyn/cm} \quad .$$

Note that if δ were taken to be 0.3 μm, σ would only decrease to 8 dyn/cm.

The shear stress acting over the cylindrical part of the cell need be considered only to calculate the cell velocity U. According to Eq. (7)

$$U = \frac{\Delta P_c (D-2\delta)\delta}{4\mu_p \ell'} \quad . \tag{8}$$

Take μ_p = 1 cp = 0.01 dyn·sec/cm^2, ℓ' = 7 μm and δ = 0.3 μm. For the same pressure drop of 100 mm Hg, the formula gives U = 34 cm/sec, which, as mentioned above, is about 100 times greater than the highest red cell speeds observed in the microcirculation in vivo. At a velocity of 34 cm/sec a cell would traverse a 10 μm pore in about 3×10^{-5} sec. This would also be the duration of the tension generated in the membrane.

POSSIBILITY OF HEMOLYSIS

It was mentioned above that significant hemolysis has been observed when a driving pressure of 100 mm Hg is applied to a Nuclepore filter with 3 μm pores. According to the preceding numerical example, these conditions can lead to a maximum membrane tension on the order of 10 dyn/cm. However, this tension occurs impulsively, almost as a step function. Owing to the viscoelastic nature of the red cell membrane a finite time is required, following a step increase in tensile stress, for a stressed membrane element to reach a certain critical strain and rupture. The time to rupture, i.e., for hemolysis, decreases as the applied stress is increased.

The well known data of Rand (5) indicate that, on the average, membrane tension in the range 20-25 dyn/cm would cause immediate hemolysis. However, some cells were observed to hemolyze rapidly at considerably lower stresses. The scatter in Rand's calculated membrane tensions and the time required to hemolyze was attributed partly to experimental error in the measurement of membrane radii and partly to natural variations in the cell population. It can be concluded, therefore, that the tension of 10 dyn/cm calculated in the preceding simplified model is in order of magnitude agreement with the values determined by Rand.

CONCLUSION

Filtration of human erythrocytes through cylindrical micropores generates maximum membrane tension in the convex leading end of the capsule-like cell. A simple model based on an axisymmetric geometry and quasi-static equilibrium of forces shows that passage through a 3 μm diameter pore under a pressure differential of 100 mm Hg can generate membrane tensions sufficient to produce immediate hemolysis.

REFERENCES

1. CHIEN, S. Principles and techniques for assessing erythrocyte deformability. Blood Cells 3, 71-95, 1977.

2. VELKER, J.A., MCINTIRE, L.V. and LYNCH, E.C. Alteration of erythrocyte deformability due to shear stress as assessed by Nuclepore filters. Trans. Amer. Soc. Artif. Int. Organs XXIII, 732-735, 1977.

3. HOCHMUTH, R.M., MARPLE, R.N. and SUTERA, S.P. Capillary blood flow, I. Deformable model cells compared to erythrocytes in vitro. Microvasc. Res. 2, 434-442, 1970.

4. SESHADRI, V., HOCHMUTH, R.M., CROCE, P.A. and SUTERA, S.P. Capillary blood flow, III. Deformable model cells compared to erythrocytes in vitro. Microvasc. Res. 2, 434-442, 1970.

5. RAND, R.P. Mechanical properties of the red cell membrane. II. Viscoelastic breakdown of the membrane. Biophys. J. 4, 303-316, 1964.

Vol. 17
1980

BLANK
PAGE

Vol.
198

BIORHEOLOGY, Vol. 17, pp. 289-291, 1980
Printed in the USA. All rights reserved.

0006-355X/80/030289-03$02.00/0
Copyright (c) 1980 Pergamon Press Ltd

THE SEDIMENTATION VELOCITY OF INDIVIDUAL HUMAN ERYTHROCYTES AS A FUNCTION OF TEMPERATURE

R. Glaser and A. Herrmann

Humboldt-Universität zu Berlin,
Sektion Biologie, Bereich Biophysik,
Invalidenstr. 43, DDR 104 Berlin

(Received 28.5.1979; in revised form 27.5.1980.
Accepted by Editor Y.C. Fung)

INTRODUCTION

In the investigation of basic haemorheological mechanisms, the sedimentation velocity of human red blood cells is studied frequently. Often a modified Stokes' equation is utilised to explain this phenomenon. Since the Reynolds' number of this movement is extremely small ($< 10^{-5}$), only a shape and orientation factor is to be taken into consideration, reflecting the nonspheric shape of the human red blood cells.

Surprisingly it can be shown that the sedimentation velocity of living red blood cells, in contrast to yeast cells and fixed erythrocytes, is a complicated function of temperature, even if the temperature dependence of the viscosity of the suspension medium is taken into account (1, 2). The product of the sedimentation velocity and the viscosity of the medium, called the "calibrated sedimentation velocity" has a well marked minimum near 20°C in Krebs-Ringer-solution at pH 7.4.

The reason for this unusual sedimentation behaviour is unknown, but it seems reasonable to assume that it somehow correlates with phase transitions of lipids and therefore some changes of mechanical properties of the membrane. A critical and careful reexamination of these measurements is undertaken to exclude the possibility that the effect observed might be due to methodical errors or to variations of sedimentation measurements caused by biological variability.

MATERIAL AND METHODS

A detailed description of the method used in these experiments was given previously (1, 2). Human erythrocytes, either taken from fresh canned blood, or after storage at 4°C, were used. After centrifugation at 750 g the erythrocytes were washed twice at 2000 g and then incubated at 37°C for one hour in the corresponding PBS-solution by a PCV of 0.45. The sedimentation of individual cells in a U-shaped capillary was observed by a horizontally orientated microscope and recorded photographically by a sequence of light flashes. The measurements of the sedimentation velocity were performed by a PCV of 10^{-4}. The shape of the erythrocytes was examined. The following solution was used: 140.0 mol $\cdot$ m^{-3} NaCl, 20.0 mol $\cdot$ m^{-3} saccharose, 5.8 ml $\cdot$ m^{-3} phosphate buffer (pH 7.4), 5.0 mol $\cdot$ m^{-3} glucose.

RESULTS

In order to distinguish between pure methodical variations from variations due to different properties of blood samples, the sedimentation rate of erythrocytes of identical blood samples was measured in two sedimentation setups under the same conditions. For every temperature point the individual sedimentation rate of 100 cells was recorded. The results of two representative experiments are shown in the Figures 1 and 2. The measurements shown in Figure 1 were made one day and those of Figure 2 two days after blood sampling (in both cases erythrocytes of the same blood sample were used).

The curves in Figures 1 and 2 clearly indicate that the function obtained by experiments in two test chambers with little experimental deviations reflects the true properties of erythrocytes. A statistical comparison of the frequency distribution of the sedimentation rate and of its kurtosis and skewness confirms this assertion because no significant differences between the corresponding measurements occurred. The standard deviation of the individual measurements is about 20% of the mean value. This corresponds to a standard error of the recorded points (Figures 1 and 2) of about 2%. These values are in accordance with those which can be obtained from the range of variations in volume, radius and density of erythrocytes (4).

In both experiments (Figures 1 and 2) the erythrocytes had the shape of echinocytes.

The minimum of the curves of $v_s \eta$ in Figure 1 at 20°C is not so drastic as found by BEUTEL (1, 2), but it occurs at the same temperature as found by Beutel. The differences of the calibrated sedimentation velocity ($v_s \eta$) at 20°C and 19°C seen in Figure 1 are significant (t-test with $\alpha = 0.01$). This minimum was reproduced in a further series of experiments.

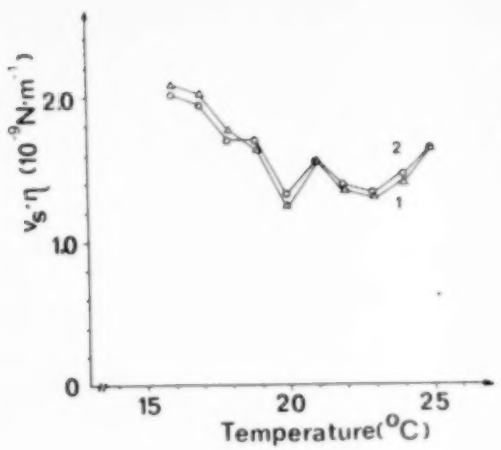

FIG. 1

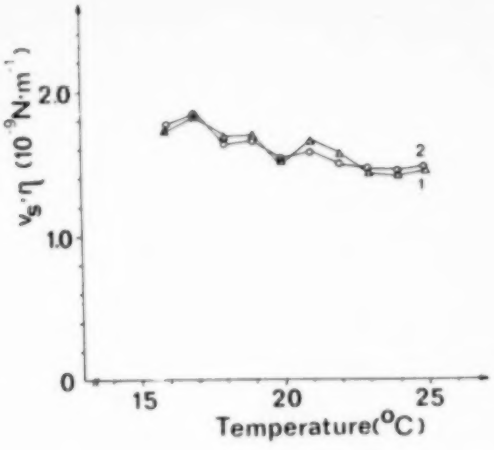

FIG. 2

The product of the sedimentation velocity v_s of human erythrocytes and the viscosity η of the suspension medium as a function of temperature. The sedimentation velocity was measured in two sedimentation chambers under the same conditions: Δ — Δ1 - chamber I
0 — 02 - chamber II
In both cases erythrocytes of the same blood sample were used. The measurements shown in Figure 1 were made one day and those of Figure 2 two days after blood sampling. (The standard deviation, usually about 20%, is not shown in the figures for reason of clarity.)

After storage of the conserved blood at 4°C, this significant sedimentation minimum at 20°C disappears (Figure 2). The same results were obtained in experiments with blood samples, stored for seven or ten days. However, even the curves obtained by stored blood are not parallel to the abscissa as predicted by Stokes' law and as indicated by fixed erythrocytes and yeast cells (1, 2). To get an objective indicator for this we fitted these data according to the method of the least-squares with the following function:

$$v_s \cdot \eta = a \cdot T + b$$

(v_s - sedimentation velocity in $m \cdot s^{-1}$, η - viscosity of the suspension medium in $N \cdot s \cdot m^{-2}$, T - temperature in °C). The values obtained for the constants a and b are listed in Table 1. The standard error of the estimate indicates the quality of fitting. The correlation coefficient is a standard measure of the degree of correlation between the temperature and the calibrated sedimentation velocity relative to the regression line defined by the equation above.

Further experiments were carried out to test the influence of human serum albumin (HSA) on the process of sedimentation. For this purpose 37 $kg \cdot m^{-3}$ HSA (Institut für Impfstoffe Dessau) were added to the incubation and sedimentation medium. The measurements were made at once after blood sampling. The values for the regression line are listed in Table 1. The low correlation coefficient indicates similarly to Figure 3 that in this case no temperature dependence was observed. The erythrocytes had a discoid shape.

TABLE 1

Sample characteristics	a (10^{-11} $N \cdot m^{-1} \cdot °C^{-1}$)	b (10^{-9} $N \cdot m^{-1}$)	Correlation coefficient	Standard error of estimate
1 day after blood sampling	- 6.73	2.98	- 0.707	0.22
2 days " " "	- 4.35	2.49	- 0.903	0.07
7 " " " "	- 3.03	2.00	- 0.942	0.04
10 " " " "	- 3.00	2.19	- 0.942	0.04
HSA-treatment (Figure 3)	- 0.28	2.00	0.189	0.05

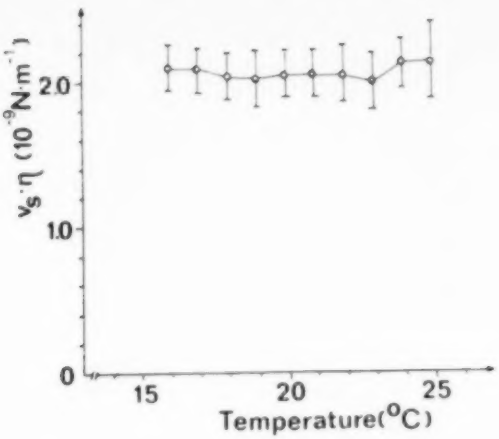

FIG. 3

The influence of human serum albumin (37 kg • m^{-3}) on the temperature dependence of the calibrated sedimentation velocity $v_s \cdot \eta$ of human erythrocytes. The measurements were made at once after blood sampling. (The standard deviation is marked.)

DISCUSSION

The measurements presented here clearly support the results published previously (1, 2) indicating that the sedimentation velocity of living red blood cells is a complicated function of the temperature. The marked minimum in the sedimentation velocity at 20°C differs in amplitude, but under identical conditions, does not differ in position. This variation is due to differences in the blood samples themselves and not to methodical reasons. Obviously it disappears even during blood storage. In older blood samples, however, a significant temperature dependence of the calibrated sedimentation velocity occurs but disappears after treatment with HSA.

The reason for this phenomenon observed remains unclear. As pointed out previously (1, 2) it cannot be explained as a result of any real density deviation or volume shift. The influence of orientation changes and the orientation preference of erythrocytes depending on membrane properties (3, 4) is only important in case of a discoid shape of erythrocytes. The occurrence of minimum at 20°C suggests a possible role of phase transitions of membrane components. This is underlined by the disappearance of the minimum during the storage of blood samples. It should be pointed out, however, that the statistically better proved data of the present publication indicate that in the previous studies (1, 2) some differences between minimal and maximal sedimentation velocities seem to have been overestimated. In Figure 1 (taken as representative of any other) the ratio between the maximal and minimal values is only about 1.6.

It is well-known that erythrocytes during sedimentation wobble randomly back and forth depending on membrane properties (3, 4). Perhaps the mechanical properties of the membrane including vibration ("flickering") are responsible for the effect observed.

REFERENCES

1. BEUTEL, U. Die Temperaturabhängigkeit der Sedimentationsgeschwindigkeit menschlicher Erythrozyten. Acta biol. med. germ. 35, 1393-1397, 1976.

2. BEUTEL, U. and GLASER, R. Die Sedimentationsgeschwindigkeit von Erythrozyten als Indikator für Phasenübergänge in der Membran. Acta biol. med. germ. 36, 321-324, 1977.

3. CANHAM, P. B., JAY, A. W. L. and TILSWORTH, E. The rate of sedimentation of individual human red blood cells. J. Cell. Physiol. 78, 319-332, 1971.

4. JAY, A. W. L. and CANHAM, P. B. Sedimentation of single human red blood cells. Differences between normal and glutaraldehyde fixed cells. J. Cell. Physiol. 80, 367-372, 1972.

Vol. 17
1980

BLANK
PAGE

Vol.
198

BIORHEOLOGY, Vol. 17, pp. 293-296, 1980
Printed in the USA. All rights reserved.

0006-355X/80/030293-04$02.00/0
Copyright (c) 1980 Pergamon Press Ltd

Vol. 17
1980

REPORT: SYMPOSIUM ON "HEMORHEOLOGY AND DISEASES", Nancy, France, 1979

J.F. Stoltz and P. Drouin Chairmen, Scientific Committee

Groupe hemorheologie, Centre Regional de Transfusion Sanguine, Brabois, 54500 Vandoeuvre-les-Nancy, and Dept Nutrition, INSERM U.59, 54000 Nancy - France

A Symposium on Hemorheology and Diseases was held in Nancy, France on October 17, 18 and 19 1979. The aim of the Symposium was to bring together different clinical and pharmacological teams and laboratory researchers in theoretical hemorheology. More than 200 researchers from universities and industry in Europe and America were present during the three days of the Symposium.

The 10 sessions, making up the scientific program, totaled 97 plenary lectures and papers which can be grouped into 6 main themes.

1) Theoretical Hemorheology

The 12 papers which came under this heading could be divided into three sub-groups : blood rheology and constitutive equations, visco-elasticity, cellular microrheology.

As concerns blood rheology, a model of the effects of sedimentation was proposed, as was a constitutive equation for diluted suspensions of spherocytes which enabled the authors (Chhim and Barthes-Biesel) to deduce the macroscopic rheological parameters of the suspension in relation to the microrheological factors (viscosity, membrane elasticity), according to Batchelor's theory. Lerche et al described a method of rheological characterization of washed erythrocyte suspensions.

The viscoelastic properties of blood and rouleaux formation were examined in 6 papers presented after an introductory conference by G.B. Thurston. These papers evoked the connections between viscoelasticity, the relaxation process and blood's tendency to form "rouleaux". Obrecht et al. described a method for determining apparent complex dynamic viscosity for a stationary structure condition from one measurement to the next and therefore obtain results covering a circumspect structure series. Lucius and Stoltz presented a new rheological model which takes into account the blood's main viscoelastic properties. Certain concepts developed in the liquid polymer kinetic theory are applied in this model ; this theory concerns materials arranged in networks in which junctions may rupture under the effect of shear. The authors have found that the shear stress experiments reported in available literature, are not sufficient to characterize the structure fully and the subsequent behaviour of normal structures must also be taken into consideration.

On a parallel with work on models, the research carried out by Schmid-Schönbein et al , Mills et al and Dintenfass et al. on erythrocyte aggregation and rouleaux formation should also be mentioned. In this context, methods for ascertaining the size of rouleaux by using a relation between size and shear rate have also been described.

Finally, the third aspect covered the problems of cellular hemorheology which may be referred to under the term of microrheology. This highly important problem was mainly investigated during three plenary discussions. S. Chien studied the rheological properties of erythrocytes and leucocytes in transient flow by means of the micropipette technique. The viscoelastic parameters were then calculated using Kelvin's model.

Teitel examined the problems of standardization and terminology in studying erythrocyte rheology. He pointed out, in particular, the importance of the experimental conditions for interpreting the results. For their part, Schmid-Schönbein et al introduced the concept of blood fluidity and the alterations produced by erythrocyte aggregation and rigidification.

2) Methods used in Hemorheology

The second topic covered the various approach methods used in hemorheology which can be divided into two distinct groups. The first group deals with the new methods of studying blood and erythrocyte rheology, whilst the second group concerns the papers which examined what could be termed as molecular hemorheology.

Kiesewetter described a method for studying the rigidity of one erythrocyte

passing through a 3 to 5 micron pore, whilst Mussler presented an instrument (filtrometer) which gives an approach to the flow properties of erythrocytes at low shear rates.

Erythrocyte filterability was investigated by Hanss using an automatized version of Reid and Dormandy's initial method (hemorheometer). Duvivier et al. attempted to interpret cellular aggregation measurements after measuring screen filtration pressure. Fourcade et al. proposed investigating the rate of sedimentation and rouleaux formation by means of electric conductivity.

Three papers described more general methods of approach, such as the study of blood in oscillating flow (Meier) and the use of ultrasound techniques for investigating the size of erythrocyte rouleaux (Cathignol et al., Boynard et al.).

The second group of papers was concerned with molecular approach methods : Bouchy et al. reviewed the possibility of using fluorescence polarization as a method of investigating membrane fluidity. André et al. also examined this field in their synthesis on the contribution of molecular fluorescence to the study of local microviscosity.

Leterrier reviewed the characteristics of Spin-label methods and their use as an approach to local microviscosity. Leterrier also reviewed the primary results obtained using these methods in relation to the rheological properties of red cells.

Caprani suggested that the electrochemical method of the rotating disc at modulated speed might be applied to hemorheology. This method consists in studying the response to sinusoïdal perturbation of the electrode's rotation speed, using ferro-cyanide anion as the substance transmission tracer. Experiment has shown that red blood cell morphology, for physiological values of the hematocrit, results in a highly characteristic flow.

3) Blood Flow and Models

Two plenary lectures illustrated and further defined the understanding of blood flow.

In the first lecture, Gaehtgens examined the micro-hemodynamics of capillary circulation in relation to blood cell microrheology. The results, which were illustrated by a film, showed that the hydrodynamic conductance of capillary flow depends largely on micro-rheological effects. Distribution of the erythrocyte flow in a capillary network in erythrocyte deformability or in any other rheological characteristic thus results in redistribution of erythrocyte flow. All these aspects were illustrated in the 30 minute film shown for the first time in its French version by Brånemark. This work showed, in particular, the fundamental part played by rouleaux formation and by rouleaux dissociation in the venules, as well as the fundamental importance of erythrocyte deformability in passing through obstacles in small blood vessels partially obstructed by leucocytes. New vessel formation was also illustrated.

Capillary circulation in relation to erythrocyte deformability was also defined in the work conducted by Seshadri, Jaffrin et al., whilst Duffaux et al. determined the thickness of the peripheral plasma layer in plane capillary vessels measuring between 100 and 500 microns. Nakache et al. studied a flow model and investigated the diffusion processes in blood flow, using a rigid tube with enzyme protein fixation on the inside surface. Variations in catalytic activity were expressed by an equation relating enzyme Michaelis constant to the flow.

Doffin et al. studied the influence of viscosity on the vortical zones in models of stenoses. It was shown, in particular, that the increase in viscosity resulted in a decrease of the whole circulation zone of oscillating flow, and in an increase in the ratio of vortical rate to oscillating rate.

4) Hemorheology and Diseases

The papers devoted to this topic can be roughly grouped under two chapters : Hematology and Ischaemic Diseases.

a) Hemorheology and Hematology

In his introduction to this session, P.F. Leblond reviewed the factors involved in various hemopathies. The respective roles played by the hematocrit, erythrocyte aggregation and the decrease in cellular deformability were examined. The author emphasized the need for setting up yet more accurate techniques in this field.

Berga et al. emphasized the decrease in erythrocyte deformability during hereditary spherocytosis, whilst Teitel et al. insisted on the advantage of determining erythrocyte filterability as a parameter for indirect evaluation of the rate of destruction of erythrocytes during hemolytic syndromes. In his investigation on 21 patients suffering from β-thalassemia, Tillman emphasized the constant decrease in erythrocyte deformability and revealed a decrease in the erythrocyte flexibility of blood transfused into patients suffering from homozygote β-thalassemia.

Leblond et al. revealed a correlation between the filterability of erythrocytes through 3-micron filters and the level of reticulocytes in hemolytic anaemia. The authors insist on the importance of this parameter in any study which may include a determination of erythrocyte filterability.

b) Hemorheology and Ischaemic Diseases

The plenary lecture given by A.L. Copley dealt with understanding the rheological mechanisms of ischaemic and thrombotic diseases. The physiopathological importance of the concept of endoendothelial fibrin lining (EEFL) and of fibrinogen gel clotting was emphasized and the participants were reminded that any perturbation of EEFL homeostasis can lead to vascular obstruction or hemorrhagic phenomena. Copley also emphasized the importance of fibrinogen gel clotting (clotting without thrombin) as an initiating factor for thrombosis and hemostasis in small blood vessels. A new theory on atherogenesis pertaining to the two preceding concepts was developed.

The frequency of the association of blood hyperviscosity with various cardiovascular degenerative diseases or with disorders which are considered to have a high vascular risk factor was emphasized by Stoltz and Drouin in a general review. This frequency was confirmed by the study on blood viscosity conducted by Drouin, Stoltz et al. on 383 diabetics. The results of the study showed a significant increase in blood viscosity measured at low shear rates in diabetics, as compared with healthy controls. The increase was even more marked in patients affected by microangiopathy.

Le Devehat et al. carried out similar observations by measuring erythrocyte filterability in 146 diabetics.

Identical results were obtained by Rieger et al. on 194 patients with risk factors associated with an ischaemic disorder and on 49 patients with risk factors and no perceptible vascular complications.

Lagrue et al. also studied erythrocyte filterability in 72 patients and noted a correlation between this parameter and the number of cardiovascular risk factors observed. The influence of smoking was clearly revealed by the research conducted by Lowe et al, who noted a decrease in erythrocyte deformability in 90 apparently healthy patients after inhaling the smoke of 3 cigarettes.

Gaillard, Rousselle et al. studied blood and plasma viscosity in 45 patients with primitive hyperlipoproteinaemia and noted a significant increase in these two parameters as compared with normolipidic controls.

The problem of arteriopathy of the lower limbs was examined by several authors. Ehrly emphasized the advantage of associating the determination of hemorheological parameters with the measurement of partial oxygen pressure in the tissues in ischaemic arteriopathy.

An investigation conducted by Schneider et al. on 40 patients with arteriopathy confirmed the increase in blood and plasma viscosity and the authors emphasized the advantages of using such measurements both for detecting and for the clinical follow-up of this type of disorder.

During the acute phase of myocardial infarction, Schäbitz and Krosh have shown that a correlation exists between blood viscosity and plasma cholesterol. Dormandy et al. confirmed the existence of blood hyperviscosity in the immediate follow-up period of myocardial infarction and have shown the prognostic value of erythrocyte deformability.

The results of the French group on erythrocyte filterability reported by Marcel revealed a decrease in filterability during strokes, arteriopathy, diabetes and contraception using oestro-progestagens.

Abnormalities in the rheological parameters have also been reported during various disorders, as for example, Raynaud's syndrome (Verry et al.), genetic muscular dystrophy (Donner et al., Leterrier et al.).

Several investigations on animals emphasized the importance of the rheological factors in lipid abnormalities (Dehlon et al.) in spontaneous arterial hypertension of the rat (Seifge et al.) or in the aging process (Terranova et al.).

c) Dynamic and Therapeutic Aspects

In an investigation on blood and plasma viscosity and erythrocyte filtration in insulin-dependent diabetics connected to an artificial pancreas during 30 to 52 hours, Drouir and Stoltz have shown the influence of the metabolic control of diabetes on the hemorheological parameters.

Vague et al. observed comparable results when investigating whole blood filterability using identical methodology. The authors emphasized the increase in A.T.P. erythrocyte level during feed back control of diabetes using an artificial pancreas.

Vol. 17
1980

The therapeutic interest of normovolemic hemodilution in peripheral arteriopathy was emphasized by several authors, particularly by Dormandy et al., Rieger et al., Schooneman et al., Wrabetz-Wölke et al. In an investigation on 5 000 surgical procedures, Duruble et al. showed that normovolemic hemodilution was well tolerated and that there was a decrease in the risk of thromboembolic complications. These results would appear to have considerable importance in the light of the investigation conducted by Dormandy et al. which revealed a significant decrease in erythrocyte filterability during surgical procedures. These results were confirmed by Drummond et al. during general and spinal anaesthesia on patients undergoing surgery for femoral neck fracture.

The influence of the rheological parameters on blood flow as determined by means of mercury strain gauge and venous occlusion plethysmography, was illustrated by Sgries et al after erythrocytopheresis in patients suffering from "polycythemia vera", and by Pointel et al. in diabetics controled via an artificial pancreas.

5) Platelet aggregation and blood clotting

This theme was the subject of two sessions regrouping 13 papers which were presented during a plenary conference given by Colwell on platelet functions during diabetes. Among the principal aspects reported was platelet hypersensitivity to aggregating agents and an increase in the synthesis of prostaglandin E_2-like material, and in thromboxane. The author reported his own experience as well as a multicentric investigation on the effect of an aspirin-persantin treatment. The problem of platelet aggregation in diabetes was also examined by Lecrubier et al. in a study on 174 diabetics, by Voisin et al. on malonaldehyde (MDA) increase in 44 patients and by Stoltz, Drouin et al. in a study on βTG level in 106 patients. In this last paper, the authors reported a mean increase in the circulating βTG level in a comparative study between patients with no complications, patients with micro-angiopathy and a group of patients with both micro-angiopathy and distal arteritis possibly resulting in amputation.

Wurtzinger et al. defined the influence of hemolysis on "in vitro" thrombus formation in a viscometric system, with parallel quantity determination of serotonin and βTG. Plouvier studied clot retraction and kinetics by means of an electric conductivity method, and revealed that clot retraction depends on the fibrinous substrata and platelet count. Stoltz, Gille et al. also defined research in platelet alterations and rheological changes during surgical extracorporeal circulation , and emphasized the existence of hyper-aggregability and blood hyper-viscosity phenomena 6 to 7 days post-operatively. Bubble oxygenators and membrane oxygenators were compared.

In an epidemiological survey on 382 case files, Humbert et al. studied the relation between blood rheological parameters and hematological data and also the connections with certain meteorological data. The authors particularly reported finding a correlation between blood viscosity and the thromboelastogram parameters. Lorient et al. studied platelet alterations in thrombotic diseases using cellular electrophoresis measurements. This study, conducted on 26 patients with a risk of thrombosis, was carried out after altering the shape of the platelets using ADP and platelet fixation with glutaraldehyde.

6) Drugs active on rheological parameters

Various drugs are capable of altering the blood's rheological properties. In a general review, Stoltz and Larcan examined the various substances which have an overall action on blood viscosity. These substances are primarily plasma substitutes, glucose parenteral solutions, anticoagulants, vasomotor drugs, contraceptives, radioiodinated substances, hypolipidemic drugs, antibiotics, anaesthetics and neuroleptics. The substances which act on a specific rheological parameter are grouped according to their type of action (sedimentation, rouleaux formation, cellular adhesion, erythrocyte deformability).

The numerous papers which dealt with this problem emphasized the fragmentary nature of the various studies carried out in this field and insisted on the absolute necessity of establishing clearly defined in vivo protocols for testing techniques, observation conditions, discussion and interpretation of results. It must be emphasized that any new drug, particularly if it is intended for treating chronical disorders, must be systematically investigated from the rheological point of view, in order to evaluate the beneficial or, on the contrary, worsening effects of the drug on the rheological conditions of blood circulation.

The Symposium ended with a Round Table presided by A.L. Copley where the main aspects developed during the three days of the conference were discussed : hemorheology and theory (G.B. Thurston), hemorheology and methods (H. Schmid-Schönbein), hemorheology and diseases (A.M. Ehrly), hemorheology and therapy (J.F. Stoltz) and hemorheology and drugs (P. Drouin).

BIORHEOLOGY, Vol. 17, pp. 297-300, 1980
Printed in the USA. All rights reserved.

0006-355X/80/040297-04$02.00/0
Copyright (c) 1980 Pergamon Press Ltd

Vol. 17
1980

OBITUARY

ALAN CHADBURN BURTON (1904 - 1979)

Alan Burton, M.B.E., B.Sc., M.A., Ph.D., LL.D., D.Sc., F.R.S.C., F.R.S.A.(U.K.), Professor-Emeritus at the University of Western Ontario, and one of Canada's distinguished biophysicists, collapsed and died June 27, 1979 on his way home from work. For those of us who knew Alan Burton over the years it is a time to reflect on him as a scientist and teacher and on what his special contributions were.

He was born in London, England, grew up in a large middle class family, and through two wars and the Great Depression, was exposed to a spectrum of social changes and economic circumstances. Variety was important to him in his life and scientific work. He received First Class Honors in Physics and Mathematics from the University of London, and came to Canada to do postgraduate work in Physics at the University of Toronto. He received his M.A. for research on 'The absorption spectra of the major planets', and his Ph.D. for his research 'Heating of electrolytes by high frequency currents'. His entry into the world of biology and the start of his career as a biophysicist, was, in his words 'more or less

Portrait of Alan Burton, on the occasion of his retirement, drawn by Dr. Alfred Jay. Dr. Jay was a graduate student of Dr. Burton.

accidental'. He began by explaining to physiologists and physicians the heating of body tissues by shortwave radiation. Alan Burton was quickly attracted and committed to the physical challenges of biology; he trained with Professor Martin at the University of Rochester to work on heat exchange in man and animals, and later with Professor Bazett at the Medical School of the University of Pennsylvania to study peripheral blood flow, followed by a research fellowship for four years at the Johnson Foundation for Medical Physics at the University of Pennsylvania, working with Dr. Detlev Bronk on human temperature regulation. At the outbreak of World War II he returned to Canada as a Research Associate of the National Research Council to work at the Banting Institute, Toronto. For his war researches in aviation medicine and on protective clothing he was awarded the M.B.E.

After the War, Alan Burton was invited to join the Department of Medical Research at the University of Western Ontario. He came, and three years later, was appointed Professor and Head of the new Department of Biophysics in the medical school. He was strongly committed to postgraduate education; the University, with his leadership, established the first Canadian postgraduate program in biophysics. Over the years he personally trained 14 M.Sc. and 22 Ph.D. students. He worked to establish Canada's first Honors Biophysics program at the University which began in 1966.

Alan Burton earned an international reputation as a scientist and received many awards in recognition of his scientific contributions. He was elected a Fellow of the Royal Society of Canada (1950), President of the American Physiological Society (1956), President of the Canadian Physiological Society (1959) and President of the Biophysical Society (1966). He served as Chairman of the Federation of the American Societies for Experimental Biology (1957-58) and of the Canadian Federation of Biological Societies (1963). He received a Gairdner Foundation Award (1961) and the degree (Honoris Causa) of LL.D. from the University of Alberta (1964) and D.Sc. from the University of Western Ontario (1974). The major areas of his published work were temperature regulation and blood flow, the equilibrium mechanics of the blood vessel wall, the mechanics and geometry of erythrocytes, the deformability of membranes and permeability, and in recent years, intercellular communication and the theories and epidemiology of cancer. He was perceptive about basic mechanisms in science and enjoyed writing. His book, published with Edholm in 1955, "Man in a Cold Environment" is regarded as a classic. His second book "The Physiology and Biophysics of the Circulation", published in 1965 (and revised in 1972) has been widely used by medical students and was translated into French, German, Italian, Japanese and Spanish. His third book, which draws together the thrust of his research on cancer, will be published late in 1980, "Understanding Human Cancer: The Physiological and Biophysical Point of View".

During the years since his retirement in 1970 he continued to teach. He vigorously pursued his new field of research on cancer

and argued his theories with colleagues and lectured about his ideas at other universities. He was uncomplaining about his declining health, and his deteriorating eyesight.

Association with Alan Burton over the years leaves an accumulation of memories of a rare man, a man whose scientific perception commanded international respect, and yet whose humility made him accessible to every level of student. He would give willingly of his time for a frustrated student and never judged anyone's efforts unworthy of his attention. Because he was always an avid learner, he was a fine teacher who welcomed questions as an opportunity for a fresh examination of the material and felt it his responsibility to bring the students to a comprehensive understanding of his subject. In his department, coffee breaks were obligatory periods of rigorous training for all aspiring scientists. He would range about the group requesting up-dates on experimental progress, assessments of lectures attended, input on problems encountered by any individual, and frequently would present aspects of papers he was reviewing as targets for departmental brainstorming. On these occasions the professor would join right in and exercise his own formidable and wide-ranging talents -- sometimes forcing students and faculty alike to return to fundamental concepts to find the significance of amassed data, making an original attack on old material with a deceptively simple question, seeing relationships in apparently disassociated studies, and allowing his humorous side to create a party atmosphere so all could respond to his challenges in the spirit of shared fun. He would often draw hilarious comparisons, invent rhyming couplets, plunge into an impromptu demonstration with any available materials such as cigarettes, matches, or coffee cups (with messy if not disastrous results), and thus infect everyone with his joy in science.

The study of science so enriched Alan Burton's life that he was tireless in initiating others in this fraternity. From science he derived challenge, purpose, values, adventure, worth, and profound joy. He lamented the modern trend to specialization as dessicating the pursuit of science. He welcomed variety and change and saw a growing need to reach across the isolation of specialties and synthesize facts into true knowledge. His most treasured quotation was Francis Bacon's description of a scientific mind:[1]

> *A Mind, Nimble and Versatile enough to catch the Resemblances of things, which is the chief point, and at the same time Steady enough to Fix and Discern their Subtle Differences; endowed by Nature with the Desire to Seek, Patience to Doubt, Fondness to Meditate, Slowness to Assert, Readiness to Reconsider, Carefulness to Set in Order, and neither Affecting what is New nor Admiring what is Old, and Hating every kind of Imposture.*

In 1975, Alan Burton said, "It has been my aspiration to live up

Vol. 17
1980

to Bacon's description, which explains, perhaps, how anyone could so spread his efforts on such a variety of topics in science."[2] He considered himself a most fortunate man to have been able to live his life as he did. And we have been fortunate to share in it.

Peter B. Canham, Ph.D.,
Professor of Biophysics,
University of Western Ontario.

[1]Selected Writings on the Interpretation of Nature. Francis Bacon. Random House, New York. 1955. p. 151.

[2]Variety -- the spice of science as well as of life. The disadvantages of specialization. A.C. Burton. Ann. Rev. Physiol. 37, 1975.

Vol.
1980

BIORHEOLOGY, Vol. 17, pp. 301-319, 1980
Printed in the USA. All rights reserved.

0006-355X/80/040301-19$02.00/0
Copyright (c) 1980 Pergamon Press Ltd

Vol. 17
1980

OVERVIEW

HEMORHEOLOGY OF TURBULENCE

Paul D. Stein and Hani N. Sabbah

Department of Medicine (Division of Cardiovascular Medicine) and
Department of Surgery, Henry Ford Hospital, Detroit, Michigan, 48202, USA

Interest in the measurement of turbulent blood flow in the cardiovascular system has largely been stimulated by its potential detrimental effects upon the arterial endothelium and upon blood constituents. Turbulence signifies chaotic and random fluctuations of fluid flow. A more precise definition may be as follows: "Turbulent fluid motion is an irregular condition of flow in which the various quantities show a random variation with time and space coordinates, so that statistically distinct values can be discerned" (1). In accordance with standard terminology (1), $U = \overline{U} + u$, where U is the instantaneous momentary velocity, $\overline{U}$ is the average (nonfluctuating) velocity, and u is the fluctuating velocity, it is usual to define the intensity of turbulence as the root-mean-square value of the fluctuating velocity: $u' = \sqrt{\overline{u^2}}$. The relative turbulence intensity is defined (1) as the ratio $u'/\overline{U}$.

In the case of viscous fluids such as blood, viscosity effects will result in the conversion of kinetic energy of flow into heat. Thus turbulent flow, like all flows of such fluids is dissipative in nature (1). If there is no continuous external source of energy for the continuous generation of the turbulent motion, the motion will decay. Other effects of viscosity, however, are to make the turbulence more homogeneous and to make it less dependent on direction. In the extreme case, if the turbulence has quantitatively the same structure in all parts of the flow field; the turbulence is said to be homogeneous. The turbulence is called isotropic if its statistical features have no preference for any direction, so that perfect disorder reigns. In all other cases, the turbulence will be nonisotropic or anisotropic (1).

The evaluation of turbulence in the cardiovascular system is complex due to many variables not commonly encountered in engineering applications. Such variables include pulsatile flow, non-Newtonian fluid, compliant vessels, complex structure of entrance regions, tapering of vessels, curvatures and branches. All of these factors interact in the determination of flow characteristics of the arterial system. Many undergo changes in various disease states, and additional factors such as irregularity of the vessel wall and stenoses may develop which alter the characteristics of flow. For these reasons, turbulence in the cardiovascular system is dependent upon more factors than are applied to the assessment of turbulence in smooth straight pipes. Because high velocities occur only during systole, the breakdown of laminar flow is transient during each cardiac cycle.

The existence of turbulence in the cardiovascular system has been suspected by some physicians for many years because of its likely association with cardiac murmurs (2). It is only in recent years, however, that turbulence or disturbed flow has been measured in laboratory animals (3-6), and human beings (7-10) (Table I).

Hot film anemometry for the detection of high frequency velocity fluctuations was first used in animals to measure disturbances of flow in 1968 (4), and the device for use in cardiovascular studies has been described (4, 11). The technique was subsequently applied to humans during open heart surgery (7). Invasion of the artery near the site of measurement was necessary for the introduction of the velocity sensor (4, 5, 7). Hot-film probes that could be introduced through catheters during cardiac catheterization enhanced the accessability of the great vessels, but to a certain extent compromised the exactness with which the axial velocity could be determined. The catheter-tip method, however, provided a satisfactory means for the determination of the magnitude of flow disturbances in the great vessels. The worst possiblity with this technique would be an underestimation rather than an overestimation of the magnitude of turbulence.

With this overview in mind, the following discussion will consider: 1) The nature of flow disturbances in normal states. 2) Disturbances of flow in abnormal conditions. 3) Factors that tend to augment or minimize disturbances, and 4) The potential of disturbed flow to initiate or potentiate cardiovascular abnormalities.

DISTURBANCES OF FLOW IN THE NORMAL STATE

Disturbed or turbulent flow in the region of a normal aortic valve was demonstrated during peak systole in a patient during open heart surgery by traversing the aorta with a hot-film probe (7) (Table I). The Reynolds number was 7800, and peak velocity was 130 cm/sec (7). Seed and Thomas, using a catheter-tip hot-film probe, reported turbulent blood flow in the ascending aorta of a man with a normal aortic valve at a peak Reynolds number of 11,000, and a peak velocity of 150 cm/sec (8). We studied the characteristics of flow in the region of normal aortic valves in six patients during cardiac catheterization (9). Disturbed or turbulent flow occurred in all patients during peak flow. The peak Reynolds numbers ranged from 5,700 to 8,900, and the unsteadiness parameter, α , ranged from 16 to 21. (The unsteadiness parameter is defined as $\alpha = r\sqrt{\rho\omega/\mu}$, where r = radius, ρ = density, μ = viscosity, ω = frequency = 2× heart rate/60 .) Our observations indicated the persistence of turbulent flow during the deceleration phase (9); and decelerating flow is thought to be unstable (12). Turbulence was present near the aortic valve, but was minimal or absent in the mid-ascending aorta and always absent in the proximal aortic arch. In a subsequent study in which aortic velocity was measured in 10 patients with normal aortic valves, we demonstrated that turbulence intensity, calculated as the root-mean-square value of the systolic fluctuations of velocity, ranged between 1.4 and 4.2 cm/sec. Peak aortic velocity ranged between 71 and 143 cm/sec (10). The relative turbulence intensity, calculated as the ratio of the absolute turbulence intensity to the instantaneous non-fluctuating velocity, ranged between 0.06 and 0.10 (10).

The assessment of the characteristics of velocity in the main pulmonary artery has received little attention. Using a circumferentially mounted hot film probe we demonstrated in 10 patients during cardiac catheterization that disturbed flow occurs in the region of normally functioning pulmonary valves as well as normal aortic valves (10). The turbulence intensity, however, was lower in the main pulmonary artery than in the ascending aorta. It ranged from 1.0 to 2.8 cm/sec. One factor that may have contributed to the higher turbulence in the aorta may be the higher velocity in the aorta. Peak velocity in the pulmonary artery ranged from 27 to 78 cm/sec; whereas in the aorta it ranged from 71 to 143 cm/sec (10). Even though volumetric flow is identical in the pulmonary artery and aorta, maximal velocity is lower in the pulmonary artery due to several factors. Among these are the larger diameter of the main pulmonary artery (13, 14) and pulmonary valve (15), and a longer systolic ejection period within the pulmonary artery (16-18). On this basis alone, mean velocity would be approximately 29 percent lower in the pulmonary artery than in the aorta, and a lower velocity has been measured by others (16-18) as well as by us (10). In addition, the greater distensibility of the pulmonary artery (13, 14) may have a damping effect upon turbulence that is independent of velocity, since compliant surfaces themselves appear to have a damping effect upon turbulence (19, 20). Turbulence or disturbed blood flow in humans in the region of a normal mitral or tricuspid valve has not, to our knowledge, been documented in patients. We believe, however, that such disturbances in the left and right ventricle are likely. Velocity measurements within the left ventricle of horses revealed highly disturbed flow (6).

Disturbed or turbulent blood flow in the cardiovascular system has been related to the transitional and critical Reynolds number (7, 21), and the unsteadiness parameter, α, (21). Greater flow disturbances occur in the region of the aortic valve in patients with an elevated stroke volume, and perhaps there is also an effect of the heart rate (9). In the presence of a high cardiac output, disturbances of flow start earlier during ejection and continue throughout the ejection phase. In the mid-ascending aorta, velocity fluctuations occur during peak velocity and persist into the deceleration phase. Isoproterenol in dogs augmented flow disturbances in the aorta. This was associated with an increased peak velocity, Reynolds number, and α number (21). The increased blood velocity would augment the Reynolds number and the increased heart rate would augment the unsteadiness parameter (21).

Only a few studies of blood flow characteristics have been performed in arteries other than the proximal portion of the great vessels. Measurements of flow characteristics have been made in the abdominal aorta and common iliac arteries of human beings (22) and animals (6), and the carotid arteries and coronary arteries of animals (6, 23). Hot film anemometry in anesthetized dogs showed disturbed blood flow in the descending thoracic aorta, which in several instances was augmented by isoproterenol (21). The Reynolds number exceeded 2000 (range 2060 to 5400) and peak velocity ranged from 71 to 252 cm/sec, with the exception of one case in which the flow was not disturbed and the Reynolds number was 1240 (21). Disturbed flow also occurred in the descending thoracic aorta of horses (6). The Reynolds numbers ranged between 1514 and 2357, the α numbers ranged between 13.9 and 25.8, and peak velocity ranged between 22 and 33 cm/sec. Measurements of blood velocity in the abdominal aorta proximal to the iliac bifurcation showed an absence of velocity disturbances (6). At various sites within the abdominal aorta, peak velocity ranged between 3 and 63 cm/sec and the Reynolds number ranged between 67 and 2250.

We evaluated the characteristics of velocity in the abdominal aorta and iliac artery of resting human subjects undergoing diagnostic cardiac catheterization (22). In each of eight patients, measurements by hot-film anemometry showed no disturbances of flow in the abdominal aorta or in the common iliac artery. One of these patients had prominent irregularities of the aorta due to atherosclerosis (22). Peak velocity recorded in the aorta in the region of the renal artery was 28 ± 3 cm/sec (mean ± SEM). Just proximal to the aortic bifurcation it was 27 ± 4 cm/sec. Velocity was only somewhat lower in the proximal portion of the common iliac artery (24 ± 4 cm/sec). The Reynolds number at the aortic bifurcation was 730 (range 400-1100). In the common iliac artery the average Reynolds number in four patients was 540 (range 390-620). The unsteadiness parameter, (α), measured just proximal to the iliac bifurcation was 9.3 (range 8.3-10.9).

Dye injected in the abdominal aorta of rabbits showed turbulence (3). Also in dogs, disturbances of flow were recorded in the abdominal aorta near the bifurcation of the common iliac arteries (24). However, velocity in the abdominal aorta of horses uniformly was undisturbed (6), and it was also undisturbed in resting patients (22). The observed differences, we speculate, may relate to anatomic and hemodynamic differences among species. In the patients in whom we were able to calculate a peak Reynolds number in the abdominal aorta, it was found to be below the transition Reynolds number established for steady pipe flow. The blood velocity that we recorded was comparable to the velocity previously reported in the descending aorta of human beings (25).

In horses, carotid artery flow was undisturbed; whereas it was disturbed or highly disturbed just distal to the aortic valve (6). The Reynolds number within the carotid artery ranged from 200 to 960 (6). Undisturbed flow was present in both the internal and external iliac arteries (6). In these arteries the peak velocity ranged from 9 to 53 cm/sec and the Reynolds number ranged from 202 to 1180.

The predisposition of the coronary arteries to develop atherosclerosis has led some investigators to assess the nature of flow in these vessels. A proper determination of flow disturbances in the coronary arteries with hot film probes presents major technical difficulties. Nevertheless, an attempt was made in anesthetized horses (23). In both the left anterior descending coronary artery and the left circumflex coronary artery, flow was generally free of disturbances. Flow was varied in character, however, and exhibited large amplitude low frequency oscillations (23). Peak velocities in the range of 9 to 83 cm/sec and Reynolds numbers of 188 to 1671 were reported at various distances from the coronary ostium. Similar observations were reported using a pulsed ultrasound Doppler velocity meter in ponies (26).

TABLE I

NORMAL FLOW CHARACTERISTICS AT REST

Site	Species	No.	Maximal Velocity (cm/sec)	Peak Reynolds Number	Character of Flow	Method	Ref.
Pulmonary artery	Man	10	27-78		Disturbed	Hot-film catheter	(10)
Proximal ascending aorta	Man	6	96-141	5700-8900	Highly disturbed	Hot-film catheter	(9)
	Man	10	71-143	-	Highly disturbed	Hot-film catheter	(10)
	Man	1	150	11,000	Highly disturbed	Hot-film catheter	(8)
	Man	1	68-130	4300-7800	Undisturbed; Highly disturbed on 2nd measurement	Needle or catheter hot-film	(7)
	Dog	6	-	-	Disturbed	Hot-film L-shaped	(5)
	Dog	1	75	3230	Disturbed	Hot-film L-shaped	(21)

TABLE I (Continued)

Site	Species	No.	Maximal Velocity (cm/sec)	Peak Reynolds Number	Character of Flow	Method	Ref.
Proximal ascending aorta (continued)	Horse	3	33-78	7130-9460	Highly disturbed	L-shaped or catheter hot-film	(6)
Mid-ascending aorta	Man	7	-	-	Undisturbed	Hot-film catheter	(9)
	Horse	2	41-83	3490-6380	Disturbed	L-shaped or catheter hot-film	(6)
Aortic arch	Man	7	-	-	Undisturbed	Hot-film catheter	(9)
	Horse	3	38-85	1388-2830	Disturbed, 2* Undisturbed, 1	L-shaped or catheter hot-film	(6)
Descending thoracic aorta	Dog	5	56-252	1240-5400	Disturbed, 4* Undisturbed, 1	L-shaped or catheter hot-film	(21)
	Dog	6	-	-	Turbulent, 1* Undisturbed, 5	Hot-film L-shaped	(5)
	Horse	6	22-33	1514-2357	Disturbed, 4* Undisturbed, 2	L-shaped or catheter hot-film	(6)
Abdominal aorta near renal artery	Man	7	19-52	-	Undisturbed	Hot-film catheter	(22)
	Horse	4	3-30	67-788	Undisturbed	L-shaped or catheter hot-film	(6)
	Rabbit	-	$\leq$60	$\leq$550	Turbulent	Dye injection	(3)
Abdominal aorta proximal to bifurcation	Man	7	13-52	400-1100	Undisturbed	Hot-film catheter	(22)
	Horse	2	14-63	212-2250	Undisturbed	L-shaped or catheter hot-film	(6)
Common iliac artery	Man	7	14-48	390-620	Undisturbed	Hot-film catheter	(22)
	Horse	6	9-53	202-1181	Undisturbed	L-shaped or catheter hot-film	(6)
Carotid artery	Horse	3	38-83	200-960	Undisturbed	L-shaped or catheter hot-film	(6)
Renal artery	Horse	1	77	1028	Undisturbed	L-shaped or catheter hot-film	(6)

Vol. 1980

TABLE I (Continued)

Site	Species	No.	Maximal Velocity (cm/sec)	Peak Reynolds Number	Character of Flow	Method	Ref.
Mesenteric artery	Horse	1	85	2148	Undisturbed	L-shaped or catheter hot-film	(6)
Left main coronary	Horse	10	11-83	188-1384	Undisturbed	L-shaped hot-film	(23)
	Pony	12	-	-	Undisturbed	Doppler ultrasound	(26)
Left circumflex coronary	Horse	7	12-40	308-790	Undisturbed	L-shaped hot-film	(23)
Left anterior descending coronary	Horse	7	9-70	103-1671	Undisturbed	L-shaped hot-film	(23)
Left ventricle	Horse	3	48-70	-	Highly disturbed	L-shaped or catheter hot-film	(6)

Key: No. = number of animals or patients
Ref. = reference number
*The number indicates the number of animals in which the indicated observation was made.

Vol. 17
1980

Flow Studies in Models of Arteries

Studies in glass models indicated that turbulent or disturbed flow would be expected at branches, and that turbulence would occur at lower velocities than expected with comparable fluids in straight tubes (27-29). Stehbens showed that turbulent flow can occur in glass models of arterial bifurcations at Reynolds numbers ranging from 347 for a T-shaped model to 1473 for a Y-shaped model with a 165° angle (27). The transition to turbulence in glass bifurcations can occur at critical Reynolds numbers as low as 1000 depending on whether flow is pulsatile or steady and depending upon the angle of bifurcation (28). The tendency for the breakdown of laminar flow was enhanced by both pulsatile flow (28) and an increased angle of bifurcation (28, 30). Based upon studies of unsteady flow in tubes, some investigators were led to speculate that turbulence or at least nonlaminar flow, probably exists in all arteries greater than one or two mm in diameter (31). Even though turbulence in glass tubes occurred at Reynolds numbers below 2000, the critical Reynolds number was above that which we observed in patients at the aortic bifurcation (22), particularly in view of the fact that Roach and associates based their calculations of the Reynolds number upon mean velocity (30) and we based our calculations of the Reynolds number on peak velocity (22).

Arterial Molds

In view of the difficulties that may be encountered in the assessment of flow characteristics in vivo, particularly in the coronary arteries, the use of models is a reasonable alternative in spite of the inherent drawbacks. The use of molds of arterial segments for the assessment of flow characteristics appears to be an improvement over previous techniques (32-36). We described a method for the construction of complex arterial molds in which the casting compound consists of paraffin and a synthetic polymer (32). The use of a casting compound which readily can be removed from a polyester resin mold, makes it possible to duplicate the lumen of complex branches of arteries for in vitro flow studies. There is no limitation on the number of branches, roughness of the internal surface, or curvature of the vessels. Such a capability was not present in the past. Previous techniques were restricted to duplicating branches of vessels that lay in a single plane. The only method that was able to duplicate irregularities in such vessels was the method described by Lutz and associates (36). The technique involved the fabrication of

plaster half-molds, and this was both tedius and time consuming. The technique was not applicable to a complex configuration of vessels such as in the coronary circulation. Other less complex methods for duplicating the lumen of arteries have been employed for in vitro studies (33-35). Such methods, however, are restricted to one or two branches of relatively smooth and short segments (33-35).

The availability of clear molds of human arterial segments provides a method for the detailed analysis of flow behavior which may not be possible in vivo. The use of laser Doppler anemometer systems in such measurements eliminates the necessity of entering the lumen and thus allows a better assessment of flow along the cross-section. Although molds of arteries by no means permit an ultimate assessment of characteristics of flow, such methods permit a more advanced evaluation over simple geometrical models.

DISTURBANCES OF FLOW UNDER ABNORMAL CONDITIONS

Valvular abnormalities almost invariably cause an augmentation of disturbances of flow. In patients with aortic valvular disease, disturbed or turbulent blood flow is markedly increased in comparison to normal subjects (9) (Table II). In patients with pure aortic insufficiency the intensity of turbulence was three times greater than in normal subjects (9). In these patients, flow disturbances may be attributed to an increased forward flow across the valve productive of high ejection velocities. Peak aortic velocities in the range of 231 to 256 cm/sec were recorded in these patients, and prominent levels of turbulence extended to the mid-ascending aorta and proximal aortic arch. Others also demonstrated prominent flow disturbances in a patient with severe aortic incompetence (7). In this patient the peak velocity during ejection was 88 cm/sec, which appears to be lower than velocities measured in the group of patients that we have studied.

In patients with aortic stenosis the level of turbulence was approximately ten times that observed in normal subjects (9). Peak velocities ranged from 358 to 459 cm/sec (9). It is possible that in patients with aortic stenosis, turbulence may extend into the carotid arteries thus explaining the physical manifestation of carotid shudder. Others have measured highly turbulent flow in the region of a congenitally stenosed pulmonary valve (7). They reported a peak velocity of 275 cm/sec.

The association of turbulent blood flow with high frequency pressure fluctuations (2, 37) productive of murmurs (2) suggests the presence of turbulent blood flow wherever murmurs are heard. This would include such conditions as mitral stenosis and insufficiency, tricuspid stenosis and insufficiency, ventricular or even atrial septal defects, coarctation of the aorta and hypertrophic obstructive cardiomyopathy to name only a few. Measurements of fluctuating pressures and intracardiac sound in the region of such defects clearly implies the presence of turbulent flow (38, 39). The pathological development of any type of obstruction to flow, unless the flow is extremely low, will result in the development of turbulence distal to the obstruction.

Turbulence in the region of aortic prosthetic valves has also been shown both in vivo (9) and in vitro (40). The structural configuration of many prosthetic valves contributes to flow separation which results in the breakdown of flow distal to the prosthesis. The amount of turbulence depends upon the configuration of the valve (40). Some newer prosthetic valves have designs which minimize turbulence (41).

PHYSIOLOGICAL AND HEMORHEOLOGICAL FACTORS THAT AUGMENT OR MINIMIZE TURBULENT BLOOD FLOW

The hemodynamic factors that tend to affect the magnitude of disturbances, and are typically evaluated in engineering systems, are parameters included in the Reynolds number. This includes the velocity, viscosity, and density of the blood, and diameter of the vessel. Any changes that would increase blood velocity or diminish blood viscosity would increase the intensity of turbulence. Lesions that produce an obstruction to flow, or produce an irregularity of the vessel would also augment disturbances distal to the obstruction. The normal aortic valve cusps also appear to act as a source of instability (42, 43). The effects of unsteady flow upon the transition from laminar to turbulent flow have been evaluated by several investigators (12, 44, 45); but an understanding of the stability of unsteady flow, even in pipes is still poor (12). Several other factors also affect the character of flow in the cardiovascular system, and these have received less attention. These include the branch-to-trunk area ratio at branches, the angle of branching, arterial tapering, and vessel distensibility. Among the hematological factors are the concentration and deformability of the erythrocytes.

Effect of Normal Semilunar Valve Leaflets Upon Flow Disturbances

The effect of the normal semilunar leaflets upon the production of disturbed or turbulent flow was investigated in vitro in the region of a stent-mounted normal porcine aortic valve (42). Maximal turbulence occurred in close proximity to the free margins of the semilunar cusps during systole (42). This can be explained by the tripping of flow at the free margin of the cusps. Fluttering of the free margin of the leaflets may contribute

to this effect, and we have observed such fluttering on high speed cine in vitro. These observations are consistent with the speculations made by McDonald (43). The observed flow disturbances can be considered to result from the semilunar cusps acting as natural projections into the stream of flow, and thereby acting as a source of instability (42). An increased Reynolds number would augment disturbances that occur at the free margin of the leaflets.

TABLE II

FLOW CHARACTERISTICS IN DISEASE STATES IN MAN

Pathology	No. Pts.	Site	Maximal Velocity (cm/sec)	Peak Reynolds Number	Character of Flow	Method	Ref.
Aortic stenosis	3	Aortic valve	308-459	10,000-20,000*	Highly turbulent	Hot-film catheter	(9)
	3	Mid-ascending aorta	-	-	Turbulent	Hot-film catheter	(9)
	3	Aortic arch	-	-	Turbulent	Hot-film catheter	(9)
Aortic insufficiency	4	Aortic valve	231-256	-	Turbulent	Hot-film catheter	(9)
	1	Aortic valve	88	7350	Turbulent	L-shaped hot-film probe	(7)
	4	Mid-ascending aorta	-	-	Turbulent	Hot-film catheter	(9)
	4	Aortic arch	-	-	Highly disturbed	Hot-film catheter	(9)
Pulmonary stenosis	1	Pulmonary valve	275	-	Turbulent	L-shaped hot-film probe	(7)
Atherosclerosis	1	Abdominal aorta proximal to iliac artery	25	950	Undisturbed	Hot-film catheter	(22)
	1	Iliac artery	18	390	Undisturbed	Hot-film catheter	(22)

Key: No. Pts. = number of patients
Ref. = reference number
*These values are approximations based upon the calculated diameter of the stenotic valve and velocity near the orifice.

Effect of Branch-to-Trunk Area Ratio Upon Flow Disturbances

The effects of different branch-to-trunk area ratios on the transition to turbulent flow were studies in glass models of the iliac bifurcation (46). A distinct effect of the branch-to-trunk area ratio upon the flow disturbances was observed in the branches. The Reynolds number in the trunk at which transition occurred in the branch was nearly halved when the branch-to-trunk area ratio increased from 0.8 to 1.4. For branch-to-trunk area ratios of 0.4 to 0.8, the critical Reynolds number in the trunk at which the transition to turbulence in the branch occurred was relatively constant at approximately 2100. As the branch-to-trunk area ratio increased beyond 0.8, the critical Reynolds number decreased until, at a ratio of 1.4, the critical Reynolds number was 1200 (46). Based upon arteriograms in 17 patients, of the aortic bifurcation, we showed a branch-to-trunk area ratio of 0.45 to 0.95 (0.71 ± .03) (mean ± SEM) (46). A branch-to-trunk area ratio of 0.52 to 1.08 (0.75 ± .04) was reported by Caro and associates (47) and a ratio of 0.77 ± .04 was

reported by Beales and Steiner (48). Others measured a branch-to-trunk area ratio of 0.4 to 1.0 (0.6 ± 0.1) (49).

A number of investigators have shown that the critical Reynolds number is diminished due to the presence of a branch (27-29). However, all of these studies were performed with branch-to-trunk area ratios of one or more (27-29). Studies in our laboratory showed that the critical Reynolds number is lower in the branches than in unbranched straight tubes for branch-to-trunk area ratios greater than one (46). Conversely, in the range of physiological branch-to-trunk area ratios observed in the abdominal aorta, there was no reduction of the critical Reynolds number.

Effect of Branch Angles Upon Flow Disturbances

The effects of angles of bifurcation in glass models with a branch-to-trunk area ratio of one showed that the critical Reynolds number decreased with increasing angles of bifurcation (28). During steady flow, there was a reduction of the critical Reynolds number in the trunk from 2500 with no bifurcation to 1500 with a bifurcation angle of 180^{o}. During pulsatile flow, the reduction of the critical Reynolds number was greater. It was approximately 2100 with no bifurcation and about 1100 with a bifurcation angle of 180^{o}. These observations indicate that flow disturbances at bifurcations are enhanced by both an increased angle of bifurcation and by pulsatile flow. The investigators recognized that a major problem in relating their study to the cardiovascular system was a lack of available data that showed the anatomic values of the branch-to-trunk area ratio and angle of branching (28). Subsequently, we measured the angle of branching of the aortic bifurcation in 19 patients; it ranged from 37^{o} to 80^{o} (46). The branch-to-trunk area ratio was usually less than one (46-49). In view of this, it is difficult to relate the results of many studies in glass tubes to disturbances that may occur at the aortic bifurcation because both the branch-to-trunk area ratio and the angle of bifurcation often exceeded the range observed in normal subjects.

Effect of Arterial Tapering Upon Flow Disturbances

Tapering of arteries has received little attention with regard to the stability of flow in the cardiovascular system. It has been recognized for hundreds of years that arteries are actually portions of truncated cones rather than cylinders (50, 51), and studies of flow have been performed in tapered tubes (52, 53). Engineers have recognized that tapering has a tendency to stabilize the laminar mode of flow (54). Some investigators, however, have calculated that the amount of tapering of vessels in the cardiovascular system, particularly in the aorta, is insufficient to diminish disturbances (29). The effect of vessel tapering on the transition to turbulent flow was studied in this laboratory in a glass model of the abdominal aorta (55). The models were constructed based upon angles of tapering observed in the descending aorta of 19 normal subjects (range 0^{o} to 3^{o}). Physiological angles of tapering had a definite stabilizing effect upon flow (55). The transition Reynolds number at which the flow was fully turbulent was nearly doubled when the angle of tapering was increased from 0.5^{o} to 2.5^{o}.

The pressure drop appeared to be primarily responsible for the stabilization of flow. Calculations based upon Bernoulli's equation indicate that the pressure drop would increase with an increased angle of tapering. The pressure gradient exerts an overwhelming influence on the stability of a laminar boundary layer; a decreased pressure in the downstream direction has a stabilizing effect (56).

Effect of Vessel Distensibility Upon Flow Disturbances

An additional physiological factor that may tend to dampen disturbances is the compliance of the arterial wall. The possibility that the compliance of the blood vessels may attenuate turbulence is suggested by observations of damping of turbulence by compliant coatings over flat plates (19). However, there is a paucity of information related to the effects of compliant tubing upon the characteristics of flow. We studied the effects of compliant walls upon turbulent flow in latex rubber tubes (20). In a tube with distensibility characteristics comparable to the human aorta, the absolute intensity of turbulence was 10% to 14% lower than in a rigid tube, depending upon the Reynolds number (20). The relative intensity of turbulence was also 10% to 14% lower than in a rigid tube. These observations suggest that the compliance of arteries may be a physiological factor that participates in reducing turbulence in the cardiovascular system.

The possibility that compliant surfaces may reduce turbulence, or turbulence induced skin friction drag, has been explored by aerodynamicists and naval engineers (19). It was suggested that the dolphin's compliant skin was responsible for its ability to swim at high speeds (57). The dolphin's skin was thought to absorb and dissipate the oscillatory energy from the boundary layer, and this retarded the transition to turbulent flow and extended the area of laminar flow over the dolphin's body (57).

Theoretical analyses suggest that the stability of laminary boundary layers can be altered by compliant boundaries. These analyses have been summarized in a review of skin friction drag reduction by compliant surfaces (58). Turbulence over compliant plates was found to be less than turbulence over a plate with a rigid surface (19). On the other hand, some investigators failed to find a reduction of drag induced by compliant surfaces (58). It was concluded that the percentage of successful drag reduction experiments was "not too high" and little theory was available to guide experiments (58).

Effect of Red Cell Concentration Upon Turbulent Flow

An assessment of the factors that may affect flow stability in the cardiovascular system requires an evaluation of the effects of the blood, since blood is a non-Newtonian fluid. We attempted to separate the effects of the erythrocytes upon turbulence from the effects produced by the viscosity and density of the blood. Blood of various hematocrits and plasma of a comparable viscosity and density were caused to flow in a turbulent fashion through an in vitro flow system (59). The viscosity of the plasma was made equal to that of blood by the addition of dextrose, and the density of the mixture was within 0.5% of that of blood. The intensity of turbulence of the blood was compared to that of the equally viscous plasma at equal Reynolds numbers. At hematocrits between 20 and 30 ml/100 ml (levels indicative of anemia) the intensity of turbulence of the blood was greater than that of comparably viscous plasma (59). At a normal hematocrit (40 ml/100 ml) blood was not more turbulent than comparably viscous plasma. This indicates that at normal hematocrits, blood does not tend to cause greater disturbances than expected with a Newtonian fluid; but at hematocrits observed in anemic patients, disturbances are augmented by the red cells (59).

The observed augmentation of turbulence with a diminished number of erythrocytes may be partially explained by the slip postulate (60). Newtonian non-slipping plasma is constrained to the wall, which promotes the stability of flow. In the case of blood, on the other hand, the red cells may skid along the wall, which would suggest a less stable condition according to this theory (60). Blood would, therefore, be more prone to turbulence than plasma under equivalent conditions of flow until a higher hematocrit tended to stabilize the flow, perhaps by virtue of the inertia of the red cell mass. Other factors also may contribute to this effect. For example, the size of the particles in suspension plays a role in the stability of flow (61). Smaller particles tend to destabilize the flow of some fluids (gases); whereas larger particles tend to stabilize it (61).

Effect of Red Cell Deformability Upon Turbulent Flow

To determine whether the deformability of normal red cells may have a modifying effect upon flow disturbances, we evaluated the characteristics of flow, in vitro, of normal cells and cells that were hardened by glutaraldehyde. The intensity of turbulence of blood composed of hardened cells was higher than that of blood composed of an equal number of fresh normal cells (62). The relative intensity of blood composed of the hardened cells was approximately twice that of blood composed of the normal cells; and this relationship was shown at various Reynolds numbers (62).

The mechanism of a relative suppression of turbulence by normally deformable cells in comparison to hardened cells appears to be related to the viscoelastic properties of the membrane of the red cells. Turbulence suppression by viscoelastic fluids is a function of the ratio of elastic to viscous forces (63). This ratio is reduced in blood containing hardened cells, because the viscosity of the hardened cells is increased and the elasticity reduced. High rates of collision among red cells would invariably occur in turbulent flow. Deformation of human red cells upon collision has been observed (64). Deformation of the cells, as a result of impact, would tend to cause the cells to act as an energy sink by absorbing some of the kinetic energy generated by the turbulent flow. This cushion effect may result in the reduction of vortex sizes and, therefore, in the suppression of turbulence.

The absence of deformability of the hardened cells may result in collisions within the turbulent field, and this presumably results in changes of the orientation and paths of the red cells. Hardened cells tumble, orbit and collide in an irregular fashion, when subjected to high shear; whereas deformable cells tend to align their major axes parallel to the direction of flow (65). Changes of the direction of motion of cells, due to collisions, may result in the generation of vortices, thus augmenting the chaotic state associated with turbulence. This effect would be even more pronounced with non-deformable cells because such cells may rotate and present their discoid surfaces at right angles to the velocity vector. Larger vortices, therefore, may be generated by non-deformable cells than would be generated by normal cells in the same turbulent field (62).

Vol. 17
1980

THE POTENTIAL OF TURBULENT BLOOD FLOW IN THE PERPETUATION OF CARDIOVASCULAR ABNORMALITIES

Disturbances of flow in normal human beings appear to be restricted to the great vessels and possibly the heart. Anatomic and hemorheologic factors in the normal cardiovascular system appear to contribute to a stabilization of flow. Nevertheless, significant levels of disturbances of flow may occur in disease states. Once turbulence occurs, there may be detrimental effects which could result from the high frequency velocity fluctuations, and high frequency pressure fluctuations; and perhaps the most important effect would be the high shear stresses (Reynolds stresses).

The Reynolds stresses in the region of a stenotic aortic valve may transiently reach 20,000 dynes/cm^2 within the jet, which is orders of magnitude higher than shear stress near the aortic wall, which was 110 dynes/cm^2 (66). During mid-ejection the root-mean-square value of the Reynolds stress was 3500 dynes/cm^2, and higher values undoubtedly will be shown when the jet is completely mapped. There is sufficient evidence in the literature to suggest that such stresses may have a detrimental effect upon blood elements.

Effect of Shear Stresses Upon Erythrocytes

Hemolysis of red cells occurs in patients with aortic stenosis (67, 68) and is thought to be caused by mechanical effects related to turbulence. It has been suggested that the frequency and severity with which the red cells encounter the wall of the vessels are factors that determine the rate of hemolysis. The latter may depend upon the chemical and physical character of the wall and upon the velocity gradient (69). It is possible that the chaotic and random motion of turbulent blood flow would increase the rate of red cell interaction with the vessel surfaces (69). Red cell lysis perhaps may occur within the turbulent field (69). The extent of red cell damage produced by shear is a function of the magnitude and duration of the shear stresses (69) (Table III). A formed element such as a red blood cell if it adheres to a vessel wall or a foreign surface may be damaged by shear stresses as low as 10 to 100 dynes/cm^2 (69). Following an exposure of erythrocytes to a shear stress of about 90 dynes/cm^2 for five minutes, the survival time diminished 22%, and after an exposure of 60 minutes, there was a 60% reduction of the half-life of these cells (70). Increased osmotic fragility and a reduction of the acetylcholinesterase activity in the cell membrane was also observed following exposure of the red cells to shear stresses (70).

A few spherocytes and poikilocytes were detected in human blood exposed to a shear stress of 1,500 dynes/cm^2 for two minutes (71). Stresses that exceeded 2,500 dynes/cm^2 for two minutes resulted in the appearance of a large number of abnormal erythrocytes as well as red cell fragments (71). The morphological changes of erythrocytes traumatized by shear were quite similar to the abnormalities observed in patients with hemolytic anemia related to prosthetic cardiac valves (71). Little hemolysis occurred with shear stresses below 3,000 dynes/cm^2 for a duration of two minutes, although at higher shear stresses hemolysis was greatly increased (71).

Human red cells began to lose their biconcavity with turbulent shear flow productive of stresses of 500 dynes/cm^2 for a duration of four minutes, and a majority of the cells assumed a prolate ellipsoidal shape when the stress exceeded 1,500 dynes/cm^2 (72). As the stresses were increased, the ellipsoidal shapes became more prominent. Above 2500 dynes/cm^2 for four minutes, fragmentation of the cells occurred (72). It was suggested that the red cells were ruptured in the bulk flow, although the effects of cell encounter with the wall were not completely excluded (72). Exposure of erythrocytes to viscous shear stresses of over 40,000 dynes/cm^2 for 0.01 msec, in the absence of wall effects, has been shown to cause hemolysis (73).

Lysis of red cells, whether caused by an interaction with the walls or high shear stresses, may contribute to thrombus formation by the release of the cellular contents (74), such as adenosine triphosphate (ATP) (75). Released ATP is converted to adenosine diphosphate (ADP) causing platelet aggregation (74). Partial thromboplastin also may be released from damaged red cells, thereby activating prothrombin to thrombin (74). This event would allow the platelet aggregates to become irreversible (74). Release of the content of red cells was found to occur even with sublethal erythrocytic hemolysis (76). Coincident with the damage of erythrocytes, therefore, is the release of factors that can produce irreversible platelet aggregation.

Turbulent blood flow and its inherent high Reynolds stresses may be detrimental in patients with some hematological disorders. In patients with hereditary spherocytosis, the red cells are less deformable than normal erythrocytes (77) and mechanical fragility is increased (78). Lysis of normal erythrocytes occurs when the critical strain of the membrane yield strength is exceeded (79). If the cells are abnormally fragile, a lower lethal shear stress would be expected. The increased turbulence due to the non-deformable cells perhaps would augment the rate of hemolysis in such patients. Sickled erythrocytes in patients with sickle cell disease are also less deformable than normal red cells (80). Turbulent flow has been found to augment the sickling process (81). The diminished number

of red cells in sickle cell disease and the diminished deformability of sickled red cells would contribute to the magnitude of turbulence in such patients (59, 62).

TABLE III

EFFECTS OF SHEAR STRESS ON ERYTHROCYTES

Method	Shear Stress (dynes/cm^2)	Duration Of Shear Stress	Effect	Reference
Viscometer	90	5 min	22% reduction in survival time	(70)
	90	60 min	60% reduction of the half-life. Increased osmotic fragility. Reduction of acetylcholinesterase activity of cell membrane	
Viscometer	1,500	2 min	Few spherocytes poikilocytes	(71)
	>2,500	2 min	Many abnormal erythrocytes and red cell fragments	
	>3,000	2 min	Hemolysis	
Viscometer	>500	4 min	Loss of biconcavity	(72)
	>1,500	4 min	Prolate cells	
	>2,500	4 min	Cell fragmentation	
Jet fragility test	>40,000	0.01 msec	Hemolysis	(73)

Vol. 17
1980

Effect of Shear Stresses Upon Platelets

High shear stresses inherent in turbulent flow may have a direct effect upon the platelets as well as the red cells (Table IV). Platelets subjected to a shear stress of 16.5 dynes/cm^2 for 20 minutes showed an appreciably higher thrombin-induced release of C^{14}-serotonin than in control suspensions (82). A possible activation of platelets by exposure to high shear stress in annular vortices has also been suggested (83). Platelet suspensions that have undergone oscillatory flow at an estimated wall shear stress of 26 dynes/cm^2 showed enhanced platelet aggregation (84). A substantial number of structural changes occurred in platelets when exposed to shear stresses in the order of 100,000 dynes/cm^2 for a few milliseconds (85). At higher shear stresses, both functional and structural evidence of severe platelet injury were observed (85).

When platelet rich plasma was exposed for a few milliseconds to shear stresses above 7,000 dynes/cm^2, the plasma serotonin level increased (86). Higher shear stresses, above 15,000 dynes/cm^2, caused a measurable diminution of the platelet count and increased lactic dehydrogenase activity in the plasma due to lysis of platelets (86). Platelet aggregation in response to ADP was impaired following this level of shear (86). For smaller exposure times, much higher shear stresses were required to yield measurable changes (86). Others have shown that platelet lysis, as indicated by lactic dehydrogenase release, began shortly after exposure to shear stresses above 165 dynes/cm^2; whereas at lower shear stresses of 50 to 100 dynes/cm^2, lactic dehydrogenase loss was not measurable even following an exposure to such shear stresses of 60 to 75 minutes (87).

To establish the premise that turbulence is a hydrodynamic factor that may contribute to the formation of thrombi, we performed studies in dogs using extracorporeal shunts (88, 89). Two arteriovenous shunts were established, each from the femoral artery to the contralateral femoral vein. In one shunt, a device for creating turbulent flow was incorporated. In the other shunt, a similar length of tubing with no constriction was inserted so that flow would be undisturbed. More thrombi occurred within the shunt that produced turbulence

than within the laminar flow shunt. Thrombi invariably occurred in the region of the turbulence generator, and most of the thormbi were located just distal to the orifice (88, 89). A linear relation was observed between the Reynolds number in the region of the turbulence producing orifice and the weight of the thrombi within the turbulent shunt (88). The relative intensity of turbulence distal to the turbulence generator was also linearly related to the Reynolds number. The weight of thrombi that accumulated within the turbulent system, therefore, appeared to be related to the intensity of turbulence (88).

Microthrombi with evidence of organization were shown on several calcific aortic valves obtained at surgery during aortic valve replacement (90). Subsequently, deposits of platelets were also observed by scanning electron microscopy, on stenotic valves from occasional patients (91). The repetitive deposition and organization of such thrombi may be an important cause of the continuing process of calcific aortic valvular stenosis of previously deformed aortic valves, and turbulent flow may be a factor that contributes to the platelet deposition. The hydrodynamic patterns of flow in the region of the aortic valve, including normal reversed flow, regurgitant flow (with aortic insufficiency) and captive annular eddies (with aortic stenosis) would cause various elements in the blood to interact with the valve surface and become deposited as a result of their increased adhesiveness. Abnormal valve surfaces, with exposure of the subendothelial layer, would further enhance the deposition of the platelets (91).

Platelet reactivity was evaluated in 30 patients who required replacement of their aortic valves (92). Sixty percent of the patients had a hyperactive platelet response as indicated by an increased percentage of spread type platelets and decreased numbers of dendritic forms, following exposure of the platelets to a stimulus in vitro. Patients both with aortic stenosis and aortic insufficiency had more hyperactive platelets than normal subjects (92). The occurrence of hyperactive platelets in patients with aortic stenosis and aortic insufficiency is compatible with the observation of platelet deposition on stenotic valves removed at surgery (90, 91). Turbulence, high shear stresses, and exposed abnormal surfaces may contribute to the increased platelet reactivity.

TABLE IV

EFFECTS OF SHEAR STRESS ON PLATELETS

Method	Shear Stress (dynes/cm^2)	Duration Of Shear Stress	Effect	Reference
Laminar oscillatory flow in tubes	17	20 min	Elevated thrombin-induced release of C^{14} serotonin	(82)
Laminar oscillatory flow in tubes	26	20 min	Enhanced platelet aggregation	(84)
Device for cell interaction with wall	100,000	msec	Structural changes	(85)
	>100,000	msec	Functional and structural evidence of severe injury	
Capillary flow system	>7,000	5 msec	Increased plasma serotonin level	(86)
	>15,000	5 msec	Reduction of platelet count, increased LDH, platelet lysis	
Viscometer	>165	msec	Increased LDH	(87)

Key: LDH = lactic dehydrogenase

Turbulence as a Cause of Poststenotic Dilatation and Aneurysm

Turbulent blood flow has been suggested to have a direct effect upon the arterial wall. Poststenotic dilatation was attributed to progressive weakening of the wall by turbulence (93). The association of turbulence with a poststenotic dilatation is likely because it

commonly occurs with aortic or pulmonary stenosis (94, 95) and may be found distal to aortic coarctations (96-98) where turbulence is known to occur. The mechanism by which turbulence may contribute to the development of a poststenotic dilatation, is conjectural. Several factors, when combined, may produce the dilatation (99). The conversion of the high kinetic energy of the swiftly moving stream into high potential energy or lateral pressure was postulated to be one factor in the development of a poststenotic dilatation. Shocks of impacts of alternating high and low pressure eventually may contribute to arterial distension. The lower velocity due to the widening of the vessel, according to the Bernoulli equation, would itself increase lateral pressure and cause even greater dilatation (99). High frequency pressure fluctuations within a turbulent field may act upon the wall of a vessel causing structural fatigue and dilatation. Although some studies have been performed in vitro in an attempt to quantitate the turbulent pressure fluctuations (100, 101), whether such pressures cause structural fatigue is undetermined.

Potential Role of Turbulence in Atherogenesis

In view of the absence of turbulent blood flow in the abdominal aorta and iliac arteries of normal resting human subjects, and its probable absence throughout the cardiovascular system with the exception of the vicinity of the cardiac valves and possibly the carotid sinus (the latter being the only region where an arterial expansion occurs), there is little to suggest that turbulence initiates atherosclerosis. It is possible that local areas of separation may be present which contain flow disturbances that cannot be detected in vivo. Such areas have been described in flow models (102). It is not clear, however, whether disturbances of flow in such zones of separation, even if present, could cause intimal injury. Endothelial proliferation has been produced in areas of high shear stress (103). On the other hand, it has also been suggested that low shear rates may contribute to atherosclerosis through its effects upon the mass transport of cholesterol (47).

Irrespective of the initial cause of atherosclerosis, once plaques or irregularities of the intima develop, turbulence perhaps may occur. One may conjecture that turbulent flow could accelerate the disease process. Several mechanisms by which the presence of turbulence within the arterial tree may lead to a progression of atherosclerosis have been suggested. High frequency pressure fluctuations inherent to turbulence may have a destructive effect directly upon the arterial wall (99). This could produce a critical injury which leads to a type of healing manifested as the lesion of atherosclerosis (99). Another mechanism by which turbulence within the arterial tree could be involved in the acceleration of atherosclerosis is by the production of localized areas of increased lateral wall pressure (local hypertension) (99). Around areas of turbulence there may occur areas of increased lateral pressure at sites of relative stasis (Bernoulli's principle) or at sites of jet streams (99). A local elevation of wall pressure perhaps may cause a critical injury, or may affect lipid synthesis within the arterial wall (104). This could result in a local accumulation of lipids often described as the first phase of the pathogenesis of the atherosclerotic lesion.

Endothelial cell damage, considered by some to be an initial factor in the formation of atherosclerotic plaques (105) has been related to high shear stresses (103), boundary layer separation (106) and/or stagnation (107). On the other hand, Copley (108), in his theory of atherogenesis, emphasized that vascular injury is not necessary for the early development of atheroma. Turbulence may contribute to platelet activation through high shear stresses and the interaction of blood elements with the arterial wall (109). Platelet deposits on the endothelial surface, according to the encrustation theory of atherogenesis, may participate in the disease process (110, 111). All of the various mechanisms by which turbulence or other hemodynamic factors may contribute to atherosclerosis are speculative, and experimental evidence is limited.

Turbulence Reducing Chemicals

With the possibility in mind that there may be potential detrimental effects of turbulence in the cardiovascular system, several investigators have considered the potential use of turbulence producing chemicals. Long-chain polymers, such as polyethylene oxide, have been shown to reduce turbulence in vitro (81, 112) as well as in laboratory animals (113). Polyethylene oxide, however, despite its effectiveness in quantities as low as one part per million, is a toxic substance. Desoxyribonucleic acid is a long chain compound that may have comparable turbulence reducing effects, and conceivably could be used with less hazard (114). The use of chemicals for the reduction of turbulence, however, is a remote therapeutic goal because the detrimental effects of turbulence have not yet been fully evaluated.

Conclusion

Disturbed or turbulent blood flow occurs in the cardiovascular system normally and in disease states. Under normal physiological conditions, turbulence occurs in the region of the cardiac valves. In disease states, turbulence may occur in peripheral vessels distal to

Vol. 17
1980

obstructions. Turbulent flow has detrimental effects upon blood elements, in particular erythrocytes and platelets. Turbulent blood flow may play a role in causing poststenotic dilatations and possibly in the production of intimal injury. Its role in atherosclerosis, is speculative.

REFERENCES

1. HINZE, J.O. Turbulence. New York: McGraw-Hill, 1959, pp. 1-4.

2. SABBAH, H.N. and STEIN, P.D. Turbulent blood flow in humans: Its primary role in the production of ejection murmurs. Circ. Res. 38, 513-525, 1976.

3. McDONALD, D.A. The occurrence of turbulent flow in the rabbit aorta. J. Physiol. (London) 118, 340-347, 1952.

4. LING, S.C., ATABEK, H.B., FRY, D.L., PATEL, D.J., and JANICKI J.S.: Application of heated-film velocity and shear probes to hemodynamic studies. Circ. Res. 23, 789-801, 1968.

5. SEED, W.A. and WOOD, N.B. Velocity patterns in the aorta. Cardiovasc. Res. 5, 319-330, 1971.

6. NEREM, R.M., RUMBERGER, J.A., JR., GROSS, D.R., HAMLIN, R.L. and GEIGER, G.L. Hot-film anemometer velocity measurements of arterial blood flow in horses. Circ. Res. 34, 193-203, 1974.

7. SCHULTZ, D.L., TUNSTALL-PEDOE, D.S., LEE, G., DeJ., GUNNING, A.J. and BELLHOUSE, B.J. Velocity distribution and transition in the arterial system. In: Circulatory and Respiratory Mass Transport. G.E.W. Wolstenholme and J. Knight, (Eds.) Boston: Little, Brown & Company, 1969, pp. 172-202.

8. SEED, W.A. and THOMAS, I.R. The application of hot-film anemometry to the measurement of blood flow velocity in man. In: Fluid-Dynamic Measurements in the Industrial and Medical Environments. D.J. Cockrell (Ed.): Leicester, England, 1972, pp. 298-304.

9. STEIN, P.D. and SABBAH, H.N. Turbulent blood flow in the ascending aorta of humans with normal and diseased aortic valves. Circ. Res. 39, 58-65, 1976.

10. STEIN, P.D., SABBAH, H.N. and ANBE, D.T. Comparison of disturbances of flow in the main pulmonary artery and ascending aorta of man. Biorheology 16, 357-362, 1979.

11. SEED, W.A. and WOOD, N.B. Development and evaluation of a hot-film velocity probe for cardiovascular studies. Cardiovasc. Res. 4, 253-263, 1970.

12. PARKER, K.H. Instability in arterial blood flow. In: Cardiovascular Flow Dynamics and Measurements. N.H.C. Hwang and N.A. Normann (Eds.) Baltimore: University Park Press, 1977, pp. 633-664.

13. GREENFIELD, J.C., JR. and GRIGGS, D.M., JR. Relation between pressure and diameter in main pulmonary artery of man. J. Appl. Physiol. 18, 557-559, 1963.

14. GREENFIELD, J.C., JR. and PATEL, D.J. Relation between pressure and diameter in the ascending aorta of man. Circ. Res. 10, 778-781, 1962.

15. DAVIES, M.J., POMERANCE, A. and LAMB, D. Techniques in examination and anatomy of the heart. In: The Pathology of the Heart. A. Pomerance and M.J. Davies (Eds.) Oxford: Blackwell Scientific Publications, 1975, p. 21.

16. MURGO, J.P., ALTOBELLI, S.A., DORETHY, J.F., LOGSDON, J.R. and McGRANAHAN, G.M. Normal ventricular ejection dynamics in man during rest and exercise. In: Physiologic Principles of Heart Sounds and Murmurs. AHA Monograph No. 46, 1975, pp. 92-101.

17. SHAVER, J.A., NADOLNY, R.A., O'TOOLE, J.D., THOMPSON, M.E., REDDY, P.S., LEON, D.F. and CURTISS, E.I. Sound pressure correlates of the second heart sound. Circulation 49, 316-325, 1974.

18. FRANKLIN, D.L., VAN CITTERS, R.L., and RUSHMER, R.F. Balance between right and left ventricular output. Circ. Res. 10, 17-26, 1962.

19. FISHER, K.H. and BLICK, E.F. Turbulent damping by flabby skins. J. Aircraft 3, 163-164, 1966.

Vol. 198

20. STEIN, P.D., WALBURN, F.J. and BLICK, E.F. Damping effect of distensible tubes on turbulent flow: Implications in the cardiovascular system. Biorheology (In Press).

21. NEREM, R.M. and SEED, W.A. An in vivo study of aortic flow disturbances. Cardiovasc. Res. 6, 1-14, 1972.

22. STEIN, P.D., SABBAH, H.N., ANBE, D.T. and WALBURN, F.J. Blood velocity in the abdominal aorta and common iliac artery of man. Biorheology 16, 249-255, 1979.

23. NEREM, R.M., RUMBERGER, J.A., GROSS, D.R., MUIR, W.W. and GEIGER, G.L. Hot film coronary artery velocity measurements in horses. Cardiovasc. Res. 10, 301-313, 1976.

24. GUTSTEIN, W.H., FARRELL, G.A. and SCHNECK, D.J. In vivo demonstration of junctional blood flow disturbances by hot wire anemometry. Atherosclerosis 11, 485-496, 1970.

25. GABE, I.T., GAULT, J.H., ROSS, J., JR., MASON, D.T., MILLS, C.J., SHILLINGFORD, J.P. and BRAUNWALD, E. Measurement of instantaneous blood flow velocity and pressure in conscious man with a catheter-tip velocity probe. Circulation 40, 603-614, 1969.

26. WELLS, M.K., WINTER, D.C., NELSON, A.W. and MCCARTHY, T.C. Hemodynamic patterns in coronary arteries. In: Fluid Dynamic Aspects of Arterial Disease. R.M. Nerem (Ed.) Columbus: Ohio State University, College of Engineering, 1974, pp. 36-38.

27. STEHBENS, W.E. Turbulence of blood flow. Quart. J. Exptl. Physiol 44, 110-117, 1959.

28. ROACH, M.R. The effects of bifurcations and stenosis on arterial disease. In: Cardiovascular Flow Dynamics and Measurements. N.H.C. Hwang and N.A. Normann (Eds.) Baltimore: University Park Press, 1977, pp. 489-539.

29. WESOLOWSKI, S.A., FRIES, C.C., SABINI, A.M. and SAWYER, P.N. Turbulence, intimal injury, and atherosclerosis. In: Biophysical Mechanisms in Vascular Homeostasis and Intravascular Thrombosis. P.N. Sawyer (Ed.) New York: Appleton-Century-Crofts, 1965, pp. 147-157.

30. ROACH, M.R., SCOTT, S. and FERGUSON, G.G. The hemodynamic importance of the geometry of bifurcation in the circle of Willis (glass model studies). Stroke 3, 255-267, 1972.

31. KROVETZ, L.J. The effect of vessel branching on haemodynamic stability. Phys. Med. Biol. 10, 417-427, 1965.

32. WALBURN, F.J., SABBAH, H.N., HAWKINS, E.T. and STEIN, P.D. Construction of molds of complex arterial segments. J. Biomech. Engin. (In Press).

33. DETERS, O.J., BARGERON, C.B., HUTCHINS, C.M., MARK, F.F. and FRIEDMAN, M.H. Velocities in unsteady flow through casts of human arteries. Proc. 32nd Ann. Conf. Engin. Med. & Biol. Denver, 1979, p. 101.

34. FRIEDMAN, M.H., BARGERON, C.B., DETERS, O.J. and MARK, F.F. LDV measurements of velocity profiles in arterial casts. Proc. 31st Ann. Conf. Engin. Med. & Biol. Atlanta, 1978, p. 42.

35. FRIEDMAN, M.H., BARGERON, C.B., DETERS, O.J., MARK, F.F. and HUTCHINS, C.M. Hemodynamic measurements in human arterial casts: Geometric effects and morphological correlates. 1979 Biomechanics Symposium. W.C. Van Buskirk (Ed.) Niagra Falls: Am. Soc. Mech. Engin., 1979, pp. 165-168.

36. LUTZ, R.J., CANNON, J.N., BISCHOFF, K.B., DEDRICK, R.L., STILES, R.K. and FRY, D.L. Wall shear stress distribution in a model canine artery during steady flow. Circ. Res. 41, 391-399, 1977.

37. SABBAH, H.N., BLICK, E.F. and STEIN, P.D. High frequency pressure fluctuations: Their significance in the documentation of turbulent blood flow. Cathet. Cardiovasc. Diagn. 3, 375-384, 1977.

38. STEIN, P.D., SABBAH, H.N., ANBE, D.T., KHAJA, F., and FOLGER, G.M., JR. Intracardiac sound as a diagnostic adjunct in subaortic stenosis. Angiology 30, 825-833, 1979

39. SABBAH, H.N., BLICK, E.F., ANBE, D.T. and STEIN, P.D. Effect of turbulent blood flow on systolic pressure contour in the ventricles and great vessels: Significance related to anacrotic and bisferious pulses. Am. J. Cardiol. 45, 1139-1147, 1980.

Vol. 17
1980

40. WEITING, W.D., HALL, W.C., LIOTTA, D. and DE BAKEY, M.E. Dynamic flow behavior of artificial heart valves. In: Prosthetic Heart Valves. L.A. Brewer, III (Ed.) Springfield, Ill.: C.C. Thomas Publisher, 1969, pp. 34-49.

41. RIEF, T.H. and HUFFSTUTLER, M.C. A preliminary flow study of a two-dimensional model of a concave-convex pivoting disc prosthetic heart valve. Proc. 7th Ann. New Eng. Bioengin. Conf. 1979, pp. 209-211.

42. SABBAH, H.N. and STEIN, P.D. Contribution of semilunar leaflets to turbulent blood flow. Biorheology 16, 101-108, 1979.

43. MCDONALD, D.A. Blood Flow in Arteries. 2nd ed., Baltimore: Williams & Wilkins Co., 1974, pp. 95-97.

44. HALE, J.F., MCDONALD, D.A. and WORMERSLEY, J.R. Velocity profiles of oscillating arterial flow, with some calculations of viscous drag and the Reynolds number. J. Physiol. (London) 128, 629-640, 1955.

45. YELLIN, E.L. Laminar-turbulent transition process in pulsatile flow. Circ. Res. 19, 791-804, 1966.

46. WALBURN, F.J., BLICK, E.F. and STEIN, P.D.: Effect of the branch-to-trunk area ratio on the transition to turbulent flow: Implications in the cardiovascular system. Biorheology 16, 411-417, 1979.

47. CARO, C.G., FITZ-GERALD, J.M. and SCHROTER, R.C. Atheroma and arterial wall shear: Observations, correlation and proposal of a shear dependent mass transfer mechanism for atherogenesis. Proc. Roy. Soc. London 177, 109-159, 1971.

48. BEALES, J.S.M. and STEINER, R.E. Radiological assessment of arterial branching coefficients. Cardiovasc. Res. 6, 181-186, 1972.

49. LALLEMAND, C., BROWN, K.G.E., and BOULTER, P.S. Vessel dimensions in premature atheromatous disease of aortic bifurcation. Br. Med. J. 2, 255-257, 1972.

50. HALL, M. A Critical and Experimental Essay on the Circulation of the Blood Especially as Observed in the Minute and Capillary Vessels of the Batrachia and of Fishes. E.L. Carey and A. Hart (Eds.) Philadelphia, 1935, Chapter I, Plates II, IV, and V.

51. JEFFORDS, J.V. and KNISLEY, M.H. Concerning the geometric shapes of arteries and arterioles. Angiology 7, 105-136, 1956.

52. CERNY, L.C. and WALAWENDER, W.P. The flow of a viscous liquid in a converging tube. Bulletin of Mathematical Biophysics 28, 11-24, 1966.

53. CHARM, S., and KURLAND, G. Blood flow in nonuniform tapered capillary tubes. Biorheology 4, 175-183, 1967.

54. PRANDTL, L. and TIETJENS, O.G. Applied Hydro- and Aeromechanics. New York: McGraw-Hill, 1934, p. 52.

55. WALBURN, F.J. and STEIN, P.D. Effect of vessel tapering on the transition to turbulent flow: Implications in the cardiovascular system. Fed. Proc. 39, 1068, 1980..

56. SCHLICHTING, H. Boundary-Layer Theory. New York: McGraw-Hill, 1968, pp. 123, 443, 445, 468-469.

57. KRAMER, M.O. The dolphin's secret. J. Am. Soc. Naval. Engrs. 73, 103-107, 1961.

58. BLICK, E.F. Skin friction drag reduction by compliant coatings. Intl. Conf. Drag Reduction. Cranfield, Bedford, England: Sponsored by BHRA Fluid Engineering, 1974, pp. F2-23 - F2-36.

59. STEIN, P.D., SABBAH, H.N. and BLICK, E.F. Contribution of erythrocytes to turbulent blood flow. Biorheology 12, 293-299, 1975.

60. NUBAR, Y. Blood flow slip and viscometry. Biophys. J. 11, 252-264, 1971.

61. MICHAEL, D.H. The stability of plane Poiseuille flow of a dusty gas. J. Fluid Mech. 18, 19-32, 1964.

62. SABBAH, H.N. and STEIN, P.D. Effect of erythrocytic deformability upon turbulent blood flow. Biorheology 13, 309-314, 1976.

63. METZNER, A.B. and PARK, M.G. Turbulent flow characteristics of viscoelastic fluids. J. Fluid Mech. 20, 291-303, 1964.

64. FUNG, J.S.K, and CANHAM, P.B. The mode and kinetics of the human red cell doublet formation. Biorheology 11, 241-251, 1974.

65. SCHMID-SCHÖNBEIN, H., WELLS, R. and GOLDSTONE, J. Influence of deformability of human red cells upon blood viscosity. Circ. Res. 25, 131-143, 1969.

66. STEIN, P.D., SABBAH, H.N. and WALBURN, F.J. Reynolds stresses near a stenotic aortic valve. (Abstract) Fed. Proc. (In Press).

67. EYSTER, E, MAYER, K. and MCKENZIE, S. Traumatic hemolysis with iron deficiency anemia in patients with aortic valve lesions. Ann. Intern. Med. 68, 995-1104, 1968.

68. FORSHAW, J. and HARWOOD, L. Red blood cell abnormalities in cardiac valvular disease. J. Clin. Pathol. 20, 848-853, 1967.

69. BLACKSHEAR, P.L., JR. Mechanical hemolysis in flowing blood. In: Biomechanics Its Foundation and Objectives. Y.C. Fung, N. Perrone and M. Anliker (Eds.) Englewood Cliffs: Prentice-Hall, 1972, pp. 501-528.

70. NANJAPPA, B.N., CHANG, H.K. and GLOMSKI, C.A. Trauma of the erythrocyte membrane associated with low shear stress. Biophys. J. 13, 1212, 1973.

71. NEVARIL, C.G., LYNCH, E.C., ALFREY, C.P., JR., and HELLUMS, J.D. Erythrocyte damage and destruction induced by shearing stress. J. Lab. Clin. Med. 71, 784-790, 1968.

72. SUTERA, S.P. and MEHRJARDI, M.H. Deformation and fragmentation of human red blood cells in turbulent shear flow. Biophys. J. 15, 1-10, 1975.

73. FORSTROM, R.J. A New Measure of Erythrocyte Membrane Strength - The Jet Fragility Test. Ph.D. dissertation, University of Minnesota, 1969.

74. JOHNSON, S.A. Platelets in hemostasis. In: Blood Clotting Enzymology. W.H. Seegers (Ed.) New York: Academic Press, 1967, Chapter 9.

75. BRAIN, M.C. Microangiopathic hemolytic anemia. New Eng. J. Med. 281, 833-835, 1969.

76. HJELM, M., ÖSTLING, S.G. and PERSSON, A.E.G. The loss of certain cellular components from human erythrocytes during hypotonic hemolysis in the presence of dextran. Acta Physiol. Scand. 67, 43-49, 1966.

77. MURPHY, J.R. Erythrocyte shape and blood viscosity. In: Hemorheology. Oxford: Pergamon Press, 1968, pp. 469-478.

78. YOUNG, L.E., IZZO, M.J. and PLATZER, R.F. Hereditary spherocytosis I. Clinical, hemotologic and genetic features in 28 cases, with particular reference to the osmotic and mechanical fragility of incubated erythrocytes. Blood 6: 1073-1098, 1951.

79. BLACKSHEAR, P.L., JR., DORMAN, F.D., STEINBACH, J.H., MAYBACH, E.J., SINGH, A. and COLLINGHAM, R.E. Shear, wall interaction and hemolysis. Trans. Amer. Soc. Artif. Intern. Organs 12, 113-120, 1966.

80. CHIEN, S., USAMI, S. and BERTLES, J.F. Abnormal rheology of oxygenated blood in sickle cell anemia. J. Clin. Invest. 49, 623-634, 1970.

81. STEIN, P.D., SABBAH, H.N. and MANDAL, A.K. Augmentation of sickling process due to turbulent blood flow. J. Appl. Physiol. 40, 60-66, 1976.

82. GOLDSMITH, H.L., YU, S.S.K. and MARLOW, J. Fluid mechanical stress and the platelet. Thrombos. Diathes. Haemorrh. 34, 32-41, 1975.

83. GOLDSMITH, H.L. and KARINO, T. Platelets in a region of disturbed flow. Trans. Am. Soc. Artif. Intern. Organs 23, 632-638, 1977.

84. YU, S.K., LATOUR, J.G., MARCHANDISE, B. and BOIS, M. Shear stress-induced changes in platelet reactivity. Thrombosis. Haemostas. 40, 551-560, 1978.

85. BERNSTEIN, E.F., MARZEC, U. and JOHNSTON, G.G. Structural correlates of platelet functional damage by physical forces. Trans. Amer. Soc. Artif. Intern. Organs 23, 617-625, 1977.

Vol. 17
1980

86. COLANTUONI, G., HELLUMS, J.D., MOAKE, J.L. and ALFREY, C.P., JR. The response of human platelets to shear stress at short exposure times. Trans. Amer. Soc. Artif. Intern. Organs 23, 626-631, 1977.

87. HUNG, T.C., HOCHMUTH, R.M., JOIST, J.H. and SUTERA, S.P. Shear-induced aggregation and lysis of platelets. Trans. Amer. Soc. Artif. Intern. Organs 22, 285-291, 1976.

88. STEIN, P.D. and SABBAH, H.N. Measured turbulence and its effect on thrombus formation. Circ. Res. 35, 608-613, 1974.

89. SMITH, R.L., BLICK, E.F., COALSON, J. and STEIN, P.D. Thrombus production by turbulence. J. Appl. Physiol. 32, 261-264, 1972.

90. STEIN, P.D., SABBAH, H.N. and PITHA, J.V. Continuing disease process of calcific aortic stenosis. Role of microthrombi and turbulent flow. Am. J. Cardiol. 39, 159-163, 1977.

91. RIDDLE, J.M., MAGILLIGAN, D.J., JR. and STEIN, P.D. Surface topography of stenotic aortic valves: A scanning electron microscopic study. Circulation 6, 496-502, 1980.

92. RIDDLE, J.M. and STEIN, P.D. Platelet reactivity in patients with aortic valve disease. (Submitted for publication).

93. ROACH, M.R. An experimental study of the production and time course of poststenotic dilatation in the femoral and carotid arteries of adult dogs. Circ. Res. 13, 537-551, 1963.

94. WOOD, P. Diseases of the Heart and Circulation. ed. 2. London: Eyre and Spottiswoode, 1956.

95. KJELLBERG, S.R., MANNHEIMER, E., RUDHE, U. and JONNSON, B. Diagnosis of Congenital Heart Disease. Chicago: Year Book Publishers, 1955.

96. SKANDALAKIS, J.E., EDWARDS, B.F., GRAY, S.W., DAVIS, B.M. and HOPKINS, W.A. Coarctation of the aorta with aneurysm. Intern. Abstra. Surg. 111, 307-326, 1960.

97. ZAROFF, L.I., KREEL, I., SOBEL, H.J. and BARONOFSKY, I.D. Multiple and infraductal coarctations of the aorta. Circulation 20, 910-917, 1959.

98. KIEFFER, S.A., LINDE, L.M., KEGEL, S.M. and LATTA, H.J. Mycotic aneurysm distal to coarctation of the aorta. J. Thorac. Surg. 42, 507-513, 1961.

99. HOLMAN, E. The development of arterial aneurysms. J. Surg. Gyn. and Obstr. 100, 599-611, 1955.

100. TOBIN, R.J. and CHANG, I.D. Wall pressure spectra scaling downstream of stenoses in steady tube flow. J. Biomech. 9, 633-640, 1976.

101. PITTS, W.H., III and DEWEY, C.F., JR. Spectral and temporal characteristics of post-stenotic turbulent wall pressure fluctuations. In: Publication of American Society of Mechanical Engineers, 77-Bio-8, 1977.

102. GUTSTEIN, W.H., SCHNECK, D.J. and MARKS, J.O. In vitro studies of local blood flow disturbance in a region of separation. J. Atheroscler. Res. 8, 381-388, 1968.

103. FRY, D.L. Acute vascular endothelial changes associated with increased blood velocity gradients. Circ. Res. 22, 165-197, 1968.

104. HOLMAN, R.L., MCGILL, H.C., STRONG, J.P. and GEER, J.C. Filtration versus local formation of lipids in pathogenesis of atherosclerosis. J.A.M.A. 170, 416-420, 1959.

105. JØRGENSEN, L. and SVENDSEN, I. Endothelial cell injury. In: International Conference on Atherosclerosis. L.A. Carlson (Ed.) New York: Raven Press, 1978, pp. 561-566.

106. FOX, J.A. and HUGH, A.E. Localization of atheroma: A theory based on boundary layer separation. Br. Heart J. 28, 388-399, 1966.

107. PINCHAK, A.C. and OSTRACH, S. Blood flow in branching vessels. J. Appl. Physiol. 41, 646-658, 1976.

108. COPLEY, A.L. Fibrin(ogen) platelets and a new theory of atherogenesis. Thromb. Res. 14, 249-263, 1979.

109. JØRGENSEN, L. Platelets and endothelial cell injury. In: International Conference on Atherosclerosis. L.A. Carlson (Ed.) New York: Raven Press, 1978, pp. 615-621, 1978.

110. MURPHY, E.A., ROWSELL, H.C., DOWNIE, H.G., ROBINSON, G.A. and MUSTARD, J.F. Encrustation and atherosclerosis: Analogy between early in vivo lesions and deposits which occur in extracorporeal circulations. Can. Med. Assoc. J. 87, 259-274, 1962.

111. MUSTARD, J.F., MURPHY, E.A., ROSWELL, H.C. and DOWNIE. H.G. Factors influencing thrombus formation in vivo. Am. J. Med. 33, 621-647, 1962.

112. STEIN, P.D., PARSONS, E.D. and BLICK, E.F. Modifications of dynamic flow properties of turbulently flowing human blood by long chain polymers. Med. Res. Eng. 11, 6-10, 1972.

113. MOSTARDI, R.A., GREEN, H.L., NOKES, R.F., THOMAS. L.C. and LUE, T. The effect of drag reducing agents on stenotic flow disturbances in dogs. Biorheology 13, 137-141, 1976.

114. WHITE, W.D. and HOYT, J.W. The effect of linear high molecular weight polymers on turbulent flow properties of human blood. Proc. 22nd Annual Conf. Engin. Med. Biol., Chicago, 1969.

Vol. 17
1980

BLANK
PAGE

Vol.
198

BIORHEOLOGY, Vol. 17, pp. 321-329, 1980
Printed in the USA. All rights reserved.

0006-355X/80/040321-09$02.00/0
Copyright (c) 1980 Pergamon Press Ltd

RHEOLOGICAL BEHAVIOUR OF SYNOVIAL FLUIDS

D.P. LY, D. BELLET, P. BOYER, C. ROQUES

Groupe de Rhéologie, I.M.F.T., 2 rue Camichel, 31071 Toulouse Cedex, FRANCE

(Received 3.2.1980; in revised form 10.5.1980.
Accepted by Editor J.C. Healy)

ABSTRACT -

This work is relating to rheometrical studies of 108 specimens of synovial fluids sampled on 59 patients. These studies allow to show up and to precise the ROPES's and BAUER's classification for arthrosis cases or arthritis ones or even for intermediate cases of complex rheumatoïd pathologies. The liquids, put through simple shear tests on a cone-plate rheometer, have all a non newtonian inelastic behaviour. In each studied case one proposes a power law model associated with coefficients n (index behaviour) and K (consistency), the shear stress/shear rate curves smoothing being made by numerical way. We have lay down a regression law between the parameters n and K, allowing to collect many results and to precise the diagnosis of the rheumatoïd disease which is at the origin of the sampled liquid. The mechanical behaviour of the synovial fluid can change naturally or artificially in the course of the time. One can follow the modifications by rheometrical measures on patients submitted to therapeutics of radionucleidi synoviolisis.

INTRODUCTION

The synovial fluid which moistens the joints of a "diarthrosis" plays an important role in the organism since it is the lubricant of the relative movements between the members. Its rheological behaviour must be known since it is subjected to various sollicitations of stresses, strains or shear-stresses. Moreover, its mechanical behaviour associated with its molecular structure must bring some informations useful for diagnosis to the clinicians and allows to choose the appropriate therapeutics.

Many studies have been made on rheological behaviours of this liquid (1, 2, 3, 4, 5, 6) However, they deal rarely with the relations between the rheological properties of the synovial fluid and the rheumatoïd diseases to which the sampled liquid is associated. Moreover the small number of tested samples during these studies doesn't allow generally to obtain significant conclusions.

The work presented here is the synthesis of results published separately (7, 8), and of a serie of rheometrical experiments made on 108 samples of human synovial fluids from different origins. Its purpose is to determine the rheological behaviours of this pathologic fluid, to precise, using rheometry, the classification proposed by ROPES and BAUER and to represent the classical cases of arthropathies. By the other hand, it allows to show up the rheological and then clinical results of local active treatments of synoviorthesis.

RECALL OF THE ROPES'S AND BAUER'S CLASSIFICATION

Relation between the arthropathies and the mechanical behaviour of the associated synovial fluid

In the case of a healthy person, the synovial fluid is a plasma (water, mineral salts, organic molecules), containing an "hyaluronic acid" which gives it some original physicomechanical properties. The synovial discharges in joints are owing to various pathologies which engender 3 types of different fluids. According to ROPES and BAUER, the following classification can be adopted :

Key words:
Synovial fluid, rheological behaviour, rheometry, arthropaties, radionucleidi synoviolisis.

- The mechanical liquid named Model I, "viscous", clear, poor in white globules (<1000/mm3) and containing :

  . less than 15 % of polynuclear "neutrophiles" ;
  . more than 85 % of "lymphocites" ;
  . less than 10 % of "ragocytes".

  This liquid is engendered by an overworking of the concerned joint, itself associated to a faultiness in the distributer of strains : the cartilage. A discharge of synovial fluid must supply to a bad repartition of strains by an increase of lubrification, which conduces to the opposite of discharge : it is the arthrosis.

- The inflammatory liquid named Model II, "fluid", turbid, rich in white globules (>3000/mm3) and containing :

  . less than 50 % of polynuclear "neutrophiles" ;
  . less than 50 % of "lymphocites" ;
  . more than 15 % of "ragocytes".

  This liquid is associated to an inflammation from various origin. If the increase of the liquid volume seems to engender the damage of the lubrificant properties, the presence of the discharge explains in fact the vascular phenomena of the inflammation : it is the arthritis.

- The mixed liquid named so intermediate or model II, showing a variable aspect. It is more or less clear. It contains :

  . between 1000 and 3000 white globules by mm3 ;
  . 15 % to 50 % of polynuclear "neutrophiles" ;
  . 10 % to 15 % of "ragocytes".

  Its existence is associated to cases of more complex diagnosis.

EXPERIMENTAL METHOD

108 specimens of synovial fluids have been studied. They have been sampled in the knee of 59 patients from the Rheumatologic Clinic Toulouse-Purpan - men and women. On the side of the cytological type, one notes liquids of model I, liquids of model II, liquids of model III (models of the ROPES's and BAUERS's classification).

For every case, many series of rheometrical measures with simple shear have been made on a cone-plate rheometer type Shirley-Ferranti thermostated at 37°C. An X-Y recorder associated with the rheometer allows to obtain directly the shear-stress/shear rate curves : $\tau_{r\theta} = f\left(\frac{du}{dr}\right)$. In every case the obtained curves showed the inelastic and pseudoplastic character of the behaviour which can be modeled by an Ostwald power law. As a matter of fact the transcription of these graphes in a logarithmical coordinates system conduces to linear graphes with the form :

$$\text{Log}\,\tau_{r\theta} = n\,\text{Log}\left(\frac{du}{dr}\right) + \text{Log}\,K$$

$$\text{i.e.} \qquad \tau_{r\theta} = K\left(\frac{du}{dr}\right)^{n}$$

where K is the consistency of fluid and n its index behaviour. The determination of K and n has been made with a method of least squares on a computer.

The samples are studied "new" in the hour following the sampling. An earlier work has shown the lack of significative differences in Rheology between liquids collected on a dry tube and on a heparined one and between the liquids studied "new" and after congelation (7).

Two extreme forms of the obtained shear -stress/shear rate curves are shown on figure 1. The first one is relative to the liquid Model I (Mechanical liquid). This liquid presents good lubricant qualities shown by a distinctly pseudoplastic behaviour (Fig. 1.a). This pseudoplastic character of the behaviour is met again in the majority of cases. The other form, associated to an inflammatory case, squares with a liquid Model II. This liquid is affected by a degradation of its mechanical properties and its behaviour is very near the newtonian one (Fig. 1.b).

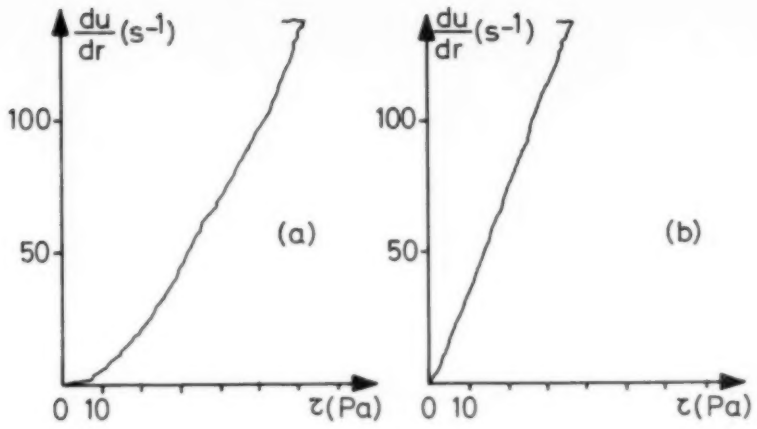

FIG. 1

Shear stress/shear rate curves obtained by cone-plate rheometer.
(a) : graph of a mechanical fluid.
(b) : graph of a inflammatory fluid.

RESULTS

1. Correlation between the consistency K and the behaviour index n

The Ostwald's model is proving completely adapted to the pseudoplastic behaviour of synovial fluids subjected to simple shears. After having determined for each case the values of the consistency K and the behaviour index n , we write the parameters in a semi-logarithmical coordinates system, we note there is a linear relation between n and Log K for every form of met diseases and whatever the nature of the studied support. So :

$$n = -\alpha \log K + \beta \quad \text{with} \quad \alpha > 0 \quad ; \quad \beta > 0$$

Let us note we can establish this fact for the rheological behaviour of aqueous high polymers solutions and give a thermodynamical explanation (9) ; others mechanicians have mentionned similar properties for some preparations of starchpaste or milk during the coagulation (10).

2. Rheological results associated to mechanical liquids, Model I (Table N° 1 and FIG. 2)

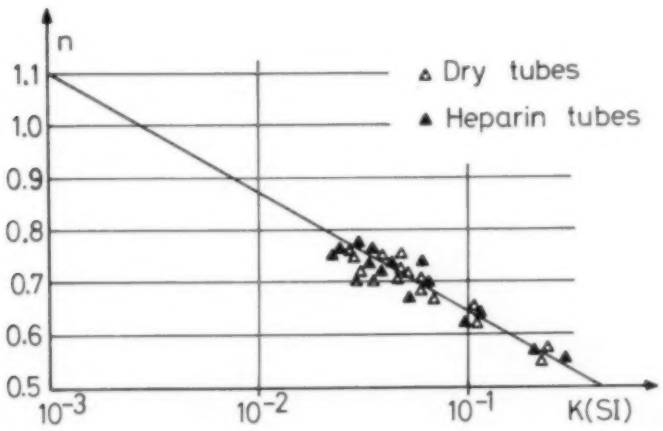

FIG. 2

Situation of rheological parameters associated to mechanical liquids on the " regression " straight line.

The table N° 1 presents the values of the behaviour index, the consistency, the number of globules by mm3 of synovial fluid and also the age and the sex of 16 patients suffering from arthrosis.

TABLE 1

Mechanical Liquids

Patients	Sex	Age	White Globules /mm3	n	K(S.I.)
9.L	M	63	200	0,276	0,0439
10.M	F	71	270	0,638	0,1217
16.B	F	54	200	0,698	0,060
19.U	F	45	30	0,663	0,0828
26.C	F	64	150	0,634	0,117
28.0	M	40	200	0,565	0,243
48.B	F	64	600	0,750	0,0407
49.R	M	52	190	0,568	0,305
51.C	M	82	420	0,559	0,399
56.P	M	72	200	0,675	0,0864
65.G	M	62	110	0,683	0,0550
67.F	M	56	350	0,750	0,0334
71.C	M	73	480	0,750	0,0544
73.C	M	73	350	0,727	0,0681
75.C	M	29	300	0,749	0,0471
77.U	F	46	40	0,744	0,0487

The rheological results show that the mechanical liquids poor in white globules (< 1000/mm3) have : a weak behaviour index : $n < 0.75$ and a high consistency : $K > 3,10^{-2}$ S.I.

The liquids are clearly pseudoplastic (FIG. 2). The patient who is affected by an arthrosis is suffering from a mechanical failing, but the fluid is undamaged. It keeps its good lubricant properties and its possibilities of adaptation to different physiological strains and even experimental ones.

3. Rheological results linked to inflammatory liquids, Model II (Table N° 2 and FIG. 3)

The table N° 2 presents the values of the rheological parameters K and n , the number of globules by mm3 of synovial fluid and also the age, the sex of 25 patients suffering form arthrosis.

TABLE 2

Inflammatory Liquids

Patients	Sex	Age	White Globules /mm3	n	K(S.I.)
1.B	M	48	11.000	0,988	0,0023
4.L	F	32	5.000	0,968	0,0039
7.C	M	19	10.700	0,942	0,0057
8.M	M	67	11.200	1,094	0,0010
11.C	F	56	11.800	0,935	0,0042
12.P	M	55	3.540	0,887	0,0100
13.C	F	56	16.800	0,954	0,0038
25.S	M	60	7.960	1,022	0,0030
29.M	F	70	25.800	0,877	0,0073
32.C	F	77	32.400	0,851	0,0101
33.L	F	58	5,740	0,856	0,0094
36.R	M	78	9.800	0,933	0,0041
37.A	M	83	15.500	0,921	0,0063
41.M	F	70	18.250	0,859	0,0100
44.M	M	27	8.700	0,858	0,0099
68.B	M	69	12.800	0,981	0,0045
74.L	M	41	29.300	0,937	0,0072
76.B	M	66	3.800	0,885	0,0098
39.B	M	30	7.200	0,869	0,0099
66.P	F	33	5.600	0,895	0,0074
61.D	M	74	3.840	0,891	0,0058
43.C	M	61	25.200	0,944	0,0044
70.C	M	61	24.300	0,939	0,0059
78.C	M	61	30.700	0,914	0,0072
84.C	M	61	23.300	0,853	0,0099

The rheological obtained results show that the inflammatory liquids, rich in white globules, always higher than 3000/mm3, present : a behaviour index n near unity : $n > 0.85$ and a weak consistency : $K < 10^{-2}$ S.I.

The pseudoplastic behaviour of these fluids is less characterized, some of them have the same behaviour as a newtonian fluid (FIG. 3). In the inflammatory diseases, the synovial fluid cannot play its lubricant role because of the clear degradation of its mechanical properties.

Vol. 17
1980

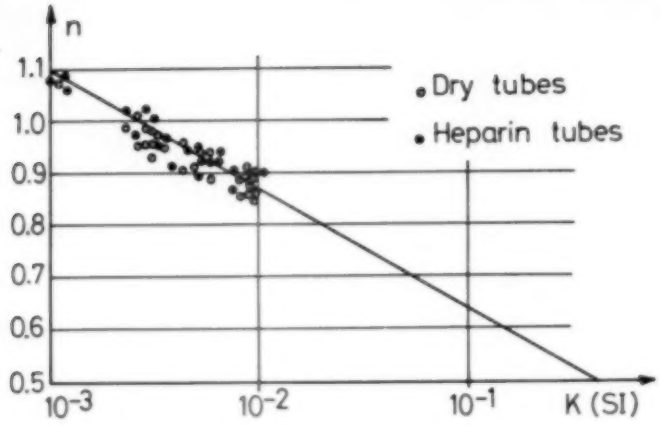

FIG. 3

Situation of rheological parameters associated to inflammatory liquids on the " regression " straight line.

For the Model I and Model II liquids, there is a good agreement between the rheological measures and the given clinical informations. One can propose a diagnosis at the sight of the shear stress/shear rate curve and confirms it having the values of the parameters K and n (FIG. 2 and 3).

4. Rheological results linked to mixed liquids, Model III (Table N° 3 and FIG. 4)

The Table N° 3 gives the rheological and cytological results of synovial liquids sampled from 8 patients suffering from a polyarthrisis and no having be subjected to a local treatment.

TABLE 3

Mixed Liquids

Patients	Sex	Age	White Globules /mm3	n	K(S.I.)
45.M	M	18	2750	0,834	0,0202
52.B	M	57	2680	0,753	0,0276
63.B	M	32	1820	0,773	0,0269
64.M	F	47	1800	0,762	0,0264
72.C	F	64	2900	0,799	0,0289
82.N	M	67	2300	0,777	0,0311
2.I	M	44	2000	0,732	0,0318
60.H	M	47	1240	0,789	0,0281

One indices that the number of white globules is between 1000 and 3000 by mm3 and that $0.74 \leqslant n \leqslant 0.85$ and 10^{-2} S.I. $\leqslant K \leqslant 3.1, 10^{-2}$ S.I.

In fact, these liquids are associated in general to clinical evolutions or complex cases. The patients are suffering from mixed diseases, successively or simultaneously. Moreover, the synovial fluid behaviour can be modified by the disease evolution.

The rheological results given by the tables 1, 2 and 3 are presented on Figure 4. One sees distinctly here the liquids (Model I, II, III) according to the situation of their rheological parameters on the " regression " straight line, and so the determination of the rate of pseudoplasticity can bring a noticeable help to diagnosis.

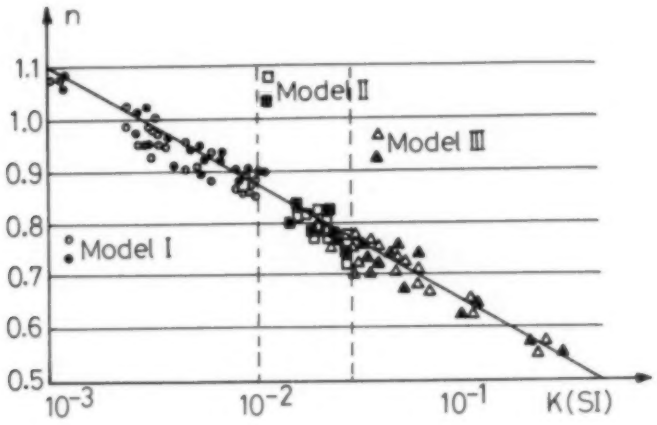

FIG. 4

Situation of rheological parameters of Model I, II, III on the " regression " straight line.

5. Some particular cases

On 54 studied cases, 5 cases have given results difficult to explain. Indeed, when the number of white globules (and the clinical remarks too) seems to demonstrate the synovial fluids to have an inflammatory origin, the values of the behaviour index and the consistency show them in the mechanical liquids class. We are not able to explain this discordance. At last, an other met case has been this one :

Patient : M.G. - 54 years old ; white globules : 120/mm3 ;

$n = 0.82$; $K = 0.023$ SI

The samples fluid is mechanical if we consider the number of white globules. If we consider K and n , it is inflammatory. On this patient, an arthroscopy and a synovial biopsy were practised :

Synovial biopsy shows numerous fragments having a greasy aspect, very rich in fatty elements and recovered with a coat of " mesothelial cells ". Others fragments have a connective tissue more fibrous, rich in vascular elements. At last, in other ones, one sees inflammation. One notes the presence of some fibrous remains.

These greasy and fatty characters are compatible whith an arthrosis.

This histological analysis allows to explain, in this definite case, the discordance between the cytological and rheological results.

INFLUENCE OF TREATMENTS BY SYNOVIOLISIS

The synoviolisis is a local active therapeutic often used in rheumatology : the radioisotopes lead to the destruction of the traumatic synovial fluid putting fibrous tissues in place of it. This method allows to destroy the inflammatory place : the synovial membrane of the joint.

We have studied the variations of synovial fluid rheological behaviour before the synoviolisis and after the application of this therapeutic. The study bears upon 10 patients who have given two samples at least. There is only a small number of studied cases because the synoviolisis gives clinical and rheological results only after 3 or 6 months : it is

Vol. 17
1980

necessary to wait for several years to have interesting conclusions. Six cases only give us interesting results. On the figure 5, we show separately the results linked to these six patients. Four studied patients A, B, C, D presented before treatment an arthritical syndrome (on the Figure 5, the number 1 corresponds to the time t which is equal to t_1). After treatment, i.e. to moments t_2 and t_3 ($t_1 < t_2 < t_3$) one sees a very net amelioration of mechanical lubricant synovial properties associated to an increasing pseudoplasticity, but there is not recovery of the patient. So, for every patient A, B, C and D, one goes from inflammatory liquids to liquids with mechanical behaviour, this is increased by the presence of many collagenic substances. The patients E and F presented, before the treatment, mixed liquids which run their course to the Model I with recovery of the mechanical properties after treatment.

The liquids of the other four cases give less significant results. For some ones, the behaviour index n varies so few that the transition to the liquid Model I cannot be seen. For others, n doesn't vary, either because the second sample has been made too early (the synoviolisis having not yet had a good effect), either because the used synoviolical therapeutics are a check.

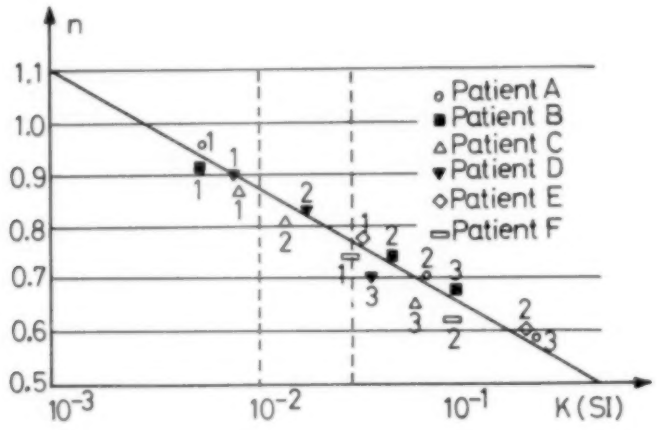

FIG. 5

Evolution on rheological behaviour of 6 specimens of synovial fluids submitted to therapeutics of radionucleidi synoviolisis.

CONCLUSIONS

ROPES and BAUER have made the synovial liquid classification with 3 models from the measurements of biological elements. The rheological study of synovial fluids allows to show a good agreement.

- the mechanical liquids (Model I) are pseudoplastic with a weak behaviour index and an high consistency ;
- the inflammatory liquids (Model II) are very near the newtonian behaviour with a near unity behaviour index and a weak consistency ;
- the mixed liquids (Model III) have a behaviour intermediate between the mechanical liquids and the inflammatory ones.

In other words, the inflammatory liquids are liquids which have lost their physical properties and cannot play their part of lubricant of moving joints. The mechanical liquids keep all their physical properties and are not responsable of the synovial discharge. The discharge proceeds only from the overworking of the joint itself.

Associated to the articular Physiology field, the presented rheological study allows to do a distinction between various types of synovial liquids. In particular, the establishment of a regression law between the parameters as the consistency K and the behaviour index n allows to collect many results and helps effectually the clinician. The interest of diagnosis of these determinations is important. In fact, linked to biological elements, the synovial rheological characteristics allow to distinguish without doubt different types of arthropathis and to precise the diagnosis of the rheumatoïd disease to which is associated the sampled liquid. It is also possible to follow regularly the effects of the used therapeutics as the synoviolisis by characterizing the mechanical evolutive possibilities of synovial fluid.

It would be interesting to establish the correlations between clinical date, rheological parameters and physico-chemical nature of the liquid ; from which, the interest of the fluid biochemical study, in particular the study of the hyaluronic acid which seems to play an important part in the fluid behaviour.

As a result of the intensive knowledge of synovial fluid mechanical properties, one can take under consideration the future works dealing with artificial liquid creation of articular lubrication, from macromolecule solutions for example.

On the one hand, this liquid would allow to renovate the articular failing function, on the other hand to prevent the damage of the molecular structure. It would be necessary to make important mechanical and biomechanical perfectings.

REFERENCE

1. SCOTT BLAIR, G.W. An Introduction to Biorheology. Amsterdam, Oxford and New-York : Elsevier Scient. Publ. Co., 1974, 222 pp.

2. ROPE, M. W. and BAUER, W. Synovial fluid changes in joint diseases. Harward University Press, Cambridge, Massachussets, 1953.

3. OGSTON, A. G., STANIER, J. E., TOMS, B. A. and STRAWBRIDGE. Elastic properties of ox synovial fluid. Nature, Lond. 165, 571, 1950.

4. DINTENFASS, L. Lubrification in synovial joints. J. Bone Joint Surgery 45A, 1241-1256 pp. 1963.

5. THURSTON, G. B. and GREILING, H. Viscoelastic properties of pathological synovial fluids for a wide range of oscillatory shear rates and frequencies. Rheologica Acta 17, 433-445 1978.

6. OGSTON, A. G. and STANIER, J. E. Some effects of hyaluronidase on the hyaluronic acid of ox synovial fluid and their bearing on the investigation of pathological fluids. J.Physiol. 119, 253-258 pp., 1953.

7. BELLET, D. BOYER, P., BOUSQUET, A. and ROQUES, C. Etude rhéologique de liquide synovial d'origine humaine. J. Fr. Biophys. et Med. Nucl. 1, 69-73 pp. 1978.

8. BELLET, D., BOYER, P., D.P. LY and ROQUES, C. Biorhéologie du liquide synovial : influence de synoviorthèse. J. Fr. Biophys. et Med. Nucl. 3, 169-171 pp.,1979.

9. BELLET, D. Relation entre comportements rhéologiques pseudoplastiques et échanges thermiques. Paul Sabatier University Thesis. Toulouse, (France), 1973.

10. NEDONCHELLE, Y. and SCHUTS. De l'homogénéité dimensionnelle de l'équation caractérisant le comportement rhéologique de systèmes aqueux de carbohydrate macromoléculaire. C.R. Acad. Sc. 265 D : 16, 1967.

Vol. 17
1980

BLANK
PAGE

Vol.
198

BIORHEOLOGY, Vol. 17, pp. 331-342, 1980
Printed in the USA. All rights reserved.

0006-355X/80/040331-12$02.00/0
Copyright (c) 1980 Pergamon Press Ltd

Vol. 17
1980

BLOOD FLOW IN CAPILLARY TUBES: CURVATURE AND GRAVITY EFFECTS

Ting-Cheng Hung, Tin-Kan Hung,
and George Bugliarello

University of Pittsburgh, Pittsburgh, Pennsylvania 15261
Polytechnic Institute of New York, Brooklyn, New York 11201

(Received 30.4.1979; in revised form 21.5.1980.
Accepted by Editor Y.C. Fung)

ABSTRACT The flow characteristics of human blood in curved capillary glass tubes are studied by means of high-speed microcinematography and pressure/flow measurements, and are compared with those in straight tubes. The velocity profiles of erythrocytes are analyzed as a function of the hematocrit, the Kármán or Reynolds number, the tube orientation (and hence gravity effects), and the station along the tube. In a 90° bend, at low Reynolds numbers, an initially symmetric velocity profile moves its peak toward the inner wall of the bend and then toward the outer wall of the straight segment after the bend. The asymmetry of velocity profile is more pronounced at the higher hematocrit (40%) than at lower ones. At higher Reynolds number, the velocity profile in the curve is blunter near the inner wall. The ratio of the peripheral plasma layer thickness in the outer region to that in the inner region of the bend is dominated by curvature rather than gravity. When the plasma viscosity is used to define a characteristic Reynolds number, the resistance coefficient for blood flowing upward increases with hematocrit. With downward flow, resistance is significantly reduced by gravity.

INTRODUCTION

The first observations of blood flow in peripheral vessels made by Malpighi in 1661 found the presence of an erythrocyte-free plasma layer (the peripheral plasma layer,PPL) adjacent to the vessel wall. Poiseuille in 1835 concluded that the thickness of the peripheral plasma layer in arterioles decreased as the rate of flow reduced. This layer results in a reduction of the apparent viscosity (refer to equation 3 below)(1,2). In 1929, Krogh (3) observed that the thickness of the peripheral plasma layer depended upon the flow rate and the relative size of the erythrocyte to the vessel. Subsequently, Copley et al.(4,5,6), using microphotographic techniques, measured the peripheral plasma layer in the microvessels (10-114 micra in lumen) of the hamster's cheek pouch and confirmed the findings of Poiseuille (7). Bloch et al. (8,9) studied the microcirculation in the mesentery, lung, and skeletal muscles of frogs, mice, rats, and rabbits. Their results showed that the ratio of the PPL thickness to the diameter of arterioles increased as the vessel diameter decreased, while a wide variation in flow rate did not cause significant alteration in the size of the layer.

Some aspects of the dynamic characteristics of the complicated flow processes in the microcirculation can be obtained by in-vitro studies of blood flow. The major advantage of such studies is the ease with which various parameters, such as hematocrit, flow rate, tube curvature can be controlled, and pressure drop measured. Detailed characteristics of in-vitro blood flow in straight glass fibers have been reported in a number of systematic studies by Bugliarello et al. (10-12). These studies have shed light on the deviation of the velocity profile of erythrocytes from that of Poiseuille flow and on the differences in the rheological characteristics of blood in small tubes and in rotating cylinder viscometers.

To acquire a more complete understanding of the flow in small vessels, it is important, however, to consider flow not only in straight tubes, but also in other geometries. Furthermore, given the fact that erythrocytes are not neutrally buoyant in plasma, it is important to assess how gravity affects the flow resistance (13). To the best of our knowledge, no

KEY WORDS: Blood - Capillary - Curvature - Gravity - Resistance - Velocity.

information exists on how the orientation of the capillaries--and hence gravity--affect the flow resistance of blood.

Before the present study, neither theoretical analyses nor in-vitro experiments had been reported for blood flow through curved capillary tubes. Recently, in-vivo studies by Schmid-Schoenbein and Zweifach (14) reported nonsymmetric erythrocyte velocity profiles for mammalian arterioles and venules. Changes in microvessel configuration, such as increased tortuousity and meandering, have been reported with various clinical disorders (15-17). For patients with systemic lupus erythematosus, the tortuous microvessels in the human nailfold may increase from the normal 25% to 44%, and the meandering microvessel to 32% from the normal 2% (18). Under these conditions, an understanding of the flow characteristics of blood in curves--starting with in-vitro studies--becomes even more significant.

The present study compares the characteristics of human blood flowing in straight and curved capillary glass tubes, with the flow occurring both with and against gravity. The task of determining the influence of curvature and gravity on all the flow characteristics of blood in capillaries, as a multiphase fluid, is extremely complex, as will be evident from the dimensional considerations in the next section. The purpose of the present study is to present some exploratory results in an area that, until now, has been terra incognita.

DIMENSIONAL CONSIDERATION

Let us, for our purposes, consider blood to be an erythrocyte suspension in plasma. The velocities, V_e, of erythrocytes and those of plasma can be assumed to be nearly steady when the blood flow rate remains unchanged. The parameters that affect V_e fall in four groups:

- -the position $(r.\theta.z)$[+] of the erythrocyte, its density ρ_e, undistorted diameter d, shape S_e, the hematocrit H, the rheological characteristics of the erythrocyte (represented here for simplicity by the membrane modulus E and the viscosity η of hemoglobin if treated as a linear fluid);
- -the density ρ_o and the viscosity μ_o of the plasma (including fibrinogen and other chemical compounds);
- -the capillary tube diameter D, its shape (through a shape parameter S_t), and the orientation θ of the tube;
- -the mean pressure gradient[++] $\Delta p/L$ between the ends of the capillary tube of length L, and the difference, $g(\rho_e-\rho_o)$, between the specific weight of erythrocytes (of density ρ_e) and that of plasma.

The flow rate of blood and the erythrocyte velocity are by no means independent. Also, the choice of μ_o rather than of the apparent viscosity μ of blood as an independent variable is based on the fact that μ_o can be taken to be independent from the shear-rate, while μ depends strongly on Δp, Q, D, and H.

The dimensionless velocity $V_e^*(=\rho_e V_e D/\mu_o)$, of the erythrocyte, defined as the ratio of the magnitude of the inertial force of the erythrocyte to the magnitude of the viscous force, can be expressed in terms of the parameters listed above, as:

$$V_e^* = f_1\left(H, \frac{\rho_o D^3 \Delta p}{\mu_o^2 L}, \frac{\rho_o D^3 g(\rho_e-\rho_o)}{\mu_o^2}, \frac{d}{D}, \frac{\rho_e}{\rho_o}, S_e, S_t, \theta, \frac{\rho_o D^2 E}{\mu_o^2}, \frac{\eta}{\mu_o}, \frac{r}{D}, \phi, \frac{z}{D}\right). \qquad (1)$$

For the flow of a given sample of blood in a tube, ρ_e/ρ_o, d/D, η/μ_o and $\rho_o D^3 g(\rho_e-\rho_o)/\mu_o^2$ can be considered constants, even though H and the Kármán number, $\mathbb{K}(=\rho_o D^3 \Delta p/\mu_o^2 L)$, may vary from one experiment to the other. Variations of $\rho_o D^2 E/\mu_o^2$ and S_e depend very much on the biochemical characteristics of blood and the stress and moment distributions on the erythrocytes. The latter will vary with the geometric, kinematic and dynamic characteristics of the flow. In this case, neither E nor S_e can be measured. However, for low Reynolds numbers, one may assume that $\rho_o D^2 E/\mu_o^2$ and S_e remain essentially unchanged, or that their effects on the velocity field are included in H and $\mathbb{K}$. Since the curved segment of the tube is practically circular, S_t is then represented by the ratio of the radius of curvature to the tube diameter, R_c/D.

Thus, the profile of the dimensionless velocity V_e^* in the diametrical plane depends in first approximation on the five variables on the right hand side of equation (2):

[+] r and θ are the polar coordinates of the cross-section of the tube and z is the tube axis

[++] The effect of elevation is included in Δp.

Vol. 1
1980

$$V_e^*(\frac{r}{D}) = \frac{\rho_e V_e D}{\mu_o} = f_2(H, \mathbb{K}, \theta, \frac{R_c}{D}, \frac{z}{D}) \tag{2}$$

A first purpose of our study is to explore the effects of the parameters on the right side of the equation on experimentally determined velocity profiles of the erythrocytes and on peripheral plasma layer dimensions.

On the basis of the mean blood velocity $\bar{V}_b$ in the tube (calculated from the measured discharge Q), and the blood apparent viscosity,

$$\mu = \frac{\pi D^4 \Delta p}{128 Q L} = \frac{D^2 \Delta p}{32 \bar{V}_b L} \tag{3}$$

the Reynolds number of the flow can be defined as:

$$\mathbb{R} = \frac{\rho \bar{V}_b D}{\mu} , \tag{4}$$

where ρ is the blood density. Substituting $\bar{V}_b$ (from equation (3)) into equation (4), one can obtain a simple relationship between $\mathbb{R}$ and $\mathbb{K}$ ($= \rho_o D^3 \Delta p / \mu_o^2 L$) as:

$$\mathbb{R} = \frac{\rho \mu_o^2}{32 \rho_o \mu^2} \mathbb{K} \tag{5}$$

Clearly, the evaluation of $\mathbb{K}$ does not require any arbitrary assumption for the flow field, while the calculation of $\mathbb{R}$ does, since the value of μ in $\mathbb{R}$ is based on Poiseuille flow. Also, the Reynolds number includes the effects of the hematocrit on the flow field while $\mathbb{K}$ does not, making it preferable to use the latter as an independent variable in equation (2).

In order to appreciate the dynamic effects of the erythrocyte suspension on blood flow, we define a characteristic Reynolds number

$$\mathbb{R}_o = \frac{\mu}{\mu_o} \mathbb{R} = \frac{\rho \mu_o \mathbb{K}}{32 \rho_o \mu} \tag{6}$$

which helps us in analyzing the pressure/flow relationship, or more specifically, the resistance coefficient (i.e. a dimensionless friction factor):

$$f = \frac{D \Delta P}{\frac{1}{2} \rho \bar{V}_b^2 L} = \frac{2 \rho \mathbb{K}}{\rho_o \mathbb{R}_o^2} = \frac{64}{\mathbb{R}_o} \cdot \frac{\mu}{\mu_o} = \frac{C}{\mathbb{R}_o} \tag{7}$$

In essence, a second purpose of our study is to determine the variations in C or in the apparent viscosity μ as the orientation of the tube and/or the hematocrit changes.

EXPERIMENTAL PROCEDURE

The results of two sets of experiments are presented in this paper (Table 1). The first (Set A), for a 90° bend in a 45 micra tube 8.07 cm. long with $R_c/D = 13.4$, consisted of 72 runs under upward (Case 1), and downward (Case 2) flow conditions, three different hematocrits were tested for each case (all coming out of the same blood sample), and at three to four different flow rates or Reynolds numbers. All 72 runs were conducted within 32 hours. Velocity profiles and peripheral plasma layer dimensions were measured only for this set of experiments.

In the second set of experiments (Set B), at $R_c/D = 6.8$, two capillary tubes of the same diameter and length (9.3 cm.) were used - one straight and the other with a 90° bend in the middle; all the experiments were performed again for upward and downward flow.

The tubes used were glass capillaries 45 micra in diameter. The curves were obtained by heating the tubes in the middle and bending them to a 90° angle along a circular curve (see Figure 1). The diameter of the curved segment was found to be almost uniformly reduced to 43 micra. The straight segment upstream was 4.3 cm. long and that downstream was

3.7 cm. The capillary tube was mounted on a glass slide which was mounted in turn on a vertical circular aluminum plate, whose rotation allowed changes in orientation of the capillary in order to study gravity effects (Figure 2).

TABLE 1.
Experimental Groups

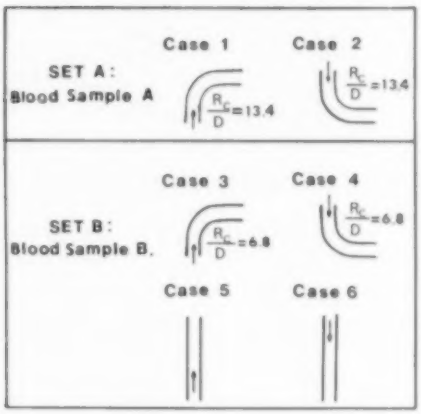

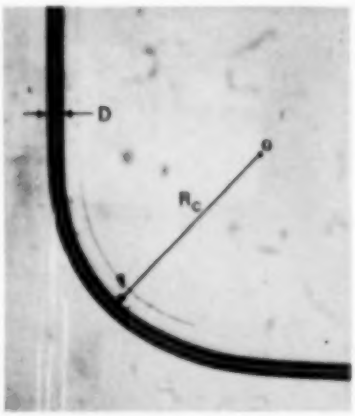

FIG. 1.

Photograph of a curved capillary glass tube ($R_c/D = 13.4$)

Vol. 1
1980

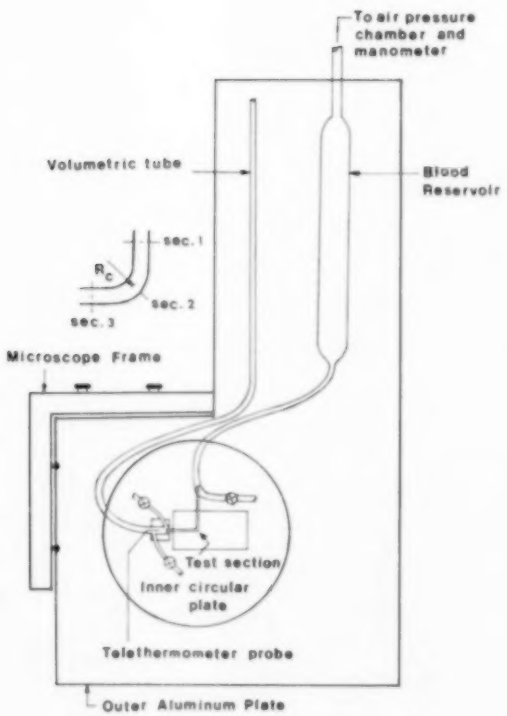

FIG. 2.

Experimental arrangement

A glass plate covering the test section of the capillary kept a uniform thickness of immersion oil between it and the glass slide, so as to reduce refraction errors. A bright field microscope was focused on the diametrical plane of the tube, and a Beckman and Whitely high-speed motion picture camera was placed in series with the microscope and operated at approximately 3000 frames per second. The erythrocyte motion was filmed on Kodak TRI-X reversal black and white movie films (ASA 200).

The experiments were conducted with citrated human blood with 30% ACD anti-coagulant solution. The blood was diluted to the desired hematocrits by adding plasma of the same sample.

Before being filled with blood, the flow system was washed by the flow of a 0.5% water solution of detergent (for 10-20 min.), then of distilled water (for 20-30 min.) and finally of plasma (for 5-10 min.). These procedures resulted in a significant reduction of the possibility of erythrocytes adhering to the capillary wall. The mean flow rate was determined by timing the advance of the meniscus of the flow blood column in a 370 micron tube downstream. In the upstream reservoir of blood sample, the pressure of the compressed air (approximately 3 to 30 cm. Hg) was measured using a mercury manometer. Since the blood in the conduits upstream of the capillary tube was practically motionless, the pressure at the entrance of the capillary tube is nearly hydrostatic. Before each steady flow experiment, the blood in the flow system was pumped back and forth so as to keep the hematocrit uniform. The steady flow rate and the pressure gradient were measured and rechecked after filming the blood motion. The blood temperature, measured with a YSI telethermometer at the outlet of the test tube, was kept constant at $25^{o} \pm 0.5^{o}C$.

The films were analyzed by following the motion of selected red blood cells, frame by frame. The images on film were corrected for refraction at the inner boundary of the tube (10). The velocity of an erythrocyte was computed from the length of pathline segment described in the unit time by the center of the erythrocyte. To obtain a statistical mean velocity profile (with approximately 150 points for velocity measurements), the cross-section of the median plane of the tube was divided into 20 laminae (each approximately 2 micra thick) and the mean velocity and standard deviation of the erythrocytes in each layer were computed. A 95% Student's "t" distribution function was used in the analysis of the confidence level. The thickness of the peripheral plasma layer (PPL) was measured for the upstream and downstream straight segments, and for the curved segment. The thickness was determined as the ratio of the integrated area (over the segment) between the wall of the tube and the edge of the cells (19).

CHANGES IN VELOCITY PROFILES AS FLOW PROGRESSES THROUGH THE BEND

To facilitate comparisons of the erythrocyte velocity profiles in the curved tubes, the velocity profiles on the diametrical plane of the tubes measured for the set of experiments A have been plotted dimensionlessly, using as a reference the measured maximum temporal mean velocity of the erythrocytes, $(\bar{V}_e)_{max}$. In the peripheral plasma layer the velocity profiles were extrapolated and do not represent primary data.

For upward flow in Case 1, the velocity profile of the erythrocytes at normal hematocrit (H = 40%) and at $\mathbb{R} \simeq 0.04$ (or $\mathbb{K} \simeq 6.9$) in the initial straight segments is nearly symmetrical, and blunter than for Poiseuille flow (Figure 3a). The PPL-thickness is practically identical for both sides of the diametrical plane. As the blood moves into the curve, the peak velocity shifts toward the inner half of the curved tube (Figure 3b), and the PPL becomes thicker at the outer wall (Figure 3b). Analytical studies have indicated that a similar velocity profile configuration occurs for creeping flow of homogeneous Newtonian fluids in a curved two-dimensional channel (20). It also occurs in the flow through coiled tubes (21,22) where, for the ratio of radius of curvature to tube diameter ($R_c/D = 13.4$) which characterized our observations, the peak velocity near the inner wall persists unless the Reynolds number $\mathbb{R}$ exceeds 21. In our case, the asymmetry of the profiles is accentuated by gravitational effects on the erythrocytes.

Proceeding beyond the curve to the straight segment downstream, the higher velocity region tends to "overshoot" the tube axis, moving to the outer portion of the cross-section (Figure 3c).

On the basis of the straight tube findings of Bugliarello and Hayden (10), one might expect that if the flow were not influenced by the curvature, the peak of the velocity profile would be encountered in the lower half of the downstream horizontal segment (because of gravity effects) - a situation that would therefore occur far downstream from the curve. We believe that in our case the shift of the velocity peak from the inner half of the middle section in the curve to the outer half in the straight section immediately downstream is due to spiral motion of the flow generated by local variations in the centrifugal force and by tube-erythrocyte interactions. However, the secondary flow was too weak to be measured.

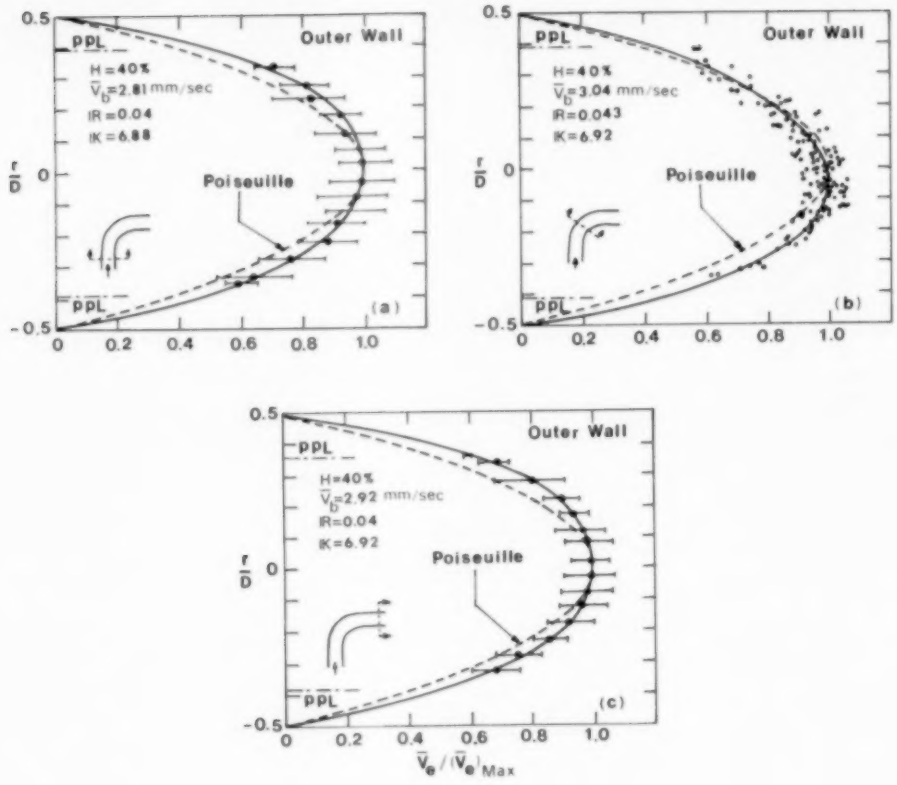

FIG. 3

Dimensionless velocity profiles for Case 1: (a) upstream, (b) in the curve, (c) downstream (H = 40%).

HEMATOCRIT EFFECTS

At small d/D blood can be considered to be homogeneous. As d/D increases, the interaction of erythrocytes among themselves and with the wall is bound to be significantly influenced by hematocrit. Indeed, measurements of V_e show hematocrit to be a major parameter affecting the motion of the erythrocytes.

In the straight segment upstream of the curve, the $\bar{V}_e$ profiles for 40% hematocrit deviate from the Poiseuille velocity profile, becoming more pronounced than those for H = 20%. Similarly, in the curve, the degree of asymmetry of the peak (toward the inner wall) is greater at 40% than at 20% and 10% hematocrit (Figure 4). This is so even though the gravitational effect works against the effect of tube orientation. In the straight segment, the $\bar{V}_e$ profiles become blunt as the hematocrits increase (Figure 5).

The peripheral layer thickness decreases rapidly with increasing hematocrit (Figure 6). The strong dependence on the hematocrit of the PPL dimensions had been already observed in straight tubes by Bugliarello et al. (11). Our data of PPL-thickness concur with those reported for steady and pulsatile blood flow in 40 and 70 micron straight tubes by Bugliarello and Sevilla (23), and Sevilla (24) in showing a decrease in the peripheral layer thickness with increasing hematocrit. However, at higher hematocrits (H = 20% and 40%) our average PPL values ($o.5(\delta_o + \delta_i)$) for the curved segment (where δ_o is the thickness at the outer wall and δ_i at the inner one) are approximately one micron larger than the corresponding ones by Bugliarello and Sevilla for a straight segment. The difference is probably due to the increase in PPL-thickness δ_o adjacent to the outer wall, and may also be due in part to different measurement techniques; the mean peripheral layer thickness was calculated from 100 successive measurements from 100 frames at a given section, while in the present study, δ_i and δ_o were based on the mean ratio for 10 frames of PPL-area to the segment (or frame length).

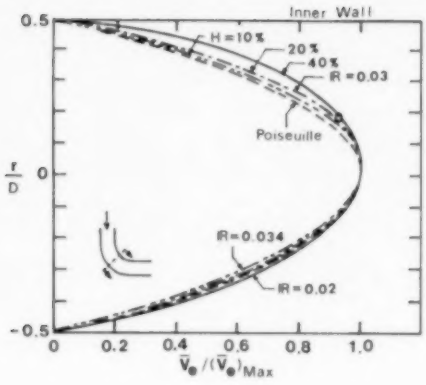

FIG. 4.

Dimensionless velocity profiles for Case 2 in the middle section of the curve (H = 10%, 20%, and 40%).

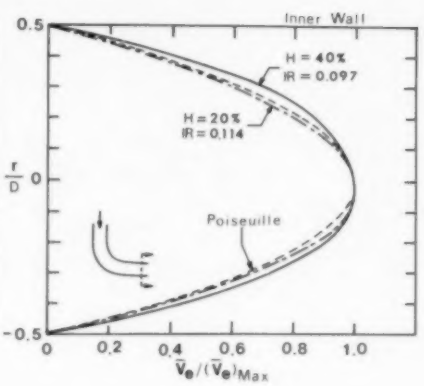

FIG. 5.

Dimensionless velocity profiles for Case 2 in the downstream straight segment of the curved tube (H = 20% and 40%).

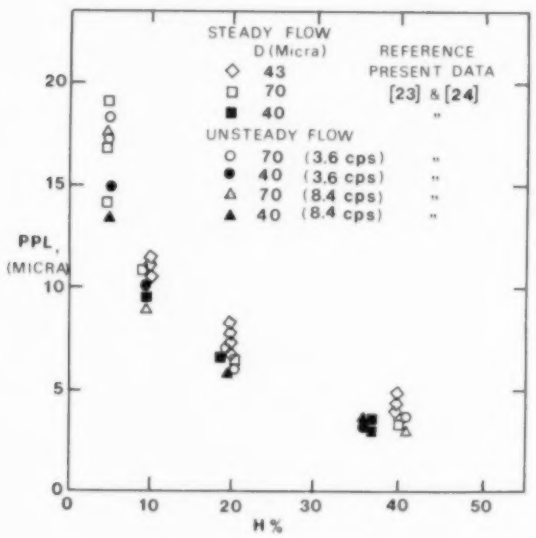

FIG. 6.

Mean values of PPL thickness near the outer wall and that near the inner wall in curved segment of the tube (Data from (23) and (24) are for straight tube).

REYNOLDS NUMBER EFFECTS

As mentioned earlier, in the straight segment upstream no significant differences were found in the shapes of the velocity profiles as the Reynolds number varied within the range considered in these experiments. In the curves, on the other hand, a comparison at H = 40% between the velocity profiles of blood for $\mathbb{R}$ = 0.019 and $\mathbb{R}$ = 0.097 (or $\mathbb{K}$ = 2.34 and 14.79) indicates that for lower $\mathbb{R}$ or $\mathbb{K}$, the peak of the velocity profile occurs closer to the inner wall (Figure 7). A similar trend is also observed at lower hematocrits, 20% and 10%.

Application of Dean's theoretical equation (21,22) for fully developed laminar flow in a coiled tube yields a peak velocity nearer to the inner wall at small $\mathbb{R}$. One might assume

this trend to persist for homogeneous flow downstream of the curve. The shift of the peak velocity from the inner region toward the outer one as blood flows through the curve must be attributed to momentum transfer effects due to the particulate nature of the flow.

The data in Figures 8a and 8b show that in the curve there is no significant variation of the peripheral layer thickness δ_o or δ_i with average wall shear stress τ, or more precisely, with the quantity $0.25D\Delta p/L$ (or $\mathbb{K}$). For τ ranging from 5 to 35 dynes/cm^2 (or $\mathbb{K}$ from 2.3 to 15.4), the average dimensions of the peripheral layer are practically not affected by wall shear stress or $\mathbb{R}$. Similar results were obtained upstream and downstream of the curve for 40% hematocrit, and in 40 and 70 micron straight vertical tubes by Bugliarello and Sevilla (23) for the wall shear stress ranging from 10 to 60 dynes/cm^2 ($\mathbb{K}$ = 3.18 to 58.4). At higher τ in the range from 33 to 100 dynes/cm^2 ($\mathbb{K}$ = 10.5 to 31.8), the peripheral layer in 40 micron tubes reported by Bugliarello et al. (11), increased with wall shear stress at normal and median hematocrits (40% and 28%), whereas at a lower range of stresses (12 to 50 dynes/cm^2), no significant effects were observed in 66.6 and 83 micron tubes. Similarly, Thomas (25), experimenting with bovine blood at 40% hematocrit flowing through two different tubes (58 and 102 micra in diameter) inferred that the thickness of the peripheral plasma layer decreased with increasing wall shear stress when the stress was greater than 50 dynes/cm^2, and approached a constant when the shear stress was below 50 dynes/cm^2. All these findings are consistent with the present results.

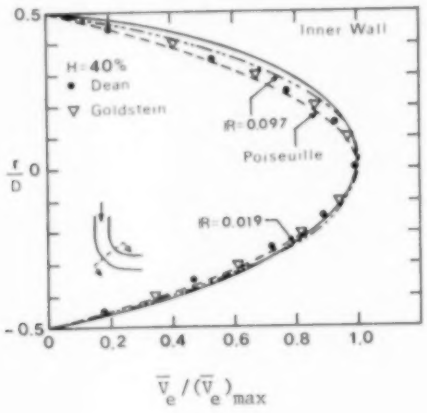

FIG. 7.

Effects of Reynolds number on the dimensionless velocity profiles at the middle section of the curved tube for H = 40%, and R_c/D = 13.4 (Case 2).

GRAVITY AND RADIUS OF CURVATURE EFFECTS

The effects of gravity have been ascertained by comparing the results for upward flow and downward flow. As expected, the resistance for the latter is smaller than that for the former (Figure 9). In our studies the Froude number (the ratio of $\rho_o\mathbb{R}_o/\rho$ to the square root of the third term on the right hand side of equation 1).

$$F = \frac{\overline{V}_b}{\sqrt{gd(\rho_e - \rho_o)/\rho_o}} \tag{8}$$

which, as is well-known, expresses the relative magnitude of inertia to gravity forces, was not small (between 0.5 to 6). Thus, the flow is dominated by inertia rather than gravity, and the degree of bluntness of the erythrocyte velocity profiles in a straight vertical segment could not be noticeably affected by gravity. In a curve, on the other hand, gravity favors higher velocities in the inner half of the curve for Case 1, and in the outer (lower) half of the curve for Case 2.

A comparison between Cases 1 and 2 of the velocity profiles in the curve for H = 40% and $\mathbb{R}$ = 0.09 ($\mathbb{K}$ = 15) in Figure 10 shows the velocity profiles in the inner and the outer sides to differ only slightly for the two cases. Thus, the effect of gravity is relatively small as compared with the curvature effect, V_e on the side of the inner wall being only

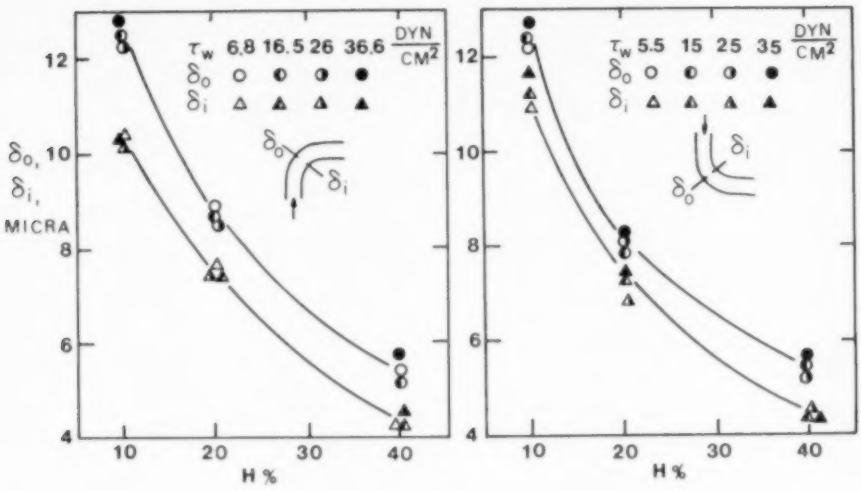

FIG. 8.

Peripheral layer thickness at the midsection of a curved tube with $R_c/D = 13.4$; (a)Case 1, and (b) Case 2.

slightly larger for Case 1 than for Case 2. However, the differences between the PPL thickness in the curved segments for the two cases indicate that the peripheral layer thickness is affected not only by the curvature of the tube, but also by gravity (Figure 8).

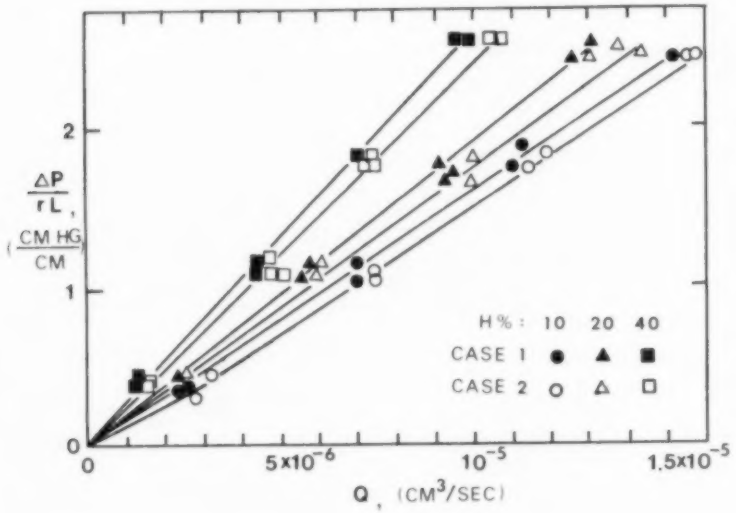

FIG. 9.

Drop of pressure head per unit length against flow rate.

The ratio δ_o/δ_i of the peripheral plasma layer thickness in the outer region to that in the inner region of the tube is not sensitive to hematocrit being about 1.20, 1.16, and 1.24 for Case 1 at 10%, 20%, and 40% hematocrit, respectively. The corresponding ratios for Case 2 are 1.12, 1.11, and 1.25.

To separate the increase in resistance due to gravity from that due to curvature, the experiments in Set B (Cases 3 to 6) were performed. The results are shown in Figure 11.

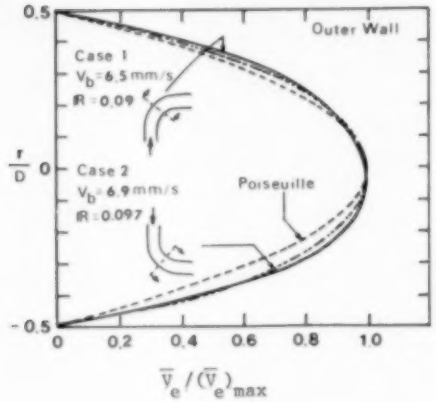

FIG. 10.

Comparison of dimensionless velocity at midsection of a curved tube for Cases 1 and 2 (H = 40%).

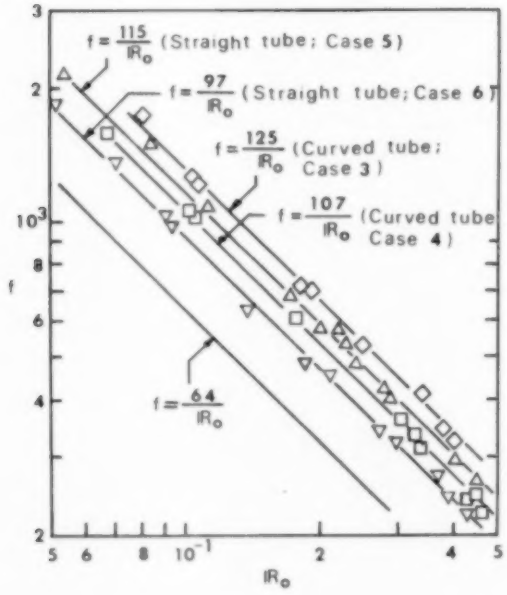

FIG. 11.

Gravity and curvature effects on resistance coefficient; H = 40%.

For the flow of plasma in the straight tube the resistance coefficient f is the same as for Poiseuille flow. At 40% hematocrit, f increases by 52% for a downward flow and by an additional 28% for upward flow. A simple estimate of the net gravitational force acting on erythrocytes can be obtained from $g(\rho_e - \rho_o)H\mathbb{L}$, which yields about 3.3% of the pressure drop when $\mathbb{R}_o = 0.1$. Although the ratio of $g(\rho_e - \rho_o)H\mathbb{L}$ to Δp decreases linearly with $\mathbb{R}_o$, the value of C in Equation 7 remains constant as $\mathbb{R}_o$ increases, indicating that the apparent viscosity $\mu(= C\mu_o/64)$ is independent of the Reynolds number (or shear rate) in this range.

The increment of resistance per unit length due to the curve (with $R_c/D = 6.8$) is due in part to the increase in resistance in the curve and in part to the asymmetry of the

velocity profiles after the curve. The mean increment of resistance coefficient per unit length due to these two effects can be expressed by

$$\Delta f = \frac{D(\Delta p - \Delta p_s)}{\frac{1}{2}\rho \bar{V}_b^2 (\frac{1}{2}\pi R_c + L_1)} = \frac{45}{R_o} \tag{9}$$

where L_1 is the length of the segment of the tube after the curve, and Δp and Δp_s are the pressure drops respectively for curved (Cases 3 and 4) and straight tubes (Cases 5 and 6) of the same length.

CONCLUSIONS

This study extends our knowledge of in-vitro behavior of blood flowing in small tubes by providing information on the effect of orientation and curvature of a glass capillary on flow resistance and detailed flow characteristics. In a curve, the peak erythrocyte velocity is found to occur away from the outer wall - similar to what we know of creeping flow in a coiled tube or in a two-dimensional curved channel. The asymmetry of the erythrocyte velocity profile increases with curvature and concentration (hematocrit). In the straight segment immediately downstream of the curve, the peak velocity of the erythrocyte shifts to the outer region.

At essentially normal hematocrits (H = 40%), the peripheral plasma layer (PPL) adjacent to the outer region of the diametrical plane is about 20% thicker in the outer region than in the inner region of the curve. At lower hematocrits (H = 20% and 10%), the outer PPL thickness is about 10% larger than the inner one. At a given hematocrit, furthermore, the PPL thickness is controlled primarily by the curvature effect.

Gravity effects on the velocity profile in the curve are generally small in comparison to curvature effects. However, the effect of gravity is noticeable in the total resistance of the flow. In a straight 45 micron tube, the resistance coefficient for an upward flow is about 18% larger than that for a downward flow. With the introduction of a 90° bend (with 6.8 ratio of the radius of curvature to the tube diameter), the resistance coefficient increases further by 10%.

ACKNOWLEDGEMENT

The work was initiated at Carnegie-Mellon University under NIH Grant #HE-05557 to G. Bugliarello. NSF Grant #GK-31514 to T.K. Hung and support to T.C. Hung under NIH training Grant #GMO-1455 during part of this investigation are also acknowledged. The authors would like to thank Dr. G.C.C. Hsiao of the University of Delaware for his assistance during the early phase of this study, and to acknowledge the assistance of Mrs. Hilda Diamond.

REFERENCES

1. FÅHRAEUS, R. The suspension stability of blood. Physiol. Rev. 9, pp. 241-274, 1929.

2. FÅHRAEUS, R. and LINDQUIST, T. The viscosity of the blood in narrow capillary tubes. Am. J. Physiol. 96, p. 462, 1931.

3. KROGH, A. The Anatomy and Physiology of Capillaries. Hafner Publishing Company, New York, 1929.

4. COPLEY, A.L. and SCOTT BLAIR, G.W. Rheol. Acta. (Suppl. Koloid-Zschr.) 1, p. 170, 1958.

5. COPLEY, A.L. and STAPLE, P.H. Hemorheological studies on the plasmatic zone in the microcirculation of the cheek pouch of Chinese and Syrian Hamster. Biorheology, 1, pp. 3-14, 1962.

6. COPLEY, A.L. Flow Properties of Blood and Other Biological Systems, Copley, A.L. and Stainsby, G. (Eds.) London: Pergamon Press, p. 97, 1960.

7. POISEUILLE, J.L.M. C.R. Acad. Sciences, seance 28, p. 12, 1935, tome VII, Savants estrangers, Paris. Impr. Royal. Quoted by Copley et al. (4).

8. BLOCK, E.H. A quantitative study of the hemodynamics in the living microvascular system. Am. J. Anatomy, 110, pp. 125-153, 1962.

9. BLOCK, E.H. Analysis of blood flow with high-speed cinephotography. Proc. 4th European Conf. Microcirculation, Cambridge, 1966.

10. BUGLIARELLO, G. and HAYDEN, J.W. Detailed characteristics of the flow of blood in-vitro. Trans. Soc. Rheol., 7, p. 209, 1963.

11. BUGLIARELLO, G., KAPUR, C., and HSIAO, G. The profile viscosity and other characteristics of blood flow in a non-uniform shear field. (Symp. on Biorheology). Proc. 4th Int. Cong. Rheology (Pt. 4), New York: Interscience, 1965.

12. BUGLIARELLO, G. and SEVILLA, J. Velocity distribution and other characteristics of steady and pulsatile blood flow in fine glass tubes. Biorheology, 7, pp. 85-107, 1970.

13. HUNG, T.C., HUNG, T.K., and BUGLIARELLO, G. The flow of blood in small curved tubes. Proc. 24th ACEMB, 13, p. 169, 1971.

14. SCHMID-SCHOENBEIN, H. and ZWEIFACH, B. RBC velocity profiles in arterioles and venules of the rabbit omentum. Microvasc. Res., 10, pp. 153-164, 1975.

15. BECKER, M.H., REDISCH, W., and MESSINA, E.J. Bone and microcirculatory changes in a child with benign pheochromocytoma. Radiol., 88, pp. 487-490, 1967.

16. DOFT, B.H., MESSINA, E.J., and REDISCH, W. Quantitation of some observations of surface microvessels of man. Microvasc. Res., 1, pp. 266-267, 1969.

17. REDISCH, W., MESSINA, E.J., HUGHES, G., and MCEWEN, C. Capillaroscopic observations in rheumatic disease, Ann. Rheum. Dis., 29, p. 244, 1970.

18. ROUEN, R.L., TERRY, E.N., DOFT, B.H., CLAUSS, R.H., and REDISCH, W. Classification and measurement of surface microvessels in man. Microvasc. Res., 4, pp. 285-292, 1972.

19. HUNG, T.C. Characteristics of blood flows in curved hollow glass fibers. Ph.D. Thesis Carnegie-Mellon University, 1972.

20. GOLDSTEIN, S. Modern Developments in Fluid Dynamics. Dover Publications, 1, p. 315, 1965.

21. DEAN, W.R. Note on the motion of fluid in a curved pipe. Phil. Mag. S. 7, 4(20), p. 208, 1927.

22. DEAN, W.R. The streamline motion of fluid in a curved pipe. Phil. Mag. S. 7, 5(30), p. 673, 1928.

23. BUGLIARELLO, G. and SEVILLA, J.F. The peripheral plasma layer in pulsating flow in hollow glass tubes. Adv. Microcirc., 2, pp. 80-88, 1969.

24. SEVILLA, J.F. Detailed characteristics of pulsatile blood flow in small glass capillaries. Ph.D. Thesis, Carnegie-Mellon University, Pittsburgh, PA, 1968.

25. THOMAS, H.W. The wall effect in capillary instruments: An improved analysis suitable for application to blood and other particulate suspensions. Biorheology, 1, pp. 41-56, 1962.

Vol. 1
1980

BIORHEOLOGY, Vol. 17, pp. 343-354, 1980
Printed in the USA. All rights reserved.

0006-355X/80/040343-12$02.00/0
Copyright (c) 1980 Pergamon Press Ltd

MAXWELL FLUID BEHAVIOR OF BLOOD AT LOW SHEAR RATE

Donald E. McMillan and Nyle Utterback
Sansum Medical Research Foundation, Santa Barbara, California

(Received 6.3.1980; in revised form 5.6.1980.
Accepted by Editor Y.C. Fung)

ABSTRACT Blood's non-Newtonian behavior is usually attributed to the predilection of red blood cells to aggregate and their ability to deform when exposed to shear stress. Aggregation has been considered more important at very low shear rate, and it has been suggested that blood acquires solid properties on standing and is converted from a solid to a liquid by application of a minimum of yield shear stress. This response pattern is usually referred to as plastic behavior. Blood has also been found to perform as a viscoelastic fluid during oscillatory flow. Viscoelasticity may produce non-Newtonian viscosity without plastic (yield stress) behavior. We performed studies in a Couette viscometer to test the relative importance of viscoelastic and plastic behavior at low shear rate. The torque delivered to the outer cylinder was measured following the onset and cessation of motion of the inner cylinder at its lowest available rotation rate, .02 revolutions per minute. The pattern of delivery of torque to the outer cylinder with Newtonian fluids of various viscosities has been characterized and pattern of motion of the outer cylinder in response to the delivered torque recorded. Blood and red blood cell suspensions at 60%and 90% concentrations were studied.An approximately exponential onset of torque transfer was found. As rotation ceased, diminished exponential decay led to an incomplete return to baseline consistent either with a small yield stress or a second slower relaxation. The exponential rise and fall of shear stress indicate that Maxwell fluid behavior predominates at low shear rate. Observation of an exponential onset and dissipation of torque for red cells suspended in phosphate-buffered saline indicates that this property is not due to aggregation and disaggregation of erythrocytes. Maxwell fluid behavior allows blood to develop flow velocity rapidly as shear stress begins. Determination of the physiologic consequences of this property will require additional studies of blood's behavior at higher shear rate.

INTRODUCTION

Blood has long been recognized to be a non-Newtonian fluid. Its increase in viscosity at low shear rate is mediated by two processes, a predilection of erythrocytes to aggregate when blood stands and the ability of each individual erythrocyte to deform when exposed to a shearing force (1). Erythrocyte aggregation is considered important in raising blood's viscosity at very low shear rates. Aggregation is thought to generate a structure in standing blood which must be disrupted for blood to begin flow (2, 3). This response, often referred to as Bingham plastic behavior, has been supported by the observation of linear regression of the square root of shear stress with the square root of shear rate (below 1 sec^{-1}) to a yield stress value of approximately .02 $dynes/cm^2$ (2), a relation similar to that described by Casson for printer's ink (4). Whole blood, but not erythrocytes suspended in serum, has been reported to follow the Casson relationship at very low shear rate (3). The model generated by this concept is that as a critical shearing stress is applied to blood it is disorganized from its normally aggregated state and flow develops.

Another model of blood flow, also non-Newtonian, has evolved from observations of blood's viscoelastic performance during oscillatory flow. Several investigators have reported that a phase shift between shear stress and shear rate develops during oscillatory flow (5,6,7). The phase shift, strain rate preceding stress, varies in a non-linear fashion with both amplitude and frequency of oscillation. Other viscoelastic fluids, whose non-Newtonian behavior does not depend on aggregation of suspended elements, undergo viscosity changes at different shear rates which are more regular and of lesser magnitude (8). The possibility that low shear rate flow behavior, linked by the Casson relationship to aggregation, might actually be due to erythrocyte deformability has attracted our attention. We performed studies in a Couette viscometer whose outer torque-sensing cylinder returns quickly to its original position because of its electronic feedback design. We have investigated the behavior of blood in response to the initiation and cessation of an approximately step function pattern of shearing motion. We have found that blood performs like a Maxwell fluid under these conditions, an observation having potential implications for blood's flow in the body.

Key Words: Blood viscosity, rheology, erythrocyte aggregation, erythrocytes, viscosity

MODELS OF FLOW BEHAVIOR

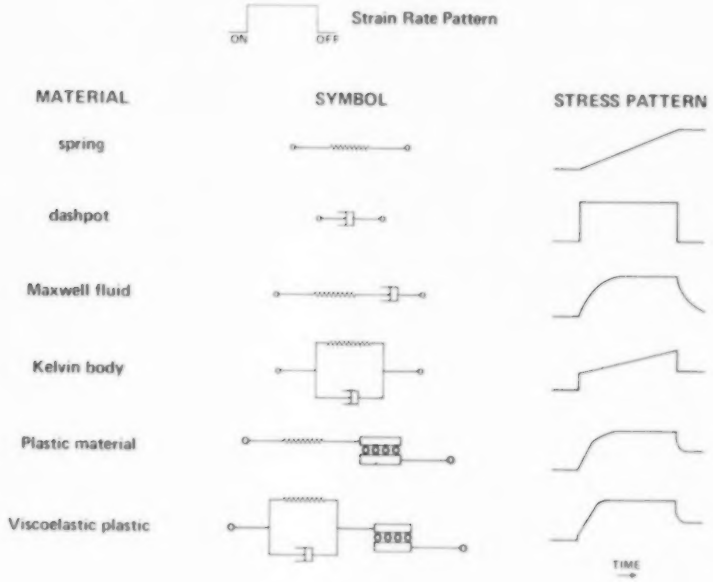

FIG. 1. The response of simple and more complex materials to step function strain rate is shown. The name of the material and its usual symbolic representation are shown using a roller to symbolize a structure which requires a minimum force (yield stress) to undergo motion and then undergoes constant slippage as additional force is placed on it. The applied stress required to induce constant strain rate and the residual stress after the displacement has been completed are shown at the right. In plastic materials a small amount of nearly exponential relaxation will occur if the roller acts as a viscous body after its motion begins, becoming, in essence, a Maxwell fluid in series with a plastic element.

Conceptualization of the development and dissipation of stress in viscoeleastic and viscoplastic materials can be accomplished using the simple models shown in Figure 1. Linear materials, symbolized by the usual conventions, are exposed to constant strain rate. After fluids (dashpot) are exposed to strain they fail to retain any stress, in contrast with simple solids (spring) exposed to the same pattern which retain the stress placed on them. When the spring and dashpot are linked in series, a simple Maxwell fluid is modelled. The Maxwell fluid's elastic element responds to initiation of strain rate by moving and generating stress which is applied to the dashpot causing it to move. As strain rate ceases, the stress stored in the spring causes the dashpot to change dimension reciprocally. Maxwell pointed out the importance of relaxation processes to the viscous behavior of gases (9). Materials represented by a parallel spring and dashpot (Kelvin or Voigt body) retain the stress applied to the spring but lose that applied to the dashpot as motion ceases. Bodies whose initiation of motion requires a yield stress have been symbolized by a roller. The force required to cause motion of the roller is applied through a spring in the model since initial elastic response is a general property of solids. As motion ceases, force persists in the system because of yield stress. A dashpot added parallel to the spring slows the onset of motion of the roller but cannot dissipate the residual stress. At onset and cessation of motion the roller's behavior is complex because of its change in state. Two basic differences exist between fluids with solid properties (Maxwell fluids) and plastic or viscoplastic solids. Stress develops exponentially during the initiation of motion of a Maxwell fluid and dissipates itself exponentially as motion ceases. In a viscoplastic material exponential behavior is dwarfed by viscous response and complete relaxation cannot occur because of yield stress.

MATERIALS AND METHODS

Blood Processing

Blood was obtained from healthy donors immediately before each study. Whole blood studies were done on fasting blood and red cell suspension studies were carried out using non-fasting blood. For whole blood studies hematocrit was determined on arrival at the laboratory and adjusted to 41.1% by addition or subtraction of plasma using a trapping correction of .013 (10). After the hematocrit was rechecked, 6.3 ml of blood was placed in the viscometer for study. For cell suspension studies red cells were washed initially in 0.15M saline to remove plasma proteins and subsequently in phosphate-buffered saline (PBS) (11). They were then mixed with phosphate-buffered saline containing 0.5% bovine plasma albumin. Microhematocrit was measured and suspending fluid added or removed to produce the desired hematocrit.

Viscometer Description

The viscometer used is a Couette viscometer patterned after the GDM design (12). It is diagrammed in Figure 2. Its inner cylinder is 2.226 cm. in diameter and its outer cylinder is 2.446 cm. in diameter leaving an 1100 micron gap. The length of the inner cylinder below the guard ring is 2.667 cm. The inner cylinder is caused to rotate by one of two motors which contain 6 gear ratios giving a total of 12 rotations from .02 to 100 RPM. The inner cylinder is made of brass and plated with gold. The outer cylinder is a lucite cup/ its inner surface has fine vertical scorings introduced by sandpapering. The cup is screw mounted into an air bearing which is enclosed by a protective housing. A capacitance sensor detects outer cylinder motion. Voltage applied to parallel plates generates an electrostatic force to return the outer cylinder to its original position. The electronic system amplifies the original capacitance sensor signal to one millivolt per microradian; the amplified signal is used to determine the position of the outer cylinder. It is also used to drive an opamp system which produces the voltage applied to the parallel plates (maximum 600 volts). One half the final amplification system is used to correct clockwise and the

Vol. 17
1980

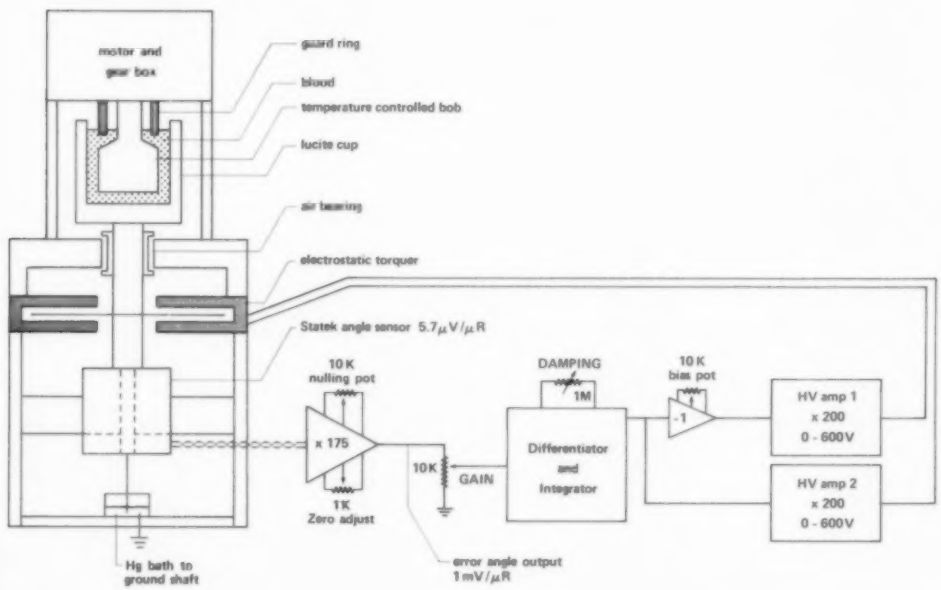

FIG. 2. The organization of our Couette viscometer is shown here. At the top is the electric motor driving the inner cylinder. Fluid at 37° C is passed through the inner cylinder to stabilize the system's temperature. With inner cylinder rotation, torque is generated through the fluid in the chamber to the outer cylinder. A guard ring prevents torque transmission by surface substances. The torque transmitted to the outer cylinder causes rotation of the air bearing system. This rotation generates a signal in the capacitance sensor which is amplified to produce a voltage on the electrostatic plates to return the outer cylinder to its original position. Amplification occurs in such a way that response increases with time so that the outer cylinder always returns to its original position.

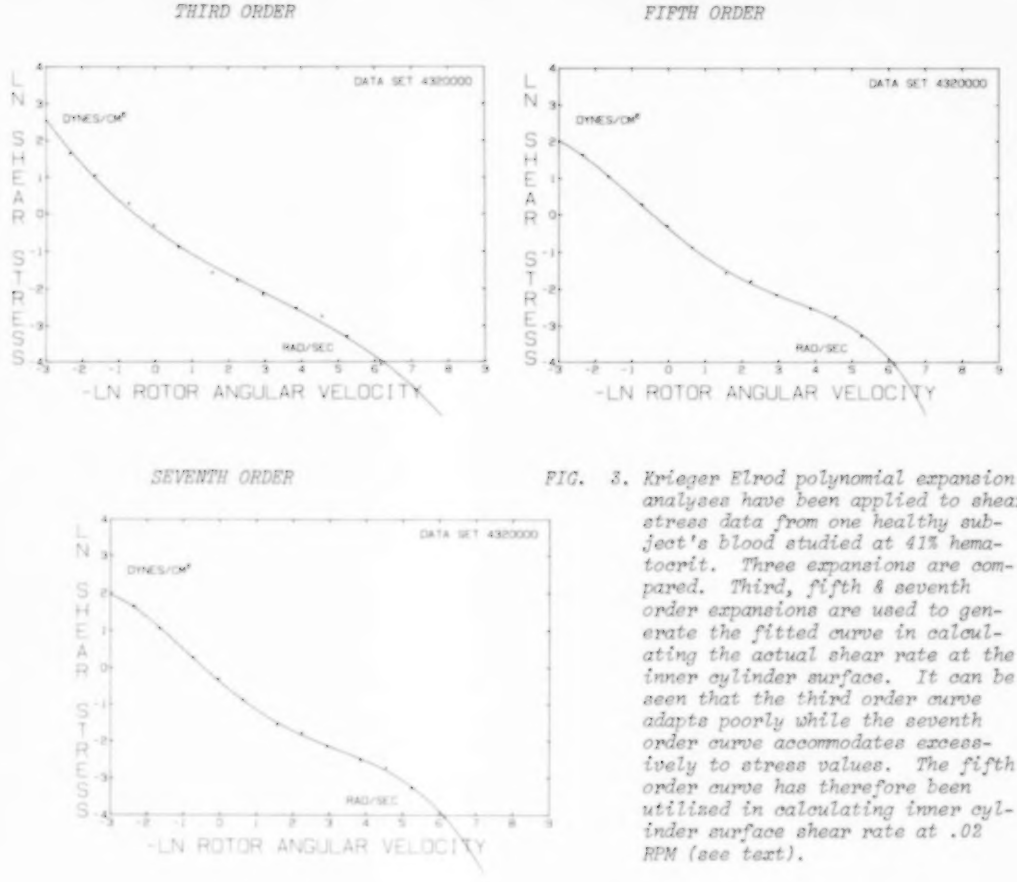

FIG. 3. Krieger Elrod polynomial expansion analyses have been applied to shear stress data from one healthy subject's blood studied at 41% hematocrit. Three expansions are compared. Third, fifth & seventh order expansions are used to generate the fitted curve in calculating the actual shear rate at the inner cylinder surface. It can be seen that the third order curve adapts poorly while the seventh order curve accommodates excessively to stress values. The fifth order curve has therefore been utilized in calculating inner cylinder surface shear rate at .02 RPM (see text).

other half to correct counterclockwise deflections. The system's feedback is designed so that the voltage applied increases with time. Any deflection of the outer cylinder will eventually generate a sufficient voltage to return the outer cylinder to its original position as long as the voltage capacity of the amplifier is not exceeded. The voltage being applied to the electrostatic plates is measured every 200 milliseconds by a digital voltmeter. The system is usually used to measure blood viscosity at 12 shear rates. A Krieger Elrod calculation, as adapted by Cokelet, is used to determine shear rate after obtaining 12 shear stress values (13). Comparison of 7th, 5th and 3rd order polynomial expansions has demonstrated that good fit without excessive curvature in the low shear rate range is obtained by 5th order expansion (Figure 3). Calculations were made comparing shear rate at .02 RPM of Newtonian fluids, blood and red cell suspensions. A 4 poise viscosity standard silicone oil (Brookfield Engineering Laboratories, Stoughton, MA) gave a shear rate of .0244 sec^{-1}. Whole blood (41% hematocrit) from eight healthy subjects had a shear rate of .0251± .0006 $sec.^{-1}$ (mean standard deviation). Red blood cells from six healthy subjects at 60% hematocrit in PBS gave a shear rate of .0256± .0005 sec^{-1}, while a single study at 90% hematocrit gave a shear rate of .029. sec^{-1}.

In the studies of response to development and cessation of shearing strain, mixing of the blood by vertical motion of the inner cylinder is done before each measurement. Baseline data are collected for 40 data points over 8 seconds. A signal then activates a solid state relay to turn on the motor driving the inner cylinder. Data acquisition continues for 100 more data points (20 seconds); then another signal causes the solid state relay to turn the motor off. A final 100 voltage values are then recorded. The voltmeter can read either the voltage being applied to the electrostatic plates or the voltage indicating the deflection of the outer cylinder. In order to acquire a representative sample, six replicate measurements are averaged for each analysis. The 240 mean values obtained are stored on 8 inch flexible discs. The entire data processing system consists of Tektronix 501 voltmeter, 502 digital clock, 31 programmable calculator, 4922 disc drive, and 4661 XY plotter.

ANALYSIS MODEL

As shown in Figure 1, a Maxwell fluid undergoes an exponential rise in stress as a constant strain rate is applied: a constant value is approached as time passes. With a cessation of strain rate, an exponential decline of stress is seen. The constitutive equation of a simple Maxwell fluid is (14)

$$\sigma + p_1 \dot{\sigma} = q_1 \dot{\varepsilon} \tag{1}$$

where σ is stress, $\dot{\varepsilon}$ strain rate, p_1 a constant in time units, and q_1 is the viscosity approached by the system at constant strain rate. The equation for a constant strain rate is therefore

$$\sigma + p_1 \dot{\sigma} = \text{constant} \tag{2}$$

and at cessation of strain rate is

$$\sigma + p_1 \dot{\sigma} = 0 \tag{3}$$

Solutions to the two differential equations, with σ_{A_o} and σ_{A_c} the change in stress being approached at onset and cessation of motion, are

for (2) $$\sigma = (1 - e^{-\frac{t}{p_1}})\, q_1 \dot{\varepsilon}_C = \sigma_{A_o}(1 - e^{-\frac{t}{p_1}}) \tag{4}$$

and for (3), while complete relaxation would give $\sigma = \sigma_C e^{-\frac{t}{p_1}}$, a residual stress, σ_R, must be introduced to match the experimental results so that

$$\sigma = \sigma_R + (\sigma_C - \sigma_R)\, e^{-\frac{t}{p_1}} \tag{5a}$$

and since $\sigma_C = \sigma_{A_c} + \sigma_R$ $$\sigma = \sigma_C - \sigma_{A_c}(1 - e^{-\frac{t}{p_1}}) \tag{5b}$$

where σ_C and $\dot{\varepsilon}_C$ are the stress and strain rate values at the cessation of strain rate. The value for p_1 can therefore be obtained by determining the difference in time x stress product between the response of a simple fluid (Figure 1) and the exponential rise and fall of the Maxwell fluid. For the onset of flow the time area, A_T, can be defined as:

$$A_T = \int_0^T \sigma \, dt = \int_0^T \sigma_{A_o}(1 - e^{-\frac{t}{p_1}})\, dt \tag{6}$$

and for a segment

$$A_{T_1}^{T_2} = \sigma_{A_o}(T_2 - T_1) - \sigma_{A_o} p_1 (e^{-\frac{T_1}{p_1}} - e^{-\frac{T_2}{p_1}}) \tag{7}$$

After cessation of flow the time area is

$$A_T = \int_0^T \sigma \, dt = \int_0^T (\sigma_C - \sigma_{A_c} + \sigma_{A_c} e^{-\frac{t}{p_1}})\, dt \tag{8}$$

and for a segment

$$A_{T_1}^{T_2} = (\sigma_C - \sigma_{A_c})(T_2 - T_1) + \sigma_{A_c} p_1 (e^{-\frac{T_1}{p_1}} - e^{-\frac{T_2}{p_1}}) \tag{9}$$

Values for p_1 and the fluid's apparent elastic modulus can be obtained by using an area fit and estimating the asymptotic stress, σ_A. Since inner cylinder motion does not actually develop instantly at .02 RPM the time required for both inner cylinder and fluid to begin and cease motion requires assessment. The system response time may be measured using Newtonian fluids (see below). An exponential onset model has been used for analysis. To calculate the area appropriate to specific values of p_1 and σ_A the constitutive relation assumed is

$$\sigma + p_1 \dot{\sigma} = q_1 \left(1 - e^{-\frac{t}{p_1'}}\right) \dot{\varepsilon}_A \tag{10}$$

where $\dot{\varepsilon}_A$ is the shear rate approached with time. For the onset of rotation a solution which meets appropriate boundary conditions including $\sigma_A = q_1 \dot{\varepsilon}_A$ is

$$\sigma = \sigma_A \left(1 - \frac{p_1 e^{-\frac{t}{p_1}} - p_1' e^{-\frac{t}{p_1'}}}{p_1 - p_1'}\right) \tag{11}$$

and for cessation with $\dot{\varepsilon}_C$ and σ_C the shear rate and stress values at the time of cessation and $\sigma_C - \sigma_A$ the stress approached over time.

$$\sigma = \sigma_C - \sigma_A \left(1 - \frac{p_1 e^{-\frac{t}{p_1}} - p_1' e^{-\frac{t}{p_1'}}}{p_1 - p_1'}\right) \tag{12}$$

The similarity allows one program to be used to solve for both onset and cessation of p_1 and σ_A. An iteration program with increments of 1 msec is used to derive the characteristic time, p_1, of the fitted curve. The area of the last 20 data points, $A_{T_1}^{T_2}$ and the trial p_1 value are used to calculate the trial σ_A value. The area calculated using the entire data array, observed $A_0^{T_2}$ is then compared with the area calculated using the trial p_1 and σ_A, trial $A_0^{T_2}$. For onset the increment in each stress measurement above baseline is accumulated to determine observed $A_0^{T_2}$, while for cessation the difference between σ_C and each measured stress is summed to determine observed $A_0^{T_2}$. Trial σ_A is calculated using assigned values for T_1, T_2, and p_1' as

$$\sigma_A = \frac{A_{T_1}^{T_2} (p_1 - p_1')}{p_1^2 \left(e^{-\frac{T_1}{p_1}} - e^{-\frac{T_2}{p_1}}\right) - p_1'^2 \left(e^{-\frac{T_1}{p_1'}} - e^{-\frac{T_2}{p_1'}}\right)} \tag{13}$$

The calculated area under the entire curve, observed A_0^T, is then compared with the trial area calculated as

$$A_0^{T_2} = \sigma_A \frac{p_1^2 \left(1 - e^{-\frac{T_2}{p_1}}\right) - p_1'^2 \left(1 - e^{-\frac{T_2}{p_1'}}\right)}{p_1 - p_1'} \tag{14}$$

This value decreases as p_1 is made larger and the last value of p_1 in milliseconds which produces an area as large as the observed value (100 data points) is accepted as p_1 and the associated σ_A value used to calculate q_1 based on an assumed value to $\dot{\varepsilon}_A$ of .025 sec^{-1}. The method is applied to onset initially and σ_C calculated from σ_A, p_1, p_1' and T_2. For cessation σ_C is used as baseline, p_1' changes, and new values of p_1 and σ_A are calculated using the same T_1 and T_2. Curves generated by this approach are compared with observed stress (torque) patterns in Figures 8, 9, 12, 14, and 15. Cessation shear rate, $\dot{\varepsilon}_C$, is calculated as $\dot{\varepsilon}_A \times \sigma_C \div \sigma_A$ using onset estimates.

Finally the apparent shear elastic modulus is estimated, ignoring vertical motion, as

$$G = \frac{q_1}{p_1} \tag{15}$$

for both onset and cessation using the derived values for q_1 and p_1. It should be noted that a number of simplifying assumptions have been made to allow the model's application to the observed data. The actual geometry of the Couette viscometer is not considered. Shear rate is lower at the outer cylinder surface than where calculated (inner cylinder) and its development pattern is not exactly the same for Newtonian and non-Newtonian fluids. The convention of dividing the measured countertorque by the product of the radius and external surface of the inner cylinder (20.76cm) to obtain shear stress has been followed as has the use of a shear rate, $\dot{\varepsilon}_A$, at this surface of .025 $seconds^{-1}$ in all calculations.

Vol. 17
1980

EXPERIMENTAL RESULTS

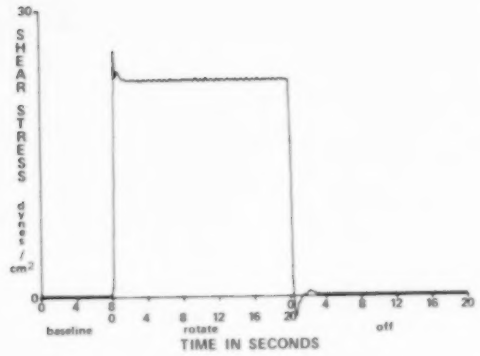

FIG. 4. The Couette system response to onset and cessation of rotation at 50 RPM (61 sec $^{-1}$ shear rate) is shown. A slight delay in torque development at onset is followed by a short period of excessive response. The opposite pattern is seen after rotation ceases.

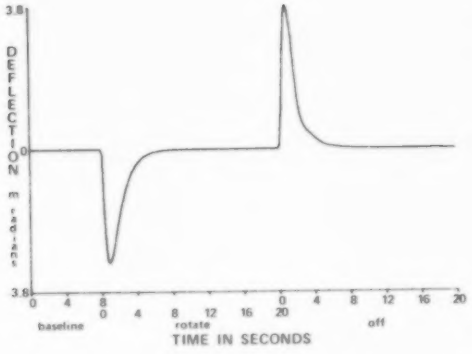

FIG. 5. The angular movement of the outer cylinder during the same study is presented. An initial deflection of less than 4 milliradians in the direction of inner cylinder rotation is restored to the original position in about 8 seconds. With cessation of rotation an opposite pattern occurs.

Shown in Figure 4 is the observed countertorque response of the viscometer system to a 20 second 50 RPM rotation; it is recorded over 48 seconds. A 0.4 poise silicone fluid is examined. There is an initial delay in torque development followed by an overshoot both at the onset and at the cessation of motion. The measured time area delay, p_1, is approximately 150 milliseconds for onset and 200 milliseconds for cessation of flow. It is attributable to the time required to cause the fluid to move. As fluid viscosity decreases, the delay is increased, as predicted by boundary layer theory (15). It can be seen that delay in onset of countertorque is followed by an excess response and that the two events are associated with motion of the outer cylinder first in the direction of flow and then in the other direction. At cessation of inner cylinder rotation a deflection response in the opposite direction is seen (Figure 5).

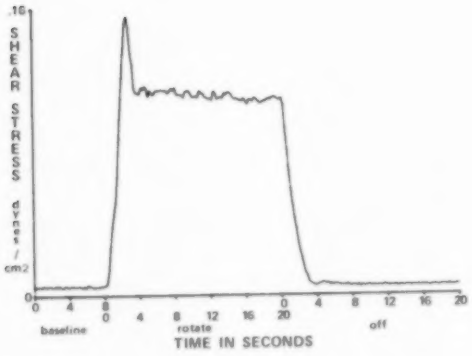

FIG. 6. The system's response at .02 RPM (.0244 sec $^{-1}$ shear rate) is shown. The shear stress values are smaller and more moment to moment variation is seen. The initial overshoot is proportionately larger and delayed. With cessation of rotation return to baseline occurs over 3 sec.

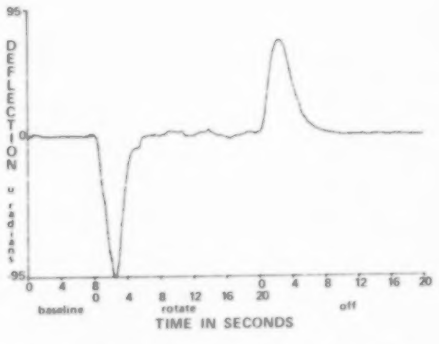

FIG. 7. The system's outer cylinder deflection under the same conditions is shown. Deflection is now less than 100 microradians. Maximum deflection time is slowed but return to baseline is comparable to Figure 5.

The response of the viscometer, now containing a more viscous silicone fluid (4 poise), at .02 RPM rotation is shown in Figure 6. The onset of countertorque is delayed and its amplitude (shear stress) is reduced. The time area delay, p_1', is increased to 1.3 seconds (mean of 36 determinations) at onset and 1.6 seconds (mean of 36 determinations) at cessation of flow. Deflection and return of the outer cylinder follow the same pattern but are slightly delayed (Figure 7). Outer cylinder deflection never exceeds 100 microradians, a value equivalent to less than 1.3 microns of linear motion of the outer surface.

An investigation was made to determine the basis for the substantial delay at .02 RPM rotation compared to 50 RPM. A strain gauge-lever system was used to measure the onset of motion of the inner cylinder at .02 RPM. It was found that an approximately exponential onset of motion develops with a reaction time of 600 milliseconds. A cessation decline is also exponential with a one second reaction time . The patterns appear to be caused by spring-like behavior of the metal gears in the motor system. At the onset of motor rotation the force applied by the gear mechanism must be increased steadily to overcome the drag of the inner cylinder drive mechanism. With cessation of the force applied by the electrical motor the strain energy stored in the gears slowly dissipates.

When 41% hematocrit blood is placed in the viscometer under the same study conditions as in Figure 6, it can be seen that the rise in countertorque (shear stress) remains incomplete over the 20-second rotation period (Figure 8). Both the rise and decline of stress are exponential in shape, and it is apparent that relaxation is incomplete in 20 seconds. Because the viscosity and shear stress were much lower than for the 4 poise silicone oil, a 0.8 poise sucrose solution was studied for comparison.

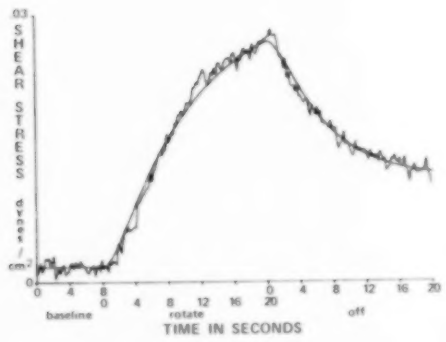

Fig. 8. The response of the system containing normal human blood at 41% hematocrit is shown. A marked delay in onset and loss of stress (torque) is seen. In addition, return to baseline is incomplete; extension of the fitted curve projects well above the baseline. The fitted curve is based on an exponential difference model (see analysis model).

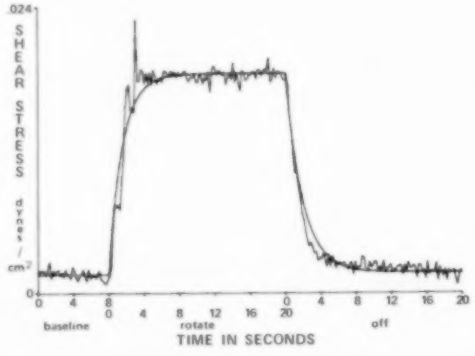

Fig. 9. The system's response to .02 RPM rotation with a 0.8 poise sucrose solution is studied and shown for comparison to Figure 8. The magnitude of shear stress is the same. It can be seen that difference in viscosity is not the basis for the slow response of blood.

An effort at curve-fitting was made initially using a simple exponential function. Before a time area fit was used the half-rise time was identified by calculation of σ_A based on each data point (Figure 10). Asymmetry was observed so that an area fit with p_1' = 0 was substituted (Figure 11). Area fit improved the asymmetry but the delay in onset and cessation of torque development compared to the fitted curve were apparent in all studies. Addition of the onset and cessation delay times found in the 4 poise oil studies generated the curves shown in Figure 8 (see analysis model).

Because the shear stress (countertorque) is so small at 41% hematocrit the associated deflection of the outer cylinder is difficult to measure. For that reason, and because blood is an aggregating fluid, studies were performed on red cell suspensions at 60% and 90% concentrations in phosphate-buffered saline (PBS). The 60% red cell suspension studies were carried out in PBS containing 0.75% dextran (M.S. 100,000 - 200,000 J. T. Baker) as well as no dextran, to determine the effect of mild erythrocyte aggregation.

Vol. 17
1980

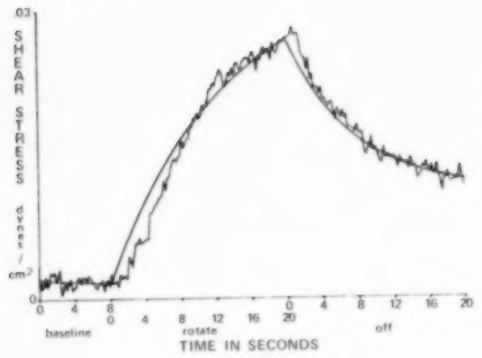

FIG. 10. *The system response study of blood shown in Figure 8 is fitted with two simple exponential curves. The half rise time was identified and a curve which passes through the mean of the last ten data points fitted. A difference in the area under the fitted and actual curves is apparent.*

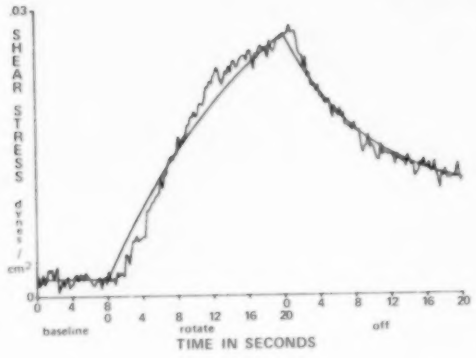

FIG. 11. *The same study shown in Figures 8 and 10 is fitted using a simple exponential model and an area fit. The delay onset of stress is now balanced by an excessive rise in the second half in both the onset and cessation curves. Addition of a response delay clearly improves curve fit as shown in Fig. 8.*

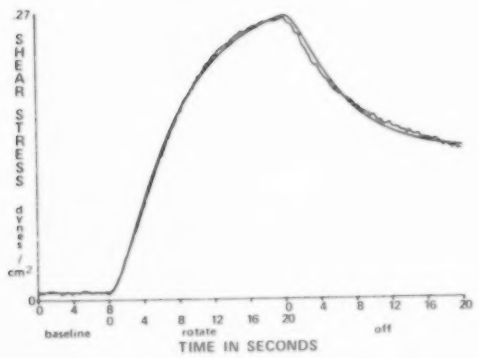

FIG. 12. *The system's response at .02 RPM to a 90% suspension of healthy human erythrocytes in phosphate-buffered saline is shown. Curve fitting is carried out as in Fig. 8. Incomplete relaxation of shear stress after cessation of rotation is more apparent.*

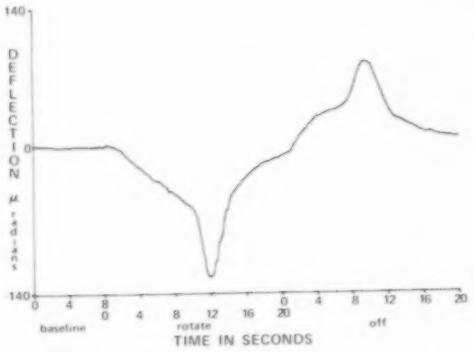

FIG. 13. *The deflection pattern during the study in Figure 12 shows a delay in development of maximal deflection until 12 seconds after onset and 9 seconds after cessation of rotation. (compare with Fig. 7)*

A 90% suspension of red cells is placed in the viscometer directly from the centrifuge. Shear stress is substantially larger than for blood, but the general shape of the response curve is the same (Figure 12). The time constant for rise and decline are similar but relaxation is less complete in 20 seconds than for blood. The outer cylinder deflection response can now be measured because of its larger amplitude (Figure 13); it is found to be delayed and has a magnitude similar to the 4 poise oil (Figure 7).

60% red cell suspensions show the same exponential response pattern (Figures 14 and 15). When dextran is added there is a substantial rise in low shear rate viscosity. Delay in the development of shear stress was longer with dextran present. The time constants, p_1, calculated using a time-area fit with a 1.3 second delay for p_1' were 3.8 and 5.1 seconds at onset and with a 1.6 second delay for cessation were 3.9 and 4.9 seconds for the zero and .75% dextran suspensions respectively.

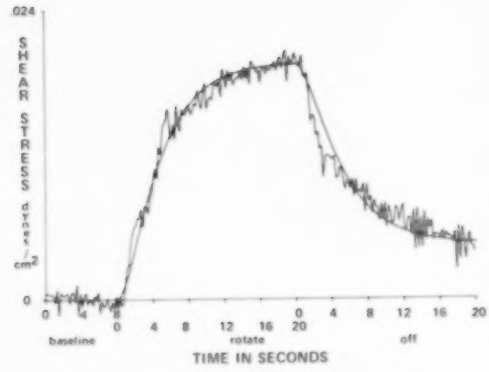

FIG. 14. *The system's response at .02 RPM to a 60% concentration of healthy human erythrocytes in phosphate-buffered saline without dextran is shown. Maxwell fluid behavior in the absence of erythrocyte aggregation and failure to dissipate stress completely after cessation of rotation are still seen.*

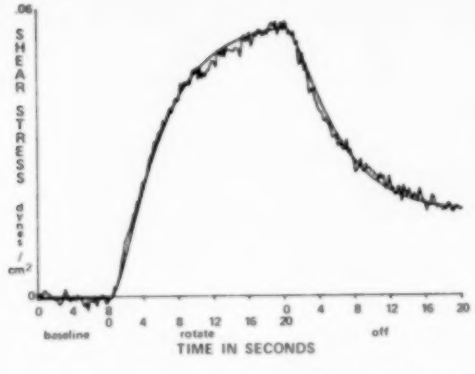

FIG. 15. *The system's response at .02 RPM to a 60% concentration of healthy human erythrocytes in phosphate-buffered saline with .75% dextran added is shown. Aggregation propensity substantially increases viscosity and mildly increases response time.*

Curve fitting was also carried out using the above p_1' values on 41% hematocrit blood from eight healthy subjects. The reaction time, p_1, following onset of rotation was 5.78± 3.35 seconds (mean ± S.D.) and the mean reaction time for cessation was 4.25 ±1.16 seconds. The calculated viscosity, q_1, for the onset was 96.4 ± 14.6 centipoise and for relaxation was 74.2 ± 6.5 centipoise. The apparent elastic modulus was 0.20 ± .08 dynes/cm² for onset and 0.19 ± .05 dynes/cm² for relaxation.

Elastic moduli were also calculated for 90% red cells (Figure 12); they were found to be 1.5 dynes/cm² for onset and 1.0 dynes/cm² for cessation. For the 60% red cell suspension without dextran onset was 0.21 dynes/cm² and cessation was 0.16 dynes/cm² while with 0.75% dextran onset was 0.4 dynes/cm² and cessation was 0.3 dynes/cm².

It was noted in all blood and red cell studies that relaxation was incomplete at 20 seconds following cessation of inner cylinder rotation. For 41% hematocrit blood the mean apparent residual shear stress value was .0051 ± .0018 dynes/cm² compared to a maximum shear stress, σ_{A_o}, of .0241 ± .0037 dynes/cm².

DISCUSSION

When our observations are compared with the Maxwell fluid and plastic models shown in Figure 1, it is apparent that blood's response to step function shear is closer to a Maxwell fluid than to a plastic material. Yield stress values for blood have been reported to be approximately 2×10^{-2} dynes/cm² in the past (2,3), but exponential dissipation of stress at cessation of flow produces a value only a third this amount in 20 seconds. The lower value is more consistent with the yield stress calculated by Copley et al (16). Exponential onset of stress is inconsistent with any viscoplastic model and indicates that blood performs at low shear rate predominantly as a viscoelastic fluid and not as a Bingham plastic.

It is not clear whether the stress still present 20 seconds after cessation of rotation is truly a yield stress or is due to a more prolonged relaxation process. Thurston has calculated the relaxation time of particles the size of human erythrocytes suspended in plasma. He found it to be 43 seconds (6). Red blood cells in more viscous suspensions would have even longer relaxation times. It is therefore possible that the residual shear stress at 20 seconds is linked to a gradual random reorientation of erythrocytes. Further studies will be required to demonstrate whether a true residual yield stress is present or whether a slower relaxation is responsible.

Vol. 1
1980

Our observation of viscoelastic performance at onset and cessation of constant shear rate is constistent both with the reports of others (5, 7) using oscillatory motion studies and with observations of the response pattern in Couette viscometer studies reported by two groups (17, 18). In both prior Couette reports cessation of motion was followed by a more complete early dissipation of stress, but nothing was said about previous mixing or about possible slippage due to wall effects. In the first report shear rates were not as low as in this study (17). In the second report shear stresses as low as those we observed were obtained using a different electronic feedback design; the visoelastic nature of the response was recognized (18). We tested for possible wall effects (red cell concentration lowering near the viscometer wall) by examining a 90% erythrocyte suspension. At this concentration each individual erythrocyte is both deformed and pressed toward the viscometer wall reducing markedly, or eliminating entirely, local hematocrit changes. The pattern we observed was comparable to lower hematocrit studies suggesting that wall effects were not important in producing the 41% hematocrit pattern.

In a recent analysis of viscoelastic behavior of blood, Bureau et al (19) extended their group's previous Couette observations (18) in a systematic study of blood's elastic and thixotropic behavior. Incomplete relaxation was suggested both at .05 sec^{-1} shear rate in viscoelastic response and in hysteresis analyses which used a ramp onset and decline of shear rate. Deutsch and Phillips have found a four constant viscoelastic constitutive equation inadequate in describing low shear rate Couette "steady state" blood viscosity (20). Thurston (21) has recently developed a model of viscoelastic behavior of blood using six Maxwell elements. Thixotropic behavior is treated as a power law degradation function. Each viscous element is changed in value with changing shear rate based on the concept that red cell aggregation changes with shear rate. His experiments (6) are used to establish values for the Maxwell elements. Our study suggests that a single Maxwell element between his elements 1 and 2 dominates behavior at very low shear rate.

The reaction times (p_0 values) that we observed at low shear rate were long compared to elastic deformation of the membranes of individual erythrocytes. Hochmuth et al have measured the relaxation time of individual erythrocytes following elongation; they found a Kelvin body response with time constant of about 0.1 second (19). Stretching of individual erythrocytes also requires forces substantially larger than those being transmitted through the blood at .025 sec^{-1} shear rate.

Nor can elastic energy storage during Maxwell fluid behavior be attributed to erythrocyte aggregation. Our studies of red cells at 60% and 90% concentrations in non-aggregating phosphate-buffered saline (Figure 12 and 14) indicate that this kind of cell interaction is not required. It seems reasonable to attribute the elastic energy storage of Maxwell fluid-behaving blood to a deformation of erythrocytes more subtle than that occurring in Hochmuth's experiments (22). Sutera et al have studied the appearance of individual erythrocytes during a progressive increase in shear force (23). Their observations,which begin at higher shear stress than we studied, suggest that the red cells in our system should be undergoing only mild bending. Direct observation of erythrocytes during low shear rate flow would be helpful in determining the basis for the relaxation process.

Viscoelastic behavior of blood at low shear rate, which dominates any true plastic behavior, is useful in facilitating its onset of flow. A plastic material requires application of a finite force before any flow occurs so that required work at onset of flow is greater than for a Newtonian fluid. A viscoelastic (Maxwell) fluid begins motion with less applied stress than a Newtonian fluid of similar viscosity (Figure 1). The work done in the initial flow period is smaller. Acceleration of blood flow should therefore be facilitated by Maxwell fluid behavior. With slowing or cessation of flow, relaxation would occur. It is interesting to point out the parallelisms between blood and thicker viscoelastic fluid such as bread dough and silicone putty. All three can store energy from an initially applied force dissipating it as conditions of motion change.

ACKNOWLEDGEMENTS

This work was supported by the Kroc Foundation, the Doris Fay Palmer Trust, and the American Heart Association - Southern California Affiliate. Technical assistance was accomplished by Mr. Christopher Wulff.

REFERENCES

1. CHIEN, S., USAMI, S., DELLENBACK and MAGAZINOVIC. V. Blood rheology after hemorrhage and endotoxin. Adv. Exper. Med. Biol. 33, 75-93, 1973.

2. MERRILL, E. W., BENIS, A. M., GILLILAND, E. R., SHERWOOD, T. K., SALZMAN, E. W., Pressure flow relations of human blood in hollow fibers at low flow rates. J. App. Physiol. 20, 954-967, 1965.

3. COKELET, G. R. The rheology of human blood. In: Biomechanics: Its Foundations and Objectives. Y. C. Fung, N. Perrone & M. Anliker (Eds.) Englewood Cliffs, Prentice-Hall Inc., pp. 63-103.

4. CASSON, N. A flow equation for pigment-oil suspensions of the printing ink type. In: Rheology of Disperse Systems. C. C. Mill (Ed.), London, Pergamon Press, 1959, pp. 84-104.

5. LESSNER, A., ZAHAVI, J., SILBERBERG, A., FREI, E. H., DREYFUS, F. The viscoelastic properties of whole blood. In: Theoretical and Clinical Hemorheology. H. H. Hartert and A. L. Copley (Eds.), Heidelberg, Springer-Verlag, 1971, pp. 194-205.

6. THURSTON, G. B. Viscoelasticity of human blood. Biophys. J. 12, 1205-1217, 1972.

7. CHIEN, S., KING, R. G., SKALAK, R., USAMI, S., COPLEY, A. L. Viscoelastic properties of human blood and red cell suspensions. Biorheology, 12, 341-346, 1975.

8. THURSTON, G. B., MARTIN, A. Rheology of pharmaceutical systems; oscillatory and steady shear of non-Newtonian viscoelastic liquids. J. Pharmaceutical Sci. 67, 1499-1506, 1978.

9. MAXWELL, J. C. On the dynamical theory of gasses. Royal Society of London Philosophical Transactions, Series A. 157A, 49-88, 1867.

10. GARBY, L., VUILLE, J. C. The amount of trapped plasma in high speed microcapillary hematocrit centrifuge. Scand. J. Clin. Lab. Invest. 13, 642-645, 1961.

11. COKELET, G. R., MEISELMAN, H. J. Rheological comparison of hemoglobin solutions and erythrocyte suspensions. Science 162, 275-277, 1968.

12. GILINSON, P. J., DAUWALTER, C. R., MERRILL, E. W. A rotational viscometer using an A.C. torque to balance loop and air bearing. Trans. Soc. Rheology 7, 319-331, 1963.

13. COKELET, G. R. The rheology of human blood. Sc. D. Thesis, Mass. Inst. Tech., 1963.

14. FLUGGE, W. Viscoelasticity. Second edition, Springer-Verlag, New York, 1975, p. 22.

15. SCHLICHTING, H. Boundary Layer Theory. Seventh edition, McGraw-Hill, New York, 1979, pp. 90-93.

16. COPLEY, A. L., HUANG, C. R., KING, R. G. Rheogoniometric studies of whole human blood at shear rates from 1000 to 0.00009 Sec Part 1--Experimental Findings. Biorheology 10, 17-22, 1973.

17. HUANG, C. R., SISKOVIC, R. W., ROBERTSON, W., FABISIAK, W., SMITHERBERG, E. H., COPLEY, A. L. Quantitative characterization of thixotropy of whole human blood. Biorheology 12 , 279-282, 1975.

18. HEALY, J. C., JOLY, M. Rheological behavior of blood in transient flow. Biorheology 12, 335-340, 1975.

19. BUREAU, M., HEALY, J.C., BOURGOIN, D. JOLY M. Etude experimentale IN VITRO du comportment rhéologique du sang en régime transitoire à faible vitesse de cisaillement. Rheol. Acta 17, 612-625, 1978.

20. DEUTSCH, S., PHILLIPS, W. M. The use of the Taylor-Couette stability problem to validate a constitutite equation for blood. Biorheology 14, 253-266, 1977.

21. THURSTON, G.B. Rheological parameters for the viscosity, viscoelasticity, and thixotropy of blood. Biorheology 16, 149-162, 1979.

22. HOCHMUTH, R. M., WORTHY, P.R., EVANS, E. A. Red cell extensional recovery and the determination of membrane viscosity. Biophys. J. 27, 101-114, 1979.

23. SUTERA, S., MEHRJARDI, M., MOHANDAS, N. Deformation of erythrocytes under shear. Blood Cells 1, 369-374, 1975.

Vol. 17
1980

BIORHEOLOGY, Vol. 17, pp. 355-362, 1980
Printed in the USA. All rights reserved.

0006-355X/80/040355-08$02.00/0
Copyright (c) 1980 Pergamon Press Ltd

LOW SHEAR RATE BLOOD VISCOSITY IN DIABETES

Donald E. McMillan, Nyle G. Utterback, and Jerzy Stocki
Sansum Medical Research Foundation, Santa Barbara, California

(Received 6.3.1980; in revised form 5.6.1980.
Accepted by Editor Y.C. Fung)

ABSTRACT: Analysis of blood viscosity in diabetes has been extended to shear rates as low as .025 sec^{-1} using a Couette rotational viscometer with guard ring. The measurement system utilizes an air bearing to eliminate friction, a differentiator-integrator amplification system to minimize response time, and a digital voltmeter and programmable calculator to collect data. It applies a Krieger Elrod shear rate correction and calculates yield shear stress using the Casson equation (shear rates 0.07 to 1.3 sec^{-1}) and power law coefficient (shear rates 2.5 to 125 sec^{-1}). In order to eliminate hematocrit-based variation in viscosity, red cell concentration was adjusted to a final hematocrit of 41% by addition or removal of plasma. Twenty diabetic subjects were compared to twenty nondiabetics. All subjects were selected to avoid any recent illness which might affect plasma protein composition. In the higher shear rate range diabetic blood did not differ significantly in viscosity from nondiabetic blood. It was more viscous than nondiabetic blood at shear rates of 0.3, 0.7 and 1.3 sec^{-1}. At the lowest shear rates studied, .03 and .07 sec^{-1}, diabetic blood viscosity was actually lower than nondiabetic. No effect of age on blood viscosity was observed in either diabetics or nondiabetics. There was a significant inverse correlation between duration of diabetes and degree of elevation of blood viscosity at 0.7 sec^{-1} shear rate. Diabetic blood viscosity was positively correlated with fasting blood sugar at 0.7 and 70 sec^{-1}. Yield shear stress did not differ between diabetic and nondiabetic subjects and was not correlated with sedimentation rate. Substantial elevation of diabetic blood viscosity over such a narrow range would be expected to have its major direct effect on blood flow in large vessels.

INTRODUCTION

Blood's viscosity has usually been studied using either rotational cone-plate or Couette viscometers (1,2). Either type, lacking a guard ring, can give high readings at low shear rate because additional torque is transmitted by surface proteins (3). When the measured viscous force is small, it is also extremely important that the sensing element move freely in order to allow accurate measurement (1). For these reasons some doubt exists about the reliability of most past studies of low shear rate blood viscosity in diabetes. Past reports of blood viscosity observations in diabetes do not present a clear picture. The Aalborg group used a Wells-Brookfield cone-plate viscometer, which has no guard ring, to study diabetic blood viscosity. They initially found a 20% elevation in diabetes (4) then no increase (5), and finally a 4-8% increase, greater at low shear rates (range 23-230 sec^{-1}) and higher in diabetics with proliferative retinopathy (6). Rees et al used a Couette viscometer with guard ring. Reporting their observations only in abstract form, they described an increased yield stress of diabetic blood, limited to cases of infection and proliferative retinopathy (7). Bollinger et al found a slight decrease in blood viscosity in diabetes, measuring only at 11.5 sec^{-1} shear rate (8). Langer et al found diabetic blood viscosity to become elevated during exercise (9). Labib et al, using a capillary viscometer, found a 6% elevation (10). Zingg et al studied viscosity at 0.1 and 2 sec^{-1} shear rates and found an elevation in diabetes (12). Volger et al, measuring between 8 and 160 sec^{-1} shear rates, found no blood viscosity elevation in diabetes (13). Hoare et al examined diabetic blood viscosity over a wide shear rate range (0.77 - 230 sec^{-1}) and found an elevation at high shear rate only after applying a correction for hematocrit; at the lowest shear rate a difference, greater in diabetics with retinopathy, was found even before correction (14). Isogai et al also reported an elevated diabetic blood viscosity associated with retinopathy (15). Dintenfass and Davis have reported values for diabetic blood viscosity without comparison to nondiabetics (16). Lowe et al found a relation between increased diabetic blood viscosity and retinopathy (17), while Stoltz et al have shown that a substantial elevation in diabetic blood viscosity at constant hematocrit in the range 0.1 - 0.8 sec^{-1} was improved by close control of blood glucose level (18). Taken together, these studies show a greater tendency to blood viscosity elevation in diabetes at low compared to high shear rate. A frequent conclusion has been an association of increased viscosity with

Key Words: Blood viscosity, rheology, viscosity, diabetes mellitus

diabetic retinopathy. A major difficulty in interpretation has been wrought by differences in mean hematocrit levels between groups studied. Only two groups adjusted blood's hematocrit before study to avoid this problem (7,18).

We have studied diabetic blood viscosity at constant hematocrit over an extensive shear rate range. Rotational viscometry using a Couette system was selected for three advantages. The system is not very sensitive to blood sedimentation, known to be increased in diabetes; it has a guard ring to avoid surface effects; and it has an air bearing to maximize precision of the sensing system. An unusual pattern of viscosity elevation was found in diabetes with no increase in blood's yield shear stress.

MATERIALS AND METHODS

Subjects Studied. Fasting blood was obtained from 20 established diabetic and 20 nondiabetic subjects. Both groups were selected to exclude recent illness and require normal recent physical activity. No individuals with advanced retinopathy or nephropathy were studied. Diabetic subjects ranged in age from 15 to 84 years. Nondiabetic subjects had normal fasting glucose levels and ranged in age from 20 to 80 years. Six diabetic and eight nondiabetic subjects were male.

Blood Processing. Blood was collected in EDTA (K_3 1.5 mg/ml) vacuum containers. The microhematocrit was determined in quadruplicate immediately on arrival at the laboratory. The subject's own plasma was added to or subtracted from an eight ml volume of blood to bring the hematocrit to 41.6%. The value, which was rechecked directly, corresponds to 40% if a trapped plasma fraction of .04 is chosen and 41.1% if .013 is assumed. Viscosity determinations were regularly completed within six hours of specimen collection. Sedimentation of blood was measured by placing a fraction of the blood prepared for viscosity analysis in a Westergren tube and measuring its vertical descent at room temperature (23°C) in one hour.

Viscometer Description. The design of the viscometer is similar to that of Gilinson, Dauwalter, and Merrill (19). Its chamber requires 6.3 ml of blood to be filled to the guard ring. The cylinder-to-cylinder gap is 1100 microns. The rotating inner cylinder (bob) is gold-plated and 2.226 cm in diameter. Its length below the guard ring is 2.667 cm. The outer lucite cup is 2.446 cm in diameter. The bob is driven by one of two synchronous electric motors with 6 gear ratios each (2, 5, 10, 20, 50, and 100). They produce sylinder rotation rates between .02 and 1 and between 2 and 100 revolutions per minute (RPM). Heated ethylene glycol is circulated through the bob to keep the blood at 37°C. The lucite cup is mounted on a vertical coaxial cylinder air bearing puchased from Professional Instruments Co. (Minneapolis, MN). Air enters the bearing through perforations in the center of the outer cylinder, passes between the cylinders, and is diverted outward by circular plates at either end. The original inner cylinder has been replaced by a smaller one of polished steel to improve an initially unsatisfactory performance. Below the air bearing is a capacitance angle sensor and two 15 cm diameter aluminum discs which have 6 pie-shaped 30° sectors missing. The entire air bearing system is grounded through a wire to a small mercury bath in the base of the protective housing. Four plates are mounted in the protective housings 1mm above and below the two discs. When voltage is placed on similarly shaped sectors of the plates, electrostatic torque applied to the discs restores the air bearing to one of two initial positions. The torque is proportional to the square of the applied voltage. The capacitance angle sensor output is amplified in the first stage of the electronic system to produce a signal of one millivolt per microradian which may be used to determine its degree of rotation. The initial deflection was found to be less than five milliradians at 100 RPM and less than 100 microradians at .02 RPM. The electronic system differentiator-integrator circuit amplifies short-term signals less than persistent signals; the system therefore returns in a few seconds to its original position. The voltage being applied to the electrostatic torquer is measured every 200 milliseconds by a digital voltmeter (Tektronix 501). A digital clock (Tektronix 502) is used to time each viscosity measurement The digital data are acquired, processed and stored by a Tektronix model 31 programmable calculator.

Viscometer Operation. Two different algorithms are used, one with the high and the other with the low rotation motor. At high rotation, two measurements of shear stress are made using both clockwise and counterclockwise rotation. After the motor is started the calculator system tests every two seconds to determine when a stable voltage is reached. Then the correlation coefficient (r) of 100 voltage measurements with time is determined. If it is found to be more than ±0.26, the measurement is repeated until stable. Accepted data are stored on a flexible 8 inch disc (Tektronix 4922). Because considerable time is required for the low motor gears to mesh, only clockwise rotation is used. Blood mixing is accomplished before each observation by moving the bob up and down six to eight times. Care is taken to avoid the introduction of bubbles. Immediately after mixing is completed the calculator begins collecting voltage values at 200 millisecond intervals to determine stability by calculating the standard deviation of the 100 most recent values. When a value equivalent to a shear stress of .003 dynes/cm^2 is obtained, rotation is begun. Five second analyses are made until it is determined that the applied countertorque is no longer rising. One hundred voltage readings are then obtained and their mean and standard deviation printed out by the calculator. If the standard deviation is satisfactorily low

Vol. 1
1980

the datum is accepted and stored. At .02 RPM six torque values are collected and averaged, at .05 RPM five values, at .1 RPM four values, at .2 RPM three values, and .5 RPM and 1 RPM two values.

Data Processing. After shear stress (torque ÷ bob area ÷ bob radius) values at the 12 rotation rates are acquired, a fifth order polynomial Krieger Elrod fit (20, 21) is carried out to determine mean shear rate. Viscosity values (shear stress/shear rate) are then calculated. A Casson regression (square root of shear stress versus square root of shear rate) (22) is calculated using the .05 to 1 RPM data points and a power law regression (log shear stress vs. log shear rate) using the 2 to 100 RPM values. Printouts of a study of a 0.4 centipoise Newtonian oil and of nondiabetic blood are compared in Figures 1 and 2.

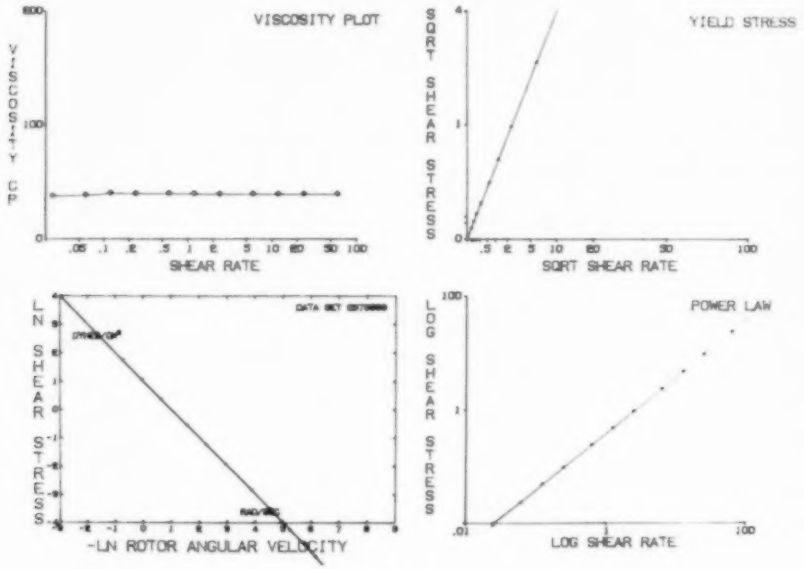

FIG. 1

Study of 0.4 poise silicone oil

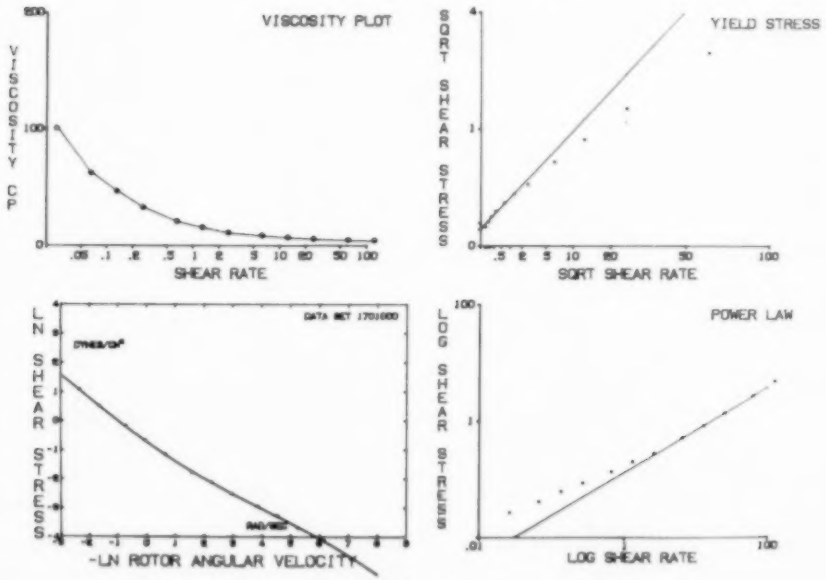

FIG. 2

Study of nondiabetic blood

Calculations. Programs prepared for the Tektronix 31 programmable calculator and stored on 8 inch flexible discs were used. Probability of similarity was calculated by iteration using a program supplied by Tektronix as each t (student) test was carried out. To simplify data presentation, P values obtained by this means are reported while t and df are omitted. To avoid prolonged iteration, only values of t greater than 1.0 were analyzed. For lower values of t the symbol P>.3 is used. In all cases variance ratio was tested and df reduced if there was evidence of inhomogeneity (23).

RESULTS

Diabetic and nondiabetic viscosity means, standard deviations, and tests of similarity are listed in Table 1. Means are also graphed in Figure 3. The slight viscosity elevation in diabetes at high shear rate does not achieve statistical significance. As shear rate falls diabetic blood viscosity rises more rapidly than nondiabetic. Significant increases are present at 1, 0.5, and 0.2 RPM. At the two lowest rotation rates, .05 and .02 RPM, diabetic blood is non-significantly less viscous than nondiabetic blood. The components used to calculate viscosity, shear stress and shear rate, are also listed in Table 1. The increase in shear stress, which is measured directly, is the basis for the elevated diabetic blood viscosity. Statistically significant elevations of shear rate, present at 0.3, 0.7 and 1.3 - 1.4 sec^{-1}, are small, ranging from 1 to 4%. The shear stress pattern is different in diabetes. When it is used in calculating shear rate, a second difference is automatically produced. No diabetic elevation of yield shear stress or power law regression coefficient was found (bottom of Table 1). Yield shear stress was actually slightly higher than the mean shear stress measured at .02 RPM.

The completion time of viscosity measurement was analyzed at 6 rotation rates to be certain that measurement time difference was not the basis for blood viscosity changes found in diabetes. Viscosity is calculated using the 100 observations obtained in the 20 seconds before measurement completion. Viscosity values were obtained in the two groups at comparable periods after flow was initiated (Table 2).

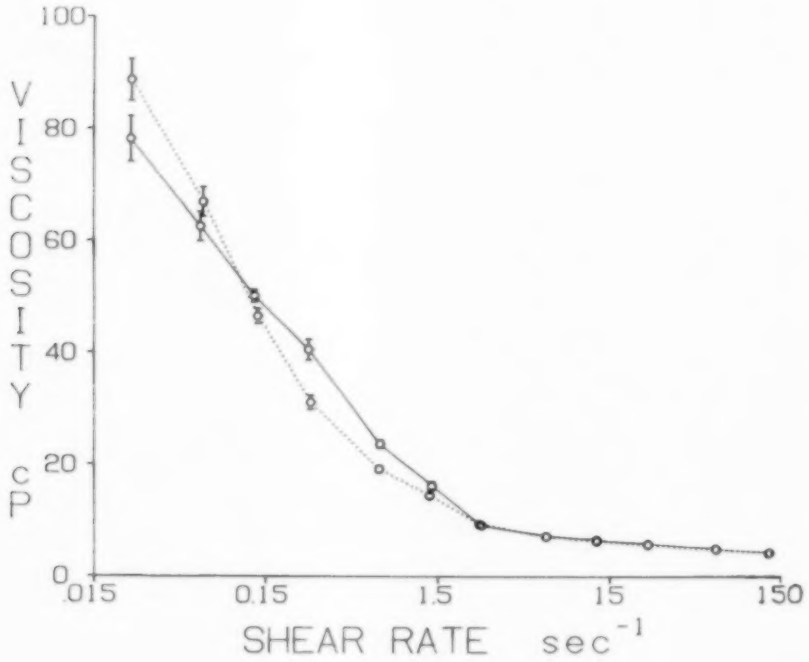

FIG. 3

The mean viscosity values of the diabetic (solid line) and nondiabetic (dotted line) groups at twelve shear rates are compared. The ordinate, viscosity, is linear in scale; the abscissa is logarithmic. At shear rates below 1.5 sec^{-1} one standard error is indicated by brackets. The elevation of blood viscosity in diabetes is limited to the shear rate range 0.2 - 2 sec^{-1}. Below 0.1 sec^{-1} diabetic blood viscosity is lower than nondiabetic viscosity.

Male and female mean shear stress, shear rate, viscosity, yield stress and power law coefficient values were compared by t tests. Both diabetic and nondiabetic groups were examined; 76 tests were made. Only one test exceeded chance at the $P<.05$ level; diabetic males had a lower blood viscosity than females at 20 RPM. The nondiabetic male mean was non-significantly higher than female mean at 20 RPM. A trend to slightly greater viscosity values at low shear rate in males, seen in both groups did not achieve statistical significance. The effect of age on nondiabetic and diabetic blood viscosity level was also tested (Table 3). No age-related trends were found. In the diabetic group high shear rate viscosity values tended to be lower in older individuals.

The relation between fasting plasma glucose and viscosity was studied at 4 rotation rates. Positive correlations were found at .7 sec^{-1}; where diabetic blood viscosity elevation was striking (Figure 1) and at 70 sec^{-1} where no increase was found. The diabetic group varied widely in duration of diabetes (2-52 years); the mean duration was 14.6 years. The relation between duration of diabetes and viscosity was examined at the same four rotation rates. A significant negative correlation was found at a shear rate where diabetic viscosity is elevated, .7 sec . The effect of type of treatment - insulin, oral agents, or diet alone - on blood viscosity in diabetes was examined by analysis of variance; no relation could be found. The sedimentation rate of blood was measured on 17 diabetics and 18 nondiabetics. Although sedimentation rate of diabetic blood was significantly elevated (22.6 ± 3.2 vs. 10.1 ± 2.3 mm/hr mean ± S.E., P = .003); sedimentation rate was not correlated with yield stress or low shear rate blood viscosity in either group.

TABLE 1

Viscosity Parameters in Diabetes

Mean ± Std. Dev., Probability of Similarity

	VISCOSITY CENTIPOISE AT 37°C			SHEAR STRESS DYNES/CM^2			SHEAR RATE SECONDS^{-1}		
RPM	Nondiabetic	Diabetic	P	Nondiabetic	Diabetic	P	Nondiabetic	Diabetic	P
100	4.10±.24	4.14±.33	>.3	5.16±.28	5.32±.36	.12	126 ± 2	129±4	.003
50	4.76±.28	4.93±.32	.068	2.95±.17	3.05±.20	.10	62.1±.3	61.9±.4	.08
20	5.63±.40	5.86±.51	.110	.140±.10	1.45±.12	.15	24.8±.2	24.7±.1	>.3
10	6.33±.47	6.55±.54	.188	.79 ±.06	.81 ±.07	.3	12.5±.1	12.5±.1	.8
5	7.17±.69	7.2 ±1.0	>.3	.45 ±.05	.46 ±.07	.3	6.33±.06	6.40±.07	.003
2	9.4 ±2.2	9.2 ±1.2	>.3	.245±.056	.246±.028	.3	2.60±.04	2.68±.06	.0001
1	14.6 ±1.8	16.4±2.8	.023	.195±.026	.225±.041	.008	1.34±.03	1.38±.04	.0008
.5	19.3 ±2.7	23.8±3.8	.0001	.131±.019	.164±.027	.0001	.68±.02	.69±.02	.18
.2	31.1 ±5.9	40.6±8.6	.0002	.086±.016	.108±.023	.0007	.274±.008	.266±.008	.002
.1	46.5 ±6.4	50.2±5.5	.060	.062±.010	.065±.008	.3	.135±.005	.129±.005	.001
.05	67 ±12	63 ±12	.260	.044±.009	.039±.008	.11	.065±.002	.063±.002	.001
.02	89 ±17	78 ±19	.073	.022±.004	.019±.005	.059	.025±.001	.025±.001	>.3
				Yield Stress .024±.005	.023±.007	P>.3	dynes/cm^2		
				Power Law Coeff. .80 ±.04	.81 ±.03	P>.3	unitless ratio		

TABLE 2

Viscosity Measurement Completion Time

RPM	20 Diabetic Subjects	20 Control Subjects	P
5	28.8 ± 1.5 secs	28.1 ± 1.2 secs	>.3
2	31.2 ± 2.0 secs	30.1 ± 1.5 secs	>.3
.5	30.1 ± 1.0 secs	29.7 ± 0.7 secs	>.3
.2	35.8 ± 1.8 secs	32.7 ± 1.5 secs	.187
.05	44.7 ± 2.0 secs	43.5 ± 2.1 secs	>.3
.02	45.7 ± 2.5 secs	45.0 ± 2.2 secs	>.3

Mean ± S.E.

TABLE 3

Correlations Between Parameters

Parameters	RPM	Diabetic r	Diabetic p	Nondiabetic r	Nondiabetic p
age vs. viscosity	50	-.27	.24	+.05	>.3
age vs. viscosity	.5	-.25	.30	-.05	>.3
age vs. viscostiy	.2	+.12	>.3	-.01	>.3
age vs. viscosity	.05	-.04	>.3	+.12	>.3
age vs. yield stress	---	+.04	>.3	+.18	>.3
age vs. power law coefficient	---	+.31	.19	+.10	>.3
sed. rate vs. viscosity	50	-.08	>.3	+.33	0.19
sed. rate vs. viscosity	.5	-.22	>.3	+.05	>.3
sed. rate vs. viscosity	.2	-.32	-.22	+.35	0.16
sed. rate vs. viscosity	.05	-.27	>.3	+.28	0.26
sed. rate vs. yield stress	---	-.35	0.17	+.35	0.16
sed. rate vs. power law coefficient	---	+.25	0.33	+.09	>.3
plasma glucose vs. viscosity	50	+0.52	.022	---	---
plasma glucose vs. viscosity	.5	+0.54	.017	---	---
plasma glucose vs. viscosity	.2	+0.36	.13	---	---
plasma glucose vs. viscosity	.05	-0.11	>.3	---	---
diabetes duration vs. viscosity	50	-0.10	>.3	---	---
diabetes duration vs. viscosity	.5	-0.48	.033	---	---
diabetes duration vs. viscosity	.2	-.21	>.3	---	---
diabetes duration vs. viscosity	.05	-.29	.21	---	---
diabetes duration vs. plasma glucose	---	-0.20	>.3	---	---

DISCUSSION

The most striking feature of the diabetic blood viscosity pattern is substantial increase in a narrow shear rate range from approximately 0.2 to 2 sec^{-1} (Figure 1). In the lower part of this range diabetic blood viscosity exceeded nondiabetic blood viscosity by 30 percent. Disproportionate increase in diabetic blood viscosity at low shear rate is consistent with past reports (6,11,14), but as shear rate falls below 0.1 sec^{-1} the pattern fails. Diabetic blood actually becomes less viscous than nondiabetic blood at the two lowest shear rates studied. Lack of further increase at very low shear rate is paralleled by absence of an increased yield stress. Yield stress was reported to be elevated in diabetes in a past study using a similar instrument (7). It is known to be made higher both by increases in hematocrit and in fibrinogen level (24). Hematocrit was held constant in this study. Blood sedimentation, strongly influenced by fibrinogen level, was found to be elevated in diabetes but uncorrelated with yield stress in either group (Table 3). One possible reason for the difference in the results of this study and the previous GDM study is a difference in calculation technique. At low shear rate blood's observed shear stress falls with time (1), a phenomenon which has been attributed to development of a cell-free zone at the bob surface (21). Our technique minimized measurement time (Table 2) and shear stress was obtained without extrapolation. In the previous study extrapolation to zero time was apparently used to calculate shear stress (21). Earlier development of the cell-free zone in diabetic blood could contribute to its lower viscosity at .025 and .06 sec^{-1}.

Hematocrit differences may be important in reports by other groups of a substantial high shear rate blood viscosity elevation in diabetes (4,6,10,15,17). The limit of error of our observations does not exclude a high shear rate viscosity elevation of 2-4%. A small elevation would be expected, since serum viscosity is increased 8 percent in diabetes (26).

The correlation between fasting plasma glucose and diabetic blood viscosity is not easily explained. No relationship of serum viscosity elevation (26) to hyperglycemia was found. A tendency for high fasting glucose to be associated with greater reduction in red cell deformability did not achieve statistical significance (27).

An inverse relation of duration of diabetes to elevation of blood viscosity was found at only a single rotation rate, 0.5 RPM. Considering the number of correlations attempted, the observation is not absolutely convincing. For that reason blood from four additional diabetics of 50 or more years duration has been studied and found to be normal in viscosity (28), supporting the validity of the negative correlation. Diabetics who survive many

Vol. 17
1980

years without serious microvascular sequelae do not have as profound a disturbance of blood viscosity as diabetics who develop microangiopathy.

What effect could the observed pattern of blood viscosity change in diabetes have on the diabetic's circulation? The increase in diabetic blood viscosity occurs over a narrow shear rate range, from 0.2 to 2 sec^{-1}. Flow resistance would be increased principally in the area of each blood vessel in which shear rate is in this range. The effect is best estimated by analysis of shear stress rather than shear rate. Diabetic blood viscosity is elevated nearly one third above normal between shear stresses from 0.1 to 0.2 dynes/cm^2 (Table 1). Shear stress rises linearly from the vessel's center to the wall. Blood flow in a vessel with a wall shear stress close to 0.2 dynes/cm^2 would require about one fourth more energy in diabetes. As wall shear stress rises substantially above 1 dyne/cm^2 the cost becomes very small, less than 5%. Wall shear stresses less than 1 dyne/cm^2 occur principally in the large veins and between heartbeats in the large arteries.

ACKNOWLEDGEMENTS

This work was supported by the Kroc Foundation, the Doris Fay Palmer Trust, the American Diabetes Association - Southern California Affiliate and the California Heart Association. We are very indebted to Drs. Giles Cokelet and Philip Gilinson for their advice during the design of our viscometer.

REFERENCES

1. MEISELMAN, H. J. and COKELET, G. R. Blood rheology. Adv. Microcir. 5, 32-61, 1973.

2. VAN WAZER, J. R., LYONS, J. W., KIM, K. Y. and COLWELL, R. W. Viscosity and Flow Measurement. In: A Laboratory Handbook of Rheology. New York: Interscience Publ. 1963, pp. 47-96.

3. McMILLAN, D. E. Surface effects of proteins in cone plate viscometry. Biorheology 11, 149-150, 1974.

4. SKOVBORG, F., NIELSEN, A. V., SCHLICHTKRULL, J., and DITZEL, J. Blood viscosity in diabetic patients. Lancet 1, 129-131, 1966.

5. DITZEL, J. Whole blood viscosity and related components in diabetes mellitus. Dan. Med. Bull. 15, 49-53, 1968.

6. SKOVBORG, F. Blood viscosity in normal and diabetic subjects. Kovenhaven: FADL'S Forlag, 1974.

7. REES, S. B., SIMON, L., PELTIER, A. GLEASON, R., BALODIMOS, M., MARBLE, A., and MERRILL, E. W. Hemorheologic studies during the progression and remission of diabetic retinopathy. Biorheology 4, 102, 1967

8. BOLLINGER, A., BERCHTOLD, P., and BERGER, W. Untersuchungen der blutviskositat bei diabetikern. Praxis 58, 1104-1107, 1969.

9. LANGER, L., BERGENTZ, S. E., BJURE, J., and FAGERBERG, S. E. The effect of exercise on haematocrit, plasma volume and viscosity in diabetes mellitus. Diabetologia 7, 29-33, 1971

10. LABIB, M. A. M., HIGAZI, A. M., EL-EBRASHY, N., EL-ASHMAWY, S., MADKOUR, M. K, and BARHOOM, G. A. Studies on diabetic retinal vascular changes with special reference to blood coagulation and viscosity. Bull. Ophthalmol. Soc. Egypt. 64, 457-482, 1971.

11. ZINGG, W., SULEV, J. C., MORGAN, S. D., and EHRLICH, R. M. Blood viscosity in diabetic children. Diabetologia 7, 461-462, 1971.

12. STORMER, B., CHMIEL, H., POTTHOFF, D., KREMER, K. and BRUSTER, H. Viskositatsumtersuchungen an gesundem and pathologischem menschlichem blut im bereich niedriger beanspruchungern. Z. Exp. Chir. 6, 237-247, 1973.

13. VOLGER, E., SCHMID-SCHONBEIN, H., and MEHNERT, H. Microheological changes in blood in diabetes mellitus. Bibl. Anat. 13, 97-98, 1975.

14. HOARE, E. M., BARNES, A. J., and DORMANDY, J. A. Abnormal blood viscosity in diabetes mellitus and retinopathy. Biorheology 13, 21-25, 1976.

15. ISOGAI, Y., IIDA, A., MICHIZUKI, K. and ABE, M. Hemorheological studies on the pathogenesis of diabetic microangiopathy. Throm. Res. 8, Suppl. II, 17-24, 1976.

16. DINTENFASS, L., and DAVIS, E. Genetic and ethnic influences on blood viscosity and capillaries in diabetes mellitus. Microvasc. Res. 14, 161-172, 1977.

17. LOWER, G. D. O., DRUMMOND, M. M., BELCH, J. J. F., LOWE, J. M., MACCUISH, A. C., and MANDERSON, W. G. Abnormal blood rheology in young male diabetics with and without retinopathy. Microvasc. Res. 17, S58, 1979.

18. STOLTZ, J. F., DROUIN, P., GAILLARD, S., ROUSSELLE, D., and POINTEL, J. W. Study of blood viscosity of insulin-dependent diabetics by means of an artificial pancreas. Microvasc. Res. 17, S57, 1979.

19. GILINSON, P. J., DAUWALTER, C. R., and MERRILL, E. W. A rotational viscometer using an A. C. Torque to balance loop and air bearing. Trans. Soc. Rheol. 8, 319-331, 1963.

20. KRIEGER, I. M., and ELROD, H. Direct determination of the flow curves of non-Newtonian fluids. II Shear rate in the concentric cylinder viscometer. J. Appl. Physics 24, 134-136, 1952.

21. COKELET, G. R. The rheology of human blood. ScD. Thesis, Department of Chemical Engineering, Massachussetts Institute of Technology, 1963.

22. CASSON, M. A flow equation for pigment-oil suspension of the printing ink type. In: Rheology of Disperse Systems. C. C. Mill, (Ed.) London, Pergamon Press, 1959, pp. 84-104.

23. DIEM, K., and LENTNER, C. Scientific Tables, Basle, Switzerland, Ciba-Geigy Ltd., 1970, p. 193.

24. McMILLAN, D. E. Plasma protein changes, blood viscosity, and diabetic microangiopathy. Diabetes 25, 895-901, 1976.

25. MERRILL, E. W. Rheology of blood. Physiol. Rev. 49, 863-888, 1969

26. McMILLAN, D. E. Disturbance of serum viscosity in diabetes mellitus. J. Clin. Invest. 53, 1071-1079, 1974.

27. McMILLAN, D. E., UTTERBACK, N. G., and LaPUMA, J. Reduced erythrocyte deformability in diabetes. Diabetes 27, 895-901, 1978.

28. McMILLAN, D. E., UTTERBACK, N. J. and WULFF, W. W. Blood viscosity in young and old diabetics. Diabetic Angiopathy in Children. Bruno Weber (Ed.) S. Karger AG, Basel, in press.

Vol. 17
1980

BIORHEOLOGY, Vol. 17, pp. 363-375, 1980
Printed in the USA. All rights reserved.

0006-355X/80/040363-13$02.00/0
Copyright (c) 1980 Pergamon Press Ltd

RELAXATION BEHAVIOR OF SPUTUM STUDIED USING THE RAISED COSINE PULSE METHOD

S. Shimura*, S. Sato*, T. Takishima*,
Y. Otsubo** and K. Umeya**

* First Department of Internal Medicine, Tohoku University School of Medicine
** Department of Applied Chemistry, Faculty of Engineering, Tohoku University, Sendai, Japan

(Received 7.4.1980; in revised form 11.6.1980.
Accepted by Editor S. Oka)

ABSTRACT

Using the newly developed Raised Cosine Pulse method, the dynamic viscoelastic properties of sputum were studied at 37°C within 2-4 hours of expulsion. It was possible to study sputum behavior in only 2-3 minutes at angular frequency $\omega = 10^{-3}$ -10^{0} rad·sec^{-1}. The measured values and frequency dependence were roughly similar to those previously reported by others, but a relaxation region was found at $\omega = 3 \times 10^{-2} \sim 3 \times 10^{-1}$ rad·sec^{-1} which was not indicated in any previous reports using the dynamic method. In purulent sputum, the relaxation region was more evident and was at a lower frequency than that in mucoid sputum. A comparison was made between the conventional dynamic method and the Raised Cosine Pulse method at $\omega = 10^{-2} - 10^{0}$ rad·sec^{-1}. Using the former method, roughly 40-60 minutes were needed for measurements of each test sample, and it was difficult to detect the behavior indicating a relaxation region. The measured values using both methods were roughly in agreement in almost all samples. Our study revealed that this new method had the advantage of determining the dynamic viscoelasticity of sputum at a wide range of frequencies within 2-3 minutes.

INTRODUCTION

Excessive sputum is a characteristic clinical manifestation of chronic obstructive lung disease, particularly chronic bronchitis, and occasionally the failure of expulsion accompanying excessive sputum leads to a serious situation of respiratory failure. Furthermore, it is known that the rheological properties of sputum have a strong influence on pulmonary function (1, 2, 3, 4, 5). That is, sputum reaches the upper trachea by ciliary movement and is expelled by coughing, and this process is thought to be heavily influenced by the rheological properties of sputum. Viscoelasticity is the most important factor determining the rheological behavior of sputum, and it is desirable to be able to consider the situation of sputum within the airways in terms of its dynamic properties. Since the introduction of the oscillation test for sputum (6), it has become possible to measure the dynamic viscoelasticity of sputum and bronchial mucus by various instruments (7, 8, 9). One of the difficulties involved in such measurements is the "highly shear-sensitive structure" of sputum, but among so-called "non-destructive" methods, a number are thought to have achieved a certain degree of success (10). However, the lapse of a considerable amount of time is inevitable when the dynamic viscoelasticity at a wide range of frequencies is obtained by any method reported previously.

On the other hand, with regard to the clearance through ciliary movements and coughing it is necessary first to understand dynamic viscoelastic behavior at a wide range of frequencies in order to estimate the changes in the internal structure of sputum. For that purpose, in the conventional dynamic method, measurements are needed of the sinusoidal strains at various frequencies in a single specimen of sputum, and this demands a considerable amount time, particularly in determining the behavior at low frequencies. Previously, there have been many reports indicating that changes of rheological properties occur in sputum or bronchial mucus following collection (10, 11, 12, 13), so it is possible that the changes occur while the measurements are being made. Consequently, the authors developed a new method by which dynamic viscoelasticity at a wide range of frequencies can be determined within a few minutes by only pulse strain and with no destruction of the samples (14). Here we report an investigation comparing the values for sputum obtained by the Raised Cosine Pulse method (R.C.P. method) and by the conventional dynamic method.

KEY WORDS: Sputum viscoelasticity, dynamic method, relaxation region

THEORY, MATERIALS AND METHOD

Theory

The complex shear modulus is commonly written as

$G^*(i\omega) = G'(\omega) + iG''(\omega)$

where ω is angular frequency in $rad \cdot sec^{-1}$ and $i = \sqrt{-1}$. In this equation, $G'(\omega)$ is storage modulus (dynamic elasticity) and $G''(\omega)$ loss modulus.

From the linear viscoelasticity theory, the complex shear modulus is defined as the product of $i\omega$ and complex viscosity $\eta^*(i\omega)$.

$$G^*(i\omega) = i\omega\eta^*(i\omega) = i\omega \int_0^\infty \psi(s) e^{-i\omega s} ds \qquad (1)$$

where $\psi(s)$ is an after-effect function often called the relaxation modulus.

According to the Boltzmann superposition principle, stress can be represented by a convolution integral of the after-effect function and the rate of strain. Therefore, the Fourier transform of the stress $\Sigma(i\omega)$ is given by

$$\Sigma(i\omega) = \eta^*(i\omega) \quad i\omega\Gamma(i\omega) \qquad (2)$$

where $\Gamma(i\omega)$ is the Fourier transform of the strain. In this equation, supposing

$$\Gamma(i\omega) = 1 \qquad (3)$$

Eq.(2) becomes

$$\Sigma(i\omega) = i\omega\eta^*(i\omega) = G^*(i\omega) \qquad (4)$$

Consequently, the complex shear modulus is determined by the Fourier transform of the stress $\sigma(t)$ as the response to a given strain function. The strain function which gives Eq.(3) is a delta-function. The delta-function would be useful because it includes all the frequency components from $-\infty$ to $+\infty$. In practice, however, it is difficult to apply the delta-function strain.

From these considerations, the following equation is adopted, which is called "The Raised Cosine Pulse".

$$\gamma(t) = \begin{cases} 1 + \cos\omega_0 t & (-\pi/\omega_0 \leq t \leq \pi/\omega_0) \\ 0 & (t < -\pi/\omega_0,\ t > \pi/\omega_0) \end{cases} \qquad (5)$$

Figure 1A shows the Raised Cosine Pulse. The Fourier transform of the Raised Cosine Pulse is given by

$$\Gamma(i\omega) = \frac{2\omega_0^2}{\omega(\omega_0^2 - \omega^2)} \sin\left(\frac{\omega}{\omega_0}\pi\right) \qquad (6)$$

and is shown in Figure 1B. This function is almost constantly a real number in a range of frequency less than ω_0.

$$\frac{\omega_0}{2\pi}\Gamma(i\omega) = 1 \qquad (\omega << \omega_0) \qquad (7)$$

Under these conditions, Eq.(4) is acceptable when the strain of the Raised Cosine Pulse is applied.

It is concluded that the complex shear modulus over a wide range of frequencies less than ω_0 can be directly determined by Fourier transformation of the stress observed as the response to the Raised Cosine Pulse strain at the frequency of ω_0.

In the conventional dynamic method, in order to obtain the frequency dependence of the complex shear modulus, sinusoidal strains at various frequencies must be applied. Whereas, in the present method, if only one strain pulse is applied to samples, the resultant stress can be analyzed by following the above principle.

Vol. 17
1980

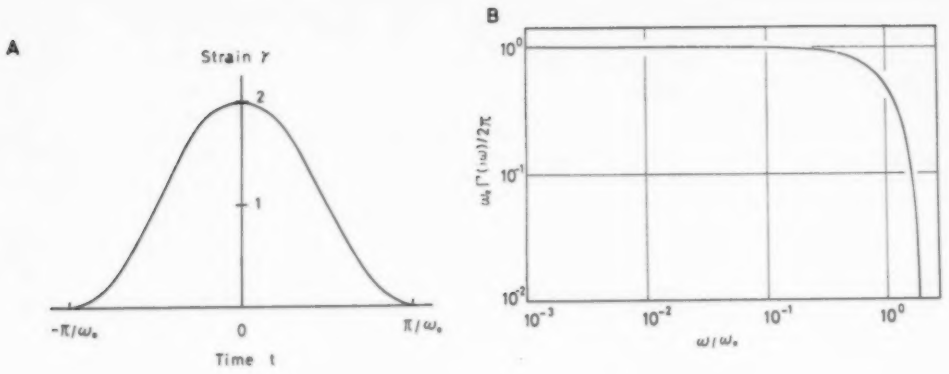

FIG. 1

A: Raised Cosine Pulse. B: Angular frequency dependence of Fourier transform of Raised Cosine Pulse (see text).

Materials

Materials included sputum obtained from 39 patients with chronic obstructive lunt diseases (26 cases of chronic bronchitis, 9 cases of chronic pulmonary emphysema and 4 cases of bronchial asthma). 10, 31 and 12 (total 53) samples of mucoid sputum (M_1 by the classification of Miller & Johnes (15)), mucopurulent sputum (M_2, P_1 and P_2) and purulent sputum (P_3), respectively, were used. Measurements of sputum obtained fresh in the morning were made within 2-4 hours of expulsion; the sputum was stored in close containers at room temperature (about 20°C) to preserve it from the change of rheological behaviour until use.

Method

A coaxial cylinder rheometer developed by the author was used for the experiments. This rheometer used is outlined in Figure 2. It is composed of four portions: a cylinder system, a power source consisting of a servomotor and a gear transmission, a torque recorder and a heat regulator. A sample of fluid to be measured is placed in the space between the bob and the cup. The torsional oscillation of the cup is transmitted to the bob through the sample, and induces shear stress at the surface of the bob. The resultant stress is converted into a torsional motion sufficient to equilibrate the rigidity of the torsion wire, and the motion is converted into an electric signal by use of a differential transformer. In the cylinder portion, the bob and the cup are 4 and 5 mm. in radius, respectively, with an effective sample depth of 30 mm. Measurements can be made with about 1.5 ml. of sputum. In addition to the sample directly involved in the measurements, excess sample is added and exposed to saturation humidity. End-effect of the coaxial cylinder rheometer used is calculated to be below 2% of the stress. Various constant temperatures for the experiments are possible, but here only 37°C was chosen to reflect the in vivo condition. The torsion wire has a 0.4 ϕ mm and a torsion constant of 2.6554×10^6 dyne·cm·rad^{-1}. Using this instrument it is possible to make a comparative investigation of the R.C.P. method and the conventional dynamic method using a single sputum sample.

In the dynamic method, by giving the cup a sunusoidal oscillation with an amplitude of 2 degree of the cup (a strain amplitude of 0.097), the bob caused the same period of oscillation but with a phase difference. The torsion angle of the cup was recorded on the x-axis of an x-y recorder and the torque of the bob on the y-axis. From the hysteresis loop obtained in this manner, the phase angle and amplitude ratio could be found and the dynamic viscoelasticity was calculated using the Markovitz equation (16). Measurements were made from a region of low frequency to one of high frequency and 7-9 points between $\omega = 10^{-2}$ and 10^0 rad·sec^{-1}. In the R.C.P. method, the measurements were carried out at a strain pulse frequency $\omega_0 = 1.05$ rad·sec^{-1}. The Raised Cosine Pulse strain was obtained by giving only 1 cycle oscillation with an amplitude of five degrees of the cup (a strain amplitude 0.2424)

in the above mentioned dynamic method. That is, the Pulse strain was taken as the single wave from the maximum value of the cup until the next maximum value. A recording was made using a transient recorder with time on the x-axis and the torque of the bob, i.e., stress, as the y-axis. The Fourier transformation of the stress curve was obtained by a digital computer (see appendix). Compensation values of $\omega = 3 \times 10^{-1} - 10^{0}$ rad·sec^{-1} were used.

This investigation was composed of the following three experiments:

i) The samples of sputum were classified macroscopically by grades, M_1, M_2, P_1, P_2 and P_3 type described by Miller and Johnes (15). The relationship between the macroscopic appearances and dynamic viscoelastic properties was then studied.

ii) Using the same samples, a comparison was made between the R.C.P. method and the conventional dynamic method. The values obtained by the R.C.P. method before and after the measurements by the conventional dynamic method were compared with those measured by the conventional dynamic method.

iii) The values were obtained by the R.C.P. method at intervals of 10 minutes until 60 minutes --- the time needed for measurements of each sample using the conventional dynamic method. During this experiment, sputum samples were kept at 37°C.

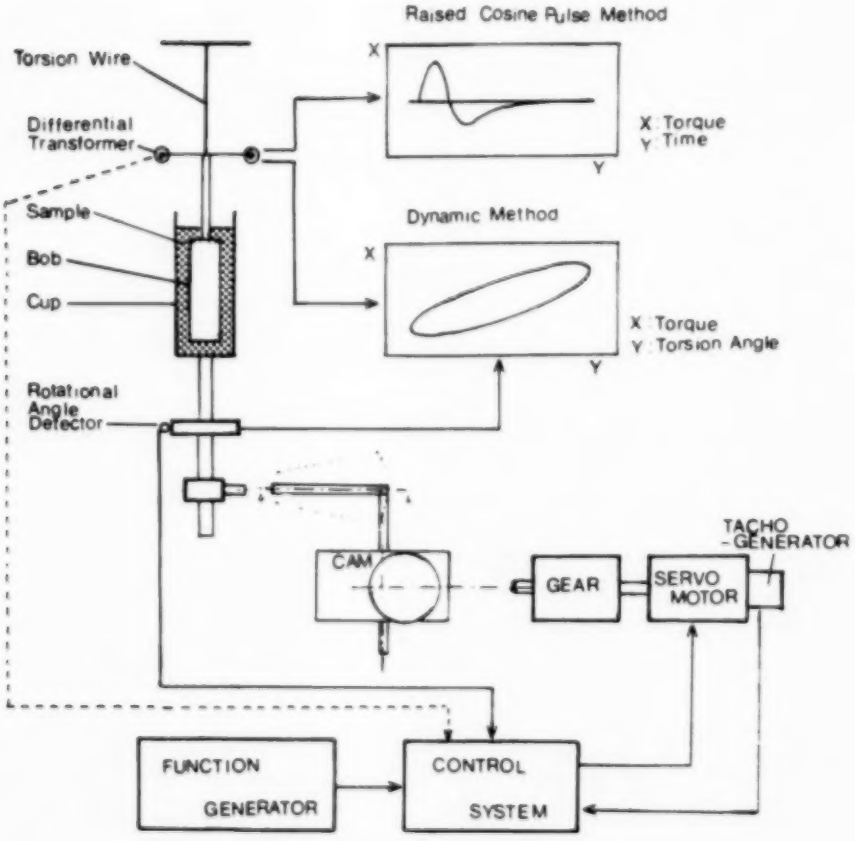

FIG. 2

Schematic representation of rheometer used. Broken line showing a feedback system which is necessary to get the behavior at frequencies higher than 1.05 rad·sec^{-1} in the Raised Cosine Pulse method (see text).

RESULTS

Applied strain could be approached with the Raised Cosine Pulse (Fig. 3a & 3b). Examples of typical stress curves obtained by the Raised Cosine Pulse are shown in Figures 3A & 3B. As the torsion wire used was highly sensitive to vibration, noises were often recorded in the stress curve obtained (Fig. 3B). However, they were too samll to be an obstacle to analysis of stress curves. From the Fourier transforms of these stress curves, dynamic viscoelastic behaviors at $\omega = 10^{-3} - 10^{0}$ rad·sec^{-1} were obtained. Figure 4 shows examples of G', G" and dynamic viscosity η' ($=G"/\omega$) against ω on a logarithmic scale obtained for a mucoid (M_1) and a purulent (P_3) sputum sample. The absolute values for G', G" and η' were found to vary widely among the samples, but fundamentally the following analogous frequency dependency was seen: G': at $\omega = 10^{-3} \sim 3 \times 10^{-2}$ rad·sec^{-1}, a plateau region of $10^{0} - 5 \times 10^{-1}$ dyne·cm^{-2} was seen and an increase was seen at $\omega = 3 \times 10^{-2} - 3 \times 10^{-1}$ rad·sec^{-1}. G": G" increased together with ω, but in many samples, a peak was seen at the region where the frequency corresponded to an increase of G'. From the behavior of G' and G", the presence of a relaxation region at $\omega = 3 \times 10^{-2} - 3 \times 10^{-1}$ rad·sec^{-1} could be assumed. η': at $\omega = 10^{-3} - 3 \times 10^{-2}$ rad·sec^{-1}, a plateau region of $10^{1} \sim 10^{3}$ poise was seen, but at the region $\omega = 3 \times 10^{-2} \sim 10^{0}$ rad·sec^{-1}, a sharp decrease was found as ω increased, and values approached $5 \times 10^{0} - 10^{1}$ poise. Within the sharp decrease, another narrow plateau region was often seen at a frequency which corresponded to the end of the peak of G" (Fig. 4B).

The macroscopic type difference of G' and G" thus obtained is shown in Figures 5 and 6. Although there was a general impression that the absolute values of G' and G" for mucoid sputum were somewhat lower than for the other sputa, the differences among individual samples were so large that no clear tendency could be seen. However, from the differences in macroscopic type, the following could be deduced. The peak of G", which indicated a relaxation region, was more evident at lower frequencies (near $\omega = 3 \times 10^{-2}$ rad·sec^{-1}) in purulent sputum. As the purulence decreased, the G" peak disappeared, and in the mucoid sputum, the peak, although indistinct, was seen at higher frequencies (near $\omega = 3 \times 10^{-1}$ rad·sec^{-1}). Frequencies showing a slight increase of G' were also higher in mucoid sputum and those showing a steep increase were lower in purulent sputum. This tendency corresponded to that seen in the peak of G". In some samples of P_2 and P_3 type sputum, the values of G' were very small relative to those of G", particularly at lower frequencies (Fig. 5C).

In the conventional dynamic method, almost all of the samples showed values in rough agreement with the R.C.P. method, but it was difficult to discern the behavior of G' and G" showing the relaxation region using the dynamic method (Fig. 7). In about 3/4 of the samples, the values measured using both methods were roughly in agreement and the values obtained by the R.C.P. method before and after measurements by the dynamic method were not so different --- the examples are shown in Figure 7A and 7B. However, in about 1/4 of the samples, the values were very different from those obtained by the R.C.P. method before and after measurements by the dynamic method and the degree of agreement between the two methods was somewhat lower than in the other samples (Fig. 7C & 7D). The values obtained by the R.C.P. method after measurements by the conventional dynamic method were clearly lower in many samples of purulent sputa, whereas there was an increase in a few samples of mucoid sputa and mucopurulent sputa. An example of the former is shown in Figure 7D and the latter in Figure 7C.

Between 40 and 60 minutes were needed for the measurement of each sample using the conventional dynamic method, but during this time the value obtained at intervals of 10 minutes at 37°C by the R.C.P. method showed the following sequential changes: Figure 8A shows the changes in time in a sample of mucopurulent (P_1) sputum whose G' and G" had sequential increases all over frequencies of about 40% and 50% of their original values after 30 minutes and 60 minutes, respectively. The G' and G" of a few mucoid and mucopurulent sputa (about 1/8 of samples) showed increases of less than 50 ~ 60% of their original values over all frequencies. In contrast, in 2/3 of the purulent sputum samples, those showing changes of that degree were all decreases, some of them being decreases of more than 60% of their original values. Figure 8B shows an example of purulent (P_3) sputum whose G' and G" underwent a decrease of about 30% and about 60% of their original values after 30 minutes and 50 minutes, respectively. The sample shown in Figure 8B, whose values had time-related decrease, in the same sample shown Figure 7D in which the degree of agreement between the two methods was somewhat lower than in the samples shown in Figure 7A and 7B. In samples showing sequential changes such as those described above, the values obtained by the R.C.P. method before and after measurement by the dynamic method showed a lower rate of agreement than in the other samples.

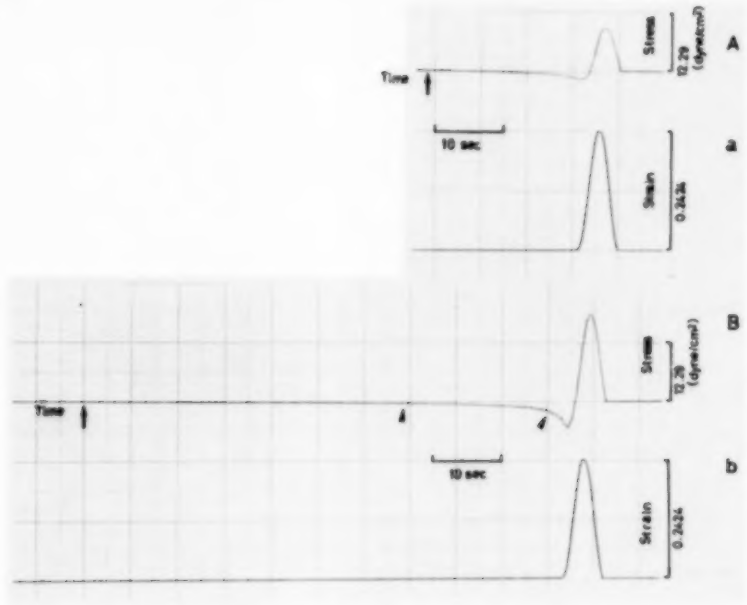

FIG. 3

a & b: Measured strains obtained by giving 1 cycle oscillation at frequency ω_0 = 1.05 rad·sec^{-1} with an amplitude of 5 degrees of the cup in the conventional dynamic method, which can be approached with the Raised Cosine Pulse. A & B: Measured stresses under the strain of Raised Cosine Pulse in a sample of mucoid (M_1) sputum (A) and mucopurulent (P_1) sputum (B). The stress becomes zero value at 28 sec in the former and at 93 sec in the latter (arrows). Small noises (arrow-heads) seen in the stress curve. Strains and stresses were recorded simultaneously, but the former shifted very slightly to the left of the recording papers.

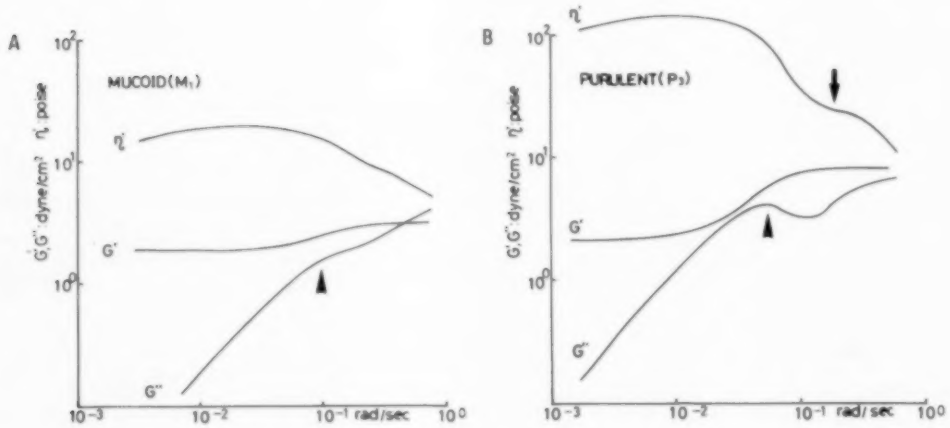

FIG. 4

Frequency dependences of dynamic viscosity (η'), storage modulus (G') and loss modulus (G'') of a sample of mucoid (M_1) sputum (Fig. A) and purulent (P_3) sputum (Fig. B). Increases with a frequency of G' and a peak of G'' near $\omega = 5 \times 10^{-2}$ rad·sec^{-1} (arrow-heads) are more prominent in purulent sputum. Within the sharp decrease of η' as frequency increases between $10^{-2} \sim 10^{0}$ rad·sec^{-1}, another narrow plateau region is seen in Fig. B (arrow).

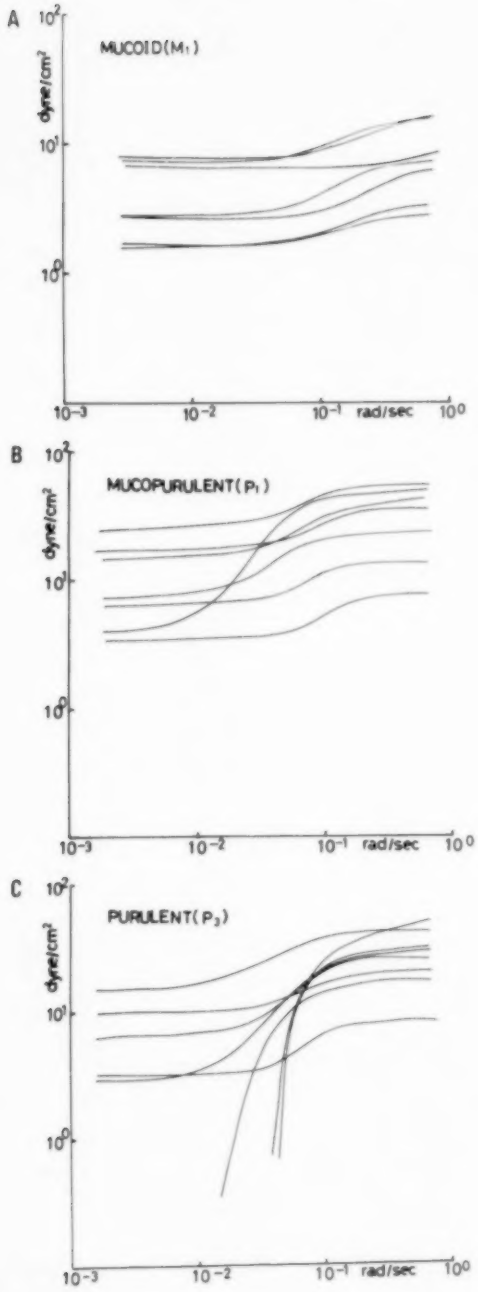

FIG. 5

Frequency dependences of storage modulus (G') of 7 mucoid (M_1), 7 mucopurulent (P_1) and 8 purulent (P_3) sputum samples. As the purulence increases, the increases with frequency become more steep and are seen at lower frequencies.

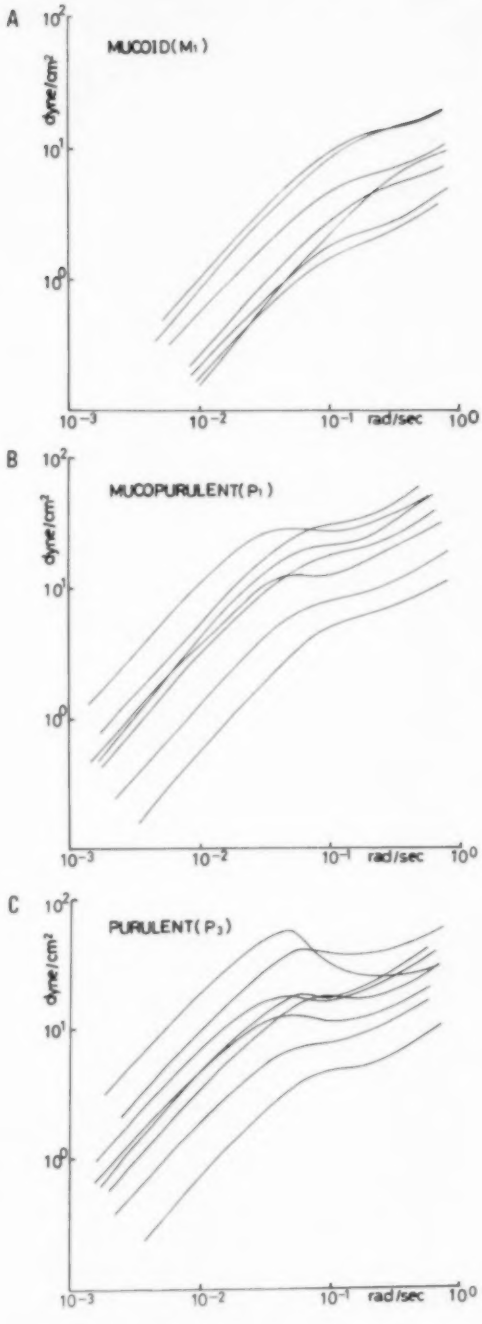

FIG. 6

Frequency dependences of loss modulus (G") of 7 mucoid (M_1), 7 mucopurulent (P_1) and 8 purulent (P_3) sputum samples. As the purulence increases, the peaks become more distinct and are seen at lower frequencies.

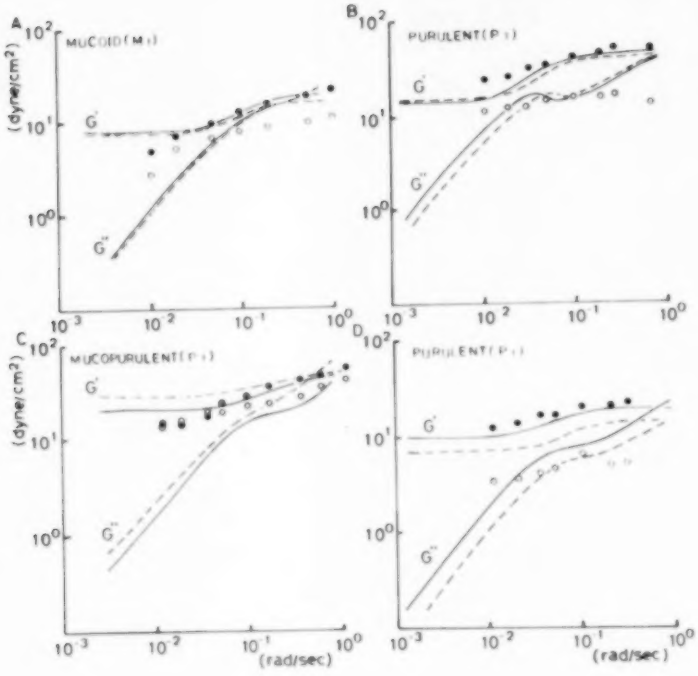

FIG. 7

Comparison of Raised Cosine Pulse method (——:before, and ----:after measurements by the conventional method) with the conventional dynamic method (G':●, G'':o) in a sample of mucoid (M_1), mucopurulent (P_1) and purulent (P_3) sputum. Figure A & B showing the examples in which the values obtained by the Raised Cosine Pulse method before and after measurements by the conventional dynamic method were roughly in agreement, and Figure C & D showing the examples not in agreement.

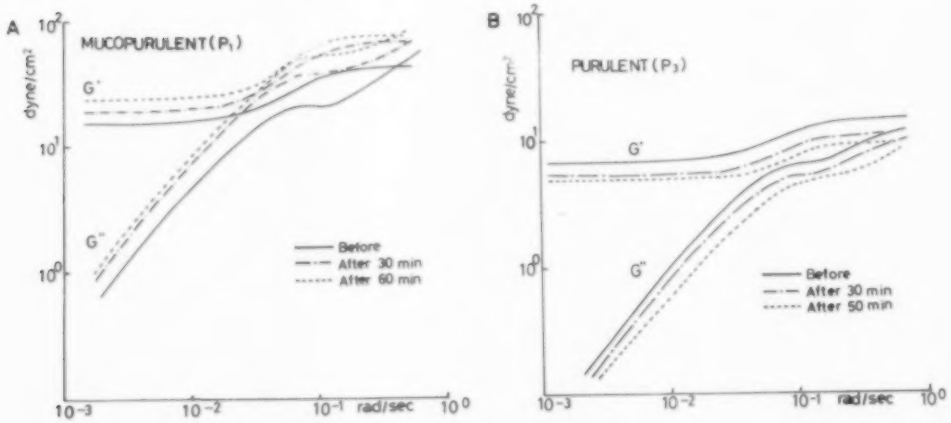

FIG. 8

A: Time-related increase of dynamic viscoelasticity seen in a sample of mucoid (M_1) sputum (——:before, —·—:after 30 minutes, ----:after 60 minutes). B: Time-related decrease of dynamic viscoelasticity seen in a samples of purulent (P_3) sputum which is the same sample as shown in Figure 7D (——:before, —·—:after 30 minutes, ----:after 50 minutes).

Vol. 17
1980

DISCUSSION

Validity of the method

It has been well known that sputum exhibits "non-linear" viscoelastic properties under large deformations (17). In the present investigation, physical properties of sputum were studied at small deformations in the range of "linear" viscoelasticity. That is, the R.C.P. method based on the linear viscoelasticity theory is available for the measurements of sputum viscoelasticity.

With regard to the shear rate applied to mucociliary transport in airways, there is not yet agreement of opinion, although it has been suggested as 1 sec^{-1} by Dulfano (17), 3 sec^{-1} by Pham et al. (1) and 20 sec^{-1} by Litt (18). Theoretically, it should be possible to measure any frequency region using the R.C.P. method, but with the apparatus used in the present study, "rotation of the bob" and "slippage of the samples and the cup" cannot be ignored as the frequency (ω_0) of pulse strain given to the cup increases. The strain at frequencies higher than ω_0 = 1.05 $rad \cdot sec^{-1}$ cannot be approached with the Raised Cosine Pulse and its influence appears chiefly in values of G'. With ω_0 = 1.05 $rad \cdot sec^{-1}$ used in this study, the error limits of G' are thought to be within ±5%, so that the measured values have sufficient validity. However, in order to accurately reflect the in vivo condition within the airways, it is necessary to follow the dynamic viscoelastic behavior in higher frequency regions. For that purpose, we found it necessary to develop another apparatus which has a feedback mechanism, as shown by the broken line in Figure 2.

Sputum is a mixture primarily of airway secretions but is also composed of various other secretions, particularly saliva. The non-uniformity of its composition is frequently said to be a major obstacle to understanding its rheological characteristics. Nevertheless, the dynamic viscoelastic curves obtained for sputum by the R.C.P. method showed a fundamentally similar frequency dependence despite the wide distribution of absolute values and differences in macroscopic findings. This fact is thought to indicate that mechanically sputa have a common internal structure and that the R.C.P. method can indeed detect it, despite the lack of uniformity within the samples.

For a simple mechanical model of bronchial mucus and sputum, a model combining Maxwell and Voigt elements in series is well-known (8, 10, 19, 20) and is shown in Figure 9A. Drawing the dynamic viscoelasticity curve of the mechanical model in rough agreement with the results obtained at the frequency region of $\omega = 10^{-3} - 10^{0}$ $rad \cdot sec^{-1}$ gives the solid line shown in Figure 9B. That is, assuming that a relaxation region exists around $\omega = 10^{-1}$ $rad \cdot sec^{-1}$, one other such region can be found at the low frequency region below $\omega = 10^{-4}$ $rad \cdot sec^{-1}$. By calculating the stress under the Raised Cosine Pulse of ω_0 = 1.05 $rad \cdot sec^{-1}$ given to this model and drawing the stress curve thus obtained, Fourier transforms can be performed on the stress curve and the dynamic viscoelasticity behavior thus obtained is as shown by the broken line in Figure 9B. This is found to closely resemble the results obtained for sputum and to clearly reflect the behavior of G' and G" showing a relaxation region at $\omega = 10^{-1}$ $rad \cdot sec^{-1}$. This fact demonstrates that the results obtained by the R.C.P. method can approximate the mechanical model described above. It also shows that the peak of G" and accompanying changes in G' seen in almost all sputum samples is not an artifact of the quantitation method itself, that is the result of the compensation values used for $\omega = 3 \times 10^{-1} - 10^{0}$ $rad \cdot sec^{-1}$, but rather that this method detects relaxation regions existing in the internal structure of the sputum. Furthermore, it shows that the reliability of values obtained are not sufficient in the frequency region near 10^{-3} or 10^{0} $rad \cdot sec^{-1}$, and this tendency is more prominent in the values of G" than in those of G'.

Relaxation region

Using a magnetic rheometer, Hwang et al. (21) have indirectly found the dynamic viscoelasticity curve by performing mathematical operations on the values obtained from the creep test. They found a relaxation region in the vicinity of 10^{-2} $rad \cdot sec^{-1}$ which was one half magnitude lower than that found by the authors. Subsequently, Davis (6, 10) and Denton et al. (22) obtained similar results and Davis maintained that the creep test was a convenient method for indirectly finding dynamic viscoelasticity at low frequencies. Judging from the behavior of G' and G" at $\omega = 10^{-3} - 10^{-2}$ $rad \cdot sec^{-1}$ found by the authors and from previous reports of dynamic measurements, it is thought to be impossible to determine one more relaxation region in that frequency region. The relaxation region found by S.H. Hwang et al. may be the same as that found by the authors. It is possible that differences in the samples or the involvement of variations are the source of this contradiction, but it is also thought that differences in the measuring method play a role. Besides the fact that the creep test is a static method whereas the R.C.P. method is one of the dynamic methods, there is a fundamental difference in that the strain under stress or the stress under strain is measured. The creep test measures the former and dynamic methods measure the latter. Currently, it is not clear which method is superior in determining the viscoelasticity of sputum. If in the future it becomes possible to compare a method for measuring sinusoidal strain under forced sinusoidal stress with a conventional dynamic method applied to sputum, presumably a single answer will be obtained. Nevertheless, in general, when considering the "flow" properties

of matter, a method for detecting stress under strain is used, and considering the situation of sputum within the airways, current dynamic measurements including the R.C.P. method are thought to be more appropriate.

In our study, a relaxation region at $\omega = 3 \times 10^{-2} \sim 3 \times 10^{-1}$ rad·sec^{-1} was evident, but this was not clearly indicated in any previous report using dynamic methods. Nevertheless, among those reports, there were two which can be considered as supporting the presence of a relaxation region such as was found in our study. The first is the report of Mitchell-Heggs and Lopez-Viderieto et al. which showed elasticity over frequencies from 0.01 to 0.8 sec^{-1}, a plateau region over the lower shear rates and then a steep increase together with an increase in frequency around 10^{-1} sec^{-1} (13, 23). The second is the report of Sturgess et al. (7), Lopez-Videriero et al. (13) which showed a "fluctuation" or "notched plateau region" of η' near the same frequency region. The latter work is particularly thought to correlate with the narrow plateau region seen in the measurements by the R.C.P. method and thought to indicate the existence of a peak of G". The relaxation region suggested by these two reports may be at a somewhat higher frequency than found by us, but such a small difference is thought to be within the range of experimental error.

Macroscopic type difference

Sturgess et al. (7) and Picat et al. (24) found no significant difference between the viscosity of purulent and mucoid sputum. Mitchell-Heggs et al. (23) reported that there was no level of elasticity characteristic of one macroscopic appearance and there was wide variation between samples. On the other hand, Dulfano (17) reported that elastic recoil of purulent sputum was smaller than that of mucoid. This tendency may be found in some samples of P_2 and P_3 type sputum whose G' was small relative to those of G" in this study. As a general rule, in comparison with other sputa, the dynamic viscoelasticity of mucoid sputum tended to be smaller at each frequency, but due to the wide distribution of values among the samples, this tendency was not pronounced. It was evident, however, that the peak of G" became more marked as the degree of purulence increased and a low frequency region (near 3×10^{-2} rad·sec^{-1}) was approached. In mucoid sputum, the indistinct peak of G" was seen at higher frequencies (near 3×10^{-1} rad·sec^{-1}). The behavior of G' corresponded to the peak of G". Furthermore, Mitchell-Heggs et al. (23) have also reported that the frequency region where G' sharply increased was often seen in zone 2 (0.5 sec^{-1} to 10 sec^{-1}) for mucoid sputum and zone 1 (up to 0.5 sec^{-1}) for purulent sputum. Based upon electron microscopic observations, Bürgi et al. (25) maintained that the fundamental structure of sputum was a network of glycoprotein fibers and in purulent sputum DNA fibers increased in number. It is thought that such differences in internal structure lengthen the relaxation time and narrow the spectrum of the relaxation time. In the model analysis of mucociliary pumping by Ross et al. (26), it was predicted that mucociliary transport velocity would decrease with increasing mucus relaxation time. Furthermore, the experimental study of mucociliary transport using a frog pharyngeal palate and sputum from bronchitics by Dulfano et al. (27) demonstrated that purulent sputum, as a group, was transported at a slower rate than mucoid sputum. Therefore, the results obtained from the present study on the relaxation regions of differing macroscopic types of sputum samples are thought to indicate a different mucociliary transport rate for purulent sputum from for mucoid sputum.

Comparison with the conventional dynamic method and changes with time

With regard to the direct measurements of the dynamic viscoelasticity of sputum, various reports have been published thus far. The majority have reported a combination of G' and η' on a log-log scale, and roughly similar results have been obtained in all of them. Our results agree with those of previous reports with regard to frequency dependence, but the absolute values obtained by us are somewhat lower than those in other reports. The main reason for this is thought to be due to the difference in temperature at measurements --- previous studies have been undertaken at 20°C or 25°C, whereas our study was performed at 37°C. When we adjusted the values obtained by Sturgess (7) in a study on mucoid sputum using Weissenberg rheogoniometer at 20°C to 37°C, viscosity diminished by half.

Both methods of measurement agree closely with one another at least with regard to the 20 wt% polystyrene solution in diethylphthalate, which has uniformity and does not change within the time needed for measurements (Fig. 10). In the present investigation using sputum, there was rough agreement at $\omega = 10^{-2} - 10^{0}$ rad·sec^{-1}, but there were large differences in the degree of agreement depending upon the given sample. The causes of the lack of agreement are thought to be both the non-uniformity of samples and the peculiarity of the R.C.P. method which was described under "validity of the method". Furthermore, many of the samples in which agreement was poor were purulent sputum; in such samples, the R.C.P. values obtained following measurements by the dynamic method were lower. It is not likely that the very small strain itself used in the dynamic method was responsible for the changes in the internal structure of the sputum, and the sequential changes during 60 minutes at 37°C were found in G' and G" by the R.C.P. method. Therefore, one probable cause of the lack of agreement was the changes in the sample with time. A number of reports have indicated a reduction in the viscosity of sputum or bronchial mucus when kept at room temperature. Lopez-Videriero et al. (12, 13) maintained that the viscosity in purulent sputum decreased more rapidly than in mucoid sputum because of the presence of proteolytic enzymes and bacterial exozymes.

Vol. 17
1980

It is possible that at 37°C, as in these experiments, the activity of these enzymes will be accelerated further. On the other hand, Sturgess et al. (7) and Lopez-Videriero et al. (13) reported that after shearing at a low shear rate, viscosity in sputum obtained from chronic bronchitics showed a striking (10-fold) increase. The increase with time of the dynamic viscoelasticity seen in a few mucoid and mucopurulent sputum samples was so small that the cause cannot be shearing, but it may be evaporation. The time factor is an important source of differences in rheological studies of sputum, so that it is mandatory that measurements be made at a defined period from expulsion of sputum and completed in a short time. The average time needed for measurement of a single sample using the R.C.P. method was 2 minutes, whereas it was roughly 1 hour using the conventional dynamic method. With the R.C.P. method, if measurements of the behavior at $\omega = 10^{-3} - 10^{-2}$ rad·sec^{-1} were attempted, 5~6 times that amount of time would be needed for the latter method. Consequently, that clinical approach becomes inconvenient because of the time factor, so that most reports to data have been comparative investigations using a constant shear rate (28, 29, 30). That, however, means that it is impossible to understand the changes in internal structure and to determine the mechanism of expectorants related to the treatment of, for example, expulsion failure. In the R.C.P. method, a sample volume of 1-2 times expelled sputum is sufficient and accumulated sputum is not necessary. It is therefore possible to measure the dynamic viscoelastic behavior which determines the internal structure within an extremely short period of time. Therefore, the R.C.P. method is thought to be an effective method for clinical use.

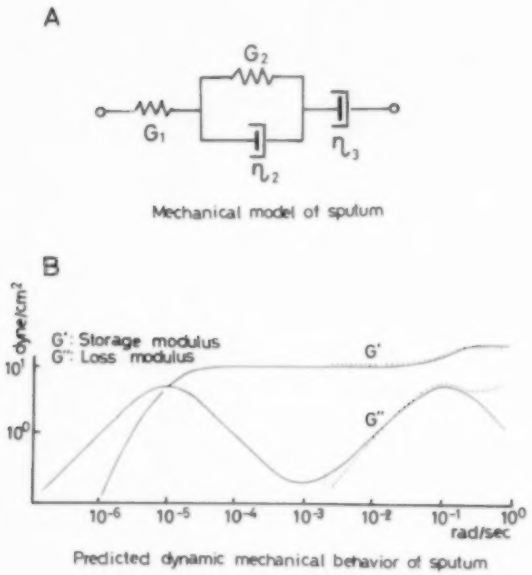

FIG. 9

A: Mechanical model of sputum combining Maxwell and Voigt elements in series. B: Predicted dynamic mechanical behavior of sputum as shown in solid line (G_1: 5.99 × 10 dyne/cm^2, G_2: 1.13 × 10^{-1} dyne/cm^2, η'_2: 6.79 × 10 poise, η'_3: 9.5 × 10^5 poise in Fig. A) and the behavior calculated by the Raised Cosine Pulse method using the predicted model as shown in the broken line. The latter closely resembles the frequency dependence obtained from sputum samples.

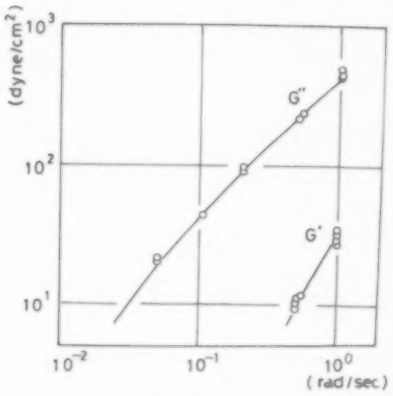

FIG. 10

Frequency dependence of storage modulus (G') and loss modulus (G'') of 20% polystyren solution at 20°C. Comparison of Raised Cosine Pulse method (——) with the conventional dynamic measurement (o). Both methods of measurement agree with one another.

APPENDIX

Generally, the Fourier transformation is obtained by using a digital computer. The discrete Fourier transform (DFT) is defined by

$$\Sigma_k = 1/N \sum_{j=0}^{N-1} \sigma j \exp(-2\pi ijk/N) \qquad j=0.1.....N-1 \qquad (1)$$

$$N = 1/\Delta t$$

where Σ_k is the k-th coefficient of the DFT and σ_j denotes the j-th sample of the time series which consists of N samples. The σ_j can be a complex number and Σ_k is almost always complex. In the present study, the σ_j was always a real number. Since the σ_j is often the value of a function at a discrete time point, the index k is sometimes called the frequency coefficient of the DFT. In the relationship between σ_j and Σ_k, σ_j is supposed to be defined in the time interval $0 \leqq t \leqq 1$ and the frequency of the DFT is limited in ranges higher than 2π (k=1).

However, as evident from theory, the Raised Cosine Pulse is defined at $t < 0$, besides $t \geqq 0$, and the Fourier transform of the stress is available under the condition of $\omega << \omega_0$. Therefore, Eq. (1) shall be so extended to satisfy these conditions. For this purpose, the following equation is employed as the Fourier transformation of σ (t) which is defined in the time interval $-T \leqq t \leqq T$.

$$\Sigma_k (\omega_k) = 2T/N \sum_{j=-N/2}^{j=N/2} \sigma (j\Delta t)\exp(-2\pi ijk/AN) \qquad (2)$$

$$t = j\Delta t$$

where $2T/N = \Delta t$, and A is a coefficient which is introduced to get the Fourier transform in the frequency range of $\omega_k << \omega_0$. In practice, the Fourier transformation was carried out in terms of the cosine and sine functions.

The frequency dependence of the complex shear modulus is given by the following equations.

$$G'_k (\omega_k) = 2T/N \sum_{j=-N/2}^{j=N/2} \sigma (j\Delta t)\cos(2\pi jk/AN) \qquad (3)$$

$$G''_k (\omega_k) = 2T/N \sum_{j=-N/2}^{j=N/2} \sigma (j\Delta t)\sin(-2\pi jk/AN) \qquad (4)$$

$$\omega_k = 2\pi k/AN\ \Delta t$$

Although the Fourier transform of stress was obtained by a straight-forward procedure according to Eqs. (3), (4) in this study, the Fast Fourier transform (FFT) is an efficient procedure for computing the DFT of a time series.

REFERENCES

1. PHAN, Q.T., PESLIN, R., PUCHELLE, E., SALMON, D., CARAUX, G., and BENIS, A.M. Respiratory function and the rheological status of bronchial secretions collected by spontaneous expectoration and after physiotherapy. Bull. Physiopathol. Respir. 9, 293-314, 1973.

2. POLGAR, G., and DENTON, R. Cystic fibrosis in adults. Studies of pulmonary function and some physical properties of bronchial mucus. Amer. Rev. Resp. Dis. 85, 319-327, 1972.

3. FEATHER, E.A., and RUSSEL, G. Sputum viscosity and pulmonary function in cystic fibrosis. Arch. Dis. Child. 45, 807-808, 1970.

4. CHODOSH, S., MEDICI, T.C., ISHIKAWA, S., and ENSLEIN, K. Relationship of physical sputum characteristics and ventilatory capacity in chronic bronchial disease. Chest 63, Suppl., 1973.

5. LOPEZ-VIDRIERO, M.T. Individual and group correlations of sputum viscosity and airways obstruction. Bull. Physiopathol. Respir. 9, 339-346, 1973.

6. DAVIS, S.S. and DIPPY, J.E. The rheological properties of sputum. Biorheology 6, 11-21, 1969.

7. STURGESS, J., PALFREY, A.J., and REID, L. Rheological properties of sputum. Rheol. Acta 10, 36-43, 1971.

Vol. 17
1980

8. MALCOLM, K., and MACKLEM, P.T. Rheological properties of microliter quantities of normal mucus. J. Appl. Physiol. 42, 797-802, 1977.

9. POWELL, R.L., AHARONSON, E.F., SCHWARZ, W.H., PROCTOR, D.F., ADAMS, G.K., and REASOR, M. Rheological behavior of normal tracheobronchial mucus of canines. J. Appl. Physiol. 37, 447-451, 1974.

10. DAVIS, S.S. Rheological examination of sputum and saliva and the effect of drugs. In: Rheology of Biological Systems, edited by Gabelnick, H.L., and Litt, M. Springfield, Ill.: Charles C Thomas, 1973, pp. 157-194.

11. MEYER, F.A. Mucus structure: relation to biological transport function. Biorheology 13, 49-58, 1976.

12. LOPEZ-VIDRIERO, M.T., and REID, L. Chemical markers of mucous and serum glycoproteins and their relation to viscosity in mucoid and purulent sputum from various hypersectory disease. Amer. Rev. Respi. Dis. 117, 465-477, 1978.

13. LOPEZ-VIDRIERO, M.T., and DAS, I. Airway secretion: Source, biochemical and rheological properties. In: Lung Biology in Health and Disease, Respiratory Defence Mechanism Part I, edited by Joseph D. Brain, Donald F. Procter, and Lynne M. Reid. New York, Marcel Dekker, 1978, pp. 289-356.

14. UMEYA K, and OTSUBO Y. Time dependent behaviour of viscoelastic suspensions. Journal of Rheology, 1980. in press.

15. MILLER, D.L., and JOHNES, R. A study of techniques for the examination of sputum in a field survey of chronic bronchitis. Amer. Rev. Resp. Dis. 88, 473-483, 1963.

16. MARKOVITS, H. A property of Bessel functions and its application of the theory of two rheometers. J. Appl. Physics 23, 1070-1077, 1952.

17. DULFANO, M.J. Physical properties. In: Sputum. Edited by Dulfano, M.J. Springfield, Ill.: Charles C Thomas, 1973, pp. 201-242.

18. LITT, M. Mucus rheology and mucociliary clearance. Mod. Probl. Paediat. 19, 175-181, 1977.

19. LUTZ, R.J., LITT, M., and CHAKRIN, L.W. Physical-chemical factors in mucus rheology. In: Rheology of Biological Systems, edited by Gabelnick, H.L., and Litt, M. Springfield, Ill: Charles C Thomas, 1973, pp. 119-157.

20. ALFREY, T. Jr., Mechanical Behavior of High Polymers, New York: Interscience, 1948, part B.

21. HWANG, S.H., LITT, M., and FORSMAN, W.C. Rheological properties of mucus. Rheol. Acta 8, 438-448, 1969.

22. DENTON, R., FORSMAN, W., HWANG, S.H., LITT, M., and MILLER, C.E. Viscoelasticity of mucus, its role in ciliary transport of pulmonary secretions. Amer. Rev. Resp. Dis. 98, 380-391, 1968.

23. MITCHELL-HEGGS, P., PALFREY, A.J.,and REID, L. The elasticity of sputum at low shear rates. Biorheology 11, 417-426, 1974.

24. PICOT, R., DAS, I., and REID, L. Pus, deoxyribonucleic acid and sputum viscosity. Thorax 33, 235-242, 1978.

25. BÜRGI, H. Fibre systems in sputum. Bull. Physiopathol. Respir. 9, 191-196, 1973.

26. ROSS, S.M., and CONSIN, S. Results of an analytical model of mucociliary pumping. J. Appl. Physiol. 37, 333-340, 1974.

27. DULFANO, M.J., and ADLER, K.B. Physical properties of sputum-rheological properties and mucociliary transport. Amer. Rev. Resp. Dis. 112, 341-347, 1975.

28. CHEN, T.M., and DULFANO, M.J. Mucus viscoelasticity and mucociliary transport rate. J. Lab. Clin. Med. 91, 423-431, 1978.

29. HIRSCH, S.R., and KORY, R.C. An evaluation of the effect nebulized N-acetylcysteine on sputum consistency. J. Allergy 39, 265-273, 1967.

30. HAMILTON, W.F.D., PALMER, K.N.V., and GENT, M. Expectorant action of Bromhexine in chronic obstructive bronchitis. Brit. Med. J. 3, 260-261, 1970.

BLANK
PAGE

Vol. 17
1980

BIORHEOLOGY, Vol. 17, pp. 377-384, 1980
Printed in the USA. All rights reserved.

0006-355X/80/040377-08$02.00/0
Copyright (c) 1980 Pergamon Press Ltd

THEORETICAL ANALYSIS OF PULSATILE BLOOD FLOW IN SMALL VESSELS

Noriko Iida* and Tadayoshi Murata**

* Nurse School, Sapporo South Hospital, Sapporo 061-22, Japan
** Department of Physics, Faculty of Science, Tokyo Metropolitan University, Setagaya-ku, Tokyo, Japan

(Received 27.12.1979; in revised form 13.6.1980.
Accepted by Editor S. Oka)

ABSTRACT Non-Newtonian effects of blood on pulsatile flow in arterioles are theoretically considered using a simplified model. The effects of the plasma layer are also considered. It is assumed that blood is a non-Newtonian fluid obeying the Herschel-Bulkley equation and plasma is a Newtonian fluid. On these assumptions the shear stress and velocity distributions at any time are obtained for small values of the Womersley frequency parameter. We also obtain the flow rate, the wall shear stress and the radius of plug core. The results are shown in figures by taking the values of parameters based on experimental data in arterioles.

INTRODUCTION

Blood flow in the body circulation system is a pulsatile flow with the same frequency as the heart beat. Pulsatile behaviors can be measured even within arterioles of less than 100 μm diameter[1]. The pulsatile action of tension and shear stress on the vessel wall following pulsatile pressure is closely connected with the myogenic and passive change of the vessels diameter and with the injury on internal surface of vessels. The pulsatile behavior of blood flow is found to directly influence the flow resistance in arterioles.

The Reynolds number is about 0.09[2] and the blood velocity is very slow in arterioles. The shear rate around the vessel axis is observed to be low enough. On the other hand, blood is a non-Newtonian fluid and the non-Newtonian behavior shows a remarkable increase at low shear rate. Thus, in the case of analysing the flow behavior of blood in arterioles, the yield stress and the nonlinear relationship between the shear stress and shear rate are very important. To understand the flow condition in microcirculation, the pulsatile flow should be investigated in relation to the non-Newtonian behavior of blood and the physiological and dynamical behavior of the vessel wall.

Aroesty and Gross [3,4] examined theoretically the influence of pulsatile pressure on blood flow in small vessels by assuming that blood is a non-Newtonian fluid obeying the Casson equation. The shear stress and velocity distributions and the flow rate were calculated as a function of time on the basis of a quasi-steady theory by assuming that the Womersley frequency parameter [5] is less than 1.0.

Scott Blair [6] reported that blood obeys the Casson equation only in the limited range, except at very high and very low shear rate and that there is no difference between the Casson plots and the Herschel-Bulkley plots of experimental data over the range where the Casson plot is valid. He also suggested that the assumptions included in the Casson equation are unsuitable for cow's blood and that the Herschel-Bulkley equation represents fairly closely what is occurring in the blood. Since the Herschel-Bulkley equation contains one more parameter than the Casson equation does, it would be expected that more detailed information about blood properties can be obtained by the use of the Herschel-Bulkley equation. Furthermore, the Herschel-Bulkley equation is reduced to the mathematical models which describes the behavior of Newtonian fluid, Bingham fluid and power law fluid by taking appropriate values of the parameters. Therefore, in this paper we use the Herschel-Bulkley equation for the analysis of pulsatile blood flow and investigate in detail the effects of the yield stress, the parameter which expresses the degree of shear thinning and the thickness of plasma layer on the blood flow, as well as the effects of the flow conditions.

Thurston [7,8] has shown that blood exhibits nonlinear viscoelastic properties in pulsatile and steady tube flows. Therefore, considering unsteady motion of blood we must take

Key words: pulsatile flow, arterioles, plug core, wall shear stress.

into account the nonlinear viscoelastic properties of blood. However, in the case where the value of the Womersley frequency parameter is very small compared with unity and the ratio of the amplitude of oscillatory component to steady component of pulsatile pressure gradient is small, it seems probable that there is little effect of the elastic properties in comparison with the viscous properties. Therefore, we neglect the elastic properties of blood in this paper.

The purpose of this paper is to examine theoretically the rheological properties of pulsatile blood flow in arterioles in comparison with steady blood flow by assuming that blood is a non-Newtonian fluid obeying the Herschel-Bulkley equation.

ASSUMPTIONS

To simplify the problem, we shall use the following assumptions:

(1) Blood vessels are straight and long rigid circular tubes whose radii are constant (Fig.1).
(2) The flow of blood is axially symmetric and is in the $\tilde{x}$-direction.
(3) The blood in arterioles consists of the plasma layer near the tube wall and the central core of a non-Newtonian fluid.
(4) The thickness of the plasma layer is constant and independent of time and location.
(5) Plasma is a Newtonian fluid.
(6) Blood obeys the Herschel-Bulkley equation. The shear stress ($\tilde{\tau}$) - shear rate ($\tilde{\dot{\varepsilon}}$) relationship is given by

$$\tilde{\dot{\varepsilon}} = \frac{1}{k}(\tilde{\tau} - f_H)^n \qquad \text{if} \quad \tilde{\tau} \geq f_H ,$$

$$= 0 \qquad \text{if} \quad \tilde{\tau} \leq f_H ,$$

where k,n and f_H are parameters which represent non-Newtonian effects and f_H is the yield stress. The equation is reduced to that for a Bingham fluid when n = 1, to that for a power law fluid when $f_H = 0$, and to that for a Newtonian fluid when n = 1 and $f_H = 0$.

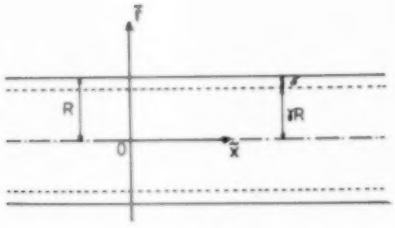

FIG. 1

Blood vessel and cylindrical coordinate system

MOMENTUM EQUATIONS AND BOUNDARY CONDITIONS

As shown in Figure 1, we shall take cylindrical coordinate system ($\tilde{r}$, $\tilde{x}$, ψ) whose origin is located on the vessel axis. The fully developed laminar flow of fluid is considered. From the assumption (2) the momentum equation and the continuity equation are given as follows:

$$\rho \frac{\partial \tilde{u}}{\partial \tilde{t}} = - \frac{\partial \tilde{p}}{\partial \tilde{x}} + \frac{1}{\tilde{r}} \frac{\partial}{\partial \tilde{r}} (\tilde{r} \tilde{\tau}), \tag{1}$$

$$0 = \frac{\partial \tilde{p}}{\partial \tilde{r}} , \tag{2}$$

$$\frac{\partial \tilde{u}}{\partial \tilde{x}} = 0 , \tag{3}$$

where $\tilde{u}$ is the axial component of the velocity, $\tilde{p}$ the pressure, $\tilde{t}$ time, and ρ is the fluid density. Body force is neglected in Eqs. (1) and (2). The boundary conditions are:

$$\tilde{u}^p = 0 \qquad \text{at} \quad \tilde{r} = R , \tag{4}$$

Vol. 17
1980

$$\tilde{u}^{p} = \tilde{u}^{H} \qquad \text{at } \tilde{r} = \gamma R , \tag{5}$$

$$\tilde{\tau}^{p} = \tilde{\tau}^{H} \qquad \text{at } \tilde{r} = \gamma R , \tag{6}$$

$$\frac{\partial \tilde{u}^{H}}{\partial \tilde{r}} = 0 \qquad \text{at } \tilde{r} = 0 , \tag{7}$$

$$\gamma = 1 - \frac{\delta}{R} , \tag{8}$$

where R is the vessel radius, δ the thickness of the plasma layer. The quantities in the plasma layer and in the central core are denoted by superscripts p and H, respectively.

We give the pressure gradient as follows:

$$\frac{\partial \tilde{p}}{\partial \tilde{x}} = p'p(\tilde{t}) = p' (1 + A \sin \omega \tilde{t}) , \tag{9}$$

where ω is the angular frequency, p' and A are constant.

Let us introduce the following nondimentional variables and parameters:

$$r = \frac{\tilde{r}}{R} , \quad t = \omega \tilde{t} , \quad u = \frac{2\eta_p}{R^2 p'} \tilde{u} , \quad \tau = \frac{2}{Rp'} \tilde{\tau} . \tag{10}$$

$$\alpha_p^2 = \frac{\rho_p R^2 \omega}{\eta_p} = \frac{\rho_p}{\rho_b} \alpha^2 , \quad \theta = \frac{2 f_H}{Rp'} , \quad \eta_H = k \left(\frac{2}{Rp'} \right)^{n-1} , \tag{11}$$

where η_p is the viscosity of plasma, ρ_p and ρ_b the density of plasma and blood, respectively.

In arterioles the Womersley frequency parameter (α or α_p) is very small compared with unity. Then, the velocity u and the shear stress τ are assumed to possess expansions in terms of the parameter α^2, which are of the form

$$u = u_0 + \alpha^2 u_1 , \quad \tau = \tau_0 + \alpha^2 \tau_1 , \tag{12}$$

all terms of order α^4 will be neglected.

VELOCITY AND SHEAR STRESS

The solutions of Eq.(1) which satisfy the boundary conditions (4) ~ (7) can readily be obtained by tedious calculations.

The shear stress distribution is given by

$$\tau = p(t)\, r[\, 1 + \alpha^2 \frac{1}{p} \frac{dp}{dt} \phi(r,t) \,] , \tag{13}$$

where $\phi(r,t)$ is the known function of r and t. The shear stress on the vessel wall τ_w is a physiologically important quantity and is given by $\tau_w = \tau(r=1)$.

The velocity distribution is given by

$$u = p(t) \, [\, \phi_0(r,t) + \alpha^2 \frac{1}{p} \frac{dp}{dt} \phi_1(r,t) \,] , \tag{14}$$

where $\phi_0(r,t)$ and $\phi_1(r,t)$ are the known functions of r and t.

The velocity gradient ($\partial u^H / \partial r$) vanishes at a location of distance from the vessel axis, which is called plug core radius. The plug core radius R_y is given by solving the equation

$$| \tau^H (r = R_y , t) | = 0. \tag{15}$$

Substituting Eq. (13) into Eq. (15) and neglecting the terms of order α^4 and higher, we get

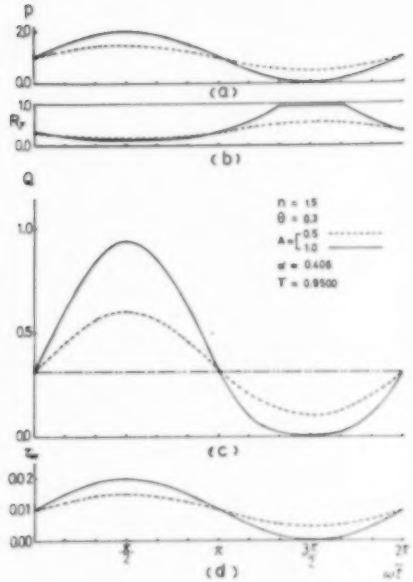

FIG. 2

The influence of reduced amplitude on blood flow. (a) Reduced pressure gradient, (b) Reduced plug core radius, (c) Reduced flow rate, (d) Reduced wall shear stress during one cycle. The quantities in steady state flow conditions (A=0) are denoted by the line — -- — .

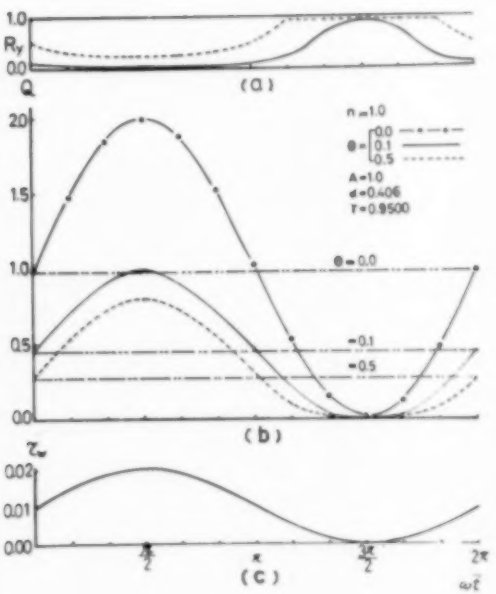

FIG. 3

The influence of reduced yield stress on reduced plug core radius (a), reduced flow rate (b) and reduced wall shear stress (c). The quantities in steady state flow conditions (A=0) are denoted by the line — -- — .

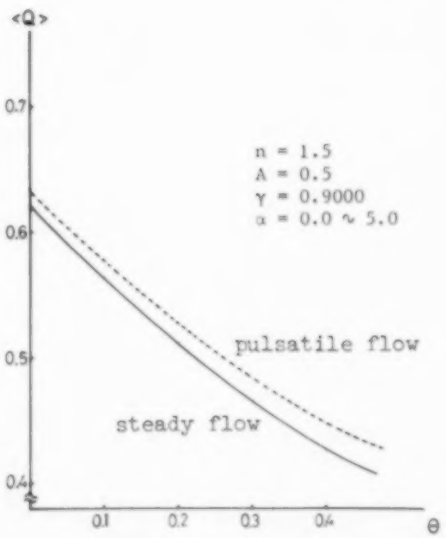

FIG. 4

The influence of reduced yield stress on mean and steady flow rate.

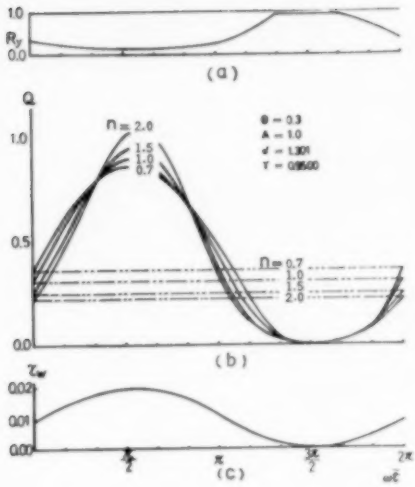

FIG. 5

The influence of parameter n on reduced plug core radius (a), reduced flow rate (b) and reduced wall shear stress (c). The quantities in steady state flow conditions (A=0) are denoted by line — -- — .

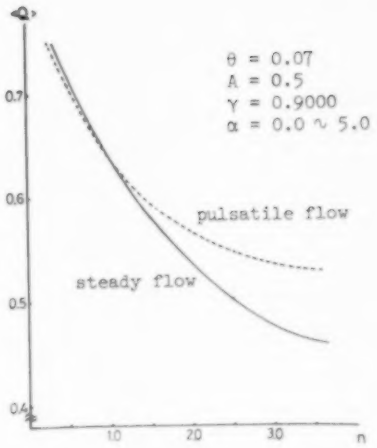

FIG. 6

The influence of parameter n on mean and steady flow rate.

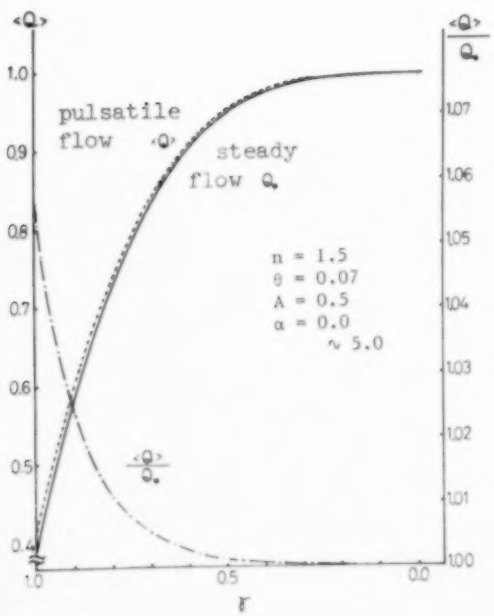

FIG. 7

The influence of the plasma layer thickness δ on mean and steady flow rate (γ=1-δ/R).

$$R_y = R_0 \left[1 + \alpha^2 \frac{1}{p}\frac{dp}{dt} \left\{ \frac{1}{4}(1-\gamma^2) + \frac{\eta_p}{2\eta_H} \frac{|p|^{n-1}}{n+1} \times (\gamma - R_0)^n (n\gamma + R_0) \right\} \right] \quad \text{for } R_y \le \gamma ,$$
$$= \gamma \quad \text{for } R_y \ge \gamma , \tag{16}$$

where

$$R_0 = \frac{\theta}{|p|} \tag{17}$$

FLOW RATE AND MEAN FLOW RATE

The volume $\overset{\gamma}{Q}$ of the fluid flowing per unit time across the cross section of the vessel is given by

$$Q(t) = \frac{\overset{\gamma}{Q}(t)}{Q_p} = p(t)\left[M(t) + \alpha^2 \frac{1}{p}\frac{dp}{dt} N(t) \right] , \tag{18}$$

where

$$Q_p = \frac{\pi R^4 p'}{8\eta_p} , \tag{19}$$

and M(t) and N(t) are the given functions of t.

Mean flow rate $\langle \overset{\gamma}{Q} \rangle$ is the average quantity of the flow rate $\overset{\gamma}{Q}(t)$ over a periode of one cycle of the periodic pressure gradient. The mean flow rate is a physiologically important quantity. The dimensionless mean flow rate $\langle Q \rangle$ is given by

$$\langle Q \rangle = \frac{1}{2\pi}\int_0^{2\pi} Q(t)\, dt . \tag{20}$$

The steady flow rate Q_0 is obtained by substituting p(t) = 1 into Eq. (18). That is, Q_0 is the flow rate under the constant pressure gradient p' which is equal to the mean pressure gradient $\langle p'p(t) \rangle$.

DISCUSSION

It is easily shown that our solution reduces to the Womersley's result which was obtained for the pulsatile flow of a Newtonian fluid, when the parameters in the Herschel-Bulkley equation are taken as n = 1, $f_H = 0$. Let's consider the case of vessel radius $R = 5 \times 10^{-3}$ cm, mean pressure gradient $p' = 0.6200 \times 10^4$ dyne/cm^3 of which plasma viscosity $\eta_p = 0.01$ poise in analytic values [9] obtained from steady blood flow in small vessels less than 100 μm diameter[10]. The difference between ρ_b and ρ_p is so small that we put $\rho_b = \rho_p$. We use values of the reduced amplitude A in Eq. (9) ranging from 0.5 to 1.0 to investigate the influence of amplitude on blood flow. The value of Womersley frequency parameter α [11] is about 0.1 in arterioles. In order to investigate the influence of α on blood flow, however, we use large values of α which satisfy the condition that the ratio of the second term to the first term in brackets of Eqs. (13),(14) and (18) is small compaired with unity. The yield stress f_H is about 0.14 dyne/cm^2 [12]. The reduced yield stress θ is about 0.1 in the case of $R = 0.5 \times 10^{-3}$ cm [9], $p' = 0.6200 \times 10^4$ dyne/cm^3. In this paper, we use values of θ ranging from 0.0 to 1.0 to investigate the influence of θ on blood flow. Parameter n [9] is 0.7 ∿ 2.0. We choose $\eta_H/\eta_p = 4.0$ as the typical value. The ratio of thickness of the plasma layer to the vessel radius δ/R may be 0.05 because the average thickness of the plasma layer is in the range between blood cell radius and blood cell diameter.

From Eqs. (13),(16) and (18) it can be seen that the influence of α on Q, τ_w and R_y is very small in the range of α<1.0. Because of the inertial effect the phase lag of Q and τ_w increases with the increase in α. Fig.2 shows the influence of the reduced amplitude A of pressure gradient on pulsatile blood flow. It can be seen that the values of Q, R_y and τ_w vary greatly with time for large value of A. It can also be seen that the mean flow rate $\langle Q \rangle$ increases with the increase in A. This is due to the increase of pressure gradient.

Vol. 17
1980

The change of the value of yield stress corresponds to the change of blood structure. The blood having a lower value of yield stress exhibits weaker structures. The value of τ_w is not affected very much with θ because of the presence of plasma layer. However, the value of R_y increases with the increase in θ throughout one cycle of pressure gradient (Fig. 3). As the result, the mean flow rate $\langle Q \rangle$ decreases with the increase in θ (Fig.4). As can be seen from Fig.4, the influence of α on $\langle Q \rangle$ is very small in the range of $\alpha<5$, and $\langle Q \rangle/Q_0$ is larger than unity.

The parameter n expresses a measure of shear thinning and the change of the value of n corresponds to the change of blood structure. From our analysis we can point out that the time dependence of Q is influenced by the value of n but R_y and τ_w are not influenced in the considered range of n (Fig.5). From Fig.6 it can be seen that the values of $\langle Q \rangle$ and Q_0 decrease with increase in n but the ratio $\langle Q \rangle/Q_0$ is larger than unity in the range $n > 1$.

The plasma layer serves as a lubricating layer. From our analysis we can point out that Q and $\langle Q \rangle$ increase with increase in the thickness of plasma layer δ but no significant change in R_y and τ_w occurs. We can also point out that in the range $n>1$ the ratio $\langle Q \rangle/Q_0$ is larger than unity and decreases monotonously with the increase in δ (Fig.7).

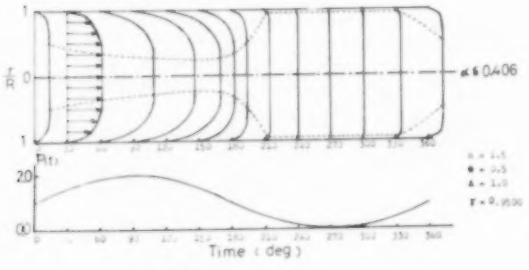

FIG. 8

Velocity profile during a cycle

Fig.8 shows velocity profiles during one cycle, where we assume A=1, θ=0.5 and n=1.5. The dashed lines indicate the radius of plug core R_y. The cardiac pulsation of blood flow velocity may be small in actual microvessels, but we use A=1 to show clearly the probable effects of non-Newtonian properties of blood on the velocity distribution. In this figure the blunt velocity profiles are seen. Although the degree of the bluntness is slight, the presence of the blunt profile in small living vessels is reported by some workers [10, 13,14,15]. The bluntness is probably attributable to the yield stress of blood. The mechanical generation of yield stress comes from the formation of rouleaux and aggregation of red blood cells.

From the results shown above, it seems probable that the flow properties in a small vessel are affected by the value of n and θ, as well as by the flow conditions.

REFERENCES

1. INTAGLITTA, M., RICHARDSON, D.R., and TOMPKINS, W.R. Blood pressure, flow and elastic properties in microvessels of cat omentum. Amer. J. Physiol. 221, 922-928, 1971.

2. CARO, C.G., REDLEY, T.J., SCHROTER, R.C., and SEED,W.A. The mechanics of the circulation. Oxford University Press, New York, 1978.

3. AROESTY, J. and GROSS, J.F. The mechanics of pulsatile flow in small vessel. I. Casson theory. Microvasc. Res. 4, 1-12, 1972.

4. AROESTY, J. and GROSS, J.F. Pulsatile flow in small blood vessels. I. Casson theory. Biorheology 9, 33-43, 1972.

5. WOMERSLEY, J.R. Oscillatory motion of a viscous liquid in a thin-walled elastic tube - I: The linear approximation for long waves. Phil. Mag. 46, 199-221, 1955.

6. SCOTT BLAIR, G.W. and SPANNER, D.C. An Introduction to Biorheology. Elsevier Scientific Publishing Company, Amsterdam, 1974, 51pp.

7. THURSTON, G.B. Elastic effects in pulsatile blood flow. Microvasc. Res. 9, 145-157, 1975.

8. THURSTON, G.B. The viscosity and viscoelasticity of blood in small diameter tubes. Microvasc. Res. 11, 133-146, 1976.

9. IIDA, N. Influence of plasma layer on steady blood flow in microvessels. Japan J. Appl. Phys. 17, 203-214, 1978.

10. EINAV, S., BERMAN, H.J., FUHRO, R.L., DIGIOVANI, P.R., FINE, S. and FRIDMAN, J.D. Measurment of velocity profiles of red blood cells in the microcirculation by Laser Doppler Anemometry (LDA). Biorheology, 12, 207-210, 1975.

11. McDONALD, D.A. Blood flow in arteries, 2nd edition. Edward Arnold London, 1974, 133pp.

12. CHARM, S. and KURLAND, G.S. Viscosity of human blood for shear rates of 0 - 100,000 sec^{-1}. Nature (London) 206, 617-618, 1965.

13. GAETHGENS, P., WAYLAND, H. and MEISELMAN, H.J. Theoretical and clinical hemorheology, Eds. Hartert, H.H. and Coply, A.L., Springer-Verlag, Berlin, Heidelberg, New York, 1971.

14. HORIMOTO, M., KOYAMA, T., MISHINA, H. and ASAKURA, T. Pulsatile blood flow in arterioles of frog web. Biorheology 16, 163-170, 1979.

15. HASEGAWA, M. and WAYLAND, H. Erythrocyte flow velocity in the microvessels of the rat mesentery. Angiology (in Japan) 20, 3-9, 1980.

Vol. 17
1980

BIORHEOLOGY, Vol. 17, pp. 385-390, 1980
Printed in the USA. All rights reserved.

0006-355X/80/040385-06$02.00/0
Copyright (c) 1980 Pergamon Press Ltd

FLOW OF BLOOD IN TRANSFUSION SYSTEMS

S. Palosaari* and K. Linko**

* Department of Chemical Technology, Lappeenranta University of Technology, Box 20, Lappeenranta 85, Finland

** Department of Anaesthesia, Helsinki University Central Hospital, Haartmaninkatu 4, 00290 Helsinki 29, Finland

(Received 1.5.1980; in revised form 7.7.1980.
Accepted by Editor G.V.F. Seaman)

ABSTRACT

The flow resistances caused by commercial elements used in blood transfusion systems were measured. These elements are comprised of microfilters, blood warmers, transfusion sets, and a venous cannula. In the absence of any occlusion in the filter it was found that the flow resistances caused by microfilters were low and without practical importance. Two warming devices were tested. The Fenwall^{R} "dry-heat" warmer was found to create a high flow resistance whereas the Portex^{R} Coil created only one third of the resistance of the Fenwal "dry-heat" warmer. Calculations from the experiments show that it is possible to substantially reduce the overall flow resistance created by the transfusion set and warmer. This may have practical importance although in practice the limiting factors to the flow may still be occlusion in the microfilter as well as flow resistance in the veins of the patient. In this work a simple method was developed enabling the flow resistance measurements to be made by the use of water or any Newtonian liquid. These values can be used to estimate the flow resistances to blood.

INTRODUCTION

Previous results on the flow rates of aggregate-free blood [1, 2] suggest that the flow resistance caused by in-line blood warmers limits their usefulness. Since these devices are already in general use it is important to study their flow properties in more detail. It is also necessary to acquire more information concerning the resistances of other elements of the transfusion system and to discuss blood flow in order to find out ways to minimize the overall flow resistance.

THE RHEOLOGICAL PROPERTIES OF BLOOD

According to experimental evidence by Walburn and Schneck [3] the general power law, i.e. the Ostwald-de Waele equation is valid for blood for shear rates above 23 reciprocal seconds:

$$\tau = K \left(\frac{dv}{dy} \right)^{n} \qquad (1)$$

where K is the flow consistency index, Pas^{n} ; τ is the shear stress, Pa ; n is the flow behaviour index, dimensionless ; and dv/dy is the shear rate, i.e. the rate of change of the velocity of the liquid with the distance from the solid wall.

Often the concept of apparent viscosity , η_{app} , is being used. It is defined as follows:

$$\eta_{app} = \tau/(dv/dy) \qquad (2)$$

Walburn and Schneck [3] developed various experimental expressions for the quantities K and n of equation (1) for blood. For the accuracy sufficient in the present work, the following expressions can be used, for blood at a temperature of 37°C.

Key Words: BLOOD TRANSFUSION , BLOOD FLOW VELOCITY

$$K = C_1 \exp(C_2 H) \quad (3\ A)$$

$$n = 1 - C_3 H \quad (3\ B)$$

where $C_1 = 1.48$ mPas^n, $C_2 = 0.0512$, $C_3 = 0.00499$, and H is hematocrit, per cent.

In order to calculate the pressure drop of blood at temperatures below 37°C it is necessary to know the values of K and n at lower temperatures. Rand et al. [4] and Schmid-Schönbein, Klose, Volger, and Weiss [5] have made measurements of apparent viscosity as a function of shear rate. Of these values only the ones in which the shear rate was at or above 23 reciprocal seconds were accepted, to ensure the validity of the general power-law, equation (1). These values of apparent viscosity as a function shear rate were fitted to equations (1) and (2). The results are shown in Table 1.

TABLE 1. The flow consistency index, K, and the flow behaviour index, n, of equation (1) for blood for shear rates at or above 23 reciprocal seconds.

Calculated from the experiments of	Hemato-crit, per cent	37°C K	37°C n	22°C K	22°C n	20°C K	20°C n	4°C K	4°C n
Schmid-Schönbein et al [5]	45	9.67	0.846	-		(18.5	0.776)	37.1	0.791
Rand et al [4]	40	11.4	0.795	20.7	0.776	-		-	
Walburn et al [3]	45	14.8	0.776	-		-		-	
	40	11.5	0.800	-		-		-	

The Schmid-Schönbein values in brackets in Table 1, at 20°C, are calculated as follows. At this temperature only one measurement is available from which the quantities K and n cannot both be calculated. The value of n was assumed to be the same as obtained by Walburn and Schneck [3] at 37°C. The value of K can then be calculated.

TURBULENCE IN FLOWING BLOOD

Eurenius and Smith [6] found increasing hemolysis taking place with increasing pressure of infusion. Under pressure of 40 kPa and with a 1.3 mm needle bore they found the plasma hemoglobin for fresh blood rising from 10.9 mg/100 cm^3 to 27.5 mg/100 cm^3 when the blood was at room temperature. For blood stored for seven days the corresponding values were 22.3 and 44.5 mg/100 cm^3. It is probable that the hemolysis is related to the Reynolds number of flow. Unfortunately, the information in the work of Eurenius and Smith is not sufficient for the construction of the hemolysis versus Reynolds number relationship. These authors mention that hemolysis above the level of 75 mg/100 cm^3 is of clinical significance, pointing out that the maximum value in their experiments was at room temperature. This means that blood at 37°C would have had nearly twice the Reynolds number, and a higher level of hemolysis would have occurred.

The Reynolds number for a power-law fluid can be calculated from the following equation:

$$Re' = 2^{7-5n}\, \pi^{n-2} \left(\frac{4n}{3n+1}\right)^n \frac{d^{3n-4}\, Q^{2-n}\, \rho}{K} \quad (4)$$

where d is the tube diameter, Q is the rate of flow, and ρ is the density of the fluid.

When a laminar flow enters a narrower tube where turbulence occurs it takes a length of about 100 tube diameters for the transition zone to end until the turbulence is even throughout the tube diameter. Infusion cannulas are usually shorter and thus blood may not be in a thoroughly turbulent state even though the Reynolds number exceeds the value above which the flow is turbulent in a straight tube. According to Longwell [7] the flow is turbulent if the Reynolds number is greater than 2219 with n = 0.8 . The flow properties of blood are here approximated by the power-law. Actually blood is a thixotropic fluid and this property may influence the value of the critical Reynolds number. Thus, though the maximal possible Reynolds number is not known for blood flow in a short cannula, it is reasonable to assume that the flow conditions below the Reynolds number of 2200 do not cause hemolysis of blood.

In Fig. 1 the laminar flow region is shown in the flow rate - cannula diameter -coordinates.

Vol. 17
1980

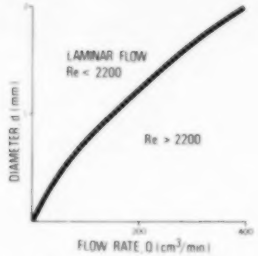

FIG. 1 The region of laminar flow, Re<2200, for blood, Hct 0.40, 37°C, as a function of the flow rate and tube diameter.

PRESSURE DROP IN BLOOD FLOW

Pressure drop in a tube for a power-law fluid can be calculated from the following equation:

$$\Delta p = \frac{2^{3n+2}}{\pi^n} \left(\frac{3n+1}{n}\right) K \left(\frac{L}{d^{3n+1}}\right) Q^n \qquad (5)$$

Values for the quantities K and n are given in Table 1. Using equation (5) and Table 1, Figures 2 and 3 have been calculated to show the pressure drop in the flow of blood in a straight tube.

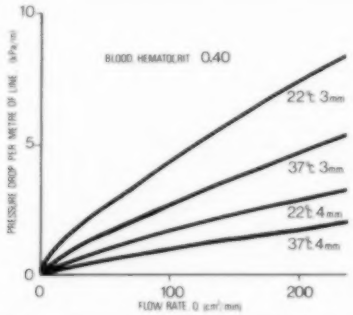

FIG. 2 Pressure drop of 0.40 hematocrit blood at 22°C and 37°C through 3 mm and 4 mm (internal diameter) lines per one metre of line as a function of flow rate.

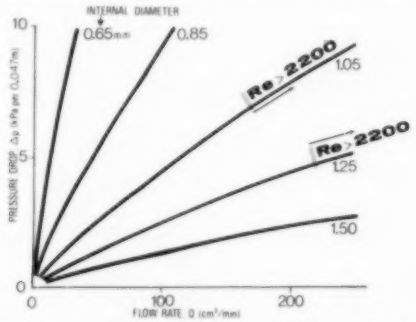

FIG. 3 Pressure drop of 0.40 hematocrit blood at 37°C in flow conduits of various internal diameters per a length of 0.047 m. This was the length of the venous cannula used in the experiments.

Equation (5) is valid only if the flow is laminar and if the power-law is valid, i.e. the shear rate is above 23 reciprocal seconds. The relationship between the flow rate and the shear rate can be calculated from the known relationship between the shear rate and the velocity of bulk flow, as given by Longwell [7, p.386], here given in terms of flow rate:

$$\left(-\frac{dv}{dy}\right)_o = \left(\frac{3n+1}{4n}\right)\frac{32\,Q}{\pi d^3} \qquad (6)$$

where the subscript o refers to the shear rate by the wall where it attains its greatest value. In Figures 2 and 3 a shear rate of less than 23 reciprocal seconds occurs at very low flow rates, for example in a tube of 3 mm diameter the flow rate is about 3 cm^3/min.

FLOW RESISTANCES

It is not a simple matter to calculate the pressure drop for every element of the flow line. For example, a filter consists of a configuration of flow conduits of various lengths and diameters. It is therefore more convenient to determine the pressure drop experimentally.

Measurements were made of the flow resistances created by various elements of the transfusion line. In the first series of measurements the liquid used was glycerol-water mixture of 10 mPas(=cP) viscosity. The results of the measurements are shown in Fig. 4.

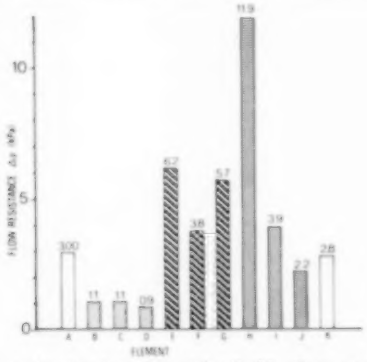

FIG. 4 Flow resistances to a Newtonian liquid of 10 mPas viscosity at the flow rate of 35.8 cm^3/min of the following elements of the transfusion system:

A Straight tube of circular cross section, length one metre, internal diameter 3 mm.

Microfilters:

B Fenwal^R (F4C 2423)
C MF10B^R (740255 Biotest-Serum-Institut GmbH, Frankfurt a.M.)
D Intersept^R (Johnson & Johnson, HRI 8137-00(1322))

Transfusion Sets:

E Fenwal^R (recipient set FDC 2115), length of line 204 mm, internal diameter 3 mm.
F MF 10B^R, 154 mm, internal diameter 3 mm.
G Intersept^R , length 178 mm, internal diameter 3 mm.

Warming Devices:

H Fenwal^R Blood Warmer (F4R 4306) and plastic blood warming unit (F4C 2416).
I Portex^R Coil (Portex Limited, Ref. 200/700/000)
J Double Portex^R Coil , made by cutting the coil into two halves in the middle, and by connecting the two halves for parallel flow. The resulting pressure drop is about half that of a single full coil, as expected.

Venous Cannula:

K Venflon^R (Viggo AB, No. 2) with 1.50 mm internal diameter and 47 mm length.

Vol. 17
1980

Because blood is not a Newtonian liquid, Fig. 4, as such, cannot be used to estimate the blood flow resistances of the various elements. According to equation (5), the flow behaviour index, n, appears in the exponent of the diameter of the flow conduit, which is not known. To overcome this difficulty it is necessary to determine the flow resistance of the element for two liquids of different viscosities. Subsequently, the equivalent length and equivalent diameter of the flow channel can be calculated from equation (5). This method was adopted and the length and the internal diameter of a venous cannula was calculated from the pressure drop measurements with glycerol-water and blood. Unfortunately, this method proved to be rather sensitive to measurement errors, and erroneous values were obtained for the length and diameter, i.e. slight inaccuracies in measurement create great inaccuracies in length and diameter.

Therefore, it was necessary to develop a simple approximate method for quick estimation of the flow resistance of the various elements to blood, starting from the flow resistances to Newtonian liquid as shown in Fig.4. In this way it is possible to avoid using blood in the making of measurements.

Perhaps the simplest possible assumption of the relationship between the pressure drops in Newtonian and non-Newtonian liquids is as follows:

$$(\Delta p_s/\Delta p_{el})_N \approx (\Delta p_s/\Delta p_{el})_{non\text{-}N} \qquad (7)$$

where Δp_s is the pressure drop of a straight line, Δp_{el} is the pressure drop in the element studied, and the subscript N refers to Newtonian liquid.

The above equation is approximately valid if the effective flow radii in the straight line and in the channels of the element do not differ greatly.

In the above equation (7) the first term, the quotient $(\Delta p_s/\Delta p_{el})_N$ is available for some elements in Fig.4 , whereas in the second term the pressure drop Δp_s for a non-Newtonian liquid, in this case blood, is available in Fig.2.

In this work the flow resistances of various elements to 20°C blood were measured. The measured values, together with the predicted values from equation (7) using the method described above, are shown in Table 2. According to the results the present method is sufficiently accurate to enable the flow resistances for a Newtonian liquid to be used to predict the flow resistances for blood.

TABLE 2. Experimentally determined values of flow resistance to blood at 20°C compared with the values calculated by the approximate method presented in this work.

Element	Measured flow resistance, kPa with 35.8 cm^3/min, at 20°C	Predicted flow resistance kPa with 35.8 cm^3/min, at 20°C
Intersept Filter	0.6±0.3	0.6
Intersept Transfusion Set	3.4±0.2	3.8
Portex Coil	2.6±0.2	2.6
Venous Cannula, Viggo No. 2	1.3±0.3	0.96

An unknown flow resistance of an element of a transfusion line can be measured, for any Newtonian liquid, and for any convenient rate of flow. From the obtained value the approximate flow resistance of this element to blood can be calculated with equation (7), and Figs. 4 and 2.

In the following example the flow reistance of an element X is measured to be 4 kPa for 20°C water at 200 cm^3/min flow rate. The flow resistance of the same element is then calculated for 37°C blood of 0.40 hematocrit when the flow rate is 100 cm^3/min, as follows:

$$\frac{4\ \text{kPa}\ \left(\frac{10\ \text{mPas}}{1\ \text{mPas}}\right)\left(\frac{38.5\ cm^3/min}{200\ cm^3/min}\right)}{3\ \text{kPa}} \cdot 2.7\ \text{kPa} \approx 6.9\ \text{kPa}$$

In the above expression the viscosity of 10 mPas and the flow rate of 38.5 cm^3/min pertain to the glycerol-water mixture, for which the pressure drops shown in Fig.4 were measured. The viscosity of 1 mPas and the flow rate of 200 cm^3/min pertain to the flow of water.

Furthermore, the pressure drop of 3 kPa is that of the glycerol-water mixture through a 3 mm tube per metre, whereas the pressure drop of 2.7 kPa is the flow of blood at 37°C through a 3 mm tube with 100 cm^3/min flow rate as given in Fig. 2.

DISCUSSION

The above calculations show that blood flow under ordinary transfusion conditions is laminar, and that this enables the flow resistances to blood to be calculated.

Fig.2 shows that the flow resistance falls to less than half if the internal diameter of the transfusion line is increased from 3 mm to 4 mm. An additional decrease in flow resistance gained by increasing the internal diameter of the transfusion line above 4 mm does not decrease the total resistance very effectively, as the flow resistance of the line already falls below that of the venous cannula and the Portex Coil, Fig. 4. Also Fig.2 shows that blood at 37°C causes about two thirds of the flow resistance of blood at room temperature.

Comparison of Figs. 3 and 4 shows that a venous cannula with an internal diameter of 1.05 mm already creates the greatest flow resistance in the system,excluding the Fenwal Blood Warmer which has a very high flow resistance. Cold whole blood should be microfiltered and warmed during massive transfusions. The blood flow rates, however, tend to remain low even if the Portex Coil is used for warming, as shown by Linko [8]. The high flow resistances created in the Fenwal Warmer , Fig.4, thus make it less suitable for rapid blood replacement.

The flow resistance of the microfilters accounts for only 5 to 11 per cent of the resistance of the total transfusion equipment. This indicates that their flow resistances are of minor practical implication until they become occluded by aggregates. Microfilters with the highest filtration capacities, e.g. Bentley^R PFF-100 and Fenwal^R 4C2423, tolerate up to three litres of 21-day-old blood until they become so obstructed by debris that the blood flow rate begins to decrease significantly, as shown by Linko [9].

Vol. 17
1980

REFERENCES

1. LINKO, K. In-line blood warming and microfiltration devices I. Testing of flow and warming properties by pressure transfusion of aggregate-free blood. Acta Anaesthesiol. Scand. 23,40-45,1979.

2. LINKO, K. In-line blood warming and microfiltration devices II. Influence of blood temperature on flow rate and hemolysis during pressure transfusion through microfilters and transfusion sets. Acta Anaesthesiol. Scand. 23,46-50,1979.

3. WALBURN, F.J. and SCHNECK,D.J. A constitutive equation for whole human blood. Biorheology 13,201-210,1976.

4. RAND, P., LACOMBE, H.E. and AUSTIN, W.H. Viscosity of normal human blood under normothermic and hypothermic conditions. J.Appl. Physiol. 19 ,117-122,1964.

5. SCHMID-SCHÖNBEIN, H.,KLOSE,H.J., VOLGER, E. and WEISS, J. Hypothermia and blood flow behavior. Res.Exp.Med. 161,58-68,1973.

6. EURENIUS, S. and SMITH, R.M. Hemolysis in blood infused under pressure. Anesthesiology 39, 650-651,1973.

7. LONGWELL, P.A., Mechanics of Fluid Flow.New York:McGraw-Hill Book Company, 1966, pp. 386,391.

8. LINKO, K. Warming of stored blood for massive transfusions.Dissertation. University of Helsinki, 1979.

9. LINKO, K. An in vitro comparison of six microaggregate blood filters. Acta Anaesthesiol. Scand., 23,603-612,1979.

BIORHEOLOGY, Vol. 17, pp. 391-396, 1980
Printed in the USA. All rights reserved.

0006-355X/80/040391-06$02.00/0
Copyright (c) 1980 Pergamon Press Ltd

MATHEMATICAL ANALYSIS OF THE HYSTERESIS RHEOGRAM OF HUMAN BLOOD

W. Fabisiak and C. R. Huang

Department of Chemical Engineering and Chemistry
New Jersey Institute of Technology
323 High Street
Newark, N. J. 07102

(Received 11.12.1979; in revised form 5.8.1980.
Accepted by Editor Y.C. Fung)

ABSTRACT

Human blood is a thixotropic fluid whose apparent viscosity is a function of the shear rate and the duration of shear. One of the most important characteristics of human blood is that its rheogram of shear stress versus shear rate exhibits a hysteresis loop. This hysteresis loop is obtained from a plot of shear stress versus shear rate in which the shear rate is steadily and linearly increased to a maximum value and then immediately decreased at the same rate toward the starting value. Recently, hysteresis loop analysis has been used to characterize the thixotropic behavior of human blood. In this paper, we obtain an analytical solution of the Navier-Stokes equation for the case of transient flow in a Couette viscometer under the conditions of a ramp function angular velocity. This ramp function is used to generate the hysteresis loop rheogram. Analysis of the solution shows that it is possible for a Newtonian fluid to exhibit a hysteresis loop under certain experimental conditions. The size and shape of this generated loop was found to be controlled by a dimensionless group. From this analysis, we are able to determine the true hysteresis loop for human blood. Our analysis can also be used to detect and eliminate the presence of any artificial hysteresis loops generated by Newtonian fluids.

INTRODUCTION

Whole human blood has been experimentally characterized as a thixotropic fluid whose apparent viscosity is a function of the shear rate and the duration of shear (1). The rheological behavior of human blood can be demonstrated in the form of two rheograms, a hysteresis loop and a torque-decay curve. The hysteresis loop is obtained from a plot of shear stress versus shear rate in which the shear rate is steadily and linearly increased to a maximum value and then immediately decreased at the same rate toward the starting value. The torque-decay curve is obtained from a plot of the shear stress versus time under conditions of constant shear rate. Recent investigations (2,3,4) have incorporated hysteresis loop and torque-decay analysis with a generalized rheological equation (5) to characterize the rheological behavior of human blood in terms of various thixotropic parameters.

In this paper, we focus our attention on the mathematical analysis of the hysteresis loop rheogram. We have obtained an analytical solution of the Navier-Stokes equation for the case of transient flow in a Couette viscometer under the conditions of a ramp function angular velocity. The ramp function is used to generate the hysteresis loop rheogram. Analysis of the solution indicates that it is mathematically possible for a Newtonian fluid to exhibit a hysteresis loop under certain experimental conditions. The size and shape of this artificial hysteresis loop generated by a Newtonian fluid was found to be controlled by a dimensionless group. Theoretical hysteresis loop rheograms for Newtonian, pseudoplastic, and thixotropic fluids are shown in Figure 1. Human blood will display pseudoplastic behavior after an extended period of shear, but will regain its thixotropic behavior once the shear field is removed. Under high rates of shear, human blood may display Newtonian behavior.

Transient flow of an incompressible Newtonian fluid in a Couette viscometer was first investigated by Bird and Curtiss (6). They obtained an exact

Key Words: Hysteresis loop, analysis, thixotropic behavior, blood

solution to the Navier-Stokes equation under the conditions of a step change in angular velocity. Their analysis describes the mathematics of the torque-decay curve. Recently, Ramkissoon and Majumdar (7) examined the transient flow of a micropolar fluid in a Couette viscometer using a sinusoidal angular velocity. In this paper, we extend the analysis of transient flow in a Couette viscometer to consider the case of a ramp function angular velocity.

THEORY

For an incompressible, Newtonian fluid undergoing isothermal flow, the equations of continuity and motion are:

$$\nabla\cdot\vec{v} = 0 \tag{1}$$

$$\rho \frac{\partial\vec{v}}{\partial t} = -\rho[\nabla\cdot\vec{v}\vec{v}] - \nabla p + \mu\nabla^2\vec{v} + \rho\vec{g} \tag{2}$$

where ρ is the fluid density, $\vec{v}$ is the velocity vector, p is the static pressure, μ is the Newtonian viscosity, and $\vec{g}$ is the gravitational force per unit mass.

In a Couette viscometer, the fluid occupies the annular region between a pair of concentric cylinders with radii κR, R and length L (see Figure 2. At time $t < 0$, the fluid within the annulus is at rest. At $t > 0$, the inner cylinder remains stationary and the outer cylinder is subjected to a ramp function change in its angular velocity (see Figure 3). The ramp function change in angular velocity is required to generate the hysteresis loop rheogram. For an incompressible, Newtonian fluid in this application, the equation of motion becomes

$$\rho \frac{\partial v_\theta}{\partial t} = \mu \frac{\partial}{\partial r}\left[\frac{1}{r}\frac{\partial (r v_\theta)}{\partial r}\right] \tag{3}$$

The initial and boundary conditions are as follows:

$$v_\theta(r,0) = 0 \tag{3-1}$$

$$v_\theta(\kappa R,t) = 0 \tag{3-2}$$

$$v_\theta(R,t) = F(t) \tag{3-3}$$

where

$$F(t) = aRt \; ; \; 0 \le t \le t_1 \tag{3-4}$$

$$F(t) = 2aRt_1 - aRt \; ; \; t_1 \le t \le 2t_1 \tag{3-5}$$

and a is the angular acceleration of the outer cylinder with t_1 being the time necessary for the angular velocity of the outer cylinder to reach its maximum value.

Since one of the boundary conditions is time-dependent, it is necessary to use Duhamel's Theorem (8) to obtain a solution to equation (3). According to Duhamel's Theorem, the velocity function in the angular direction may be obtained from the relationship

$$v_\theta(r,t) = \int_0^t F'(t-\xi)V(r,\xi)\,d\xi \tag{4}$$

where F' is the time derivative of the time-dependent boundary condition and V represents a velocity function in the angular direction which satisfied equation (3) with the following initial and boundary conditions:

$$V(r,0) = 0 \tag{5-1}$$

$$V(\kappa R,t) = 0 \tag{5-2}$$

$$V(R,t) = 1 \tag{5-3}$$

Applying the method of separation of variables to equation (3) subject to the above initial and boundary conditions, the velocity function V becomes

$$V(r,t) = \frac{\chi r}{R} - \frac{\psi R}{r} + \sum_{n=1}^{\infty} E_n Z_1(\zeta\beta_n r)\exp[-\beta_n^2 t] \tag{6-1}$$

where

$$\chi = 1/(1-\kappa^2) \tag{6-2}$$

$$\psi = \kappa^2/(1-\kappa^2) \tag{6-3}$$

$$\zeta = \sqrt{\rho/\mu}$$

$$Z_1(\zeta\beta_n)r = J_1(\zeta\beta_n r)Y_1(\zeta\beta_n\kappa R) - Y_1(\zeta\beta_n r)J_1(\zeta\beta_n\kappa R) \tag{6-4}$$

Vol. 17
1980

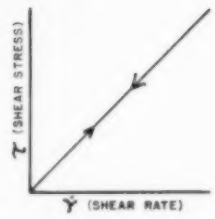

Figure Ia. Hysteresis Loop Rheograms For A Newtonian Fluid

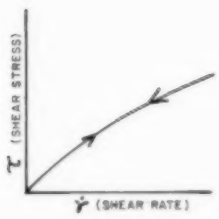

Figure Ib. Hysteresis Loop Rheogram For A Pseudo Plastic Fluid

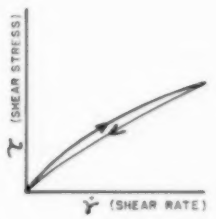

Figure Ic. Hysteresis Loop Rheogram For A Thixotropic Fluid

Figure I. Hysteresis Loop Rheograms

FIGURE 2: Couette Viscometer

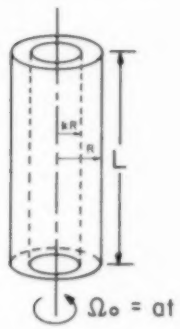

FIGURE 3: Ramp Function Angular Velocity

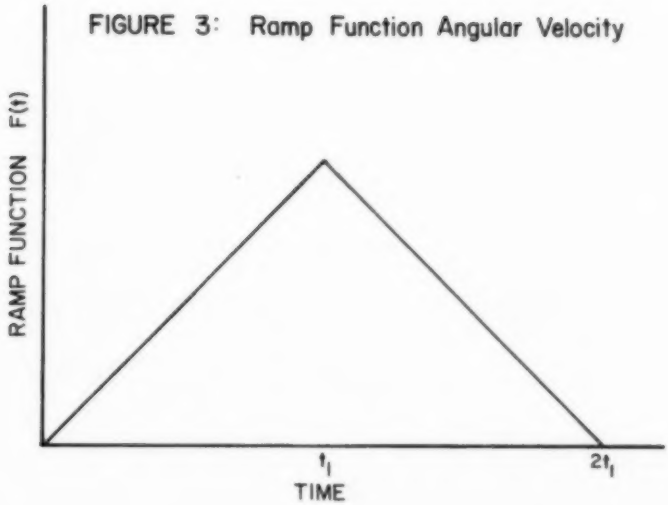

with J_1 and Y_1 being first order Bessel functions of the first and second kind, respectively. The eigenvalues β_n satisfy the relationship

$$J_1(\zeta\beta_n\kappa R)Y_1(\zeta\beta_n R) = J_1(\zeta\beta_n R)Y_1(\zeta\beta_n\kappa R) \tag{7}$$

The series constants E_n are obtained by means of a Sturm-Liouville analysis which yields

$$E_n = \frac{\frac{\chi}{R}[R^2Z_0(\zeta\beta_n R) - \kappa^2R^2Z_0(\zeta\beta_n\kappa R)] - \psi R[Z_0(\zeta\beta_n R) - Z_0(\zeta\beta_n\kappa R)]}{\frac{1}{2}\zeta\beta_n[R^2Z_0^2(\zeta\beta_n R) - \kappa^2R^2Z_0^2(\zeta\beta_n\kappa R)]} \tag{8}$$

Applying Duhamel's Theorem to the present situation, the angular velocity function becomes, when $0 \leq t \leq t_1$,

$$v_\theta(r,t) = a[\chi r - \frac{\psi R^2}{r}]t + \sum_{n=1}^{\infty} \frac{aRE_n}{\beta_n^2} Z_1(\zeta\beta_n r)[1 - \exp[-\beta_n^2 t]] \tag{9}$$

and when $t_1 \leq t \leq 2t_1$,

$$v_\theta(r,t) = a(\chi r - \frac{\psi R^2}{r})(2t_1 - t) + \sum_{n=1}^{\infty} \frac{aRE_n}{\beta_n^2} Z_1(\zeta\beta_n r)(1 - 2\exp(-\beta_n^2 t_1) + \exp(-\beta_n^2 t)) \tag{10}$$

Once the velocity function $v_\theta(r,t)$ has been determined, the shear stress distribution $\tau_{r\theta}(r,t)$ and the torque $T(t)$ applied by the fluid to the inner cylinder may be obtained from the following relationships:

$$\tau_{r\theta}(r,t) = -\mu r \frac{\partial}{\partial r}(v_\theta(r,t)/r) \tag{11}$$

$$T(t) = 2\pi\kappa^2R^2L\{-\tau_{r\theta}(r,t)\}_{r=\kappa R} \tag{12}$$

Therefore, when $0 \leq t \leq t_1$,

$$\tau_{r\theta}(r,t) = -\mu(\frac{2a\psi R^2 t}{r^2} - \sum_{n=1}^{\infty} \frac{\zeta aRE_n}{\beta_n} Z_2(\zeta\beta_n r)\{1 - \exp(-\beta_n^2 t)\}) \tag{13}$$

$$T(t) = 4\pi aL\psi R^2\mu t + 2\pi aL\kappa^2R^3\sqrt{\rho\mu}(\sum_{n=1}^{\infty} \frac{E_n}{\beta_n} Z_0(\zeta\beta_n\kappa R)\{1 - \exp(-\beta_n^2 t)\}) \tag{14}$$

and for $t_1 \leq t \leq 2t_1$,

$$\tau_{r\theta}(r,t) = -\mu(\frac{2a\psi R^2}{r^2}(2t_1 - t) - \sum_{n=1}^{\infty} \frac{\zeta aRE_n}{\beta_n} Z_2(\zeta\beta_n r)\{1 - 2\exp(-\beta_n^2 t_1) + \exp(-\beta_n^2 t)\}) \tag{15}$$

$$T(t) = 4\pi aLR^2\mu\psi(2t_1 - t) + 2\pi aL\kappa^2R^3\sqrt{\rho\mu}(\sum_{n=1}^{\infty} \frac{E_n}{\beta_n} Z_0(\zeta\beta_n\kappa R)\{1 - 2\exp(-\beta_n^2 t_1) + \exp(-\beta_n^2 t)\}) \tag{16}$$

Since both torque functions consist of two groups of terms, we may express the torque function as

$$T(t) = T_1(t) + T_2(t) \tag{17}$$

where the functions $T_1(t)$ and $T_2(t)$ are defined by equations (14) and (16). Examination of these equations indicates that the function $T_1(t)$ is a linear function of time for both the upcurve and the downcurve of the hysteresis loop rheogram. These equations also show that the function $T_2(t)$ is a series of first order responses with successively diminishing amplitudes. Typical representations of these classes of functions are shown in Figure 4. The total measured torque is simply the graphical sum of these two response functions. This graphical addition is demonstrated in Figure 5.

For a Newtonian fluid, the linear response function $T_1(t)$ represents the theoretically anticipated response of the shear stress under a ramp input in the shear rate. This indicates that $T_1(t)$ is the primary response function for a Newtonian fluid and that the first order response function $T_2(t)$ represents secondary responses of the shear stress under a ramp input in the shear rate. These secondary responses would be responsible for the presence of any hysteresis loops that may be observed. This analysis indicates that it is possible for a Newtonian fluid to exhibit time-dependent non-Newtonian behavior under certain experimental conditions.

In order to minimize or eliminate the presence of any artificial non-Newtonian effects, it would be necessary to demonstrate that these secondary responses are negligible with respect to the primary response function under the prevailing experimental conditions. This may be readily accomplished by the

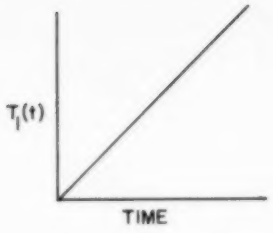

Figure 4a. Linear Response Function $T_1(t)$

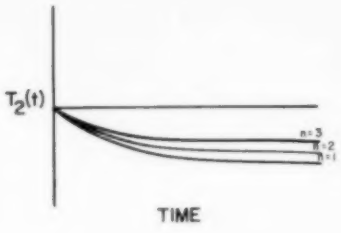

Figure 4b. First Order Response Function $T_2(t)$

Figure 4. Response Functions

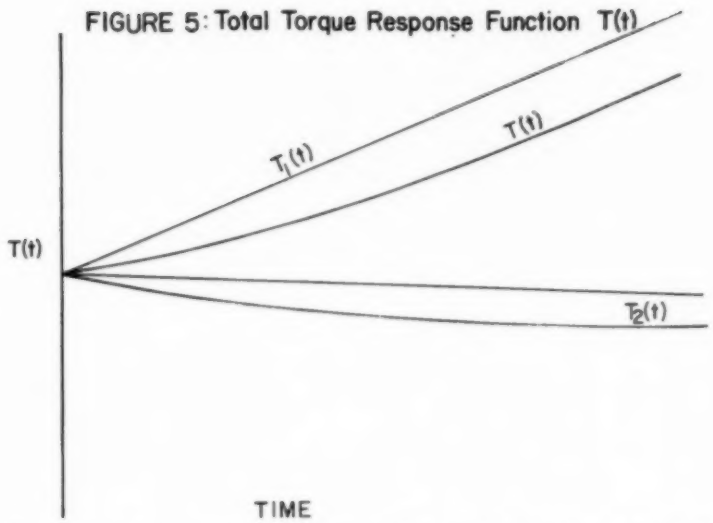

numerical evaluation of a dimensionless group. The appropriate dimensionless group is formed by rewriting the total torque functions in a dimensionless form. Thus equation (14) becomes

$$T^*(\sigma) = \sigma + \frac{(1 - \kappa^2)R\zeta}{2t_1}\left(\sum_{n=1}^{\infty} \frac{E_n}{\beta_n} Z_0(\zeta\beta_n\kappa R)\{1 - \exp(-\beta_n^2 t_1\sigma)\}\right) \tag{18}$$

where

$$\sigma = t/t_1 \tag{19-1}$$

$$T^*(\sigma) = \frac{(1 - \kappa^2)T(t)}{4\pi aL\kappa^2 R^2 \mu t} \tag{19-2}$$

The quantities σ and $T^*(\sigma)$ represent dimensionless time and torque, respectively. Similarly, equation (16) becomes

$$T^*(\sigma) = (2 - \sigma) + \frac{(1 - \kappa^2)R\zeta}{2t_1}\left(\sum_{n=1}^{\infty} \frac{E_n}{\beta_n} Z_0(\zeta\beta_n\kappa R)\{1 - 2\exp(-\beta_n^2 t_1) + \exp(-\beta_n^2 t_1\sigma)\}\right) \tag{20}$$

The series portions of equations (18,20) are monotonic decreasing functions in total torque. The first term in these types of functions is normally the controlling term, such that the following dimensionless group, N_{HF},

$$N_{HF} = \frac{(1 - \kappa^2)R\zeta E_1 Z_0(\zeta\beta_1\kappa R)}{2t_1\beta_1} \tag{21}$$

may be considered to be the controlling factor for the magnitude of these secondary responses for both the upcurve and the downcurve of the hysteresis loop rheogram. If this dimensionless group is small with respect to unity, then the experimentally observed rheological behavior is representative of the material being examined. Therefore, the dimensionless group, N_{HF}, may be used to detect and minimize the presence of any artificially induced non-Newtonian behavior.

RESULTS AND DISCUSSION

We have examined the relative magnitude of the dimensionless group, N_{HF}, for two cases which are representative of the experimental conditions under which we have investigated the thixotropic behavior of human blood. We have concentrated our investigation on the viscosity as our variable of interest because our Couette geometry was fixed and the density of our samples remained essentially constant. Since most of our experimentally investigated blood samples possessed an apparent viscosity between 0.1 and 0.2 poise, it was felt that these two cases would be sufficiently representative of our experimental analysis of the thixotropic behavior of human blood. These results are shown in Table 1.

TABLE 1

Case I	Case II
R = 1.6 cm	R = 1.6 cm
ρ = 1.06 g/cm^3	ρ = 1.06 g/cm^3
μ = 0.10 poise	μ = 0.20 poise
κ = 0.95	κ = 0.95
N_{HF} =-0.000862	N_{HF} =-0.000427
t_1 = 10 sec	t_1 = 10 sec

For both sets of conditions, the magnitude of the dimensionless group was small compared to unity and indicated that a Newtonian fluid, under these experimental conditions, would not generate an artificial hysteresis loop. Therefore any hysteresis loop observed under these conditions must be attributed to the thixotropic nature of the material being examined. Thus, the hysteresis loop behavior we have observed is a direct result of the thixotropic nature of human blood.

This dimensionless group may be used to determine the relative magnitude of the secondary responses that are present during any desired set of experimental conditions. We have used this dimensionless group in our analysis of the thixotropic behavior of human blood. This group was evaluated to insure that any observable hysteresis loop was truly a result of the thixotropic nature of blood and not an artifact created by the prevailing set of experimental conditions. This analysis is not restricted to blood, but may be applied to any thixotropic material.

REFERENCES

1. HUANG, C.R., SISKOVIC, N., ROBERTSON, R.W.J., WANG, H.H., and OROSZ, P.J., Jr., "Thixotropy of Human Blood," presented at the 1st International Congress of Biorheology, Lyon, France, August, 1972.

2. HUANG, C.R. SISKOVIC, N., ROBERTSON, R.W.J., FABISIAK, W., SMITHBERG, E.H., and COPLEY, A.L., Biorheology, 12, 279 (1975).

3. HUANG, C.R. and FABISIAK, W., "A Rheological Equation Characterizing Both the Time-Dependent and the Steady State Viscosity of Whole Human Blood," AIChE Symposium Series, 182, Vol. 74, 19-21, (1978).

5. HUANG, C.R., Chem. Eng. J., 3, 100 (1971).

6. BIRD, R.B. and CURTISS, C.F., Chem. Eng. Sci., 11, 108 (1959).

7. RAMKISSOON, H. and MAJUMDAR, Can. J. Chem. Eng., 55, 408 (1977).

8. CHURCHILL, R.V., "Operational Mathematics," 2nd Edition, McGraw-Hill, New York (1958).

Vol. 1
1980

BIORHEOLOGY, Vol. 17, pp. 397-398, 1980
Printed in the USA. All rights reserved.

0006-355X/80/050397-02$02.00/0
Copyright (c) 1981 Pergamon Press Ltd

ol. 17
980

EDITORIAL

WELCOME TO NEW EDITORS. THE NEW FORMAT OF BIORHEOLOGY AND COMMUNICATIONS PERTAINING TO CLINICAL BIORHEOLOGY OTHER THAN CLINICAL HEMORHEOLOGY

The Editorial published in issue 3 of volume 17, 1980 dealt among others, under separate headings, with the following topics: Revised editorial policy concerning additional Editors, communications concerning clinical hemorheology and the new journal CLINICAL HEMORHEOLOGY. A Companion Journal of BIORHEOLOGY , and revised Instructions to Authors.

New Editors Alice Maroudas and Yukio Hiramoto

We are pleased to welcome Professor Maroudas (United Kingdom) and Professor Hiramoto (Japan) as additional Editors of the Editorial Board.

The New Format of BIORHEOLOGY

This double issue 5/6 of volume 17 is published in the old size. However, any communications and other texts will be published in the smaller format given in the Instructions to Authors. It is, therefore, necessary that Authors submit communications in accordance with the Aims and Editorial Policy and Instructions to Authors printed in each issue of BIORHEOLOGY. Any communications typed on the laysheets of the present size and format can no longer be considered for publication by an Editor. The new size will make it handier to our Readers. Laysheets can be secured from any of the Editors of BIORHEOLOGY or from the Executive Editorial Office.

We should like to emphasize that a communication must adhere strictly to the Instructions to Authors. We have advised our Editors not to consider a manuscript and return it to the Author(s), if it does not follow fully the Instructions to Authors. A date of receipt of a manuscript can be given by an Editor only, if it follows strictly these Instructions. We, therefore, must re-emphasize that Authors as well as the typists of manuscripts must acquaint themselves in every detail with the Instructions to Authors. This will make it possible for an Editor to consider a communication for publication without delay and, if accepted by the Editor, lead to its rapid publication.

Communications of Clinical Biorheology Other than Clinical Hemorheology

Communications on theoretical and experimental hemorheology will be published as before in BIORHEOLOGY. This is also the case with communications on clinical biorheology other than clinical hemorheology. However, communications on clinical hemorheology will need to be submitted from now on to an Editor of CLINICAL HEMORHEOLOGY.

Since CLINICAL HEMORHEOLOGY is a companion journal of BIORHEOLOGY, as stated in its subtitle, a communication on clinical hemorheology submitted to an Editor of BIORHEOLOGY can be sent by this Editor to an Editor of his/her choice to an Editor of CLINICAL HEMORHEOLOGY. Conversely, a communication on theoretical hemorheology or experimental hemorheology can be sent by an Editor of

CLINICAL HEMORHEOLOGY, if submitted to an Editor of CLINICAL HEMORHEOLOGY, to an Editor of his/her choice of BIORHEOLOGY. In both cases the Author will need to be informed to this effect by the Editor, to whom it was originally submitted, and by the Editor, who receives it. This procedure will make possible most rapid handling of a manuscript in the event it is not submitted to the proper journal. Such a transfer of manuscripts will be possible, because the Instructions to Authors for both journals are identical, as are the laysheets and the size of the journals.

Alfred L. Copley Alex Silberberg

Editors-in-Chief

Vol. 1
1980

BIORHEOLOGY, Vol. 17, pp. 399-402, 1980
Printed in the USA. All rights reserved.

0006-355X/80/050399-04$02.00/0
Copyright (c) 1981 Pergamon Press Ltd

A NOTE ON PLANE POISEUILLE FLOW OF COUPLE STRESS FLUID

P. CHATURANI

Department of Mathematics
Indian Institute of Technology, Bombay 400 076, INDIA

(Received 25.1.1980; in revised form 15.5.1980.
Accepted by Editor J.C. Healy.
Received by Executive Editorial Office 25.7.1980)

ABSTRACT

Plane Poiseuille flow of a couple stress fluid has been studied in this note. It is shown that the variation of couple stress parameter a can be interpreted in a more meaningful way. The existence of critical value of a has been predicted.

INTRODUCTION

Stokes (1) has considered various viscometeric flow problems to study the qualitative and quantitative effects of couple stresses on the flow. In the study of plane Poiseuille flow, the non-dimensional velocity U is given by

$$U(\xi) = \frac{u(\xi)}{u_o} = 1 - \xi^2 - \frac{2}{a^2}\left(1 - \frac{\cosh(a\xi)}{\cosh a}\right) , \qquad (1)$$

where

$$u_o = -\frac{h^2}{2}\frac{dp}{dx} , \quad a^2 = \frac{\mu h^2}{\eta} = \frac{h^2}{\ell^2} , \quad \xi = \frac{y}{h} , \qquad (2)$$

2h is the distance between the plates, μ is shear viscosity, η is couple stress parameter, u is velocity, y is a co-ordinate normal to flow direction and dp/dx is constant pressure gradient. The variation of velocity profiles with a, a couple stress parameter, has been computed from equation (1) and shown graphically. It is concluded that due to couple stresses 'size effect' comes in which is absent in Newtonian fluids. Here, it may be noticed from equation (2) that the non-dimensionalising velocity u_o, used in Ref. (1), is not constant with respect to h (apparatus size) - it contains h^2 [equation (2)]. Hence, one cannot study the effects of the variation of h on the velocity u with this non-dimensionalising velocity u_o. It is, therefore, necessary to find a new non-dimensionalising velocity, independent of h, if the effects of the variation of h are to be studied. Further, it is also important to note that there are some other interpretations of the variation of a which have physical meaning and are of importance from application point of view. Somehow these interpretations have been missed by Stokes, and this has led to serious misunderstanding. In the following text, some of these interpretations of variation of a have been discussed.

DISCUSSION

It is of interest to note that by definition [equation (2)] a is a function of three parameters, viz., h, μ and η. Therefore, any variation in a can be interpreted in seven different ways. Here, we shall restrict

Key Words: Plane Poiseuille Flow, Couple Stress Fluid, Size Effects, Viscometric Flows, Non-dimensionalising Velocity.

our studies to the variation of a to be interpreted in only three ways, i.e., we keep the two parameters fixed and allow the variation in third. Physically, this means to study the influence of each individual parameter on the flow. We shall now discuss these three cases separately.

Cowin (2) has shown that couple stress fluids are the special cases of polar fluids and their shear viscosity μ is given by

$$\mu = \mu_s + \frac{1}{2}\mu_R \ , \tag{3}$$

where μ_s is solvent viscosity and $\frac{1}{2}\mu_R$ is rotational viscosity. Ariman et al (3) have shown that μ_R is related with suspension concentration [Fig. 1, Ref. (3)]. At this stage, it must be made clear that μ_R depends on concentration and is independent of the size and shape of the particles. Hence, by virtue of equation (3), μ is a function of concentration and is independent of the size and shape of the particles. Let us now consider the case in which h and μ (concentration) are held fixed and η is allowed to vary, i.e., the shape and size of the particles is allowed to vary. This situation is of particular significance in blood flow. In such situations, it is observed that even though the concentration is fixed, the change in the size and shape of the particles leads to a change in the value of effective viscosity (increase in effective viscosity as the particle size increases) and change in the shape of velocity profiles. Since h and μ are fixed, the change in the value of effective viscosity, due to the change in the particle size and shape, could be attributed to the variation of η. Because an increase in the value of η leads to an increase in the value of the effective viscosity (from theoretical calculations) and an increase in the size of particles also gives rise to an increase in the effective viscosity, it appears to be logical to expect that the increase in the size of particle is related with the increase in η. Further, it means η is an increasing function of particle diameter. However, one feels that for a given value of μ and h, there will exist a critical value of η (particle size $\simeq h/5$); if the value of η, i.e., particle size, is increased (a decreased) beyond this, then the validity of continuum approach to the problem may be questionable. In the limiting case when $\eta \to 0$, i.e., particle size tends to zero and $a \to \infty$, the velocity tends to become Newtonian (Newtonian velocity of fluid with viscosity μ and not μ_s).

We shall now consider another case of variation of a. Let h and η be constant and μ is allowed to vary (concentration variation under consideration). It may be noted from equation (2) that an increase in μ (concentration) leads to an increase in a. The velocity U increases with a, as shown in Fig. 1 of Ref. (1), i.e., velocity increases with μ. This is contrary to the experimental observations and intuitive expectations (velocity decreases as the concentration increases). The reason for this controversy is improper non-dimensionalisation of velocity in Ref. (1) - the non-dimensionalising quantity u_o is not constant with respect to μ [equation (2)]. We, therefore, suggest a new non-dimensionalising velocity u_1 which is constant with respect to μ and is given by

$$u_1 = -\frac{h^2}{2\mu_s}\frac{dp}{dx}. \tag{4}$$

The non-dimensional velocity U_μ is

$$U_\mu = \frac{u}{u_1} = \frac{\mu_s}{\mu}\left[1 - \xi^2 - \frac{2}{a^2}\left\{1 - \frac{\cosh(a\xi)}{\cosh a}\right\}\right]. \tag{5}$$

Now, it can be easily shown from equation (5) that U_μ decreases as a increases, e.g.,

$$S = \frac{U_{\mu 5}(0)}{U_{\mu 2}(0)} = \frac{0.1474}{0.6329}, \tag{6}$$

where S is the ratio of the axial velocities for $a = 5$ and 2. As expected, S is less than one. In the limiting case when the concentration c tends to zero, $\mu \to \mu_s$, and $a \to \infty$, the velocity tends to become Newtonian velocity (Newtonian velocity of the fluid with viscosity μ_s and not μ). The other limiting case is when $\mu \to \infty$, i.e., $a \to \infty$. In this case, the velocity U_μ tends to zero because the expression on the right hand side of equation (5) is zero – first term is zero and the term in square brackets is finite as $a \to \infty$. But, much before this limit ($\mu \to \infty$) is reached, suspension will become semi-solid and the continuum theory will cease to be valid for the deformations.

Finally, we shall discuss the effects of the variation of h (apparatus size). It may be noticed that an increase in h leads to an increase in a which in turn increases U [equation (1) or Fig. 1, Ref. (1)]. But this increase of U, given by equation (1), does not represent the full effect of the variation of h on velocity. Because the non-dimensionalising velocity u_o, used in Ref. (1), is not constant with respect to h - it contains h^2 [equation (2)]. Hence, one cannot study the effects of the variation of h on the velocity with this non-dimensionalising velocity u_o. Since ℓ, the material characteristic length [equation (2)], does not change with h, one can use the following expression for the non-dimensionalising velocity in such situations :

$$u_h = -\frac{dp}{dx} \cdot \frac{\ell^2}{2\mu}. \tag{7}$$

Now the form of the non-dimensional velocity U_h is

$$U_h = \frac{u}{u_h} = a^2 \left[1 - \xi_1^2 - \frac{2}{a^2} \left\{ 1 - \frac{\cosh (a\xi_1)}{\cosh (a)} \right\} \right]. \tag{8}$$

The ratio of axial velocities for $a = 5$ and 2 is

$$\frac{U_{h5}(0)}{U_{h2}(0)} = \frac{25}{4} (1.46) = 9.125. \tag{9}$$

For the corresponding ratio of Newtonian velocities, the number in the parentheses in equation (9) is one. Thus, one can see the difference at glance between the couple stress fluids and the Newtonian fluids.

It may be noticed from equations (2) and (8) that when $a \to \infty$, i.e., $h \to \infty$, the flow tends to become Newtonian flow (fluid with viscosity μ) and when $a \to 0$, i.e., $h \to 0$, $U \to 0$. But much before the second limit, i.e., $h \to 0$, is reached, a critical value of h – say, h_{crit} (depending on the nature of suspension) – will be reached, such that, for the values of h lower than h_{crit}, the flow between the plates cannot be considered by continuum theory (for blood flow $h_{crit} \simeq 5\ \mu$). Hence, in this case also, one can expect the existence of a_{crit}.

CONCLUSION

For Poiseuille flow of couple stress fluid, Stokes has related the variation of couple stress parameter a with the 'size effects'. In this note, it has been shown that besides 'size effects', the variation of a has two

more interpretations which are physically meaningful and are of importance from application point of view. It is of interest to note that without the present interpretations, the results of Ref. (1) can be mistaken, for example, the statement of Valanis and Sun (4) (p. 95, II para): "Before we close this section we make what we feel is an important observation. Keeping v_o^n [$v_o^n = a^2(dp/dx)/4\mu$, a is tube radius] constant for all concentrations implies, by virtue of equation (3.32d) [Perhaps, they mean equation (3.23d)], that μ is independent of the concentration for the fluid with couple stress. This may sound almost heretical to the people who have been, in the past, calculating the dependence of μ on the concentration. However, one must recall that they were not dealing with a fluid with couple stress which obviously gives another avenue for accommodating the effect of concentration on the flow." This statement is very strange and incorrect.

Further, it has been shown that when the variation in a is due to the change of concentration, the non-dimensionalising velocity u_o used by Stokes is unsuitable. An appropriate non-dimensionalising velocity u_1 has been obtained for this case. The existence of the critical value of a, depending on the fluid, has been predicted.

Stokes (1) has studied the influence of the variation of a, due to change in h, on velocity [only this variation of a has been studied in Ref. (1)]. Since the non-dimensionalising velocity u_o, used in Ref. (1), is a function of h, it cannot be used to study this particular variation of a. Hence, the results obtained there are only qualitatively true – quantitatively they are not. An appropriate non-dimensionalising velocity u_h has been suggested and the existence of a critical value of a, depending on h, has been predicted.

It is of interest to note that the non-dimensionalising velocity u_o, used in Ref. (1), is suitable to study the effects of the variation of a, due to the change in η, on velocity. But, for some reasons, it has not been discussed there [Ref. (1)]. In the present analysis, it is observed that this variation of a may be related to the variation of particle size.

It may be noticed that, in this paper, we have interpreted only three variations of a which are due to the change in individual parameter (only one of the three parameters μ, η and h is allowed to vary). The remaining four variations of a are the combinations of these three basic variations. These variations of a comprise variation of flow conditions and suspension (concentration, particle size). For a given situation, μ, η and h are fixed. Therefore, a can be determined uniquely. However, the converse is not true. In view of the present interpretations of the variation of a, it appears that the couple stress theory, suggested in Ref. (1), may serve as a powerful tool for the study of the flow of suspensions.

ACKNOWLEDGMENTS

This research was made possible by the support from C.S.I.R. through research grant no. 3(430)/78/EMR II.

REFERENCES

1. STOKES, V.K. Couple stresses in fluids. Phys. of Fluids 9, 1709-1715, 1966.

2. COWIN, S.C. The theory of polar fluids. Advan. Appl. Mech. 14, 279-347, 1974.

3. ARIMAN, T., TURK, M.A. and SYLVESTER, N.D. On steady and pulsatile flow of blood. J. Appl. Mech. (ASME) 41, 1-7, 1974.

4. VALANIS, K.C. and SUN, C.T. Poiseuille flow of a fluid with couple stress with applications to blood flow. Biorheology 6, 85-97, 1969.

Vol. 17
1980

BIORHEOLOGY, Vol. 17, pp. 403-410, 1980
Printed in the USA. All rights reserved.

0006-355X/80/050403-08$02.00/0
Copyright (c) 1981 Pergamon Press Ltd

BIORHEOLOGICAL ASPECTS OF BLOOD FLOW THROUGH ARTERY WITH MILD STENOSIS : EFFECTS OF PERIPHERAL LAYER

J.B. Shukla, S.P. Gupta and B.S. Parihar

Department of Mathematics, Indian Institute of Technology
Kanpur-208016, INDIA.

(Received 6.11.1979; in revised form 25.8.1980.
Accepted by Editor S. Oka)

ABSTRACT

The blood flow through an artery with mild stenosis has been analysed by characterising it as a power-law fluid. It has been shown that the resistance to flow and the wall shear stress, as compared to non-stenosis case, decrease as the consistency of peripheral layer fluid decreases and this decrease is enhanced due to the pseudoplastic nature of the blood.

INTRODUCTION

Several workers have studied the flow characteristics of blood in an artery with mild stenosis by considering it as a Newtonian fluid [Young (1,2), Forrester and Young (3)]. However, it has been observed that blood, being a suspension of cells, behaves as a non-Newtonian fluid at low shear rates in tubes of smaller diameters [Hershey et al. (4), Huckaba et al. (5), Charm and Kurland (6), Whitmore (7), Han and Barnett (8)]. It has been reported that the suspension of red cells in serum, the behaviour of which is similar to the whole blood for shear rates more than 1 sec^{-1}, obey power-law model [Whitmore (7), Han and Barnett (8)]. Han and Barnett (8) pointed out that the power law exponent for blood serum may vary between .2 to .9 depending upon the pathological conditions, while Whitmore (7) quoted this value between .68 - .80. The exponent for plasma has been reported to be .95 - .995. The consistency of the suspension of red cells in serum is found to be ten times the viscosity of the suspending medium [Whitmore (7), p. 73].

Keeping in view the non-Newtonian power-law behaviour of blood, its flow characteristics in an artery with mild stenosis have been investigated by Shukla et al. (9). However, they did not take into account the effects of radial distribution of cells and the existence of the peripheral plasma layer near the wall whose thickness may be of the order 40 μ in tubes of diameter 1 to 6 mm [Hershey et al. (10), Lih (11), Middleman (12)]. In this paper, an attempt has been made to study these effects on the characteristics of the blood flow in an artery with mild stenosis.

ANALYSIS

Consider an axially symmetric flow of blood (fluid) through an artery (circular tube) with mild stenosis (constriction) as shown in Fig. 1. The blood flow is assumed to be characterised by the power-law model whose consistency varies symmetrically along the radial direction. As pointed out by Caro et al. (13, p. 111), the time average value of the shear would have similar spatial distribution as associated with steady flow, hence, the flow studied here is assumed to be laminar and steady.

$$\frac{R(z)}{R_0} = 1 - \frac{\delta_s}{2R_0}\left[1 + \cos\frac{2\pi}{L_0}\left(z - d - \frac{L_0}{2}\right)\right]; \quad d \leq z \leq L_0 + d$$
$$= 1 \quad ; \quad \text{elsewhere} \qquad (1)$$

where $R(z)$ is the radius of the artery in the stenotic region, R_0 is the constant radius elsewhere, L_0 is the length of the stenosis and δ_s is its maximum height ($\delta_s \ll R_0$, Fig. 1).

KEY WORDS : Blood Flow, Peripheral Layer

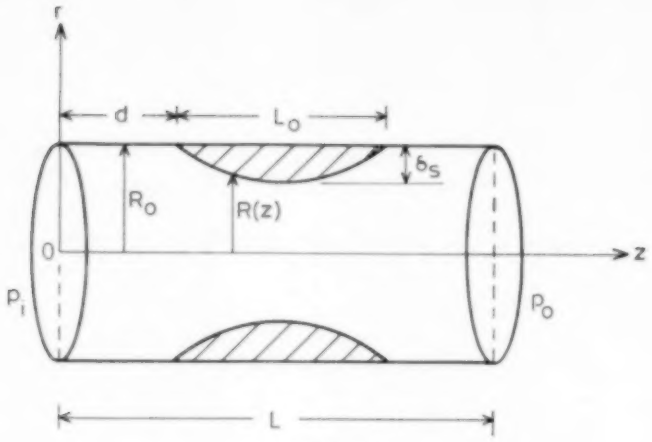

FIG. 1

Geometry of arterial stenosis

The basic equation governing the flow is [Shukla et al. (9)]

$$\frac{1}{r}\frac{\partial}{\partial r}(r\tau) = -\frac{dp}{dz}, \tag{2}$$

where τ, for power-law fluid is given by

$$\tau = -m(r)\left|\frac{\partial w}{\partial r}\right|^{n-1}\frac{\partial w}{\partial r}$$

$$= m(r)\left(-\frac{\partial w}{\partial r}\right)^{n} ; \left(\frac{\partial w}{\partial r} < 0\right), \tag{3}$$

w is the axial velocity, p is the fluid pressure, m(r) is the consistency function and n is the power-law exponent, assumed to be a constant and may be taken as the mean of the flow behaviour indices over the radius.

Solving equation (2) and using the boundary conditions

$$\frac{\partial w}{\partial r} = 0 \quad \text{at} \quad r = 0,$$

$$w = 0 \quad \text{at} \quad r = R(z), \tag{4}$$

the axial velocity w is obtained as

$$w = \left(-\frac{1}{2}\frac{dp}{dz}\right)^{\frac{1}{n}} \int_{r}^{R(z)} \left(\frac{r}{m(r)}\right)^{\frac{1}{n}} dr. \tag{5}$$

The volumetric flow rate, Q, is defined as

$$Q = \int_{o}^{R(z)} 2\pi rw\, dr = -\pi \int_{o}^{R(z)} r^{2}\frac{\partial w}{\partial r}\, dr, \tag{6}$$

which on using equation (5) gives

$$Q = \pi\left(-\frac{1}{2}\frac{dp}{dz}\right)^{\frac{1}{n}} \int_{o}^{R(z)} \frac{r^{\frac{1}{n}+2}}{\{m(r)\}^{1/n}}\, dr. \tag{7}$$

It can be seen from equation of continuity that the flow flux Q is constant across any cross section of the tube.

Rearranging equation (7), we get

$$\frac{dp}{dz} = -2\left[\frac{Q}{\pi I(z)}\right]^{n}, \tag{8}$$

Vol. 17
1980

where

$$I(z) = \int_0^{R(z)} \frac{r^{\frac{1}{n}+2}}{\{m(r)\}^{\frac{1}{n}}}\, dr. \tag{9}$$

Integrating equation (8) and using the condition $p = p_i$ at $z = 0$ and $p = p_o$ at $z = L$, we have

$$p_i - p_o = 2\left(\frac{Q}{\pi}\right)^n \int_0^L \frac{dz}{\{I(z)\}^n}. \tag{10}$$

The resistance to flow, λ, is defined as

$$\lambda = \frac{p_i - p_o}{Q}, \tag{11}$$

which on using equation (10) gives

$$\lambda = \frac{2}{Q}\left(\frac{Q}{\pi}\right)^n \int_0^L \frac{1}{\{I(z)\}^n}\, dz. \tag{12}$$

In the case of no stenosis ($\delta_s = 0$ or $R(z) = R_o$) and with constant consistency of the fluid ($m = m_1$, say), the resistance to flow, λ_N, is calculated from equation (12) as

$$\lambda_N = \frac{2}{Q}\left(\frac{Q}{\pi}\right)^n \left(\frac{3n+1}{n}\right)^n \frac{m_1 L}{R_o^{3n+1}}. \tag{13}$$

From equations (12) and (13), we have

$$\bar{\lambda} = \frac{\lambda}{\lambda_N} = \left(\frac{n}{3n+1}\right)^n \frac{R_o^{3n+1}}{m_1 L} \int_0^L \frac{1}{\{I(z)\}^n}\, dz. \tag{14}$$

The shearing stress, τ_R, on the wall of the tube is given by

$$\tau_R = \left[m(r)\left(-\frac{\partial w}{\partial r}\right)^n\right]_{r=R(z)}, \tag{15}$$

which on using equations (5) and (8) gives the shearing stress, τ_s, at the maximum height of the stenosis (i.e. at $z = d + L_o/2$), as

$$\tau_s = \left[R\left\{\frac{Q}{\pi I(z)}\right\}^n\right]_{z = d + \frac{L_o}{2}}. \tag{16}$$

The wall shearing stress, τ_N, in the case of no stenosis with the constant consistency m_1 is calculated from equation (15) as

$$\tau_N = \left(\frac{3n+1}{n}\right)\left(\frac{Q}{\pi}\right)^n \frac{m_1}{R_o^{3n}}. \tag{17}$$

From equations (16) and (17), we have

$$\bar{\tau}_s = \frac{\tau_s}{\tau_N} = \left(\frac{n}{3n+1}\right)^n \left(1 - \frac{\delta_s}{R_o}\right) \frac{R_o^{3n+1}}{m_1}\left[\frac{1}{\{I(z)\}^n}\right]_{z = d + \frac{L_o}{2}}. \tag{18}$$

The resistance to flow and the wall shear stress at the maximum height of the stenosis can be studied from equations (14) and (18) respectively for any general consistency function $m(r)$.

EFFECTS OF PERIPHERAL LAYER

As pointed out earlier, the existence of cell depleted layer near the arterial wall has been suggested by many workers [Hershey et al. (10), Middleman (12)]. To see the effects

of consistency of such a peripheral layer fluid on the flow behaviour, the function m(r) may be assumed as follows :

$$m(r) = m_1 \quad ; \quad 0 \leq r \leq R_1(z)$$
$$= m_2 \quad ; \quad R_1 \leq r \leq R(z) \tag{19}$$

where m_1, m_2 are the consistencies of the fluids of the central and the peripheral layers respectively. It may be noted that the value of the power-law exponent, n, in this case is taken to be the mean of the flow behaviour indices of the central and peripheral layers.

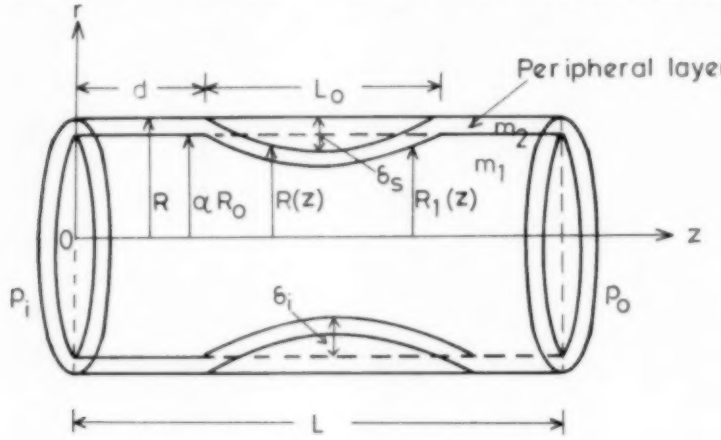

FIG. 2

Geometry of arterial stenosis with peripheral layer

The function $R_1(z)$ represents the geometry of the interface and may be given by (see Fig. 2)

$$\frac{R_1(z)}{R_o} = \alpha - \frac{\delta_i}{2R_o}\left[1 + \cos\frac{2\pi}{L_o}\left(z - d - \frac{L_o}{2}\right)\right] \quad ; \quad d \leq z \leq L_o + d$$
$$= \alpha \quad ; \text{ elsewhere} \tag{20}$$

where α is the ratio of the central layer radius to the tube radius in the unobstructed region and δ_i is the maximum bulging of the interface due to stenosis which is to be determined as follows :

Using the consistency function (19), the fluid velocities w_c, w_p of the central and the peripheral layers respectively have been calculated from equation (5) to obtain the corresponding fluxes Q_c and Q_p as

$$Q_c = \int_0^{R_1} 2\pi r w_c \, dr$$
$$= \pi\left(-\frac{1}{2m_1}\frac{dp}{dz}\right)^{\frac{1}{n}} \cdot \frac{n}{n+1} \cdot \frac{1}{\beta^{1/n}} \cdot R_1^2\left[\frac{1}{R^n} + 1 - \left(1 - \frac{n+1}{3n+1}\beta^{\frac{1}{n}}\right)R_1^{\frac{1}{n}} + 1\right], \tag{21}$$

$$Q_p = \int_{R_1}^{R} 2\pi r w_p \, dr$$
$$= \pi\left(-\frac{1}{2m_1}\frac{dp}{dz}\right)^{\frac{1}{n}} \cdot \frac{n}{3n+1} \cdot \frac{1}{\beta^{1/n}}\left[\frac{1}{R^n} + 3 - \frac{3n+1}{n+1}R_1^2 R^{\frac{1}{n}} + 1 + \frac{2n}{n+1}R_1^{\frac{1}{n}} + 3\right], \tag{22}$$

where

$$\beta = \frac{m_2}{m_1}.$$

The total flux, Q is

$$Q = Q_c + Q_p$$

Vol. 17
1980

$$= \pi\left(-\frac{1}{2m_1}\frac{dp}{dz}\right)^{\frac{1}{n}} \frac{n}{3n+1} \frac{1}{\beta^{1/n}} \left[\frac{1}{R^{n}}^{\frac{1}{n}+3} - (1-\beta^{\frac{1}{n}})\, R_1^{\frac{1}{n}+3}\right]. \tag{23}$$

This flux Q can also be obtained from equation (7) on using the consistency function (19).

It can be seen by integrating the equation of continuity appropriately that not only Q but Q_c and Q_p are also constants separately.

Now, integrating equations (21), (22) and (23) and remembering that the pressure drop, $(p_i - p_o)$, across the tube length is the same in each case, we get

$$Q_c = \left(\frac{p_i - p_o}{2m_1}\right)^{\frac{1}{n}} \frac{\pi}{\beta^{1/n}} \frac{n}{n+1} \frac{1}{(I_1)^{1/n}}, \tag{24}$$

$$Q_p = \left(\frac{p_i - p_o}{2m_1}\right)^{\frac{1}{n}} \frac{\pi}{\beta^{1/n}} \frac{n}{3n+1} \frac{1}{(I_2)^{1/n}}, \tag{25}$$

$$Q = \left(\frac{p_i - p_o}{2m_1}\right)^{\frac{1}{n}} \frac{\pi}{\beta^{1/n}} \frac{n}{3n+1} \frac{1}{(I_o)^{1/n}}, \tag{26}$$

where

$$I_1 = \int_o^L \left[\frac{1}{R_1^2\left\{R^{\frac{1}{n}+1} - (1 - \frac{n+1}{3n+1}\beta^{1/n})\, R_1^{\frac{1}{n}+1}\right\}}\right]^n dz, \tag{27}$$

$$I_2 = \int_o^L \left[\frac{1}{R^{\frac{1}{n}+3} - \frac{3n+1}{n+1} R_1^2 R^{\frac{1}{n}+1} + \frac{2n}{n+1} R_1^{\frac{1}{n}+3}}\right]^n dz, \tag{28}$$

$$I_o = \int_o^L \left[\frac{1}{R^{\frac{1}{n}+3} - (1-\beta^{1/n})\, R_1^{\frac{1}{n}+3}}\right]^n dz. \tag{29}$$

Since $Q = Q_c + Q_p$, from equations (24), (25) and (26), we obtain the following equation to determine δ_i,

$$\frac{3n+1}{(I_1)^{1/n}} + \frac{n+1}{(I_2)^{1/n}} = \frac{n+1}{(I_o)^{1/n}}. \tag{30}$$

It can be seen by direct substitution that

$$R_1 = \alpha R \tag{31}$$

satisfies equation (30), which on using equations (1) and (20) gives

$$\delta_i = \alpha\delta_s. \tag{32}$$

Using the consistency function (19) in equation (9) and making use of the relation (32) in equations (14), (18), the expressions for $\bar{\lambda}$, $\bar{\tau}_s$ can be written in a simplified form as follows :

$$\bar{\lambda} = \left\{\frac{\beta^{1/n}}{1 - (1-\beta^{1/n})\,\alpha^{\frac{1}{n}+3}}\right\}^n \left[1 - \frac{L_o}{L} + \frac{L_o}{L}\, G\right], \tag{33}$$

$$\bar{\tau}_s = \left\{\frac{\beta^{1/n}}{1 - (1-\beta^{1/n})\,\alpha^{\frac{1}{n}+3}}\right\}^n \frac{1}{(1 - \frac{\delta_s}{R_o})^{3n}}, \tag{34}$$

where

$$G = \frac{1}{L_o}\int_d^{d+L_o} \frac{dz}{(R/R_o)^{3n+1}}$$

$$= \frac{1}{2\pi} \int_0^{2\pi} \frac{d\phi}{(a + b\cos\phi)^{3n+1}}, \qquad (35)$$

$$\phi = \pi - \frac{2\pi}{L_0}\left(z - d - \frac{L_0}{2}\right), \quad a = 1 - \frac{\delta_s}{2R_0}, \quad b = \frac{\delta_s}{2R_0}.$$

It may be noted that for general value of n, the integral (35) cannot be evaluated analytically. But when 3n+1 is an integer, this integral can be evaluated by using the method of calculus of residues. In such a case, $\bar{\lambda}$, from equation (33), can be written as

$$\bar{\lambda} = \left\{ \frac{\beta^{1/n}}{1 - (1 - \beta^{1/n})\,\alpha^{\frac{1}{n}+3}} \right\}^n \left[1 - \frac{L_0}{L} + \frac{L_0}{L}\left\{ \frac{1}{b\sqrt{c^2-1}} \right\}^{3n+1} \sum_{s=0}^{3n} (-1)^s \frac{(3n+s)!}{(s!)^2\,(3n-s)!}\, \nu^s \right], \qquad (36)$$

where

$$c = \frac{a}{b}, \quad \nu = \frac{-c + \sqrt{c^2-1}}{2\sqrt{c^2-1}}.$$

It is seen that equations (34) and (36) reduce to the case of Shukla et al. (9) for $\beta = 1.0$ and to the case of Young (1) for $n = 1.0$, $\beta = 1.0$.

RESULTS AND DISCUSSION

To see the effects of various parameters on $\bar{\lambda}$, $\bar{\tau}_w$, the following values have been used [Whitmore (7), Han and Barnett (8), Hershey et al. (10), Middleman (12)] :

$n = 0.667, 0.75, 1.0;$

$\beta = 0.1, 0.3, 1.0;$

$\frac{L_0}{L} = 0.1, 0.5, 1.0;$

$\alpha = 0.95;$

$\frac{\delta_s}{R_0} = 0.0 - 0.20.$

Using these data the values of $\bar{\lambda}$ from equation (33) or (36) have been calculated numerically and plotted against δ_s/R_0 in Figs. 3 and 4. From these figures, it is noted that $\bar{\lambda}$ increases as the stenosis size (δ_s/R_0 or L_0/L) increases for fixed β and n. It is also noted from Fig. 3 that $\bar{\lambda}$ decreases as β or n decreases for fixed stenosis size.

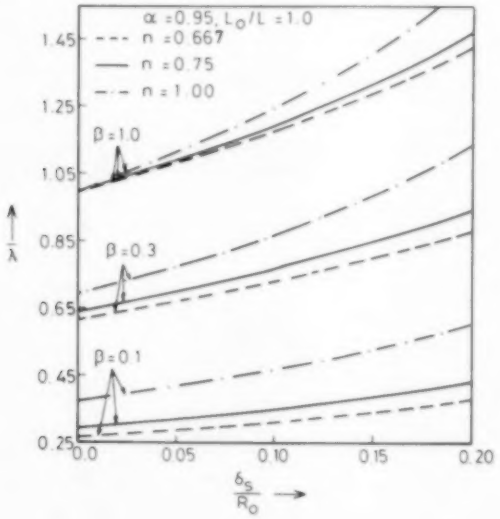

FIG. 3

Variation of $\bar{\lambda}$ with δ_s/R_0 for different n and β

Vol. 1
1980

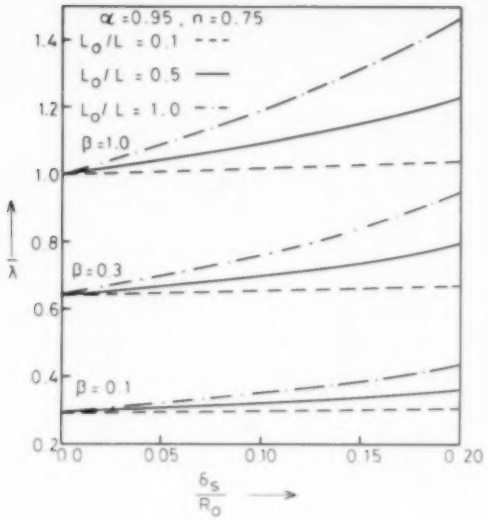

FIG. 4

Variation of $\bar{\lambda}$ with δ_s/R_0 for different β and L_0/L

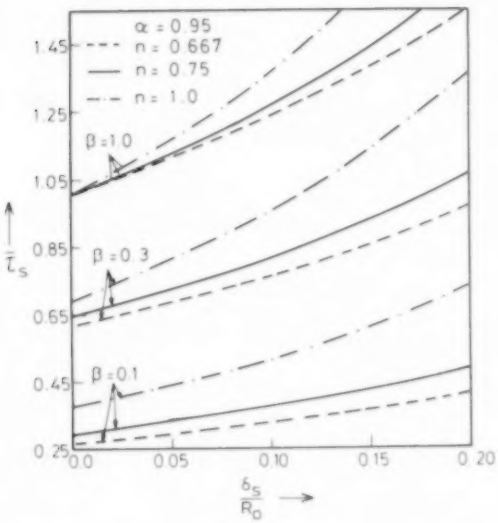

FIG. 5

Variation of $\bar{\tau}_s$ with δ_s/R_0 for different n and β

The values of $\bar{\tau}_s$ from equation (34) have been plotted in Fig. 5 for various values of n, β and δ_s/R_0. It is seen from this figure that $\bar{\tau}_s$ also increases as the stenosis height increases but decreases as β or n decreases.

CONCLUSION

The flow characteristics of blood flow through an artery with mild stenosis have been investigated by modelling the blood as a non-Newtonian power-law fluid with variable consistency. By assuming the existence of a peripheral layer with a fluid of smaller consistency, it has been shown that the resistence to flow and the wall shear stress, as compared to non-stenosis case, (though increase with stenosis size) decrease as the consistency of the peripheral layer fluid decreases and this decrease is enhanced due to the pseudo-plastic nature of the fluid.

Thus, it appears that nature has provided a self controlling mechanism by associating favourable conditions to the system so that it may function smoothly as far as possible even under diseased conditions.

REFERENCES

1. YOUNG, D.F. Effects of a time-dependent stenosis on flow through a tube. J. Engng. Ind. Trans. ASME 90, 248-254, 1968.

2. YOUNG, D.F. Fluid mechanics of arterial stenoses. J. Biomechanical Engng., Trans. ASME 101, 157-175, 1979.

3. FORRESTER, J.H. and YOUNG, D.F. Flow through a converging-diverging tube and its implications in occlusive vascular disease. J. Biomech. 3, 297-316, 1970.

4. HERSHEY, D., BYRNES, R.E., DEDDENS, R.L. and RAO, A.M. Blood rheology : Temperature dependence of the power-law model. Paper presented at A.I.Ch.E. meeting.Boston, December, 1964.

5. HUCKABA, C.E. and HAHN, A.W. A generalized approach to the modelling of arterial blood flow. Bull. Math. Biophys. 30, 645-662, 1968.

6. CHARM, S.E. and KURLAND, G. Viscometery of human blood for shear rates of 0 -100,000 sec^{-1}. Nature 206, 617-618, 1965.

7. WHITMORE, R.L. Rheology of the Circulation. Pergamon Press Ltd., 1968.

8. HAN, C.D. and BARNETT, B. Measurements of the rheological properties of biological fluids. IN : Rheology of Biological Systems. Henry L. Gabelnick and Mitchel Litt (Ed.).Illinois, U.S.A. : Charles C. Thomas. Publisher.1973, pp. 195-217.

9. SHUKLA, J.B., PARIHAR, R.S. and RAO, B.R.P. Effects of stenosis on non-Newtonian flow of the blood in an artery. Bull. Math. Biol. 42, 283-294, 1980.

10. HERSHEY, D. and CHO, S.J. Blood flow in rigid tubes : thickness and slip velocity of plasma film at the wall. J. Appl. Physiol. 21, 27-32, 1966.

11. LIH, M.M. Transport Phenomena in Medicine and Biology. New York : John Wiley & Sons,1975.

12. MIDDLEMAN, S. Transport Phenomena in the Cardiovascular System. New York : John Wiley & Sons, 1972.

13. CARO, C.G., FITZ-GERALD, J.M. and SCHROTER, R.C. Atheroma and arterial wall shear : Observation, correlation and proposal of a shear dependent mass transfer mechanism for atherogenesis. Proc. Roy. Soc. Lond. B 177, 109-159, 1971.

Vol. 1
1980

BIORHEOLOGY, Vol. 17, pp. 411-418, 1980
Printed in the USA. All rights reserved.

0006-355X/80/050411-08$02.00/0
Copyright (c) 1981 Pergamon Press Ltd

METABOLIC REQUIREMENTS OF CONTRACTILE FORCE GENERATION IN PLATELET RICH PLASMA - A RHEOLOGICAL STUDY

J. P. Kirkpatrick, L. V. McIntire, *J. L. Moake and *D. M. Peterson
Biomedical Engineering Laboratory, Rice University, Houston, Texas 77001
*Division of Hematology, University of Texas Medical School

(Received 1.10.1980. Accepted by Editor E. Fukuda)

ABSTRACT

Inhibitors of platelet metabolism were used to investigate energy requirements of platelet-fibrin interaction and contractile force development utilizing a rheological technique. Glycolysis inhibitor 2-deoxy-D-glucose and respiration inhibitor KCN had little effect on clot structure formation in PRP when used separately. When employed together, there was a dramatic decrease in the maximum elastic modulus attained (G'_{max}). Results indicate that platelet-fibrin attachment is not strongly dependent on platelet metabolic activity, but that contractile force generation can be eliminated if both glycolysis and respiration are interrupted.

INTRODUCTION

Platelets metabolize carbohydrates primarily via aerobic glycolysis and respiration (1, 2). Inhibitors of these processes interfere with the platelet functions of aggregation, viscous metamorphosis and clot retraction (3-10). Monoiodoacetic acid (IAA) and 2-deoxy-D-glucose (DDG), inhibitors of glycolysis, reduce platelet aggregation and induce a shape change (4, 5). In the presence of another glycolytic inhibitor, 3,5-dinitrobenzoyl glucosamine, clot retraction is decreased (6). While agents which inhibit oxidative phosphorylation, such as cyanide or antimycin, have been shown to cause a platelet shape change (4), they have little effect on platelet aggregation (5, 7). When both inhibitors of glycolysis and respiration are employed, e.g., IAA and cyanide (4, 7), DDG and antimycin (5, 9), or DDG and cyanide (8), normal platelet function is suppressed totally.

To determine the effect of metabolic inhibitors (IAA, DDG, KCN) on the platelet-fibrin interaction during clot structure formation, we have employed a dynamic rheological testing technique. Using this method, the initiation, rate of development, and extent of the platelet-mediated contractile force can be determined. In addition, alterations of platelet aggregation in response to the addition of exogenous ADP were observed in the presence of these agents, in accord with previous work (4, 5, 7-9).

MATERIALS AND METHODS

Blood was drawn from healthy adult volunteers into siliconized glassware containing 3.8% trisodium citrate (9 parts blood: 1 part anticoagulant). Platelet-rich plasma (PRP) was produced by centrifugation of citrated blood at 150 X g for 10 minutes. Platelet-free plasma (PFP) was obtained by centrifugation of citrated blood for 15 minutes at 1500 X g and centrifugation of the resultant supernatant at

KEY WORDS: platelet metabolism, clot rheology, platelet-fibrin interaction.

11,000 X g for an additional 15 minutes. Platelet counts were performed using a Coulter Counter, Model ZBI (Coulter Electronics, Hialeah, Fla.)

Solutions of potassium cyanide (KCN), 2-deoxy-D-glucose (DDG) and sodium monoiodoacetic acid (IAA) were prepared daily in phosphate buffered saline (PBS, 0.014 M Na_2HPO_4 + 0.003 M KH_2PO_4 + 0.125M NaCl, pH 7.4).

Fifteen or 60 minutes prior to testing, 1 part inhibitor solution of PBS and 9 parts PRP or PFP were incubated at 37°C. Immediately following pre-incubation, ADP-induced platelet aggregation studies were performed by the turbidimetric technique of Born (11, 12).

In the rheological experiments 0.165 ml of .25 M $CaCl_2$ was added to 2.0 ml of the preincubated PRP-inhibitor solution mixture to initiate thrombin formation. The recalcified plasma was then subjected to dynamic oscillatory testing as described by Glover (13). In this method, following the addition of calcium, the plasma is placed between the stainless steel parallel platens of a Weissenberg Rheogoniometer, Model R18. A forced sinusoidal oscillation was then applied to the bottom platen. This motion was transmitted to the upper platen (held in a frictionless air-bearing rotor and restricted only by a torsion bar), by the test material. The movement of the platens was monitored continuously, using displacement transducers.

As fibrin undergoes polymerization and crosslinking and the fibrin network is tightened isometrically by platelets, the motion of the upper platen increases in amplitude and is more nearly in-phase with the oscillatory movement of the bottom platen. If the shear strain is sufficiently small, such that the sample behaves as a linear viscoelastic material (14), the amplitude ratio and phase angle between the motions of platens may be employed to calculate the dynamic shear moduli (15). The dynamic shear storage modulus, G', is a measure of the elasticity of the material, and the loss modulus, G", gives an estimate of the importance of dissipative (viscous) processes in the network. In platelet-fibrin clots, G' increases as platelets interact with polymerizing fibrin and subject the forming network to a contractile force (13, 16). This technique permits quantitative measurement of the initiation, rate of development and extent of fibrin polymerization, and the contractile force generated in the platelet-fibrin network. In a prior study (17), we have shown this technique to be significantly more sensitive than clot retraction measurements in the study of the platelet fibrin interaction.

RESULTS

The maximum shear storage moduli (G'_{max}) of PRP clots containing increasing concentrations of IAA decreased progressively (Fig. 1). However, this effect does not appear to be due solely to inhibition of platelet function. In PFP, the presence of 2 X 10^{-3} M IAA results in a clot with G'_{max} only 30% that of the control (Fig. 2). In neither PFP nor PRP was the time between the addition of calcium and the rapid rise in G' increased significantly by IAA. In PRP containing 2 X 10^{-3} M IAA, some platelet aggregation in response to the addition of 2 µM ADP occured, but was followed by spontaneous disaggregation (Fig. 3). At IAA concentrations of 2 X 10^{-5} and 2 X 10^{-4} M, the platelets did not disaggregate after ADP exposure. However, at 2 X 10^{-4} M IAA the extent of aggregation was somewhat less than in the control samples.

In PRP containing 10^{-2} M DDG, G'_{max} was only slightly less than the control value (Fig. 4). 10^{-3} M KCN had no apparent effect on the rheology during coagulation (Fig. 5). However, in the presence of both DDG and KCN at concentrations of 5 X 10^{-3} M, G'_{max} was 25% that of the control and $\Delta G'$ (G'_{max} - G' at 90 minutes) was only 21% (Fig. 5, 6 and Table 1). Neither the coagulation of PFP nor the time required to initiate clotting were affected significantly by these agents (Fig. 6).

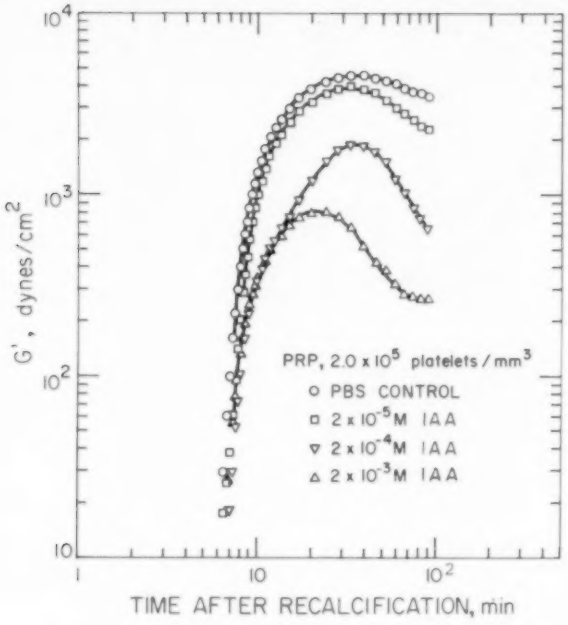

FIG. 1
Dynamic shear storage modulus (G') of PRP incubated with 2 X 10^{-5}, 2 X 10^{-3} M monoiodoacetic acid (IAA), or PBS for 15 minutes prior to recalcification.

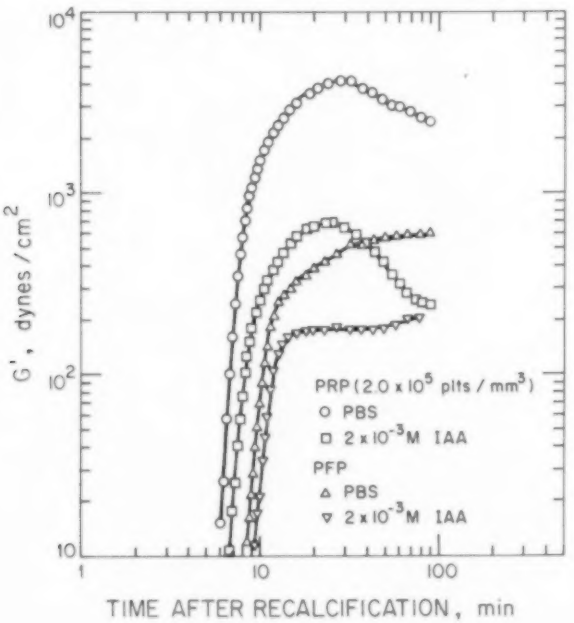

FIG. 2
Dynamic shear storage modulus (G') of PRP and PFP incubated with 2 X 10^{-3} M monoiodoacetic acid (IAA) or PBS for 15 minutes prior to recalcification.

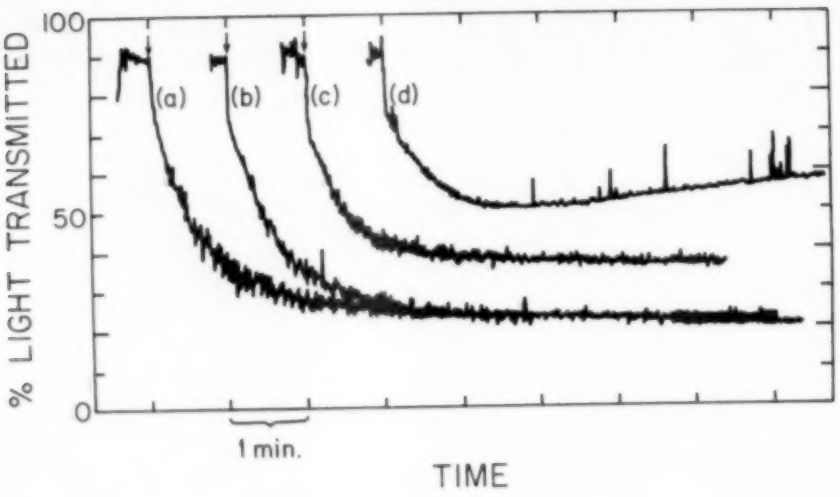

FIG. 3

Platelet aggregation in response to addition (↓) of 0.1 ml 10 μM ADP to 0.4 ml PRP (2.0×10^5 platlets/mm^3) incubated for 15 minutes with a) PBS; b) 2.0×10^{-5} M monoiodoacetic acid (IAA); c) 2.0×10^{-4} IAA; d) 2.0×10^{-3} M IAA.

Vol. 1
1980

While platelet aggregation to 2 μM ADP was not inhibited in the presence of 10^{-2} M DDG, in PRP containing 5×10^{-3} M KCN and 5×10^{-3} M KCN + 5×10^{-3} M DDG no aggregation to ADP was observed. The number of platelets and the platelet size distribution were not affected significantly at these concentrations of inhibitors.

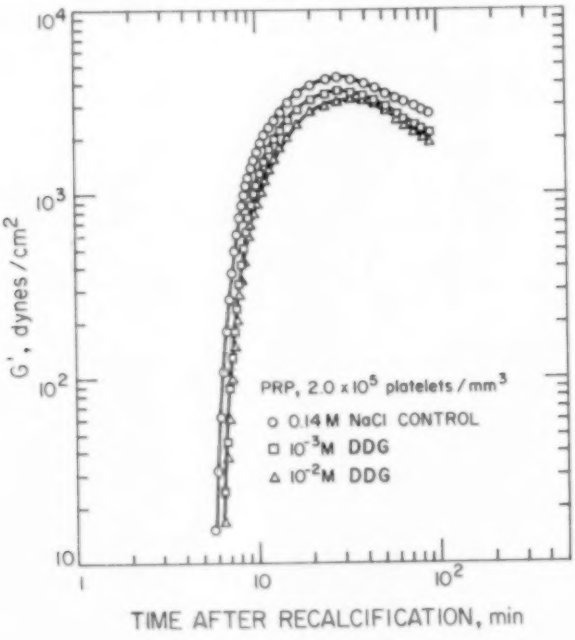

FIG. 4
Dynamic shear storage modulus (G') of PRP incubated with 10^{-3} M, 10^{-2} M 2-deoxy-D-glucose or 0.14 M NaCl for 60 minutes.

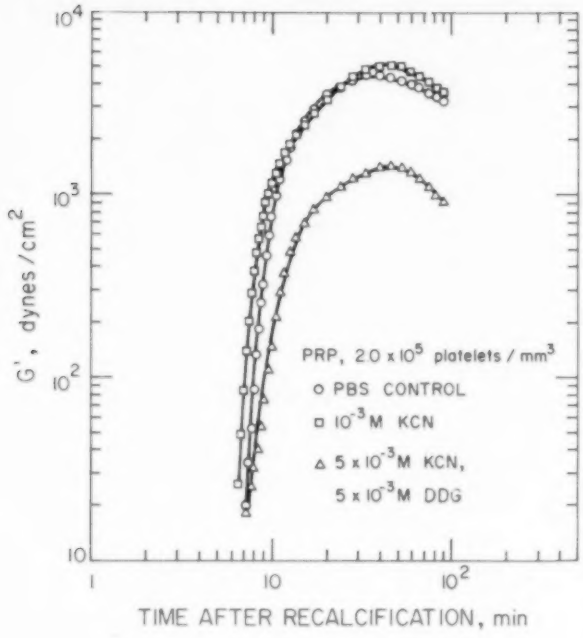

FIG. 5
Dynamic shear storage modulus (G') of PRP incubated for 60 minutes with PBS, 10^{-3} M KCN, or 5 X 10^{-3} M KCN + 5 X 10^{-3} M 2-deoxy-D-glucose.

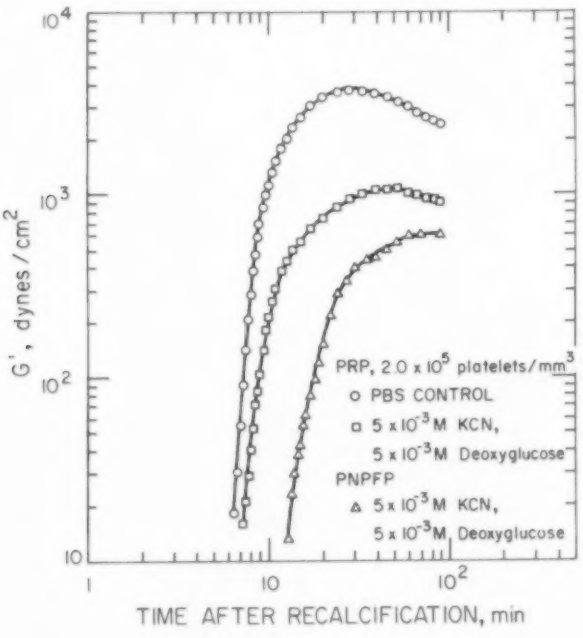

FIG. 6

Dynamic shear storage modulus of PRP or PFP incubated for 60 minutes with PBS or 5 X 10^{-3} M KCN + 5 X 10^{-3} M 2-deoxy-D-glucose before recalcification.

TABLE 1

The development and extent of the platelet contractile force in PRP containing 5 X 10^{-3} M KCN + 5 X 10^{-3} M DDG. G'_{max} - G' (90 minutes). The drop in elastic modulus is due to network relaxation as platelet contractile action decreases. t_o is the time between recalcification and the time at which G' = 15 dynes/cm^2. The subscript "c" denotes the control. Results are ± one S.D. (5 observations).

$\frac{G'_{max}}{(G'_{max})_c}$	$\frac{\Delta G'}{(\Delta G')_c}$	$\frac{t_o}{(t_o)_c}$
0.253 ± 0.045	0.217 ± 0.113	1.08 ± 0.15

DISCUSSION

Recent studies (5, 18) have shown the effects of inhibition of both glycolysis (DDG) and respiration (KCN or antimycin A) on intraplatelet adenine nucleotide levels, using both washed platelets and PRP. DDG interferes with glycolysis by competing with glucose in the phosphohexose isomerase reaction without being a substrate. Thus the ratio of glucose/DDG is important in systems which contain glucose (such as PRP) and drops in platelet ATP are minimal if this ratio is 2 or greater (18). Intraplatelet ATP drops dramatically if both DDG and a respiration inhibitor are present (18).

In our work the dramatic reduction of G'_{max} in PRP but not PFP containing 5 X 10^{-3} M KCN and 5 X 10^{-3} M DDG indicates that these agents inhibit platelet contraction but do not interfere with fibrin network formation. The decrease in G' of 78% relative to controls in the presence of KCN + DDG (Table 1) suggests that the large decline in G' after G'_{max} is attained - seen in normal PRP - is due to depletion of the energy stores of the platelet. Glover (13, 19) has shown that this drop in elastic modulus is due neither to an unrecoverable strain of the crosslinked fibrin network nor fibrinolysis, but rather due to a network relaxation as platelet contraction decreases. Similar decreases in G'_{max} and $\Delta G'$ have been found in PRP incubated with cytochalasin B (17), an agent which directly disrupts the contractile proteins, but has minimal effect on nucleotide levels. Thus, these results show that the platelet-mediated contractile mechanism is an energy-requiring process, involving cytochalasin B sensitive proteins and utilizing ATP.

IAA appears to affect fibrin polymerization as well as platelet function. G'_{max} of both PRP and PFP clots are reduced significantly in the presence of 2 X 10^{-3} M IAA. However, $\Delta G'$ of PRP containing this concentration of IAA is comparable to $\Delta G'$ found in normal PRP. It appears that the primary effect of IAA in the concentration range investigated is the disruption of the fibrin network upon which the platelets are anchored, rather than an alteration of platelet contractility.

The increased rigidity of clots formed from PRP is not due solely to the energy-requiring contractile mechanism. Even when the ability of platelets to tighten the fibrin network is inhibited almost completely ($\Delta G' \approx 0$), the rigidity of fully-formed PRP clots is at least twice that of PFP clots. The observation that platelets attach to fibrin strands (13, 16) implies that they serve as mechanical crosslinks as well as actively contracting the fibrin network. Thus, the possible conformations of the polymer chains are restricted in number, and the entropy of the system is decreased. From rubber elasticity theory (20), this is equivalent to an increase in the apparent crosslink density and modulus of the material.

Vol. 1
1980

Platelets have been shown to accelerate coagulation by contributing platelet factors (21, 22), by promoting the activation of Factors XII, XI, and X, specifically (23-26), and by providing a catalytic surface for factor activation in general (27). In all rheological studies, the length of time between recalcification and the initial rapid rise in G' is shorter for PRP than PFP from a given donor (13) (7-9 minutes vs. 10-14 minutes). When chemical agents are present that inhibit the platelet metabolism (KCN + DDG), depolymerize microtubules (colchicine, vinblastine (28)) or disrupt contractile microfilaments (cytochalasin B, (17)), this initiation time is not prolonged significantly. Apparently, the procoagulant role of platelets is not diminished by decreased energy production or by the absence of assembled cytoskeletal and contractile proteins.

CONCLUSION

Platelets appear to have three primary thromboplastic functions. First, they promote and accelerate coagulation. Second, they serve as passive mechanical crosslinks, thereby increasing clot rigidity. Third, by contracting the fibrin network, they further enhance clot strength and reduce clot volume in vivo. Each of these functions can be independently followed using the dynamic materials testing rheological technique described. Alterations in any one platelet function, caused by biochemical or clinical changes, can be easily differentiated from the others employing this method. The first two functions appear unaffected by the metabolic state of the platelet and the condition of the microfilament and microtubule networks, while the contractile function is strongly dependent on these factors.

ACKNOWLEDGMENT

This work was supported by grant HL 18672 from the National Heart, Lung and Blood Institute.

REFERENCES

1. KARPATKIN, S. and LANGER, R. M. Biochemical energetics of simulated platelet plug formation: Effect of thrombin, adenosine diphosphate, and epinephrine on intra- and extracellular adenine nucleotide kinetics. J. Clin. Inv. 47, 2158, 1968.

2. KITCHENS, C. S. and NEWCOMB, T. F. Human platelet respiration. J. Appl. Physiol. 25, 581, 1968.

3. ZUCKER, M. B. and BORELLI, J. Viscous metamorphosis, clot retraction and other morphologic alterations of platelets. J. Appl. Physiol. 14, 575, 1959.

4. BEHNKE, O. Effects of some chemicals on blood platelet microtubules, platelet shape and some platelet functions in vitro. Scand. J. Haemat. 7, 123, 1970.

5. HOLMSEN, H., SETKOWSKY, C. A. and DAY, H. J. Effects of antimycin and 2-deoxyglucose on adenine nucleotides in human platelets. Biochem. J. 144, 385, 1974.

6. BETTEX-GALLAND, M. and LUSCHER, E. F. Studies on the metabolism of human blood platelets in relation to clot retraction. Thromb. Diath. Haemmorh. 4, 178 (1960).

7. ZUCKER, M. B. and JERUSHALMY, Z. Studies on platelet shape and aggregation; effect of inhibitors on these and other platelet characteristics. In Physiology of Hemostasis and Thrombosis. S.A.Johnson and W.H.Seegers (Eds). Charles C. Thomas, Springfield, IL, 1967, 249.

8. KATTLOVE, H. E. Platelet ATP in ADP-induced aggregation. Am. J. Physiol. 226, 325, 1974.

9. CHAO, F. C., SHEPRO, D., TULLIS, J. L., BELLAMARICH, F. A., and CURRY, W. A. Similarities between platelet contraction and cellular motility during mitosis; role of platelet microtubules in clot retraction. J. Cell. Sci. 20, 569, 1976.

10. MURER, E. H. Clot retraction and energy metabolism of platelets. Effect and mechanism of inhibitors. Biochim. Biophys. Acta, 172 266, 1969.

11. BORN, G. V. R. Aggregation of blood platelets by adenosine diphosphate and its reversal. Nature 194, 927, 1962.

12. BORN, G. V. R. and HUME, M. Effects of the numbers and sizes of platelet aggregates on the optical density of plasma. Nature 215, 1027, 1967.

13. GLOVER, C. J., McINTIRE, L. V., BROWN, C. H., and NATELSON, E. A., Dynamic coagulation studies; influence of normal and abnormal platelets on clot formation. Thromb. Res. 7, 185, 1975.

14. FERRY, J. D. Viscoelastic Properties of Polymers. J. Wiley and Sons, New York, NY, 1971.

15. WALTERS, K. and KEMP, R. A. On the use of a rheogoniometer III - oscillatory shear between parallel plates. Rheol. Acta 7, 1, 1968.

16. NIEWIAROWSKI, S., REGOECZI, E., STEWART G. J., SENYI, A. F. and MUSTARD, J. F. Platelet interaction with polymerizing fibrin. J. Clin. Invest. 51, 685, 1972.

17. KIRKPATRICK, J. P., McINTIRE, L. V., MOAKE, J. L. and CIMO, P. L. Differential effects of cytochalasin B on platelet release, aggregation and contractility. Thrombosis and Haemostasis 42, 1483, 1980 .

18. HOLMSEN, H. and ROBKIN, L. Effects of antimycin A and 2-deoxyglucose on energy metabolism in washed human platelets. Thrombosis and Haemostasis 42, 1460, 1980.

19. GLOVER, C. J. Dynamic shear moduli during normal and abnormal plasma clot formation. Ph.D. thesis, Rice University, 1975.

20. TRELOAR, L. R. G. The Physics of Rubber Elasticity. Oxford University Press, London, 1958.

21. NIEWIAROWSKI, S. A., POPLAWSKI, A., KIPINSKI, B. and FARBISZEWKI, R. The release of platelet clotting factors during aggregation and viscous metamorphosis. Exp. Biol. Med. 3, 121, 1968.

22. HARDISTRY, R. M. and HUTTON, R. A. Platelet aggregation and the availability of platelet Factor III. Br. J. Haematol 12, 764, 1960.

23. SCHIFFMAN, S. RAPAPORT, S. I. and CHONG, M. M. Y. Platelets and the initiation of intrinsic clotting. Br. J. Haematol 24, 633, 1973.

24. WALSH, P. N., and BIGGS, R. The role of platelets in intrinsic Factor Xa formation. Br. J. Haematol 22, 743, 1972.

25. WALSH, P. N. Platelet coagulant activities and hemostasis: a hypothesis. Blood 43, 597, 1974.

26. VECCHIONE, J. and ZUCKER, M. B. Procoagulant activity of platelets in recalcified plasma. Br. J. Haematol 31, 423, 1975.

27. SILVER, M. J. Role of calcium ions and phospholipids in platelet aggregation. Am. J. Physiol 201, 1128, 1965.

28. KUNTAMUKKULA, M. S., MOAKE, J. L., McINTIRE, L. V., and CIMO, P.L. Effects of colchicine and vinblastine on platelet contractility and release. Thromb. Res. In press, 1980.

BIORHEOLOGY, Vol. 17, pp. 419-430, 1980
Printed in the USA. All rights reserved.

0006-355X/80/050419-12$02.00/0
Copyright (c) 1981 Pergamon Press Ltd

ON THE RHEOLOGY OF VISCOUS DROPS SURROUNDED BY AN ELASTIC SHELL

P. BRUNN

Department of Chemical Engineering
Columbia University
New York, N.Y. 10027

(Received 1.6.1979; in revised form 6.10.1980.
Accepted by Editor A. Silberberg)

ABSTRACT

Neglecting inertial effects the problem studied concerns an elastic spherical shell with viscous material inside, suspended in a viscous fluid, when the general undisturbed flow is time dependent. The rheological behavior of a highly dilute suspension of such particles constitutes a linear viscoelastic fluid, as long as the deformation is neglected. Explicit constitutive equations are derived with special attention paid to the case of a rigid interior, gaseous interior, a purely elastic sphere and a viscous sphere with a thin elastic membrane.

1. INTRODUCTION

The rheological properties of a suspension are strongly influenced by whether the suspended particles are rigid or deformable. As far as the latter case is concerned two kinds of particles have so far received considerable consideration: purely elastic particles [1-3] and droplets with surface tension [4,5]. And it is the model of a drop which serves to estimate the internal viscosity of the red cells. A red cell, however, is a deformable particle with a membrane as the interface and not pure liquid. Thus it is not surprising to find discrepancies between the predictions of the drop-theory and experiments [6].

The deformation of a red cell has successfully been studied by taking the elastic nature of its membrane into consideration [e.g. 7,8,9]. On the other hand virtually no studies have been concerned with the rheological response of viscous particles surrounded by an elastic shell. Brennen [10] tried his hand at that problem by assuming the cells to be and remain spherical for a simple shear flow. Using membrane analysis and a "cell" model for a concentrated solution of such particles he thus obtained the (steady state) shear viscosity. Unfortunately, the flow employed is too special and not suited to furnish a rheological classification of the suspension in question.

To remedy this situation we have to start all over again. Focusing attention on a dilute suspension implies that we need to consider only a particular particle in detail. Following Brennen, we assume that without any flow this particle (and all the others) are spherical in shape, having a viscous inside surrounded by an elastic shell. Imposing no restrictions on the thickness of this shell means that we cannot use membrane analysis. But it is worth the effort since it will enable us to obtain results for purely elastic particles by taking proper limits.

In order to obtain the rheological equation of state we need to know the response of our characteristic particle in a spatially homogeneous flow, whose time dependence may be arbitrary. But this is a problem which cannot be solved exactly. The reason being that the particle will in general deform (in a time dependent manner). And the deformation of the particle has to be calculated simultaneously along with the solution of the equations of motion. This renders the overall problem nonlinear, even though inertial effects will be neglected. However, for small deformations we can adopt the same iteration scheme which has been found useful for droplets [5]. In this paper only the first iteration will be considered, in which the particle can still be approximated by the undeformed sphere (cf. [1,4]).

Keywords: Dispersion, microrheology, viscoelastic fluid

2. AN ELASTIC SPHERICAL SHELL WITH VISCOUS MATERIAL INSIDE IN A GENERAL TIME DEPENDENT FLOW

Let us assume that an elastic spherical shell of radii r_i and r_o, respectively ($r_i < r_o$) obeys Hooke's law (shear modulus μ). The inside of the shell shall consist of an incompressible newtonian fluid, characterized by the shear viscosity η_i. The particle itself is suspended in a newtonian fluid having the shear-viscosity η_o. The situation we consider is one in which the particle center is fixed at the origin (particle is macroscopically at rest), while the undisturbed flow of the solvent is homogeneous, i.e. a linear function of position,

$$\underset{\sim}{V}^\circ = \underset{\sim}{\Omega} \times \underset{\sim}{r} + \underset{\sim}{r} \cdot \underset{\sim}{E}^\circ . \tag{1}$$

Here $\underset{\sim}{\Omega}$ is one half the vorticity vector and $\underset{\sim}{E}^\circ$ is the rate of strain dyadic, each of which will in general depend upon time.

Clearly, the stresses acting on the particle surface tend to deform it. For small departures from spherical shape an iteration scheme similar to the one used for droplets [5] seems appropriate. We will do the same and focus in this paper attention on the first iteration, in which our particle can be approximated by the original sphere.

Assuming inertial effects to be negligible the mathematical statement of our problem thus reads

$$\frac{\partial}{\partial \underset{\sim}{r}} \cdot \underset{\sim}{w} = 0,$$

$$-\frac{\partial}{\partial \underset{\sim}{r}} p + \zeta \nabla^2 \underset{\sim}{w} = 0, \tag{2}$$

with

$$\begin{aligned} \underset{\sim}{w} &= \underset{\sim}{v}^i, \; p = p^i, \; \zeta = \eta_i \quad \text{for} \quad r < r_i, \\ \underset{\sim}{w} &= \underset{\sim}{u}, \; p = p_e, \; \zeta = \mu \quad \text{for} \quad r_i < r < r_o, \\ \underset{\sim}{w} &= \underset{\sim}{v}^\circ, \; p = p^\circ, \; \zeta = \eta_o \quad \text{for} \quad r_o < r . \end{aligned} \tag{3}$$

The boundary conditions are

$$\underset{\sim}{v}^i, \; p^i \quad \text{finite at} \quad r = 0, \tag{4a}$$

$$\left.\begin{aligned} \underset{\sim}{v}^\circ &= \underset{\sim}{V}^\circ, \\ p^\circ &= \text{const.}, \end{aligned}\right\} \quad \text{for} \quad r \to \infty , \tag{4b}$$

$$\left.\begin{aligned} \underset{\sim}{v}^i &= \dot{\underset{\sim}{u}}, \\ \underset{\sim}{n} \cdot \underset{\sim}{T}^i &= \underset{\sim}{n} \cdot \underset{\sim}{T}^e, \end{aligned}\right\} \quad \text{at} \quad r = r_i, \tag{4c}$$

$$\left.\begin{aligned} \underset{\sim}{v}^\circ &= \dot{\underset{\sim}{u}}, \\ \underset{\sim}{n} \cdot \underset{\sim}{T}^\circ &= \underset{\sim}{n} \cdot \underset{\sim}{T}^e, \end{aligned}\right\} \quad \text{at} \quad r = r_o . \tag{4d}$$

Vol. 1
1980

While $\underset{\sim}{n}$ stands for the surface normal, the dyads $\underset{\sim}{T}^i$, $\underset{\sim}{T}^e$ and $\underset{\sim}{T}^o$ are the stress dyads of the inside, the elastic and the outside region.

The general solution of (2) has been given by Lamb [11]. In conjunction with the boundary conditions (4) we thus find that the flow and displacement fields, respectively, can only be of the form*

$$\underset{\sim}{v}^i = \underset{\sim}{\Omega} \times \underset{\sim}{r} + \underset{\sim}{r} \cdot \underset{\sim}{E}^i + \frac{1}{\eta_i}\left[\frac{3}{5} r^2 \underset{\sim}{r} \cdot \underset{\sim}{C}^i - \frac{2}{105} r^7 \underset{\sim}{\chi} : \underset{\sim}{C}^i\right], \tag{5}$$

$$\underset{\sim}{u} = \underset{\sim}{A}^e \times \underset{\sim}{r} + \underset{\sim}{r} \cdot \left[\frac{3}{5\mu} r^2 \underset{\sim}{C}^e + \underset{\sim}{E}^e + \frac{3}{5\mu r^3} \underset{\sim}{c}^e\right] + \underset{\sim}{\chi} : \left[-\frac{2}{105\mu} r^7 \underset{\sim}{C}^e + \frac{r^2}{10\mu} \underset{\sim}{c}^e + \underset{\sim}{b}^e\right], \tag{6}$$

and

$$\underset{\sim}{v}^o = \underset{\sim}{V}^o + \frac{3}{5\eta_o r^3} \underset{\sim}{r} \cdot \underset{\sim}{c}^o + \underset{\sim}{\chi} : \left[\frac{r^2}{10\eta_o} \underset{\sim}{c}^o + \underset{\sim}{b}^o\right]. \tag{7}$$

Here $\underset{\sim}{\chi}$ is the third order tensor

$$\underset{\sim}{\chi} = -\frac{\partial^3}{\partial \underset{\sim}{r} \partial \underset{\sim}{r} \partial \underset{\sim}{r}} r^{-1},$$

which is completely symmetric and irreducible.

Since

$$\dot{\underset{\sim}{A}}^e = \underset{\sim}{\Omega}, \tag{8}$$

we see that the particle rotates with the fluid. For the freely suspended sphere we are considering this was to be expected. For the remaining eight symmetric and irreducible dyads $\underset{\sim}{E}^i$, $\underset{\sim}{C}^i$, $\underset{\sim}{E}^e$, $\underset{\sim}{C}^e$, $\underset{\sim}{b}^e$, $\underset{\sim}{c}^e$, $\underset{\sim}{b}^o$ and $\underset{\sim}{c}^o$ the boundary conditions (4.c) and (4.d) furnish the following eight relations

At $r = r_o$:

$$\underset{\sim}{E}^o + \frac{3}{5\eta_o r_o^3} \underset{\sim}{c}^o = \dot{\underset{\sim}{E}}^e + \frac{3}{5\mu} r_o^2 \dot{\underset{\sim}{C}}^e + \frac{3}{5\mu r_o^3} \dot{\underset{\sim}{c}}^e, \tag{9a}$$

* This is most readily seen if Lamb's solution is expressed in cartesian coordinates and the independence of the multipole potentials is utilized (cf. [12]).

$$\underset{\sim}{b}^{o} + \frac{r_o^2}{10\eta_o}\underset{\sim}{c}^{o} = -\frac{2}{105\mu}r_o^7\dot{\underset{\sim}{C}}^{e} + \dot{\underset{\sim}{b}}^{e} + \frac{r_o^2}{10\mu}\dot{\underset{\sim}{c}}^{e}, \tag{9b}$$

$$2\eta_o\underset{\sim}{E}^{o} - \frac{9}{5r_o^3}\underset{\sim}{c}^{o} = 2\mu\underset{\sim}{E}^{e} + \frac{6}{5}r_o^2\underset{\sim}{C}^{e} - \frac{9}{5r_o^3}\underset{\sim}{c}^{e}, \tag{9c}$$

$$8\eta_o\underset{\sim}{b}^{o} + \frac{4}{5}r_o^2\underset{\sim}{c}^{o} = \frac{19}{105}r_o^7\underset{\sim}{C}^{e} + 8\mu\underset{\sim}{b}^{e} + \frac{4}{5}r_o^2\underset{\sim}{c}^{e}, \tag{9d}$$

and similarly at $r = r_i$

$$\underset{\sim}{E}^{i} + \frac{3}{5\eta_i}r_i^2\underset{\sim}{C}^{i} = \dot{\underset{\sim}{E}}^{e} + \frac{3}{5\mu}r_i^2\dot{\underset{\sim}{C}}^{e} + \frac{3}{5\mu r_i^3}\dot{\underset{\sim}{c}}^{e}, \tag{9e}$$

$$-\frac{2}{105\eta_i}r_i^7\underset{\sim}{C}^{i} = -\frac{2}{105\mu}r_i^7\dot{\underset{\sim}{C}}^{e} + \dot{b}^{e} + \frac{r_i^2}{10\mu}\dot{\underset{\sim}{c}}^{e}, \tag{9f}$$

$$2\eta_i\underset{\sim}{E}^{i} + \frac{6}{5}r_i^2\underset{\sim}{C}^{i} = 2\mu\underset{\sim}{E}^{e} + \frac{6}{5}r_i^2\underset{\sim}{C}^{e} - \frac{9}{5r_i^3}\underset{\sim}{c}^{e}, \tag{9h}$$

$$\frac{19}{105}r_i^7\underset{\sim}{C}^{i} = \frac{19}{105}r_i^7\underset{\sim}{C}^{e} + 8\mu\underset{\sim}{b}^{e} + \frac{4}{5}r_i^2\underset{\sim}{c}^{e}. \tag{9i}$$

Although these dyads are independent of position they all depend upon time. Since the relations resulting from the continuity of the velocity across the interphase (i.e. (9.a), (9.b), (9.e) and (9.f) involve time derivatives of the displacement field $\underset{\sim}{u}$ the boundary conditions (9) constitute an initial value problem. We will assume that at time t=0 the flow was started so that all dyads vanish for t=0.

Applying the Laplace operation

$$\int_0^\infty dt\, e^{-st}$$

to each of the equations (9) and characterizing the Laplace transform of a function f (t) by $\bar{f}$ (s), i.e.

$$\bar{f}(s) = \int_0^\infty dt\, e^{-st} f(t), \tag{10}$$

the resulting eight algebraic equations for the dyads $\underset{\sim}{E}^{i}$, $\underset{\sim}{C}^{i}$, $\underset{\sim}{E}^{e}$, $\underset{\sim}{C}^{e}$, $\underset{\sim}{b}^{e}$, $\underset{\sim}{c}^{e}$, $\underset{\sim}{b}^{o}$ and $\underset{\sim}{c}^{o}$ are readily solved in terms of the given dyad $\underset{\sim}{E}^{o}$.

Instead of listing all these results it seems worthwhile to recall that our primary interest concerns the rheological response of a suspension. And it is relatively simple to show that the bulk stress $\underset{\sim}{\Sigma}$ of a homogeneous dilute suspension of identical particles is [13]

Vol. 1
1980

$$\underset{\sim}{P} = -P\underset{\sim}{\delta} + 2\eta_0 \underset{\sim}{E} - 4\pi n \underset{\sim}{\varepsilon}^0 . \tag{11}$$

Here $\underset{\sim}{E}$ is the volume average of rate of strain dyadic and n the member-density of the particles. Consequently it is the dyad $\underset{\sim}{\varepsilon}^0$ (the stresslet) we need to know. Since this is multiplied by n we can replace the $\underset{\sim}{E}^\infty$, appearing in the explicit final expression for $\underset{\sim}{\varepsilon}^0$, by $\underset{\sim}{E}$ and thus obtain the desired constitutive equation valid to first order in the concentration.

For the Laplace transform of $\underset{\sim}{\varepsilon}^0$ we find

$$\overline{\underset{\sim}{\varepsilon}^0} = \frac{10}{9}\eta_0 r_0^3 \overline{\underset{\sim}{E}^\infty} - \frac{25}{27}\eta_0 r_0^3 \bar{f}(s)\overline{\underset{\sim}{E}^\infty} , \tag{12}$$

with

$$\bar{f}(s) = \alpha \frac{s^3 + q_2 s^2 + q_1 s + q_0}{s^4 + p_3 s^3 + p_2 s^2 + p_1 s + p_0} \equiv \alpha \frac{f_1(s)}{f_2(s)} . \tag{13}$$

The constitutive equation for the deviatoric stress dyad

$$\underset{\sim}{T} \equiv \underset{\sim}{P} + P\underset{\sim}{\delta} , \tag{14}$$

thus becomes

$$\underset{\sim}{T}(t) = 2\eta_0\left[1 - \frac{5}{3}\phi\right]\underset{\sim}{E}(t) + \frac{25}{9}\eta_0\phi\int_0^t dt' f(t-t')\underset{\sim}{E}(t') , \tag{15}$$

where ϕ is the volume fraction of the spheres and f (t) is the inverse of $\bar{f}$ (s) (cf. (10)). The suspension thus comprises a linear viscoelastic material. Due to the fact that deformation of the particle was neglected such a linear relation was indeed to be expected.

For the explicit results f (t) has to be known. Since $\bar{f}$ (s) is a quotient of the two polynomials f_1 and f_2 we need the roots of the denominator f_2. However, the coefficients p_i (which in addition to α and q_i are listed in the appendix) are functions of the parameters

$$\tau_0 = \eta_0/\mu , \quad \lambda = \eta_0/\eta_i \quad \text{and} \quad x = \frac{r_0}{r_i} . \tag{16}$$

Consequently, the roots will be so complicated expressions that they are of little practical use. Thus we will consider only a few special cases in detail.

Before doing so it seems worthwhile to point out the fact that for steady state flows our suspension asymtotically (i.e. for $t \to \infty$) approaches the behavior of a suspension of rigid spheres (Einsteinian viscosity). Although this was to be expected on physical grounds, care is needed to prove that result mathematically. Thus, while in general the ratio of q_o and p_o is needed for the $s \to 0$ limit of $\bar{f}(s)$, i.e. for f(o), (this limit leads to the Einsteinian formula) the ratio of q_2 and p_2 determines f(o) for the λ =0 case. Yet the Einsteinian viscosity emerges in either case, i.e. irrespective of λ , x or τ_o.

3. EXAMPLES

3.1 The Elastic Sphere

In this case there is no viscous inside and the sphere is solely composed of elastic material. Taking the limit $x \to \infty$, it is readily checked that the numerator f_1 of (13) is contained in the denominator f_2 such that $\bar{f}(s)$ becomes

$$\bar{f}(s) = \frac{\alpha}{s + \alpha/3} ,$$

with

$$\alpha = 2/\tau_0 \tag{17}$$

Consequently, our constitutive equation (15) reads

$$\underset{\sim}{T}(t) = 2\eta_0\left[1 - \frac{5}{3}\phi\right]\underset{\sim}{E}(t) + \frac{50}{9}\mu\phi\int_0^t dt'\,\underset{\sim}{E}(t')\exp\left[-\frac{2}{3}\frac{t-t'}{\tau_0}\right] \tag{18}$$

To first order in the volume fraction this equation (i.e. the differential version of it) is identical to the relation Fröhlich and Sack [1] derived in a different way.

It also follows from (17) and eqs (9) that the only nonzero dyads are

$$\underset{\sim}{b}^0 = -\frac{\tau_0^2}{10\eta_0}\underset{\sim}{c}^0 ,$$

and

$$\underset{\sim}{E}^e = \tau_0\underset{\sim}{E}^0 - \frac{9}{10\mu\tau_0^3}\underset{\sim}{c}^0 . \tag{19}$$

This implies that the particle deforms homogeneously (cf. eq. (6)). The basic assumption customarily used in the study of elastic particles [1-3] thus follows rigorously from our analysis. The resulting ellipsoidal shape of the particle could be accounted for in the next iteration. In this way the constitutive equation can be extended into the nonlinear regime (3).

Vol. 1
1980

3.2 Rigid Interior

The $\lambda = 0$ limit characterizes the situation in which the viscosity η_i of the inner region by far exceeds the viscosity η_0 of the solvent, i.e. in which the inside is rigid. While α is unaffected by λ the coefficients q_1, q_0, p_1 and p_0 all vanish for $\lambda = 0$. This implies that the denominator f_2 has a double zero at s=0. Since f_1, too, has a double zero at s=0 for $\lambda = 0$, we have

$$\lim_{\lambda\to 0}\bar{f}(s) = \alpha\frac{s + q_{20}}{s^2 + p_{30}s + p_{20}} , \tag{20}$$

where the additional subscript zero characterizes the $\lambda = 0$ limit under investigation. It is readily proven that the two roots of the denominator of (20) are real and negative, so that the constitutive equation for such a suspension is

$$T(t) = 2\eta_0\left[1 - \frac{5}{3}\phi\right]\underset{\sim}{E}(t) + \frac{25}{9}\eta_0\phi\sum_{i=1}^{2}\frac{A_i}{\tau_i}\int_0^t dt'\,\underset{\sim}{E}(t')\,e^{-\frac{t-t'}{\tau_i}} . \tag{21}$$

If s_i^*, i=1,2 denotes one of the two roots of the denominator of (20) (i.e. of $s^{-2}f_{20}(s)$) the relaxation times τ_i appearing in equation (21) are simply the negative inverse of the s_i^*, i.e.

$$\tau_i = -(s_i^*)^{-1} \tag{22}$$

Knowing the s_i^* (or τ_i) immediately furnishes the coefficients A_i,

$$\frac{A_1}{\tau_1} = \alpha\frac{s_1^* + q_{20}}{s_1^* - s_2^*} = \frac{1}{\tau_1}(3 - A_2) \tag{23}$$

The last equality sign of (23) guarantees that the Einsteinian viscosity is recovered by taking appropriate limits.

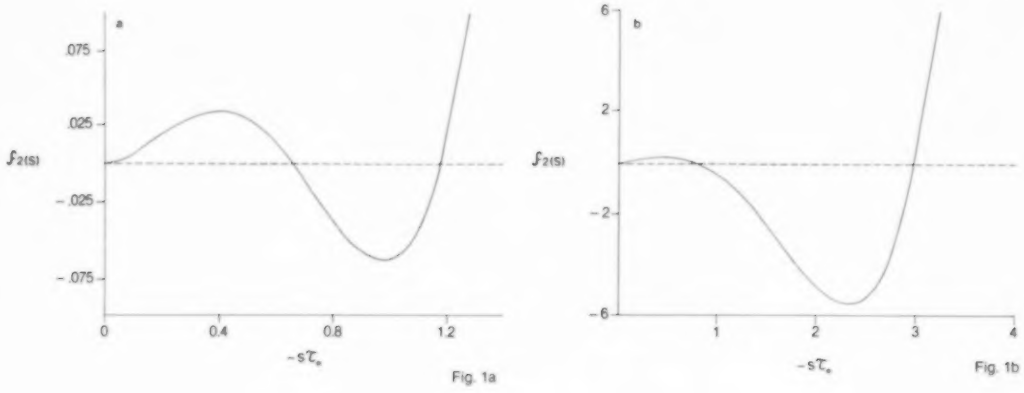

Fig. 1a Fig. 1b

FIG. 1

The denominator $f_2(s)$ for $\lambda = 0$ for different thicknesses of the shell
a, x=100; b, x=2

In figure 1 the function $f_{20}(s)$ is plotted versus $-s\tau_o$. As said before, only the two nonzero roots s_i^* matter. Starting from the values -19/16 and -2/3, respectively, at $x = \infty$ (the first root is also a root of $f_{10}(s)$ for $x = \infty$) for the roots $s_i^* \tau_o$, the roots increase in magnitude as x decreases, i.e. as the thickness of the elastic shell becomes smaller. This implies that the relaxation times τ_i get smaller and smaller. But the rate of strain dyadic $\underline{E}$ has to vary appreciably over a time period of the order of the τ_i in order to reveal the viscoelastic nature of our suspension. Thus, unless the elastic region is sufficiently thick (large τ_i) or the external flow is rapidly varying one will encounter nothing but the $\tau_i = 0$, i=1,2 limit of (21), i.e. the same rheological behavior as for a suspension of rigid spheres. Note that if ϵ denotes the thickness of the elastic region made dimensionless with r_o i.e.

$$X = \frac{1}{1 - \epsilon} \tag{24}$$

the two relaxation times vanish for $\epsilon \to 0$ like ϵ and ϵ^3, respectively.

3.3 Gaseous Inside

If the inside consists of a gas its viscosity η_i will be much smaller than the solvent viscosity η_o. Thus, we have to take the $\lambda \to \infty$ limit with the result

$$\lim_{\lambda \to \infty} \bar{f}(s) = \alpha \frac{q_{1\infty} s + q_{0\infty}}{p_{2\infty} s^2 + p_{1\infty} s + p_{0\infty}}, \tag{25}$$

where the subscript ∞ on the coefficients q_i and p_i, respectively indicates the $\lambda \to \infty$ limit of the corresponding quantity (i.e. q_i or p_i) divided by λ^2. The two roots of the denominator of (25) are again real and negative. The constitutive equation will therefore

be of the same form as eq. (21). Denoting by τ_3 and τ_4, respectively, the two relaxation times and by A_3 and A_4, respectively, the corresponding coefficients, we explicitly have

$$\tau_{3/4} = -\frac{1}{s_{3/4}} = 2\,\frac{P_{2\infty}}{P_{1\infty}}\left[1 \pm \left(1 - 4\,\frac{P_{2\infty}P_{0\infty}}{P_{1\infty}^2}\right)\right]^{-1},$$

$$\frac{A_3}{\tau_3} = \frac{\alpha}{P_{2\infty}}\,\frac{q_{1\infty}s_3^* + q_{0\infty}}{s_3^* - s_4^*} = \frac{1}{\tau_3}(3 - A_4). \qquad (26)$$

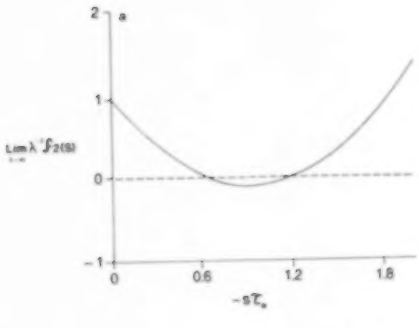

Fig. 2a

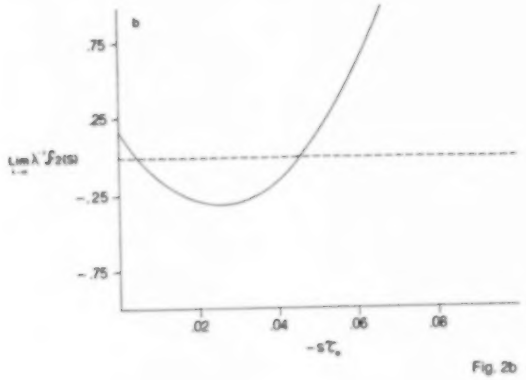

Fig. 2b

FIG. 2

The function $\lim_{\lambda\to\infty}\left[\lambda^{-2} f_2(s)\right]$ for different thicknesses of the shell a, x=100, x=1.01

From these results and from Fig. 2 it follows that the relaxation times increase if the thickness ϵ of the elastic shell decreases. Starting from the values

$$\tau_3/\tau_o = \frac{16}{19} \quad \text{and} \quad \frac{\tau_4}{\tau_o} = \frac{3}{2} \quad \text{for} \quad \epsilon \to 1$$

(the corresponding coefficient A_3 vanishes as it should by the results of §3.1) the relaxation times increase as ϵ^{-1} for $\epsilon \to 0$. Consequently, our suspension will in general behave as a Maxwell fluid with two relaxation times. Especially if the elastic region is extremely thin the memory for this suspension is so large that only truly steady state flows will lead to the Einsteinian result.

3.4 General Case

For arbitrary viscosity ratio λ and arbitrary thickness ϵ of the elastic region four roots of the denominator f_2 of $\tilde{\xi}$ have in general to be reckoned with. As seen from the table and from Fig. 3 these roots can be grouped in pairs of two, one pair of small roots (say, s_1^* and s_2^*) and one pair of large roots (say s_3^* and s_4^*).

Vol. 1
1980

TABLE: The roots $-s_i^* \tau_o$ of the function f_2

λ \ x	100	2	1.01	1.002
0	.67; 1.19	.80; 3.0	25; 35 x 10^4	
.2	.17; .30; .67; 1.19	.11; .17; .83; 3.7	.91 x 10^{-3}; .73 x 10^{-2} 29; 46 x 10^4	.18x10^{-3}; .15 x 10^{-2}; .14 x 10^3; 55 x 10^6;
5	.67; 1.19; 4.3; 7.6	.40; .87 4.33; 23	.37 x 10^{-2}; .37 x 10^{-1} 1.25 x 10^3; 3.04 x 10^7	
∞	.67; 1.19	.44; .90	.44 x 10^{-2}; .453 x 10^{-1}	

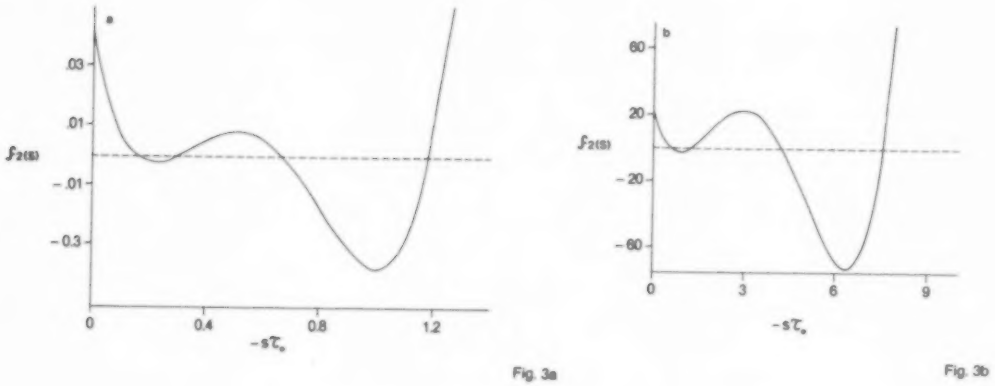

Fig. 3a Fig. 3b

FIG. 3

The function $f_2(s)$ for x=100 for different viscosities
a, λ =.2 b, λ =5

Keeping λ fixed and decreasing ϵ separates the two pairs more and more, since the two smaller roots get smaller while the two larger roots get larger. Consequently, for ϵ sufficiently small it makes sense to approximate τ_3 and τ_4 by zero (recall (22)). For $\epsilon \ll 1$ the constitutive equation thus reads

$$\underset{\sim}{T}(t) = 2\eta_0\left[1+\frac{5}{2}\frac{1-\lambda}{1+\frac{3}{2}\lambda}\phi\right]\underset{\sim}{E}(t) + \eta_0\phi\sum_{i=1}^{2}\frac{B_i}{\tau_i}\int_0^t dt'\,\underset{\sim}{E}(t')\,e^{-\frac{t-t'}{\tau_i}}, \quad \text{with}$$

$$\frac{\tau_{1/2}}{\tau_0} = \frac{2}{5\epsilon}\frac{(1+\frac{16}{19}\lambda)(1+\frac{3}{2}\lambda)}{\lambda(1+\frac{24}{19}\lambda)}\left\{1 \mp \frac{\left[\frac{283}{19}\left(1+\frac{14256}{5377}\lambda+\frac{9792}{5377}\lambda^2\right)\right]^{\frac{1}{2}}}{5(1+\frac{24}{19}\lambda)}\right\}^{-1},$$

$$B_1 = \frac{25}{4}\frac{\lambda}{1+\frac{3}{2}\lambda}\left\{1+\frac{7}{5}\left(1+\frac{312}{133}\lambda\right)\left[\frac{283}{19}\left(1+\frac{14256}{5377}\lambda+\frac{9792}{5377}\lambda^2\right)\right]^{-\frac{1}{2}}\right\} = \frac{25}{2}\frac{\lambda}{1+\frac{3}{2}\lambda} - B_2. \quad (27)$$

This again, constitutes a generalized Maxwell fluid with two relaxation times. As seen from figure 4 the ratio τ_1/τ_2 is of the order of 10 and this in general will be too small to warrant our additional taking the $\tau_2 \to 0$ limit.

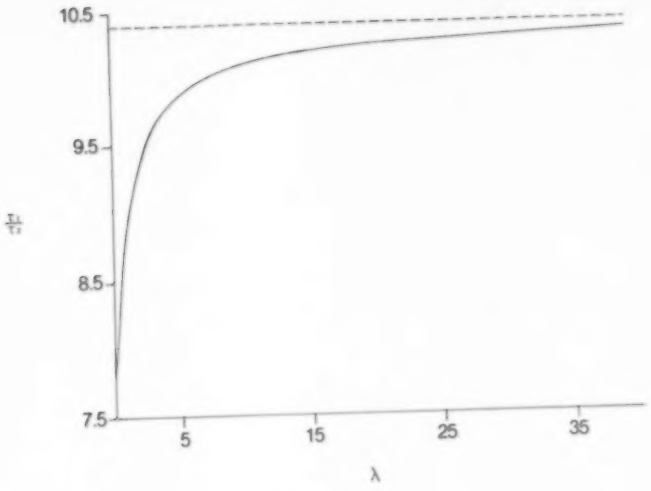

FIG. 4

The ratio of the dominant relaxation times τ_{1/τ_2} for a thin membrane

Vol. 17
1980

If we compare (27) with the linear constitutive equation for a suspension of droplets (use eqs. (3.4) and (3.5) of [5] in their linearized form)

$$\underline{T}(t) = 2\eta_0\left[1+\frac{5}{2}\frac{1-\lambda}{1+\frac{3}{2}\lambda}\phi\right]\underline{E}(t) + \eta_0\phi\frac{B}{\tau}\int_0^t dt'\,\underline{E}(t')\,e^{-\frac{t-t'}{\tau}},$$

$$\tau = \frac{19}{20}\frac{\eta_0\tau_0}{\sigma}\frac{(1+\frac{3}{2}\lambda)(1+\frac{16}{19}\lambda)}{\lambda(1+\lambda)}, \qquad B = \frac{19}{2}\frac{\lambda(1+\frac{16}{19}\lambda)}{(1+\lambda)(1+\frac{3}{2}\lambda)}, \tag{28}$$

where σ is the surface tension, two differences immediately become apparent.* First, in case of droplets only one relaxation time appears and second, the steady state viscosity of droplets explicitly shows a dependence upon λ while nothing but the Einsteinian viscosity results if the interface consists of linear elastic material. Whether or not these differences become immaterial or not in the nonlinear regime (non-linear rheology) remains to be shown.

3.4 Summary and Conclusion

A dilute suspension of spherical particles, consisting of a newtonian fluid which is surrounded by a Hookean elastic shell of arbitrary thickness constitutes a generalized Maxwell fluid. Since particles of this kind will in general deform we are restricted to the case in which the deformation will be small. For $\lambda = 0$ (1) the deformation will indeed be small if $\tau_0 |E| << 1$, although this condition may be too stringent, especially for arbitrary λ and ϵ. Consequently we defer that point to a future study.

No more than four relaxation times characterize the fluid. Especially, if the elastic region is thin only two survive the $\epsilon << 1$ limit. For example, using $\epsilon = 2 \times 10^{-3}$ and $\lambda = .2$ we extract from eq. (27) or from the numerical results in the table

$$\tau_{1/\tau_0} = 5.52 \times 10^3; \quad \tau_{2/\tau_0} = 6.81 \times 10^2 \tag{29}$$

* The characteristic time $\eta_0\tau_0/\sigma$ corresponds to τ_0/ϵ in case of a membrane.

For a dilute suspension of red cells in plasma λ =.2 is generally accepted [6]. Taking r_o = 5 x 10^{-6} m as cell radius, ϵ = 2 x 10^{-3} requires a membrane thickness of 100Å, again a reasonable value [14]. Consequently, the relaxation times given by (29) should be relevant for a dilute suspension of red cells. With η_i =6 cpoise [6] and $\mu\epsilon r_o$=10^{-5} N/m [7] we obtain for the characteristic time τ_o a value of 10^{-6} sec. Even if, as Richardson [7] points out, the value for $\mu\epsilon r_o$ may be in error by at least one order of magnitude the τ_o would nevertheless be so small that viscoelastic behavior would be found only in extremely rapidly varying flows. Otherwise one finds rheologically identical behavior to a suspension of rigid spheres, at least as long as any deformation is neglected. But as said before deformation will constitute the subject of a future study.

APPENDIX

Using (16) and defining the quantities a and b by

$$a = 4x^{10} - 15x^7 + 42x^5 - 25x^3 - 6, \tag{A.1}$$

$$b = a - 10(x^7 - 1), \tag{A.2}$$

we have

$$\alpha = \frac{2}{\tau_o}\frac{a}{b}, \tag{A.3}$$

$$P_3 = \frac{1}{\tau_o b}\left\{\frac{89}{12}x^{10} + \frac{25}{4}x^7 - 14x^5 + \frac{25}{3}x^3 - 8 + \lambda\left[\frac{178}{19}x^{10} + \frac{75}{19}x^7 - \frac{126}{19}x^5 + \frac{25}{19}x^3 - 8\right]\right\}, \tag{A.4}$$

$$P_2 = \frac{1}{\tau_o^2 b}\left\{\frac{19}{6}x^{10} + \frac{75}{4}x^7 - 28x^5 + \frac{50}{3}x^3 + 4 + \lambda\left[\frac{7921}{456}x^{10} - \frac{75}{76}x^7 + \frac{42}{19}x^5 - \frac{25}{57}x^3 + 16\right] + \lambda^2\left[\frac{96}{19}x^{10} + \frac{400}{19}x^7 - \frac{672}{19}x^5 + \frac{450}{19}x^3 + 4\right]\right\}, \tag{A.5}$$

$$P_1 = \frac{\lambda}{\tau_o^3 b}\left\{\frac{89}{12}x^{10} - \frac{225}{76}x^7 + \frac{84}{19}x^5 - \frac{50}{57}x^3 - 8 + \lambda\left[\frac{178}{19}x^{10} - \frac{100}{19}x^7 + \frac{224}{19}x^5 - \frac{150}{19}x^3 - 8\right]\right\}, \tag{A.6}$$

$$P_0 = \frac{\lambda^2}{\tau_o^4 b}\left\{4x^{10} - \frac{300}{19}x^7 + \frac{448}{19}x^5 - \frac{300}{19}x^3 + 1\right\}, \tag{A.7}$$

and

$$q_2 = \frac{1}{\tau_o a}\left\{\frac{19}{4}x^{10} + \frac{225}{8}x^7 - 42x^5 + 25x^3 + 6 + \lambda\left[\frac{178}{19}x^{10} + \frac{45}{19}x^7 - \frac{126}{19}x^5 + \frac{25}{19}x^3 + 12\right]\right\}, \tag{A.8}$$

$$q_1 = \frac{\lambda}{\tau_o^2 a}\left\{\frac{89}{8}x^{10} - \frac{675}{152}x^7 + \frac{126}{19}x^5 - \frac{25}{19}x^3 - 12 + \lambda\left[\frac{96}{19}x^{10} + \frac{240}{19}x^7\right.\right.$$

$$- \frac{672}{19}x^5 + \frac{450}{19}x^3 - 6 \Big] \Big\}, \qquad \text{(A.9)}$$

$$q_0 = \frac{3}{\alpha} p_0 \quad . \qquad \text{(A.10)}$$

ACKNOWLEDGEMENT

I thank Mr. B. Guzman for preparing the graphs and the table.

REFERENCES

1. FRÖHLICH, H. and SACK, R. Theory of the rheological property of dispersions. Proc. Roy. Soc. Lond. A. 185, 415-430, 1946.

2. ROSCOE, R. On the rheology of a suspension of viscoelastic spheres in a viscous liquid. J. Fluid Mech. 28, 273-293, 1967.

3. GODDARD, J.D. and MILLER, CH. Nonlinear Effects in the rheology of dilute suspensions. J. Fluid Mech. 28, 657-673, 1967.

4. TAYLOR, G.I. The viscosity of a fluid containing small drops of another fluid. Proc. Roy. Soc. Lond. A 138, 41-48, 1932.

5. FRANKEL, N.A. and ACRIVOS, A. The constitutive equation for a dilute emulsion. J. Fluid Mech. 44, 65-78, 1970.

6. GOLDSMITH, H.L. and MASON, S.G. Some model experiments in hemodynamics IV. In: Theoretical and clinical hemorheology. H.H. Hartert and A.L. Copley (Eds.) Berlin: Springer Verlag 1971, 47-59.

7. RICHARDSON, E. Deformation and haemolysis of red cells in shear flow. Proc. Roy. Soc. Lond. A 338, 129-153, 1974.

8. FUNG, Y.C. and TONG, P. Theory of the sphering of red blood cells. Biophys. J. 8, 175-197, 1968.

9. ZARDA, P.R., CHIEN, S. and SKALAK, R. Elastic deformations of red blood cells. J. Biomed. 10, 211-221, 1977.

10. BRENNEN, CH. A concentrated suspension model for the Conette rheology of blood. Can. J. Chem. Engng. 53, 126-133, 1975.

11. LAMB, H. Hydrodynamics, Cambridge: Cambridge Univ. Press 1932, 594-602.

12. BRUNN, P. The effect of Brownian motion for a suspension of spheres. Rheol. Acta 15, 104-119, 1976.

13. BATCHELOR, G.K. The stress system in a suspension of force-free particles. J. Fluid Mech. 41, 545-570, 1970.

14. MIDDLEMAN, S. Transport phenomena in the cardiovascular system, New York: Wiley-Interscience, 1972, 50-86.

Vol. 17
1980

BIORHEOLOGY, Vol. 17, pp. 431-444, 1980
Printed in the USA. All rights reserved.

0006-355X/80/050431-14$02.00/0
Copyright (c) 1981 Pergamon Press Ltd

STERIC HINDRANCE EFFECTS ON THE TIME DEPENDENT DIFFUSION OF PLASMALEMMA VESICLES ACROSS VASCULAR ENDOTHELIUM

Leslie Arminski*, Shu Chien**, Robert Pfeffer*, Sheldon Weinbaum*

*The City College of The City University of New York
New York, New York 10031
**Columbia University, College of Physicians and Surgeons
New York, New York 10032

(Received 20.5.1980; in revised form 10.10.1980.
Accepted by Editor M. Litt)

ABSTRACT

The time dependent theory of Arminski, Weinbaum and Pfeffer (1) for the vesicular transport of macromolecules across endothelial cells is modified to include the effects of steric hindrance of vesicles attached at the plasmalemma membranes of the cells. The spatial variation of the diffusion coefficient near the plasmalemma membranes of an endothelial cell layer is determined experimentally by measuring velocities of spheres settling under gravity perpendicular to a single plate fitted with an array of attached spheres that model the ultrastructural features of a plasmalemma membrane and its attached vesicles. The spatial variation of the diffusion coefficient in the central part of the cell is determined by the recent hydrodynamic theory of Ganatos, Weinbaum and Pfeffer (2) for the creeping motion of a sphere between two plane parallel walls. This improved description of the vesicle dynamics is used to generate vesicle concentration profiles using the theoretical formulation of Arminski et al. (1). A comparison of the present solutions with the time dependent tracer data of Casley-Smith and Chin (3) shows substantially improved agreement over previous models in which the effect of the steric hindrance of attached vesicles is neglected.

1. INTRODUCTION

Electron microscopic studies (4,5) and perfusion studies (6,7,8) have shown that the endothelial cell layer is the rate limiting barrier in the transport of macromolecules across the artery wall. Since the initial description by Palade (9), there has been increasing evidence (3,10) that the transendothelial transport of macromolecules, especially those larger than 40Å in diameter, cross the cell by vesicular transport.

With some deviation for vascular heterogeneity, electron dense markers larger than 40Å are seen to traverse endothelial cells via plasmalemma vesicles rather than through the intercellular clefts (5). Vesicles are spherical, 700Å, membrane bound intracellular bodies. When unimpeded by cytoplasmic structure, unattached (free) vesicles undergo a diffusional migration across the cell which is strongly influenced by a hydrodynamic and molecular force interaction with the plasmalemma membranes of the endothelial cell. The time dependent tracer studies of Casley-Smith and Chin (3) and Simionescu, Simionescu and Palade (5) indicate that vesicles are attached long enough at both the luminal and tissue fronts for the marker molecules horseradish peroxidase and exogenous myoglobin to come to concentration equilibrium with the surrounding luminal and interstitial fluid respectively. Current evidence indicates that larger tracer macromolecules, e.g., ferritin, do encounter molecular sieving effects in the vesicle neck.

Laboratory experiments to study vesicular transport are usually conducted by introducing a uniform source of labeled macromolecules at the luminal

KEY WORDS: vesicular transport, theoretical model, vascular endothelium

surface and then studying the subsequent advance of the labeled vesicles at different time intervals across the cell. Tomlin (11) estimated that the loading of the vesicles in the absence of molecular sieving occurs on the order of 10^{-2} sec. The only investigation that quantitatively attempts to follow this sequence of events is the transport data of Casley-Smith and Chin (3). These authors measured the relative concentration of labeled cytoplasmic vesicles at increasing distances across some heart endothelium and diaphragmatic mesothelium using the tracers ferritin, horseradish peroxidase, and sodium ferrocyanide. The cells were incubated in Hank's solution containing the tracer for periods of 2 sec up to 30 min at 37°C.

Although there have been a variety of theoretical models to quantitatively study both steady state and time dependent vesicular transport (11,12,13, 14,15,16), the only theory which can follow the transient sequence of events leading to steady state labeling is that of Arminski, Weinbaum and Pfeffer (1). The time dependent solutions of Rubin (16) are valid only for very short times since the influence of the plasmalemma on the tissue side of the cell is neglected. Rubin's analysis also does not consider the spatial variation of the vesicle diffusion coefficient due to the hydrodynamic interaction of a free vesicle with the boundary plasmalemma or the additional resistance a vesicle encounters due to the steric hindrance of attached vesicles.

The earliest of the steady state models were based on one-dimensional continuum diffusion theory (11) or random walk computer simulation experiments (12) in which the interaction of the vesicle with the boundary plasmalemmas was neglected entirely and a constant diffusion coefficient was assumed based on infinite domain Stokes-Einstein diffusion theory.

The first dynamic model of the steady state vesicular transport process which attempts to account for the hydrodynamic and molecular force interaction between the vesicle and the plasmalemma, is presented in Weinbaum and Caro (15). This more complete model still neglects the chemical, elastic and viscoelastic energies involved in the formation and dissolution of the vesicle attachment stalks. These latter processes, the formation and dissolution of the vesicle neck, are treated as a free energy barrier within the framework of absolute reaction rate theory in Rubin (16).

The more recent time dependent theory of Arminski, Weinbaum and Pfeffer (1) combines the reaction rate theory approach of Rubin (16) modified to take account of asymmetry of the vesicle attachment/detachment process (17) with the spatially non-uniform diffusion theory of Weinbaum and Caro (15) extended to unsteady one-dimensional diffusion.

In this model, a theoretical expression is derived for the spatial variation of the diffusion coefficient, which considers the increased hydrodynamic resistance of the vesicle as it approaches the plasma membranes on each side of the cell, and the van der Waals electrodynamic attractive force between the vesicle and the boundary plasmalemmas. The agreement of this more complete theory with the steady state labeling data of Casley Smith and Chin (3) was disappointing although the results for early times were satisfactory. This discrepancy was attributed in part to the resistance due to steric hindrance of attached vesicles at the plasmalemmas.

The freeze cleavage electron micrograph shown in Fig. 2 of Simionescu, Simionescu and Palade (18) and the extensive data on the density of vesicular openings provide clear evidence that a vesicle attempting to attach at a plasmalemma membrane must experience significant steric resistance effects. However, all existing theoretical models have neglected this effect because there was no available theory or experiment to describe the spatial variation of the vesicle diffusion coefficient as a function of the vesicle attachment density.

It is the purpose of this paper to determine more realistic expressions for the spatial variation of the vesicle diffusion coefficient and hence obtain an improved description of transient vesicle dynamics by combining laboratory experiments, which model the ultrastructural features of a plasmalemma and its attached vesicles, with the theory of Ganatos, Weinbaum and Pfeffer (2) for a sphere translating perpendicularly between two parallel walls. Section 2 reviews the relevant parts of the theory presented in Arminski at al. (1) which are pertinent to the proposed model. Section 3 is a description of the experimental apparatus and method. In section 4 we present the predic-

Vol. 1
1980

tions of the new model and a discussion of these results.

2. THEORETICAL MODEL

The essential features of the theoretical formulation of the overall transendothelial vesicle transport presented in Arminski, Weinbaum and Pfeffer (1) are summarized in this section. The motion is characterized by five different length scales (see Fig. 1): a short length ϵ_o, representative of

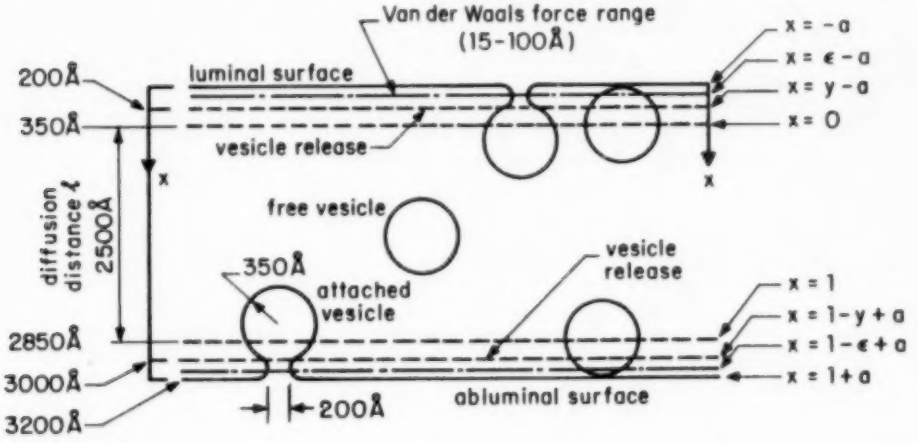

FIG. 1

Schematic illustration showing coordinates and geometry for mathematical model of plasmalemma vesicle migration across border region of endothelial cell. Dimensions are based on canine carotid artery.

London van der Waals electrodynamic forces, a hydrodynamic interaction length characteristic of the vesicle-cell membrane interaction, the vesicle radius a, the vesicle release distance y, and the transendothelial diffusion distance ℓ.

The simplified geometry and typical dimensions for the diffusion of a vesicle across an endothelial cell are shown schematically in Fig. 1. The origin of coordinates is measured from the vesicle center assuming the outer edge of the vesicle touches the luminal surface. The vesicles are assumed to be released from the lumen at a finite distance y=200Å equal to the length of the vesicle attachment stalk. The distance between the plasmalemmas is equal to the diffusion distance of the center of the vesicle ℓ plus the vesicle diameter 2a representing the excluded distance of the vesicle center from the two boundary membranes. In the vicinity of each plasmalemma narrow regions are hypothesized to exist where electrodynamic forces are important. As discussed later the effective center of interaction, ϵ_o, of these layers lies from 15 to 100Å from the plasmalemma surface although the long range effect of the van der Waals forces can be felt as far as 400-500Å from this surface. The interior surface of the plasmalemma and the exterior surface of the vesicle are believed to contain little negative charge. For this reason electric double layer forces have been neglected in the model.

The conservation equation for the vesicle number density c on each side of the plane of release x=y can be described by a continuum equation (1) of the form (all quantities in dimensional form)

$$\frac{\partial c}{\partial t} + \frac{\partial c u_{vw}}{\partial x} = \frac{\partial}{\partial x}\left(D(x)\frac{\partial c}{\partial x}\right) \qquad \begin{matrix} 0 < x < y \\ y < x < \ell \end{matrix} \qquad (1)$$

where u_{vw} can be thought of as a convective velocity for the vesicles created by the macroscopic London-van der Waals force and D(x) is a spatially dependent diffusion coefficient that describes the fluid resistance a spherical vesicle experiences in performing a one-dimensional Brownian motion between parallel plasmalemmas. All distances in equation (1) will henceforth be scaled relative to the diffusion distance ℓ.

The expression for D(x) is obtained by introducing an effective viscosity $\mu(x) = \lambda(x)\mu_o$ into the Stokes-Einstein relation for the diffusion coeffi-

cient where μ_o is the unbounded fluid viscosity and λ is a hydrodynamic interaction parameter describing the variation in fluid resistance for the perpendicular motion of a spherical particle between the plasmalemmas. Thus:

$$D(x) = D_o/\lambda(x) \tag{2}$$

where D_o is the vesicle diffusion coefficient in an infinite medium.

The derivation of an accurate expression for λ, even when the steric hindrance of attached vesicles is neglected, is a formidable mathematical problem. Exact solutions to the hydrodynamic problem for the creeping motion of a sphere between infinite plane parallel boundaries have recently been obtained by Ganatos, Weinbaum and Pfeffer (2). Previous to this the only available strong interaction solution was that of Brenner (19) for the motion of a sphere approaching a single plane wall in an infinite fluid.

In Arminski, Weinbaum and Pfeffer (1) $\lambda(x)$ is represented by:

$$\lambda = \beta + \frac{\theta a}{x} + \frac{\theta a}{1-x} \tag{3}$$

where the constants β and θ are selected to provide an optimum root mean square curve fit with the exact results of Ganatos et al. (2). In the present paper the values of β and θ will be modified as described in section 3 to take account the effect of steric hindrance of the attached vesicles.

Laboratory experiments to study vesicular transport are usually conducted by introducing at some time t = 0 a labeled marker molecule and then studying the subsequent advance of the labeled vesicles at different time intervals across the cell. The boundary and initial value problem described by such an experiment is much more difficult than its steady state counterpart solved by Weinbaum and Caro (15). One simplifying feature, easily demonstrated by an order of magnitude analysis (1), is that the characteristic time required to achieve a quasi-steady vesicle concentration profile in the thin van der Waals force layers near each plasmalemma is of $0(\varepsilon_o a/\ell^2)$ shorter than the time required to achieve a steady state profile for the entire cell. The narrow van der Waals force layers near each plasmalemma therefore develop in a quasi-steady manner with a nearly steady state concentration profile that is slowly changing in response to events that occur in the cell interior.

The quasi-steady solution to equation (1) derived in (15) is:

$$\frac{cD_o}{\theta a A(t)} = \frac{1}{3} \ln\left[1+(x/\varepsilon_o)^3\right] \tag{4}$$

where A(t) is a slowly varying function of time that is obtained by matching with the unsteady solution in the cell interior.

As shown in Fig. 6 of (15) the effective van der Waals force layer thickness ε_o is defined as the distance from the plasmalemma at which the free vesicle concentration would appear to vanish for the solution in the cell interior if electrodynamic forces were not present. The dimensionless distance $\varepsilon = \varepsilon_o/\ell$ plays the same role as a displacement thickness in fluid boundary-layer theory. Though ε is small it can not be set equal to zero since the fluid resistance is infinite as x approaches zero and the concentration (see equation (4)) would be logarithmically singular at the origin. Long range electrodynamic forces are therefore essential to overcome hydrodynamic resistance at close spacing.

In the interior of the cell, outside the van der Waals layers, equation (1) can be non-dimensionalized by introducing the scaled variables $x^* = x/\ell$, $t^* = tD_o/\ell^2$ and $c^* = cD_o/\varphi\ell$, where φ is the vesicle release rate per unit area of luminal surface. The dimensionless vesicle conservation equation for vesicles released at the luminal surface (asterisk dropped) is:

$$\frac{\partial c}{\partial t} = \frac{\partial}{\partial x}\left(\frac{1}{\lambda(x)}\frac{\partial c}{\partial x}\right) \qquad \begin{matrix}\varepsilon \le x \le y^- \\ y^+ \le x \le 1-\varepsilon\end{matrix} \tag{5}$$

In this interior region $u_{vw} = 0$ since the van der Waals forces vanish. The effect of the van der Waals forces can be approximated by simply relocating the position at which the free vesicle concentration vanishes in accord with the above definition of the van der Waals displacement distance. Thus:

$$c(\varepsilon,t) = 0 \tag{6a}$$

$$c(1-\varepsilon,t) = 0 \tag{6b}$$

Initially there are no labeled vesicles so that:

$$c(x,0) = 0 \tag{7}$$

At x = y, the average intrusion distance for vesicles released from the

luminal membrane, the concentration of free vesicles is continuous:

$$c(y^-,t) = c(y^+,t) \tag{8}$$

but there is a discontinuity in concentration gradient. In dimensionless form this discontinuity is given by:

$$1 = \frac{1}{\lambda(y)}\left[\frac{\partial c(y^-,t)}{\partial x} - \frac{\partial c(y^+,t)}{\partial x}\right] \tag{9}$$

Equation (9) states that the difference in diffusive flux at each side of the plane x=y is equal to the vesicle release rate which has been scaled to unity by the nondimensionalization.

Equation (5) is also valid in the range $\varepsilon \le x < 1-y$ and $1-y < x \le 1-\varepsilon$ for vesicles released at the tissue front, where at $x = 1-y$ equivalent matching conditions to (8) and (9) hold. Statistical studies performed by Bruns and Palade (20) and Casley-Smith (21) for the number density profile of free vesicles at each plasmalemma show that the vesicle transport is nearly symmetric.

In the steady state, equation (5) can be reduced to a constant coefficient equation by introducing the transformation

$$d\xi = \lambda(x)\,dx \tag{10}$$

This steady state diffusion equation is

$$\frac{d^2c}{d\xi^2} = 0 \qquad \begin{matrix}\varepsilon \le x < y \\ y < x \le 1-\varepsilon\end{matrix} \tag{11}$$

In the transformed ξ coordinate matching condition (9) and the other boundary and matching conditions are all independent of $\lambda(x)$. Thus, the steady state solution to equation (11), given later by equations (14a,b), is valid for an arbitrary one-dimensional spatial distribution for $\lambda(x)$ and hence $D(x)$.

For the time dependent case the introduction of the coordinate transformation (10) gives the more convenient form:

$$\frac{\partial c}{\partial t} = \lambda(\xi)\,\frac{\partial^2 c}{\partial \xi^2} \qquad \begin{matrix}\xi(\varepsilon) \le \xi(x) < \xi(y) \\ \xi(y) < \xi(x) \le \xi(1-\varepsilon)\end{matrix} \tag{12}$$

When λ is given by equation (3), equation (10) is readily integrated to give

$$\xi(x) = \theta(x-\varepsilon) + \theta a \ln\left[\frac{x(1-\varepsilon)}{(1-x)\varepsilon}\right] \tag{13}$$

where the origin $\xi = 0$ is chosen for convenience to be at $x = \varepsilon$.

To circumvent the considerable time and expense that would be required in a finite difference solution scheme, Arminski, Weinbaum and Pfeffer (1) use an approximate integral solution technique in which (12) is converted to two coupled first order ordinary differential equations. The outline of the solution procedure is shown in Fig. 2. One considers two concentration boundary layers of thickness $\delta_1(t)$ and $\delta_2(t)$ spreading with time from the vesicle plane of release x=y. There are three different time domains of solution. For $t \le t_1$ both boundary layers diffuse until the one on the left reaches $x = \varepsilon$ and $\delta_1(t_1) = y-\varepsilon$. The boundary layer to the right of x=y has not yet reached $x = 1-\varepsilon$. This marks the beginning of the second time domain $t_1 \le t \le t_2$. In this time domain the boundary layer on the right continues to grow towards $x = 1-\varepsilon$, while the one on the left remains fixed at $x = \varepsilon$, where it satisfies condition (6a), but with a time dependent concentration gradient $\alpha_1(t)$ at $x=\varepsilon$. This behavior continues until the boundary layer on the right reaches $x = 1-\varepsilon$ and $\delta_2(t_2) = 1-\varepsilon-y$. In the third time domain $t_2 \le t \le t_\infty$ both boundary layers satisfy equation (6) at their ends $x = \varepsilon$ and $x = 1-\varepsilon$, but their concentration gradients at these locations will vary until a steady state concentration profile is asymptotically achieved. The details of the integration procedure are given in Arminski et al. (1). One can also show that the undetermined function A(t) in the profile (4) for the van der Waals force layer at the luminal membrane is zero for $t < t_1$ and $\alpha_1(t) \neq 0$ for $t > t_1$.

To compare the predictions of the theory with the time dependent tracer studies of Casley-Smith and Chin (3) one needs to determine the proportion of labeled vesicles to total concentration of vesicles at any distance across the endothelium. The total concentration at any point is obtained by adding the steady state concentration profiles due to vesicle release at both the lumen and tissue fronts. Integration of (11) with boundary and matching conditions (6), (8) and (9) yields

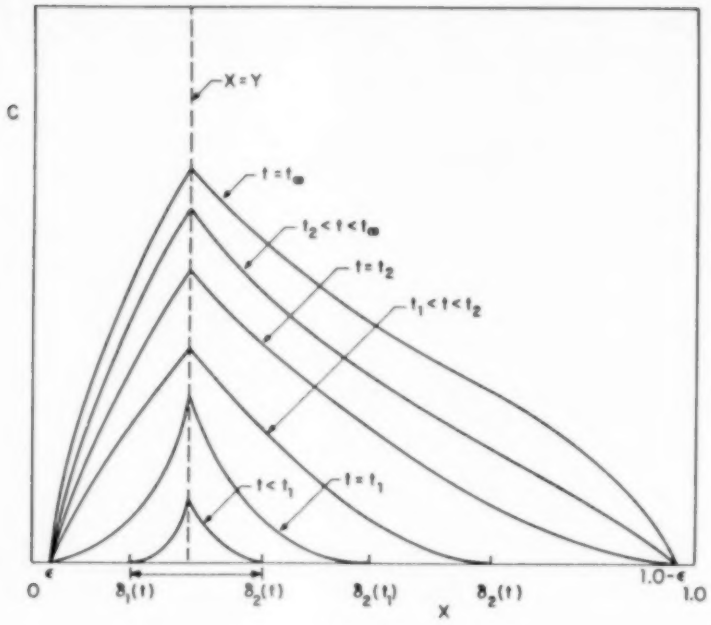

FIG. 2

Three time domains for concentration profiles of integral solution technique.

$$c(\xi(x)) = \left[1 - \frac{\xi(y)}{\xi(1-\epsilon)}\right] \xi(x), \quad \epsilon \le x < y \tag{14a}$$

$$c(\xi(x)) = \left[1 - \frac{\xi(x)}{\xi(1-\epsilon)}\right] \xi(y), \quad y < x \le 1-\epsilon \tag{14b}$$

The corresponding expressions for the vesicles released at the tissue front are:

$$c(\xi(x)) = \left[1 - \frac{\xi(1-y)}{\xi(1-\epsilon)}\right] \xi(x), \quad \epsilon \le x < 1-y \tag{15a}$$

$$c(\xi(x)) = \left[1 - \frac{\xi(x)}{\xi(1-\epsilon)}\right] \xi(1-y), \quad 1-y < x \le 1-\epsilon \tag{15b}$$

Fig. 7 of Arminski, Weinbaum and Pfeffer (1) compares the theoretically predicted concentration profiles and the experimental data of Casley-Smith and Chin (3). The curves are based on the exact solution of Ganatos, Weinbaum and Pfeffer (2) for $\lambda(x)$ in which the effect of steric hindrance of attached vesicles is neglected. These solutions provide reasonable agreement with the experiment for short times, but show a much poorer agreement as the steady state is approached. A reasonable explanation of this discrepancy is the increased value for $\lambda(x)$ as a vesicle approaches a plasma membrane due to the steric hindrance of attached vesicles.

The next section is concerned with the experimental determination of $\lambda(x)$ in which the effects of steric hindrance are included. From these values for $\lambda(x)$ new values for θ and β in relation (3) are found and new time dependent concentration profiles are generated and compared with the data of Casley-Smith and Chin (3).

3. LABORATORY MODEL EXPERIMENTS

This section is devoted to a description of the experimental apparatus and method.

A nylon test sphere measuring 0.5 in. in diameter was dropped through a tube into a rectangular tank filled with UCON 50-HB-5100 fluid where viscosity was high enough so that the Reynolds number based on particle diameter did not exceed 0.01. The test sphere, randomly released, settled under gravity onto an array of identical acrylic spheres which were attached by connecting

Vol. 17
1980

rods to a plexiglass plate at the bottom of the tank (see Fig. 3). The plate

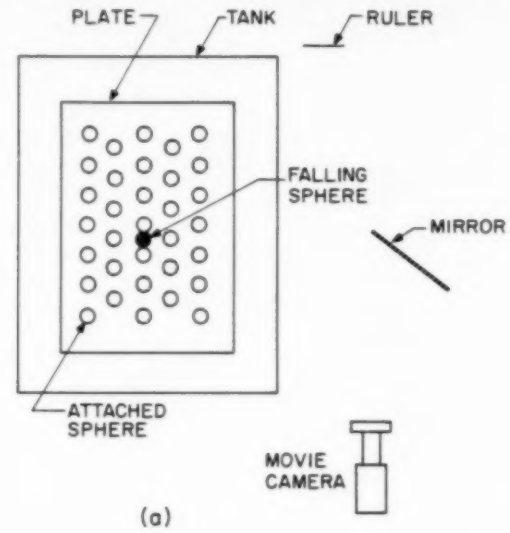

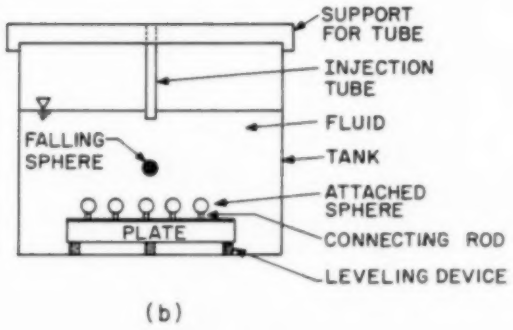

FIG. 3

Schematic illustration of experimental apparatus. (a) Top view of tank with tube support removed, ruler, mirror and movie camera. (b) Front view of tank.

and attached spheres were designed to model the ultrastructural features of a plasmalemma membrane and its attached vesicles. The sphere diameter of 0.5 in. corresponded to a vesicle diameter of 700Å. All other dimensions were scaled according to these figures, including the length of the connecting rod between the plate and attached spheres so that a vesicle neck was simulated.

Three different plates were used each with a different center-to-center spacing between attached spheres. The relationship between center-to-center distance, χ, and vesicle number density per μm^2, ρ, is shown in Fig. 4. A hexagonal pattern was chosen for the array after carefully viewing the freeze-cleaved preparations of Simionescu, Simionescu and Palade (18) showing broken vesicle necks (see for example, Fig. 2 in that paper).

The tank was placed on a fatigue mat in order to damp out vibrations. Care was taken to insure that the plate was parallel to the surface of the fluid. The experimental set-up was maintained at constant temperature so that the viscosity and density of the fluid were nearly uniform. Temperature and viscosity measurements were made at the beginning and end of each series of runs to insure that there were no changes in viscosity during the runs and no temperature gradients in the tank.

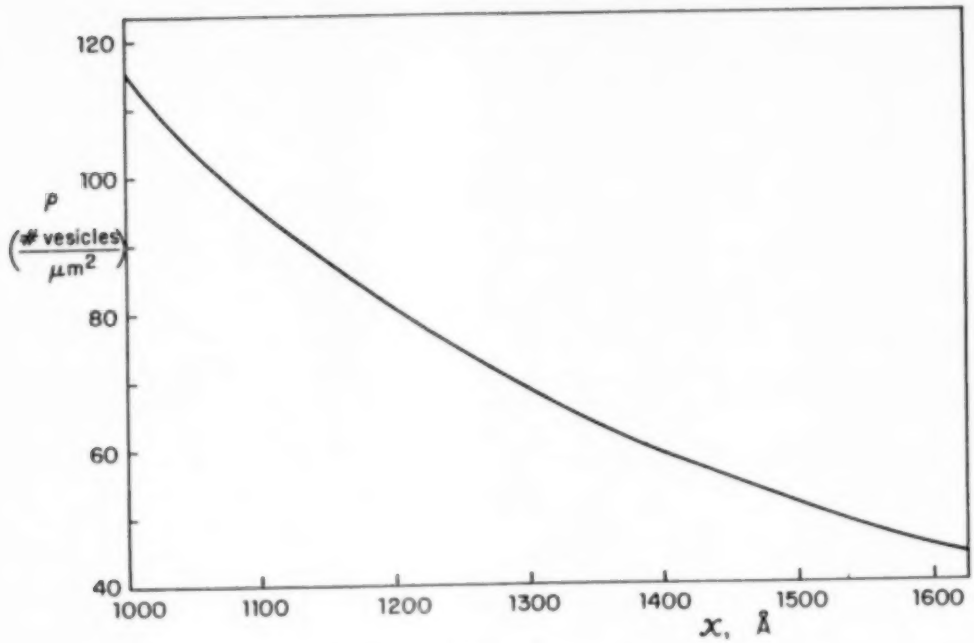

FIG. 4

Vesicle density per μm^2 ρ as a function of vesicle center-to-center distance χ in a hexagonal array.

A Bauer C Royal 6-Zoom Super 8 movie camera was used to take continuous motion pictures of each run. The camera was mounted on a variable height tripod which was lowered during every run so that the sphere would remain at right angles to the camera so as not to introduce any parallax. In order that a reference scale could be introduced into the picture frame it was decided not to take a direct shot of the falling sphere. Rather, a properly leveled front surface mirror was placed at a location equidistant to the falling sphere and the reference (ruler). By proper placement a split-screen image was produced. This procedure resulted in a picture of far better resolution than that of a direct image because the focal length for the images of the sphere and the reference were identical.

A Kodak Ektagraphic MFS-8 movie projector was used to project the films onto a grid from which measurements were taken. For each .125 in. the sphere traveled, the number of frames on the film were counted. Knowing the number of frames passing per second, velocities at the mean position of the sphere for every .125 in. of travel were calculated. The ratio of the terminal settling velocity, which was calculated from the physical parameters of the fluid and falling sphere, to the actual measured velocity gave the correction to the Stokes drag, λ, as a function of distance from the plate.

Simionescu, Simionescu and Palade (18) measured the average density of vesicular openings per μm^2 within the endothelium of both muscular (diaphragm, myocardium) and visceral (pancreas, jejunal villi) capillaries in rats. Their data indicated the number of openings per μm^2 was 78 in diaphragm, 89 in myocardium, 25 in pancreas, and 10 in jejunal mucosa capillaries. Drs. K.M. Jan and S. Chien at the Columbia University School of Medicine have measured approximately 120 openings per μm^2 in canine carotid artery. On the basis of the above results, we chose spacings of 1100, 1300 and 1500 Å corresponding to vesicle number densities of 95, 68 and 51 vesicles/μm^2 respectively as representative values for our experiments.

Many spheres were dropped on each plate so that a statistical average for λ could be obtained. All runs were discontinued once the falling sphere

Vol. 17
1980

touched an attached sphere; thus only hydrodynamic effects were considered.

4. RESULTS AND DISCUSSION

Experimentally determined values for the hydrodynamic interaction parameter λ of a sphere settling under gravity onto a plate fitted with an array of identical spheres are shown in Fig. 5 for simulated vesicle center-to-

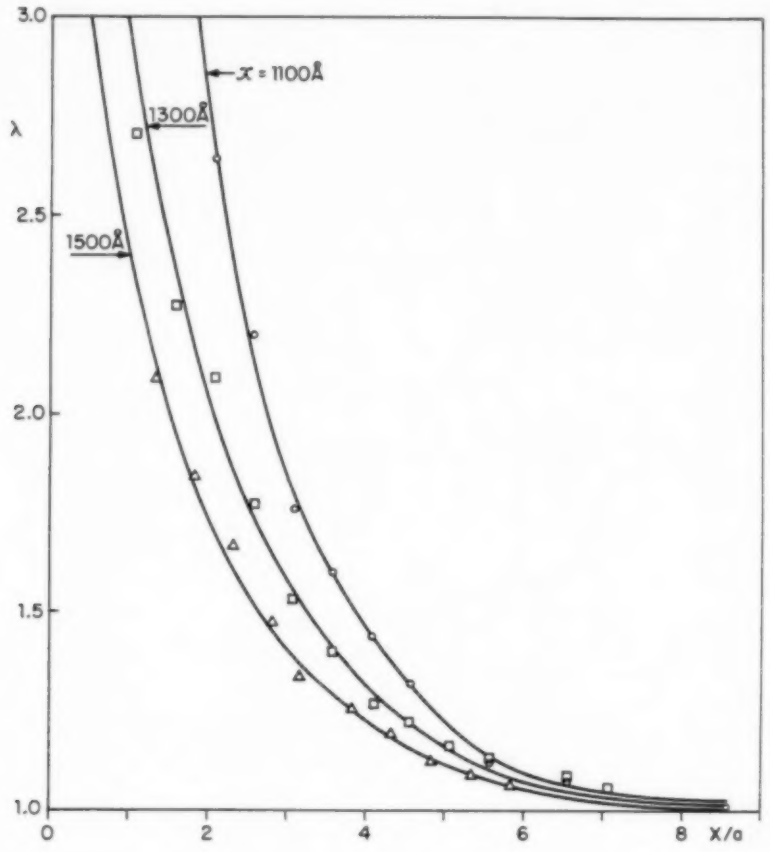

FIG. 5

Correction to Stokes drag as a function of the number of vesicle radii (x/a) from plasma membrane for various vesicle center-to-center, χ, distance. Experimental data: o - χ = 1100Å; □ - χ = 1300Å; Δ - χ = 1500Å.

center spacings of 1100, 1300 and 1500Å. These results are shown for increasing distances from the plate as number of sphere radii (x/a). Fig. 5 shows that the vesicle center-to-center spacing χ has an important effect on the hydrodynamic interaction parameter close to the plasmalemma but has little or no influence far away from the plasmalemma. One can see that for small values of x/a, decreasing the vesicle center-to-center distance and hence increasing the steric hindrance due to the steric crowding of attached vesicles significantly increases the correction to the Stokes drag. However, for large values of x/a the value of λ asymptotes to 1 for all values of x.

The results given in Fig. 5 are valid only for one plasmalemma and its attached vesicles with the second being removed. Close to the plasmalemma, the increased hydrodynamic resistance due to the presence of attached vesicles is so great that the influence of the other plasma membrane can be neglected. But, in the interior part of the cell these experimental values underestimate the value of λ because of the absence of the second wall. Thus, it was decided to use the results of the experiment to estimate λ close

to the plasmalemma and the exact solution for a sphere translating perpendicularly between two planar walls (2) to estimate λ in the interior region.

Expression (3) has been plotted as the solid curve in Fig. 6 to approximate λ for a vesicle center-to-center spacing of 1100Å and a transendothelial

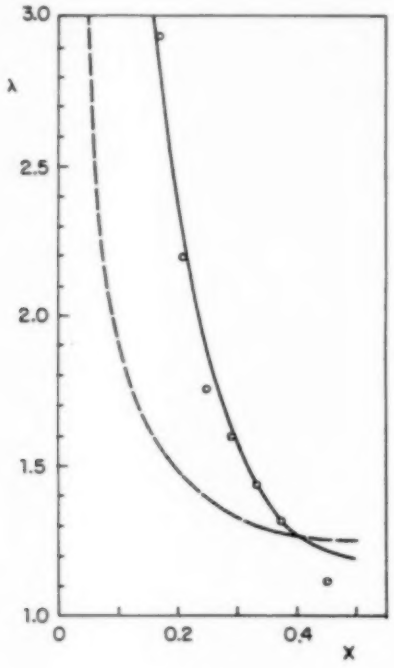

FIG. 6

Correction to Stokes drag across endothelial cell for a vesicle center-to-center distance of 1100Å and a transendothelial diffusion distance ℓ of 4300Å. o - experimental data; ---theory of Ganatos, Weinbaum and Pfeffer (2); ___curvefit.

diffusion distance of 4300Å. The constants β and θ for the spacing of 1100Å are -0.99 and 6.6 respectively and were obtained by a least squares curve fit of our experimental results near the plate and the theoretical results of Ganatos et al. (2) (indicated by the dashed curve) in the interior. Values for β and θ for other vesicle spacings can be found in Arminski (22). A comparison of the solid and dashed curves in Fig. 6 shows a significant increase in the value of the hydrodynamic resistance parameter when the effects of steric hindrance are taken into account.

A comparison of the theoretically predicted concentration profiles with the data of Casley-Smith and Chin (3) is shown in Fig. 7 for an assumed transendothelial diffusion distance of 4300Å and a van der Waals cut-off distance of 15Å. The time to reach steady state is taken to be the time at which the peak concentration has reached 98% of its final value. One observes that there is a marked improvement over the agreement shown in Fig. 7 of Arminski, Weinbaum and Pfeffer (1). Whereas the agreement in Arminski et al. (1) was good only for short times, it is good for all times in the present study.

The times shown in Fig. 7 are real times (not non-dimensionalized). These were obtained using the relation $t^* = tD_o/\ell^2$. In order to calculate D_o from the Stokes-Einstein relation, one needs to know the intracellular viscosity. Unfortunately, there is a great deal of uncertainty in the value of this physical quantity. Values in the literature range from 0.2 poise (3) to 8 poise (12) and higher. Since the dimensionless time t^* to reach steady state can be estimated from the 98 percent criterion mentioned previously and

Vol. 1
1980

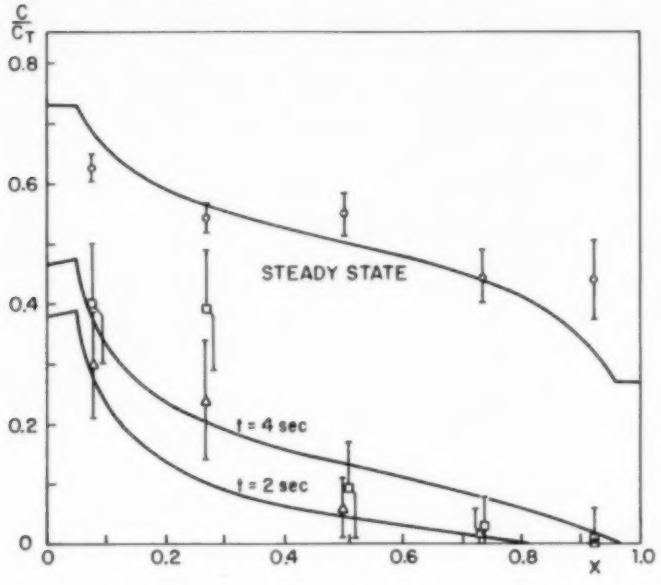

FIG. 7

Theoretical and experimental time dependent proportion of labeled vesicles c/c_T as a function of distance x for an effective van der Waals cut-off distance ϵ_o of 15Å, a transendothelial diffusion distance ℓ of 4300Å and a vesicle center-to-center distance χ of 1100Å. Experimental data: Δ, 2s; □, 4s; 0 ≥ 16s (Casley-Smith and Chin (3)): vesicles labeled with horseradish peroxidase). Vertical bars represent ± 1 standard error.

Casley-Smith and Chin (3) found experimentally that it took approximately 10 sec for steady state to be reached, one can calculate D_o and hence μ_o from the relation $t^* = tD_o/\ell^2$. Values for μ_o of 638, 780 and 845 cp were found for center-to-center distances of 1100, 1300 and 1500Å respectively. All these values are lower, as would be expected, than the value 895 cp found in Arminski, Weinbaum and Pfeffer (1) where steric exclusion was not considered.

If the constants β and θ in (3) are chosen to be unity, the steady state solutions (14a,b) are identical to equations (3.25a,b) in Weinbaum and Caro (15). In Fig. 8 this solution is compared to the present steady state concentration profile. Fig. 8 shows that the modified mathematical model developed in the present study gives better agreement with the data of Casley-Smith and Chin (3), especially near the plasmalemma membranes where the effects of steric hindrance are important. Although this improved agreement of theory and experiment is encouraging, we point out that exact numerical comparisons with the electron microscopic data of Casley-Smith and Chin (3) must be interpreted cautiously. As pointed out in Simionescu, Simionescu and Palade (18) it is extremely difficult to distinguish an attached from a free vesicle when close to the plasmalemma if the location of the cutting plane is not known.

In Fig. 9 the effect of the van der Waals cut-off parameter ϵ_o is examined. Steady-state concentration profiles have been plotted for van der Waals cut-off distances of 15, 50 and 100Å. The proportion of free labeled vesicles is higher at the luminal side and lower at the tissue side for the case ϵ_o = 100Å than for the smaller van der Waals cut-off distances. This occurs because a vesicle is more likely to reattach at the vesicle plane of release (x=y) the closer ϵ is to x=y. Thus more labeled vesicles are located near x=y and less are transported across the cell to the tissue side.

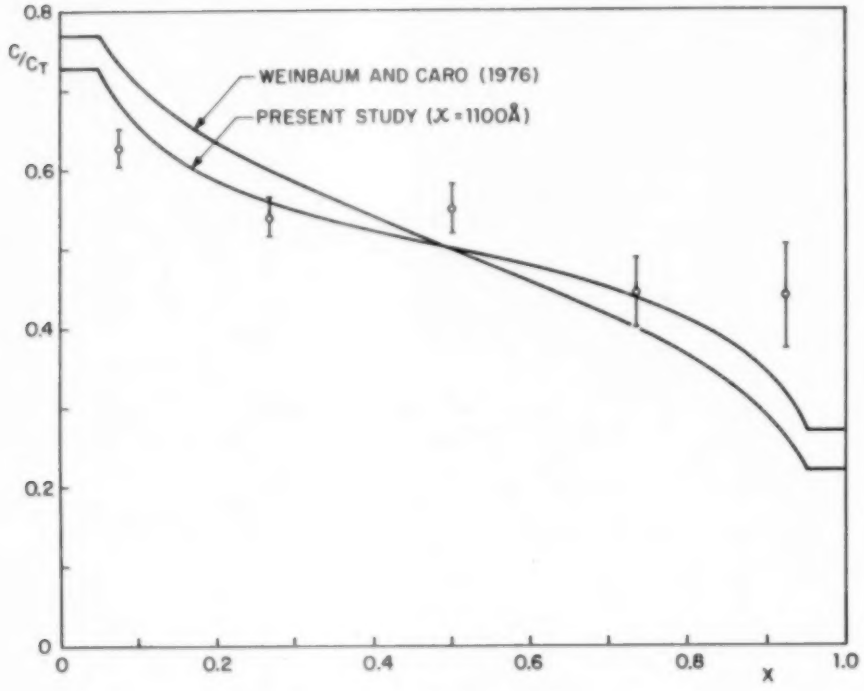

FIG. 8

Comparison of steady state proportion of labeled vesicles c/c_T as a function of distance x of Weinbaum and Caro (15) and present study (χ = 1100Å) for an effective van der Waals cut-off distance ϵ_o of 15Å and a transendothelial diffusion distance ℓ of 4300Å. Experimental data: 0 ≥ 16s (Casley-Smith and Chin (3): vesicles labeled with horseradish peroxidase). Vertical bars represent ± 1 standard error.

One important factor which has not been considered is that an incoming vesicle may not be able to fuse directly with a plasma membrane. Experimental evidence indicating this possibility is found in the paper of Simionescu, Simionescu and Palade (18). In a hexagonal pattern the minimum spacing required for a vesicle to just squeeze in is 1212Å corresponding to an attached vesicle density of 79 per μm^2. This suggests that incoming vesicles may fuse with already attached vesicles instead of fusing directly with the plasma membrane (18). It is also possible that a vesicle may detach just as another one is attaching. In addition, plasmalemma vesicles, though relatively thick-walled structures (membrane thickness roughly one-fifth of the vesicle radius), do deform under Brownian motion and thus are capable of penetrating an attached vesicle array that would be impermeable for rigid spheres. These effects were beyond the sophistication of our experiment.

Finally, it should be pointed out that vesicles are not identical. Simionescu, Simionescu and Palade (18) found a range of 640-720Å for the diameter of plasmalemma vesicles in rats. In addition, there appeared to be areas where the vesicle density was extremely high and no vesicle could fit through, while other areas left enough room for attachment. This non-homogeneity of attached plasmalemma vesicles may have to be considered in future theoretical models or laboratory model experiments.

In summary, we have modified the time dependent vesicle labeling theory of Arminski, Weinbaum and Pfeffer (1) to include some of the effects of steric hindrance. When experimentally determined values of the hydrodynamic

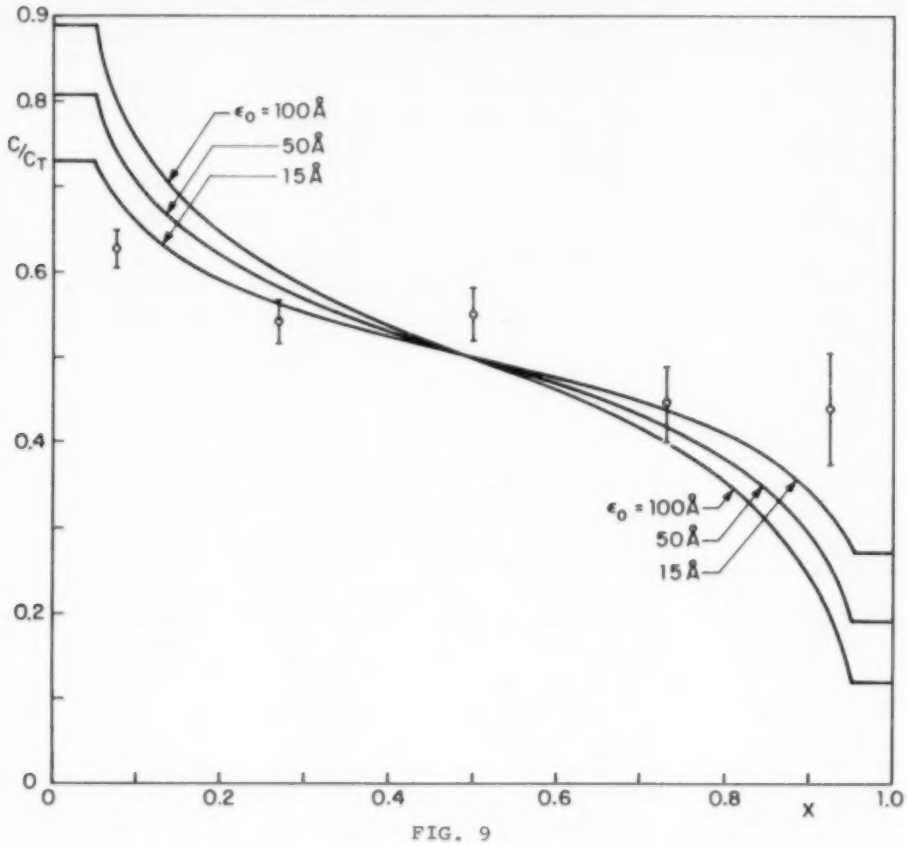

FIG. 9

Effect of van der Waals cut-off parameter ϵ_o on steady state proportion of labeled vesicles c/c_T as a function of distance x for a transendothelial diffusion distance ℓ of 4300Å and a vesicle center-to-center distance γ of 1100Å. Experimental data: 0 ≥ 16s (Casley-Smith and Chin (3): vesicles labeled with horseradish peroxidase). Vertical bars represent ± 1 standard error.

interaction parameter are included in the above theoretical formulation, substantially improved agreement with the data of Casley-Smith and Chin (3) is obtained.

The authors wish to thank Mr. Jonah Smith who performed the experimental runs, Mr. John Da Silva, Artist in Residence, at the Leonard Davis Center for Performing Arts (Picker Film Institute) for his assistance in lighting and Drs. C. Caro, K.M. Jan, M. and N. Simionescu and R. Skalak for their many helpful comments. This work was jointly supported by NSF Grant ENG 75-19243 and NIH Grant HL 19454. The above work has been performed in partial fulfillment of the requirements for the Ph.D. degree of L. Arminski at The City University of New York

5. REFERENCES

1. ARMINSKI, L., WEINBAUM, S. and PFEFFER, R. Time dependent theory for vesicular transport across vascular endothelium. J. Theor. Biol. 85, 13-43, 1980.

2. GANATOS, P., WEINBAUM, S. and PFEFFER, R. A strong interaction theory for the creeping motion of a sphere between plane parallel boundaries. Part 1. Perpendicular motion. J. of Fluid Mech. 99, 739-753, 1980.

3. CASLEY-SMITH, J.R. and CHIN, J.C. The passage of cytoplasmic vesicles across endothelial and mesothelial cells. J. Microsc. 93, 167-189, 1971.

4. KARNOVSKY, M.J. The ultrastructural basis of capillary permeability studied with peroxidase as a tracer. J. Cell Biol. 35, 213-236, 1967.

5. SIMIONESCU, N., SIMIONESCU, M. and PALADE, G.E. Permeability of muscle capillaries to exogenous myoglobin. J. Cell Biol. 57, 424-452, 1973.

6. FRY, D.L. Localizing factors in arteriosclerosis. In: Atherosclerosis and Coronary Heart Disease. W. Likoff, B. Segal, W. Insull and J.H. Mayer (Eds.), New York: Grune and Stratton 1972, pp. 40-83.

7. SIFLINGER, A., PARKER, K. and CARO, C.G. Uptake of ^{125}I albumin by the endothelial surface of the isolated dog common carotid artery: effect of certain physical factors and metabolic inhibitors. Cardiovasc. Res. 9, 478-489, 1975.

8. CARO, C.G. Specialists meeting at the Ohio State University, Columbus, Ohio, August 24-25, 1978.

9. PALADE, G.E. Fine structure of blood capillaries. J. Appl. Phys. 24, 1424 (Abstr.), 1953.

10. PALADE, G.E. Transport in quanta across the endothelium of blood capillaries. Anat. Record 136, 254 (Abstr.), 1960.

11. TOMLIN, S.G. Vesicular transport across endothelial cells. Biochim. Biophys. Acta 183, 559-564, 1969.

12. SHEA, S.M., KARNOVSKY, M.J. and BOSSERT, W.H. Vesicular transport across endothelium: Simulation of a diffusion model. J. Theor. Biol. 24, 30-42, 1969.

13. GREEN, H.S. and CASLEY-SMITH, J.R. Calculations on the passage of small vesicles across endothelial cells by brownian motion. J. Theor. Biol. 35, 103-111, 1972.

14. SHEA, S.M. and BOSSERT, W.H. Vesicular transport across endothelium: A generalized diffusion model. Microvasc. Res. 6, 305-315, 1973.

15. WEINBAUM, S. and CARO, C.G. A macromolecule transport model for the arterial wall and endothelium based on the ultrastructural specialization observed in electron microscopic studies. J. Fluid Mech. 74, 611-640, 1976.

16. RUBIN, B.T. A theoretical model of the pinocytotic vesicular transport process in endothelial cells. J. Theor. Biol. 64, 619-647, 1977.

17. PALADE, G.E. and BRUNS, R.R. Structural modulations of plasmalemmal vesicles. J. Cell Biol. 37, 633-649, 1968.

18. SIMIONESCU, M., SIMIONESCU, N. and PALADE, G.E. Morphometric data on the endothelium of blood capillaries. J. Cell Biol. 60, 128-152, 1974.

19. BRENNER, H. The slow motion of a sphere through a viscous fluid towards a plane surface. Chem. Eng. Sci. 16, 242-251, 1961.

20. BRUNS, R.R. and PALADE, G.E. Studies on blood capillaries. II. Transport of ferritin molecules across the wall of muscle capillaries. J. Cell Biol. 37, 277-299, 1968.

21. CASLEY-SMITH, J.R. Endocytosis: the different energy requirements for the uptake of particles by small and large vesicles into peritoneal macrophages, J. Microsc. 90, 15-30, 1969.

22. ARMINSKI, L. The transport of macromolecules across the vascular endothelium. Ph.D. Dissertation, The City University of New York, 1980.

Vol. 17
1980

BIORHEOLOGY, Vol. 17, pp. 445-454, 1980
Printed in the USA. All rights reserved.

0006-355X/80/050445-10$02.00/0
Copyright (c) 1981 Pergamon Press Ltd

THIXOTROPY OF BLOOD AND RED BLOOD CELL SUSPENSIONS

Donald E. McMillan, Nyle G. Utterback, and James B. Baldridge
Sansum Medical Research Foundation, Santa Barbara, California

(Received 7.29.1980; in revised form 14.10.1980.
Accepted by Editor Y.C. Fung)

ABSTRACT Thixotropy is an attribute that describes a fluid's decreasing viscosity with time as flow becomes established and its return to a higher flow resistance after shearing ceases. Blood's thixotropy is usually recognized as stress decay, a fall in apparent viscosity after the onset of viscometric flow at constant shear rate. We have operated a Couette viscometer at different constant shear rates and for different shearing durations to characterize the change with time in the shear stress response of blood and red blood cell suspensions. In examining post-shearing stress relaxation, we have observed stress decay during shearing and a relation between the two processes. Exponential stress relaxation following shearing at .024 inverse seconds shear rate has been found to be incomplete because of continuing slow relaxation rather than persistent post-shearing stress. As duration of shearing is shortened the proportion of stress released in the rapid and slow relaxation processes is maintained. Longer post-cessation observation demonstrates complete stress relaxation at .60 hematocrit and incomplete relaxation at .84-.90 hematocrit. The difference between the two post-shearing relaxation processes becomes striking when shear rate is increased while shearing duration is kept constant. Rapid relaxation decreases in duration while the slow relaxation is little affected. Stress decay during shearing also becomes prominent at higher shear rates, decreasing in duration as shear rate increases. When red blood cell suspensions are studied at constant total shear, stress decay is greater in magnitude at higher shear rate and disappears after a total shear of about 10. Studies using repetitive shearing show that stress decay diminishes after the first shearing period. Stress decay almost disappears when the interval between shearing periods is shortened to the point that shearing is reinstituted early in the slow relaxation process. We attribute both blood's thixotropy and its slow post-shearing stress relaxation to an association between rapidly developing elastic erythrocyte deformation and more slowly developing orientation of erythrocytes along shearing planes as flow becomes established.

INTRODUCTION

The term thixotropy was originally developed to describe fluids that decrease in resistance with time when they flow and revert to their original resistance to shearing after flow ceases (1). The universal method by which thixotropy has been studied is observation of stress (torque) decay, a decline in the force being transmitted by the thixotropic fluid to the viscometer wall following the onset of constant shear rate flow (1). The recording of stress hysteresis during a patterned increase and decrease of shear rate has recently been added as an alternative (2-4). Neither of these techniques for observing thixotropy obliges investigation of the change which occurs in the fluid on standing. Thixotropy has been linked both to viscoelasticity and to shear-thinning, the decline in steady-state observed viscosity seen as shear rate rises (5,6). We have recently demonstrated Maxwell fluid behavior of blood at very low shear rate (7). A monotonic onset of shear stress was observed at the onset of shearing and an exponential stress relaxation was seen after shearing ceased, but post-shearing relaxation was incomplete. We have encountered thixotropy in an investigation of the asymmetry of blood's Maxwell fluid behavior. Thixotropic stress decay has been linked to slow post-shearing stress relaxation which was found responsible for the asymmetry of Maxwell fluid behavior at low shear rate. Our observations suggest that stress decay during shearing, slow post-shearing stress relaxation, and the "yield stress" behavior of blood are linked to each other through the need for erythrocytes to establish and maintain an orientation during flow and their tendency to randomize when flow ceases.

KEY WORDS: blood viscosity, erythrocyte aggregation, erythrocytes, rheology, viscosity

MATERIALS AND METHODS

Fresh blood was used in both whole blood and red blood cell suspension studies. It was collected in EDTA vacutainers by venesection from two different individuals without known health impairment (DEM, JBB). Fasting blood was used in whole blood studies; non-fasting blood was used for red cell suspension studies. Silicone oils used for comparison were not detectably viscoelastic; they had a low shear rate stress onset similar to glycerol. All studies were done at 37°C. Hematocrit was modified as previously described; the design and operation of the Couette viscometer have been reported in detail (7,8).

A Tektronix 31 programmable calculator controls the onset and cessation of motion of the bob by signalling a solid state relay system. The sequence of study is mixing by vertical movement of the bob, collection of baseline stress values (40 or 20) starting less than 30 seconds later, bob rotation for a specified time with continuing collection of stress values, cessation of rotation (repeated rotation and cessation if appropriate), and completion of the study when a total of 240 stress values have been collected. A digital voltmeter records every 200 milliseconds the electrostatic torque being applied to restore or maintain the cup position so that 240 observations are made in multiples of 48 seconds. The electrostatic torque being applied to the cup is shown in each figure as shear stress, a value calculated by dividing the measured torque in dyne-cm by 20.76 cubic cm, the product of the radius and exposed surface area of the bob.

Onset and cessation of rotation of the bob have been studied in detail. Delay in development of motion after solid state relay activation was found to be approximately 100 milliseconds, due principally to retardation of physical movement of the electric motor. For that reason, a time delay was built into the controlling algorithm so that the first datum is collected 95-105 milliseconds after the actual onset of rotation of the bob. A similar delay occurs following the cessation signal and is similarly compensated. Data was processed by the Tektronix 31 calculator and stored on 8 inch flexible discs as previously described (7,8). In most studies more than one stress profile was averaged; the number of replicate analyses averaged is shown in each legend.

RESULTS

1. Maxwell Fluid Behavior - Shorter Duration of Shearing

The pattern of response of a .90 hematocrit red blood cell suspension in high potassium phosphate-buffered saline (PBS) is compared in Figure 1 to a 4 poise viscosity standard silicone oil at .024 inverse seconds shear rate. Monotonic onset of stress is observed at each shearing duration studied. Incomplete relaxation following early exponential decline is also seen. The impairment of relaxation is proportional to the peak stress achieved.

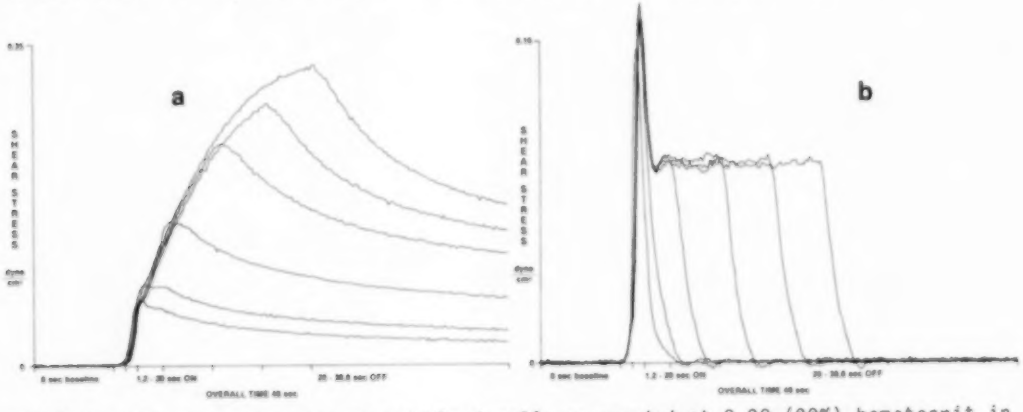

FIGURE 1. The stress response of red blood cells suspended at 0.90 (90%) hematocrit in phosphate-buffered saline (PBS) decreases as duration of shearing shortens (a). The response is compared to that of a 4 poise silicone oil (b). Shearing durations are 20, 15, 10, 5, 2.4 and 1.2 seconds. The shear rate is .024 inverse seconds for the silicone oil. Each plot is the mean of 6 individual stress profiles. The red cell suspension generates a monotonic stress pattern at low shear rate. At cessation of shearing both the exponential decline and the incomplete relaxation diminish similarly in magnitude as duration of shearing is shortened. The silicone oil stress pattern is dominated by early compensatory overshoot (7). At onset of shearing the sensing system (cup) moves a few microns; the electronic response system then generates sufficient excess countertorque to reestablish its original position. This adjustment produces the excess stress seen 2-4 seconds after shearing onset. Because the bob and gap fluid require more than a second to stop much less compensatory overshoot is observed at cessation of shearing.

Vol. 17
1980

2. Longer Post-Shearing Observation

To visualize the relaxation process more effectively the observation period at low shear rate (.024 inverse seconds) was extended to 480 seconds. An 86% red blood cell suspension in PBS (Figure 2a) was studied under the same conditions as a 4 poise silicone oil (Figure 2c). At cessation of shearing an early rapid decrease in stress is followed by a much slower decline which persists for 400 seconds. Whole blood generates stress levels too low for stable recording over an extended period. A 60% red blood cell suspension containing 0.75% dextran (MW 100,000 - 200,000) to raise low shear rate viscosity was studied as a substitute for blood. The dextran concentration chosen causes slight aggregation, demonstrated by a sedimentation of 3mm in one hour at 41% hematocrit in Westergren tubes. At 60% hematocrit post-shearing stress is completely released (Figure 2b).

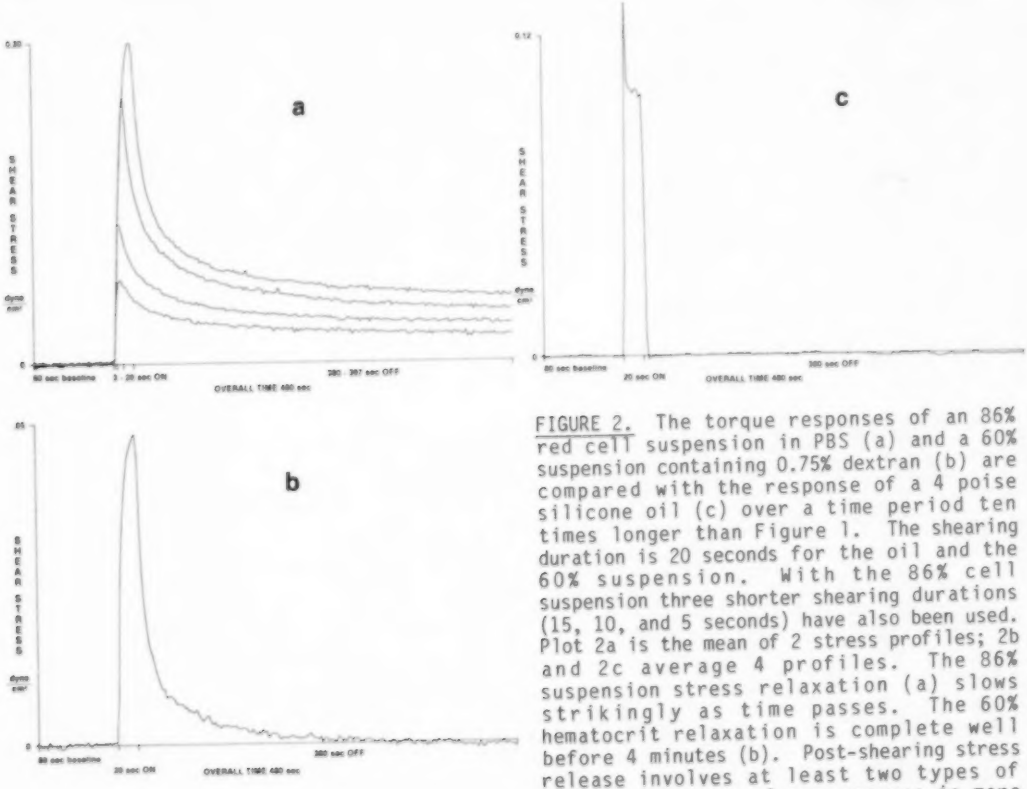

FIGURE 2. The torque responses of an 86% red cell suspension in PBS (a) and a 60% suspension containing 0.75% dextran (b) are compared with the response of a 4 poise silicone oil (c) over a time period ten times longer than Figure 1. The shearing duration is 20 seconds for the oil and the 60% suspension. With the 86% cell suspension three shorter shearing durations (15, 10, and 5 seconds) have also been used. Plot 2a is the mean of 2 stress profiles; 2b and 2c average 4 profiles. The 86% suspension stress relaxation (a) slows strikingly as time passes. The 60% hematocrit relaxation is complete well before 4 minutes (b). Post-shearing stress release involves at least two types of relaxation; the slower process is more prominent at high red cell concentration than when mild aggregation is present.

3. Response to Increasing Shear Rate

Whole blood and an 88% red blood cell suspension in PBS were studied at six shear rates ranging from 0.24 to 1.2 inverse seconds (Figures 3,4). As shear rate rises monotonic stress development is replaced by stress decay. Stress decay persists longer in blood than it does in the 88% red cell suspension; in both cases it shortens in duration as shear rate increases. An early stress overshoot is seen at the two highest shear rates in red cell studies and in most oil studies. It is due to the countertorque required to return the cup to its original position. Early post-shearing relaxation occurs more quickly at higher shear rate, while blood's slow relaxation has almost the same rate and magnitude at all shear rates. For red blood cells at 88% hematocrit the residual stress 20 seconds after cessation of shear is actually less at high than at low shear rate.

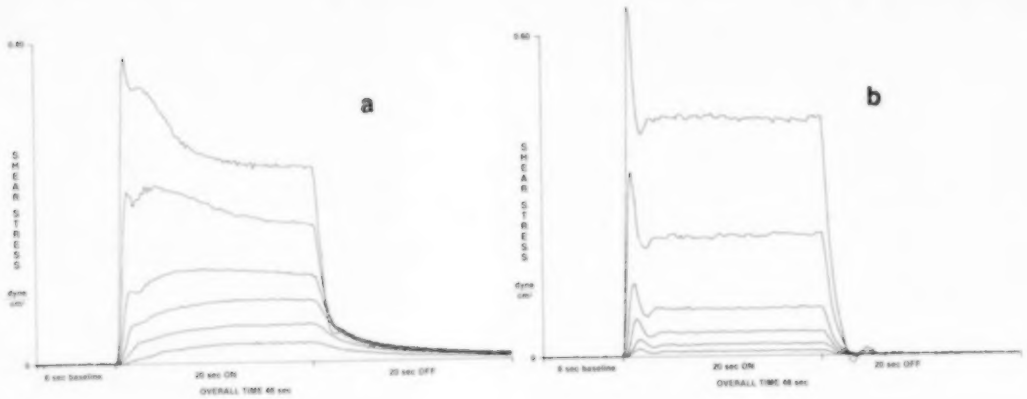

FIGURE 3. The response of 41% hematocrit blood (a) to 20 seconds of shearing at 6 different shear rates is compared with that of a 0.4 poise silicone oil (b). Shear rates are 1.2, .6, .24, .12, .06, and .024 inverse seconds for the oil. Shear rates for blood are slightly higher (8). Each plot is the mean of 4 to 6 stress profiles. The overshoot seen regularly with oil also occurs in blood studies at higher shear rates. Following the initial overshoot blood undergoes stress decay at the three highest shear rates. The duration of stress decay shortens as shear rate rises. Early post-shearing relaxation also becomes more abrupt as shear rate increases, but slow relaxation is similar in pattern at all six shear rates.

Vol. 17
1980

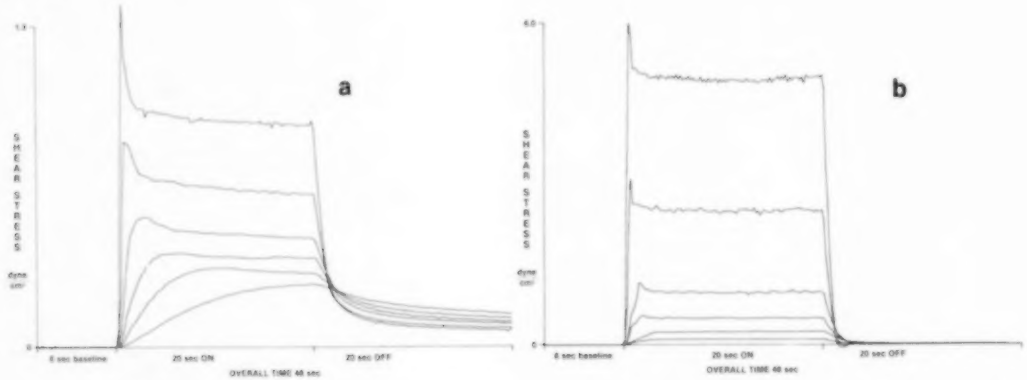

FIGURE 4. The study shown in Figure 3 is now carried out on an 88% red cell suspension in PBS (a) and a 4 poise oil (b). Each red blood cell plot is the mean of 6 stress profiles and each oil plot the mean of 4 profiles. The 4 poise oil shows less early overshoot than the 0.4 poise oil in Fig. 3b. At low shear rate the red cell suspension's stress onset is monotonic while at high shear rate stress overshoot is seen. Stress decay at high shear rate is shorter in duration than in the blood study (Fig. 3a). Slow relaxation is more prominent at low shear rate than at high despite absence of red cell aggregation.

4. Torque Decay at Constant Total Shear

Because the duration of stress decay appears to be influenced by shear rate, stress responses of an 84% red cell PBS suspension (Figure 5a) and a 60% red cell suspension in PBS containing 0.75% dextran (Figure 6a) were studied at a constant total shear (shearing time x shear rate) of 24. A 50 fold difference in shear rate was compensated by increasing the total observation time from 48 seconds at 1.2 inverse seconds shear rate to 2400 seconds (40 minutes) at .024 inverse seconds. Stress decay disappears more slowly in total shear units at low than at high shear rate at 60% hematocrit. The total area under the stress decay curve is smaller at low than at high shear rate in both studies. Stress decay is both larger in magnitude and more abrupt in onset at high shear rate and therefore more easily detectible. Persistence of stress decay is much less striking for the 84% red cell PBS suspension (Fig. 5a) than for the 60% hematocrit dextran-containing suspension (Fig. 6a). At 84% hematocrit the slow relaxation process is also strikingly incomplete. Residual stress at the end of the observation period is large at all shear rates despite the marked difference in the actual passage of time.

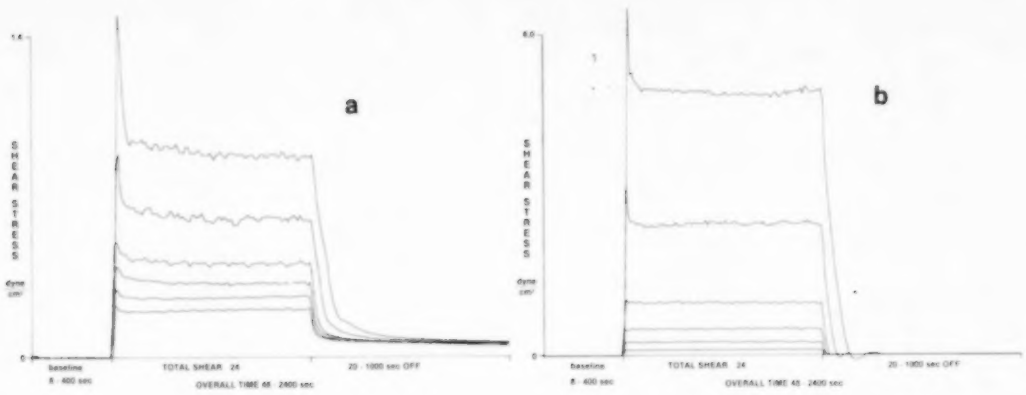

FIGURE 5. Figures 3 and 4 suggested that stress decay might develop and disappear very slowly at low shear rate. An 84% red cell suspension in PBS (a) was therefore compared to a 4 poise oil (b) at 6 shear rates with constant total shear. Red blood cell plots are a single stress profile while oil plots are the mean of 2 to 4 profiles. The shearing duration of 20 seconds at 1.2 inverse seconds shear rate is doubled at 0.6 inverse seconds, and increased progressively up to 50 fold at .024 inverse seconds. With this shearing pattern the total bob rotation is the same at each shear rate and total shear (shearing time x shear rate) is always 24 for the oil and slightly more for the non-Newtonian cell suspensions. The stress decay process is now similar in duration at all shear rates. An initial abrupt stress decrease is followed by a small but prolonged stress decay lasting for a total shear of 10 to 15. The total shear constancy of the stress decay pattern at different shear rates suggests that the red cells are becoming aligned into planes of flow as shearing develops so that they present less resistance to flow.

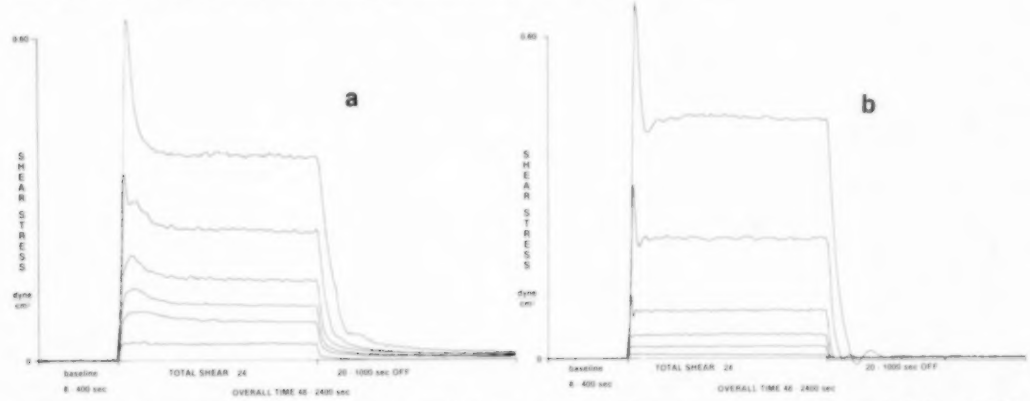

FIGURE 6. The total shear response of a 60% red blood cell suspension in PBS containing 0.75% dextran (a) is compared to that of a 0.4 poise oil (b). The pattern of observation is the same as for Figure 5. Red blood cell plots are the mean of 2 stress profiles and oil plots of 2 to 6 profiles. Stress decay behavior is more easily recognized in the 60% red cell suspension than in the 84% cell suspension. It also clearly persists longer at low than at high shear rate but is smaller in magnitude. Post-cessation stress relaxation is also more complete than with the 84% cell suspension.

5. Response to Repetitive Shearing

The response to four repetitive shearing periods was examined. Blood (Fig. 7) and an 84% red cell suspension in PBS (Fig. 8) were studied at six shear rates. The initial shearing response differs from the 3 subsequent responses, which are similar to each other. The first shearing interval follows mixing of the suspension while the others occur without intervening randomization. Stress decay decreases in magnitude after the initial shearing and has nearly the same pattern in later shearing periods. The difference is more striking for blood than for the concentrated red cell suspension. Delay in stress onset at low shear rate is reduced by repetitive shearing. Each response starts from the residual stress of the previous relaxation. The silicone oil response is not affected by repetition.

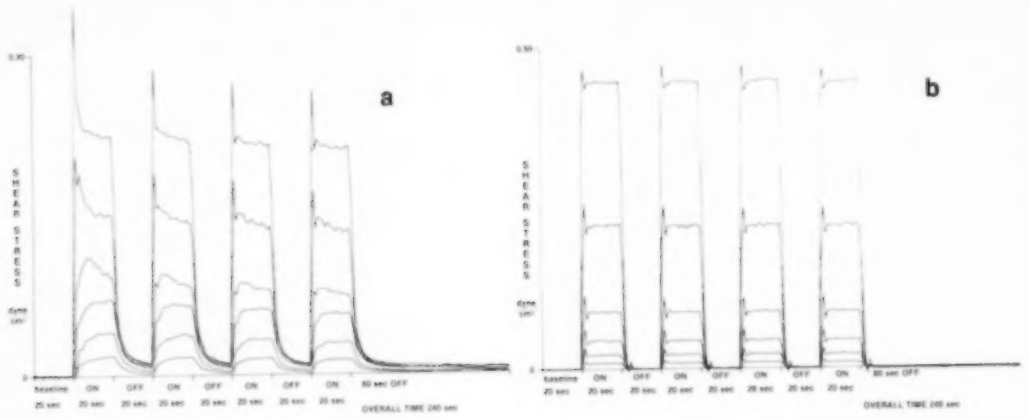

FIGURE 7. The response of blood at 41% hematocrit (a) and of a 0.4 poise silicone oil (b) to four repetitions of shearing is compared at 6 shear rates, 1.2, .6, .24, .12, .06, and .024 inverse seconds. Plots for blood are the means of 2 to 3 stress profiles and for oil the mean of 4 to 6 profiles. The overshoot seen with each silicone oil repetition is followed by a stable stress that disappears quickly as shearing ceases. In the initial shearing period blood shows stress decay at high shear rate, but stress decay is much less striking in subsequent shearings. The three shearing repetitions differ little from each other.

Vol. 17
1980

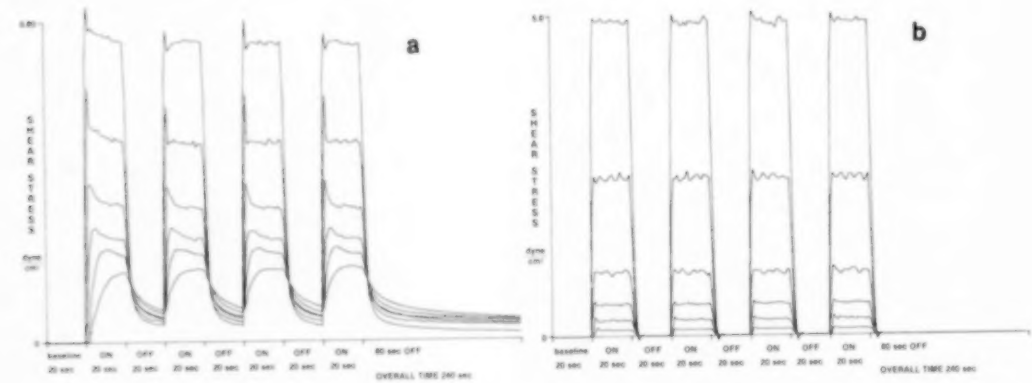

FIGURE 8. Response of an 84% red cell suspension in PBS (a) is compared to that of a 4 poise oil (b) using the same repetitive shearing pattern and six shear rates shown in Figure 7. At high shear rate stress decay observed in the first shearing period diminishes in the three subsequent shearing periods. At lower shear rates stress decay is less diminished and post-shearing relaxation is also less complete. At very low shear rate a disparately high relaxation stress is seen in all post-shearing periods. When total shear was constant (Figure 5a), the stress relaxation pattern was similar at all shear rates. The differences observed in the study suggest that during early shearing cell orientation is not established and that cell deformation strain energy is greater than when established cell orientation allows stable flow at lower shear stress.

6. Shortening the Interval Between Shearing Periods

Whole blood and a 60% red blood cell suspension in PBS containing 0.75% dextran were studied in a sequence in which 50 seconds of shearing was followed after two different non-shearing intervals by another 50 seconds of shearing. In Figures 9 and 10, blood and a silicone oil are compared at 0.6 inverse seconds shear rate. Intervening non-shearing times are 50 and 10 seconds. In Figures 11 and 12, the 60% red cell suspension is studied at a shear rate of 0.24 inverse seconds using similar non-shearing intervals. A stress decay response nearly half the size of that seen during the initial shearing period is observed after the longer non-shearing interval. Shortening the time between shearing periods almost obliterates stress decay in both studies.

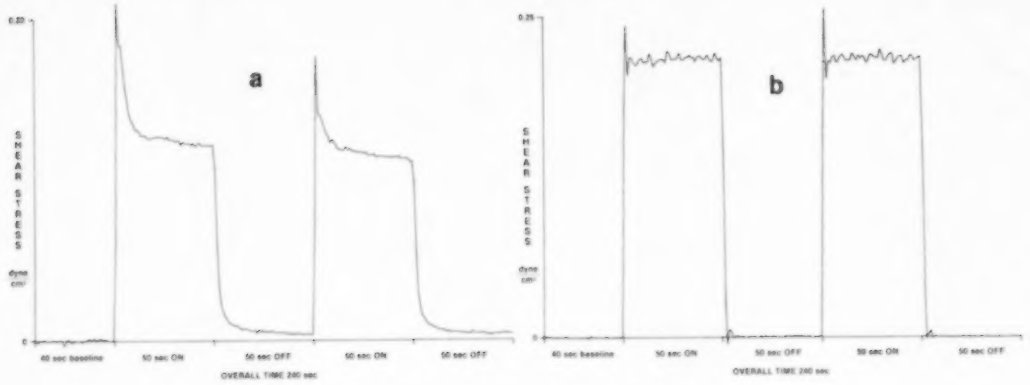

FIGURE 9. The response of blood (a) to two shearing periods of 50 seconds each with a 50 second non-shearing interval at 0.6 inverse seconds shear rate is compared to that of a 0.4 poise silicone oil (b). Both plots are the mean of 3 stress profiles. Stress decay is recognizable during both shearing periods and clearly reduced in magnitude in the second.

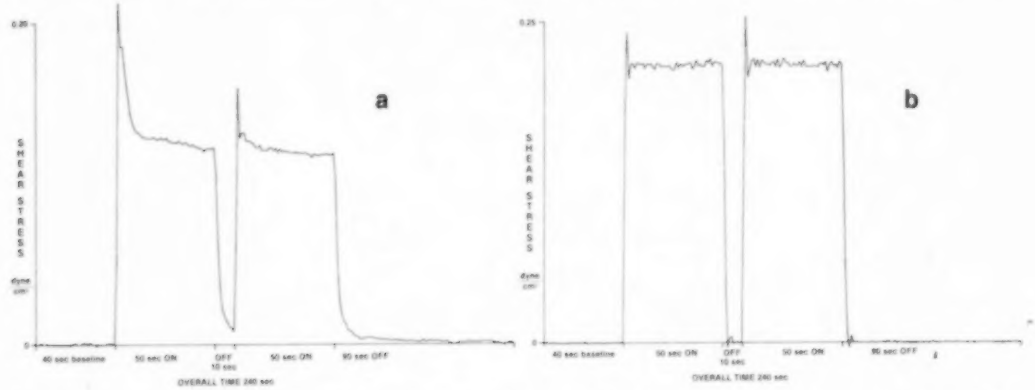

FIGURE 10. The interval between the shearing periods in Figure 9 has now been shortened to 10 seconds. Blood (a) is again compared with a 0.4 poise oil (b). Both plots are the mean of 3 stress profiles. Stress decay nearly disappears when the interval between shearings is shortened.

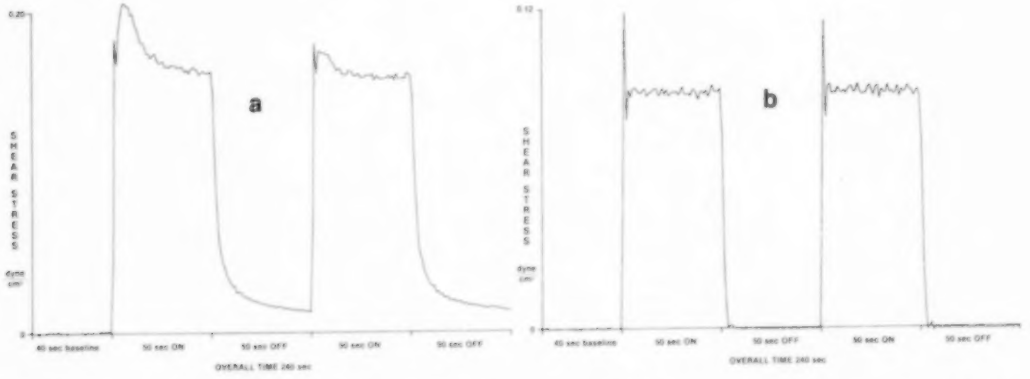

FIGURE 11. The response of a 60% red cell suspension in PBS containing .75% dextran (a) to recurrent shearing is compared to a 0.4 poise silicone oil (b). The shear rate is now 0.24 inverse seconds. Fifty seconds of shearing, a 50 second non-shearing interval, and a repeat 50 second shearing are used once again. Both plots are the mean of 3 stress profiles. Stress decay, more prolonged at lower shear rate, is again diminished in the second shearing period.

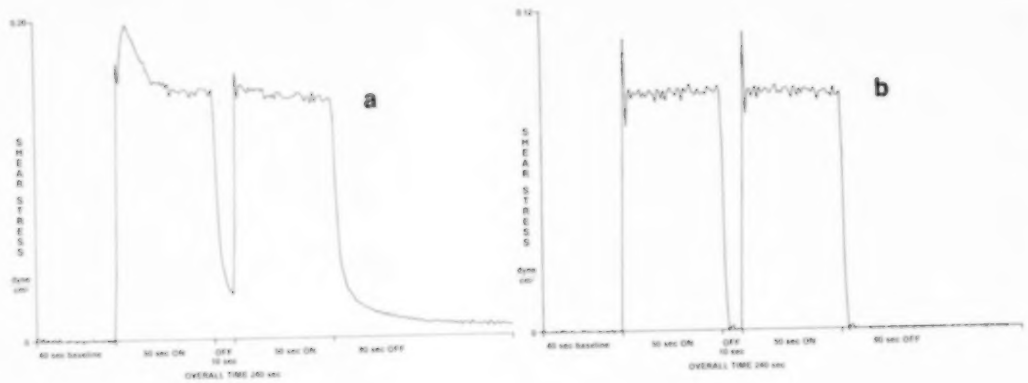

FIGURE 12. The interval between the shearing periods in Figure 11 has now been shortened to 10 seconds. Both plots are the mean of 3 stress profiles. In the second shearing period stress decay nearly completely disappears. The onset of blood flow initiates the orientation of cells as shearing planes become established. Before the red cells have become oriented the observed shear stress is higher than when a steady flow is achieved. Once erythrocyte flow orientation has been established it is lost very slowly, so that stress decay is much less prominent when shearing is repeated.

Vol. 17
1980

DISCUSSION

In studying the Maxwell fluid behavior of blood at low shear rate, we were unable to determine whether the observed incomplete post-shearing relaxation observed was due to a yield stress residual or to a second slower relaxation process (7). Studies with shorter shearing periods (Fig 1a) and longer post-shearing observations (Fig. 2a,b) indicate that a second slower relaxation follows the early exponential relaxation. The shear stress released in the slow relaxation process is proportional to the maximum shear stress achieved. Residual Bingham plastic stress would generate a constant post-shearing plateau at all shearing durations. When red blood cells are packed together the rate of slow relaxation decreases so strikingly that residual stress persists after 6 minutes (Fig. 2a) and even 16 minutes (Fig. 5a).

The early and slow relaxation processes differ. Early relaxation decreases in duration as shear rate rises, while slow relaxation has a magnitude and duration little influenced by preceding shear rate (Figs. 3a, 4a). The lack of shear rate influence gives blood's slow relaxation process a yield stress-like appearance (Fig. 3a).

Stress decay increases in magnitude and shortens in duration as shear rate rises (Figs. 3a, 4a). It can be seen at very low shear rate when the shearing period's duration is sufficiently long (Figs. 5a,6a). The constant total shear studies (Figs. 5a,6a) show a general relation between duration of stress decay and the viscometer's total rotation path. Repetitive shearing (Figs. 7a,8a) produces a marked diminution in higher shear rate stress decay, and studies comparing short and long intervals between shearing periods (Figs. 9a-12a) link stress decay to post-shearing slow relaxation. Stress decay is regained as residual post-shearing stress declines.

Four causes have been suggested for the thixotropic behavior of blood. Development of a cell-free zone adjacent to the rotating viscometer bob has been suggested to be the basis for stress decay (9). We have observed the described plasma-coated bob when mixing blood between studies, but not when mixing the 60% or 90% red cell suspensions. Close examination of Figure 7a reveals that blood undergoes a decrease in shear stress with each shearing repetition. The 90% red cell suspension (Figure 8a) shows no such decline. We attribute the stress decline seen when blood is repetitively sheared to cell-free zone formation but conclude that stress decay (the early rapid decline in torque) is not related to development of a cell-free zone.

The commonest explanation offered for blood's thixotropy has been that red blood cells must disaggregate as flow develops and that they aggregate again as flow ceases (2-4, 10-14). Experimental support for this conclusion has been given by the observation that addition of sodium salicylate to blood lowers its low shear rate viscosity and obliterates its thixotropic behavior (10). While disaggregation probably contributes to stress decay it does not appear to be the major process causing blood's high early flow resistance. We have observed thixotropy when erythrocytes are suspended in a non-aggregating medium at 84-90% concentration. The time required for repetitive shearing stress decay recovery (Fig. 9-12) is also considerably longer than that required for the restoration of cell aggregation.

A linkage between blood's viscoelastic behavior and its thixotropy has been proposed. Two groups have examined viscoelastic models with thixotropic properties using Oldroyd constitutive equations. The first group showed that shear-thinning could not be explained by a four constant Oldroyd equation (three element fluid model) without using a shear rate dependent term; they could fit a six constant Oldroyd equation (four element fluid model) to the observed data (5). The second group utilized a three constant Oldroyd equation with exponentiated shear rate terms, basing the values selected on an analysis of exponential stress decay at various shear rates (6). Neither group's descriptive equation contains a time constant sufficient to explain the observed slow restoration of stress decay.

The fourth cause, favored by this study, is progressive orientation of red blood cells as flow develops. Both direct visual analysis (15) and measurements of change in electrical resistance following onset of blood flow (16,17) have demonstrated that erythrocytes in nondilute suspensions become oriented in the direction of flow. While the time required for the development of this orientation was not clearly established in these studies the observed changes in electrical resistance with time (16) are consistent with our observations. The nearly constant total path required for completion of stress decay at different shear rates is far more consistent with development of cell orientation than with disaggregation; the orientation of red cells along planes of shearing must develop over a minimum path length. The red blood cells achieve a flow orientation through the constraint generated by their moving neighbors. Flow-mediated red cell disaggregation would add to the extra work necessary at the onset of shearing. Since degree of aggregation diminishes as shear rate rises, the work required to disaggregate blood should increase with rising shear rate. A comparison of Figures 5a and 6a suggests that stress decay's magnitude increases with shear nearly as much in the absence of erythrocyte aggregation (84%) as in its presence (60% with dextran).

Thurston has suggested that blood undergoes slow relaxation at the completion of flow. Using unconstrained rotary Brownian motion as a model, he calculated the relaxation time for an oblate ellipsoid the size of a red blood cell to be 43 seconds in plasma at 25°C (18). Cell orientation established by flow would be lost by such a mechanism after shearing ceases. In the absence of surrounding cells the calculated time constant may be appropriate, but in nondilute blood and red cell suspensions cell-cell constraint will quickly slow the relaxation rate, especially at high hematocrit. Our observations (Figs. 2a,b,3a) support Thurston's hypothesis that slow stress relaxation after blood flow ceases is due to a gradual loss of cell orientation. A coupling between flow-induced elastic cell deformation and cell orientation links the early and slow post-shearing relaxation processes. As shearing ceases, lack of cell-cell constraint allows considerable cell deformation elastic strain energy to be released. Rapid development of cell-cell constraint slows subsequent energy release since the cell movement necessary for further energy loss develops slowly since it is linked to rotary Brownian motion through cell-cell constraint. The dependence of stress decay on post-shearing slow relaxation suggests that both phenomena are based on flow-mediated cell orientation. Thixotropy of blood should therefore reflect the work required to develop cell orientation as flow becomes established. Because cell orientation is lost only slowly after flow ceases this work is diminished in repetitive shearing.

The insensitivity of post-shearing slow relaxation to shear rate changes in the shear rate range from 0.1 to 1 inverse seconds indicates that a component of the conversion of mechanical to thermal energy both during flow is nearly shear rate independent. Cell orientation can be lost by rotary Brownian motion during flow as well as after flow ceases. For the efficiency of flow to be maintained, a small shear rate-insensitive component of the applied shearing force appears to be utilized to restore Brownian motion-mediated loss of erythrocyte orientation. The shear-rate insensitive nature of the stress component required to maintain red cell orientation creates shear-thinning similar in pattern to the yield stress response of a Bingham plastic (19). We suggest that both blood's yield stress behavior and its retention of a small amount of shear stress long after cessation of flow are linked to its thixotropy through flow-mediated red cell orientation and Brownian randomization.

ACKNOWLEDGEMENTS

This work was supported by the Kroc Foundation and the Doris Fay Palmer Trust.

REFERENCES

1. MEWIS, J. Thixotropy - a general review. J. Non-Newtonian Fluid Mech. 6, 1-20, 1979.

2. HUANG, C. R., SISKOVIC, N., ROBERTSON, R. W., FABISIAK, W., SMITHERBERG, E. H., and COPLEY, A. L. Quantitative characterization of thixotropy of whole human blood. Biorheology 12, 279-282, 1975.

3. JOLY, M. Remarques sur le comportement rheologique en cisaillement de certaines classes de systemes condenses et sur ses methodes d'etude. Industrie Minerale, 176-181, 1977.

4. FUKADA, E. and KAIBARA, M. Viscoelastic study of aggregation of red blood cells. Biorheology 17, 177-182, 1980.

5. DEUTSCH, S. and PHILLIPS, W.M. The use of the Taylor-Couette stability problem to validate a constitutive equation for blood. Biorheology 14, 253-266, 1977.

6. STOLTZ, J.F., GAILLARD, S., and GUILLOT, M. An approach of the viscoelastic properties of blood in transient flow. AIChE Symposium Series No. 182, Vol. 74, 4-9, 1978.

7. McMILLAN, D.E. and UTTERBACK, N.G. Maxwell fluid behavior of blood at low shear rate. Biorheology 17, 343-354, 1980.

8. McMILLAN, D.E., UTTERBACK, N.G. and STOCKI, J. Low shear rate blood viscosity in diabetes. Biorheology 17, 355-362, 1980.

9. COKELET, G. R., MERRILL, E. W., GILLILAND, E. R., and SHIN, H. The rheology of human blood-measurement near and at zero shear rate. Transactions of the Society of Rheology VII, 303-317, 1963.

10. HEALY, J.C. and JOLY, M. Rheological behavior of blood in transient flow. Biorheology 12, 335-340, 1975.

11. HUANG, C.R. and FABISIAK, W. A rheological equation characterizing both the time dependent and the steady state viscosity of whole human blood. AIChE Symposium Series No. 182, Vol. 74, 19-21, 1978.

12. BUREAU, M., HEALY, J.C., BOURGOIN, D., and JOLY, M. Etude experimentale IN VITRO du comportement rheologique du sang en regime transitoire a faible vitesse de cisaillement. Rheol. Acta. 17, 612-625, 1978.

13. THURSTON, G.B. Rheological parameters for the viscosity, viscoelasticity, and thixotropy of blood. Biorheology 16, 149-152, 1979.

14. BUREAU, M., HEALY, J.C., BOURGOIN, D., and JOLY, M. Rheological hysteresis of blood at low shear rate. Biorheology 17, 191-203, 1980.

15. GOLDSMITH, H. L. and MASON, S. G. Some model experiments in hemodynamics - V: microrheological techniques. Biorheology 12, 181-192, 1975.

16. DELLIMORE, J. W. Conductimetric investigation of erythrocyte behavior during shear flow of concentrated suspensions through a large tube. Proc. R. Soc. Lond. B. 193, 359-385, 1976.

17. DELLIMORE, J.W. and CAMPBELL, D.A. Apparent suspension viscosity and the orientation and deformation of erythrocytes in shear flow. AIChE Symposium Series No. 182, Vol. 74, 65-73, 1978.

18. THURSTON, G. B. Viscoelasticity of human blood. Biophysical J. 12, 1206-1217, 1972.

19. BINGHAM, E.C. Fluidity and Plasticity. New York: McGraw-Hill, 1922, pp. 215-240.

BIORHEOLOGY, Vol. 17, pp. 455-464, 1980
Printed in the USA. All rights reserved.

0006-355X/80/050455-10$02.00/0
Copyright (c) 1981 Pergamon Press Ltd

PRELIMINARY REPORT ON PLATELET CONCENTRATION IN CAPILLARY TUBE FLOWS OF WHOLE BLOOD

M. R. Beck, Jr. and E. C. Eckstein

Department of Biomedical Engineering
University of Miami
Coral Gables, Fla. 33124
USA

(Received 17.3.1980; in revised form 23.10.1980.
Accepted by Editor H.L. Goldsmith)

ABSTRACT Experiments are reported that study the effect of flow rate and geometry on regional platelet concentration. The flow circuit consists of a stirred reservoir, capillary tube and collected outflow. To provide a sample of tubular blood without velocity biasing of contributions from various radial locations, the flow is stopped instantaneously and the entire tubular contents are flushed into a container. Bulk reservoir and outflow blood are collected in standard ways. Measurements of the relative platelet concentration for the samples are made with an electronic cell counter and volume analyzer. Results show that reservoir and outflow have equal platelet concentrations. For small capillary tubes (125 to 302 micrometers) the tubular platelet concentration is elevated relative to the other samples. Smaller capillary tubes have larger relative platelet concentrations than larger capillary tubes; no increase is measurable for an inner diameter of 635 micrometers. Biological adhesion is not the source of the enhanced tubular concentrations; this is shown by experiments using glutaraldehyde-hardened platelets. Thorough anti-coagulation and surface treatment minimize platelet adhesion in all experiments. Hematocrit does not strongly effect the tubular platelet concentration. However, flow of platelet-rich plasma through 178 micrometer tubes produces a tubular platelet concentration of about 0.6 of the reservoir value. Fluid mechanical events centered about interactions among red cells, platelet and flow appear to be the cause of enhanced tubular platelet concentration.

INTRODUCTION

Experiments presented here establish methods of study and determine important variables that affect regional platelet concentration during the flow of whole blood from a reservoir through a capillary tube to a collecting vessel. Previous work shows that when whole blood flows through tubes of small diameter (40 to 200 micrometers), the platelet concentration of blood within the tubes is increased above the platelet concentration of blood in the supply reservoir or the collected outflow (1,2). The platelet concentrations in the supply reservoir and the collected outflow are nominally equal. Increased tubular platelet concentration occurs because of alterations in the average velocity of platelets during passage through the tube, not because of surface adhesion. Regional platelet concentration and flow rate set an upper limit on the number of platelets that can react with the surface. An understanding of flow, diameter and hematocrit effects on regional platelet concentration is essential to understand blood-surface interactions. In addition, such work is an interesting problem in multi-component suspension flow.

KEY WORDS: Platelets, Blood Flow, Suspensions, Shear Rate, Capillary Tubes.

Altered species concentrations in non-reacting flows are conveniently viewed via conservation equations for red cells and platelets. These equations interrelate the average regional concentration and flow variables:

$$C_{i,r} \cdot Q_r = C_{i,t} \cdot V_i \cdot A_t \qquad (1)$$

Here C is a volumetric concentration, Q is the volumetric flow rate from the reservoir into the tube, V_i is the average velocity of the species in the tube and A is the cross-sectional area of the tube. The subscript i serves to identify the species that is conserved in the equation; subscripts r and t show reservoir and tube locations. Phenomena that result in unequal entrance of species from the reservoir, such as "screening," (3) require more complex equations. Much work has been done on the flow of red cell suspensions and whole blood through capillary tubes. For tubes of small diameter there is a reduction in tubular hematocrit as compared to the reservoir or outflow hematocrit; this phenomenon is generally termed the Fahraeus effect. Experimental measurements of tubular hematocrit in blood flow through small tubes can be fit to Equation 1 with an appropriate value of V_{rbc}. This method of data reduction yields values of V_{rbc} that are greater than the average bulk velocity given by Q_{res}/A_{tube}. Cokelet provides a very good review of the Fahraeus effect (4).

In accord with Equation 1, an increased tubular concentration of platelets would occur when the average platelet velocity V_p is less than the average bulk velocity. Low values of V_p can occur if one portion of the tubular platelet populace is distributed as a highly concentrated, slow moving region with the remaining portion uniformly distributed across the tube. Although this is not a unique way to have a low value of V_p, it is a physically meaningful possibility. The marginal layer, i.e., the few microns closest to the wall, offers a region that could sequester large local concentrations of platelets. Through high speed cine-micrography Bugliarello and Sevilla show the marginal layer to be cell-poor and to contain a peripheral plasma layer (5). As blood flows past an observation site the peripheral plasma layer varies in height and thus must be described statistically. Their work shows the average thickness of the peripheral plasma layer to be strongly dependent on the inlet hematocrit, but relatively unaffected by variation of tube diameter or flow rate. Exact general characterization of the marginal layer remains to be done. It is clear that a statistical description is necessary, that the average hematocrit very near the tube wall is low, and that the local hematocrit increases toward core values with increasing distance from the wall. For the discussion below, the marginal layer is a region characterized by reduced velocity and, because of wall effects, low red cell concentration. If platelets are sequestered in the marginal layer, flow through tubes of small diameter will be associated with larger elevations in tubular platelet concentration than flow through larger diameter tubes. The reason for this is geometrical; an annular region of constant thickness is a larger proportion of the volume of a tube of small inner diameter.

Tubular suspension flow is associated with the phenomena of lateral migration of particles for dilute suspensions and shear-induced dispersion of particles for concentrated suspensions (6,7,8). Both phenomena scale with shear rate, but have different exponents in power-law representations. For experiments that compare platelet concentration in tubes of different diameter, a priori logic dictates the use of flows that cause equivalent wall shear rates and thereby have equal hydrodynamic mixing phenomena.

An interesting Gedanken experiment considers the marginal layer as a separate control volume of very low absolute cellular concentration located between the core flow of blood and the wall of the tube. Platelets can enter the marginal layer by diffusion or shear-induced dispersion from the core flow and by detachment from the wall. Platelets can leave the marginal layer by reaction with the wall or by diffusion toward the core. Since shear-induced dispersion requires both a shearing motion and a significant volumetric cell concentration, this transport mechanism is not available to remove platelets from the peripheral plasma region of the marginal layer. Because of the small volume of the platelet, this will be true even when platelet concentration is significant in the marginal layer. In the limit of no reaction with the wall and when dispersive fluxes are much greater than diffusive fluxes, a large concentration of platelets can accumulate in the marginal layer. In a fashion that is analogous to the flux of gas molecules from a hot region to a cold region, the dispersive flux from the core to the marginal layer is set by the shear rate of the flow. At steady state, a high concentration of platelets must occur in the marginal layer to drive a core-directed diffusive flux that balances the wall-directed dispersive flux. The fluid mechanical, wall-repulsive force is also core directed; however, it requires both significant shear rate and close wall proximity to be important (8). At high wall shear

Vol. 17
1980

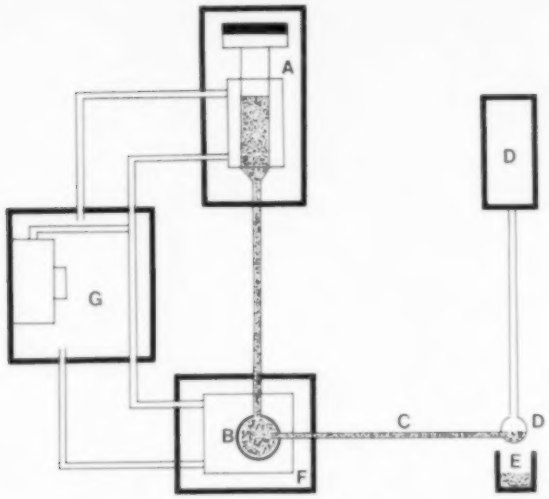

FIG. 1

Flow apparatus. The schematic diagram shows connections among a syringe pump (A), stirred reservoir (B), capillary tube (C), saline drip (D), and outflow collection vessel (E). Accessory elements are a magnetic stirrer (F) and a circulating water bath (G), which is regulated to physiological temperature.

rates it would also contribute to the core-directed flux from the marginal layer.

The outcome of the above Gedanken experiment is significantly different if platelets react with, or adhere to the wall. For highly reactive surfaces, the marginal layer acts as a "way station" between the core and the wall; accumulated platelets would react with the wall rather than reside passively near the wall. Furthermore, the scale of geometric irregularities induced by the adherent platelets or by platelet aggregates is of the same order as the peripheral plasma region of the marginal layer. This renders the use of the marginal layer as a control volume questionable. An interesting use of a control volume between a reactive wall and a core flow of red cells is presented in the literature (9).

A second aspect of reactivity occurs if the platelets are very slightly adherent to the surface. Suppose the flow provides sufficient platelets to coat the surface and that these platelets can be removed in the process of collecting the tubular blood sample. These platelets would then add to the tubular concentration. To obviate the difficulties caused by the platelet adhesion, these experiments used either anticoagulants in combination with surface treatments or platelets that had been hardened with glutaraldehyde.

The above discussion presents evidence suggesting that the tubular platelet concentration may be elevated only when red cells are present but may not be strongly dependent on hematocrit, since the marginal layer is the focus of events. Furthermore, elevations in tubular platelet concentration are expected to increase as the inner diameter decreases and to depend upon the wall shear rate. The data below support these expectations.

MATERIALS AND METHODS

This section is divided into three parts, namely: flow apparatus, blood and sampling techniques, and analysis of blood samples. Methods of data reduction are described in the third part. Descriptions are intentionally brief; further detail is contained in a thesis by Beck (10).

Flow Apparatus. A syringe pump, stirred reservoir, magnetic stirrer, circulating water bath, saline drip and a capillary tube comprise the flow apparatus (Figure 1). The reservoir has three openings: an inflow port connected to the syringe pump, an outflow connector for attachment of the capillary tube and a port for sampling and filling the reservoir at the top. After the syringe and reservoir are filled with blood, all air is purged through the sample/fill port and the port is sealed. Infusion of blood from the syringe into the reservoir causes blood to flow through the capillary

tube. At steady state the flow rate through the capillary tube is equal to the discharge rate of the syringe pump. A large range of flow rates is available through use of syringes of various sizes. Addition of a second stage of mechanical transmission to the syringe pump (Harvard model 975) permits fine gradations of syringe discharge rate. When the velocity profile is fully developed, a tube of diameter D, carrying a volumetric flow rate Q of a Newtonian fluid has a wall shear rate S, that equals $32\ Q/(\pi D^3)$. Development lengths for Newtonian fluids flowing at the Reynolds numbers of these experiments are several diameters or less. Work by Palmer and Betts shows that the entrance length for full development of the concentration/velocity profile is much longer for the flow of a concentrated suspension (blood) than for a Newtonian liquid; for channel flow with a 25 micrometer height, the entrance length is about 1 cm (11).

Most surfaces that contact blood are plastic, primarily plexiglass or teflon. Glass surfaces, such as the syringes (Hamilton gas-tight series) or the mounting tubes that hold the small capillaries are siliconized (Pierce SC-87). The magnetic stirrer is operated at its lowest speed, approximately 60 rpm. The syringe and reservoir are surrounded by water jackets that are fed by a circulating pump in a water bath thermostatically regulated to physiological temperature. All surfaces are scrupulously cleaned and rinsed with normal saline prior to filling the apparatus with blood.

Capillary tubes of glass (Corning 5 microliter disposable glass pipettes) and polyvinyl chloride tubing (Tygon Microbore or Elkay Autoanalyzer tubing) are used. The inner diameter of tubing and glass capillaries are measured with a metallurgical microscope. Polyvinyl chloride (pVC) tubes are mounted in thinwall glass tubes for support. After mounting, the ends of the pVC tubing are cut off squarely with a razor blade. Glass capillary and support tubes are siliconized with SC-87; pVC tubing is soaked overnight in 1% (wt/vol.) species specific albumin solution. Tubes are connected to the reservoir with modified Luer fittings. In all cases the capillary tube extends into the stirred core of the reservoir. The saline drip provides and renews a droplet that covers the exit of the capillary tube. It also provides easy visual proof of flow through the capillary tube. In most experiments blood flowed for ten minutes prior to collecting samples.

Blood and Sampling Techniques. Bovine and human blood were used; whole blood experiments used one part of 3.9% sodium citrate solution to nine parts of blood to provide anticoagulation. Later experiments with human blood used HEPES buffer to maintain pH in the anticoagulated blood. Experiments were also performed with reconstituted bovine blood suspensions. In these experiments, red cells and platelets were centrifugally separated from whole bovine blood collected with heparin and EDTA anticoagulation, triply washed with saline, hardened with 2.5% glutaraldehyde solution and finally washed twice to remove excess glutaraldehyde. Bovine blood suspensions were made as either saline suspensions of hardened red cells and hardened platelets (HCP suspensions) or as saline suspensions of hardened platelets and fresh, washed bovine red cells (FCHP suspensions). One set of experiments used platelet rich plasma (PRP) prepared by lightly centrifuging fresh human blood that was anticoagulated with sodium citrate. The nature of the blood suspension is identified with each set of experiments described below.

Experiments with whole human blood are performed great care to minimize activation of the coagulation process. Blood is collected in Vacutainers (Becton-Dickinson), which are quickly, but gently, inverted to mix the blood and anticoagulant. The blood samples are then stored at 37°C until use. All experiments with human blood are performed within four hours of blood collection. As drawing human blood with citrated vacutainers tends to produce a hematocrit of 35 to 37, most human blood experiments have been at a hematocrit of 35. Phosphate-buffered normal saline is used for the minor dilution of the blood to a hematocrit of 35. This procedure was determined advantageous to minimize trauma by handling and to expedite use after collection. Hematocrits are determined using a microhematocrit technique, which accurately corrects for included plasma among flexible red cells, but not among hardened red cells. A packing factor of 0.61 is used to correct the microhematocrit reading of the HCP suspensions.

To collect the reservoir sample, a siliconized pasteur pipette is inserted through the sample/fill port at the top of the reservoir. About one half milliliter of blood is removed and transferred to a clean disposable sample cup. Outflow blood samples are collected by catching the blood-laden saline drip in a siliconized volumetric flask for a measured period of time. To use the electronic cell counter, blood samples must be diluted at about 50,000:1. The outflow collection uses the saline drip as the first stage of dilution; the dilution is easily calculated from the flask volume, the blood flow rate and the time of collection.

Collection of tubular blood samples is more involved. The tube sample

Vol. 17
1980

must represent all blood in the tube or in a section of the tube at a given instant of time. To achieve this, the tube flow is instantaneously stopped either by blocking or clamping the exit. The entire contents of the section or the whole tube are flushed into a volumetric flask. A small amount of saline is initially placed in the flask to minimize the loss of cells onto the flask surface. Typically, hundreds of tube volumes of saline are gently flushed through the tube to insure that all blood components are removed. Microscopic examination of tubular surfaces after flushing shows that only a few red cells and platelets remain on the tube surface. Inspection of blood smears made with whole blood flushed from tubes during experiments shows that red cells and platelets are intact and have appropriate morphological shapes.

Tube samples were collected by two methods. The first method, used for the largest number of samples, involved flusing contents from the entire length of the tube. Samples collected in this manner are termed "whole tube" samples. Samples collected by the second method characterize the tubular platelet concentration at various stations along the tube length. Blood is flushed from 2.5 cm segments that are cut from the tube. Typically, three segments, located at the entrance, middle and exit portions of the tube were obtained from each experimental run. This type of tubular sample, termed a segmental sample, is a local average.

Analysis of Blood Samples. The blood samples are analyzed to determine the distribution of cell volumes. The assumption is made that differences in relative concentration of platelets and red cells can be determined by volume analysis because the size distributions of the two cell types are quite widely separated. Calibration studies with mixtures of washed red blood cells and platelet rich plasma validate this assumption for the available blood sources. Indeed, blood without adequate separation of platelet and red cell distributions would not be used for these experiments. Measurements of the cell volume distribution are made with an electronic cell counter and size analyzer (Model ZBI and a Channelyzer C-1000, Coulter Electronics). For whole-blood samples a high resolution orifice with a diameter of 50 microns and a length of 60 microns is used as a part of the counter; for platelet-rich plasma an orifice diameter of 30 microns is selected. All samples are diluted to approximately 50,000:1 prior to analysis; actual concentrations are calculated using exact values for the dilutions of the individual samples. Instrument settings are selected so the volume differential histogram displays portions of both the red cell and platelet distributions. Settings are selected to minimize noise and adverse biological effects; generally, the procedure is that suggested by the manufacturer.

As a cell passes through the orifice the counter produces an electronic signal of amplitude proportional to the cell volume. The volume analyzer separates these electronic signals into one hundred classes by amplitude and displays the number of cells (signals) in each class (y-axis) versus the characteristic amplitude of the class (x-axis). This display is the cell-volume distribution. The cell counter is operated in a mode that draws a preset volume of diluted cell suspension through the orifice to provide the signals used for the cell-volume distribution; thus, concentrations can be calculated from the measured distributions and dilutions. Associated instruments provide graphical and printed permanent records of the cell-volume distribution.

The assumption is made that flow alters the relative proportion of species in the tube, but does not change the volume distributions of the species that are present in the tube. With this assumption it is possible to compare the number of platelets in various samples by comparing concentration of particles within identical volume regions of the cell-volume distributions. On this basis two ratios have been defined; the first ratio compares two samples using the absolute concentrations of particles in the volume region from approximately 4 to 20 cubic microns. This volume range corresponds to a portion of the platelet volume distribution that extends upwards from approximately the modal volume. This ratio is computed to compare the samples from the tube and the reservoir and from the collected outflow and the reservoir. Use of particle counts in restricted volume regions (rather than the total count over the entire range of platelet or red cell volumes) allows exclusion of volume regions where spurious events such as electronic or biological noise cause a significant contribution to the displayed cell volume distribution.

The second ratio uses the number of platelets per red cell as an index of platelet concentration. The height of the red cell peak scales the volume of original blood sample that was diluted and processed by the counter and volume analyzer. In this way it avoids the need to calculate the absolute concentration of platelets in the sample. To calculate the second ratio an index value is calculated for each sample; it is the number of platelets within the volume region from 4 to 20 cubic microns divided by the number of

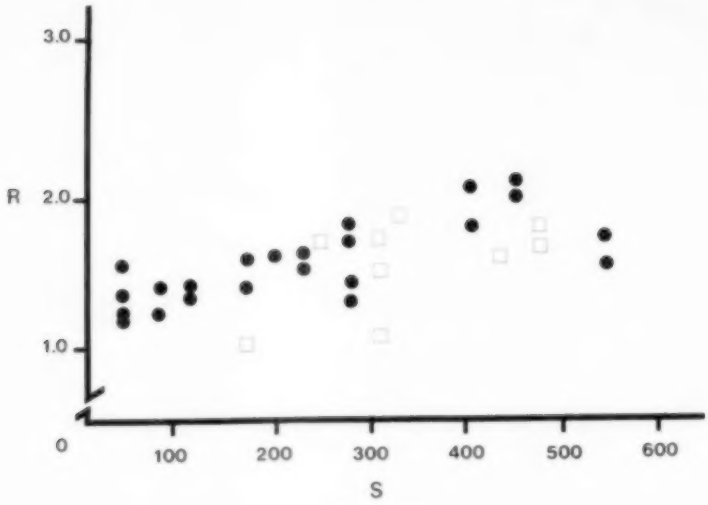

FIG. 2

Relative tubular platelet concentration, R vs. wall shear rate, S. Experiments use 302 micrometer siliconized glass tubes. Closed circles are FCHP suspensions at hematocrit of 35; open squares are HCP suspensions at hematocrit of 14. Tube length is 12.6 cm.

red cells in the modal channel of the red cell distribution. Obviously, the number of red cells in the tube sample must be corrected for the Fahraeus effect; values from Barbee have been used (12). The second ratio is calculated by dividing indices for two samples, such as the tube and reservoir or the collected outflow and the reservoir. Values of the two ratios calculated for the same samples typically agree to within 10%; comparison of the two ratios shows no apparent statistical trends. Calibration studies using mixtures of PRP and washed red cells show that the ratios measure relative populations of platelets in samples with an accuracy of $\pm$ 10%. Except for the experiments with PRP the second ratio is used to calculate the data presented here. The symbol R is used on the figures of this paper to represent the platelet-concentration ratio for tube and reservoir samples. The formulation of R obviates differences in reservoir concentration between experiments, i.e. R is a normalized or relative tubular platelet concentration. Values of R greater than one indicate that the tube sample has a greater platelet concentration than the reservoir sample.

RESULTS AND DISCUSSION

Carefully controlled techniques must be used in platelet experiments to prevent platelet loss or reaction, especially at the boundaries. In these experiments it is crucial to minimize biological adhesion since this may give erroneous values of tubular platelet concentrations. Physical sequestration of platelets in the red-cell depleted marginal layer is a complementary mechanism that would increase tubular platelet concentration. These experiments used anticoagulants and surface pre-treatment with siliconizing solutions or surface absorption of albumin to minimize biological platelet-surface interaction. Three observations demonstrate the efficacy of these measures. First, over the course of a 4-hour set of experiments, the reservoir concentration of platelets does not change significantly. Second, microscopic observation of the tube surfaces after flushing to remove the tube sample shows only isolated platelet deposits, which seldom have more than a few loosely bound platelets. Third, over the course of the experiments, samples of collected outflow blood have essentially the same cell-volume distribution and cell concentrations as the samples of reservoir blood. This fact is important not only because it implies minimal reaction, but also because it indicates a change of average transit velocity for the platelets. Occasional microscopic examination of smears of reservoir, tube and outflow samples shows that the platelets have the expected morphology for the anticoagulant: discoid for citrate and spheroid for EDTA and heparin. The smears also show that the vast majority of platelets are single with few pseudopods.

Vol. 17
1980

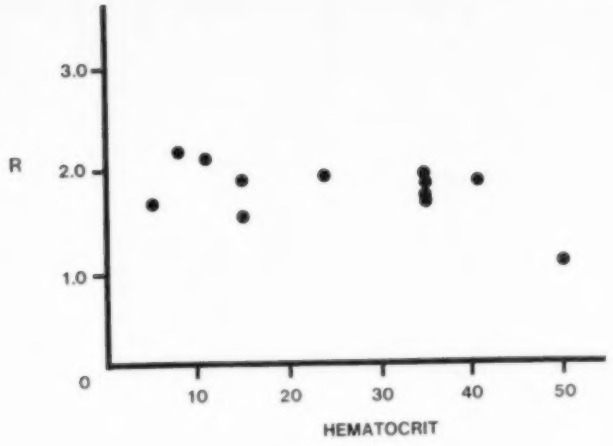

FIG. 3

Relative tubular platelet concentration, R vs. hematocrit. Data was obtained using 302 micrometer siliconized glass tubes and FCHP suspensions; wall shear rate is 400 inverse seconds. Tube length is 12.6 cm.

Additionally, some experiments used saline suspensions of fresh, washed bovine red cells and bovine platelets that had been hardened with glutaraldehyde (FCHP suspension); other experiments used saline suspensions of bovine red cells and platelets that had been separately treated with glutaraldehyde to harden them (HCP suspension). Hematocrits are 35 and 14, respectively. Since platelet reactivity is eliminated by the glutaraldehyde treatment, platelet adhesion to surfaces is not the source of increased tubular concentrations displayed in Figure 2. The value of R for the FCHP suspensions appears to increase with shear rate up to approximately 450 sec^{-1}. More work is needed to determine if there truly is a shear rate dependence and to demonstrate if there is a shear rate where R is maximum. Furthermore, R is elevated for both FCHP and HCP suspensions. (Scatter in the HCP data is larger than that in the FCHP data because the higher sedimentation rate of the HCP suspensions makes these experiments technically difficult.) These results suggest that increased concentration of small particles is a general feature of suspension flow through tubes when the suspensions have two distinct sizes of particle and when the tube diameter is only a small multiple of the larger size of particle. Flows of both rigid and flexible particles exhibit a marginal layer. The hypothesized mechanism of sequestration of small particles (platelets) in the marginal layer is thus feasible for suspensions having either rigid or flexible particles.

Experiments were performed with bovine blood suspensions of various hematocrits. The FCHP suspension was diluted with saline to adjust the hematocrits. Accordingly, the ratio of platelets to red cells in the reservoir samples is approximately the same for all data points shown in Figure 3. All tests used 302 micrometer siliconized glass tubes 12.6 cm long; flow was set to produce a wall shear rate of 400 sec^{-1}. Actual hematocrit appears to be of minor importance. Saline suspensions lack protein to mediate intercellular events, such as rouleaux formation, thus experiments with whole blood may show a greater dependence on hematocrit.

In one set of experiments, platelet-rich plasma (PRP) flowed through 25.5 cm. lengths of Elkay polyvinyl chloride tubing with an inner diameter of 178 micrometers. Because of the low dilution required to count platelets, the whole tube sampling technique was used. Data for these experiments are shown in Table I. Values are remarkably consistent with $R \simeq 0.6$ despite variation of shear rate by over two orders of magnitude. Examination of the data for whole human blood (Figure 4) shows R to be greater than one over a wide range of shear rates. (High pressure drops precluded measurements at $S=8000$ sec^{-1} in 125 micrometer tubing). Scatter in the data prevents clear interpretation of effects due solely to variation of wall shear rate. Over restricted ranges of S, e.g., from 500 to 1200 sec^{-1}, R increases as the inner diameter decreases. Lateral migration away from the wall may cause R to decrease to 1 for $S \geq$ 10,000 sec^{-1}. Experiments with tubes having a larger inner diameter, such as 635-micron Elkay pVC tube, produce R values that are scattered about 1 and have no obvious shear rate dependence. These observations are consistent with

TABLE I

Data for Flow of Human PRP Through 178 μm Tubing at Various Shear Rates.

Wall Shear Rate, S (sec^{-1})	Platelet Concentration Ratio, R
81	0.67
511	0.61
1000	0.61
3330	0.64
9590	0.62

sequestration of platelets in the marginal layer. For large diameter tubes, the sequestered amount is a very small proportion of the total platelet populace, thus extremely sensitive techniques are required to measure or observe the phenomenon. Similar events occur for Fahraeus-effect studies in large tubes.

Work with tube flows must consider entrance effects, which Palmer and Betts have demonstrated can occur over a substantial length (11). When experiments with tube lengths under 2 cm are excluded, no significant variation of R occurs with respect to axial position of the segmental sample or with respect to the total tube length. Data for tube lengths less than 2 cm are inconclusive because of scatter associated with experimental difficulties related to connector size, sample volume and sampling error. Future work will improve experimental methods to study this interesting region of the tube.

Dimensional analysis suggests time as a variable. No time dependent changes in the value of R were found in experiments in 178 micrometer Elkay tubing at S = 8000 sec^{-1}; flow duration prior to sampling was varied from 10 to 1200 seconds. In early experiments to develop effective protocols, no apparent variation in R was observed with experiments that had different times of through flow (up to 40 minutes) prior to sampling. When values of platelet diffusivity that include shear-induced dispersion are used to scale concentration boundary layers in blood flow through tubes of this small diameter (13), non-dimensional parameters indicate that transient events should occur in very short times, on the order of ten seconds. Such data cannot be taken due to the washout of saline from the tube at the start of the experiments.

The marginal layer offers a reasonable location to sequester the excess platelets that cause the enhanced tubular platelet concentration. As noted

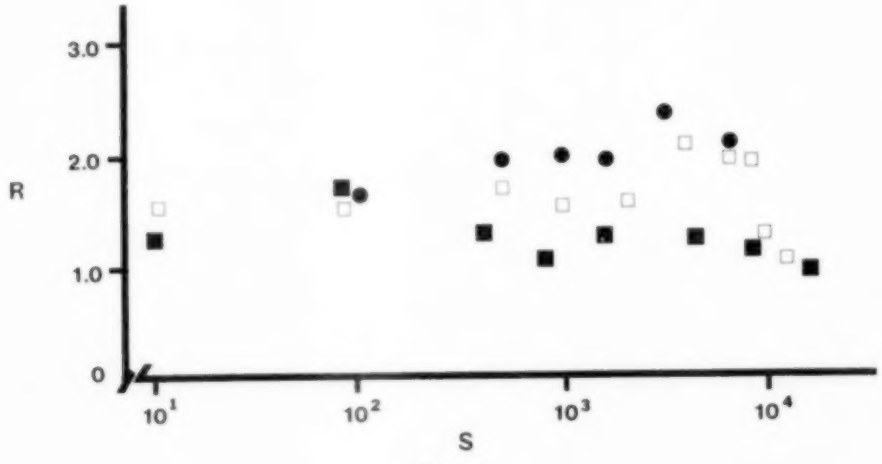

FIG. 4

Relative tubular platelet concentration, R vs. wall shear rate (logarithmic scaling). Experiments use citrated whole human blood at hematocrit of 35 in 128 micrometer Elkay tubing (closed circles), 178 micrometer Elkay tubing (open squares), or 254 micrometer Elkay tubing (closed squares). Data points are the average value of three or more segmental samples.

Vol. 1
1980

above, this region is statistically depleted of red cells by an amount that depends on the distance from the wall. Via several simplifying assumptions, the platelet concentration near the wall can be estimated. For calculative ease, assume that at any instant the platelets in the tube are separable into two groups. One group moves through the tube at the same velocity as the plasma, is uniformly distributed across the tube, and has the correct number to provide by itself a tubular platelet concentration equal to the reservoir platelet concentration. The second group, which is formed by the excess platelets, is stationary and located in the three micrometers closest to the wall. Separation of the platelets into such groups automatically satisfies mass conservation. To provide an estimate of the maximum wall concentration, the maximum value of R for each tube size is chosen; this controls the number of platelets in the second group. For the three pVC tube diameters, the average wall concentration of platelets is 15.7 times the reservoir concentration (standard deviation is 0.7). Decreasing the thickness of the marginal layer increases the wall concentration. The many assumptions of such a model bear critically on the predicted outcome in platelet concentrations; accordingly, their predictions should be used with great caution.

The simple model described below explains the results obtained with platelet rich-plasma (PRP). Individual rigid and flexible particles avoid the region close to the wall in flows similar to those reported here. Segre and Silberberg (14) show individual particles achieve a stable location at 60% of the tube radius (14); flexible particles move to the axis (6). These motions are caused by interactions among the flow, boundary and particle; inter-particle events are unnecessary. Assuming inter-particle events are insignificant for PRP, the platelets will leave the wall region like flexible or rigid particles. Accordingly, the average platelet velocity, V_p, increases and the relative tube concentration, R, decreases. Using a parabolic velocity profile, V_p can be related to an average radial location, which for the PRP experiments is 45% of the tube radius. This indicates a significant shift of the platelet distribution to the central region. (A uniform platelet distribution has an average radial location of 71% of tube radius). Redistribution to the axis is limited because of finite space in the core region. The frequency of particle interactions, a key feature of concentrated suspensions, increases as the core becomes filled with platelets, which then necessarily spread over a wider region. The small average radial location of 45% is consistent with a model wherein platelets behave as flexible particles that attempt to move to the center. In the sense that there is only one type (size) of particle, the PRP experiments are analogous to traditional Fahraeus-effect experiments with very low reservoir hematocrit.

The dramatically different outcomes for flows of PRP and whole blood have a major impact on models of blood-surface interaction. Typical analyses of platelet adhesion assume uniform platelet concentration in the blood approaching a reactive surface (13). Enhanced platelet transport to the surface is incorporated to account for flow and hematocrit induced increases in diffusivity. This work suggests that, over a wide range of shear rates, flow past a non-reactive surface prior to the reactive surface causes a non-uniform distribution of platelets. Furthermore, the distributions will be dramatically different for flows of PRP and whole blood.

Finally, note that these are initial experiments. In general, values of R are elevated above 1, unless experiments such as the PRP series are performed. Scatter in the data prevents detailed interpretation of changes in R with fundamental parameters such as shear rate and diameter. At this time we have opted to improve methods and have set aside such questions. What is clear from this work is that microrheological events in a two-component suspension are critical to the increased tubular concentrations. Other experimental studies have shown the interaction of two-components in a suspension; the studies are shear-induced increases in platelet diffusivity (dispersivity) (6,7) and platelet adhesion tests using glass bead columns (15). These are respectively a bulk phenomenon and a surface-reaction phenomenon; the enhancement of tubular concentration appears to be surface-layer phenomenon.

CONCLUSIONS

When blood flows through small tubes (less than 302 microns) there is a measurable, increased concentration of platelets in tubular samples as compared to reservoir or collected outflow samples, which have nominally equal platelet concentrations. Work with hardened platelets and effectively anticoagulated blood shows that this effect is not due to surface adhesion. Red cells are necessary to the increased tubular concentrations, but hematocrit is not a major variable. Generally, very low and high shear rates are associated with lower values of relative tubular platelet concentration.

The increase in tubular platelet concentration is largest in tubes with small inner diameters; work with larger inner diameters, such as 635 microns, shows no increase in tubular platelet concentration. The observations are consistent with sequestration of platelets in a slowly moving zone such as the marginal layer.

ACKNOWLEDGEMENTS

This research was funded by grant HL 22455 from the National Heart, Lung and Blood Institute. Instrumentation and laboratory facilities were provided by the Institute for Cell Analysis, University of Miami. Human blood was drawn by the Clinical Hematology Lab. of University of Miami Hospitals and Clinics following appropriate human-subjects protocol. We thank the many people who aided us.

REFERENCES

1. ECKSTEIN, E. C., BECK, M. R., Platelet concentration in blood flow through capillary tubes, In: Biofluid Mechanics: First Mid-Atlantic Conference on Biofluid Mechanics, D. J. Schneck.(Ed.), Blacksburg, Va: VPI & SU Press 1978, pp. 9-18.

2. BLACKSHEAR, P. L.,PATANKAR, S. V., HEIL, R. W., IVANDVIC, M., NIPPOLDT, T. and ROSENSTEIN, A., Fluid dynamics of blood cells and applications to hemodialysis, available Nat. Tech. Inform. Ser. PB-288 587 Jan. 1978.

3. GAEHTGENS, P., ALBRECHT, K. H., KRENTZ, F., Fahraeus effect and cell screening during tube flow of humam blood. I. Effect of variation of flow rate, Biorheology 15: 147-154, 1978.

4. COKELET, G. R., Microscopic rheology and tube flow of human blood. In: Microcirculation. J. Grayson and W. Zingg (Ed.) New York: Plenum, 1976, pp. 9-30.

5. BUGLIARELLO, G., SEVILLA, J., Velocity distribution and other characteristics of steady and pulsatile blood flow in fine glass tubes, Biorheology, 7: 85-107, 1970.

6. GOLDSMITH, H. L., Red cell motions and wall interactions in tube flow. Fed. Proc. 30: 1578-1588, 1971.

7. TURITTO, V. T., BENIS, A. M., LEONARD, E. F., Platelet diffusion in flowing blood, Ind. Eng. Chem. Fundam. 11: 216-223, 1972.

8. FORSTROM, R. J., VOSS, G. O., BLACKSHEAR, P. L., Fluid dynamics of particle (platelet) deposition for filtering walls: Relationship to atherosclerosis, Trans. Amer. Soc. Mech. Eng., J. Fluids. Eng. 96 Ser. I: 168-172, 1974.

9. KELLER, K. H., LAUFFENBURGER, D., The effect of flow channel thickness on surface-induced blood damage, J. Bioeng. 2: 205-217, 1978.

10. BECK, M. R., Platelet concentration in blood flow through capillary tubes, M. S. Thesis, University of Miami, December, 1979.

11. PALMER, A. A., BETTS, W. H., The axial drift of fresh and acetaldehyde-hardend erythrocytes in 25 μm capillary slits of various lengths, Biorheology 12: 283-292, 1975.

12. BARBEE, J. H., COKELET, G. R., The Fahraeus effect, Microvasc. Res. 33: 6-16, 1971.

13. FRIEDMAN, L. I., LIEM, H., GRABOWSKI, E. F., LEONARD, E. F., and McCORD, C. W., Inconsequentiality of surface properties for initial platelet adhesion, Trans. Amer. Soc. Artif. Int. Org., 16: 63-76, 1970

14. SEGRE, G., SILBERBERG, A., "Behavior of macroscopic rigid spheres in Poiseuille flow; Part 2: Experimental results and interpretation, J. Fluid Mech. 14: 136-157 1962.

15. HELLUM, A. J., The adhesiveness of human blood platelets in vitro, Scand. J. Clin. Lab. Investig. 12 (Suppl. 51) : 1-117, 1960.

BIORHEOLOGY, Vol. 17, pp. 465-478, 1980
Printed in the USA. All rights reserved.

0006-355X/80/050465-14$02.00/0
Copyright (c) 1981 Pergamon Press Ltd

NON-LINEAR VISCOELASTIC PROPERTIES OF CERVICAL MUCUS

P.Y. Tam[1]*, D.F. Katz[2]† and S.A. Berger[1]

[1]Department of Mechanical Engineering, University of California, Berkeley, California 94720
[2]Department of Obstetrics and Gynecology, School of Medicine, University of California, Davis, California 95616

(Received 13.6.1980; in revised form 13.11.1980.
Accepted by Editor M. Litt)

ABSTRACT

A capillary tube rheometer was constructed, capable of applying variable shear rates to fluid samples with volumes less than 1 ml. Samples of fresh human and bovine cervical mucus were studied in terms of power-law viscous and elastic rheological moduli. Bovine cervical mucus exhibited fairly linear viscous behavior, but its elastic behavior tended to be non-linear. The degree of non-linearity depended upon the native hydration of the mucus. An effective shear modulus increased and an effective viscosity decreased with increasing hydration. An effective stress relaxation time ranged from approximately 0.5 - 15 sec., and increased as hydration decreased. The viscous and elastic rheological behavior of the samples of human cervical mucus was more linear than that for the bovine. The effective viscosity of the human mucus exhibited more variation and tended to be somewhat higher. The effective shear modulus of the human mucus was significantly higher than that for the bovine. Effective relaxation times in the range 1 - 10 sec. were calculated for the human mucus.

INTRODUCTION

There is substantial biological motivation for studying the rheological and other biophysical properties of cervical mucus. In those mammals where this mucus is abundant, it functions as an accepting, filtering, and nurturing environment for spermatozoa en route to the site of fertilization in the oviduct (1,2). Cervical mucus accomplishes this role via the sophisticated architecture of its glycoprotein-dominated microstructure. At the time of ovulation, that microstructure is optimized to receive spermatozoa. During the non-ovulatory phases of the reproductive cycle, the organization of the mucus micro-structure is altered, thereby rendering it impenetrable to sperm. These microscale changes in the macromolecular architecture of cervical mucus are manifested in macroscale alterations in rheological properties. Attention to the rheological properties of cervical mucus is, therefore, directly relevant to the determination of the phase of the female reproductive cycle. Indirectly, it also pertains to understanding of the sperm-mucus interaction.

There have been a number of studies, initially by Scott-Blair et al. (3) and subsequently by other investigators, of the fundamental viscoelastic properties of human and bovine cervical mucus. Human mucus has been investigated using a rheometer in which a small iron sphere undergoes forced oscillations, e.g. (4,5,6). The frequency spectra of the storage (elastic) and loss (viscous) components of the dynamic stress relaxation modulus were obtained. Bovine cervical mucus has been studied using a concentric cylinder rheometer which also underwent forced sinusoidal oscillations (7). Values of the dynamic moduli were obtained at several different frequencies, and the spectrum of stress relaxation times was subsequently investigated.

Inherent to all these preceding studies was the assumption that the visco-elastic behavior of cervical mucus is linear. However, there exist situations in which cervical mucus is subjected to shear rates that are sufficiently high such that the assumption of linear visco-elastic properties may not be valid. For example, shear rates estimated from

*Now with the Center for Bioengineering, University of Washington, Seattle, Washington.
†To whom correspondance should be addressed.
Key Words: Cervical mucus, non-linear viscoelasticity, rheometer.

data (8) on pressure gradients across the cervix due to contractions of the vaginal, cervical and uterine musculature during coitus yield values in the range of 40-60 sec^{-1}. Mucus shear rates due to undulations of individual spermatozoa may reach the range of 40-200 sec^{-1} (9). The present investigation was designed to address whether the assumption of linear viscoelasticity is valid in this biologically relevant range of shear rates. A capillary rheometer was designed and constructed which was capable of characterizing a fluid in terms of power-law viscous and elastic moduli. The rheometer was applied to samples of fresh human and bovine cervical mucus.

RHEOMETER

The reheometer is a variation of the traditional configuration, cf. (10,11,12). In our instrument, the applied stress is not controlled directly by a vacuum pump. Rather, it is controlled indirectly, and does not remain constant for the duration of the measurement. The rheometer is represented by the schematic drawing, Figure 1. The system can be roughly divided into subsystems: (1) viscometric test section, (2) vacuum, and (3) vacuum monitoring.

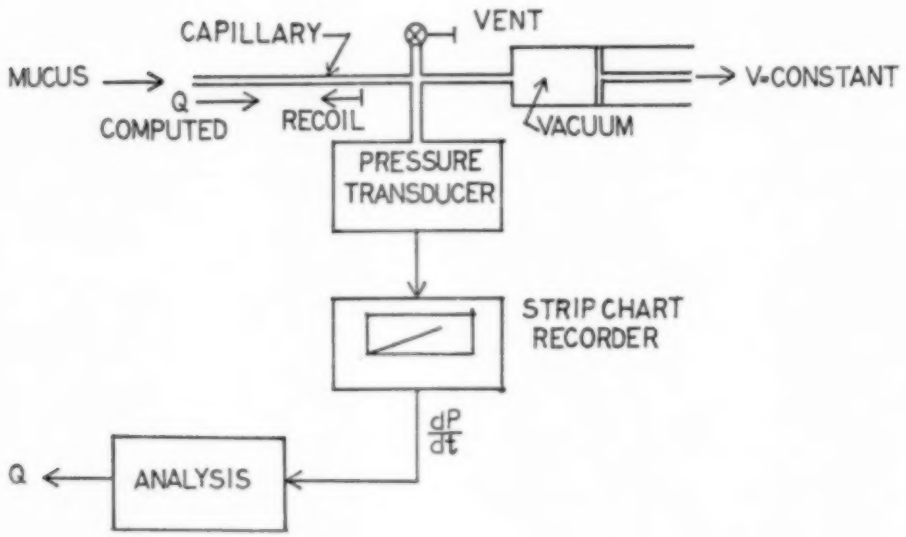

FIG. 1
Schematic of capillary rheometer.

(1) The viscometric test section consists of a circular capillary tube of 0.09 cm internal diameter. One end of the capillary is attached to an air vent (a three-way valve) which is normally closed to the atmosphere. The free end of the capillary is introduced to the sample during a test. A measuring scale with 0.5 mm resolution is attached to the side of the capillary for monitoring the recoil of the sample. The scale also measures the length of the mucus aspirated into the capillary.

(2) The suction required to aspirate the mucus into the test section is provided by the vacuum created by a moving syringe plunger. The rate of plunger movement is controlled by an infusion pump with variable speeds. The syringe is connected to the test section by an adapter, to effect a vacuum in the capillary.

(3) A pressure transducer is attached to monitor the suction used to aspirate the mucus. The output of the pressure transducer is plotted on a strip-chart recorder such that the rate of change of the vacuum with respect to time is readily measured.

A set of measurements for each mucus sample is obtained in the following manner:

Vol. 17
1980

(1) The apparatus is checked for air leaks. In place of the mucus sample is an air-tight seal which renders the system closed to the atmosphere. The infusion pump is turned on until an arbitrary vacuum is achieved. When the infusion pump is turned off, the vacuum should be maintained, provided there is no air leak. The system is then vented so that the pressure everywhere in the system is atmospheric.

(2) A mark is drawn on the capillary, indicating a standard, pre-determined length of the mucus column. During a measurement, the seal is removed and the free end of the capillary is introduced into a reservoir of mucus. The infusion pump is turned on and maintained at a pre-determined rate. The mucus is aspirated into the capillary and the vacuum is monitored and plotted on the strip-chart recorder. The volume flow rate of the mucus is calculated from the rate of change of vacuum.

(3) When the mucus meniscus reaches the mark on the capillary, the vacuum is released (by opening the three-way valve to the atmosphere) so that the mucus recoils. The length of recoil is measured by the attached measuring scale.

(4) The original capillary is removed from the adapter and a new capillary is put in its place. Steps (2) and (3) are repeated at different settings of infusion pump speed.

(5) For each sample, a set of four measurements are taken. Each measurement contains the volume flow rate, recoil, mucus column length and the infusion pump rate.

THEORY

The quantities which characterize the viscoelastic properties of mucus, i.e. shear stress, shear strain, and shear rate, can be derived from the experimentally determined flow rate, recoil, etc. Such derivations have been discussed in detail by Van Wazer et al. (10) and Dunn and Picologlou (12). The key results are:

$$-\left(\frac{du}{dr}\right)_{r = R_c} = \left(\frac{3 + v}{4}\right)\left(\frac{4Q}{\pi R_c^3}\right) , \tag{1}$$

where

$-\left(\frac{du}{dr}\right)_{r = R_c}$ = shear rate at the capillary wall (at $r = R_c$)

Q_c = volume flow rate

R_c = radius of capillary

L_c = length of mucus column

v = correction of factor determined by the slope of a log-log plot of $\left(\frac{4Q}{\pi R_c^3}\right)$ versus $\frac{\Delta P \cdot R_c}{2L_c}$, the shear stress at the wall; or

$$v = \frac{d\left(\log \frac{4Q_c}{\pi R_c^3}\right)}{d\left(\log \frac{\Delta P \cdot R_c}{2L_c}\right)} , \tag{2}$$

and

$$-\gamma = \left(\frac{3 + e}{4}\right)\left(\frac{4V}{\pi R_c^3}\right) , \tag{3}$$

where

$-\gamma$ = recoverable shear strain

V = recoil volume

R_c = radius of capillary tube

e = correction factor determined by the slope of a log-log plot of $\frac{4V}{\pi R_c^3}$ versus shear stress, or

$$e = \frac{d\left(\log \frac{4V}{\pi R_c^3}\right)}{d\left(\log \frac{\Delta P \cdot R_c}{2L_c}\right)} \tag{4}$$

In capillary rheometry, the viscous and elastic properties of the material are separable. Equation 1 describes the viscous component and Equation 3 the elastic component of the response. The correction factors v and e are equal to unity for a Newtonian fluid and a Hookian solid, respectively. Note that Equations 1 and 3 are entirely general expressions irrespective of the models one may assume to describe the material. From Equations 1 and 3, one can obtain the relationship between shear stress, shear strain and shear rate. Theoretical models can then be applied to analyze these empirical relationships. Rheological behavior of non-linear viscoelastic materials can be approximated by power-law relations (12). For the viscous property, the power-law relation can be expressed as:

$$-\frac{du}{dr} = \frac{\tau}{\kappa}\left|\frac{\tau}{\kappa}\right|^{a-1}, \tag{5}$$

while the elastic property is represented by

$$\gamma = \frac{\tau}{\beta}\left|\frac{\tau}{\beta}\right|^{b-1} \tag{6}$$

Here τ is shear stress, and κ and β denote the equivalent of viscosity and shear modulus for the non-linear case. For $a > 1$, the material is pseudoplastic, and for $a < 1$ it is dilatant. When $a = 1$, it behaves like a Newtonian fluid.

It can be shown (12) that the exponent a is equal to v, and b is equal to e (the viscous and elastic correction factor in Equations 2 and 4, respectively). Therefore the degree of non-linearity, i.e. the value of the exponents in the power-law model, is readily obtained from experimental data. Rheological data are often presented as an apparent viscosity κ_{app} and apparent shear modulus β_{app}. These are defined as:

$$\tau = \kappa_{app} \frac{4Q_c}{\pi R_c^3} \tag{7}$$

and

$$\beta = \beta_{app} \frac{4V}{\pi R_c^3} \tag{8}$$

where $\frac{4Q_c}{\pi R_c^3}$ and $\frac{4V}{\pi R_c^3}$ are the uncorrected shear rate and shear strain. However, if we compare Equations 5, 6, 7 and 8 we see that κ is related to κ_{app} by Equation (9) and β to β_{app} by Equation (10)

$$\kappa^a = \frac{4\,\kappa_{app}}{a+3}\left|\frac{\Delta P \cdot R_c}{2L_c}\right|^{a-1}, \tag{9}$$

$$\beta^b = \frac{4\,\beta_{app}}{a+3}\left|\frac{\Delta P \cdot R_c}{2L_c}\right|^{b-1}, \tag{10}$$

Since β and κ are values which are independent of the applied shear stress τ, they are more representative of material properties. We have chosen to present rheological data by β and κ.

Alternatively, one may assume a simple Maxwell model, in which a "dash-pot" (representing the fluid component) and a "spring" (representing the solid component) are connected in series, to analyze the data. The Maxwell model is expressed mathematically by:

$$\tau + \frac{\eta}{G}\frac{\partial \tau}{\partial t} = \eta \frac{\partial \gamma}{\partial t} \tag{11}$$

where τ = shear stress, γ = shear strain, η = viscosity of the fluid component, and G = shear modulus of the elastic component. The fluid component is considered to be Newtonian

Vol. 17
1980

and the elastic one is assumed to be Hookian. We may further define $\eta/G = \lambda$, a relaxation time constant. The constant λ represents the time required for a viscoelastic material to relax to 1/e of the peak stress during a stress-relaxation test. It is true that if the stress-strain and stress-shear rate relationships obey the power-law description, it is not strictly correct to consider a simple Maxwell model. However if one wishes to have an order of magnitude estimation of the relaxation time, it is possible to obtain η and G from average values of τ, γ, and $\dot{\gamma}$. In presenting the values of relaxation time in the following section, we will designate them by $\hat{\lambda}$ to signify that they are obtained from averaged values.

When one assumes a simple Maxwell model of the viscoelastic material, it is possible to calculate the dynamic moduli based on the relaxation time (13). The dynamic moduli G^* and η^* are calculated according to the following equations (11):

$$G^* = G' + iG'' \tag{12}$$

$$\eta^* = \eta' - i\eta'' \tag{13}$$

$$G' = \omega\eta'' = \frac{\eta\omega^2\lambda}{1 + (\lambda\omega)^2} \tag{14}$$

$$G'' = \omega\eta' = \frac{\eta\omega}{1 + (\lambda\omega)^2} \tag{15}$$

where G' is the storage modulus, G'' is the loss modulus and ω is frequency.

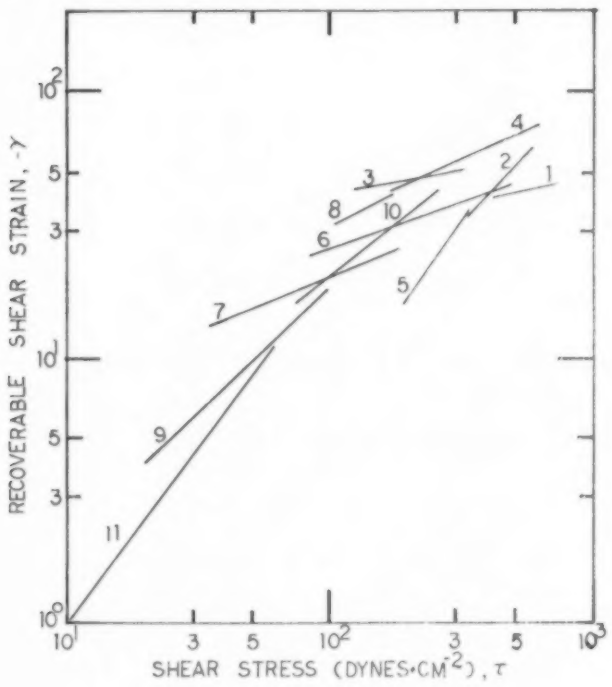

FIG. 2

Relationship between recoverable shear strain and applied shear stress for bovine cervical mucus. H is native hydration (weight of water/weight of non-dializable dry solid).

Curve #1	H = 63	Curve #6	H = 102
2	H = 69	7	H = 151
3	H = 79	8	H = 181
4	H = 80	9	H = 213
5	H = 92	10	H = 226
		11	H = 247

RESULTS

The results will be presented in two categories: (1) bovine cervical mucus (BCM), and (2) human cervical mucus (HCM). Samples of estrous bovine mucus were collected by aspiration into a glass catheter, c.f. (14). Samples of midcycle human mucus were obtained by gentle suction into a polyethylene catheter (15). All mucus samples were maintained in small sealed containers at 4°C from the time of collection until the onset of the rheological measurements. The latter commenced within 24 hours of collection, and were performed at 21° ± 1°C.

The bovine cervical samples collected were of large enough volume that it was possible to determine the effective native hydration and viscoelastic properties on the same sample. By hydration, we refer to the ratio of wet mucus weight to dry weight, after exhaustive dialysis against distilled water. The native hydration of the samples ranged from about 60 to 250. There were eleven samples tested. The values of recoverable shear strain (as measured by the recoil volume) versus the applied shear stresses (measured from the pressure tracing on the strip-chart recorder) are shown in Figure 2. All such data on relationships between shear or shear rates vs shear stress are graphically presented using linear regression lines. The linearity of these lines was consistently good. (The linear correlation coefficients r were generally greater than 0.95 with $P < 0.05$). Applied shear stresses ranged from 10 dynes/cm^2 to 600 dynes/cm^2; while the recoverable shear strain varied from 1- 10 for samples with high native hydration, to 40-70 for the ones with low hydration. The stress and shear rate relationship is shown in Figure 3. In this log-log plot, the data obtained for each sample (4 data points) fall within experimental error on a straight line. The shear rate imposed on the samples falls between 1-30 sec^{-1}, and the corresponding shear stress between 30-3000 dynes/cm^2. Applying Equations 2 and 4, the correction factors v (i.e.a) and e (i.e.b) for equations 1 and 3 , respectively, can be calculated.

Vol. 17
1980

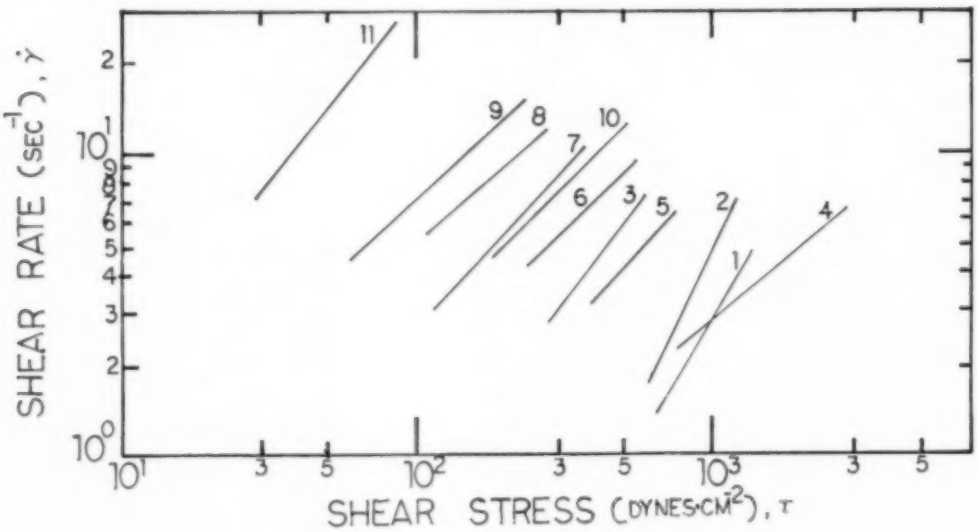

FIG. 3

Relationship between shear rate $\dot{\gamma}$ and applied shear stress τ for bovine cervical mucus (numbers on curves correspond to those in FIG. 2).

Figure 4 shows the calculated values of the exponent b for the elastic component, and Figure 5 shows the values for the viscous exponent a. The error bars at the data points denote the 95% confidence intervals. The values for the viscous exponent remain close to a = 1, except for one sample with low native hydration, where the value of a = 2.2 was obtained. The elastic exponent does not show such constancy. Rather it tends to increase with increasing native hydration. Values of the elastic exponent ranged from b = 0.2 - 1.4.

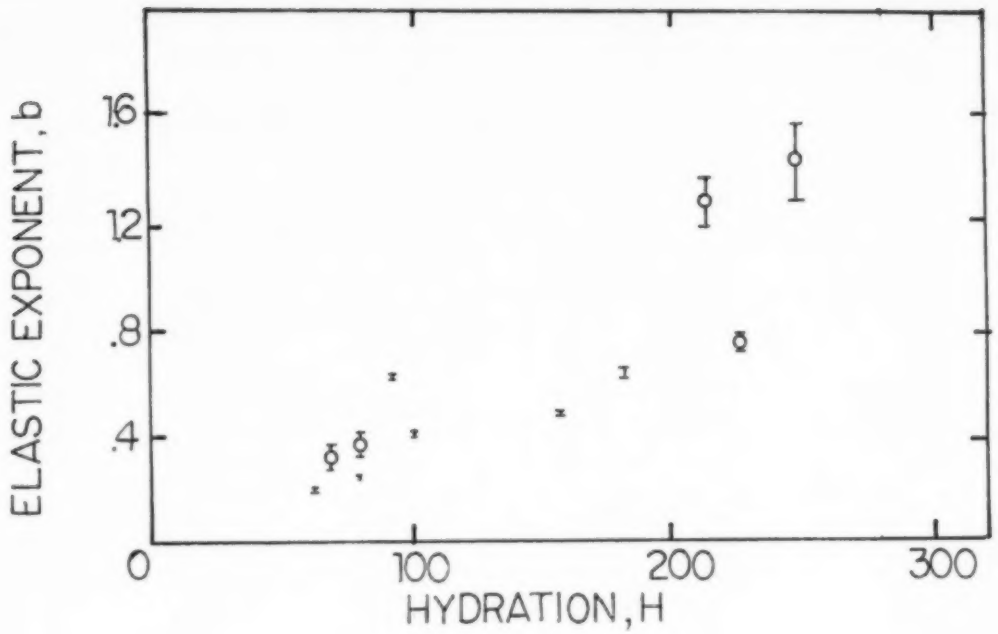

FIG. 4

Experimental values of elastic exponent "b" of power-law model for bovine cervical mucus. Error bars indicate 95% confidence interval.

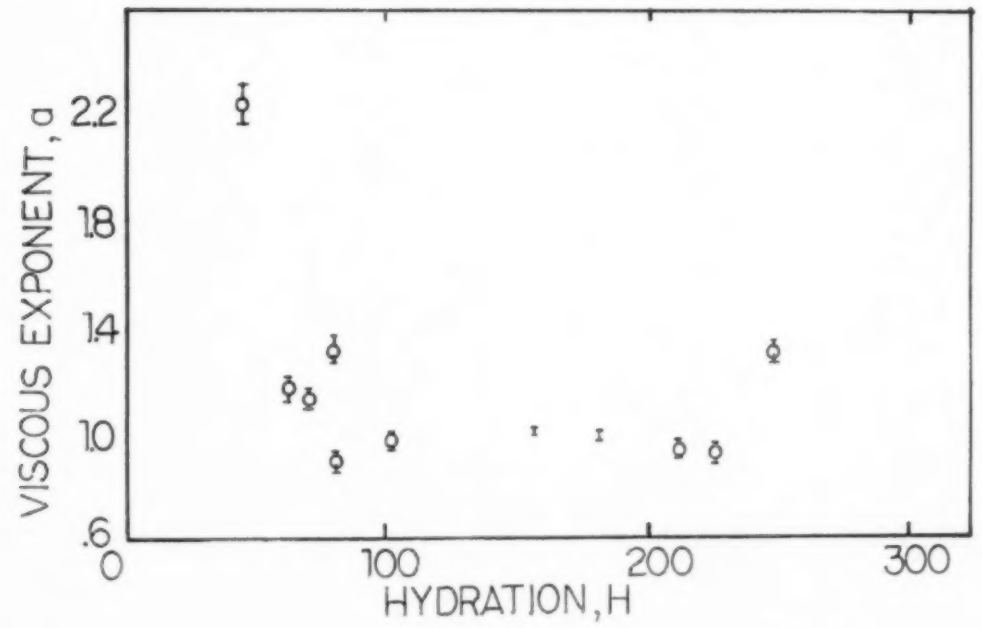

FIG. 5

Experimental values of viscous exponent "a" of power-law model for bovine cervical mucus. Error bars indicate 95% confidence interval.

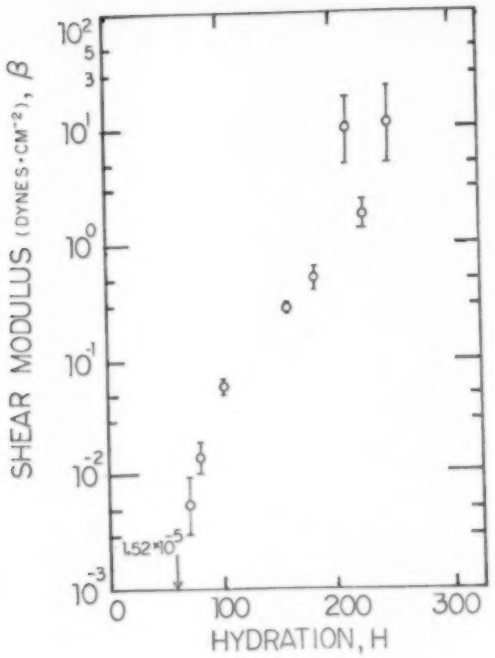

FIG. 6

Distribution of "shear modulus" β (Equation 6 in text) versus native hydration for bovine cervical mucus.

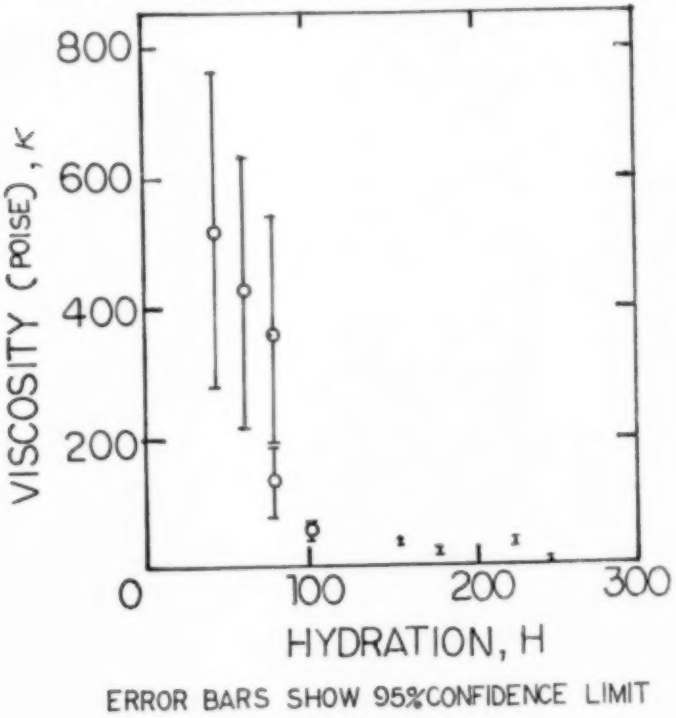

FIG. 7

Distribution of "viscosity" κ (Equation 5 in text) versus native hydration for bovine cervical mucus.

Vol. 17
1980

The values of β and κ are shown in Figures 6 and 7 respectively. The shear modulus β shows a wide excursion of values from 10^{-5} to 20 dynes/cm^2. However these values follow a fairly linear pattern in a semi-log scale for samples tested ($y = -4.27 + 0.5x$, $r = 0.71$, $P < 0.05$). The viscosity κ for the same samples shows a dramatic increase for native hydration less than eighty. For these samples, κ reaches the values of 700 poise, while in those with $H > 100$, κ remains in the range 10-50 poise. This increase was shown to be statistically significant by analysis of variance, $P < 0.05$. Table 1 summarizes the results obtained for BCM.

TABLE 1

Rheological Parameters for Bovine Cervical Mucus

NATIVE HYDRATION	$\hat{\eta}$	$\hat{G}$	$\hat{\lambda} = \frac{\hat{\eta}}{\hat{G}}$	G'	G"
44	239.4	58.9	4.1	58.74	2.89
63	326.0	17.8	18.4	17.75	0.19
69	226.7	9.3	24.5	9.25	0.08
79	71.7	4.8	14.8	4.84	0.07
80	378.9	7.2	53.0	7.14	0.03
102	56.0	76.2	0.7	70.94	19.29
157	36.2	5.8	6.3	5.75	0.18
181	21.8	3.8	5.8	3.79	0.13
213	14.9	5.9	2.5	5.86	0.47
226	44.2	5.5	8.1	5.50	0.14
247	3.4	6.8	0.5	5.84	2.36

$\hat{\eta}$ = average viscosity (poise); G = average shear modulus (dynes/cm^2);
$\hat{\lambda}$ = average relaxation time (sec); G' = dynamic storage modulus (dynes/cm^2);
G"= dynamic loss modulus (dynes/cm^2); G' and G" are evaluated at $\omega = 30$ rad/sec

Because of the small sample volume (100-200 $\mu\ell$), the native hydration of the samples of human cervical mucus was not determed. However, careful records were kept of the collection day with respect to the stage of the menstrual cycle as assessed by pelvic examination at the time of mucous collection, and by referral to the normal basal body temperature curves of each mucous donor. On visual inspection, the HCM seemed more "sticky" than the BCM. HCM also tended to have less optical clarity.

The experimentally determined rheological parameters for HCM are shown in Table 2. The values of recoverable shear strain show a higher range than those for BCM. For applied stresses from 250-1800 dynes/cm^2, the corresponding recoverable strains extend from 12 to 35.

The shear rate measured for this range of applied stress varies from 4.5 to 25 sec^{-1}. Figure 8 gives the relationship between stress and recoverable strain, while Figure 9 shows the variation of volume flow rate versus shear stress. There is more scatter in the data for HCM than for BCM. However, despite the increased scatter, the data still fit onto the straight lines well in the log-log plots for both volume flow rate and recoverable shear strain versus wall stress (with coefficients of linear correlation $r > 0.95$; $P < 0.05$). The values of the power-law exponents a and b, corresponding to the viscous and elastic components, show less variation. The values of b for the HCM samples measured do not fall off from a high value of 2, as in the case of BCM. Instead they remain approximately equal to unity. Similarly, the elastic exponents a are consistently higher than those for BCM, and do not show an increasing trend (see Table 2). This difference in the non-linear viscoelastic characteristics of HCM and BCM may be a true qualitative difference between the

TABLE 2

Rheological Parameters for Human Cervical Mucus

SAMPLE	VISCOSITY κ		SHEAR MODULUS β		ELASTIC EXPONENT b ± error	VISCOUS COMPONENT a ± error	$\hat{\eta}$	$\hat{G}$	$\hat{\lambda} = \hat{\eta}/\hat{G}$	G'	G"
	min	max	min	max							
+4	56.34	162.42	10.41	55.84	0.83 ± 0.06	0.9 ± 0.02	221.71	38.34	5.78	38.29	1.32
+3	229.39	1267.2	70.73	102.70	1.01 ± 0.01	1.57 ± 0.08	231.43	84.81	2.73	84.36	6.183
+2	201.68	274.77	30.36	87.98	1.43 ± 0.06	1.30±0.01	165.32	25.67	6.44	25.65	0.796
+2	1.35	139.24	46.09	178.93	1.27 ± 0.06	1.79 ± 0.02	41.41	49.28	0.84	46.64	11.10
+1	15.15	18.76	33.50	75.02	0.86 ± 0.03	0.95 ± 0.01	15.81	71.09	0.22	39.30	35.32
0	11.70	28.11	54.93	70.92	1.37 ± 0.01	1.73 ± 0.08	4.46	35.12	0.13	10.09	15.89
-2	44.24	314.32	8.94	95.31	0.92 ± 0.10	1.25 ± 0.17	159.09	32.97	4.83	32.91	1.364
-2	26.03	201.54	153.93	324.43	1.08 ± 0.08	1.01 ± 0.08	57.82	64.44	0.9	61.39	13.68
-2	132.00	249.76	36.78	53.30	1.06 ± 0.02	1.24 ± 0.03	126.80	36.95	3.41	36.82	2.158
-2	73.09	218.43	23.69	46.63	0.98 ± 0.03	1.02 ± 0.04	121.60	36.00	3.38	35.87	2.12

*Minimum and maximum values of κ and β indicate 95% confidence limits. Day "0" of sample corresponds to ovulation.
$\hat{\eta}$ = averaged viscosity (poise); G = average shear modulus (dynes/cm^2); $\hat{\lambda}$ = average relaxation time (sec);
G' = dynamic storage modulus (dynes/cm^2); G" = synamic loss modulus (dynes/cm^2); G' and G" are evaluated at ω = 30 rad/sec.

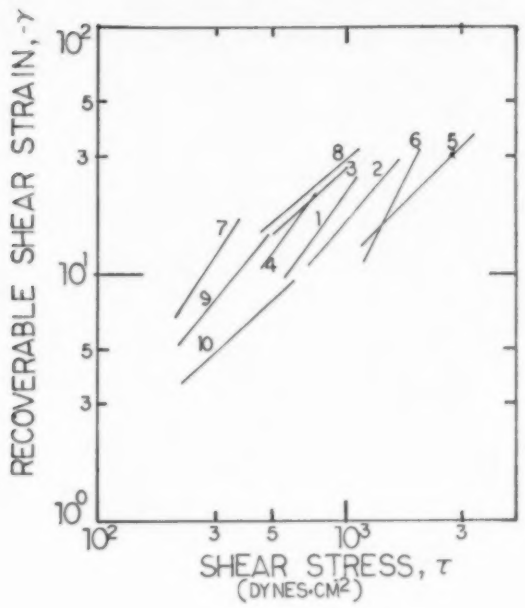

FIG. 8
Relationship between recoverable shear strain γ and applied shear stress τ for human cervical mucus. Samples used were collected from different days of the menstrual cycle. Day 0 (zero) corresponds to ovulation.

Curve	#1	Day +4	Curve	#6	Day 0
	2	Day +3		7	Day -2
	3	Day +2		8	Day -2
	4	Day +2		9	Day -2
	5	Day +1		10	Day -2

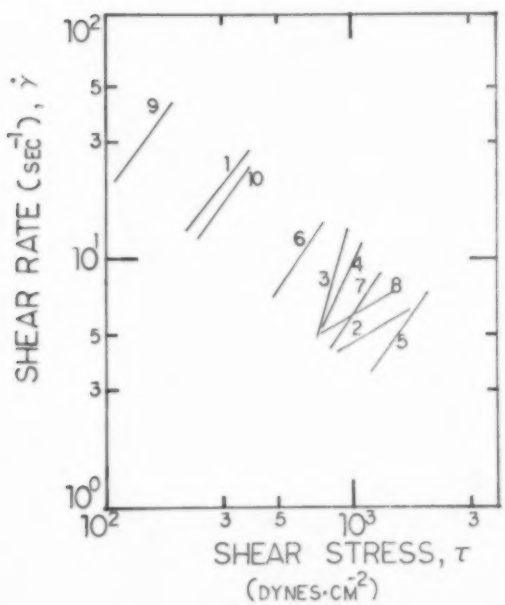

FIG. 9
Relationship between shear rate $\dot{\gamma}$ and applied shear stress τ for human cervical mucus. The number on the curves corresponds to that on FIG. 8.

two kinds of mucus, or it may be incidental that the solids content of the tested HCM did not exhibit great variation.

The viscosity κ for HCM has values similar to those for BCM with $H < 80$. For HCM there is a wide range of values for κ (17 - 600 poise). In Table 2 these values are shown as the mid-point within a 95% confidence interval. The dispersion of the values for the shear modulus β for HCM is much less than for BCM. While values of β for BCM vary from 10^{-5} to 30 dyne/cm^2, those for HCM fall within the narrower range of 20 to 250 dynes/cm^2.

Dynamic moduli G' and G" were calculated from characteristic relaxation times measured from capillary rheometry. In so doing a simple Maxwell model was assumed. For a set of four measurements of stress versus shear rate, an arithmetic average was calculated for the shear stress and shear rate. Average values of recoverable shear strain were obtained analogously. From each pair of average values, i.e. shear stress versus shear rate and shear stress versus recoverable strain rate pair, a viscosity η and shear modulus G were calculated. In so doing, the fluid component was assumed to behave like a Newtonian fluid, and the elastic component like a Hookian solid. The characteristic relaxation time λ is defined as η/G, and is also shown in Table 2. From the relaxation time for each sample, dynamic moduli G' and G" were calculated according to Equations 14 and 15. Wolf et al. (6) have pointed out that at frequencies of about 30 rad/sec, G', G" best characterize the material properties of mucus. Therefore, G' and G" at 30 rad/sec were selected to be presented in Table 2. The values compare well with Wolf's data obtained from the magnetic microrheometer. The relaxation times calculated for the HCM samples range from 1 - 10 sec. The G' and G" values for BCM are generally lower than those for HCM (except for the sample with H = 44 and two anomalous values for the sample of H = 92 and 102).

DISCUSSION

The log shear rate versus log shear stress relationships for both the BCM and the HCM samples display linear behavior within the range of shear stresses measured (the coefficients of correlation for linear regression are $r > 0.95$; $P < 0.05$). This indicates that the power-law adequately describes the behavior of both BCM and HCM. In general, the curves for HCM, in comparison with those of BCM, are slightly shifted towards the right. This implies that higher shear stresses are necessary to induce a similar shear rate. However, one may conclude that the viscous behavior of HCM is very similar to BCM, judging from the similar domain into which these sets of curves fall. Although the native hydrations of the HCM samples were not determined, we suspect that they vary over a similar range as the BCM samples tested. This is inferred from the similar shifts in the curves in BCM and HCM samples, if one assumes that native hydration plays a dominant role in the viscous behavior of the material.

The log-log plots of recoverable shear strain versus shear stress display quite different results for BCM and HCM. The data for BCM span the low shear stress-strain domain, with the majority of the data points found at regions of shear stress from 100-1000 dynes/cm^2, and strains of 10-100. For the HCM samples, the range of shear stresses is 200 to 3000 dynes/cm^2, and the range of strains is 3-40. There is much more scatter in the data for the elastic recoil than those for stress-shear rate. Furthermore, data for HCM samples show more scatter than those from BCM. This may be due to the inherently smaller sample size of the HCM. The general characteristic of HCM is that there is a higher stress observed for shear strains similar to BCM samples. This implies that BCM deforms more easily and to a greater extent for a given applied shear stress, and is consistent with the visual observation the HCM seemed "thicker."

From the stress-shear rate curves, one has the qualitative impression that the viscous component of HCM does not differ to a great extent from that of BCM. If the power-law exponents a of the viscous components are compared (Figure 6 and Table 2), the values for BCM fall within the range of 0.9 - 1.8, while for HCM they range from 0.9 - 1.6. These values do not differ substantially from those for Newtonian fluids, which have the value of a equal to unity. The viscosity κ of BCM and HCM, calculated according to Equations 9 and 10, has values from 10-500 poise. The minimum and maximum values of κ are 1.9 and 517.7 poise respectively for BCM, and 17.0 and 748.3 poise for HCM. The maximum value of κ for HCM is lower than the zero-shear viscosity of 1000 - 2000 poise obtained by Hwang et al. (4). In general, the viscosity, as measured by capillary rheometry, does not differ significantly between BCM and HCM.

The power-law exponent b of the elastic component of BCM differs significanlty from that of HCM. The values of b for BCM extend from 0.2 to 1.4, while those of HCM fall within a narrower range of 0.83 to 1.4. The wide excursion of b for BCM accounts for the tremendous variation in the shear modulus, β. The values of β change from 10^{-5} dyne/cm^2 for the thicker samples to about 20 dynes/cm^2 for the thinner ones. The values of β for HCM are generally higher than those of BCM. They vary from 20 - 230 dynes/cm^2. These results indicate that the difference in the viscoelastic behavior between BCM and HCM lies predominantly in the elastic component. The smaller values of β for BCM imply that for a

given applied stress, the recoverable shear strain is smaller than for HCM. Alternatively, this indicates that when HCM is stressed, a more significant portion of energy is stored in the elastic component.

Dynamic viscoelastic moduli can be calculated from continuous shear or stress-relaxation data. The simplest such approach is to assume that the material behaves as a simple Maxwell model. This approach requires that a relaxation time be calculated from the viscosity and shear modulus measured from shear or stress-relaxation tests. Since our data indicate that mucus behaves like a power-law material, an average value of viscosity and shear modulus, independent of shear rate and strain, must be calculated. One can obtain an average viscosity by taking the ratio of the averaged-stress-to-averaged-shear rate. Similarly the average shear modulus can be calculated. The relaxation times, λ, based on these average viscosities and shear moduli, range from 0.1 to 6.44 sec for HCM and 0.5 to 53 sec for BCM. The value of $\lambda = 53$ for BCM is for a sample with very high native hydration, and may be an anomalous data point. The majority of data for BCM fall in the range from 0.5 to 15 (see Tables 1 and 2). This range of relaxation times is consistent with those quoted by Eliezer (7) (i.e. 1 - 100 sec).

The values of G' for HCM calculated for $\omega = 30$ rad/sec do not differ significantly from those obtained by Wolf et al. (6). Eliezer (7) performed dynamic testing on BCM using a concentric cylinder configuration. No value of G' was given for ω beyond 4.5 rad/sec. However, the curve presented showed an asymptotic behavior toward higher frequencies. If one extrapolates on the curve, a value of G' for $\omega = 30$ rad/sec of 4.5 dynes/cm^2 is obtained. This compares well with our calculations for BCM with high native hydration (Table 1). For samples with low native hydrations, $H < 100$, our calculated values lie considerably higher.

From the good agreement with data from dynamic testing, the capillary rheometer has been shown to be a useful apparatus for measuring viscoelastic properties of mucus. There are a number of advantages in using this device, viz. 1) small sample volume; 2) variable shear rate via use of different tube sizes as well as applied shearing; 3) simplicity and low cost of construction; 4) amenability to analysis of non-linear viscoelastic behavior. The small sample volumes required render it particularly attractive for testing human samples. Moreover the ability of this instrument to take into account non-linear rheological behavior may be of particular relevance in the mechanistic assessment of the biological role of cervical mucus.

ACKNOWLEDGEMENT

This work was supported by NIH grant HD 12971 (D.F.K.) and an NIH Bioengineering Traineeship (P.Y.T)

We thank Drs. J.W. Kendrick and B. BonDurant, Department of Reproduction, School of Veterinary Medicine, and Drs. F.W. Hanson and J.W. Overstreet, Department of Obstetrics and Gynecology, School of Medicine, University of California at Davis, for the collection of the bovine and human cervical mucus, respectively.

REFERENCES

1. DAVAJAN, V., NAKAMURA, R.M. and KHARMA, K. Spermatozoan transport in cervical mucus. Obstet. Gynec. Survey 25, 1-43, 1970.

2. OVERSTREET, J.W. and KATZ, D.F. Sperm transport and selection in the female genital tract. In: Mammalian Development, M.H. Johnson (Ed.) Amsterdam: Elsevier/North Holland. 1977, pp. 31-65.

3. SCOTT-BLAIR, G.W., FOLLEY, S.J., COPPEN, F.M.V. and MALPRESS F.H. Rheological properties of bovine cervical secretions during the oestrous cycle. Nature, London, 147, 453-454, 1941.

4. HWANG, S.W., LITT, M. and FORSMAN, W.C. Rheological properties of mucus. Rheolog. Acta 8, 438-448, 1969.

5. WOLF, D.P., BLASCO, L., KHAN, M.A. and LITT, M. Human cervical mucus. I. Rheological characteristics. Fertil. & Steril. 28, 41-46, 1977.

6. WOLF, D.P., BLASCO, L., KHAN, M.A. and LITT, M. Human cervical mucus. II. Changes in viscoelasticity during the ovulatory menstrual cycle. Fertil. & Steril. 28, 47-52, 1977.

7. ELIEZER, N. Viscoelastic properties of mucus. Biorheology 11, 61-68, 1974.

8. FOX, C.A., WOLFF, H.S. and BAKER, J.A. Measurement of intra-vaginal and intra-uterine pressures during human coitus by radiotelemetry. J. Reprod. Fert. 22, 243-251, 1970.

9. DRESDNER, R.D. and KATZ, D.F. Relationships of mammalian sperm motility and morphology to hydrodynamic aspects of cell function. Biol. Reprod. 22, Suppl. 1, 73A, 1980.

10. VAN WAZER, J.R., LYONS, J.W., KIM, K.Y. and COLWELL, R.E. Viscosity and Flow Measurement - A Laboratory Handbook of Rheology. New York: John Wiley & Sons, Inc., 1963.

11. PHILIPPOFF, W.D. and GASKINS, F.H. The capillary experiment in rheology. Trans. Soc. Rheol. II, 263-271, 1967.

12. DUNN, P.C. and PICOLOGLOU, B.F. Investigation of the rheological properties of human semen. Biorheology 14, 277-292, 1977.

13. BIRD, R.B., ARMSTRONG, R.C. and HASSAGER, O. Dynamics of Polymeric Liquids, Vol. I. Fluid Mechanics. New York: John Wiley & Sons, Inc., 1976.

14. KATZ, D.F. and SINGER, J.R. Water mobility in bovine cervical mucus. Biol. Reprod. 18, 843-849, 1978.

15. KATZ, D.F., OVERSTREET, J.W. and HANSON, F.W. A new quantitative test for sperm penetration into cervical mucus. Fertil. & Steril. 33, 179-186, 1980.

16. WOLF, D.P., BLASCO, L., KHAN, M.A. and LITT, M. Human cervical mucus. IV. Viscoelasticity and sperm penetrability during the ovulatory menstrual cycle. Fertil. & Steril. 30, 163-169, 1978.

Vol. 1
1980

BIORHEOLOGY, Vol. 17, pp. 479-484, 1980
Printed in the USA. All rights reserved.

0006-355X/80/050479-06$02.00/0
Copyright (c) 1981 Pergamon Press Ltd

CHANGES IN SURFACE AREA AND VOLUME MEASURED BY MICROPIPETTE ASPIRATION FOR ERYTHROCYTES AGEING IN VIVO.

G.B. NASH and S.J. WYARD
Department of Physics, Guy's Hospital Medical School
London Bridge SE1 9RT England.

(Received 9.10.1980; in revised form 31.10.1980.
Accepted by Editor R.D. Harkness)

INTRODUCTION

During in vivo ageing, erythrocytes decrease in volume and lipid content whilst their mean cell haemoglobin concentration (MCHC) and density increase (1, 2, 3). At the same time their enzymatic and metabolic activities lessen (4). The variation in density has made it possible for populations of red cells of differing age to be separated centrifugally, either using density gradients (2, 5) or by sedimenting whole blood (3, 6) and the success of the separation has been tested by cohort labelling of cells with radioactive iron and glycine.

The dominant process by which senescent red cells are removed from the circulation is not certainly known. It has been suggested that a decrease in the deformability of aged cells may impair their ability to pass through the microcirculation, especially of the spleen, hence facilitating their removal by that organ (7, 8). In general, erythrocyte deformability depends on the elastic properties of the plasma membrane, on the fluidity of the cell contents and on the cell surface area/volume ratio (and hence shape) (9). It has been shown that aged cells require greater pressure to force them through narrow pipettes ($< 3\ \mu m$ internal diameter) (10), and that the rate at which they initially enter similar micropipettes is reduced (11). It has also been demonstrated that membrane fluidity, assessed by ESR methods, is lower in older cells (12). In addition it has recently been demonstrated that the increase in MCHC with age is linked to a disproportionately large rise in the internal viscosity of the cells (13) which would decrease the rate at which they can be deformed.

With respect to changes in size and shape, the decrease in cell volume which accompanies ageing has been well documented (2, 14). It has been suggested that erythrocyte fragmentation (10, 15) occurs which would be accompanied by a loss in membrane area and surface area/volume ratio. This would result in a decrease in the minimum cylindrical diameter which an erythrocyte could attain and might lead to mechanical lysis if a blood vessel of smaller diameter was encountered (7). In any case, sphering of red cells has been shown to decrease their ease of deformation (9) and it has been reported that separated aged cells appear to lose their biconcavity (12).

In this study we have carried out direct measurements of individual red cell surface area and volume, in order to see if quantitative shape changes occur during ageing. A micropipette aspiration technique similar to that of Jay & Canham (16) was used to measure these parameters for erythrocytes confined to a cylindrically symmetrical geometry. Both human and rabbit blood were fractionated according to density to provide populations of cells of differing age.

KEYWORDS: Erythrocyte Ageing, Erythrocyte Volume, Erythrocytes analysis

MATERIALS AND METHODS

Materials

Blood was obtained from the marginal vein of the ear of rabbits and from humans by venepuncture. Anticoagulant was sodium EDTA (1mg/ml whole blood) except in the case of one of the human donors when heparin was used. Experiments were carried out immediately at room temperature, lasting 4-6 hours.

The basic medium for density separation was Percoll (Pharmacia Ltd., Hounslow, England), a polyvinylpyrrolidone coated silica colloid (density 1.129 g/ml). Stock percoll solution (SPS) was made up by adding one part of ten fold concentrated phosphate buffered saline (PBS) (Dulbecco A., Oxoid Ltd., Basingstoke, England) to nine parts Percoll. The pH was adjusted to 7.4 using HCl and final osmolarity was approximately 300 mOsm/l. Fractionated cells were suspended in Krebs Ringer (NaCl 120mMol/l, $NaHCO_3$ 25mMol/l, $CaCl_2$ 2.5mMol/l, KCl 2.6mMol/l, $MgSO_4$ 1.2mMol/l, KH_2PO_4 1.2mMol/l plus 2mg/ml glucose) containing 2mg/ml human serum albumin (HSA) (Fraction V, Sigma Chemicals, Poole, England). The above media also contained penicillin (1000 U/ml) and streptomycin (0.1mg/ml) (Flow Labs Ltd., Irvine, Scotland).

Fractionation

Rabbit Blood. To separate rabbit erythrocytes according to age a simplified version of the method of Piomelli et al. (2) was used. Percoll, a low viscosity, non-toxic, colloidal medium with low osmotic activity, was used in place of bovine serum albumin. Only two layers of SPS diluted with normal strength PBS were used (typically 77% and 85% SPS, but varying between rabbits). 0.1ml of whole blood was mixed with the upper layer (5ml) before the denser medium was injected beneath it and finally 2ml of PBS was added on top using a pasteur pipette. The concentrations for the dense layers were chosen from experience so that most ($\sim$ 90%) of the cells came to rest at the interface between them after centrifugation at 800g for 15 minutes. In addition a thin band formed above the less dense layer and a small pellet rested at the bottom of the denser portion. Three cell layers were retrieved (upper, middle and lower pellet) using pasteur pipettes, the middle sample also containing cells suspended between the layers. These samples were washed twice in PBS and finally suspended in 10ml KRBG plus HSA.

Human Blood. Since the above method had poor resolution for human red cells (judging by the differences in cell volume between the fractions), a different technique was devised. Using swing out rotors shallow density gradients can be formed from Percoll suspensions (17). Thus 0.1ml of whole blood was mixed with 10ml of 80-85% SPS diluted with PBS (the concentration required varying between donors) and 1ml of PBS was layered on top. The suspension was centrifuged at 2000g for 30 minutes using a swing out rotor. This resulted in the formation of a thin layer of cells at the top interface and of striations near the bottom. Some cells also remained dispersed throughout the gradient. If the centrifugation was repeated then the striations were moved up the tube as the density near the bottom of the gradient tended to increase. The top layer was harvested, followed by the majority of the suspension and striations, and finally the bottom layer or pellet was collected. The samples were washed twice with PBS and finally suspended in 10ml KRBG plus HSA. The SPS dilutions were chosen so that between 5-10% of the least and most dense cells could be separated from the remainder.

Measurements on Separated Cells

Aliquots from the cell suspensions were placed in a glass chamber on a microscope stage. The chamber was closed from above with a coverslip, and a micropipette, mounted on a motorised micromanipulator (Micro Instruments Ltd., Oxford, England), was introduced via a channel in its side. Cells and pipette were observed using a X40, long working distance, water immersion lens (Carl Zeiss Ltd., London). Photomicrographs were recorded on 35mm film. The pipette was connected to a liquid filled, spring loaded reservoir which was moved vertically by a micrometer barrel. The pressure head was read directly from the micrometer scale after zero pressure had been adjusted by observing the behaviour of cells adjacent to the pipette tip. Micropipette internal diameter, approximately 1.8-2.0μm, was measured by head on photography using a X40 objective lens before the pipette was filled with Isoton (Coulter Electronics Ltd., Harpenden, England).

The correct pressure for deforming the erythrocytes was obtained by gradually increasing the suction for a trapped cell. Initially cells tend to fold as they enter the pipette but at a negative pressure of about 1cmH_2O (depending on pipette diameter) a smooth outline with a spherical outer

Vol. 1
1980

and cylindrical inner portion is obtained. Having attained the correct suction, the reservoir was set at this level and cells were photographed a few seconds after entrapment. Subsequently they were ejected by raising the reservoir against its spring. The effects of further increasing the suction pressure and of prolonged cell attachment were tested to see whether these would alter the cells' behaviour. Later the developed film negatives were projected and the diameters of the spherical portions and the lengths of the cylindrical portions of the cells were measured. From the values obtained the surface area, volume and surface area/volume ratio were calculated for each cell (assuming the tips of the cylindrical portions to be hemispherical). In addition undeformed cell diameter was measured for erythrocytes settled on the bottom of the chamber.

A Coulter Counter Model ZF with Channelyser and volume distribution plotter (Coulter Electronics Ltd.) was also used to measure cell volume and to count the cells in the fractionated samples. These were diluted with KRBG and compared to freshly suspended whole blood. Volume calibration was carried out using latex spheres (median diameter 4.9μm) and thus to calculate absolute cell volume a shape factor was required for the cells (18, see also Results). As the sphere diameter quoted by the manufacturers was the median value, we decided also to use the median value for the red cell volume. Finally reticulocyte counts were made microscopically after staining concentrated cell suspensions with brilliant cressyl blue, by counting approximately one thousand cells.

RESULTS

Blood samples from each of three rabbits and three humans were fractionated according to density on two occasions. The more dense cells had markedly smaller volumes and reticulocytes were concentrated in the uppermost layers (see Table 1). The separation procedure did not alter overall median cell volume compared to freshly suspended cells (see Table 2) and the fractionated cells appeared morphologically normal.

When ejected from the micropipette tips, cells returned quickly to their original shapes. It was noted however, that if larger suction pressures were used (about 5-7cmH_2O for a 2μm diameter pipette) cells were crenated or deformed after release. Nevertheless, the measured cell volume was not dependent on suction pressure for freshly suspended cells if this was not raised above 2cmH_2O. Nor was volume significantly altered if cells were attached to the pipette for periods up to one minute. Values obtained for cell surface area were not affected by suction pressure or time of attachment at any of the levels mentioned above.

TABLE 1
Data Obtained Microscopically

SAMPLE	FRACTION	+RETICULOCYTE COUNT (%)	*MICROPIPETTE MEASUREMENTS VOLUME (μm^3)	SURFACE AREA (μm^2)	AREA/VOLUME RATIO	ǵ DIAMETER (μm)
HUMAN BLOOD	UPPER	1.5	111 ± 13%	141 ± 7%	1.27 ± 5%	8.3 ± 5%
	MIDDLE	0.3	105 ± 11%	136 ± 6%	1.34 ± 6%	8.1 ± 5%
	LOWER	0	99 ± 14%	130 ± 8%	1.32 ± 7%	7.85 ± 5%
RABBIT BLOOD	UPPER	13	84 ± 14%	120 ± 8%	1.43 ± 7%	7.5 ± 6%
	MIDDLE	0.9	72 ± 15%	109 ± 7%	1.52 ± 7%	6.9 ± 8%
	LOWER	0	70 ± 14%	105 ± 9%	1.49 ± 6%	6.6 ± 7%

+ Freshly suspended samples of human and rabbit blood contained 0.4% and 1.6% reticulocytes respectively.

* Values represent the means from six experiments. Each of three donors had 20 cells measured on two separate occasions. These are followed by average coefficients of variation from the six sets of measurements.

ǵ As for * except 36 cells were measured on each occasion.

Data from the micropipette analysis of cell size are summarised in Table 1. These show that mean cell volume was approximately 20% greater for the least dense rabbit erythrocytes compared to the most dense and that for human red cells the equivalent difference was about 12%. Surface area was also greater in the upper fractions but the surface area/volume ratio was essentially constant for all fractions from a given donor. The ratio also varied little between cells in a given sample as cells with larger volumes tended also to have larger surface areas. The rabbit cells were smaller than those from human donors and had a significantly greater area/volume ratio. Although the denser cells were of smaller diameter for both types of donor, spherical cells were not found in any samples. However, a relatively large number of cup-shaped cells (stomatocytes) were found in the most dense fractions. These were especially evident in the rabbit blood samples, which are known to exhibit anisocytosis (19).

The Coulter Counter cell volume and cell count data are summarised in Table 2 and the former are compared to the equivalent values obtained by micropipette analysis. Latex spheres were used to calibrate the Coulter Counter and thus an equivalent sphere or sensed volume for each cell sample was initially obtained. To determine absolute volume data a shape factor of 1.08 was assigned for the red cells (20, 21), compared to 1.5 for the spherical particles (18). A multiplicative correction factor of approximately 1.4 (= 1.5/1.08) was thus applied to the initial sensed volume. Data obtained in this way verified that erythrocyte volume decreased with increasing cell density.

TABLE 2

* Coulter Counter Measurements

SAMPLE	FRACTION	CELL COUNT (% of total)	+ø COULTER VOLUME (μm^3)		MICROPIPETTE VOLUME (μm^3)	
HUMAN BLOOD	UPPER	12.5	105	(1.14)	111	(1.12)
	MIDDLE	79.5	99	(1.08)	105	(1.06)
	LOWER	8.0	91	(1.0)	99	(1.0)
RABBIT BLOOD	UPPER	6.0	83	(1.2)	84	(1.2)
	MIDDLE	89.0	73	(1.06)	72	(1.03)
	LOWER	5.0	68.5	(1.0)	70	(1.0)

* Values represent the means from six experiments. Blood from three donors of each type was measured on two separate occasions. Figures in brackets represent the volumes expressed relative to those for the lower (least dense) samples.

ø Coulter data represent the median cell volumes and were calculated from the equivalent sphere volumes initially measured, by using appropriate shape factors (see text).

\+ For freshly suspended samples of human and rabbit blood, the Coulter volumes were $100\mu m^3$ and $73\mu m^3$ respectively.

DISCUSSION

Since reticulocytes were concentrated in the uppermost layer and cell volume was smaller in the lower layers, as expected for denser ageing cells (2, 14), it is concluded that both human and rabbit red cells were successfully fractionated according to age. In addition the separation procedure had no apparent harmful effect on the cells.

Micropipette analysis yielded reproducible values for mean cell surface area, volume and their ratio. These properties were not altered by the measurement procedure as the suction pressures used were less than those required to significantly alter cell volume or area (22, 23). The volume data obtained in this way were consistent with the Coulter Counter measurements, though slightly greater in the case of human blood samples. The micropipette measurements of cell surface area are in agreement with other studies of human blood (7, 16) and though no comparable data is available for rabbit erythrocytes, the volumes determined for these cells are similar to values previously published (19).

Vol. 1
1980

Volume, surface area and diameter were all smaller for older cells and these differences were more marked for the rabbit blood samples. However, the cell surface area/volume ratio did not decrease with age thus precluding the possibility that erythrocytes become sphered during this process. Moreover spherical cells of the diameter measured in this study would have much greater volumes than those found here. Nevertheless it was noted that a relatively large proportion of the oldest cells were cup shaped stomatocytes with deep depressions in them. These cells can appear roughly spherical but in fact have large surface area/volume ratios.

It has been shown previously that membrane lipid is lost whilst red cells age (1, 12). The data presented here also suggest some loss of membrane material. However, cell fragmentation (10, 15) cannot account totally for the changes in surface area and volume since in that case surface area/volume ratio would also decrease (9). It has also been shown that membrane protein is not lost during ageing (12) and that cell haemoglobin content remains constant (2, 12). Thus any fragments lost during ageing would essentially have to be lipid vesicles devoid of haemoglobin. Protein contraction (24) might then account for the decrease in membrane area. Further loss of cell water and electrolytes, causing decreases in cell volume without membrane loss, would also need to occur to explain the values for the surface area/volume ratio observed in this study.

With respect to erythrocyte deformability, the reported decreases with age (10, 11) cannot be linked to geometric factors. The cell surface area/volume ratio does not decrease with age and for the values obtained in this study, the minimum cylindrical diameter which the erythrocytes could achieve is slightly smaller for the older cells. That is, for example, the minimum diameter for a cylindrical tube through which the upper sample (youngest) of rabbit cells could pass is 3.05μm whereas the oldest cells could on average pass through a tube of diameter 2.9μm without their volume or surface area having to be altered. On the other hand, the decrease in cell volume and concurrent increase in haemoglobin concentration lead to a large increase in internal viscosity as the cells age (13) and this will slow the rate at which the cells can be deformed, as shown by Shiga et al. (11). Another property which could affect erythrocyte deformability and which might alter with age is the cell membrane elasticity. It has previously been demonstrated that membrane fluidity and lipid/protein ratio decrease with age (12) and we hope shortly to report results of relevant studies of membrane elasticity carried out in this laboratory.

In summary, we have shown that whereas surface area and volume decrease with increasing cell age, the ratio of these parameters remains approximately constant. Thus red cells do not become spherical as they approach senesence and their decreased deformability cannot be explained by a change in shape.

ACKNOWLEDGEMENTS

This work was supported by MRC Project Grant No. G978/659/N. We gratefully acknowledge the help and advice given by Dr. M. Adinolfi and the aid of Miss S. Dodds, Mrs. S. Bayer and Miss N. Dobson in obtaining blood samples.

REFERENCES

1. PRANKRED T.A.J. The ageing of red cells. J. Physiol., 143, 325-331, 1958.

2. PIOMELLI S., LURINSKY G. and WASSERMAN L.R. The mechanism of red cell ageing. I. Relationship between cell age and specific gravity evaluated by ultracentrifugation in a discontinuous density gradient. J. Lab. Clin. Med., 69, 659-674, 1967.

3. BORUN E.R., FIGUEROA W.G. and PERRY S.M. The distribution of Fe59 tagged human erythrocytes in centrifuged specimens as a function of cell age. J. Clin. Invest., 36, 676-679, 1957.

4. WINTROBE M. Clinical haematology (7th Edition). Lea & Febiger, Philadelphia. 1974, pp. 200-204.

5. LEIF R.C. and VINOGRAD J. The distribution of buoyant density of human erythrocytes in bovine albumin solutions. Proc. Nat. Acad. Sci. (US), 51, 520-528, 1964.

6. RIGAS D.A. and KOLER M.D. Ultracentrigal fractionation of human erythrocytes on the basis of cell age. J. Lab. Clin. Med., 58, 242-246, 1964.

7. CANHAM P.B. and BURTON A.C. Distribution of size and shape in populations of normal human red cells. Circ. Res., 22, 405-422, 1968.

8. LACELLE P.L. and ARKIN B. Acquired rigidity: a possible determinant of normal RBC lifespan. Blood, 36, 837-840, 1970.

9. LACELLE P.L. Effect of sphering on red cell deformability. Biorheology, 9, 51-59, 1972.

10. LACELLE P.L., KIRKPATRICK F.H., UDKOW M.D. and ARKIN B. In: Red cell shape. M. Bessis, R.I. Weed and P.F. Leblond (Eds). Springer Verlag, New York, Heidelberg and Berlin. 1973, pp. 69-78.

11. SHIGA T., MAEDA N., SUDA T., KON K., SEKIYA M. and OKA S. A kinetic measurement of red cell deformability: A modified micropipette technique. Jap. J. Physiol., 29, 705-720, 1979.

12. SHIGA T., MAEDA N., SUDA T., KON K. and SEKIYA M. The decreased membrane fluidity of in vivo aged human erythrocytes. Biochimica Biophysica Acta, 553, 84-95, 1979.

13. WILLIAMS A.R. and MORRIS D.R. The internal viscosity of the human erythrocyte may determine its lifespan in vivo. Scand. J. Haematol., 24, 57-62, 1980.

14. GANZONI A.M., OAKES R. and HILLMAN R.S. Red cell ageing in vivo. J. Clin. Invest., 50, 1373-1378, 1971.

15. ROUS P. Destruction of the red blood cell corpuscles in health and disease. Physiol. Rev., 3, 75-105, 1923.

16. JAY A.W.L. and CANHAM P.B. Viscoelastic properties of the human red blood cell. II. Area and volume of individual red cells entering a micropipette. Biophys. J., 17, 169-178, 1977.

17. PERTOFT H., LAURENT T.C., LAAS T. and KAGEDAL L. Density gradients prepared from colloidal silica particles coated by PVP (Percoll). Anal. Biochem., 88, 271-282, 1978.

18. GROVER N.B., NAAMAN J., BEN-SASSON S. and DOLJANSKI F. Electrical sizing of particles in suspension. I. Theory. Biophys. J., 9, 1398-1414, 1969.

19. MITRUKA B.M. and RAWNSLEY H.M. Clinical and haematological reference values in normal experimental animals. Masson Inc., New York, Paris, Barcelona and Milan. 1977.

20. KACHEL V. Optical investigation of form factors during Coulter volume measurement. Microscopica Acta, 75, 419-428, 1974.

21. NASH G.B. Measurement of cell volume and shape by electronic sensing and light scattering methods in flow systems. PhD Thesis, University of London. 1979, chapter 5.

22. EVANS E.A., WAUGH R. and MELNIK L. Elastic area compressibility modulus of red blood cells. Biophys. J., 16, 585-595, 1976.

23. EVANS E.A. and WAUGH R. Osmotic correction to elastic area compressibility measurements on red cell membrane. Biophys. J., 20, 307-313, 1977.

24. ROSENTHAL A.S., KREGENOW E.M. and MOSES H.L. Some characteristics of a Ca (2+) - dependent ATP-ase activity associated with a group of erythrocyte membrane proteins which form fibrils. Biochimica Biophysica Acta, 196, 254-262, 1970.

BIORHEOLOGY, Vol. 17, pp. 485-499, 1980
Printed in the USA. All rights reserved.

0006-355X/80/050485-15$02.00/0
Copyright (c) 1981 Pergamon Press Ltd

INFLUENCE OF MEMBRANE FLUIDITY ON ERYTHROCYTE FUNCTIONS

Takeshi Shiga and Nobuji Maeda
Department of Physiology
School of Medicine, Ehime University
Shigenobu, Onsen-gun, Ehime, Japan 791-02

ABSTRACT The close relationship between the membrane fluidity and functions of erythrocytes was briefly discussed: (1) general consideration, (2) spin label study on membrane and (3) examples, of cholesterol effect, aging and protein cross-linking, were presented.

The purpose of this review is to describe how the membrane fluidity is estimated and how its changes correlate with the erythrocyte functions, such as rheological properties and oxygen transport activity.

It is difficult to define and quantify the degree of membrane rigidity (hardness-softness properties). In the case of erythrocyte membrane, however, (i) the viscoelasticity and other properties could be physically defined and successfully determined [1,2], and (ii) the "membrane fluidity" ("internal viscosity or microviscosity of membrane" or simply "membrane viscosity") was frequently measured, in order to express the state of membrane[3].

The fluidity may be simply defined as the reciprocal of the viscosity for isotropic liquid, but in the case of biomembrane the friction tensor is difficult to be realized, because the constituents of membrane are heterogeneous and do not distribute uniformly. Therefore, the fluidity is often operationally measured on the basis of spectral parameters, reflecting the motion of extrinsic molecular probes incorporated into the membrane. Such measures do consequently differ each other, depending on the probes and the methods used [4]; in addition, most of these techniques concern with the lipid portion of membrane [3]. However, the methods are applicable to various types of membrane; thus the comparison among different membranes (e.g., artificial vesicles of known composition and biomembranes) is possible.

Recently, several review articles on erythrocyte membrane have been collected with emphasis to structure-function relation of membrane proteins [5]. Therefore, this review deals with (1) the relation between the membrane fluidity and erythrocyte functions, (2) the measurement (estimation) of membrane fluidity by spin label technique, using electron paramagnetic resonance[EPR] (since the dynamic structure of membrane is represented by the movements of lipid-like spin labels very well), and finally (3) the representative examples demonstrating the close relation between the membrane fluidity and erythrocyte functions, i.e., (i) the effect of membrane cholesterol, (ii) the effect of aging (both in vivo and in vitro), and (iii) the effect of glutaraldehyde (as a cross-linking reagent).

Correlation between membrane fluidity and erythrocyte functions

According to the Singer-Nicolson model, the biomembrane is composed of lipid bilayer in which the membrane proteins are floated (peripheral or extrinsic proteins) or penetrated (intrinsic proteins), and are moving (rotation and lateral diffusion). In the erythrocyte membrane, furthermore, the cytoskeletal network (mainly, spectrin and actin) interacts with

Abbreviations: electron paramagnetic resonance (EPR), nuclear paramagnetic resonance (NMR), 2,3-diphosphoglycerate (2,3-DPG).
Key words: erythrocytes, membrane, spin label, cholesterol, aging.

the inner layer; thus the network is believed to serve for the mechanical stability of the membrane.

The dynamic, supramolecular organization of membrane is primarily determined by the biochemical composition and modulated by the interactions with other constituents. The membrane fluidity may regulate the important functional properties of erythrocytes, such as the mechanical and rheological properties, the oxygen transport activity, the cellular metabolism (in relation to life span), further the intracellular interactions (Fig. 1).

Cellular functions	Subcellular phenomena	Compositions
Rheology suspension viscosity deformability	Membrane fluidity	Lipids: cholesterol phospholipids
	Intracellular viscosity	Proteins: enzymes carriers hemoglobin
Life span		
	Metabolic activity	Metabolites: 2,3-DPG ATP, etc.
Oxygen transport		
	Hemoglobin allosterism	Ions: H^+, K^+, Ca^{++}, etc.
Surface responce immunological aggregation fusion		Carbohydrates, etc.
	Shape	(Drugs)

FIG. 1. Erythrocyte functions, subcellular (supramolecular) phenomena and biochemical composition.

(1) Mechanical properties of erythrocyte membrane: (a) the rigidity of membrane is an important factor for determining the cell deformability, together with other factors such as the intracellular viscosity and the cell shape (or the ratio of surface area vs. volume) [6,7]. (b) The viscosity of erythrocyte suspension increases at lower shear rates because of cell aggregation, and decreases at higher shear rates because of the cell deformation to ellipsoid (probably as to reduce the rheological resistance against shear) [8,9]. (c) The tank-tread movement of erythrocyte membrane may be directly related to the membrane fluidity, though the physiological meaning of the movement is unclear [10]. (d) the mechanical strength of membrane may be influenced by the membrane fluidity.

(2) The membrane as a barrier: (a) In the case of passive diffusion, for example, the diffusion of oxygen through the lipid bilayer has been shown to depend on the composition and the states of membrane, i.e., it reduces when the membrane cholesterol is increased [11]. (b) The carrier-mediated transport may be affected by alteration of membrane fluidity (vide infra), e.g., the activity of glucose carrier in reconstituted vesicles depends on membrane fluidity [12].

(3) The activities of membrane enzymes: (a) The rotational and lateral diffusion in membrane, (b) the conformational changes and (c) the association-dissociation phenomena, of membrane proteins are influenced by the modification of lipid-protein interaction [13-18]. If the activities of the proteins, either enzymes or carriers, are modified dependently on membrane fluidity, the cellular metabolism changes. Consequently, the intracellular concentrations of ATP, 2,3-DPG, inorganic ions and pH will be varied.

(4) The state of cell surface: The changes of membrane fluidity (a) may influence the immunological responces, though it is not a sole controlling factor [19,20] and (b) may modify the ability of intercellular aggregation, of interaction with plasma proteins and of cell fusion. Further, the change in surface charge may occur. On the other hand, at the inner surface, the interaction between the cytoskeletal network and other membrane components may be affected by the change in membrane fluidity [21].

In short, these cellular and subcellular functions are closely related to the membrane fluidity, which is determined primarily by the composition and organization of the membrane constituents and is modulated by the interactions with the intracellular substances.

Measurement of membrane fluidity by the spin label method

In general, the methods using molecular probes have to fulfil the following requirements.

(i) The method must be non-destructive and the molecular probes must be detected selectively . Further, the quickness of (spectral) measurement is recommended for living materials.
(ii) The probe molecules have to be easily incorporated into membrane, without perturbing the structure and function of the membrane.
(iii) The molecular motion of probes must be sensitive to the state of their close environments; thus their molecular size and structure must be suitably selected.
(iv) The observed spectra (or spectral parameters) must be converted, either theoretically or empirically, to the appropriate measures related to the molecular motion.
(v) The probes are preferred either to be distributed uniformly in whole membrane or to be selectively located in (or excluded from) the defined loci.

In order to look through the ability and limitation of the methods and to obtain the informations from inside of membrane, the application of the spin label technique will be briefly described below (for details, see recent publications [22-25]). Since most of spin label molecules are derivatives of natural lipids [see footnote], they satisfy the above requirements (though the overloading of some spin labels induces echinocytosis and hemolysis [26]). In addition, EPR is an unique method in a sence that it detects only paramagnetic species and does not require any pretreatment (e.g., solubilization, etc.).

(1) Measurements of spin label motion in membrane:

The observable movements of spin label molecules, which are resembled those of natural lipids in membrane, are summarized in Fig. 2.

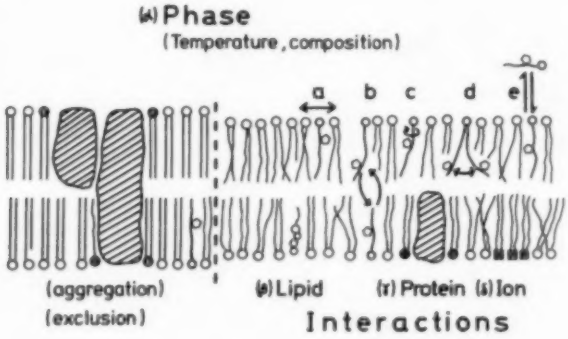

FIG. 2. Scheme of spin label motion in membrane.
(left part) representing the solid, crystalline phase; the acyl chain immobilizes, the thickness of bilayer increases, and the membrane proteins may tend to be excluded from lipid layer and to aggregate together.
(right part) representing the fluid phase; the acyl chain motion increases, the thickness decreases, and the proteins are dispersed.
(a) - (e): representing the types of spin label motion [see text].
(α) - (δ): representing the phases and the interactions between lipids and other components [see text].

(a) The lateral diffusion of the spin label is a two-dimensional movement in the plane of lipid bilayer: the rate of lateral diffusion is 10^{-8} - 10^{-7} cm^2/sec for spin-labeled phospholipids in fluid bilayer of phosphatidylcholine membrane [27,28].
(b) The flip-flop transmembrane motion between the outer and inner lipid layers: the half time for exchange of spin-labeled phosphatidylcholine in phosphatidylcholine membrane is estimated as ca. 6.5 hr at 30 °C [29].

Representative spin labels are shown below:
Stearate spin labels, denoted as I(m,n), are perhaps uniformly dispersed in lipid portion.
Phospholipid spin labels may locate heterogeneously, depending on the properties of their head groups.
Androstane spin label, denoted as ASL, gradually immobilizes, as increasing its concentration in erythrocyte membrane [33].
Tetramethyl-piperidine-oxyl (TEMPO) is often used for measurement of partition parameter, since it is believed to be excluded from the solid phase to the medium.

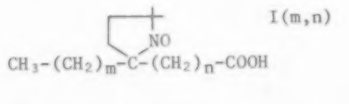

I(m,n)

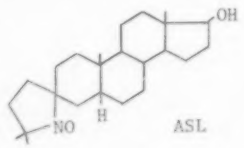

ASL

TEMPO

(c) and (d) The motion of nitroxide group in membrane differs depending on the position attached to the acyl chain, because the hydrocarbon chain motion increases as approaching to the terminal methyl ("flexibility gradient" [22,30]), as confirmed by deuterium-NMR [31]. (c) When the nitroxide group is attached near the head group anchored to bilayer surface (e.g., COO^- of stearate spin label), the movements around each C-C bond of acyl chain (trans-gauche transformation) dominate and give the tilted structure, and the nitroxide group rotates around the long molecular axis perpendicular to the bilayer plane. This movement can be expressed by order parameter (S) calculated from the observed spectra [32]. (d) When the nitroxide group is attached near the terminal methyl group, located in the middle portion of bilayer, the nitroxide group moves more freely. This motion is usually expressed by the correlation time (τ_c) (for details, see ref. [23]).
(e) The spin label molecules present in equilibrium between membrane and solvent medium (in different environments and with different mobilities), thus two EPR signals overlap. The partition parameter (f) may be determined from the observed spectra (TEMPO is used often) [34].

For obtaining the measures of membrane fluidity, the spin label motions [(c) and (d)] are commonly monitored, because of simplicity of EPR measurement. On the other hand, the motion of other membrane components, especially the membrane proteins, is hard to determine by such simple technique: i.e., when a spin label is covalently attached to some groups of protein, the motion of nitroxide group is predominantly affected by the mobility of (and around) the binding site, thus the motion does not reflect the movement of whole protein in membrane. In order to measure the rotational and lateral diffusion of membrane proteins, more elaborate techniques have been developed [16].

Corresponding to the lateral diffusion of order of 10^{-8} cm^2/sec, the estimated "micro-viscosity" of human erythrocyte ghosts varied (2.6 - 6.0 Poise at 25°C, if converted to the viscosity of isotropic liquid [35]). On the other hand, the lateral diffusion coefficient of membrane proteins ranges 10^{-11}- $10^{-10}$$cm^2/sec$ [16].

(2) Factors influencing the molecular motion of lipids:

The fluidity, as measured through the motion of the lipid-like molecules in membrane, is influenced by many factors. The representative phenomena are as follows (see Fig. 2).

(α) The phase and the phase separation: At lower temperature the membrane is in solid, crystalline phase; thus the spin label molecules are immobilized. In contrast, at higher temperature, the molecules are mobilized as the membrane fluidizes (in fluid or liquid phase). In certain tempearture range around transition temperature (T_c), the membrane is in intermediate, liquid-crystalline phase [36]. The thickness of bilayer, the molecular packing and the acyl chain motion depended on the phase. Therefore, the solubility and the permeability of other solutes change, e.g., some molecules such as proteins may be excluded from lipid portion and may form aggregates in solid phase. The transition temperature varies with the composition of membrane.

Further, the lateral phase separation occurs in membrane composed of mixture of phospholipids, i.e., the phases and the lipid composition of the microscopic loci differ each other, resulting the microscopic mosaic structure with different phases [37,38]. The phase separation should be frequently observed in biomembrane, being consisted of many kinds of lipids and interacted with others (proteins, ions, etc.). However, in intact erythrocyte membrane, the averaged spectral parameter is usually obtained and the molecular organization of every loci cannot be estimated, unless a drastic change takes place in some specified portion.

(β) The lipid-lipid interaction: The fluidity of artificial membrane depends on the composition of lipids, i.e., the head groups, the length and the degree of unsaturation of acyl chains, the molar ratios of the constituents, etc. For example, cholesterol modifies the membrane phase [38-41]: below the transition temperature, it shows the condensing effect on phospholipid bilayer. The cholesterol effect on human erythrocyte membrane and functions will be discussed later.

(γ) The protein-lipid interaction: At the vicinity of membrane protein, lipid molecules interact with protein to form boundary (annular) lipids and the motion of such lipids is restricted. Some proteins show strict lipid specificity for the structure of acyl chain (like cofactor) [17] or exclude cholesterol from their boundaries [42]. Not only the lipids adjacent to proteins are strongly affected, but also the surrounding lipids are influenced in some extent, therefore the phase separation is induced.

(δ) The ion-lipid interaction: Ca^{++} interacts with certain group of phospholipid and induces the lateral phase separation (clustering of phospholipids) in bilayer [43,44]. Recently, proton-induced phase separation is found [25,45]. Since the phospholipids are asymmetrically distributed between inner and outer layers [46], the effect of divalent cations and H^+

cannot be uniform and symmetric. In addition, the interaction between ions and membrane proteins must be accounted.

The above interactions are representative phenomena occuring in biomembrane. They are correlating each other and modulating the membrane fluidity in a complex way. At the present stage, it is impossible to estimate the weights of these factors. Furthermore, in erythrocytes, the effect of the cytoskeletal network on the lipid bilayer (including proteins) is not clearly understood.

Examples demonstrating the dependence of erythrocyte functions on the membrane fluidity

The changes in membrane fluidity of erythrocytes occur by various causes and often modify the erythrocyte functions, in particular the rheological properties. From the patho-physiological points of view, three examples are discussed below, concerning with (1) the quantitative variation of membrane lipid (cholesterol effect), (2) the erythrocyte aging and blood storage and (3) the modification of membrane proteins ("fixation" by glutaraldehyde).

(1) Effect of membrane cholesterol.

The condensing effect of cholesterol on phospholipid membrane, above transition temperature, has been established by various methods. When the membrane cholesterol of erythrocyte ghosts was artificially increased, the "membrane viscosity" (measured by fluorescence method) increased [47]. Cooper and Jandl [48] demonstrated the high resistance of cholesterol-loaded erythrocytes against hypotonic hemolysis and the alteration of mechanical properties of membrane.

In our recent in vitro study on human erythrocytes [33,49], the cholesterol contents in membrane could be modified, without altering the cell shape and volume, without varying the intracellular H^+, 2,3-DPG and adenylates and without changing the amounts of membrane phospholipids. The representative results are summarized in Table I.

TABLE I. Effect of membrane cholesterol on the erythrocyte functions*[1].

		A	B
Cholesterol (C)	(x 10^{-10} µmoles/cell)	2.70	6.96
Phospholipids (P)	(x 10^{-10} µmoles/cell)	4.06	3.86
C/P	(molar ratio)	0.67	1.80
MCV	(μm^3)	96.8	96.5
MCH	(pg/cell)	32.9	32.2
ATP	(mM/l of packed cells)	1.65	1.56
ADP	(mM/l of packed cells)	0.128	0.123
AMP	(mM/l of packed cells)	0.014	0.016
2,3-DPG	(mM/l of packed cells)	4.89	5.04
O_2 affinity (P_{50})	(mmHg, at 37°C; pH_{out}=7.38)	29.5	29.8
pH (intracellular)		7.06	7.06
Depormability	(relative value, at 34°C)	1.07	0.85
Viscosity of suspension	at γ=376 sec^{-1}	4.17	4.53
(cP at 37°C, Ht = 55 %)	at γ= 37.6 sec^{-1}	6.40	7.11
	at γ= 3.76 sec^{-1}	11.95	11.95

* Representative data are chosen from ref. [49].

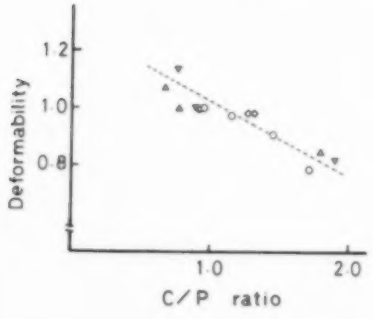

FIG. 3. Deformability vs. C/P ratio

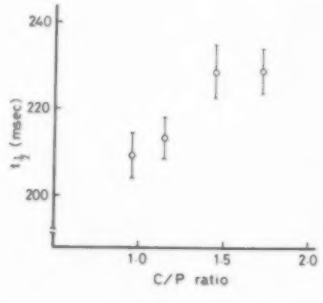

FIG. 4. Half time of oxygen release vs. C/P ratio

The following functional impairments were observed with the cholesterol-loaded erythrocytes: (a) the decreased deformability, measured by the method of Braasch [50] with some modification [51] (Fig. 3), (b) the slight increase of suspension viscosity, determined by a cone-plate viscometer (Table I) and (c) the retarded rate of oxygen release from erythrocytes, detected by a stopped flow experiment [49,52] (Fig. 4).

Concerning the membrane fluidity, the decreased motion of stearate spin label was detected, as increasing the membrane cholesterol [33] (Fig. 5). Also, the motion of cholesterol analogue (ASL) was immobilized in cholesterol-loaded erythrocyte membrane, as well as in cholesterol-rich phospholipid vesicles [33].

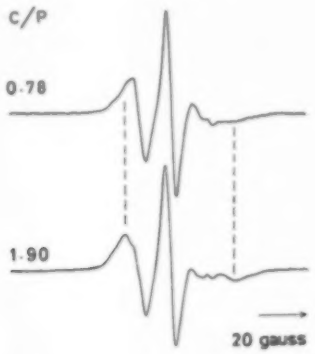

FIG. 5. EPR spectra of I(5,10)-labeled erythrocytes at 39°C [33].
(Top) C/P = 0.78; S = 0.435 (order parameter)
(Bottom) C/P = 1.90; S = 0.550 (order parameter)

Vol. 17
1980

These functional impairments induced by cholesterol-loading can be interpreted as follows (Fig. 6)

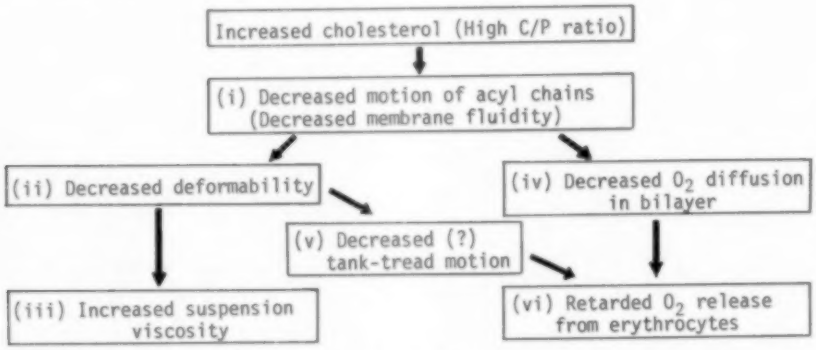
Increased cholesterol (High C/P ratio)
(i) Decreased motion of acyl chains (Decreased membrane fluidity)
(ii) Decreased deformability
(iv) Decreased O_2 diffusion in bilayer
(v) Decreased (?) tank-tread motion
(iii) Increased suspension viscosity
(vi) Retarded O_2 release from erythrocytes

FIG. 6. Effect of cholesterol-loading in erythrocyte membrane.

(i) The increase of membrane cholesterol decreases the motion of acyl chains of phospholipids; in addition, deuterium-NMR study has shown that the effect is stronger in C_2 - C_{12} regions, probably due to the increase of hydrophobic interaction between acyl chains and cholesterol-skeleton [53,54]. Consequently, the membrane fluidity decreases.
(ii) The decreased deformability can be explained by the decreased membrane fluidity, because other important determinants (such as the cell shape and the intracellular viscosity) unaltered.
(iii) The suspension viscosity at higher shear rates increases, probably due to the difficulty of transformation under high shear stress.
(iv) The rate of oxygen release from erythrocytes (half time = 200 msec at 25 °C, in normal cells) is far slower than that of purified hemoglobin (half time < 20 msec), because the oxygen affinity of intracellular hemoglobin is modulated by the intracellular pH and 2,3-DPG content and because there is "oxygen diffusion barrier" [55] (the intracellular viscosity, the membrane and the stagnant layer outside of membrane). Since the diffusion coefficient of oxygen in membrane reduces as the fraction of cholesterol increases [11], the retarded rate of oxygen release must be correlated with the decreased membrane fluidity.

(v) Furthermore, the change of tank-tread motion of membrane [10] might occur by cholesterol -loading (due to the decreased fluidity) and might contribute to the increased oxygen diffusion barrier.
(vi) In our series of experiments, the oxygen affinity of hemoglobin (represented by P_{50}) unchanged by cholesterol-loading (since the intracellular pH and 2,3-DPG content were similar for all samples); thus the increased oxygen diffusion barrier in cholesterol-loaded membrane would be a main cause for the decreased rate of oxygen release. Recently, we have developed a method for obtaining the parameter of oxygen diffusion barrier and shown that the cholesterol-loading certainly increases the barrier [56].

In short, our results showed that the increase of membrane cholesterol in twice amount induced the decreased deformability (in some 10 %), the slight increase in suspension viscosity (in the range of $18 < \dot{\gamma} < 752\ sec^{-1}$) and the retarded oxygen release (of about 10 %). The pathophysiological significance of these dysfunction must be studied further.

Our preliminary, clinical study revealed that the correlation coefficients among the membrane fluidity (expressed by τ_c of I(1,14)), the deformability and the molar fraction of membrane cholesterol were 0.5 - 0.6. Therefore, the membrane cholesterol is certainly important, as one of the determinant factors for deformability [57].

The cholesterol effect on the activity of membrane proteins and on the protein-lipid interaction is also important for the erythrocyte functions. However, the studies on Na^+-K^+ flux for erythrocytes are controversial (see references quoted in [58]); a part of discrepancies may arise from the materials (animal species) and methods (for the modification of cholesterol contents).

Cholesterol may be excluded from the vicinity of membrane proteins [59]: in erythrocyte ghosts, the fluorescence of protein tryptophan is quenched by paramagnetic spin labels incorporated into membrane, but the sterol label is less sensitive than stearate labels, suggesting that the distribution of sterol is away from membrane proteins, further the process is sensitive to temperature and pH (i.e., local phase).

Similarly, no significant changes in the rotational diffusion of band 3 protein are observed following variation of membrane cholesterol [60], though the specific binding niche on this protein surface is suggested [61]. On the other hand, the binding capacity of surface reactive groups of membrane protein (including band 3 protein, etc.) changes with cholesterol content, depending on their location (endofacial or exofacial) of individual proteins [62].

The onset temperature of membrane phase separation depends on cholesterol/phospholipid molar ratio: a freeze fracture study [63] reveals that the intramembrane proteins of erythrocytes aggregate below the onset temperature, even in the presence of intact cytoskeletal network. Such phase separation forms the protein-free areas in membrane, thus the membrane cholesterol may enhance cell fusion [64].

TABLE II. Comparison between younger and older human erythrocytes [65].

		Younger cells	Older cells
Cholesterol(C)	(x 10^{-10}μmoles/cell)	3.81	3.54
Phospholipids(P)	(x 10^{-10}μmoles/cell)	3.80	3.14
C / P	(molar ratio)	1.00	1.13
Membrane proteins	(x 10^{-13}g/cell)	6.86	6.94
Lipids/proteins	(weight ratio)	0.644	0.546
Diameter	(μm)	7.55	6.72
MCV	(μm^3)	122	91
MCH	(pg/cell)	32.3	33.9
ATP	(mM/l of packed cells)	0.899	0.713
ADP	(mM/l of packed cells)	0.119	0.195
AMP	(mM/l of packed cells)	0.018	0.060
2,3-DPG	(mM/l of packed cells)	5.22	4.06
O_2 affinity(P_{50})	(mmHg, at 37°C; pH_{out}=7.36)	25.6	20.4
Deformability	(relative value, at 33°C)	1.00	0.75
Fluidity; S of I(5,10) at 39°C		0.480	0.515
τ_c of I(1,14) at 39°C (ns)		2.20	2.52

For details, see tables in ref.[65].

(2) Influence of erythrocyte aging

Erythrocytes aged in circulation are easily fractionated by the density gradient centrifugation. Our representative results of comparison between younger and older human erythrocytes [65] are summarized in Table II.

In in vivo aged erythrocytes, the following functional impairments were observed: (a) the decreased oxygen transport activity, represented by decreased P_{50}, (b) the decrease in general metabolic activity, represented by decreased ATP, increased ADP and AMP (with loss of total adenylates) and (c) the decreased deformability, leading the difficulty for capillary passage (thus the aged cells would be trapped and destroyed in spleen). (d) The membrane fluidity of aged cells decreased, as proved by slight increase in order parameter of I(5,10) and by increase in correlation time of I(1,14).

Many causes could be counted for these dysfunctions of in vivo aged erythrocytes (for references, see [65]), as follows.

(i) The amounts of membrane lipids, both cholesterol and phospholipids, decreased during aging, but their molar ratio unchanged. However, the amounts of membrane proteins unaltered . Consequently, the surface area and the cell volume (MCV) decreased in aged cells, but no significant change of mean corpuscular hemoglobin (MCH) was observed. Therefore, the diameter reduced, the biconcavicity decreased and the intracellular density increased (this made the centrifugal fractionation possible).

(ii) The decreased activities of enzymes accompanying in vivo aging have been reported: the decreased 2,3-DPG and ATP were noticed. The decrease of 2,3-DPG led the increased oxygen affinity of hemoglobin (decreased P_{50}).

(iii) The decreased membrane fluidity would be resulted from the following causes: the modification of protein-lipid interaction due to the reduction of lipid/protein ratio in membrane, the alteration of free divalent cations due to the decreased organic phosphate [66], the contribution of decreased glycolytic activity to maintain the membrane states, the influences of conformational changes of membrane proteins (possibly protein denaturation), and so forth (vide infra).

(iv) The decreased deformability could be due to the shape change (loss of biconcavicity), the increased intracellular viscosity (high density) and the decreased membrane fluidity.

In short, every factors tended to impair the functions during in vivo aging.

During the blood storage in appropriate medium at 4°C (i.e., in the case of Bank Blood) , a number of biochemical changes was produced. The most of phenomena observed during storage were similar to those observed for in vivo aging.

(i) The diameter of erythrocytes decreased, the thickness increased and finally spherocytes appeared [67-69]. The specific gravity also increased[70].

(ii) The loss of lipids was reported, but cholesterol/phospholipid ratio unaltered[68].

(iii) The metabolic state changed considerably: the most striking changes related to functions were the decrease of 2,3-DPG and ATP. The decrease of 2,3-DPG reduces the oxygen transport activity, which can be restored by regenerating 2,3-DPG [71] or by incorporating the allosteric effector of hemoglobin [72,73]. The decrease of ATP lessened the post-transfusion survival, which can be improved by incubation with adenine and purine nucleosides [74]. In addition, the decrease of K^+ and increase of Na^+ in erythrocytes were observed [69].

(iv) The rheological impairments were demonstrated by various methods: the increased viscosity [6,68,70,75], the decreased deformability [76] and the decreased filtrability [68]

Further, the osmotic fragility increased during storage [69,77].

The close relation between ATP level and shape change was pointed out earlier [67]. Further studies revealed the rheological impairments of ATP-depleted erythrocytes [68]. The acute ATP depletion (in vitro incubation without glucose at 37°C) has been shown to produce similar changes in shape and mechanical properties (rheological) [78,79], i.e., the echinocytic transformation, the fragmental loss of membrane components, the decreased K^+ and Ca^{++} flux (Ca^{++} accumulation) and the cross-linking of membrane proteins. Therefore, in order to study the mechanism maintaining the normal shape and deformability, a number of works on (acute) ATP depletion has been conducted. Many factors must be considered, as below.

(i) Spectrin (probably in favor of tetramer [80]) and other proteins (actin oligomer, etc.) undergoes an irreversible aggregation to yield large polymer (>10^6 dalton; perhaps disulfide bridge is formed) during ATP depletion[81].

Spectrin is distributed uniformly throughout the cytoplasmic surface, and it retains its submembranous location in the spiny processes of echinocytes produced by ATP depletion [82], though the spectrin-free vesicles are released during ATP depletion [83].

When the membrane proteins (mainly, spectrin, band 3 and 4.2 proteins) are cross-linked by bifunctional, permeable SH-reagents, the deformability decreases [84].

(ii) The phospholylation of spectrin may modify the shape and modulate the additional interaction with actin[85-87], though the in vitro turnover rates of spectrin phosphate (of dog erythrocytes) are higher than the rates observed in vivo [88]. On the other hand, the importance of spectrin phospholylation, for the shape and binding to membrane components, is

Vol. 17
1980

recently contradicted [89].
(iii) Ca^{++}-activated cytoplasmic transglutaminase cross-links the protein, yielding glutamine-lysine bond but a considerably high Ca^{++} is required [90]. Therefore, when the intracellular Ca^{++} is increased (e.g., by ionophore), this process may be operative for alteration of erythrocyte properties [91].
(iv) Phosphatidyl-serine and -ethanolamine are distributed in favor of inner layer, while phosphatidylcholine is rich in outer layer of erythrocytes [46]. The head group of phosphatidylserine interacts with Ca^{++} and H^{+}, inducing the phase separation to form cluster of spin-labeled phospholipids in model membrane [43-45]. In this interaction, Ca^{++} and H^{+} seem to be competitive and Mg^{++} is less effective, further the process depends on ionic strength.

Spectrin also interacts with certain phospholipids in inner layer [92,93]. This interaction may protect the bilayer against the action of divalent ions, in the reconstituted vesicles [94]. Recently, Ca^{++} (and Mg^{++})-induced, conformational change of SH-spin-labeled spectrin is reported [95].
(v) The intracellular Ca^{++} level is controlled by Ca^{++}-Mg^{++} ATPase utilizing ATP; thus the intracellular pH, ATP, Mg^{++} and calmodulin modulate the activity of Ca^{++} flux [96].
(vi) The mobility of the intrinsic proteins (probably, band 3 protein and glycophorin) decreases by ATP depletion [97]. Since band 3 protein is linked with spectrin through ankylin (or syndein), the decreased protein motion may be due to spectrin polymerization.
(vii) Concerning the shape changes, the importance of the ratio of the inner and outer surface areas is suggested, especially for drug-induced transformation [98,99].
(viii) The decreased (cellular) deformability produced by ATP depletion has been accepted. However, surprizingly, no significant differences are observed in the intrinsic mechanical properties (i.e., surface shear modulus of elasticity, elastic area compressibility and shear viscosity in the plastic domain) between fresh and ATP-depleted human erythrocyte membrane [100], though the differences of techniques may be the reason of discrepancy. Also , a report showed the maintenance of normal biconcavicity with normal deformability after rapid ATP depletion in the presence of iodoacetate, suggesting that the shape change is secondary to ATP depletion [101].

Altogether, it is difficult to draw an overall picture on the relation among cell shape , deformability, cytoskeletal network, lipid bilayer and ATP, Ca^{++}, pH, etc., at the present stage. Further careful studies are required.

(3) Influence of cross-linking of membrane proteins (by glutaraldehyde)
Glutaraldehyde is commonly used for electron microscopy, and also applied to harden the

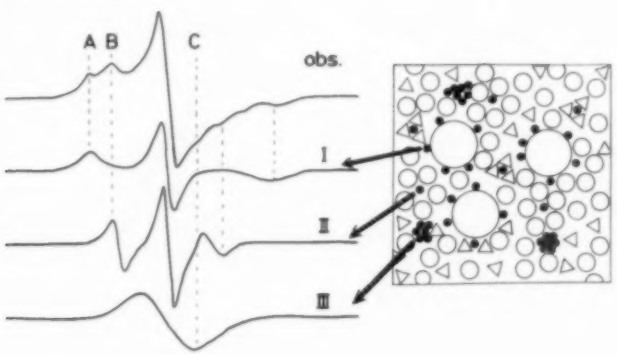

FIG. 7. Effect of glutaraldehyde pretreatment on EPR spectrum (6°C) of ASL in erythrocyte membrane [33].
(Left) (top) The observed spectrum; the erythrocytes were incubated with glutarladehyde (2 %) for 30 min at 0°C, then washed three times, The spectrum consisted of
(I) the strongly immobilized signal; originated from "frozen sites", persisting at 40°C, probably interacting with modified protein surface,
(II) the normal signal, same as observed with intact membrane; originated from the lipid portion, perhaps unperturbed by protein cross-linking, and
(III) the broad signal, due to the spin-spin interaction; originated from ASL cluster in lipid portion, and reversibly disappeared at higher temperature.

(Right) Scheme of surface view of membrane: lipids (○, △), ASL (●) and modified proteins (large circles).

erythrocyte and to fix the cell shape for model rheological experiments and for observation of cells deformed by physical forces. We would like to comment on the use of glutaraldehyde for rheological study, because a considerable modification of membrane organization was observed.

Glutaraldehyde cross-links the membrane proteins, as shown by Steck [102]. When stearate spin labels were incorporated into the glutaraldehyde-pretreated erythrocyte membrane (after washing out the excess of reagents), the strongly immobilized EPR signal ("frozen sites") appeared besides of normal signal [103]. When a cholesterol analogue (ASL) was incorporated, the following phenomena were observed [33]; (i) the appearance of strongly immobilized signal, which arose from temperature-independent "frozen sites", (ii) the formation of ASL cluster, which showed a broad EPR signal due to the spin-spin interaction, i.e., the ASL molecules were aggregated at lower temperature but reversibly dispersed at higher temperature, and (iii) the amount of ASL incorporation, from phospholipid vesicles (containing excess amount of ASL) to erythrocyte membrane, increased without hemolysis. The representative EPR spectrum is shown in Fig. 7.

The frozen sites for these lipid-like spin labels may be produced by modification of proteins (probably due to direct interaction at protein surface). The reversible ASL cluster formation, primarily due to overloading of ASL into membrane, clearly indicated the change in ASL-lipid interaction. As the glutaraldehyde concentration increased, these change in lipid organization became more evident: at 0.01 % glutaraldehyde pretreatment, these changes were observable. Further, not only the cross-linking of membrane proteins, but also the polymerization of tetrameric hemoglobin in erythrocytes was detected by the molecular sieve study [unpublished observation].

Therefore, in order to visualize the cell deformation, glutaraldehyde may be used inevitably, but it is strongly recommended to compare the cell shape before and after fixation. Especially, when mechanical forces is applied to erythrocytes, for the purpose of measuring the force-equilibrium in deformed condition, one must be careful to the use of glutaraldehyde; even if the membrane could be "fixed" instantaneously, the mechanical properties of fixed membrane would not be same as those of intact membrane. The other cross-linking reagents might show similar phenomena as glutaraldehyde.

As the results of glutaraldehyde fixation of erythrocytes, the following functional changes occur: (a) the decreased deformability and the increased suspension viscosity, due to protein cross-linking and (b) the increase of oxygen affinity and the retarded oxygen release, due to polymered hemoglobin formation (even in the absence of methemoglobin which is the oxidized product by R-CHO). The detailed mechanism of these dysfunction could not be clarified by the spin label method, since the EPR spectra indicated the considerable modification of protein, but they would be "shadows on the bilayer film".

Concluding remarks

Membrane fluidity, quantified from spectral parameter of lipid-like probes in membrane, is one of reliable measure for expressing the rigidity of erythrocyte membrane, although it represents the state of membrane lipid portion.

When the amount of one membrane component (e.g., cholesterol) is varied, keeping others constant, the correlation between the fluidity and the functions can be successfully interpreted. On the other hand, when many factors alter, as in the case of aged erythrocytes, the changes in membrane fluidity are certainly linked to the functional disturbances, though the definite role remains uncertain.

The membrane fluidity is sometimes insufficient for explaining the phenomena concerned with membrane proteins. Therefore, the development of elaborate methods for measuring the state of proteins, especially the dynamic structure of cytoskeletal network, is necessary.

Further experimental efforts will be required to clarify the correlation between the supramolecular structure of membrane and the rheological (mechanical) properties of erythrocytes. Also, the ability to modulate the activities of membrane proteins, e.g., enzymes and carriers, must be extensively studied; in this connection the measure of membrane fluidity will be useful.

Acknowledgement

The authors are indebted for the encouragement of Professors Syoten Oka and Eiichi Fukada. They are grateful to their colleagues, Drs. Takeo Suda and Kazunori Kon and Miss Misuzu Sekiya.

The work has been supported in part by grants from Ministry of Education of Japan and Ehime Medical Foundation.

Vol. 17
1980

REFERENCES

1. EVANS,E.A. and HOCHMUTH,R.M., Membrane viscoelasticity. Biophys.J.,16,1-11,1976.
2. WAUGH,R. and EVANS,E.A., Thermoelasticity of red blood cell membrane. Biophys.J.,26,115-132,1979.
3. ANDERSON,H.C., Probes of membrane structure. Ann.Rev.Biochem.,47,359-383,1978.
4. HARE,F., \MIELL,J. and LUSSAN,C., Is an average viscosity tenable in lipid bilayers and biomembranes ? A comparison of semi-empirical equivalent viscosities given by unbound probes: a nitroxide and a fluorophore. Biochim.Biophys.Acta,555,388-408,1979.
5. See review articles included In:Blood cell membranes, Semin.Hematol.,vol.16(no.1 and 2), H.S.Jacob(Ed).1979,pp.1-139.
6. CHEN,S. Biophysical behavior of red cells in suspension. In:The red blood cells. D.M. Surgenor(Ed). New York:Academic Press. 2nd ed.,1975,pp.1032-1133.
7. STOLTZ,J.F. and VIGNERON,C. Viscosité sanguine et déformabilité des hématies. Paris:Lab. Hoechst.1976,p.18.
8. SCHMID-SCHÖNBEIN,H. Microrheology of erythrocytes, blood viscosity and the distribution of blood flow in the microcirculation. In:Cardiovascular Physiology II. A.C.Guyton and A.W.Cowley(Eds).Baltimore:University Park Press.1976,pp.1-62.
9. BESSIS,M. and MOHANDAS,N. A diffractometric method for the measurement of cellular deformability. Blood Cells,1,307-313,1975.
10. FISCHER,T.M., STÖHR-LIESEN,M. and SCHMID-SCHÖNBEIN,H. The red cell as a fluid droplet: Tank tread-like motion of human erythrocyte membrane in shear flow. Science,202,894-896, 1978.
11. FISCHKOFF,S. and VANDERKOOI,J.M. Oxygen diffusion in biological and artificial membrane determined by the fluorescence pyrene. J.gen.Physiol.,65,663-676,1975.
12. MELCHIOR,D.L. and CZECH,M.P. Sensitivity of the adipocyte D-glucose transport system to membrane fluidity in reconstructed vesicles. J.Biol.Chem.,254,8744-8747,1979.
13. SANDERMANN,H. Regulation of membrane enzymes by lipids. Biochim.Biophys.Acta,515,209-237, 1978.
14. GENNIS,R.B. and JONES,A. Protein-lipid interactions. Ann.Rev.Biophys.Bioengn.,6,195-238, 1977.
15. CHAPMAN,D., GÓMEZ-FERNÁNDEZ,J.C. and GOÑI,F.M. Intrinsic protein-lipid interaction. FEBS Lett.,98,211-223,1979.
16. CHERRY,R.J. Rotational and lateral duffusion of membrane proteins. Biochim.Biophys.Acta, 559,289-328,1979.
17. CHAPMAN,D. and HOFFMANN,W. Enzyme function and membrane lipids. Biochem.Soc.Transact.,8, 32-34,1980.
18. LEVITZKY,A. and HELMREICH,J.M. Hormone-receptor adenylate cyclase interaction. FEBS Lett. 101,213-219,1979.
19. SHIN,M.L., PAZNEKAS,W.A. and MAGER,M.M. On the mechanism of membrane damage by complement. J.Immunol.,120,1996-2002,1978.
20. ESSER,A.F., BARTHOLOMEW,R.M., PARCE,J.W. and McCONNELL,H.M. The physical state of membrane lipids modulates the activation of the first component of complement. J.Biol.Chem., 254,1768-1770,1979.
21. BOROCHOV,H., ABBOTT,R.E., SCHACHTER,D. and SHINITZKY,M. Modulation of erythrocyte membrane proteins by membrane cholesterol and lipid fluidity. Biochemistry,18,251-255,1979.
22. GAFFNEY,B.J. and CHEN,S.C. Spin label studies of membrane. In:Methods in membrane biol. vol.8, E.D.Korn(Ed). New York and London:Plenum Press,1977.pp.291-358.
23. SCHREIER,S., POLNASZEK,C.F. and SMITH,I.C.P. Spin labels in membrane. Problems in practis. Biochim.Biophys.Acta,515,375-436,1978.
24. BERLINER,L.J. (Ed). Spin labelling, theory and application. New York:Academic Press,1976.
25. OHNISHI,S. and TOKUTOMI,S. Calcium- and proton-induced phase separations in phosphatidyl serine-phosphatidylcholine membrane. In:Biol.Magnetic Resonance,vol.3, L.J.Berliner and J.Reuber (Eds). New York and London:Plenum Press,1980, in press.
26. BIERI,V.G., WALLACH,D.F.H. and LIN,P.S. Focal erythrocyte membrane perturbations caused by nitroxide lipid analogues. Proc.Natl.Acad.Sci.,71,4797-4801,1974.

27. KORNBERG,R.D. and McCONNELL,H.M. Lateral diffusion of phospholipids in a vesicle membrane. Proc.Natl.Acad.Sci.,68,2564-2568,1971.

28. SHEATS,J.R. and McCONNELL,H.M. A photochemical technique for measuring lateral diffusion of spin-labeled phospholipids in membranes. Proc.Natl.Acad.Sci.,75,4661-4663,1978.

29. KORNBERG,R.D. and McCONNELL,H.M. Inside-outside transitions of phospholipids in vesicle membranes. Proc.Natl.Acad.Sci.,70,1111-1120,1971.

30. McCONNELL,H.M. Membrane motion in biological membrane. In:Spin labeling. L.J.Berliner (Ed). New York:Academic Press,1976,pp.525-560.

31. SEELIG,A. and SEELIG,J. The dynamic structure of fatty acyl chains in a phospholipid bilayer measured by deuterum magnetic resonance. Biochemistry,13,4839-4845,1974.

32. HUBBEL ,W.L. and McCONNELL,H.M. Molecular motion in spin-labeled phospholipids and membranes. J.Am.Chem.Soc.,93,314-326,1971.

33. SUDA,T., MAEDA,N. and SHIGA,T. Effect of cholesterol on human erythrocyte membrane. A spin label study. J.Biochem.(Tokyo),87,1703-1713,1980.

34. HUBBEL,W.L. and McCONNELL,H.M. Spin-label studies of the excitable membranes of nerve and muscle. Proc.Natl.Acad.Sci.,61,12-16,1968.

35. DEMBO,M., GLUSHKO,V., ABERLIN,M.E. and SONENBERG,M. A method for measuring membrane microviscosity using pyrene excimer formation. Application to human erythrocyte ghosts. Biochim.Biophys.Acta,522,201-211,1979.

36. LEE,A.G. Lipid phase transition and phase diagram. Biochim.Biophys.Acta,472,273-344,1977.

37. WU,S.H. and McCONNELL,H.M. Phase separation in phospholipid membranes. Biochemistry,14, 847-854,1975.

38. SHIMSHICK,E.J. and McCONNELL,H.M. Lateral phase separation of binary mixtures of cholesterol and phospholipids. Biochem.Biophys.Res.Commun.,53,496-451,1973.

39. LADBROOK,B.D., WILLIAMS,R.M. and CHAPMAN,D. Studies on lecithin - cholesterol-water interactions by differencial scanning calorimetry and X-ray diffraction. Biochim.Biophys Acta,150,333-340,1968.

40. DEMEL,R.A. and DE KRUYFF,B. The function of sterols in membranes. Biochim.Biophys.Acta, 457,109-132,1976.

41. McINTOSH,T.J. The effect of cholesterol on the structure of phosphatidylcholine bilayers. Biochim.Biophys.acta,513,43-58,1978.

42. WARREN,G.B., HOUSLAY,M.D., METCALFE,J.C. and BIRDSALL,N.J.M. Cholesterol is excluded from the phospholipid annulus aurrounding an active calcium transport protein. Nature, 255,684-687,1975.

43. OHNISHI,S. and ITO,T. Clustering of lecithin molecules in phosphatidylserine membranes induced by calcium ion binding to phosphatidylserine. Biochem.Biophys.Res.Commun.,51, 132-138,1973.

44. TOKUTOMI,S., EGUCHI,G. and OHNISHI,S. Disappearance of calcium-induced phase transition in phosphatidylserine-phosphatidylcholine membranes caused by protonation and by electric current. Biochim.Biophys.Acta,552,78-88,1979.

45. TOKUTOMI,S., OHKI,K. and OHNISHI,S. Proton-induced phase separation in phosphatidylserine/phosphatidylcholine membranes. Biochim.Biophys.Acta,569,192-200,1980.

46. OP DEN KAMP,J.A.F. Lipid asymmetry in biomembranes. Ann.Rev.Biochem.,48,47-71,1979.

47. COOPER,R.A., LESLIE,M.H., FISCHKOFF,S., SHINITZKY,M. and SHATTIL,S.J. Factors influencing the lipid composition and fluidity of red cell membranes in vitro: production of red cells possessing more than two cholesterols per phospholipids. Biochemistry,17,327-331,1978.

48. COOPER,R.A. and JANDL,J.H. Bile salts and cholesterol in the pathogenesis of target cell in obstructive jaundice. J.Clin.Invest.,47,809-822,1968.

49. SHIGA,T., MAEDA,N., SUDA,T., KON,K. SEKIYA,M. and OKA,S. Rheological and kinetic dysfunctions of the cholesterol-loaded, human erythrocytes. Biorheology,16,363-369,1979.

50. BRAASCH,D. Deformability and traversing time of shape-transformed single red cell passing through a 4 μ glass-capillary. Pflügers Arch.,329,167-171,1971.

Vol. 17
1980

51. SHIGA,T., MAEDA,N., SUDA,T., KON,K., SEKIYA,M. and OKA,S. A kinetic measurement of red cell deformability: a modified micropipette aspiration technique. Jap.J.Physiol.,29,707-722,1979.

52. SHIGA,T., MAEDA,N., SUDA,T., KON,K. and SEKIYA,M. Rheological and functional impairments in cholesterol-loaded human erythrocytes. Experientia,36,127-128,1980.

53. STOCKTON,G.W. and SMITH,I.C.P. A deutrium nuclear magnetic resonance study of the condensing effect of cholesterol on egg phosphatidylcholine bilayer membrane. I. Perdeutrated fatty acid probes. Chem.Phys.Lipids,17,251-263,1976.

54. OLDFIELD,E., MEADOWS,M., RICE,D. and JACOBS,R. Spectroscopic studies of specifically deutrium labeled membrane system. Nuclear magnetic resonance investigation of the effect of cholesterol in model systems. Biochemistry,17,2727-2740,1978.

55. NICOLSON,P. and ROUGHTON,F.J.W. A theoretical study of the influence of diffusion and chemical reaction velocity on the rate of exchange of CO and oxygen between the red blood corpuscle and surrounding fluid. Proc.Roy.Soc.,B138,241-264,1951.

56. KON,K., MAEDA,N., SEKIYA,M., SHIGA,T. and SUDA,T. A method for studying oxygen diffusion barrier in erythrocytes: effect of hemoglobin content and membrane cholesterol. J.Physiol. (London),in press,1980.

57. SUDA,T., MAEDA,N., SEKIYA,M., MATSUOKA,K., TOKITA,R. and SHIGA,T. Influences of membrane cholesterol on the human red cell properties. Med.J.Osaka Univ.,29,21-27,1978.

58. GREG,J.E. and LAUF,P.K. Membrane cholesterol depletion and K^+ transport in high and low potassium sheep red cells. Membr.Biochem.,3,21-35,1980.

59. BIERI,V.G. and WALLACH,D.F.H. Variations of lipid-protein interactions in erythrocyte ghosts as a function of temperature and pH in physiological and non-physiological ranges .A study using paramagnetic quenching of protein fluorescence by nitroxide lipid analogues. Biochim.Biophys.Acta,406,415-423,1975.

60. NIGGS,E.A. and CHERRY,R.J. Influence of temperature and cholesterol on the rotational diffusion of band 3 in the human erythrocyte membrane. Biochemistry,18,3457-3465,1979.

61. KLAPPAUF,E. and SCHUBERT,D. Interactions of band 3 protein from human erythrocytes with cholesterol and cholesterol analogues. Z.Physiol.Chem.,360,1225-1235,1979.

62. BOROCHOV,H., ABOTT,R.E., SCHACHTER,D. and SHINITZKY,M. Modulation of membrane proteins by membrane cholesterol and lipid fluidity. Biochemistry,18,251-255,1979.

63. HUI,S.W., STEWART,C.M., CARPENTER,M.P. and STEWART,T.P. Effects of cholesterol on lipid organization in human erythrocyte membrane. J.Cell Biol.,85,283-291,1980.

64. HOPE,M.J., BRUCKDORFER,K.R., HART,C.A. and LUCY,J.A. Membrane cholesterol and cell fusion of hen and guinea-pig erythrocytes. Biochem.J.,166,255-263,1977.

65. SHIGA,T., MAEDA,N., SUDA,T., KON,K. and SEKIYA,M. The decreased membrane fluidity of in vivo aged, human erythrocytes. A spin label study. Biochim.Biophys.Acta,553,84-95,1979.

66. LA CELLE,P.L., KIRKPATRICK,F.H., UDKOW,M.P. and ARKIN,B. Membrane fragmentation and Ca^{++} membrane interaction: potential mechanism of shape change in the senescent red cells. Nouv.Rev.Franç.Hématol.,12,789-798,1972.

67. NAKAO,M., NAKAO,T., and YAMAZOE,S. ATP and maintenance of shape of the human red cells. Nature,187,945-947,1960.

68. HARADIN,A.R., WEED,R.I. and REED,C.F. Changes in physical properties of stored erythrocytes. Relationship to survival in vivo. Transfusion,9,229-237,1969.

69. RAPOPORT,S. Dimensional, osmotic and chemical changes of erythrocytes in stored blood. J.Clin.Invest.,26,591-615,1947.

70. DE VENUTO,F., WILSON,S.M. and LOWE,C.V. Relative viscosity and specific gravity of human blood during cold storage. Proc.Soc.Exp.Biol.Med.,134,169-173,1970.

71. VALERI,C.R. Liquid and freeze preservation of human red blood cells. In:The red blood cells, 2nd ed.,vol.1, D.M.Surgenor(Ed).New York:Academic Press,1974,pp.511-574.

72. MAEDA,N., KON,K., SEKIYA,M. and SHIGA,T. Restoration of the poor oxygen transport function of ACD-stored blood by pyridoxal 5'-phosphate. Experientia,35,1245-1246,1979.

73. MAEDA,N., KON.K., SEKIYA,M. and SHIGA,T. Functional restoration of ACD-blood by pyridoxal 5'-phosphate. Brit.J.Haematol.,45,467-480,1980.

74. SIMON,E.R. Adenine and purine nucleosides in human red cell preservation. Transfusion, 7,395-400,1967.

75. AZELVANDRE,F., MANDRET,G. and PETERS,A. Rheological behavior of stored blood cells. Biorheology,16,435-446,1979.

76. LA CELLE,P.L. Alteration of deformability of the erythrocyte membrane in stored blood. Transfusion,9,238-245,1969.

77. STOLTZ,J.F., VIGNERON,C.V. and STREIFF,F. Alteration od red blood cell osmotic fragility during storage of blood drawn on ACD solution. Vox Sang.,21,86-89,1971.

78. WEED,R.I., LA CELLE,P.L. and MERRILL,E.W. Metabolic dependence of red cell deformability J.Clin.Invest.,48,795-809,1969.

79. MEISELMAN,H.J. and BAKER,R.T. Flow behavior of ATP-depleted human erythrocytes. Biorheology,14,111-126,1977.

80. LIU,S-C. and PALEK,J. Spectrin tetramer-dimer equilibrium and the stability of erythrocyte membrane skeletons. Nature,285,586-588,1980.

81. PALEK,J., LIU,S-C. and SNYDER,L.M. Metabolic dependence of protein arrangement in human erythrocyte membranes. I. Analysis of spectrin-rich complexes in ATP-depleted red cells. Blood,51,385-395,1978.

82. ZIPARO,E., LEMAY,A. and MARCHESI,V.T. The distribution of spectrin along the membranes of normal and echinocytic human erythrocytes. J.Cell Sci.,34,91-101,1978.

83. LUTZ,H.U., LIU,S-C. and PALEK,J. Release of spectrin-free vesicles from human erythrocytes during ATP depletion. I. Characterization of spectrin-free vesicles. J.Cell Biol., 73,548-560,1977.

84. FISCHER,T.M., HAEST,C.W.M., STÖHR,M. KAMP,D. and DEUTICKE,B. Selective alterations of erythrocyte deformability by SH-reagents. Evidence for an involvement of spectrin in membrane shear elasticity. Biochim.Biophys.Acta,510,270-282,1978.

85. SHEETZ,M.P. and SINGER,S.J. On the mechanism of ATP-induced shape changes in human erythrocyte membrane. I. The role of spectrin complex. J.Cell Biol.,73,638-646,1977.

86. BIRCHMEIER,W. and SINGER,S.J. On the mechanism od ATP-induced shape changes in human erythrocyte membrane. II. The role of ATP. J.Cell Biol.,73,647-659,1977.

87. PINDER,J.C., UNGEWICKELL,E., BRAY,D. and GRATZER,W.B. The spectrin actin complex and erythrocyte shape. J.Supramolec.Str.,8,439-445,1978.

88. SMITH,J.E. and MOORE,K. In vivo and in vitro turnover of spectrin phosphate in erythrocytes. J.Lab.Clin.Med.,95,808-815,1980.

89. ANDERSON,J.M. and TYLER,J.M. State of spectrin phosphorylation does not effect erythrocyte shape or spectrin binding to erythrocyte membranes. J.Biol.Chem.,255,1259-1265,1980

90. LORAND,L., WEISSMANN,L.B., EPEL,P.L. and BRUNER-LORAND,J. Role of the intrinsic transglutaminase in the Ca-mediated cross-linking of erythrocyte proteins. Proc.Natl.Acad. Sci.,73,4479-4481,1976.

91. COETZER,T.L. and ZAIL,S.S. Cross-linking of membrane proteins of metabolically-depleted and Ca-loaded erythrocytes. Brit.J.Haematol.,43,375-390,1979.

92. HAEST,C.W., PLASA,G., KAMP,D. and DEUTICKE,B. Spectrin as a stabilizer of the phospholipid asymmetry in the human erythrocyte membrane. Biochim.Biophys.Acta,509,21-32,1978.

93. MARINETTI,G. and CRAIN,R.C. Topology of amino-phospholipids in the red cell membrane. J.Supramoles.Str.,8,191-213,1978.

Vol. 17
1980

94. MOMBERS,C., VAN DIJCK,P.W.M., VAN DEENEN,L.L.M., DE GIER,J. and VERKEIJ,A.J., The interaction of spectrin-actin and synthetic phospholipids. Biochim.Biophys.Acta,470, 152-160,1977.
95. LAMMEL,B. and MAIER,G. A spin labeling study of the effects of inorganic ions and pH on the conformation of spectrin. Biochim.Biophys.Acta,622,245-258,1980.

96. ROUFOGALIS,B.D. Regulation of calcium translocation across the red cell membrane. Can. J.Physiol.Pharmacol.,57,1331-1349,1979.

97. FOWLER,V. and BRANTON,D. Lateral mobility of human erythrocyte integral membrane proteins. Nature,268,23-26,1977.

98. SHEETZ,M. and SINGER,S.J. Biological membrane as bilayer couples. A molecular mechanism of drug-erythrocyte interactions. Proc.Natl.Acad.Sci.,71,4457-4461,1974.

99. MOHANDAS,N. GREENQUIST,A.C. and SHOHET,S.B. Bilayer balance and regulation of red cell shape changes. J.Supramolec.Str.,9,453-458,1978.

100. MEISELMAN,H.J., EVANS,E.A. and HOCHMUTH,R.M. Membrane mechanical properties of ATP-depleted human erythrocytes. Blood,52,499-504,1978.

101. FEO,C. and MOHANDAS,N. Clarification of role of ATP in red-cell morphology and function Nature,265,166-168,1977.

102. STECK,T.L. Cross-linking the major proteins of the isolated erythrocyte membrane. J.Mol.Biol.,66,2950305,1972.

103. SHIGA,T., SUDA,T. and MAEDA,N. Spin label studies on the human erythrocyte membrane. Two sites and two phases for fatty acid spin labels. Biochim.Biophys.Acta,466,231-244, 1977.

l. 17
980

BLANK
PAGE

Vol. 17
1980

BIORHEOLOGY, Vol. 17, pp. 501-509, 1980
Printed in the USA. All rights reserved.

0006-355X/80/050501-09$02.00/0
Copyright (c) 1981 Pergamon Press Ltd

ABSTRACTS OF PAPERS PRESENTED AT THE 1980 ANNUAL MEETING OF JAPANESE SOCIETY OF BIORHEOLOGY

(June 28—29, 1980, Shinshu University School of Medicine, Matsumoto, Japan.)

1. NUMERICAL ANALYSIS OF FLOW IN THE VERTEBRAL ARTERY

T. Fukushima, T. Matsuzawa* and T. Azuma
Research Laboratory for Cardiovascular Diseases, Department of Physiology and Department of Public Health* , Shinshu University School of Medicine, 3-1-1 Asahi, Matsumoto 390, Japan.

Abnormal hemodynamic forces related to distortions of blood vessel lumen have been thought to play an important role in the pathogenesis of focal vascular lesions. In the vertebral artery, segments located between the osseous rings become more ectatic with age compared with segments surrounded by bone. Based on the assumption of quasi-steady flow, this work is undertaken to investigate the structure of flows through arterial models with single and multiple sinusoidal stenoses. Numerical analysis was made by an integral-momentum method. The validity of the method was examined by comparison of experimental and calculated values obtained with a mild sinusoidal stenosis. Theoretical predictions of separation and reattachment characteristics in this model are in good agreement with experimental observations. Velocity and wall shear stress distributions were explored in a model with multiple stenoses simulating the vertebral artery. The wall of the ectatic segment of the vertebral artery has been known as a predilection site of atherosclerotic lesions. The present results indicate that the wall is under unstable shear stresses, the direction of which is dependent upon the magnitude of Reynolds number.

2. NUMERICAL STUDY ON PERISTALTIC FLOW OF A VISCOUS FLUID

S. Nakanishi and M. Kawaguti*
Hiroshima Institute of Technology, Saekigun, Hiroshima 738, Japan. * Dept. of Physics, Keio Univer-sity, Kohhoku-ku, Yokohama 223, Japan.

The flow of a viscous fluid in a channel with progressive wave of contraction of walls is numerically studied as a two-dimensional model of peristaltic flow. In order to clarify the flow connected with peristaltic motion, the peristaltic flow of a viscous fluid through a channel with progressive wave of contraction of walls is investigated for various parameters : the Reynolds number, wave length, amplitude of contractive wave, and pressure gradient along the channel. The rate of fluid transport by the peristaltic motion is shown as a function of these parameters.

3. NUMERICAL STUDY ON THE WALL SHEAR STRESS DUE TO A PULSATILE BIFURCATING FLOW

Y. Matunobu and N. Takemitsu
Dept. of Physics, Keio Univ., Kohhoku-ku, Yokohama 223, Japan.

It is well known that the blood-vessel wall is subject to vascular lesions near the site of bifurcation and that its origin seems to lie primarily in the wall-shear-stress intensification due to the flow pulsation. Here, as a model of bifurcating flow, the two-dimensional pulsatile flow of an incompressible Newtonian fluid with a narrow side-branch is considered. It is, for example, a simulation of the descending aorta with an intercostal artery. This model is analyzed by numerical procedure based on the Navier-Stokes equation. It can be concluded from the results that the vessel wall can be undergone by the back stress more violently at the downstream side of the branch. This may be a possible cause of vascular lesion there.

4. FINITE ELEMENT ANALYSIS OF VASCULAR WALL DEFORMATION UNDER PULSATILE PRESSURE WAVE

E. Nakamachi
Dept. of Mechanical and Electrical Engineering, Yatsushiro Technical College, Yatsushiro, Kumamoto 866, Japan.

In this paper the nonlinear-elastic and visco-nonlinear-elastic analysis of vascular wall which undergoes a pulsatile pressure wave is studied by the use of the incremental finite element method based on the membrane shell theory. The geometric nonlinearity is treated with incremental method denoted by the orthogonal surface convected coordinate. The cylindrical element is used owing to the restriction of axisymmetrical deformation. From the comparison with the results for human abdominal aorta and dacron graft tube, the availability of the artificial blood vessel is discussed. And the applicability of this numerical method employed to visco-nonlinear-elastic model for the investigation of the vascular disease is shown.

5. TURBULENCE IN CANINE ASCENDING AORTA-EFFECT OF MEAN VELOCITY ON MEAN TURBULENCE INTENSITY

T. Yamaguchi, T. Yoshikawa*, S. Kikkawa, K. Tanishita and M. Sugawara
Dept. of Surgical Science, Heart Institute Japan, Tokyo Women's Medical College, Shinjuku-ku, Tokyo 162, Japan.* Dept. of Cardiovascular Surgery, 2nd Hospital, Tokyo Women's Medical College.

The turbulence intensity near the central axis of the canine ascending aorta was measured with a hot-film anemometer. The cardiac output and the heart rate were controlled at will by the use of an extracorporeal circulation and of an atrial pacing. The mean turbulence intensity during the deceleration phase of the blood flow velocity was calculated. The ralative mean turbulence intensity I^* (mean turbulence intensity divided by the time mean sectional average velocity in the aorta) is constant in most animals regardless of the changes in fluid mechanical parameters. In some animals, however, it is dependent upon the peak Reynolds number. The correlation between the frequency parameter and I^* is weakly positive for the pooled data. The effect of the amplitude ratio on I^* is not clear in the present experiments.

6. DISTRIBUTION OF MURAL THROMBI IN ABDOMINAL ANEURYSM.

N. Muraki, H. Yoshida, K. Taguchi, S. Yamazaki, M. Shukuya, Y. Masuda, Y. Inagaki, T. Fukushima* and T. Azuma*
Dept. of the 3rd Int. Med., Chiba Univ., School of Med., Chiba 280, Japan.* Dept. of Physiol., Shinshu Univ., Med. School, Matsumoto 390, Japan

It is well known that mural thrombi exist in most abdominal aortic aneurysms. Our clinical observation with ultrasonotomography suggested that the mural thrombi would be formed beginning from distal area of aneurysm. In aneurysmal glass model experiment, a strong vortex formation was observed in the distal portion of the aneurysmal glass and wall shear stress changed abruptly near this portion. Therefore, it was indicated that the distal area of aneurysm was a proper site for thrombus formation and these hemodynamic changes might injure the endothelium of this area causing thrombus formation.

7. BLOOD RHEOLOGY AT STAGNATION

H. Niimi
National Cardiovascular Center Research Institute, Suita, Osaka 565, Japan

Structures of blood flow at stagnation were investigated theoretically in relation to thromboatherogenesis. The viscous shear stress in two-dimensional stagnation flow was calculated to determine the area of non-flow or rigid region due to non-Newtonian viscosity of blood. A factor of legional metabolic disorder probably due to oxygen defficiency was proposed.

8. MEASUREMENT OF ARTERIAL FLOW VELOCITY BY LASER DOPPLER VELOCIMETRY WITH AN OPTICAL FIBER

G. Tomonaga, N. Hoki, O. Hiramatsu, K. Mito and F. Kajiya
Dept. of Medical Engineering and Systems Cardiology, Kawasaki Medical School, Kurashiki, Okayama 701-01, Japan

In order to measure blood flow velocity in an artery with a thick wall and/or a large diameter, we have developed a laser Doppler velocimetry using an optical fiber, by which the light can be introduced into any sampling point in a vessel. At first, known blood velocities in a circular groove on a rotating turntable were measured at various revolution speeds to evaluate the accuracy of the present method. As a result, a good linear relation was obtained the Doppler shift frequency and the blood velocity ($r=0.998$). Then, the blood flow velocity was measured in various arteries of mongrel dogs such as femoral and coronary arteries. It was demonstrated that the measurements were accurately achievable in small sampling volume across a vessel, even at the points near the vessel wall. The blood flow velocity obtained in the coronary artery was diastolic dominant which is characteristic of the coronary arterial flow.

9. FLUID DYNAMIC CLASSIFICATION OF SUPRAVALVULAR AORTIC STENOSIS.

M. Sugawara, S. Hanya*, T. Yamaguchi, K. Tanishita, Y. Sakurai and A. Ishihara*
The Heart Institute Japan, Tokyo Women's Medical College, Shinjuku-ku, Tokyo 162, Japan.* Dept. of Thoracic & Cardiovascular Surgery, Univ. of Kitasato, Kitasato, Sagamihara.

To clarify the hemodynamic difference between the hourglass and hypoplastic types of supravalvular aortic stenosis, model experiments in fluid dynamics were performed. From the distribution of the total pressure along the model tubes and the flow as visualized by the aluminium powder method, it has become clear that the pressure loss in hourglass type is caused by the flow separation resulting from the rapid increase in cross-section distal to the stenosis and will be well improved by the surgical correction of the local stenosis. In the hypoplastic type, on the other hand, the pressure loss occurring in the ascending aorta is neither large nor due to a localized cause. Therefore, the surgical correction does not seem to be effective.

10. CORONARY ARTERIAL FLOW DYNAMICS UNDER LOADING CONDITION OF ELASTIC AND RIGID CONSTRICTIONS

N. Hoki, G. Tomonaga, O. Hiramatsu, K. Mito and F. Kajiya
Dept. of Medical Engineering and Systems Cardiology, Kawasaki Med. School, Kurashiki 701-01, Japan

Using mongrel dogs, the pressure-flow relationships were analysed in the coronary artery with an elastic constriction and the results were compared with those in a rigid constriction. In the case with an elastic constriction the vascular self-exciting oscillation (SEO) developed when the extravascular loading pressure exceeded the diastolic aortic pressure, and the blood flow rates fell abruptly with an occurrence of the SEO. In the case with a rigid constriction the SEO did not develop and the blood flow rates kept well until just before the degree of coronary stenosis became around 80%. These results indicate that in the former the SEO have a potent influence on the decrease of the coronary arterial flow, while in the latter the coronary blood flow is affected mainly by the degree of coronary arterial stenosis.

11. A POSSIBLE MECHANISM OF CEREBRAL BLOOD FLOW REGULATION.—CHANGES IN FLOW DISTRIBUTION BETWEEN THE INTERNAL AND EXTERNAL CAROTID ARTERIES INDUCED BY VASOACTIVE AGENTS——

Y. Kawai, T. Fukushima, T. Ohhashi and T. Azuma
Dept. Physiol. and Res. Lab. Cardiovasc. Disease, Shinshu Univ. Sch. Med., Asahi 3-1-1, Matsumoto, 390 Japan

Y-shaped canine arterial preparations consisting of the common, internal, and external carotid arteries were suspended in an organ bath and perfused with arterial blood led from support dogs at a constant rate of flow. Administration of some vasoactive substances into the perfusate induced redistribution of flow between the internal and external carotid arteries (steal-like phenomenon). Norepinephrine increased the rate of flow in the internal carotid artery and decreased that in external carotid artery. 5-hydroxytryptamine, on the other hand, brought about a change of opposite direction : i. e. a decrease of internal carotid flow and an increase in external carotid flow. A simple mathematical model is developed to investigate the steal-like phenomenon. Based on the pure resistance theory, we calculated the changes in diameters of the internal and external carotid arteries. Assuming that the diameter of the internal carotid artery was kept unchanged, norepinephrine reduced the diameter of the external carotid artery by about 60%. Under the reciprocal condition, 5-hydroxytryptamine decreased the diameter of the internal carotid artery by about 50%. These findings suggest that the steal-like phenomenon occuring between the internal and external carotid arteries may take part in the regulation of cerebral blood flow.

12. RHEOLOGICAL STUDIES ON CHROMOSOME MUTATION II. UNRAVELING ASSAY OF RHEOLOGICAL LESIONS IN CHROMATIN.

M. Watanabe and Y. Kinjo
Tokyo Metropolitan Isotope Research Institute, Setagaya-ku, Tokyo 158, Japan

Some rheological lesions of DNA molecule (single-strand break and/or double-strand break, cross-linking and aberrant distortion) induced by ionizing radiations in the chromatin network isolated from mouse leukemic cell line L5178Y, rat thymocytes, cellular slime mold amoeboid cells and sea urchin sperms were studied employing improved technigues of "unraveling assay". The irradiated chromatin was unraveled by some "rheological agents", i. e., alkaline solution (TEAH, pH 12), polyanions (heparine, sodium dextran sulfate), and 8-ethoxy caffeine. The broken and eluted DNA molecules as well as the retained molecules within the chromatin network were assayed by scintillation counting, microfluorometry and whole-mount electron microscopy. The condensed DNA and chromatin fibril in the entangled chromatin network is supposed to give various rheological effects, i. e., accumulating latent lesions, promoting latent lesions, immediate restitution of primary lesions and interfering repairing.

13. DIAGNOSIS OF JOINT DISEASE BY THE DIELECTRIC SPECTROMETER

T. Tateishi, Y. Shirasaki and Y. Miyanaga*
Mechanical Engineering Laboratory, Sakura-mura, Niihari-gun, Ibaraki,* Dept. Orthopaedic Surgery, University of Tokyo, Hongo, Bunkyo-ku, Tokyo

The dielectric properties of synovial fluids, cancellous bone and articular cartilage at frequencies 33Hz to 1.7 MHz have been measured by means of a psuedorandom noise dielectric spectrometer, which processes the data on the response of a sample to a psuedorandom noise. Both the dielectric increment and the dielectric loss of synovial fluids are increased by heating at temperatures above 0℃. The obvious dielectric differences between osteoarthritic and reumatoid synovial fluids are found. The magnitude of the dielectric constant of the synovial fluid aspirated from osteoarthritic human knee joints has greater value than that of the reumatoid fluids. Both the dielectric constant and the dielectric loss of the osteoarthritic fluids increase after the aspiration.

14. VISCOELASTIC PROPERTY OF CRYSTALLINE LENS (THE CONSIDERATION BY THE KINEMATIC MODEL)

A. Takami,
Yamawaki Gakuen Junior College, Minato-ku, Tokyo 107, Japan.

Human crystalline lenses in vitro have viscoelastic properties. When an external force was applied on the lens, the strain (deformation) occured rapidly at first, then it increased gradually with time until even several minutes. When the force is unloaded, following rapid partial recovery, the deformation of the lens gradually recovers (Fukuda, 1962 ; Kikkawa and Sato, 1963 ; Itoi, 1965). On the other hand, it is known that the kinematic models of viscoelastic bodies are generally expressed by the Maxwell model, the Voigt model, three elements' model or four elements' model. In this report, three elements' model has been used as the model of the lense. From observations, the rigidity and the viscosity of the model have been calculated, while the calculated values have the considerable deviations by the force in spite of the same lens. It seems that the viscoelastic properties of the lens are very complicated.

15. ESTIMATION OF THE SMOOTH FIBER ORIENTATION IN CANINE ARTERY.

O. Hiramatsu, N. Hoki, G. Tomonaga, K. Mito, and F. Kajiya,
Dept. of Medical Engeering and Systems Cardiology, Kawasaki Med. School, Kurashiki 701-01, Japan.

The fiber orientation of vascular smooth muscle has been considered to play an important role in a vascular spasm and its critical closing. It was difficult, however, to evaluate the mechanical meaning of fiber orientation in arterial contraction in situ. In the present study, we have proposed a new simple method to elucidate the physical effect of the pitch angle of smooth muscle on vascular closing. Axial stretching was made in arteries of mongrel dogs and the axial strain-flow relations were analyzed in each artery. An index to evaluate the pitch angle was calculated from the degree of axial strain corresponding to the cessation of the flow. The indices of the pitch angle estimated were 43.5 , 36.7 and 50.5 in femoral, carotid and left circumflex coronary arteries, respectively. These values were similar to those reported from the morphological experiments.

16. ON THE UNSTABLE PHENOMENA OF CANINE INFERIOR VENA CAVA UNDER EXTRAVASCULAR PRESSURE

M. Sato and N. Ohshima
Institute of Basic Medical Sciences, The University of Tsukuba, Ibaraki 305, Japan.

Mechanical behaviors of fresh and 1% glutaraldehyde (GA)-treated vena cava excised from mongrel dogs were examined at 37 C under transmural pressure from -8 to 10 cmH_2O. Their intravascular volume and transmural pressure were controlled by infusing a proper amount of saline solution by a micropump. We obtained the pressure-volume relations and observed the configurations of cross section from photographs taken by ultrasono-tomography. Unstable phenomena began to reveal with a partial collapse unexpectedly at slightly positive transmural pressure of about 0.3 cmH_2O. From complete collapse to circular sections, the perimeter and the area of cross section increased for the fresh vena cava. For the GA-treated specimens, on the other hand, the rate of perimeter increase was small during collapsed states. These data suggested that both the bending and the tensile characteristics were important for the fresh vena cava and the bending was dominant for the stiffened one.

17. PARAMETRIC DESCRIPTION OF MECHANICAL BEHAVIOR OF ARTERIAL WALLS

K. Hayashi, S. Nagasawa* , Y. Naruo* , K. Moritake* , A. Okumura* , and H. Handa*
National Cardiovascular Center Research Institute, Suita, Osaka 565, Japan.* Kyoto University Medical School, Department of Neurosurgery, Kyoto 606, Japan.

Although arterial walls usually yield nonlinear relations between the intraluminal pressure (P) and the diameter (D), linear relations are obtained between the logarithm of pressure ratio (P/Ps) and the distension ratio (D/Ds) in the physiologically normal pressure range and are described as follows : $ln\ (P/Ps)=\beta\ (D/Ds-1)$, where Ds is the standard diameter at the standard pressure, Ps. The generalized form of this equation is : $\beta = (dP/P)/(dD/Ds)$, which can be used for a wider pressure range as well as for pathological cases. The coefficient, β, has been proved to represent the apparent stiffness of arterial walls. Physical meaning of this stiffness parameter and its feasibility are discussed using the pressure-diameter data of various human and canine arteries.

18. THE AORTIC BARORECEPTOR ACTIVITY IN RABBITS AND THE DISTENSIBILITY OF THE AORTIC WALL.

M. Minamiyama and M. Hasegawa
Dept. of Vascular Physiology, National Cardiovascular Center Research Institute, Suita, Osaka 565, Japan.

Baroreceptor activities and outer diameter were examined after the application of square wave pressure

Vol. 17
1980

steps to the in situ aortic arch-aortic nerve preparation. Aortic diameter showed a sharp increase at the initial step pressure rise followed by a small additional increase at the subsequent constant pressure level. Impulse frequency reached its peak at the maximal rate of diameter change followed by a slow rise with increasing diameter. This increased sensitivity of the baroreceptor is dependent on both the pressure level and the change in tone of the smooth muscle fibers of the wall. Stress-strain curves and stress relaxation curves were obtained with circumferential strips from the baroreceptor area and its vicinities. The region-dependent difference in mechaical behavior was not significant in the aortic arch. Only a slight degree of relaxation was observed in the aortic wall.

19. MECHANICAL PROPERTIES OF HUMAN CEREBRAL ARTERIES SUBJECTED TO SUBARACHNOID HEMORRHAGE.

S. Nagasawa, Y. Naruo, A. Okumura, K. Hayashi* , K. Moritake, and H. Handa
Department of Neurosurgery, Kyoto University Medical School,Kyoto 606, Japan, *National Cardiovascular Center Research Institute, Suita, Osaka 565, Japan

Mechanical properties of human intracranial vertebral arteries subjected to subarachnoid hemorrhage were studied. Their pressure-diameter curves are biphasic and have sharp flexion at the pressure of 181 ± 10 mmHg when their smooth muscle is activated by KCl 50 mM. The strong vaso-constriction accompanied with little change in the vascular diameter is retained up to the pressure level at the flexion point, above which the constriction is released abruptly. The existence of the flexion point at a high pressure level is an important feature in considering the development and the treatment of the cerebral ischemia produced by the vaso-spasm.

20. CHANGES OF BASILAR ARTERY MECHANICS AND COMPOSITION AFTER SUBARACHNOID INJECTION OF BLOOD IN THE DOG

Y. Naruo, S. Nagasawa, A. Okumura, K. Moritake, H. Handa, K. Hayashi* , and T. Takeda**
Dept. of Neurosurgery, Kyoto Univ. Med. School, Kyoto 606,* National Cardiovasc. Center Res. Instit., Suita, Osaka 565, **Dept. of Pathology, Kyoto Univ. Chest Disease Res. Instit., Kyoto 606.

Passive mechanical properties and connective tissue composition of the canine basilar artery were chronologically studied after subarachnoid injection of fresh autogenous blood through the cisterna magna. Stress-strain curves were shifted to the right and stiffness parameters and incremental elastic moduli were lower in the blood-injected groups than in the control. While both collagen content and elastin content increased chronologically after the blood injection, the increase in elastin content appeared earlier and more markedly than that in collagen content. Ratios of collagen content to elastin content, which were found to be lower in the blood-injected groups, correlated well with the stiffness parameters and the incremental elastic moduli.

21. BIORHEOLOGICAL APPROACHES IN NON-INVASIVE AND QUANTITATIVE MEASUREMENT OF ARTERIO-SCLEROSIS IN THE CAROTID AND CEREBRAL ARTERIES (CCA)

S. Yoshimura, H. Furuhata, R. Kanno, K. Kodaira, K. Ohara, and K. Fujishiro
4 th Dept. of Int. Med., ME Lab., Jikei Univ. School of Med.

Arterio-sclerotic changes of CCA could be measured by a method using both of the carotid blood flow informations(CBF)and an electric simulation model for CCA. (1) CFB is the absolute values and waveforms of velocity V_b, diameter $D_b$and flow volume Q_b which can be non-invasively measured by a newly-developed ultrasonic 'QFM' system. (2) The volume elastance of carotid artery (V_E) has been determine from D_b, $\Delta D_b$and the pressure pulse wave. (3) The compliance of cerebral vascular system (C_P) has been obtained from the value of model parameter at the optimum approximation of Q_b in an analog simulation method. It has been otained from clinical measurement that the elder subjects showed a large increase 4 times in $V_E$and decrease 70% in $C_P$in comparison with the younger ones. This non-invasive method will be routinely applied to clinical fields as a useful method to measure the arterio-sclerotive changes of CCA.

22. COMPLIANCE OF THE PULMONARY "VENOUS" SYSTEM ESTIMATED FROM PULMONARY ARTERY WEDGE PRESSURE TRACINGS.

T. Tanaka, M. Arakawa, K. Gotoh, T. Suzuki, M. Gotoh, H. Miyamoto, M. Yamaguchi, T. Nakano, H. Itoh and S. Hirakawa
The 2nd Dept. of Internal Medicine, Gifu University, Gifu 500, Japan

There is a paucity of data concerning the compliance ($\Delta V/\Delta P$) of the pulmonary "venous" system, consisting of the pulmonary veins and left atrium. We estimated the compliance of the human pulmonary "venous" system from the pulmonary artery wedge pressure tracings. The slope compliance was given by an equation, $\Delta V/\Delta P = 0.4 \cdot k'' \cdot SV/(v-d)$ (Hirakawa), where $k'' = 0.075 \cdot \overline{PAW} + 0.9$, SV = stroke volume, v = v wave of PAW pressure tracings, d = diastasis (pre-a) of PAW pressure tracings.

$\Delta V/\Delta P$ of the pulmonary "venous" system in man was normally 10—20 ml/mmHg, and in 40 cases of mitral stenosis, we found a relation of $\Delta V/\Delta P = 1/(0.0079 \cdot \overline{PAW} + 0.0183)$.

23. A STUDY ON FLOW COMPONENTS OF AORTIC PRESSURE PULSE

R. Nakayama, H. Toyoshima, S. Ozawa, Y. Ishikawa and T. Fukushima*
Dept. of Intn. Med. Nat. Cardiovasc. Cent., Suita, Osaka 565, Japan. *Dept. of Physiol. Shinshu Univ. Med. School, Asahi 3—1—1, Matsumoto 390, Japan**

The motion of fluid in arteries is governed by the Navier-Stokes equations under the condition of continuity in cylindrical coordinates. From the theoretical discussion it appears justified that the pressure pulse wave P(x, t) consists of a forward wave $\Delta P_1(x=x_0, t)$ or $\Delta P_1(x, t=t_0)$ $(=\rho cv)$ and a retrograde wave $\Delta P_2(x=x_0, t)$ or $\Delta P_2(x, t=t_0)$ produced by reflection. The ΔP_2 wave should interfere with the ΔP_1 wave. According to analysis of actual waves the minimum points of the oscillatory wave $\{P(x, t)-\Delta P_1(x)\}$ were seen at ascending aorta, middle part of aortic tree and distal part of abdominal aorta, corresponding to the pressure nodes. One maximum point of the oscillation seen at the middle of the thoracic aorta (trough) was 180° out of phase compared with another maximum point of the wave observed at the middle of abdominal aorta (peak). That is, the wave obtained by the subtraction of $\Delta P_1(x, t=t_0)$ from P(x, t) appears to be a "standing wave" which is an evidence of "interference".

24. A TRIAL OF QUANTITATIVE MEASUREMENT OF AORTIC COMPLIANCE IN MAN

S. Ozawa, Y. Ishikawa, H. Toyoshima and R. Nakayama
Dept. of Intn. Med. Nat. Cardiovasc. Cent., Suita, Osaka 565, Japan

Elastic properties of the aorta are of basic importance for the dynamics of the arterial pulsations, and the quantitative measurement of aortic compliance is essential for the physiologic diagnosis of elastic abnormalities observed in the arterial diseases. The pressure volume behavior of the aorta was studied by means of the manometer implanted at the cathetertip and the linear ultrasonic tomography (LUT). M mode scan at a point of the aorta selected by the LUT longitudinal scan sectional observation was simultaneously recorded with the pressure wave at the point. From the record of M mode scan the maximum diameter ($2R_1$) and the minimum diameter ($2R_2$) were measured, and the pressure pulse (ΔP) was obtained from the pressure pulse wave. The aortic compliance was calculated by the following equation: $C=\pi(R_1^2-R_2^2)/\Delta P$ ml/mmHg. The value of C (abdominal aorta) obtained from a normal subject (53 y.o.M) was 0.004784, while that from an ASO patient (64 y.o.M) was 0.000991.

25. RELATION OF COMPLIANCE CALCULATED FROM PULSE WAVE TRAVEL TIME TO THAT OF THREE COMPONENT MODEL

O. Okai
Department of Physiology, Kyorin University School of Health Science, Mitaka, Tokyo 181, Japan

Dogs were anesthetized with penthobarbital. Arterial pressure was measured at the ascending aorta and the femoral artery. From the travel time t of pulse wave between both pressure-measuring points the compliance can be calculated: $C=k_1t^2/D$ where D is diameter of the vessel, k_1 is constant; abbreviated compliance is defined as $C'=k_2t^2$. On the other hand the three component model is composed of aortic resistance R_1 in series with Windkessel model i. e., a parallel circuit of compliance C_0 and a resistance R_2. Then impedance is expressed as $Z=R_1+R_2/(1+j\omega R_2C_0)$. Using cardiac output F we get mean pressure $P=ZF$, $P_1=R_1F$, $P_2=R_2F$. Thus $C_0=FT(1/P_1+1/P)$ where $T=R_1C_0P_2/(P_1+P_2)$. The results were that (1) close agreement between compliances C and C_0 was observed; (2) the compliance C' was related almost linearly to C_0.

26. DECREASE IN CBV AND RBC AGGREGATION IN ACUTE ISCHEMIA OF CEREBRO-CORTICAL TISSUE IN CATS

M. Tomita, F. Gotoh, N. Tanahashi, K. Tanaka and M. Kobari
Dept. of Neurol., Keio Univ. School of Med., Shinjuku-ku, Tokyo 160, Japan

Changes in cerebral blood volume (CBV) observed by our photoelectric method after clipping of a middle cerebral artery at its origin, may be masked by a factor related to RBC aggregation in sluggishly flowing blood. Separation of the factor from decrease in optical density in the ischemic area was attempted by calculating the relative decrease in shear rate of the blood on which RBC aggregation depends. This was accomplished in the ischemic area by frequent determinations of tissue hemodilution curves produced by saline injection into the carotid artery. The vascular bed was assumed to comprise a simple tube, the diameter of which was related to the square root of CBV (calculated from changes in optical density) and through which blood flowed at a relative velocity of 1/t. The in vitro relationship between shear rate and RBC aggregation was employed for estimation of the RBC aggregation (%). It is concluded that the vascular bed decreases in the face of the autoregulatory mechanism in response to abrupt occlusion of the artery.

27. HEMORHEOLOGICAL OBSERVATIONS ON CUTANEOUS MICROCIRCULATION IN CHOLESTEROL-FED RABBITS. 1. ACUTE AND SUBCHRONIC CHANGES.

M. Asano, A. Hirokawa, S. Ogawa, C. Ohkubo and K. Sawanobori
Dept. of Physiological Hygiene, the Institute of Public Health, Minato-ku, Tokyo 108, Japan.

Vol. 17
1980

Intravascular behaviors of cellular elements of blood were observed vital-microscopically in a transparent rabbit ear chamber for a period of 30 days during which the rabbit was fed cholesterol-supplemented (1.5%, W/W) standard diet. About 6 hours after the initiation of feeding the cholesterol diet, leukocytes became highly adhesive in post-capillary vessels. In the venular area leukocytes adhered in pile to the lumenal wall places for long periods. The mass of leukocytes looked like a thrombus, but platelets appeared not to participate in forming it. Following 1 week's cholesterol loading, leukocytes became considerably adhesive even in arterioles, though not forming large masses, and erythrocytes were apt to make aggregates such as sludges and rouleaux. These changes in behaviors of leukocytes and erythrocytes were observed invariably till the 30 th day of the cholesterol loading.

28. PHYSIOLOGICAL AND MORPHOLOGICAL STUDIES OF BLOOD FLOW REDISTRIBUTION IN MICROCIRCULATORY BEDS OF THE STRIATED MUSCLE OF DOG'S HIND LIMBS.

H. Yokoyama, T. Inui, M. Stoh, and S. Hirakawa
Department of Medicine, Gifu University School of Medicine, Gifu 500, Japan

As a physiological approach, we measured the diffusion capacity PS (permeability P, surface area S pruduct) for ^{22}Na or ^{86}Rb, using "indicator diffusion" method with a single injection into the femoral artery. PS was decreased by about 30–40 % both at the end of 6 minutes after the venous pressure was acutely elevated and at the end of 20 minutes after the blood was shed in amount of 20 ml/kg. As a morphological approach, the minute blood vessels of the striated muscle of dog's hind limbs were visualized, employing low-viscosity silicone rubber injection method, and the capillary fiber ratio (C/F ratio) was measured. C/F ratio was decreased about 20% only when blood was shed in amount of 20 ml/kg. It is suggested that the blood flow is redistributed in favor of non-exchange vessels during both venous congestion and hemorrhagic hypotension.

29. VISCOSITY OF A SUSPENSION OF MODEL RED CELLS

T. Murata
Dept. of Physics, Tokyo Metropolitan University, Setagaya-ku, Tokyo 158, Japan

The defomation of a solid particle (as a model of red cell) freely suspended in an unbounded incompressible Newtonian fluid undergoing a simple shearing motion is investigated theoretically under some assumptions. It is assumed that the undeformed particle is spherical in shape and is a homegeneous, isotropic elastic body obeying Hooke's law. It is shown that for small values of the deformation parameter the particle deforms into a spheroid and rotates at a constant velocity. The apparent viscosity of a dilute suspension of these deformable particles is also calculated. It is shown that the apparent viscosity decreases with increase in the rate of shear. This non-Newtonian behavior is due to the deformation of the individual particles.

30. DEFORMATION PROCESS OF RED CELLS IN THE INFLOW AND OUTFLOW AT THE TIP OF MICROPIPETTE

H. Niimi and T. Yamakawa.
National Cardiovascular Center Research Institute, Suita, Osaka 565, Japan

The deformation of human red cells was examined when the they flowed into and out the tip of micropipette. Their change in shape was determined in the high seed motion picture photography(240 frames/sec). It was found that the deformation process of red cells in the outflow was different from that in the inflow.

31. RELATION BETWEEN RED CELL SHAPE AND SUSPENSION VISCOSITY

T. Suda, N. Maeda and T. Shiga.
Dept. of Physiology, Med. Sch., Ehime Univ., Ehime 791-02, Japan

Some cationic drugs, e. g., chlorpromazine (CPZ) and isoxsuprine (ISOX), modified the cell shape to stomatocyte, then to spherostomatocyte, depending on drug concentration. The suspension viscosity decreased, as transformation to spherostomatocyte proceed (i. e., induced by 0.2 mM CPZ or 3 mM ISOX). The membrane fluidity, monitored by fatty acid spin label motion, increased by CPZ at higher concentration, but unaltered by ISOX. Therefore the fluidity change was not essential but the spherostomatocyte formation was important for the deceased suspension viscosity (the cell volumes were similar). Quantitative data of drug uptake by red cells and ghosts revealed that both drugs were present in membrane and in cytoplasm (partly bound with hemoglobine, as proved by equilibr. dialysis). Although the above effective doses were different, the estimated drug conc. in membrane was similar for both drugs (ca. 2 mM/l of packed ghosts).

32. EFFECT OF TEMPERATURE AND VISCOSITY OF SUSPENDING MEDIUM ON ERYTHROCYTE FILTERABILITY

Y. Isogai, K. Mochizuki, T. Yokose, T. Maeda, and M. Akiyama
Third Dept. of Med. Jikei University School of Medicine, Tokyo 105, Japan

To observe the effect of temperature on erythrocyte filtrability (EF) a negative pressure filtration system

using polycarbonate membrane filter and variable inductive transducer was deviced. In degree of temperature between 10°C and 37°C, the raising EF was observed as it was going to higher : there was around 45% raised EF observed when the temperature was changed from 21°C to 37°C. On the other hand EF was decreased with negative correlation with increasing viscosity of suspending medium which was obtained by adding low molecular dextran, Rheomacrodex into medium in concentration between 2% and 20%. These results suggested that it was important to make constant in temperature and viscosity of suspendig medium as well as concentration of erythrocytes at all the time when EF was examined.

33. AN EXPERIMENT TO USE A NEW TYPE VISCOMETER (BIORHEOLIZER LVT 1000)

K. Mochizuki, M. Akiyama, T. Maeda, S. Ikemoto, M. Ashikaga, H. Okabe, T. Yokose, and Y. Isogai
Dept. of Internal Medicine, Jikei University School of Medicine, Tokyo 105, Japan.

We had a chance to test a viscometer named Biorheolizer type 1000 newly developed by Tokyo Keiki co-op. The tool is a cone-plate rotational viscometer, and the rate of revolution of cone is set between 3 RPM and 100 RPM, the shear rate is 22.5 sec^{-1} to 750 sec^{-1}. The volume of sample is 0.5 ml and the temperature is controlled to 37±0.15°C. The reading is taken by photodetecter, and the results of measurement are printed out automatically. Sample exchange is easy by autowashing system. When standard oil (JS 10) is measured at 3 RPM, the coefficient of variation of results is 1.22%, and that of blood is 2.84%. In conclusion, this viscometer is useful to deal with a large number of samples in clinical study.

34. RELATIONSHIP BETWEEN FIBRINOGEN LEVELS IN BLOOD AND ELEVATION OF BLOOD VISCOSITY AT LOWER TEMPERATURE

T. Matsuda, M. Ogawara, R. Miura, T. Seki, and M. Yokouchi
Dept. Physiology, Tokyo Metropolitan Institute of Gerontology, Tokyo 173, Japan.

Viscosity of blood at 37°C and 25°C was compared at shear rate of 0.39 sec^{-1}. There was a significant correlation between ratios of blood viscosity determined at 25°C to one at 37°C and fibrinogen levels in blood in 49 blood samples taken from hospitalized patients randomly, although those did not correlate with hematocrit values. Effects of fibrinogen on elevation of blood viscosity at lower temperature were confirmed in erythrocyte suspension which contained various amount of fibrinogen. Prothrombin times and activated partial thromboplastin times of normal plasma measured at 25°C prolonged to levels of 25–30 per cent activity on saline dilution curves at 37°C. From these results, it was concluded that low temperature elevated blood viscosity, especially when plasma fibrinogen content increased, although hypocoagulability of blood canceled risk of thrombosis.

35. NONLINEAR VISCOELASTICITY OF CLOTTING BLOOD.

Y. Sugiura, and E. Fukada
The Institute of Physical and Chemical Research, Wako-shi, Saitama 351, Japan.

The time variation of dynamic viscoelastic properties of thrombin-fibrinogen solution and blood was investigated during clotting with special attention of nonlinearity between stress and strain. Viscoelastic nonlinearity of thrombin-induced fibrin gel was observed to become pronounced as the gelation reaction proceeded, while viscoelastic nonlinearity of clotting blood was observed to diminish as the clotting reaction proceeded. The major origin of the viscoelastic nonlinearity appears to be caused by stretching out of network chains of fibrin gel. In blood and plasma, which contain factor XIII and Ca^{2+}, the formation of cross-links due to covalent bonds leads to more elastic and harder network which shows less nonlinearity.

36. EFFECTS OF DRUGS ON BLOOD VISCOSITY.——Attempt of easy measuring method in vitro——

S. Kobayashi, Y. Kanakubo and T. Yamaguchi*
Hospital Pharmacy, Chiba Uhiversity.* Pharmacy, Dōjinkai, 1-8-1 Inohana, Chiba 280, Japan

In comparison of Pentoxifyllin with Isoxsuprine, long lasting of the former and immediate effect of the latter on stored blood viscosity were suggested by easy measuring method. Viscosity of corpuscle value was lowered by LMWD in vitro.

37. BLOOD VISCOSITY IN ABNORMAL FETUSES

M. Kaibara, Y. Marumoto, I. Taniguchi and T. Kobayashi
Dept. of Obstet. and Gynecol., Tokyo University Branch Hospital, Bunkyo-ku, Tokyo 112, Japan.

Viscosity was measured in the cord blood from normal and abnormal fetuses at a shear rate of 1 sec^{-1} and at temperature of 24°C. The mean value for blood viscosity of small for dates fetuses (SFD) and that of fetuses with intrauterine infection was 29.8±14.7 (mean±SD) cp and 27.1±7.8 cp respectively and was significantly higher than that of normal fetuses (19.8±7.5 cp). Elevation of blood viscosity in SFD was due to incresed hematocrit level and in fetuses with intrauterine infection was due to increased fibrinogen level. It was suggested that feto-placental circulation would be impaired due to elevated blood viscosity in these abnormal fetuses.

Vol. 17
1980

38. BLOOD RHEOLOGY AND RIGIDITY OF ERYTHROCYTES

N. Iida, and S. Shigehiro
Div. of Biomedical Control, Research Institute of Appl. Electri., Hokkaido Univ., Sappro 063, Japan
Dept. of Internal Medicine, Kitasato Univ. Med. School, Kanagawa 228, Japan

The rheological properties of blood in cardiac diseases (myocardial infarction and angina pectoris) were analysed by using Casson and Herschel-Bulkley (H-B) models. It was found that parameter n contained in H-B model is a function of hematocrit and the value is $n \cong 1.2$ in 45% whole blood and $n \cong 1.0$ in plasma and that parameter k represents the apparent viscosity of blood above shear rate $50s^{-1}$.Furthermore, it was found from the fluid emulsion model of blood that the abnormal viscosity of blood in the cardiac diseases is closely related with the change of rigidity of erythrocytes and that the shear stress and the apparent viscosity of blood flow in high shear rate increase remarkably with the increase of rigidity of erythrocytes. The finding suggests that the increase of rigidity of erythrocytes influences directly on the flow resistance, the damage of the wall in small vessels and the hemolysis of erythrocytes.

39. HEMORHEOLOGICAL ABNORMALITIES IN DIABETICS WITH MACROANGIOPATHY

S. Ikemoto, M. Akiyama, T. Maeda, M. Ashikaga, H. Okabe, T. Yokose, K. Mochizuki and Y. Isogai
3rd Dept. of Int. Med., Jikei Univ. Sch. of Med., Tokyo 105, Japan

This research aimed at elucidating the role of hemorheological factors in the pathogenesis of vascular disease in diabetics. Some hemorheological factors were observed in diabetics with macroangiopathy and/or microangiopathy. In the diabetics with macroangiopathy, fibrinogen, plasma viscosity, factor Ⅷ related antigen and the maximum dynamic elastic modulus of the blood clot were increased significantly. These changes were correlated with those in diabetics with microangiopathy. These factors are considered to be related with the vascular endothelial damage. It is suggested that diabetic macroangiopathy may be related at least partially with microangiopathy, influenced by some hemorheological factors.

The annual meeting was held under the presidency of Dr. T. Azuma, Professor of Physiology, Shinshu University School of Medicine. The attendance numbered about one hundred.

The meeting consisted of the following eight sections at which a total of forty three papers were presented : (1) Numerical analysis and biorheology, (2) Rheological evaluation of blood flow measurements, (3) Regulation of blood flow, (4) Rheology of cells and tissues, (5) Structure and function of blood vessel walls, (6) Pulse wave and blood vessel hemorheology, (7) Hemodynamic aspects of microcirculation, and (8) Rheology of blood. All the abstracts listed here were written on the author's own responsibility.

The next annual meeting will be held in Tokyo under the presidency of Dr. K. Taniguchi, Associate Professor of Internal Medicine, Tokyo Medical and Dental University.

BLANK
PAGE

Vol. 17
1980

BIORHEOLOGY, Vol. 17, pp. 511-512, 1980
Printed in the USA. All rights reserved.

0006-355X/80/050511-02$02.00/0
Copyright (c) 1981 Pergamon Press Ltd

ANNOUNCEMENT

Second European Conference on Clinical Haemorheology

London, England. 30. September - 2. October, 1981

The principal aim of this conference will be to encourage further links between the rapidly expanding science of haemorheology and the clinical practice of medicine and surgery. Sessions will be primarily arranged around individual disease processes such as diabetes, cerebrovascular disorders, myocardial and limb ischaemia. There will also be sessions on methodology and therapy as well as other clinical topics of haemorheological interest.

An exciting social and ladies' programme is being arranged for the participants of the conference.

For further details, please write to:

Miss B. Komoniewska BA, Conference Secretary
Second European Conference on Clinical Haemorheology
Royal Society of Medicine
1 Wimpole Street, London W1M 8AE, United Kingdom

President of the Conference: Sir John Stallworthy

Vice Presidents: A.L. Copley and G.W. Scott Blair

Organising and Scientific Advisory Committees: J.A. Dormandy (Chairman), P.T. Flute (Vice Chairman), A.J. Barnes (Programme Secretary), J.R. Pattison (Treasurer), B. Komoniewska (Conference Secretary), G. Bennette, A. Bloom, G.V.R. Born, N.L. Browse, C.G. Caro, S. Chien, N. Cristal, T. di Perri, J. Ditzel, L. Dintenfass, P. Drouin, A. Ehrly, C. Forbes, S. Forconi, E. Fukada, P. Gaehtgens, C. George, M. Hanss, H. Hartert, G. Holti, E. Housley, E. Housset, Irene Juhan, Z.S. Latallo, P. Leblond, G. Lowe, G.A. Marcel, J. Marshall, H. Meiselman, T.C. Pearson, M. Samama, H. Schmid-Schönbein, G.V.F. Seaman, A. Silberberg, J. Sirs, J.F. Stoltz, J. Stuart, D.J. Thomas, D.P. Thomas, M. Verstraete.

The Alan C. Burton Prize Fund

The following information was supplied by Professor P.B. Canham in a letter of October 10, 1980. However, it was sent too late for inclusion as a footnote to the Obituary of Alan Burton, which was published in BIORHEOLOGY Volume 17, Number 4, pages 297-300, 1980. Since the information given in Professor Canham's letter will be of interest to our Readers, it is as follows:

> "The Alan C. Burton Prize Fund was established when Dr. Burton became Professor Emeritus in 1976. The prize consists of a scroll and $300, awarded to the student with the top marks in third-year Biophysics courses. Dr. Burton's family have requested that memorial contributions should go to the Prize Fund, c/o The University of Western Ontario, London, Ontario, Canada N6A 5C1."

1981 Advances in Bioengineering

American Society of Mechanical Engineers (ASME) Winter Annual Meeting

Washington, D.C. 15. - 20. November 1981

Vol. 17
1980

The Bioengineering Division of the American Society of Mechanical Engineers will be pleased to receive original abstracts for publication and presentation at the ASME Winter Annual Meeting to be held at the Sheraton Park Hotel in Washington, D.C. Although the theme of this meeting focuses on the effect of government and regulations on the engineer, all forms of original bioengineering work will be accepted in the areas of biofluid and biosolid mechanics, biohea⁺ and mass transfer, instrumentation and controls, rehabilitation engineering, medical devices and standards, biomechanics of sport, and industrial applications of bioengineering. Technical sessions will include invited keynote lectures by recognized scientists and bioengineers.

Authors are encouraged to submit manuscripts in compact format on author-prepared mats limited to two pages of text and two pages of figures. Accepted abstracts will be published in "1981 Advances in Bioengineering."

Authors may write or call for guidelines and abstract mats to:

David C. Viano, Ph.D.
Biomedical Science Department
General Motors Research Laboratories
Warren, MI 48090

Deadline for receipt of completed abstracts is June 1, 1981.

l. 17
80